



Targeting transcriptional addiction in cutaneous melanoma

Max Cigrang

► To cite this version:

Max Cigrang. Targeting transcriptional addiction in cutaneous melanoma. Cancer. Université de Strasbourg, 2023. English. NNT : 2023STRAJ048 . tel-04286456

HAL Id: tel-04286456

<https://theses.hal.science/tel-04286456>

Submitted on 15 Nov 2023

HAL is a multi-disciplinary open access archive for the deposit and dissemination of scientific research documents, whether they are published or not. The documents may come from teaching and research institutions in France or abroad, or from public or private research centers.

L'archive ouverte pluridisciplinaire **HAL**, est destinée au dépôt et à la diffusion de documents scientifiques de niveau recherche, publiés ou non, émanant des établissements d'enseignement et de recherche français ou étrangers, des laboratoires publics ou privés.

ÉCOLE DOCTORALE DES SCIENCES DE LA VIE ET DE LA SANTÉ

Institut de Génétique et de Biologie Moléculaire et Cellulaire

Thèse présentée par :

Max CIGRANG

soutenue le : **20 septembre 2023**

pour obtenir le grade de : **Docteur de l'université de Strasbourg**

Discipline/ Spécialité : Sciences de la Vie et de la Santé

**Targeting transcriptional addiction in
cutaneous melanoma**

THÈSE dirigée par :

M. COIN Frédéric

Directeur de recherche INSERM, IGBMC, Illkirch

RAPPORTEURS :

M. JANJI Bassam

Directeur de recherche, LIH, Luxembourg

Mme. KREIS Stephanie

Professeur, Université du Luxembourg, Esch-sur-Alzette

AUTRES MEMBRES DU JURY :

Mme. CHAN Susan

Directeur de recherche INSERM, IGBMC, Illkirch

“Nothing in life is to be feared, it is only to be understood. Now is the time to understand more, so that we may fear less.”

- Marie Curie

“Science knows no country, because knowledge belongs to humanity, and is the torch which illuminates the world.”

- Louis Pasteur

“I do not know what I may appear to the world, but to myself I seem to have been only like a boy playing on the seashore, and diverting myself in now and then finding a smoother pebble or a prettier shell than ordinary, whilst the great ocean of truth lay all undiscovered before me.”

- Isaac Newton

Table of contents

Table of contents.....	3
Acknowledgments.....	6
Publications and oral communications	7
Résumé en français.....	9
List of figures	13
Abbreviations and Acronyms.....	16
Preface: Thesis structure.....	21
Introduction	23
Section I: Cutaneous Melanoma	25
A. Notions about the skin, melanocytes, and melanoma.....	27
1. Skin anatomy and physiology	27
1.1. Overview of main functions.....	27
1.2. Histological structure and cellular components.....	27
2. Melanocyte Biology	29
2.1. Roles and functions of melanocytes	29
2.2. UV radiation and protection by melanogenesis.....	31
2.3. Embryonic origins and transcriptional regulation of the melanocyte identity	35
3. Skin cancers and melanoma.....	39
3.1. Clinical Classifications and Epidemiology	39
3.2. Genomic classification and driver mutations	43
B. Cutaneous melanoma disease progression	45
1. The evolving nature of melanoma progression understanding	45
2. Initiation: From melanocytes to melanocytic precursor lesions	47
2.1. Cell of origin and somatic mutations	47
2.2. Precursor lesions: Melanocytic naevi	49
3. Progression: Towards invasive melanoma	53
3.1. Melanoma in situ	53
3.2. Invasive melanoma.....	55
4. Dissemination: Melanoma metastasis	59
4.1. Melanoma spreading trajectories.....	59
4.2. Cell states, migration, and dormancy	61
4.3. The metastatic niches in melanoma and their establishment.....	65
C. Aspects of melanoma biology through the lens of Hanahan and Weinberg's hallmarks of cancer	69
1. Functional hallmarks – Core attributes.....	69
1.1. Sustained proliferative signaling, immortalization, and evading growth suppressors	69
1.2. Deregulating cellular metabolism.....	73
1.3. Resisting cell death and avoiding immune destruction	77
1.4. Angiogenesis and senescence	81
2. Enabling hallmarks – Driving forces.....	85
2.1. Tumor-promoting inflammation	85
2.2. Polymorphic microbiomes	87
3. Genetic and epigenetic hallmarks – Phenotypic plasticity.....	89
3.1. Genetic melanoma heterogeneity	89
3.2. Melanoma plasticity, phenotype switching, and cell states	91
3.2. Multi-layered reprogramming in phenotype switching.....	99

D. The clinical management of cutaneous melanoma and therapy resistance mechanisms	103
1. Melanoma treatment in 2023	103
1.1. Surgical treatment and a historical perspective for metastatic disease	103
1.2. Targeted therapy through small-molecule MAPK inhibitors	105
1.3. Immune checkpoint inhibitors.....	107
2. Mechanisms behind treatment resistance in melanoma.....	111
2.1. Different types of resistances	111
2.2. Resistance to targeted therapy.....	113
2.3. Resistance to immunotherapies	115
3. Potential prospects and future treatments	119
Section II: Gene expression, its dysregulation in cancer, and targeting transcriptional addiction	121
A. Transcription and its regulation	123
1) Genome architecture and regulatory elements of transcription	123
1.1. The importance of gene expression regulation and chromatin condensation	123
1.2. Chromatin accessibility and remodeling.....	129
1.3. Regulatory elements of transcription.....	131
2. The transcription cycle and the role of TFIID	137
2.1. Pre-initiation complex formation	137
2.2. The multiple functions of TFIID and its role in transcription initiation.....	139
2.2. Promoter proximal pausing and release into productive elongation	143
2.3. Transcription termination	147
3. Diseases associated with transcriptional dysregulations.....	147
B. Transcriptional addiction in cancer and its targeting	151
1. Gene expression dysregulation in cancer cells.....	151
1.1. Deregulation of trans-acting factors	151
1.2. Deregulation of cis-regulatory elements	159
2. Targeting transcriptional dependencies in cancer	167
2.1. Inhibiting transcription: From undruggable to reality.....	167
2.2. Targeting transcription and SEs through TFIID: THZ1 and Triptolide	173
2.3. Inhibiting oncogenic gene expression with DNA-binding molecules: Lurbinectedin	177
C. Targeting transcriptional addiction in melanoma: Research context and objectives	181
Results	183
Section I: Targeting TFIID in melanoma	185
Preface to Article 1: Context and contributions.....	186
Article 1: CDK7 and MITF repress a transcription program involved in survival and drug tolerance in melanoma.....	187
Addendum: The role of XPB in super-enhancer dependent gene expression in melanoma.....	230
Article 2: Pharmacological inhibition of XPB and CDK7 differentially disrupt super-enhancer dependent gene expression in melanoma cells.....	231
Section II: Targeting transcriptional addiction in melanoma with novel marine-derived drugs	259
Preface to Article 3: Context and contributions.....	260
Article 3: Targeting master regulator genes with Lurbinectedin and its derivatives as a novel therapeutic strategy against targeted therapy-resistant melanoma.....	261
Addendum: Mechanisms of resistance towards Lurbinectedin and its analogues.....	306

Article 4: Resistance to novel transcriptional inhibitor Lurbinectedin and its derivatives is mediated by the efflux pump ABCB1.....	307
General conclusions and remarks	340
Annexes	344
Preface to annexed Articles 5 and 6: Context and contributions.....	345
Article 5: Super-enhancer driven expression of BAHCC1 promotes melanoma cell proliferation and genome stability.....	346
Article 6: Active mRNA degradation by EXD2 nuclease elicits recovery of transcription after genotoxic stress.....	403
Bibliography	433

Acknowledgments

As I write the last few words of this manuscript, and I look back upon the last four years of my life, I realize that despite some lows, there have been a great number of amazing moments, not least because of the people that surrounded and supported me during this journey.

I would first like to thank **Dr. Susan Chan**, **Dr. Stephanie Kreis**, and **Dr. Bassam Janji** for agreeing to evaluate this manuscript. I am grateful to **Dr. Frédéric Coin**, who allowed me to work in conditions most other PhD students would be jealous of, and who found a perfect balance between solid guidance and allowing his PhD students a great deal of creative freedom. A big thank you to **Dr. Emmanuel Compe** for our many funny scientific and non-scientific discussions, and for his mentoring advice. Thanks also to **Dr. Jean-Marc Egly**, for his encouraging words. To the present and former lab engineers **Maguelone Nogaret**, **Cathy Braun** and **Philippe Catez**, I am extremely grateful for your constant readiness to help me out, and for our excellent teamwork. Thanks a lot to my fellow PhD students **Clémence Elly**, **Amélie Zachayus**, **Léane Seno**, **Pietro Berico**, **Jérémy Sandoz**, **Alexandra Helleux**, **Alexandre Haller**, **Antonin Lallement**, and **Guillaume Davidson**, from the Coin and Davidson teams, for sharing these last four years with me, and for the friendships we forged. Finally, I would like to express my deep gratitude to the many interns I had the privilege of mentoring. They showed me that the scientific process is worthless in a vacuum, and only unfolds its potential when it is shared and transmitted. A special thanks goes to **Clara Maréchal** and **Julian Obid**, whom I wish the best of luck on their PhD journeys.

Ech soen mengen **Frënn zu Lëtzebuerg** een kollektiven Merci dass dir emmer fir mech do wart, och wann ech net emmer sou disponibel war wei ech dat gewollt hätt. Ech sinn immens dankbar doriwwer esou vill Leit ze kennen, op dei ech zielen kann. Een groussen Merci och un ex an present Memberen vun der **ALUS**, dei mech firun allem dei leschten Joeren moralesch ennerstetzt an jonk gehalten hunn.

Un grand merci aussi à ma **famille étendue**, surtout à mes cousins **Valentine**, **Kelly** et **Sébastien**, et à mes deux jeunes tatas, **Meixin** et **Kerstin**, que je considère comme mes grandes sœurs. **Lizi**, ech wees dass et net emmer einfach ass mat mir als Brudder, mee ech hoffen du wees dass ech stolz op dech sinn. **Mama** et **Papa**, merci pout tout. C'est grâce à votre soutien que j'ai décidé de continuer en thèse, et donc ce manuscrit vous est dédié.

Publications and oral communications

Published articles:

1) Berico P, **Cigrang M**, Davidson G, Braun C, Sandoz J, Legras S, Vokshi BH, Slovic N, Peyresaubes F, Gene Robles CM, Egly JM, Compe E, Davidson I, Coin F. CDK7 and MITF repress a transcription program involved in survival and drug tolerance in melanoma. *EMBO Rep.* 2021 Sep 6;22(9):e51683. doi: 10.15252/embr.202051683. Epub 2021 Jul 23. PMID: 34296805; PMCID: PMC8419699.

2) Sandoz J, **Cigrang M**, Zachayus A, Catez P, Donnio LM, Elly C, Nieminuszczy J, Berico P, Braun C, Alekseev S, Egly JM, Niedzwiedz W, Giglia-Mari G, Compe E, Coin F. Active mRNA degradation by EXD2 nuclease elicits recovery of transcription after genotoxic stress. *Nat Commun.* 2023 Jan 20;14(1):341. doi: 10.1038/s41467-023-35922-5. PMID: 36670096; PMCID: PMC9859823.

Submitted articles:

1) Berico P, Nogaret M, **Cigrang M**, Lallement A, Rajabpour FV, Flores-Yanke A, Gambi G, Davidson G, Seno L, Obid J, Vokshi BH, Le Gras S, Mengus G, Ye T, Fernandez Cordero C, Dalmaso M, Compe E, Bertolotto C, Hernando E, Davidson I, Coin F. Super-enhancer driven expression of BAHCC1 promotes melanoma cell proliferation and genome stability. In Review at *Cell Reports*.

Articles in preparation:

1) **Cigrang M**, Catez P, Nogaret M, Berico P, Davidson G, Egly JM, and Coin F. Pharmacological inhibition of XPB and CDK7 differentially disrupt super-enhancer dependent gene expression in melanoma cells.

2) **Cigrang M**, Obid J, Nogaret M, Berico P, Catez P, Davidson G, Egly JM, Davidson I, Garrido-Martin EM and Coin F. Targeting master regulator genes with Lurbinectedin and its derivatives as a novel therapeutic strategy against targeted therapy-resistant melanoma.

3) **Cigrang M**, Nogaret M, Obid J, Catez P, Berico P, Davidson G, Egly JM, and Coin F. Resistance to novel transcriptional inhibitor Lurbinectedin and its derivatives is mediated by the efflux pump ABCB1.

Oral and poster presentations:

1) **Cigrang M**, Nogaret M, Coin F. Targeting Transcriptional Addiction in Melanoma with a new marine derived drug. Poster presented at the 21st Science Day of ‘La Ligue contre le Cancer’ (9th November 2021, Strasbourg, France) and the 2021 IGBMC poster session (25th November 2021, Illkirch-Graffenstaden, France). Both times voted ‘Best Poster’.

2) **Cigrang M**, Nogaret M, Obid J, Coin F. Resistance to novel transcriptional inhibitor Lurbinectedin is mediated by the efflux pump ABCB1. Virtual poster presentation at the EMBO workshop Persistent cancer cell: Molecular mechanisms, dynamic models towards therapy (28th June – 1st July 2022, Cavtat, Croatia). An updated version of this poster was also presented at the 22nd Science Day of ‘La Ligue contre le Cancer’ (14th November 2022, Strasbourg, France), the 2022 IGBMC poster session (15th November 2022, Illkirch-Graffenstaden, France).

Résumé en français

Le mélanome est la forme la plus grave et la plus mortelle de cancer de la peau. Les traitements actuels (immunothérapie et ciblage de la voie MAPK) sont limités par l'émergence de diverses sous-populations cellulaires qui diffèrent par leurs degrés de sensibilité aux traitements, ainsi que par leurs capacités d'invasion et d'expression de gènes clés. On distingue ainsi deux principaux phénotypes cellulaires dans le mélanome. D'une part, les cellules mélanocytaires sont souvent sensibles aux drogues utilisées en clinique et expriment des gènes d'identité tels que *MITF* ou *SOX10*. D'autre part, les cellules mésenchymateuses présentent une multirésistance aux traitements, une mobilité accrue et un phénotype de type cellule souche caractérisée par l'extinction de *MITF/SOX10* et l'expression de gènes tels que *AXL* et *EGFR*. À l'heure actuelle, il n'existe aucun moyen efficace et généralisé pour cibler les cellules mésenchymateuses en clinique. A ce titre, il est important de découvrir de nouvelles approches thérapeutiques. Le fait que des cellules du mélanome dépendent fortement du niveau d'expression élevé de certains gènes pour maintenir leur phénotype unique, fait que cette dépendance transcriptionnelle pourrait être l'objet d'un ciblage thérapeutique. Ainsi, l'objectif principal de ma thèse a été de tester les effets de différents types d'inhibiteurs transcriptionnels sur les cellules de mélanome. Deux stratégies distinctes d'inhibition transcriptionnelle ont été étudiées. Premièrement, l'inhibition des protéines CDK7 et XPB du facteur général de transcription TFIID, par les molécules THZ1 et Triptolide respectivement, a été étudiée (I). La deuxième stratégie a consisté à tester des inhibiteurs transcriptionnels d'origine marine qui se lient de façon covalente à l'ADN : la Lurbinectedine et deux de ses dérivés. Ces molécules ont été récemment synthétisées par l'entreprise pharmaceutique PharmaMar S.A., avec laquelle nous collaborons sur ce projet (II).

I- Le premier sujet de ma thèse, dont une partie des résultats a été publié dans *EMBO Reports* en 2021, se focalise sur le ciblage de TFIID dans le mélanome, un facteur qui est impliqué dans différentes fonctions cellulaires telles que l'initiation de la transcription et la réparation de l'ADN. Fait intéressant, il a été montré que la sous-unité kinase CDK7 est fortement recrutée dans les cellules du mélanome sur des régions appelées super-enhancers (SE), ce qui entraîne l'expression intense d'oncogènes, tels que les facteurs de transcription MITF et SOX10. Nous nous sommes donc concentrés sur le rôle de CDK7 dans le mélanome et les effets de son ciblage par la molécule THZ1. Nos résultats montrent qu'à des concentrations nanomolaires

de THZ1, les cellules à phénotype mélanocytaire présentent une forte inhibition de la croissance cellulaire, alors que les cellules mésenchymateuses sont insensibles. Pour étudier le mécanisme moléculaire de cette insensibilité, nous avons généré des cellules résistantes en exposant des cellules mélanocytaires de manière chronique au THZ1. Étonnamment, ces cellules sont devenues mésenchymateuses. L'analyse comparative du transcriptome de ces cellules devenues résistantes a montré une augmentation de l'expression d'un ensemble de gènes régulés par le facteur de transcription GATA6, comme notamment le gène codant pour la pompe d'efflux ABCG2. De manière remarquable, l'inactivation de GATA6 entraîne une baisse d'expression d'ABCG2, et resensibilise partiellement les cellules à l'inhibition de CDK7. Nous avons constaté que l'ensemble des gènes régulés par GATA6 est enrichi dans la sous-population mésenchymateuse de cellules de mélanome. L'expression de GATA6 étant anti-corrélée à celle de MITF, nous avons invalidé l'expression de MITF dans les cellules mélanocytaires et observé une augmentation de l'expression de GATA6. Conformément à notre hypothèse selon laquelle MITF pourrait réprimer l'expression de GATA6, nous avons démontré par ChIP-Seq que MITF est recruté dans une région intronique du gène GATA6, ce qui inhibe son expression. En conclusion, l'inhibition de CDK7 par THZ1 conduit à une régulation négative des gènes SE-dépendants tels que MITF et SOX10 dans les cellules mélanocytaires, ce qui favorise un switch phénotypique vers l'état mésenchymateux et résistant dans lequel le facteur GATA6 est activé.

Des inhibiteurs pharmacologiques ciblant d'autres sous-unités enzymatiques de TFIIH existent. La triptolide (TPL) est une molécule qui se lie de manière covalente à la translocase XPB et inhibe son activité ATPase. Bien qu'il y ait récemment eu des indications que l'inhibition de XPB pourrait perturber les SEs dans le cancer du pancréas, il n'est pas clair si XPB est directement recruté dans ces régions et si ses activités enzymatiques entrent en jeu. De plus, l'interaction potentielle entre XPB et les SEs n'a pas été étudiée dans d'autres cancers tels que le mélanome, et on ne sait toujours pas si les différentes sous-unités de TFIIH comme CDK7 et XPB auraient la même importance dans l'activation des SEs, et si, en conséquence, leurs inhibitions auraient des effets similaires. Nos résultats montrent que contrairement à THZ1, toutes les cellules de mélanome testées, qu'elles soient mélanocytaires ou mésenchymateuses, sont sensibles à TPL à de faibles doses nanomolaires, avec un fort effet antiprolifératif même dans des mélanosphères (cellules de mélanome cultivées en conditions 3D). THZ1 et TPL affectent communément un nombre de gènes dans des cellules mélanocytaires, tels que des facteurs cruciaux SE-dépendants comme MITF et SOX10. Néanmoins, la réponse

transcriptionnelle pour les deux drogues diffère modérément, TPL dérégulant moins de gènes. Enfin, alors que l'exposition chronique au TPL conduit également à l'émergence de cellules résistantes, aucun changement de phénotype vers un état mésenchymateux n'a été observé, comme ce fut le cas pour la résistance au THZ1. Collectivement, ces données préliminaires indiquent que l'inhibition de XPB pourrait être un candidat plus intéressant pour la perturbation des SEs dans le mélanome que l'inhibition de CDK7. S'agissant d'un projet de recherche en cours, certaines questions cruciales n'ont pas encore de réponse : Quel est l'impact de TPL sur les gènes SE-dépendants dans les cellules mésenchymateuses ? XPB est-il directement recruté au niveau des SEs et de la même manière que CDK7 ? Quelles sont ses fonctions moléculaires exactes au niveau des SEs ? Quels sont les mécanismes à l'origine de la résistance au TPL ?

II – La deuxième stratégie d'inhibition transcriptionnelle étudiée fait appel à des molécules se liant directement à l'ADN. J'ai notamment étudié les effets sur le mélanome d'un nouveau type d'inhibiteur transcriptionnel d'origine marine, la Lurbinectedine. Celle-ci se lie spécifiquement et de manière covalente au niveau des gènes hautement exprimés, où elle bloque l'ARN polymérase II, induit des cassures d'ADN et conduit à l'apoptose. La Lurbinectedine a récemment reçu l'approbation accélérée de la FDA dans le traitement du cancer de poumon à petites cellules métastatique. Cependant, ses effets sur d'autres types de cancer tels que le mélanome sont largement inconnus. Collaborant avec PharmaMar S.A., nous avons eu à disposition exclusive des dérivés structuraux de cette molécule, à savoir les molécules PM14 et PM54, afin de potentiellement les breveter contre le mélanome. Compte tenu de la dépendance transcriptionnelle de ce cancer, nous avons supposé que ces molécules pourraient être très efficaces dans ce cancer. En effet, nous avons vu que toutes les cellules testées étaient extrêmement sensibles à des doses nanomolaires, quel que soit leur phénotype mélanocytaire ou mésenchymateux. Une forte inhibition de la prolifération et des capacités d'invasion, ainsi qu'une forte induction d'apoptose, ont été observées à la fois dans des cellules cultivées en 2D ou en 3D. De plus, des traitements courts de souris xénogreffées provoquent des diminutions importantes de marqueurs de mitose et des augmentations de marqueurs d'apoptose dans les tumeurs. L'exposition aux drogues entraîne une diminution d'expression significative de gènes connus pour être surexprimés dans le mélanome, tels que MITF dans les cellules mélanocytaires ou EGFR dans les cellules mésenchymateuses. En conclusion, la Lurbinectedine et ses dérivés semblent montrer une haute efficacité initiale dans le mélanome et devraient être étudiés pour l'utilisation clinique contre des mélanomes résistants à des thérapies conventionnelles.

Bien que la Lurbinectedine soit utilisée en clinique pour le traitement de cancers du poumon, aucune information n'existe sur des mécanismes de résistances. Par ailleurs, l'éventuelle future utilisation dans le traitement du mélanome renforce d'autant plus l'intérêt d'étudier ces mécanismes potentiels. Nous avons donc chroniquement exposé quatre différentes cultures de cellules de mélanomes à des doses croissantes de Lurbinectedine ou de ses dérivés. De manière intéressante, nous avons réussi à générer des cellules résistantes à partir d'un seul type de cellules mésenchymateuses, les traitements ayant été trop cytotoxiques pour les autres cultures. Des analyses RNA-Seq ont montré que l'expression d'un grand nombre de gènes était impactée, notamment le gène codant pour la pompe d'efflux ABCB1 qui se retrouve hautement surexprimée. L'utilisation d'agents pharmacologiques inhibant ABCB1 restaure complètement la sensibilité des cellules résistantes envers la Lurbinectedine et ses dérivés. A l'inverse, la surexpression de cette pompe rend résistantes des cellules initialement sensibles, révélant qu'ABCB1 contribue au mécanisme de résistance à la Lurbinectedine. De manière intéressante, la surexpression d'ABCB1 semble être inhibée dans la plupart des cellules mélanocytaires par des phénomènes de dégradation par le protéasome. Nous étudions donc actuellement les mécanismes derrière la dégradation d'ABCB1 en essayant d'identifier les ubiquitine ligases impliquées. De plus, nos résultats préliminaires laissent entendre que la surexpression d'ABCB1 dans les cellules mésenchymateuses est régulée par les facteurs AP-1/TEAD, déjà connus pour jouer des rôles importants dans le phénotype invasif des cellules de mélanome.

En conclusion, mes travaux pendant ces quatre années de thèse ont porté sur l'efficacité de plusieurs types d'inhibiteurs de la transcription sur des modèles *in vitro* et *in vivo* de mélanome, en étudiant aussi les effets potentiellement néfastes associés à ces traitements comme l'émergence de résistances. Plus précisément, ces travaux ont permis de montrer l'implication de CDK7 dans la commutation phénotypique des cellules du mélanome, et ont mis en lumière le fait que l'inhibition de XPB serait potentiellement plus bénéfique. J'ai également travaillé sur un nouveau traitement potentiel du mélanome, démontrant une grande efficacité. Cependant, nous avons aussi caractérisé un mécanisme de résistance contre la Lurbinectedine. En dehors de ce travail principal, mes autres travaux en collaboration ont également porté sur la caractérisation de BAHCC1, une protéine codée par un gène SE-dépendant surexprimé dans le mélanome, et impliquée dans sa prolifération. Enfin, j'ai également travaillé sur EXD2, une nucléase impliquée dans la réponse transcriptionnelle au stress génotoxique, qui interagit avec l'ARN polymérase II bloquée par une lésion pour dégrader l'ARNm synthétisé.

List of figures

Figure 1. The histological structure of human skin.	26
Figure 2. The stratified nature of the epidermis.	26
Figure 3. The dendritic morphology of melanocytes.	28
Figure 4. Non-classical (potential) roles of melanocytes.	28
Figure 5. Melanocytes in skin immunity.	30
Figure 6. The melanogenesis cascade.	30
Figure 7. Nucleotide Excision Repair.	32
Figure 8. Supranuclear melanin-caps.	34
Figure 9. Ontogeny of the melanocyte lineage from the neuroectoderm/neural tube.	34
Figure 10. Structural characterization of the MITF DNA-binding and assembly region.	36
Figure 11. Schematic diagram of transcription factors regulating the MITF-M promoter positively or negatively and their response to signaling pathways.	36
Figure 12. Skin cancer classification and approximative incidence rates.	38
Figure 13. Cutaneous melanoma and rising incidence rates.	38
Figure 14. Melanoma 5-year relative survival rates by stage at diagnosis and sex.	40
Figure 15. Overview of the four major cutaneous melanoma subtypes.	40
Figure 16. CSD and non-CSD melanomas are distinct subtypes of melanoma.	42
Figure 17. Landscape of driver mutations in cutaneous melanoma.	42
Figure 18. Main molecular pathways involved in melanomagenesis and associated mutations.	44
Figure 19. Levels of tumor heterogeneity.	44
Figure 20. The Clark Model of linear melanoma progression.	46
Figure 21. Distinct trajectories of melanoma initiation.	46
Figure 22. Characteristics of melanocytic neoplasms across the morphological spectrum.	48
Figure 23. Proposed mechanisms of growth arrest of melanocytic naevi.	50
Figure 24. Clinical features of atypical/dysplastic naevi.	50
Figure 25. Proposed model of the genetic evolution of melanoma from precursor lesions to metastatic disease, and mutation burden and type at each step of progression.	52
Figure 26. Evolutionary model of genetic intratumoral heterogeneity, and examples of individual progression cases and mutation acquisitions.	54
Figure 27. Breslow depth.	54
Figure 28. Incremental alterations of signaling pathways during melanoma progression.	56
Figure 29. Model of metastatic trajectories in melanoma.	58
Figure 30. A journey through lymph vessels could boost melanoma cell metastasis.	58
Figure 31. Phenotype switching and melanoma invasion and metastasis.	60
Figure 32. The metastatic cascade.	60
Figure 33. Distinct modes of melanoma cell intra- and extravasation.	62
Figure 34. Heterotypic clusters and collective cell migration versus phenotype switching in melanoma metastasis.	62
Figure 35. The role of dormancy in melanoma.	64
Figure 36. Establishment of the lung pre-metastatic niche (PMN) and molecular players involved. ..	66
Figure 37. The fourteen hallmarks of cancer (2022 version) and subdivision into functional and enabling hallmarks (Included is the important TME).	68
Figure 38. Positions of the three typical classes of BRAF mutations and BRAF protein structure.	70
Figure 39. Metabolic reprogramming and the Warburg effect in melanoma.	72
Figure 40. Adaptive tumor metabolism supports multiple steps of the metastatic cascade.	74
Figure 41. Various types of cell death (A) and apoptosis signaling (B).	76
Figure 42. Immune dysfunctions contributing to melanoma progression.	78
Figure 43. Key angiostatic or angiogenic signals (A) and the multiple origins of tumor-neovascularization (B).	80
Figure 44. Cell senescence pathways associated with genes altered in melanoma (red).	82

Figure 45. SASP in tumor progression.	82
Figure 46. Induction of tumor-associated immune cells such as myeloid-derived suppressor cells (MDSCs) (A) and the influence of inflammatory signaling on cancer progression and signaling (B).	84
Figure 47. Microbiomes and the hallmarks of cancer.	86
Figure 48. Mechanisms of microbial immunomodulation during tumor progression.	86
Figure 49. Clonal sweeps can give rise to intra-tumoral driver-gene mutation homogeneity (A). Models of genetic heterogeneity and metastatic evolution (B).	88
Figure 50. The rheostat model of MITF function and target gene regulation.	90
Figure 51. Phenotypic states of melanoma cells identified in different studies.	90
Figure 52. Basics of melanoma phenotype switching.	92
Figure 53. Markers of phenotypic states in epithelial cancers and melanoma.	92
Figure 54. Potential arrangement of six different melanoma cell states, their relative expression of MITF and SOX10 (A) and other characteristics (B+C).	94
Figure 55. Phenotype switching trajectories and TME stimuli.	96
Figure 56. Changing intercellular contacts during melanoma progression.	96
Figure 57. TME stress signals and translational reprogramming in melanoma plasticity.	98
Figure 58. Epigenetic Regulation of EMT and melanoma phenotype switch.	98
Figure 59. Stress-specific pathways and transcriptional networks driving melanoma phenotype switching.	100
Figure 60. Approved treatments for melanoma and associated overall survival at 2 years.	102
Figure 61. Treatments for unresectable metastatic melanoma and BRAF mutation status.	104
Figure 62. Targeted therapies approved by the FDA (in white) or in trials (in gray).	106
Figure 63. Immunotherapies approved by the FDA (in white) or in trials (in gray).	106
Figure 64. Immune checkpoint inhibitor associated toxicities.	108
Figure 65. Intrinsic vs acquired (A) and genetic vs epigenetic (B) treatment resistances.	110
Figure 66. Common mechanisms of resistance to targeted therapies.	112
Figure 67. Minimal Residual Disease (MRD) and associated phenotype plasticity.	114
Figure 68. ICI resistance mechanisms (A) and associated dedifferentiation (B).	116
Figure 69. Transcriptional dysregulation in melanoma cells and their addiction to it as fundamental drivers of the malignant hallmarks of cancer.	118
Figure 70. Nucleosome and chromatin organization.	122
Figure 71. Higher-order chromatin organization.	124
Figure 72. Transcription condensates (or factories/hubs).	126
Figure 73. Chromatin accessibility and remodeling (A+B) and histone modifications (C).	128
Figure 74. Properties and function of core promoters and enhancers.	130
Figure 75. Regulation of PIC assembly by enhancers (A) and the function of the Mediator (B).	130
Figure 76. Differences between Super-Enhancers and Typical Enhancers.	132
Figure 77. Schematic representation of transcription initiation.	134
Figure 78. TFIIH subcomplexes and role in RNAPII transcription.	136
Figure 79. XPB and promoter opening.	138
Figure 80. CDK7 functions during the Pol II transcription cycle.	140
Figure 81. Transcription initiation, RNAPII pausing, and elongation.	142
Figure 82. The RNAPII transcription cycle.	144
Figure 83. Current model of transcription termination.	146
Figure 84. Transcription machinery mutations and associated diseases.	148
Figure 85. Components of gene expression control altered in cancers.	150
Figure 86. Major cancer-associated signaling pathways and their interactions.	152
Figure 87. Common transcriptional dysregulation mechanisms involving trans-factors: (A) TF dysregulation, (B) chromatin remodeler dysregulation, and (C) cohesin and CTCF mutations.	154
Figure 88. Transcriptional amplification through elevated MYC levels.	156
Figure 89. Different functions of lncRNAs (A) and miRNAs (B) in cancer.	156
Figure 90. Common transcriptional dysregulation mechanisms involving cis-factors: (A) Promoter mutations, (B) disruption of insulated neighborhood anchor sites, and (C) acquisition of super-enhancers.	158
Figure 91. Rewiring of a single enhancer can deregulate two unrelated disease genes.	160

Figure 92. Enhancer rewiring by genome structural alterations.....	160
Figure 93. SEs and core transcriptional regulatory circuitries in different human cancers.	162
Figure 94. SE-dependent transcriptional addiction.	164
Figure 95. Mutations leading to oncogenic SE formation.	164
Figure 96. Differential effects of transcriptional inhibitors on cancer cells versus normal cells as a rationale for using transcriptional therapeutics.	166
Figure 97. Assembly and disassembly of nuclear condensates by mutations or inhibitors (A) and SE vulnerability (B).	168
Figure 98. Partitioning of cancer therapeutics in nuclear condensates.	170
Figure 99. Drugs targeting TFIID subunits (A) and their potential effects on the transcriptional addiction of cancer cells (B).	172
Figure 100. Rationale for using THZ1 to target transcriptional addiction (A), ChIP-Seq data showing the high enrichment of CDK7 at SEs (B) and the SE-decommissioning effect of THZ1 in cancers such as MYCN-amplification driven neuroblastoma (C).	174
Figure 101. The potential role of XPB in SE-associated oncogene expression.	176
Figure 102. Processes reported to be activated (green arrows) or inhibited (red arrows) by Triptolide (TPL) and key genes belonging to pathways targeted by TPL.	176
Figure 103. Structure of Lurbinectedin (A), its mechanism of action (B) and its effects on immune cells of the TME (C).....	178
Figure 104. Selective targeting of transcriptional addiction of SCLC cells.....	178
Figure 105. Targeting transcriptional addiction in melanoma: Broad aims of the project.	180

Abbreviations and Acronyms

6,4PP	pyrimidine-6,4-pyrimidone photoproducts
AD	Activation domain
AID	Activation-Induced Cytidine Deaminase
ALK	Anaplastic lymphoma kinase
ANGPT2	Angiopoietin 2
AP-1	Activator Protein 1
APAF-1	Apoptotic Protease Activating Factor 1
AQP1	Aquaporin 1
ARF	Alternative Reading Frame
ARID1A/2	AT-rich interaction domain 1A/2
ASCL1	Achaete-Scute Homolog 1
ATF4	Activating Transcription Factor 4
ATP	Adenosine triphosphate
BAF	BRG1/BRM-associated factor
BCL2/6	B-cell lymphoma 2/6
BET	Bromodomain and Extra-Terminal domain
BMDC	Bone marrow-derived cell
BMF	Bcl-2 Modifying Factor
bp	Base pairs
BR	Basic Region
BRAF	B rapidly accelerated fibrosarcoma
BRD2/4	Bromodomain-containing protein 2/4
BRG1	Brahma-related gene-1
BRN2	Brain-specific homeobox/POU domain protein 2
CAF	Cancer-associated fibroblasts
CAK	CDK-activating kinase
cAMP	Cyclic adenosine monophosphate
CNA	Copy number alterations
CBF β -SMMHC	Core Binding Factor Beta-Smooth Muscle Myosin Heavy Chain
CBP	CREB-binding protein
CCL2/20	Chemokine (C-C motif) ligand 2/20
CD4/8/31/36	Cluster of differentiation 4/8/31/36
CDH2	Cadherin 2
CDK	Cyclin-dependent kinase
CDKN2A	Cyclin-dependent kinase inhibitor 2A gene
CPD	Cyclobutane pyrimidine dimers
CPF	Cleavage and Polyadenylation Factor
CPSF	Cleavage and polyadenylation specificity factor
CREB	cAMP response element-binding protein
CRH	Corticotropin-releasing hormone
CS	Cockayne syndrome
CSD	Chronically sun-damaged
CTC	Circulating tumor cell
CTCF	CCCTC-binding factor

CTD	C-terminal Domain
CTLA-4	Cytotoxic T-lymphocyte-associated protein 4
CXCL8/12	C-X-C motif chemokine 8/12
CXCR4	C-X-C chemokine receptor type 4
DAMP	Damage-associated molecular pattern
DAPI	4',6-diamidino-2-phenylindole
DBD	DNA binding domain
DCT	Dopachrome tautomerase
DEL-1	Developmental Endothelial Locus-1
DNA	Deoxyribonucleic acid
DSIF	DRB sensitivity-inducing factor
DTC	Disseminated Tumor Cells
ECM	Extracellular matrix
EGFR	Epidermal growth factor receptor.
EGR3	Early Growth Response 3
EMT	Epithelial-mesenchymal transition
ENCODE	Encyclopedia of DNA Elements
ERK	Extracellular Signal-Regulated Kinase
EVI1	Ecotropic Viral Integration Site 1
EVM	Extravascular Migration
EWS/FLI	Ewing sarcoma/friend leukemia integration
FACT	Facilitates Chromatin Transcription complex
FDA	Food and Drug Administration
FGFR	Fibroblast growth factor receptor
FOS	FBJ murine osteosarcoma viral oncogene homolog
FOXD3	Forkhead Box D3
GATA2/3/6	GATA-binding protein family 2/3/6
GFRA1	GDNF Family Receptor Alpha 1
GG-NER	Global Genome Nucleotide Excision Repair
GHR	Growth hormone receptor
GLUT1	Glucose transporter 1
GNA11	G protein subunit alpha 11
GNAQ	Guanine Nucleotide-Binding Protein Q Polypeptide
gp100	Glycoprotein 100
GSH	Glutathione
GTP	Guanosine Triphosphate
HGFR	Hepatocyte growth factor receptor
HIF1 α	Hypoxia-Inducible Factor 1 α
HLH	Helix-Loop-Helix
HSP	Heat Shock Protein
i	Inhibitor/inhibition
ICI	Immune checkpoint inhibitor
IDH	Isocitrate Dehydrogenase
IFN- α /- β /- γ	Interferon- α /- β /- γ
IGF1R	Insulin-like growth factor 1 receptor
IL-1 β /-2/-6/-8/-10/-16	Interleukin-1 β /-2/-6/-8/-10/-16
IPRES	Innate-anti-PD-1 resistance signature
IRF	Interferon Regulatory Factor

ITGAV	Integrin alpha V
JAK	Janus Kinase
JNK	c-Jun N-terminal kinase
kb	Kilobase
KDM1B/5A/5B	Lysine Demethylase 1B/5A/5B
LAG-3	Lymphocyte-activation gene 3
LATS2	Large Tumor Suppressor Kinase 2
LENOX	lncRNA-enhancer of oxidative phosphorylation
LMO1	LIM Domain Only 1
lncRNA	long non-coding RNA
Lurbi	Lurbinectedin
LZ	Leucine zipper
MAPK	Mitogen-Activated Protein Kinase
MC1R	Melanocortin one receptor
MCT	Monocarboxylate Transporter
MDM2/4	Mouse Double Minute 2/4
MDSC	Myeloid-derived suppressor cell
MED1	Mediator Complex Subunit 1
MET	Mesenchymal–epithelial transition
MHC	Major Histocompatibility Complex
miRNA	micro RNA
MITF	Microphthalmia-associated transcription factor
MLANA	Melanoma Antigen-A
ML-IAP	Melanoma inhibitor of apoptosis protein
MMP	matrix metalloproteinases
mol	Mole
MRD	Minimal Residual Disease
mRNA	Messenger RNA
MSPR	Macrophage-stimulating protein receptor
mTOR	Mechanistic target of rapamycin
NC	Neural crest
ncRNA	non-coding RNA
NCSC	Neural crest stem cell
NELF	Negative elongation factor
NER	Nucleotide excision repair
NEUROD1	Neurogenic Differentiation 1
NF1	Neurofibromatosis type 1
NFATC2	Nuclear Factor of Activated T Cells 2
NF-κB	Nuclear Factor-kappa B,
NGFR	Nerve Growth Factor Receptor
NLRP3	Nucleotide-binding oligomerization domain-like receptor family pyrin domain-containing 3
NMSC	Non-melanoma skin cancers
NURF	Nucleosome remodeling factor
OXPPOS	Oxidative phosphorylation
PAF1	RNA polymerase II-associated factor 1
PAMP	Pathogen-associated molecular pattern
PAS	Polyadenylation signal

PAX3/5	Paired box gene 3/5
PDGFRA	Platelet-Derived Growth Factor Receptor Alpha
PGC1 α	Peroxisome Proliferator-Activated Receptor Gamma Coactivator 1-Alpha
PI3K	Phosphoinositide 3-kinase
PIC	Preinitiation Complex
PM14/PM54	PharmaMar14/54
PMN	Pre-metastatic niche
PRC2	Polycomb Repressive Complex 2
PROTAC	Proteolysis Targeting Chimeras
P-TEFb	Positive Transcription Elongation Factor b
PTEN	Phosphatase and Tensin Homolog
PTM	Post-Translational Modification
RAC	Ras-Related C3 Botulinum Toxin Substrate
RAS	Rat sarcoma
RB1	Retinoblastoma 1
RELA	v-Rel Avian Reticuloendotheliosis Viral Oncogene Homolog A
RNA	Ribonucleic acid
RNAPII	RNA Polymerase II
ROS	Reactive oxygen species
RPB1	RNA polymerase II subunit B1
RTK	Receptor tyrosine kinase
RUNX1/3	Runt-related transcription factor 1/3
RXRG	Retinoid X Receptor Gamma
SAGA	Spt-Ada-Gcn5-acetyltransferase
	Survival Associated Mitochondrial Melanoma-Specific Oncogenic Non-Coding RNA
SAMMSON	
SCLC	Small cell lung cancer
SE	Super-enhancer
SEC	Super elongation complex
Ser	Serine
SERPINE1	Serpin family E member 1
	SWI/SNF-related, matrix-associated, actin-dependent regulator of chromatin, subfamily A, member 4
SMARCA4	
SMC	Starved melanoma cell
SNP	Single Nucleotide Polymorphism
SOX2/6/9/10	SRY-related HMG-box 2/6/9/10
STAT	Signal Transducer and Activator of Transcription
SWI/SNF	Switch/Sucrose Non-Fermentable
TAD	Topologically associating domains
TAF	TBP-associated factors
TAL1	T-cell Acute Lymphoblastic Leukemia 1
TBP	TATA-binding protein
TCF4	Transcription Factor 4
TC-NER	Transcription-coupled nucleotide excision repair
TEAD	TEA Domain
TERT	Telomerase Reverse Transcriptase
TF	Transcription Factor
TFAP2A	Transcription factor AP-2 alpha

TGFβ	Transforming growth factor β
THZ1	Triazolopyrimidine-1 compound
TIGIT	T cell Immunoreceptor with Ig and ITIM domains
TIM-3	T-cell immunoglobulin and mucin domain-containing protein 3
TIME	Tumor immune microenvironment
TME	Tumor microenvironment
TNF-α	Tumor Necrosis Factor alpha
TP53	Tumor protein P53
TPL	Triptolide
TSP-1	Thrombospondin-1
TSS	Transcription start site
TTD	Trichothiodystrophy
TYR	Tyrosinase
UV	Ultraviolet
VE-cadherin	Vascular endothelial cadherin
VEGFA	Vascular endothelial growth factor A
VEGFR	Vascular endothelial growth factor receptor
VISTA	V-domain Ig suppressor of T cell activation
WNT	Wingless/Integrated
WT	Wild type
XIAP	X-linked inhibitor of apoptosis protein
XPB/C/D	Xeroderma pigmentosum B/C/D
XRN2	5'-3' Exoribonuclease 2
YAP/TAZ	Yes-associated protein/Transcriptional co-activator with PDZ-binding motif
ZEB-1	Zinc finger E-box binding homeobox 1
Zip	Zipper
α-MSH	α-melanocyte stimulating hormone

Preface: Thesis structure

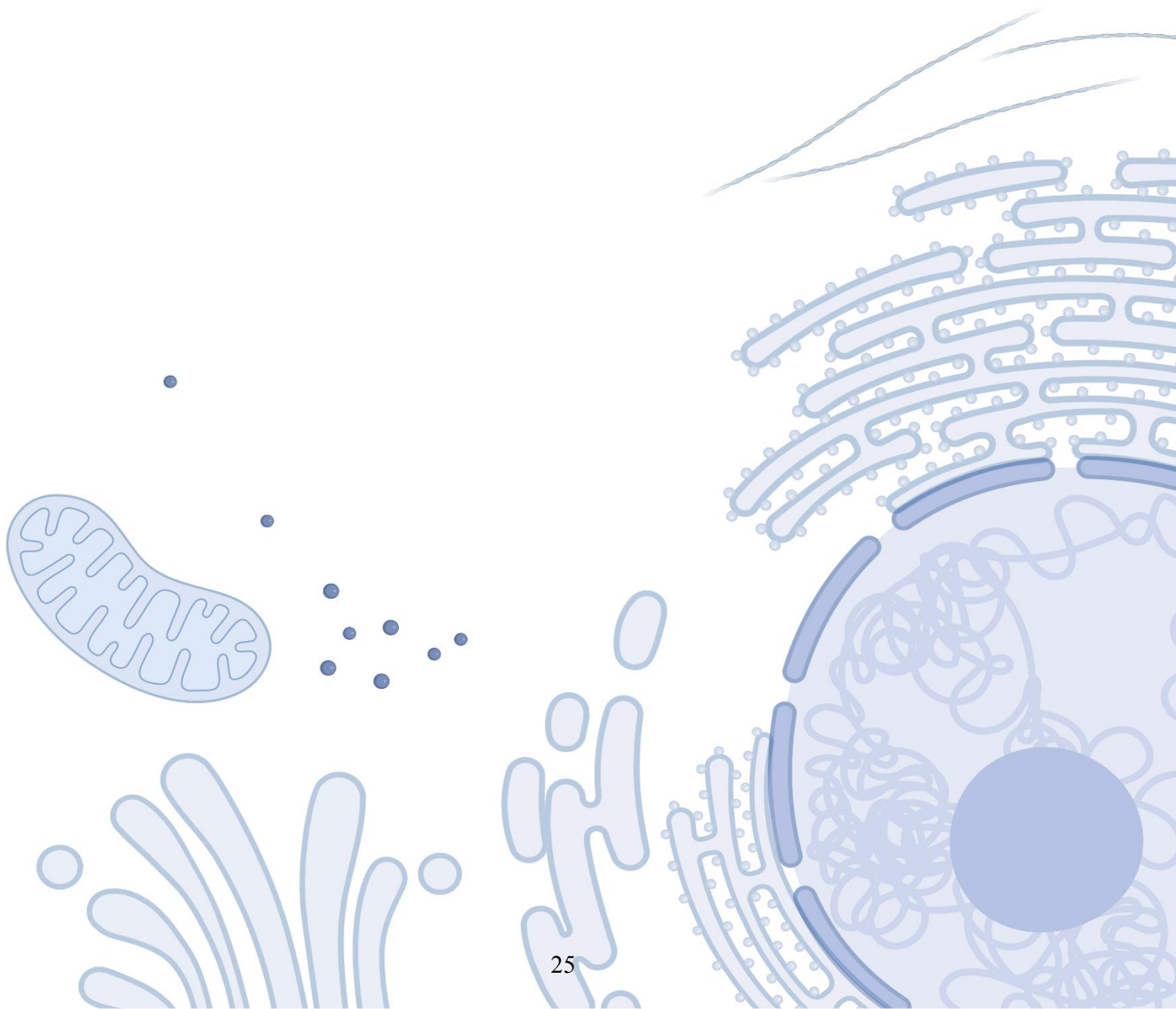
This thesis manuscript focuses on investigating the effects of various types of transcriptional inhibitors on melanoma cells. Although there have been remarkable advancements in the treatment of advanced melanoma over the past decade, the development of therapeutic resistances remains a prevalent issue. These resistances often stem from the inherent cell state plasticity observed in melanoma cells, which exhibit a state of 'transcriptional addiction' to sustain their abnormal phenotypes. Therefore, the objective of this thesis is to explore the potential utility of transcriptional inhibitors in treating metastatic melanoma, comprehending their impact on melanoma cells, and deciphering the mechanisms through which melanoma cells might acquire insensitivities to them.

The manuscript begins with an exhaustive introduction to the topic of melanoma, beginning with a discussion on melanocyte biology and positioning cutaneous melanoma in the context of other skin cancers. Subsequently, molecular and cellular events driving melanoma disease progression are described, with a particular focus on the role of cell state plasticity and the associated gene expression programs. Current treatment strategies for melanoma and their limitations are explained, and followed by the introduction of the concept of targeting the 'transcriptional addiction' of cancer cells as a potential innovative treatment approach. After providing a comprehensive depiction of the normal regulation of the transcriptional process, the oncogenic mechanisms leading to transcriptional dysfunctions are elucidated, along with the resulting dependencies of cancer cells on these dysfunctions. Finally, three different strategies to target these 'transcriptional addictions' are presented, which constitute the framework for my thesis work.

Following the introduction, I present the main results we obtained either as published studies or as preliminary drafts of manuscripts. The first part of the results aims to understand the role of the CDK7 and XPB subunits of the general transcription factor TFIID in melanoma biology and in super-enhancer-associated oncogene expression, by utilizing the two covalent inhibitors THZ1 and Triptolide. In the second part of the results, the focus is primarily on a novel kind of DNA-binding transcriptional inhibitor, Lurbinectedin. We show very encouraging preclinical data but also uncover, for the first time, a cellular resistance mechanism against this promising drug. After presenting the results, a concise conclusion summarizes and discusses the main findings of the studies. Finally, two additional projects in which I participated are included as annexes, and the bibliography is found at the end of the manuscript.

Introduction

Section I: Cutaneous Melanoma



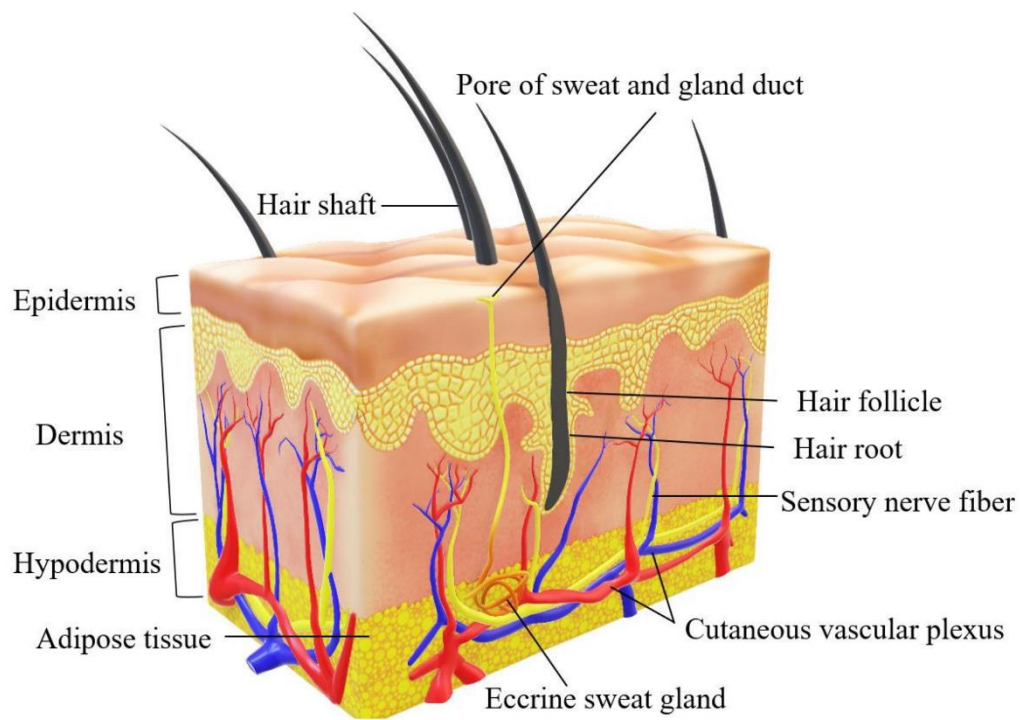


Figure 1. The histological structure of human skin.

From Masri et al., 2022.

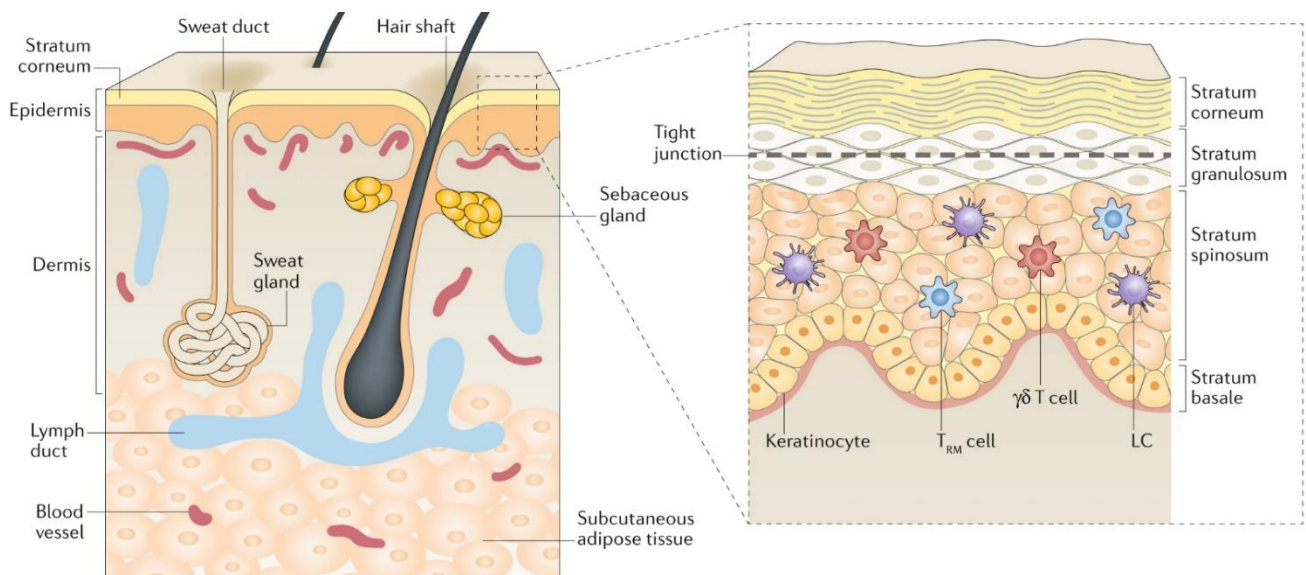


Figure 2. The stratified nature of the epidermis.

From Kabashima et al., 2019.

A. Notions about the skin, melanocytes, and melanoma

1. Skin anatomy and physiology

1.1. Overview of main functions

The skin represents the heaviest and superficially largest organ of the human body. In adults, this complex structure covers approximately 2 m² and can make up to 20 % of the body weight (Ibrahim *et al.*, 2020). The skin is composed of a wide range of cells, reflecting its various physiological functions that go beyond its role as a first line of defense and communication with the outside environment. Its different functions include hydro- and thermoregulation (Kenny and McGinn, 2017), Vitamin D synthesis (Bikle, 2011), microbiome interactions (Gallo, 2017), excretion and absorption of various molecules (Halling-Overgaard *et al.*, 2017), acting as a blood reservoir (Deschamps and Magder, 1990) and a sensory organ (Zimmerman, Bai and Ginty, 2014), and protection against a vast array of threats.

Apart from its role as a physical and mechanical barrier, the skin represents a biological and immunological obstacle against environmental pathogens. Complex cross-talks between skin cells such as keratinocytes or melanocytes, nerve cells, immune cells (either residing in or being recruited to the skin), and the skin microbiome ensure efficient immunological protection against viruses, bacteria, fungi, and parasites (Belkaid and Segre, 2014; Kabashima *et al.*, 2019). The skin is also a chemical barrier, synthesizing and secreting important protective biomolecules. Various dermal enzymes such as Cytochrome P450 or alcohol dehydrogenase, as well as antimicrobial peptides, help protect against outside harmful chemicals or microorganisms (Pyo and Maibach, 2019). The skin's sebaceous glands produce sebum-containing lipids and enzymes also involved in this process and in the dehydration response. Finally, skin melanocytes produce melanin, a pigment crucial for shielding the organism from the harmful effects of UV-radiation.

1.2. Histological structure and cellular components

Human skin is structured into three distinctive layers (Wong *et al.*, 2016; Kabashima *et al.*, 2019), with the hypodermis being the innermost one (Figure 1). The hypodermis is composed of loose connective areolar and adipose tissue and contains blood vessels irrigating the moresuperficial layers, as well as various types of immune cells and somatosensory nerves. The dermis is the thickest layer and provides most of the mechanical strength and elasticity to

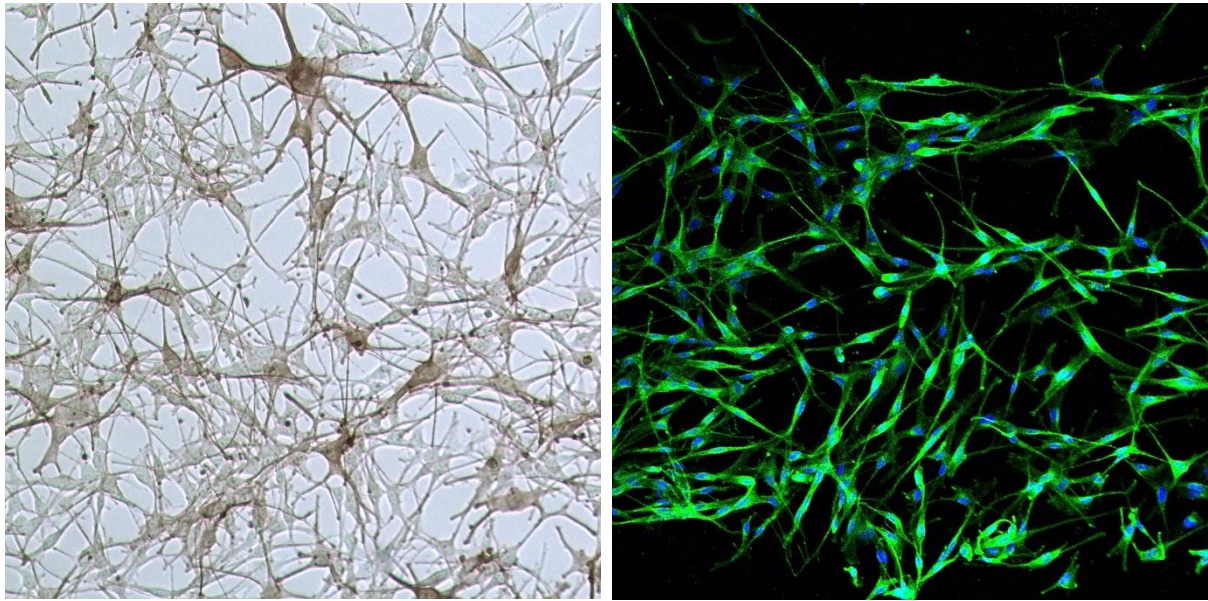


Figure 3. The dendritic morphology of melanocytes. Right: Phase contrast microscopy of NHMs (Normal human melanocytes) in monolayer culture, 100x. Left: Immunohistochemical analysis of NHM cells. MEL-5 (specific melanocyte antigen, green), DAPI (blue), 100x. From <https://www.mattek.com/products/human-melanocytes/>

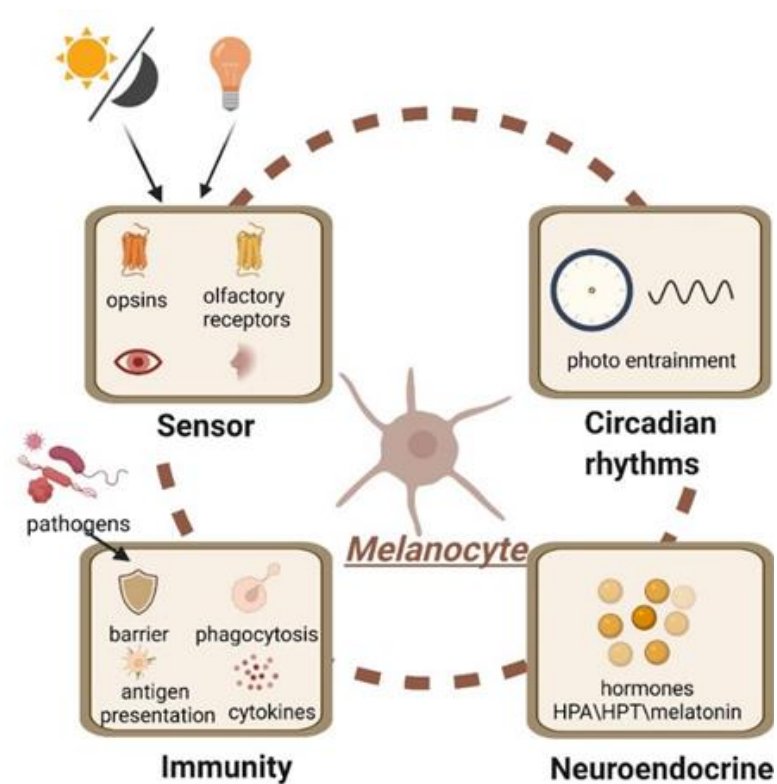


Figure 4. Non-classical (potential) roles of melanocytes.

Adapted from Chen et al., 2022.

the skin, as it is composed mainly of dense connective tissue with dermal fibroblasts producing a compact extracellular matrix (ECM, collagen, and elastin fibers). Other components are immune cells, blood and lymphatic vessels, sensory receptors, and epidermal appendages such as nails, hair follicles, sebaceous and sweat glands (Tortora, 2017). The epidermis is the outermost and most biologically active layer of the skin, a constantly renewing squamous and keratinized epithelium separated from the underlying dermis via the dermal-epidermal junction. It is subdivided into four sublayers, called strata, which are defined by the developmental stage of their composing keratinocytes (Figure 2). While the more stem-like cells of the deeper basal stratum continually divide and push older and more differentiated cells upwards, the more mature keratinocytes in superior strata produce keratin, a fibrous and resistant protein protecting the skin. The uppermost part of the skin, the stratum corneum, consists of layers of squamous and flattened keratinocytes filled and surrounded by keratin (also called corneocytes), which protect the body from friction, water loss, and pathogens (Gould, 2018). Apart from keratinocytes, which make up 90 % of epidermal cells, other cell types are found in the skin, including Langerhans (4 %) and Merkel cells (3 %), which are respectively involved in immune homeostasis and touch sensation, and melanocytes (3 %), whose functions will be detailed hereinafter (Sulaimon and Kitchell, 2003).

2. Melanocyte Biology

2.1. Roles and functions of melanocytes

Melanocytes are non-epithelial, neuroectoderm-derived cells displaying a highly polarized and dendritic morphology (Li, Knapp and Iden, 2020) (Figure 3). They have the unique capability to synthesize melanin, a complex pigment capable of scattering and absorbing UV radiation, thereby ensuring the protection of neighboring cells from UV-associated DNA damage (Lin and Fisher, 2007). Although primarily found in the basal stratum of the epidermis (1500 cells per mm²) (Kanitakis, 2002), melanocytes are also encountered in significant numbers in hair follicles and the iris of the eye (Shain and Bastian, 2016). Surprisingly, melanocytes are also present in deeper parts of the body that are not directly exposed to UV radiation, such as inside the ear (Zhang et al., 2013), the brain (Adameyko and Lallemand, 2010), the heart (Yajima and Larue, 2008; Levin et al., 2009), adipose tissue (Ikeda et al., 2021) as well as in several mucosae (Ma et al., 2021). Nevertheless, these ‘nonclassical’ melanocytes differ phenotypically from those found in the skin (Colombo et al., 2011; Yamaguchi and Hearing, 2014; Gudjohnsen et

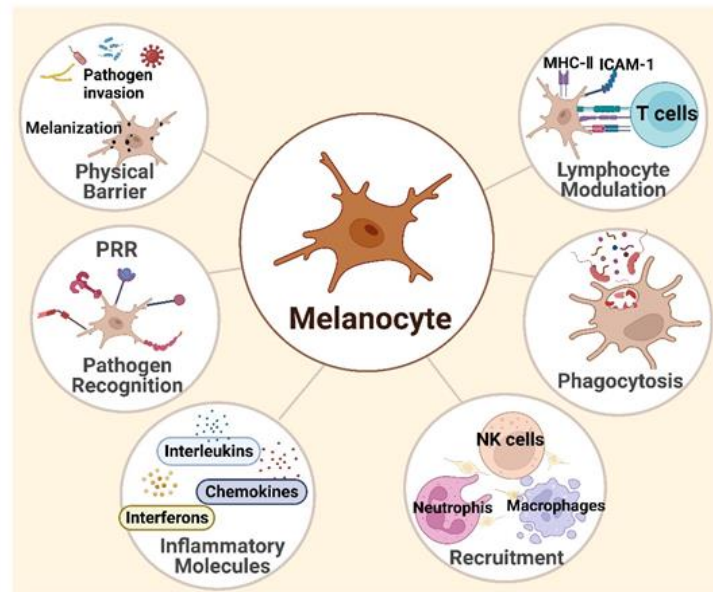


Figure 5. Melanocytes in skin immunity.

From Chen et al., 2022.

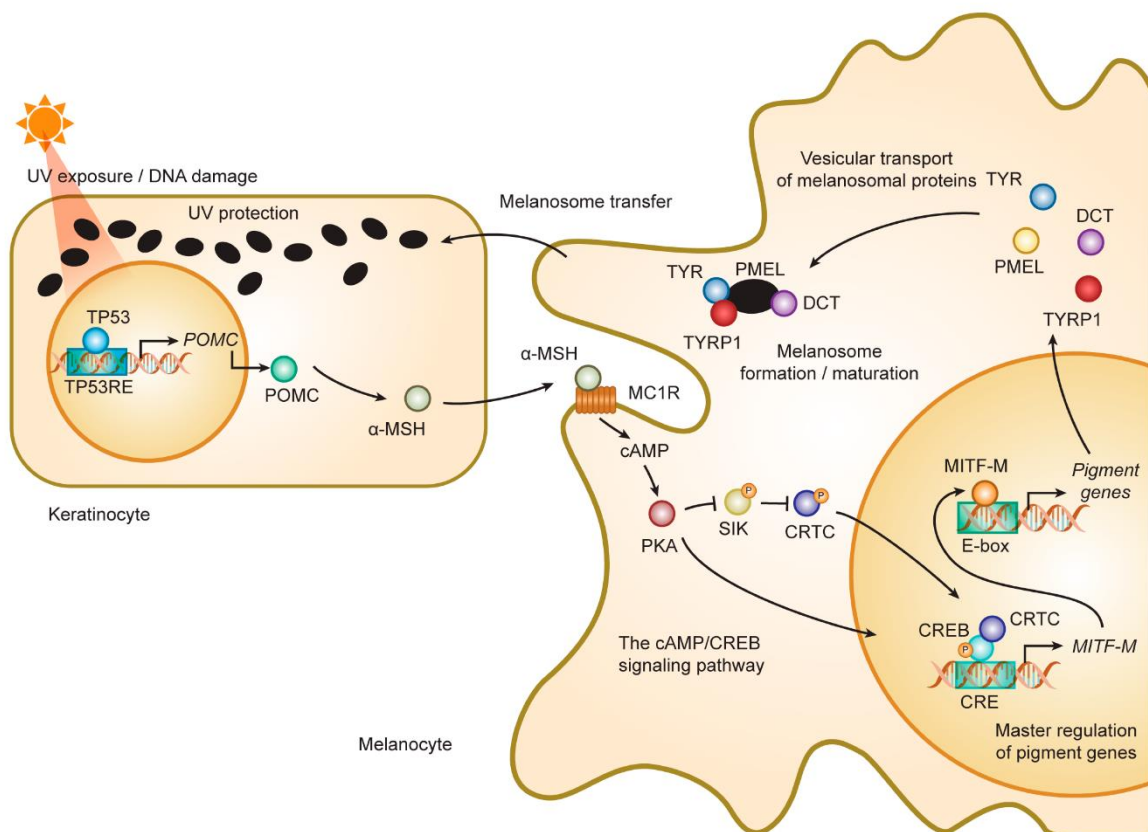


Figure 6. The melanogenesis cascade.

From Hida et al., 2020

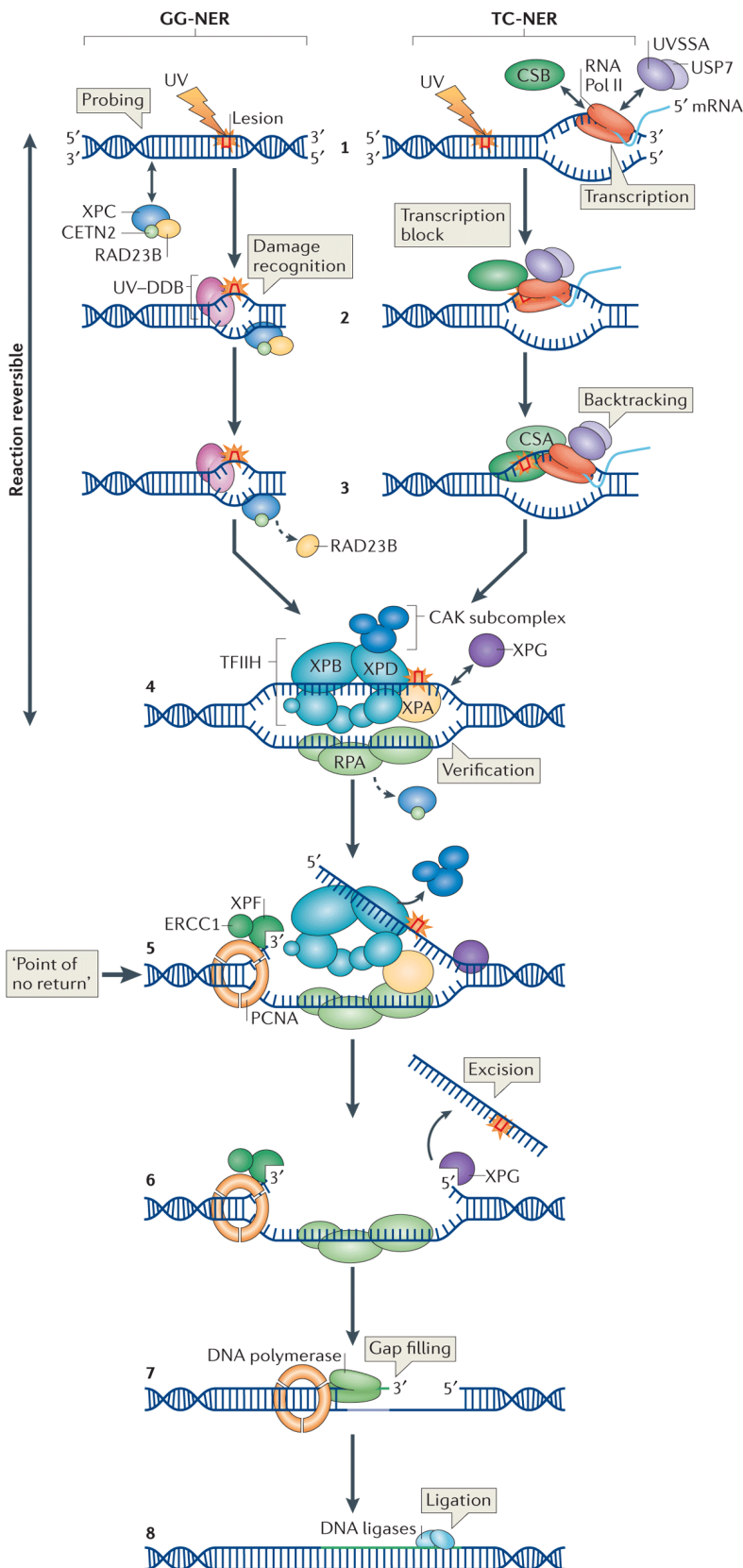
al., 2015; Anbar, Hegazy and Shalaby, 2019).

Whereas the primary function of dermal and ocular melanocytes seems to be pigmentation and associated UV-protection, various other less studied roles have been uncovered (Slominski, Paus and Schadendorf, 1993; Plonka et al., 2009; Chen et al., 2022) (Figure 4). Melanocytes are increasingly recognized as vital players in skin immunity (Figure 5), as they express many different pattern recognition receptors, which can initiate the inflammatory cascade once activated (Gasque and Jaffar-Bandjee, 2015). Additionally, melanocytes can secrete cytokines (TNF- α , CCL2, CCL20, CXCL8, CXCL12), interferons (IFN- α and IFN- β), and interleukins (IL-6, IL-10, IL-16) (Tam, Dzierżęga-Lęcznar and Stępień, 2019), and are capable of pathogen phagocytosis and antigen presentation to CD4+T cells, indicating their role as ‘nonprofessional’ antigen-presenting cells (Le Poole et al., 1993; Kabashima et al., 2019). Melanocytes also have neuroendocrine functions as they can secrete a vast range of hormones and neurotransmitters such as catecholamines or corticotropin-releasing hormone (CRH) (Takeda, Takahashi and Shibahara, 2007; Slominski, 2009). Interestingly, melanocytes also seem to possess elaborate environmental sensor abilities by expressing photosensitive opsins (Regazzetti et al., 2018) and olfactory receptors (Gelís et al., 2016), with potential roles in the regulation of the peripheral circadian rhythm. However, this claim remains contested (Chen et al., 2022). Some of these melanin-production-independent roles may be a predominant task for extracutaneous melanocytes, such as oxidative stress regulation for cardiac melanocyte-like cells (Hwang et al., 2015).

An active area of research in recent years has been to characterize the origin and functions of extracutaneous melanocytes. Additionally, many questions remain largely unanswered, even about classical melanocytes. For example, it is not well understood how neuroendocrine and sensory functions are regulated, what their exact systemic physiological effects are, and if they have clinical relevance. Be that as it may, the best-studied function of melanocytes remains their capacity to produce melanin.

2.2. UV radiation and protection by melanogenesis

As the skin represents the organ that is the most exposed to the dangers of UV-mediated mutagenesis, the multi-step process of melanin production and distribution called melanogenesis (Figure 6) is of crucial importance. UV radiation is classified into three subtypes depending on the wavelength: UVA (400-315 nm), UVB (315-280 nm), and UVC (280-100 nm) (Lee et al., 2020). While the energetic UVC radiation is absorbed by the earth’s ozone



In the global genome nucleotide excision repair (GG-NER) subpathway, the damage sensor XPC, in complex with RAD23B and CETN2, constantly probes the DNA for helix-distorting lesions (**step 1, left**). Upon recognition (**step 2, left**) and binding of the XPC complex to the damage, RAD23B dissociates from the complex (**step 3, left**). In the transcription-coupled NER (TC-NER) subpathway, damage is indirectly recognized during transcript elongation by the stalling of RNA Pol II at a lesion. During transcript elongation, UVSSA, USP7 and CSB transiently interact with RNA Pol II (**step 1, right**). Upon stalling at a lesion, the affinity of CSB for RNA Pol II increases (**step 2, right**) and the CSA-CSB complex is formed, which results in backtracking of RNA Pol II (**step 3, right**) that renders the DNA lesion accessible for repair. After damage recognition, TFIIH is recruited to the lesion in both GG-NER and TC-NER (**step 4**). The XPG endonuclease binds to the pre-incision NER complex (**step 4**). Upon binding of TFIIH, its CAK subcomplex dissociates from the core TFIIH complex. The helicase activity of TFIIH opens the double helix around the lesion, and 5'–3' unwinding of the DNA by the TFIIH helicase subunit XPD verifies the existence of lesions with the help of the ATPase activity of the XPB subunit and XPA (**step 4**). In this step, RPA is also recruited and coats the undamaged strand. XPA recruits an endonuclease — the XPF-ERCC1 heterodimer, which is directed to the damaged strand by RPA to create an incision 5' to the lesion (**step 5**). Once this 'point of no return' is reached, XPG is activated and cuts the damaged strand 3' to the lesion, which excises the lesion within a 22–30 nucleotide-long strand (**step 6**). Then, DNA Pol δ , DNA Pol κ or DNA Pol ϵ are recruited for gap-filling DNA synthesis (**step 7**). Gap filling can begin immediately after the 5' incision is made. The NER reaction is completed through sealing the final nick by DNA ligase 1 or DNA ligase 3 (**step 8**).

Figure 7. Nucleotide Excision Repair.

From Marteijn et al., 2014

layer, UVB and UVA radiation can penetrate the skin in a wavelength-dependent manner. UVA radiation, while very abundant and able to penetrate deep into the dermis and cause photoaging by generating reactive oxygen species (ROS) that can damage DNA (D’Orazio et al., 2013), is far less carcinogenic than the higher-energy UVB radiation (Anna et al., 2007; Ikehata et al., 2018). Mostly absorbed by the epidermis, UVB photons can directly damage DNA by causing covalent bonds to form between adjacent pyrimidine bases (photodimers), creating primarily cyclobutane pyrimidine dimers (CPDs) and pyrimidine-6,4-pyrimidone photoproducts (6,4PPs) (Mullenders, 2018). These bulky and DNA-distorting photolesions, if not removed by the complex cellular repair mechanism known as such as nucleotide excision repair (NER) (Compe and Egly, 2012; Marteijn et al., 2014) (Figure 7), can cause UV-specific mutations, primarily C→T substitutions at dipyrimidine sites (Ikehata and Ono, 2011; Brash, 2015).

The primary role of epidermal melanocytes is to protect neighboring cells from these genotoxic dangers. UV-damaged keratinocytes activate TP53, which stimulates the secretion of α -melanocyte stimulating hormone (α -MSH), a ligand of the melanocortin one receptor (MC1R) expressed by melanocytes (Cui et al., 2007; Shain and Bastian, 2016) (Figure 6). The activation of MC1R sets in motion a cAMP/CREB-dependent signaling cascade resulting in the expression of the microphthalmia-associated transcription factor (MITF), the master regulator of the melanocyte lineage (D’Mello et al., 2016; Goding and Arnheiter, 2019). MITF then stimulates the expression of pigmentation genes such as tyrosinase (TYR) and dopachrome tautomerase (DCT), which synthesize melanin from tyrosine (Sturm, Teasdale and Box, 2001). Of note, two different types of melanin exist in humans, brown-black eumelanin and yellow-red pheomelanin, the production ratios of which genetically depend on polymorphisms of the MC1R gene. The eumelanin/pheomelanin ratio represents the primary determinant of skin/hair pigmentation and phototype, an assessment of sun sensitivity (Ito and Wakamatsu, 2003; Maresca, Flori and Picardo, 2015). Although having different biosynthetic pathways, both types of melanin are eventually packed into lysosome-like structures called ‘melanosomes’ and transported through the melanocytic dendrites to adjacent keratinocytes of the hair bulb or epidermis (Hida et al., 2020). Interestingly, the exact molecular mechanisms of melanosome transport remain unresolved (D’Alba and Shawkey, 2019; Moreiras, Seabra and Barral, 2021). Inside the keratinocytes, melanosomes can be strategically positioned over the ‘sun-exposed’ side of nuclei to form umbrella-like structures called ‘supranuclear melanin-caps’ (Kobayashi et al., 1998; Byers et al., 2003; Castellano-Pellicena et al., 2021) (Figure 8), which scatter and absorb UV-radiation. This is possible because of the melanin polymer’s exceptional refractive index value and broad absorption spectrum (Solano, 2014).

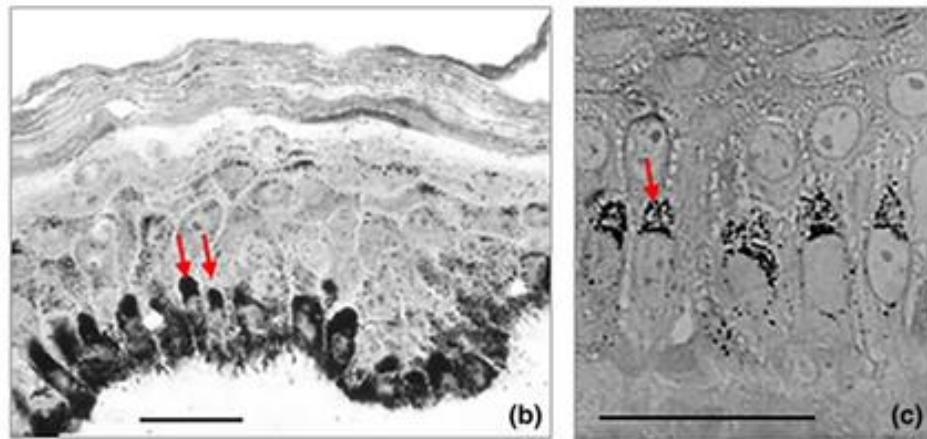


Figure 8. Supranuclear melanin-caps. Skin stained with melanin-specific Warthin Starry stain. Melanin is concentrated in keratinocytes as supranuclear caps (red arrows).

Adapted from Joly-Tonetti et al., 2018.

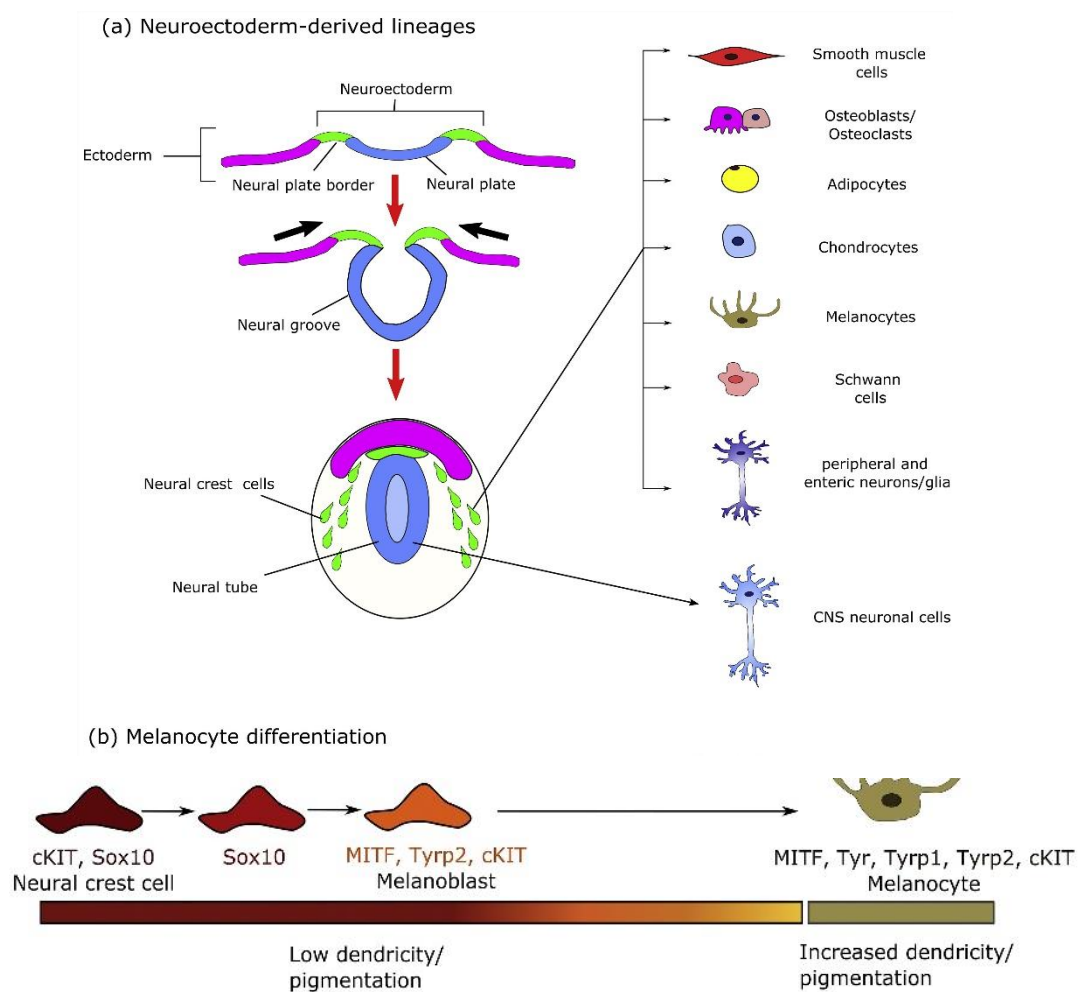


Figure 9. Ontogeny of the melanocyte lineage from the neuroectoderm/neural tube.

Adapted from Li, Knapp and Iden, 2020.

2.3. Embryonic origins and transcriptional regulation of the melanocyte identity

Approximately two weeks after fertilization, the gastrulation phase of embryonic development leads to the emergence of three main embryonic germ layers: the endoderm, mesoderm, and ectoderm (Tyser and Srinivas, 2022). After gastrulation, the complex process of neurulation differentiates the ectoderm into two parts, the surface ectoderm and the neuroectoderm, which is further divided into the neural plate and the neural plate border, delimiting the non-neural ectoderm. It is at this border that the neural crest (NC) cells arise, from which the melanocyte lineage descends (Milet and Monsoro-Burq, 2012) (Figure 9). Later stages of neurulation result in the formation of the neural tube (the precursor of the central nervous system) from the neural plate, leading the NC cells to reside in the dorsal region of the neural tube and to begin expressing neural crest specifier transcription factors (TFs) like SOX10, PAX3, TFAP2A, and FOXD3 (Bronner and LeDouarin, 2012; Simões-Costa and Bronner, 2015). This subsequently allows the NC cells to undergo an epithelial-to-mesenchymal transition (EMT) with the expression of factors like SNAIL, SLUG or SOX9 and to transform into a multipotent, highly migratory stem-cell-like progenitor population which delaminates and leaves the neural tube region (Theveneau and Mayor, 2012; Mort, Jackson and Patton, 2015).

The stereotypic viewpoint today is that these migratory NC cells move along highly defined pathways to settle in diverse distant final sites, while progressively differentiating into distinct cell types depending on the microenvironmental cues the cells encounter by a mesenchymal-to-epithelial-like process (Sommer, 2011; Green, Simoes-Costa and Bronner, 2015; Shellard and Mayor, 2019). Most NC cells would migrate dorsoventrally to differentiate into for example Schwann cells or peripheral neurons. On the other hand, cells moving along a dorsolateral path, colonizing the tissues that will later become the skin epidermis, would eventually give rise to melanocytes (Erickson and Goins, 1995; Ernfors, 2010). Interestingly however, it seems that a number of melanocytes (termed ‘second-wave’) can also arise from Schwann cell precursors having migrated dorsoventrally (Adameyko et al., 2009; Adameyko and Lallemand, 2010; Colombo et al., 2022). Conversely, Schwann cells are able to transdifferentiate into melanocytes (Dupin et al., 2003). This underscores the proneness to phenotypic instability and transcriptional plasticity of even seemingly fully differentiated NC-derived cells like melanocytes (Luo et al., 2015; Vandamme and Berx, 2019).

In any case, NC cells migrating to the future epidermis differentiate into melanocyte precursors called melanoblasts by losing the expression of many early NC cell specifiers, including FOXD3, while beginning to express the master regulator TF and specification marker

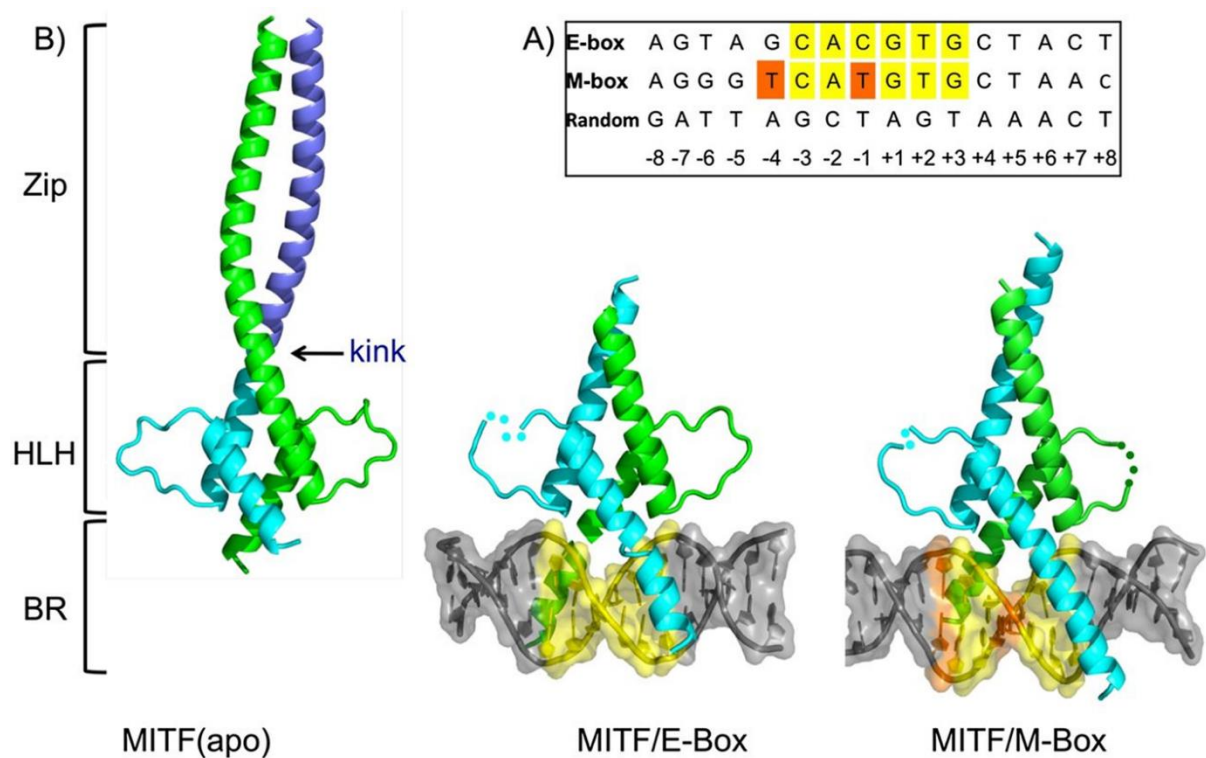


Figure 10. Structural characterization of the MITF DNA-binding and assembly region.

A) E-/M-box DNA sequences. B) Crystal structure of MITF in absence (apo) or presence of DNA. From Pogenberg et al., 2012. BR: Basic Region, HLH: Helix-Loop-Helix, Zip: Zipper.

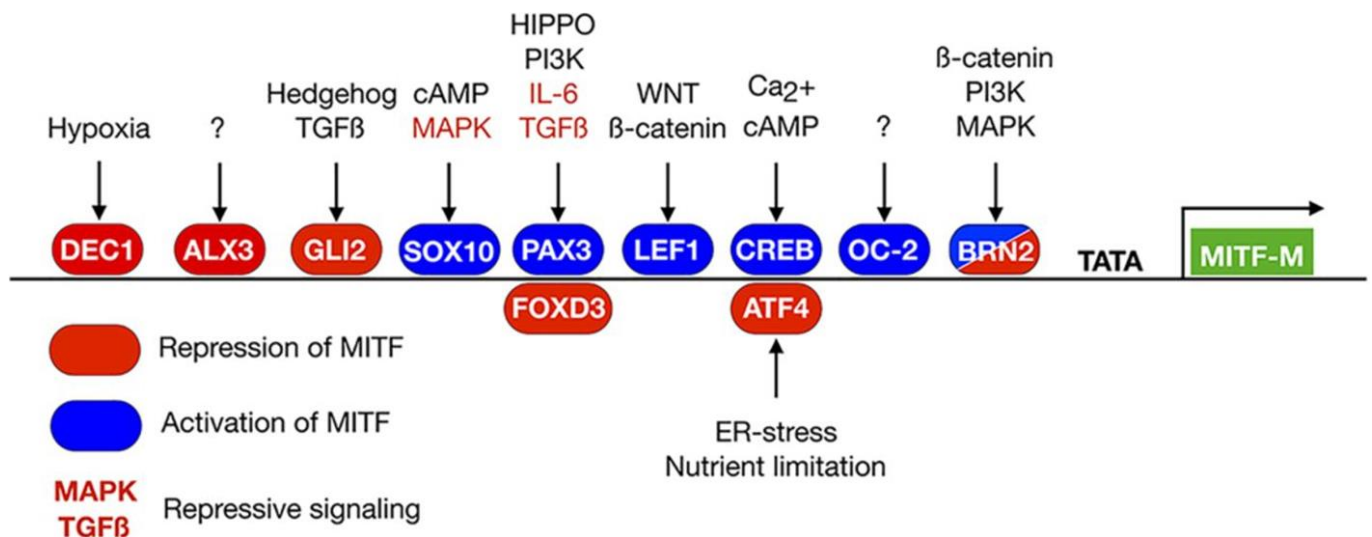


Figure 11. Schematic diagram of transcription factors regulating the MITF-M promoter positively or negatively and their response to signaling pathways.

From Goding and Arnheiter, 2019.

MITF (specifically the MITF-M isoform). This happens by the direct action of the remaining NC specifier TFs SOX10 and PAX3 as well as WNT/ β -catenin and KIT signaling (Potterf et al., 2000; Hou and Pavan, 2008; Betancur, Bronner-Fraser and Sauka-Spengler, 2010; Colombo et al., 2022). While some melanoblasts translocate to hair follicles to become melanocyte stem cells, others become mature, dendritic, and pigmented interfollicular melanocytes through the MITF/SOX10/PAX3 positive feedback-loop circuit resulting in the expression of terminal differentiation factors such as TYR or DCT, (Murisier and Guichard, 2007; Simões-Costa and Bronner, 2015). Importantly, open questions remain about the precise gene-expression programs specific to different developmental time points and anatomical locations which govern these melanocytic stages, although spatial single-cell transcriptomics have begun to give insight into this matter (Belote et al., 2021; Theodoridis et al., 2022).

Although there are nine isoforms of MITF (due to nine alternative promoters), with varying degrees of expression tissue specificity (Flesher et al., 2020), the MITF-M isoform is almost exclusively present in melanocytes. First discovered in mice exhibiting small ‘microphthalmic’ red eyes and loss of pigmentation (Hodgkinson et al., 1993), the MITF gene is located on chromosome 3q13 and implicated in a wide range of functions. From cell survival, pigmentation, proliferation, migration, differentiation, senescence, metabolism, and DNA damage repair, MITF-M coordinates key aspects of melanocyte biology (Goding and Arnheiter, 2019; Gelmi et al., 2022). MITF is a basic domain helix–loop–helix leucine zipper (bHLH-LZ) TF belonging to the MYC superfamily that binds DNA as homo- or heterodimers with the related TFEB, TFE3 and TFEC TFs (Pogenberg et al., 2012). The MITF bHLH domain can recognize 6-bp E-box sequences (CACGTG) present in promoters of a wide plethora of target genes, implicated in melanocyte homeostasis and survival (Cheli et al., 2010). However, MITF displays a higher affinity for an E-box variant named ‘M-box’ (TCATGTG) which is specifically present in promoters of melanogenesis-related genes like *TYR*, *DCT* or *MLANA* (Lowings, Yavuzer and Goding, 1992; Bentley, Eisen and Goding, 1994) (Figure 10). To regulate the expression of its target genes, MITF interacts with various cofactors such as the chromatin-remodeling NURF and pBAF/BRG complexes or lysine acetyltransferases like p300/CBP (Sato et al., 1997; Koludrovic et al., 2015; Laurette et al., 2015). As the activity of MITF-M is of crucial importance to melanocytes, its expression is finely regulated at different levels. An intricate network of signaling pathways and TFs converge on the MITF-M promoter (Figure 11), either repressing or activating its expression (Kawakami and Fisher, 2017). Of note, the cAMP/CREB cascade activated by α -MSH, as well as the NC-specifiers PAX3 and

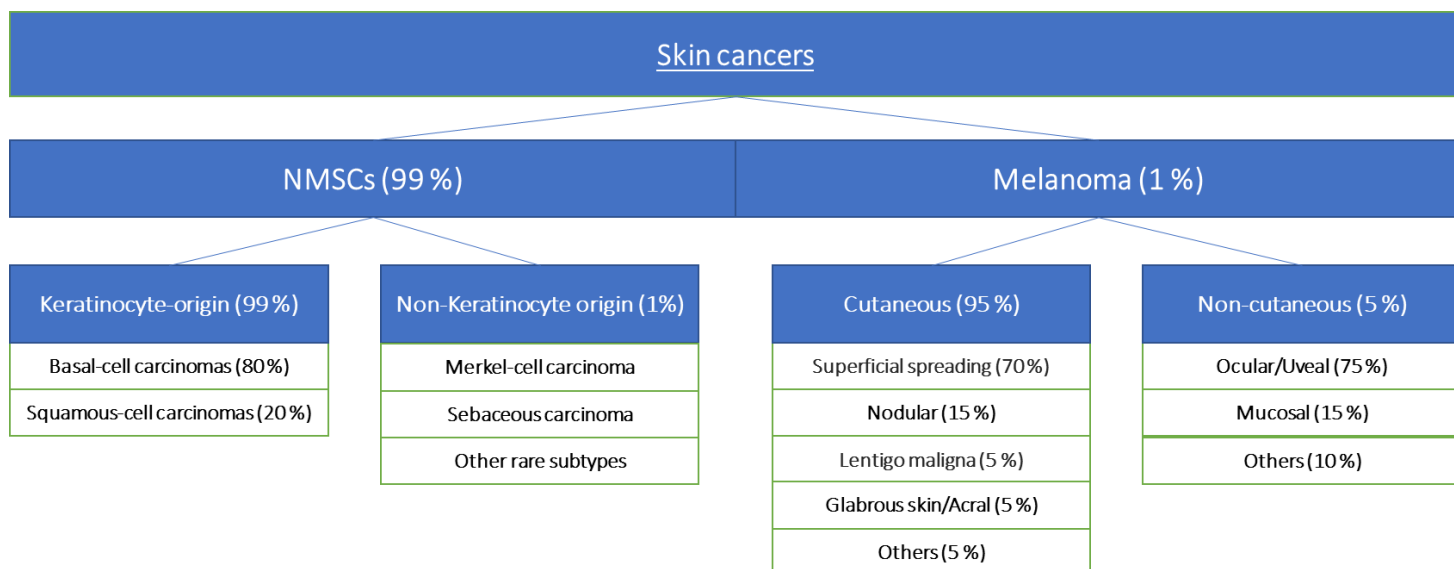


Figure 12. Skin cancer classification and approximative incidence rates. No information was found for non-keratinocyte NMSCs. Data from Saginala et al., 2021 and Scatena, et al., 2021.

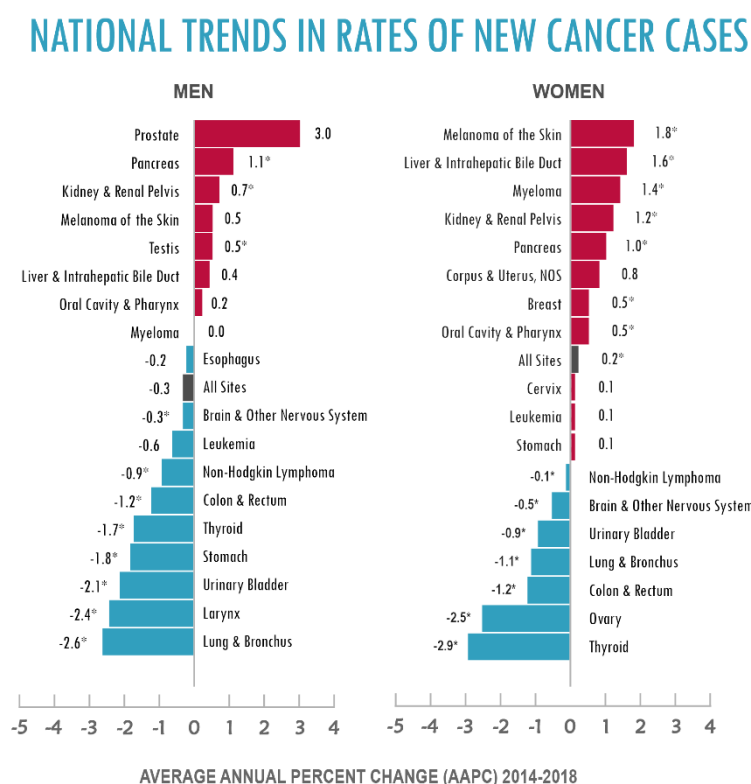


Figure 13. Cutaneous melanoma and rising incidence rates.

Adapted from the ‘Annual Report to the Nation 2022: National Trends in Rates of New Cancer Cases’ (https://seer.cancer.gov/report_to_nation/infographics/trends_incidence.html).

Accessed February 9th, 2023.

SOX10 positively stimulate MITF expression (Bondurand et al., 2000; Potterf et al., 2000; Betancur, Bronner-Fraser and Sauka-Spengler, 2010), whereas stress-response signaling, as for example through HIF1 α or AP-1 factors such as ATF4, represses MITF expression (Riesenberg et al., 2015; Falletta et al., 2017; Ferguson et al., 2017; Maurus et al., 2017). Significantly, the early NC-specifier FOXD3 also represses *MITF*. As such, the loss of expression of FOXD3 by NC cells migrating to the epidermis allows for their differentiation into melanoblasts and mature melanocytes (Thomas and Erickson, 2009; Curran et al., 2010). Other mechanisms regulating MITF expression and activity include cytoplasmic mRNA polyadenylation (Pérez-Guijarro et al., 2016), the action of microRNAs (Kunz, 2013), and posttranslational modifications, which can for example modulate MITF nuclear export (Ngeow et al., 2018) or DNA-binding affinity and genome distribution (Louphrasitthiphol et al., 2020). Given its primordial role as the master TF of the melanocytic lineage, it comes as no surprise that mutations of *MITF* and its regulators like SOX10 and PAX3 can lead to pigmentary and developmental pathologies such as Waardenburg syndrome (Huang et al., 2022). Significantly, deregulations of the expression of these factors are heavily involved in the emergence of melanoma (Hartman and Czyz, 2015), the cancer developing from melanocytes. The aforementioned properties of melanocytes (their immune functions, their neuroendocrine capacities, their neural crest origin from multipotent, highly migratory stem-cell-like cells capable of EMT, and their proneness to phenotypic instability and associated transcriptional plasticity) help to explain why melanoma is particularly aggressive and by far the deadliest type of skin cancer (Mort, Jackson and Patton, 2015).

3. Skin cancers and melanoma

3.1. Clinical Classifications and Epidemiology

Skin cancers are the most common neoplasms diagnosed worldwide, especially in Caucasian populations (Ciężyńska et al., 2021). They are broadly subdivided into either melanoma or non-melanoma skin cancers (NMSC), with the latter type being far more frequent (99 % of skin cancers). NMSC are further classified into basal cell carcinoma and squamous cell carcinoma, also called ‘keratinocyte carcinomas’ and which comprise the vast majority of NMSC cases (Nagarajan et al., 2019; Ciężyńska et al., 2021). Other rarer and more aggressive subtypes exist, such as Merkel-cell carcinomas, which emerge from non-keratinocytic and non-melanocytic cells. NMSCs vary vastly from each other in terms of biological characteristics, genetic

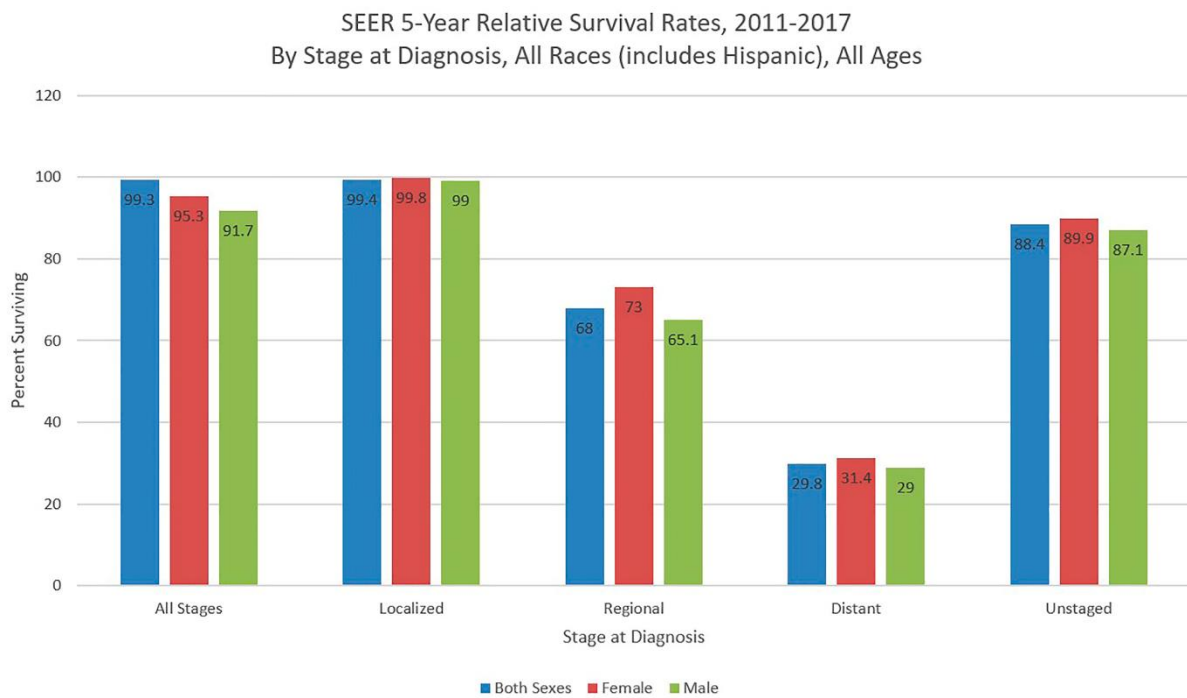


Figure 14. Melanoma 5-year relative survival rates by stage at diagnosis and sex.
Adapted from Saginala et al., 2021.



Figure 15. Overview of the four major cutaneous melanoma subtypes.

From Schadendorf, Kochs and Livingstone, 2013.

landscapes, pathogenesis, and disease progression. Most are usually treated with surgery or radiotherapy (Madan, Lear and Szeimies, 2010). While an estimated 5.5 million people are diagnosed with an NMSC every year in the U.S., with rising incidence rates, the mortality rate lies only at 0.03 % (Skin Cancer (Non-Melanoma) - Statistics, cancer.net, 2022). This is mainly because NMSCs develop slowly and rarely spread (Cives et al., 2020).

Malignant melanoma, on the other hand, while representing only 1 % of skin cancers, accounts for 80 % of deaths (NCI-SEER-Database, 2023) due to its high proclivity for metastasis (Atkins et al., 2021; Radke et al., 2022). Worryingly, cutaneous melanoma incidence rates are rising substantially every year (320 % since 1975 in the U.S.), especially in women (Saginala et al., 2021) (Figure 13). An estimated 100,000 people are diagnosed yearly in the U.S., with the average age being 65. Nevertheless, cutaneous melanoma represents one of the most common cancers in young adults (Del Fiore et al., 2021). Although mortality rates have declined over the last decade (almost 18 % from 2013 to 2016) due to the introduction of revolutionary new treatments, an estimated 8000 people still die every year from cutaneous melanoma in the U.S. (Berk-Krauss et al., 2020; Melanoma Skin Cancer Statistics, cancer.org, 2023). Most cases are detected at an early stage and present very high survival chances, however, 5 % of patients are diagnosed with advanced distally spread disease and face a somber 5-year relative survival rate of about 30 % (Saginala et al., 2021) (Figure 14). Of note, non-cutaneous melanoma, which can arise from mucosal or ocular tissue, and a rare subtype of cutaneous melanoma of glabrous skin, acral melanoma (Figure 12), show even poorer prognosis. For example, the 5-year relative survival rate for distally spread uveal melanoma is 18 % (Eye Melanoma - Statistics, cancer.net, 2023). These rare non-cutaneous or acral melanoma types differ clinically, phenotypically, and genetically from those of hair-bearing skin (Hayward et al., 2017; Rabbie et al., 2019; Chacón et al., 2020; Weiss et al., 2022; Vergara et al., 2022), and will not be further discussed here.

Among cutaneous, non-acral melanoma, the traditional Clark classification presents three main subtypes based on pathological morphology and primary sites: superficial spreading melanoma (the most common form), nodular melanoma, and lentigo maligna melanoma (Figure 15) (Scolyer, Long and Thompson, 2011). Of note however, in the current clinical staging system of cutaneous melanoma of the American Joint Committee on Cancer (Keung and Gershenwald, 2018), these subtypes are not mentioned as prognostic factors, as clinicians instead focus on aspects like vertical tumor thickness (Breslow's depth) or the deepness of invasion (Clark's level) (Scatena, Murtas and Tomei, 2021). In contrast, in the newest World Health organization classification of skin tumors (Elder et al., 2020; Yeh and Bastian, 2021),

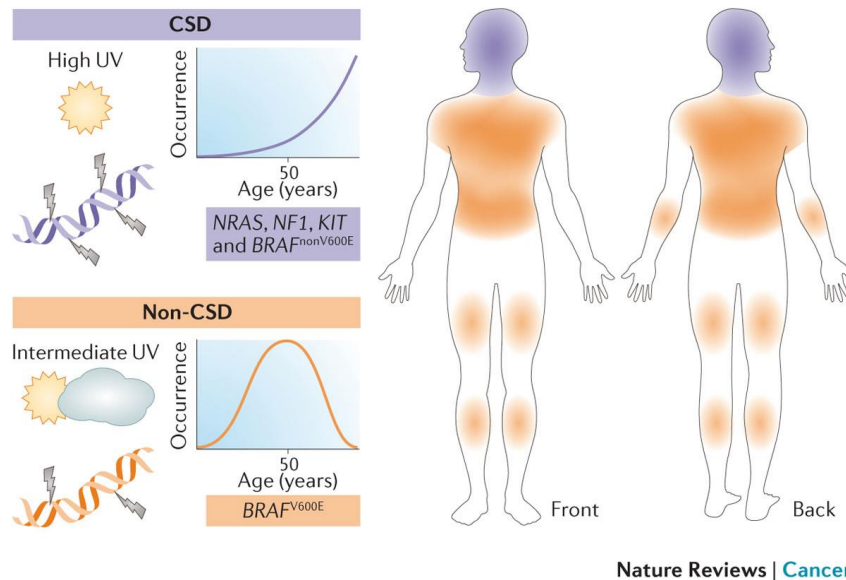


Figure 16. CSD and non-CSD melanomas are distinct subtypes of melanoma.

From Shain and Bastian, 2016.

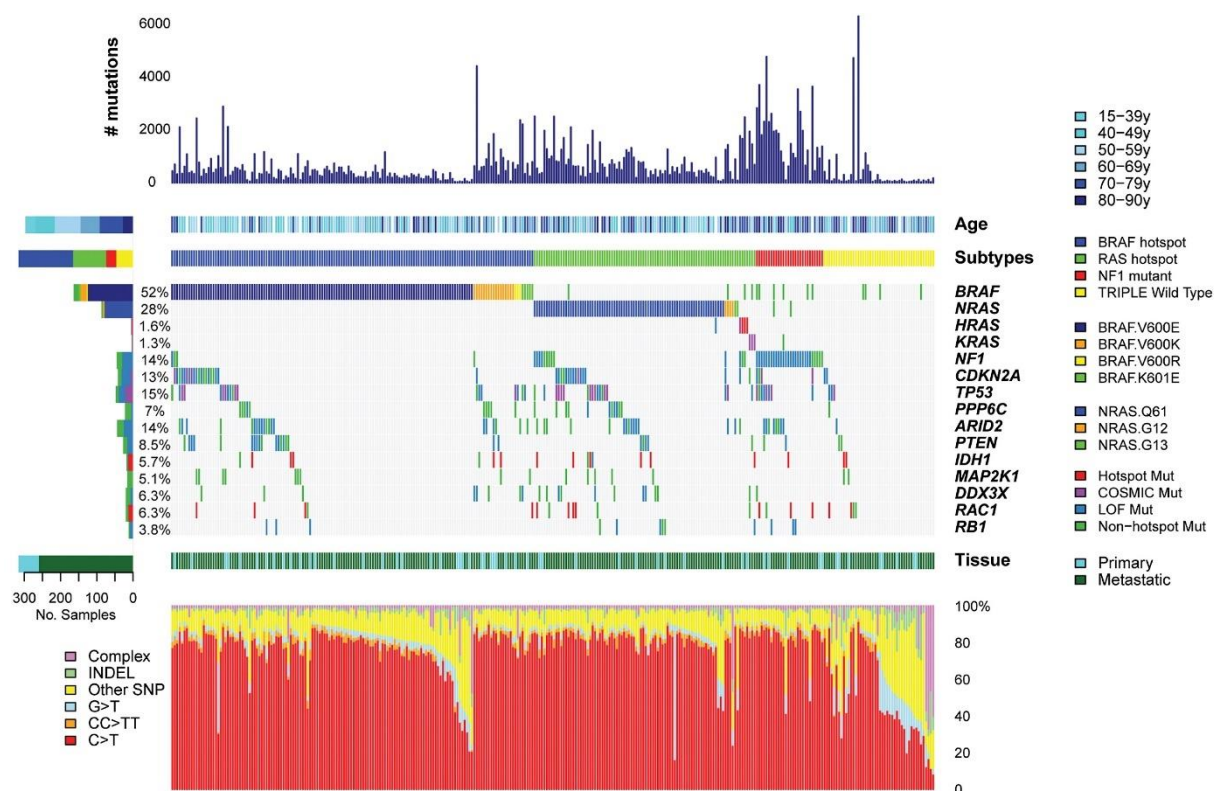


Figure 17. Landscape of driver mutations in cutaneous melanoma.

Tumor samples from 333 cutaneous primary and/or metastatic melanomas were used to establish mutational landscapes. Total number of mutations, age at melanoma accession, mutation subtype (BRAF, RAS [N/H/K], NF1, and Triple-WT), color-coded matrix of individual mutations, type of melanoma specimen (primary or metastasis), and mutation spectra are indicated for each sample (from top to bottom). Adapted from Akbani et al., 2015.

cutaneous melanoma is classified according to its origin from either chronically sun-damaged (CSD) or non-CSD skin and associated genomic alterations and mutational pathways (Figure 16). CSD-melanomas show high UV-mutation burden and arise on parts of the body like the head, neck, and dorsal extremities, usually in older people. On the other hand, non-CSD melanomas show fewer UV mutations and affect the less sun-exposed areas, such as the trunk and proximal extremities of younger people (< 55 years) (Bastian, 2014; Shain and Bastian, 2016). Significantly, these two types of melanomas differ in clinical aspects and oncogenic alterations (Curtin et al., 2005).

3.2. Genomic classification and driver mutations

Underlying the pathophysiological manifestations of the diverse melanoma subtypes are genes that, when their expression is altered, allow melanoma cells to maintain their deregulated phenotypes, like increased proliferation and survival (Hodis et al., 2012; Ding et al., 2014). While for a given case, hundreds or thousands of genes can be found to be altered, only specific few somatic mutations are recurrently considered proper ‘drivers’ of tumor growth and progression (Guan, Gupta and Filipp, 2015; Shain et al., 2015; Birkeland et al., 2018). The most common classification of genomic alteration landscapes divides melanoma cases according to the most prevalently mutated genes: mutant BRAF (55 %), mutant H/N/KRAS (25 %), mutant NF1 (10 %), and Triple-WT (wild-type, 10 %) (Figure 17) (Akbani et al., 2015). RAF, RAS, and NF1 proteins are essential regulators of the MAPK and PI3K/AKT proliferation and survival pathways (Figure 18), with one or both found hyperactivated in over 90 % of melanomas (Davies, 2012; Sullivan and Flaherty, 2013). The most common mutation in melanoma is the BRAFV600E substitution, associated with the 400-fold increased activity of this kinase (Al Hashmi et al., 2020). BRAFV600E is primarily found in non-CSD melanomas. On the other hand, RAS (mostly G12 or Q61), NF1 (loss of function), and non-BRAFV600E mutations are commonly found in CSD-melanomas, and are more related to UV damage (Bastian, 2014). The Triple-WT subtype represents a more heterogeneous group characterized by a lack of BRAF, RAS, or NF1 mutations. Instead, alterations in genes such as *GNAQ*, *GNAI1*, *KIT* or *TP53* and more copy-number and structural genome changes are found relative to the other subgroups. Other melanoma driver mutations affect genes such as *ARID2*, *CDKN2A*, *PTEN*, and *TERT* (Akbani et al., 2015). While these pathogenic drivers have been well cataloged in recent years, the order of occurrence, evolutionary pathways, and biological implications for melanoma progression are incompletely understood.

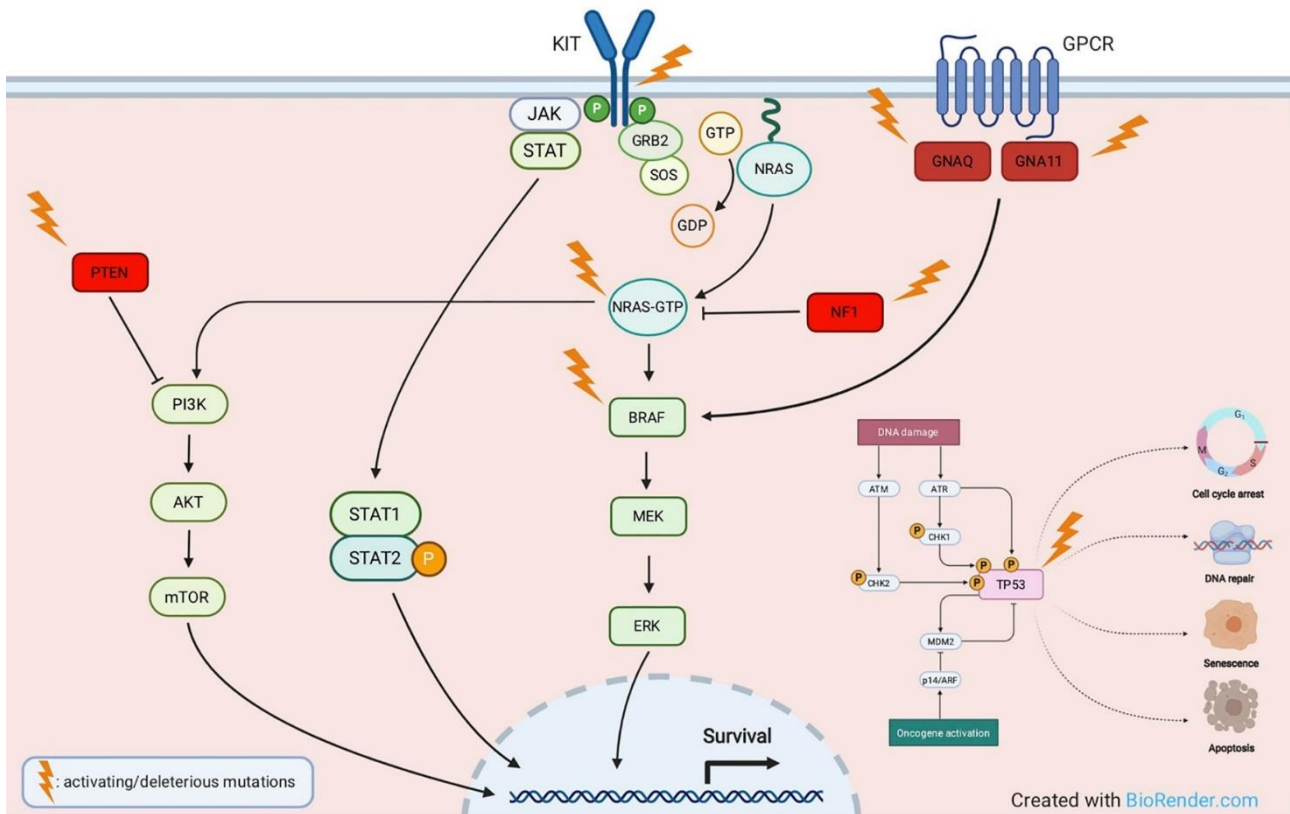


Figure 18. Main molecular pathways involved in melanomagenesis and associated mutations.

From Scatena, Murtas and Tomei, 2021.

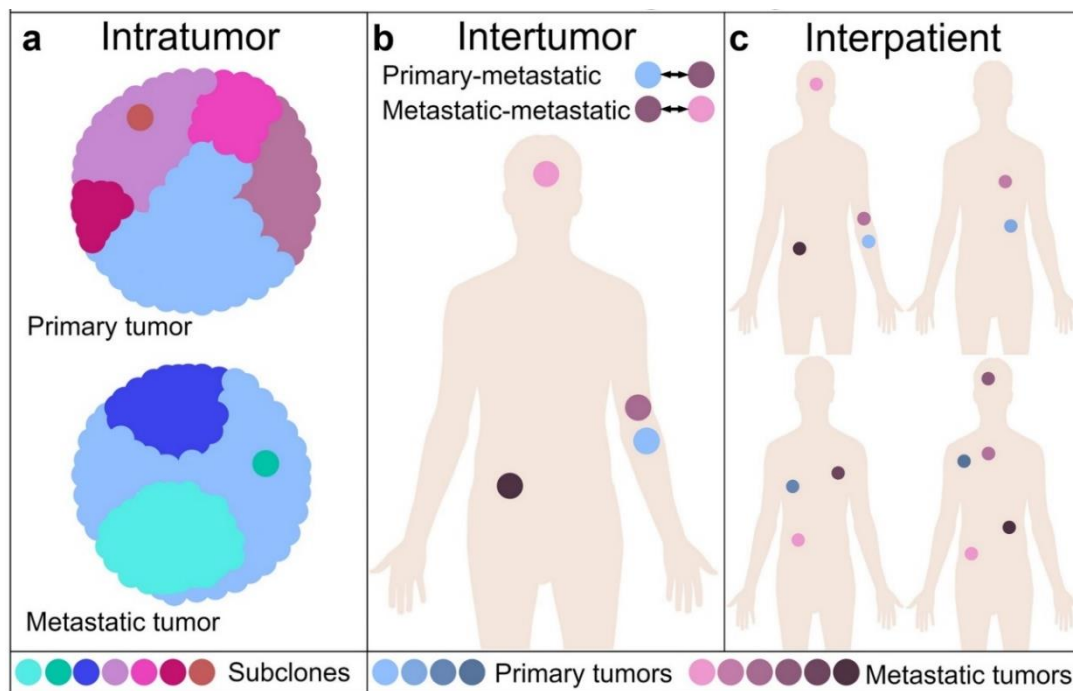


Figure 19. Levels of tumor heterogeneity.

Adapted from Grzywa, Paskal and Włodarski, 2017.

B. Cutaneous melanoma disease progression

1. The evolving nature of melanoma progression understanding

Carcinogenesis towards a primary cutaneous melanoma (hereafter called melanoma), capable of invasion and metastasis, is a complex process. It is important to note that for the longest time, researchers tried to model cancer progression along a stepwise, gradual, one-dimensional path from initiating lesion to final metastatic cancer, with closely associated genetic alterations (Clark et al., 1984). However, the emerging data indicates a more complicated reality of different melanoma subsets, with many different evolutionary pathways, cell types, pathophysiological manifestations, and genomic alterations, whose diseases trajectories can vary substantially, even among patients with supposedly similar clinical melanoma subtypes (Sanborn et al., 2015; Harbst et al., 2016; Birkeland et al., 2018; Belote et al., 2021; Eddy, Shah and Chen, 2021; Loras et al., 2022; Rogiers et al., 2022). Furthermore, other layers of complexity arise from the fact that genotype-phenotype connections are hard to infer (Hodis et al., 2022), and that oncogenic changes to DNA are not transforming in all circumstances (Baggiolini et al., 2021; Fowler et al., 2021). Instead, the precise anatomic location of a melanocyte dictates a transcriptional state which renders it more or less susceptible to specific oncogenic effects (Weiss et al., 2022). Hence, a one-fits-all progression model for melanoma seems outdated in the light of important interpatient, intertumor, as well as intratumor heterogeneity (Figure 19) (Grzywa, Paskal and Włodarski, 2017; Ng, Simmons and Boyle, 2022; Gavish et al., 2023). Importantly, anatomical position, microenvironmental factors, and transcriptional cell states must be considered when talking about melanoma development. As such, our understanding of progression models has expanded tremendously in recent years and is more heavily taken into account by the newest WHO melanoma classification (Elder et al., 2020; Yeh and Bastian, 2021). However, to provide a more schematic view of the process in the following pages, the progression model outlined hereinafter is based on the well-known, simplified, but still widely accepted one proposed by Clark et al. in 1984, which proposed a five-step development from melanocytes to metastatic melanoma (Figure 20). This progression includes: 1) benign naevus; 2) dysplastic naevus; 3) radial growth phase; 4) vertical growth phase; and 5) metastatic melanoma. Nevertheless, it is crucial to remember the more complex, evolving, less-linear nature of this subject, and the crucial aspect of tumor heterogeneity.

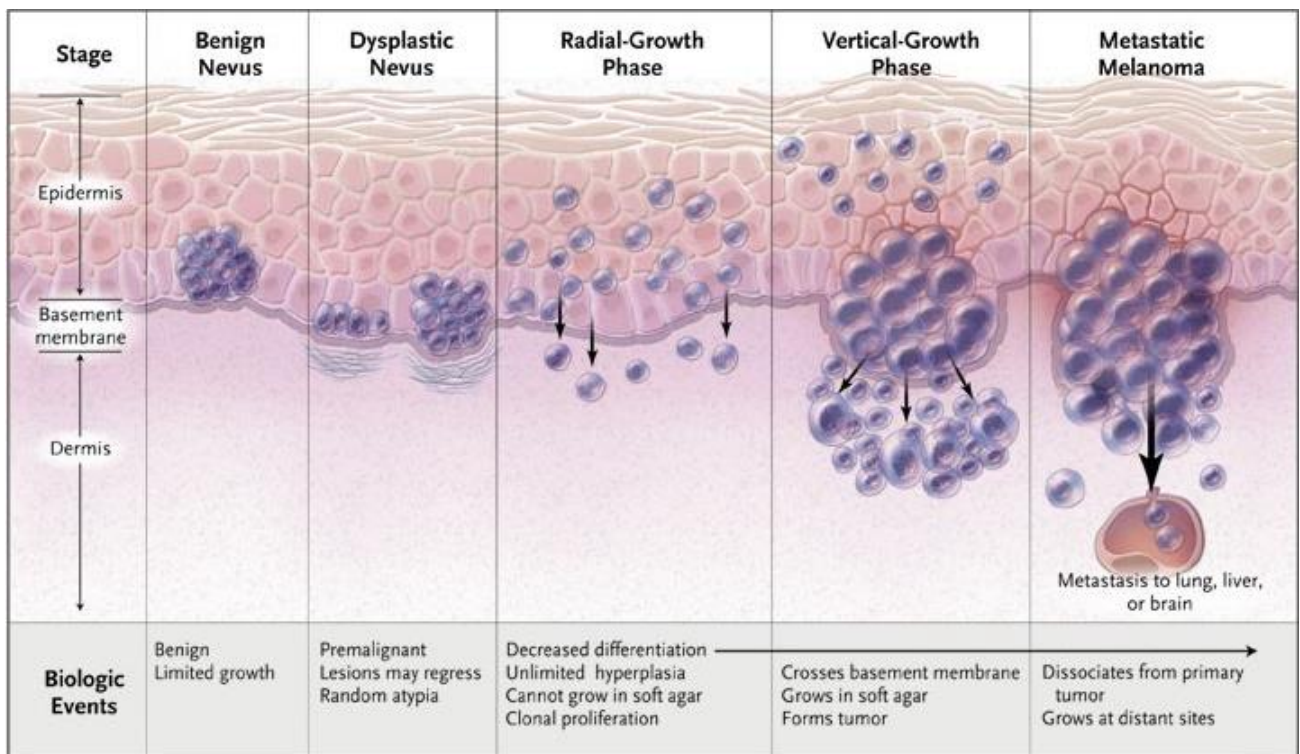


Figure 20. The Clark Model of linear melanoma progression.

Adapted from Miller and Mihm, 2006.

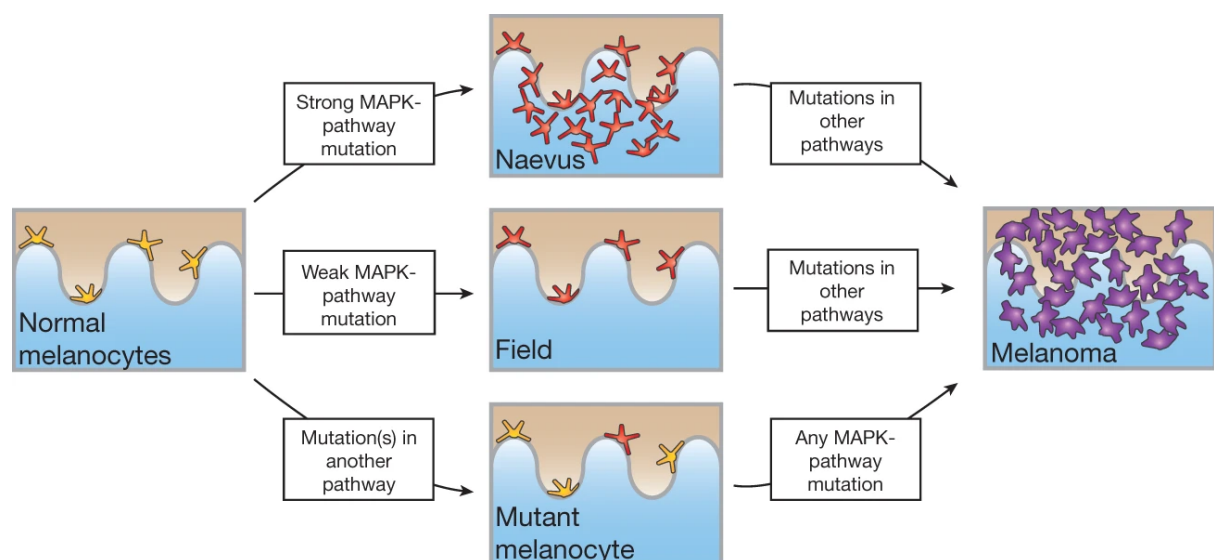


Figure 21. Distinct trajectories of melanoma initiation.

From Tang et al., 2020.

2. Initiation: From melanocytes to melanocytic precursor lesions

2.1. Cell of origin and somatic mutations

Under normal circumstances, epidermal melanocytes divide twice a year (Jimbow et al., 1975). However, as they are located at the very barrier to the outside environment, skin cells like melanocytes are chronically exposed to UV radiation (Wei et al., 2021). Seeing that DNA repair processes weaken in elderly individuals, UV-related somatic mutations accumulate exponentially with increasing age (Hernando et al., 2021). Ultradeep bulk-sequencing of cutaneous biopsies revealed that despite the protection mechanism of melanin production, non-cancerous, sun-exposed aged skin cells like keratinocytes already harbor a very high burden of mutations, more than in many cancer types, with strong positive selection for skin cancer driver mutations (Martincorena et al., 2015). Thus, it comes as no surprise that melanoma presents, with lung cancers, the highest average mutational burden of any cancer (Alexandrov et al., 2013), and that the most significant risk factors are excessive sun exposure and a light phototype (Schadendorf et al., 2018). Although most are ‘passenger mutations’ without any noticeable phenotypic effects, rare ‘driver mutations’ can confer a selective advantage to some melanocytes, leading to preferential growth or survival of a clone (Martincorena and Campbell, 2015). Interestingly, the predominant cell-of-origin of melanoma is still debated. While it seems that melanocyte stem cells can act as cancer-initiating cells (Moon et al., 2017), other data suggest that fully mature melanocytes are better-suited candidates (Köhler et al., 2017).

In a landmark study in 2020, Tang et al. shed light on the mutational dynamics of the first steps of melanoma initiation by overcoming the technical difficulties related to sequencing individual pre-neoplastic skin melanocytes. They confirmed that sun-exposed melanocytes display an astonishing average of 20,000 UV-radiation-induced mutations per cell, which is similar to the mutational burden found in transformed malignant melanoma cells. This suggested that melanoma cells display similar numbers of mutations to neighboring normal melanocytes, with the difference being the nature and degree of oncogenicity of the mutations. Expectedly, there was substantial heterogeneity between anatomical sites, but surprisingly there were also marked differences in mutation burdens between groups of melanocytes taken from the same skin location, assumed to be subject to similar amounts of UV radiation. The authors found that the differential expression of genes regulating p53, like *MDM2* or *MDM4*, correlated with mutation burdens. Unexpectedly, chronically sun-exposed skin (like on the face) had lower numbers of mutations than intermittently sun-exposed skin (like on the back),

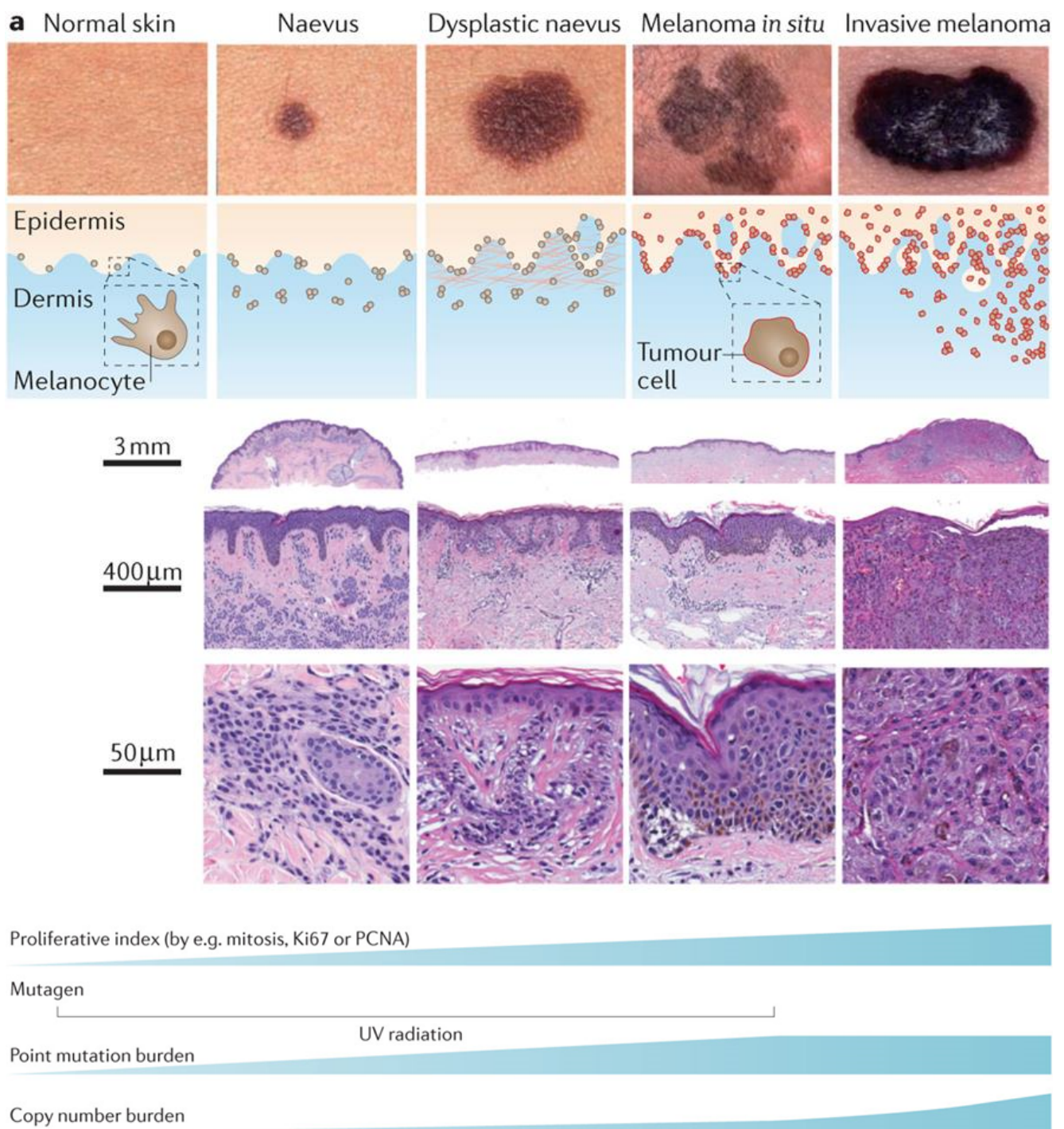


Figure 22. Characteristics of melanocytic neoplasms across the morphological spectrum.

Adapted from Shain and Bastian, 2016.

possibly due to divergences in UV protection, mutation rates, DNA repair, or melanocyte turnover. This finding could explain why most melanomas develop in intermittently sun-exposed areas (Elwood and Gallagher, 1998). Another interesting finding of Tang et al. was that one-fifth of analyzed melanocytes in sun-exposed skin already harbored diverse weak activator mutations in MAPK pathway genes like *BRAF*, *NRAS*, or *NF1* (Krauthammer et al., 2015; Yao et al., 2017). These cells were often found to be slightly more proliferating and created ‘clonal fields’ or clusters of pathogenically mutated melanocytes in the skin. However, the authors did not detect the strong MAPK activator BRAFV600E or NRAS Q61(K/R/L)/Q12D mutations. This might be explained by the fact that this study did not analyze melanocytes from naevi (moles), which often present the BRAFV600E mutation.

Based on these observations, the authors proposed a model of three distinct trajectories of melanoma initiation, depending on the order of driver mutation occurrence (Figure 21). Firstly, somatic UV-dependent mutations (or in rare cases inherited germline mutations) may affect genes besides MAPK effectors, such as by increasing the expression of TERT, the catalytic subunit of telomerase (Huang et al., 2013), or by disabling tumor suppressor genes like *ARID2* (Carcamo et al., 2022) or *CDKN2A* (Zeng et al., 2018), which alone are not sufficient to generate a neoplasm. They might however prime the melanocytes for transformation once an activating MAPK mutation is acquired. Secondly, UV-mutations can also ‘weakly’ increase MAPK signaling (for example with BRAFV600K, BRAFK601E, NF1 loss-of-function, or KIT gain-of-function) (Shain et al., 2018), leading to melanocyte growth and creation of melanocyte clusters/fields, which progress to malignant melanoma if additional driver mutations are acquired. These two trajectories rely on UV mutations and might immediately progress into ‘de novo’ high-CSD-in-situ melanomas without a discernible precursor lesion (Figure 22). Thirdly however, low-CSD melanoma tend to arise from strong MAPK activator mutations like BRAFV600E, which are not directly caused by UV radiation and initially significantly increase melanocyte proliferation to form precursor lesions like benign naevi (Figure 22). These are defined as preliminary, partially transformed neoplasms in which further development is halted, at least until additional somatic mutations accumulate.

2.2. Precursor lesions: Melanocytic naevi

Approximately one-third of melanomas can be directly traced back to naevi precursors, which are benign, usually pigmented proliferations of melanocytes (Lee et al., 2021). Although only a tiny percentage of naevi progress to malignant melanoma (about 1 in 3000 for men and 1 in

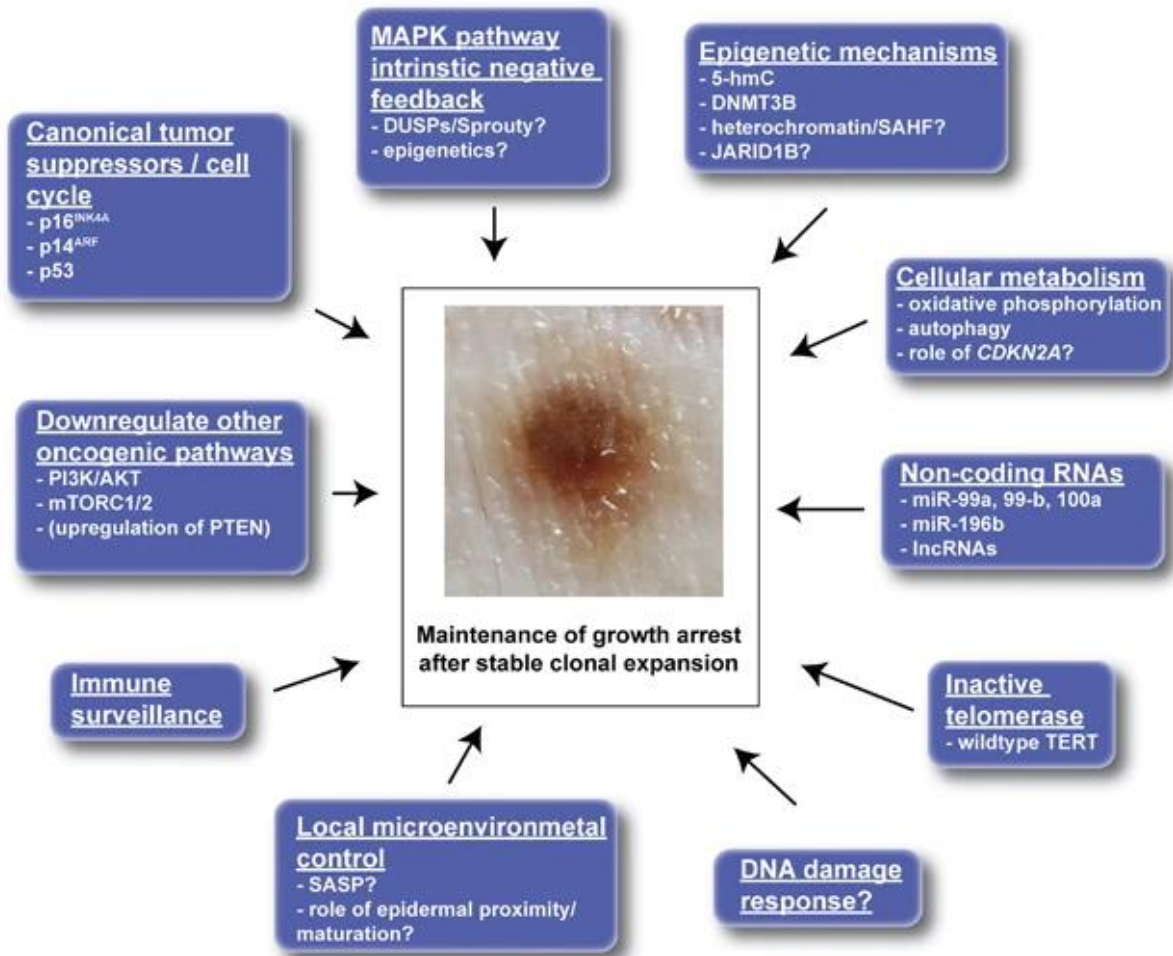


Figure 23. Proposed mechanisms of growth arrest of melanocytic naevi.

From Damsky and Bosenberg, 2017.

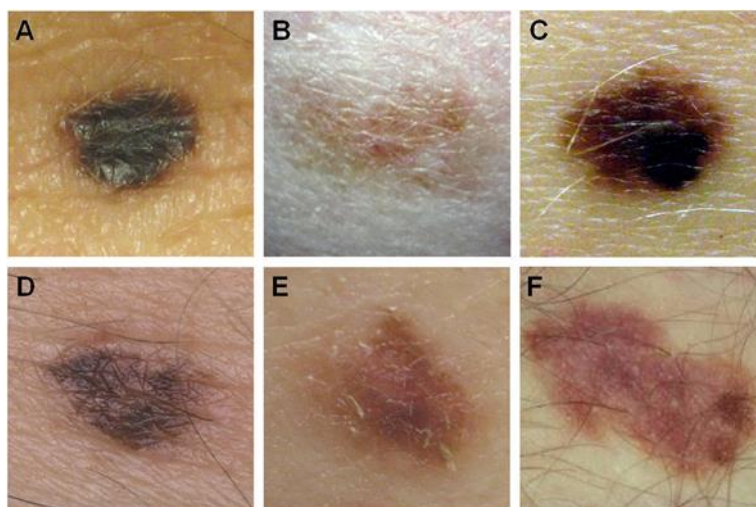


Figure 24. Clinical features of atypical/dysplastic naevi.

From Duffy and Grossman, 2012.

11000 for women), having a high number of them presents a decisive risk factor for melanoma development, including ‘de novo’ melanomas not deriving from naevi (Tsao et al., 2003; Gandini et al., 2005; Shreberk-Hassidim, Ostrowski and Fisher, 2023). Rarely, naevi can be congenital, but most arise during the first two decades of life and tend to regress after age sixty, by mechanisms not entirely understood (Damsky and Bosenberg, 2017).

About 80 % of naevi form because of MAPK pathway hyperactivation by the BRAFV600E mutation in a single melanocyte (the remaining 20 % are mainly due to *H/N/KRAS* mutations, mutually exclusive with *BRAF* mutations) (Yeh, von Deimling and Bastian, 2013; Roh et al., 2015; Cisowski et al., 2016). Of note, the etiology of BRAFV600E is still debated. While the T→A transversion leading to the V600E mutation is not a classic UV signature mutation, atypical and rare UV photoproducts or ROS generation could still implicate UV radiation in this process (Laughery et al., 2020). Constitutive MAPK pathway activation, as for example through BRAFV600E, is sufficient to give a strong proliferative signal for melanocytes to clonally expand (Dankort et al., 2009). However, after this period of initial mitotic burst, several mechanisms usually lead to growth arrest and the formation of a mature, stable naevus (Michaloglou et al., 2005), in which the proliferation rate however is not entirely zero but rather in equilibrium with inhibitory factors (Glatz et al., 2010). This process can take months and more than 16 rounds of cell division to create a naevus of 2 to 6 mm comprised of more than 100,000 melanocytes (Damsky and Bosenberg, 2017).

Several tumor suppressive mechanisms explaining this dramatically reduced melanocyte proliferation have been proposed in recent years (Figure 23), but their individual contributions and dynamics are still incompletely understood. While for a long time oncogene-induced cellular senescence has been seen as the leading cause of cell cycle arrest, this view is being challenged by observations that melanocytes lacking senescence-inducing proteins, such as *CDKN2A* proteins p16^{INK4A} and p14^{ARF} or p53, keep the ability to enter a growth-arrested state (Damsky et al., 2015). Other mechanisms include activation of the Hippo/YAP/TAZ (Vittoria et al., 2022) or DNA damage response pathways (Gorgoulis et al., 2005), actions of miRNAs (Xu et al., 2012), metabolic rewiring (Haq et al., 2013), immune surveillance (Duffy et al., 2010; Katlinskaya et al., 2016), and the role of telomeres (Ramirez et al., 1999; Huang et al., 2013). In conclusion, all these overlapping mechanisms lead to naevi being growth arrested, potentially for many years or indefinitely. For a naevus to develop into a melanoma, several of these tumor suppression mechanisms must be overcome simultaneously, through the acquisition of supplemental driver mutations.

Of note, there seem to exist precursor neoplasms in an intermediary state between the common

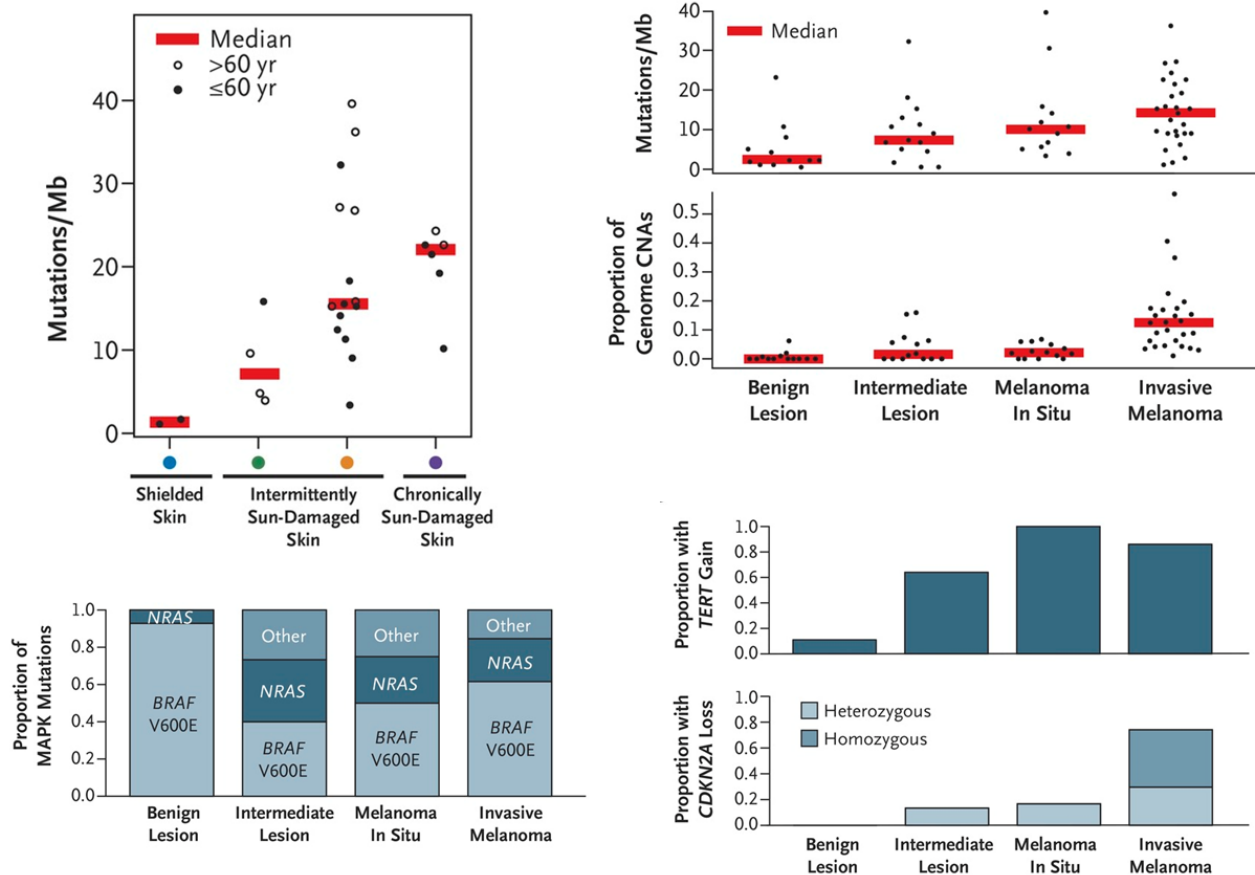
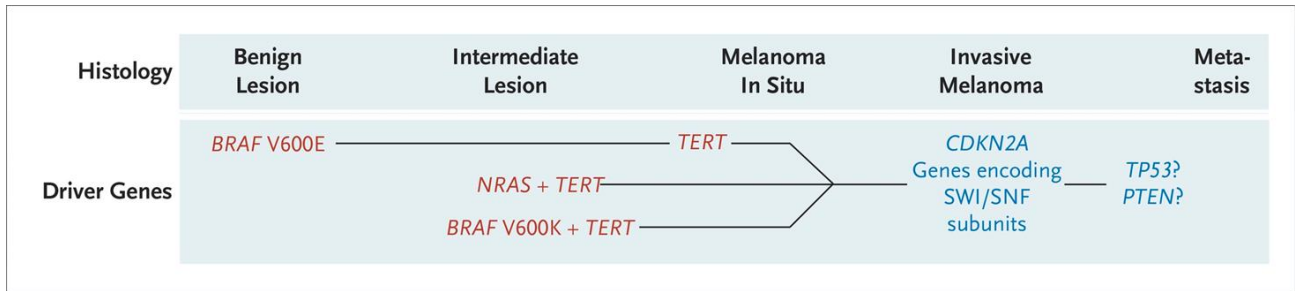


Figure 25. Proposed model of the genetic evolution of melanoma from precursor lesions to metastatic disease, and mutation burden and types at each step of progression.
CNAs = copy number alterations. Adapted from Shain et al., 2015.

naevus and melanoma, denominated as ‘dysplastic naevi’ (Figure 22 and 24), presenting malignant histologic or clinical features like severe dysplasia, irregular borders, or variable pigmentation (Duffy and Grossman, 2012). Individuals with multiple dysplastic naevi seem to show increased melanoma risks (Tucker et al., 1997). While there is still debate about the clinical significance of these enlarged and atypical naevi, sequencing analyses by Shain et al. in 2015 have shown that, in contrast to benign naevi, which invariably harbored a singular driver mutation like BRAFV600E, the intermediary lesions/dysplastic naevi presented multiple driver mutations and increased mutation burden (Figure 25). In the majority of cases, non-BRAFV600E MAPK mutations were found, pointing to the fact that dysplastic naevi do not usually arise from previous benign naevi, and instead follow another initiation trajectory, which might explain their propensity for appearing ‘de novo’ on CSD skin (Figure 21). Also, heterozygous mutations in cell cycle genes like *CDKN2A* were detected in a significant subset of lesions (Shain et al., 2015; Shain and Bastian, 2016) (Figure 25). Additionally, most dysplastic naevi presented mutations in the *TERT* promoter, substantially elevating telomerase expression and thus telomere length, which very probably induced their malignant features by causing immortalization and genomic instability (Huang et al., 2013, Chiba et al., 2017). Interestingly, *TERT* promoter mutations are found in nearly all melanomas (Shain et al., 2018). Based on this, Shain et al. propose a model in which *TERT* mutations emerge very early in melanoma progression and are positively selected as the initial secondary driver mutation prompting the malignant transformation of melanocytes (Figure 25). In growth-halted naevi, this would allow to bypass mechanisms such as oncogene-induced-senescence. The telomerase-dependent increased survivability of melanocytes (naevi-associated or not) would enable them to accumulate subsequent mutations, with progression towards malignant melanoma in-situ (Figure 21).

3. Progression: Towards invasive melanoma

3.1. Melanoma in situ

Melanomas in situ are defined as malignant and irregular hyperplasia of melanocytes which entirely reside in the epidermis (Figures 20 and 22). In the Clark progression model, this phase is called ‘radial growth phase’, as the cells have become highly proliferative through senescence escape and immortalization, but they cannot yet invade underlying tissues by crossing the dermo-epidermal junction (Hall and LeBoit, 2014). Clinically, they can represent

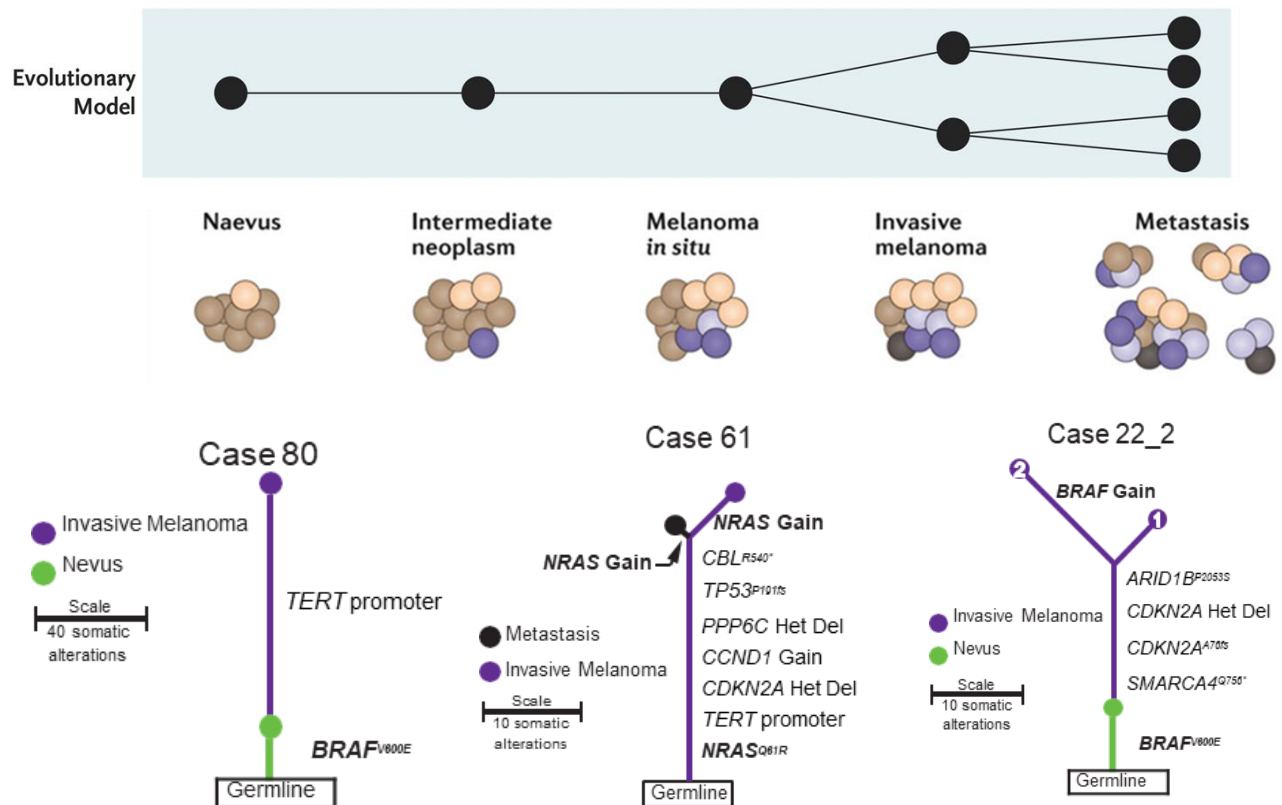


Figure 26. Evolutionary model of genetic intratumoral heterogeneity, and examples of individual progression cases and mutation acquisitions.

Adapted from Shain et al., 2015, Shain and Bastian, 2016 and Shain et al., 2018.

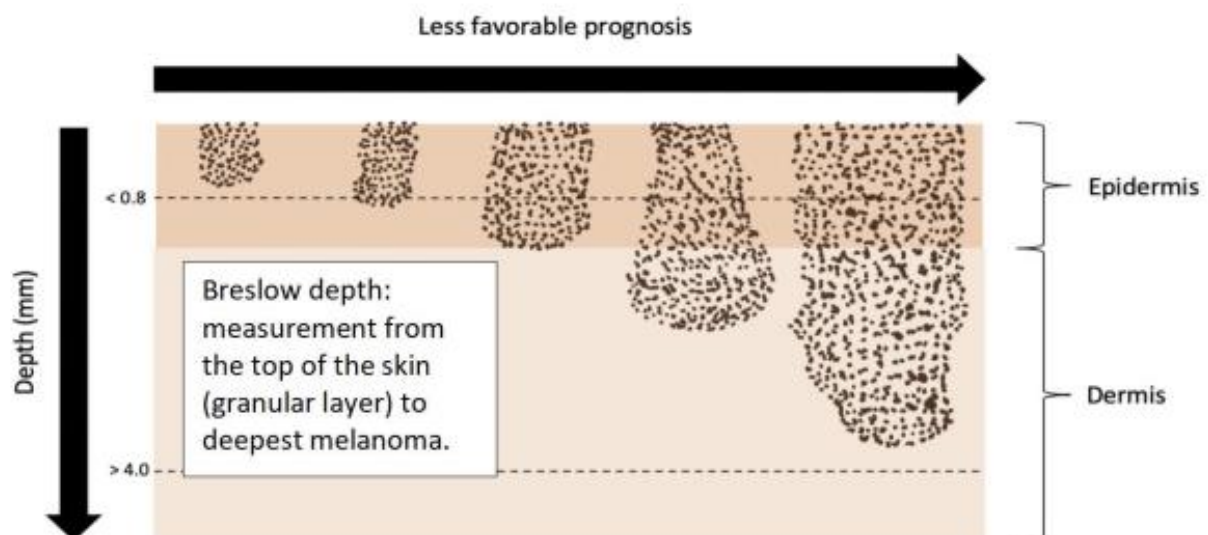


Figure 27. Breslow depth.

From <https://www.nm.org/conditions-and-care-areas/dermatology/moles-and-melanoma/treatment>

raised lesions in the skin, and the survival rates when totally resected are near 100 % (Guerry et al., 1993). Although different evolutionary paths can lead to melanoma in situ, either with associated naevi precursor lesions or de novo apparitions (Figure 21), they are genetically characterized by the presence of a MAPK-stimulating mutation and *TERT* promoter mutations (Shain et al., 2015) (Figure 25). It may take years for in situ melanoma to become invasive, showcasing the need for additional genomic alterations for this specific capacity (Weinstock and Sober, 1987). These may be necessary to overcome additional inhibitory mechanisms other than oncogene-induced-senescence, such as immune surveillance. This immune escape is helped by the fact that melanoma tumors tend to become more heterogeneous during these later progression stages, as polyclonality through differently branched evolutionary cell trajectories increases (Figure 26). This leads to the probable coexistence of various subclones with differently activated genetic driver pathways (Shain et al., 2018; Hodis et al., 2022), but also allows for the emergence of multiple cellular phenotypes with divergent levels of melanocytic differentiation and distinct governing transcriptional programs (Grzywa, Paskal and Włodarski, 2017; Hinohara and Polyak, 2019). The mechanisms underlying this epigenetic plasticity will be further elucidated later on.

3.2. Invasive melanoma

The vertical growth phase of melanoma begins once malignant cells breach the epidermal basement membrane and invade the subjacent mesenchymal tissue, the dermis, forming a bona fide 3-dimensional tumor. At this stage, the invasion depth serves as a primary determinant of cancer staging and for prognosticating survival, metastasis, and disease management (Balch et al., 2009). As such, invasive melanomas are subcategorized by their thickness, the distance in millimeters between the granular layer of the epithelium and the deepest point of the invasive tumor front, also called Breslow depth (Figure 27), mainly into thin (<1mm), intermediate (1-4mm) and thick (>4mm) melanoma. Thick melanoma represents invasion into subcutaneous fat and is the most likely to spread, with 5-year survival dropping to around 50 % (Erkurt et al., 2009; Montagnani et al., 2016; Bozsányi et al., 2022).

Compared to melanoma in situ, invasive melanoma shows an even increased mutational burden. Of note, as the tumor develops into deeper skin regions, it is less exposed to UV radiation. As such, UV-dependent point mutations become rarer as larger chromosomal rearrangements and copy number alterations (CNAs) become more frequent (Bauer and Bastian, 2006; Montagnani et al., 2016) (Figures 22 and 25). This can potentially be explained

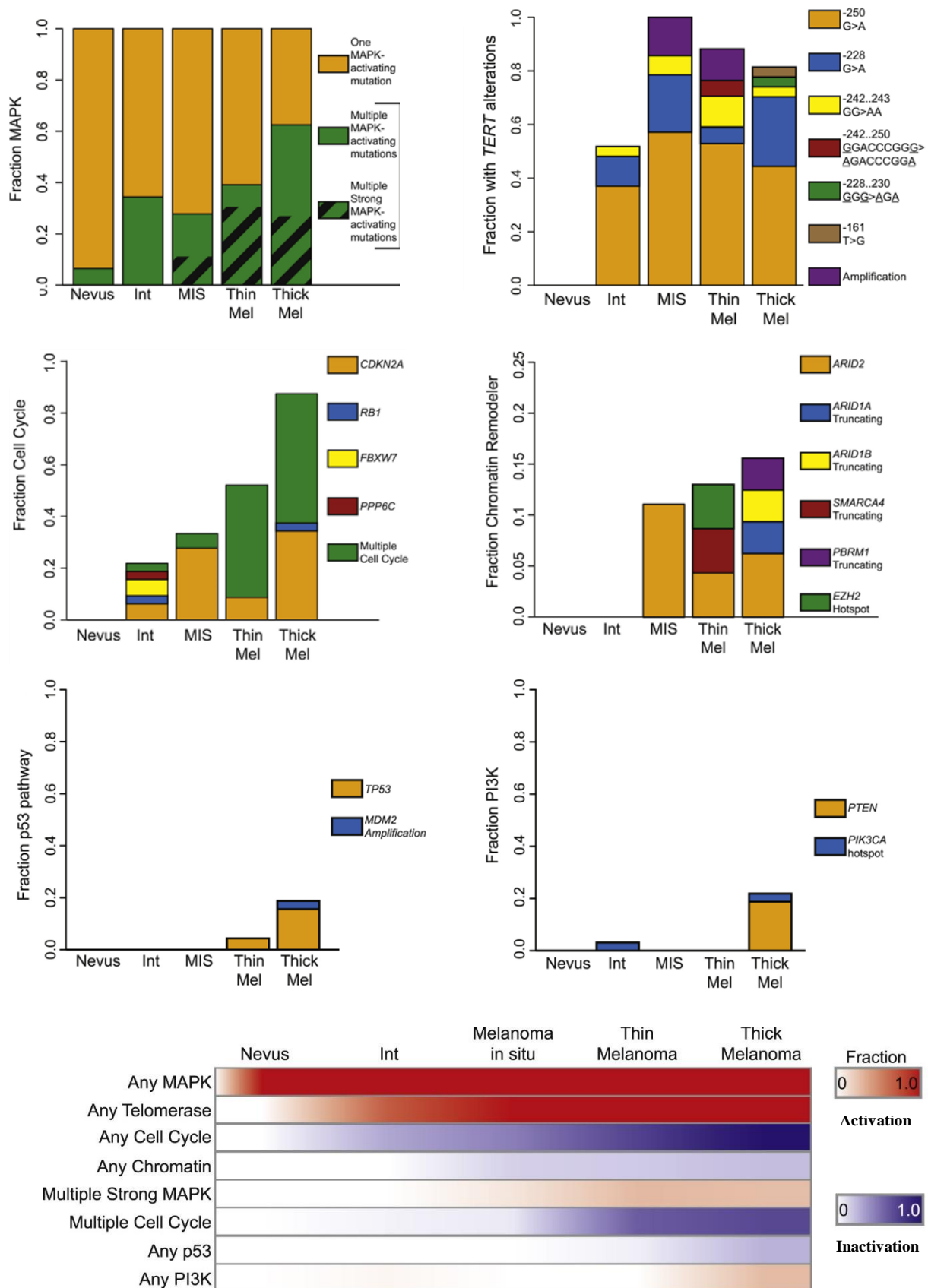


Figure 28. Incremental alterations of signaling pathways during melanoma progression.

Data presented as fractions of mutations at a given stage. Adapted from Shain et al., 2018.

by the fact that at this stage of melanoma development, inactivating alterations of cell-cycle-regulating checkpoint genes are observed in almost all cases, such as bi-allelic mutations for the *CDKN2A* protein p16^{INK4A} or the retinoblastoma protein RB1, both implicated in the G1/S checkpoint. Their mutations lead to abnormal cell cycle progression and potential chromosomal aberrations (Reed et al., 1995; Pavey et al., 2002) (Figure 28). Additionally, invasive melanomas often display secondary driver mutations in genes related to maintaining chromatin structure, such as in SWI/SNF chromatin-remodeling complex members ARID2, ARID1A, or SMARCA4, further contributing to genomic instability (Wang, Haswell and Roberts, 2014). Furthermore, the disabling of SWI/SNF complexes gives rise to a more stem-cell-like chromatin landscape dominated by PRC2 remodeling complexes (Wilson et al., 2010; Shain et al., 2018). Additional weak or strong MAPK-activating mutations are frequently acquired during this malignant progression, ramping up oncogenic MAPK signaling even more (Joseph et al., 2010; Shain et al., 2018) (Figure 28). During later stages of melanoma invasion, alterations in the p53 (Lassam, From and Kahn, 1993) and PI3K/AKT/mTOR (Goel et al., 2006) pathways also tend to appear (each found altered in approximately 25 % of melanomas), respectively contributing to genomic instability and the diversification of oncogenic signaling.

During this stage of melanoma development, the different above-mentioned genetic changes as well as a host of microenvironmental factors such as increased hypoxia (Cheli et al., 2012), acidic surroundings (Andreucci et al., 2020), decreased nutrient availability (Ferguson et al., 2017), increased inflammation (Landsberg et al., 2012), and differences in stromal interactions (Bellei, Migliano and Picardo, 2020; Romano et al., 2021), all contribute to a pseudo-EMT with profound metabolic (Avagliano et al., 2020; Tasdogan et al., 2020) and epigenetic (Arozarena and Wellbrock, 2019) changes. Melanoma cells having undergone this so-called phenotype switch present a less differentiated, more stem-like phenotype by starting to express TFs found during the neural-crest developmental stage like SNAIL, SLUG, or SOX9, while losing the expression of differentiation markers like MITF (Pedri et al., 2022). These cells show increased mobility and invasive capacities, as they can for example secrete matrix metalloproteinases (Moro, Mauch and Zigrino, 2014). Interestingly, the genetic and epigenetic causes of increased invasiveness are in some cases closely linked, such as in the case of the more stem-like chromatin landscape induced by SWI/SNF mutations. Another example would be that mutations in *CDKN2A* cause the E2F1-dependent expression of BRN2, a TF repressing *MITF*, and an important driver of the dedifferentiated state and thus of melanoma invasion and metastasis (Zeng et al., 2018; Fane et al., 2019; Hamm et al., 2021).

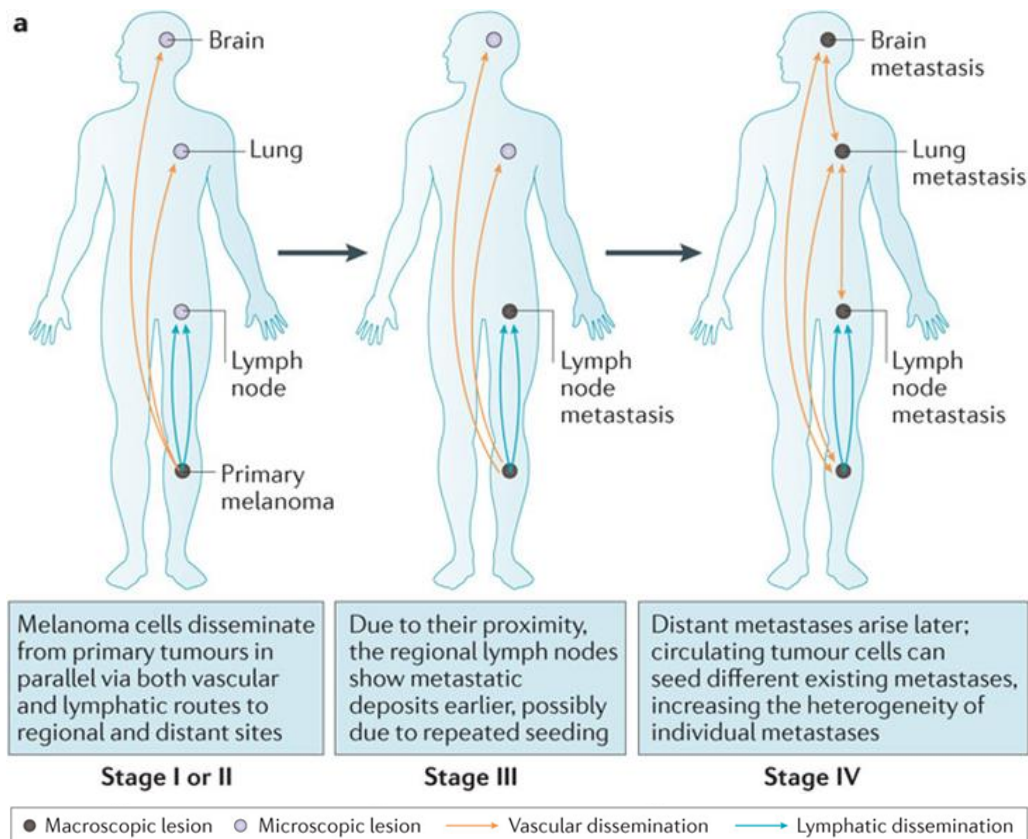


Figure 29. Model of metastatic trajectories in melanoma.

Adapted from Shain and Bastian, 2016.

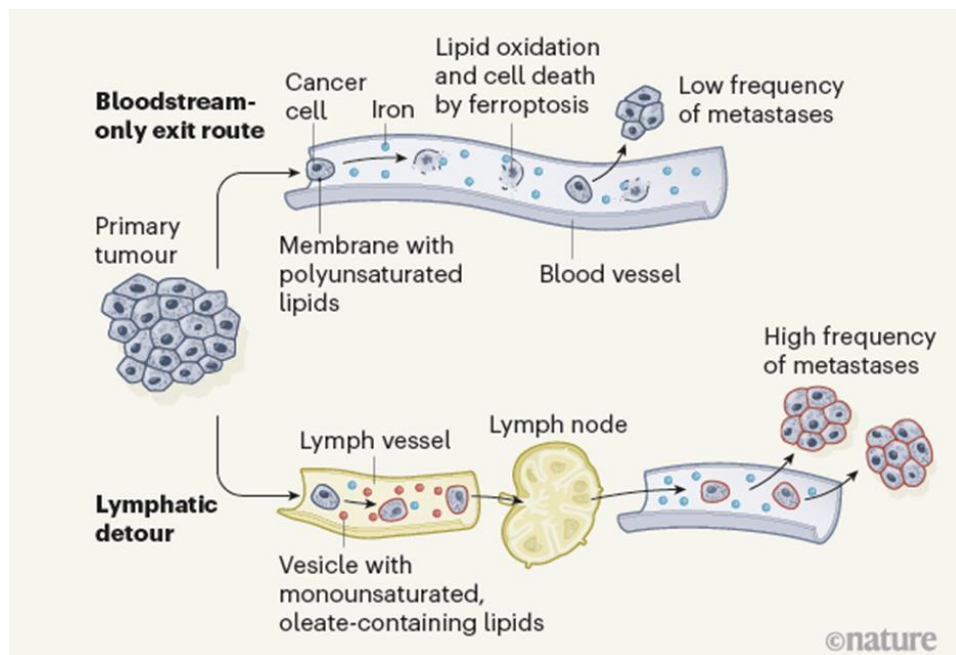


Figure 30. A journey through lymph vessels could boost melanoma cell metastasis.

From Grüner and Fendt, 2020.

4. Dissemination: Melanoma metastasis

4.1. Melanoma spreading trajectories

Melanoma is defined as metastatic once cells leave the local primary tumor site via the lymphatic and then circulatory systems and disseminate to other tissues to grow secondary tumors. Compared to other cancers, melanoma has a very high risk of early and rapid spreading, due to the fact that it develops from melanocytes which themselves originate from the highly migratory neural-crest cells (Damsky, Rosenbaum and Bosenberg, 2010; Damsky, Theodosakis and Bosenberg, 2014; Sundararajan et al., 2022). This final stage of cancer progression is the deadliest and displays the highest rates of mitotic indexes, mutational burdens (especially with sharp increases in large-scale genomic alterations), and intra- and intertumoral genetic and epigenetic heterogeneities (Paluncic et al., 2016; Thompson, Mozzillo and Ross, 2020; Vergara et al., 2021). Metastases tend first to be macroscopically observed in the lymph nodes surrounding the primary tumor, before appearing in more distant organs such as the liver, bones, lungs, or brain. This led to the historical assumption that metastatic progression follows a linear, temporal trajectory of melanoma cells starting from the primary tumor to enter the lymphatic system and then mainly invade regional lymph nodes (regional metastasis) and subsequently proceed towards distant metastasis (Damsky, Theodosakis and Bosenberg, 2014). However, this view is being challenged by the fact that early precautionary resections of regional lymph nodes do not prevent the outcome of distant metastasis and do not significantly improve patient survival (Morton et al., 2014; Leiter et al., 2016; Faries et al., 2017). Furthermore, blood-circulating melanoma cells can already be found in patients without lymph node metastases (Reid et al., 2013; Keller and Pantel, 2019), indicating a parallel mode of tumor dissemination via both the lymph and blood (Figure 29) (Werner-Klein et al., 2018). One proposed explanation as to why regional lymph nodes develop earlier metastases might just be due to the closer proximity of the primary tumor, simply increasing the probability of tumor cells passing through, leading to repeated seeding (Shain and Bastian, 2016).

However, recent, elegantly performed studies in rodent models (Brown et al., 2018; Pereira et al., 2018) showed that while melanoma cells can spread directly from the primary subcutaneous tumor, cells can be dispersed from lymph node metastases as well. Dissemination via/from the lymph nodes seemed to be responsible for more lung metastases than cells that took an immediate route from the primary tumor. In these models, the lymph nodes seemed to serve as efficient direct entry points to the blood circulation, as tumor cells did not need to first

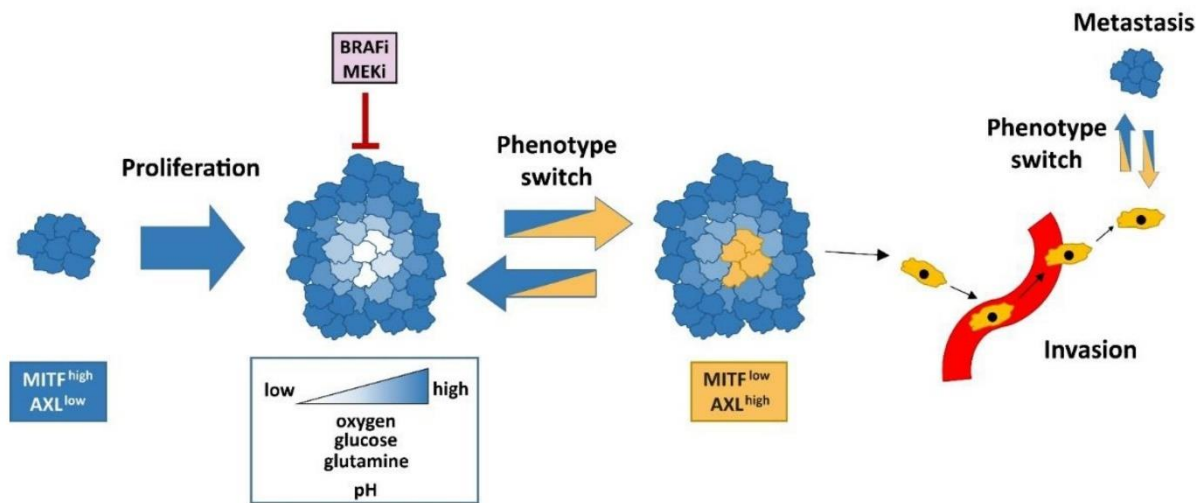


Figure 31. Phenotype switching and melanoma invasion and metastasis.

From Wessely et al., 2021.

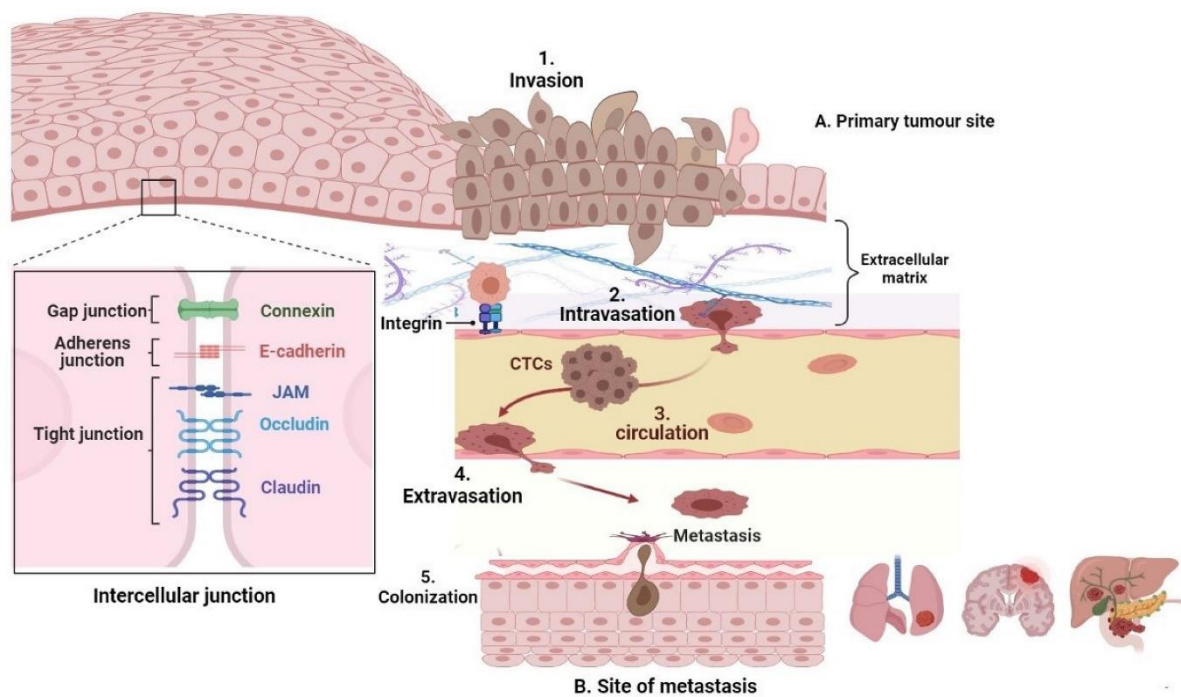


Figure 32. The metastatic cascade. (CTCs = circulating tumor cells)

From Imodoye et al., 2021.

make a detour through lymphatic vessels. This contradicted the widely accepted view that metastatic cells can only reach the bloodstream by first passing through lymphatic circulation. Furthermore, another study (Ubellacker et al., 2020) showed that melanoma cells first passing through the lymphatic system (high in oleic acid and glutathione, while low in free iron) seemed to display increased subsequent survival in the blood circulation by becoming more resistant to ferroptosis and oxidative stress, which represent major obstacles for tumor cells taking a direct bloodstream route (Piskounova et al., 2015; Tsoi et al., 2018; Talty and Bosenberg, 2022) (Figure 30). An explanation for those observations might be the fact that melanoma cells adapt to the lymphatic environment by metabolically shifting towards fatty acid oxidation and increasing YAP/TAZ signaling, which are known drivers of the dedifferentiated and resistant cell state (Aloia et al., 2019; Lee et al., 2019; Thompson, 2020; Li et al., 2021). These studies thus also confirmed that melanoma cells spreading from lymph nodes were more likely to form secondary tumors than those that did not and that metastases have the capacity to reseed each other, which would help explain the exponential emergence of secondary tumors during the final stages of disease progression (Kim et al., 2009; Sanborn et al., 2015) (Figure 29). Whether these in vitro and rodent observations also occur in humans remains to be explored, as they seem contradictory to the clinical data mentioned above, which showed that regional lymph node dissection has little patient benefit. In conclusion, many unanswered questions remain about the complexities of metastatic trajectories in melanoma.

4.2. Cell states, migration, and dormancy

Although numerous genetic alteration steps are needed to progress toward metastatic melanoma, no recurrent metastasis-specific mutations have been found, as none seem to specifically drive melanoma dissemination (Reiter et al., 2018; Shain et al., 2018). Nevertheless, reactivation of pathways associated with embryonic melanocyte development such as increased WNT/ β -Catenin or AP-1 signaling tend to be implicated (Damsky et al., 2011; Gajos-Michniewicz and Czyz, 2020; Suresh et al., 2023). As such, before-mentioned epigenetic changes such as the EMT-like phenotype switch to more invasive, stem-like, dedifferentiated MITF^{low} cell states, displaying altered expression of matrix metalloproteinases (MMP) and cell adhesion molecules (Hao et al., 2012; Das et al., 2017), seem to be indispensable in the metastatic process (Huang et al., 2021) (Figure 31). Like in most other cancers, this metastatic cascade follows the key steps of invasion, intravasation, circulation, extravasation, and colonization at secondary sites (Lambert, Pattabiraman and Weinberg,

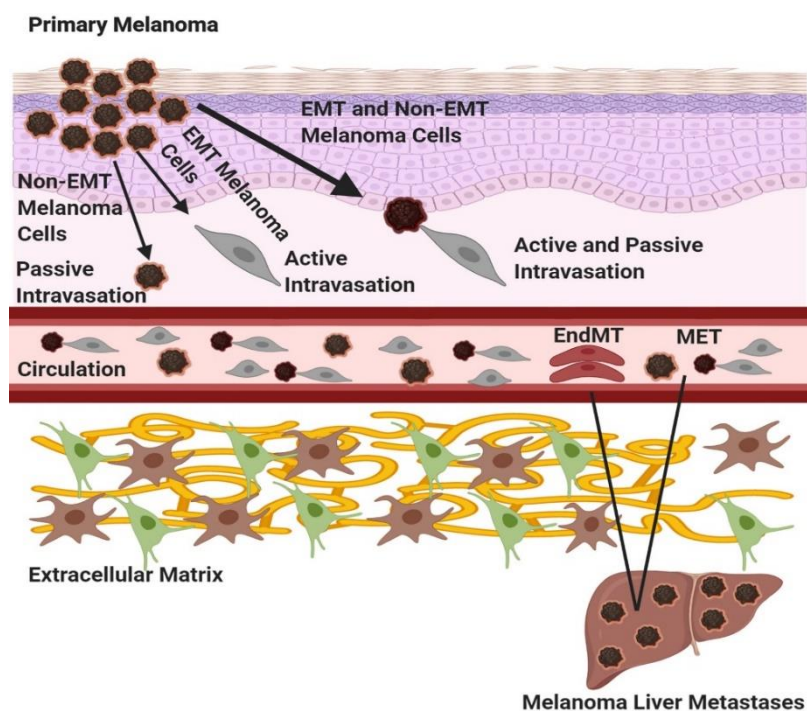


Figure 33. Distinct modes of melanoma cell intra- and extravasation.

EndMT = Endothelial-to-Mesenchymal transition. From Eddy, Shah and Chen, 2021.

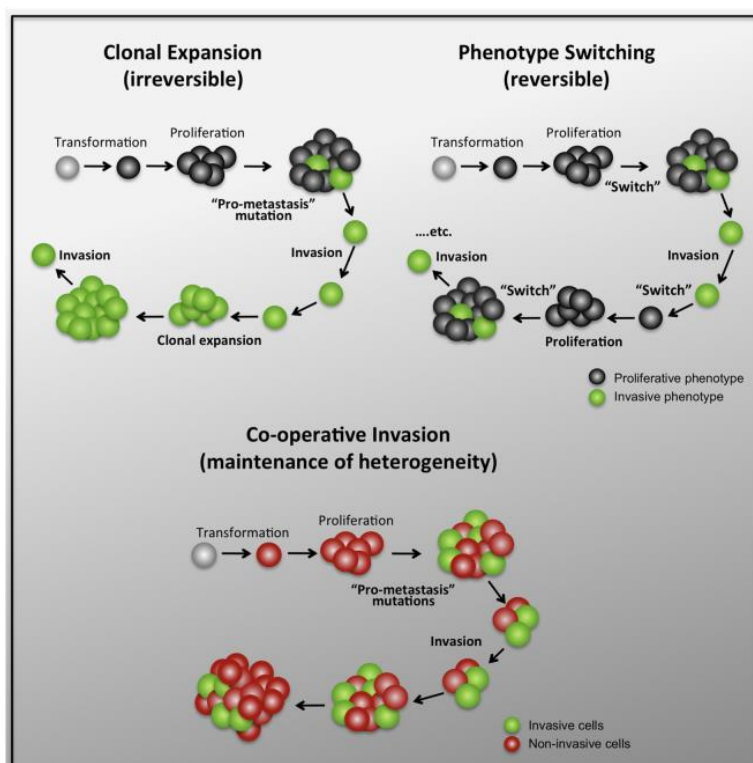


Figure 34. Heterotypic clusters and collective cell migration versus phenotype switching in melanoma metastasis.

From Chapman et al., 2014.

2017) (Figure 32). While the EMT-like invasive cells are well suited for the first four steps of this process, their capacity to re-establish colonies in secondary sites seems limited (Rambow, Marine and Goding, 2019; Karras et al., 2022). As such, the conundrum of the exact contributions of the different cell states in the metastatic progress becomes apparent, and various models addressing this problem have emerged over the years (Vandyck et al., 2021). Some studies propose that differentiated melanoma cells might passively intravasate into circulation, whereas dedifferentiated cells display active intravasation. Once in circulation, both cell types would cooperate to migrate to an adapted niche to establish a secondary tumor, with differentiated cells ‘riding along’ dedifferentiated cells (Bockhorn, Jain and Munn, 2007; Tsuji, Ibaragi and Hu, 2009) (Figure 33). Recent studies showcase this cooperation by identifying heterotypic clusters of both melanoma cell states that extravasate efficiently due to the dedifferentiated cells and, once they arrived in a favorable niche, grew rapidly to form metastases because of the differentiated cells (Chapman et al., 2014; Campbell et al., 2021) (Figure 34). Another model proposes however that the dedifferentiated melanoma cells can reverse back to a differentiated and proliferative state by a mesenchymal-to-epithelial-like (MET-like) phenotype switch to form secondary growths (Yao, Dai and Peng, 2011; Brabletz et al., 2018; Vandamme et al., 2020) (Figure 34). In this model, a delicate balance between EMT- and MET-like phenotype switches is paramount (Cook and Vanderhyden, 2020; Vandyck et al., 2021), and metastases here would more likely result as a consequence of the seeding of a single cell, rather than of a heterogeneous cell cluster (Cheung and Ewald, 2016). Recent data suggest these two mechanisms might be intertwined (Rowling et al., 2020).

Remarkably, a subset of dedifferentiated melanoma cells displaying neural-crest-stem-like characteristics can remain inactive in circulation for a long time (Rambow, Marine and Goding, 2019). Some of these cells seem to be able to transdifferentiate into a quiescent state with fibroblastic or endothelial characteristics (as evidenced by the expression of CD31 or VE-Cadherin), which can remain dormant in the intravascular niche of the pre-metastatic organs for years and may explain delayed metastatic disease or melanoma relapse (Li et al., 2020). Melanoma cells seem to enter this state in different ways, such as by the targeted expression of tumor suppressor genes, leading to cellular dormancy (Horak et al., 2008; Sosa, Bragado and Aguirre-Ghiso, 2014; Triana-Martínez, Loza and Domínguez, 2020), by induction of cytostasis by the immune system, leading to immunogenic dormancy (Eyles et al., 2010; Senft and Ronai, 2016), or by insufficient nutrient access, leading to angiogenic dormancy (Naumov et al., 2006) (Figure 35). Once these dormant mesenchymal-like or endothelial cells become re-awakened by external stimuli, they can extravasate into the metastatic niches. To do this, endothelial-like

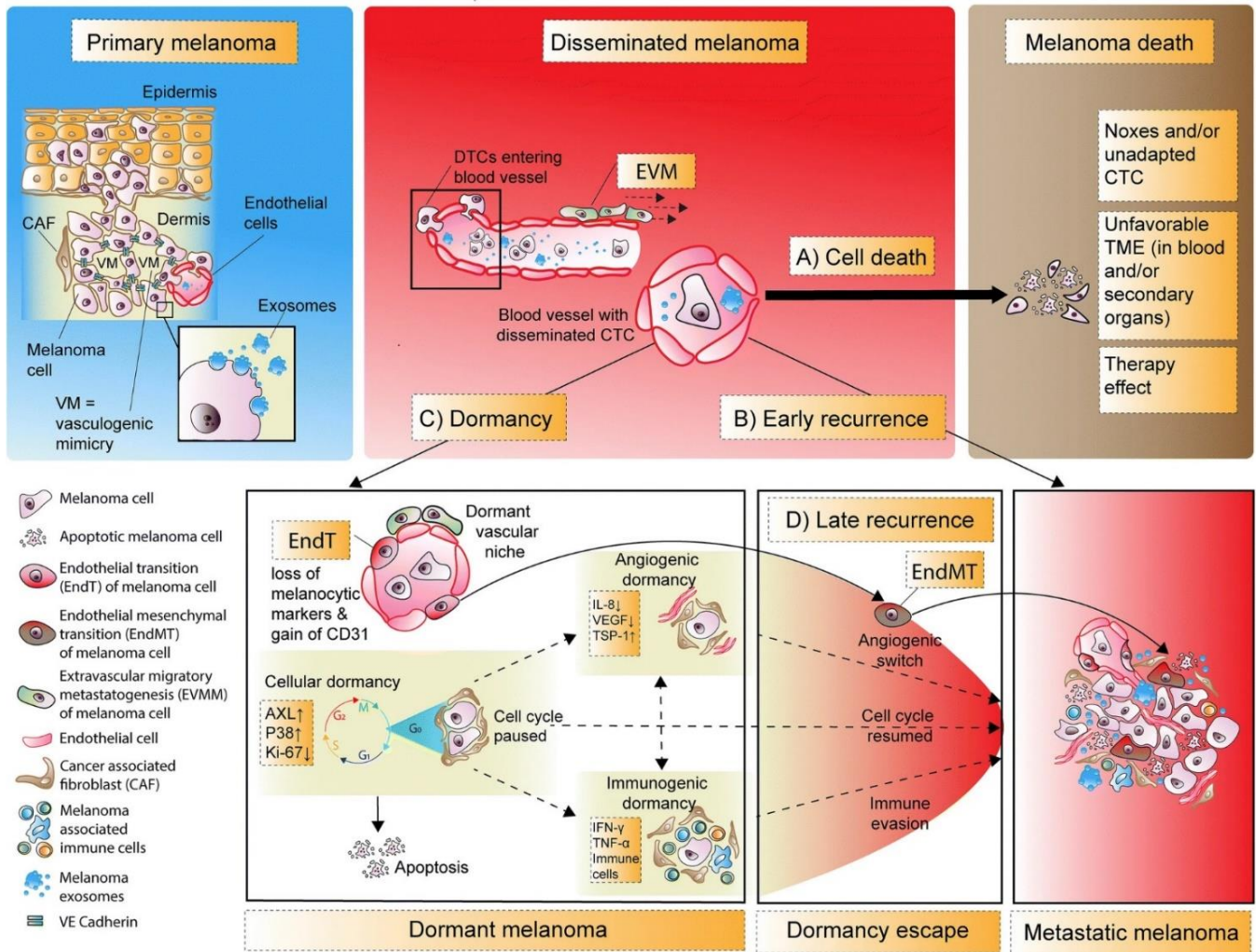


Figure 35. The role of dormancy in melanoma.

The majority of disseminated melanoma cells die (A); however, a fraction possesses the potential to adapt to various new environments, followed either by early recurrence (B) with metastasis or induction of dormancy (C), which can yield in late recurrence (D) of metastatic disease. Dormancy can be subdivided in cellular dormancy and tumor mass dormancy due to angiostasis (angiogenic dormancy) or immuno surveillance (immunogenic dormancy). Escape from dormancy is the result of immune evasion, angiogenic switch and/or endothelial mesenchymal transition (EndMT) and will ultimately lead to a metastatic state of the disease. CTC = Circulating Tumor Cells, DTC = Disseminated Tumor Cells, EVM = Extravascular Migration. From Vandyck et al., 2021.

cells need to undergo an endothelial-to-mesenchymal-like transition first (Giancotti, 2013) (Figure 33). While these activating signals are relatively unexplored, recent work in mice seems to show that age-induced changes in the microenvironment of key niches, such as the lung, have an essential role in re-awakening dormant cells (Fane et al., 2022). It has also been shown that the endothelial-like melanoma cells, by a phenomenon known as vasculogenic mimicry, can form their own pseudo-vascular networks which allow for improved blood circulation to the tumors, the promotion of cancer cell dissemination and the auto-establishment of a dormant vascular niche (Fernández-Cortés, Delgado-Bellido and Oliver, 2019; Zhang et al., 2019).

4.3. The metastatic niches in melanoma and their establishment

Melanoma displays a strong proneness for specific distant metastasis to the liver, lungs, and brain (Damsky, Rosenbaum and Bosenberg, 2010). Pulmonary metastasis causing respiratory failure and intracranial hemorrhages resulting from brain metastases are the two most common causes of death in melanoma (Sundararajan et al., 2022). Organ specificity, or organ tropism, is a phenomenon that has been known for a long time, with the historical “seed-and-soil” theory positing that cancer cells (the seeds) display inherent characteristics allowing them to specifically grow in organs fulfilling certain micro-environmental conditions (the soil). Whereas some mechanisms behind this process remain mysterious to this date (Peinado et al., 2017), integrins and chemokines have been shown as major players responsible for these seed-and-soil interactions (Dittmar et al., 2008; Huang and Rofstad, 2018; Jacquelot et al., 2018). For example, among many others, some melanoma cells express the chemokine receptor CXCR4, which enables chemotaxis towards niches with high expression of its CXCL12 ligand, such as in the liver or lungs (O’Boyle et al., 2013; McConnell et al., 2016). It has also been shown that melanoma cells specifically expressing the ITGAV integrin adhere strongly to the brain vasculature and penetrate the blood-brain barrier easily, allowing for brain metastasis (Berghoff et al., 2013). It is important to note that microenvironmental niches are not static and can change over time. As such, the effects of for example surgery, infection, chronic inflammation, stress, and aging can all alter the local milieu so that it becomes sufficiently receptive to colonization by circulating, potentially dormant, tumor cells (Sleeman, 2012).

Recently, this model has gained another layer of complexity, as it becomes increasingly clear that tumor cells, before metastasis even occurs, actively send out signals to prepare the pre-metastatic niches (PMNs) for future colonization. This is often mediated by tumor-secreted soluble pro-angiogenic or inflammatory factors, such as VEGFA or TGFβ, or extracellular

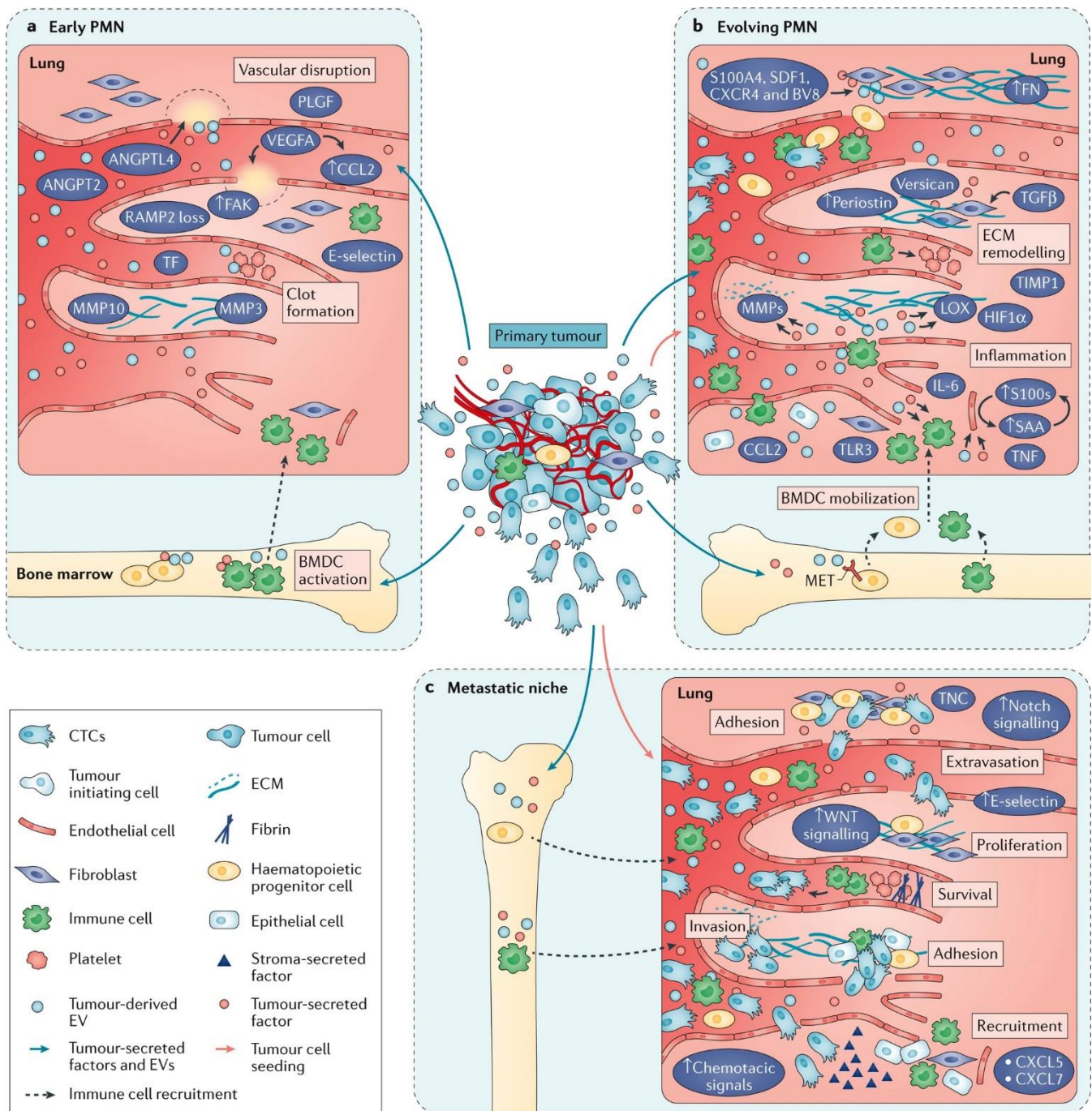
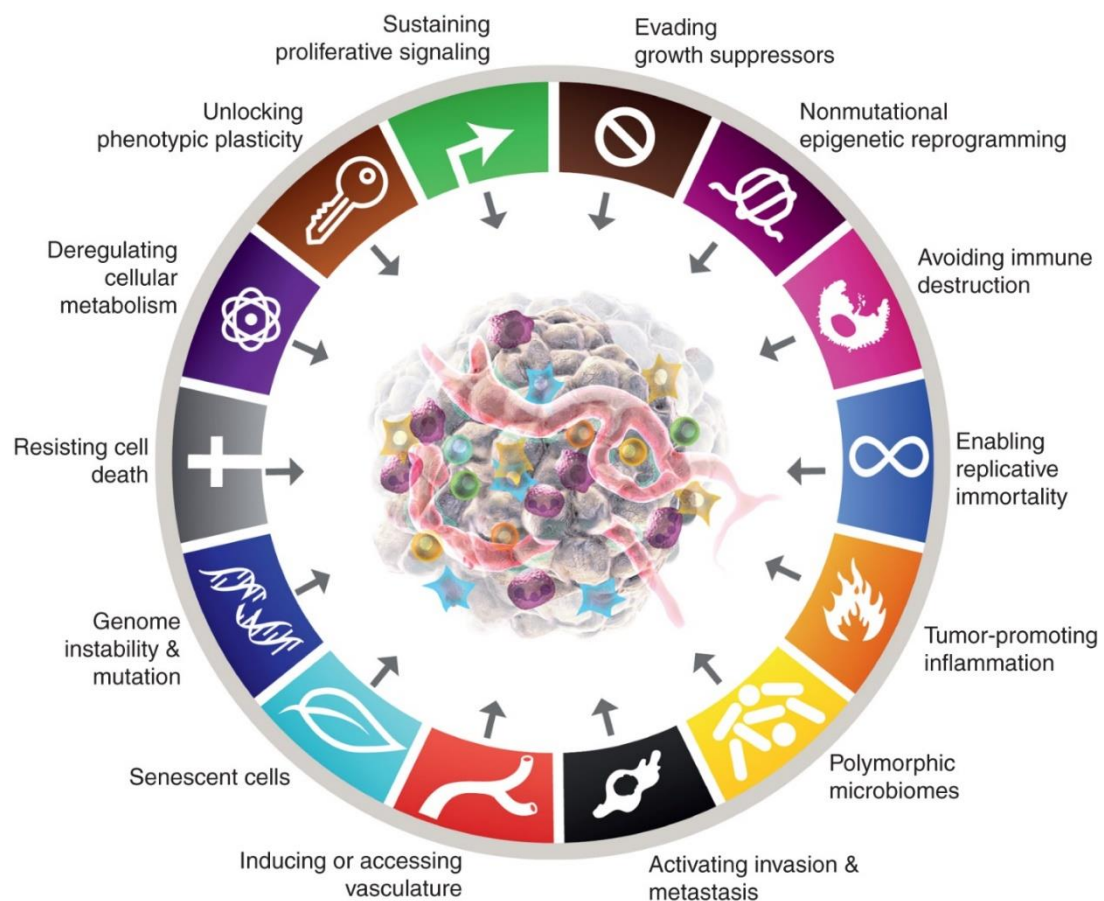


Figure 36. Establishment of the lung pre-metastatic niche (PMN) and molecular players involved.

Establishment of the PMN requires clot formation and vascular disruption, through FAK signaling induction and recruitment of various bone marrow-derived cell (BMDC) populations (A). Evolution of the PMN through active extracellular matrix (ECM) remodeling and increased inflammation (B). Metastatic niche formation which increases cancer cell docking, survival, and proliferation (C). From Peinado et al., 2017.

vesicles such as exosomes (Kaplan et al., 2005; Psaila and Lyden, 2009; Chin and Wang, 2016; Peinado et al., 2017). These niche inductions tend to happen in a progressive manner, involving many different molecular pathways (Peinado et al., 2012; Hoshino et al., 2015) (Figure 36). To prepare the lungs for subsequent invasion, melanoma tumors secrete factors such as MMPs, VEGFA, or ANGPT2 to induce vascular disruptions and leakiness, increasing accessibility to the niche for circulating cells (Huang et al., 2009). This is further facilitated by tumor-dependent platelet reprogramming and blood clot formation, which can act as docking sites for metastatic cells, and a source of inflammatory signals (Gay and Felding-Habermann, 2011; Gil-Bernabé et al., 2012; Labelle, Begum and Hynes, 2014). Melanoma-derived exosomes contain various bioactive molecules from cytokines to miRNAs (Walbrecht et al., 2020), which can specifically be released in target tissues due to integrin-dependent homing and docking (Hoshino et al., 2015). These exosomes can for example recruit bone marrow-derived cells (BMDCs) to premetastatic niches at distant organs, which then help to shape the microenvironment in favor of melanoma cell colonization (Peinado et al., 2012). Melanoma-derived exosomes can transfer receptor tyrosine kinases (RTKs) such as ALK and MET to target cells such as BMDCs, to give them increased survivability (Cesi et al., 2018). Stromal cells such as fibroblasts, immune and endothelial cells at these sites have been shown to take up exosomes, thereby being reprogrammed to function as cancer-associated cells by degrading or remodeling the surrounding ECM, increasing local inflammation, and secreting pro-tumoral factors such as chemokines or signaling molecules (Shu et al., 2018). Finally, during later phases of metastasis, these exosomes also affect tumor heterogeneity, as they are involved in melanoma phenotype switching (Xiao et al., 2016). In conclusion, melanoma tumors can affect different PMNs through various mechanisms, often by reprogramming stromal cells to begin malignant signaling. These PMN formations frequently lead to tissue micro-damages such as thromboses and hemorrhages as well as increased inflammation. Importantly, this results in a devious cycle of metastasis formation and signaling, as additional secondary tumors emerge and themselves start secreting pro-metastatic factors, facilitating additional PMN formation and cancer cell seedings (Peinado et al., 2017).

To sum up, melanoma progression from melanocytic precursor lesions to large-scale metastasis recapitulates many malignant features of other types of cancers as well, and is therefore often used as a prime model to study the so-called ‘hallmarks of cancer’, biological capabilities gained during tumor progression, which were defined by Hanahan and Weinberg in three consecutive landmark papers in 2000, 2011 and 2022.



The hallmarks of cancer	
Functional hallmarks	Enabling hallmarks
Sustaining proliferative signalling	Tumor-promoting inflammation
Evading growth suppressors	Polymorphic microbiomes
Enabling replicative immortality	Genome instability and mutation
Deregulating cellular metabolism	Nonmutational epigenetic reprogramming
Resisting cell death	
Avoiding immune destruction	(Tumor Microenvironment)
Inducing or accessing vasculature	
Activating invasion and metastasis	
Senescent cells	
Unlocking phenotypic plasticity	

Figure 37. The fourteen hallmarks of cancer (2022 version) and subdivision into functional and enabling hallmarks (Included is the important TME).

Adapted from Hanahan, 2022.

C. Aspects of melanoma biology through the lens of Hanahan and Weinberg's hallmarks of cancer

The hallmarks of cancer are defined as fourteen distinct capabilities and characteristics which are commonly acquired in a progressive way in virtually all types of neoplastic diseases. They serve as an organizing framework for the underlying molecular and cellular principles governing tumor progression and have been updated roughly every decade to include the newest emerging concepts in cancer research (Hanahan and Weinberg, 2000, 2011; Hanahan, 2022). These hallmarks can be divided into two distinct categories. On the one hand, the functional hallmarks define distinct but complementary capabilities causing the malignant phenotypes of survival, proliferation, and dissemination, observed during tumor progression (Figure 37). On the other hand, the enabling hallmarks drive the acquisition of these functional traits. The following pages will address the different hallmarks while showcasing their respective roles in melanoma biology. Given that the most critical aspects of melanoma invasion and metastasis have already been elucidated, these will be skipped, and the more novel and underlying enabling hallmarks will be more thoroughly explored, especially the aspects of melanoma phenotype plasticity.

1. Functional hallmarks – Core attributes

1.1. Sustained proliferative signaling, immortalization, and evading growth suppressors

Perhaps the most well-defined feature of cancer cells lies in their capacity of unlimited proliferation and growth. In contrast to normal tissues, cell cycle control has become uncoupled from the mitogenic signals usually emanating in a controlled manner from outside the cells. This autonomously sustained and chronic cell division can be enabled through various mechanisms. Autocrine signaling, by which melanoma cells produce themselves the ligands activating RTKs such as EGFR, VEGFR, FGFR, HGFR, IGF1R, GHR, c-MET, ERBB3/4, AXL or MSPR, has been frequently observed throughout various phases of melanoma progression (Molhoek et al., 2011; Sensi et al., 2011; Zhang et al., 2012; Czyz, 2018; Buckels et al., 2019). Signaling can also be increased through receptor overexpression, rendering the cells hyperresponsive to even small amounts of ligands, as evidenced by AXL and EGFR amplification, especially in dedifferentiated invasive melanoma cells (Revach et al., 2019;

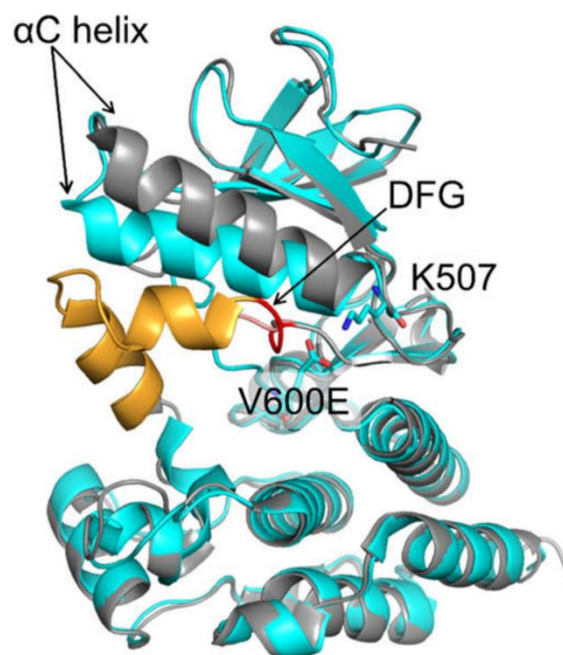
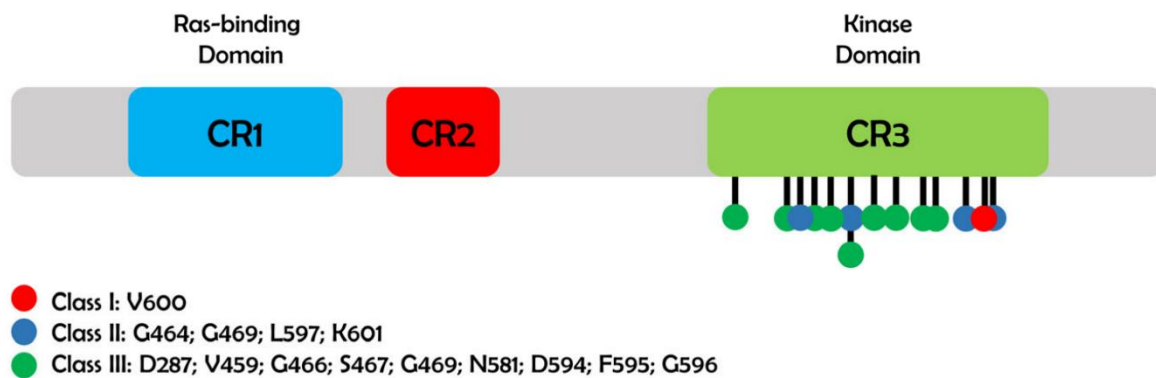


Figure 38. Positions of the three typical classes of BRAF mutations and BRAF protein structure. There are three classes of BRAF mutations. Class I mutations allow BRAF to act as a constitutively active monomer. Class II mutations allow for constitutively active dimers. Class III are inactivating mutations. CR = Conserved region. In the 3D structure, gray and orange represent the inactive form of BRAF, in which the activation segment (in orange, with its Asp-Phe-Gly DFG motif in red) is stabilized due to various hydrophobic interactions. Cyan represents activated BRAF, in which phosphorylation of the activating segment leads to destabilization of the hydrophobic interactions and conformational changes of the α -helices are induced, opening the catalytic cleft. The V600E mutation forms a salt-bridge with the K507 amino acid that permanently changes the position of the α C helix, rendering the catalytic cleft permanently exposed.

From Śmiech et al., 2020.

Pastwińska et al., 2022). Alternatively, melanoma cells can send signals to neighboring stroma cells such as fibroblasts, stimulating them to become tumor-associated cells that release growth factors, benefiting tumor growth through paracrine signaling (Papaccio et al., 2021; Mazurkiewicz et al., 2022). Through ECM remodeling, cell-matrix communications are altered, and growth factors sequestered in the ECM can be released (Winkler et al., 2020; Popovic and Tartare-Deckert, 2022). Constitutive, ligand-independent activation of key signaling pathways can result from structural alterations of receptors and downstream effectors, such as in the case of KIT or BRAF mutations, respectively (Pham, Guhan and Tsao, 2020). The BRAFV600E mutation, as mentioned before, affects roughly half of all melanomas, and permanently exposes the catalytic site of this kinase, thereby constitutively activating MAPK signaling and cell proliferation (Kiel et al., 2016; Śmiech et al., 2020) (Figure 38). Finally, overexpression by various mechanisms such as gene amplification and promoter hypomethylation, can lead to the overexpression of oncogenic transcription factors such as MYC, driving melanoma growth (Zhuang et al., 2008; Kfoury et al., 2018).

To sustain proliferation, melanoma cells must become immortalized, which mostly happens through *TERT* overexpression, counteracting telomere shortening and chromosomal end-to-end fusions. Interestingly, telomerase seems to display various non-canonical, extratelomeric roles including implications in NF- κ B and WNT/ β -Catenin signaling, DNA damage response, ROS protection and regulation of MYC and VEGF expression (Ségal-Bendirdjian and Geli, 2019; Dratwa et al., 2020; Guo et al., 2022). Tumor progression also depends on the capacity to evade growth-inhibitory mechanisms mediated by tumor suppressor genes. Inactivating alterations of negative regulators of diverse pathways are often observed, such as loss of PTEN activity by mutations or promoter methylation, leading to increased PI3K/AKT/mTOR signaling (Shull et al., 2012; Roh et al., 2016). MAPK pathway overactivation can be caused by RASA2 or NF1 alterations (Arafeh et al., 2015; Cirenajwis et al., 2017). Other often found tumor suppressors inactivated in melanoma are TP53, CDKN2A, or RB, governing important DNA damage and cell cycle checkpoints. Additionally, many other essential genes and pathways have been found to be inhibited during tumor progression in recent years (Ha et al., 2007; Gobeil et al., 2008; Fung et al., 2009; Fang et al., 2013; Olvedy et al., 2017; Güvenç et al., 2021). For example, Hippo pathway repression, through YAP/TAZ and TEAD overexpression, enables escape from contact inhibition (Zanconato, Cordenonsi and Piccolo, 2016; Vittoria et al., 2022). Remarkably, melanoma cells can in some cases repurpose canonical tumor suppressor pathways so that they turn into positive enablers of various cancer

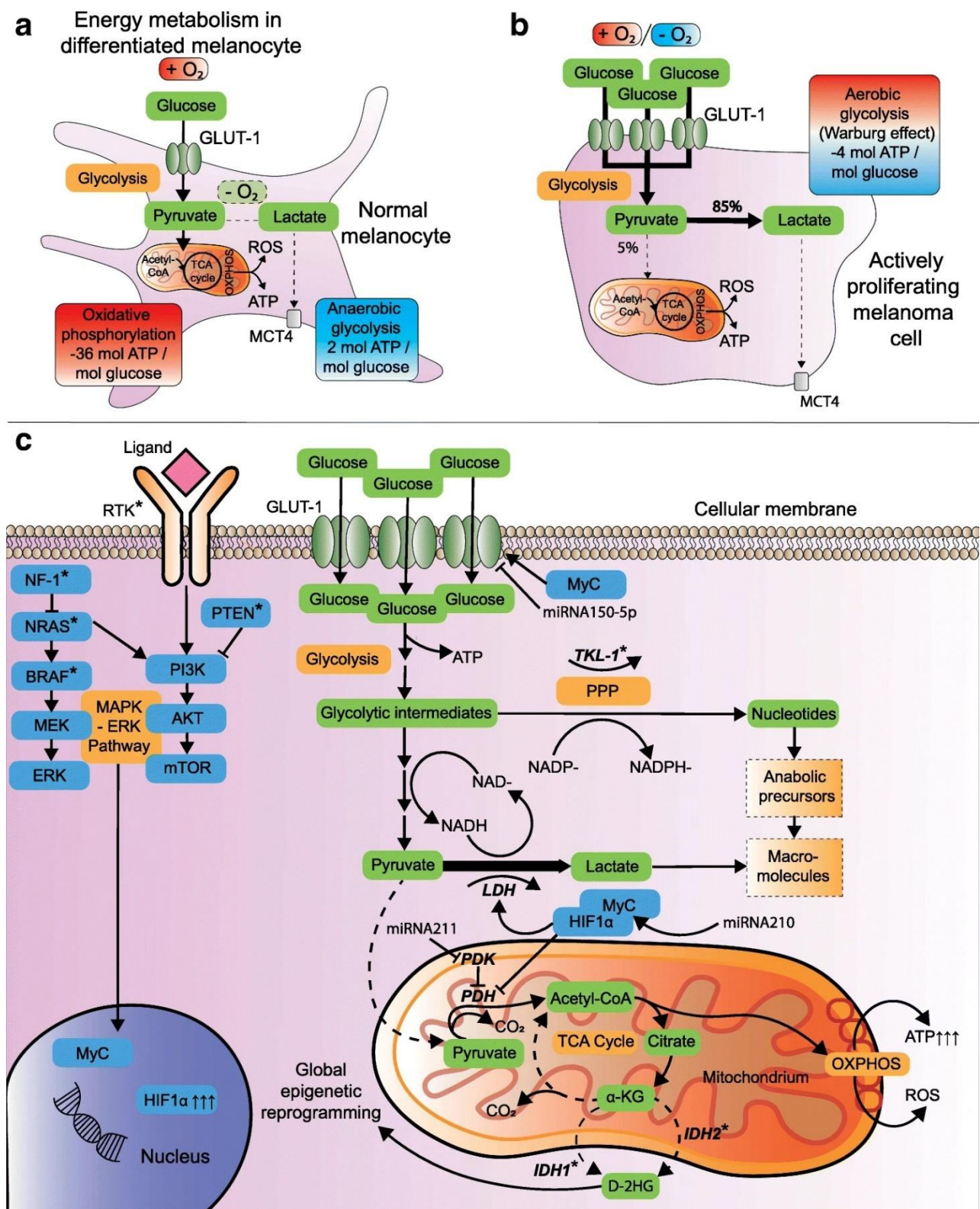


Figure 39. Metabolic reprogramming and the Warburg effect in melanoma.

A) OXPHOS metabolism in normal melanocytes. B+C) The Warburg effect.

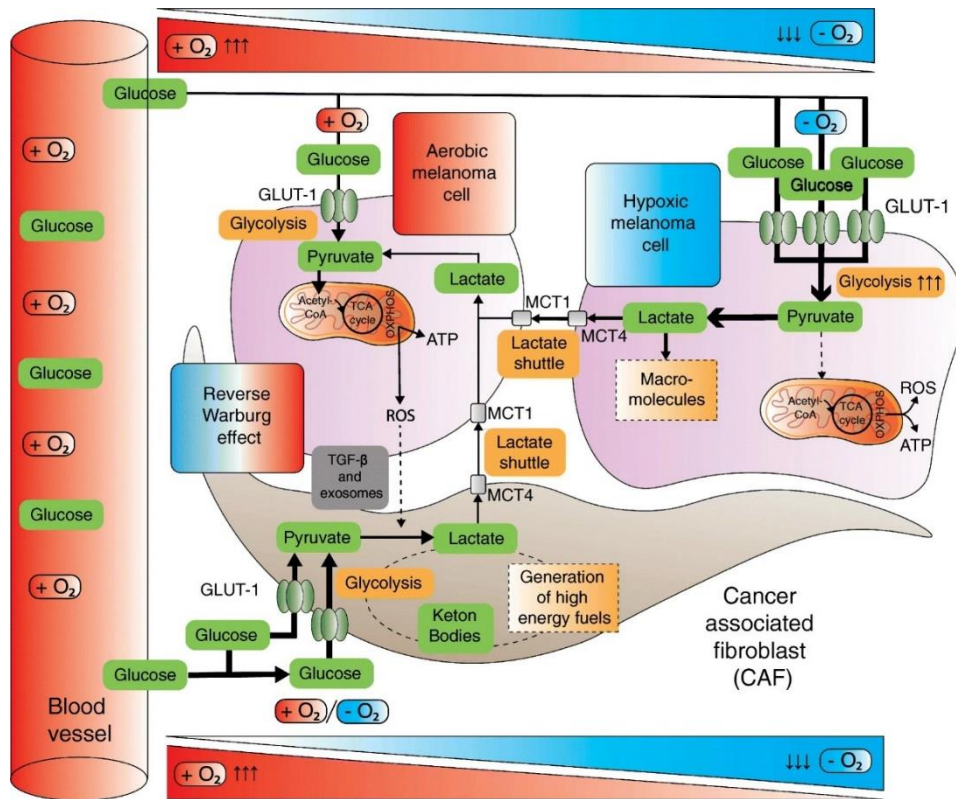
From Vandyck et al., 2021.

hallmarks. For example, the TGF β pathway seems to exert cytostatic effects during early melanoma stages, whereas during later progression, TGF β becomes a driver of invasion and phenotype switching (Busse and Keilholz, 2011; Lebrun, 2012; Golan et al., 2019).

1.2. Deregulating cellular metabolism

In normal physiological conditions, most cellular energy is provided by mitochondrial oxidative phosphorylation (OXPHOS), generating 36 mol of ATP for 1 mol of glucose (Nath and Villadsen, 2015). Alternatively, a lower yield of ATP (2 mol ATP per mol glucose) can be achieved by anaerobic glycolysis, which produces lactate under hypoxic conditions (Figure 39). Somewhat counterintuitively, actively proliferating melanoma cells, even in the presence of oxygen, tend to display high glucose uptake, glycolysis, and lactate secretion rates, which Otto Warburg a century ago defined as aerobic glycolysis (Warburg, 1924). This paradoxical appearing propensity of various types of cancer cells for utilizing glycolysis even in normoxic conditions, a less energy-effective metabolic pathway than OXPHOS, is called the Warburg effect (DeBerardinis and Chandel, 2020; Faubert, Solmonson and DeBerardinis, 2020). Several different reasons why cancer cells would prefer aerobic glycolysis have been proposed (Liberti and Locasale, 2016). High mitotic rates correlate with increased nutrient and biosynthesis demands, and the Warburg effect provides more recyclable intermediate metabolites for macromolecule biosynthesis than other anabolic pathways (Ratnikov et al., 2017). Additionally, aerobic glycolysis produces less ROS than OXPHOS, which benefits high proliferation activity (Kluza et al., 2012). The lower ATP yield is also countered by faster production rates enabled through mechanisms such as overexpression of glycolysis enzymes and glucose transporters such as GLUT1, by the action of various miRNAs and TFs, including TP53, MYC, and especially HIF1 α . This factor is usually expressed in hypoxic conditions but can be stabilized by increased MAPK signaling even in normoxia (Kietzmann, Mennerich and Dimova, 2016). As such, hypoxia can further amplify the Warburg effect by upregulating hypoxia-inducible factors (HIFs), with significant effects on cell plasticity (Yang et al., 2008; Widmer et al., 2013). Furthermore, aerobic glycolysis allows for the generation of significant amounts of lactate which can be secreted, profoundly affecting the TME through acidification (Rolver and Pedersen, 2021). For example, extracellular lactate impairs tumor-infiltrating immune cell function, contributing to melanoma immune escape (Feichtinger and Lang, 2019; Wang et al., 2021; Xie et al., 2022). Circulating lactate can be taken up via MCT transporters and used by neighboring cancer or stromal cells as energetic fuel that is converted into pyruvate

A



B

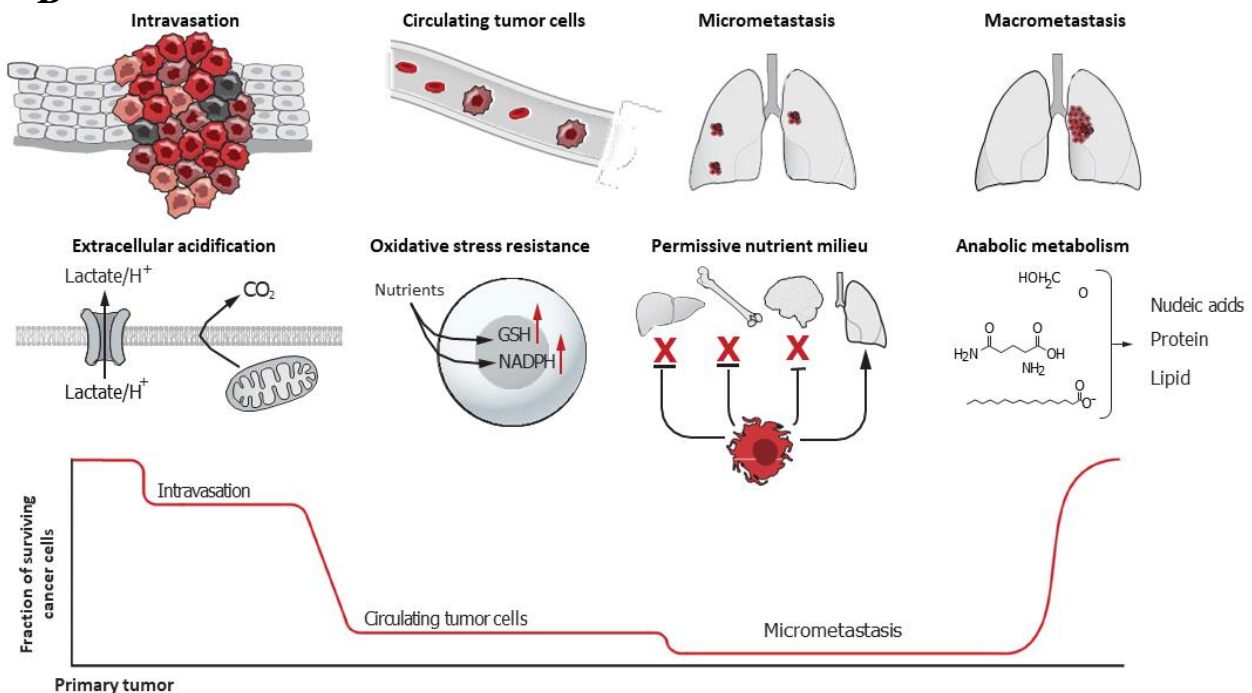


Figure 40. Adaptive tumor metabolism supports multiple steps of the metastatic cascade.

Metabolic symbiosis through nutrient trade-offs and metabolite shuttling between different melanoma cell subsets and adjacent CAFs (A). Overcoming of survival bottlenecks through metabolic reprogramming (B). Adapted from Faubert, Solmonson and DeBerardinis, 2020 and Vandyck et al., 2021.

used in the mitochondrial TCA/OXPHOS cycle (Avagliano et al., 2020). This underlines the fact that within a tumor, a high degree of metabolic heterogeneity can be observed, as distinct subpopulations of cancer cells depend on different forms of energy production, with important phenotypical consequences (Tasdogan et al., 2020). Similar to melanoma phenotype switching, cells have the capacity for metabolic plasticity and adaptability by dynamically switching their oxygen use, energy sources, and metabolic states depending on the TME (Fischer et al., 2018; Ruocco et al., 2019). Whereas the primary energy source for more differentiated, proliferative melanoma cells seems to be aerobic glycolysis by the Warburg effect, more slow cycling, dedifferentiated cells display a hybrid metabolic state with increased OXPHOS and exogenous fatty acid metabolism, while maintaining intermediate levels of glycolysis (Roesch et al., 2013; Feichtinger et al., 2018). However, the interconnection and regulation between metabolic and differentiation states is not clear-cut and requires further investigation (Falletta, Goding and Vivas-García, 2022).

Regarding melanoma progression, these complex metabolic reprogramming processes can be boiled down to the following schematic oversimplification (Figure 40). During tumor progression, when nutrients are abundant, cells gain biosynthetic advantages through the Warburg effect and reach maximal proliferative capacities. Through exosomes and other signaling molecules, stromal cells such as fibroblasts are reprogrammed towards aerobic glycolysis and secrete lactate as well, thereby contributing to the acidifying of the TME (Ruocco et al., 2019; Faubert, Solmonson and DeBerardinis, 2020). As the cancerous mass grows, oxygen and nutrient supplies vary between the outskirts and centers of the tumors. Cells in the tumor periphery are closer to the vasculature and are therefore exposed to a more aerobic TME, whereas in other locations, oxygen and nutrients become scarce. Hypoxia through HIFs stimulates aerobic glycolysis but can also contribute, in interaction with many other factors, to phenotype switching towards the more migration-prone dedifferentiated phenotype in a subset of cells (Ratnikov et al., 2017; Malekan, Ebrahimzadeh and Sheida, 2021). At this point, a metabolic symbiosis arises, in which it becomes advantageous for some cells to be able to take up and metabolize the abundance of extracellular lactate. In this context, some cells undergo a reverse Warburg effect by elevating OXPHOS, decreasing glycolysis, and gaining increased migratory capacities and thus access to more aerobic, but less nutrient-rich TMEs such as the lymphatic or blood circulation (Feichtinger and Lang, 2019; Kumar et al., 2021). It has been shown that melanoma cells overexpressing the MCT1 transporter, allowing for increased lactate uptake, had higher metastatic and ROS-resistance capacities (Tasdogan et al., 2020).

Switching to lactate-dependent OXPHOS allows for more efficient ATP production

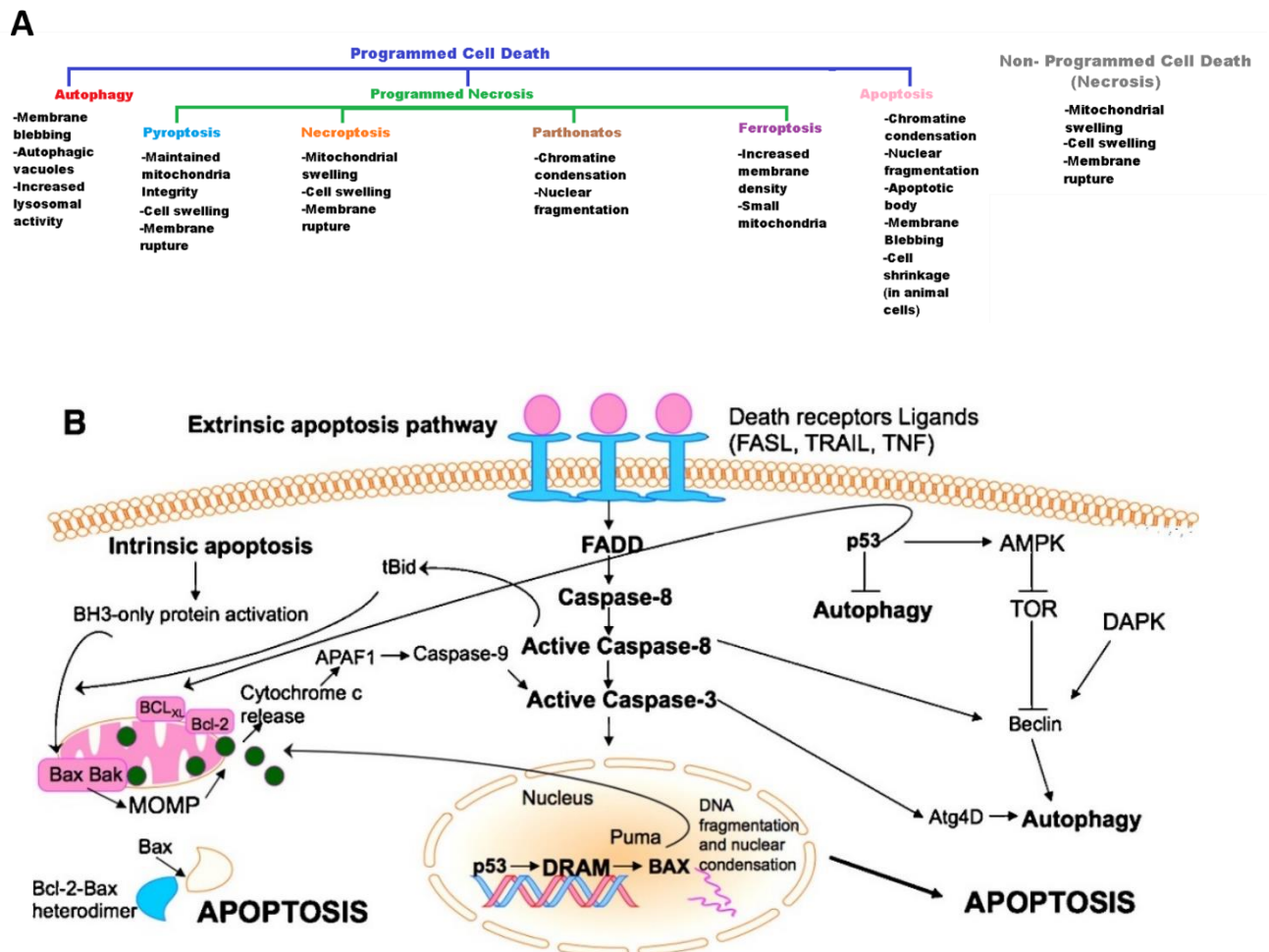


Figure 41. Various types of cell death (A) and apoptosis signaling (B).

Adapted from Mohammad et al., 2015.

even under challenging conditions, such as during metastasis, improving survival rates at the cost of diminished proliferation (Elia, Doglioni and Fendt, 2018). Circulating cells acquire increased oxidative stress resistance through increases in factors such as GSH, to counter the oxidizing TME of the bloodstream (Le Gal et al., 2015; Piskounova et al., 2015). Once they arrive in the metastatic niches, cells are confronted once again with different metabolic needs, dependent on the permissive nutrient milieu. For example, melanoma brain micro-metastases display high levels of OXPHOS, but lung metastases less so (Fischer et al., 2019). To establish macroscopic secondary tumors however, the need for proliferation and increased macromolecule synthesis re-emerges, made possible by a metabolic shift back towards the Warburg effect and aerobic glycolysis (Faubert, Solmonson and DeBerardinis, 2020).

1.3. Resisting cell death and avoiding immune destruction

For melanoma progression to be successful, tumor cells must overcome and resist various intrinsic or extrinsic mechanisms which are supposed to defend the organism from neoplastic growths. Cell-cycle and DNA damage checkpoints can induce growth arrest through senescence or programmed cell death such as apoptosis (Figure 41A). The immune system is constantly surveilling cells for tumor antigens and destroys transformed cells in the majority of cases (Soengas and Lowe, 2003; Chen and Mellman, 2013). Multiple different escape mechanisms have been described in the last decades, many of which are implicated in melanoma therapy resistance, and which will be further elucidated later on. A short overview of the deregulations leading to host defense evasion is given here. Concerning escape from apoptosis, melanoma cells often deregulate the intricate balance between pro- and antiapoptotic effectors (Broussard et al., 2018) (Figure 41B). For example, the expression of cell-death effectors, such as APAF-1, is often lost (Soengas et al., 2001). On the other hand, the overexpression of apoptosis-inhibiting BCL2 family proteins leads to increased survival and significant cell signaling changes, such as more elevated NF- κ B, IL-8 and AKT activity (Mohammad et al., 2015). Increased AKT signaling in turn activates other anti-apoptotic proteins such as BCL2 family members through phosphorylation, creating a PI3K/AKT-BCL2 survival signaling loop. Therefore, alterations in upstream regulators of AKT, such as PTEN or EGFR, can activate this survival circuit (Neophytou et al., 2021). Although inactivating mutations in the critical checkpoint gene *TP53* tend to appear more rarely in melanomas compared to other cancers, its regulators such as ARF or MDM2 are often found altered (Ha et al., 2007; Rajabi, Karimian and Heidarpour, 2012). So-called Inhibitors of Apoptosis

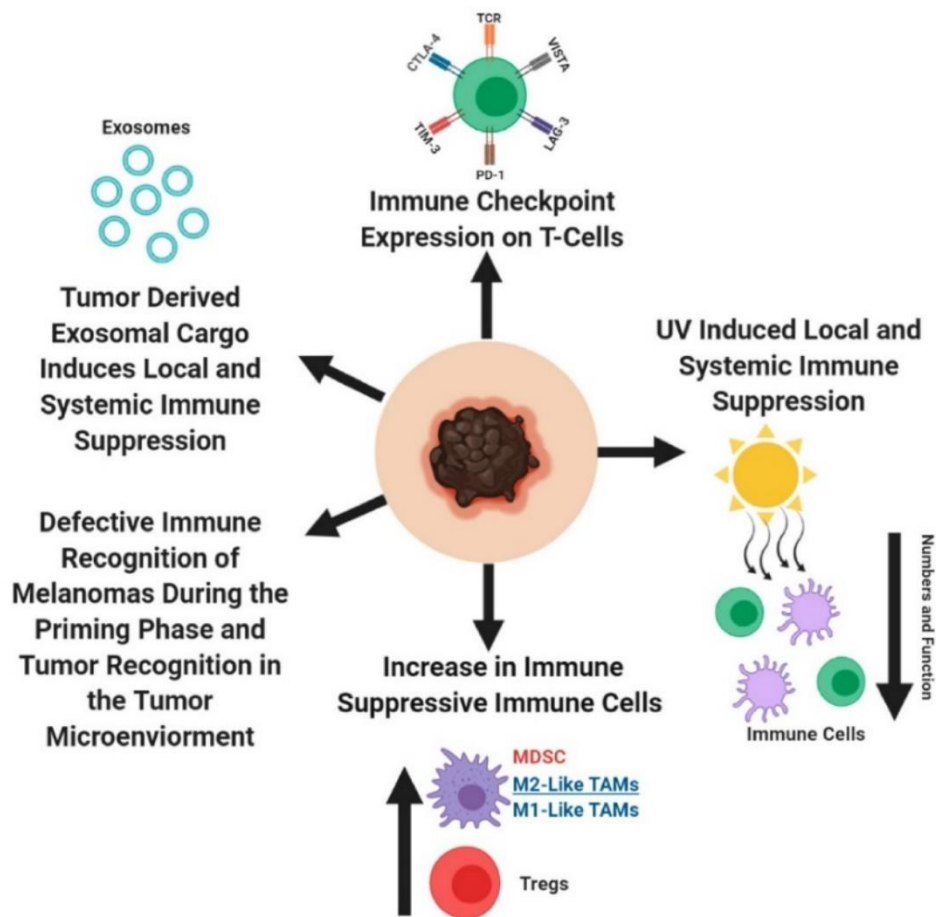


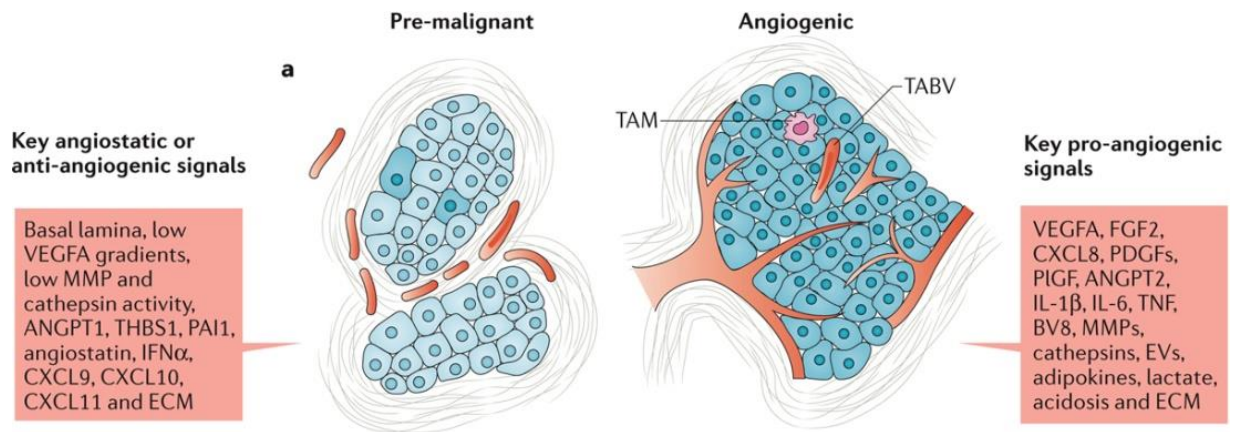
Figure 42. Immune dysfunctions contributing to melanoma progression.

From Eddy and Chen, 2020.

Proteins (IAPs) including ML-IAP, XIAP and Survivin are often deregulated in melanoma (Abd-Elrahman et al., 2009; McKenzie and Grossman, 2012; Daoud et al., 2022). As in virtually all other aspects of melanoma development, the TME and cellular stroma also play essential roles in modulating apoptotic escape. Cancer-associated fibroblasts (CAF)-derived extracellular vesicles containing miRNAs, lncRNAs, interleukins, growth factors and other signaling molecules inhibiting various effectors of apoptotic signaling have been observed in multiple cancers including melanoma (Neophytou et al., 2021). Remarkably, starting the apoptotic cascade without successfully completing it might benefit melanoma progression. Melanoma cells undergoing failed apoptosis become more invasive because of a JNK/AP-1 mediated phenotype switch (Berthenet et al., 2020). Of note, apoptosis is not the only type of programmed cell death with implications in melanoma (Figure 41A). Necroptosis, pyroptosis, ferroptosis, parthanatos, and autophagy all represent barriers that melanoma cells need to circumvent (Hartman, 2020).

Melanoma tumors are infiltrated by immune cells of both the adaptive and innate response, constituting the tumor immune microenvironment (TIME) (Binnewies et al., 2018; Wang et al., 2022). The TIME is very dynamic and variable, as highly infiltrated tumors are defined as ‘hot’, whereas poorly infiltrated tumors are termed ‘cold’ (Duan et al., 2020; Noman et al., 2020). Melanoma cells utilize multiple strategies of immune evasion (Figure 42), such as taking profit from immune checkpoints. Various immune cells such as T-lymphocytes, macrophages, dendritic cells, or NK cells express the PD-1 receptor, which inhibits their tumor-detecting and eliminating functions when activated by its PD-L1 or PD-L2 ligands. These can be expressed by melanoma cells themselves or be carried by tumor-released vesicles. (Baumeister et al., 2016; Ghoneim et al., 2017; Chen et al., 2018; Hartley et al., 2018). PD-L1 and PD-L2 expression in melanoma cells has been linked to IFN- γ exposure and subsequent JAK/STAT/IRF1 signaling. TFs such as MYC, AP-1, HIF-1, and NF- κ B are also involved, depending on melanoma cell phenotype (Casey et al., 2016; Garcia-Diaz et al., 2017; Eddy and Chen, 2020; Tsai et al., 2023). In addition to PD-1, multiple other immune checkpoint molecules dampening cytotoxic activity against tumor cells exist, such as CTLA-4, LAG-3, TIM-3, or VISTA (Lines et al., 2014; Rotte, 2019; Chocarro et al., 2022). Remarkably, PD-1 and CTLA-4 can also be expressed by melanoma cells themselves, with implications for increased immune evasion and tumor progression and pathogenesis through mTOR regulation (Kleffel et al., 2015; Clark et al., 2016; Mo et al., 2018; Pistillo et al., 2020). Another mechanism used by melanoma cells is to recruit or induce immune suppressive immune cells.

A



B

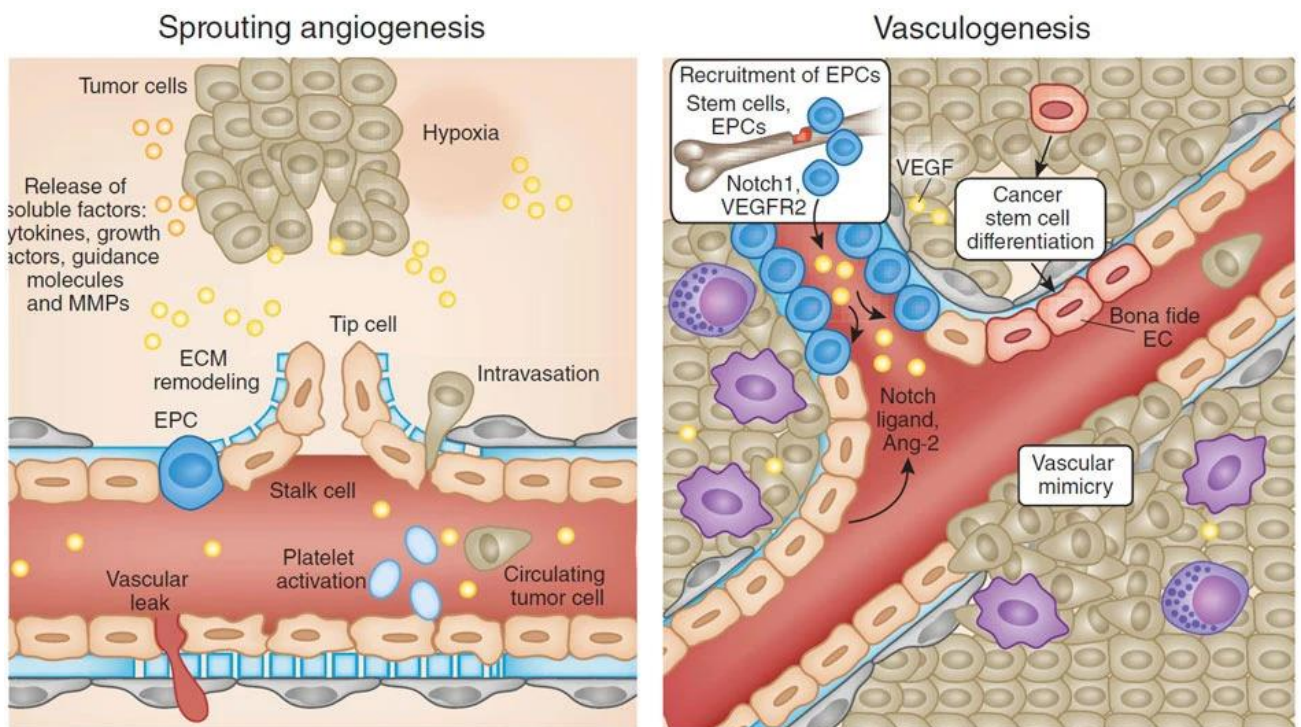


Figure 43. Key angiostatic or angiogenic signals (A) and the multiple origins of tumor-neovascularization (B).

Adapted from De Palma, Biziato and Petrova, 2017 and Weis and Cheresh, 2011.

For example, regulatory T-cells inhibit the activity of other T-cells in the TIME, after being recruited and activated by melanoma-secreted chemokines and cytokines (Huang et al., 2021). Melanoma cells can also recruit bone marrow-derived myeloid-derived suppressor cells to the TIME or pre-metastatic niches (Veglia, Sanseviero and Gabrilovich, 2021; Tomela et al., 2023) and convert them into tumor-associated macrophages, beneficial for tumor progression (Zhou et al., 2020; Mantovani et al., 2022). Additional immune suppressive mechanisms include reduced immunogenicity by decreasing presentation of melanoma-specific antigens, such as MLANA, gp100, or TYR (del Campo et al., 2014; Escors, 2014), and secretion of various locally or systemically acting suppressive signals. Most significantly, melanoma-derived exosomes can effectively induce immune dysregulation by several different ways, such as by containing immunosuppressive cytokines or inducing tumor-supporting immune cell populations (Isola, Eddy and Chen, 2016; Sharma et al., 2020).

1.4. Angiogenesis and senescence

Accessing or inducing vasculature is crucial for tumor progression because of the increasing needs for oxygen, nutrients, and waste evacuation. Once the growing tumor mass reaches a threshold of nutrient availability and hypoxia, a so-called ‘angiogenic switch’ is turned on and remains constitutively activated (Weis and Cheresch, 2011). Similar to most types of cancer, melanoma cells and their TME begin secreting angiogenic growth factors such as VEGF or FGF which sustain the formation of a neoplastic vasculature through gene expression changes in endothelial cells (Shibuya, 2011; Simons, Gordon and Claesson-Welsh, 2016; Eddy, Shah and Chen, 2021). Mechanistically, loss of p53 and increased RAS and HIF-1 signaling can induce the production of VEGF (Rak et al., 1995; Ravi et al., 2000; Oladipupo et al., 2011). Whereas in normal tissues, a well-regulated equilibrium of angiostatic and angiogenic signaling is maintained (Figure 43A), the angiogenic switch in tumors maintains the production of an aberrant, leaky vasculature contributing to many malignant hallmarks of melanoma such as increased metastasis and intratumoral heterogeneity (Nagy et al., 2010; Cooke et al., 2012; Cho, Jour and Aung, 2019; Quaresmini and Guida, 2020). Different forms of tumor neovascularization can occur (Figure 43B). The most well-known form is sprouting angiogenesis, whereas endothelial cells from mature, normal blood vessels are activated and form new aberrant tubes which begin sprouting toward tumor cells. However, de novo tumor-associated blood vessels, which eventually connect to a pre-existing network, can be formed by the recruitment of bone marrow-derived endothelial precursor cells (EPCs) (Lyden et al.,

2001; Butler, Kobayashi and Rafii, 2010). Additionally, melanoma cells have the capacity to differentiate into endothelial-like cells and participate in the formation of new vessels through vasculogenic mimicry (Hendrix et al., 2003; Vartanian et al., 2011). Recently, the description of non-angiogenic mechanisms such as vessel co-option have also been described to favor the neo-vascularization of tumors (Kuczynski et al., 2019).

Cellular senescence is defined in normal conditions as a programmed, irreversible, and stable cell cycle arrest due to various internal or external stresses such as telomere shortening, non-repaired DNA damage, or oncogene activation, to stop the growth of abnormally behaving cells (Di Micco et al., 2021). Importantly, in addition to many other morphological and behavioral changes, affected cells activate a senescent-associated secretory phenotype (SASP) whereby many different signaling molecules, such as cytokines and chemokines, are released to create a pro-inflammatory microenvironment (Coppé et al., 2010). Whereas senescence was long regarded as a tumor-suppressive mechanism, nowadays it becomes clear that cancers like melanoma can take profit of certain aspects of senescence. As stated before, oncogene-induced senescence plays a major role in inhibiting the progression of melanocytic precursor lesions such as naevi into malignant melanoma. Important molecular players involve p53, p21^{WAF1/CIP1}, p27^{Kip1}, p16^{INK4A}, p15^{INK4B} and RB, whose mutations allow for senescence bypass (Leclerc, Ballotti and Bertolotto, 2017) (Figure 44). However, during cancer progression, and especially the later stages of development, melanoma cells can actively benefit from the SASP of tumor and TME cells (Faget, Ren and Stewart, 2019; Yang et al., 2021). Through multiple mechanisms, the secreted factors can stimulate virtually all malignant aspects of melanoma cells such as increases in proliferation, stemness, angiogenesis, invasion or migration, in primary tumors or metastatic sites (Ghosh and Capell, 2016; Sun et al., 2018; Kyjacova et al., 2021; Hu et al., 2022; Homann et al., 2022) (Figure 45). Importantly, melanoma cells can enter a transitory and reversible slow-cycling senescent-like phenotype, by which they are of benefit to surrounding proliferating malignant cells with their SASP (Yang et al., 2021). The induction of this more dormant and resistant phenotype can result from increased DNA damage signaling, or from extrinsic factors such as hypoxia, starvation, or anti-cancer therapies (Faget, Ren and Stewart, 2019). It has been shown that cancer cells, upon their escape from this senescent-like state, become much more invasive and retain an increased stem-like dedifferentiated phenotype (Medema, 2018; Milanovic et al., 2018). As the senescence signaling programs significantly overlap with those responsible for dedifferentiation and stem-cell phenotypes, senescence is a potent driver of melanoma phenotype switching (De Blander et al., 2021).

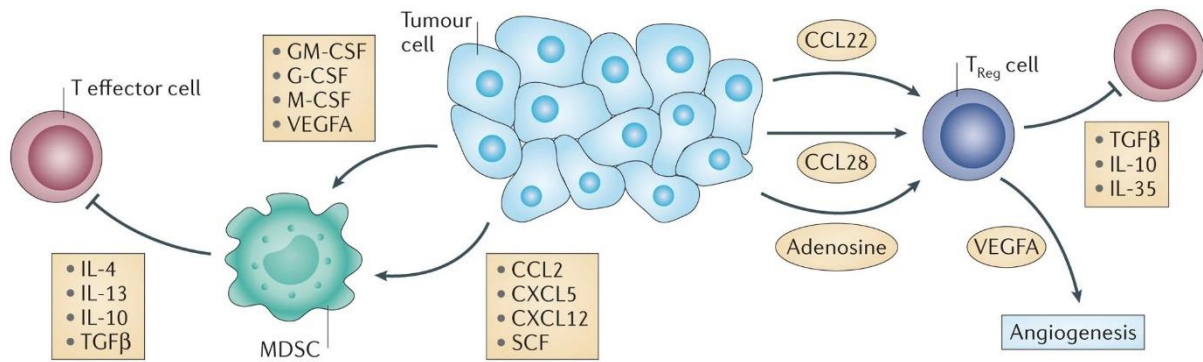
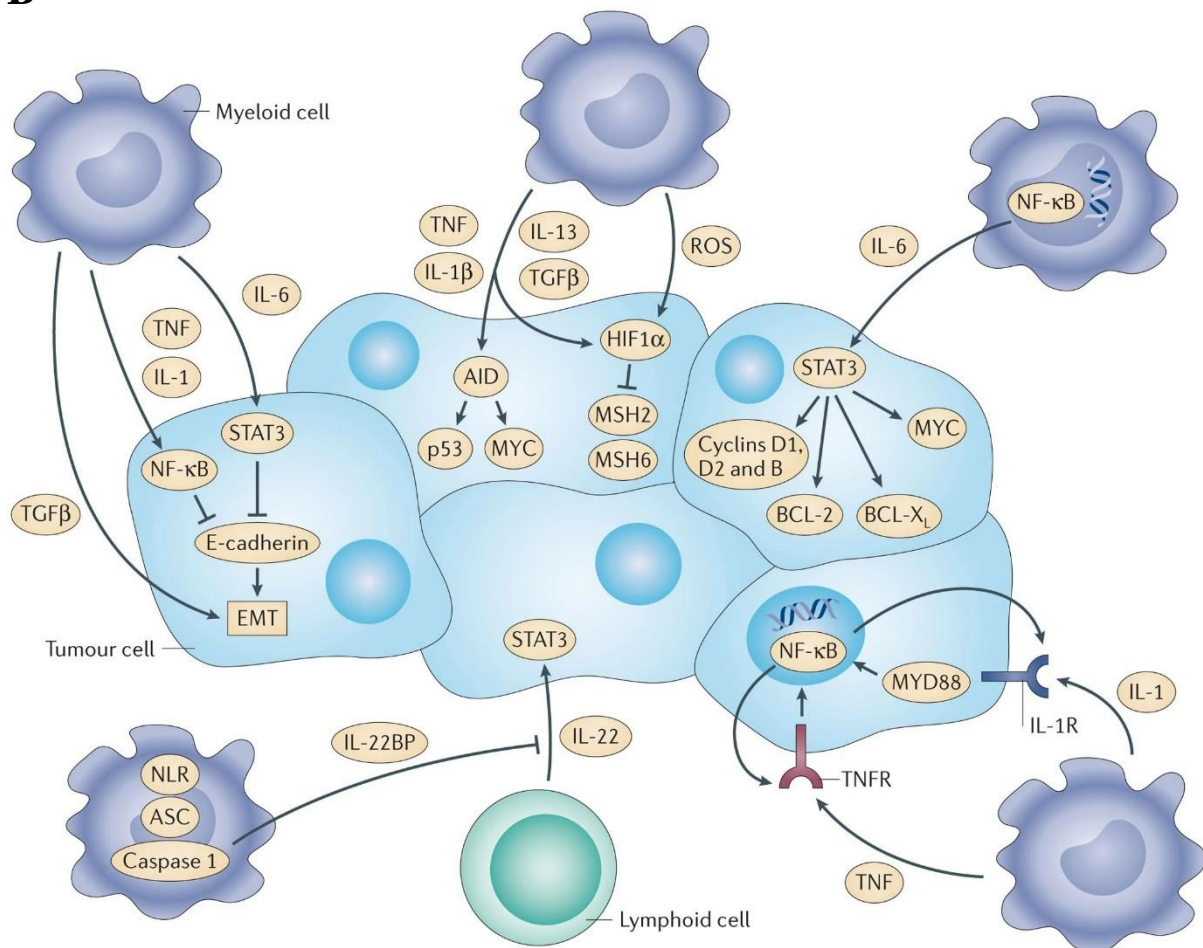
A**B**

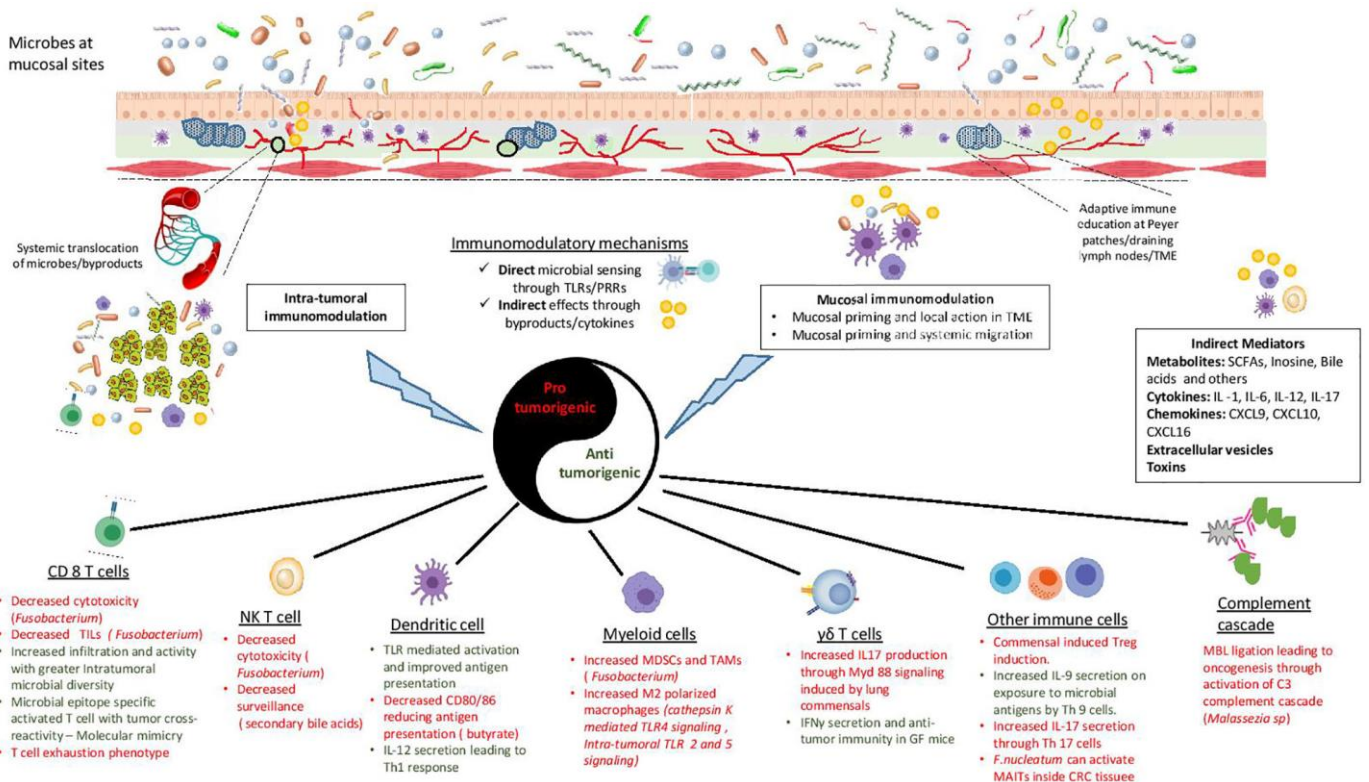
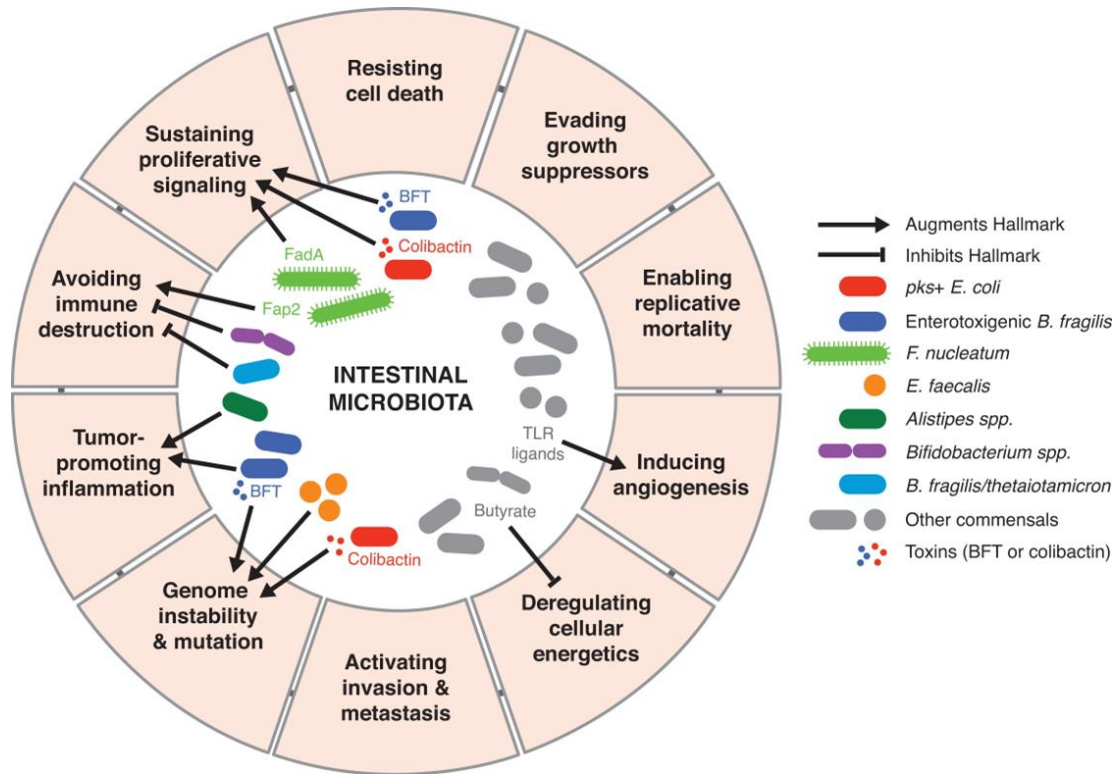
Figure 46. Induction of tumor-associated immune cells such as myeloid-derived suppressor cells (MDSCs) (A) and the influence of inflammatory signaling on cancer progression and signaling (B).

From Elinav et al., 2013.

2. Enabling hallmarks – Driving forces

2.1. Tumor-promoting inflammation

Inflammation during melanoma progression is a double-edged sword. On the one hand, anti-tumoral immune surveillance usually efficiently detects and removes malignant cells, but various escape and immunomodulating mechanisms can lead to cancer cells becoming resistant and even being aided by chronic inflammation (Dunn, Old and Schreiber, 2004; Zitvogel, Tesniere and Kroemer, 2006). The term of ‘cancer immunoediting’ was coined to describe this duality of action of the immune system by which it can both inhibit and stimulate tumor development. This incremental process passes through three phases: elimination, equilibrium, and escape. Notably, these steps can also be recapitulated in patients developing treatment resistance after receiving immunotherapies (Vesely and Schreiber, 2013; O’Donnell, Teng and Smyth, 2019; Gubin and Vesely, 2022). The mechanisms by which cancer cells avoid immune destruction and reach an equilibrium state, in which tumor-suppressive mechanisms are inhibited, have been touched upon previously. Several different studies have shown that in later phases of progression, melanoma cells actively modulate the composition and activity of the TIME, especially by recruiting and inducing tumor-associated myeloid (including macrophages, neutrophils, and dendritic cells) and lymphoid cells (including T-cells and B-cells) (Arango Duque and Descoteaux, 2014; Jiang et al., 2015; Greten and Grivennikov, 2019; Griss et al., 2019; Hibino et al., 2021) (Figure 46A). For example, melanoma cells can express the inflammasome component NLRP3 which contributes to the production and release of IL-1 β . This proinflammatory cytokine stimulates the expansion of myeloid-derived suppressor cells (MDSC) which inhibit NK- and T-cell activity, while recruiting immune suppressive regulatory T-cells (Tengesdal et al., 2021). These tumor-associated immune cells can in turn secrete a host of tumor-promoting inflammatory cytokines affecting for example STAT3, HIF-1, or NF- κ B signaling, enhancing melanoma survival, proliferation, or phenotypic plasticity (Melnikova and Bar-Eli, 2009; Elinav et al., 2013; Hölzel and Tüting, 2016; Landsberg et al., 2016) (Figure 46B). Several studies also link inflammation and pre-metastatic niche formation. Endothelial cells in the lung express the anti-inflammatory factor DEL-1, which is downregulated upon inflammatory stress, causing neutrophil recruitment and reduced NK-cell numbers, constituting a more permissive metastatic melanoma environment (Hyun et al., 2020). As stated before, melanoma cells can actively send out inflammatory cytokines and chemokines such as TGF β or TNF to pre-metastatic niches (Figure 36). These factors can for

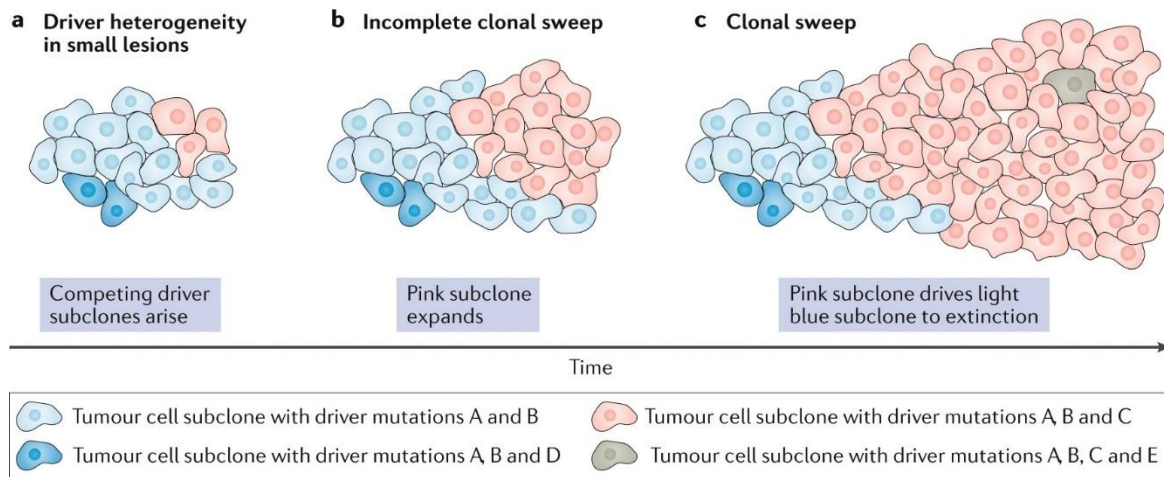


example induce the expression of S100 proteins by local stroma cells, which recruits pro-inflammatory myeloid immune cells and bone marrow progenitors (Peinado et al., 2012, 2017). Increased lung neutrophil counts result in the degradation of the anti-metastasis and anti-inflammatory factor TSP-1, further enabling a hospitable metastatic niche (El Rayes et al., 2015). Of note, tumor-promoting inflammation does not necessarily need to be induced by the cancer cells themselves, as many external factors such as UV-radiation (Bald et al., 2014; Ansary et al., 2021), aging (Franceschi et al., 2018) and obesity (Quail and Dannenberg, 2019; Smith et al., 2020) have been shown to be involved as well.

2.2. Polymorphic microbiomes

One of the perhaps most novel observations in melanoma biology and cancer research in general is the profound impact of tumor-intrinsic or -extrinsic microbiota on disease progression, associated inflammation, and therapy resistance (Elinav et al., 2019). Multiple hallmarks of cancer, such as proliferative signaling or genomic instability, have been observed to be modulated by bacteria-secreted factors in multiple types of neoplasms, with both oncogenic and tumor-suppressive properties (Fulbright, Ellermann and Arthur, 2017) (Figure 47). In melanoma cases, it has been shown that the skin and gut microbiomes are significantly changed compared to controls, and that these dynamically evolve during tumor progression to reach a state of microbial ecosystem disturbance, referred to as “dysbiosis” (Vitali et al., 2022; Makaranka et al., 2022; Mekadim et al., 2022). Different mechanisms by which microorganisms affect melanoma progression have been proposed. Disruption of the skin barrier, paracrine signaling, DNA damage mediated by microbial toxins, or increased inflammation due to damage-associated molecular patterns (DAMPs) or pathogen-associated molecular patterns (PAMPs), are among the most studied ones (Li et al., 2019; Knippel, Drewes and Sears, 2021; Woo et al., 2022). In melanoma especially, this last point of immunomodulation, either through direct interactions or by indirect signaling induction through metabolites or cytokines, has important effects on immune cells and immunotherapy (Jain et al., 2021; Villemin et al., 2023) (Figure 48). In the last five years, several important publications have established a strong link between the composition of the gut/skin microbiomes and anti-melanoma immunity or clinical responses to immunotherapy treatments (Gopalakrishnan et al., 2018; Matson et al., 2018; Routy et al., 2018; Spencer et al., 2021; Lee et al., 2022). The exact reasons why this is the case seem complex and no scientific consensus has yet been reached. In another study, it was observed that microbiome depletion in a

A



B

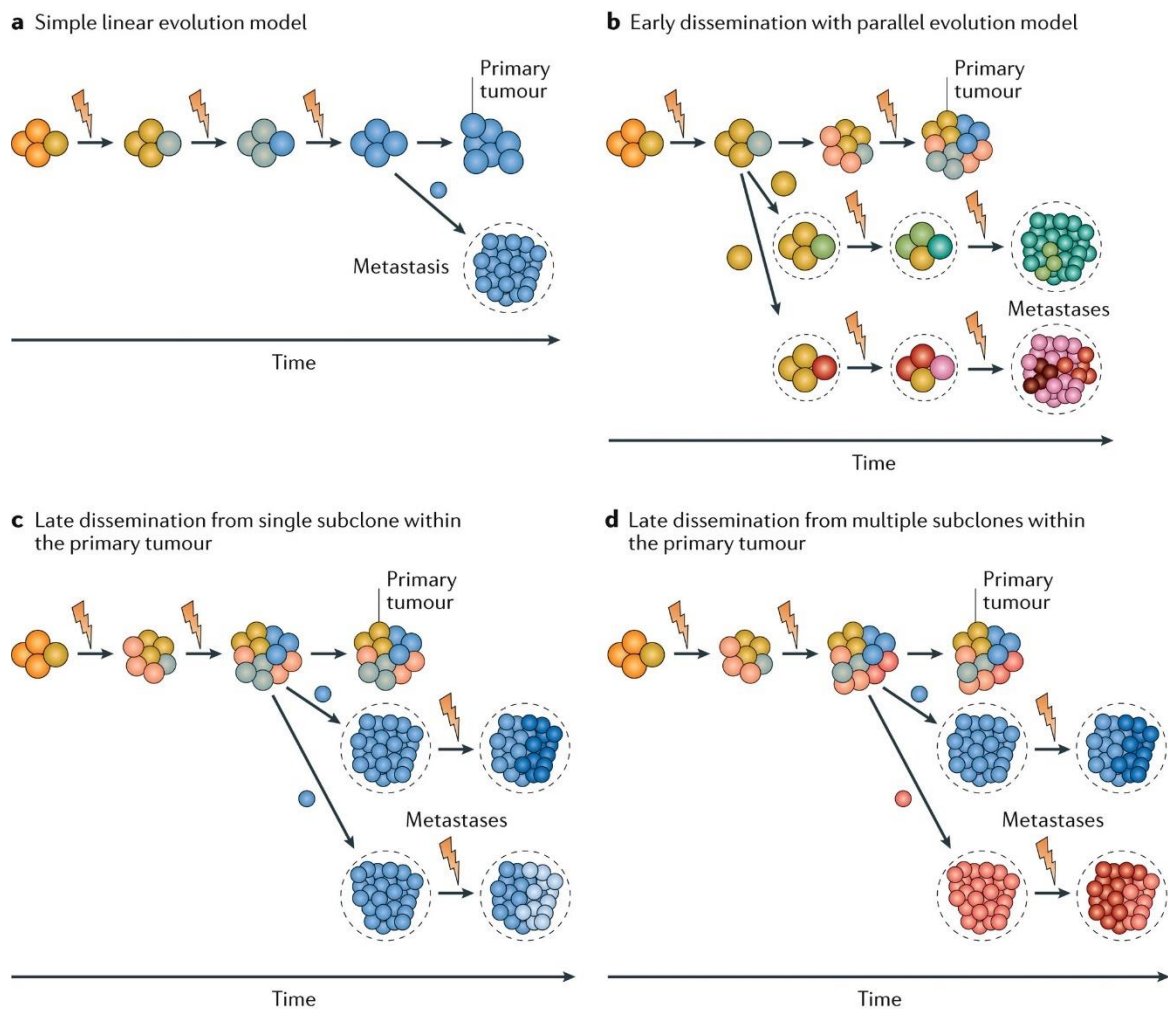


Figure 49. Clonal sweeps can give rise to intra-tumoral driver-gene mutation homogeneity (A). Models of genetic heterogeneity and metastatic evolution (B).

From Hunter et al., 2018; and Reiter et al., 2019.

melanoma mouse model led to increased bone metastasis, as more tumor-promoting immune cells were recruited from the gut to the bone marrow, showing a potential risk of excessive antibiotics treatment in melanoma patients (Pal et al., 2022). Of note, microorganisms are also a part of the immediate TME, as intra-tumor bacteria are often present inside both cancer and immune cells, where they can exert metabolic and detoxifying functions (Nejman et al., 2020).

3. Genetic and epigenetic hallmarks – Phenotypic plasticity

3.1. Genetic melanoma heterogeneity

As stated before, melanoma is characterized by both genetic and epigenetic inter- and intra-tumoral heterogeneity (Figure 19). However, significant differences exist between these modes of melanoma diversity. Genetic heterogeneity mainly describes differences in driver mutations whose dynamic progressive acquisition is mediated by the core hallmark of genomic instability, which is mainly driven by UV-exposure in melanoma. Other players include defective DNA damage repair, telomere alterations, and defects in chromosome segregation (Jeggo, Pearl and Carr, 2016). Importantly, genetic changes are irreversible, and their effects and outcomes are highly context dependent. Hence, the same genetic variant might confer advantages or disadvantages depending on the specific cell environment, and complex natural selection dynamics are in play (Turajlic et al., 2019). High genetic heterogeneity is linked to poor prognosis because Darwinian selection during tumor progression favors highly proliferative, resistant, or dissemination-prone subclones to emerge. As such, differences in the genotypes and driver mutations can manifest themselves in distinct degrees of malignant potential and various branched evolutionary disease progression pathways (Kwong et al., 2017; Osrodek and Wozniak, 2021; Dharanipragada et al., 2023) (Figures 25 and 26). Remarkably, in some tumors, specific subclones can acquire mutations that endow such a strong survival or growth advantage that they can ‘sweep’ through a tumor and outcompete all other genetic subpopulations, even to the point of extinction. Thus, high initial intra-tumoral genetic diversity seems to favor the emergence of clonal sweeps, leading in turn to subsequent reduced genetic heterogeneity with specific selection of the context-dependent most advantageous driver-mutations in a specific tumor (Reiter et al., 2019) (Figure 49A). However, matters are more complicated when considering secondary tumor emergence, where several modes of genetic heterogeneity have been observed, leading to intra- and inter-metastatic genetic heterogeneity (Figure 49B). This complexity arises because of different seeding mechanisms, including

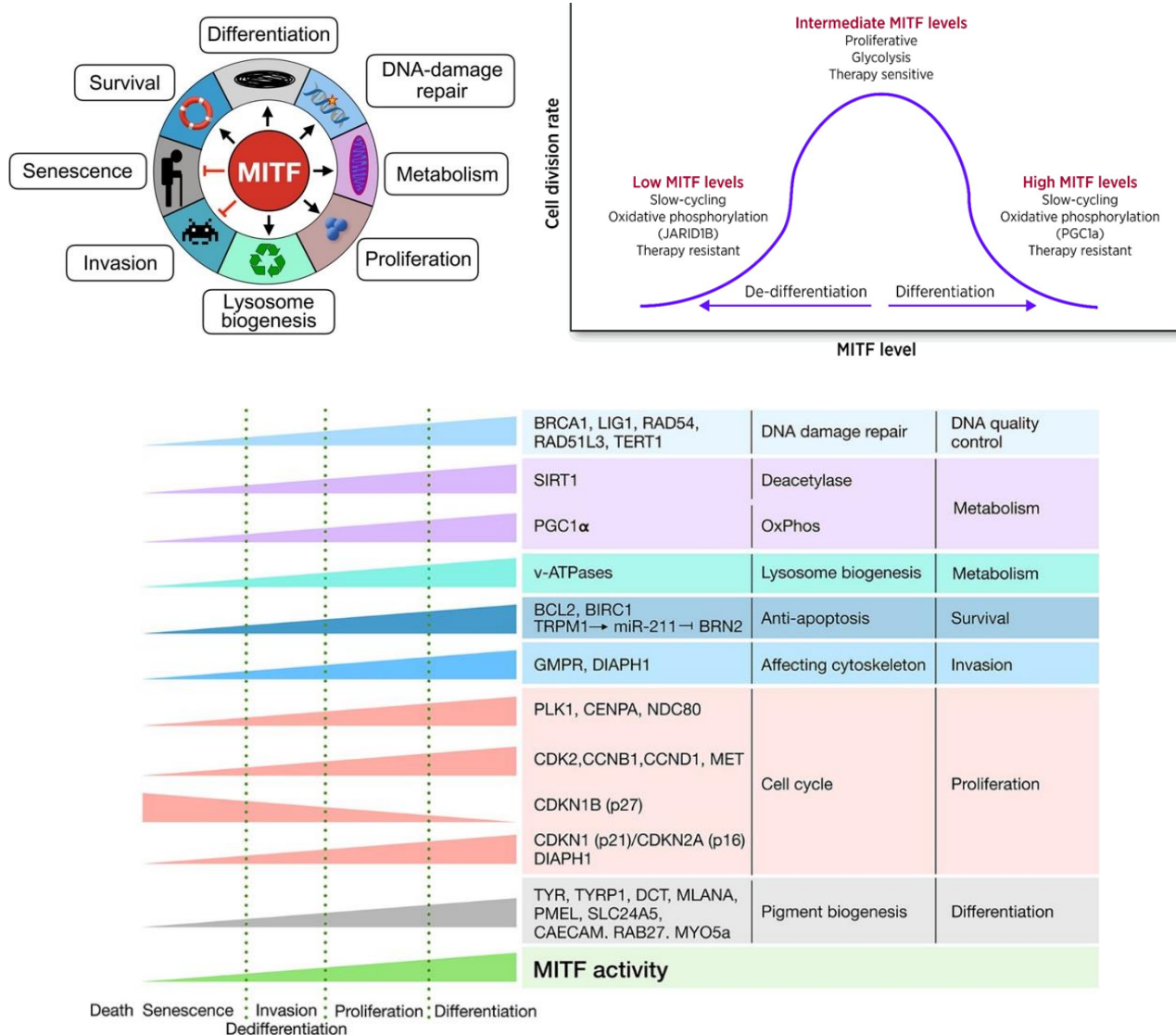


Figure 50. The rheostat model of MITF function and target gene regulation.

Adapted from Ahn, Chatterjee and Eccles, 2017; and Goding and Arnheiter, 2019.

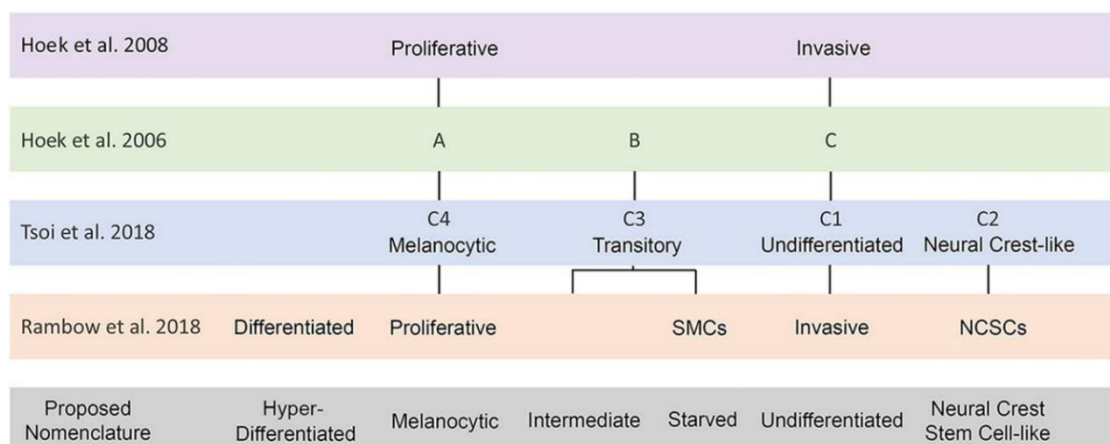


Figure 51. Phenotypic states of melanoma cells identified in different studies.

From Rambow, Marine and Goding, 2019.

polyclonal seeding and metastasis-to-metastasis reseeding, somatic mutation dynamics, and metastatic niche-dependent clonal selections (Hunter et al., 2018; Reiter et al., 2018). Importantly however, de novo mutations conferring selective advantages are stochastic events that usually take a long time to appear and are not sufficient to explain the high degree of melanoma adaptability and phenomena such as the rapid appearance of therapy resistance (Marusyk, Janiszewska and Polyak, 2020; Feinberg and Levchenko, 2023). As such, the other main source of melanoma heterogeneity is phenotypic plasticity, mediated by non-mutational transcriptional and epigenetic reprogramming, representing the final two hallmarks of cancer.

3.2. Melanoma plasticity, phenotype switching, and cell states

To adjust to surrounding microenvironmental challenges, melanoma cells can dynamically set up adaptive phenotypical responses by shifting between different transcriptional and epigenetic programs, leading to fundamental changes in cell behaviors and biological capacities (Flavahan, Gaskell and Bernstein, 2017). As such, high degrees of intra-tumoral cell-state heterogeneity are prevalent in melanoma, with distinct temporally shifting and spatially localized cell subpopulations displaying different malignant capacities, depending on specific niche cues (Karras et al., 2022). These dedifferentiation/differentiation processes are made possible by the intrinsic plasticity of melanoma cells due to their neural crest ontogeny and are regulated by the expression and activity of different master regulators (Imodoye et al., 2021; Najem et al., 2022). In contrast to time-consuming, irreversible genetic variation and adaptation, phenotypic plasticity is a relatively quick, reversible, and graded phenomenon, meaning that cells can dynamically switch between different phenotypes by activating distinct transcriptional signatures (Rambow, Marine and Goding, 2019). Importantly, in melanoma, well-defined markers of the different phenotypic cell states have been identified and have given key insights into the molecular mechanisms driving phenotype switching and its profound role in metastasis and therapy resistance (Arozarena and Wellbrock, 2019; Tang et al., 2020; Pedri et al., 2022).

Although phenotypic cell diversity was already observed in the 1980s (Fidler et al., 1981; Bennett, 1983), a molecular and transcriptional characterization of the different melanoma cell states only became possible with the advent of high-throughput sequencing (Fattore et al., 2019) and the characterization of MITF, the master regulator of phenotype plasticity in melanoma (Hodgkinson et al., 1993; Hughes et al., 1994). As stated before, MITF plays a key role in melanocyte differentiation and virtually every other physiological function

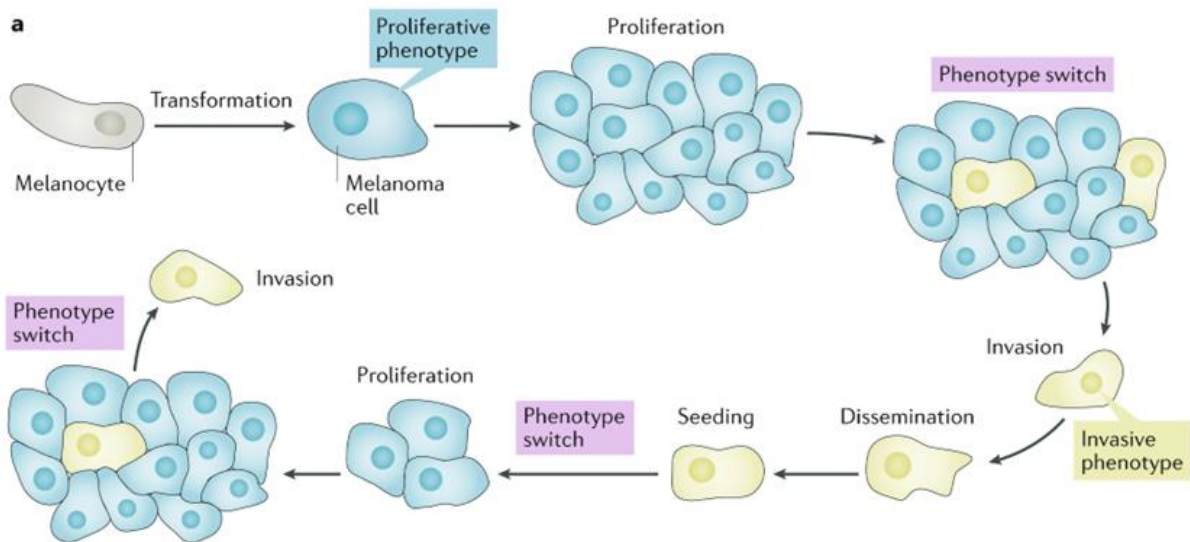


Figure 52. Basics of melanoma phenotype switching.

From Arozarena and Wellbrock, 2019.

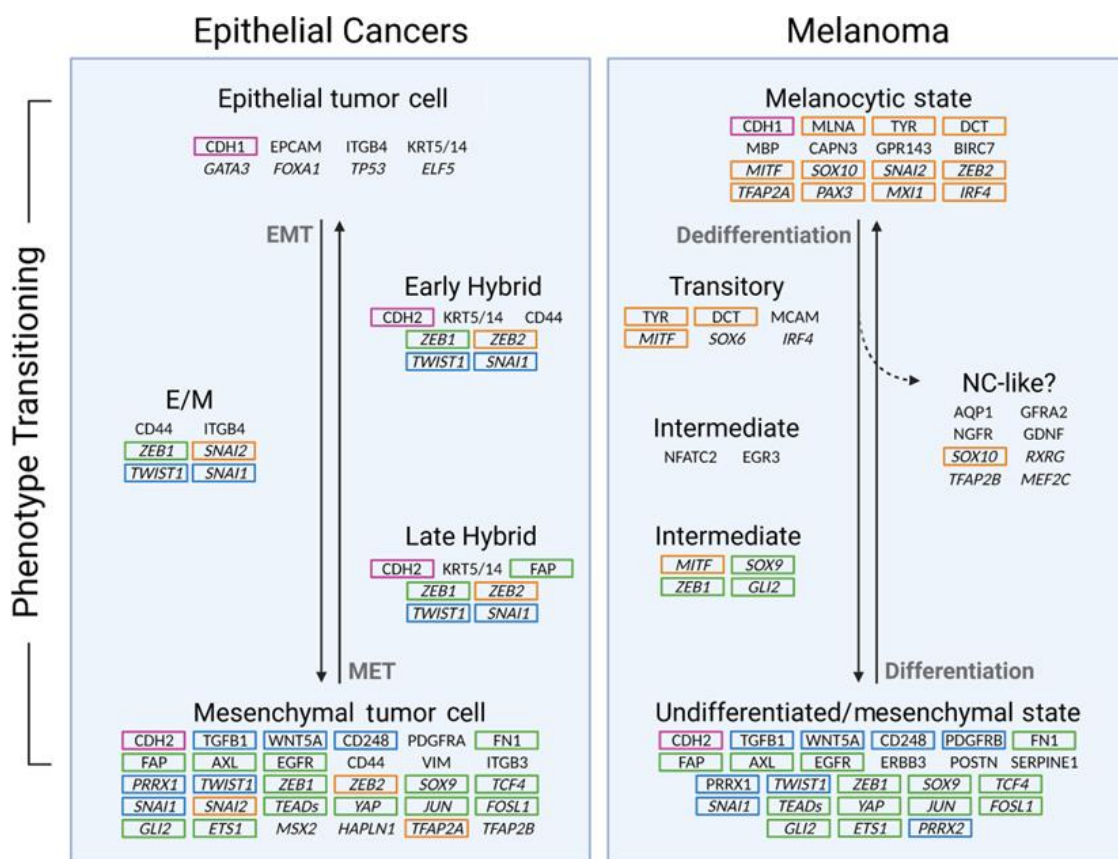


Figure 53. Markers of phenotypic states in epithelial cancers and melanoma.

Transcriptional regulators in *italics*. Mesenchymal markers in blue. Common markers between epithelial cancer EMT factors and undifferentiated melanoma states in green. Melanocytic markers in orange. From Pedri et al., 2022.

of melanocytes and melanoma cells, by promoting survival, proliferation and the suppression of senescence and invasive capacities (Goding and Arnheiter, 2019; Chauhan et al., 2022). Thus, its loss of expression or activity leads to profound epigenetic changes and dedifferentiation (Riesenberg et al., 2015; Tsoi et al., 2018). Initial studies on the functions of MITF appeared contradictory as its perceived role in stimulating cell proliferation was at odds with its contribution to a differentiation-mediated cell cycle arrest (Garraway et al., 2005; Loecherer et al., 2005). However, this paradox was resolved by the “rheostat model hypothesis” that stipulates that high levels of MITF activity promote differentiation and reduced proliferation, intermediary levels promote intense proliferation accompanied by the Warburg effect, and low-level activity induces a slow-cycling, dedifferentiated state characterized by invasive behavior and senescence (Carreira et al., 2006; Seberg, Van Otterloo and Cornell, 2017) (Figure 50).

Around the same time of the rheostat model description, key studies from Hoek et al. in 2006 and 2008 confirmed this theory by broadly identifying two main *in vivo* cell states based on differential gene signature expression profiles, corresponding to the proliferative and invasive phenotypes. The transcriptomes of these cell states were thoroughly analyzed in various subsequent studies, with significant contributions from the Jean-Christophe Marine and Stein Aerts research groups, and with different nomenclatures emerging and evolving over time (Widmer et al., 2012; Verfaillie et al., 2015; Tirosh et al., 2016; Pastushenko et al., 2018; Rambow et al., 2018; Tsoi et al., 2018; Wouters et al., 2020; Marin-Bejar et al., 2021; Karras et al., 2022) (Figure 51). The initially identified proliferative/differentiated melanoma cells display high proliferation rates but poor migratory and invasive properties and express intermediary to high expression and activity levels of MITF and its regulator TFs SOX10 and PAX3. On the other hand, the invasive/un- or dedifferentiated/mesenchymal-like melanoma cells display a more stem-like state characterized by the loss of melanocytic markers while overexpressing RTKs such as AXL and EGFR and being dominated by BRN2 and AP-1/TEAD TF activity. Additionally, they express EMT-like genes, including SNAI1, ZEB-1, SERPINE1, CDH2, or SOX9, and display heightened TGF- β , TNF- α , Hippo, WNT, HIF-1, and NF- κ B signaling, related to high invasiveness, ECM modulation, and drug tolerance (Caramel et al., 2013; Richard et al., 2016; Lüönd et al., 2022). Importantly, these studies also demonstrated that melanoma cells can move back and forth among these phenotypes, with profound consequences for tumor progression (Figure 52). While the distinct gene expression signatures and cell-state markers were reminiscent of the EMT encountered in epithelial cancers (Figure 53), this phenomenon was named phenotype switching in melanoma, since melanoma cells

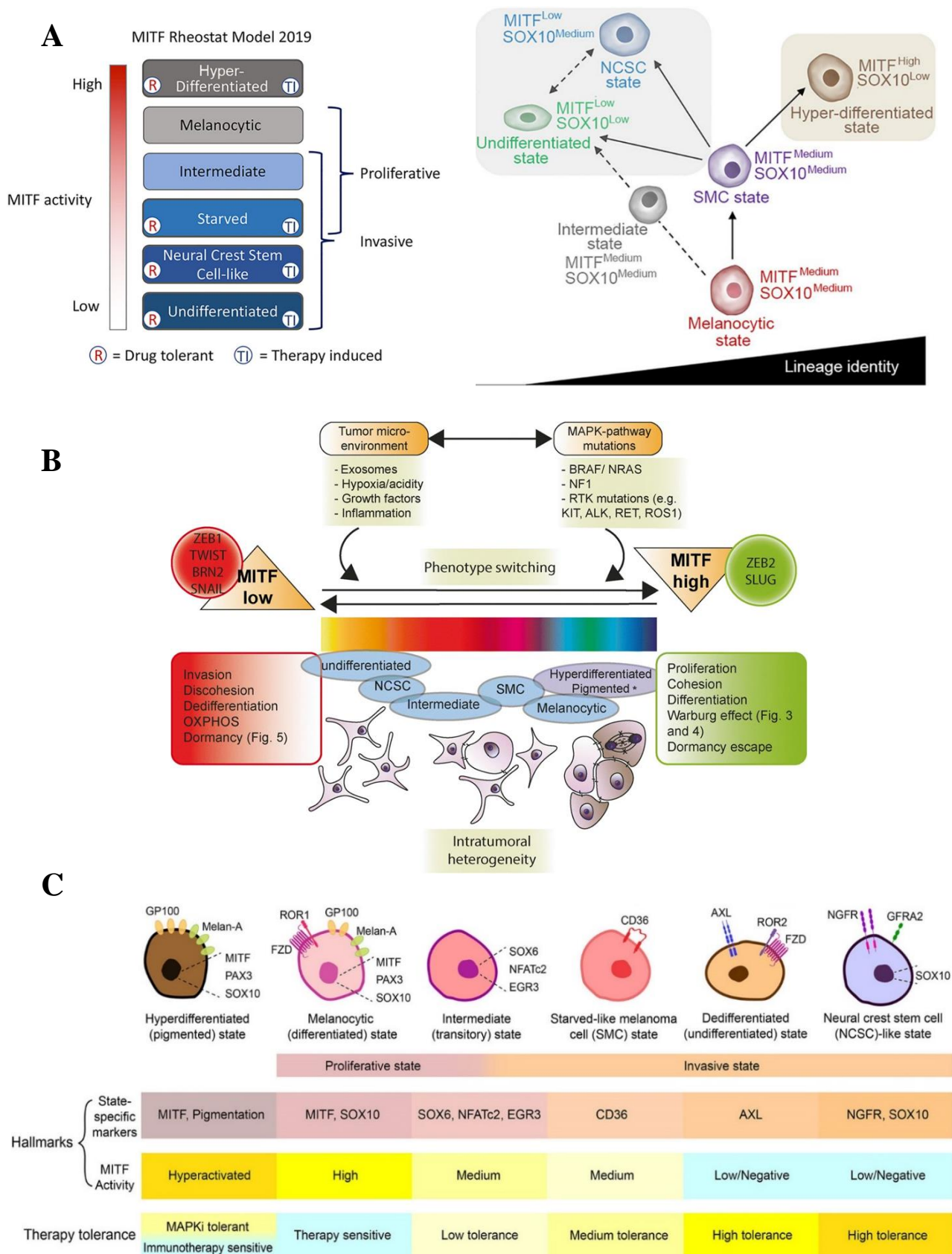


Figure 54. Potential arrangement of six different melanoma cell states, their relative expression of MITF and SOX10 (A) and other characteristics (B+C).

From Rambow, Marine and Goding, 2019; Huang et al., 2021; and Vandyck et al., 2021.

are not truly epithelial or mesenchymal cells (Hoek & Goding, 2010). As such, this term does not refer to a switch between two pre-defined states but rather indicates a general transition between different melanoma cell states.

Indeed, more recent studies utilizing single-cell RNA-sequencing on melanoma tumors detected cells with intermediary or transitory phenotypes, expressing genes of both the previously identified proliferative and invasive signatures, as well as other outlier cell states. This proved the existence of additional cell phenotypes and a greater complexity beyond the simple black-and-white proliferative/invasive switch in melanoma (Tirosh et al., 2016; Ennen et al., 2017; Rambow et al., 2018; Tsoi et al., 2018; Wouters et al., 2020; Karras et al., 2022). In 2019, Rambow, Marine and Goding proposed the following human melanoma cell state classification into six phenotypes, based on increasing MITF and SOX10 activity levels: Mesenchymal-like or dedifferentiated (or undifferentiated), Neural Crest Stem Cell (NCSC)-like, Starved melanoma cell (SMC), Intermediate, Melanocytic or differentiated, and Hyper-differentiated or pigmented (Figure 54). In this new nomenclature, the dedifferentiated and NCSC-like cells correspond to the broader invasive phenotype discovered a decade earlier by Hoek et al., whereas the SMC and intermediary cells describe a transitory state between the invasive and the differentiated/melanocytic (previously called proliferative) phenotypes (Verfaillie et al., 2015). While melanocytic, intermediate, and dedifferentiated cells are detectable in drug-naïve tumors (Ennen et al., 2017), NCSC-like, SMC and pigmented cells are rarer subpopulations that more likely arise with drug treatments (Rambow et al., 2018).

For example, MAPK inhibitor treatments have been shown to promote an important PAX3-dependent upregulation of MITF activity (Smith et al., 2016), leading to the emergence of melanin-producing hyper-differentiated melanoma cells, characterized by a slow-cycling and therapy-resistant terminal differentiation state. As high MITF activity upregulates mitochondrial-biogenesis genes such as PGC1 α , these cells become highly dependent on OXPHOS (Haq et al., 2013). This fundamentally differentiates these hyper-differentiated cells from the fast-cycling, Warburg-effect-dependent melanocytic population, which constitutes the majority of cells encountered in treatment-naïve tumors (Rambow et al., 2018). Intermediate melanoma cells with moderate migratory capacities were initially only defined as a mixed transition state between the proliferative and invasive phenotypes, expressing genes of both. However, it has since become clear that it is rather its own discrete and stable cell state, regulated by a distinct open chromatin landscape and a specific and unique set of transcription factors, including SOX6, EGR3, NFATC2, and RXRG, whose loss leads these cells towards a more dedifferentiated fate (Wouters et al., 2020). As stated before, stress factors such as

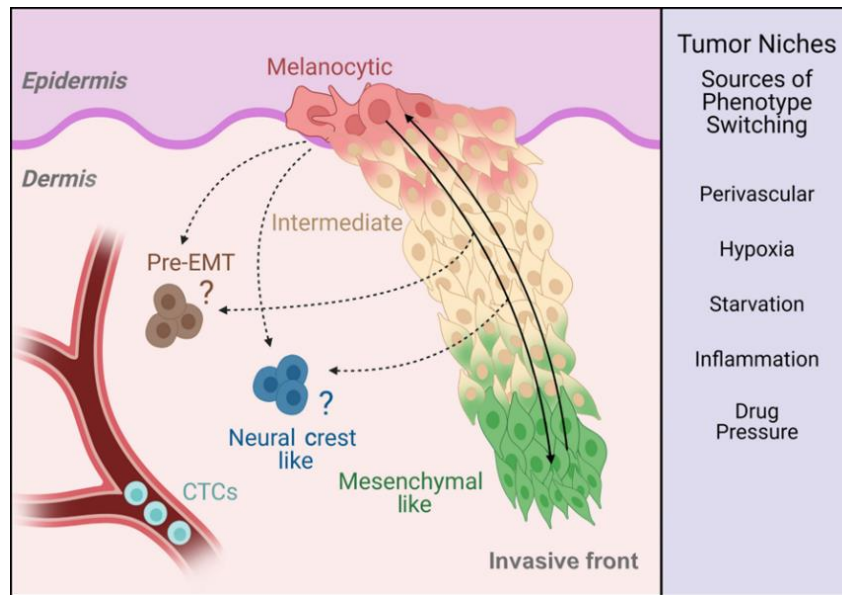


Figure 55. Phenotype switching trajectories and TME stimuli.

From Pedri et al., 2022.

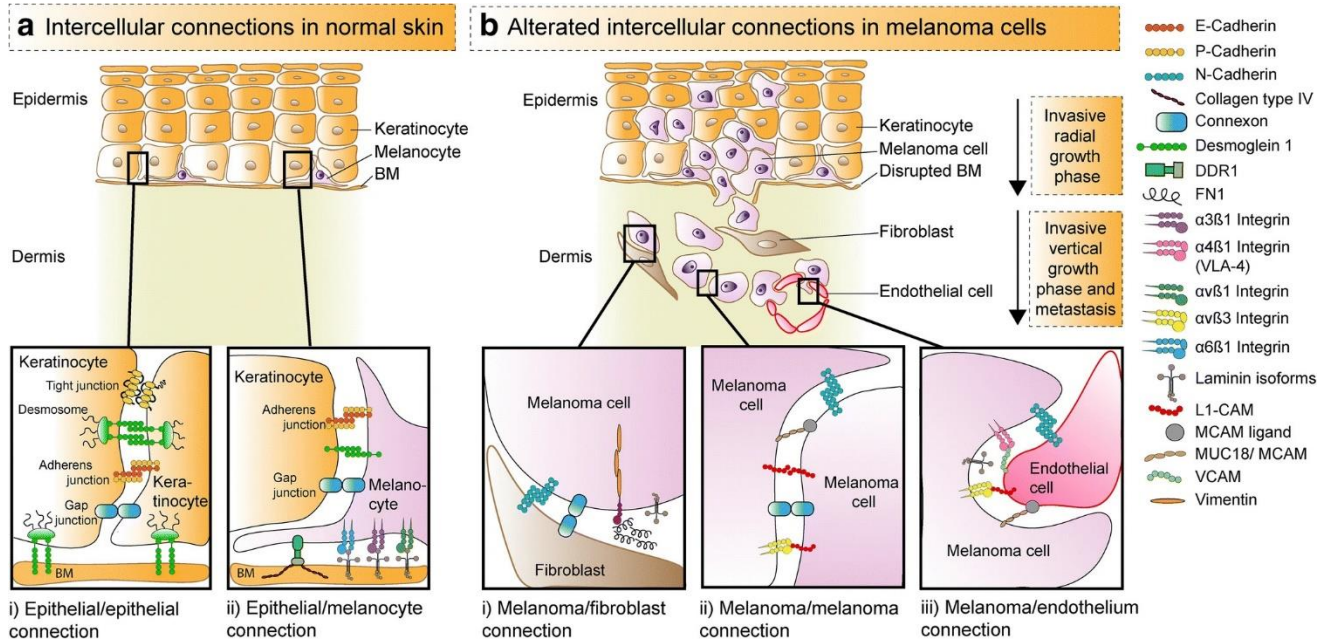


Figure 56. Changing intercellular contacts during melanoma progression.

From Vandyck et al., 2021.

hypoxia, drug treatment or nutrient limitation often give rise to slower cycling and more resistant states through epigenetic and metabolic reprogramming, which often passes through a transitory starved melanoma state (Rambow et al., 2018). As such, SMCs display a PAX3-dependent mixed expression of proliferative, invasive and NC marker genes while reducing their cancer cell metabolism signature (Kim et al., 2016). Instead, they increase the expression of angiogenesis and fatty acid catabolism genes such as the fatty acid translocase CD36, rendering them highly metabolically adaptive. As such, they are uniquely poised to act as a founder or waypoint state toward more stress- or treatment-resistant phenotypes, including the hyper-differentiated, dedifferentiated, or NCSC-like cell states (Aloia et al., 2019; Huang et al., 2021). Consistent with this, in patient-derived xenograft (PDX) models, drug treatments induced the initial apparition of SMCs which disappeared concomitantly to the appearance of these more resistant phenotypes, predominantly NCSC-like melanoma cells (Rambow et al., 2018). Together with the dedifferentiated cells, NCSC-like cells also lack MITF activity and display a mesenchymal/invasive signature with the expression of AXL. However, they also express an NC-like gene signature that includes SOX10, NGFR, GFRA1, SOX2, RXRG, and AQP1 (Fallahi-Sichani et al., 2017; Restivo et al., 2017; Larribère and Utikal, 2019; Wessely et al., 2021). Both the dedifferentiated and NCSC-like states have been shown to be slow-cycling, intrinsically drug-resistant, and, as mentioned before, they are able to transdifferentiate into dormant CAF- or endothelial-like cells, the latter being able to perform vasculogenic mimicry (Rambow, Marine and Goding, 2019). It is however the NCSC-like subpopulation that is mainly found enriched upon therapy and is thought to be the main culprit of melanoma resistance and relapse (Rambow et al., 2018; Tsoi et al., 2018; Boshuizen et al., 2020; Liu et al., 2021). Importantly, NCSC-like cells have been strongly associated with stem-cell-like dormancy and quiescence (Diener and Sommer, 2020; Liu et al., 2021; Marin-Bejar et al., 2021). Additionally, a landmark study from Karras et al. in 2022 demonstrated different functions of dedifferentiated and NCSC-like cells in a melanoma mouse model. In this study, NC-like cells were preferentially found in proximity of perivascular endothelial cells, where Notch-dependent intercellular signaling maintained their stemness. These NC-like cells displayed important tumorigenic and self-renewal capacities, and they could also give rise to more proliferative cells to fuel tumor growth, in a function reminiscent of cancer stem cells (Batlle and Clevers, 2017). On the other hand, the dedifferentiated/mesenchymal-like cells did not contribute to primary tumor growth but, instead, displayed important migratory and dissemination capacities. This phenotype was however incapable of giving rise to secondary tumors, as these mesenchymal-like cells had to switch back to a more tumorigenic and

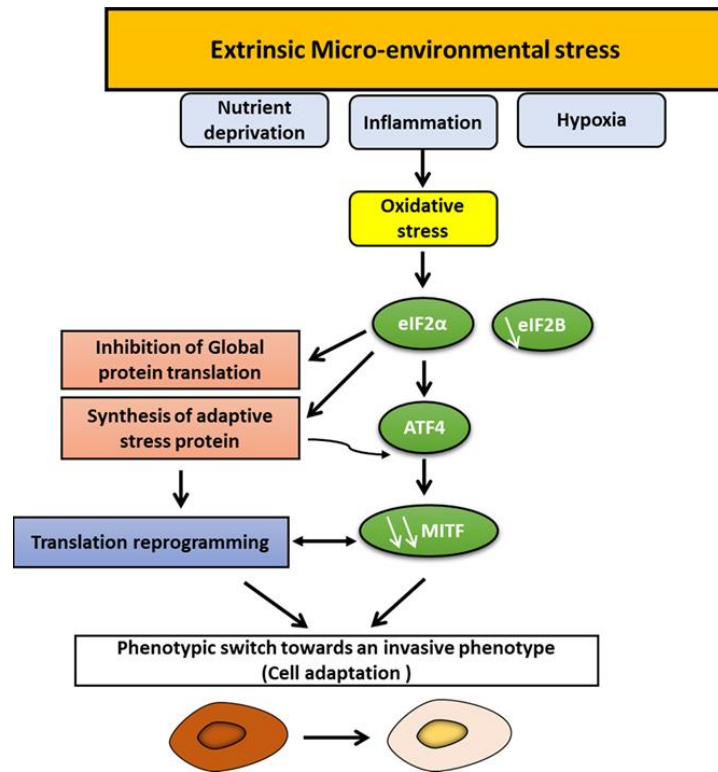


Figure 57. TME stress signals and translational reprogramming in melanoma plasticity.

From Najem et al., 2022.

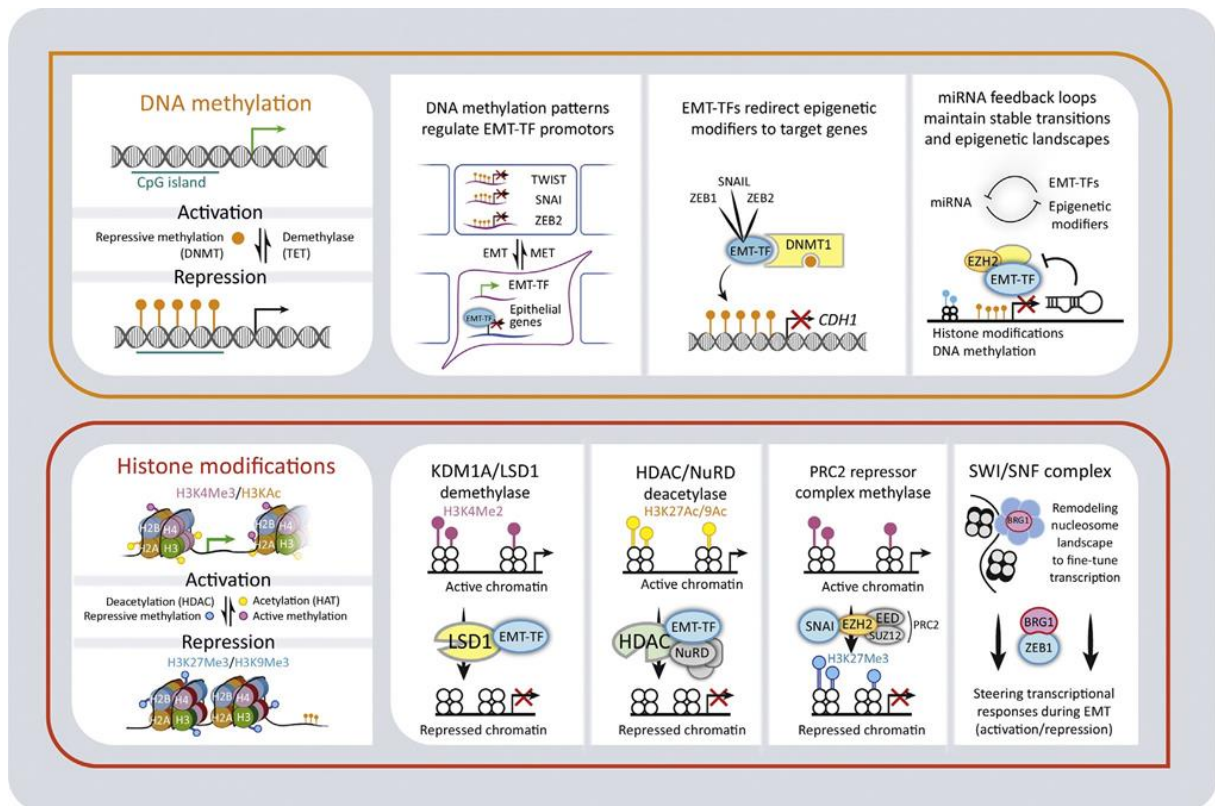


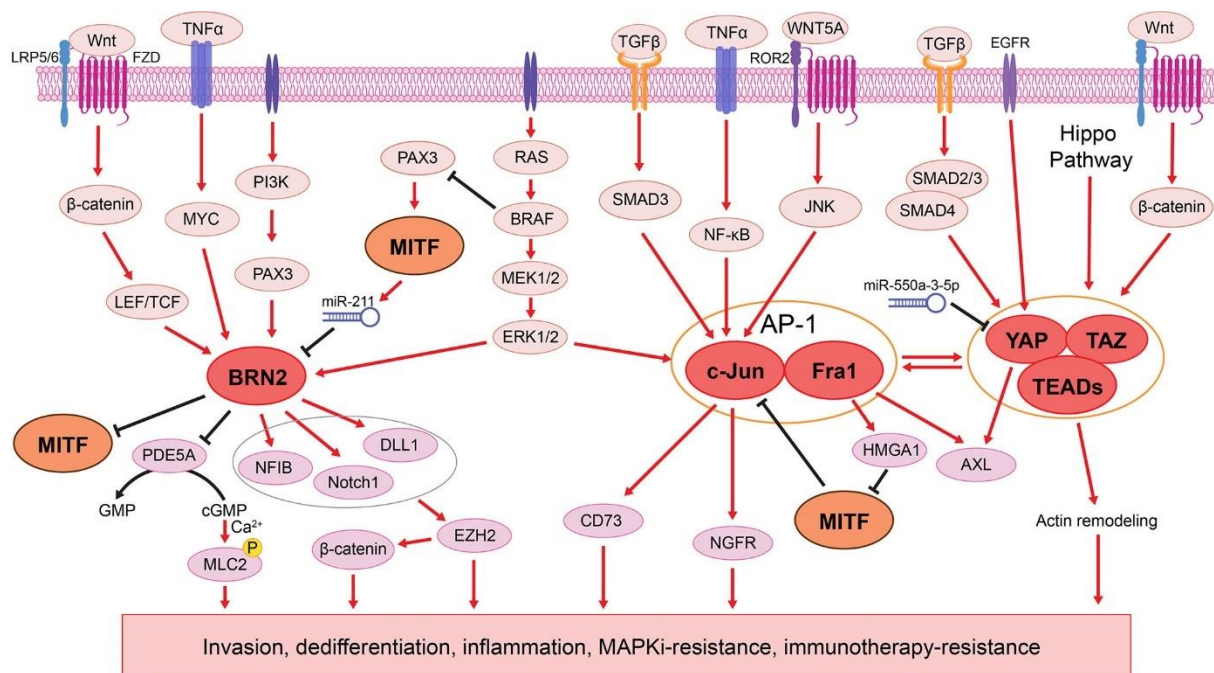
Figure 58. Epigenetic Regulation of EMT and melanoma phenotype switch.

From Skrypek et al., 2017.

proliferative state in a MET-like manner to successfully seed to metastatic niches. Of note, this study also identified additional phenotypic subpopulations, indicating the progressively evolving nature of this field. Additionally, the authors emphasized the non-random geographic distribution of cell states within melanoma tumors, hinting at the profound implications of TME niche cues on phenotype switching (Figure 55).

3.2. Multi-layered reprogramming in phenotype switching

As the connections between extrinsic factors and the large-scale reprogramming necessary to induce melanoma cell state transitions have become increasingly more apparent in recent years, the molecular mechanisms behind phenotype switching are an active area of investigation. During tumor progression, melanoma cells are exposed to dynamically changing dialogs with stromal cells and the TME. Once the basement membrane is breached, invading cells can for example establish novel integrin and laminin interactions with cell populations not usually encountered, such as other melanoma cells, fibroblasts, and immune or endothelial cells (Golan et al., 2015; Attieh et al., 2017; Vannini et al., 2019) (Figure 56). While normal adhesion to keratinocytes through E-cadherin is lost (Haass et al., 2005), N-cadherin interactions get the upper hand, along with the activation of various other adhesion and signaling pathways through changes in the TME. Many of these novel interactions and exposures have been shown to downregulate MITF activity and promote dedifferentiation, such as increased TGF- β (Javelaud et al., 2011), inflammation (Landsberg et al., 2012; Riesenberger et al., 2015), hypoxia (Feige et al., 2011; Cheli et al., 2012; O'Connell et al., 2013; Louphrasitthiphol et al., 2019), altered ECM stiffness (Kaur et al., 2019; Diazi, Tartare-Deckert and Deckert, 2023), or nutrient availability (Falletta et al., 2017; Ferguson et al., 2017). This happens through a complex network of multiple molecular mechanisms, including changes in membrane receptors or intracellular signaling (Najem et al., 2022; Pagliuca, Di Leo and De Zio, 2022; Hossain and Eccles, 2023). Many of these stimuli, including glucose, amino acid, and oxygen deprivation, seem to converge through oxidative stress on eIF2 α , a translation initiation factor that, when phosphorylated, leads to global protein translation inhibition (Falletta et al., 2017) (Figure 57). As translation is a high-energy process, this stress and starvation response aims to minimize the energy consumption of cells by reprogramming translation toward selective transcripts needed for adaptation and survival (Pathria et al., 2019). This leads to the inhibition of eIF2B and the activation of the AP-1 factor ATF4, both of which suppress MITF activity, while stimulating the expression of invasive signature genes such as AXL (Ferguson et al., 2017;



Conditions	Factors	Master regulators	Signaling pathways/mechanisms
Metabolic stress	Hypoxia	HIF1 α	HIF1 α \rightarrow BHLHE40/BHLHB2 (-MITF) \rightarrow dedifferentiation HIF1 α \rightarrow WNT5A-ROR2 \rightarrow invasion Akt \rightarrow NF- κ B (+HIF1 α) \rightarrow Notch1 \rightarrow phenotype switching
	Nutrient starvation	p-eIF2 α ATF4	p-eIF2 α (-eIF2B) \rightarrow ATF4 \rightarrow AXL \rightarrow invasion p-eIF2 α (-eIF2B) \rightarrow ATF4 (-MITF) \rightarrow dedifferentiation
	Oxidative stress	NRF2	NRF2 \rightarrow ATF4 (-MITF) \rightarrow dedifferentiation, inflammation
Inflammation & cytokines	TNF α	BRN2 AP-1 (c-Jun)	TNF α \rightarrow BRN2 \rightarrow phenotype switching TNF α \rightarrow c-Jun \rightarrow phenotype switching
	TGF β	ATF4 AP-1 (c-Jun) HIF1 α	TGF β \rightarrow ATF4 (-MITF) \rightarrow proliferation, differentiation TGF β \rightarrow c-Jun (or JunB) \rightarrow phenotype switching TGF β (-IPHD2) \rightarrow HIF1 α \rightarrow phenotype switching
	IL-1	NF- κ B AP-1	IL-1 \rightarrow phospho-I κ B \rightarrow NF- κ B \rightarrow phenotype switching IL-1 \rightarrow JNK \rightarrow AP-1 (c-Jun) \rightarrow phenotype switching IL-1 \rightarrow MMP-9 \rightarrow invasion IL-1 (-MITF) \rightarrow dedifferentiation
	IL-6	WNT5A CA-IX	IL-6 \rightarrow MAPK \rightarrow WNT5A \rightarrow phenotype switching IL-6 \rightarrow CA-IX \rightarrow phenotype switching

Extracellular Ligands.
Receptors.
Transcription factors.
Transcriptional repressors.
Epigenetic regulators.
Translational factors.
Others.

Figure 59. Stress-specific pathways and transcriptional networks driving melanoma phenotype switching.

Adapted from Huang et al., 2021.

García-Jiménez and Goding, 2019; Phung et al., 2019). Concurrently with the translational reprogramming, a crucial metabolic rewiring regarding fatty acid usage helps the emergence of the above-mentioned highly adaptive SMC state, poised to switch to other phenotypes (Vivas-García et al., 2020; Oren et al., 2021; Falletta, Goding and Vivas-García, 2022). MITF activity can be regulated through several other mechanisms, such as through nuclear export (Ngeow et al., 2018), miRNAs (Arts et al., 2015; Qian, Yang and Yang, 2017), or differential DNA binding affinity (Louphrasitthiphol et al., 2020).

Multiple epigenetic mechanisms contribute to phenotype switching, leading to profound chromatin and transcriptional remodeling (Strub, Ballotti and Bertolotto, 2020) (Figure 58). Whereas in proliferative cells, the enhancer landscape resembles that of melanocytes, invasive cells acquire a mesenchymal-like chromatin landscape reminiscent of fibroblasts, in which the *SOX10* promoter for example acquires the repressive H3K27me3 mark, whereas the invasive marker TF SOX9 is expressed through the loss of promoter hypermethylation and novel long-range enhancer interactions (Cheng et al., 2015; Verfaillie et al., 2015). Various histone modifiers and chromatin remodelers, including KDM1B, KDM5A, KDM5B or BRG1 are altered during phenotype switching (Sharma et al., 2010; Roesch et al., 2013; Laurette et al., 2015; Emmons et al., 2019). Additionally, a great number of miRNAs and lncRNAs have been shown to either up- or downregulate proliferative or invasive signature genes (Segura et al., 2009; Li et al., 2018; Coe et al., 2019; Siena et al., 2019; Varrone and Caputo, 2020). Remarkably, on the single-cell level, not all melanoma cells seem to display the same levels of transcriptional adaptability, which would explain why oftentimes just a subset of cells in a tumor manages to survive certain stresses such as exposure to melanoma treatments. In important studies by Shaffer et al. in 2017 and Torre et al. in 2021, it was shown that the cells which were pre-destined to adapt and become drug-resistant were the ones already displaying increased transcriptional variations and fluctuations in MITF and SOX10 levels, and which sporadically and stochastically expressed invasive and resistance markers such as AXL, EGFR, NGFR, JUN, LATS2, or RUNX3. These studies further consolidated the notion of transition states and postulated that phenotype switching operated through an initial rare cell subpopulation primed for cell fate transition, which displays increased transcriptional flexibility. In these cells, stress exposure would lead to cellular reprogramming, giving rise to stable new phenotypes. This epigenetic remodeling is due primarily to the incremental loss of the MITF/SOX10 regulon, which lifts the inhibition of crucial dedifferentiation TFs such as JUN (Riesenberg et al., 2015) (Figure 59). This is followed by the activation of new signaling pathways, mediated by the activity of TEAD and AP-1 factors (Verfaillie et al., 2015).

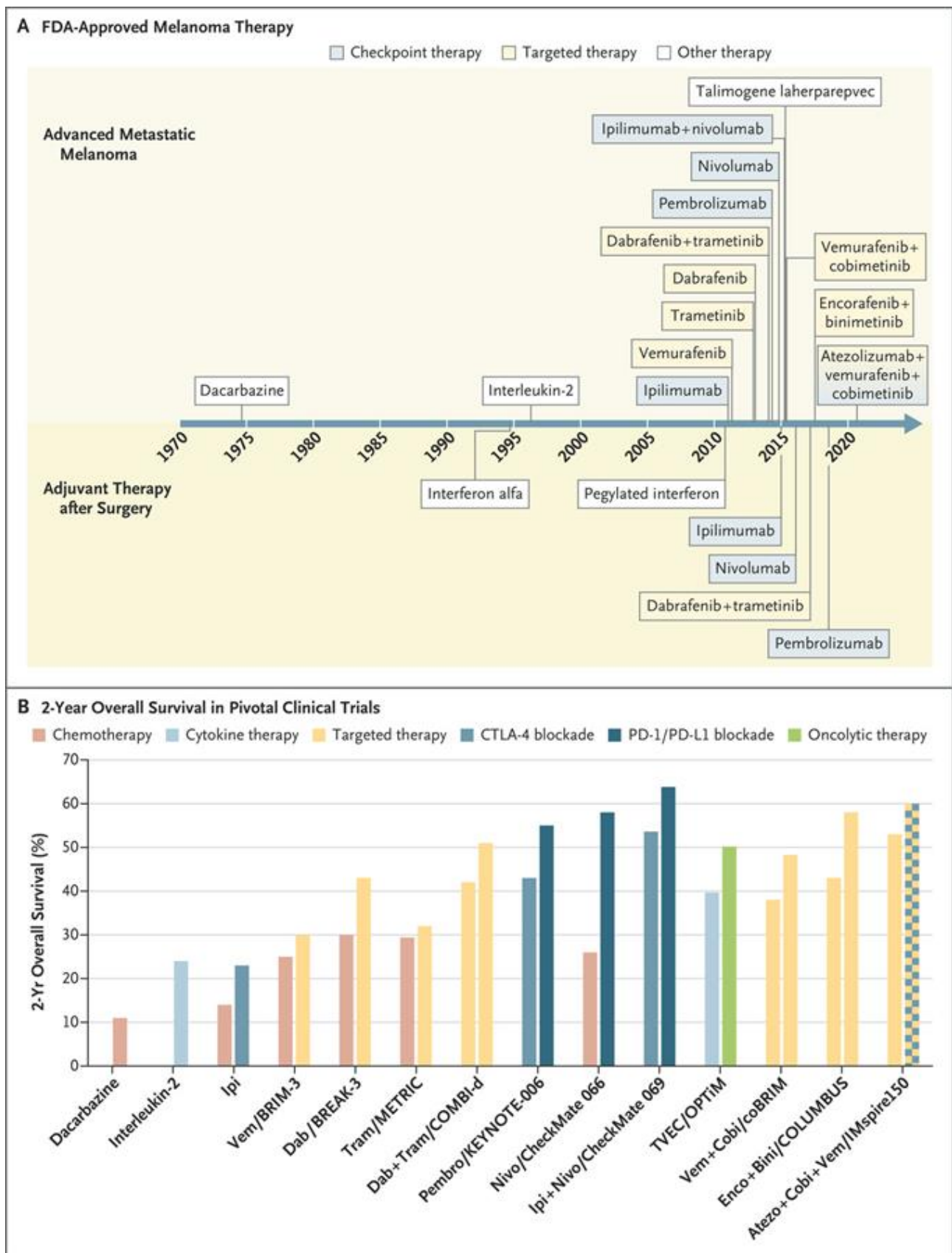


Figure 60. Approved treatments for melanoma and associated overall survival at 2 years.
From Curti and Faries, 2021.

D. The clinical management of cutaneous melanoma and therapy resistance mechanisms

1. Melanoma treatment in 2023

1.1. Surgical treatment and a historical perspective for metastatic disease

More than 90 % of melanoma patients are diagnosed with localized or regional disease, for which the standard care is surgery. Tumor resection usually leads to complete remission and an excellent 5-year survival rate of over 95 % (Joyce, 2017). The resection margin required for local excision is determined by Breslow depth, as wider and deeper surrounding tissue sections are removed depending on how far the tumor has progressed (Gillgren et al., 2011). Currently, patients with risk of lymphatic nodal metastases undergo wide excisions with 1- or 2-cm margins depending on tumor thickness, accompanied with sentinel-node biopsy, meaning that lymph nodes receiving direct drainage from the tumor site are removed and examined for metastatic presence (Faries et al., 2017). In some cases of higher-risk melanoma, IFN- α adjuvant therapy can be of benefit (Ives et al., 2017). Unfortunately, tumor resections become impossible with widespread metastatic melanoma, and survival chances look bleaker.

Nevertheless, melanoma has been pointed to as a prime example of how the understanding of underlying biological mechanisms, such as how cancer cells evade the immune system or which driver genes are responsible for tumor growth, gives rise to the development of novel therapeutics (Luke et al., 2017; Leonardi et al., 2018). Until roughly a decade ago, metastatic melanoma presented an overall survival of less than 10 % (Dickson and Gershenwald, 2011), with only two FDA-approved treatments available until 2011: the chemotherapeutic drug dacarbazine and high-dose IL-2 immunotherapy. Unfortunately, these did not significantly improve overall survival and were limited by meager response rates and severe toxicity (Benjamin, 1979; Finn, Markovic and Joseph, 2012). However, with the revolutionary introduction of MAPK pathway and immune checkpoint inhibitors as the new standard of care for metastatic melanoma since 2011, patient survival has dramatically increased, as today over half of patients experience significant clinical benefits (Curti and Faries, 2021; Jenkins and Fisher, 2021) (Figure 60). In some distinct cases, oncolytic viruses or radiotherapy are also used (Ernst and Giubellino, 2022), but these will not be discussed here.

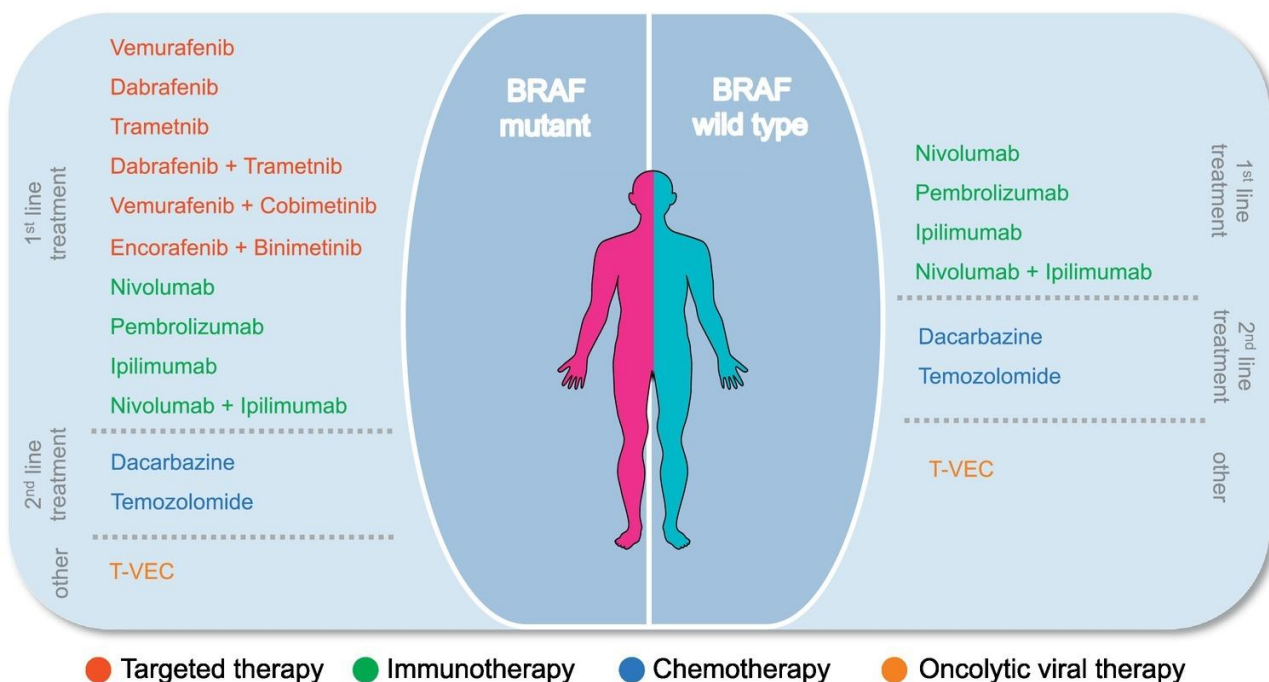
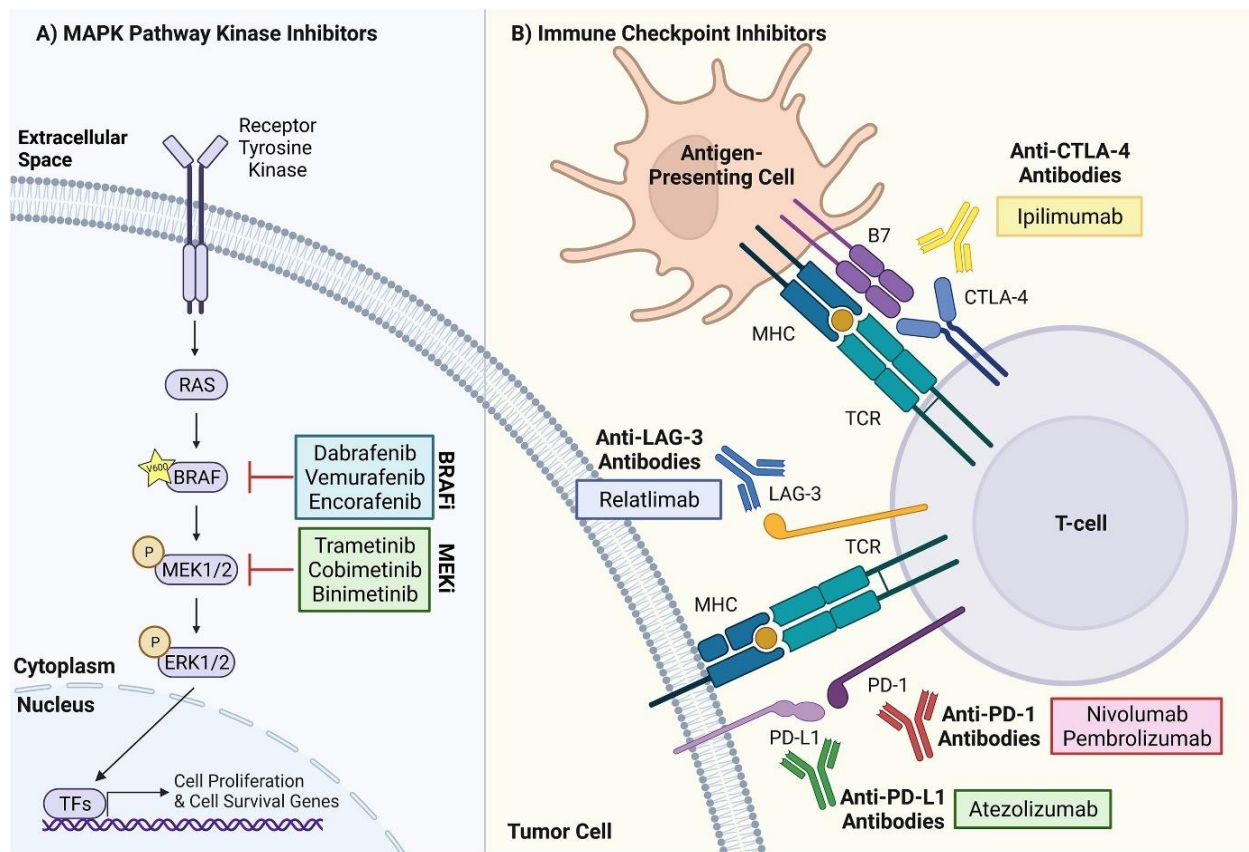


Figure 61. Treatments for unresectable metastatic melanoma and BRAF mutation status.

From Kozar et al., 2019; and Caksa, Baqai and Aplin, 2022.

1.2. Targeted therapy through small-molecule MAPK inhibitors

The discovery in the early 2000s that the MAPK pathway is hyper-activated in 90 % of melanoma cases (Davies et al., 2002), ultimately led to the development of Vemurafenib, a first-in-class orally available and selective inhibitor of V600E-mutated BRAF, displaying high-affinity binding to its ATP-binding pocket (Figures 61 and 62) (Bollag et al., 2010; Chapman et al., 2011). This leads to strong cytostatic and cytotoxic effects through abrogation of the MAPK pathway in BRAF-mutated cells (Yang et al., 2010; Marchetti et al., 2018). This agent provided a clinical benefit previously unheard of in metastatic melanoma, by efficiently abrogating MAPK signaling. Compared to dacarbazine chemotherapy, the response rate was 48 % versus 5 %, the median progression-free survival was 5.3 months versus 1.6 months; and the median overall survival was of 13.3 months versus 10.0 months (McArthur et al., 2014). A second BRAFV600 inhibitor, Dabrafenib, was approved in 2013 and showed very similar clinical benefits, albeit having a slightly broader inhibition spectrum, as rarer BRAF mutations such as V600K were shown to be efficiently targeted (Hauschild et al., 2012; Long et al., 2012). In 2018, a second-generation BRAFV600 inhibitor named Encorafenib was approved, which displays distinct pharmacological properties and a higher efficacy through prolonged target suppression (Koelblinger, Thuerigen and Dummer, 2018). Besides BRAF inhibitors, small molecules targeting the downstream MEK1/2 kinase have also been approved, in the hopes of blocking a wider array of upstream oncogenic mutations. Trametinib was the first MEK inhibitor to be approved in 2013, resulting in progression-free survival of 4.8 months vs. 1.5 months compared to dacarbazine (Flaherty et al., 2012). This was then followed by the development of Cobimetinib and Binimetinib (Garnock-Jones, 2015; Tran and Cohen, 2020). Today, combination treatment between BRAF and MEK inhibitors constitute the standard of care for targeted therapy in BRAF-mutated melanoma patients (Figure 61), as response rates exceeding 60 % and a complete response rate of up to 18 % can be achieved (Curti and Faries, 2021). Despite these modestly promising results, survival gains are still mainly counted in months, and major drawbacks limit the clinical efficacy of MAPK inhibitors (MAPKi). First, there is a severe lack of efficient targeted therapies for *BRAF* wild-type melanoma cases, such as for the 25 % of patients carrying *NRAS* mutations (Randic et al., 2021). For these patients, BRAFV600 inhibitors cannot be used, and MEK inhibitors display significantly reduced potency (Solit et al., 2006; Dummer et al., 2017), so that targeted therapy is not used as a first-line treatment for non-BRAFV600 melanomas (Kozar et al., 2019) (Figure 61). Many adverse effects have been documented over the years, including rashes, photosensitivity, arthralgia,

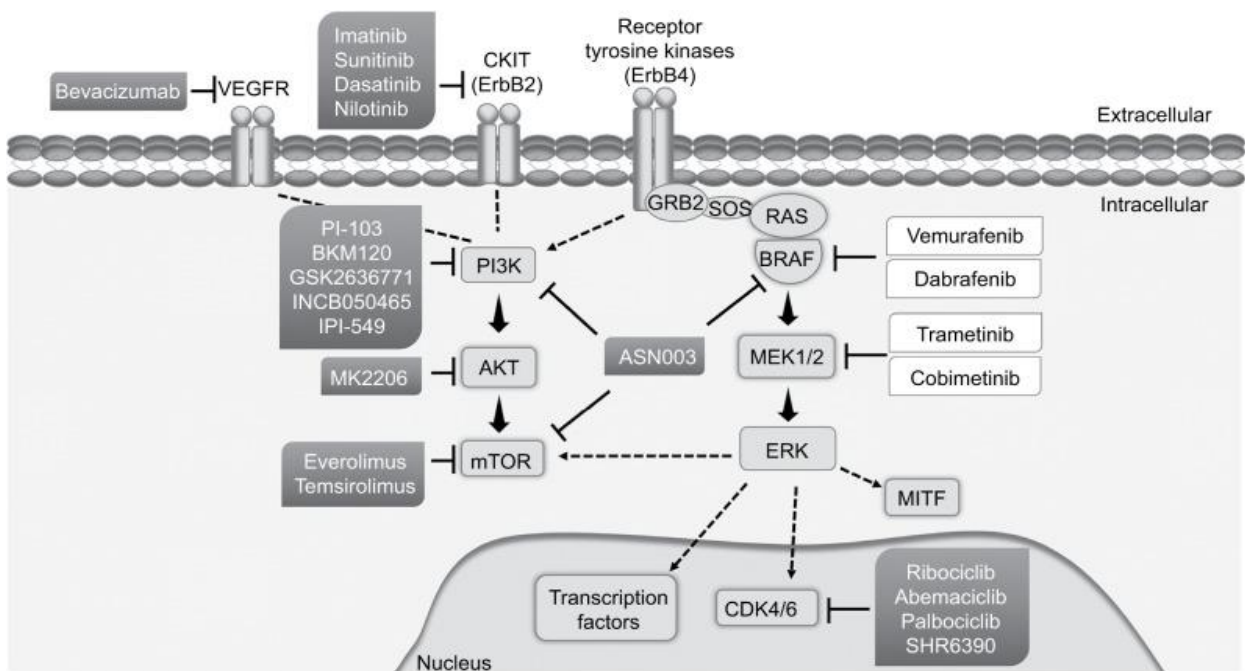


Figure 62. Targeted therapies approved by the FDA (in white) or in trials (in gray).

From Domingues et al., 2018.

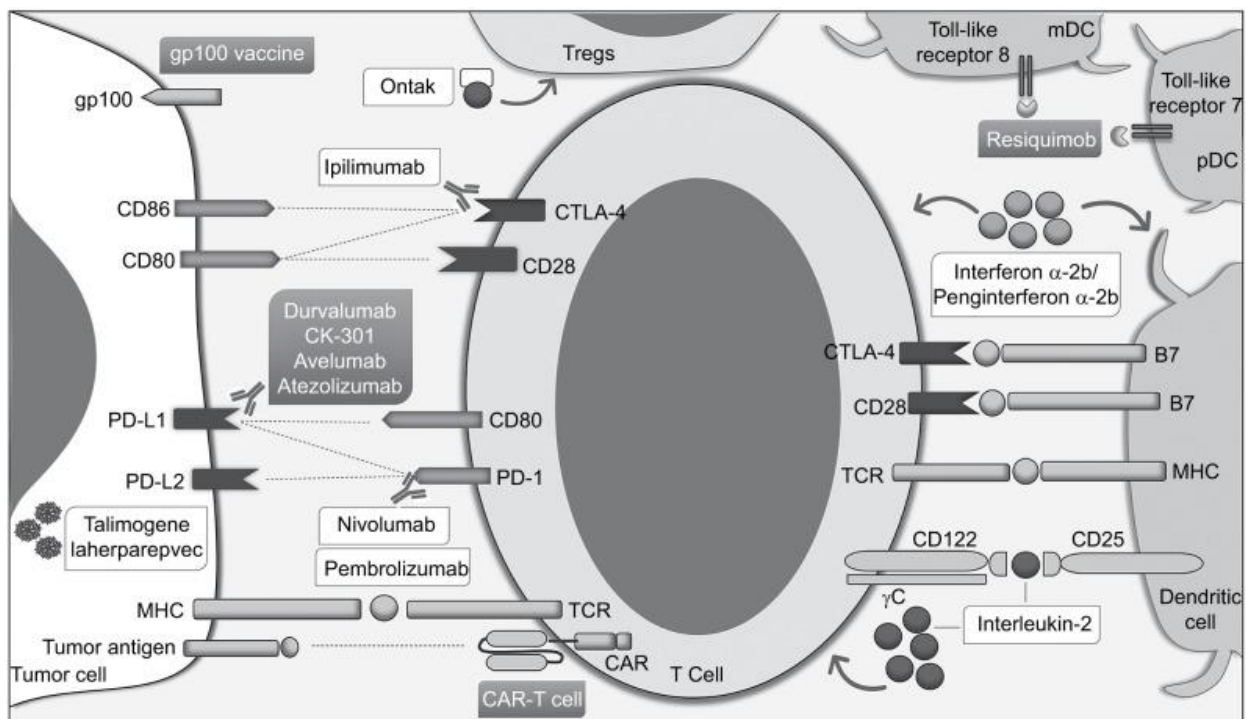


Figure 63. Immunotherapies approved by the FDA (in white) or in trials (in gray).

From Domingues et al., 2018.

fatigue, fever, as well as hepatic, ocular, cardiovascular, and immune-related toxicities (Luke et al., 2017; Boutros et al., 2020; Subbiah, Baik and Kirkwood, 2020). Worryingly, a paradoxical hyper-activation of MAPK signaling in BRAF wild-type cells through RAF dimerization (CRAF homodimers or CRAF-BRAF heterodimers) and auto-activation, was shown to be induced in patients receiving BRAF inhibitor treatments such as Vemurafenib (Hatzivassiliou et al., 2010; Poulikakos et al., 2010). In some cases, this led to the emergence of cancers, such as squamous cell carcinomas, keratoacanthomas, new primary melanomas, leukemias, and colon carcinomas (Callahan et al., 2012; Holderfield, Nagel and Stuart, 2014; Zhang et al., 2015). Fortunately, these developments could be mitigated by BRAF/MEK inhibitor combinations, which increase the progression-free survival by approximately three months when compared to BRAF inhibitor monotherapy and delay the onset of drug resistance (Subbiah, Baik and Kirkwood, 2020; Tanda et al., 2020). However, while these combination treatments seem to slow down the onset of treatment insensitivity (Griffin et al., 2017), this fate seems in most cases still inevitable, as most patients develop resistance to MAPKi treatments within a year (Villanueva, Vultur and Herlyn, 2011; Rebecca and Herlyn, 2020).

1.3. Immune checkpoint inhibitors

Multiple biological insights have propelled immunotherapies, in addition to MAPK inhibitors, to become one of the two cornerstones of modern melanoma clinical management (Domingues et al., 2018). Melanoma is recognized as having one of the highest mutational burdens of any cancer and is therefore thought to be highly immunogenic, as higher mutation rates result in more neo-antigens, increasing T-cell recognition (Jardim et al., 2021). As such, melanomas, compared to other neoplasms, tend to be ‘hot tumors’ displaying high levels of immune infiltrates and a more inflamed tumor microenvironment (Vareki, 2018; Kang et al., 2020; Niknafs et al., 2023). However, as stated before, melanoma cells utilize multiple mechanisms to evade immune destruction, including the subversion of the immune-regulatory PD-1 and CTLA-4 receptors. As such, monoclonal antibodies that function as immune checkpoint inhibitors (ICIs) have been developed to increase the natural cytotoxic response against cancer cells, especially for melanoma non-BRAF patients (Pardoll, 2012; Carlino, Larkin and Long, 2021; Huang and Zappasodi, 2022) (Figures 61 and 63). The first ICI to receive FDA approval was the CTLA-4 inhibitor Ipilimumab in 2011. CTLA-4 is an immune-inhibitory receptor expressed on the surface of activated T cells through chronic tumor antigen presentation, mainly by dendritic cells, which inhibits the mounting of an anti-cancer response (Snyder et

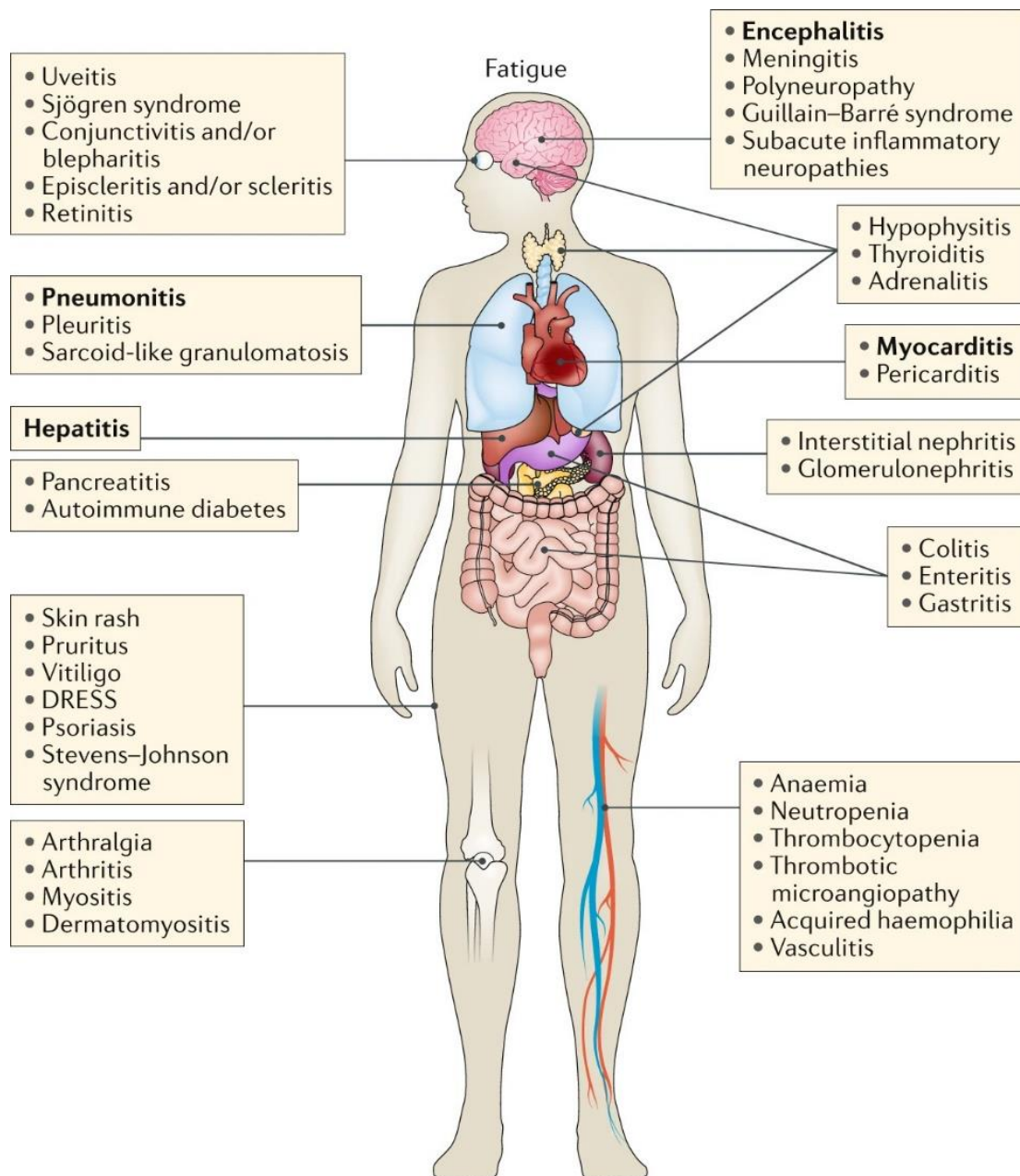
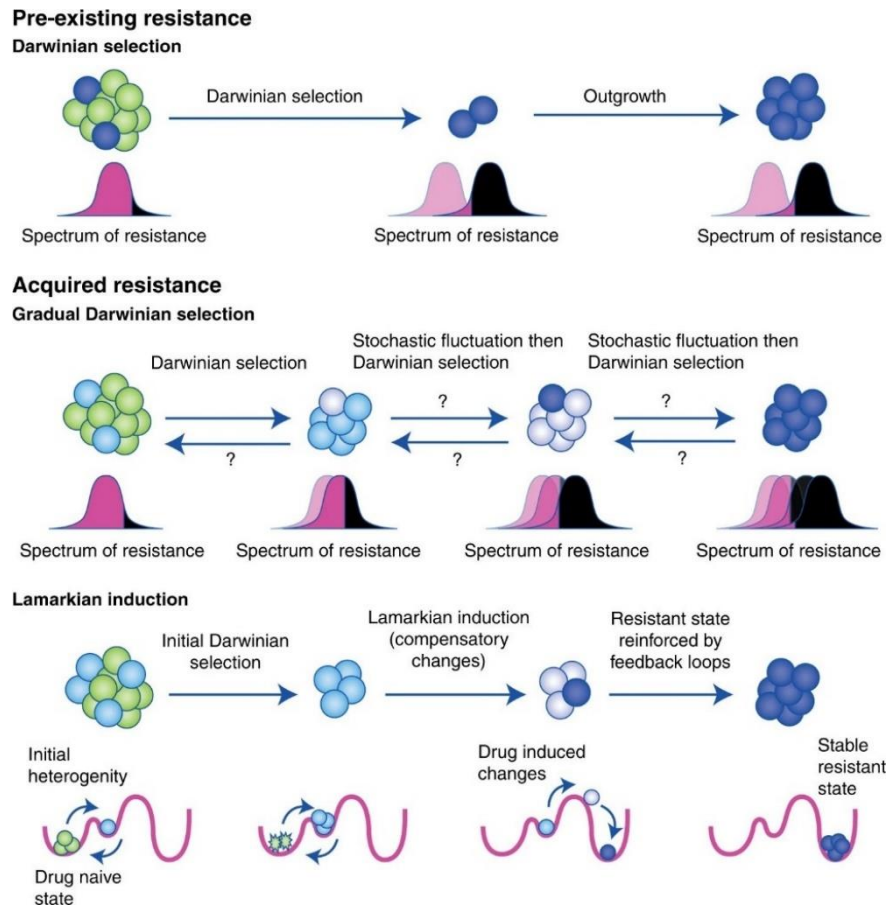


Figure 64. Immune checkpoint inhibitor associated toxicities.

From Martins et al., 2019.

al., 2014). CTLA-4 blockade by Ipilimumab showed an increase in the 3-year overall survival rate to 22 %, compared to 5 % with chemotherapy (Hodi et al., 2010; Schadendorf et al., 2015). Importantly, survival rates seemed to plateau after three years, demonstrating for the first time that long-term disease management is possible for a subset of melanoma patients through ICIs (Eggermont et al., 2019). Unfortunately however, response rates for monotherapy are only about 10 %, and autoimmune-related side effects are observed in up to 80% of patients, of which over one-third experience severe-grade toxicities such as dermatitis, encephalitis, or hepatitis (Ernst and Giubellino, 2022) (Figure 64). In 2014, two anti-PD-1 monoclonal antibodies, Pembrolizumab and Nivolumab were approved. Importantly, they displayed increased efficacy compared to Ipilimumab, with superior response rates (20-40 %), better overall survival (up to 44 %) and more durable antitumor immune activities, even in BRAF-WT tumors, while displaying reduced toxicities (Ribas et al., 2015; Robert et al., 2015, 2019; Weber et al., 2017; Hodi et al., 2018). More recently, the PD-L1 inhibitor Atezolizumab and the LAG-3 inhibitor Relatlimab were also approved (de Azevedo et al., 2021; Paik, 2022). Due to the ineffectiveness of MAPKi in BRAF-WT melanomas, these patients only receive immunotherapies, whereas ICIs followed by MAPKi constitute the preferred treatment sequence for most BRAF-mutated patients today (Atkins et al., 2023). However, in very rapidly advancing cases, MAPKi seems to be the more optimal first-line option, as clinical responses to ICIs may take longer to manifest (Kozar et al., 2019). Combining CTLA-4 and PD-1 inhibitors was shown to be effective, with less non-responders and 5-year survival rates of roughly 50 % compared to 25 % for monotherapies (Larkin et al., 2019). However, these combinations are also associated with significantly higher risks of severe toxicity, for up to 70 % of patients (Zimmer et al., 2020). This can be attenuated using drug treatment delays, glucocorticoids, and anti-TNF antibodies (Brahmer et al., 2018). The most recent clinical trials are looking at the possibility of combining MAPKi with ICIs, based on data that these might display synergistic effects, but initial results have been somewhat disappointing (Griffin et al., 2017; Yu et al., 2019; Ribas et al., 2020; Welte et al., 2022). In conclusion, although ICIs improve survival in many patients, severe toxicities limit their clinical use in a significant subset of patients (Carlini, Larkin and Long, 2021; Curti and Faries, 2021). Additionally, still less than half of patients experience complete remissions, due to intrinsic or acquired treatment insensitivities, and maximal response rates only being at roughly 50 % (Moreira et al., 2021). As such, the onset of resistances constitutes the biggest hurdle that needs to be overcome to improve clinical benefits of both targeted and immunotherapies against melanoma (Ernst and Giubellino, 2022; Knight, Karapetyan and Kirkwood, 2023).

A



B

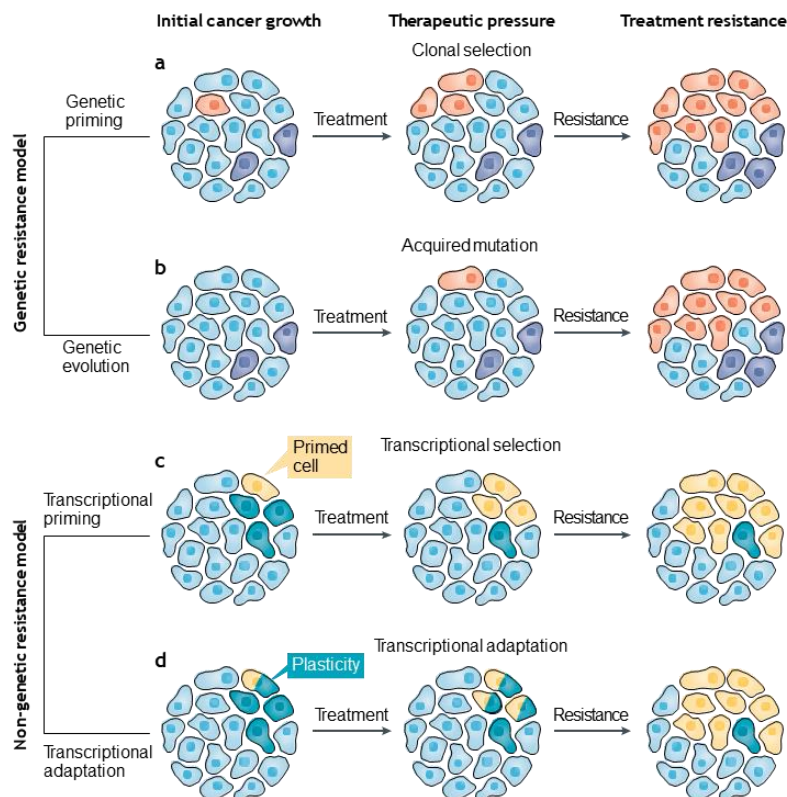


Figure 65. Intrinsic vs acquired (A) and genetic vs epigenetic (B) treatment resistances.

Adapted from Bell and Gilan, 2020; and Marine, Dawson and Dawson, 2020.

2. Mechanisms behind treatment resistance in melanoma

2.1. Different types of resistances

Therapy escape mechanisms can be broadly sub-categorized into either intrinsic or acquired and genetic or epigenetic resistances (Sharma et al., 2017; Marin-Bejar et al., 2021; Emran et al., 2022). Intrinsic resistance indicates a pre-existing drug-insensitive state, caused by either genetic or epigenetic mechanisms, that concerns the entire cancer cell population or only a subset thereof, which then becomes enriched due to Darwinian selection through drug exposure (Figure 65A). In most cases, this happens because of the absence of the targeted mutation or the independence regarding the inhibited pathway (Bagrodia, Smeal and Abraham, 2012; Kalbasi and Ribas, 2020). On the contrary, acquired resistance refers to cancer cells that initially respond to the drug, but which can over time adapt to become insensitive. This can happen through a stepwise selection for gradually more resistant cells that have an increasingly stable genetically or epigenetically mediated resistance profile, from a starting pool in which some rare cells are more drug-refractory in a stochastic and dynamically fluctuating manner (Kelderman, Schumacher and Haanen, 2014; Bell and Gilan, 2020). On the other hand, in highly plastic cancers such as in melanoma, an initially sensitive subpopulation can adapt, in a Lamarckian fashion, via epigenetic changes in response to drug treatments, which result in the cells acquiring a new cell state through phenotype switching (Rebecca and Herlyn, 2020; Rubanov, Berico and Hernando, 2022). As such, genetic resistance mainly relies on mutations that either pre-exist the drug treatment or are acquired during it (Van Allen et al., 2014) (Figure 65B). Non-mutational/epigenetic mechanisms allow for phenotypic heterogeneity, with certain cells expressing specific transcriptional programs providing increased resistance. These cell states can either be already present before the therapy or be induced by drug exposure (Marine, Dawson and Dawson, 2020; Boumahdi and de Sauvage, 2020; Shi et al., 2023). Over the last decades, many different either intrinsic, acquired, genetic, or epigenetic resistance mechanisms have been identified (Shen, Vagner and Robert, 2020), which are utilized by melanoma cells to evade therapies. Hereinafter, a concise overview of the well-characterized escape mechanisms is given. However, it is essential to keep in mind their varied nature, as phenomena such as drug efflux pumps (Chen et al., 2009), autophagy (Mgrditchian et al., 2017), antioxidant or detoxification enzymes (Pizzimenti et al., 2021), cell-death signaling deregulations (Hartman, 2020) cell-environment remodeling (Brighton et al., 2018), or cytoskeleton changes (Orgaz and Sanz-Moreno, 2020) can also be implicated.

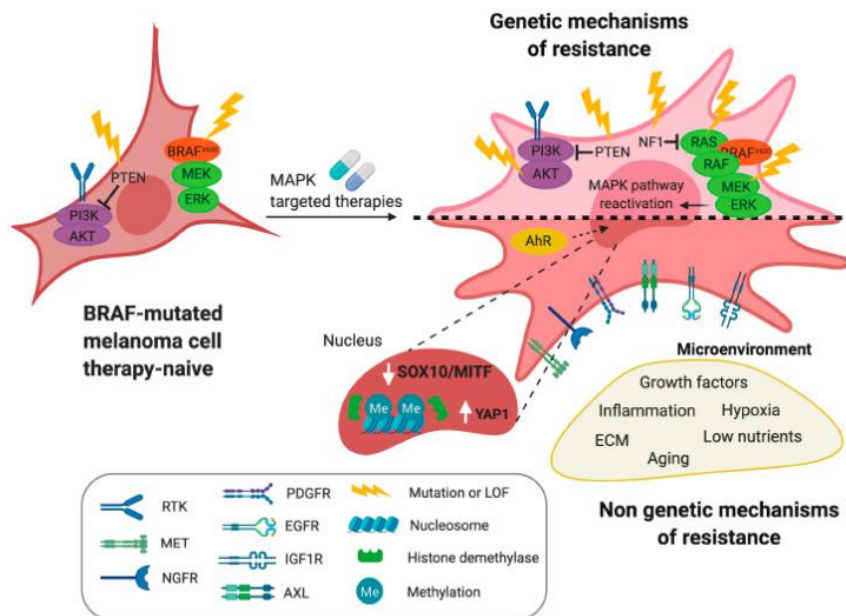
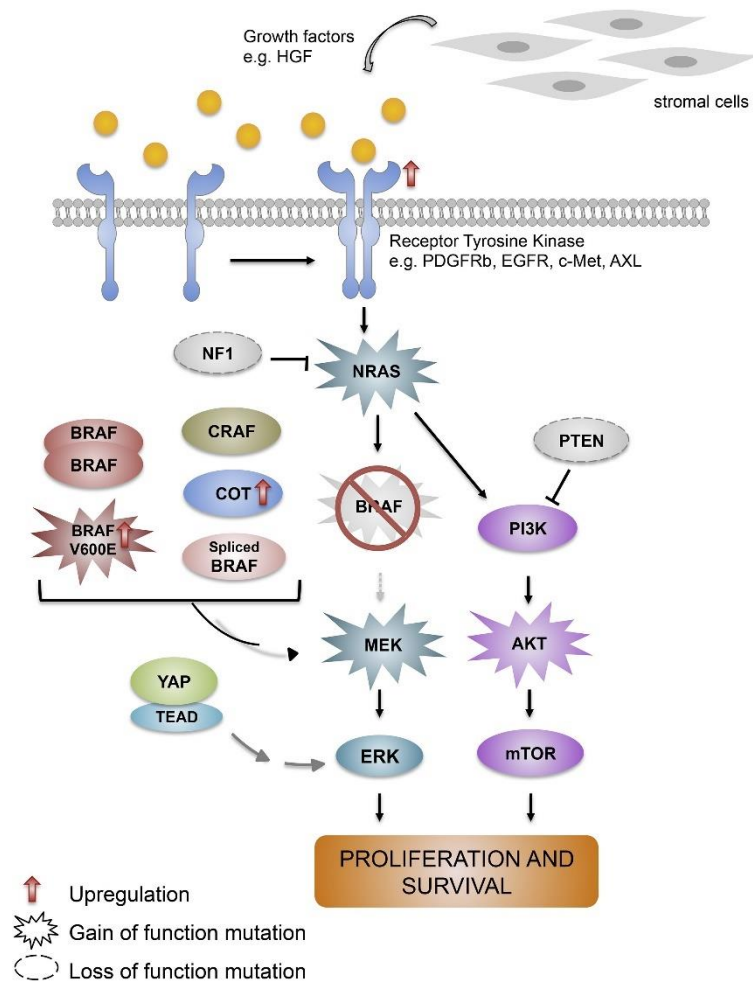


Figure 66. Common mechanisms of resistance to targeted therapies.

From Kozar et al., 2019; and Diazzi, Tartare-Deckert and Deckert, 2020.

2.2. Resistance to targeted therapy

Intrinsic resistance to BRAF inhibition is observed in 50 % of patients with BRAF-mutant melanoma, mainly because of the pre-existence of additional alterations in genes such as *GNAQ*, *PTEN*, *NF1*, *RAC*, *AKT*, or *RB* (Gibney and Smalley, 2013; Turajlic et al., 2014; Watson et al., 2014; Roesch, 2015). These hyper-activate the MAPK and/or the PI3K pathways independently of the BRAFV600E mutation, which is also possible by action of the TME. CAFs were shown to heavily secrete HGF, which stimulates these two pathways as well (Straussman et al., 2012). Regarding acquired resistance towards MAPKi, analyses of tumors from relapsed patients revealed that in 80 % of cases, resistance was due to reactivation of the MAPK pathway through several mechanisms (Moriceau et al., 2015; Lim, Menzies and Rizos, 2017; Kozar et al., 2019) (Figure 66). Additional mutations in MAPK effectors such as BRAF, NRAS, MEK and NF1 (Dietrich et al., 2018), BRAF splice variants (Vido et al., 2018), overexpression of RAF isoforms (Doudican and Orlow, 2017) or of other activators of MAPK signaling such as COT (Gruosso et al., 2015), can all lead to sustained ERK signaling. Additionally, melanoma cells can activate alternative signaling pathways to bypass the MAPK pathway and promote survival and growth, with the PI3K/AKT/mTOR pathway being usually found activated in drug-resistant melanomas (Shi et al., 2014). This happens through the loss-of-function of tumor suppressors such as PTEN, or by the activation of RTKs such as EGFR or AXL (Sun et al., 2014; Cesi et al., 2018; Irvine et al., 2018; Zuo et al., 2018).

Although MAPKi leads in many cases to significant initial melanoma tumor shrinking, a small residual subpopulation of resistant cells, which are referred to as “minimal residual disease” (MRD), remain viable upon drug exposure, and cause subsequent relapse (Marin-Bejar et al., 2021; Smith, Sheppard and McArthur, 2021) (Figure 67). Whereas this MRD can be due to mutational mechanisms outlined above, various studies have shown that relapse can happen without genetic alterations, and rather depend on non-mutational cell state heterogeneity (Shaffer et al., 2017). Single-cell analyses of melanoma MRD performed by Rambow et al. in 2018 have shown that phenotypic heterogeneity already present in therapy-naïve tumors is exacerbated upon the treatment with MAPKi, as pre-existing resistant cell states are selectively enriched, or new cell states emerge by phenotype switching. While the melanocytic cells, constituting the bulk of the tumor mass, are susceptible to MAPKi effects, a subset of these cells initially switch to the starved melanoma (SMC) state through drug-induced metabolic, translational, and transcriptional reprogramming, driven by ATF4-dependent stress signaling (Roesch et al., 2013; Liguoro et al., 2020; Oren et al., 2021; Yang

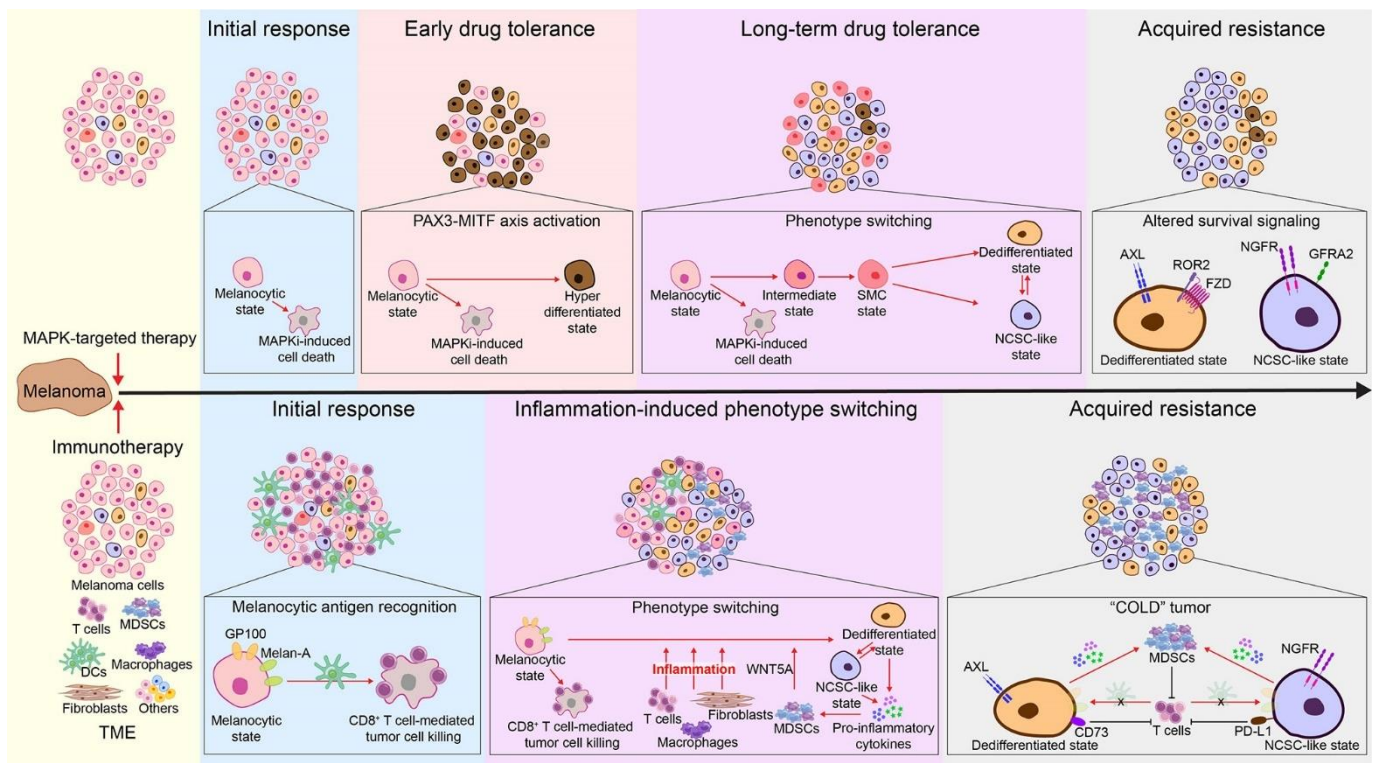
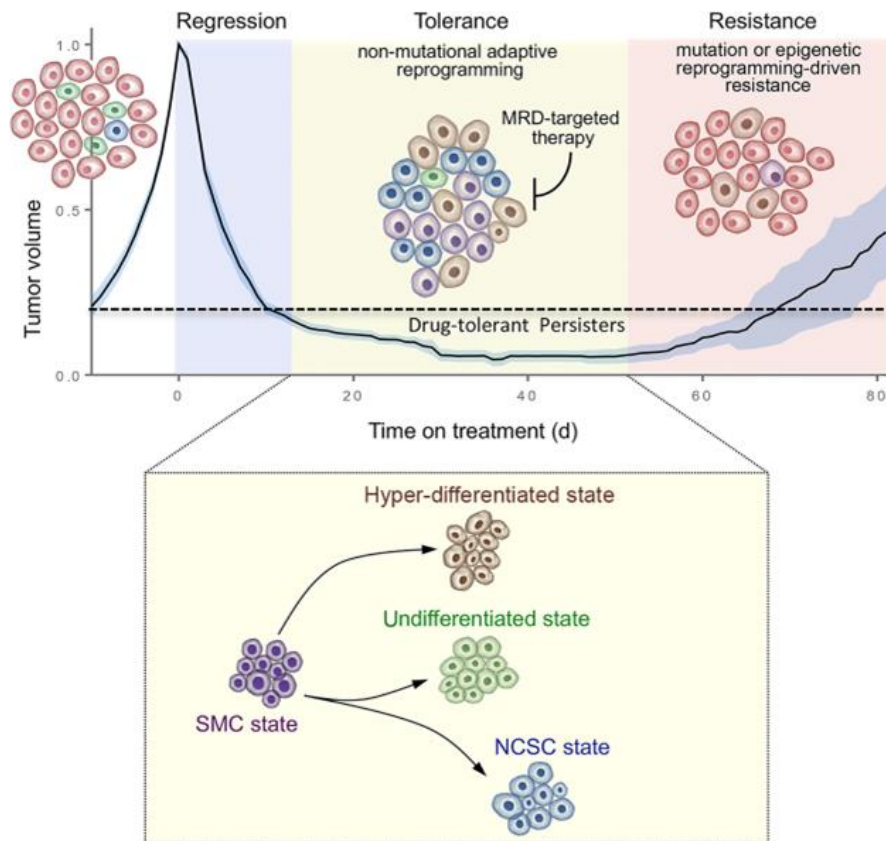


Figure 67. Minimal Residual Disease (MRD) and associated phenotype plasticity.

Adapted from Rambow, Marine and Goding, 2019; and Huang et al., 2021.

et al., 2021; Hossain and Eccles, 2023). This is mediated among other mechanisms by increased ROS presence (Cesi et al., 2017), fatty acid oxidation and CD36 expression (Aloia et al., 2019), and MITF modulation through abrogated ERK signaling (Haq et al., 2013; Smith et al., 2019). Starting from the highly adaptable SMC state, cells can either differentiate into pigmented cells or dedifferentiate into undifferentiated or NCSC-like cells (Pillai et al., 2022). During early drug tolerance, the switch to the pigmented state seems more favorable, as a PAX3-MITF-*PGC1 α* axis allows for hyperactivated MITF and reduced apoptotic signaling, thus representing an immediate survival advantage in these cells (Rose et al., 2016; Smith et al., 2016). Additionally, heightened melanosome production might allow for the sequestration of drugs (Chen et al., 2006). Longer-term drug resistance was however shown to be rather mediated by cell dedifferentiation into particularly the NCSC-like state during prolonged MAPKi treatment, through mechanisms including oxidative stress and FAK signaling (Hugo et al., 2015; Su et al., 2017; Tsoi et al., 2018; Marin-Bejar et al., 2021). These cells express increased levels of RTKs such as AXL, EGFR, or NGFR, allowing them to bypass MAPK signaling, as well as displaying other stem-like features permitting MAPKi resistance (Konieczkowski et al., 2014; Müller et al., 2014; Dugo et al., 2015; Fallahi-Sichani et al., 2017). Collectively, the intrinsically resistant cell states can emerge concomitantly during tumor adaptation and display far lower proliferation rates than sensitive melanocytic cells and are thereby less affected by the cytostatic effects of MAPKi (Ahn, Chatterjee and Eccles, 2017; Perego et al., 2018). Additionally, they seem to rely on multiple survival pathways rather than depending mostly on MAPK signaling (Arozarena and Wellbrock, 2017; Guo, Wang, and Li, 2021). Consequently, resistant cell states become gradually enriched and thus, at the relapse stage, melanomas tend to display decreased MITF/SOX10/PAX3 expression while increasing AP-1/TEAD-driven gene signatures, including a predominant expression of AXL and NGFR (Shaffer et al., 2017; Boshuizen et al., 2018). Importantly, drug-induced phenotype switching can happen in parallel with mutational resistance mechanisms (Marin-Bejar et al., 2021). Furthermore, recent data indicates that acquired MAPKi resistance can cause an immune-evasive TME and cross-resistance to immunotherapies (Haas et al., 2021).

2.3. Resistance to immunotherapies

Compared to MAPKi, the mechanistic underpinnings of ICI resistance remain less well understood, but so-called ‘cold’, less-inflamed, and immune cell-desert tumors show weaker responses to immunotherapies (Sharma et al., 2017; Bonaventura et al., 2019). In recent years,

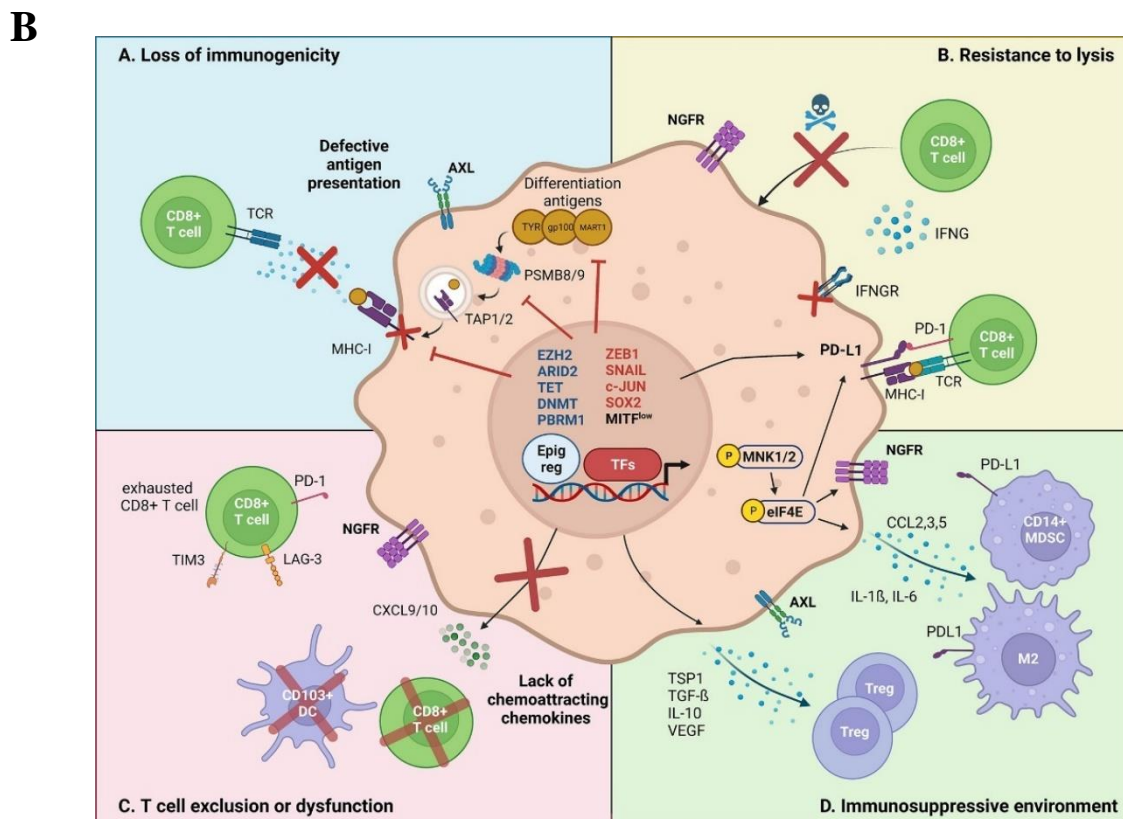
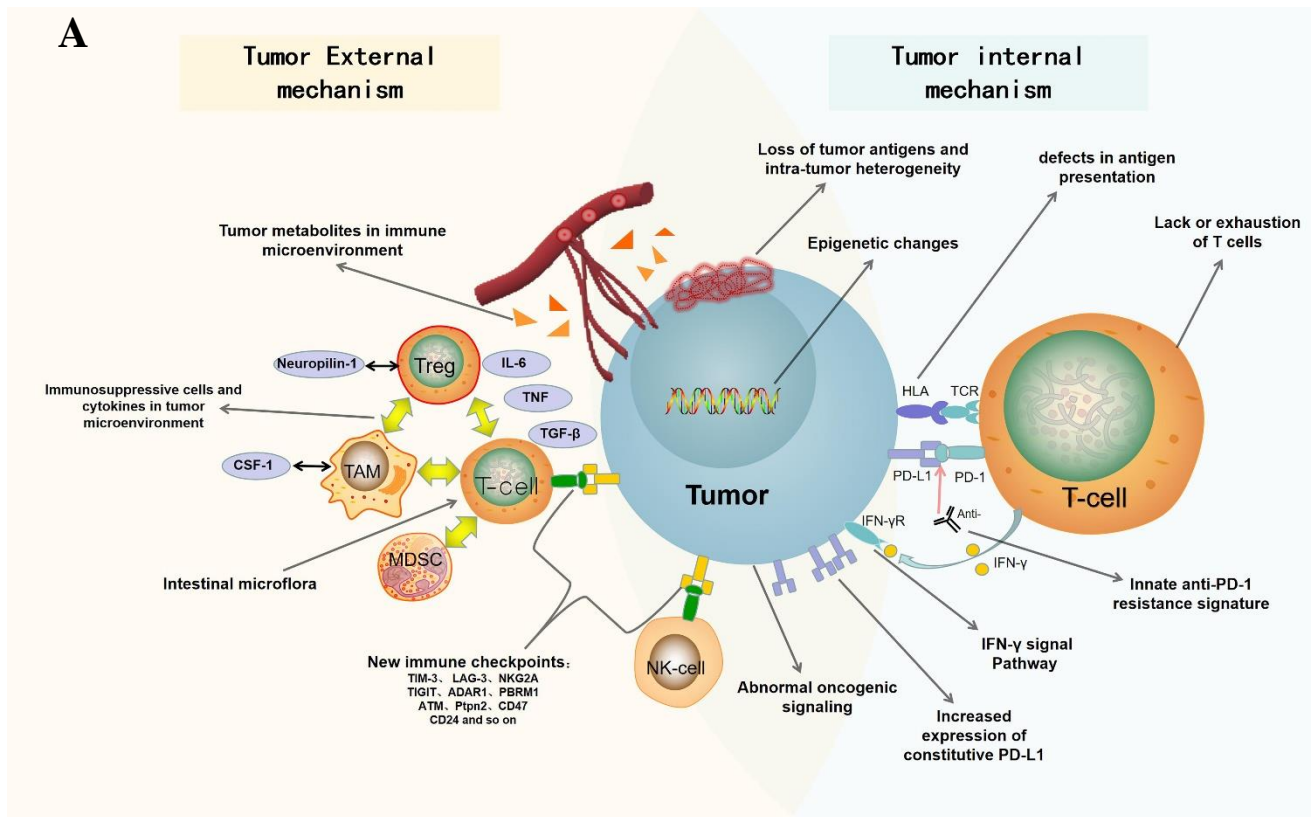


Figure 68. ICI resistance mechanisms (A) and associated dedifferentiation (B).

From Huang et al., 2020; and Benboubker et al., 2022.

several characteristics of these cold tumors have been elucidated (Huang et al., 2020; Benboubker et al., 2022; Thornton et al., 2022; Lim et al., 2023) (Figure 68A). They tend to display lower mutational burdens and thus reduced tumor antigen presentation (Ning et al., 2022), which can also be due to MHC polymorphisms and mutations, or because of alterations in JAK/STAT signaling effectors (Zaretsky et al., 2016; Shin et al., 2017; Chowell et al., 2018). Other pathways can be found to be abnormally activated and hindering the anti-tumor immune response. Wnt/ β -Catenin signaling was shown to favor T-cell exclusion (Spranger, Bao and Gajewski, 2015; Spranger et al., 2017), and loss of PTEN and subsequently elevated PI3K signaling results in increased immunosuppressive cytokine release (Trujillo et al., 2019). While initially favoring anti-tumor immunity, chronic IFN γ exposure leads to T-cell depletion and immunosuppression while transcriptomically reprogramming cancer cells toward ICI resistance (Benci et al., 2016, 2019; Grasso et al., 2020). Constitutive overexpression of PD-1/PD-L1 and CTLA-4 (Kataoka et al., 2016; Xie et al., 2019) or expression of new immune checkpoints such as LAG-3 or TIGIT, either by melanoma cells, their released vesicles, or other immune cells, have also been implicated in treatment insensitivity (Lui and Davis, 2018; Zhang et al., 2018; Andrews, Yano and Vignali, 2019). Finally, melanoma cells can evade immune destruction by recruiting immunosuppressive cells such as regulatory T-cells (Huang et al., 2021), or by the release of immunosuppressive cytokines, including TGF- β (Mariathasan et al., 2018; Batlle and Massagué, 2019) and IL-6 (Tsukamoto et al., 2018; Chan et al., 2019).

Of note, these cytokines and associated chronic inflammation have been implicated in inflammation-induced phenotype switching of melanoma cells into dedifferentiated or NCSC-like states (Landsberg et al., 2012; Arozarena and Wellbrock, 2019; Huang et al., 2021), through down-regulation of MITF and activation of AP-1/BRN2 signaling (Pierrat et al., 2012; Riesenberger et al., 2015; Qiao et al., 2016; Hamm et al., 2021). As such, initially hot melanoma tumors, mainly consisting of melanocytic cells displaying the melanoma-specific MLANA and gp100 antigens, are efficiently eliminated by immunotherapy and associated elevated T-cell function and inflammation. However, such as in MAPKi resistance, an MRD enriched in invasive cell types through chronic inflammation can persist and eventually expand, leading to the emergence of a cold tumor and eventual relapse (Mehta et al., 2018; Tsoi et al., 2018; Boshuizen et al., 2020; Liu et al., 2021; Patel et al., 2023) (Figure 67). Notably, the invasive melanoma gene signature (Verfaillie et al., 2015) displays important overlaps with the innate anti-PD-1 resistance signature (IPRES) described by Hugo et al. in 2016. Several mechanisms allow for more dedifferentiated melanoma cells to be less sensitive toward ICIs (Huang et al., 2021; Benboubker et al., 2022) (Figure 68B), including loss of melanoma antigen presentation

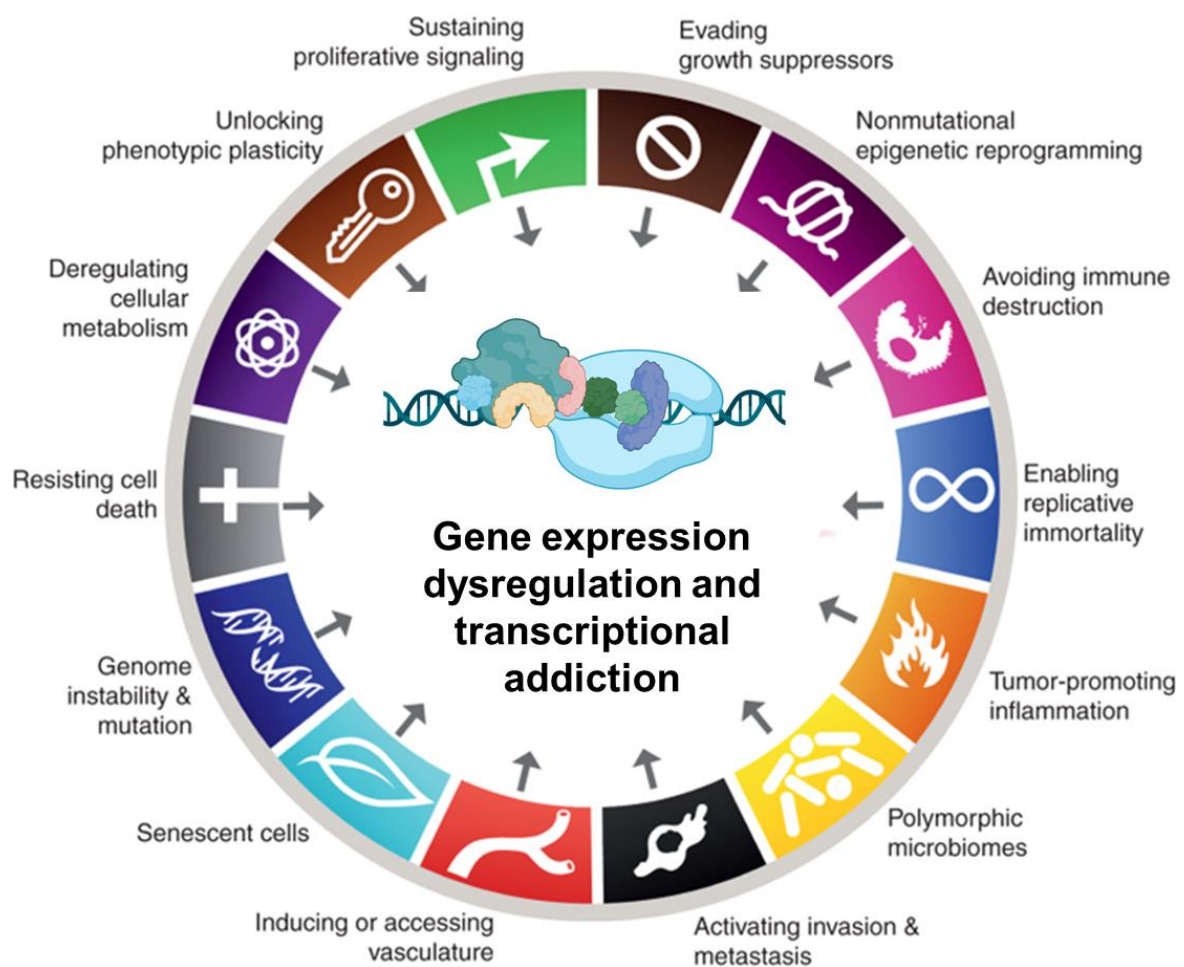
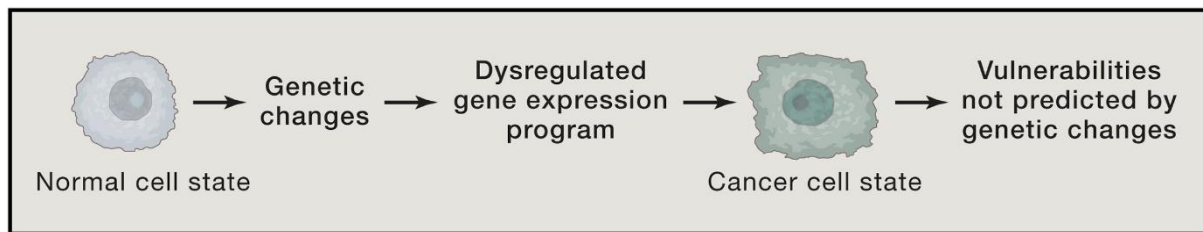


Figure 69. Transcriptional dysregulation in melanoma cells and their addiction to it as fundamental drivers of the malignant hallmarks of cancer.

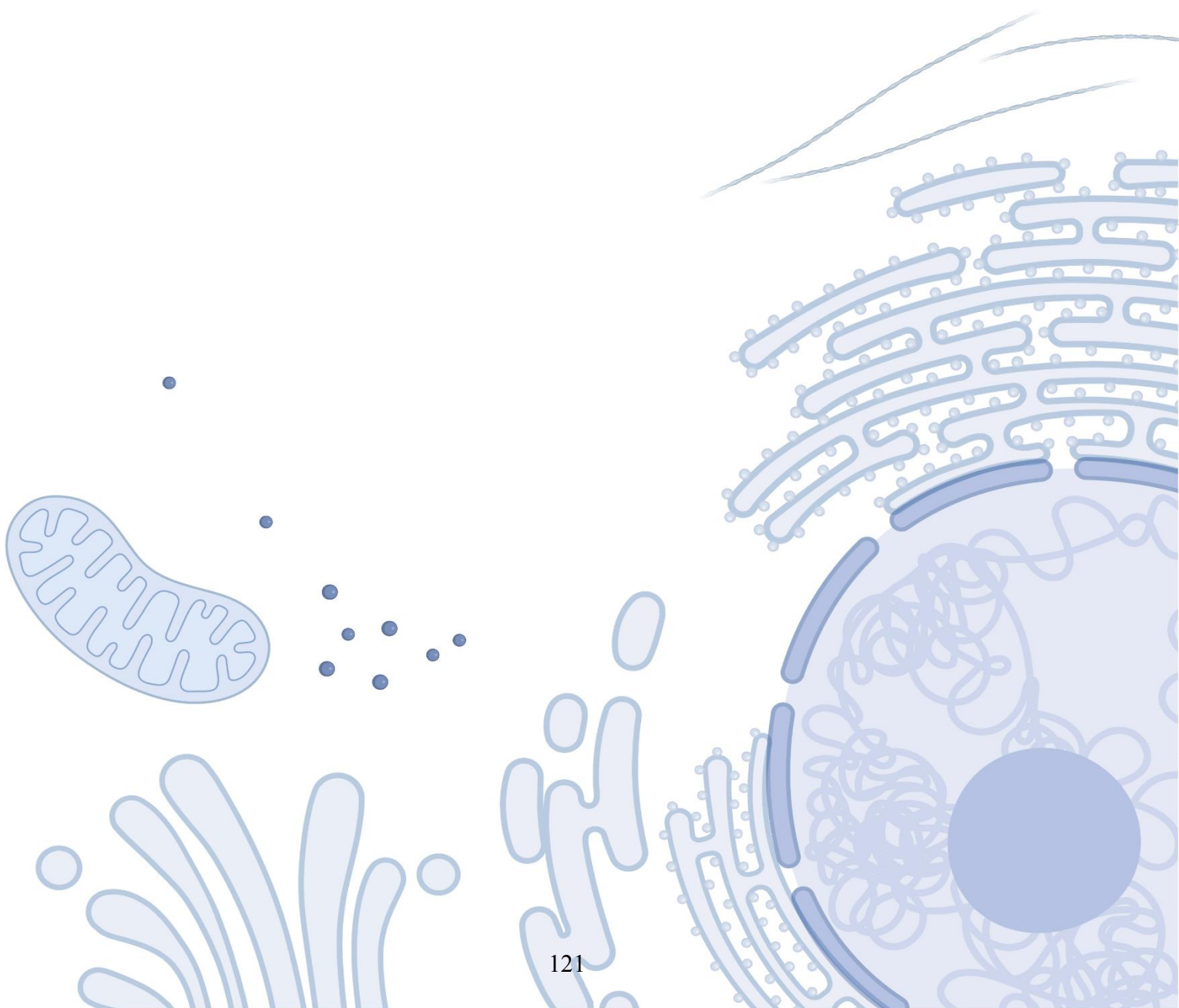
Adapted from Bradner, Hnisz and Young, 2017; and Hanahan, 2022.

(Mehta et al., 2018; Lee et al., 2020), upregulated immune checkpoint expression (Cerezo et al., 2018; Lequeux et al., 2019), increased cytotoxicity resistance (Huelgo-Zapico et al., 2018; Wu et al., 2020; Cheli et al., 2021), the establishment of an immunosuppressive cellular and cytokine environment (Ouzounova et al., 2017; Douglass et al., 2021; Huang et al., 2021), and associated T-cell dysfunction (Boshuizen et al., 2020; Plaschka et al., 2022). Importantly, one of the major research areas in recent years has been to elucidate how to reprogram the TIME to transform cold tumors back into hot ones, thus rendering them more sensitive to ICIs (Noman et al., 2020, 2022; Lequeux et al., 2021).

3. Potential prospects and future treatments

Although revolutionary advances have been made in recent years to improve the management of metastatic melanoma, clinical benefits are still only measured in months rather than in years for over half of patients (Knight, Karapetyan and Kirkwood, 2023; Pawlik, Morgenroth and Dummer, 2023). The major problem of treatment resistances underlines the urgent need for novel therapeutics which could ideally target different driver mutations as well as different melanoma cell states. Substantial progress is being made to improve targeted and immunotherapies (Xiao et al., 2018; Margue et al., 2019; Janji and Chouaib, 2021; Randic et al., 2021), and the inhibition of specific therapeutic vulnerabilities of the different melanoma cell states could wield potential clinical benefit, such as using RXR antagonists against NCSC-like melanoma cells (Rambow, Marine and Goding, 2019). Of note, interest and expertise concerning mRNA vaccines have been greatly accelerated by the recent COVID-19 pandemic, with far-reaching implications for immunogenic cancers like melanoma. Vaccines encoding various melanoma-specific antigens such as gp100 or TYR, to prime and induce host immune responses, are currently being assessed in clinical trials (Lorentzen et al., 2022; Bafaloukos et al., 2023). Additionally, another paradigm shift has emerged in cancer research in recent years. Novel insights into the pervasive role of gene expression dysregulation in virtually every aspect of cancer pathogenesis have led to the emerging concept of ‘transcriptional addiction’, which posits that the acquired dependencies on these dysregulations might be leveraged as cancer cell liabilities (Bradner, Hnisz and Young, 2017) (Figure 69). In neoplasms of a highly plastic nature such as melanoma, where every cell state seems to be highly dependent on specific gene expression programs, the inhibition of the transcriptional machinery and its associated regulators is coming into view as an attractive target of a potential new generation of drugs.

Section II: Gene expression, its dysregulation in cancer, and targeting transcriptional addiction



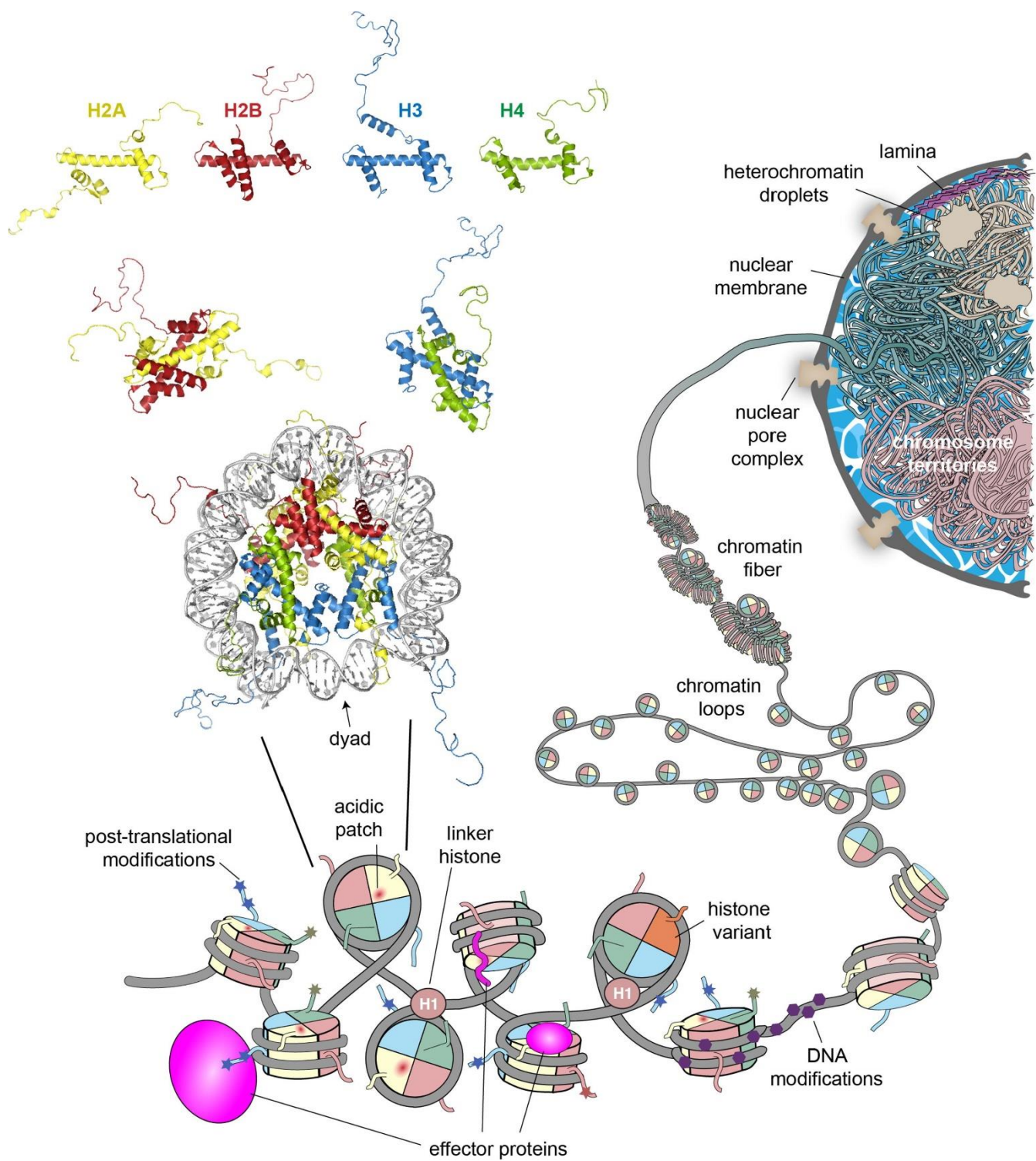


Figure 70. Nucleosome and chromatin organization.

From van Emmerik and van Ingen, 2019.

A. Transcription and its regulation

1) Genome architecture and regulatory elements of transcription

1.1. The importance of gene expression regulation and chromatin condensation

One of the most perplexing features of higher multicellular organisms, oftentimes composed of hundreds of functionally and morphologically different cell types, is the fact that this complexity can be linearly traced back to a single cell, the fertilized egg. The genetic information required for the development and maintenance of the human organism resides within genomic DNA, in the approximately 20,000 genes of the genome. As all cells in an organism contain mostly accurate copies of the genome of the initially fertilized egg, the question of how such complex cellular diversity can arise from the same genetic template has puzzled biologists for the largest part of the 20th century (Roeder, 2019). The answer that has emerged over the last 50 years lies in the fact that while different cell types, such as melanocytes or neurons, are for the most part genetically identical (in terms of DNA sequences), there is a finely regulated selective reading of the genome, as not all genes are used by a cell all of the time (Levine and Tjian, 2003; Haberle and Stark, 2018). This is made possible by the fact that the genetic information includes both protein-coding sequences of genes and as well as non-coding regulatory elements that govern when, where and to what level a given gene is expressed. As such, well-regulated gene expression is essential in cell differentiation, identity and function, and its disruption leads to diseases such as cancers (Bradner, Hnisz and Young, 2017).

Transcription is executed by RNA polymerase enzymes, which must gain access to so-called promoter regions located at the beginning of genes in order to synthesize RNA from the DNA template, acting as a blueprint to build functional proteins (Fuda, Ardehali and Lis, 2009). In basal conditions however, DNA access is often sterically limited by the condensation of chromatin (Cramer, 2019). Indeed, for the genome to fit into the limiting space of a human cell nucleus, with a diameter of 5 to 20 μm (Lammerding, 2011), the genetic material, consisting of around 2 m of DNA, needs to be compacted. Nevertheless, this nuclear condensation of DNA and associated proteins, the so-called chromatin, must be dynamically flexible enough for the correct genes to be accessible to the transcription machinery at the appropriate moments and in the proper tissues and cell types (Kim and Shendure, 2019). In 1884, the negatively

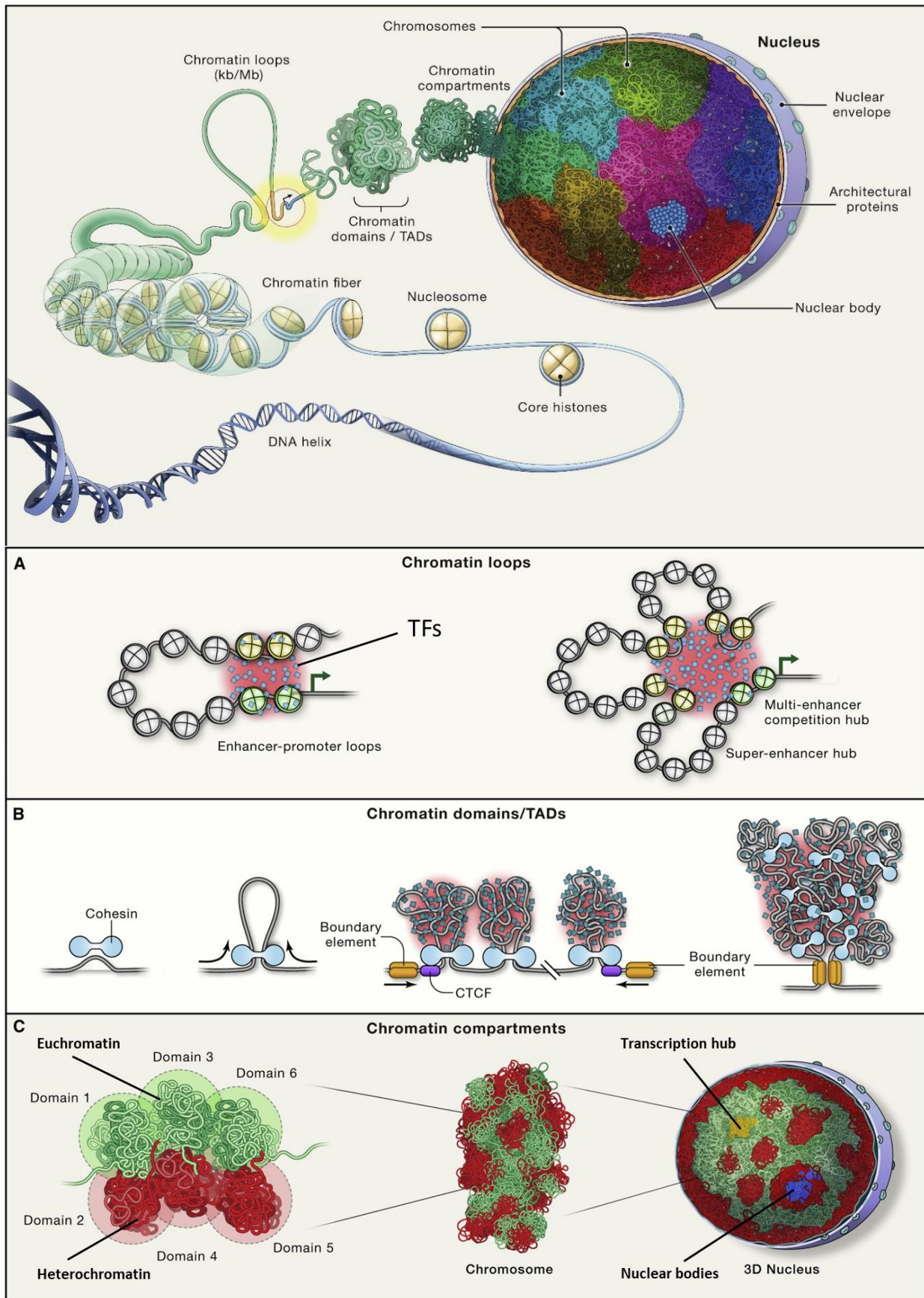


Figure 71. Higher-order chromatin organization.

Adapted from Misteli, 2020.

charged DNA was found to be associated with small, positively charged nuclear proteins named histones (Dhall and Chatterjee, 2011), which together form the primary and repeating unit of chromatin: the nucleosome (Kornberg and Thomas, 1974). The nucleosome consists of 147 DNA base pairs (bp) wrapped around an octamer containing two copies of each of the four core histones: H2A, H2B, H3, and H4 (Felsenfeld and Groudine, 2003; McGinty and Tan, 2015) (Figure 70). Small sections of nucleosome-free DNA of 20-90 bp join the nucleosomes together, leading to the ‘beads-on-a-string’ structure of the chromatin fiber, with the linker histone H1 sealing and stabilizing DNA at the nucleosome entry and exit sites (Kim and Shendure, 2019; Maeshima, Ide and Babokhov, 2019). From this basic conformation, chromatin is organized into higher-order structures such as loops, domains, and compartments (Misteli, 2020) (Figure 71).

The chromatin fiber can auto-interact to form loops of various sizes, spanning from Kbs to Mbs, with fundamental importance for gene transcription and chromatin compaction (Dekker and Misteli, 2015; Vermunt, Zhang and Blobel, 2019). Smaller loops (10 to several hundred kb) usually mediate the proximity and interactions of regulatory transcription elements, called enhancers or silencers, with gene promoters (Figure 71), thus allowing for gene expression activation or repression, as will be discussed later. Bigger loops of up to Mbs in length contribute to the formation of chromatin domains, also called topologically associating domains (TADs), which are defined as genome regions that interact preferentially with each other rather than with their surrounding sequences (Dixon et al., 2012; Dekker and Mirny, 2016; Rowley and Corces, 2018; Misteli, 2020). Inside these TADs, internal loops occur, supporting the notion of local co-regulation: genes found inside TADs are preferentially regulated by elements also inside these TADs. These are formed by loop-extrusion mechanisms, in which the cohesin protein allows for the formation of chromatin loops via its motor activity (Fudenberg et al., 2016). As such, cohesion generates chromatin contacts and allows for intermingling within TADs. The outer extremities of the TADs are defined by the presence of the architectural chromatin protein CTCF, which prevents inter-TAD contacts by setting strict boundaries (also known as TAD insulation), thus restricting the influence of outside regulatory elements on genes within the domain (Hsieh et al., 2020; Krietenstein et al., 2020).

Together, multiple chromatin domains/TADs coalesce into one of two distinct spatially segregated chromatin compartments (Dekker and Mirny, 2016; Rowley and Corces, 2018) (Figure 71). These two distinct compartments represent on one side the transcriptionally active, less condensed, and therefore RNA polymerase-accessible euchromatin, and on the other hand,

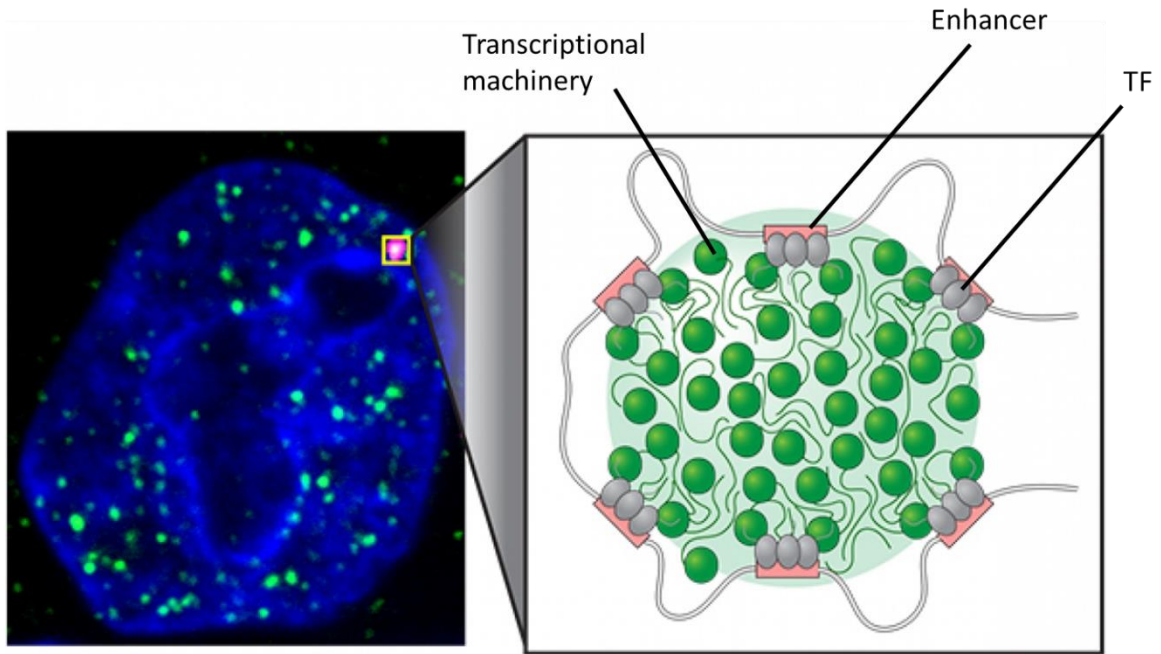
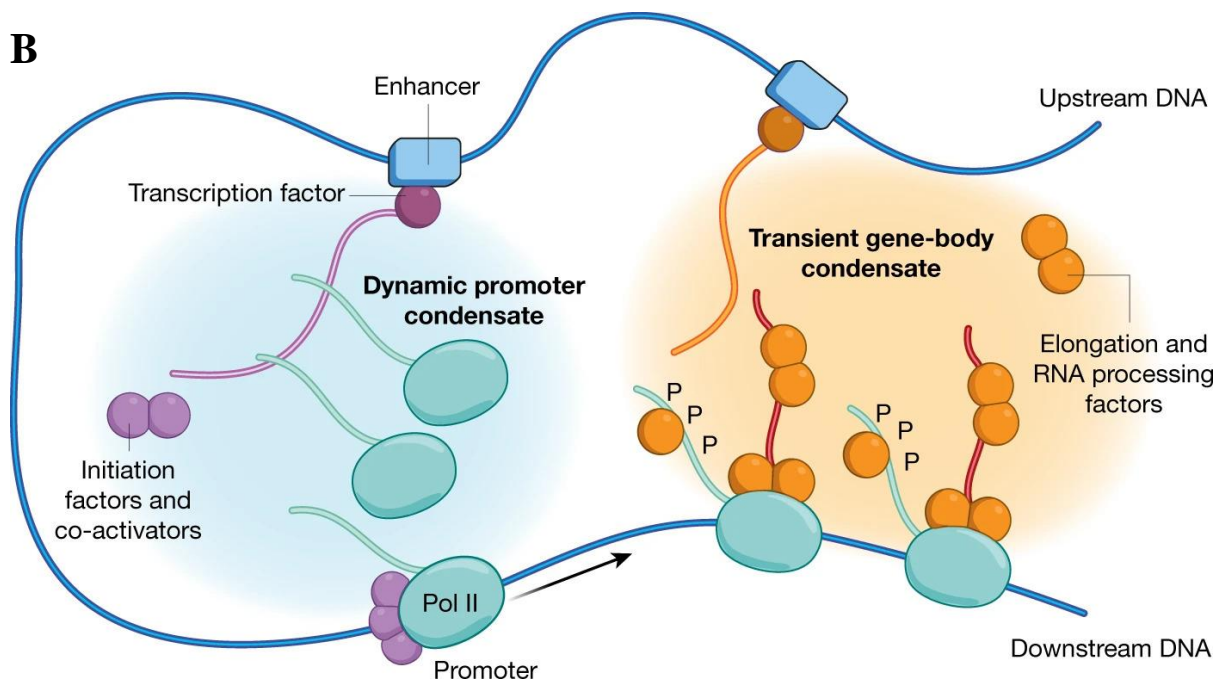
A**B**

Figure 72. Transcription condensates (or factories/hubs). Cell stained for components of the transcriptional machinery (Mediator subunit MED1 and coactivator BRD4 in green), showing the clustered nature of gene expression in the nucleus (A). Condensate-based model of transcription (B). Adapted from Sabari et al., 2018; and Cramer, 2019.

heterochromatin with silenced gene expression due to a more condensed state (Lieberman-Aiden et al., 2009; Fraser et al., 2015; Wang et al., 2016). During interphase, chromatin fibers from a given chromosome are not dispersed throughout the whole volume of the nucleus, but are restricted to a compact, spatially restricted area, called the chromosome territory (Cremer and Cremer, 2010). Importantly, the 3D organization of chromatin and the positioning of a specific TAD or gene locus within a nucleus is highly coordinated and non-random. As such, inactive genes and heterochromatin tend to be peripherally located near the nuclear envelope, whereas active genes and euchromatin are more frequently located toward the nuclear interior (Takizawa, Meaburn and Misteli, 2008; Crosetto and Bienko, 2020). Recent high-resolution microscopy and chromosomal conformation capture techniques have shown the existence of so-called transcription factories/hubs/condensates, which are formed by the coalescent clustering of genome regions with actively transcribing RNA polymerases, representing specific foci where intense transcriptional activity is concentrated (Hnisz et al., 2017; Chen et al., 2018; Shaban and Seeber, 2020) (Figure 72). As such, genes tend to be transcribed in clusters and not individually in a diffused manner throughout the nucleus. This allows for sharing of transcriptional machinery between multiple genes and improved gene expression efficiency (Sexton et al., 2007; Cho et al., 2016; Wei et al., 2020; Palacio and Taatjes, 2022). Additionally, proteins are also non-randomly concentrated in the nucleus into structures called nuclear bodies such as for example the nucleolus or nuclear speckles (Staněk and Fox, 2017) (Figure 71). Notably, these higher-order chromatin structures, such as transcription factories or nuclear bodies, are characterized by distinct biophysical characteristics whose importance emerged in recent years (Hnisz et al., 2017; Boija et al., 2018; Sabari et al., 2018; Lafontaine et al., 2021). Indeed, structures such as transcription factories behave like membrane-less organelles, formed through liquid–liquid phase separation by the high concentration of transcription machinery proteins such as TFs and their intrinsically disordered regions (Dignon, Best and Mittal, 2020). These protein-rich aggregated condensates, reminiscent of oil droplets in water, allow for a wide range of functions, including the enhancement of biochemical reactions (Lyon, Peebles and Rosen, 2021). As such, phase separation and condensation underlie the formation of transcription factories/hubs, which are nowadays rather called transcription condensates (Figure 72), allowing for amplified gene expression (Wei et al., 2020; Bhat, Honson and Guttman, 2021). Finally, although it is well established that chromatin organization tends to be cell type-specific, the precise molecular mechanisms behind the 3D-positioning of genes remain largely unknown and are an important topic of current research (Crosetto and Bienko, 2020; Shachar and Misteli, 2017).

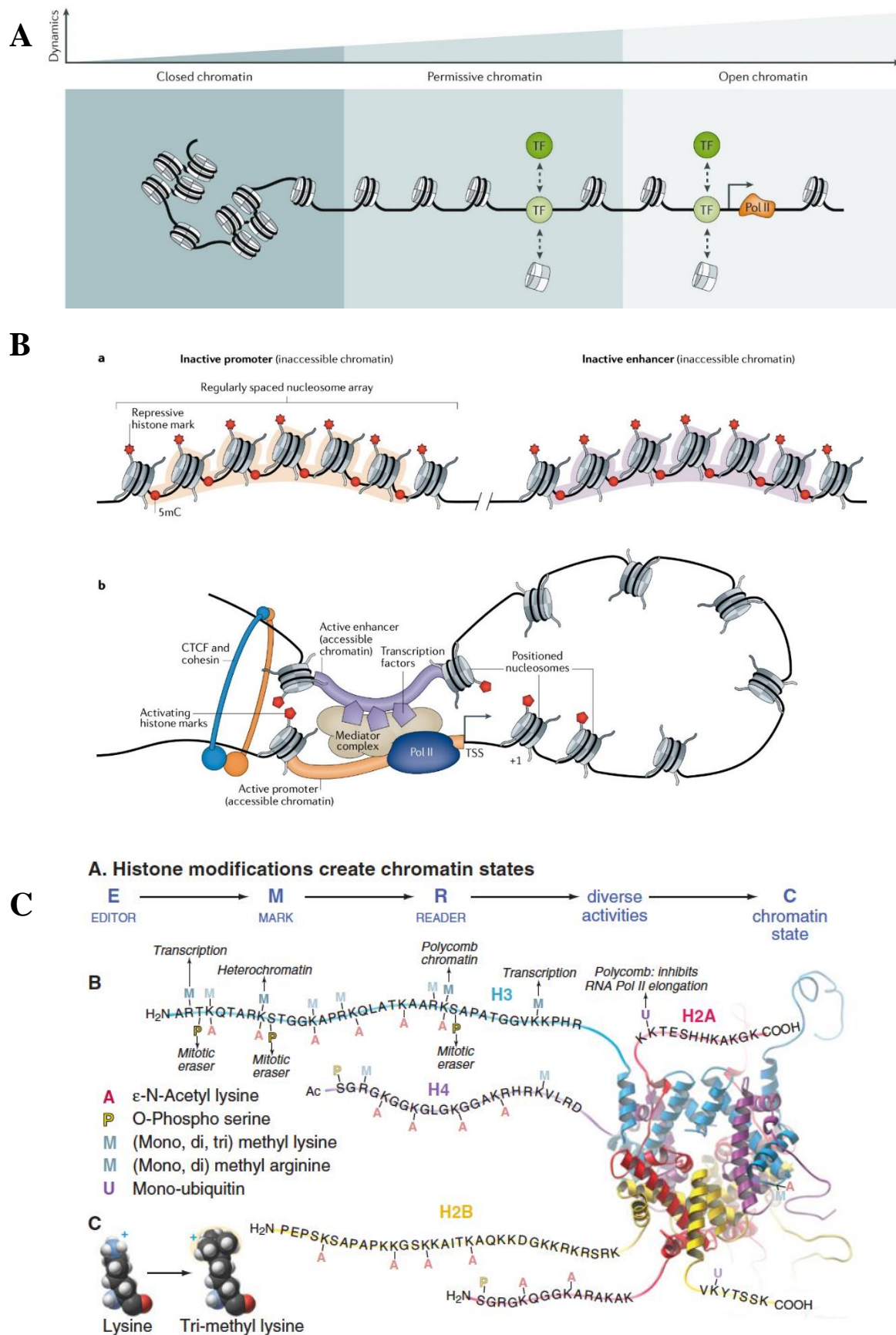


Figure 73. Chromatin accessibility and remodeling (A+B) and histone modifications (C).

From Pollard et al., 2016; Klemm, Shipony and Greenleaf, 2019; and Carter and Zhao, 2021.

1.2. Chromatin accessibility and remodeling

Within a nucleus, chromatin compaction states can range from open and hyper-accessible for the transcription machinery, through more moderate states of accessibility known as permissive chromatin, to inaccessible, very compacted and closed chromatin (Mansisidor and Risca, 2022) (Figure 73A). Open and permissive chromatin is found to be transcriptionally active and collectively represent euchromatin, whereas genes in the condensed heterochromatin are not expressed. Heterochromatin can be further subdivided into constitutive heterochromatin, which permanently silences repetitive regions in all mature cells (Lomber, Wallrath and Urrutia, 2006; Janssen, Colmenares and Karpen, 2018), and facultative heterochromatin, representing cell-type-specific compacted regions that retain their potential to switch into euchromatin under certain cues (Trojer and Reinberg, 2007; Żylicz and Heard, 2020). Of note, euchromatin includes both actively transcribed genes as well as those not being immediately expressed, but that are in a permissive state poised for transcription (Bulut-Karslioglu et al., 2018). Importantly, the physical access to DNA is a highly dynamic process, with specific facultative heterochromatin sections, harboring genes needed by the cell in a given context, becoming less compacted and thus accessible (Allshire and Madhani, 2018; Klemm, Shipony and Greenleaf, 2019). The open, accessible genome makes up for roughly 3% of the entire chromatin of a cell, however more than 90% of total bound transcription factors (TFs), proteins binding to specific regulatory DNA regions in association with cofactors, thereby activating or repressing transcription, are found in these regions (Thurman et al., 2012).

Several mechanisms allow condensed heterochromatin, displaying regularly interspaced nucleosomes, to become open euchromatin (Penagos-Puig and Furlan-Magaril, 2020; Mansisidor and Risca, 2022) (Figure 73B). Chromatin remodeling complexes such as SWI/SNF allow dynamic nucleosome shifting or eviction (Centore et al., 2020; Laurette et al., 2020). The N-terminal protruding histone tails rich in arginines and lysines can be subjected to various post-translational modifications (PTMs) by histone-modifying enzymes, forming the complex histone code (Figure 73C), which influences gene expression through two main mechanisms (Jenuwein and Allis, 2001; Fillingham and Greenblatt, 2008; Bannister and Kouzarides, 2011; Morgan and Shilatifard, 2020). First, PTMs such as acetylation modify the nucleosome's net electric charge, which alters chromatin conformation by loosening DNA-histone and histone-histone interactions. Second, specific histone readers can recognize PTMs, such as methylations, which can have repressive or activating functions. Specific chromatin states are associated with distinct histone modifications: for example, the acetylation of

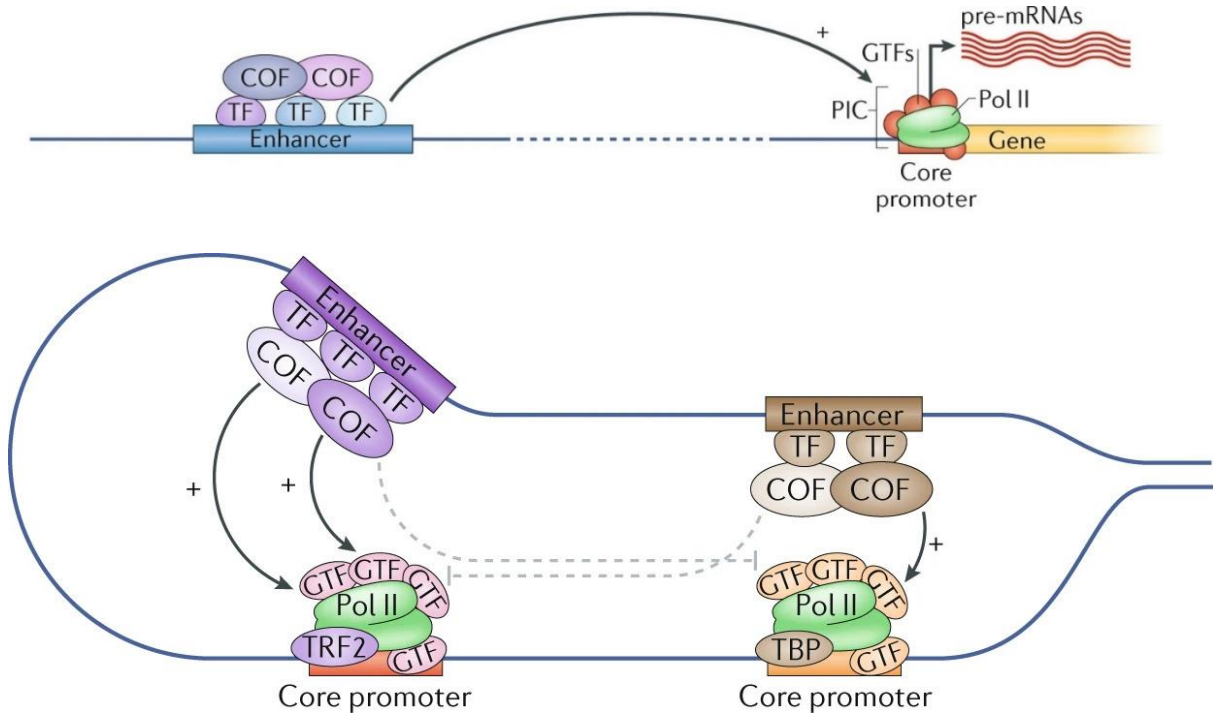


Figure 74. Properties and function of core promoters and enhancers.

Adapted from Haberle and Stark, 2018.

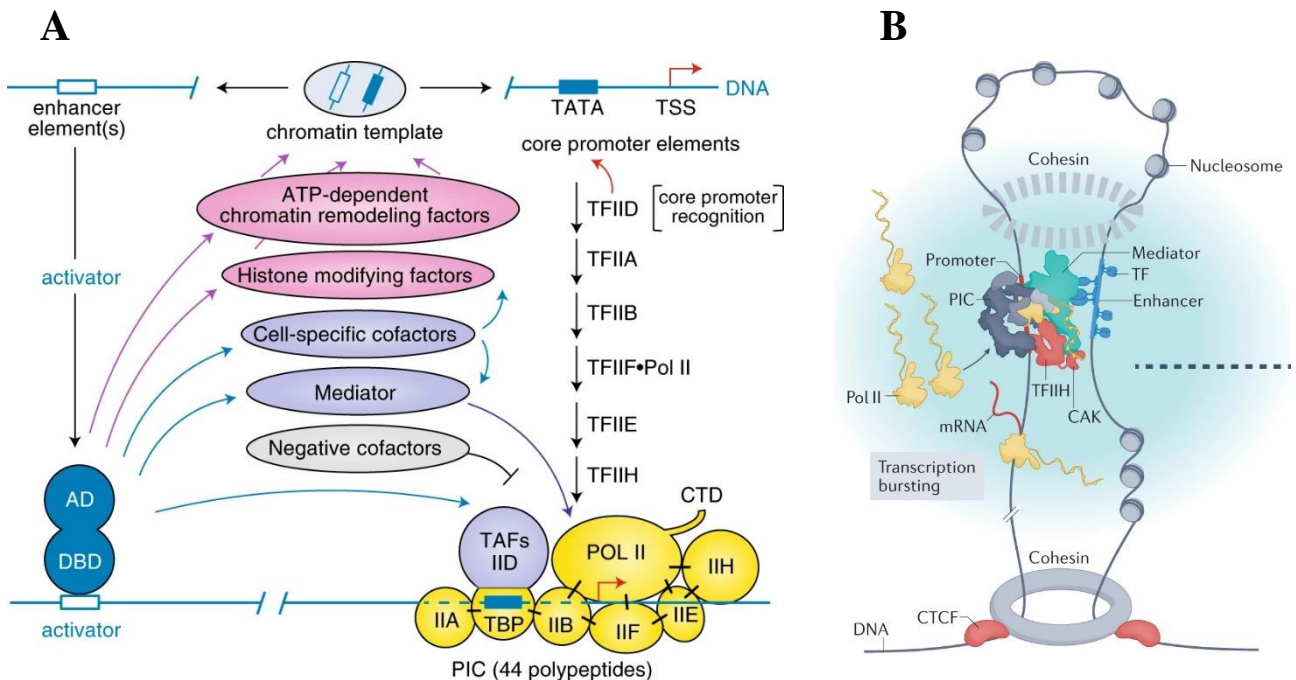


Figure 75. Regulation of PIC assembly by enhancers (A) and the function of the Mediator (B).

TAFs = TBP-associated factors. AD = TF activation domain. DBD = TF DNA binding domain. From Roeder, 2019.

lysine 27 of histone H3 (H3K27ac) is a mark of open chromatin and often associated with active gene expression, whereas constitutive heterochromatin presents high H3K9me3 deposition, and facultative heterochromatin displays high levels of H3K27me3 (Creyghton et al., 2010; Igoalkina et al., 2019; Cai et al., 2021). Other mechanisms allowing for modulating chromatin compaction levels include DNA methylation (Buitrago et al., 2021), the action of non-coding RNAs (Cernilogar et al., 2011; Dueva et al., 2019), or the incorporation of histone variants (Martire and Banaszynski, 2020).

1.3. Regulatory elements of transcription

The transcription of a gene starts at a more or less well-defined DNA position named the transcription start site (TSS), representing the location where the first DNA nucleotide is transcribed into RNA (Core et al., 2014; Kugel and Goodrich, 2017; Vo Ngoc et al., 2017). In higher organisms such as humans, different types of RNA polymerases synthesize different types of RNA, as RNA polymerase I synthesizes ribosomal RNA and RNA polymerase III synthesizes transfer and other small RNAs (Girbig, Misiaszek and Müller, 2022). However, for the sake of simplification, hereinafter only RNA polymerase II (RNAPII)-mediated gene expression is elucidated. RNAPII transcribes the totality of protein-coding genes, as well as many non-coding genes (Compe and Egly, 2021; Girbig, Misiaszek and Müller, 2022). The TSS is usually located within the core promoter of a gene, a roughly 100 bp spanning region where the transcription initiation machinery, also called the preinitiation complex (PIC), assembles (Haberle and Stark, 2018). Core promoters vary greatly in terms of DNA motif composition, functionality, and activity. For highly regulated cell-type-specific genes, a single defined and focused TSS is often observed, as well as the TATA-box motif (consensus sequence: T-A-T-A-A/TA-A/T-A/G), present in 10-15 % of core promoters, which serves as a recognition and anchor point for the PIC (Cavallini et al., 1988; Carninci et al., 2006; Müller and Tora, 2014). However, more constitutively expressed genes, such as housekeeping genes, often present core promoters with multiple dispersed TSSs and no TATA boxes. This type of core promoter is often positioned inside regions with high frequencies of CpG dinucleotide sequences, so-called ‘CpG islands’, spanning up to 1000 bp and associated with a more accessible chromatin conformation (Fenouil et al., 2012; Compe and Egly, 2021). Within these CpG-island promoters, certain types of motives such as initiator (Inr) or downstream promoter element (DPE) can be recognized by the transcription machinery (Smale and Baltimore, 1989; Landolin et al., 2010).

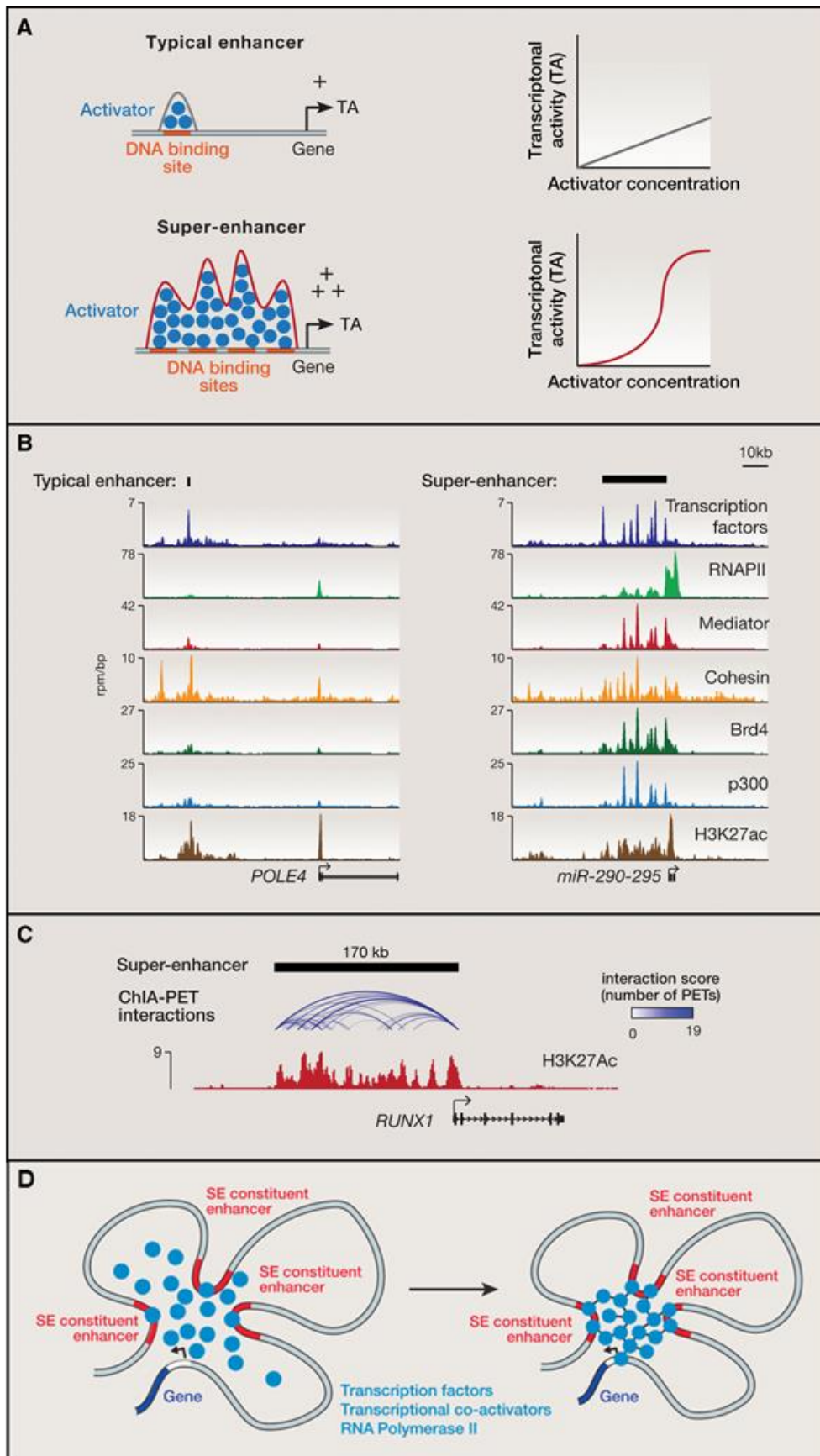


Figure 76. Differences between Super-Enhancers and Typical Enhancers.

Adapted from Hnisz et al., 2017.

The PIC is a large structure, which includes RNAPII, the general transcription factors (GTFs: TFIIA, TFIIB, TFIID, TFIIIE, TFIIF, and TFIIH), which are indispensable for proper gene expression, as well as coregulatory complexes such as the Mediator complex (Murakami et al., 2015; Chen et al., 2021). Although the core promoter can allow for PIC assembly and transcription initiation on its own, its basal activity is weak, also because of previously mentioned steric inaccessibility (Kadonaga, 2012). Increased rates of transcription require that core promoters find themselves in nucleosome-depleted regions, or regions with specific histone variants such as H3.3 or H2A.Z, and therefore rely on chromatin remodeling to remove the topological barriers hindering PIC assembly (Jin et al., 2009; Lorch and Kornberg, 2017; Mueller et al., 2017; Semer et al., 2019) (Figure 73). As such, gene expression rates can be increased or decreased by different regulatory elements of transcription, consisting of both cis-regulatory DNA elements such as enhancers, and trans-acting elements such as transcription factors (TFs). These are proteins that can recognize and bind specific cis-regulatory DNA regions, thus modulating transcription in association with cofactors (Spitz and Furlong, 2012; Shlyueva, Stampfel and Stark, 2014; Zabidi and Stark, 2016) (Figure 74).

An enhancer is defined as a DNA element spanning 50-1000 bp that strengthens the transcription of a gene, independently of its relative distance and orientation, by being bound in a sequence-specific manner by TFs (Claringbould and Zaugg, 2021). Different models of enhancer-promoter interplays have emerged over the years (Haberle and Stark, 2018; Compe and Egly, 2021). However, many studies suggest that in a first step, specific TFs called pioneer factors, such as PAX3 or SOX2, recognize their distinct binding sequences through a low-affinity scanning mechanism, even in the presence of heterochromatin (Michael and Thomä, 2021; Sunkel et al., 2021; Balsalobre and Drouin, 2022). This initiates the opening of closed chromatin in the enhancer region through the recruitment of chromatin remodelers and histone modifiers, allowing for other TFs to bind in a more high-affinity manner (Suter, 2020; Jonge et al., 2022). As multiple TFs can bind an enhancer, their combinatorial occupancy determines the specific regulation of a target core promoter (Ong and Corces, 2011; Reiter, Wienerroither and Stark, 2017). The predominant model to explain the influence of enhancers on gene expression involves cohesin/CTCF-mediated DNA loop formations, which bring enhancers physically close to core promoters (Rowley and Corces, 2018; Kim and Shendure, 2019; van Steensel and Furlong, 2019). In this proximity, the bound TFs serve as platforms to recruit additional cofactors and chromatin remodelers, such as the SWI/SNF or SAGA complexes, leading to a less compacted promoter landscape (Alver et al., 2017; Baptista et al., 2017) (Figure 74 and 75A). Additional noteworthy, recruited coactivators are for example the

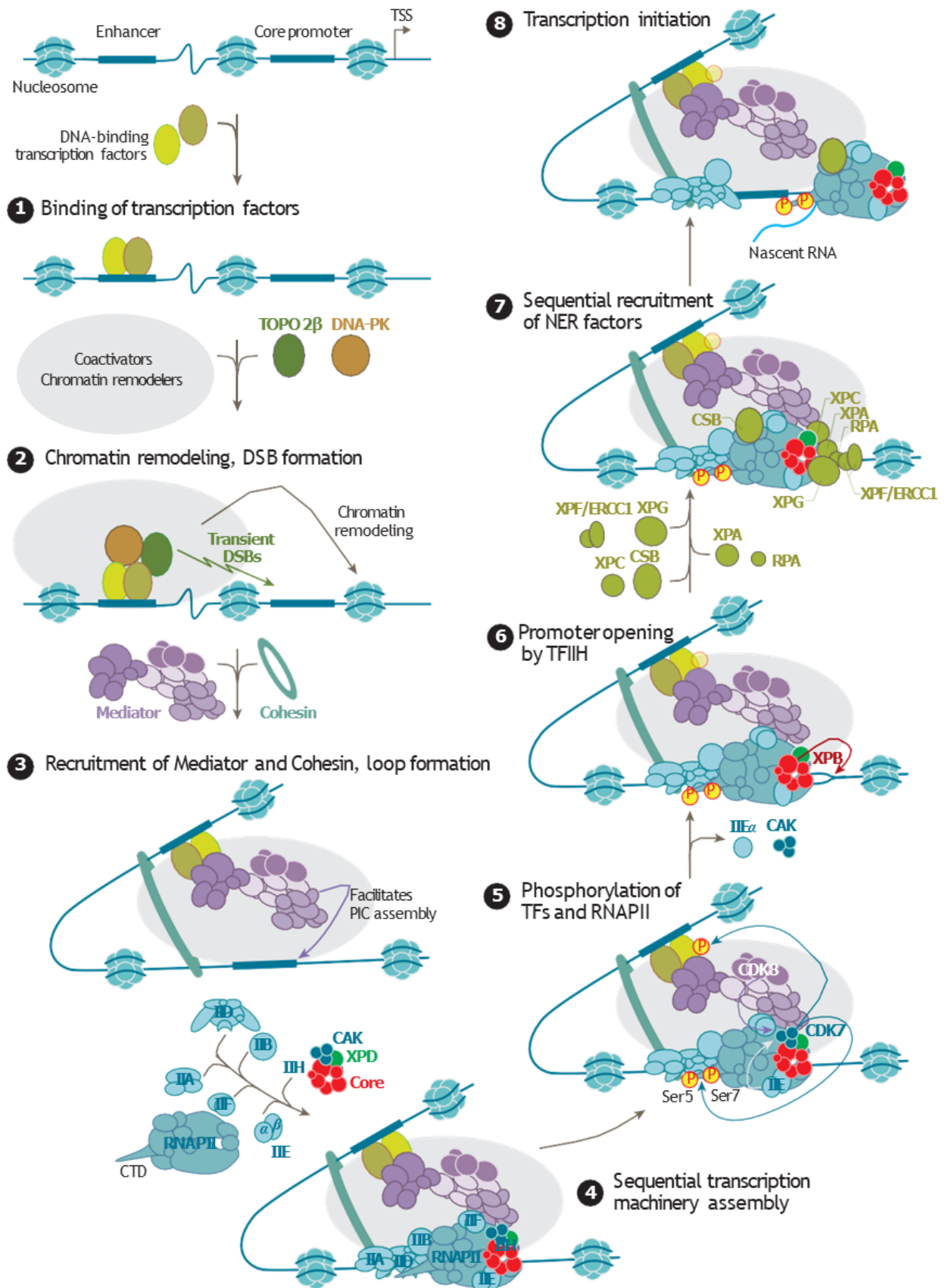
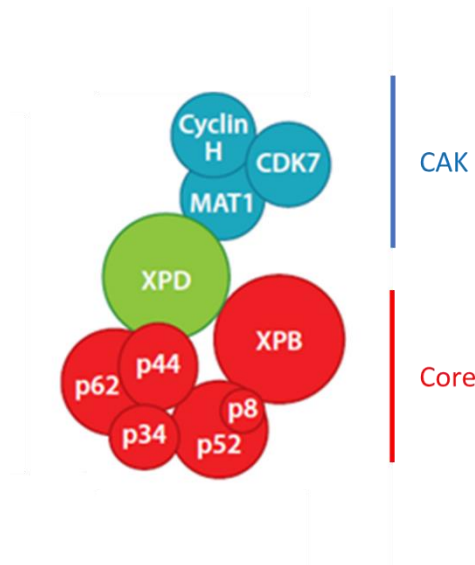


Figure 77. Schematic representation of transcription initiation.

From Compe and Egly, 2021.

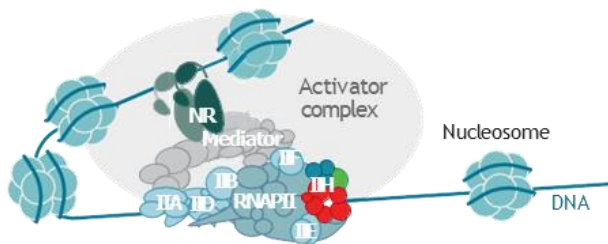
acetyltransferase p300, acetylating specific lysine residues on histones but also on TFs and RNAPII, thereby activating them (Visel et al., 2009; Schröder et al., 2013). Bromodomain and Extraterminal (BET) proteins, such as BRD4, constitute a class of coactivators interacting with acetylated histones, which in tandem with DNA-bound TFs help to recruit larger complexes that promote transcription initiation, such as the Mediator (Shi and Vakoc, 2014; Donati, Lorenzini and Ciarrocchi, 2018). This 26-subunit complex directly bridges enhancers to core promoters and improves the recruitment, positioning, and stability of different PIC components (Abdella et al., 2021; Chen et al., 2021; Nguyen et al., 2021; Rengachari et al., 2021) (Figure 75B). The Mediator also serves to transduce signals from enhancer-bound TFs towards the transcription machinery, and is indispensable for the activity of RNAPII, regulating its function at various steps (Soutourina, 2018; Cramer, 2019; Richter et al., 2022).

Whereas most enhancers span a few hundred bp, two landmark studies from Richard A. Young's lab in 2013 characterized for the first time regulatory regions with extreme enrichment of active chromatin marks such as H3K27ac and transcriptional coactivators including the Mediator, CDK7 and BRD4, thus resembling large clusters of enhancers spanning over 12 kb in size (Hnisz et al., 2013; Whyte et al., 2013) (Figure 76). They named these elements super-enhancers (SEs) and reported them to be predominantly found near key cell identity genes, while being heavily occupied by cell-type specific master TFs, representing important lineage regulators (Pott and Lieb, 2015). These studies showed that distinct SEs could be found in different cell types, and that a small number of these SEs determined cell fate by activating lineage-specifier expression patterns, such as in the case of the SE-dependent *MITF* or *SOX10* genes in melanocytes (Eliades et al., 2018; Fufa et al., 2019). More recent characterizations of SEs confirmed their distinct nature as massive networks of cooperative interactions between transcriptional co-activators (Cho et al., 2018; Chong et al., 2018), which phase-condensate to compartmentalize and concentrate the transcriptional machinery to maintain the constant expression of essential cell-identity genes, as evidenced by the massive recruitment of RNAPII (Boehning et al., 2018; Sabari et al., 2018) (Figure 76). Through their cooperative nature, SEs display emergent properties that seem distinct from the sum of their individual enhancer parts (Hay et al., 2016; Shin et al., 2016; Boija et al., 2018). SEs can thus drive much higher transcriptional activities and establish more physical contacts with core promoters than regular enhancers, and they are a critical component of the before-mentioned transcriptional condensates (Hnisz et al., 2017; Grosveld, van Staaldunen and Stadhouders, 2021; Lyons et al., 2023). Significantly, the discovery of SEs marked a conceptual shift in the field of gene expression, as this phase condensation model of transcription helped elucidate



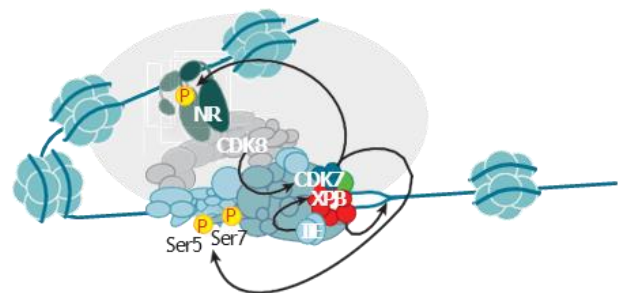
① Preinitiation complex formation

Release of transcription inhibitors and chromatin modifications
 Recruitment of transcription factors (coactivators, Mediator, NRs, etc.)
 Sequential recruitment of TF-IID, IIA, IIB, IIF, RNAPII, IIE, and IIH



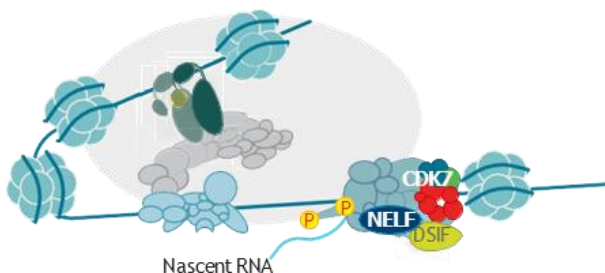
② Promoter opening

TFIIH interacts with and stabilizes NRs
 XPB opens DNA and CDK7 phosphorylates NRs and RNAPII
 TFIIH activity is regulated by Mediator (via CDK8) and TFII E



③ Transcription initiation

RNAPII produces short RNA
 Capping (m7G) of the 5' end of nascent RNA
 DSIF and NELF contribute to RNAPII pausing



④ Release from the pausing site and elongation

CDK7 phosphorylates the CDK9 kinase of p-TEFb
 CDK9 targets the NELF, DSIF and Ser2 of the CTD
 Phosphorylated NELF is released and RNAPII elongates RNA

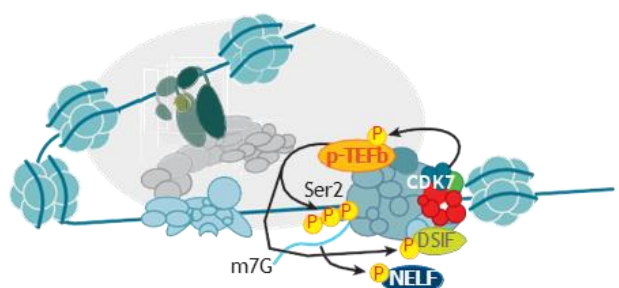


Figure 78. TFIIH subcomplexes and role in RNAPII transcription.

Adapted from Compe and Egly, 2016.

some phenomena such as the temporal dynamics of transcription machinery formation, how a single enhancer might control multiple genes, and how gene expression might be dysregulated in cancers (Shrinivas et al., 2019; Blobel et al., 2021; Boija, Klein and Young, 2021).

2. The transcription cycle and the role of TFIID

2.1. Pre-initiation complex formation

Once the chromatin context favors transcription initiation, RNAPII is guided toward gene promoters. However, as RNAPII can neither recognize specific promoter elements on its own nor accurately position itself at the TSS of a given gene, the presence of the GTFs, serving as a bridge between RNAPII and promoters, is indispensable for accurate gene expression (Orphanides, Lagrange and Reinberg, 1996). This inability of RNAPII for sequence-specific binding is exemplified by the fact that most of the genome is transcribed, leading for example to pervasive bi-directional transcription of enhancer or promoter regions into non-coding RNA (Kapranov et al., 2007; Andersson et al., 2014, 2015; Core et al., 2014). To guide and improve the specificity of gene transcription, the function of core promoters and their DNA motifs is to recruit the GTFs, mediating the assembly of a PIC primed to start RNA synthesis (Kadonaga, 2012; Schor et al., 2017). During the last decade, astonishing advances have been made to elucidate the structural basis of the intricacies of PIC formation, many of them coming from Patrick Cramer's lab (Abdella et al., 2021; Chen et al., 2021; Rengachari et al., 2021; Schilbach et al., 2021; Wang et al., 2023). Hereinafter, a simplified version of the canonical model of the sequential PIC assembly on core promoters is presented (Figures 75 and 77).

In a first step, the GTF TFIID recognizes and binds a core promoter DNA motif, thereby taking on a saddle-like form that covers and bends DNA, constituting a platform for the recruitment of subsequent GTFs (Davison et al., 1983; Patel et al., 2018). For example, TATA-boxes are recognized by the TATA-box-binding protein (TBP) subunit of TFIID, whereas other sequences, such as the before-mentioned Inr and DPE motifs, are recognized by other TFIID components, namely TBP-associated factors (TAFs) (Pugh and Tjian, 1991; Chalkley and Verrijzer, 1999; Louder et al., 2016). Importantly, TFIID recruitment and activity are regulated by many factors, such as the Mediator and SAGA complexes (Johnson et al., 2002; Allen and Taatjes, 2015; Papai et al., 2020), and its DNA binding stability is increased by the recruitment of TFIIA and TFIIB (Ozer et al., 1998; Kostrewa et al., 2009). TFIIB then binds RNAPII, which is anchored to the preformed complex by its association with TFIIF and by the action of

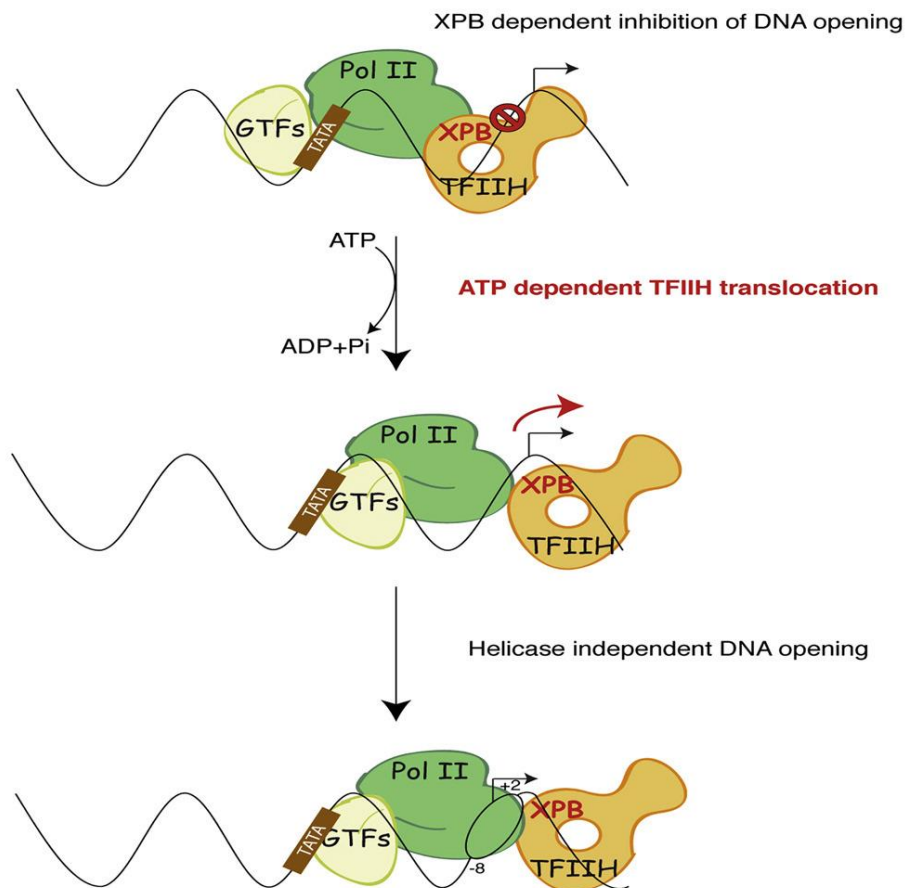


Figure 79. XPB and promoter opening.

From Alekseev et al., 2017.

the Mediator, ensuring the proper orientation of RNAPII recruitment to the PIC (Robert et al., 1998; Bushnell et al., 2004; Kostrewa et al., 2009; Sainsbury, Niesser and Cramer, 2013). TFIIIE then binds to RNAPII and TFIIIF, which allows for proper TFIIH recruitment, finally completing the PIC (Maxon, Goodrich and Tjian, 1994; Compe et al., 2019).

2.2. The multiple functions of TFIIH and its role in transcription initiation

First purified in 1989, the various roles and dynamic subunit composition of the multi-functional TFIIH complex have been intensely studied for over three decades, with important contributions from the Jean-Marc Egly/Frédéric Coin team (Gerard et al., 1991; Egly and Coin, 2011). TFIIH is composed of 10 subunits which are resolved into two sub-complexes: the core TFIIH (containing six subunits, namely XPB, p62, p52, p44, p34, and p8), linked by XPD to the cyclin-dependent kinase (CDK)–activating kinase module (CAK, containing CDK7, Cyclin H, and MAT1) (Schultz et al., 2000; Nogales and Greber, 2019) (Figure 78). The three main enzymatic subunits of TFIIH, namely the kinase CDK7, the translocase XPB and the helicase XPD, play essential roles in various cellular processes (Compe and Egly, 2016). During NER, TFIIH is recruited to DNA damage sites, where it ejects its CAK sub-complex to be able to open the DNA double strand around the lesion (Coin et al., 2008; Oksenych et al., 2009; Kokic et al., 2019). During this process, XPB serves an ATP-dependent DNA-anchoring function while the helicase activity of XPD unwinds the damaged DNA site, allowing for subsequent repair by the NER machinery (Coin et al., 2004; Coin, Oksenych and Egly, 2007; Oksenych and Coin, 2010). The TFIIH CAK subcomplex is fundamentally important in cell cycle progression control, as the CDK7 subunit phosphorylates the T-loops of CDK1, CDK2, CDK4, and CDK6, thereby activating them (Russo, Jeffrey and Pavletich, 1996; Fisher, 2005; Schachter et al., 2013). More recent studies have also shown the involvement of TFIIH subunits in processes such as mitotic regulation and chromosome segregation (Ito et al., 2010; Compe et al., 2022), chromatin condensation (Sandoz et al., 2019), or telomere replication (Yang, Sharma and de Lange, 2022).

TFIIH was first identified as an RNAPII GTF indispensable for transcription, in which its translocase and kinase activities play preponderant roles (Schaeffer et al., 1993; Coin et al., 1999; Zhovmer, Oksenych and Coin, 2010; Rimel and Taatjes, 2018) (Figure 78). Although XPB was initially recognized as a helicase involved in promoter DNA unwinding (Guzder et al., 1994), emerging models suggest that helicase-independent mechanisms are at play (Grünberg, Warfield and Hahn, 2012; Fishburn et al., 2015; He et al., 2016; Dienemann et al.,

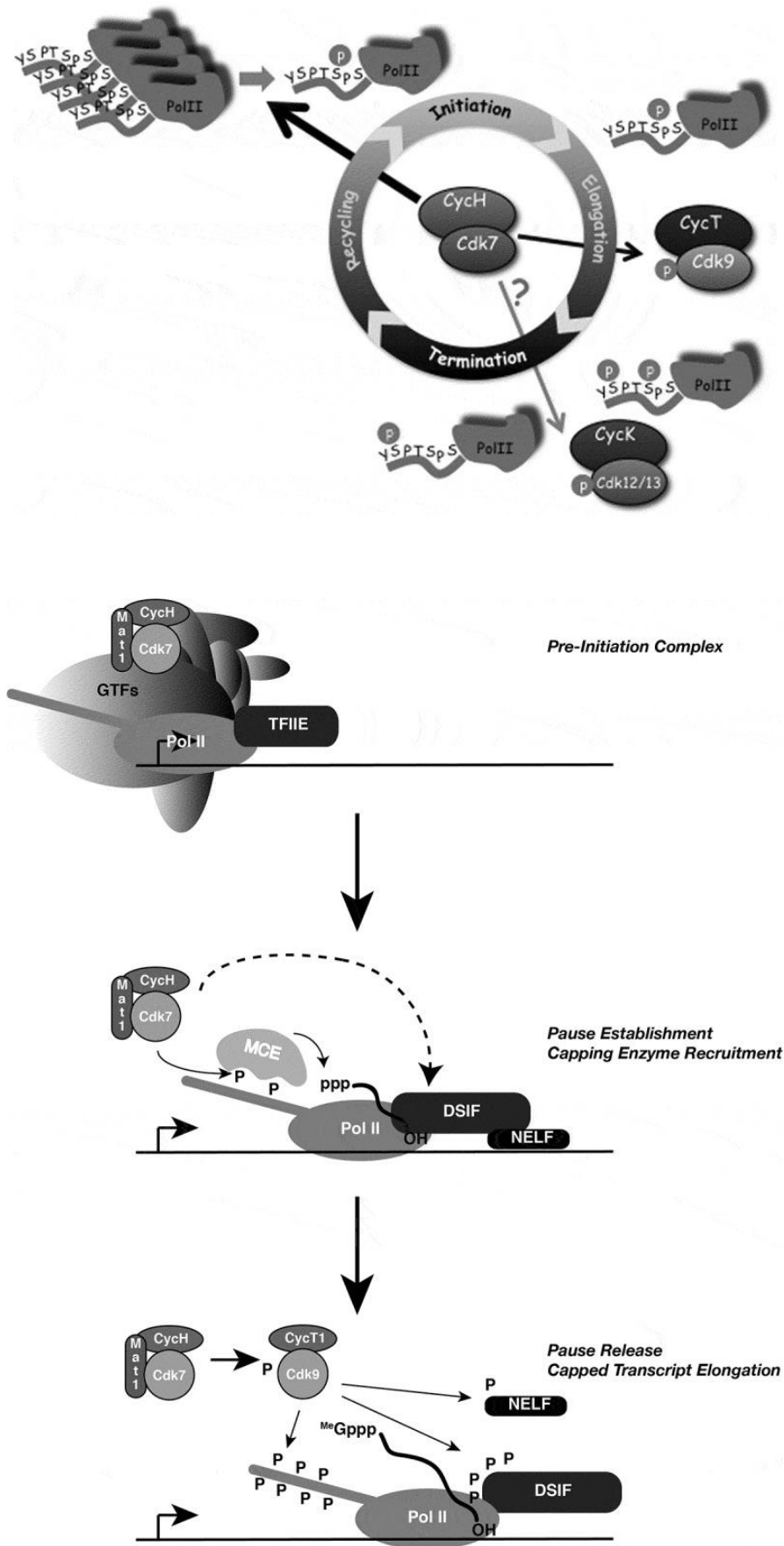


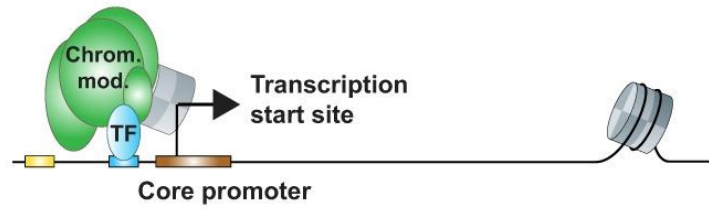
Figure 80. CDK7 functions during the Pol II transcription cycle.

Cyc = Cyclin, MCE = Mammalian Capping Enzyme. From Fisher, 2018.

2019). These models were supported by a 2017 finding by Alekseev et al. that showed that depletion of XPB had minimal effects on transcription, whereas pharmacological inhibition of its ATPase activity significantly impacted RNA synthesis. This apparently paradoxical situation seemed to fit the integrated XPB blocking model first proposed by J. Gralla, in which the presence of XPB in the PIC initially blocks promoter unwinding (Lin, Choi and Gralla, 2005). This XPB-dependent inhibition of DNA opening is overcome by its own ATP-dependent translocation along a short stretch of DNA, which then allows the released binding energy, inherent in the creation of complex condensates such as the PIC, to break the hydrogen bonds that hold the DNA strands attached (Figure 79). The opening of the DNA region converts the closed promoter complex into an open one, harboring the transcription bubble, in which the single-stranded template DNA is positioned into the RNAPII active site, allowing RNA synthesis to begin (Plaschka et al., 2016; Alekseev et al., 2017; Glyde et al., 2017; Sandoz and Coin, 2017; Dienemann et al., 2019). Recently, it has been observed that TFIIH interacts with the first nucleosome located downstream of the TSS, the co-called +1 nucleosome, whose rotation is driven by XPB to facilitate nucleosomal DNA detachment (Wang et al., 2023). Additionally, the relative position of the +1 nucleosome is an important regulator of transcription initiation, as close proximity to the TSS, a state encountered in heterochromatin, reduces transcription by affecting the assembly of the PIC and by inducing a closed TFIIH conformation, by which XPB cannot stimulate DNA unwinding and nucleosome rotation, and in which the CDK7 kinase is distanced from its targets (Abril-Garrido et al., 2023).

The CDK7 subunit of TFIIH, while being regulated among others by MAT1, Cyclin H, TFIIIE, and the CDK8 Mediator subunit, can phosphorylate multiple substrates involved in transcription initiation and elongation (Fisher, 2018). For example, CDK7 participates in the activation of p53 and many nuclear receptors such as RAR- α and PPARs (Lu et al., 1997; Rochette-Egly et al., 1997; Compe et al., 2005). Importantly, CDK7 also phosphorylates the carboxy-terminal domain (CTD) of the largest subunit of RNAPII, RPB1, which contains 52 heptad repeats (Y₁S₂P₃T₄S₅P₆S₇) in human cells (Lu et al., 1992; Glover-Cutter et al., 2009; Harlen and Churchman, 2017) (Figure 80). More specifically, during transcription initiation, the Mediator positions the TFIIH CAK submodule into a position that permits CDK7 to directly phosphorylate serines 5 and 7 (Ser5 and Ser7) of the RNAPII-CTD (Abdella et al., 2021; Chen et al., 2021; Richter et al., 2022). The phosphorylated CTD can then serve as a recruitment platform for factors involved in subsequent co-transcriptional events such as RNA capping, splicing, and polyadenylation (Cho et al., 1997; Phatnani and Greenleaf, 2006; Hsin and Manley, 2012; Guo et al., 2019). Additionally, as the Mediator cannot bind the phosphorylated

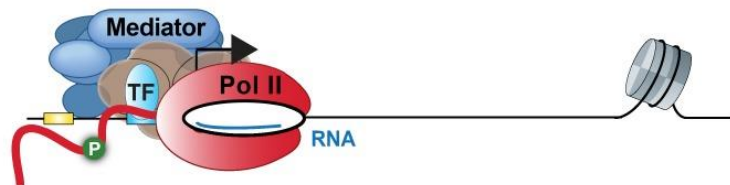
A Chromatin remodeling



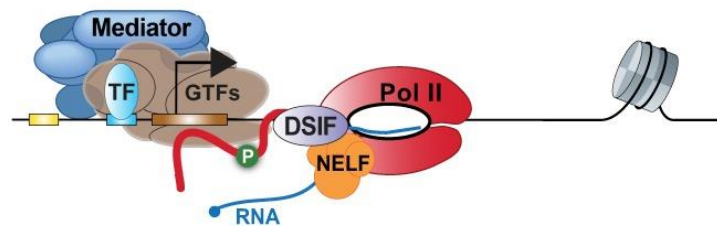
B Preinitiation complex formation



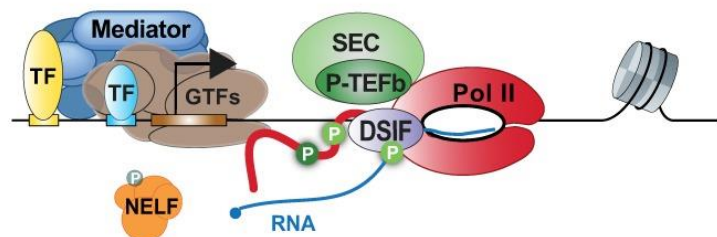
C Transcription initiation



D Promoter escape and pausing



E Pause release



F Productive elongation

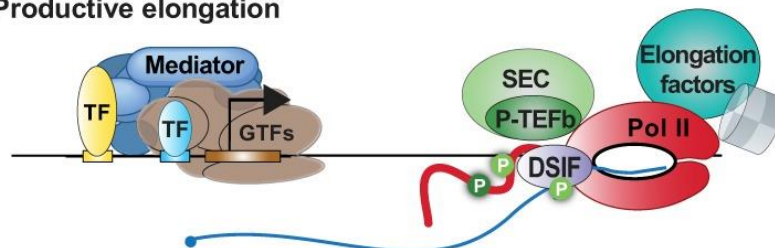


Figure 81. Transcription initiation, RNAPII pausing, and elongation.

From Core and Adelman, 2019.

CTD, CDK7 also plays an essential role in Mediator-RNAPII dissociation, which allows the release from the PIC and the promoter escape of RNAPII, paving the way for subsequent phases of the transcription process (Max, Søgaaard and Svejstrup, 2007; Eick and Geyer, 2013; Wong, Jin and Struhl, 2014).

2.2. Promoter proximal pausing and release into productive elongation

After promoter escape, RNAPII synthesizes a short initial RNA segment which is capped at the 5' end to protect it against degradation (Fabrega et al., 2003). The nascent RNA remains hybridized with its complementary DNA to form an RNA-DNA hybrid, still attached to RNAPII (Luse, 2013; Fazal et al., 2015; Core and Adelman, 2019). This hybrid represents a steric obstacle that impairs further nucleotide insertions, which can result in RNAPII promoter-proximal pausing at 20 to 60 nucleotides downstream of the TSS (Saba et al., 2019) (Figure 81). RNAPII pausing is further reinforced by the recruitment of the negative elongation factor (NELF) and its partner, the DRB sensitivity-inducing factor (DSIF), which recognize the phosphorylated RNAPII-CTD (Jonkers and Lis, 2015; Bernecky, Plitzko and Cramer, 2017; Vos, Farnung, Boehning, et al., 2018; Vos, Farnung, Urlaub, et al., 2018). RNAPII pausing constitutes a significant regulatory step of transcription, as it is a mechanism to both limit and induce gene expression (Levine, 2011; Li and Gilmour, 2011; Muniz, Nicolas and Trouche, 2021; Abuhashem, Garg and Hadjantonakis, 2022). Indeed, promoter-proximal pausing was first discovered in *Drosophila*, in which RNAPII was found enriched in a halted state near promoters of heat-shock protein (HSP) encoding genes, where it could be rapidly released into productive RNA synthesis in order to protect the organism if exposed to heat stress (Gilmour and Lis, 1986; Rougvie and Lis, 1988; Vihervaara, Duarte and Lis, 2018). Whereas the rapid expression of many stress-response genes is induced by RNAPII pause release, the same external stimuli, such as heat shocks, cause a global transcriptional downregulation of metabolic, cell-cycle or housekeeping genes to improve cell survival (Aprile-Garcia et al., 2019; Gressel, Schwalb and Cramer, 2019). Recent studies have shown that this transcriptional halting is also mediated by RNAPII pausing, resulting from stress-induced NELF phase-condensation at many gene promoters (Aoi et al., 2020; Rawat et al., 2021). As such, promoter-proximal pausing serves to position RNAPII in a poised state for rapid induction of stress response factors such as HSPs, MYC or FOS (Krumm et al., 1992; Plet, Eick and Blanchard, 1995; Mayer, Landry and Churchman, 2017), but also constitutes a checkpoint and rate-limiting step of transcription, as RNAPII can be removed from the gene by promoter-proximal

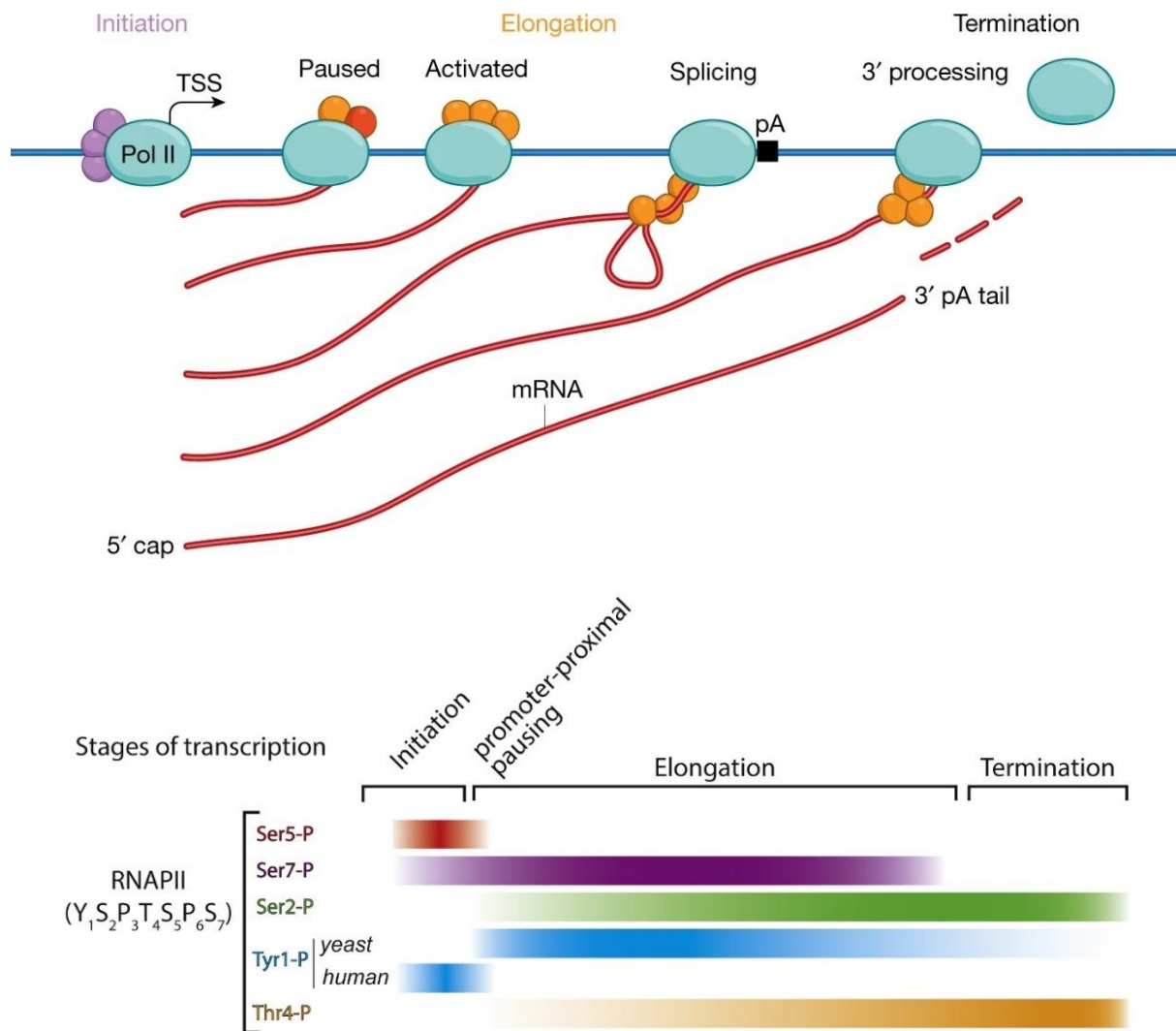


Figure 82. The RNAPII transcription cycle.

From Cramer, 2019., and Rodríguez-Molina, West and Passmore, 2023.

premature termination (Core and Adelman, 2019; Wagner, Tong and Adelman, 2023).

The release of paused RNAPII into productive RNA synthesis is mediated by the positive transcription elongation factor b (P-TEFb), found within the larger super elongation complex (SEC), which is recruited by the Mediator and several co-activators (Takahashi et al., 2011; Adelman and Lis, 2012; Luo et al., 2012; Dollinger and Gilmour, 2021) (Figure 81). P-TEFb is itself a complex that includes cyclin T1 or T2 and the CDK9 kinase (Anshabo et al., 2021). The activity of P-TEFb is tightly regulated by various factors, including MYC, BRD4 and TFIIF, whose CDK7 subunit phosphorylates CDK9, thereby activating it (Kim et al., 2002; Larochelle et al., 2012; Itzen et al., 2014). P-TEFb then phosphorylates many proteins, including NELF and DSIF, triggering NELF dissociation and turning DSIF from a negative elongation factor into a positive one, serving as a recruitment platform for elongation factors, thereby initiating RNAPII pause release (Sansó et al., 2016; Fujinaga, Huang and Peterlin, 2023). Additionally, P-TEFb participates in the phosphorylation of Ser2 of the RNAPII-CTD, but only if it has been primed before by Ser7 phosphorylation through CDK7, to ensure that only RNAPII at the appropriate transcription stage is targeted (Czudnochowski, Böskén and Geyer, 2012). As such, P-TEFb and other kinases, such as CDK12 and CDK13, which are also recruited to the elongation complex, contribute to the phase-separation-dependent hyperphosphorylation of the CTD, necessary for elongation factor recruitment and, thus, the switch into effective transcription elongation (Lu et al., 2018; Fan et al., 2020). During the elongation phase, the CTD loses Ser5 and Ser7 phosphorylation levels while accumulating higher levels of Ser2P, increasing the recruitment of further elongation, chromatin-modifying and RNA-processing factors that regulate co-transcriptional processes such as RNA splicing (Eick and Geyer, 2013; Jeronimo, Bataille and Robert, 2013; Harlen and Churchman, 2017) (Figure 82). Elongation factors, such as PAF1 or the FACT complex, are recruited after promoter-proximal pause release, mainly to help with the problem of nucleosomes, which represent inherent barriers to the elongating RNAPII (Teves, Weber and Henikoff, 2014; Weber, Ramachandran and Henikoff, 2014). For example, PAF1 is a histone modifying complex with ubiquitylation and methylation activities, recruited to RNAPII only after NELF release, whereas the FACT complex displays histone chaperone activity through disassembly and reassembly of nucleosomes as RNAPII passes through the gene body (Van Oss et al., 2016; Chen, Smith and Shilatifard, 2018; Couvillion et al., 2022). The rate of transcription elongation by RNAPII (also called ‘processivity’) has been estimated at an average speed of 2 kb per minute, ensuring a rapid and efficient synthesis of the RNA molecule (Singh and Padgett, 2009; Steurer et al., 2018).

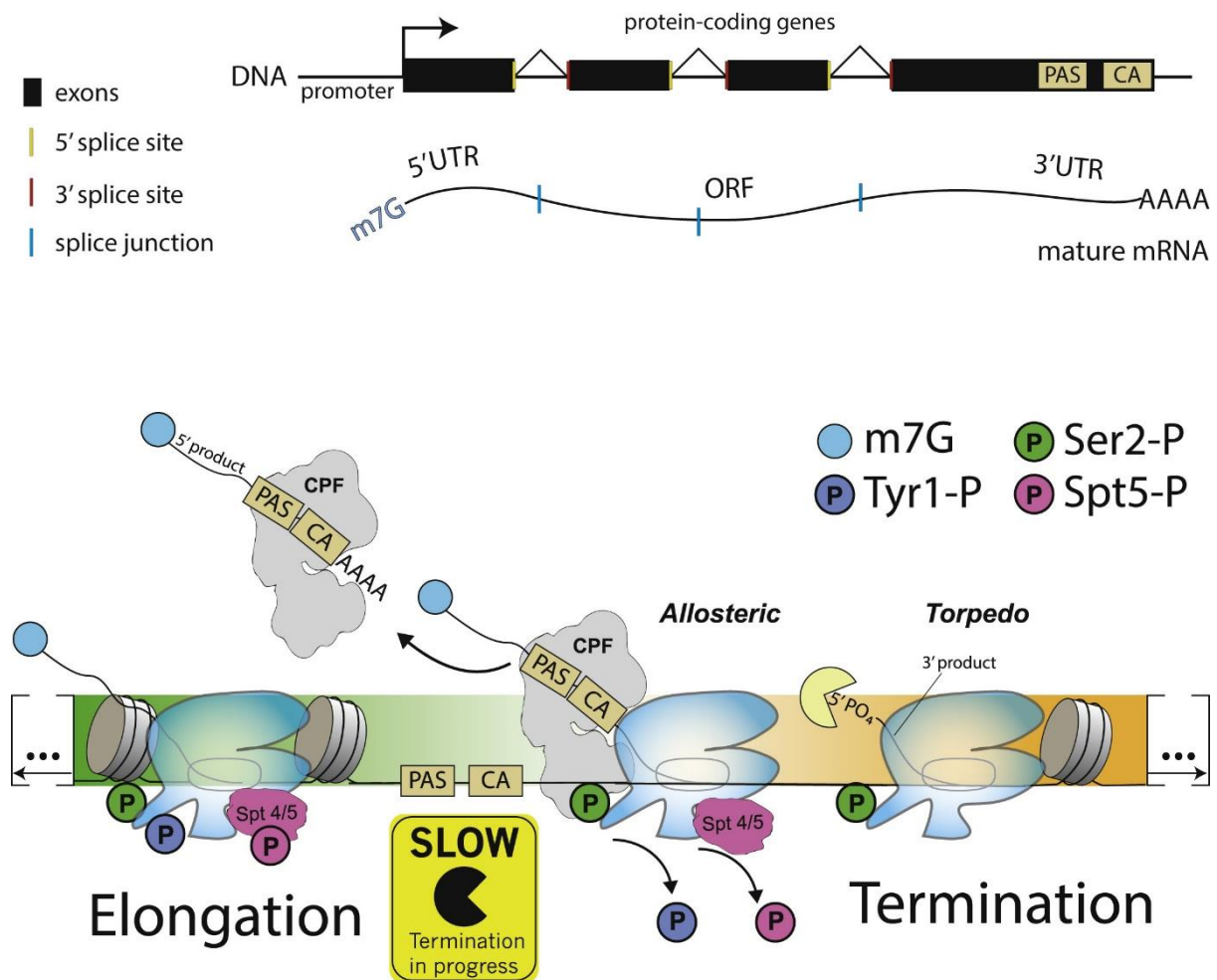


Figure 83. Current model of transcription termination.

CPF in yeast = CPSF (Cleavage and polyadenylation specificity factor) in humans, CA = Cleavage site. Adapted from Rodríguez-Molina, West and Passmore, 2023.

2.3. Transcription termination

RNAPII transcribes the remainder of the transcript throughout the elongation phase until it passes through a consensus sequence known as the polyadenylation signal (PAS) (Eaton and West, 2020). At the 3' ends of genes, pre-mRNAs are polyadenylated and cleaved to generate mature transcripts (Figures 82 and 83), and these processes are tightly coupled to transcription termination (Rodríguez-Molina, West and Passmore, 2023). After the PAS is transcribed into RNA, this sequence, as well as other factors such as phosphorylated Ser2 on the RNAPII-CTD, are recognized by the large multi-protein complex named cleavage and polyadenylation specificity factor (CPSF) (Mandel et al., 2006; Kumar et al., 2019; Sun, Hamilton and Tong, 2020). This complex, which harbors endonuclease and polyadenylation polymerase activities, binds to the AAUAAA sequence and induces RNAPII slowing and RNA 3' end processing (Shi et al., 2009). CPSF, in association with other termination factors, then cleaves the pre-mRNA, thereby releasing it from RNAPII, while an RNA segment with an open 5' phosphate remains attached to the latter (Hill et al., 2019; Schmidt et al., 2022). After this point, the exact mechanisms governing transcription termination remain unclear, however, two models have been historically outlined: the allosteric and the torpedo model (Eaton et al., 2020). Current insights propose that these two models might be unified, as they are compatible with each other (Rodríguez-Molina, West and Passmore, 2023) (Figure 83). Briefly, transcription of the PAS seems to provoke a conformational change of RNAPII, further slowing it down, which is aided by other mechanisms. For example, during this termination phase, multiple phosphatases are implicated in dephosphorylating SPT5, a subunit of DSIF, as well as the RNAPII-CTD, allowing for the recruitment of termination factors helping to dissociate elongation factors (Davidson, Muniz and West, 2014; Schrieck et al., 2014; Parua et al., 2018; Cortazar et al., 2019; Cossa et al., 2021). The slowing down of RNAPII seems to help the so-called torpedo 5'-3' exonuclease XRN2 to recognize the RNA fragment still attached to RNAPII after cleavage (West, Gromak and Proudfoot, 2004; Eaton et al., 2018, 2020). XRN2 degrades this fragment until it reaches RNAPII, forcing its release from the DNA template by unknown mechanisms, thus finishing the transcription cycle and liberating RNAPII for subsequent rounds of transcription (Eaton and West, 2020; Rodríguez-Molina, West and Passmore, 2023).

3. Diseases associated with transcriptional dysregulations

Since their initial characterization in the 1960s, our understanding of the intricate mechanisms and processes underlying gene expression control have increased dramatically (Jacob and

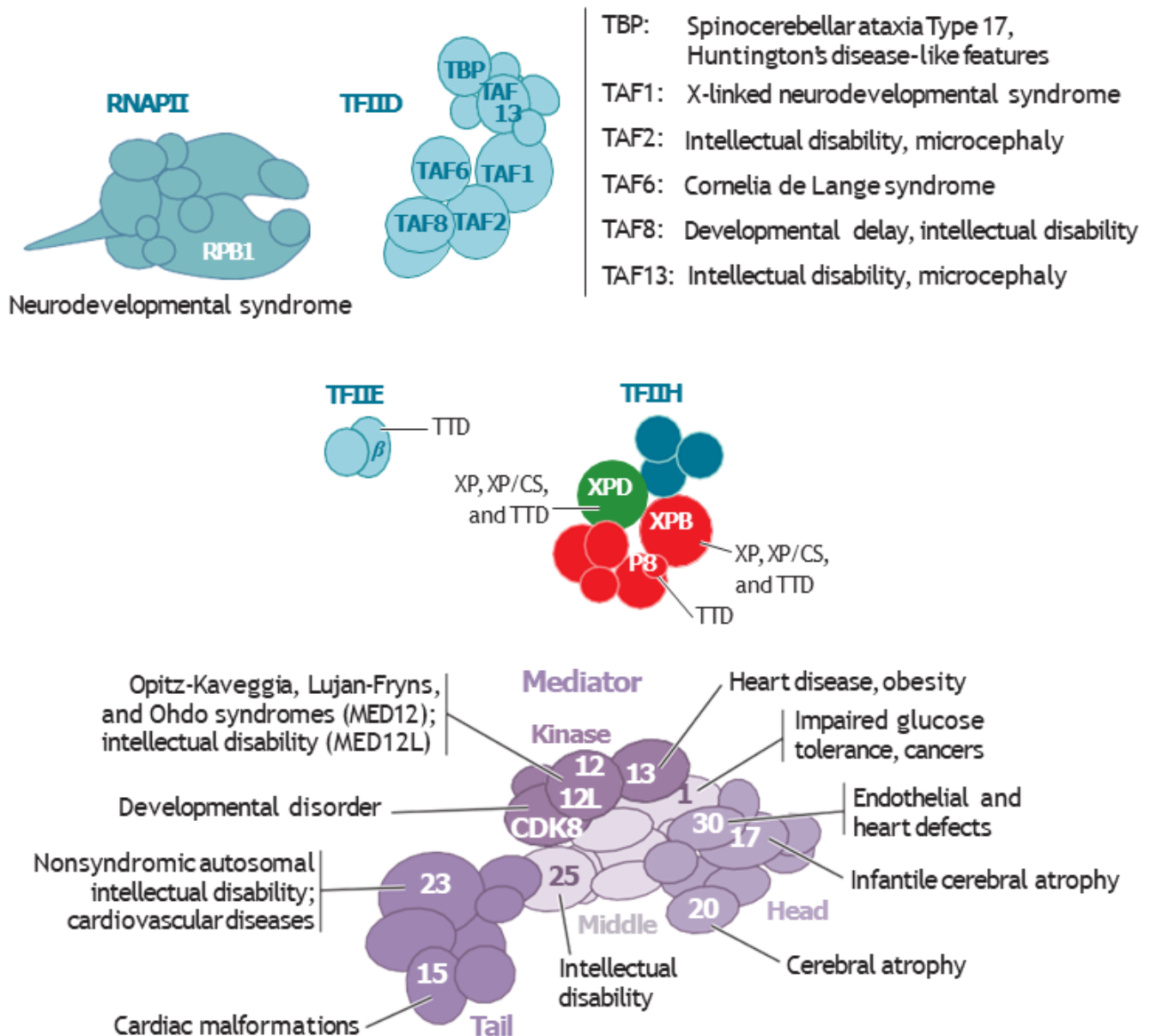


Figure 84. Transcription machinery mutations and associated diseases.

Depicted are syndromes associated with mutations in subunits of RNAPII (RPB1), TFIID (TBP, TAF1, TAF2, TAF6, TAF8, and TAF13), TFIIE (β), TFIIH (XPB, XPD, p8/TTDA), and the Mediator (MED1, MED12/12L, MED13, MED15, MED17, MED20, MED23, MED25, MED 30, and CDK8).

Adapted from Compe and Egly, 2021.

Monod, 1961; Roeder and Rutter, 1969; Lis, 2019; Roeder, 2019). In parallel to elucidating how transcription operates in normal conditions, these insights also helped to understand the preponderant role of gene expression dysregulation in the etiology of many diseases, including neurological, cardiovascular, autoimmune, infectious or metabolic disorders, and, of course, in virtually all types of cancer. As such, many mutations in diverse cis-regulatory DNA elements or trans-regulatory factors have been identified as direct causes of various pathologies (Lee and Young, 2013; Bradner, Hnisz and Young, 2017). While it was long thought to be unlikely to be possible, due to incompatibility with cell viability in most cases, specific mutations in genes encoding components of the basal transcription machinery have been found to be associated with various syndromes in recent decades, such as in the cases of TFIID, TFIIH, TFIIE, Mediator subunits, and in the *POLR2A* gene encoding RPB1 (Compe and Egly, 2021) (Figure 84). Several specific mutations in the XPB, XPD and p8 subunits of TFIIH have for example been shown to be causative of the autosomal recessive disorders trichothiodystrophy (TTD) and xeroderma pigmentosum (XP), which is sometimes associated with Cockayne syndrome (XP/CS) (Coin et al., 1998; Compe et al., 2007; Vessoni et al., 2020). The symptoms associated with these pathologies can vary substantially, from brittle hair and nails, ichthyosis, and neurological abnormalities for TTD, to heightened photo- and UV-sensitivity in patients afflicted with XP, who display greatly elevated incidence of skin cancers such as melanoma (Cleaver, 2008; Lehmann, McGibbon and Stefanini, 2011). XP/CS patients also suffer from dwarfism, skeletal abnormalities, and premature aging (Faghri et al., 2008; Schärer, 2008). Although these syndromes were initially only ascribed to DNA repair defects, various lines of evidence suggest that the observed phenotypes are also due to transcriptional anomalies (Coin et al., 1999; Dubaele et al., 2003; Singh et al., 2015). As such, a more integrated view of the role of gene expression within the larger network of cellular functions and their link with genetic diseases is becoming more and more apparent (Matharu and Ahituv, 2020).

A number of similar conceptual framework shifts have been seen in recent decades in the field of cancer research. Initially characterized on a purely cellular level, scientists soon became interested in the molecular and genetic causes behind the development of cancers (Vogelstein and Kinzler, 1993). This led to the discovery of oncogenes, and the introduction of the idea of ‘oncogene addiction’, heralding the advent of targeted therapies (Weinstein and Joe, 2006; Felsner, 2008). However, emerging data suggested that the multifaceted and dynamic hallmarks of cancers cannot be simply reduced to specific mutations, as evidenced by the temporally limited successes of most targeted therapies (Hartsough, Shao and Aplin, 2014; Vander Velde et al., 2020). Instead, it has become clear that tumor-growth-mediating

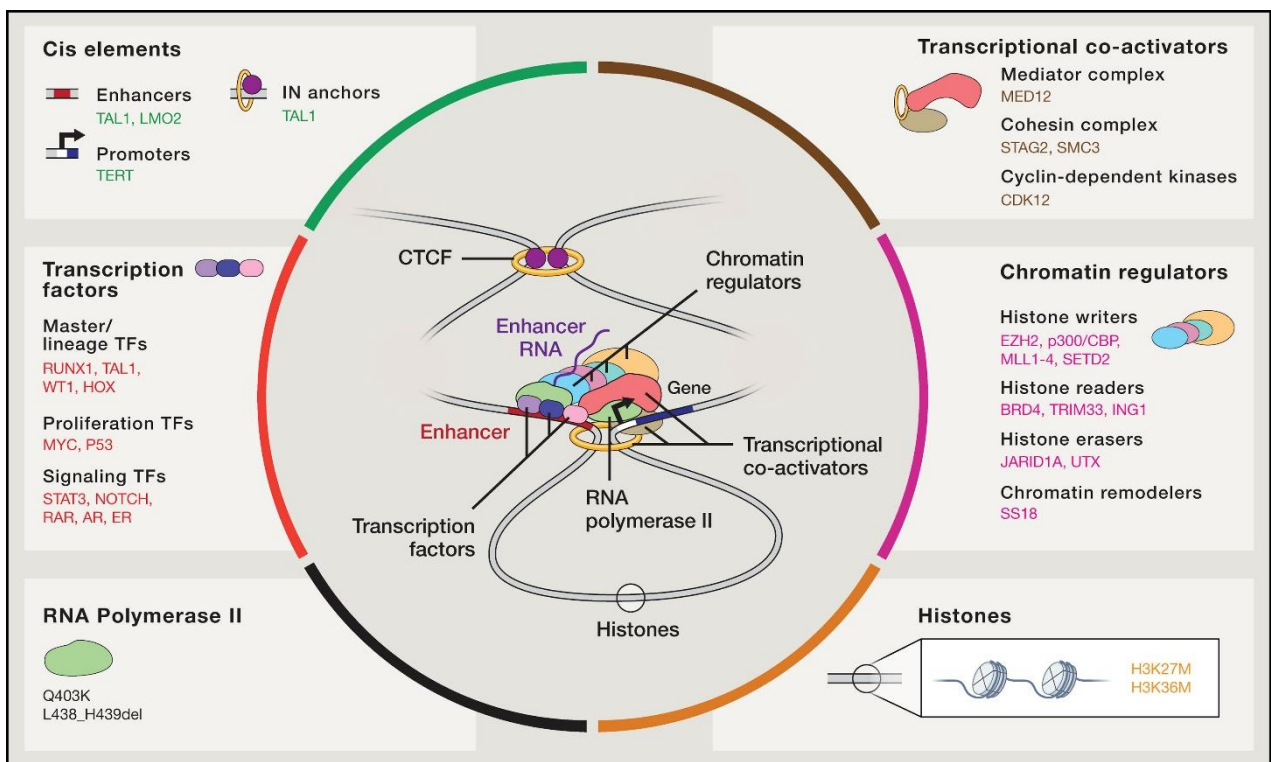


Figure 85. Components of gene expression control altered in cancers.

From Bradner, Hnisz and Young, 2017.

oncogenes operate within the larger context of epigenetic and transcriptional dysregulation, manifested through cancer-cell-specific gene expression programs (Sager, 1997; Lee and Young, 2013; Gonda and Ramsay, 2015; Okabe and Kaneda, 2021). As such, the term ‘transcriptional addiction’ was coined in 2017 by Richard A. Young, describing the increased dependencies of cancer cells towards certain regulators of gene expression in order to maintain their aberrant transcriptional programs. In the following pages, the mechanisms leading to dysregulated gene expression in cancer cells and their effects will be outlined, and how this transcriptional addiction might be leveraged for novel therapeutic interventions in cancers.

B. Transcriptional addiction in cancer and its targeting

1. Gene expression dysregulation in cancer cells

1.1. Deregulation of trans-acting factors

Cancer-associated deregulations can affect every level of transcriptional control, including trans-acting proteins implicated in gene expression regulation (Lee and Young, 2013). Signaling proteins, TFs, co-activators, chromatin regulators, or chromosome structuring proteins are recurrently found mutated in cancers, altering their activities, functions, half-lives, or relative amounts (Weinhold et al., 2014; Calabrese et al., 2020) (Figure 85). Concerning TFs, the perhaps most well-characterized type of oncogenically deregulated TFs concerns those involved in signaling control (Sever and Brugge, 2015; Sanchez-Vega et al., 2018). Their role is to bridge extra- or intracellular inputs, transmitted through a vast network of different signaling pathways, with appropriate and specific gene expression responses through enhancer binding (Trompouki et al., 2011; Huilgol et al., 2019; Weidemüller et al., 2021) (Figure 86). Countless studies have shown that dysregulation of signaling TFs can cause the hyperactivation or inactivation of specific pathways by various mechanisms, fueling tumor progression (Chen and Koehler, 2020; Islam et al., 2021). Besides signaling TFs, two other TF types are frequently deregulated in cancers, whose roles have been elucidated in more recent times: master TFs and transcriptional amplifier TFs such as MYC (Bradner, Hnisz and Young, 2017) (Figure 87A).

In normal cells, a specific few highly expressed master TFs control the gene expression programs underlying cell identity and physiological functions by cooperatively binding most active enhancers, including their own, to form auto-regulatory loops, also named core

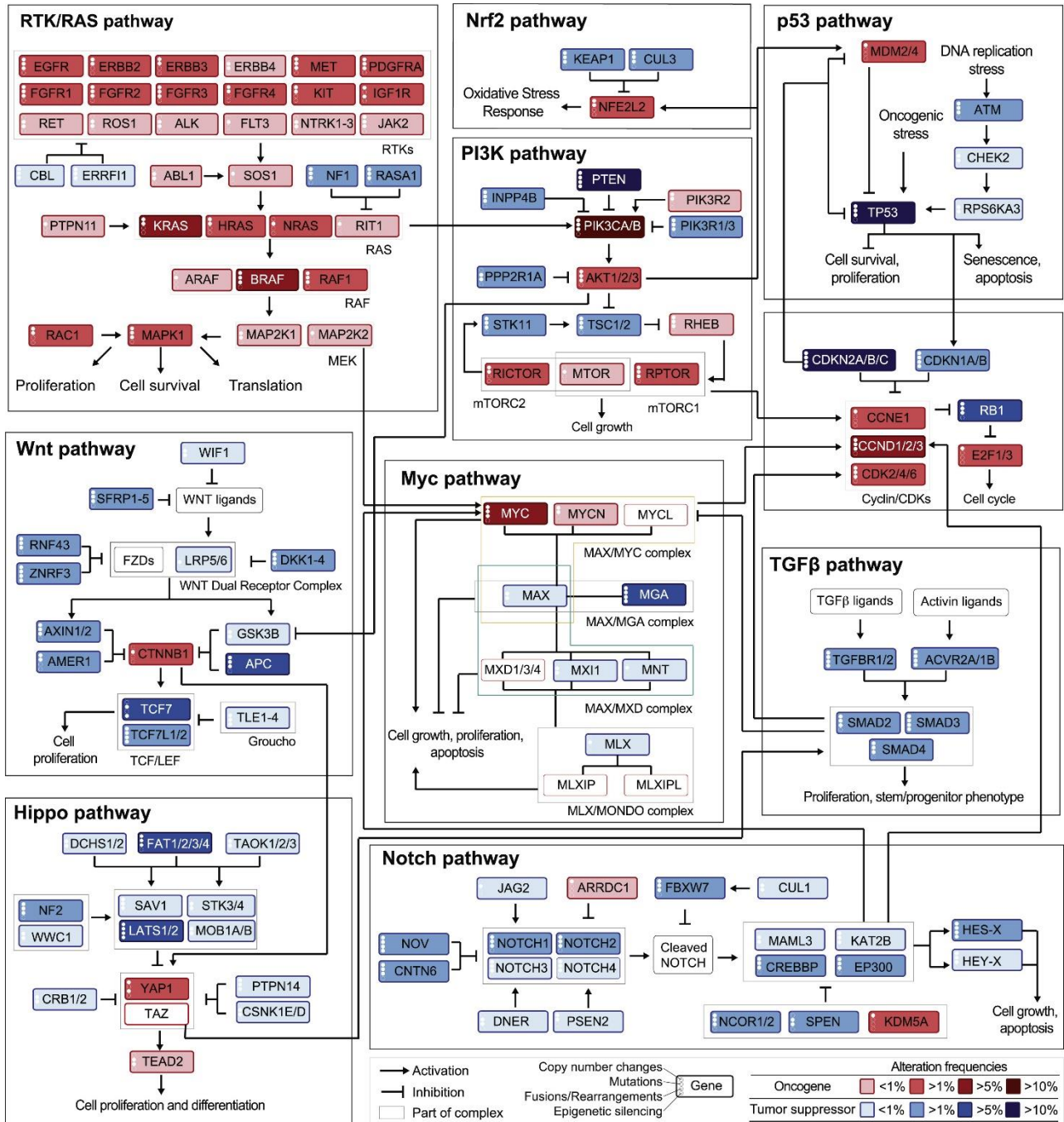


Figure 86. Major cancer-associated signaling pathways and their interactions.

Color intensity indicates the average frequency of alterations in cancers. Oncogenic activations in red and tumor suppressor inactivation in blue. The types of somatic alteration considered for each gene (copy-number alterations, mutations, fusions or epigenetic silencing) are specified using a set of four vertical dots on the left of each gene symbol. From Sanchez-Vega et al., 2018.

regulatory circuitries (Lee and Young, 2013; Whyte et al., 2013; D'Alessio et al., 2015). In cancer cells however, master TFs are often either overexpressed or abnormally repressed. In the case of melanoma for example, proliferative cells overexpress the melanocytic master TFs MITF and SOX10 involved in tumor survival and differentiation through gene amplification or acquisition of SEs (Eliades et al., 2018; Rosenbaum et al., 2021; Yokoyama et al., 2021). On the other hand, dedifferentiated melanoma cells lose MITF and SOX10 expression through various epigenetic mechanisms to gain invasion and resistance capacities (Rambow, Marine and Goding, 2019). The deletion of Ikaros, a key player in hematopoietic cell differentiation and function, constitutes another instance where the loss of a master TF furthers tumor progression (Kastner and Chan, 2011; Heizmann, Kastner and Chan, 2018). In T-cell acute lymphoblastic leukemia, Ikaros acts by repressing the transcription of Notch target genes, and thus, the loss of Ikaros drives Notch-signaling-dependent tumor progression (Jeannet et al., 2010; Geimer Le Lay et al., 2014). Many master TFs have roles in early embryonic development and are linked to pluripotency, but become repressed in mature cells (Marshall et al., 2014; Reddy et al., 2021). However, these developmental master TFs can be aberrantly re-expressed in cancer cells, thereby gaining access to more embryonic and stem-like expression programs (Monk and Holding, 2001; Yu and Xu, 2020; Islam et al., 2021). For example, T-cell development master TFs such as TAL1, GATA3, RUNX1, and MYB are highly re-expressed in T-cell acute lymphoblastic leukemias, mainly through chromosomal translocations or deletions of inhibitory sequences (Sanda et al., 2012; Mansour et al., 2014). High MYCN expression, restricted to embryogenesis in normal circumstances, is a recurrent early phenomenon in childhood neuroblastoma which leads to novel dedifferentiation-stimulating gene expression patterns (Durbin et al., 2018; Dzieran et al., 2018). MYCN overexpression is driven by many different mechanisms, including SE acquisition, gene amplification, and increased mRNA or protein stabilization through somatic mutations (Rickman, Schulte and Eilers, 2018; Liu et al., 2021; Otte et al., 2021).

MYC is one of the most frequently mutated genes in cancer (Gabay, Li and Felsher, 2014), with two landmark studies in 2012 by Lin et al. and Nie et al. shedding light on why over half of human cancers might display predilections for MYC alterations. The authors proposed a model in which at high, oncogenic levels of MYC, this TF, instead of only binding to a specific set of target genes harboring the canonically recognized E-box motif, rather accumulates in the promoter regions of virtually all actively transcribed genes, increasing global gene expression by a phenomenon named 'MYC invasion' or 'transcriptional amplification' (Littlewood, Kreuzaler and Evan, 2012; Lewis et al., 2018) (Figure 88).

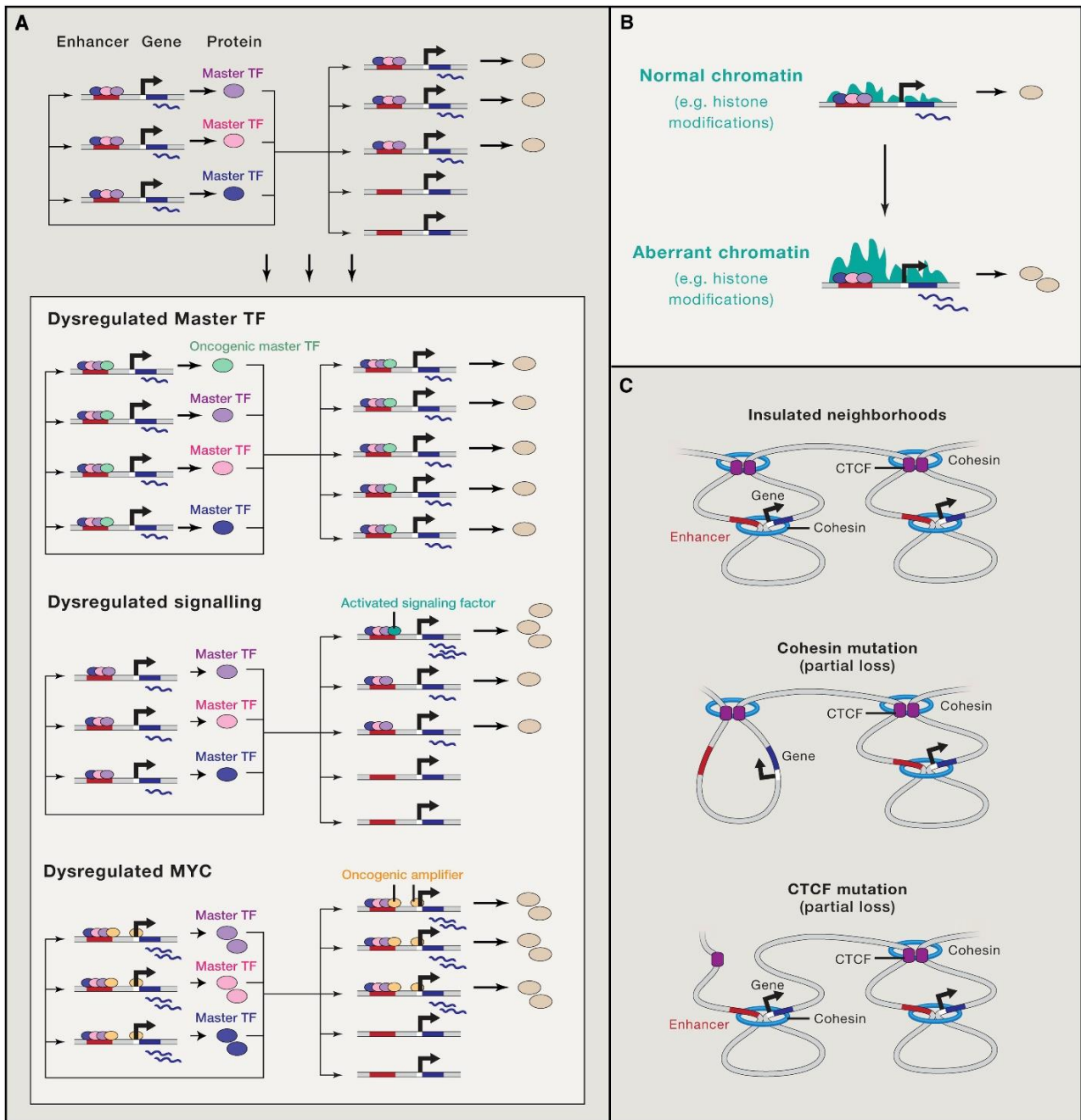


Figure 87. Common transcriptional dysregulation mechanisms involving trans-factors: (A) TF dysregulation, (B) chromatin remodeler dysregulation, and (C) cohesin and CTCF mutations.

From Bradner, Hnisz and Young, 2017.

Mechanistically, oncogenic MYC family proteins can act as universal transcription amplifiers through alteration of gene expression at nearly all levels, including TF binding dynamics, RNAPII pause release and mRNA translation, thus providing the heightened transcriptional output needed by cancer cells to sustain their aberrant phenotypes (Eick, 2018; Zeid et al., 2018; Singh et al., 2019; Lourenco et al., 2021; Patange et al., 2022; Das, Lewis and Levens, 2023). MYC overexpression can be due to a wide array of reasons, including chromosomal translocations (Boxer and Dang, 2001), gene amplifications (Dang, 2012), single point mutations leading to increased stability (Thomas and Tansey, 2011), the loss of upstream inhibitors such as TGF β (Wanzel et al., 2008) and perhaps most importantly, the establishment of novel long-range transcriptional regulation of *MYC* through SEs (Saint-André et al., 2016; Lancho and Herranz, 2018; Schuijers et al., 2018). It is however important to note that this ‘global amplification’ model is not uniformly accepted in the field, as some researchers propose a more gene-specific view of MYC activity (Kress, Sabò and Amati, 2015; Baluapuri, Wolf and Eilers, 2020).

Master TF overexpression is not the only way that it can exert increased or altered activity, as mutations can change their DNA binding specificities or affinities for example (Deplancke, Alpern and Gardeux, 2016; Ilsley et al., 2019). In 2020, Louphrasitthiphol et al. elucidated a mechanism that illustrates how altered cellular signaling can lead to TF activity changes. They showed that in melanocytes, MITF widely binds large portions of the genome through low-affinity binding sites, which act as a TF reservoir. Through MAPK signaling, oftentimes exacerbated in melanoma through the BRAFV600E mutation, p300-mediated acetylation of MITF stimulates its more specific recruitment to its high-affinity DNA binding sites to drive higher target gene expression and melanoma progression. Additionally, specific transcriptional dependencies can also be mediated by the fusion of oncogenes through chromosomal translocations or rearrangements (Tuna, Amos and Mills, 2019). For example, the main driver of Ewing sarcoma is the EWS/FLI fusion protein acting as an aberrant TF, which causes far-reaching transcriptional rewiring on which the cancer cells become highly dependent (May et al., 1993; Cidre-Aranaz and Alonso, 2015; Flores and Grohar, 2021).

Besides TFs, transcriptional cofactors such as chromatin remodelers are also frequently mutated in cancers (Figure 87B). For example, alterations in one of the SWI/SNF subunits are encountered in roughly 25 % of human cancers, the majority of which are loss-of-function mutations, suggesting a tumor-suppressive action of SWI/SNF (Centore et al., 2020; Mittal and Roberts, 2020; Andrades et al., 2023). These tumor-promoting SWI/SNF mutations are most

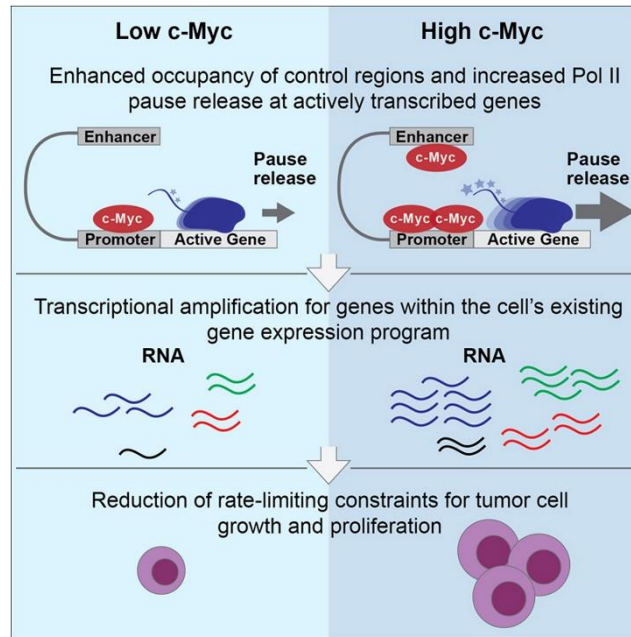
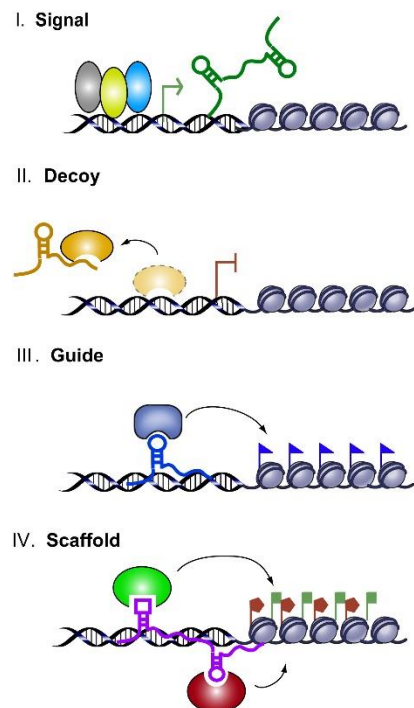


Figure 88. Transcriptional amplification through elevated MYC levels.

From Lin et al., 2012.

A



B

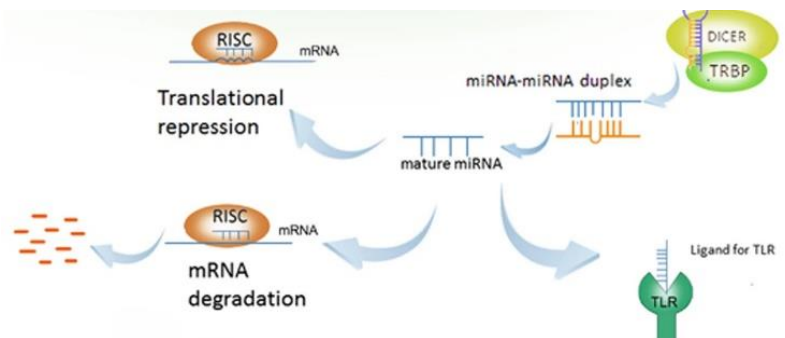


Figure 89. Different functions of lncRNAs (A) and miRNAs (B) in cancer.

Adapted from Wang and Chang, 2011; and Peng and Croce, 2016.

likely explained by the aberrant activity of the residual complex in the absence of the mutated subunit, leading to transcriptional dysregulation and genomic instability (Kadoch and Crabtree, 2015). Of note, the biallelic inactivation of the SWI/SNF BAF47 subunit is found in nearly all cases of malignant rhabdoid tumors, in which the mutated BAF47 is unable to remove the repressive Polycomb complexes from the tumor suppressor *CDKN2A* locus, leading to increased cell proliferation (Wilson et al., 2010). However, other SWI/SNF subunits tend to have more oncogenic roles, such as the BRG1 factor in melanoma cells, in which the master TF MITF actively interacts and recruits this chromatin remodeler to a large portion of actively transcribed genes, such as those encoding important melanoma identity factors. As such, the loss of BRG1 leads to major downregulation of melanoma gene expression programs, strongly inhibiting tumor growth by inducing senescence (Laurette et al., 2015, 2020). Another mechanism by which cancer cells can develop profitable transcriptional dysregulations includes aberrant histone variants (Ghiraldini, Filipescu and Bernstein, 2021). In melanocytes, the histone variant macroH2A is found to have a repressive role at the *CDK8* locus as well as at specific stem-like-associated enhancers, by blocking BRD4 access (Kapoor et al., 2010; Mohammed Ismail et al., 2023). During tumorigenesis however, macroH2A is lost at the expense of H2A.Z.2 which strongly interacts with BRD2, leading to increased CDK8 activity and cancer cell stemness and proliferation through transcriptional and epigenetic reprogramming (Vardabasso et al., 2015). Novel transcriptional dependencies can also arise through Mediator subunit mutations (Mäkinen et al., 2011), or alterations in CTCF or cohesion coding sequences, which change TAD and insulated neighborhood structure and can thus result in abnormal DNA looping and enhancer/promoter interactions (Guo et al., 2018; Fang et al., 2020; Di Nardo, Pallotta and Musio, 2022) (Figure 87C).

Finally, one of the most important shifts in the field of molecular biology in the last two decades was the recognition that non-coding RNAs (ncRNAs), representing about 90 % of total produced RNAs but initially labeled as ‘junk’, play in fact major roles in gene expression regulation and cancer progression (Anastasiadou, Jacob and Slack, 2018; Slack and Chinnaiyan, 2019). Most of the thousands of identified ncRNAs have not been functionally annotated, but they can be divided into different classes according to their size: small ncRNAs as for example microRNAs (miRNAs) have an average length of 22 bp, whereas long ncRNAs (lncRNAs) span over 200 bp (Lorenzi et al., 2021). Functionally, lncRNA are classified into four types: signaling lncRNAs which can act in many cellular processes as signaling effectors, decoy lncRNAs storing away TFs, guide lncRNA escorting TFs to their targets, and scaffold lncRNAs facilitating ribonucleoprotein complex assembly (Wang and Chang, 2011; Bhan,

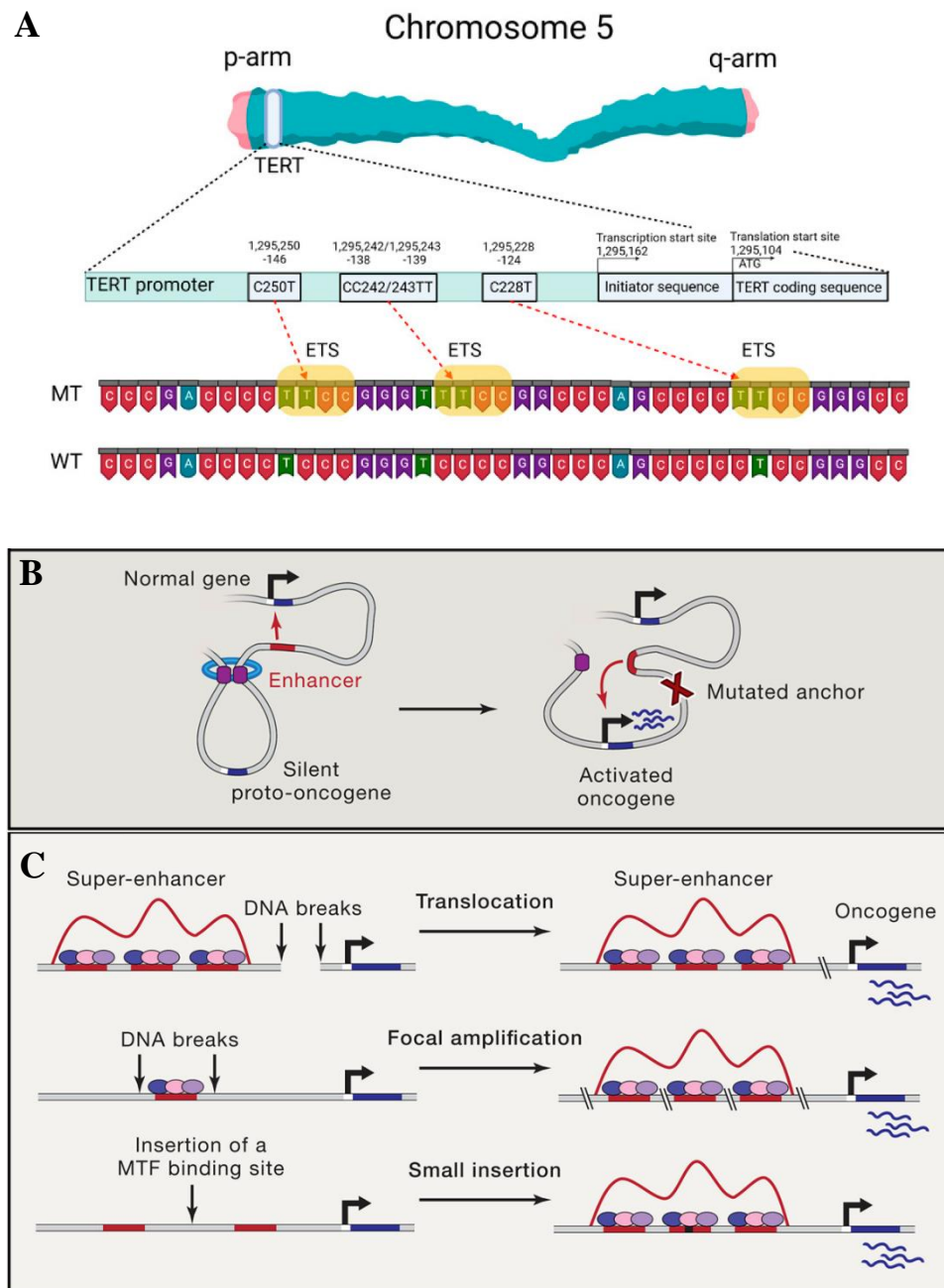


Figure 90. Common transcriptional dysregulation mechanisms involving cis-factors: (A) Promoter mutations, (B) disruption of insulated neighborhood anchor sites, and (C) acquisition of super-enhancers.

Adapted from Bradner, Hnisz and Young, 2017, and Hasanau et al., 2022.

Soleimani and Mandal, 2017) (Figure 88A). miRNAs usually downregulate the expression of specific gene targets, mainly through mRNA degradation induction or translational inhibition, although they can also function as ligands for specific signaling receptors (Peng and Croce, 2016) (Figure 88B). Importantly, the RNAPII-dependent expression patterns of both lncRNAs and miRNAs are highly regulated and tissue- or disease-specific, making them potentially interesting biomarkers or therapeutic targets in cancers such as melanoma (Philippidou et al., 2010; Nazarov et al., 2013; Varrone and Caputo, 2020; Wozniak and Czyz, 2021). For example, in most melanoma cases, several mechanisms including focal chromosome amplifications lead to the overexpression of the lncRNAs SAMMSON and LENOX, both involved in cell metabolism and survival, specifically rendering melanoma cells ‘addicted’ to their expression (Leucci et al., 2016; Gambi et al., 2022). In parallel, the loss of for example miRNA-205 has been shown to cause E2F1 overexpression and melanoma progression (Dar et al., 2011).

1.2. Deregulation of cis-regulatory elements

In the last few decades, the search for the causative mechanisms underlying cancer progression has led to the discovery of many somatic mutations lying within coding regions, which account for roughly 2% of the human genome (Plesance et al., 2010; Poulos et al., 2015). More recent insights have however shown that most cancer-associated alterations are found in non-coding cis-regulatory regions, affecting transcriptional and post-transcriptional regulation of gene expression (Cheng et al., 2021; Castro-Mondragon et al., 2022). The latest version of the ENCODE project has registered 926,535 human candidate cis-regulatory elements, classified into promoter-like (H3K27ac and H3K4me3 positive), insulator-element-like (CTCF positive, DNaseI accessible), and active or poised enhancer-like elements (H3K27ac positive, DNaseI accessible), collectively constituting 7,9 % of the human genome (Moore et al., 2020). Recurrent core promoter mutations are somewhat poorly studied, with the exception of *TERT* promoter mutations, found in over 50 different types of cancers, such as glioblastoma, bladder cancer, and melanoma (Killela et al., 2013; Kinde et al., 2013; Bell et al., 2016; Fredriksson et al., 2014, 2017). In 2013, two landmark studies described for the first time somatic cis-regulatory mutations in cancer by identifying highly recurrent *TERT* core promoter mutations, which in melanoma cells created de novo binding motifs for ETS TFs, thus upregulating *TERT* expression (Horn et al., 2013; Huang et al., 2013) (Figure 90A). Another promoter mutation affects for example the *FOXA1* gene in breast cancers, by generating an E2F binding motif

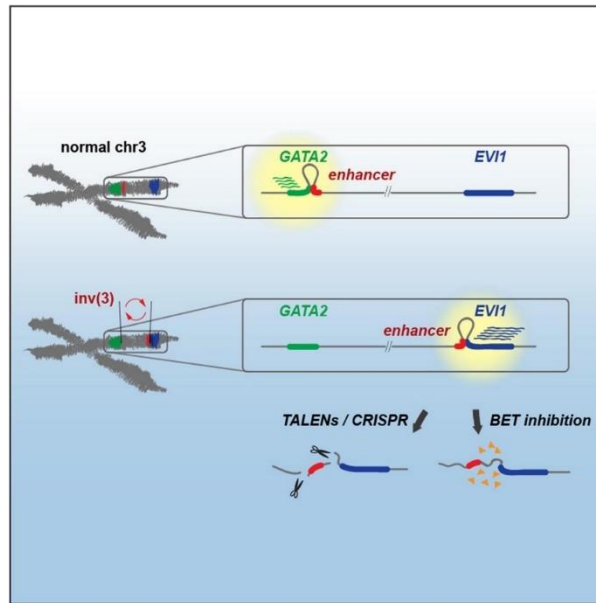


Figure 91. Rewiring of a single enhancer can deregulate two unrelated disease genes.

From Gröschel et al., 2014.

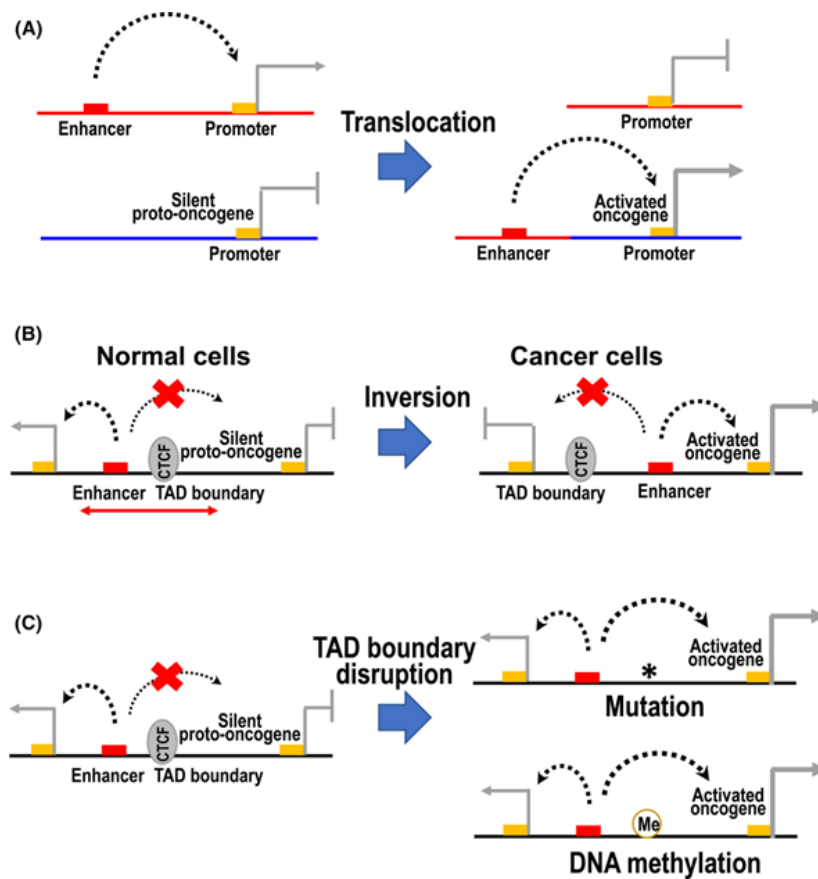


Figure 92. Enhancer rewiring by genome structural alterations.

From Okabe and Kaneda, 2021.

and driving the strong overexpression of this pioneer factor (Rheinbay et al., 2017).

Insulator sequences, recognized by CTCF and cohesin in order to define the boundaries of a TAD, are recurrently observed to be altered in different cancers, which leads to abnormal interactions between enhancers and promoters within a specific genomic region (Katainen et al., 2015) (Figure 90B). Insulator mutations allow aberrant DNA looping and chromatin 3D conformation, leading either to transcriptional activation of proto-oncogenes, or the downregulation of tumor-suppressors through loss of enhancer action (Hnisz et al., 2016). In many gliomas for example, IDH overexpression leads to the inhibition of histone demethylases, causing the hypermethylation of insulator sites and reduced CTCF binding, ultimately leading to oncogenic overexpression of the PDGFRA RTK through aberrant enhancer interactions (Flavahan et al., 2016). In leukemias, chromosomal rearrangements that disrupt TAD conformations can cause enhancer delocalization, allowing for the simultaneous loss of expression of the tumor suppressor GATA2 and the overexpression of oncogenic EVI1 (Gröschel et al., 2014) (Figure 91). EVI1 overexpression in leukemias has also been linked to the hijacking of MYC SEs, which is facilitated by abnormal CTCF-dependent looping (Ottema et al., 2021).

Soon after the first description of enhancer sequences and functions, it became apparent that their dysregulation has important roles to play in various diseases, collectively named enhanceropathies, which encompass all types of cancers (Banerji, Rusconi and Schaffner, 1981; Taub et al., 1982; Smith and Shilatifard, 2014; Chatterjee and Ahituv, 2017). Although recent high-throughput analyses have helped tremendously in that regard, it is still challenging to infer the causative links between disease phenotypes and small somatic mutations in enhancers, including single base alterations, insertions, or deletions (Claringbould and Zaugg, 2021; Okabe and Kaneda, 2021). In some instances, however, single mutations in enhancers have been linked with altered gene expression, such as in the case of an *PAX5*-associated enhancer in chronic lymphocytic leukemia (Puate et al., 2015). In another example, a polymorphism in a *LMO1*-associated enhancer causes gene expression modulation through reduced GATA3 TF binding, leading to neuroblastoma progression (Oldridge et al., 2015). However, larger genomic rearrangements such as translocations, inversions or focal amplifications have unequivocally been linked to so-called ‘enhancer hijacking or mistargeting’, in which genes are unintentionally activated by enhancer delocalization or TAD disruption (Northcott et al., 2014; Ryan et al., 2015; Drier et al., 2016) (Figure 92).

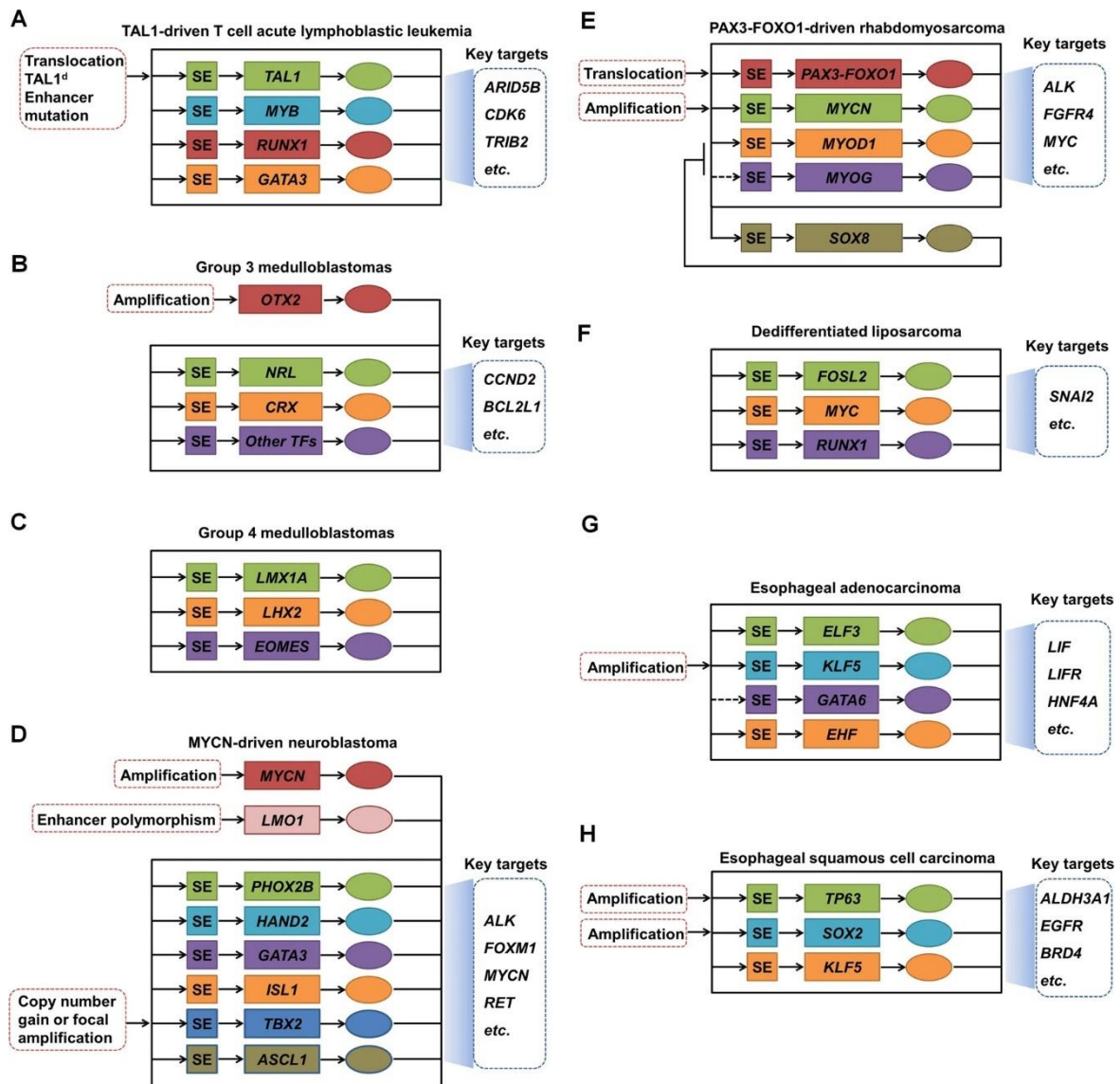
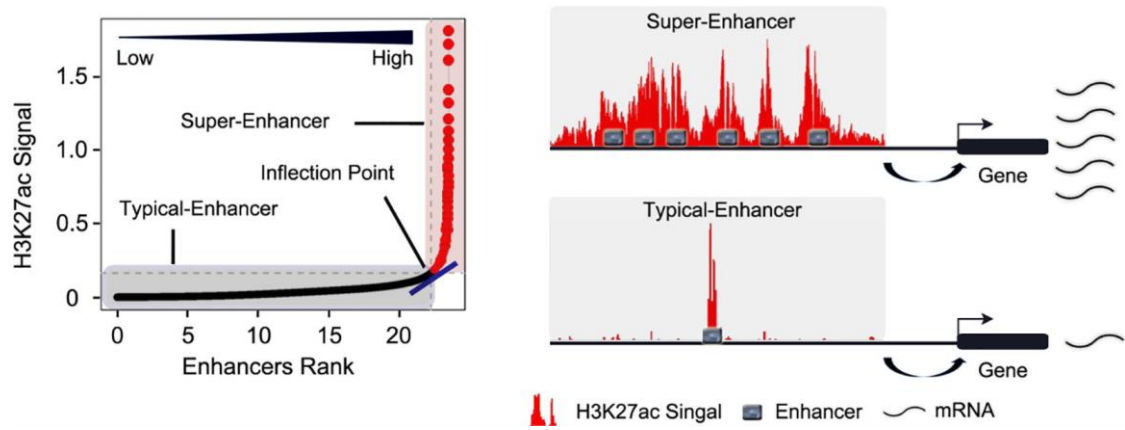


Figure 93. SEs and core transcriptional regulatory circuitries in different human cancers. Representative downstream targets of core regulatory circuitries are listed in blue dashed boxes. Gene loci and super-enhancers are depicted as rectangles.

From Chen et al., 2020.

These genetic mechanisms affecting enhancer function and activity have also been shown to cause the acquisition of SEs that activate oncogene expression in cancer cells (Figure 90C) (Jia et al., 2020; Bacabac and Xu, 2023). In normal cells, SEs act as the main drivers of core regulatory circuitries governing cell identity, as genes encoding lineage-determining master TFs are dependent on SEs, while the produced master TFs themselves bind and activate their SEs, producing cooperative feedforward loops (Adam et al., 2015; Zhang et al., 2020; Wang et al., 2022; Feng et al., 2023). However, cancer cells hijack SE-function to promote oncogenic transcription through the acquisition of aberrant, cancer-specific regulatory circuitries and feedback loops, to which they become highly addicted in order to maintain their cancer cell states (Hnisz et al., 2013; Sengupta and George, 2017; Chen et al., 2020) (Figure 93). Importantly, cancer-associated SEs differ from those encountered in normal cells at lineage genes, by their size (up to 300 kb vs 10 – 20 kb in normal cells), by their extraordinary degree of internal cooperativity but also by their less transient and more stable nature (Kwiatkowski et al., 2014; Mansour et al., 2014; Shrinivas et al., 2019). Since their first identification in myelomas as regions highly enriched in H3K27ac, BRD4, CDK7, P-TEFb, Mediator and TFs (Lovén et al., 2013), many tumor-specific SEs have been characterized in various cancers, where they were found to be driving the expression of core oncogenic drivers, such as MYC and MYCN in neuroblastoma and small cell lung cancer (SCLC) (Christensen et al., 2014; Durbin et al., 2018), RUNX1 in esophageal cancer, PAX5 in leukemias (Ott et al., 2018), or MITF, SOX10, AXL and PGC1 α in melanoma (Kaufman et al., 2016; Zhou et al., 2016; Eliades et al., 2018; Gelato et al., 2018). Importantly, these oncogene-associated SEs are absent in untransformed cells of identical lineage, suggesting that they are acquired de novo during tumorigenesis and underlie the oncogenic state (Hnisz et al., 2013; Sengupta and George, 2017). Numerous different mechanisms by which SEs drive all hallmarks of cancer progression have been uncovered, including implications in drug resistances, cellular plasticity, immune escape or metastasis (Sengupta and George, 2017; Thandapani, 2019; Wu and Shen, 2019; Tang et al., 2020; Wang et al., 2020; Li et al., 2021). As such, oncogenic SEs have been proposed as the key mechanism by which cancer cells sustain their abnormal survival and proliferative phenotypes which require increased ‘transcriptional fuel’ and gene expression (Chipumuro et al., 2014; Kwiatkowski et al., 2014; Grosveld, van Staalduinen and Stadhouders, 2021; Li et al., 2021) (Figure 94). Oncogenic SEs have been associated with the induction of key signaling pathways, such as MAPK signaling (Nakamura et al., 2017), but they also serve themselves as platforms on which oncogenic signaling converges to drive gene expression, as they tend to be enriched in specific TF-binding sites according to the distinct

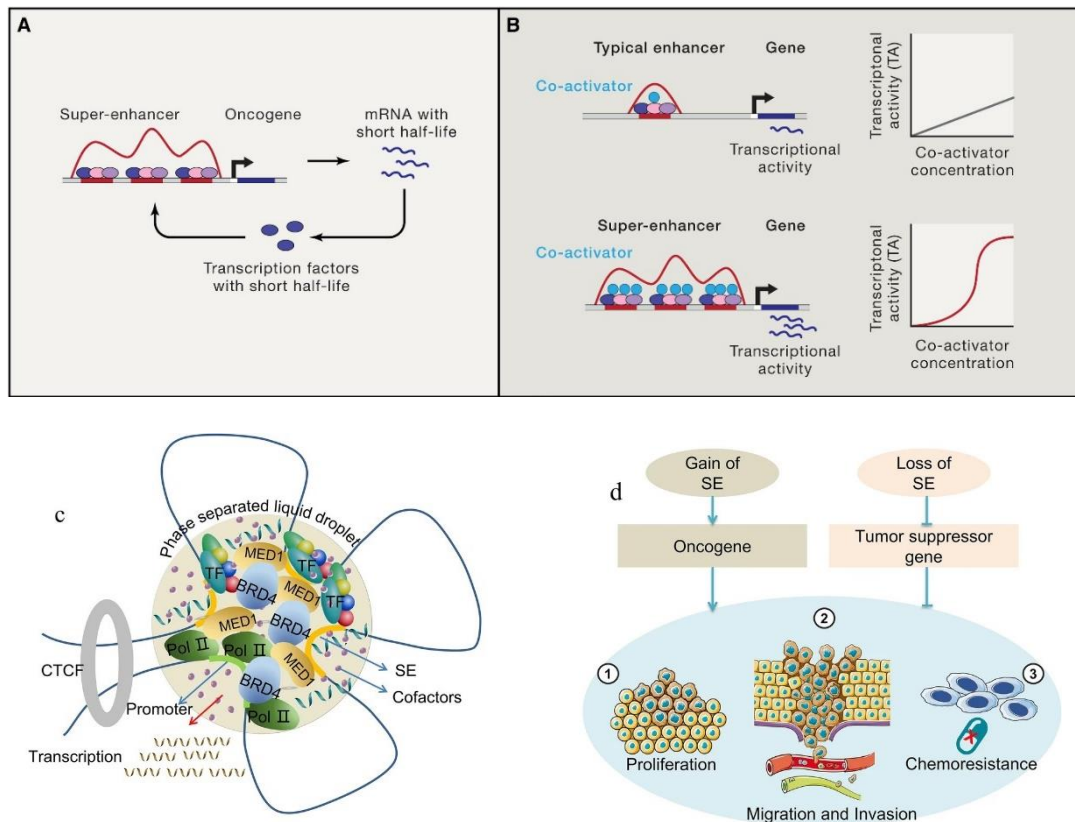


Figure 94. SE-dependent transcriptional addiction.

Adapted from Bradner, Hnisz and Young, 2017; Jia, Chng and Zhou, 2019.

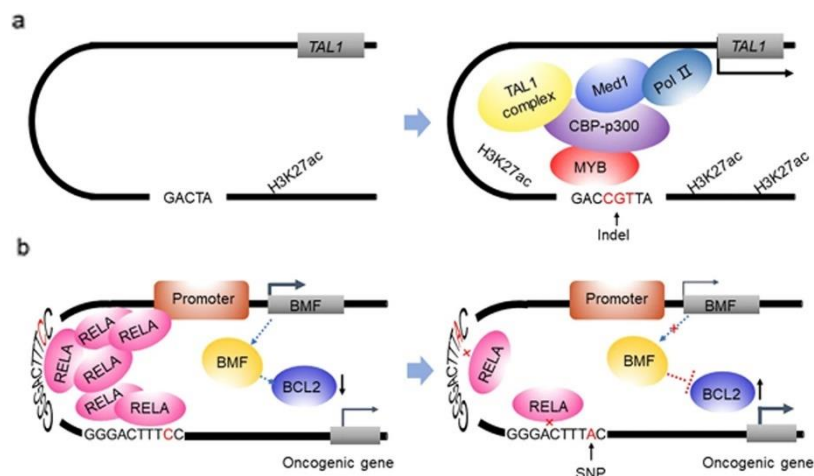


Figure 95. Mutations leading to oncogenic SE formation.

Adapted from Jia et al., 2020.

pathways on which a given type of cancer depends (Zamudio et al., 2019). In WNT-driven colorectal cancer cells for example, SEs are enriched in binding sites for TCF4, the WNT pathway terminal TF, whereas in hormone receptor-positive breast cancer cells, SE-associated genes are enriched for estrogen receptor binding sites, which is however not the case in triple-WT breast cancer cells (Hnisz et al., 2013, 2015; Wang et al., 2015). On the other hand, SE formation and function can itself be driven by deregulated signaling pathways, as aberrant MAPK signaling for example has been linked with SE induction, and altered Hippo signaling has been shown to facilitate global RNAPII pause release through SE activation (Galli et al., 2015; Nabet et al., 2015; Bojcsuk, Nagy and Balint, 2017).

During tumorigenesis, cancer cells have been shown to acquire SE dependencies through various mechanisms (Jia et al., 2020). Pre-existing enhancers can become SEs through small-scale somatic mutations, as was first observed in T-cell acute lymphoblastic leukemia, where small insertions upstream of the *TALI* oncogene introduced binding sites for the MYB TF, which recruits p300 and the Mediator, thereby forming a SE (Mansour et al., 2014) (Figure 95A). In other cases however, the mutational inactivation of a tumor-suppressor-associated SE leads to tumor progression, as is the case with a SNP within the intronic SE of the proapoptotic *BMF* gene in chronic lymphocytic leukemia, disrupting RELA binding sites and thus resulting in reduced enhancer activity and BMF expression, which leads to unrestrained antiapoptotic BCL2 function (Kandaswamy et al., 2016) (Figure 95B). Before-mentioned larger chromosomal rearrangements can lead to SE-hijacking, as in the case of adenoid cystic carcinoma, where a translocation event can reposition a distant SE in proximity to the *MYB* gene, which, in addition to activating its expression, also creates a positive feedback loop as MYB itself binds to the newly acquired SE (Drier et al., 2016). Focal amplifications of enhancer sequences can also lead to SE formation, causing for example MYC and MYCN overexpression (Chipumuro et al., 2014; Zhang et al., 2016). Importantly, the acquisition of a novel SE can result in the concomitant deregulation of multiple genes that may cooperatively contribute to tumorigenesis (Sengupta and George, 2017). Furthermore, in some cases, more ‘exotic’ mechanisms have been implicated in SE formation, such as viral infections (Gunnell et al., 2016), or increased inflammation (Brown et al., 2014; Zhou et al., 2022). Recent data also indicates that pre-existing and active SEs can become oncogenic by being highly and specifically hypermutated, as for example in diffuse large B cell lymphoma, where abnormal activity of activation-induced cytidine deaminase (AID) leads to SE alterations which inhibits the binding of transcriptional repressors and causes transcriptional dependencies via the overexpression of *BCL6*, *BCL2* and *CXCR4* proto-oncogenes (Bal et al., 2022). Finally, as SE

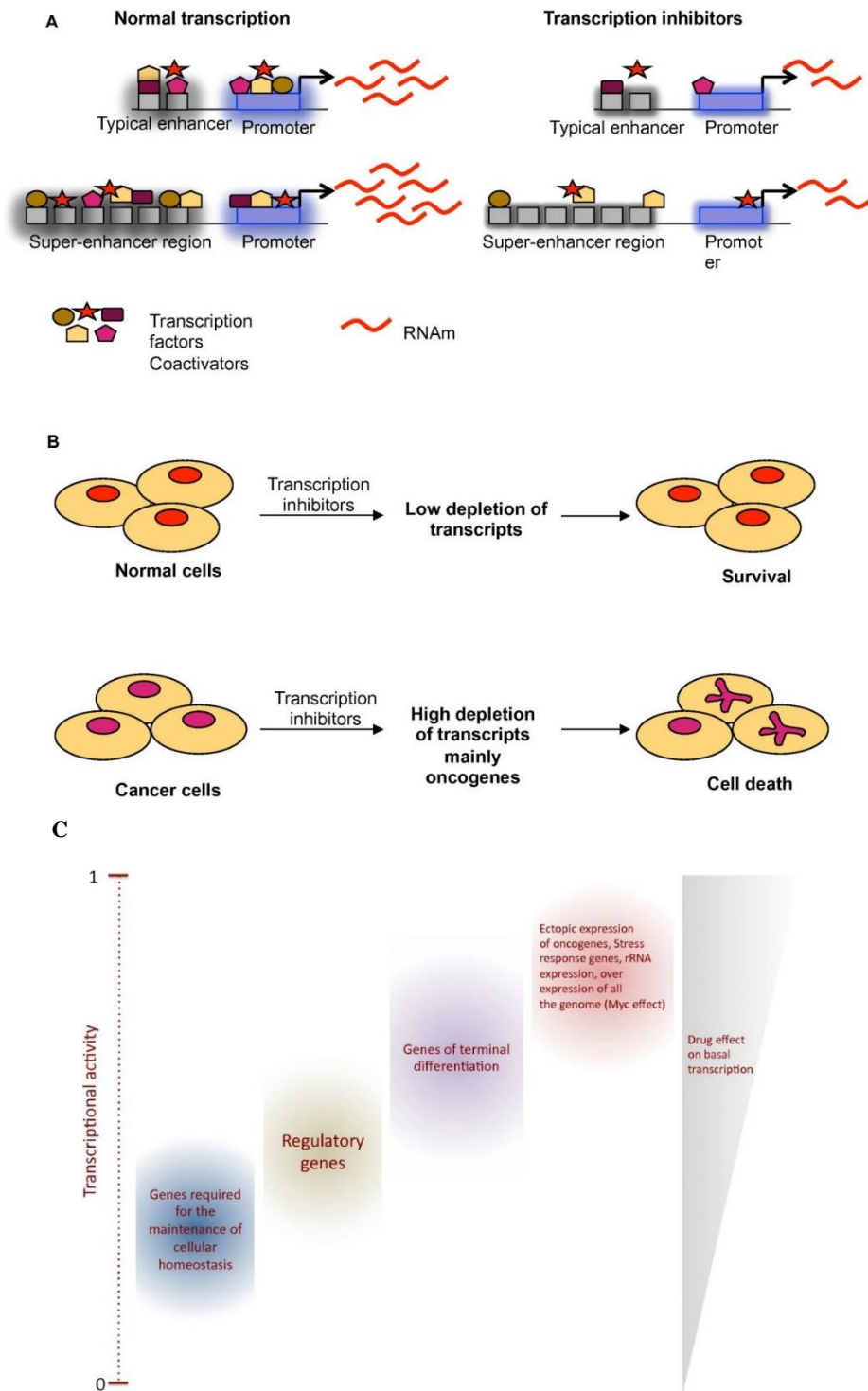


Figure 96. Differential effects of transcriptional inhibitors on cancer cells versus normal cells as a rationale for using transcriptional therapeutics.

Adapted from Villicaña, Cruz and Zurita, 2014.

acquisition is in many cases a crucial event needed to sustain the transcriptional addiction of cancer cells, profiling of SE landscapes has emerged in recent years as a powerful tool for uncovering novel target genes, particularly in cancers with few recurrently mutated genes (Mack et al., 2018; Fang et al., 2022).

2. Targeting transcriptional dependencies in cancer

2.1. Inhibiting transcription: From undruggable to reality

In recent decades, it has become more and more clear that rather than being a side-effect of tumorigenesis and tumor-progression, many neoplastic lesions depend heavily on transcription dysregulation and altered regulatory gene expression circuitries as the underlying driver of their aberrant phenotypes (Lee and Young, 2013; Gonda and Ramsay, 2015). Even though every type of cancer cell might display distinct abnormal gene regulatory networks, they potentially all share a common transcriptional addiction to the dysregulation of both trans-acting and cis-regulatory gene expression components, including altered chromatin states, the acquisition of oncogenic SEs, and a deregulated basal transcription machinery (Bradner, Hnisz and Young, 2017). These dysregulated gene expression states must be constantly upheld by tumoral cells to maintain their oncogenic hallmarks and to satisfy their high biological turnovers, making them particularly vulnerable to transcriptional inhibition (Augert and MacPherson, 2014; Franco and Kraus, 2015). As such, multiple studies in various models have demonstrated that cancer cells require higher levels of transcription than normal cells, whose lower biological activities make them less dependent on constant and high gene expression activity. Thus, the inhibition of transcriptional activity has emerged as a therapeutic avenue with substantial anti-neoplastic potential (Radhakrishnan and Gartel, 2006; Villicaña, Cruz and Zurita, 2014) (Figure 96).

Although it has been known for a long time that TFs are often deregulated in cancers, they have historically been viewed as ‘undruggable’, mainly because of challenges to develop small molecule inhibitors targeting protein–DNA or protein–protein interactions, as TFs do not possess more easily targetable enzymatic sites, and because of frequent off-targets effects (Darnell, 2002; Arkin, Tang and Wells, 2014; Chen and Koehler, 2020; Pathmanathan et al., 2022). However, recent structural insights have allowed for increased specificity through the

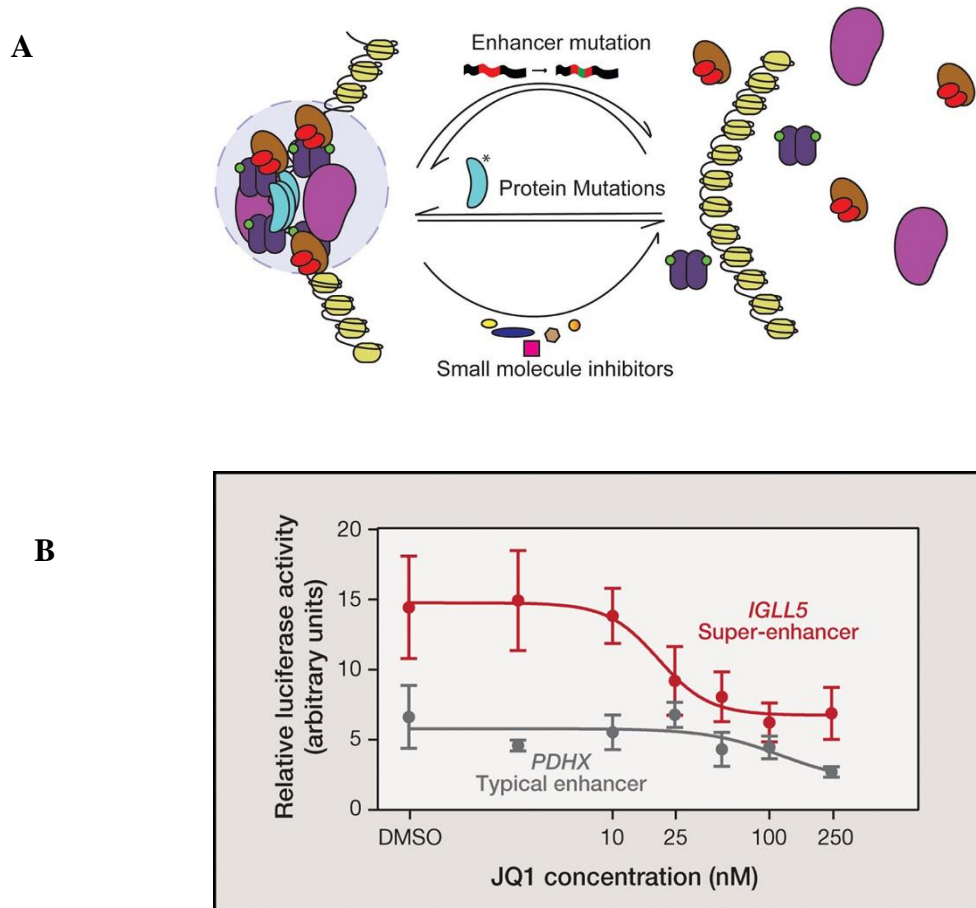


Figure 97. Assembly and disassembly of nuclear condensates by mutations or inhibitors (A) and SE vulnerability (B).

Adapted from Hnisz et al., 2017; and Mann and Notani, 2023.

identification of ‘hotspot residues’ and by using ‘allosteric modulation’, by which a small molecule binds to a location distinct from the primary site of activity of a TF in order to inhibit it (Bushweller, 2019). Besides the great successes of small molecules binding to specific nuclear hormone receptors (Burris et al., 2013), numerous recent promising in vivo results have allowed for next-generation TF inhibitors to enter clinical trials. For example, molecules inhibiting MDM2–p53 binding were shown to lead to reduced degradation and thus enhanced pro-apoptotic activity of p53 (Ding et al., 2013; Tovar et al., 2013), whereas targeting the fusion oncoprotein CBF β –SMMHC led to the reversal of cancer-associated transcription programs in leukemia (Illendula et al., 2015; Pulikkan et al., 2018). Of note, another recently developed strategy consists in using ‘proteolysis targeting chimaeras’ (PROTACs), which are bifunctional molecules, binding both to E3 ubiquitin ligases as well as to specific target proteins, leading to their proteasomal degradation (Bondeson et al., 2015; Lai and Crews, 2017). Proof-of-concept experiments showing that these molecules could be used to target transcriptional components such as BRD4 and EGFR were performed (Winter et al., 2015; Burslem et al., 2018; Shi et al., 2023), and current investigations are looking into the possibility of targeting bona fide TFs with PROTACs (Liu et al., 2021).

Besides these technological breakthroughs, other, more mechanistic and conceptual insights have emerged which allow for rationalizing the use of transcriptional inhibitors in cancer treatment by establishing that their effects, which could be presumed to act on many genes throughout the genome in a wide and indiscriminate manner, can nevertheless exert highly selective and oncogene-specific effects (Shin, 2018; Laham-Karam et al., 2020; Vervoort et al., 2022). The realization that liquid-liquid phase separation constitutes a crucial mechanism underlying the spatiotemporal coordination of biological activities such as gene expression control, but whose formation and function are heavily dysregulated in cancer cells, make them potentially promising targets (Banani et al., 2017; Kilgore and Young, 2022; Mehta and Zhang, 2022; Xie et al., 2023). Indeed, the inherent and specific properties of biomolecular condensates, i.e., their ability to compartmentalize and concentrate large numbers of molecules with related functions, thus accelerating biochemical reactions, can be leveraged for patient advantage. As such, the high degree of proneness for disassembly when structural components of condensate networks are inhibited, and distinct associated pharmacodynamics of cancer therapeutics, present an opportunity to consider new clinical hypotheses (Boija, Klein and Young, 2021; Suzuki and Onimaru, 2022; Mann and Notani, 2023).

Oncogenic SEs display exceptionally high densities of enhancer factors such as TFs, Mediator subunits, RNAPII, BRD4 or CDK7, which assemble into vast networks of

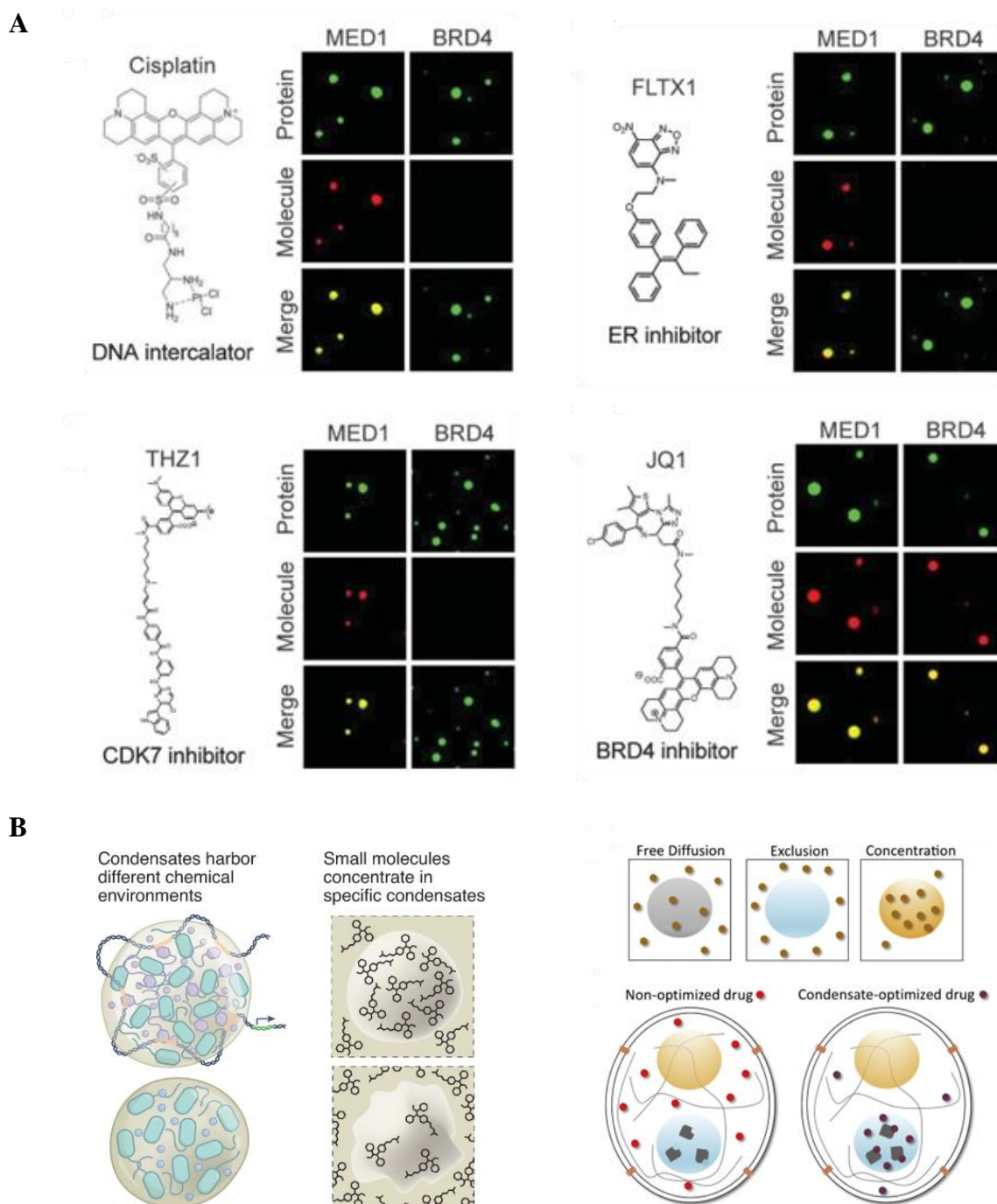


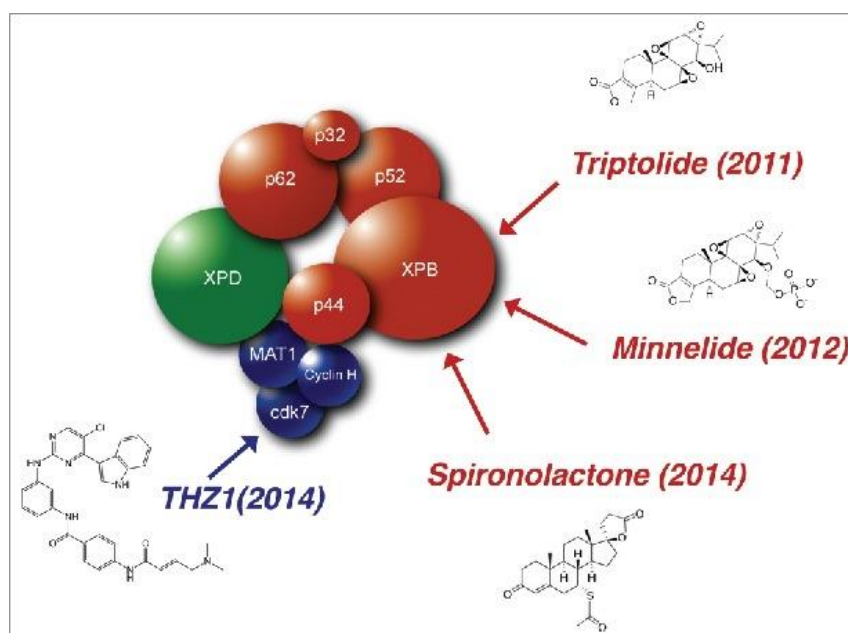
Figure 98. Partitioning of cancer therapeutics in nuclear condensates.

(A) Purified recombinant, fluorescently labeled MED1 or BRD4 formed condensation droplets in an in vitro assay where fluorescently labeled cancer drugs were added and their diffusion behavior was followed by confocal fluorescence microscopy. Results show that drugs partition selectively into specific protein condensates in vitro through physicochemical properties independent of the drug target. (B) Rationale for developing condensate-optimized drugs. Adapted from Howard and Roberts, 2020; Klein et al., 2020; and Kilgore and Young, 2022.

cooperative interactions. These aberrant networks have been shown to be remarkably vulnerable to disruption and disassembly by the pharmacological inhibition of constituent enhancer factors (Figure 97A) (Hnisz et al., 2017; Sengupta and George, 2017). Experimentally, the vulnerability of SEs to perturbation by inhibitors of common transcriptional co-factors has been demonstrated in different cancer models, in which oncogenic SEs were disrupted at drug concentrations that did not affect typical enhancers (Figure 97B). For example, while BRD4 is both encountered at typical enhancers and SEs, its inhibition in several cancer models by the small molecule JQ1 potently abrogates SE-associated gene expression at roughly 10-fold lower concentrations needed to impact non-SE-associated genes, resulting in reduced tumor growth and improved survival (Filippakopoulos et al., 2010; Chapuy et al., 2013; Lovén et al., 2013; Zanconato et al., 2018). In another very recent example, KAT8–IRF1 condensate formation was shown to cause PD-L1 overexpression and fueling tumor immune evasion, which was inhibited by condensate disruption (Wu et al., 2023).

Other SE-associated features, such as the tendency of their regulated genes to encode for TFs with short mRNA and protein half-lives, and their auto-regulatory nature, additionally explain the increased vulnerability of SEs to transcriptional inhibition (Bradner, Hnisz and Young, 2017). Furthermore, the team around Klein et al. from Richard A. Young's lab have shown in a landmark paper in 2020 that certain small-molecule therapeutics preferentially partition and concentrate into nuclear condensates, thereby enhancing drug-efficacy in these regions (Figure 98). By ingeniously creating artificial phase condensates with transcriptional regulator proteins such as the Mediator subunit MED1 or the coactivator BRD4, they observed that the addition of antineoplastic drugs did not result in a free-diffusion behavior. Instead, the drugs either concentrated or avoided different classes of condensates, based on the physiochemical properties of the scaffold proteins constituting these phase separates. For example, drugs with aromatic rings preferentially concentrated in MED1 condensates, because they phase-condensated with MED1-associated aromatic rings. These results were confirmed in cancer cells, where cisplatin, a widely used chemotherapeutic agent, was found to be concentrated 600-fold in MED1-condensates such as SEs, showcasing how a drug, previously considered an indiscriminate DNA-crosslinking agent, could in fact preferentially target these key regions of cancer-cell control. In a similar fashion, tamoxifen was shown to be partitioned into MED1-condensates, independently of the presence of its molecular target, estrogen receptor, showing that the physiochemical properties of this partitioning do not depend on those that underlie drug-protein target interactions. The authors show that this might impact drug

A



B

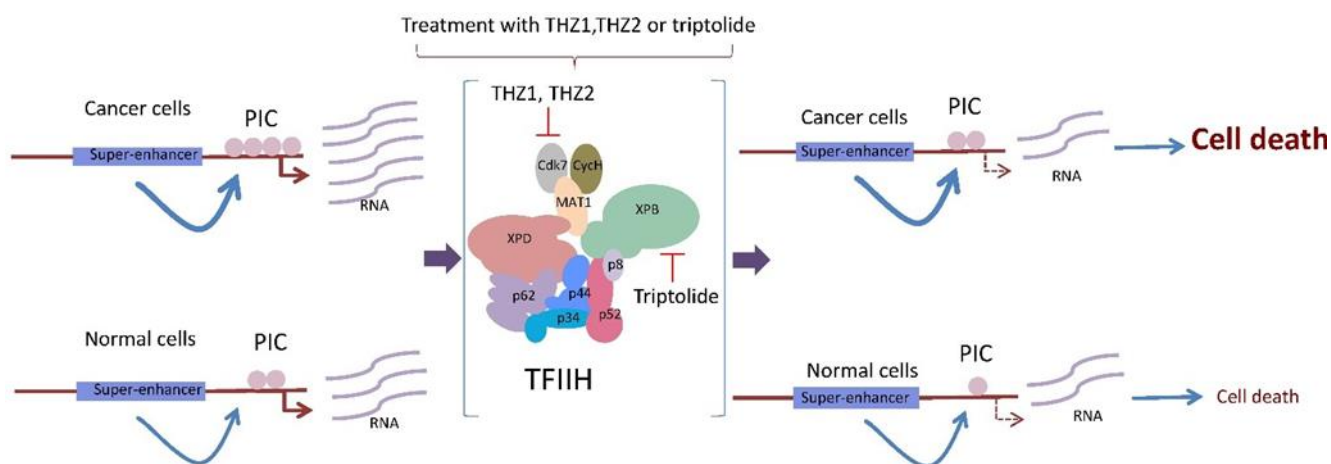


Figure 99. Drugs targeting TFIIF subunits (A) and their potential effects on the transcriptional addiction of cancer cells (B).

Adapted from Zurita and Cruz-Becerra, 2016; and Berico and Coin, 2017.

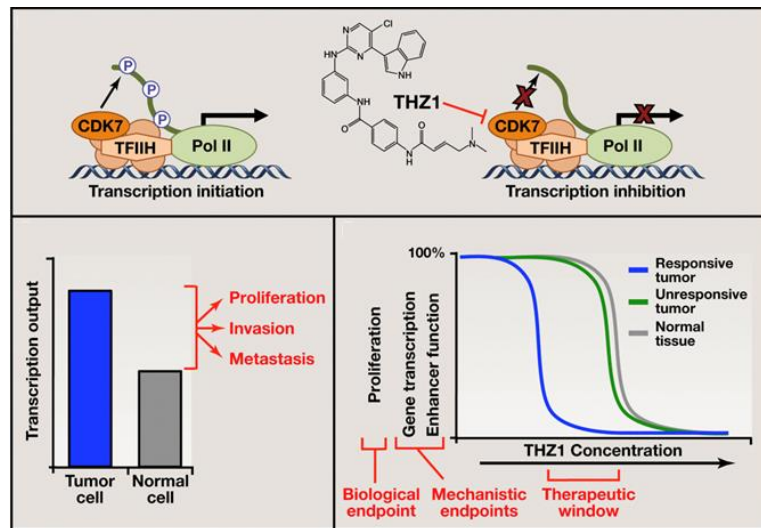
resistances, as MED1 overexpression in breast cancer cells lead to enlarged SE condensates and increased tamoxifen partitioning, impairing its overall efficacy. The inversed effect was described for drugs which partitioned into phase condensates as well, but whose targets were precisely the proteins enriched at SEs, such as BRD4 and CDK7. As such, drugs such as JQ1 and THZ1, a potent CDK7 inhibitor, partitioned selectively to SEs and preferentially disrupted transcription at those loci, further explaining how the targeting of global gene regulators such as BRD4 or CDK7 can have selective effects on oncogenes. While the exact physiochemical intricacies of condensate-mediated drug partitioning remain to be explored, these results showcase the rationale for developing condensate-optimized drugs, presenting the ability to concentrate preferentially in the same condensate as their targets (Howard and Roberts, 2020; Kilgore and Young, 2022).

In conclusion, inhibiting oncogenic transcription is more and more coming into consideration as an attractive therapeutic option, especially for cancers without clear driver mutations lacking thus available targeted therapies. Furthermore, evidence is emerging which relativizes the initial hypothesis that factors involved in gene expression are ‘undruggable’ because of their role in fundamental and ubiquitous biological processes which implies associated potentially toxic consequences on global gene expression. The discovery of oncogenic SEs and the elucidation of drug partitioning mechanisms explaining the initially confusing extraordinary vulnerability of SEs to transcriptional perturbation, opens the possibility of clinically useful transcriptional inhibitors. These drugs should optimally selectively target oncogenic gene expression and induce cancer cell death without causing excessive toxicity in normal cells. In the next pages, the mechanisms of action of three relevant transcriptional inhibitors will be further examined: THZ1 and Triptolide which selectively inhibit enzymatic subunits of the TFIIF GTF, and Lurbinectedin, a novel, marine-derived DNA-binder.

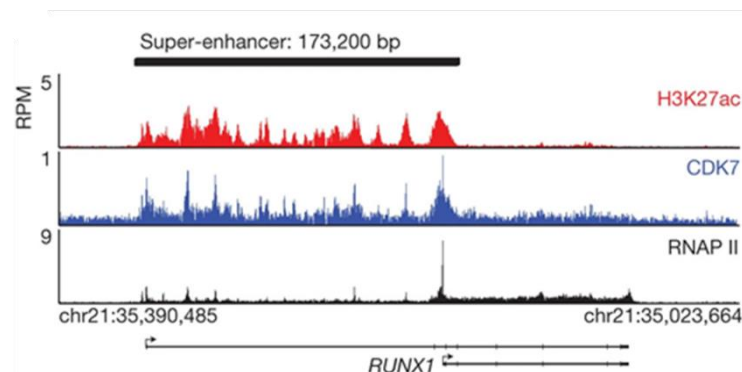
2.2. Targeting transcription and SEs through TFIIF: THZ1 and Triptolide

Due to its central role in cellular processes such as transcription, cell cycle control and DNA repair, TFIIF has become a privileged target to exploit in antineoplastic therapy (Zurita and Cruz-Becerra, 2016). Being a key actor of the basal transcription machinery, significant effort was put into finding molecules which could inhibit its activities, and to date, specific drugs targeting two of its three enzymatic subunits - CDK7 and XPB - have been relatively well characterized (Kuper and Kisker, 2021) (Figure 99A). Some of these TFIIF inhibitors have entered clinical trials for various cancers (Noel et al., 2019; Sava et al., 2020), in the hopes of

A



B



C

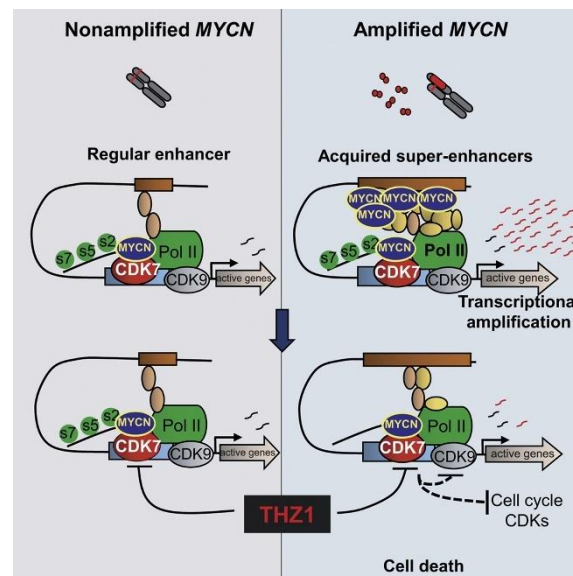


Figure 100. Rationale for using THZ1 to target transcriptional addiction (A), ChIP-Seq data showing the high enrichment of CDK7 at SEs (B) and the SE-decommissioning effect of THZ1 in cancers such as MYCN-amplification driven neuroblastoma (C).

Adapted from Chipumuro et al., 2014; Kwiatkowski et al., 2014; and Franco and Kraus, 2015.

selectively targeting their transcriptional addictions (Berico and Coin, 2017) (Figure 99B).

Cyclin dependent kinases (CDKs) have been proposed as attractive targets for cancer therapy because of their deep involvement in either transcription or cell cycle control (Parua and Fisher, 2020; Constantin et al., 2022). Uniquely amongst CDKs, the TFIIF kinase subunit CDK7 has essential roles in both of these processes, as it activates cell cycle-associated CDKs and regulates RNAPII activity by phosphorylating its CTD as well as other actors involved in gene expression control such as transcription-associated kinases CDK9, CDK12, and CDK13 (Rimel et al., 2020). Although this invokes a ubiquitous "master regulator" role in transcription, Kwiatkowski et al. in 2014 showed that multiple types of cancer cells display exceptional sensitivity to THZ1, a small molecule able to irreversibly bind CDK7 with high affinity and specificity (Figure 100A). This specificity relies on the fact that THZ1 is a phenylaminopyrimidine with a cysteine reactive acrylamide moiety that covalently binds to cysteine 312 located just outside of the catalytic domain of CDK7. This specificity was useful to further elucidate the role of CDK7 in gene expression events such as co-transcriptional capping and pausing, but it also showed that the inhibition of CDK7 at low nanomolar doses of THZ1 leads to the specific disruption SE-mediated oncogene expression without major effects on basal transcription, which requires higher doses and longer treatments (Chipumuro et al., 2014; Christensen et al., 2014; Coin and Egly, 2015; Nilson et al., 2015; Wang et al., 2015). Indeed, CDK7 was shown in various cancer cells to be heavily enriched at SEs, such as near the *RUNX1* gene in T-cell acute lymphoblastic leukemia, which was shown to be exceptionally vulnerable to THZ1 and its disruption of the core oncogenic transcriptional regulatory circuitry (Kwiatkowski et al., 2014) (Figure 100B). Another example of how CDK7 inhibition selectively targets transcriptional addiction was shown in both SCLC and neuroblastoma cells, where oncogenic SE-associated MYC or MYCN expression was potently abrogated at low doses of THZ1, causing massive suppression of MYC- or MYCN-driven global transcriptional amplification and tumor regression without the introduction of systemic toxicity in mouse models (Chipumuro et al., 2014; Christensen et al., 2014) (Figure 100C). These promising pre-clinical results led to the development of THZ1 analogues and other CDK7 inhibitors, four of which are currently undergoing clinical trials (Patel et al., 2018; Sava et al., 2020; Sharma et al., 2022). Despite this, the exact molecular functions of CDK7 at SE loci are not clear, and it is currently not settled whether CDK7 is present as an independent entity from the CAK or TFIIF in SEs or if other TFIIF subunits are recruited and have SE-associated functions as well (Berico and Coin, 2017).

Indeed, other enzymatic subunits of TFIIH such as the XPB translocase have been hypothesized to be enriched at SEs as well, but no direct evidence of that, such as through ChIP-Seq analysis, has been observed yet. The potential involvement of XPB in SE-associated oncogene expression mainly stems from a single study demonstrating that treatment of pancreatic cancer cells with Triptolide (TPL), elicited the downregulation of SE-associated genes such as *MYC* (Noel et al., 2020) (Figure 101). TPL is a diterpenoid triepoxide extracted from a vinelike Chinese medicinal herb called *Tripterygium wilfordii* or Thunder God vine, which displays efficacy against multiple diseases, including inflammatory diseases and various cancers (Kupchan et al., 1972; Noel et al., 2019; Yuan et al., 2019). Although other targets have been proposed, such as interactions with protein regulators of autophagy, EMT, or inflammation signaling (Figure 102), TPL was shown to display a very high specificity for XPB, by covalently binding to cysteine 342 and thus effectively inhibiting its ATPase and translocase activities (Titov et al., 2011). Strikingly, cells were observed to become largely insensitive to the effects of TPL by mutating Cys342 of XPB, showing that the cellular effects exerted by TPL seem to be mainly due to XPB inhibition and not the other identified proteins for which interactions were shown (He et al., 2015; Kuper and Kisker, 2021). TPL induces potent RNAPII-dependent transcription inhibition but also prevents NER, and has therefore been studied as a chemosensitization agent for cancer cells (Chen, Gao and Shilatifard, 2015; Wang, Wang and Xu, 2015; Fanelli et al., 2020). Nevertheless, the poor solubility and bioavailability, coupled with reported hepatic toxicities limit the clinical use of TPL (Xi et al., 2017). Instead, multiple water-soluble prodrugs of TPL were developed, such as Minnelide which is currently in clinical trials as a ‘SE inhibitor’ for treatment of advanced pancreatic cancers (Skorupan et al., 2022). However, the exact molecular roles of XPB in SE function remain unclear.

2.3. Inhibiting oncogenic gene expression with DNA-binding molecules: Lurbinectedin

Besides the direct inhibition of proteins involved in the transcription process, another therapeutic strategy to target gene expression consists in using DNA-binding molecules. Perhaps the prime example of anticancer DNA binders are platinum drugs, including cisplatin, carboplatin, and oxaliplatin, which elicit cytotoxic responses in multiple cancers, by forming covalent adducts with purine DNA bases (Dasari and Tchounwou, 2014). This binding is widely considered as non-specific and tends to affect the entire genome, eliciting multiple effects such as generalized DNA damage, replication stress and transcriptional inhibition,

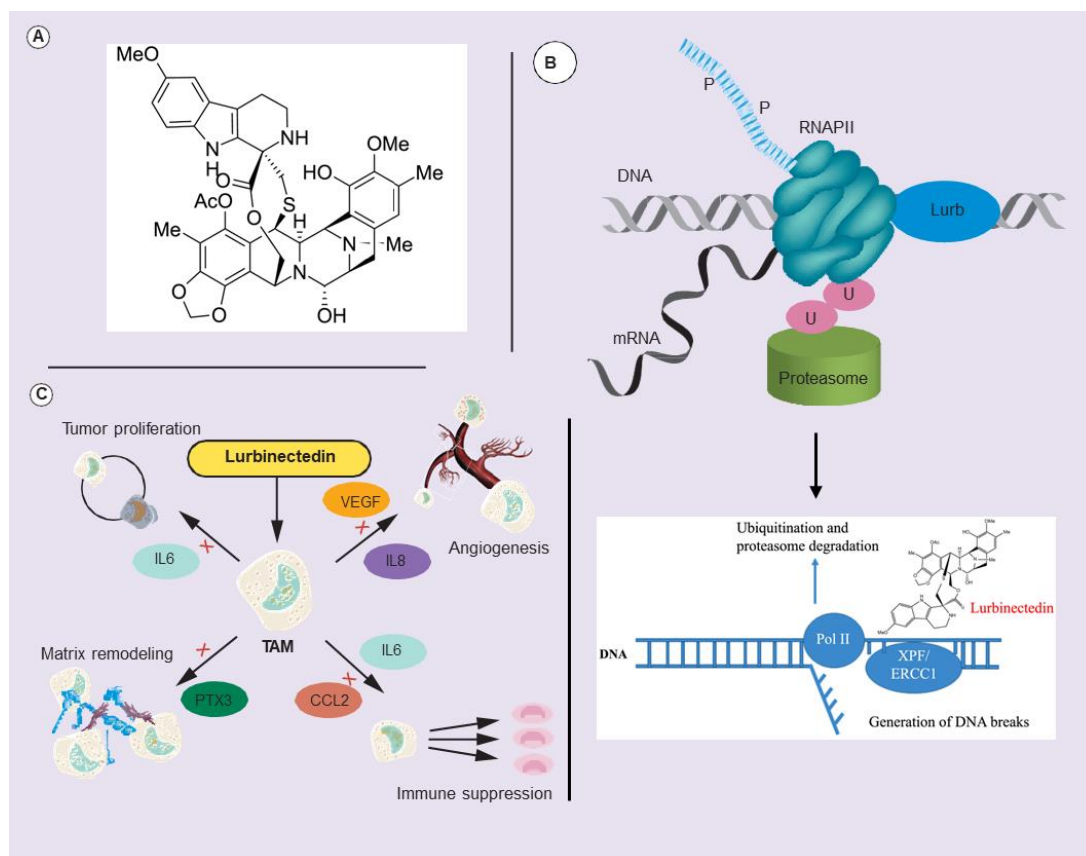


Figure 103. Structure of Lurbinectedin (A), its mechanism of action (B) and its effects on immune cells of the TME (C).

Adapted from Farago et al., 2019.

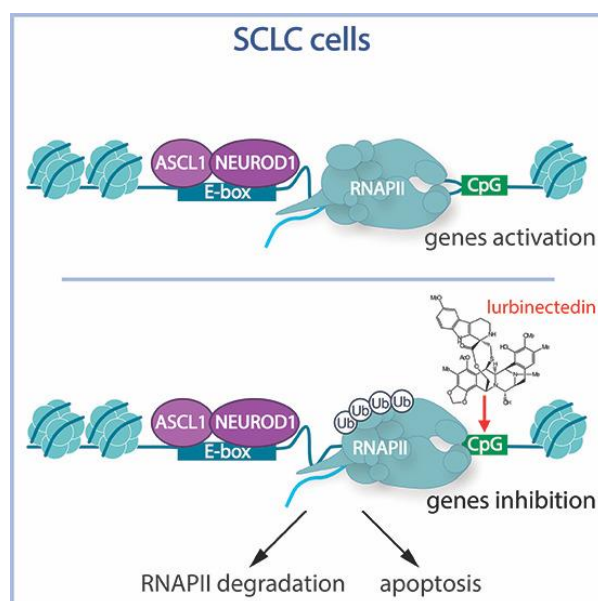


Figure 104. Selective targeting of transcriptional addiction of SCLC cells.

From Costanzo et al., 2022.

potentially explaining the severe associated toxicities, although recent condensate-based evidence might suggest a previously unsuspected specific transcriptional effect (Todd and Lippard, 2009; Klein et al., 2020; Forgie, Prakash and Telleria, 2022; Tang et al., 2023).

Among the newer generations of DNA binders, Lurbinectedin stands out because of its unique mechanism of action (Gadducci and Cosio, 2022). Developed by PharmaMar SA, Lurbinectedin is a synthetic ecteinascidin tetrahydroisoquinoline (Figure 103A) derived from Trabectedin, a marine-sourced molecule clinically used in sarcomas and ovarian cancers and extracted from the Caribbean tunicate *Ecteinascidia turbinata*, (Erba et al., 2001; Barone et al., 2017; Pereira et al., 2019). Compared to its natural counterpart, Lurbinectedin displays pharmacokinetic and pharmacodynamic advantages, and was shown to be a potent DNA minor groove covalent binder with high specificity toward CGG triplets (Leal et al., 2010; Vidal et al., 2012; Romano et al., 2013). Of note, Lurbinectedin predominantly binds to CG-rich sequences within accessible chromatin regions, as it has been shown to particularly target the vicinities of promoters of actively transcribed, protein-coding genes, enriched in CpG islands and displaying an open chromatin conformation (Costanzo et al., 2022). Thus, Lurbinectedin differs from many other alkylating DNA binders by exhibiting a clear specificity for transcribed gene regions, potentially explaining its less toxic side effects. The binding of Lurbinectedin to these regions leads to the irreversible stalling of elongating RNAPII in front of the adduct, followed by its degradation by the ubiquitin/proteasome machinery and leading to the targeted gene not being expressed (Santamaría Nuñez et al., 2016) (Figure 103B). The stalling of RNAPII leads furthermore to the recruitment of the NER machinery, with the ERCC1 and XPF endonucleases unsuccessfully trying to excise the lesion, thereby generating DNA breaks. As such, the combined effect of the resulting DNA damages and transcriptional inhibition leads to cancer cell apoptosis (Harlow et al., 2016; Lima et al., 2016; Tumini et al., 2019). This mechanism was extensively studied in SCLC, a cancer displaying important transcriptional addiction because of the dependence on the ASCL1 and NEUROD1 master TFs (Christensen et al., 2014). Lurbinectedin was shown to potently abrogate the expression of SCLC-associated oncogenes, including *MYC*, *MYB* and *BCL2* (Costanzo et al., 2022) (Figure 104). Lurbinectedin has also been observed to modulate the TIME, by depleting tumor-associated macrophages and provoking immunogenic cancer cell death, thus potentially enhancing the anti-tumor response to immunotherapies (Belgiovine et al., 2017; Xie et al., 2019; Allavena et al., 2022). Based on promising results and safety profiles, the FDA granted accelerated approval to Lurbinectedin for the second-line treatment of metastatic and relapsed SCLC in 2021, but its clinical effects on other types of cancer remain relatively unexplored (Trigo et al., 2020; Singh et al., 2021).

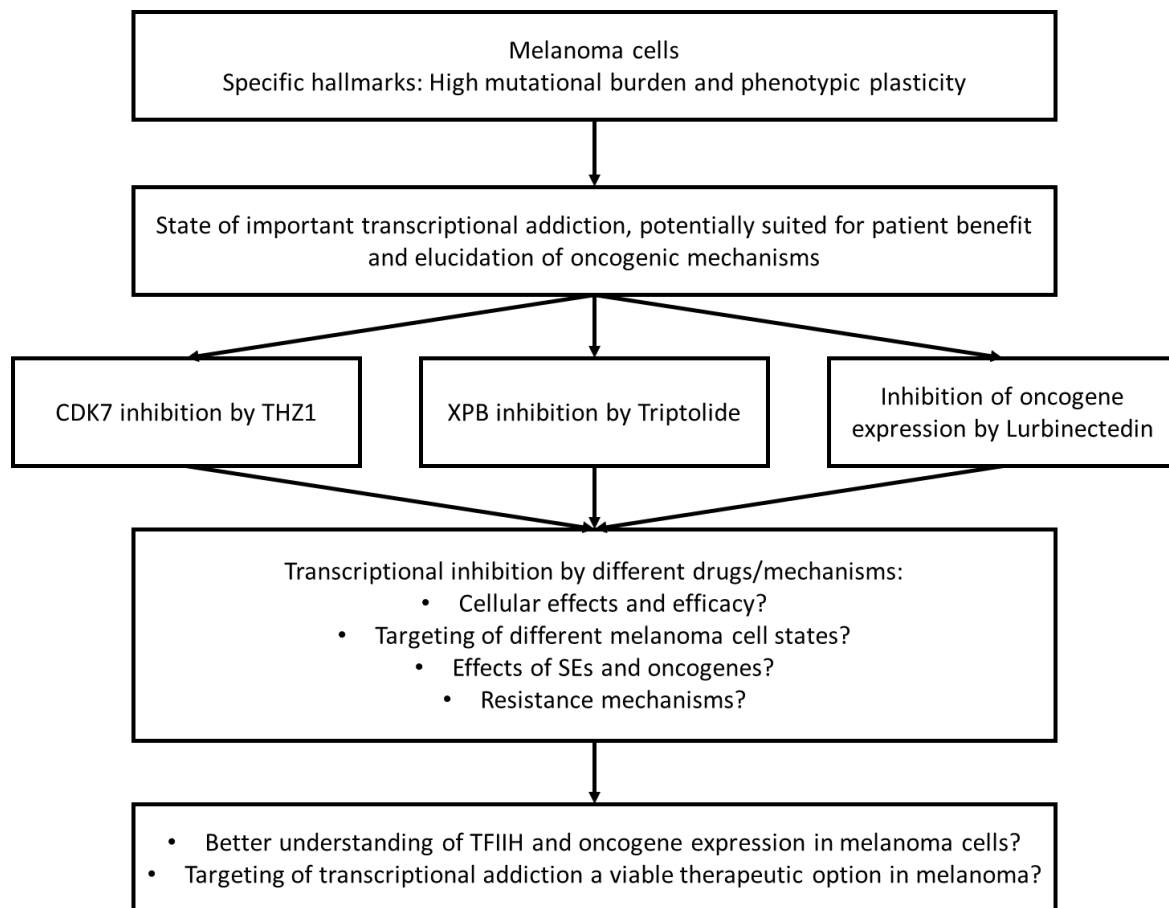


Figure 105. Targeting transcriptional addiction in melanoma: Broad aims of the project.

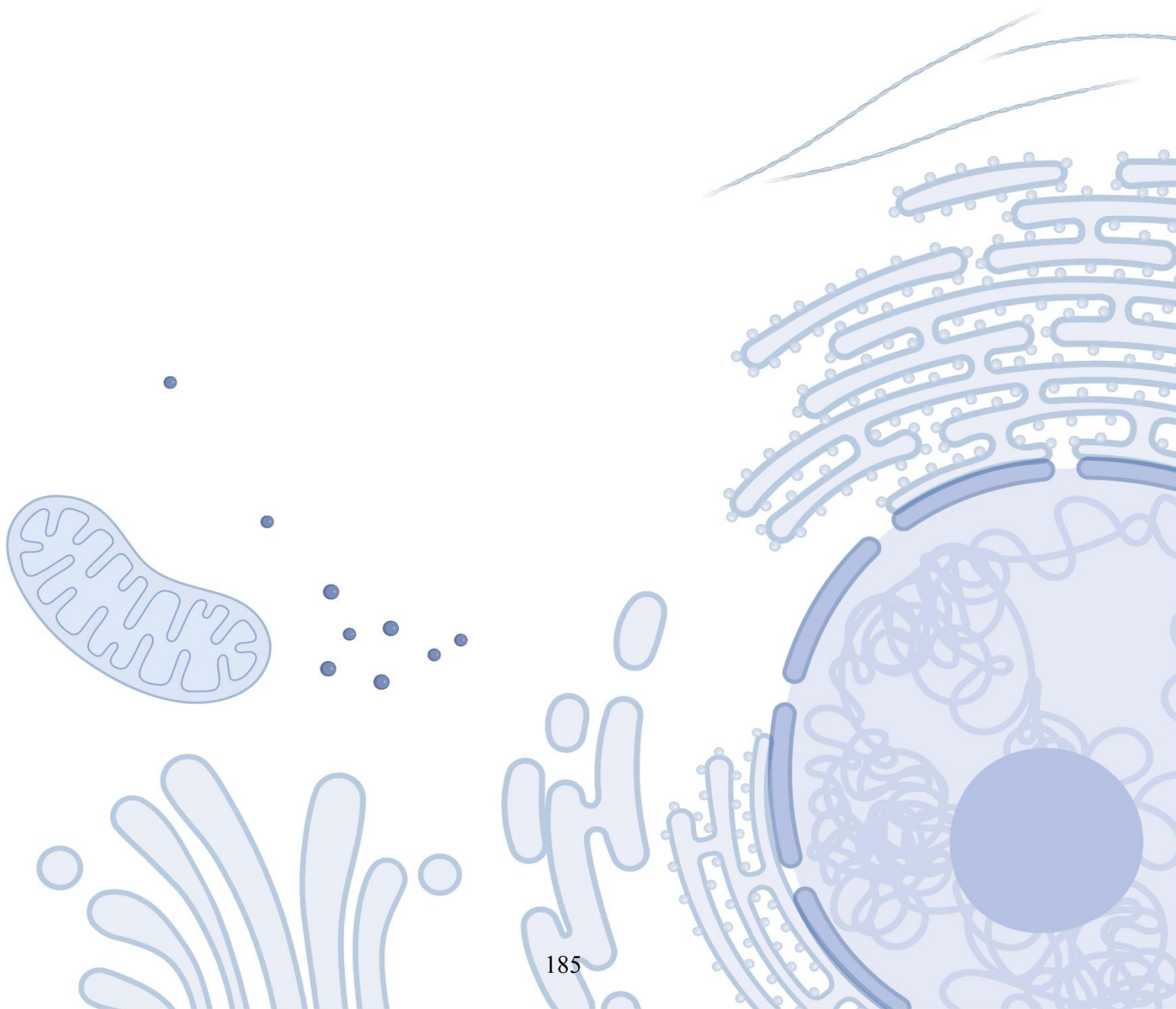
C. Targeting transcriptional addiction in melanoma: Research context and objectives

While the targeting of transcriptional addiction is becoming increasingly viewed as an attractive therapeutic option in multiple types of cancers, its effectiveness concerning melanoma remained somewhat unexplored when my thesis project was first initiated. Compared to other types of cancers, melanoma cells display very high degrees of mutational burdens, and their gene expression patterns might therefore be proportionally strongly dysregulated. Furthermore, the notorious cell-state plasticity of melanoma cells indicates a strong dependency on tightly regulated oncogenic gene expression programs, which rely on relatively well-studied, SE-dependent melanoma master TFs such as MITF or SOX10. Based on these facts, we hypothesized that melanoma might be a cancer with a high degree of transcriptional addiction, which could be potentially leveraged for patient benefit. The main roadblock to effective melanoma treatment today consists in the fact that multiple different resistant cell states emerge during drug treatments. However, while these different melanoma cell states differ phenotypically, they might all be dependent on distinct transcriptional expression patterns, whose inhibition could uniformly affect their survival. Furthermore, the use of specific molecules targeting trans- or cis-acting regulators of the transcriptional process, such as TFIID or SEs, might elucidate novel associated roles and functions, as well as provide important insights into melanoma cell core regulatory circuitries and TF dependencies. As melanoma cells are infamously prone to developing therapeutic resistances, we also argued that they might be a suitable model to study potential drug resistance mechanisms against transcriptional inhibitors, representing a somewhat untapped research area.

My thesis work thus aims to elucidate the mechanistic underpinnings of the role of transcriptional addiction in melanoma pathogenesis, by focusing especially on the function of TFIID on SE-mediated oncogene expression, and on the effects and efficacy of novel types of marine-derived DNA binders (Figure 105). By using three different types of transcriptional inhibitors (THZ1 targeting CDK7, TPL targeting XPB, and Lurbinectedin targeting actively transcribed genes), my research characterized the impacts of these drugs on melanoma cells. Furthermore, I studied whether the clinical application of transcriptional therapeutics might be a viable addition to the existing framework of treatments, and how melanoma cells might develop insensitivities against these drugs.

Results

Section I: Targeting TFIIH in melanoma










Preface to Article 1: Context and contributions

When I started my PhD in late 2019, several studies had shown that the pharmacological inhibition of CDK7 led to promising effects in various types of cancers. Eliades et al. had reported in 2018 that by exposing several melanoma cell lines to THZ1, they potently abrogated SE-dependent *MITF* and *SOX10* expression, thereby severely affecting cell survival. Before my arrival, our lab, in close collaboration with the team of Dr. Irwin Davidson (IGBMC), recapitulated these promising results by observing that the treatment of BRAFV600E/PTEN^{-/-} melanoma mouse models with THZ1 effectively blocked tumor growth (Data not shown). However, Eliades et al. exclusively studied differentiated melanoma cells and thus did not address the role of CDK7 and the effects of its inhibition on melanoma cell plasticity. Furthermore, the molecular and phenotypical consequences of prolonged CDK7 inhibition on melanoma cells remained a complete mystery.

During the first year of my PhD, I assisted Pietro Berico (at the time a doctoral candidate whose main project was to better understand the role of SEs in melanoma biology) in elucidating these outstanding questions. As such, we especially focused on investigating the differential effects of CDK7 inhibition on the two main types of melanoma cells, the differentiated/melanocytic and the undifferentiated/mesenchymal-like states, and tried to dissect the molecular roles of CDK7 in melanoma cells. We observed that the inhibition of CDK7 by THZ1 induced the dedifferentiation of melanocytic melanoma cells and gave rise to a GATA6-dependent gene expression program promoting melanoma survival and drug tolerance. We showed that CDK7 drives the expression of MITF, which in melanocytic melanoma cells binds to an intronic region of *GATA6* to repress its expression, leading to *GATA6* targets, such as the ABCG2 efflux pump, to remain silenced. My concrete and main contributions in this project, published in *EMBO Reports*, consisted in functionally characterizing GATA6 and ABCG2 in melanoma cells (Figures 3, 4, 5, 7, EV2, and EV3), helping to uncover this new transcriptional program and elucidating a role of CDK7 in melanoma phenotype switching. Strikingly, these results also underscore that while short-term in vivo treatments with transcriptional inhibitors such as THZ1 might provide initially promising benefits, it is of primordial importance that the long-term consequences are considered as well. Indeed, our results point to a potential danger of using CDK7 inhibitors in cancers prone to undergo EMT and dedifferentiation, and pushed us to investigate whether other transcriptional inhibitors might elicit similar responses in melanoma cells.

CDK7 and MITF repress a transcription program involved in survival and drug tolerance in melanoma

Pietro Berico^{1,2,3,4} , Max Cigrang^{1,2,3,4} , Guillaume Davidson^{1,2,3,4}, Cathy Braun^{1,2,3,4}, Jeremy Sandoz^{1,2,3,4}, Stephanie Legras^{1,2,3,4}, Bujamin Hektor Vokshi^{1,2,3,4} , Nevena Slovic^{1,2,3,4} , François Peyresaubes^{1,2,3,4}, Carlos Mario Gene Robles^{1,2,3,4}, Jean-Marc Egly^{1,2,3,4} , Emmanuel Compe^{1,2,3,4}, Irwin Davidson^{1,2,3,4,*}  & Frederic Coin^{1,2,3,4,**} 

Abstract

Melanoma cell phenotype switching between differentiated melanocytic and undifferentiated mesenchymal-like states drives metastasis and drug resistance. CDK7 is the serine/threonine kinase of the basal transcription factor TFIIF. We show that dedifferentiation of melanocytic-type melanoma cells into mesenchymal-like cells and acquisition of tolerance to targeted therapies is achieved through chronic inhibition of CDK7. In addition to emergence of a mesenchymal-type signature, we identify a GATA6-dependent gene expression program comprising genes such as *AMIGO2* or *ABCG2* involved in melanoma survival or targeted drug tolerance, respectively. Mechanistically, we show that CDK7 drives expression of the melanocyte lineage transcription factor MITF that in turn binds to an intronic region of *GATA6* to repress its expression in melanocytic-type cells. We show that *GATA6* expression is activated in MITF-low melanoma cells of patient-derived xenografts. Taken together, our data show how the poorly characterized repressive function of MITF in melanoma participates in a molecular cascade regulating activation of a transcriptional program involved in survival and drug resistance in melanoma.

Keywords CDK7; TFIIF; MITF; melanoma; GATA6

Subject Categories Cancer; Chromatin, Transcription & Genomics; Signal Transduction

DOI 10.15252/embr.202051683 | Received 7 September 2020 | Revised 18 June 2021 | Accepted 25 June 2021 | Published online 23 July 2021

EMBO Reports (2021) 22: e51683

Introduction

Malignant melanoma is responsible for 70% of skin cancer deaths in Western countries (Eggermont *et al*, 2014). Somatic gain-of-function mutations in the proto-oncogene kinase *BRAF* are the commonest mutations (60%) with the T → A transversion underlying *BRAF*^{V600E} comprising the majority of *BRAF* mutations (Brose *et al*, 2002; Davies *et al*, 2002). As an alternative to *BRAF* mutations, human melanomas frequently (35%) carry *NRAS* or *NF1* mutations, while the remainder (5%) shows no mutations of these three genes (Triple-Wt) (Hodis *et al*, 2012).

Melanoma is notorious for its heterogeneity based on co-existing melanoma cell phenotypes. *In vitro*, transcriptomic analysis of melanoma cells has established two main and distinct signatures defined as either melanocytic-type (proliferative) or mesenchymal-like (invasive) melanoma cell states (Carreira *et al*, 2006; Widmer *et al*, 2012; Verfaillie *et al*, 2015). At the transcriptional level, the differentiated melanocytic-type melanoma cells display high levels of lineage-specific transcription factors, including the *SRY-box 10* (*SOX10*) and the *Microphthalmia-associated Transcription Factor* (*MITF*) that drive expression of melanocyte lineage genes. Undifferentiated mesenchymal-like melanoma cells express low levels of *MITF* and *SOX10*, and their gene expression signature, including markers like the *AXL receptor tyrosine kinase* (*AXL*) and *SOX9*, is driven by AP1-TEAD factors (Verfaillie *et al*, 2015; Minnoye *et al*, 2020). The discovery of cells with intermediate signatures (Ennen *et al*, 2017; Wouters *et al*, 2020) supports the initial concept of phenotypic plasticity driving melanoma progression through conversion from one phenotype into another in response to external cues (Hoek *et al*, 2008; Ennen *et al*, 2017; Rambow *et al*, 2018).

Treatment options for patients with metastatic melanoma include combination therapies with inhibitors targeting the *BRAF* (i.e.,

¹ Institut de Génétique et de Biologie Moléculaire et Cellulaire, Equipe Labélisée Ligue contre le Cancer, Strasbourg, France

² Centre National de la Recherche Scientifique, UMR7104, Illkirch, France

³ Institut National de la Santé et de la Recherche Médicale, Illkirch, France

⁴ Université de Strasbourg, Illkirch, France

*Corresponding author. Tel: +33 3 88653445; E-mail: irwin@igbmc.fr

**Corresponding author. Tel: +33 3 88653270; E-mails: frederic@igbmc.fr

vemurafenib and dabrafenib) and MEK (i.e., trametinib) kinases (BRAFi and MEKi, respectively), whose efficiency is limited by development of resistance and subsequent progression (Menzies & Long, 2014). It is well established that tolerance to targeted therapies can involve various phenotype changes, including epithelial–mesenchymal transition(-like) (EMT) from a melanocytic to a mesenchymal state (Kemper *et al*, 2014; Arozarena & Wellbrock, 2019; Rambow *et al*, 2019). Therefore, understanding the molecular details of phenotypic plasticity and transcriptional reprogramming of melanoma cells is crucial for the development of future therapeutic approaches.

Among the protein complexes essential for gene expression in eukaryotes, the basal transcription factor TFIID is unique due to its various enzymatic activities, including helicase, translocase, and kinase functions (Villicana *et al*, 2014; Berico & Coin, 2018). The CDK7 subunit of TFIID is a kinase that phosphorylates transcription factors, including the largest subunit of RNA polymerase II, to promote gene expression (Eick & Geyer, 2013; Compe & Egly, 2016; Fisher, 2019). Surprisingly, CDK7 kinase activity inhibition (CDK7i) elicits dramatic responses in various cancers (Cao & Shilatifard, 2014; Christensen *et al*, 2014; Kwiatkowski *et al*, 2014) probably due to the contribution of the TFIID kinase in super-enhancer (SE)-linked oncogene transcription (Chipumuro *et al*, 2014). SEs are broad genomic regions that drive transcription of cell identity genes in normal tissue or oncogenes in cancer (Hnisz *et al*, 2013). SEs are enriched in specific transcription factors such as CDK7, Mediator, the BET family of bromodomain protein 4 (BRD4), or chromatin marks such as H3K27 acetylation (H3K27ac) (Whyte *et al*, 2013). Besides CDK7i, inhibition of BRD4 (BETi) with the small molecule JQ1 causes loss of expression for many SE-associated genes in cancer cells (Loven *et al*, 2013).

Here, we show that resistance to CDK7i correlated with melanoma cell dedifferentiation and acquisition of tolerance to BRAF and MEK inhibitors. Besides the mesenchymal-like signature, we observed the emergence of a transcription program comprising genes involved in melanoma survival and drug tolerance under the control of the *GATA-binding factor 6 transcription factor* (GATA6). CDK7 prevents the emergence of the GATA6-dependent transcription program in differentiated melanoma cells by promoting the SE-dependent expression of MITF that binds to an intronic regulatory sequence of the GATA6 locus to silence its expression. In agreement with findings in cell cultures, we observed that diminished MITF expression during human melanoma progression and phenotype switching promotes the progressive activation of GATA6 in patient-derived xenografts. We determined that GATA6 emerges in the MITF-low cells of the PDX showing invasive or interferon γ (IFN γ)-active phenotypes.

Results

Melanoma cultures exhibit distinct sensitivity to CDK7i

We explored the sensitivity of melanoma cells to CDK7i using cells with the two main phenotypes and most common driver mutations. The melanocytic-type patient-derived MM011 (NRAS^{Q61K}), MM074 (BRAF^{V600E}), MM117 (Triple-wt) cell cultures and the melanoma 501mel cell line (BRAF^{V600E}) exhibited moderate to high expression

of the lineage-specific transcription factors MITF and SOX10 together with low to undetectable levels of SOX9 and c-JUN (Widmer *et al*, 2012; Verfaillie *et al*, 2015) (Fig 1A). In contrast, patient-derived MM029 (BRAF^{V600K}), MM047 (NRAS^{Q61R}), and MM099 (BRAF^{V600E}) cell cultures showed a mesenchymal-like phenotype characterized by low to undetectable levels of MITF and SOX10 coupled to high levels of SOX9 and c-JUN (Widmer *et al*, 2012; Verfaillie *et al*, 2015; Wouters *et al*, 2020). We observed that all melanocytic-type cells together with the MM047 mesenchymal-like cells were sensitive to low concentrations of THZ1, the first-in-class selective and covalent inhibitor of CDK7 (Kwiatkowski *et al*, 2014) (Fig 1B). In marked contrast, the MM099 and MM029

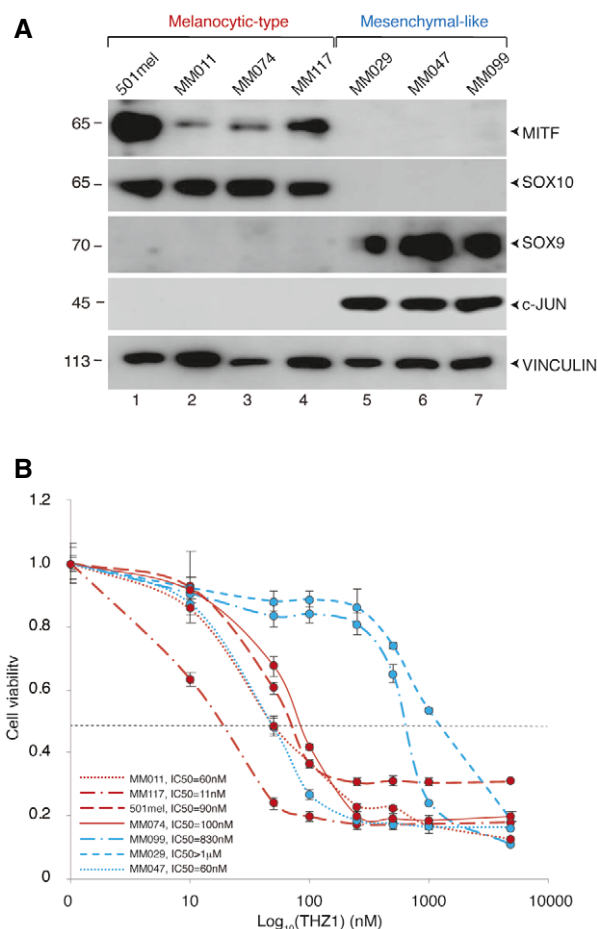


Figure 1. Melanoma cells show differential sensitivity to CDK7i.

- A** Protein lysates from the melanocytic-like melanoma cells 501mel, MM011, MM074, and MM117 or the mesenchymal-like melanoma cells MM029, MM047, and MM099 were immuno-blotted for proteins as indicated. Molecular mass of the proteins is indicated (kDa).
- B** Melanoma cells were treated with increasing concentrations of THZ1 as indicated for 72 h. Mean growth is shown relative to vehicle (DMSO)-treated cells. IC50 for each cell line is indicated. Melanocytic-type (MITF-High, proliferative) melanoma cells are shown in red, while mesenchymal-like (MITF-low, invasive) melanoma cells are shown in blue.

Data information: In (B), data are presented as mean values + standard deviation (SD) for three replicates ($n = 3$).

Source data are available online for this figure.

mesenchymal-like cells were tolerant to CDK7i, even at high concentrations of the drug. These observations demonstrated that melanocytic-type melanoma cells were highly sensitive to CDK7i, regardless of their driver mutation, while some mesenchymal-like melanoma cells were tolerant to the drug.

CDK7i promotes dedifferentiation of melanoma cells

To investigate the role of CDK7 in melanoma cells, we generated several THZ1-resistant (CDK7i) or vemurafenib-resistant (BRAFi) cell lines *ex vivo* (MM074^{CDK7i-R}, MM074^{BRAFi-R}, and MM047^{CDK7i-R}) (Fig EV1A–C). Establishment of CDK7i resistance decreased sensitivity of the MM074^{CDK7i-R} to BRAFi (vemurafenib) and MEKi (trametinib) (Fig EV1B and D), while the BRAFi-resistant MM074^{BRAFi-R} remained sensitive to both CDK7i and MEKi (Fig EV1A and D). In agreement with the involvement of CDK7 in gene expression, global transcription activity of MM047 and MM074 was strongly impacted by CDK7i treatment, in contrast to MM047^{CDK7i-R} and MM074^{CDK7i-R} where global transcription was not inhibited (Fig EV1E).

RNA-seq revealed a pronounced modification of the transcriptional programs of MM074^{CDK7i-R} and MM074^{BRAFi-R} compared to the parental MM074, but a less pronounced modification of the MM047^{CDK7i-R} compared to MM047 (Fig 2A). More than 6,000 genes were deregulated in MM074^{CDK7i-R} compared to MM074 and 1,000 genes in MM047^{CDK7i-R} compared to MM047 (Fig 2B). Despite the fact that the parental cells were of different phenotypes, 261 genes were commonly up-regulated in the two CDK7i-resistant cell cultures (Fig 2B and Dataset EV1). We hereafter defined these genes as the “CDK7i-resistant signature” (K7iRS). As shown by Gene Ontology (GO) analysis, these genes were involved in epithelial cell differentiation or in the transport of small molecules (Appendix Fig S1).

We next clustered melanoma cells based on the expression of a hundred genes corresponding to previously described signatures of melanocytic *vs* mesenchymal transcriptional cell states (Widmer *et al*, 2012). In agreement with the literature (Verfaillie *et al*, 2015; Wouters *et al*, 2020), 501mel and MM074 showed a melanocytic-type transcriptional signature (Fig 2C, lanes 1–2), while the MM047, MM099, and MM029 cells showed a mesenchymal-like signature (lanes 5–7). Surprisingly, chronic exposure of MM074 to CDK7i induced the emergence of a stable mesenchymal-like signature (compare lane 2 with 4) correlating with increased invasion capacity

(Fig EV1F). In apparent contrast with MM074^{CDK7i-R}, the melanocytic-type signature of MM074 persisted in MM074^{BRAFi-R} where we further observed a significant increase in the expression of a set of *bone fide* pigmentation genes (Fig 2C, compare lane 2 with 3). RT-qPCR confirmed the increased expression of genes involved in pigmentation such as *MLANA* in MM074^{BRAFi-R} (Fig EV1G), which correlated with higher cellular pigmentation (Fig EV1H). In agreement with mRNA, we observed that the MM074^{BRAFi-R} exhibited significantly higher amounts of the melanocyte lineage-specific proteins MITF and TFAP2A compared to MM074 (Fig 2D, compare lane 1 with 2). In contrast, MM074^{CDK7i-R} showed a dramatic decrease of these proteins together with the emergence of SOX9 (compare lane 1 with 3).

Altogether, these data showed that MM074 melanocytic-type cells chronically exposed to CDK7i dedifferentiated to adopt a mesenchymal state, whereas those exposed to BRAFi acquired a highly pigmented hyper-differentiated cell state. Furthermore, both mesenchymal-like and melanocytic-type melanoma cells chronically exposed to CDK7i displayed common altered expression of 261 genes corresponding to the K7iRS.

A GATA6-dependent transcription program in CDK7i-resistant melanoma cells

We compared the MM074^{CDK7i-R} and MM047^{CDK7i-R} gene expression programs to potentially identify a signature involved in drug tolerance that emerges as melanocytic-type cells undergo a phenotype switch and that is shared with the drug-resistant mesenchymal cells. This comparison focusing on genes commonly regulated during drug tolerance bypassing the much larger number of genes characterizing the phenotype switch *per se* identified the K7iRS genes. Merging these genes with a list of annotated transcription factors identified 16 common up-regulated transcription factors (TFs) in MM074^{CDK7i-R} and MM047^{CDK7i-R} (Fig EV2A). Analysis of their expression in RNA-seq data from melanoma cells showed that only 4 were significantly more expressed in the CDK7i-resistant MM029, MM099, MM074^{CDK7i-R}, and MM047^{CDK7i-R} cells, compared to CDK7i-sensitive cells (Fig EV2B). Of these, only GATA6 was significantly overexpressed in primary melanoma *vs* nevi (Fig EV2C). We confirmed by RT-qPCR and immuno-blot higher levels of GATA6 mRNA and GATA6 protein, respectively, in the CDK7i-insensitive cells (Fig 3A and B). We also noted that

Figure 2. Exposure to CDK7i induces melanoma dedifferentiation.

- Volcano plots were used to demonstrate differentially expressed genes as determined by RNA-seq in either MM047^{CDK7i-R} *vs* MM047 (top), MM074^{CDK7i-R} *vs* MM074 (middle), or MM074^{BRAFi-R} *vs* MM074 (bottom). Red dots show significantly over-represented (top) or under-represented (bottom) RNAs in drug-resistant cells compared to parental cells. All data were evaluated with the DESeq2 R package. The value for a given gene is the normalized gene expression value relative to the mean of all samples belonging to the same condition.
- Proportional Venn diagrams indicating the number of up-regulated (top) and down-regulated (bottom) genes in MM047^{CDK7i-R} and MM074^{CDK7i-R} compared to the parental MM047 and MM074, respectively. The number of genes overlapping between the datasets is indicated. 261 genes were found up-regulated and 241 down-regulated in MM047^{CDK7i-R} and MM074^{CDK7i-R}. Hypergeometric *P*-value is indicated.
- Genes characterizing the melanocytic-type and mesenchymal-like transcription signatures (Widmer *et al*, 2012) have been plotted on a heatmap and are shown in relation to their expression in different melanoma cells. RPKM values are represented as z-score. The group of genes related to pigmentation has been highlighted in red. The color key shows the log₂ expression values. Yellow color stands for high expression and dark violet for low expression.
- Protein lysates from MM074, MM074^{BRAFi-R}, or MM074^{CDK7i-R} were immuno-blotted for indicated proteins. Molecular sizes of the proteins are indicated (kDa). The numbers below the gel lanes represent relative protein level, which was determined from the band intensity using ImageJ software and normalized to each relative vinculin control.

Source data are available online for this figure.

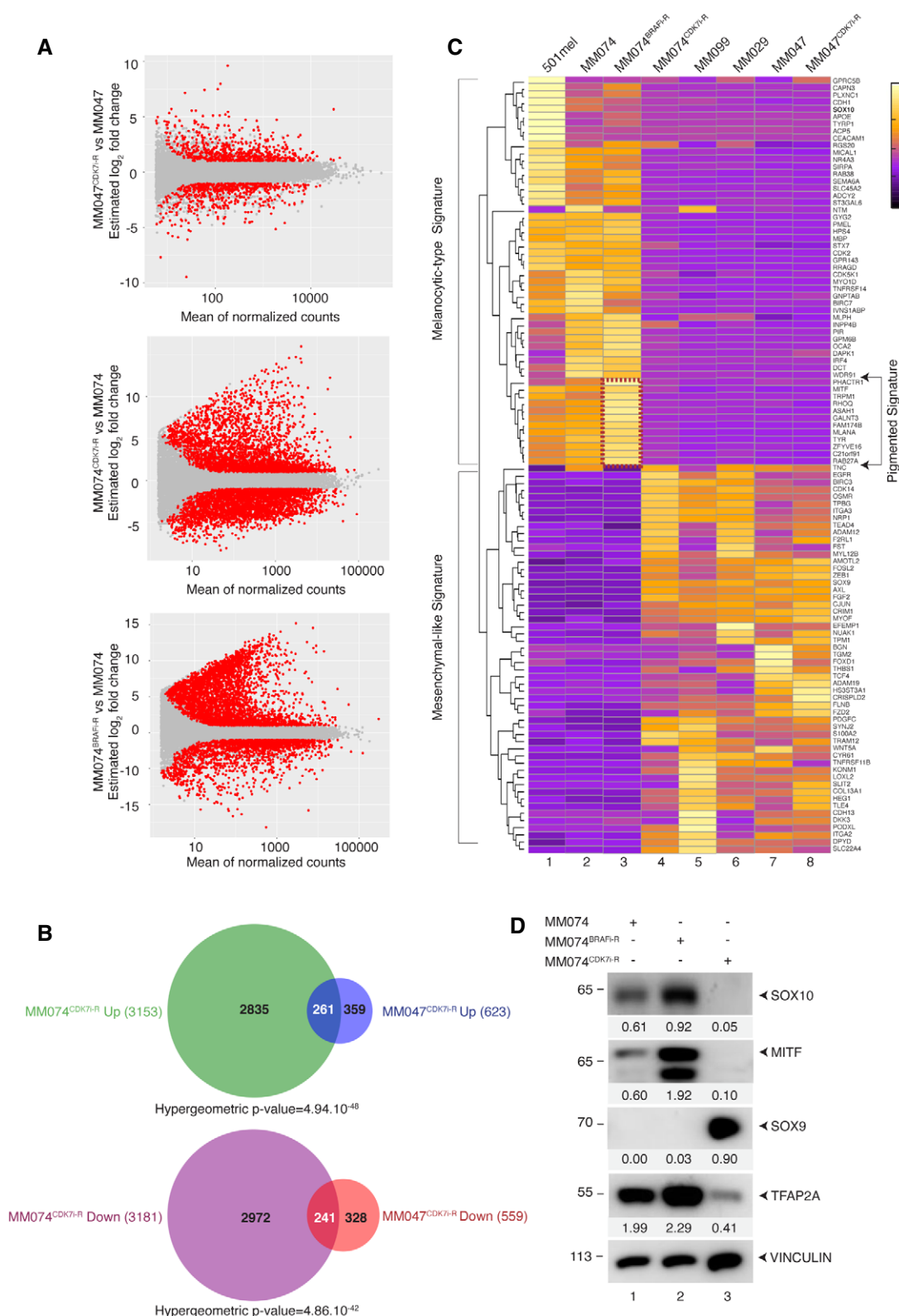


Figure 2.

GATA6 protein in MM047-sensitive cells was much lower than in the tolerant MM029 and MM099 cells and was potentially induced in MM047^{CDK7-R} (Fig 3B).

We then analyzed the transcriptomic profiles of the CDK7i-insensitive mesenchymal-like MM099 cells in which GATA6 was depleted using siRNA and observed a significant down-regulation of

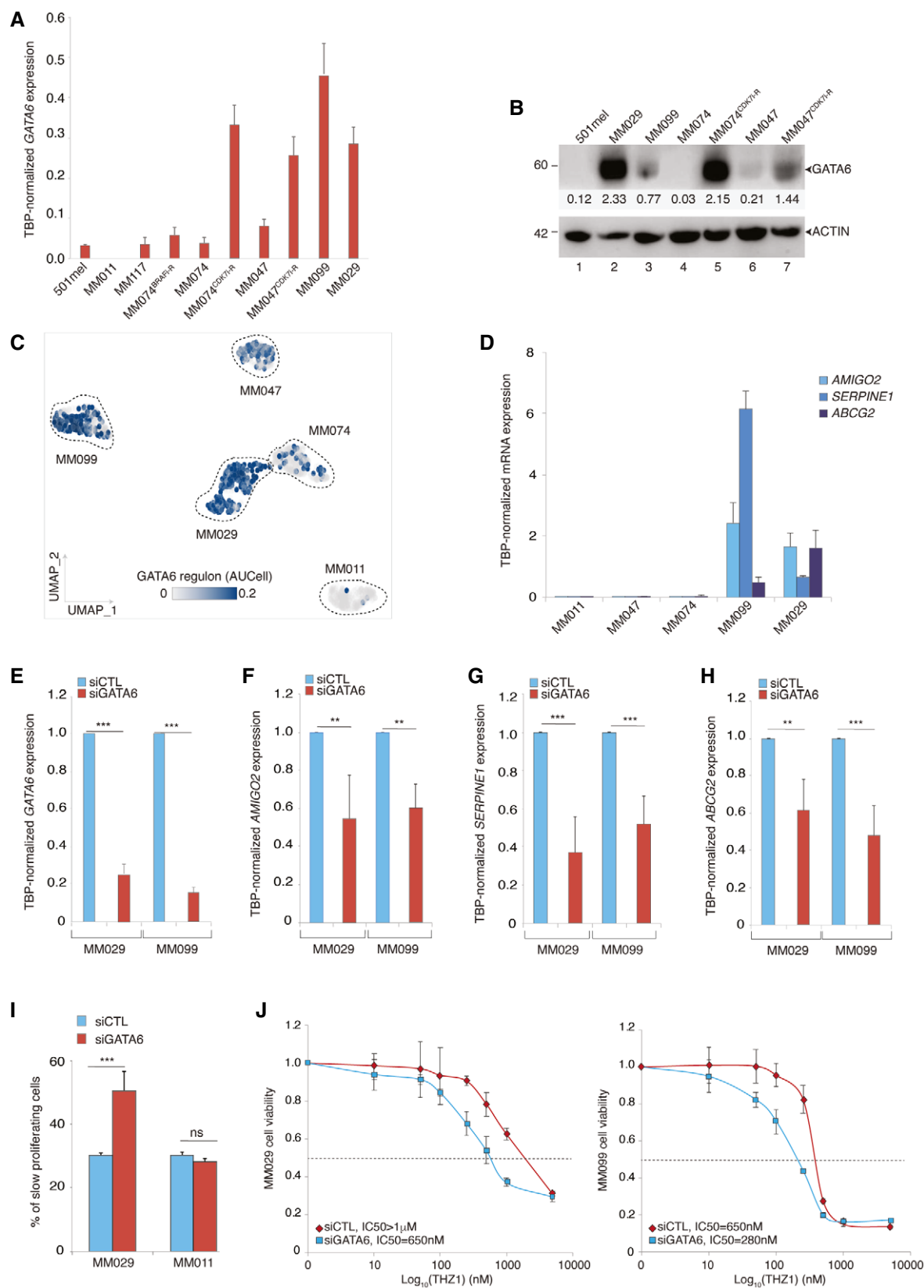


Figure 3.

Figure 3. GATA6 and its regulon are expressed in CDK7i-tolerant melanoma cells.

- A qRT-PCR analysis showing average *TBP*-normalized expression of *GATA6* in the indicated cells.
- B Protein lysates from the indicated cells were immuno-blotted for the indicated proteins. Molecular sizes of the proteins are indicated in kDa. The numbers below the gel lanes represent relative protein level, which was determined from the band intensity using ImageJ software and normalized relative to each relative actin control.
- C UMAP (Uniform Manifold Approximation and Projection) dimension reduction representative of *GATA6* regulon expression in MM011, MM029, MM047, MM074, and MM099 from Wouters dataset (Wouters *et al*, 2020). UMAP is colored according to the continuous *GATA6* AUC values (from 0 to 0.2).
- D qRT-PCR analysis showing average *TBP*-normalized expression of *AMIGO2*, *SERPINE1*, and *ABCG2* in the indicated cells.
- E–H qRT-PCR analysis showing average *TBP*-normalized expression of *GATA6* (E), *AMIGO2* (F), *SERPINE1* (G), and *ABCG2* (H) in the indicated cells treated with either siCTL or si*GATA6* for 72 h.
- I MM011 and MM029 were treated with either siCTL or si*GATA6* for 72 h. Cell proliferation was analyzed using CellTrace staining and flow cytometry in the indicated cell lines, and the % of slow proliferating cells is shown for each condition.
- J MM029 (left) and MM099 (right) were pre-treated with either siCTL or si*GATA6* for 48 h and treated with increasing concentrations of THZ1 for 72 h. Mean growth is shown relative to vehicle (DMSO)-treated cells.

Data information: In (A, D–J), data are presented as mean values + SD for six replicates ($n = 6$). The *P*-value (Student's *t*-test) is indicated, ** < 0.01, *** < 0.005, and ns, non-significant.

Source data are available online for this figure.

86 genes following *GATA6* silencing (defined below as “*GATA6* regulon”) (Dataset EV2). We next examined expression of the *GATA6* regulon in single-cell transcriptomic data recently obtained from MM011, MM029, MM047, MM074, and MM099 (Wouters *et al*, 2020). The *GATA6* regulon was more enriched in CDK7i-insensitive MM099 and MM029 cells compared to the others (Fig 3C). Within the *GATA6* regulon, we identified genes whose function was previously defined as important for melanoma such as the *Adhesion Molecule with Ig like domain 2* (*AMIGO2*) (Fontanals-Cirera *et al*, 2017) and the *SERPINE family E member 1* (*SERPINE1*) (Klein *et al*, 2012) together with genes contributing to multidrug resistance in cancer cells such as the efflux pump *ATP Binding Cassette Subfamily G member 2* (*ABCG2*) (Robey *et al*, 2018). RT-qPCR showed that expression of these genes was significantly higher in the CDK7i-resistant MM099 and MM029 cells compared to MM011, MM047, and MM074 (Fig 3D). As in MM099, *GATA6* depletion in MM029 decreased expression of *AMIGO2*, *SERPINE1*, and *ABCG2* (Fig 3E–H). Furthermore, *GATA6* depletion diminished MM029 proliferation compared to MM011 (Figs 3I and EV2D) and sensitized MM029 and MM099 to CDK7i (Figs 3J and EV2D). We also tried to overexpress *GATA6* in melanocytic-like cells; however, its expression was toxic in these cells, leading to cell cycle arrest that compromised the isolation of stably expressing clones. Therefore, we overexpressed *GATA6* in the mesenchymal-like MM047 cells and obtained stable expression of *GATA6* (Fig EV2E). Ectopic expression of *GATA6* induced expression of *ABCG2*, *AMIGO2*, and *SERPINE1* (Fig EV2E and F) and increased resistance to CDK7i (Fig EV2G). These data suggested that *GATA6* coordinated the expression of a set of genes specifically expressed in drug-tolerant mesenchymal-like melanoma cells and required for proliferation/survival and drug resistance.

***ABCG2* is involved in tolerance to CDK7i and BRAFi in melanoma cells**

The above data suggest that up-regulation of *ABCG2* expression by *GATA6* in mesenchymal-like melanoma cells may promote CDK7i resistance. RNA-seq data from melanoma tumors and *in situ* mRNA hybridization of melanoma tumor sections

demonstrated higher expression of *ABCG2* in cutaneous metastatic melanoma compared to primary tumors (Fig EV3A and Appendix Fig S2). Three ABC transporters (*ABCG2*, *ABCB1*, and *ABCC3*) were up-regulated in MM047^{CDK7i-R} and/or MM074^{CDK7i-R} (Fig EV3B and C), but only *ABCG2* was overexpressed in the CDK7i-insensitive MM099 and MM029 (Fig 4A and B). Depletion of *ABCG2* using siRNA (Fig EV3D) significantly sensitized MM099 and MM029 to CDK7i (Fig 4C and D). Interestingly, depletion of *ABCG2* also sensitized MM099 cells to BRAFi (Fig 4E), showing the potential pleiotropic impact of this efflux pump on drug resistance. Consistently, decrease of *ABCG2* in MM029 cells did not impact their sensitivity to BRAFi since they harbored the vemurafenib-resistant BRAF^{V600K} mutation (Fig 4F). Taken together, these data suggested that the ABC transporter *ABCG2* played a significant role in tolerance to CDK7i and BRAFi in melanoma cells.

CDK7 regulates expression of MITF and SOX10

We investigated the regulation of *GATA6* regulon that was repressed in melanocytic melanoma cells and activated by chronic exposure to CDK7i. Previous work suggested that CDK7 occupied SEs regulating MITF and SOX10 expression in melanoma cells (Eliades *et al*, 2018), but the presence of CDK7 at MITF/SOX10-associated super-enhancers was not observed so far. We performed ChIP-seq chromatin profiling of CDK7 using 501mel where the CDK7 locus was tagged with a Biotin-3xFlag tag by CRISPR/Cas9 genome editing (501mel^{BIO-FLAG:CDK7}) (Appendix Fig S3). FLAG ChIP-seq identified numerous CDK7-binding sites throughout the *MITF* locus and of its transcriptional activator *SOX10* (Fig 5A and B). CDK7 occupancy co-localized with H3K27ac, binding of MITF and/or of SOX10, BRG1, or H2AZ, all characterizing SE elements. A short 24 h CDK7i treatment impaired *MITF* and *SOX10* expression in 501mel, whereas exposure to BETi JQ1 had no effect (Fontanals-Cirera *et al*, 2017) (Fig 5C and D and Appendix Fig S4). Interestingly, decrease of *MITF* and *SOX10* following CDK7i occurred in parallel with increased expression of *GATA6* (Fig 5E). Moreover, expression of *CDK7*, *MITF*, and *SOX10* anti-correlated with that of *GATA6* in published RNA-seq data from human patient cutaneous melanoma (SKCM from TCGA) (Appendix Fig S5A).

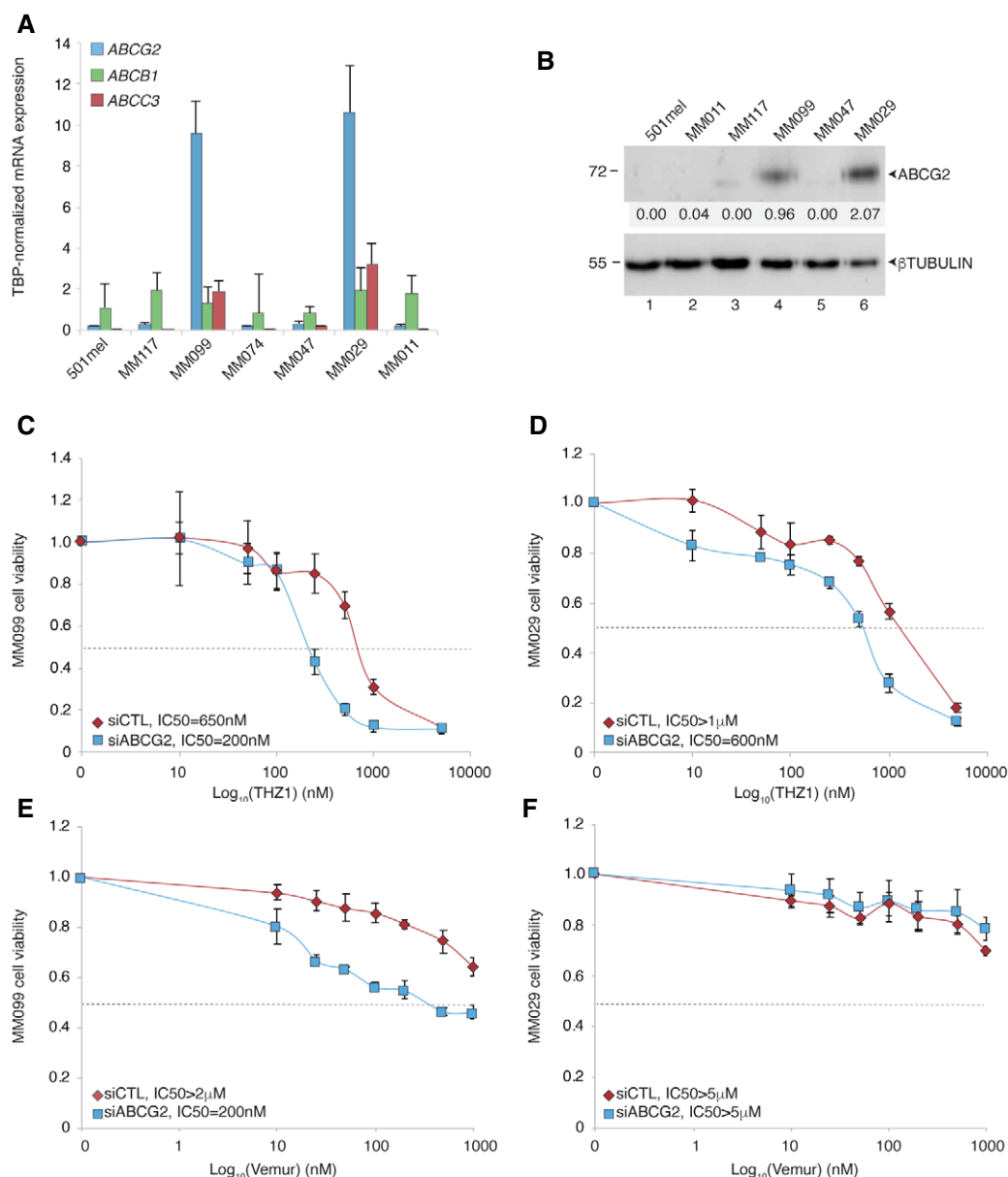


Figure 4. ABCG2 is involved in multidrug tolerance in melanoma cells.

A qRT-PCR analysis showing average TBP-normalized expression of *ABCB1*, *ABCC3*, and *ABCG2* in the indicated cells.

B Protein lysates from the indicated cells were immuno-blotted for the indicated proteins. Molecular masses of the proteins are indicated in kDa. The numbers below the gel lanes represent relative protein level, which was determined from the band intensity using ImageJ software and normalized to each relative β-tubulin control.

C, D MM099 (**C**) and MM029 (**D**) were pre-treated with either siCTL or siABCG2 as indicated and treated with increasing concentrations of THZ1 for 72 h. Mean growth is shown relative to vehicle (DMSO)-treated cells.

E, F MM099 (**E**) and MM029 (**F**) were pre-treated with either siCTL or siABCG2 as indicated and treated with increasing doses of vemurafenib for 72 h. Mean growth is shown relative to vehicle (DMSO)-treated cells.

Data information: In (**A**), data are presented as mean values + SD for six replicates ($n = 6$). In (**C-F**), data are presented as mean values + SD for three replicates ($n = 3$). IC₅₀ for each cell line is indicated.

Source data are available online for this figure.

SOX10 silencing induces release of GATA6 regulon expression

The above data suggested that decreased MITF and/or SOX10 expression may induce GATA6 expression. To test this, we depleted SOX10

with siRNA in 501mel cells and observed a significant decrease of *MITF* and induction of GATA6 expression (Fig 6A and Appendix Fig S5B). In agreement, bioinformatic analyses of published scRNA-seq performed at different times after SOX10 depletion in melanocytic-like

and E) correlated with concomitant up-regulation of *GATA6*, *ABCG2*, *SERPINE1*, and *AMIGO2* (Fig 6F–I). Altogether, these data showed an antagonism between MITF/SOX10 and GATA6 regulon in melanoma.

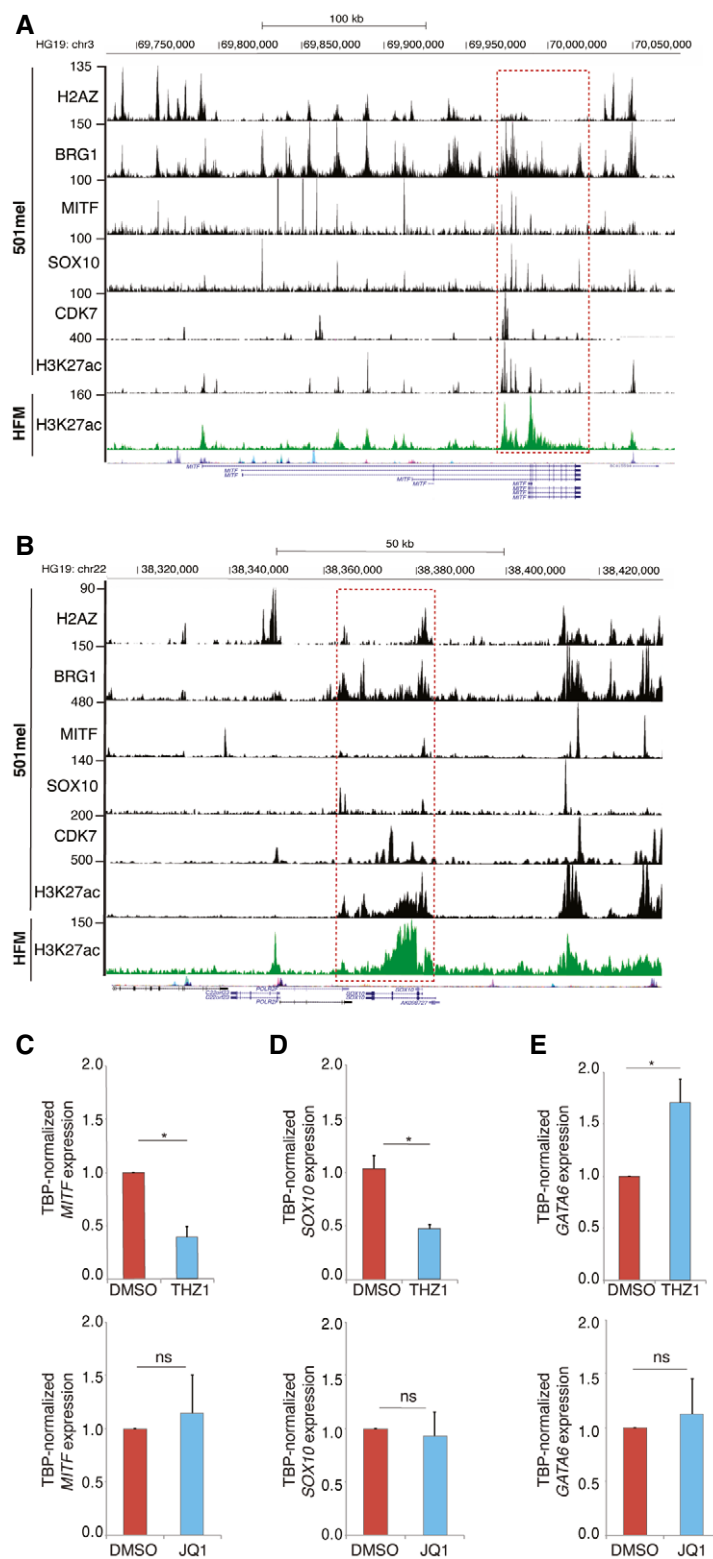


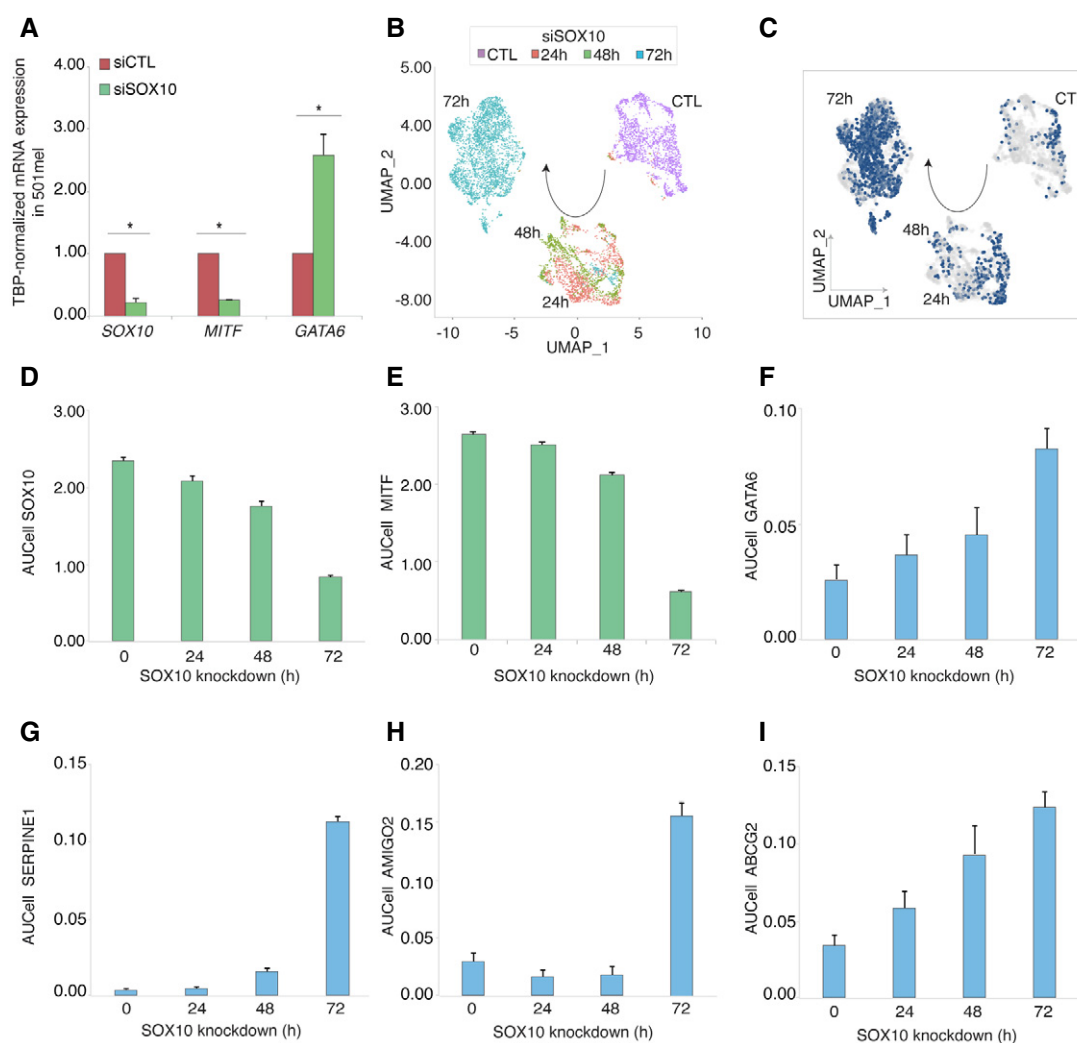
Figure 5.

Figure 5. CDK7i induced inhibition of MITF and SOX10 and release of GATA6 expression.

A, B Gene track of CDK7 occupancy at *MITF* (A) or *SOX10* (B) loci in 501mel^{BIO-FLAG:CDK7} cell line. Gene tracks of H2A.Z, BRG1, MITF, SOX10, and H3K27ac (GSE94488 and GSE61967) at the same loci in parental 501mel are indicated. SE is denoted by a red opened square. H3K27ac deposition is also shown in Hair Follicle Melanocytes (HFM) (GSE94488).

C–E qRT–PCR analysis showing average *TBP*-normalized fold expression of *MITF* (C), *SOX10* (D), and *GATA6* (E) in 501mel treated with either DMSO/THZ1 (50 nM) (upper) or DMSO/Q1 (10 μ M) (lower) for 24 h.

Data information: In (C–E), data are presented as mean values + SD for six replicates ($n = 6$). The *P*-value (Student's *t*-test) is indicated, * < 0.05 .

**Figure 6. Loss of SOX10 and MITF releases GATA6 expression.**

A qRT–PCR analysis showing average *TBP*-normalized fold expression of *SOX10*, *MITF*, and *GATA6* in 501mel treated with either siCTL or siSOX10 for 48 h.

B Seurat UMAP of MM074 treated with siCTL or siSOX10 (24, 48, and 72 h post-treatment). The arrow indicated the trajectory from control to 72 h post-siSOX10 transfection.

C UMAP of AUCCell GATA6 regulon in MM074 shows that GATA6 regulon is up-regulated along the trajectory from siCTL to 72 h post-siSOX10 treatment (GSE116237) (Wouters et al, 2020). The arrow indicated the trajectory from siCTL to 72 h post-siSOX10 transfection. We considered cell with GATA6 regulon activity of AUCCell > 0.15 as active (see Appendix Fig S5).

D–I Graphs showing the average expression of the *SOX10* (D), *MITF* (E), *GATA6* (F), *SERPINE1* (G), *AMIGO2* (H), and *ABCG2* (I) per individual melanoma cell measured by AUCCell on MM074 at different time points post-transfection of siSOX10 (GSE116237) (Wouters et al, 2020).

Data information: In (A), data are presented as mean values + SD for six replicates ($n = 6$). The *P*-value (Student's *t*-test) is indicated, * < 0.05 . In (D–I), data are presented as mean values + standard error of the mean (SEM) for six replicates ($n = 6$).

MITF drives direct transcriptional repression of GATA6

The above data suggested a direct mechanistic link between SOX10 and/or MITF and the repression of GATA6 in melanoma cells. ChIP-

seq did not reveal SOX10 binding at the GATA6 locus in 501Mel cells; however, a prominent MITF-binding site was observed in an intronic region of the GATA6 gene body (hereafter called “intGATA6r”, for intronic GATA6 locus region) containing potential

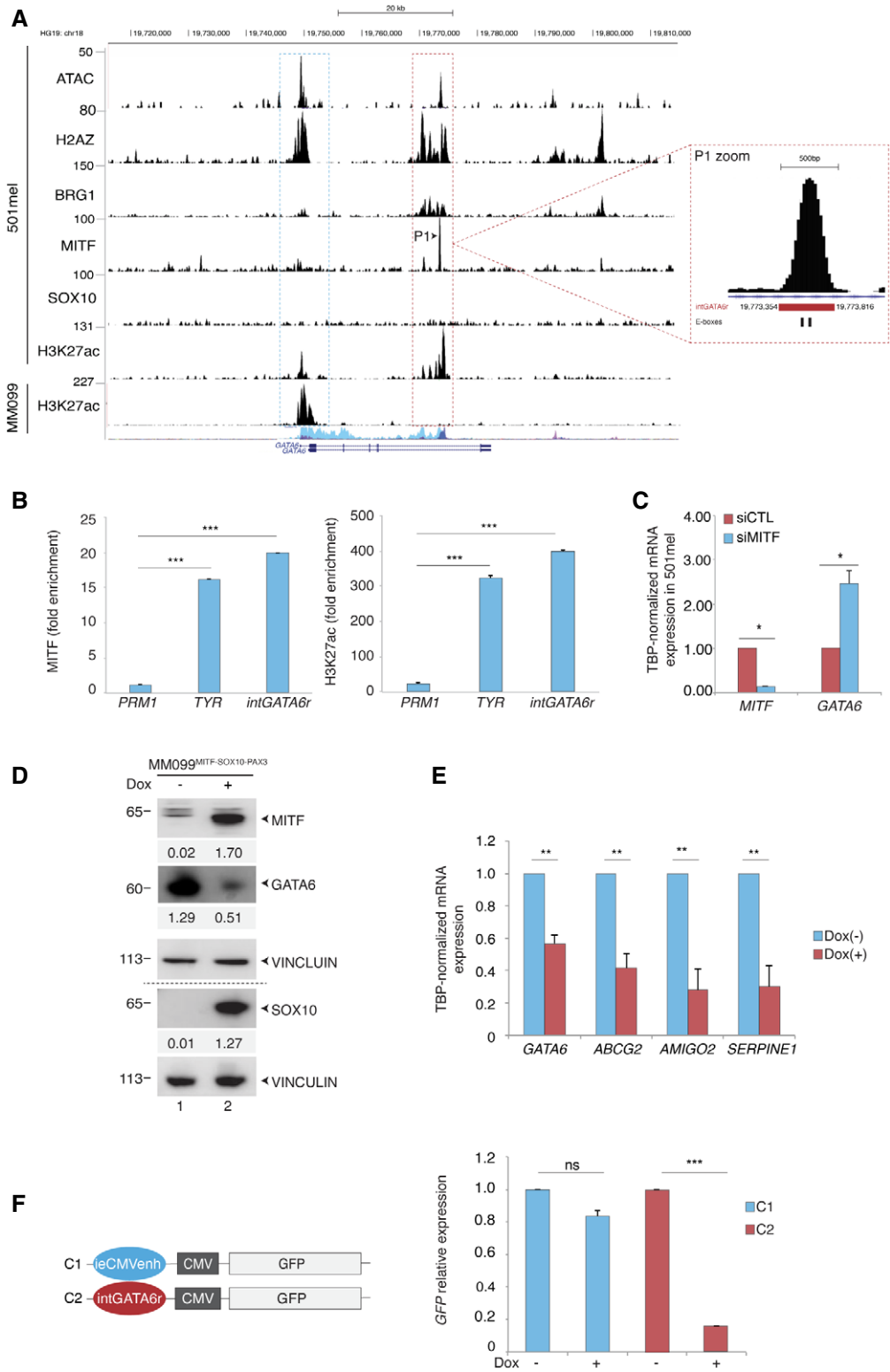


Figure 7.

Figure 7. MITF binds and represses the GATA6 locus.

- A ChIP-seq track of 3HA-MITF signal occupancy showing a significant MITF-binding peak (P1) in the GATA6 gene body in 501mel (GSE61967). Additional tracks indicate potential regulatory regions highlighted by ATAC-seq and H3K27ac, BRG1, SOX10, and H2A.Z deposition (GSE94488 and GSE61967). H3K27ac deposition is also shown in MM099 at the GATA6 locus. The scale bar indicates the size of the genomic region in kilobases (Kb). A magnification of the P1 region for MITF occupancy is shown in which the “intGATA6r” region is indicated in red and the two E-boxes in black.
- B ChIP qPCR experiment monitoring the fold enrichment (compare to control IgG) of MITF protein and H3K27ac mark at the “intGATA6r” region. *Proteamine 1* (*PRM1*) and Tyrosinase (*TYR*) regulatory regions were used as negative and positive controls, respectively (Laurette et al, 2015).
- C qRT-PCR analysis showing average *TBP*-normalized fold expression of *MITF* and *GATA6* in 501mel treated with either siCTL or siMITF for 48 h.
- D MM099^{MITF-SOX10-PAX3} expressing inducible *MITF-SOX10-PAX3* genes was treated or not with doxycycline (1 µg/ml) for 24 h, and protein lysates were immuno-blotted for the indicated protein. The numbers below the gel lanes represent relative protein level, which was determined from the band intensity using ImageJ software and normalized relative to vinculin control.
- E qRT-PCR analysis showing average *TBP*-normalized fold expression of *GATA6*, *ABCG2*, *AMIGO2*, or *SERPINE1* in MM099^{MITF-SOX10-PAX3} treated or not with doxycycline (1 µg/ml) for 24 h.
- F Left panel: Schematic representation of pCDNA-icCMVenh-CMV-GFP (C1) or pCDNA-intGATA6r-CMV-GFP (C2) reporter vectors. The icCMVenh sequence in C1 was replaced by the “intGATA6r” sequence to generate C2. Right panel: qRT-PCR analysis showing average *TBP*-normalized fold expression of *GFP* in MM099^{MITF-SOX10-PAX3} transfected with C1 or C2 vectors for 48 h before treatment or not with doxycycline (1 µg/ml) for 24 h.

Data information: In (B, C, E), data are presented as mean values + SD for three biological triplicates. The *P*-value (Student's *t*-test) is indicated, * < 0.05, ** < 0.01, and *** < 0.001. In (F), data are presented as mean values + SD for three technical replicates (*n* = 6). The *P*-value (Student's *t*-test) is indicated, *** < 0.005 and ns, non-significant (> 0.05).

Source data are available online for this figure.

MITF-binding sites (E-box motifs) (Fig 7A) (Laurette et al, 2015). In addition, “intGATA6r” was enriched in H3K27ac, BRG1, and H2AZ, marks of enhancer elements. Interestingly, in MM099 where MITF is not expressed, intronic H3K27ac was lost, but rather replaced by strong H3K27ac labeling at the *GATA6* promoter, correlating with its high expression in these cells. ChIP-qPCR confirmed enrichment of MITF and H3K27ac at the “intGATA6r” region in 501mel (Fig 7B). In agreement with a role for MITF in *GATA6* repression, siMITF silencing in 501mel induced *GATA6* expression (Fig 7C and Appendix Fig S5B).

To determine whether MITF was able to transcriptionally repress *GATA6*, we generated MM099^{MITF-SOX10-PAX3} in which MITF, SOX10, and PAX3 expression could be induced by doxycycline (Dox) treatment (Fig 7D). We co-expressed MITF, SOX10, and PAX3 as we observed that the presence of SOX10 and PAX3 stabilized MITF in these cells. Following induction of MITF-SOX10-PAX3, *GATA6* mRNA expression was repressed and level of *GATA6* protein decreased (Fig 7D and E). Consequently, the expression of the *GATA6* regulon genes *ABCG2*, *AMIGO2*, and *SERPINE1* was inhibited (Fig 7E).

To establish its repressive role, the 500bp “intGATA6r” sequence was inserted upstream of the CMV promoter of the pcDNA-CMV vector to replace the immediate early CMV enhancer (“icCMVenh”) in the context of a GFP reporter vector (Fig 7F, left panel). The reporter construct was transiently transfected into MM099^{MITF-SOX10-PAX3} with or without Dox-induced MITF-SOX10-PAX3 expression. While icCMVenh-dependent GFP expression was barely affected by MITF-SOX10-PAX3 expression, the presence of the “intGATA6r” element upstream of the promoter strongly impacted expression of the GFP compared to cells that did not express MITF-SOX10-PAX3 (Fig 7F, right panel). Altogether, these data strongly suggested that MITF transcriptionally repressed *GATA6* by binding to a negative regulatory sequence located in an intronic region of *GATA6*.

GATA6 is expressed in MITF-low cells of human melanoma

Our *in vitro* data suggested that *GATA6* and its regulon may be expressed in MITF-low melanoma cells in human tumors. To test

this hypothesis, we first performed an immunohistological (IHC) examination of human tumor samples. Because MITF antibodies are poorly efficient in IHC, we rather detected its transcriptional activator SOX10. While *GATA6* was not observed in nevi and primary melanomas that showed high SOX10 expression (Fig 8A, panels a-d), it was highly expressed in a subpopulation of cells in cutaneous metastases that did not express SOX10 (Fig 8A, panels e-f). In line with the above data, analyses of public DNA microarray (Xu et al, 2008) or RNA-seq data (TCGA) consistently revealed higher expression of *GATA6* in metastatic melanoma compared with primary melanoma (Fig EV4A).

To further define which melanoma cell subtypes express *GATA6* and its regulon, we re-analyzed scRNA-seq data from a PDX tumor before and after BRAFi (dabrafenib) and MEKi (trametinib) combination treatment (Rambow et al, 2018). An unsupervised gene clustering analysis that included more cells than in the original published analyses detected 9 different cell subpopulation clusters (Fig 8B). GO analysis attributed the four previously well characterized phenotypes to clusters 1, 5, 7, and 8, specifically starved-like melanoma cells (SMC), pigmented, invasive and neural crest-stem cells (NCSC) characterized by many of the previously described genes of each signature (Fig 8C). We attributed two additional phenotypes to clusters 4 and 6 that we defined as “Mitotic” due to the high expression of late S-phase and G2 M phase genes and “IFN-active” (previously designated as Immune (Rambow et al, 2018)) due to the enriched expression of interferon response genes. Cluster 0 corresponded to MITF-intermediate proliferative cells, while no specific ontology could be assigned to clusters 2 and 3 that were characterized by high expression of mitochondrial or pseudo-genes, respectively, and were excluded from subsequent analyses.

The frequency of cells of each phenotype was then analyzed at the different phases defined by Rambow before and after MAPKi exposure (T0 is the drug-naïve phase, phases 1 and 2 are the minimal residual disease phase (MRD), and phase 3 is the development of drug resistance (Rambow et al, 2018)). As previously described, an increase in SMC, pigmented and NCSC at minimal residual disease (MRD) phases 1 and/or 2 was observed (Fig EV4B), while the frequency of mitotic cells was strongly reduced in phases 1 and

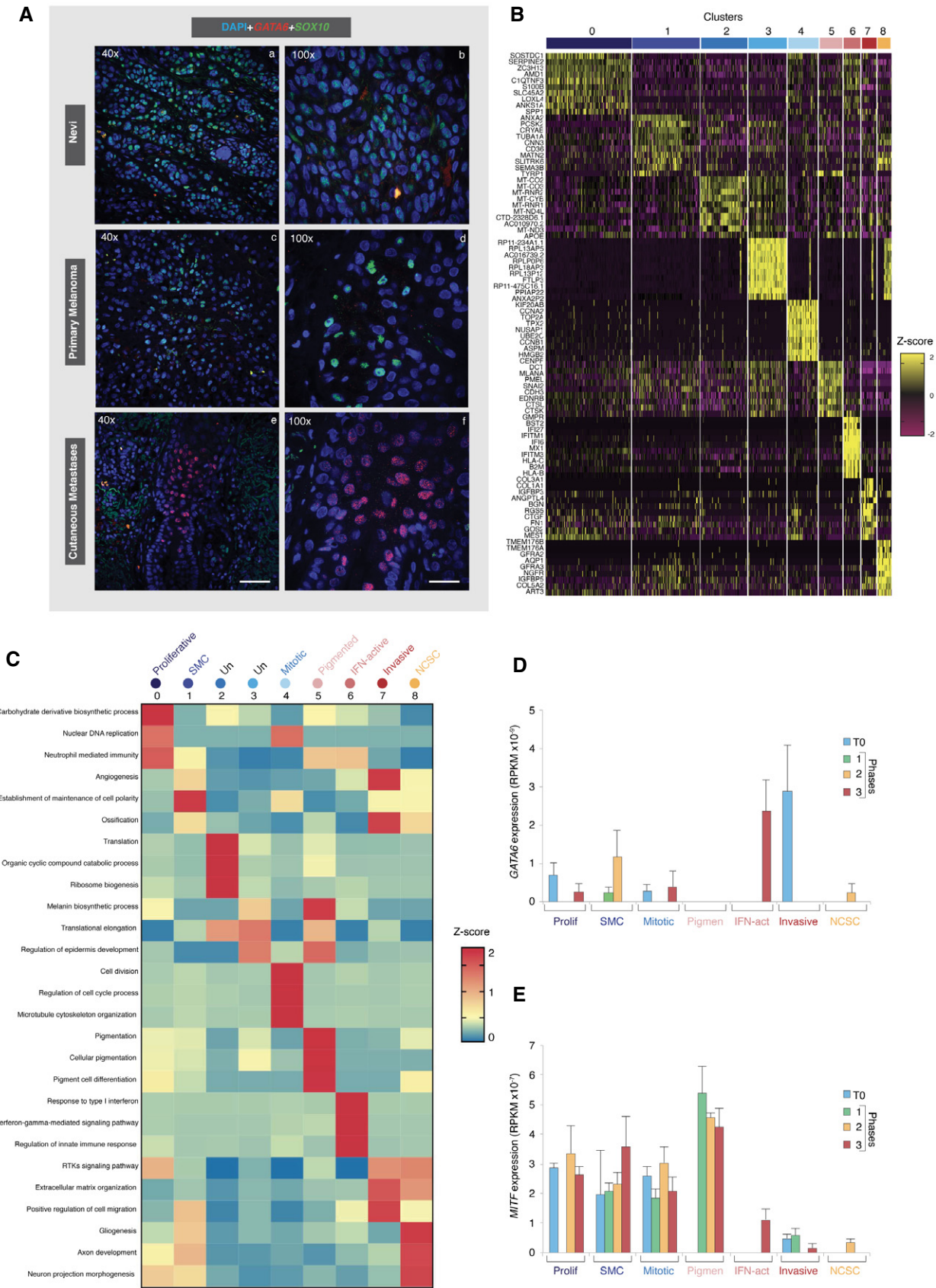


Figure 8.

Figure 8. GATA6 is expressed in MITF-low melanoma cells *in vivo*.

- A Tumor sections were immuno-labeled (IHC) with anti-GATA6 (red) and anti-SOX10 (green) antibodies, and images were captured by confocal microscopy at the indicated magnification. We analyzed six tumor sections of metastases and observed significant GATA6 expression in only one of them. Scale bar 250 μ m for 40 \times and 100 μ m for 100 \times .
- B Seurat cluster heatmap was generated from published scRNA-seq performed on PDX tumor ($n = 674$ cells) (GSE116237) (Rambow *et al*, 2018). The heatmap shows 9 different clusters into which the cells can be divided according to the expression of different referenced genes (Z-score). The top 10 genes are indicated in the left for each cluster.
- C GO was used to analyze the genes characterizing each cluster identified above. The average *P*-value was retrieved for each cluster taking the 3 best GO per cluster, and then, z-score ((*P*-value of each biological process-average of *P*-value of each biological process)/standard deviation) was calculated. Clusters 2 and 3 were undefined (un).
- D, E Graphs showing the average expression of *GATA6* (D) and *MITF* (E) (RPKM) for each phenotype cluster in T0 (drug naïve) (blue), phases 1–2 (MDR) (green and yellow), and phase 3 (drug resistance) (red).
- Data information: In (D, E), data are presented as mean values + SEM ($n = 6,574$ cells from 5 PDX).

2 but increased in the drug-resistance phase 3. The IFN-active cells were present uniquely in phase 3. MITF-intermediate proliferative cells were prevalent at the drug-naïve phase T0, but declined strongly in phase 1 before becoming more numerous in phases 2 and 3.

Analyses of GATA6 expression in the seven cell types during the defined phases indicated that GATA6 significantly emerged in cells displaying “Invasive” phenotype at T0, persisted at low levels in “SMC” cells during the MRD phase before re-emerging in cells with “IFN-active” phenotype during the drug-resistant phase 3 (Fig 8D). In contrast, MITF was expressed in cells with “SMC” or “Mitotic” phenotypes in T0, but showed essentially no expression in “Invasive” or “NCSC” cells and was strongest expressed in “Pigmented” cells with lower expression in the “IFN-active” cells at the drug-resistance phases (Fig 8E). The expression of GATA6 in “IFN-active” melanoma cells in the PDX prompted us to treat MM074 cells with the pro-inflammatory cytokine IFN γ . This treatment decreased expression of MITF and up-regulated expression of GATA6, c-JUN (Riesenberg *et al*, 2015), and the positive control PD-L1 at both mRNA (Fig EV4C) and protein levels (Fig EV4D). These data indicated an anti-correlation between MITF and GATA6 in cells from PDX tumors together with the emergence of GATA6 in MITF-low cells of the drug-resistance phase. This anti-correlation was recapitulated in cells treated with the pro-inflammatory cytokine IFN γ .

Discussion

In this work, we have shown that CDK7i sensitivity of melanoma cells was independent of driver mutation status, but strongly influenced by their phenotype. MITF-high melanocytic-type melanoma cells were highly sensitive to CDK7i, while MITF-low mesenchymal-like melanoma cells were largely insensitive. As shown before (Ennen *et al*, 2017; Wouters *et al*, 2020), mesenchymal-like MM099, MM029, and MM047 showed similar, but not identical signatures. Our current data show that MM047 differs from the MM099 and MM029 cells in its resistance to CDK7i. As each are primary cultures from different patients with a different natural history of the disease, differences between lines are only to be expected. Through the establishment of CDK7i-resistant cells from two different parental phenotypes, we defined a set of 261 genes reflecting the adaptation of melanoma cells to the exposure to CDK7i. Among these, we identified a network governed by GATA6 and containing genes such as

AMIGO2, involved in melanoma cell survival. GATA6 and its regulon were not only expressed in melanoma cells chronically exposed to CDK7i *in vitro*, but also more broadly in melanoma cells showing low expression of the lineage-specific markers SOX10 and MITF in tumors. We further observed that depletion of SOX10 or MITF proteins also activated GATA6-dependent genes, suggesting that the decommission of the CDK7-dependent SEs regulating MITF and SOX10 expression following CDK7i exposure (Eliades *et al*, 2018) is a key step in their activation. Our results also established that CDK7i more strongly inhibited *MITF* and *SOX10* expression in melanoma cells compared to BETi (Fontanals-Cirera *et al*, 2017), despite the presence of BRD4 at their corresponding SEs (Eliades *et al*, 2018), that may just be a collateral non-functional recruitment associated with strong enrichment of coactivators at SEs. Further evidence for the critical role of MITF/SOX10 in GATA6 repression comes from their ectopic expression in mesenchymal-like cells that inhibited GATA6 expression. We further identified a short regulatory sequence in a GATA6 intron that is bound by MITF and conferred MITF-driven transcriptional repression in a heterologous setting, a recognized criterion for *bone fide* repressor elements.

Consistent with our analysis showing GATA6 expression in both “invasive” and “IFN-active” PDX melanoma cells, IFN γ treatment of melanocytic cells repressed MITF/SOX10 leading to the concomitant activation of GATA6 (Son *et al*, 2014). Since MITF has been shown to participate in stabilization of CDK7 in melanocyte-type melanoma cells (Seoane *et al*, 2019; Louphrasitthiphon *et al*, 2020), our data suggest a negative feedback loop where the progressive loss of MITF during melanoma progression and inflammation triggers decreased CDK7 protein levels that in turn promotes lower MITF expression leading to de-repression of GATA6 expression in MITF/CDK7-low melanoma cells (Fig EV5). In line with this model, a negative correlation between CDK7 and GATA6 was observed in human SKCM.

GATA6 is expressed in various normal tissues derived from the mesoderm and endoderm (Almalki & Agrawal, 2016). An oncogenic role for GATA6 has been proposed in various cancers including pancreatic cancer where its knockdown reduced cell proliferation and cell cycle progression (Sun & Yan, 2020). We show that the decrease of GATA6 impaired proliferation of MITF-low mesenchymal-like melanoma cells. Since GATA6 is expressed in normal adult tissues, it is unlikely that its targeting would lead to efficient therapy. However, identification of its downstream regulon genes may help to identify molecular targets in mesenchymal-like melanoma cells that could be exploited therapeutically to prevent

acquisition of metastatic and drug resistance potential. One of the GATA6 regulon genes, *AMIGO2*, has already been identified as targetable for metastatic melanoma (Fontanals-Cirera *et al*, 2017). We observed that the GATA6-dependent multidrug transporter *ABCG2* is, at least in part, responsible for cross-resistance to targeted therapies in mesenchymal-like cells and is significantly overexpressed in metastatic melanoma tumors compared with primary tumors, suggesting that it may mediate ubiquitous cross-resistance to targeted therapies clinically.

Our results also clearly established a role for CDK7 in transcriptional reprogramming of melanoma cells. MITF-high melanoma cells exposed to CDK7i progressively lost melanocytic-type markers and acquired those of the undifferentiated mesenchymal-like state. In acquired CDK7i-resistant melanoma cells, we detected both a mesenchymal-like transcriptional signature and the acquisition of programs responsible for invasion. In apparent contrast, we observed that the acquired resistance of MITF-high melanoma cells to BRAFi was not accompanied by a loss of lineage-specific markers. In our hands, and as previously observed (Hag *et al*, 2013) (Smith *et al*, 2016), chronic exposure of melanocytic-type melanoma cells to escalating doses of BRAFi switched them to a highly pigmented state, which is likely a consequence of the increased MITF expression that we observed in these cells (Khaled *et al*, 2010).

Finally, an increasing number of studies identified CDK7 as a therapeutic target in various cancers (Fisher, 2019). However, the phenotype reprogramming observed during prolonged exposure of melanoma cells to CDK7i illustrates the potential danger of targeting this kinase in cancers where EMT plays an important role in therapeutic resistance and metastasis, an issue that has not been fully investigated so far. Future studies should therefore take into consideration the potential of CDK7i treatment to promote emergence of mesenchymal-like cells and therapeutic resistance.

Materials and Methods

A full list of reagents including antibodies, commercial kits, and oligonucleotides is supplied in Appendix Table S1.

Patients

Gene expressions in tumors and nevi were retrieved from several previously published datasets (including TCGA) indicated in the figure legends.

Cell culture and treatment

Cells were grown in 5% CO₂ at 37°C in HAM-F10 (Gibco, Invitrogen) supplemented with 10% FCS and penicillin–streptomycin. Melanoma cell line 501mel was grown in 5% CO₂ at 37°C in RPMI w/o HEPES (Gibco, Invitrogen) supplemented with 10% FCS and gentamycin.

Cells were transfected with Lipofectamine RNAiMAX following the manufacturer's instructions with 25 nM of siRNA ON-TARGETplus SMARTPool (Horizon Discovery), and cells were harvested 48 and/or 72 h after transfection. All cell lines used were mycoplasma negative.

MM099^{MITF-SOX10-PAX3}, MM047^{GFP}, and MM047^{GATA6} cells were generated as followed. Lentiviral vectors pTET-SMP encoding human untagged MITF, SOX10, and PAX3 proteins, and pLenti-EF1a-GFP and pLenti-EF1-3xFLAG-GATA6 encoding for GFP and GATA6 proteins, respectively, were transduced in either MM099 or MM047 in the presence of polybrene, and cells were selected with 3 µg/ml of puromycin. Conditional expression of pTET vector was carried out by adding 1 µg/ml of doxycycline in the medium for at least 24 h.

Generation of CDK7i- and BRAFi-resistant cells

To generate CDK7i- or BRAFi-resistant cells, we chronically exposed the MM074 (BRAF^{V600E}) melanocytic-type cells to escalating doses of THZ1 or vemurafenib over several weeks. These treatments were carried out until the cells proliferated in drug concentrations equal to at least 5 times the original IC50 values, allowing us to generate stable MM074^{CDK7i-R} and MM074^{BRAFi-R} lines, respectively. In parallel, the MM047 (NRAS^{Q61R}) mesenchymal-like cells were chronically exposed to THZ1 following the same protocol to generate stable MM047^{CDK7i-R}. Once established, the resistance was permanent and drugs can be removed without affecting cell phenotype.

CRISPR/Cas9 editing of 501mel^{BIO-FLAG:CDK7}

A 501mel were co-transfected with vector px738 (encoding Cas9-HF-GFP and two guide RNAs targeting CDK7 locus) and construct m599 linear DNA fragment carrying homology regions to CDK7 locus and puromycin-P2A-BIO-FLAG-CDK7N-termsequence (Appendix Table S1) with transfection reagent FuGENE6. Twenty-four h later, single cells GFP positive were sorted in P96-well plates in the presence of puromycin (3 µg/ml) with cell sorter. Single clones were let grown and selected for 4–6 weeks and surviving ones screened for gene editing through PCR using Phusion High-Fidelity TAQ Polymerase using different combination of primers (F1, F5, R3, R4, R5, see Appendix Table S1). PCR-positive clones were finally further amplified to perform Western blot and Co-IPs validation.

Cell proliferation assay

To measure proliferation, cells were incubated first with CellTrace Violet according to the manufacturer's instructions. Cell proliferation was detected on a BD LSRFortessa™ Flow Cytometer. Data were analyzed with FlowJo software. To define slow proliferating cells, we proceeded as follows: We considered that slow proliferating cells represented the 30% of cells with the highest concentration of BV421 in the siCTL treatment. We then calculated the % of cells that had a concentration greater than or equal to this value after treatment with siRNA.

Reporter assay

The intGATA6r element was isolated by genomic PCR using Phusion High-Fidelity TAQ polymerase (Thermo Fisher) with specific primers (Appendix Table S1). To allow the cloning within pCDNA-GFP vector, the first PCR product was further amplified by PCR with primers carrying MluI and SmaI restriction sites at the 5' and 3', respectively (MluI_F and SmaI_R primers in Appendix Table S1).

The immediate early CMV enhancer (ieEnh) in the pCDNA-GFP vector (pCDNA-ieEnh-CMV-GFP) was then replaced with the intGATA6r element (pCDNA-intGATA6r-CMV-GFP).

MITF-SOX10-PAX3 expression was induced in MM099^{MITF-SOX10-PAX3} cells with doxycycline for 48 h, and cells were subsequently transfected with pCDNA-ieEnh-CMV-GFP or pCDNA-intGATA6r-CMV-GFP vectors for 24 h with FuGENE6 following the manufacturer's instructions. RNA was then collected for qPCR, and GFP protein signal was detected on cytofluorometer. FACS data were analyzed with FlowJo software.

Histology

Human tissue sections were de-paraffinized and dehydrated with Histosol and dilutions of ethanol (100, 90, 70, and 30%) and then rehydrated with demineralized water. Subsequently, sections were boiled in sodium citrate buffer (0.1 M citric acid, 0.1 M sodium citrate) for 15 min to unmask antigens. Alternatively, cells were grown on glass slides and fixed with 4% formaldehyde. Both tissues and cells were permeabilized with PBS and 0.1% Triton X-100. Blocking was done with 10% fetal bovine serum before incubation with primary antibodies.

In situ hybridization of *ABCG2* mRNA was performed using the RNAscope assay according to the manufacturer's instructions (ACDBio). Cells and tissue sections were counterstained with DAPI and visualized using confocal microscope Spinning disk Leica CSU W1. Probes' sequences were not provided by the manufacture.

EU incorporation assay

RNA labeling by EU incorporation was performed with Click-iT RNA Imaging kit following the manufacturer's protocol. EU signal intensity was quantified using imaging system.

Cell survival assay

Normal or transfected cells were seeded at 5,000 cells/well in a 96-well plate and treated with increasing concentrations of THZ1, vemurafenib, or trametinib. After 72 h of incubation, cells were treated with PrestoBlue reagent according to the manufacturer's instructions. The absorbance per well was measured with a microplate reader. The data were then analyzed using Prism8.

RT-qPCR

Total RNA was isolated from cells using a GenElute Mammalian Total RNA Miniprep kit (Sigma) and reverse-transcribed with SuperScript IV reverse transcriptase (Invitrogen). The quantitative PCR was done using LightCycler. The primer sequences for the different genes used in qPCR are indicated in Appendix Table S1. The mRNA expression of the various analyzed genes represents the ratio between values obtained from treated and untreated cells normalized with the housekeeping genes mRNA.

ChIP

Cells were grown on 15-cm plates and, once reached 80% of confluence, were fixed with PBS + 0.4% formaldehyde solution for

10 min. Fixation reaction was stopped with 2 M Glycin pH 8. Cells were then pelleted and suspended in lysis buffer (EDTA 10 mM, Tris-HCl pH8 50 mM, SDS 1%) and sonicated with Covaris E220 AFA power 200 Hz 6 cycles 200 s to get a DNA fragmentation between 500 and 200 bp. Chromatin was then diluted in 60 µg aliquots with 8 volumes of ChIP dilution buffer (Tris-HCl pH8 16.7 mM, EDTA 1.2 mM, NaCl 167 mM, Triton X-100 1.1%, SDS 0.01%). The immuno-precipitations were done as follows. 1–5 µg of antibody was incubated overnight with chromatin, and the complex antibody-chromatin was then captured with G protein sepharose beads (Sigma-Aldrich) 1 h at 4°C. Beads were washed 2 times with low salt buffer (Tris-HCl pH8 20 mM, EDTA 2 mM, NaCl 150 mM, Triton X-100 1%, SDS 0.1%), high salt buffer (Tris-HCl pH8 20 mM, EDTA 2 mM, NaCl 500 mM, Triton X-100 1%, SDS 0.1%), LiCl buffer (Tris-HCl pH8 500 mM, EDTA 1 mM, Na deoxycholate 1%, NP40 1%, LiCl 0.25 M), and TE buffer (Tris-HCl pH8 10 mM, EDTA 1 mM), and DNA was eluted 30 min at room temperature with Elution buffer (NaHCO₃ 0.1 M, SDS 1%). DNA was finally purified through phenol-chloroform, re-suspended in 100 µl of water, and analyzed by qPCR using a set of primers indicated in Appendix Table S1.

RNA-seq

RNA-seq was performed as previously described (Laurette *et al*, 2019). Reads were preprocessed in order to remove adapter and low-quality sequences (Phred quality score below 20). After this preprocessing, reads shorter than 40 bases were discarded for further analysis. These preprocessing steps were performed using cutadapt version 1.10. Reads were mapped to rRNA sequences using bowtie version 2.2.8, and reads mapping to rRNA sequences were removed for further analysis. Reads were mapped onto the hg19 assembly of Homo sapiens genome using STAR version 2.5.3a. Gene expression quantification was performed from uniquely aligned reads using htseq-count version 0.6.1p1, with annotations from Ensembl version 75 and "union" mode. Only non-ambiguously assigned reads have been retained for further analyses. Read counts have been normalized across samples with the median-of-ratios method (Anders & Huber, 2010). Differential gene expression analysis was performed using the methodology implemented in the Bioconductor package DESeq2 version 1.16.1 (Love *et al*, 2014). *P*-values were adjusted for multiple testing by the method proposed by Benjamini and Hochberg (Benjamini & Hochberg, 1995). Deregulated genes were defined as genes with log₂(foldchange) > 1 or < -1 and adjusted *P*-value < 0.05. Heatmaps were generated with the R package pheatmap v1.0.12.

ChIP-seq

Purified DNA fragments for ChIP-seq were prepared by using the ChIP-IT High Sensitivity Kit (Active Motif) and the related antibodies. ChIP-seq was performed on an Illumina sequencer as single-end 50 base reads following Illumina's instructions. Image analysis and base calling were performed using RTA 1.17.20 and CASAVA 1.8.2. Reads were mapped onto the hg19 assembly of the human genome. Peak detection was performed using MACS (<https://github.com/macs3-project/MACS>) under settings where the input fraction was used as negative control. Peaks detected were annotated using

HOMER (<http://biowhat.ucsd.edu/homer/ngs/annotation.html>) as well as TSS protein enrichment comparison. Quantitative comparison of RNA Pol II gene body enrichment was performed using seqMINER (<http://bips.u-strasbg.fr/seqminer/>). As reference coordinates, we used the MACS-determined peaks or the annotated TSS/TTS of human genes as defined by RefSeq database. Sequence enrichment was performed using RSAT (<http://rsat.sb-roscoff.fr>) with MACS-determined peaks as reference.

Analysis of scRNA-seq data from short-cultured melanoma cells

After being downloaded, raw reads from scRNA-seq from MM011, MM029, MM047, MM074, and MM099 (Wouters *et al*, 2020) were processed using CellRanger (v 3.1) to align on the hg19 human genome, remove unexpressed genes, and quantify barcodes and UMIs. Data were then analyzed in R (v4.0.2) with Seurat v3.2.0 following the recommended workflow. Cells were filtered for feature count ranging from 120 to 2,000 and percentage of mitochondrial reads < 15%. Counts were normalized with the “LogNormalize” method and data scaled to remove unwanted sources of variation (UMI count and mitochondrial reads). The number of principal components to use was determined from the Jackstraw plots. Clustering was performed on variable features using the 25 most significant principal components and a resolution of 1.15. Regulome analyses of active transcription factors were performed using the SCENIC v1.1.2.2 package. Transcription factor activities were visualized on the UMAP using AUCell or as heatmaps using the R package pheatmap. Trajectory on the UMAP projection was resolved by monocle3 v0.2.0.

Analysis of scRNA-seq from PDX

Expression matrix with row reads counts for the single-cell experiment was retrieved from GEO (GSE116237). Then, data were normalized and clustered using the Seurat software package version 3.1.4 (Butler *et al*, 2018) in R version 3.6.1. Data were filtered, and only genes detected in at least 3 cells and cells with at least 350 detected genes were kept for further analysis. Expression of 26,661 transcripts in 674 cells was quantified. To cluster cells, read counts were normalized using the method “LogNormalize” of the Seurat function NormalizeData. It divides gene expression counts by the total expression, multiplies this by a scale factor (10,000 was used), and log-transforms the result. Then, 2,000 variable features were selected with the variance stabilizing transformation method using the Seurat function FindVariableGenes with default parameters. Integrated expression matrices were scaled (linear transformation) followed by principal component analysis (PCA) for linear dimensional reduction. The first 20 principal components (PCs) were used to cluster the cells with a resolution of 0.5 and as input to tSNE to visualize the dataset in two dimensions. The Bioconductor package AUCell v 1.6.1 (Aibar *et al*, 2017) was used to assess whether some cells from the Rambow dataset were enriched in gene sets of interest. AltAnalyze was used for the supervised clustering of TCGA samples (Olsson *et al*, 2016).

Gene ontology

Gene ontology was performed using Metascape software developed by (Zhou *et al*, 2019).

Quantification and statistical analysis

Statistical details of experimental can be found in figure legends or in the methods details. Hypergeometric distribution tests for the Venn diagrams were performed using: <https://systems.crump.ucla.edu/hypergeometric/>.

Data availability

The datasets produced in this study are available in the following databases:

Access numbers for data generated in this paper are as follows:

ChIP-Seq data CDK7: Gene expression Omnibus GSE158118.

<https://www.ncbi.nlm.nih.gov/geo/query/acc.cgi?acc=GSE158118>

RNA-seq data CDK7i cells: Gene expression Omnibus GSE158119.

<https://www.ncbi.nlm.nih.gov/geo/query/acc.cgi?acc=GSE158119>

RNA-seq data: Gene expression Omnibus GSE164431.

<https://www.ncbi.nlm.nih.gov/geo/query/acc.cgi?acc=GSE164431>.

Expanded View for this article is available online.

Acknowledgments

We thank the IGBMC antibody and cell culture facilities, Prof D. Lipsker, and the staff of the Strasbourg University Hospital dermatology clinic for tumor sections and Dr Ghanem Ghanem and J-C Marine for providing us the MM-series melanoma cultures. This study was supported by the Institut National Du Cancer (INCa) (2015-9378 and 2017-11537), the Ligue contre le Cancer (Equipe labélisée 2019, FC and équipe labélisée 2018, ID) and the ANR (START-2021), the ANR-10-LABX-0030-INRT, a French State fund managed by the Agence Nationale de la Recherche under the frame program Investissements d'Avenir ANR-10-IDEX-0002-02. Sequencing was performed by the IGBMC GenomEast platform, a member of the “France Génomique” consortium (ANR-10-INBS-0009). PB is supported by the Ligue contre le Cancer. M.C is supported by the Fondation pour la Recherche Médicale.

Author contributions

PB, ID, and FC conceived the study. PB, ID, FC, and EC analyzed the data. PB generated the resistant cells and performed the RNA-seq and the IH staining. SL, GD, BV, and PB, performed the bioinformatics analyses. PB, MC, and CMGR performed the survival assays. EC, FP, PB, and MC performed the RT-qPCR and the WB. JS performed the EU staining. NS performed the IFN γ experiments. CB provided a valuable technical assistance. JME provided valuable materials. FC and ID wrote the manuscript with input from EC.

Conflict of interest

The authors declare that they have no conflict of interest.

References

- Aibar S, González-Blas CB, Moerman T, Huynh-Thu VA, Imrichova H, Hulselmans G, Rambow F, Marine J-C, Geurts P, Aerts J *et al* (2017) SCENIC: single-cell regulatory network inference and clustering. *Nat Methods* 14: 1083–1086
- Alekseev S, Nagy Z, Sandoz J, Weiss A, Egly JM, Le May N, Coin F (2017) Transcription without XPB establishes a unified helicase-independent

- mechanism of promoter opening in eukaryotic gene expression. *Mol Cell* 65: 504–514
- Almalki SG, Agrawal DK (2016) Key transcription factors in the differentiation of mesenchymal stem cells. *Differentiation* 92: 41–51
- Anders S, Huber W (2010) Differential expression analysis for sequence count data. *Genome Biol* 11: R106
- Arozarena I, Wellbrock C (2019) Phenotype plasticity as enabler of melanoma progression and therapy resistance. *Nat Rev Cancer* 19: 377–391
- Badal B, Solovyov A, Di Cecilia S, Chan JM, Chang LW, Iqbal R, Aydin IT, Rajan GS, Chen C, Abbate F et al (2017) Transcriptional dissection of melanoma identifies a high-risk subtype underlying TP53 family genes and epigenome deregulation. *JCI Insight* 2: e92102
- Benjamini Y, Hochberg Y (1995) Controlling the false discovery rate: a practical and powerful approach to multiple testing. *J R Stat Soc Ser B Methodol* 57: 289–300
- Berico P, Coin F (2018) Is TFIH the new Achilles heel of cancer cells? *Transcription* 9: 47–51
- Brose MS, Volpe P, Feldman M, Kumar M, Rishi I, Gerrero R, Einhorn E, Herlyn M, Minna J, Nicholson A et al (2002) BRAF and RAS mutations in human lung cancer and melanoma. *Cancer Res* 62: 6997–7000
- Butler A, Hoffman P, Smibert P, Papalexi E, Satija R (2018) Integrating single-cell transcriptomic data across different conditions, technologies, and species. *Nat Biotechnol* 36: 411–420
- Cao K, Shilatfard A (2014) Inhibit globally, act locally: CDK7 inhibitors in cancer therapy. *Cancer Cell* 26: 158–159
- Carreira S, Goodall J, Denat L, Rodriguez M, Nuciforo P, Hoek KS, Testori A, Larue L, Goding CR (2006) Mitf regulation of Dia1 controls melanoma proliferation and invasiveness. *Genes Dev* 20: 3426–3439
- Chipmuro E, Marco E, Christensen C, Kwiatkowski N, Zhang T, Hatheway C, Abraham B, Sharma B, Yeung C, Altabef A et al (2014) CDK7 inhibition suppresses super-enhancer-linked oncogenic transcription in MYCN-driven cancer. *Cell* 159: 1126–1139
- Christensen C, Kwiatkowski N, Abraham B, Carretero J, Al-Shahrour F, Zhang T, Chipmuro E, Herter-Sprie G, Akbay E, Altabef A et al (2014) Targeting transcriptional addictions in small cell lung cancer with a covalent CDK7 inhibitor. *Cancer Cell* 26: 909–922
- Compe E, Egly JM (2016) Nucleotide excision repair and transcriptional regulation: TFIH and beyond. *Annu Rev Biochem* 85: 265–290
- Davies H, Bignell GR, Cox C, Stephens P, Edkins S, Clegg S, Teague J, Woffendin H, Garnett MJ, Bottomley W et al (2002) Mutations of the BRAF gene in human cancer. *Nature* 417: 949–954
- Eggermont AM, Spatz A, Robert C (2014) Cutaneous melanoma. *Lancet* 383: 816–827
- Eick D, Geyer M (2013) The RNA Polymerase II Carboxy-Terminal Domain (CTD) code. *Chem Rev* 113: 8456–8490
- Eliades P, Abraham BJ, Ji Z, Miller DM, Christensen CL, Kwiatkowski N, Kumar R, Njauw CN, Taylor M, Miao B et al (2018) High MITF expression is associated with super-enhancers and suppressed by CDK7 inhibition in melanoma. *J Invest Dermatol* 138: 1582–1590
- Ennen M, Keime C, Gambi G, Kiény A, Coassolo S, Thibault-Carpentier C, Margerin-Schaller F, Davidson G, Vagne C, Lipsker D et al (2017) MITF-high and MITF-low cells and a novel subpopulation expressing genes of both cell states contribute to intra- and intertumoral heterogeneity of primary melanoma. *Clin Cancer Res* 23: 7097–7107
- Fisher RP (2019) Cdk7: a kinase at the core of transcription and in the crosshairs of cancer drug discovery. *Transcription* 10: 47–56
- Fontanals-Cirera B, Hasson D, Vardabasso C, Di Micco R, Agrawal P, Chowdhury A, Gantz M, de Pablos-Aragoneses A, Morgenstern A, Wu P et al (2017) Harnessing BET inhibitor sensitivity reveals AMIGO2 as a melanoma survival gene. *Mol Cell* 68: 731–744.e9
- Haq R, Shoaib J, Andreu-Perez P, Yokoyama S, Edelman H, Rowe GC, Frederick DT, Hurley AD, Nellore A, Kung AL et al (2013) Oncogenic BRAF regulates oxidative metabolism via PGC1alpha and MITF. *Cancer Cell* 23: 302–315
- Hnisz D, Abraham BJ, Lee TI, Lau A, Saint-Andre V, Sigova AA, Hoke HA, Young RA (2013) Super-enhancers in the control of cell identity and disease. *Cell* 155: 934–947
- Hodis E, Watson I, Kryukov G, Arold S, Imielinski M, Theurillat J-P, Nickerson E, Auclair D, Li L, Place C et al (2012) A landscape of driver mutations in melanoma. *Cell* 150: 251–263
- Hoek KS, Eichhoff OM, Schlegel NC, Dobbeling U, Kobert N, Schaerer L, Hemmi S, Dummer R (2008) *In vivo* switching of human melanoma cells between proliferative and invasive states. *Cancer Res* 68: 650–656
- Kemper K, de Goeje PL, Peeper DS, van Amerongen R (2014) Phenotype switching: tumor cell plasticity as a resistance mechanism and target for therapy. *Cancer Res* 74: 5937–5941
- Khaled M, Levy C, Fisher DE (2010) Control of melanocyte differentiation by a MITF-PDE4D3 homeostatic circuit. *Genes Dev* 24: 2276–2281
- Klein RM, Bernstein D, Higgins SP, Higgins CE, Higgins PJ (2012) SERPINE1 expression discriminates site-specific metastasis in human melanoma. *Exp Dermatol* 21: 551–554
- Kwiatkowski N, Zhang T, Rahl PB, Abraham BJ, Reddy J, Ficarro SB, Dastur A, Amzallag A, Ramaswamy S, Tesar B et al (2014) Targeting transcription regulation in cancer with a covalent CDK7 inhibitor. *Nature* 511: 616–620
- Laurette P, Coassolo S, Davidson G, Michel I, Gambi G, Yao W, Sohler P, Li M, Mengus G, Larue L et al (2019) Chromatin remodellers Brg1 and Bptf are required for normal gene expression and progression of oncogenic Braf-driven mouse melanoma. *Cell Death Differ* 27: 29–43
- Laurette P, Strub T, Koludrovic D, Keime C, Le Gras S, Seberg H, Van Otterloo E, Imrichova H, Siddaway R, Aerts S et al (2015) Transcription factor MITF and remodeler BRG1 define chromatin organisation at regulatory elements in melanoma cells. *Elife* 4: e06857
- Louphrasitthiphol P, Siddaway R, Loffreda A, Pogenberg V, Friedrichsen H, Schepsky A, Zeng Z, Lu M, Strub T, Freter R et al (2020) Tuning transcription factor availability through acetylation-mediated genomic redistribution. *Mol Cell* 79: 472–487.e10
- Love MI, Huber W, Anders S (2014) Moderated estimation of fold change and dispersion for RNA-seq data with DESeq2. *Genome Biol* 15: 550
- Loven J, Hoke HA, Lin CY, Lau A, Orlando DA, Vakoc CR, Bradner JE, Lee TI, Young RA (2013) Selective inhibition of tumor oncogenes by disruption of super-enhancers. *Cell* 153: 320–334
- Menzies AM, Long GV (2014) Systemic treatment for BRAF-mutant melanoma: where do we go next? *Lancet Oncol* 15: e371–e381
- Minnoye L, Taskiran II, Mauduit D, Fazio M, Van Aerschoot L, Hulselmans G, Christiaens V, Makhzami S, Seltenthamer M, Karras P et al (2020) Cross-species analysis of enhancer logic using deep learning. *Genome Res* 30: 1815–1834
- Olsson A, Venkatasubramanian M, Chaudhri VK, Aronow BJ, Salomonis N, Singh H, Grimes HL (2016) Single-cell analysis of mixed-lineage states leading to a binary cell fate choice. *Nature* 537: 698–702
- Rambow F, Marine JC, Goding CR (2019) Melanoma plasticity and phenotypic diversity: therapeutic barriers and opportunities. *Genes Dev* 33: 1295–1318
- Rambow F, Rogiers A, Marin-Bejar O, Aibar S, Femel J, Dewaele M, Karras P, Brown D, Chang YH, Debiec-Rychter M et al (2018) Toward minimal residual disease-directed therapy in melanoma. *Cell* 174: 843–855.e19

- Riesenberg S, Groetchen A, Siddaway R, Bald T, Reinhardt J, Smorra D, Kohlmeier J, Renn M, Phung B, Aymans P *et al* (2015) MITF and c-Jun antagonism interconnects melanoma dedifferentiation with pro-inflammatory cytokine responsiveness and myeloid cell recruitment. *Nat Commun* 6: 8755
- Robey RW, Pluchino KM, Hall MD, Fojo AT, Bates SE, Gottesman MM (2018) Revisiting the role of ABC transporters in multidrug-resistant cancer. *Nat Rev Cancer* 18: 452–464
- Seoane M, Buhs S, Iglesias P, Strauss J, Puller A-C, Müller J, Gerull H, Feldhaus S, Alawi M, Brandner JM *et al* (2019) Lineage-specific control of TFIIH by MITF determines transcriptional homeostasis and DNA repair. *Oncogene* 38: 3616–3635
- Smith MP, Brunton H, Rowling EJ, Ferguson J, Arozarena I, Miskolczi Z, Lee JL, Girotti MR, Marais R, Levesque MP *et al* (2016) Inhibiting drivers of non-mutational drug tolerance is a salvage strategy for targeted melanoma therapy. *Cancer Cell* 29: 270–284
- Son J, Kim M, Jou I, Park KC, Kang HY (2014) IFN- γ inhibits basal and α -MSH-induced melanogenesis. *Pigment Cell Melanoma Res* 27: 201–208
- Sun Z, Yan B (2020) Multiple roles and regulatory mechanisms of the transcription factor GATA6 in human cancers. *Clin Genet* 97: 64–72
- Verfaillie A, Imrichova H, Atak ZK, Dewaele M, Rambow F, Hulselmans G, Christiaens V, Svetlichnyy D, Luciani F, Van den Mooter L *et al* (2015) Decoding the regulatory landscape of melanoma reveals TEADS as regulators of the invasive cell state. *Nat Commun* 6: 6683
- Villicana C, Cruz G, Zurita M (2014) The basal transcription machinery as a target for cancer therapy. *Cancer Cell Int* 14: 18
- Whyte WA, Orlando DA, Hnisz D, Abraham BJ, Lin CY, Kagey MH, Rahl PB, Lee TI, Young RA (2013) Master transcription factors and mediator establish super-enhancers at key cell identity genes. *Cell* 153: 307–319
- Widmer DS, Cheng PF, Eichhoff OM, Belloni BC, Zipser MC, Schlegel NC, Javelaud D, Mauviel A, Dummer R, Hoek KS (2012) Systematic classification of melanoma cells by phenotype-specific gene expression mapping. *Pigment Cell Melanoma Res* 25: 343–353
- Wouters J, Kalender-Atak Z, Minnoye L, Spanier KI, De Waegeneer M, Bravo González-Blas C, Mauduit D, Davie K, Hulselmans G, Najem A *et al* (2020) Robust gene expression programs underlie recurrent cell states and phenotype switching in melanoma. *Nat Cell Biol* 22: 986–998
- Xu L, Shen SS, Hoshida Y, Subramanian A, Ross K, Brunet JP, Wagner SN, Ramaswamy S, Mesirov JP, Hynes RO (2008) Gene expression changes in an animal melanoma model correlate with aggressiveness of human melanoma metastases. *Mol Cancer Res* 6: 760–769
- Zhou Y, Zhou B, Pache L, Chang M, Khodabakhshi AH, Tanaseichuk O, Benner C, Chanda SK (2019) Metascape provides a biologist-oriented resource for the analysis of systems-level datasets. *Nat Commun* 10: 1523

Expanded View Figures

Figure EV1. Generation of CDK7i- or BRAFi-resistant melanoma cells.

- A Dose–response curves for MM074, MM074^{CDK7i-R}, and MM074^{BRAFi-R} cells treated with increasing doses of THZ1 for 72 h. Fractions of viable cells relative to DMSO-treated cells are shown. IC50 for each cell line is indicated.
- B Dose–response curves for MM074, MM074^{BRAFi-R}, and MM074^{CDK7i-R} cells treated with increasing doses of vemurafenib for 72 h. Fractions of viable cells relative to DMSO-treated cells are shown. IC50 for each cell line is indicated.
- C MM047 cells and their CDK7i-resistant MM047^{CDK7i-R} counterparts were treated as in panel (A).
- D Dose–response curves for parental MM074, MM074^{BRAFi-R}, and MM074^{CDK7i-R} cells treated with increasing doses of trametinib for 72 h. Fractions of viable cells relative to DMSO-treated cells are shown. IC50 for each cell line is indicated.
- E Impact of CDK7i on global transcription was measured by labeling *de novo* synthesized RNA with 5-ethynyl uridine (5EU) (Alekseev *et al*, 2017). Cells as indicated were treated 4 h with either vehicle (DMSO) or THZ1 (50 nM). Transcribed RNAs were labeled by 5EU incorporation.
- F Boyden chamber assay for MM074 and MM074^{CDK7i-R} cells. Pictures are representative images of the bottom of the Boyden chamber membrane. Scale bar 400 μ m.
- G qRT–PCR analysis showing average *TBP*-normalized expression of *MLANA* in the indicated cell lines.
- H Image shows pellets of MM074, MM074^{CDK7i-R}, and MM074^{BRAFi-R} cells. The pellets of MM074^{BRAFi-R} cells have a brown color suggesting the presence of highly pigmented cells.

Data information: In (A–D), data are presented as mean values + SD for three replicates ($n = 3$). In (F, G), data are presented as mean values + SD for six replicates ($n = 6$). In (E), data are presented as mean values + SEM for three replicates. $n = \sim 2,500$ cells were analyzed in each experiment. The *P*-value (Student's *t*-test) is indicated, *** < 0.005 and ns, non-significant (> 0.05).

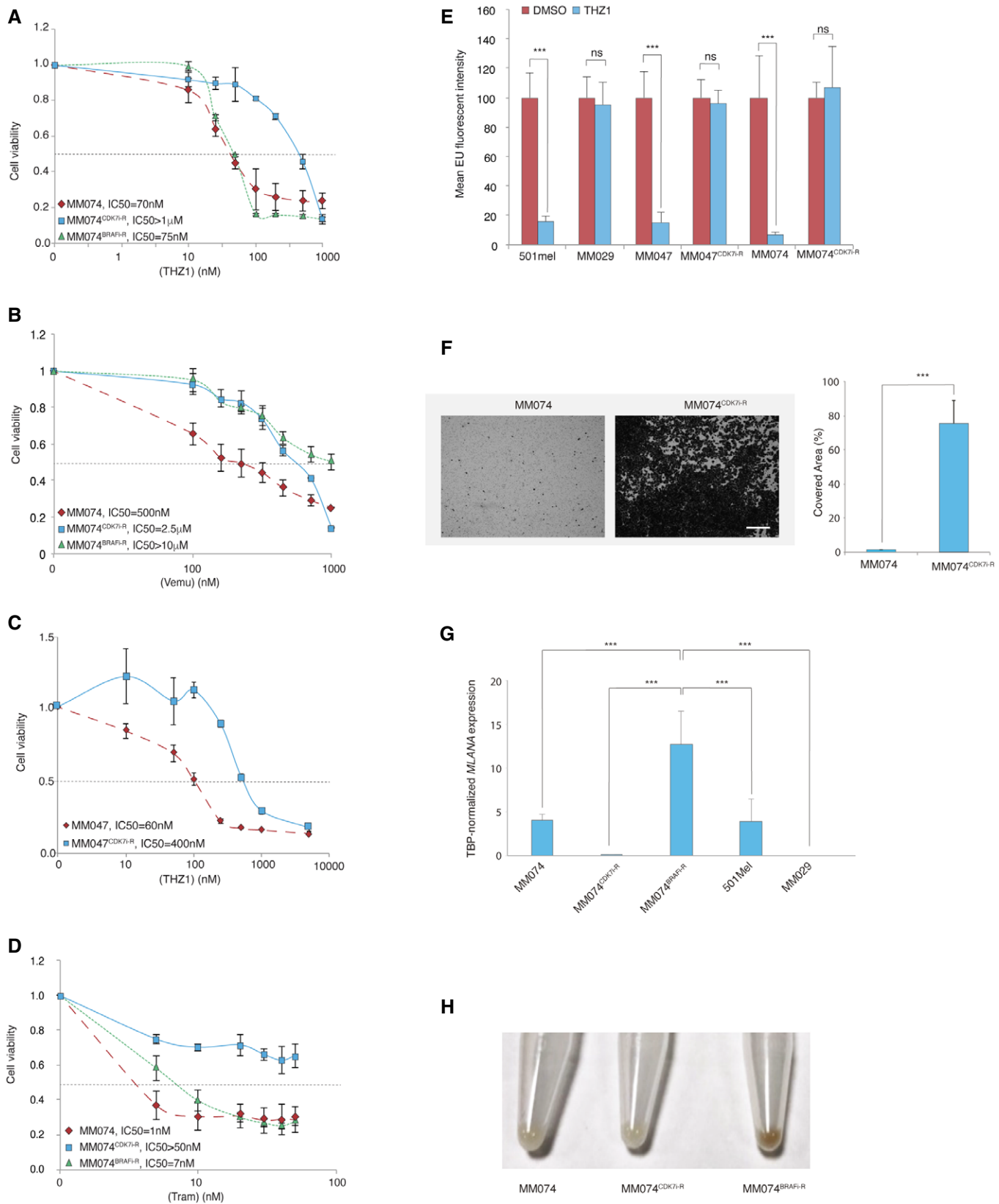


Figure EV1.

Figure EV2. GATA6 expression in melanoma *in vivo*.

- A Venn diagram merging the up-regulated genes in MM074^{CDK7i-R} and MM047^{CDK7i-R} with a list of annotated transcription factors (TFs) (<https://www.ncbi.nlm.nih.gov/pubmed/29425488>).
- B Statistical comparison of the average fold change expression of 16 TFs associated with drug resistance between sensitive (501mel, MM047, MM074) *vs.* resistant (MM029, MM099, MM074^{CDK7i-R}, MM049^{CDK7i-R}) cell lines. In red, the four TFs with *P*-value < 0.05.
- C Scatter plot expression values for *DMRTA1*, *THRB*, *TLE4*, and *GATA6* in nevi *vs.* primary melanoma extracted from public bulk RNA-seq data of treatment-naïve melanocytic tumors (*n* = 78) consisting of primary melanomas of the skin and benign melanocytic lesions (GSE98394) (Badal *et al*, 2017). The *P*-value (Student's *t*-test) is indicated, *** < 0.005.
- D MM029, MM099, and MM011 were pre-treated with either siCTL or siGATA6 for 48 h, and protein lysates from the indicated cells were immuno-blotted for the indicated proteins. Molecular masses of the proteins are indicated in kDa.
- E GFP or GATA6 were expressed in MM047 (MM047+GPF or MM047+GATA6). Following selection, protein lysates from the indicated cells were immuno-blotted for the indicated proteins. Molecular masses of the proteins are indicated in kDa.
- F qRT-PCR analysis showing average *TBP*-normalized fold expression of *GATA6*, *ABCG2*, *AMIGO2*, and *SERPINE1* in MM047+GFP or MM047+GATA6.
- G Dose-response curves for MM047+GFP and MM047+GATA6 cells treated with increasing doses of THZ1 for 72 h. Fractions of viable cells relative to DMSO-treated cells are shown. IC50 for each cell line is indicated.

Data information: In (F), data are presented as mean values + SD for six replicates (*n* = 6). In (G), data are presented as mean values + SD for three replicates (*n* = 3). The *P*-value (Student's *t*-test) is indicated, *** < 0.005.

Source data are available online for this figure.

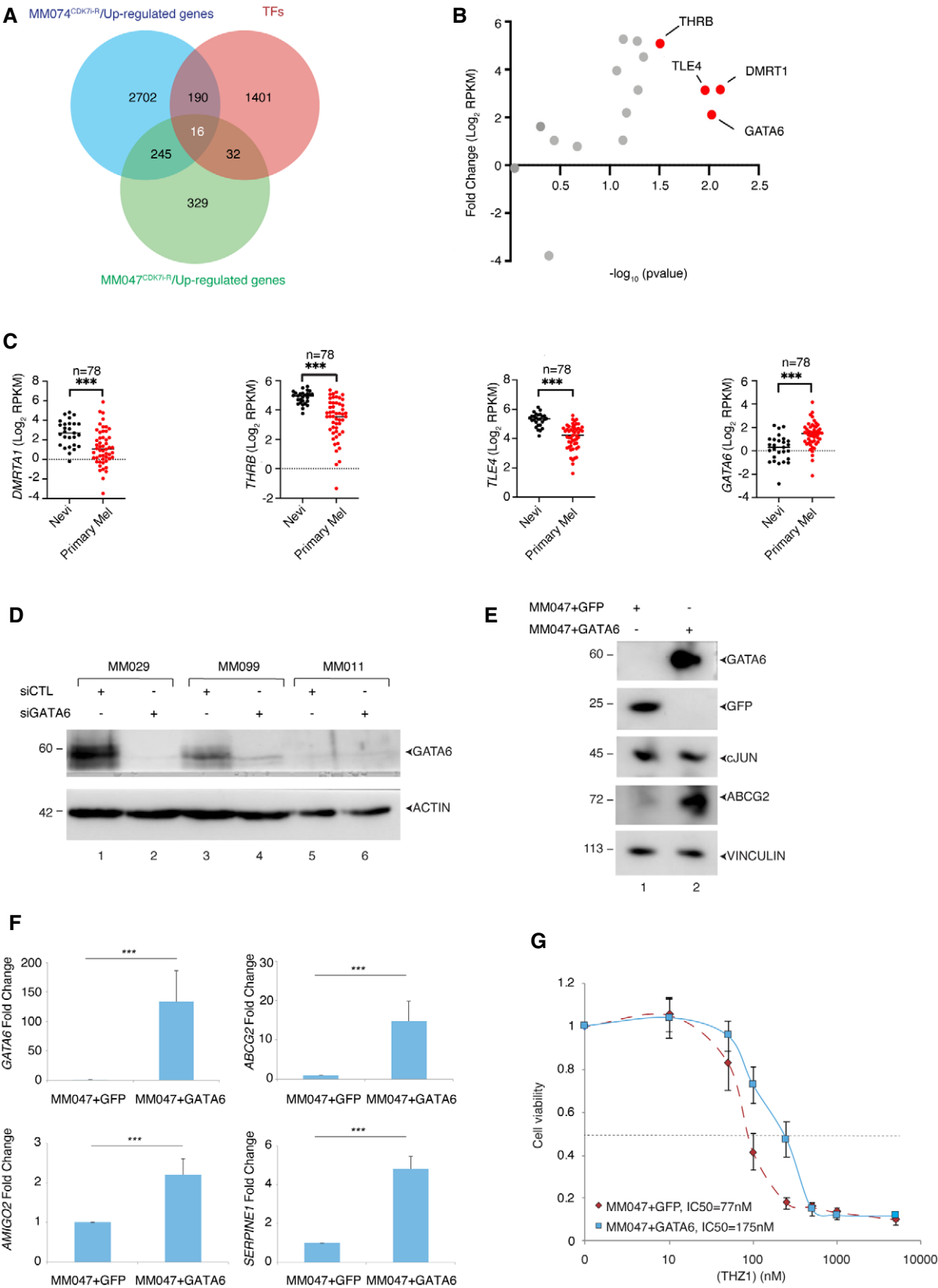


Figure EV2.

Figure EV3. ABCG2 is up-regulated in metastatic melanoma.

- A RNA FISH/mRNA *in situ* hybridization of *ABCG2*. Top panel: Probe was validated using 501mel and MM011 cells that do not express *ABCG2* *vs.* MM029 that expresses it. Scale bar 40 μm . Bottom panel: Nevi and tumor sections (primary melanoma or cutaneous metastases) were used ($n = 3$ sections from each tissue) with one representative micrograph from each tissue shown. Images were captured by confocal microscopy. Scale bar 400 μm .
- B Venn diagram merging the up-regulated genes in MM074^{CDK71-R} and MM047^{CDK71-R} with a list of all ABC transporters. Three ABC transporters are up-regulated in MM074^{CDK71-R} and/or MM047^{CDK71-R}.
- C qRT-PCR analysis showing average *TBP*-normalized expression of *ABCB1*, *ABCC3*, and *ABCG2* in the indicated cell lines.
- D MM029 and MM099 melanoma cells were treated with either siCTL or si*ABCG2*. mRNA was analyzed by qRT-PCR analysis showing average *TBP*-normalized expression of *ABCG2* (left panel). Protein level was analyzed by WB (right panel). Molecular masses of the protein ladder (lane 3) are indicated in kDa.

Data information: In (C, D), data are presented as mean values + SD for six replicates ($n = 6$).

Source data are available online for this figure.

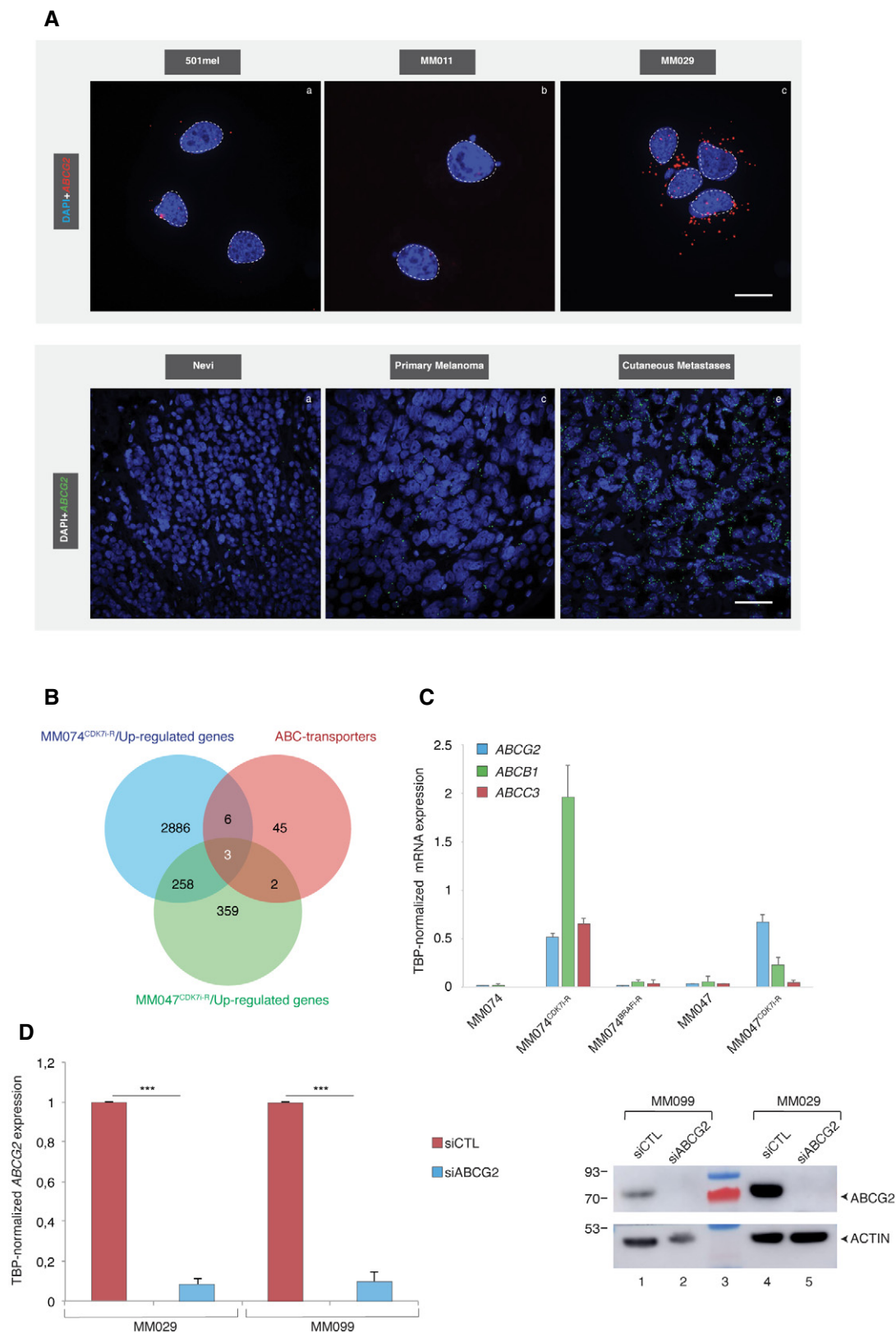


Figure EV3.

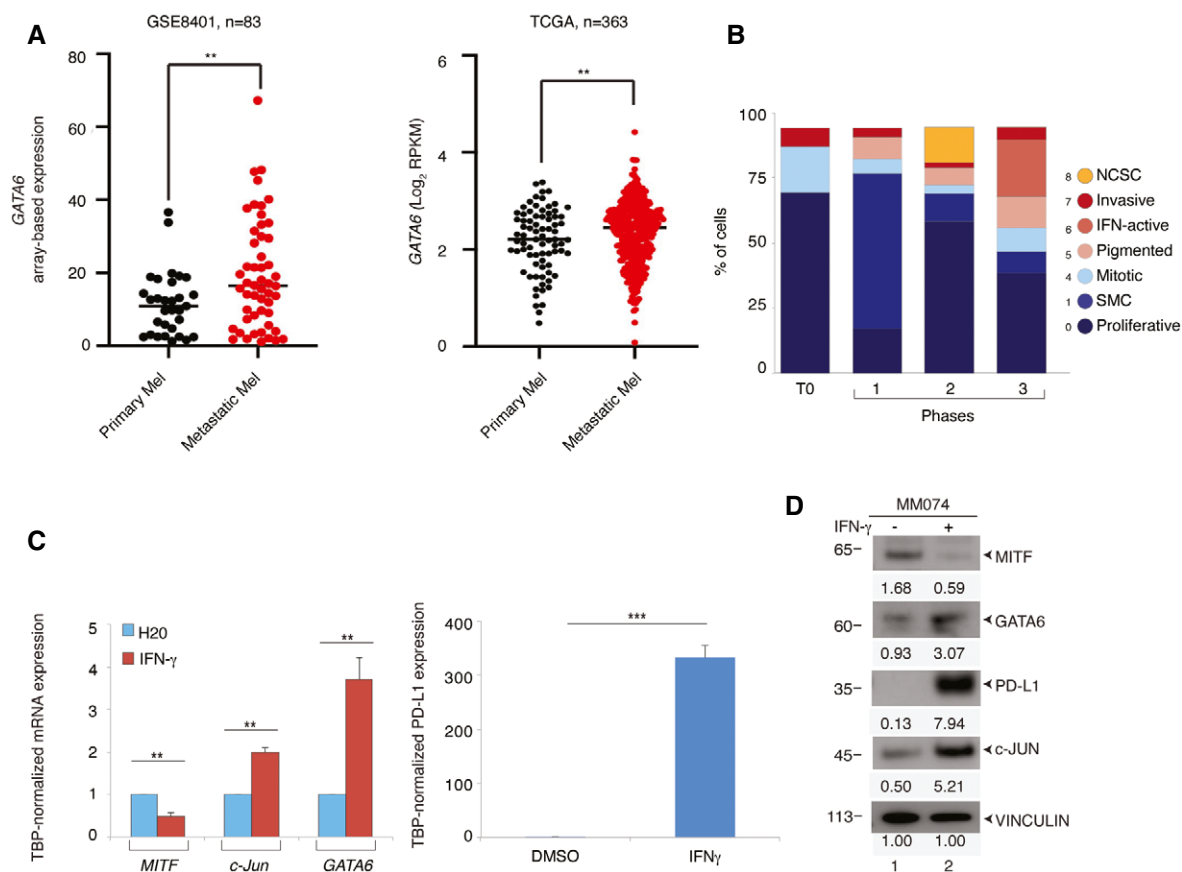


Figure EV4. GATA6 is overexpressed in metastatic melanoma.

- A Scatter plot expression values for *GATA6* in primary vs metastatic melanoma extracted either from published DNA microarray data on a cohort of patient melanomas (skin cutaneous melanoma, $n = 83$) (GSE8401) (Xu *et al*, 2008) (left panel) or from TCGA bulk RNA-seq data on a cohort of patient melanomas (skin cutaneous melanoma, $n = 363$, Pan-Cancer Atlas) (right panel). The P -value (Student's t -test) is indicated, $** < 0.01$.
- B Group histogram showing the percentage of cells belonging to phenotype clusters as indicated in T0 (drug naïve), phases 1–2 (MDR), and phase 3 (drug resistance).
- C qRT-PCR analysis showing average TBP-normalized fold expression of *MITF*, *c-Jun*, *GATA6*, and PD-L1 in MM074 treated or not with IFN- γ (20 ng/ml) for 24 h.
- D MM074 was treated or not with IFN- γ (20 ng/ml) for 24 h, and protein lysates were immuno-blotted for the indicated protein. The numbers below the gel lanes represent relative protein level, which was determined from the band intensity using ImageJ software and normalized relative to vinculin control.

Data information: In (C), data are presented as mean values + SD for six replicates ($n = 6$). The P -value (Student's t -test) is indicated, $** < 0.01$ and $*** < 0.005$.

Source data are available online for this figure.

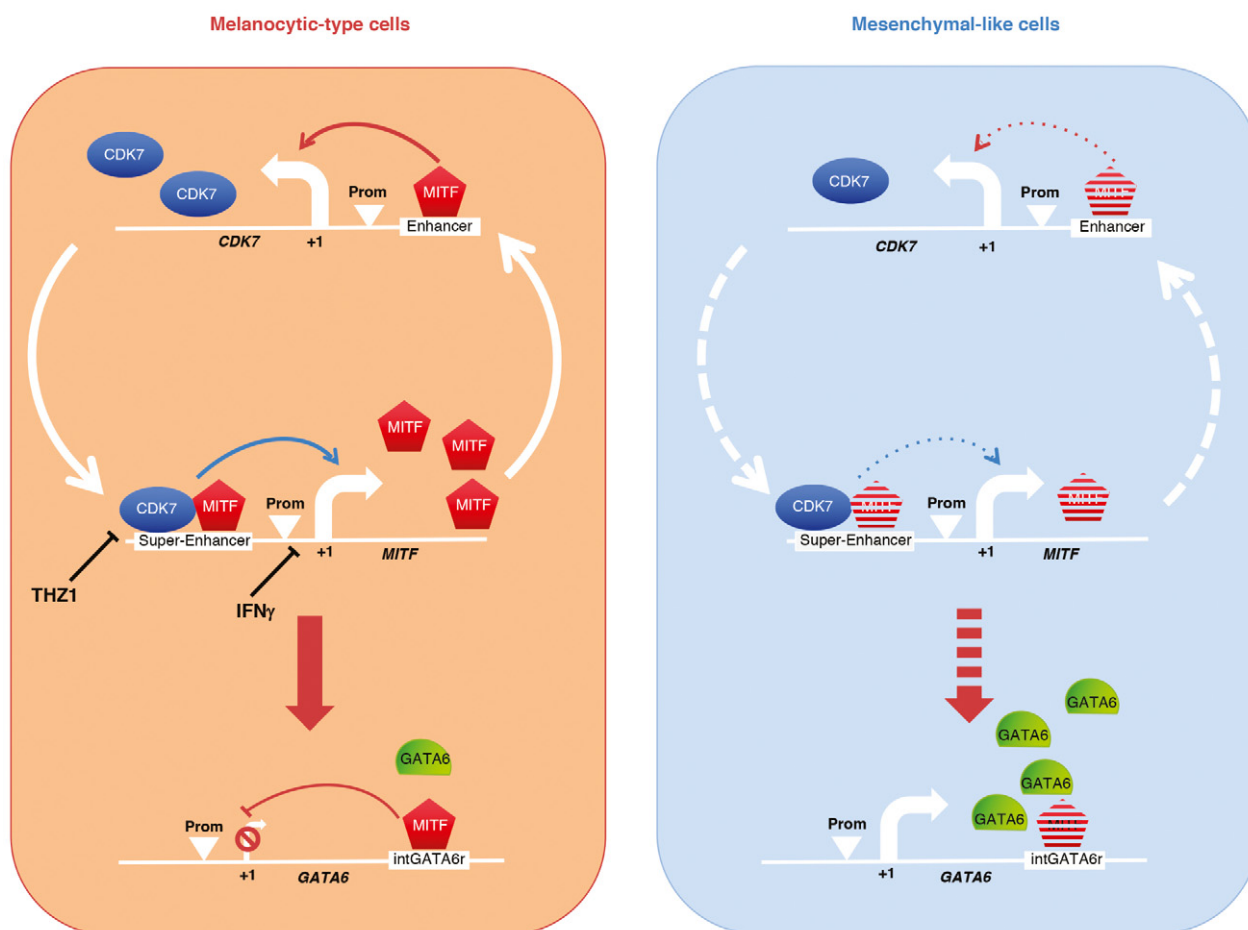


Figure EV5. Scenarios for the repression and activation of GATA6 expression in melanoma.

In melanocytic-type cells (left red panel), CDK7 and MITF mutually regulate each other in a positive feedback loop through binding to enhancers or SEs associated with each gene. In turn, MITF binds to a sequence located in an intron of GATA6 to repress its expression. Consequently, GATA6 is poorly expressed in MITF/CDK7 high cells. THZ1 or IFN γ represses MITF expression leading to GATA6 up-regulation. Upon switching to a mesenchymal-like state (right blue panel), a negative feedback loop is established where the progressive loss of MITF during melanoma progression and inflammation triggers decreased CDK7 protein levels that in turn promotes lower MITF expression leading to de-repression of GATA6 expression in MITF/CDK7-low cells.

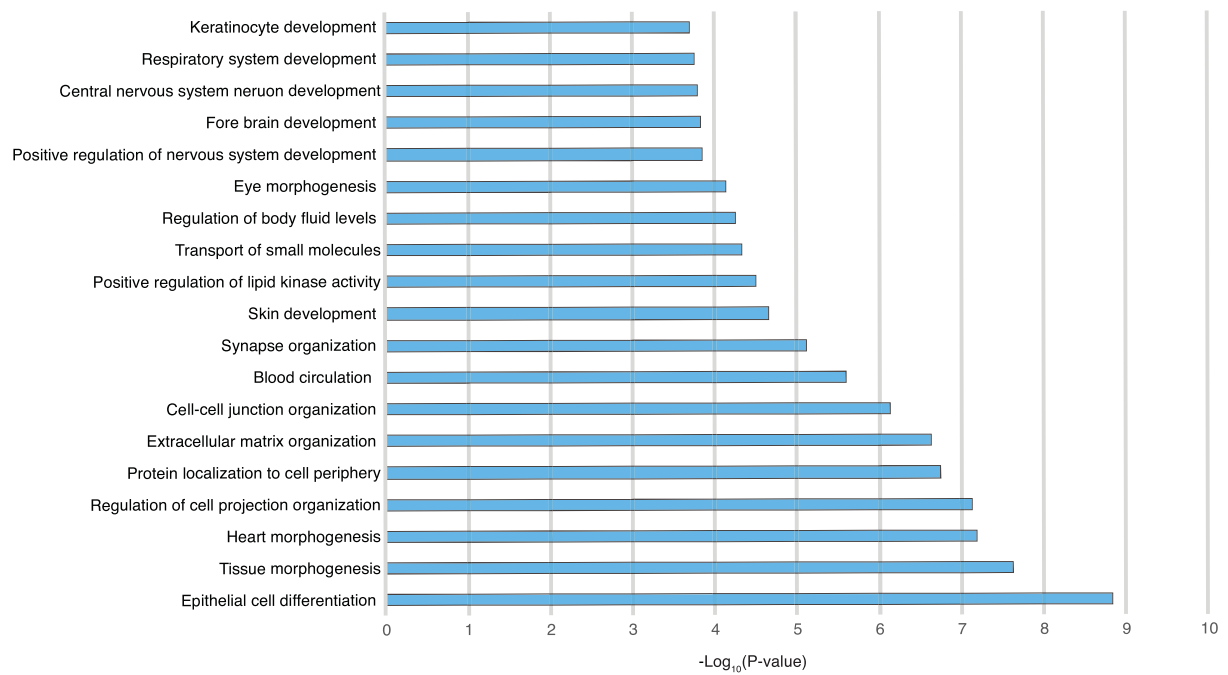
Appendix table of Content

Appendix Figure S1	Page 2
Appendix Figure S2	Page 3
Appendix Figure S3	Page 4
Appendix Figure S4	Page 5
Appendix Figure S5	Page 6
Appendix Table S1:	Page 7

Appendix Figure S1: Phenotype reprogramming of drug-resistant melanoma cells

GO was used to analyze the 261 genes up-regulated both in MM047^{CDK7i-R} and MM074^{CDK7i-R} cells. In the horizontal histograms the top 20 significant pathways obtained from the Metascape analysis are shown.

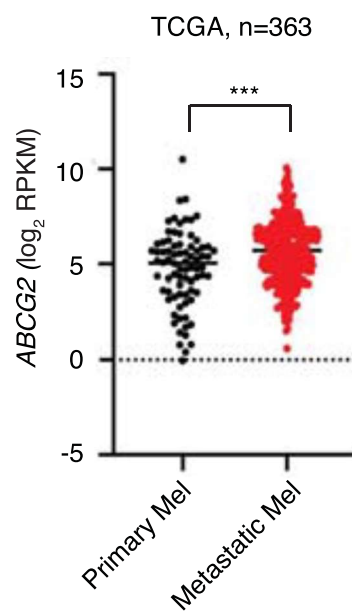
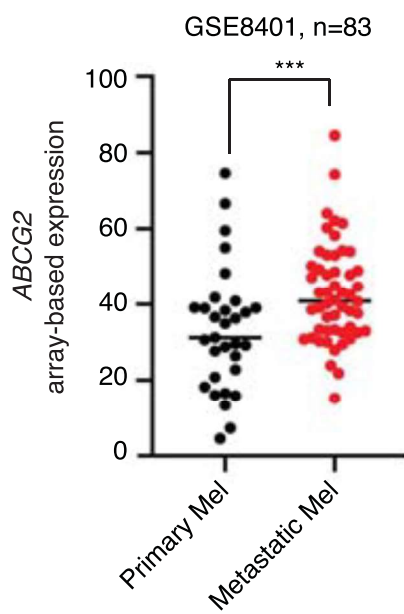
Appendix Figure S1



Appendix Figure S2: *ABCG2* is up-regulated in metastatic melanoma

Scatter plot expression values for *ABCG2* in primary vs metastatic melanoma extracted either from published DNA microarray data on a cohort of patient melanomas (skin cutaneous melanoma, n=83) (GSE8401) (Xu et al., 2008) (left panel) or from TCGA bulk RNA-seq data on a cohort of patient melanomas (skin cutaneous melanoma, n=363, Pan-Cancer Atlas) (right panel). The p-value (Student's test) is indicated, ***<0.005.

Appendix Figure S2



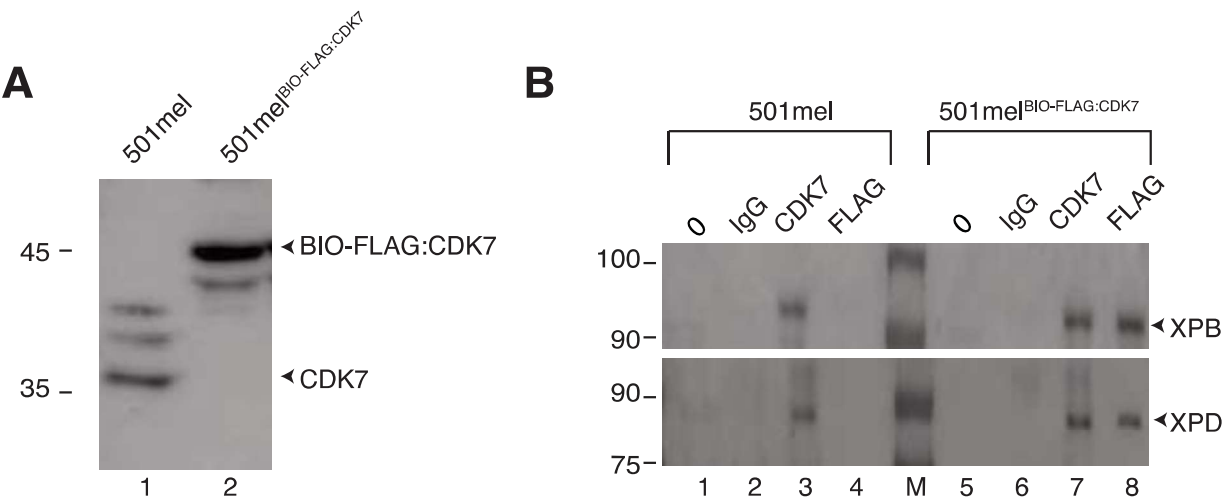
Appendix Figure S3: Characterization of 501mel^{BIO-FLAG:CDK7} cells

A. Protein lysates from 501mel and 501mel^{BIO-FLAG:CDK7} cells were immuno-blotted for CDK7.

Molecular sizes (KDa) of the proteins are indicated in kDa.

B. Immunoprecipitation was performed with anti-IgG, anti-CDK7 or anti-FLAG using whole cell extracts of 501mel and 501mel^{BIO-FLAG:CDK7} cells. Proteins on the resin were resolved by SDS-PAGE and immunoblotted using anti-XPB or anti-XPB antibodies. Molecular sizes (KDa) of the proteins are indicated in kDa.

Appendix Figure S3

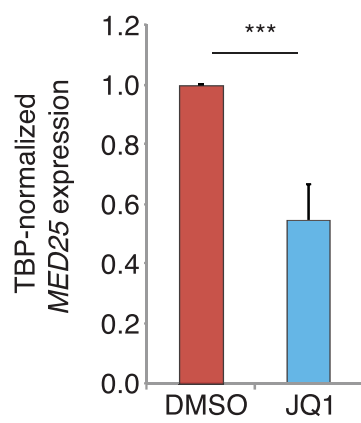


Appendix Figure S4: JQ1 affects MED25 expression

MED25 expression is used a positive control of JQ1 treatment. qRT-PCR analysis showing average *TBP*-normalized fold expression of *MED25* in 501mel treated either with DMSO or JQ1 (10 μ M) for 24h. Error bars indicate mean values + SD for three biological triplicates. The p-value (Student's t-test) is indicated, ***<0.005.

Appendix Figure S4

A



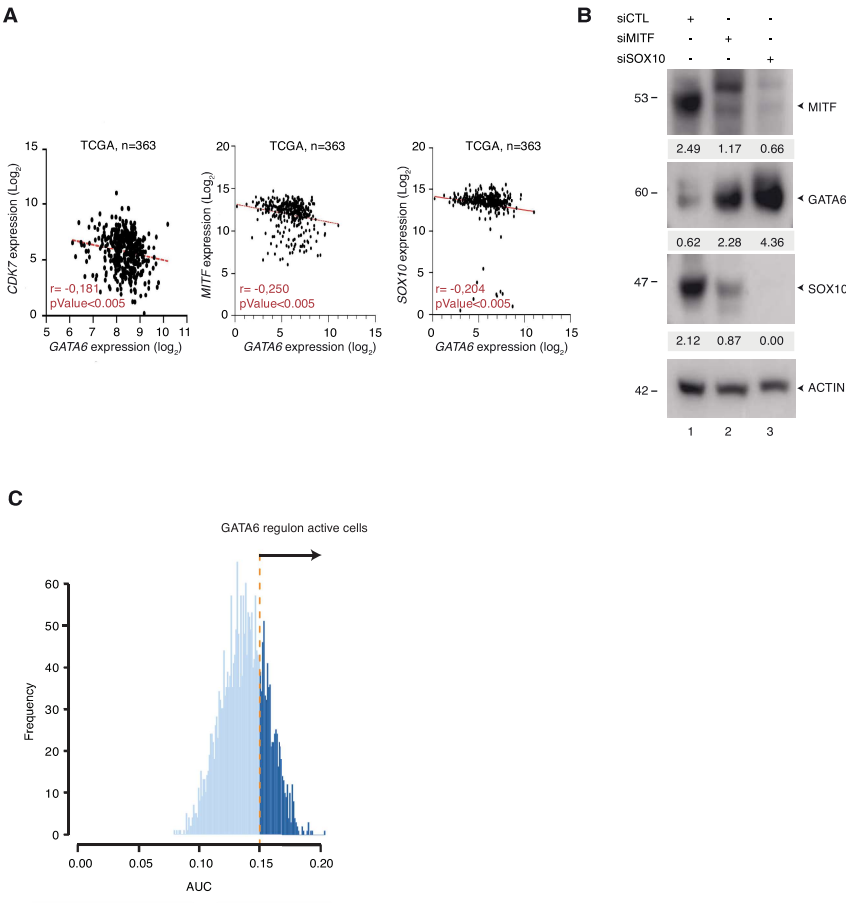
Appendix Figure S5: Decrease of SOX10 and MITF using siRNA induces GATA6 expression

A. Scatter plot expression values (in $\log_2(\text{RPKM})$) of *GATA6* against either *CDK7* (left), *MITF* (middle) or *SOX10* (right). These data were extracted from TCGA bulk RNA-seq data on a cohort of patient melanomas (n=363, Pan-Cancer Atlas). The line of best fit, the Spearman's rank correlation coefficient (r) and the p-value (Student's t-test) are indicated.

B. 501mel were pre-treated with siCTL, siMITF or siSOX10 for 48h and protein lysates from the indicated cells were immuno-blotted for the indicated proteins. Molecular masses of the proteins are indicated in kDa. The numbers below the gel lanes represent relative protein level, which was determined from the band intensity using ImageJ software, and normalized to each relative actin control.

C. Bi-modal distribution of the frequency of AUCell values of GATA6 regulon in MM074 single cells treated with siSOX10. We considered that GATA6 regulon active cells show an AUCell value > 0.15.

Appendix Figure S5



Appendix Table S1: A full list of reagents including antibodies, oligonucleotides and biological kits used in this paper is provided.

REAGENT/ RESOURCE	SOURCE	IDENTIFIER
Antibodies		
Monoclonal Anti-Vinculin antibody produced in mouse	Sigma-Aldrich	V4505
Polyclonal Anti- β Tubulin antibody produced in goat	Abcam	Ab21057
Monoclonal Anti-SOX10 antibody produced in rabbit	Cell Signaling	D5V9L
Monoclonal Anti-MITF antibody produced in rabbit	Cell Signaling	D5G7V
Monoclonal Anti-TFAP2A antibody produced in mouse	SC Biotechnology	sc-12726
Monoclonal Anti-GATA6 antibody produced in rabbit	Cell Signaling	D61E4
Monoclonal Anti-SOX9 antibody produced in rabbit	Cell Signaling	D8G8H
Monoclonal Anti-c-JUN antibody produced in rabbit	Cell Signaling	9165
Polyclonal Anti-H3K27ac antibody produced in rabbit-ChIP Grade	Abcam	Ab4729
Polyclonal Anti-HA antibody produced in rabbit-ChIP Grade	Abcam	Ab9110
Monoclonal Anti-FLAG antibody produced in mouse	Merck Millipore	F3165
Biological Samples		
Sections of nevi and melanoma samples	Prof. B. Cribier, head of the <i>Laboratoire d'histopathologie et d'immunopathologie cutanées</i> at the Hôpital Civil of Strasbourg	N/A
Chemicals, Peptides, and Recombinant Proteins		
THZ1	MedChemExpress	HY-80013
Trametinib	MedChemExpress	HY-10999

Vemurafenib	SelleckChem	PLX4032
JQ1	SelleckChem	S7110
INF γ	PeptoTech	300-02
Critical Commercial Assays		
Click-iT RNA Alexa Fluor 488 Imaging kit	Invitrogen	C10329
PrestoBlue	ThermoFisher	A13262
GenElute Mammalian Total RNA Miniprep kit	Merck	RTN70
CellTrace Violet	ThermoFisher	C34571
Phusion High-Fidelity TAQ polymerase	ThermoFisher	F-530XL
APC Annexin V	BD Biosciences	550474
BafilomycinA1	Sigma-Aldrich	B1793
FuGENE6 transfection reagent	Promega France	E2691
Lipofectamine RNAiMAX reagent	ThermoFisher	13778150
Experimental Models: Cell Lines		
Human; Short-term cultured melanoma cells		(Gembarska et al., 2012)
Human; MM099 ^{MITF-SOX10-PAX3}	This paper	N/A
Human; 501mel ^{BIO-FLAG:CDK7}	This paper	N/A
Oligonucleotides		
Primer <i>ACT1N</i> , forward, ACATCTGCTGGAAGGTGGAC	This paper	N/A
Primer <i>ACT1N</i> , reverse, CCCAGCACAAATGAAGATCAA	This paper	N/A
Primer <i>GAPDH</i> , forward, ACAACTTTGGTATCGTGGAAGG	This paper	N/A
Primer <i>GAPDH</i> , reverse, GCCATCACGCCACAGTTTC	This paper	N/A
Primer <i>MITF</i> , forward, CATTGTTATGCTGGAAATGCTAGAA	This paper	N/A
Primer <i>MITF</i> , reverse, GGCTTGCTGTATGTGGTACTTGG	This paper	N/A

Primer <i>TBP</i> , forward, CGGCTGTTTAACTTCGCTTC	This paper	N/A
Primer <i>TBP</i> , reverse, CACACGCCAAGAAACAGTGA	This paper	N/A
Primer <i>SOX10</i> , forward, CCAGTTTGACTACTCTGACCATCAG	This paper	N/A
Primer <i>SOX10</i> , reverse, ATATAGGAGAAGGCCGAGTAGAGG	This paper	N/A
Primer <i>ABCC3</i> , forward, GGAAAACGTGCTTTTCGGCAA	This paper	N/A
Primer <i>ABCC3</i> , reverse, CCCCCAGACAGGTTAATGCC	This paper	N/A
Primer <i>ABCB1</i> , forward, GGAGGCCAACATACATGCCT	This paper	N/A
Primer <i>ABCB1</i> , reverse, AGGCTGTCTAACAAGGGCAC	This paper	N/A
Primer <i>ABCG2</i> , forward, TCAGGAGGCCTTGGGATACT	This paper	N/A
Primer <i>ABCG2</i> , reverse, GTCTTCTTCTCTGTTAATGCCACA	This paper	N/A
Primer <i>GATA6</i> , forward, ACCACCTTATGGCGCAGAAA	This paper	N/A
Primer <i>GATA6</i> , reverse, ATAGCAAGTGGTCTGGGCAC	This paper	N/A
Primer <i>AMIGO2</i> , forward, GCAGTGATAGCTGAGGGCAT	This paper	N/A
Primer <i>AMIGO2</i> , reverse, CGCCACAAAAGGTGTGTCAG	This paper	N/A
Primer <i>SERPINE2</i> , forward, AGAGCGCTGTCAAGAAGACC	This paper	N/A
Primer <i>SERPINE2</i> , reverse, CTCAGAGGTGCCTTGCGATT	This paper	N/A
Primer for ChIP, intGATA6r, forward, GAAAAAGCCGTAAGCACAGTCTCA	This paper	N/A
Primer for ChIP, intGATA6r, reverse, ACGACTGTGTGATCCTTCCCA	This paper	N/A
Primer for ChIP, TYR, forward, CATCCTTCTGTAAGGCCACAG	This paper	N/A
Primer for ChIP, TYR, reverse, ACTGGGAATGAAGGGCAAG	This paper	N/A
Primer for ChIP, PRMG, forward, ACAGAGCGACACCCTGTCAT	This paper	N/A
Primer for ChIP, PRMG, reverse, AGGCGGTGGTTACACAACA	This paper	N/A
gRNA1, CDK7, tcgggctttacggcgccgga	This paper	N/A
gRNA2, CDK7, acttcacgtccagagccatc	This paper	N/A

Puromycin-P2A-BIO-FLAG-CDK7N-termsequence:ctttaaattcgtgtgtcctcctggagctcgcccttttcggctgga gtcgggctttacggcgCCGgATGACCGAGTACAAGCCCACGgt gcgcctcgccaccccgacgacgtccccagggccgtacgcaccctcgccgc cggttcgacgactaccccgccacgcccacacgctgatccggaccgcccacat cgagcgggtcaccgagctgcaagaactcttctcacgcgcgtcgggctcgaca tcggcaagggtgtgggtcgcggacgacgcccgcgggtggcggtctggaccac gccggagagcgtcgaagcggggggcggtgttcgagatcgcccgccgcgt ggccgagttgagcgggtcccgctggccgcgcagcaacagatggaaggcctc ctggcgccgcaccggcccaaggagcccggtgttcttgccaccgctcggt ctgcgccgaccaccagggcaagggtcggcgacgcgcgtgtctccccgga gtggaggcgccgagcgcgcggggtcccgccttcttggaAacctccgcgc cccggaacctcccttctacgagcggctcggctcacgcgcaccgcccgcgacgtc agggtcccgaaggaccgcgcacctgtgtcatgacccgaagcccggtgccG Gaagcggagctactaactcagcctgtgaagcaggctggagacgtggagga gaacctggacctggcctgaatgacatcttgaggccagagaagatcgagtggc atgaggagggaatggactacaaggacgacgatgacaaggaggcgaggagg agtggaggcggtggCAGCGGTGGCGGAGGGAGTGctctggacg tgaagtctcgggcaaagcgttatgagaagctggactccttggggagggacag gtg)	This paper	N/A
Single clones check, F1: GAACGCCAACCGCTGG	This paper	N/A
Single clones check, F5: AAGAACTCTTCCTCACGCGCG	This paper	N/A
Single clones check, R3: CCGAGACTTCACGTCCAGAGC	This paper	N/A
Single clones check, R4: AAACGTGGCGGGTCAGTCTCC	This paper	N/A
Single clones check, R5: CCTTCCATCTGTTGCTGCGC	This paper	N/A
MluI_F:aaaaACGCGTACGATTTGCAGGAAAGCATTTC		
SmaI_R:aaaaCCCGGGCATGGGTTCTTCGGCTTGTGG		
intGATA6r forward primer ACGATTT GCAGGAAAGCATTTC		
intGATA6r reverse primer CATGGGTTCTTCGGCTTGTGG		
Recombinant DNA		
pCDNA-ieEnh-CMV-GFP	This paper	N/A
pCDNA-intGATA6r-CMV-GFP	This paper	N/A
pTET-SMP-MITF/SOX10/PAX3	This paper	N/A
pCDNA-GFP	Thermofisher	
pLenti-EF1a-GFP	This paper	N/A
PLenti-EF1a-3xFLAG-GATA6	This paper	N/A

Software and Algorithms		
Metascape software	(Zhou et al., 2019)	
AUCCell v 1.6.1	(Aibar et al., 2017)	
Seurat software package version 3.1.4	(Butler et al., 2018)	
RSAT	http://rsat.sb-roscoff.fr	
seqMINER	http://bips.u-strasbg.fr/seqminer/	
HOMER	http://biowhat.ucsd.edu/homer/ngs/annotation.html	
MACS	http://liulab.dfci.harvard.edu/MACS/	
ImageJ	http://rsb.info.nih.gov/ij/	
Other		
FACSAria™ Fusion cell sorter	BD Biosciences	
LSRFortessa™ Flow Cytometer	BD Biosciences	
INCell Analyzer 1000 imaging system	GE Healthcare	
Mithras LB 940 microplate reader	Berthold	
LightCycler [®] 480 Instrument II	Roche Diagnostic	
HiSeq2500 system	Illumina	

Addendum: The role of XPB in super-enhancer dependent gene expression in melanoma

Our paper published in *EMBO Reports* in 2021 clearly pointed to the involvement of CDK7 in the phenotypical plasticity of melanoma cells and also showcased a previously unexpected potential risk of using CDK7 inhibitors in cancer treatments. These data led us to ask ourselves if the targeting of other TFIIH subunits might result in similar transcriptional reprogramming of melanoma cells. Surprisingly, until 2020, no data at all was available concerning the potential SE-related roles of other TFIIH subunits except CDK7. While Kwiatkowski et al. already demonstrated in 2014 that CDK7 is heavily involved in SE-dependent oncogene expression, thus far, no similarly comprehensive studies have been undertaken to elucidate whether partners of CDK7, such as the TFIIH translocase XPB, are recruited to SEs and if they might have oncogenic roles to play. In 2020, when our results began to coalesce into a model in which CDK7 is of crucial importance to maintain the melanocytic identity of melanoma cells, I was tasked to study whether the use of Triptolide (TPL), a potent inhibitor of XPB, would exert similar effects than THZ1. During that very year, a study by Noel et al. showed that the treatment of pancreatic cancer cells with TPL induced the important disruption of SE-dependent oncogene expression. However, the study did not explain whether this was a direct effect of XPB inhibition, and by which exact mechanisms SEs were affected. While the enrichment and role of XPB at SEs were not elucidated at all in that paper, these insights reinforced our hypothesis that TFIIH subunits other than CDK7 might play important roles in SE architecture and function. As such, the aims of this project were to study:

- the potential molecular roles of XPB in melanoma-associated SE function, considering CDK7-related insights.
- the potential use of XPB inhibitors in the clinical setting for melanoma patients.
- whether the inhibition of XPB leads to transcriptional reprogramming.

This project, which was put under my direct supervision, was unfortunately greatly slowed down by the COVID-19 pandemic and is thus still ongoing. Nonetheless, the preliminary data I obtained with the help of the lab engineers Maguelone Nogaret and Philippe Catez have already allowed to generate interesting insights, which are presented in the next pages as a draft of a prospective paper.

Pharmacological inhibition of XPB and CDK7 differentially disrupt super-enhancer dependent gene expression in melanoma cells

--- Work in progress ---

Max Cigrang^{1, 2, 3, 4}, Philippe Catez^{1, 2, 3, 4}, Maguelone Nogaret^{1, 2, 3, 4}, Pietro Berico^{1, 2, 3, 4}, Guillaume Davidson^{1, 2, 3, 4}, Jean-Marc Egly^{1, 2, 3, 4}, Emmanuel Compe^{1, 2, 3, 4}, and Frédéric Coin^{1, 2, 3, 4, 5}

¹ Institut de Génétique et de Biologie Moléculaire et Cellulaire Illkirch Cedex, C.U. Equipe Labélisée Ligue contre le Cancer 2022, Strasbourg, France

² Centre National de la Recherche Scientifique, UMR7104, 67404 Illkirch, France

³ Institut National de la Santé et de la Recherche Médicale, U1258, 67404 Illkirch, France

⁴ Université de Strasbourg, 67404 Illkirch, France

⁵ Corresponding author, fredr@igbmc.fr

Tel: +33 3 88 65 34 49

Key words: Melanoma, Transcription, Super-enhancers, TFIIH, XPB, CDK7, Triptolide, THZ1

Introduction

Gene expression dysregulation is a major hallmark of cancer. Various molecular mechanisms in tumor cells lead to extensive alterations in transcriptional programs which are underlying many aspects of their malignant phenotypes, such as increased proliferation, invasiveness, and therapy resistance. In recent years, the concept of ‘transcriptional addiction’ of cancer cells has emerged, which posits that their complex, dysregulated gene expression programs heavily depend on a relatively few crucial components and mechanisms, which may be therapeutically exploited (Bradner, Hnisz and Young, 2017; Sengupta and George, 2017). One of these mechanisms is the oncogenic acquisition of genomic structures known as super-enhancers (SEs). These are defined as large clusters of enhancers (>12 kb), which in normal conditions are associated with the transcription of master transcription factors maintaining tissue identity (Pott and Lieb, 2015; Eliades *et al.*, 2018; Blobel *et al.*, 2021). In cancer cells however, their acquisition at abnormal loci can lead to the strong overexpression of key oncogenes (Thandapani, 2019; Gartlgruber *et al.*, 2021). ChIP-Seq analysis has revealed that at SEs, there is unusually high enrichment of transcription factors, co-activators, and open chromatin marks such as H3K27ac (Hnisz *et al.*, 2015). Interestingly, the TFIIH kinase subunit CDK7 was also found to be enriched at SEs. Whereas the exact and intricate molecular functions of CDK7 are still an area of active investigation, its overarching role as master regulator of transcription and the cell cycle is established (Fisher, 2005; Compe and Egly, 2016, 2021; Rimel *et al.*, 2020). In the context of SEs, CDK7 inhibition was shown to heavily impact SE-dependent gene expression, however, its exact functions in this regard remain a mystery (Chipumuro *et al.*, 2014; Kwiatkowski *et al.*, 2014). Furthermore, it isn’t clear whether CDK7 is recruited at SEs by itself or in tandem with other TFIIH subunits such as the translocase XPB, which plays fundamental roles in promoter opening during transcription initiation and gene expression (Alekseev *et al.*, 2017; Sandoz *et al.*, 2019).

Melanoma is a cancer which is notoriously prone to the rapid establishment of therapy resistances (Kozar *et al.*, 2019; Rambow, Marine and Goding, 2019). This is mainly due to its intrinsic phenotypic and transcriptional plasticity, which leads to the emergence of two main cellular states: the treatment-sensitive differentiated/melanocytic cells and the treatment-insensitive dedifferentiated/mesenchymal-like cells (Verfaillie *et al.*, 2015; Rambow *et al.*, 2018). Recently, our lab showed that the pharmacological inhibition of CDK7 by the small

molecule THZ1 (Kwiatkowski *et al.*, 2014) had initial beneficial effects in melanocytic melanoma cells by abrogating the expression of SE-dependent genes such as the master regulators of the melanocytic lineage, MITF and SOX10 (Berico *et al.*, 2021). However, mesenchymal-like melanoma cells were largely resistant to THZ1. Furthermore, prolonged exposure led melanocytic cells to undergo a GATA6-dependent phenotype switch into the mesenchymal phenotype, resistant to THZ1. As this cell state is a known driver of melanoma metastasis and treatment insensitivity, targeting CDK7 in melanoma might represent a potential danger. However, pharmacological inhibitors targeting other enzymatic subunits of TFIIH exist. Triptolide (TPL) is a diterpene triepoxide isolated from the medicinal herb *Tripterygium wilfordii*, which covalently binds to XPB and inhibits its ATPase activity (Titov *et al.*, 2011). Although there have been recent hints that the inhibition of XPB disrupts SEs in pancreatic cancer, it is unclear whether XPB is directly recruited to these regions and if its enzymatic activities come into play, or if the effects observed in this singular study were of a more indirect nature (Noel *et al.*, 2020). Furthermore, the potential interaction between XPB and SEs has not been studied in other cancers such as melanoma, and it remains unknown what functions TFIIH subunits like CDK7 or XPB would have at these sites, if they have the same roles, and if, correspondingly, their inhibitions would have similar effects on SE-dependent gene expression.

Here, we show that in contrast to THZ1, all tested melanoma cells, irrespective of their melanocytic/mesenchymal-like phenotype, were sensitive to TPL at low nanomolar doses, which had strong antiproliferative effects on 2D- and 3D-cultured cells. While THZ1 and TPL commonly affected a large overlap of genes, such as crucial SE-dependent melanoma factors like *MITF*, *SOX10*, *INO80*, or *KIT*, the transcriptional response for the two drugs somehow differed, with TPL deregulating fewer genes. Finally, while chronic exposure to TPL led cells to become insensitive over time, no phenotype switch towards a more mesenchymal phenotype was observed, as was the case for CDK7-inhibition. Collectively, these preliminary data indicate that the inhibition of XPB by might be a viable strategy for the disruption of SE-networks in melanoma cells, irrespective of their cell state.

Results

Both melanocytic and mesenchymal-like melanoma cells are highly sensitive to TPL.

To compare the sensitivity of melanoma cells to THZ1 and TPL, we used cells covering the two main phenotypes and four of the most common driver mutations in melanoma. On the one

hand, differentiated melanocytic-type 501mel (BRAF^{V600E}), MM011 (NRAS^{Q61K}), and MM074 (BRAF^{V600E}) cells showed high expression of the lineage-specific SE-dependent transcription factors MITF and SOX10, coupled with low to undetectable levels of the pro-metastatic EGFR and AXL factors (Widmer et al., 2012; Verfaillie et al., 2015) (**Figure 1A, lanes 2-4**). On the other hand, dedifferentiated mesenchymal-like melanoma cells MM029 (BRAF^{V600K}), MM047 (NRAS^{Q61R}), and MM099 (BRAF^{V600E}) exhibited low levels of MITF and SOX10 coupled with high levels of EGFR and AXL (**Figure 1A, lanes 5-7**). Both cell states seemed to express similar quantities of RPB1, the largest subunit of RNA Polymerase II and of the TFIIH subunits CDK7 and XPB. Interestingly, the amounts of CDK7 and XPB were higher in all melanoma cells compared to the Hermes3A non-cancer immortalized melanocytes (**Figure 1A, compare lanes 2-7 to lane 1**). We next determined the IC50s of these cells towards either CDK7 inhibition by THZ1 or XPB inhibition by TPL, by using cell viability assays. Our results first confirmed that the melanocytic 501mel, MM011 and MM074 cells as well as the mesenchymal-like MM047 cells were sensitive to THZ1, whereas the MM029 and MM099 mesenchymal-like cells were resistant (**Figure 1B, upper panel**). Previous work from our lab determined that GATA6-mediated ABCG2 efflux pump expression causes THZ1 resistance of these cells (Berico *et al.*, 2021). On the contrary, all melanoma cells were highly sensitive towards TPL, at lower concentrations than for THZ1 (**Figure 1B, lower panel**). Strikingly, it seemed that the MM047 and MM099 mesenchymal-like cells were even more sensitive to TPL than the melanocytic cells.

Cell survival assays using Crystal Violet, in which the cells were exposed to the measured IC50 doses, confirmed these trends (**Figure 2A**). We next investigated the effects of THZ1 and TPL treatments on melanoma cell proliferation and apoptosis. CellTrace staining followed by Flow Cytometry analysis revealed that whereas THZ1 did not have anti-proliferative effects in MM029 and MM099 cells, TPL was efficient in all tested cells, regardless of phenotype (**Figure 2B**). AnnexinV staining next showed that the effects regarding apoptosis were less pronounced for both drugs (**Figure 2C**). However, it is worthwhile to notice that the NRAS-mutated MM011 and MM047 cells showed significant cell-death increases. To validate the findings that TPL is effective against mesenchymal-like cells, we treated 3D-grown melanospheres with the drugs, as it is known that these represent more accurate models of drug sensitivities. While THZ1 did not affect cell viability and apoptosis of MM029 and MM099 cells, TPL treatment severely affected all melanospheres (**Figure 2D**). In these 3D conditions, TPL induced significantly increased apoptosis (**Figure 2E**). Collectively, these data show that,

contrary to THZ1, TPL displays strong effects on the viability and proliferation of melanocytic as well as mesenchymal-like melanoma cells.

THZ1 and TPL potently inhibit MITF and SOX10 expression in melanoma.

We next aimed to study whether XPB inhibition by TPL could abrogate SE-dependent gene expression, as had already been observed for CDK7 inhibition (Kwiatkowski *et al.*, 2014; Berico *et al.*, 2021). After differentiated 501mel cells were treated with doses equivalent to 5xIC₅₀, RT-qPCR analysis showed that both drugs rapidly affected the expression of the SE-dependent melanocytic lineage-specific transcription factors MITF and SOX10, compared to the housekeeping ACTb gene whose expression remained unchanged following treatments (**Figures 3A**). In parallel, immunoblotting showed that protein products of these genes also significantly decreased following THZ1 and TPL treatment (**Supplemental Figure 1**). Interestingly, whereas THZ1 seemed to induce the rapid loss of CDK7 protein levels, the same was less obvious for TPL and XPB, potentially indicating differential degradation dynamics of the inhibited proteins. To investigate whether these treatments affected SE activity, ChIP-qPCR experiments targeting H3K27ac were performed on 501mel cells treated with 5xIC₅₀ doses of THZ1 or TPL for 12 hours (**Figure 3B**). Whereas a significant drop in H3K27ac signal was observed at the MITF and SOX10 SEs for both drugs, no significant reduction was observed at the promoters of non-SE dependent genes like ACTb or CDK7. Our previous studies showed that treatment of melanocytic melanoma cells with THZ1 induced a GATA6-dependent phenotype switch towards the mesenchymal-like phenotype, characterized by the expression of factors such as SOX9 and the loss of markers such as MITF and SOX10 (Berico *et al.*, 2021). To test whether a similar process might also occur upon TPL treatment, 501mel cells were subjected to 1xIC₅₀ concentrations of drugs for 24, 48 or 72 hours, and cell-state markers were assessed by RT-qPCR (**Figure 3C**). With both THZ1 and TPL treatments, MITF and SOX10 were impacted, and the invasive marker SOX9 was heavily upregulated. Remarkably however, no significant increase of GATA6 expression was observed in TPL-treated cells after 72 hours, in clear contrast to THZ1-treated cells. Taken together, these data suggest that both the inhibition of CDK7 and XPB rapidly impact active enhancer marks such as H3K27ac at SEs, and subsequently lead to repression of key SE-dependent melanoma identity genes such as *MITF* and *SOX10*, with the potential risk of phenotype switch activation. However, cell responses towards THZ1 and THZ1 might differ, as seen by the differential induction of GATA6 expression.

THZ1 and TPL differently affect SE-dependent genes.

To determine the genome-wide transcriptomic effects of CDK7 and XPB inhibition, we next performed gene expression profiling in 501mel cells after a short 6h treatment with 5xIC₅₀ of either THZ1 or TPL. RNA-Seq analysis revealed that THZ1 inhibition led to approximately twice as many genes being significantly deregulated (4186 genes) than in TPL treated cells (2413 genes). (**Figure 4A, Supplemental Table 1**, not included in the thesis but available upon request). Among the genes downregulated upon treatment with THZ1 (2415 genes) and TPL (1505), 979 genes were commonly downregulated. On the other hand, among the upregulated genes (1771 for THZ1 and 908 for TPL), 430 genes were commonly upregulated (**Supplemental Figures 2A and 2B**). Gene ontology analysis revealed that among the common downregulated genes for THZ1 and TPL, a very significant enrichment of genes involved in transcription was observed (**Supplemental Figures 2C**). THZ1 and TPL treatments seemed however to affect different pathways, as GSEA analysis showed that TPL exposure significantly inhibited TNF α and Notch signaling, whereas no significant negative correlation could be found for THZ1 (**Supplemental Figures 2D**). Among the upregulated gene signatures, protein localization and metabolic changes, such as in fatty acid metabolism, became apparent.

We next overlapped the sets of down- and upregulated genes by THZ1 and TPL treatments with a list of 1015 putative SE-dependent genes in 501mel cells, determined by H3K27ac ChIP-Seq (**Supplemental Table 2**, not included in the thesis but available upon request). Although TPL treatment downregulated fewer genes than THZ1 treatment, the number of downregulated SE-dependent genes was almost similar between both drug treatments (132 for TPL vs 134 for THZ1) (**Figure 4B**). Among them, 84 genes were commonly affected by both drugs (such as *MITF*, *SOX10*, or *KIT*), while 50 and 48 genes were differentially downregulated for THZ1 and TPL, respectively. Surprisingly, although THZ1 is a well-known SE inhibitor (Kwiatkowski *et al.*, 2014), the overlap between deregulated genes and SE-dependent genes did not reach statistical significance (Hypergeometric p-value < 0.165), suggesting that the inhibitory effect of THZ1 is not restricted to SE-dependent genes. On the contrary, TPL seemed to have stronger specificity towards SE-dependent genes (Hypergeometric p-value < 0.0000049). Additionally, whereas TPL treatment induced the upregulation of just 30 SE-dependent genes, THZ1 treatment lead to increased expression of 94 genes, some of which were associated with melanoma progression and phenotype switching, such as *LGALS3*, *IQGAP1*, *SEMA5A*, *SPAG9* and *LAMC1* (Braeuer *et al.*, 2012; Zhang *et al.*, 2017; D'Aguanno *et al.*, 2018; Hebert *et al.*, 2020; Bassey-Archibong *et al.*, 2023). However, scatter-plot analysis of melanocytic-like and

mesenchymal-like marker genes (Verfaillie *et al.*, 2015) didn't show a systematic overexpression of mesenchymal-like markers in either condition (**Supplemental Figure 2E**), suggesting that a potential phenotype switch isn't induced after 6 hours of drug treatments. Taken together, these data indicate that THZ1 and TPL both deregulate SE-dependent genes, albeit targeting somewhat different gene sets. Importantly, when compared to THZ1, the specificity of TPL towards SEs seems to be more important. Additionally, TPL has less overall transcriptomic effects while activating less invasion-promoting SE-dependent genes than THZ1.

Long-term exposure leads to different outcomes between THZ1 and TPL

To investigate the long-term effects of TPL treatments and potential resistance mechanisms, we chronically exposed three different types of cells (differentiated 501mel and MM074, and dedifferentiated MM047) to escalating doses of TPL until cells proliferated in 5xIC50 drug concentrations. The IC50s of TPL-resistant cells (TPL-R) were determined by cell viability assays (**Figure 5A**) and confirmed that these cells were all at least 5 times more resistant towards TPL than their respective original cells. We have previously demonstrated that MM074 cells with acquired resistance to THZ1 undergo a phenotype switch towards a mesenchymal-like state accompanied by multi-drug resistance towards clinically used MAPK inhibitors (Berico *et al.*, 2021). In clear contrast to this, TPL-R cells did not show a significantly increased resistance towards THZ, the BRAFV600E inhibitor Vemurafenib or the MEK inhibitor Trametinib. We then proceeded to investigate whether long-term XPB inhibition also led to a transcriptional reprogramming and dedifferentiation towards a more mesenchymal-like cell state, as previously observed for long-term CDK7 inhibition. RT-qPCR analysis showed that while some TPL-R cells displayed increased expression of some dedifferentiation markers compared to their non-resistant original cells, no bona fide phenotype switch with systematic increase of these markers could be observed as was the case with MM074 THZ1-R cells (**Figure 5B**). Immunoblotting confirmed these results by showcasing that originally melanocytic or mesenchymal-like cells did not change their MITF/SOX10 or AXL/EGFR protein levels, respectively, upon acquisition of resistance towards TPL, in contrast to MM074 THZ1-R cells. Furthermore, while GATA6 levels were increased in THZ1-R cells, they did not significantly change in TPL-R cells (**Figure 5C**).

Discussion

The specific targeting of SEs has been proposed in recent years as an interesting therapeutic strategy, because of their crucial roles in oncogene expression and their sensitivity to transcriptional inhibitors such as THZ1 or JQ-1 (Hnisz *et al.*, 2013; Lovén *et al.*, 2013; Kwiatkowski *et al.*, 2014). However, unanswered questions remain about the molecular architecture of SEs, and the roles of the different involved protein complexes. Although CDK7 has been well characterized as being massively recruited to SEs in different cancers (Chipumuro *et al.*, 2014; Wang *et al.*, 2015; Eliades *et al.*, 2018; Zhang *et al.*, 2020), it is unclear whether other TFIID subunits are present as well, although first hints coming from pancreatic cancer seem to indicate this (Noel *et al.*, 2020). Furthermore, the long-term effects of SE inhibition have not been thoroughly assessed. Our lab has recently shown the potential dangers of disrupting SE networks in melanoma with THZ1 (Berico *et al.*, 2021), and so the question emerged whether inhibiting another enzymatic subunit of TFIID would lead to similar dedifferentiating effects.

In this preliminary work, we show that the XPB inhibitor TPL displayed strong cytostatic activities in all studied melanoma cells, regardless of their transcriptional and phenotypic state. Similarly to THZ1, short TPL exposure impacted SE chromatin state and abrogated the expression of crucial SE-dependent TFs regulating the melanocytic phenotype such as MITF and SOX10. Further transcriptomic analysis seemed however to indicate that TPL has less genome-wide effects than THZ1, with a more specific action towards SEs and several differentially inhibited SE-dependent genes. Collectively, these data support the notion that XPB is involved in SE maintenance and that its targeting could be more beneficial in melanoma than using THZ1. Although the clinical use of TPL is limited by its poor solubility and hepatic toxicity (Xi *et al.*, 2017), more water-soluble prodrugs of TPL such as Minnelide are currently being tested for treatment of advanced pancreatic cancers (Skorupan *et al.*, 2022). As such, as the inhibition of XPB seems to heavily affect even invasive and dedifferentiated melanoma subpopulations, the use of Minnelide could potentially prove beneficial for melanoma patients after phenotype switch-mediated MAPKi or immunotherapy relapse. In conclusion, our results warrant further *in vivo* exploration into the possibility of using XPB inhibitors as second-line treatment or adjuvant therapy in the metastatic melanoma setting.

Intriguingly, we previously showed that the loss of MITF expression through prolonged inhibition of CDK7 in melanocytic melanoma cells lifts the repression of the GATA6 TF and

results in a multi-drug resistant, dedifferentiated phenotype through the expression of genes such as *AMIGO2* and *ABCG2*. Indeed, we identified a MITF binding-site in an intronic region of *GATA6* and showed a direct repressive function of MITF. Surprisingly however, cells treated with TPL, while also losing the expression of MITF, do not display an increase in *GATA6* expression. As such, it would seem that the repressive role of MITF at the *GATA6* locus is altered in TPL-treated cells when compared to THZ1-treated cells, and more extensive mechanistic studies are warranted to establish why melanoma cells respond so differently to these two drugs. Furthermore, although both melanocytic-like and mesenchymal-like cells chronically exposed to TPL gradually became insensitive to its activity, no phenotype-switch or systematic dedifferentiation was observed as for THZ1-resistant cells. While the acquired resistance to TPL treatments does not seem to be mediated by a shift towards the arguably more problematic mesenchymal-like state, the exact molecular mechanisms of the observed resistance are still unknown. Here as well, differential gene expression profiling in the generated TPL-resistant cells by RNA-Seq should provide insights into deregulated pathways and regulons, helping to potentially identify underlying and potentially targetable effectors.

Other very important questions remain unanswered as well, as the direct recruitment of XPB to SEs has not been shown yet. While we tried to perform ChIP experiments on XPB in 501mel cells, the results were repeatedly inconclusive, probably due to the fact that the several antibodies targeting endogenous XPB we used were inadequate for ChIP experiments. As such, to potentially get clearer results, we decided to induce the overexpression of HA-tagged XPB in cells we previously modified by CRISPR gene editing to express CDK7-Bio-Flag (Berico *et al.*, 2021). This ongoing task (**Supplemental Figure 3**) will hopefully allow us to study whether CDK7 and XPB are differentially recruited to SEs, and how THZ1 or TPL drug treatments might inhibit this recruitment, providing possible insights into the exact SE-related functions of these factors. At the moment, all of the transcriptomic analysis was only performed on the melanocytic 501mel cells. Ongoing work is underway to check whether the observed effects are reproducible in other cells such as MM074. Furthermore, as TPL also seems to heavily impact mesenchymal-like melanoma cells, we are checking whether SEs in these cells are also inhibited by targeting XPB. As such, the mesenchymal-like MM047 and MM099 cells, for which we have the lists of putative SEs, will be treated with TPL and RNA-Seq will be performed.

In conclusion, while significant work needs still to be done, initial data seems encouraging. This work sheds light on fundamental questions such as the role of XPB in SE architecture, but has also a more translational component, as XPB inhibitors could be considered as a potential novel therapeutic agent, capable of inhibiting multiple melanoma cell states.

Materials and Methods

Protein extraction and Western Blotting

For whole cell extracts, cells were rinsed once with cold PBS, before pelleting and resuspension in LSDB 0.5M buffer (500 mM KCl, 50 mM Tris pH 7.9, 20% glycerol, 1% NP-40, 1mM DTT and protease inhibitor cocktail). Afterwards, cells were fully disrupted with 3 cycles of heat shock (liquid nitrogen followed by 37°C water bath). Then, samples were centrifugated for 15min at 14,000rpm to remove cell debris. Lysates were subjected to SDS–polyacrylamide gel electrophoresis (SDS-PAGE) and proteins were transferred onto a nitrocellulose membrane. Membranes were incubated overnight at 4 °C with primary antibodies in PBS+ 5% milk powder + 0.01% Tween-20. The membranes were then incubated with HRP-conjugated secondary antibody (Jackson ImmunoResearch) for 1h at room temperature and visualized using the ECL detection system (GE Healthcare).

Antibodies

ACTb	Mouse Monoclonal 1:1000	IGBMC	2D7
AXL	Mouse Polyclonal 1:1000	ProteinTech	13196-1-AP
CDK7	Mouse Monoclonal 1:1000	IGBMC	2F8
EGFR	Mouse Monoclonal 1:1000	SantaCruz	sc-373746
Flag-Tag	Mouse Monoclonal 1:3000	Sigma Aldrich	F1804
GATA6	Rabbit Monoclonal 1:1000	Cell Signalling	D61E4
HA-Tag	Rabbit Polyclonal 1:1000	Abcam	ab9110
MITF	Rabbit Monoclonal 1:1000	Cell Signaling	D5G7V
RPB1	Mouse Monoclonal 1:1000	IGBMC	7C2
SOX10	Mouse Monoclonal 1:1000	SantaCruz	sc-365692
Vinculin	Mouse Monoclonal 1:1000	Sigma Aldrich	V4505
XPB	Rabbit Polyclonal 1:1000	Novus Biologicals	NB100-61060

Cell culture, treatments and generation of resistant cells

Cells were grown at 37°C in 5% CO₂ (10% for Hermes3A) and were regularly checked for mycoplasma contamination. MM patient-derived short-term melanoma cultures (MM011, MM074, MM029, MM047, MM099) were grown in HAM-F10 (Gibco, Invitrogen) supplemented with 10% Fetal Calf Serum (FCS), 25 mM HEPES, 5,2 mM GLUTAMAX and penicillin–streptomycin. Melanoma cell line 501mel was grown in RPMI w/o HEPES (Gibco, Invitrogen) supplemented with 10% FCS and gentamycin. Immortalized melanocytes Hermes3A were grown in RPMI 1640 medium (Gibco, Invitrogen) supplemented with 10% FCS, 200 nM TPA, 200 pM cholera toxin, 10 ng/ml human stem cell factor, 10 nM endothelin-1 and penicillin–streptomycin. 501mel cells were purchased from ATCC, MM and Hermes3A cells were obtained from collaborators.

To generate TPL-resistant cells, 501mel, MM074, MM029 and MM047 were chronically exposed to escalating doses of TPL over several weeks. These treatments were carried out until the cells proliferated in drug concentrations equal to at least 5 times the original IC₅₀ values. Once established, TPL-R cells were cultured with 3xIC₅₀ concentrations of TPL.

IC₅₀ estimation

Cells were seeded at 5,000 cells/well in 96- well plates and treated with increasing concentrations of THZ1 (MedChemExpress, HY-80013), TPL (Tocris, 3253), Vemurafenib (SelleckChem, PLX4032), or Trametinib (MedChemExpress, HY-10999). After 72 h of incubation, cells were treated with PrestoBlue reagent (ThermoFisher, A13262) according to the manufacturer's instructions. The absorbance per well was measured with a CellInsight CX5 microplate reader. Determination of IC₅₀ values was performed by nonlinear curve fitting using the Prism9 statistical software (GraphPad).

Cell Density Assay

Cells were seeded at 1x10⁵ or 2x10⁵ cells in 6-well plates and treated with THZ1 or TPL for 72h at respective IC₅₀ concentrations. Afterwards cells were fixed for 10 min with 4% Formaldehyde solution, washed once with PBS and stained with Crystal Violet solution 0.2% for 15 min. The wells were finally washed twice with deionized water, air dried, scanned and analyzed with Fiji to measure the covered surface %.

Cell proliferation and apoptosis analysis by Flow Cytometry

2x10⁶ cells were seeded in 6-well plates and were incubated 24h later with 1uM of CellTrace Violet reagent (ThermoFisher, C34571) according to the manufacturer's instructions, immediately before rinsing and drug treatments (1xIC₅₀). After 48h of incubation, cells were rinsed and incubated with AnnexinV-APC (BD Biosciences, 550474). Cell proliferation and apoptosis were detected on a BD LSRFortessa™ Flow Cytometer. Data were analysed with FlowJo software. To define slow proliferating or apoptotic cells, we proceeded as follows: We considered that slow proliferating cells represented the 30% of cells with the highest concentration of CellTrace Violet signal in the DMSO control. We then calculated the % of cells that had a signal greater than or equal to this value with drug treatment. For apoptotic cells, we considered the 20% of cells with the highest signal of AnnexinV-APC in the DMSO control. For apoptosis assays with 3D-grown melanoma cells, TrypLe Select 10x reagent (Gibco) was used to dissociate melanospheres to obtain single-cell suspensions. These cells were incubated with AnnexinV-APC (BD Biosciences).

Melanosphere formation and viability assay

5x10⁴ cells were seeded in ultra-low attachment hydrogel-layered 96 well plates (Corning) in KO DMEM medium supplemented with 20% KSR, AANE, 2 mM Glutamax, Penicillin/Streptomycin and 100 uM Beta-mercaptoethanol. To allow for melanosphere formation, cells were left to grow for 4 days before drug treatment (5xIC₅₀s, 72h). To analyze melanosphere viability after drug treatment, cells were treated with CellTiterGlo reagent (Promega, G7572) according to the manufacturer's instructions. Luminescence signals were measured with a Centro XS LB 960 microplate reader (Berthold).

RNA Extraction and RT-qPCR

Total RNA isolation was performed according to the manufacture protocol with NucleoSpin RNA Plus kit (Macherey-Nagel). RNA was retrotranscribed with Reverse Transcriptase Superscript IV (Invitrogen), qPCR was performed with SYBR Green (Roche) and on a LightCycler 480 (Roche). Primers for RT-qPCR were designed using Primer-BLAST.

Primers for RT-qPCR

18S	F TCAACTTTCGATGGTAGTCGCCGT R TCCTTGGATGTGGTAGCCGTTTCT
ABCB1	F GGAGGCCAACATACATGCCT R AGGCTGTCTAACAAGGGCAC

ABCC3	F GGAAAACGTGCTTTTCGGCAA R CCCCCAGACAGGTTAATGCC
ABCG2	F TCAGGAGGCCTTGGGATACT R GTCTTCTTCTCTGTTTAATGCCACA
ACTb	F ACATCTGCTGGAAGGTGGAC R CCCAGCACAAATGAAGATCAA
AMIGO2	F GCAGTGATAGCTGAGGGCAT R CGCCACAAAAGGTGTGTCAG
AXL	F CCGTGGACCTACTCTGGCT R CCTTGGCGTTATGGGCTTC
EGFR	F GCAGCGATGCGACCCTC R CCAACTGCGTGAGCTTGTTAC
GATA6	F ACCACCTTATGGCGCAGAAA R ATAGCAAGTGGTCTGGGCAC
JUN	F CCAACTCATGCTAACGCAGC R TCTCTCCGTCGCAACTTGTC
MITF	F CATTGTTATGCTGAAATGCTAGAA R GGCTTGCTGTATGTGGTACTTGG
SERPINE1	F AGAGCGCTGTCAAGAAGACC R CTCAGAGGTGCCTTGCGATT
SOX9	F AGGAAGTCGGTGAAGAACGG R CGCCTTGAAGATGGCGTTG
SOX10	F CCAGTTTGACTACTCTGACCATCAG R ATATAGGAGAAGGCCGAGTAGAGG

ChIP-qPCR

Cells were grown on 15-cm plates and, once reached 80% of confluence, were fixed with PBS + 0.4% formaldehyde solution for 10 min. Fixation reaction was stopped with 2 M Glycin pH8. Cells were then pelleted and suspended in lysis buffer (EDTA 10 mM, Tris–HCl pH8 50 mM, SDS 1%) and sonicated with Covaris E220AFA power 200 Hz 6 cycles 200 s to get a DNA fragmentation between 500 and 200 bp. Chromatin was then diluted in 100 ug aliquots with 8 volumes of ChIP dilution buffer (Tris–HCl pH8 16.7 mM, EDTA 1.2 mM, NaCl 167 mM, Triton X-100 1.1%, SDS 0.01%). The immuno-precipitations were done as follows. 5 ug of antibody was incubated overnight with chromatin, and the antibody–chromatin complex was then captured with Protein G-magnetic beads (Dynabeads, Invitrogen) for 1 h at 4°C. Beads were washed 2 times with low salt buffer (Tris–HCl pH8 20 mM, EDTA 2 mM, NaCl 150 mM, Triton X-100 1%, SDS 0.1%), high salt buffer (Tris–HCl pH8 20 mM, EDTA 2 mM, NaCl 500 mM, Triton X-100 1%, SDS 0.1%), LiCl buffer (Tris–HCl pH8 500 mM, EDTA 1 mM, Na deoxycholate 1%, NP40 1%, LiCl 0.25 M), and TE buffer (Tris–HCl pH8 10 mM, EDTA 1

mM), and DNA was eluted 30 min at room temperature with Elution buffer (NaHCO₃ 0.1 M, SDS 1%). DNA was finally purified through phenol–chloroform, re-suspended in 100 uL of H₂O, and analyzed by qPCR.

Antibodies for ChIP-qPCR

H3	Rabbit Polyclonal	Abcam	ab1791
H3K27ac	Rabbit Polyclonal	Abcam	ab4729

Primers for ChIP-qPCR

<i>ACTb</i> Promoter	F CAAAGGCGAGGCTCTGTGCT R GTGCGCCGTTCCGAAAGTT
<i>CDK7</i> Promoter	F GCAACAGAGTGACACAGCAGCC R GACCCGGATCGCGTCGAAG
<i>MITF</i> SE	F GGCCCTCTGAACAGTTTCAA R ATCCCCATTTTCAGCATGAG
<i>SOX10</i> SE	F GCACCAGGTCTTCAGCAAA R GCCACAGTTGGGTAGAGATTG

RNA-Sequencing

Library preparation was performed at the GenomEast platform at the IGBMC using TruSeq Stranded Total RNA Reference Guide - PN 1000000040499. Total RNA-Seq libraries were generated from 700 ng of total RNA using TruSeq Stranded Total RNA Library Prep Gold kit and TruSeq RNA Single Indexes kits A and B (Illumina, San Diego, USA), according to manufacturer's instructions. Briefly, cytoplasmic and mitochondrial ribosomal RNA (rRNA) was removed using biotinylated, target-specific oligos combined with Ribo-Zero rRNA removal beads. Following purification, the depleted RNA was fragmented into small pieces using divalent cations at 94°C for 8 minutes. Cleaved RNA fragments were then copied into first strand cDNA using reverse transcriptase and random primers followed by second strand cDNA synthesis using DNA Polymerase I and RNase H. Strand specificity was achieved by replacing dTTP with dUTP during second strand synthesis. The double stranded cDNA fragments were blunted using T4 DNA polymerase, Klenow DNA polymerase and T4 PNK. A single 'A' nucleotide was added to the 3' ends of the blunt DNA fragments using a Klenow fragment (3' to 5' exo minus) enzyme. The cDNA fragments were ligated to double stranded adapters using T4 DNA Ligase. The ligated products were enriched by PCR amplification. Surplus PCR primers were further removed by purification using AMPure XP beads (Beckman-

Coulter, Villepinte, France) and the final cDNA libraries were checked for quality and quantified using capillary electrophoresis. Libraries were sequenced on an Illumina HiSeq 4000 sequencer as single read 50 base reads. Image analysis and base calling were performed using RTA version 2.7.7 and bcl2fastq version 2.20.0.422.

Reads were preprocessed to remove adapter and low-quality sequences (Phred quality score below 20). After this preprocessing, reads shorter than 40 bases were discarded for further analysis. These preprocessing steps were performed using cutadapt version 1.10. Reads were mapped to rRNA sequences using bowtie version 2.2.8 and reads mapping to rRNA sequences were removed for further analysis. Reads were mapped onto the hg19 assembly of Homo sapiens genome using STAR version 2.5.3a. Gene expression quantification was performed from uniquely aligned reads using htseq-count version 0.6.1p1, with annotations from Ensembl version 75 and 'union' mode. Only non-ambiguously assigned reads have been retained for further analyses. Read counts have been normalized across samples with the median-of-ratios method proposed by Anders and Huber (Anders and Huber, 2010) to make these counts comparable between samples. Comparisons of interest were performed using the Wald test for differential expression proposed by Love et al. (Love et al., 2014) and implemented in the Bioconductor package DESeq2 version 1.16.1. Genes with high Cook's distance were filtered out and independent filtering based on the mean of normalized counts was performed. P-values were adjusted for multiple testing using the Benjamini and Hochberg method (Benjamini and Hochberg, 1995). Deregulated genes were defined as genes with adjusted P-value < 0.05. Volcano plots and scatter plots were generated using the Prism9 statistical software (GraphPad). Heatmaps were generated using Morpheus (<https://software.broadinstitute.org/morpheus>). Venn diagrams were generated using DeepVenn (<http://www.deepvenn.com/>) and representation factors and hypergeometric P-values were determined using Graeber lab software (<https://systems.crupp.ucla.edu/hypergeometric/>). Gene Ontology Analysis was performed using ShinyGO (Ge SX, Jung D & Yao, 2020).

Generation of XPB-HA overexpressing cells

The generation of 501mel Bio-FLAG:CDK7 was described previously (Berico et al., 2021). cDNA of human XPB was cloned in pLENTI-EF1-3HA vector, which was then transfected in 501mel Bio-FLAG:CDK7 using TA Xtreme 9 reagent (Roche, 06365809001) according to manufacturer instructions.

Figure Legends

Figure 1: Human melanoma cells with distinct genotypes and phenotypes are highly sensitive to TPL

A. Protein lysates from the non-cancer melanocyte Hermes3A cell line, melanocytic melanoma cells 501mel, MM011, MM074 and the mesenchymal-like melanoma cells MM029, MM047, and MM099 were immuno-blotted for proteins as indicated. Molecular masses of proteins are indicated (kDa).

B. Melanoma cells were treated with increasing concentrations of THZ1 or TPL as indicated for 72 h. Dose response curves are shown relative to vehicle (DMSO)-treated cells. IC50s for each cell type are indicated. Melanocytic melanoma cells are shown in blue, mesenchymal-like melanoma cells are shown in red and Hermes3A are shown in green. Data are presented as mean values + standard deviation (SD) for three replicates (n = 3).

Figure 2: TPL, as opposed to THZ1, exerts strong cytostatic activities in melanocytic as well as in mesenchymal-like melanoma cells

A. Representative images (left panel) and quantification (right panel) of crystal violet staining of indicated cells treated for 72 h with either DMSO or respective IC50 concentrations of THZ1 or TPL.

B+C. Indicated cells were treated for 72 h with either DMSO or respective IC50 concentrations of THZ1 or TPL. Cell proliferation was analysed using CellTrace (**B**) and apoptosis was analysed using AnnexinV staining (**C**) and flow cytometry. The % of slow proliferating and apoptotic cells are shown for each condition.

D+E. 3D-grown melanospheres consisting of mesenchymal cells were treated for 72 h with either DMSO or respective 5xIC50 concentrations of THZ1 or TPL. Melanosphere viability was then measured using CellTiterGlo assay (**D**) and apoptosis was analysed using AnnexinV staining and flow cytometry (**E**).

Data are presented as mean values + SD for three replicates (n = 3). The P-values (Two-way ANOVA) are indicated, * < 0.05 ** < 0.01 *** < 0.001 **** < 0.0001 and ns (non-significant) > 0.05.

Figure 3: Both THZ1 and TPL disrupt the MITF and SOX10 SEs in melanocytic-like cells

A. RT-qPCR analysis showing average 18S-normalized expression of *MITF*, *SOX10* and *ACTb* in 501mel cells treated for 2,4,6 or 12 h with either DMSO or 5xIC50 concentrations of THZ1 or TPL.

B. ChIP-qPCR analysis of H3K27ac signal (normalized by H3 signal) at the MITF SE, SOX10 SE, or proximal promoters of *ACTb* and *CDK7*, in 501mel cells treated for 12 h with either DMSO or 5xIC50 concentrations of THZ1 or TPL.

C. Heatmap showing 18S-normalized expression changes of indicated genes, measured by RT-qPCR, after 501mel cells were treated for 24, 48 or 72 h with either DMSO or IC50 concentrations of THZ1 or TPL. Colors represent expression fold change values versus DMSO-treated cells (blue: decreased expression; red: increased expression; white: no expression change).

Data are presented as mean values + SD for three replicates (n = 3). The P-values (Two-way ANOVA) are indicated, * < 0.05 ** < 0.01 *** < 0.001 **** < 0.0001 and ns (non-significant) > 0.05.

Figure 4: THZ1 and TPL differently impact gene expression and SEs

A. Volcano plots showing differentially expressed genes as determined by RNA-seq performed in 501mel cells treated for 6 h with either THZ1 or TPL at 5xIC50 concentrations.. Blue dots show significantly (adjusted p-value < 0.05) over-represented (positive fold change, FC) or under-represented (negative FC) RNAs in drug-treated cells compared to DMSO-treated cells. The number of deregulated genes and examples are indicated.

B. Proportional Venn diagrams indicating the number of down-regulated (left panel) or up-regulated (right panel) genes from the RNA-Seq described in (A) overlapping with a set of 1015 putative SE-dependent genes in 501mel cells, determined by H3K27ac ChIP-Seq. Representation factors, hypergeometric P-values and examples of significantly down- or up-regulated SE-dependent genes both by THZ1 and TPL are indicated.

Figure 5: TPL-resistant cells do not undergo phenotype switching

A. Indicated cells were treated with increasing concentrations of TPL, THZ1, Vemurafenib or Trametinib as indicated for 72 h. Dose response curves are shown relative to vehicle (DMSO)-treated cells. IC50s for each cell type are indicated. Data are presented as mean values + standard deviation (SD) for three replicates (n = 3).

B. Heatmap showing 18S-normalized expression changes of indicated genes, measured by RT-qPCR in indicated cells. Colors represent expression fold change values versus non-resistant original cells (blue: decreased expression; red: increased expression; white: no expression change).

C. Protein lysates from indicated cells immuno-blotted for indicated proteins. Molecular sizes of the proteins are indicated (kDa).

Supplemental Figure Legends

Supplemental Figure 1: MITF and SOX10 protein levels rapidly decline after THZ1 or TPL treatment

A+B. Protein lysates from 501mel cells treated for 6, 12, 24 or 48 with either THZ1 (**A**) or TPL (**B**) at either 1x or 5xIC₅₀ concentrations were immuno-blotted for indicated proteins. Molecular sizes of the proteins are indicated (kDa). MITF and SOX10 protein levels were quantified by analysing band intensities and were normalized to ACTb control using ImageJ software. Quantification data are presented as mean values + SD for three replicates (n = 3). The P-values (Two-way ANOVA) are indicated, * < 0.05 ** < 0.01 *** < 0.001 **** < 0.0001 and ns (non-significant) > 0.05.

Supplemental Figure 2: Transcriptional disruption by CDK7 or XPB inhibition

A. Proportional Venn diagrams indicating the number of overlapping down- or up-regulated genes from the RNA-Seq described in **Figure 4**. Representation factors and hypergeometric P-values are indicated.

B. Heatmap depicting all deregulated genes from either THZ1 or TPL treatments, from the RNA-Seq described in **Figure 4**. RPKM values are represented as z-score and common up- or downregulated genes between treatments are indicated.

C. Gene Ontology analysis of the commonly down- or upregulated genes between THZ1 and TPL treatments from the RNA-Seq described in **Figure 4**.

D. GSEA analysis of the genes deregulated either by THZ1 or TPL treatments from the RNA-Seq described in **Figure 4**.

E. Scatter plot of differentially expressed marker genes of the melanocytic (dots in blue) or mesenchymal-like (dots in red) melanoma cell states (Gene sets from Verfaillie et al., 2015) from the RNA-Seq described in **Figure 4**. Data is represented as log₂ values of the fold change

versus DMSO treatment. Negative values depict downregulated genes and positive values depict upregulated genes.

Supplemental Figure 3: XPB-HA and CDK7-Bio-Flag

501mel Bio-Flag:CDK7 cells were transiently transfected or not with vector containing pLENTI-EF1-XPB-3HA vector, and protein lysates were immunoblotted for HA-Tag, XPB, Flag-Tag or CDK7 as indicated.

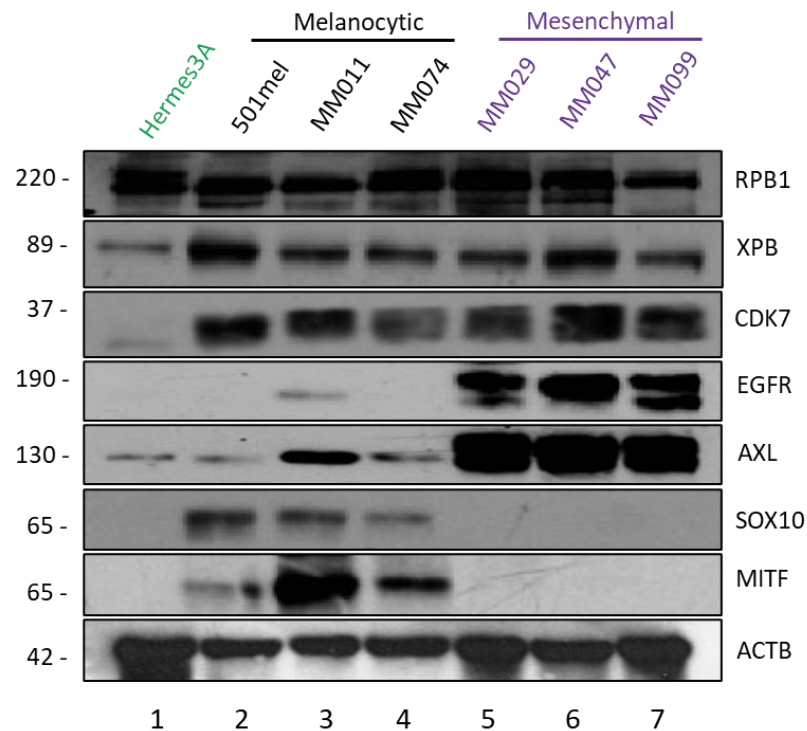
References

- Alekseev, S. *et al.* (2017) 'Transcription without XPB Establishes a Unified Helicase-Independent Mechanism of Promoter Opening in Eukaryotic Gene Expression', *Molecular Cell*, 65(3), pp. 504-514.e4. Available at: <https://doi.org/10.1016/j.molcel.2017.01.012>.
- Bassey-Archibong, B.I. *et al.* (2023) 'An HLA-G/SPAG9/STAT3 axis promotes brain metastases', *Proceedings of the National Academy of Sciences*, 120(8), p. e2205247120. Available at: <https://doi.org/10.1073/pnas.2205247120>.
- Berico, P. *et al.* (2021) 'CDK7 and MITF repress a transcription program involved in survival and drug tolerance in melanoma', *EMBO reports*, 22(9), p. e51683. Available at: <https://doi.org/10.15252/embr.202051683>.
- Blobel, G.A. *et al.* (2021) 'Testing the super-enhancer concept', *Nature Reviews Genetics*, 22(12), pp. 749–755. Available at: <https://doi.org/10.1038/s41576-021-00398-w>.
- Bradner, J.E., Hnisz, D. and Young, R.A. (2017) 'Transcriptional Addiction in Cancer', *Cell*, 168(4), pp. 629–643. Available at: <https://doi.org/10.1016/j.cell.2016.12.013>.
- Brauer, R.R. *et al.* (2012) 'Galectin-3 contributes to melanoma growth and metastasis via regulation of NFAT1 and autotaxin', *Cancer Research*, 72(22), pp. 5757–5766. Available at: <https://doi.org/10.1158/0008-5472.CAN-12-2424>.
- Chipumuro, E. *et al.* (2014) 'CDK7 Inhibition Suppresses Super-Enhancer-Linked Oncogenic Transcription in MYCN-Driven Cancer', *Cell*, 159(5), pp. 1126–1139. Available at: <https://doi.org/10.1016/j.cell.2014.10.024>.
- Compe, E. and Egly, J.-M. (2016) 'Nucleotide Excision Repair and Transcriptional Regulation: TFIIH and Beyond', *Annual Review of Biochemistry*, 85(1), pp. 265–290. Available at: <https://doi.org/10.1146/annurev-biochem-060815-014857>.
- Compe, E. and Egly, J.-M. (2021) 'The Long Road to Understanding RNAPII Transcription Initiation and Related Syndromes', *Annual Review of Biochemistry*, 90(1), pp. 193–219. Available at: <https://doi.org/10.1146/annurev-biochem-090220-112253>.
- D'Aguzzo, S. *et al.* (2018) 'Semaphorin 5A drives melanoma progression: role of Bcl-2, miR-204 and c-Myb', *Journal of Experimental & Clinical Cancer Research*, 37(1), p. 278. Available at: <https://doi.org/10.1186/s13046-018-0933-x>.
- Eliades, P. *et al.* (2018) 'High MITF Expression Is Associated with Super-Enhancers and Suppressed by CDK7 Inhibition in Melanoma', *The Journal of Investigative Dermatology*, 138(7), pp. 1582–1590. Available at: <https://doi.org/10.1016/j.jid.2017.09.056>.
- Fisher, R.P. (2005) 'Secrets of a double agent: CDK7 in cell-cycle control and transcription', *Journal of Cell Science*, 118(22), pp. 5171–5180. Available at: <https://doi.org/10.1242/jcs.02718>.
- Gartlgruber, M. *et al.* (2021) 'Super enhancers define regulatory subtypes and cell identity in neuroblastoma', *Nature Cancer*, 2(1), pp. 114–128. Available at: <https://doi.org/10.1038/s43018-020-00145-w>.
- Hebert, J.D. *et al.* (2020) 'The scaffold protein IQGAP1 is crucial for extravasation and metastasis', *Scientific Reports*, 10(1), p. 2439. Available at: <https://doi.org/10.1038/s41598-020-59438-w>.
- Hnisz, D. *et al.* (2013) 'Super-Enhancers in the Control of Cell Identity and Disease', *Cell*, 155(4), pp. 934–947. Available at: <https://doi.org/10.1016/j.cell.2013.09.053>.
- Hnisz, D. *et al.* (2015) 'Convergence of developmental and oncogenic signaling pathways at transcriptional super-enhancers', *Molecular Cell*, 58(2), pp. 362–370. Available at: <https://doi.org/10.1016/j.molcel.2015.02.014>.
- Kozar, I. *et al.* (2019) 'Many ways to resistance: How melanoma cells evade targeted therapies', *Biochimica Et Biophysica Acta. Reviews on Cancer*, 1871(2), pp. 313–322. Available at: <https://doi.org/10.1016/j.bbcan.2019.02.002>.
- Kwiatkowski, N. *et al.* (2014) 'Targeting transcription regulation in cancer with a covalent CDK7 inhibitor', *Nature*, 511(7511), pp. 616–620. Available at: <https://doi.org/10.1038/nature13393>.

- Lovén, J. *et al.* (2013) 'Selective Inhibition of Tumor Oncogenes by Disruption of Super-Enhancers', *Cell*, 153(2), pp. 320–334. Available at: <https://doi.org/10.1016/j.cell.2013.03.036>.
- Noel, P. *et al.* (2020) 'Triptolide targets super-enhancer networks in pancreatic cancer cells and cancer-associated fibroblasts', *Oncogenesis*, 9(11), pp. 1–12. Available at: <https://doi.org/10.1038/s41389-020-00285-9>.
- Pott, S. and Lieb, J.D. (2015) 'What are super-enhancers?', *Nature Genetics*, 47(1), pp. 8–12. Available at: <https://doi.org/10.1038/ng.3167>.
- Rambow, F. *et al.* (2018) 'Toward Minimal Residual Disease-Directed Therapy in Melanoma', *Cell*, 174(4), pp. 843–855.e19. Available at: <https://doi.org/10.1016/j.cell.2018.06.025>.
- Rambow, F., Marine, J.-C. and Goding, C.R. (2019) 'Melanoma plasticity and phenotypic diversity: therapeutic barriers and opportunities', *Genes & Development*, 33(19–20), pp. 1295–1318. Available at: <https://doi.org/10.1101/gad.329771.119>.
- Rimel, J.K. *et al.* (2020) 'Selective inhibition of CDK7 reveals high-confidence targets and new models for TFIID function in transcription', *Genes & Development*, 34(21–22), pp. 1452–1473. Available at: <https://doi.org/10.1101/gad.341545.120>.
- Sandoz, J. *et al.* (2019) 'Functional interplay between TFIID and KAT2A regulates higher-order chromatin structure and class II gene expression', *Nature Communications*, 10(1), p. 1288. Available at: <https://doi.org/10.1038/s41467-019-09270-2>.
- Sengupta, S. and George, R.E. (2017) 'Super-Enhancer-Driven Transcriptional Dependencies in Cancer', *Trends in Cancer*, 3(4), pp. 269–281. Available at: <https://doi.org/10.1016/j.trecan.2017.03.006>.
- Skorupan, N. *et al.* (2022) 'A phase II trial of the super-enhancer inhibitor Minnelide™ in advanced refractory adenosquamous carcinoma of the pancreas', *Future Oncology* (London, England), 18(20), pp. 2475–2481. Available at: <https://doi.org/10.2217/fon-2021-1609>.
- Thandapani, P. (2019) 'Super-enhancers in cancer', *Pharmacology & Therapeutics*, 199, pp. 129–138. Available at: <https://doi.org/10.1016/j.pharmthera.2019.02.014>.
- Titov, D.V. *et al.* (2011) 'XPB, a subunit of TFIID, is a target of the natural product triptolide', *Nature Chemical Biology*, 7(3), pp. 182–188. Available at: <https://doi.org/10.1038/nchembio.522>.
- Verfaillie, A. *et al.* (2015) 'Decoding the regulatory landscape of melanoma reveals TEADS as regulators of the invasive cell state', *Nature Communications*, 6, p. 6683. Available at: <https://doi.org/10.1038/ncomms7683>.
- Wang, Y. *et al.* (2015) 'CDK7-Dependent Transcriptional Addiction in Triple-Negative Breast Cancer', *Cell*, 163(1), pp. 174–186. Available at: <https://doi.org/10.1016/j.cell.2015.08.063>.
- Widmer, D.S. *et al.* (2012) 'Systematic classification of melanoma cells by phenotype-specific gene expression mapping', *Pigment Cell & Melanoma Research*, 25(3), pp. 343–353. Available at: <https://doi.org/10.1111/j.1755-148X.2012.00986.x>.
- Xi, C. *et al.* (2017) 'Toxicity of triptolide and the molecular mechanisms involved', *Biomedicine & Pharmacotherapy = Biomedecine & Pharmacotherapie*, 90, pp. 531–541. Available at: <https://doi.org/10.1016/j.biopha.2017.04.003>.
- Zhang, J. *et al.* (2020) 'Targeting Super-Enhancer–Associated Oncogenes in Osteosarcoma with THZ2, a Covalent CDK7 Inhibitor', *Clinical Cancer Research*, 26(11), pp. 2681–2692. Available at: <https://doi.org/10.1158/1078-0432.CCR-19-1418>.
- Zhang, Y. *et al.* (2017) 'Overexpression of LAMC1 predicts poor prognosis and enhances tumor cell invasion and migration in hepatocellular carcinoma', *Journal of Cancer*, 8(15), pp. 2992–3000. Available at: <https://doi.org/10.7150/jca.21038>.

Figure 1

A



B

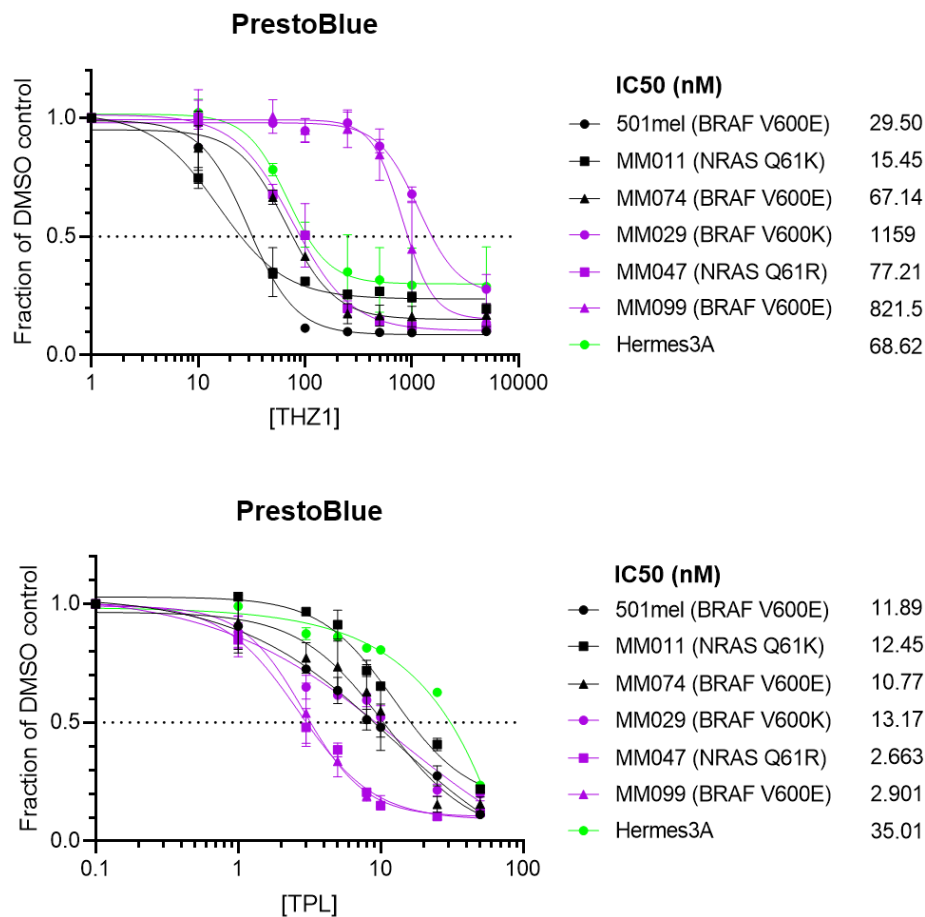


Figure 2

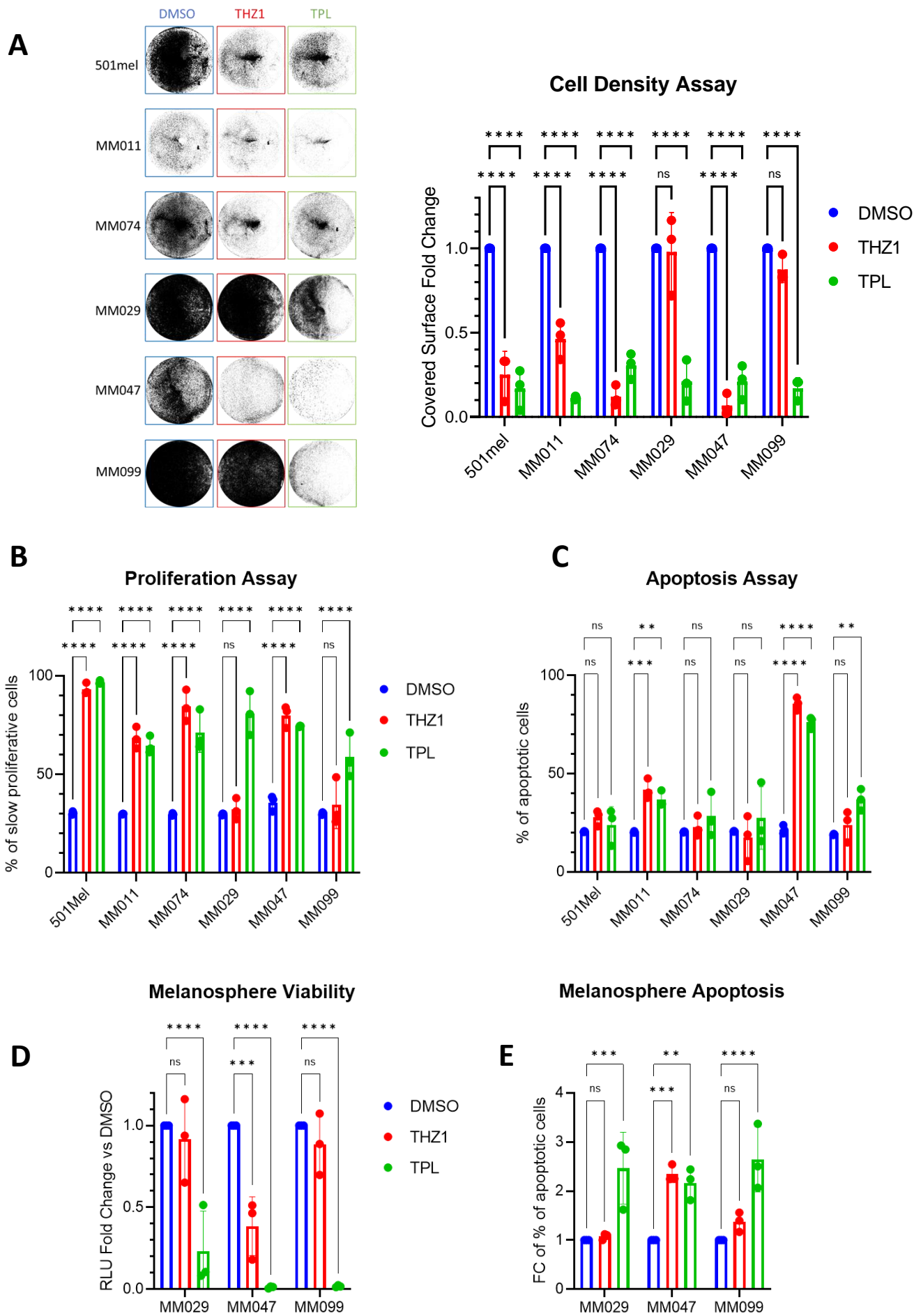
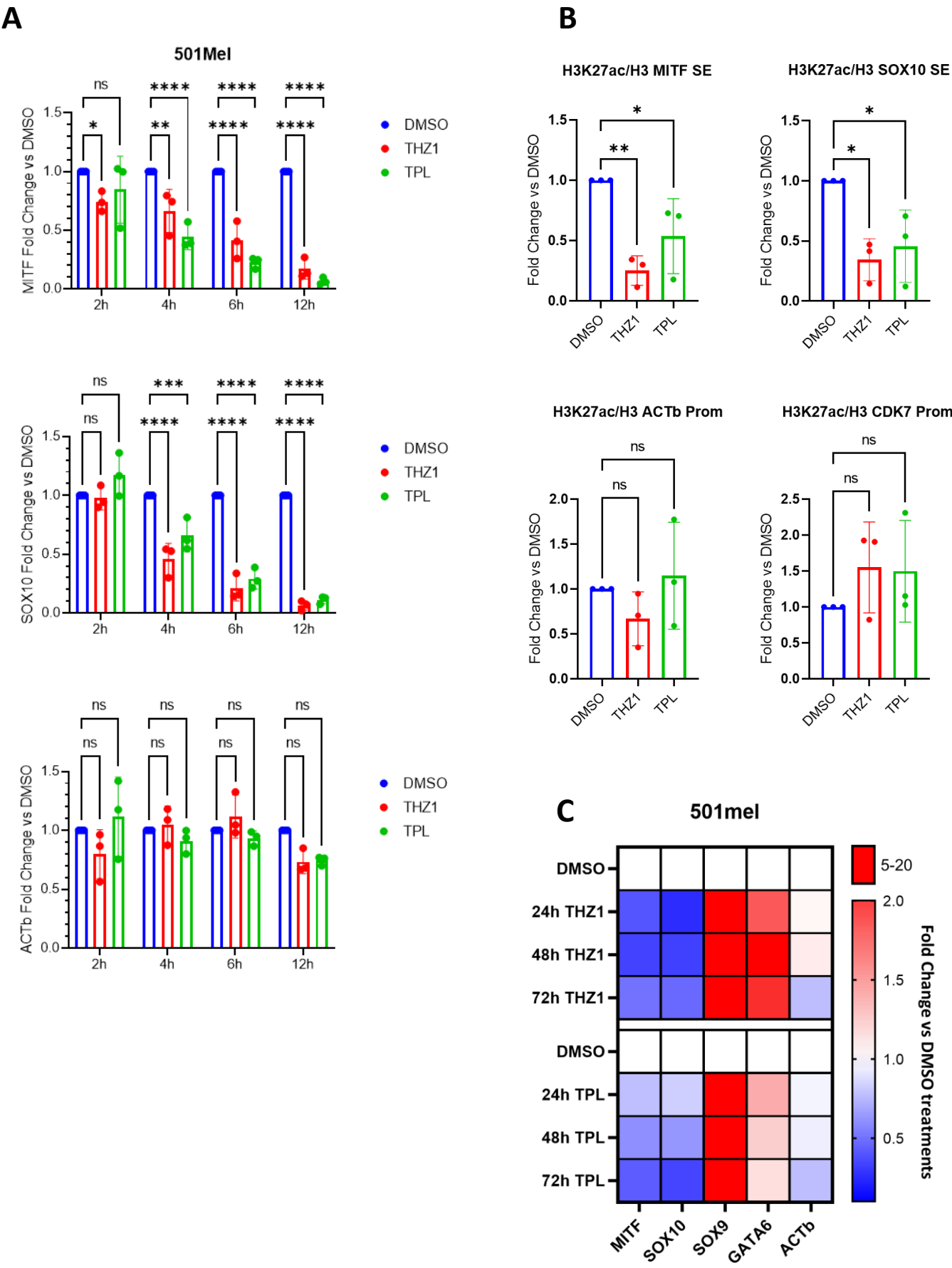


Figure 3



A

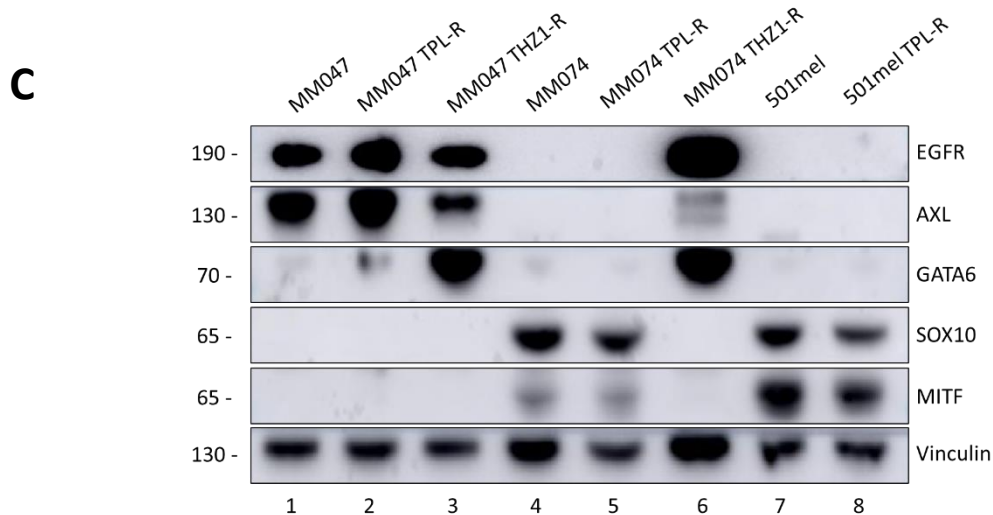
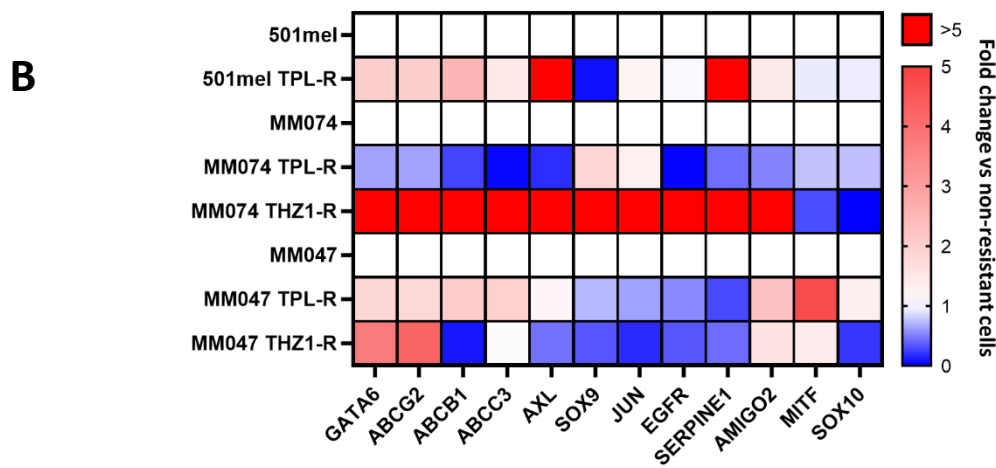
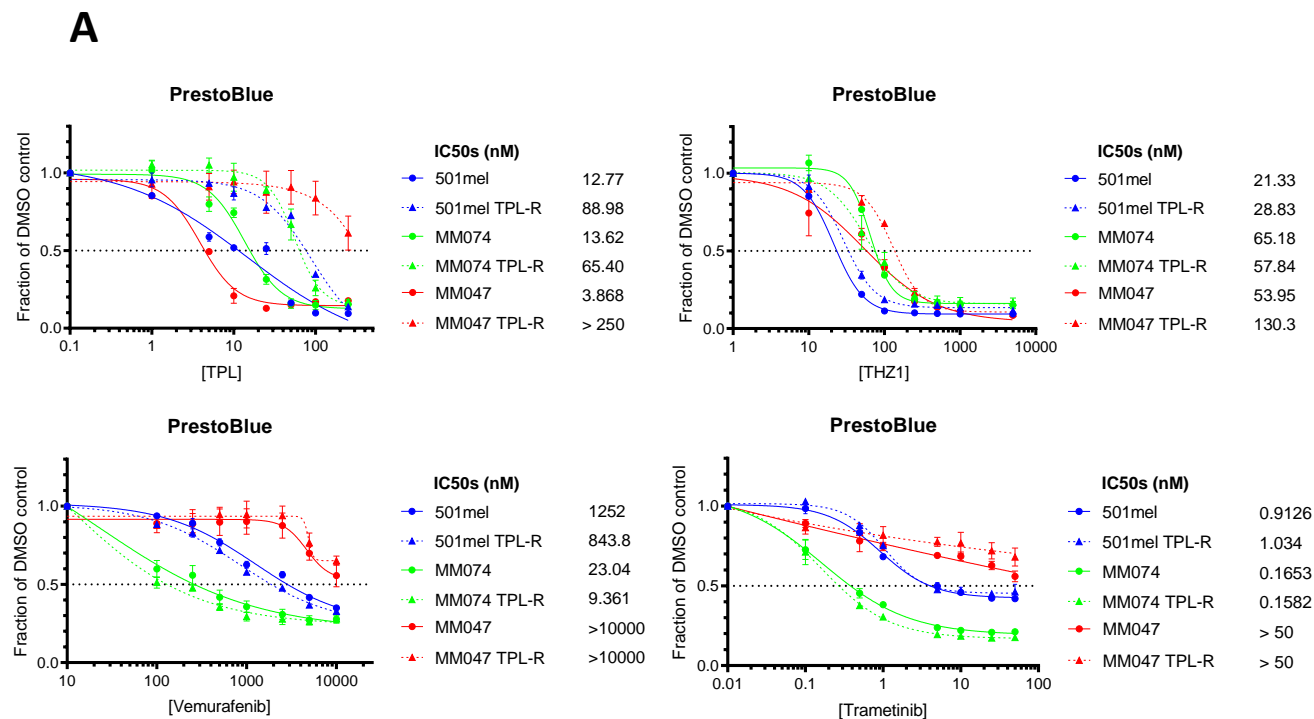
- Total genes: **14474**
 - Significantly differentially expressed with Adj-PVal < 0.05 : **4186**
 - Significantly downregulated: **2415**
 - Significantly upregulated: **1771**

- Total genes: **15651**
 - Significantly differentially expressed with Adj-PVal < 0.05 : **2413**
 - Significantly downregulated: **1505**
 - Significantly upregulated: **908**

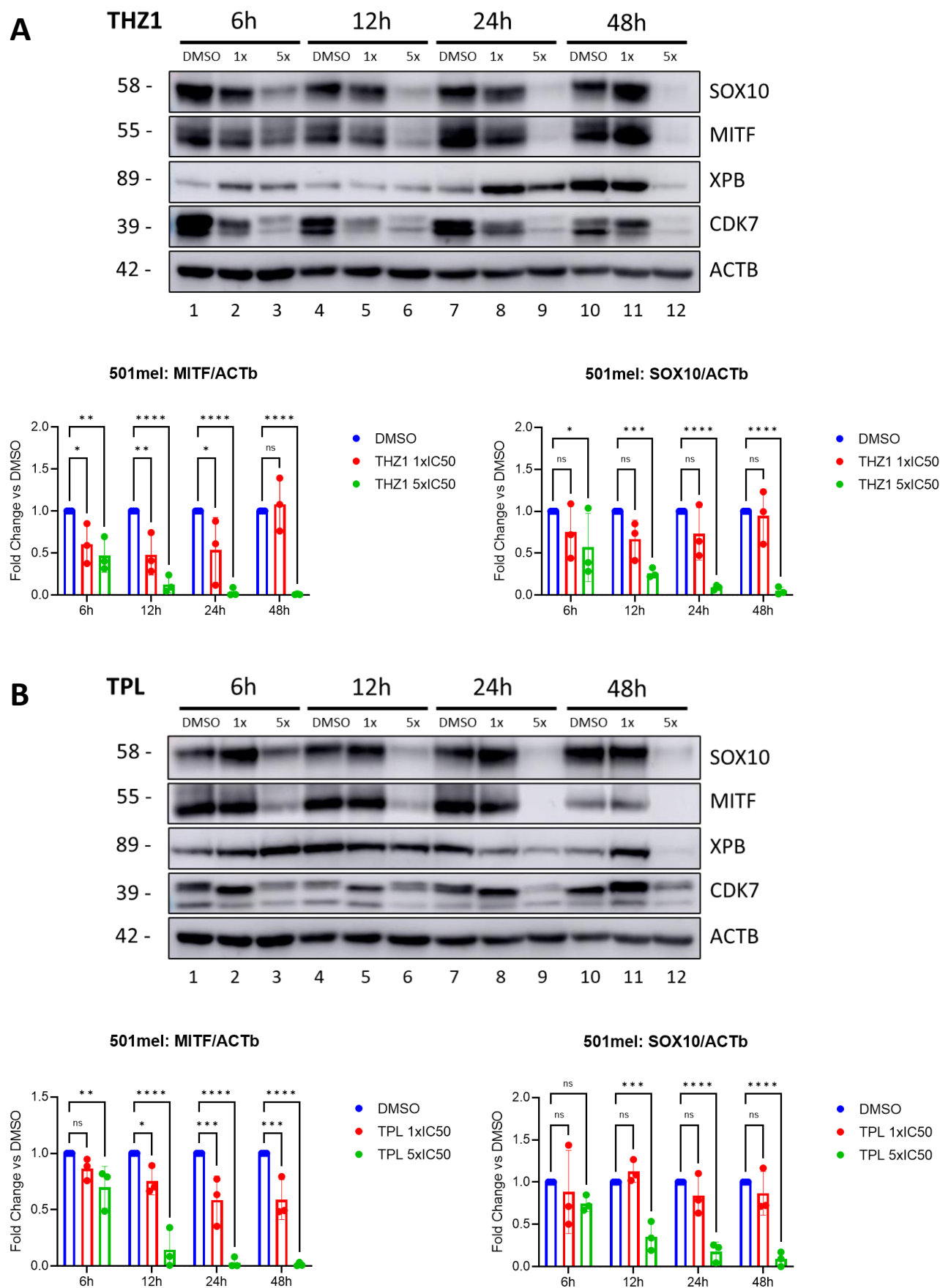
B



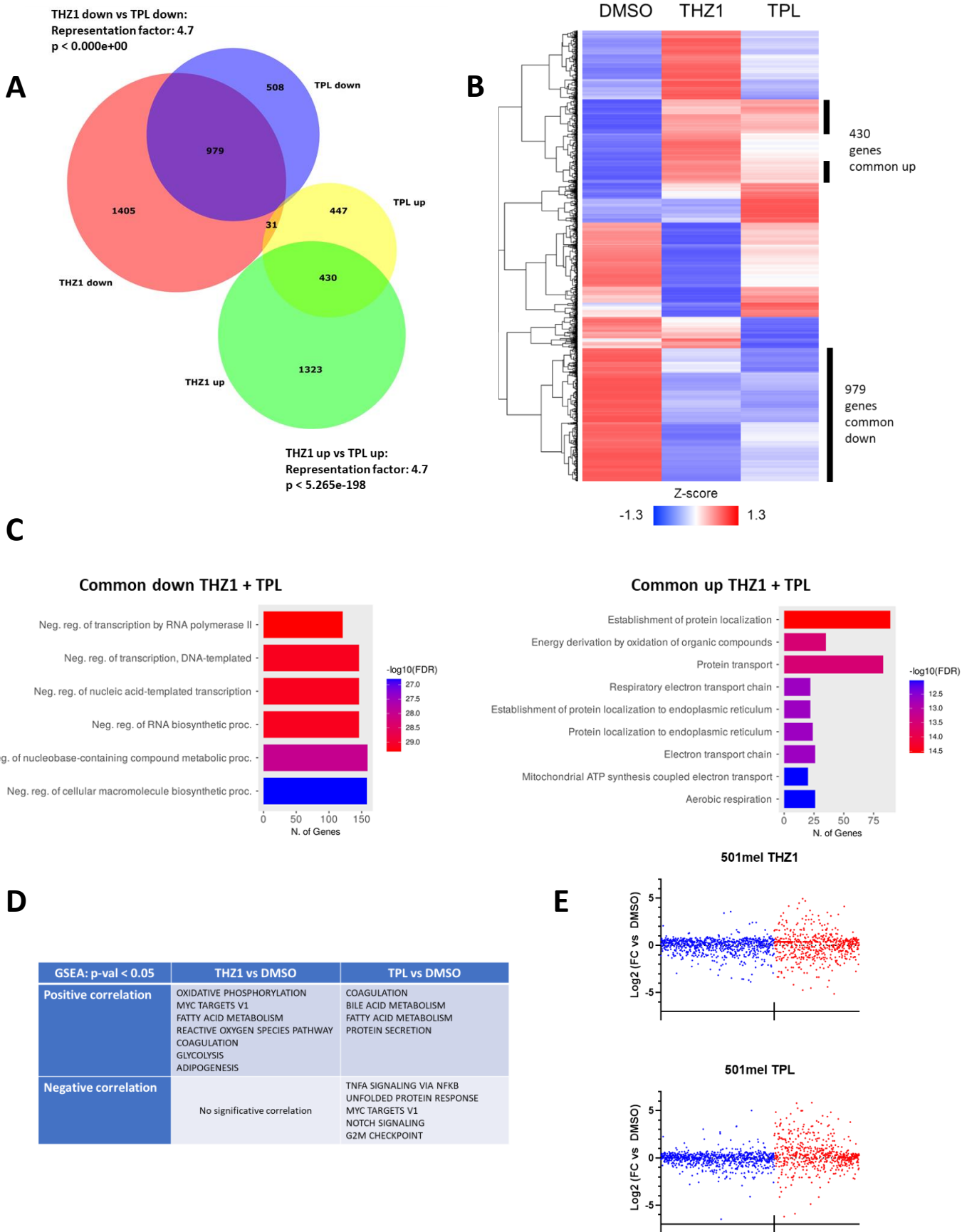
Figure 5



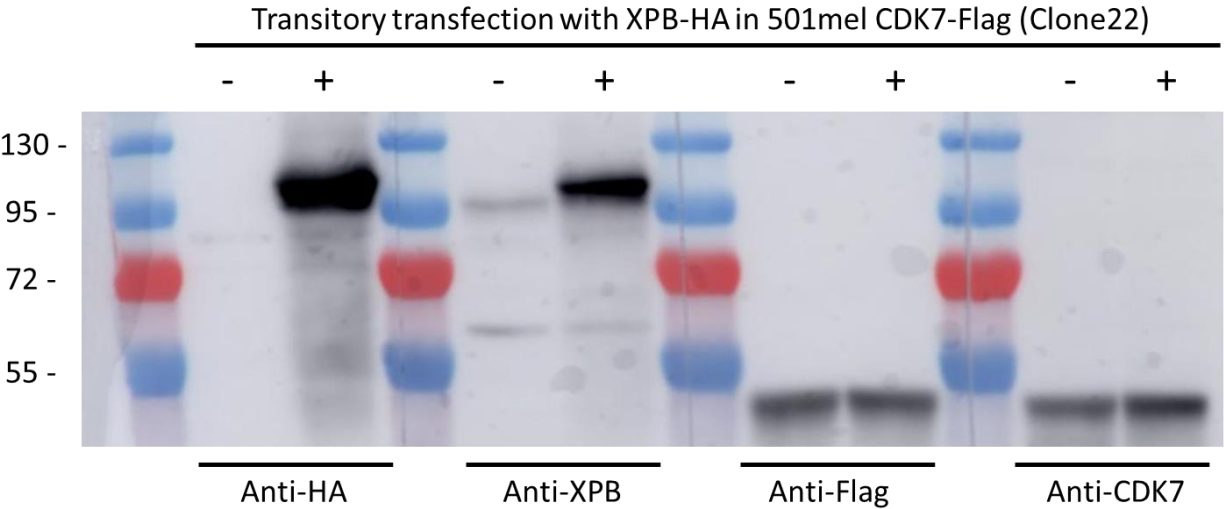
Supplemental Figure 1



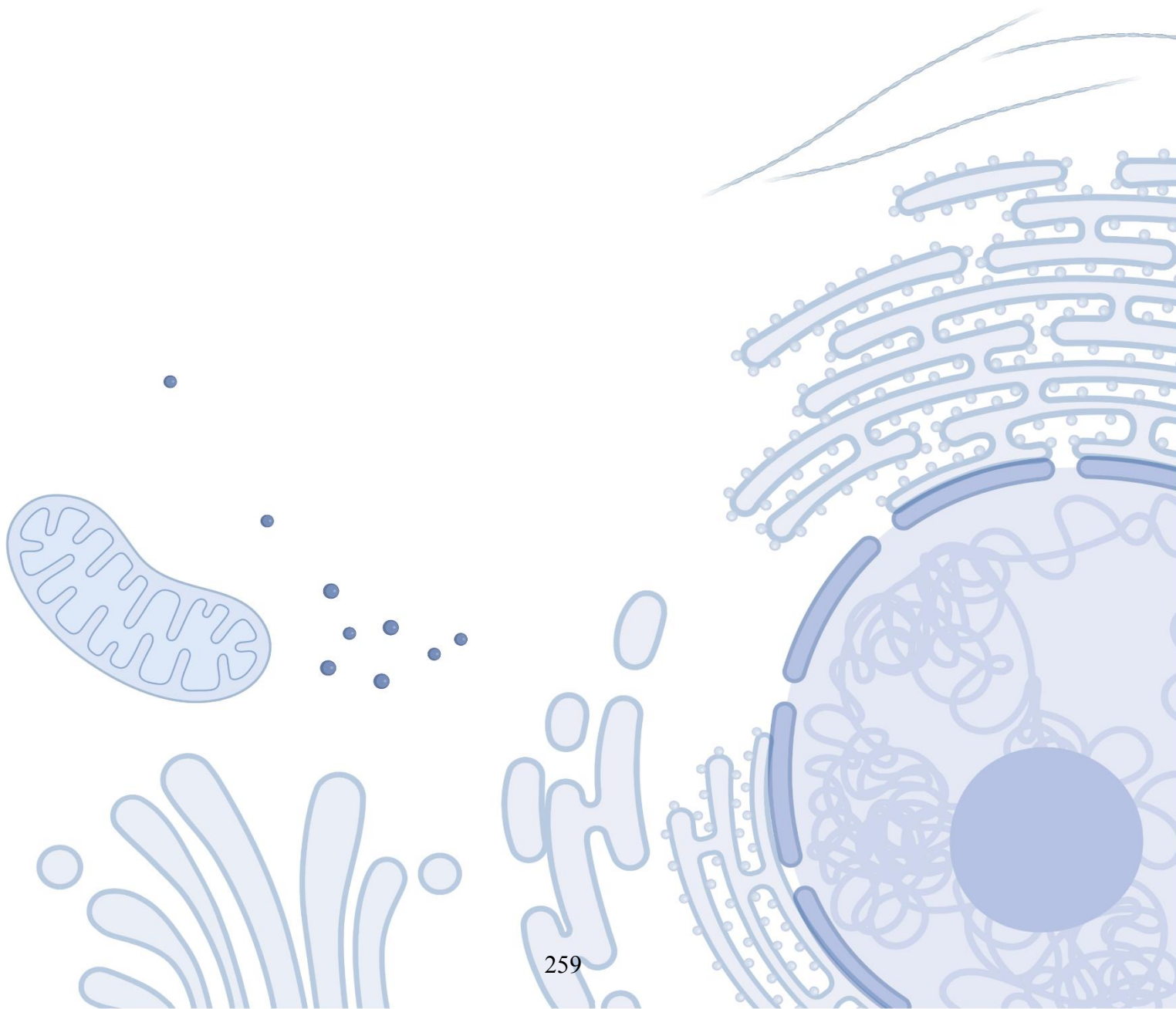
Supplemental Figure 2



Supplemental Figure 3



Section II: Targeting transcriptional addiction in melanoma with novel marine-derived drugs



Preface to Article 3: Context and contributions

PharmaMar S.A. is a Spanish pharmaceutical company specialized in developing novel marine-based cancer therapeutics, such as Trabectedin, clinically used for the treatment of soft-tissue sarcomas and ovarian cancers, and its more potent analogue Lurbinectedin, recently approved for SCLC. In the early 2010s, the exact mechanisms of actions of these drugs were still unknown. Suspecting however the involvement of DNA repair and transcriptional processes, PharmaMar reached out to Dr. Jean-Marc Egly, the former head of my lab and a renowned expert in these fields, to elucidate the molecular actions of these drugs. Consequently, in 2016, in collaboration with researchers from PharmaMar, our lab described the DNA-binding nature of Lurbinectedin, which triggers RNAPII degradation and induces DNA breaks mainly at actively transcribed genes (Santamaría Nuñez et al., 2016). A few years later, our team helped to elucidate the transcriptional effects of Lurbinectedin on SCLC (Costanzo et al., 2022), a disease which was shown to be particularly vulnerable to the targeting of its transcriptional addiction. These projects helped to set up clinical trials for the use of Lurbinectedin, which received accelerated FDA approval for treating patients with relapsed SCLC in 2021. However, due to the recent nature of this clinical approval, the effects of Lurbinectedin on other types of cancers have not been thoroughly examined yet.

Considering the encouraging clinical benefits displayed by Lurbinectedin in SCLC, PharmaMar tasked us to assess its potency and effects in other types of transcriptionally addicted cancers, such as melanoma. Thus, the second pillar of my PhD project, apart from characterizing the role of TFIIH in melanoma, was to check whether Lurbinectedin could potentially represent a useful addition to the therapeutic arsenal against this disease, and to analyze its cellular and gene expression effects on different types of melanoma cells. Furthermore, just as Lurbinectedin is a structural analogue of Trabectedin, PharmaMar recently developed two derivatives of Lurbinectedin, namely PM14 and PM54, whose effects I also assessed to find out whether these new compounds might display clinical advantages compared to the original compound. This project, which constituted the main body of work for the final two years of my PhD and in which the help of Maguelone Nogaret and Jolian Obid were indispensable, is nearing completion and will soon be submitted for publication. However, due to confidentiality reasons concerning PharmaMar, not all our results could be included in this thesis. Hereinafter is presented a first draft of the paper, although important work, such as Chem-Seq and Cut&Tag assays are currently still being analyzed to finalize the publication.

**Targeting master regulator genes with Lurbinectedin and its derivatives as
a novel therapeutic strategy against targeted therapy-resistant melanoma**

--- Work in progress ---

Max Cigrang^{1, 2, 3, 4}, Julian Obid^{1, 2, 3, 4}, Maguelone Nogaret^{1, 2, 3, 4}, Pietro Berico^{1, 2, 3, 4}, Philippe Catez^{1, 2, 3, 4}, Guillaume Davidson^{1, 2, 3, 4}, Jean-Marc Egly^{1, 2, 3, 4}, Irwin Davidson^{1, 2, 3, 4}, Eva Maria Garrido-Martin⁵ and Frédéric Coin^{1, 2, 3, 4, 6}

¹ Institut de Génétique et de Biologie Moléculaire et Cellulaire Illkirch Cedex, C.U. Equipe
Labélisée Ligue contre le Cancer 2022, Strasbourg, France

² Centre National de la Recherche Scientifique, UMR7104, 67404 Illkirch, France

³ Institut National de la Santé et de la Recherche Médicale, U1258, 67404 Illkirch, France

⁴ Université de Strasbourg, 67404 Illkirch, France

⁵ Cell Biology Department, Research and Development, PharmaMar SA, Colmenar Vejo, Spain

⁶ Corresponding author, fredr@igbmc.fr

Tel: +33 3 88 65 34 49

Key words: Melanoma, Marine-derived DNA-binders, Transcription

Abstract

Melanoma, an aggressive form of skin cancer, displays remarkable cellular phenotype plasticity. Melanoma cells have the ability to transition between various cellular states, including proliferative and invasive phenotypes, characterized by divergent levels of drug resistances and unique transcriptional signatures governed by specific master regulator genes (MRGs). This poses significant challenges to current treatments and underscores the urgent need for innovative therapeutic strategies. Lurbinectedin, a synthetic DNA-binding compound derived from a marine organism, has emerged as a promising candidate for targeting cancer cells that are characterized by a transcriptional addiction to MRGs. In our study, we demonstrated the efficacy of Lurbinectedin and two novel derivatives, PM14 and PM54, on patient-derived melanoma cells cultured in both two-dimensional and three-dimensional environments. Remarkably, our results indicate that the effectiveness of these compounds remains unaffected by the nature of the driver mutations or phenotypical status. In mouse models carrying melanoma cell-derived xenografts, these compounds significantly hindered tumor growth and prolonged survival. We observed that Lurbinectedin and its derivatives induced DNA damage that disrupted the expression of MRGs critical for cell identity. Through chemical-sequencing approaches, we discovered that Lurbinectedin exploits the transcriptional addiction of melanoma cells by selectively binding to CpG regions within MRGs located in an open chromatin environment. This binding effectively triggers DNA damage that block MRG expression and promotes the degradation of RNA Polymerase II, leading to apoptosis. In conclusion, Lurbinectedin and its derivatives hold promise as a novel therapeutical option for melanoma tumors, offering a unique mechanism of pan-melanoma action and demonstrating potent preclinical activity.

Introduction

Malignant melanoma, comprising only 1 % of skin cancer cases, is responsible for 80 % of related deaths (NCI-SEER-Database, 2023). Its high metastatic potential contributes to the significant mortality rate (Atkins et al., 2021) (Radke et al., 2022). Although incidence rates are rising, mortality rates have diminished in recent years (Schadendorf et al., 2018)(Sung et al., 2021) with the revolutionary introduction of kinase inhibitors and immunotherapy as the new standard of care for advanced disease (Curti and Faries, 2021) (Jenkins and Fisher, 2021), which until a decade ago presented an overall survival of less than 5% (Dickson and Gershenwald, 2011). Melanoma has been pointed to as a prime example of how the understanding of underlying biological mechanisms can be translated into novel therapeutics (Shain and Bastian, 2016) (Luke et al., 2017) (Leonardi et al., 2018). Comparative genomic studies have identified key targetable driver mutations in cutaneous melanoma, with aberrant activation of the Mitogen Activated Protein Kinase (MAPK) pathway observed in 90 % of cases due to somatic mutations in BRAF (50 %), RAS (20 %) and NF1 (15 %) oncogenes (Akbani et al., 2015) (Newell et al., 2022). Patients with the commonly found BRAF^{V600E/K} mutations, leading to constitutive MEK and ERK signaling, can benefit from combined treatment with targeted BRAF or MEK therapies, resulting in favorable progression-free survival rates (Guo et al., 2021) (Switzer et al., 2022). Additionally, immune checkpoint inhibitors targeting CTLA-4 and PD-1 have become the first-line treatment for metastatic melanoma, providing long-term benefits to a substantial number of patients (Carlini et al., 2021) (Huang and Zappasodi, 2022). Despite the advancements in targeted and immunotherapies, complete remission is achieved only in a small subset of patients, while severe adverse effects and limited efficacy are observed in many cases (Curti and Faries, 2021)(Saginala et al., 2021)(Ribas et al., 2013) (De Velasco et al., 2017). Moreover, non-BRAF mutated melanoma pose significant challenges, as effective treatment options are limited (Delyon et al., 2020). One of the critical barriers to clinical success is intrinsic or acquired resistance to treatment. Various mechanisms of drug resistance have been described, with intratumoral heterogeneity driven by cellular phenotypic plasticity emerging as a key contributor to relapse (Kozar et al., 2019) (Rebecca and Herlyn, 2020) (Marin-Bejar et al., 2021) (Rubanov et al., 2022), (Luskin et al., 2018) (Rambow et al., 2018). Indeed, melanoma cells can undergo phenotype switching, transitioning between melanocytic/differentiated states governed by master regulator genes (MRGs) such as the MITF and SOX10 transcription factors, and mesenchymal-like/undifferentiated states governed by

the AXL and AP-1/TEAD MRGs (Jerby-Amon et al., 2018) (Tsoi et al., 2018) (Arozarena and Wellbrock, 2019) (Benboubker et al., 2022) (Verfaillie et al., 2015) (Chauhan et al., 2022) (Comandante-Lou et al., 2022) (Karras et al., 2022). Melanoma cells can switch between these states in response to microenvironmental cues such as drug presence, complicating treatment outcomes (Hoek and Goding, 2010) (Wouters et al., 2020). The heterogeneity and phenotypic plasticity of melanoma cells underscore the need for therapeutics that can uniformly target divergent transcription programs governing different tumor cell states (Rambow et al., 2019). In recent years, the concept of ‘transcriptional addiction’ has gained attention as a novel hallmark of cancer cells. Dysregulated gene expression programs and associated transcriptional regulatory machinery are critical for sustaining cancer cell phenotypes, making them susceptible to transcriptional inhibitors (Bradner et al., 2017) (Sengupta and George, 2017) (Zanconato et al., 2018) (Hogg et al., 2020) (Vervoort et al., 2022). Several compounds targeting transcriptional factors have entered clinical trials (Laham-Karam et al., 2020) (Bushweller, 2019), including CDK7 and BRD4 inhibitors (Kwiatkowski et al., 2014) (Berico et al., 2021) (Fontanals-Cirera et al., 2017) (Donati et al., 2018).

Lurbinectedin (Lurb), a synthetic alkylating derivative of Trabectedin, binds covalently to DNA, generating adducts that stall RNA polymerase II and induce DNA double-strand breaks. Lurb was recently approved for the treatment of relapsed small cell lung cancer (SCLC). PM14 and PM54 are synthetic analogs of Lurb which were recently developed by PharmaMar SA. and which might display pharmacokinetic benefits compared to Lurb. This study aimed to analyze the sensitivity of a diverse panel of human melanoma cell lines and cultures, characterized by defined oncogenic alterations, to Lurb and its derivatives. We demonstrated potent anti-proliferative and apoptotic effects of these drugs on melanocytic or undifferentiated BRAF, NRAS and triple-wild type mutated melanoma cells in various *in vitro* 2D and 3D models and *in vivo* in xenograft mouse models. Functional genomics demonstrated that Lurb and its derivatives induced DNA damage that disrupted the expression of MRGs such as MITF and AXL, critical for cell identity. Through chemical-sequencing approaches, we discovered that Lurb exploits the transcriptional addiction of melanoma cells by selectively binding to CpG regions within MRGs located in an open chromatin environment. This binding triggers degradation of RNA Polymerase II, effectively blocking MRG expression. These findings pave the way for further research and development of these compounds as effective clinical treatment for melanoma, particularly for targeted therapy-resistant cases.

Results

Cellular models of human melanoma with distinct genotypes and phenotypes are highly sensitive to Lurb/PM14/PM54

To investigate the response of melanoma cells to Lurb and its derivatives, we examined cells representing the two primary phenotypes and the most prevalent driver mutations in melanoma. On one hand, we evaluated differentiated patient-derived melanocytic-type cultures MM011 (NRAS^{Q61K}), MM074 (BRAF^{V600E}), MM117 (Triple-wt) as well as melanoma cell lines 501mel (BRAF^{V600E}), IGR37 (BRAF^{V600E}) and SKMeI-28 (BRAF^{V600E}). These cells exhibited moderate to high expression of the lineage-specific transcription factors MITF and SOX10, coupled with low to undetectable levels of the pro-metastatic EGFR and AXL factors (Widmer et al., 2012) (Verfaillie et al., 2015) (**Table 1 and Figure 1a**). On the other hand, we examined patient-derived undifferentiated and mesenchymal-like melanoma cell cultures MM029 (BRAF^{V600K}), MM047 (NRAS^{Q61R}), MM099 (BRAF^{V600E}) and the melanoma cell line IGR39 (BRAF^{V600E}). These cells showed low to undetectable levels of MITF and SOX10, along with high levels of EGFR and/or AXL (**Table 1 and Figure 1a**).

To determine the IC50s (half maximal inhibitory concentration) of these cells to various inhibitors, we performed cell viability assays. As expected, the patient-derived cell cultures and melanoma cell lines exhibited varying sensitivities to targeted therapy agents commonly used in the clinical management of melanoma, such as the BRAF inhibitors Vemurafenib (Vemu) and Dabrafenib (Dabra) (**Table 1 and Figures 1b-c**), as well as the MEK inhibitor Trametinib (Trame) (**Table 1 and Figure 1d**). Differentiated BRAF^{V600E} melanoma cells, such as MM074 or IGR37, were the most responsive to these drugs, while undifferentiated melanoma cultures and cell lines demonstrated high resistance.

In contrast, we observed that all melanoma cells displayed high sensitivity to Lurb (**Figure 1e**), PM14 (**Figure 1f**) and PM54 (**Figure 1g**), with IC50 values in the low nanomolar range, spanning from 0.3 to 4.93 nM (**Table 1**). Additionally, we generated Vemu-resistant cells, namely 501mel^{VemuR} and MM074^{VemuR}, by exposing cells to increasing drug concentrations *in vitro* (**Table 1 and Figure 1b**) (Berico et al., 2021). These Vemu-resistant cells, displaying a hyperdifferentiated and pigmented state, exhibited cross-resistance to Dabra (in the case of MM074) and Trame (**Table 1 and Figure 1c**), but remained highly sensitive to Lurb, PM14 and PM54 (**Table 1 and Figures 1e-g**). Strikingly, when these compounds were tested on the non-cancerous Hermes3A immortalized melanocytes, we observed that this cell line was

consistently less sensitive than the melanoma cells towards Lurb, PM14 or PM54. Collectively, these findings demonstrate that melanoma cells exhibit a high sensitivity to Lurb, PM14 and PM54, with IC₅₀ values in the nanomolar ranges, irrespective of the cell phenotypes or driver mutations.

Lurb/PM14/PM54 leads to melanoma cell apoptotic death

Based on the cell viability assays conducted above, we investigated the efficacy of Lurb and its derivatives on melanoma cell proliferation and survival. Initially, a clonogenic assay was performed using a concentration of each drug equivalent to 1xIC₅₀, for 48 hours. The results demonstrated a significant impact of Lurb and its derivatives on all tested melanoma cell cultures or cell lines (**Figure 2a and Supplemental Figure 1**). Subsequently, we conducted additional experiments to elucidate the cellular responses affected in melanoma cells following drug treatments and analyzed proliferation and apoptotic induction using flow cytometry. We observed a significant inhibition of melanoma cell proliferation upon exposure to Lurb and its derivatives compared to DMSO (**Figure 2b**). Concurrently, there was a notable blockade of cell cycle progression (**Figure 2c**) and induction of apoptosis (**Figure 2d**) following treatment with Lurb, PM14 or PM54.

In SCLC, Lurb induces the degradation of the largest subunit of RNA Polymerase II (RPB1) and triggers a DNA damage response characterized by the activation of gH2AX due to drug-induced DNA breaks (Santamaria Nunez et al., 2016). We examined whether a similar response occurred in melanoma cells. Upon treatment with 5xIC₅₀ of each drug for 24 hours, we observed distinct gH2AX activation in the nucleus of differentiated 501mel melanoma cells or undifferentiated MM099 cell cultures (**Supplemental Figure 2a-b-c-d**), which was confirmed by immunoblotting in differentiated 501mel and MM074 cells (**Figure 2e and Supplemental Figure 2e**) or undifferentiated MM099 cells (**Supplemental Figure 2e**). In parallel with gH2AX accumulation, phosphorylation of ATM, the master protein involved in the DNA damage response, was observed in 501mel (**Figure 2e**). Interestingly, RPB1 degradation was minimal with Lurb, but pronounced in the presence of PM14 and PM54 (**Figure 2e**). Furthermore, Boyden chamber and wounding assays clearly indicated that all three drugs significantly affected the invasion and migration of undifferentiated melanoma cell cultures, respectively (**Figures 2f-g and Supplemental Figure 3**). These results indicate that Lurb and its derivatives exert robust cytostatic and cytotoxic effects on both differentiated and undifferentiated melanoma cells, characterized by the generation of DNA breaks and the degradation of RNAPII, particularly notable for PM14 and PM54.

Lurb/PM14/PM54 exerted strong cytotoxic activities against BRAF-mutant melanospheres

Using melanosphere culture assays, we investigated the effects of Lurb and its derivatives on three-dimension (3D) melanoma cultures. Initially, we examined the response of melanospheres to BRAF (Vemu and Dabra) and MEK (Tram) inhibitors. Melanospheres derived from BRAFi/MEKi-sensitive MM074 cells were exposed to doses equivalent to 1x, 2x and 5xIC₅₀ of the drugs, as determined in 2D cultures, for 72 hours. Cell viability was assessed using CellTiter-Glo assay. Interestingly, in stark contrast to the response observed in 2D cultures, Vemu, Dabra and Trame were unable to reduce cell viability in 3D culture, even at doses equivalent to 5xIC₅₀ (**Figure 3a**). Conversely, Lurb, PM14 and PM54 exhibited significant cytotoxic effects on MM074 melanospheres at doses equivalent to 5xIC₅₀ (**Figure 3b**). Moreover, melanospheres treated with Lurb, PM14 and PM54 displayed a substantial population of late apoptotic cells positive for annexin V and propidium iodide, indicating abundant DNA fragmentation compared to control samples (**Figure 3c**). These findings highlight the potent cytotoxic activity of Lurb, PM14 and PM54 against mutant-BRAF melanospheres, in contrast to the limited efficacy of currently used targeted therapies based on BRAF and/or MEK inhibition.

Lurb, PM14 and PM54 affect crucial melanoma genes

We aimed to investigate the mechanisms underlying the sensitivity of melanoma cells to Lurb and its derivatives. Lurb, PM14 and PM54 are known DNA binders and transcription inhibitors that have been shown to affect the expression of essential cancer-associated genes in SCLC (Costanzo et al., 2022). We hypothesized that these compounds might also deregulate critical genes in melanoma, such as the lineage-specific transcription factors MITF and SOX10, which are expressed in differentiated melanoma cells, as well as the pro-invasion/migration transmembrane protein AXL and the pro-metastatic protein EGFR expressed in undifferentiated melanoma cells. To test this hypothesis, we treated 2D cell cultures of differentiated melanoma cells (501mel, MM074 and IGR37) and undifferentiated melanoma cells (MM029, MM099 and IGR39) with doses equivalent to 5xIC₅₀ of Lurb and its derivatives for 12 hours. RT-qPCR analysis revealed that the expression of MITF and SOX10 in differentiated cells, as well as AXL and EGFR expression in undifferentiated cells, was significantly affected by Lurb and its derivatives compared to the housekeeping gene beta-actin, which exhibited stable expression following treatments (**Figures 4a-b and Supplemental Figures 4a-b**). Furthermore, immunoblotting performed 24 hours after treatment further

confirmed a significant decrease in the protein levels of melanoma marker genes (**Figures 4c-d**). Additionally, in 3D melanoma cultures, the expression of MITF and SOX10 in MM074 or EGFR in MM029 was significantly affected by Lurb and its derivatives when treated with a dose equivalent to 5xIC₅₀ for 24 hours, as compared to control genes RPL13A or TBP (**Figure 4e**). To investigate the dynamics of the dual mechanism of action of these compounds, we treated differentiated 501mel and undifferentiated MM099 cells for increasing durations with 5xIC₅₀s of drugs. We observed in 501mel cells a significant induction of gH2AX at 4 to 6 hours of treatments, which coincided with the decrease in SOX10 expression (**Supplemental Figure 4c-d**). In MM099 cells however, gH2AX levels increased at 12h, at the same time as AXL mRNA levels decreased (**Supplemental Figure 4e-f**). Collectively, these findings indicate that short-term treatments with Lurb, PM14 or PM54 can impact crucial melanoma master regulator genes (MRGs) in both 2D and 3D melanoma cell cultures. This transcriptional inhibition of key regulators of melanoma cell survival coincides with the induction of double-strand breaks, leading to cell apoptosis.

Lurb, PM14 and PM54 repress differential set of melanoma genes

To investigate the effect of Lurb and its derivatives on the transcriptional landscape of melanoma cells, we conducted gene expression profiling in 2D cultures of representative melanoma cells, MM074 and MM029, which represent differentiated and undifferentiated phenotypes, respectively. The cells were treated with 10xIC₅₀ of the drugs for a short duration of 8 hours. Treatment with Lurb, PM14 and PM54 resulted in a significant down-regulation of genes expressed in both MM074 and MM029 cells, with a smaller number of genes being up-regulated (**Supplemental Figure 5a**). Notably, Lurb, PM14 and PM54 commonly down-regulated 1,365 genes in differentiated MM074 and 1,104 genes in undifferentiated MM029 cells (**Figure 5a**). Among these genes, 757 were consistently down-regulated by all three drugs in both MM074 and MM029 cells (**Figure 5b and Supplemental Table 1**, not included in this thesis but available upon request). Gene ontology (GO) analysis revealed that many of these 757 genes were involved in transcriptional processes, indicating that a significant fraction of the genes sensitive to Lurb and its derivatives are associated with transcription factor function (**Figure 5c**). Furthermore, gene set enrichment analysis (GSEA) demonstrated that genes involved in the G2M checkpoint and WNT-beta catenin signaling pathway were particularly affected by the three drugs in both MM074 and MM029 (**Supplemental Figure 5b**).

Next, we compared the transcriptional effects of PM14 and PM54 to those of Lurb in differentiated MM074 and undifferentiated MM029 melanoma cell cultures. Lurb and PM14

exhibited very similar effects, and no genes showed significant differential expression when comparing the effects of these drugs in MM074 or MM029 cells (**Figure 6a and 6b**). Interestingly, PM54 induced distinct transcriptional effects compared to Lurb, with dissimilar and fewer genes being deregulated in both differentiated and undifferentiated melanoma cells (**Figure 6a and c**). GSEA and GO analysis revealed that PM54 more specifically targets genes involved in transcriptional regulation, whereas Lurb more broadly down-regulated genes associated with different cellular processes, such as cell cycle and protein modification (**Supplemental Figures 6a and b**). Taken together, these findings demonstrate that Lurb, PM14 and PM54 have significant impacts on the transcriptional programs of melanoma cells, with PM54 exerting the lowest levels of transcriptionally deregulated genes while displaying equally high cytotoxic activity compared to Lurb and PM14.

Anti-proliferative and pro-apoptotic impact of PM14 and PM54 in xenograft mouse melanoma models

To investigate the effects of the aforementioned tested drugs in living organisms, we decided to examine the impact of PM14 and PM54 on melanoma cell-derived xenograft (CDXs) mouse models. Human 501mel, 501mel^{VemuR} or SKMEL28 melanoma cells were subcutaneously implanted into the right flank of NSG mice. Once the tumors reached a size of 150 mm³, a single intravenous (IV) dose of either PM14 or PM54 at a concentration of 1.2mg/kg was administrated to the animals (N=3/group). After 24 hours, we assessed the level of phospho-histone H3 (pHH3) as a measure of the mitotic index (Casper et al., 2010). We found that the fraction of pHH3-positive cells decreased fourfold in the 501mel-, 501mel^{VemuR}- and SKMEL28-derived xenografts, 24 hours post-drug treatment, compared to xenografts treated with either no drug or DMSO (**Figure 7a**). Additionally, we evaluated the density of apoptotic cells 24 hours after drug-treatment using caspase-3 cleavage detection through IF. We observed a significant increase in the fraction of apoptotic cells in all three tumors treated with either PM14 or PM54, compared to the non-treated or DMSO-treated xenografts (**Figure 7b**).

Subsequently, we monitored the tumor volumes following weekly IV treatments of PM14 or PM54 at a concentration of 1.2mg/kg. Treatments commenced (Day 0) when the tumors reached 150 mm³ in female NSG mice aged 4 to 6 weeks (N=8/group). We observed statistical significant difference in the antitumor activity of both PM15 and PM54, including against the 501mel^{VemuR}-derived tumors, when comparing the groups receiving weekly treatment with the placebo-treated group (**Figure 7c and Table 2**). Concurrently, we noted a significant increase in overall survival for both drugs in all three CDX models, with a particularly pronounced

impact on the survival of mice harboring the 501mel^{VemuR}-derived tumors (**Figure 7d**). These findings indicate a potent anti-tumor activity of PM14 and PM54 in living organisms, with significant effects on animal survival.

Discussion

The treatment of metastatic melanoma fundamentally evolved with the introduction of MAPK and immune checkpoint inhibitors, which leverage recently gained insights of certain molecular hallmarks of cancer cells (Robert et al., 2019)(Jenkins and Fisher, 2021). While these treatments provided remarkable clinical benefits, their efficacy is limited by the important transcriptional and cell state plasticity of melanoma cells, giving for example rise to treatment-resistant undifferentiated/mesenchymal-like cells. Thus, considerable effort is currently being invested into finding new therapeutics to successfully target even the rarer, more stem-like cellular subpopulations. We postulated that all types of melanoma cells, irrespective of their specific phenotype and mutational status, would still be highly vulnerable to the disruption of oncogene expression because of their cancer-associated hallmark of transcriptional addiction (Verfaillie et al., 2015)(Tirosh et al., 2016)(Wouters et al., 2020). Indeed, compared to other types of cancers, melanoma cells display very high degrees of mutational burdens, and their gene expression patterns might therefore be proportionally strongly dysregulated. Furthermore, the notorious cell-state plasticity of melanoma cells indicates a strong dependency on tightly regulated oncogenic gene expression programs. As the recent clinical approval of Lurb in SCLC opened new avenues to exploit transcriptional dependencies of cancer cells, we investigated here the possibility of repurposing this novel marine-derived DNA binder for the treatment of melanoma. Furthermore, we tested whether the structural analogues of Lurb, PM14 and PM54, might provide differential or additional benefits compared to the original compound.

In the current study, we assayed the efficacy of Lurb, PM14 and PM54 against a large panel of melanoma cell cultures, recapitulating various driver mutations and phenotypes, and compared their effects against those elicited by the clinically used MAPKi Vemu, Trame and Dabra. Strikingly, undifferentiated melanoma cells displaying intrinsic resistance to MAPKi, as well as in vitro generated hyperpigmented cells with acquired MAPKi resistance (Berico et al., 2021), were sensitive to Lurb and its analogues at low nanomolar concentrations. As recent studies have also shown the involvement of undifferentiated cells in immunotherapy resistance (Mehta et al., 2018)(Benboubker et al., 2022), our results showcase a potential clinical benefit

of using these novel compounds as either a second-line treatment after MAPKi/immunotherapy relapse, or as adjuvant therapy.

Our results also shed light onto the mechanisms of action of Lurb and its analogues PM14 and PM54, while elucidating their common features but also revealing some notable differential molecular effects between these compounds. Low nanomolar doses of Lurb, PM14 or PM54 commonly decreased proliferation and invasive capacities of melanoma cells, while inducing apoptosis and cell cycle blockage in the S phase. Similarly, the viabilities of 3D-cultured melanospheres were severely affected by treatments with the three drugs. Surprisingly however, even high doses of MAPKi did not affect the viability of melanospheres containing BRAF^{V600E}-mutated melanocytic MM074 cells, which were shown to be highly sensitive to BRAFi and MEKi in 2D-settings. These results thus showcase the importance of assaying novel drugs in different settings, as factors such as hypoxic signalling or drug penetration might severely limit their therapeutic effects. However, these factors did not seem to limit the efficacy of Lurb, PM14 or PM54 in our 3D models. As Lurb covalently binds DNA at actively transcribed genes and blocks elongating RNAPII, eventually resulting in the formation of TC-NER-associated DSBs (Santamaria Nunez et al., 2016), we suspected the observed cellular effects to be at least partly due to DNA damage response signalling. Thus, we checked RNAPII degradation status and the induction of gH2AX and P-ATM. While the three compounds rapidly induced gH2AX in melanoma cells, a phenomenon not observed for MAPKi, marked differences were somewhat surprisingly observed between Lurb and PM14/PM54 treatments in some cellular models. In 501mel cells for example, RNAPII degradation and gH2AX were much more pronounced when treated with PM14 or PM54, pointing to potential differences in efficacy and intracellular pharmacodynamics, which remain to be further studied.

Our results also highlight the dual mechanism of action by which Lurb and its analogues exert their cytotoxic effects. Synchronously with the induction of DNA breaks, as highlighted through the appearance of gH2AX, drug treatments also led to the important disruption of oncogene expression. Importantly, the transcriptional effects of the compounds seemed to exhibit a high degree of specificity for distinctly overexpressed oncogenes depending on the melanoma cell state. As such, while the expression of housekeeping genes such as *ACTb*, *TBP* or *RPL13a* were not affected in 2D or 3D conditions by short-term drug treatments, oncogenically overexpressed MRGs such as MITF or SOX10 were heavily inhibited specifically in melanocytic cells. In mesenchymal-like cells however, different MRGs were affected, such as the overexpressed RTKs AXL or EGFR. To investigate and compare the exact DNA targets of the compounds, biotinylated versions of Lurbi and PM54 (**Supplemental**

Figure 7a) were used to perform Chem-Seq assays. Preliminary results show that in 501mel cells, drug enrichment was significantly higher at melanoma MRG loci with open chromatin conformation such as the *MITF* gene, as compared to housekeeping genes such as *HPRT1* (**Supplemental Figure 7b**). While these Chem-Seq results are still being analyzed for differential binding patterns between Lurbi and PM54 and compared to RNA-Seq data, these observations nevertheless reveal arguably the most interesting feature of these novel drugs. As they selectively bind to actively transcribed regions, with high specificity towards highly expressed oncogenes, probably because of their exceedingly accessible chromatin environment, these compounds may be very well suited to target cancers such as melanoma, in which various, transcriptionally very different cell populations pose a problem. Through their unique mechanism of action, they seem to selectively inhibit the distinct transcription programs on which a given cancer cell subpopulation depends on. As non-cancer cells display a less open chromatin conformation and are less ‘transcriptionally addicted’, they should experience less cytotoxic effects than cancer cells.

Delving deeper into the transcriptional effects elicited by Lurb and its analogues by performing RNA-Seq on both melanocytic and mesenchymal-like melanoma cells, two important insights were gained. Firstly, GSEA and GO analysis revealed that drug treatments elicited a strong stress response with the activation of AP-1 and EMT factors while disrupting β -catenin-signaling, which represent events related to melanoma phenotype switching. As such, not unlike for other drugs, the cellular response to Lurb and its analogues could consist in dedifferentiation. However, the negative effects of phenotype switch induction could be of a more mitigated nature for these treatments, as even mesenchymal-like cells were shown to be sensitive to these drugs. Secondly, while the gene expression changes elicited by Lurb and PM14 greatly overlapped, the transcriptional effects of PM54 significantly diverged. Notably, PM54 treatments deregulated fewer genes than Lurb or PM14, while eliciting the same cytostatic and cytotoxic effects, thus representing potentially a clinical benefit. Indeed, PM54 might cause less systemic gene expression disruptions and thus unwanted secondary effects while still potently targeting cancer cells. Consequently, we advise that particular interest be given to clinically assess the efficacy of PM54.

Considering the promising in vitro data, we confirmed the in vivo effects of PM14 and PM54. We observed potent decreases in mitotic indexes and increases in cell death and overall survival in three different melanoma CDX models. Of note, particularly beneficial effects were observed with 501mel^{VemuR} tumors, potentially because of their increased dependency on MITF expression, in line with their hyperpigmented phenotype (Berico et al., 2021). While in vivo

effects could not be assessed on mesenchymal-like cells, because of their very weak tumorigenic nature, our results demonstrate that PM14 and PM54 significantly impact melanocytic-like melanoma cells in vivo, even those with acquired resistances to MAPKi.

Collectively, our data allow for a comprehensive overview of the cellular and molecular effects of a potential novel kind of melanoma treatment, based on the dual mechanism of action of DNA damage induction and transcriptional inhibition. The current study further sheds light onto the intricacies of gene expression dependencies of different melanoma cell subpopulations and their molecular reactions towards transcriptional disruptions. While this important preclinical work might legitimize the clinical testing of Lurb outside of the SCLC setting, it also highlights the potential benefits of further exploring the effects of its structural analogues. These results provide a rationale for investigating Lurb and its analogues in a clinical setting, especially for MAPKi-relapsed melanoma, and our transcriptional data warrant that particular interest should be given to PM54 and its potentially superior clinical benefits.

Materials and Methods

Cell culture and treatment

Cells were grown at 37°C in 5% CO₂ (10% for Hermes 3A) and were regularly checked for mycoplasma contamination. MM patient-derived short-term melanoma cultures (MM011, MM074, MM117, MM029, MM047, MM099) were grown in HAM-F10 (Gibco, Invitrogen) supplemented with 10% Fetal Calf Serum (FCS), 25 mM HEPES, 5,2 mM GLUTAMAX and penicillin–streptomycin. Melanoma cell lines 501mel and SKmel28 were grown in RPMI w/o HEPES (Gibco, Invitrogen) supplemented with 10% FCS and gentamycin. Vemurafenib-resistant cells (501mel^{VemuR} and MM074^{VemuR}) were additionally supplemented with 1,5 uM of Vemu. Melanoma IGR cell lines (IGR37 and IGR39) were grown in RPMI w/o HEPES (Gibco, Invitrogen) supplemented with 15% FCS and gentamycin. Immortalized melanocytes Hermes-3A were grown in RPMI 1640 medium (Gibco, Invitrogen) supplemented with 10% FCS, 200 nM TPA, 200 pM cholera toxin, 10 ng/ml human stem cell factor, 10 nM endothelin-1 and penicillin–streptomycin. 501mel, SKmel28 and IGRs cells were purchased from ATCC, MM and Hermes-3A cells were obtained from collaborators. Vemu (PLX4032), Trame (GSK1120212) and Dabra (GSK2118436) were purchased from Selleckchem. Lurb (PM1183), PM14, and PM54 were obtained from PharmaMar S.A.

Protein extraction and Western Blotting

For whole cell extracts, cells were rinsed once with cold PBS, before pelleting and resuspension in LSDB 0.5M buffer (500 mM KCl, 50 mM Tris pH 7.9, 20% glycerol, 1% NP-40, 1mM DTT and protease inhibitor cocktail). Afterwards, cells were fully disrupted with 3 cycles of heat shock (liquid nitrogen followed by 37°C water bath). Then, samples were centrifugated for 15min at 14,000rpm to remove cell debris. Lysates were subjected to SDS–polyacrylamide gel electrophoresis (SDS-PAGE) and proteins were transferred onto a nitrocellulose membrane. Membranes were incubated overnight 4 °C with primary antibodies in PBS+ 5% milk powder + 0.01% Tween-20. The membranes were then incubated with HRP-conjugated secondary antibody (Jackson ImmunoResearch) for 1h at room temperature and visualized using the ECL detection system (GE Healthcare).

Antibodies

Western Blots assays were performed with the following antibodies: ACTb (IGBMC House-Made, 1:1000), MITF (Cell Signaling, D5G7V, 1:1000), SOX9 (Cell Signaling, D8G8H, 1:1000), SOX10 (Santa Cruz sc-365692, 1:1000), EGFR (Santa Cruz sc-373746, 1:1000), AXL (Proteintech, 13196-1-AP, 1:1000), RPB1 (IGBMC House-Made, 1:1000), ATM (Cell Signaling 2873S, 1:1000), Phospho-ATM (Cell Signaling 13050S, 1:1000), γ H2AX (EMD Millipore JBW301, 1:1000), Vinculin (Sigma-Aldrich V4505, 1:1000).

For γ H2AX immunofluorescence assay, EMD Millipore JBW301 antibody was used at 1:500 dilution.

For in vivo stainings, anti-phosphorylated histone H3 antibody (Sigma-Aldrich, 06-570 diluted 1:1000), and anti-cleaved caspase-3 (Cell Signalling, 9661 diluted 1:300) were used.

For Chem-Seq assays, anti-biotin antibody (Abcam, ab53494) was used.

IC50 estimation

Cells were seeded at 5,000 cells/well in 96- well plates and treated with increasing concentrations of Vemu, Dabra, Trame, Lurb, PM14, PM54, Biotin-Lurb, or Biotin-PM54. After 72 h of incubation, cells were treated with PrestoBlue reagent (ThermoFisher) according to the manufacturer's instructions. The absorbance per well was measured with a CellInsight CX5 microplate reader. Determination of IC50 values was performed by nonlinear curve fitting using the Prism9 statistical software (GraphPad).

Clonogenicity Assay

Cells were drug-treated at IC₅₀ concentrations during 48h before seeding 1×10^3 or 2×10^3 cells in 6-well plates without drug, where they grew for 10 days to allow for colony formation. Afterward cells were fixed for 10min with 4% Formaldehyde solution, washed once with PBS and stained with Crystal Violet solution 0.2% for 15min. The wells were finally washed twice with deionized water, air dried, scanned and analyzed with Fiji software to count the number of colonies.

Cell proliferation, apoptosis, and cell cycle analysis by Flow Cytometry

2×10^6 cells were seeded in 6 well plates and were incubated 24h later with 1uM of CellTrace Violet reagent (ThermoFisher) according to the manufacturer's instructions, immediately before rinsing and drug treatment at IC₅₀ concentrations. After 48h of incubation, cells were rinsed and incubated with AnnexinV-APC (BD Biosciences). Cell proliferation and apoptosis were detected on a BD LSRFortessa™ Flow Cytometer. Data were analysed with FlowJo software. To define slow proliferating or apoptotic cells, we proceeded as follows: We considered that slow proliferating cells represented the 30% of cells with the highest concentration of CellTrace Violet signal in the DMSO control. We then calculated the % of cells that had a signal greater than or equal to this value with drug treatment. For apoptotic cells, we considered the 20% of cells with the highest signal of AnnexinV-APC in the DMSO control. For cell cycle analysis, 2×10^6 cells were seeded in 6 well plates. After drug treatments at IC₅₀ concentrations, cells were pelleted and fixed with 70% ethanol for 1h at 4°C. After 2 washes with cold PBS, cells were incubated with RNase A and PI for 1h in the dark, before being analyzed on a BD LSRFortessa™ Flow Cytometer. Data were analysed with FlowJo software. For apoptosis assays with 3D-grown melanoma cells, TrypLe Select 10x reagent (Gibco) was used to dissociate melanospheres to obtain single-cell suspensions. These cells were incubated with AnnexinV-APC (Biolegend) and Propidium Iodide (PI, Biolegend). With bivariate dot plots, we distinguished between viable (AnnexinV⁻ / PI⁻), early apoptotic (AnnexinV⁺ / PI⁻), late apoptotic (AnnexinV⁺ / PI⁺) and necrotic cells (AnnexinV⁻ / PI⁺).

Boyden Chamber Invasion Assay

2×10^6 cells were seeded inside Boyden Chamber inserts (Fisher Scientific) with 4% Matrigel (Corning) and covered with Serum free media. The inserts were placed in 24 well plates filled with complete medium. After 24h, the inserts were fixed for 10min with 4% Formaldehyde solution, washed once with PBS and stained with Crystal Violet solution 0.2% for 15min. The

wells were finally washed twice with deionized water, air dried, and photos were collected using an EVOS xl Core microscope. The pictures were analyzed with Fiji to assess the area of occupancy of the cells.

Wound-healing assay

Confluent melanoma cell monolayers in 6-well plates were scratched with the tip of a 20- μ L pipette to create uniform, cell-free wounds. Fresh medium with lower FCS % (to mitigate proliferation), with or without drugs, was added. At 0, 24, and 48 hours, photomicrographs of the wounds were taken under an inverted microscope. The wound areas were then quantified using ImageJ software.

Melanosphere formation and viability assay

5×10^4 cells were seeded in ultra-low attachment hydrogel-layered 96 well plates (Corning 7007) in KO DMEM medium supplemented with 20% KSR, AANE, 2 mM Glutamax, Penicillin/Streptomycin and 100 μ M Beta-mercaptoethanol. To allow for melanosphere formation, cells were left to grow for 4 days before drug treatment.

To analyze melanosphere viability after drug treatment, cells were treated with CellTiterGlo reagent (Promega) according to the manufacturer's instructions. Luminescence signals were measured with a Centro XS LB 960 microplate reader (Berthold).

RNA Extraction and RT-qPCR

Total RNA isolation was performed according to the manufacture protocol with NucleoSpin RNA Plus kit (Macherey-Nagel). RNA was retrotranscribed with Reverse Transcriptase Superscript IV (Invitrogen), qPCR was performed with SYBR Green (Roche) and on a LightCycler 480 (Roche). Target gene expression was normalized using 18S as reference gene. Primers for RT-qPCR were designed using Primer-BLAST. The following primers were used:

MITF	F CATTGTTATGCTGGAAATGCTAGAA R GGCTTGCTGTATGTGGTACTTGG
AXL	F CCGTGGACCTACTCTGGCT R CCTTGGCGTTATGGGCTTC
ACTb	F ACATCTGCTGGAAGGTGGAC R CCCAGCACAATGAAGATCAA

RPL13a	F TTGAGGACCTCTGTGTATTTGTCAA R CCTGGAGGAGAAGAGGAAAGAGA
TBP	F CGGCTGTTTAACTTCGCTTC R CACACGCCAAGAAACAGTGA
SOX10	F CCAGTTTGACTACTCTGACCATCAG R ATATAGGAGAAGGCCGAGTAGAGG
EGFR	F GCAGCGATGCGACCCTC R CCAACTGCGTGAGCTTGTTAC
18S	F TCAACTTTCGATGGTAGTCGCCGT R TCCTTGGATGTGGTAGCCGTTTCT

Bulk RNA-Sequencing and analysis

Library preparation was performed at the GenomEast platform at the Institute of Genetics and Molecular and Cellular Biology using TruSeq Stranded Total RNA Reference Guide - PN 1000000040499. Total RNA-Seq libraries were generated from 700 ng of total RNA using TruSeq Stranded Total RNA Library Prep Gold kit and TruSeq RNA Single Indexes kits A and B (Illumina, San Diego, USA), according to manufacturer's instructions. Briefly, cytoplasmic and mitochondrial ribosomal RNA (rRNA) was removed using biotinylated, target-specific oligos combined with Ribo-Zero rRNA removal beads. Following purification, the depleted RNA was fragmented into small pieces using divalent cations at 94°C for 8 minutes. Cleaved RNA fragments were then copied into first strand cDNA using reverse transcriptase and random primers followed by second strand cDNA synthesis using DNA Polymerase I and RNase H. Strand specificity was achieved by replacing dTTP with dUTP during second strand synthesis. The double stranded cDNA fragments were blunted using T4 DNA polymerase, Klenow DNA polymerase and T4 PNK. A single 'A' nucleotide was added to the 3' ends of the blunt DNA fragments using a Klenow fragment (3' to 5' exo minus) enzyme. The cDNA fragments were ligated to double stranded adapters using T4 DNA Ligase. The ligated products were enriched by PCR amplification. Surplus PCR primers were further removed by purification using AMPure XP beads (Beckman-Coulter, Villepinte, France) and the final cDNA libraries were checked for quality and quantified using capillary electrophoresis. Libraries were sequenced on an Illumina HiSeq 4000 sequencer as single read 50 base reads. Image analysis and base calling were performed using RTA version 2.7.7 and bcl2fastq version 2.20.0.422.

Reads were preprocessed to remove adapter and low-quality sequences (Phred quality score below 20). After this preprocessing, reads shorter than 40 bases were discarded for further

analysis. These preprocessing steps were performed using cutadapt version 1.10. Reads were mapped to rRNA sequences using bowtie version 2.2.8 and reads mapping to rRNA sequences were removed for further analysis. Reads were mapped onto the hg19 assembly of Homo sapiens genome using STAR version 2.5.3a. Gene expression quantification was performed from uniquely aligned reads using htseq-count version 0.6.1p1, with annotations from Ensembl version 75 and 'union' mode. Only non-ambiguously assigned reads have been retained for further analyses. Read counts have been normalized across samples with the median-of-ratios method proposed by Anders and Huber (Bushweller, 2019) to make these counts comparable between samples. Comparisons of interest were performed using the Wald test for differential expression proposed by Love et al. (Love et al., 2014) and implemented in the Bioconductor package DESeq2 version 1.16.1. Genes with high Cook's distance were filtered out and independent filtering based on the mean of normalized counts was performed. P-values were adjusted for multiple testing using the Benjamini and Hochberg method (Benjamini and Hochberg, 1995). Deregulated genes were defined as genes with $\log_2(\text{Fold change}) > 1$ or < -1 and adjusted P-value < 0.05 .

Volcano plots were generated using the Prism9 statistical software (GraphPad). Heatmaps were generated using Morpheus (<https://software.broadinstitute.org/morpheus>). Venn diagrams were generated using DeepVenn (<http://www.deepvenn.com/>) and representation factors and hypergeometric P-values were determined using Graeber lab software (<https://systems.crupp.ucla.edu/hypergeometric/>). Gene Ontology Analysis was performed using ShinyGO (Ge SX, Jung D & Yao, 2020).

Immunofluorescence

After PBS-rinsing, cells grown on coverslips were fixed with 4% PFA for 10 min. Cells were then permeabilized with PBS and 0.1% Triton X-100. Blocking was done with 10% BSA. Primary antibodies were incubated overnight at 4°C, after which cells were stained for 1 hour at room temperature with AlexaFluor-488 conjugated secondary antibodies diluted 1:500 in PBS+10% FCS (Life technologies) and stained with DAPI. Image acquisition was performed on a DFC7000T widefield microscope (Leica) and analysis was done using the Fiji software. For quantification, gH2AX signals were assessed for each DAPI-positive area.

Chemical-Sequencing (Chem-Seq)

501mel cells were seeded and grown to sub-confluency in 15-cm plates before treatment for 8 h with DMSO, biotinylated Lurbinectedin (Bio-Lurbi) or PM54 (Bio-PM54) at a concentration

equivalent to 10xIC₅₀. Cells were then fixed with 0.4% of PFA for 10 min and quenched with 2 M Glycin pH 8. Cells pellets were lysed in 25 mM HEPES pH 7.8, 10 mM NaCl, 1.5 mM MgCl₂, 0.5% NP-40, 1 mM DTT. Nuclei were resuspended in 50 mM Hepes-KOH pH 7.8, 140 mM NaCl, 1 mM EDTA, 1% Triton X-100, 0.1 mM Na-deoxycholate, 0.1% SDS and sonicated at 4°C with Q500 sonicator for 90 cycles with 30 sec intervals between cycles to get DNA fragments between 100-500 bp. 100 µg of the sonicated chromatin was then diluted in Dilution buffer (1% Triton X-100, 2 mM EDTA, 20 mM Tris HCl pH 7.5, 150 mM NaCl) and incubated overnight at 4°C with 5 µg of Anti-Biotin antibody (Abcam ab53494). The complex antibody-chromatin was then captured with protein A Dynabeads (Invitrogen, 10002D) for 2 h at 4°C, and beads were washed twice in Low Salt Washing Buffer (1% Triton, 2 mM EDTA, 20 mM Tris HCl pH 7.5, 150 mM NaCl, 0.1% SDS), High salt Washing Buffer (1% Triton, 2 mM EDTA, 20 mM Tris HCl pH 7.5, 500 mM NaCl, 0.1% SDS), and TE buffer (100 mM Tris HCl pH 7.5, 10 mM EDTA). Immunoprecipitated chromatin was subsequently eluted from beads in 1% SDS and 100mM NaHCO₃ at 65°C for 30 min, and crosslinks were reversed by overnight incubation with Proteinase K (50µg/ml) at 65 °C. The DNA was finally purified with the QIAquick PCR Purification kit (QIAGEN). Library preparation was performed at the GenomEast platform at the Institute of Genetics and Molecular and Cellular Biology using Diagenode MicroPlex Library Preparation kit v3 Instruction Manual. ChIP samples were purified using SPRIselect beads (Beckman-Coulter, Villepinte, France) and quantified using the Qubit 4 fluorimeter (Thermo Fischer Scientific, Illkirch, France). ChIP-seq libraries were prepared from 10 ng of double-stranded purified DNA using the MicroPlex Library Preparation kit v3 (C05010001, Diagenode, Seraing, Belgium), according to manufacturer's instructions. In the first step, the DNA was repaired and yielded molecules with blunt ends. In the next step, stem-loop adaptors with blocked 5 prime ends were ligated to the 5 prime end of the genomic DNA, leaving a nick at the 3 prime end. The adaptors cannot ligate to each other and do not have single-strand tails, avoiding non-specific background. In the final step, the 3 prime ends of the genomic DNA were extended to complete library synthesis and Illumina compatible indexes were added through a PCR amplification (7 cycles). Amplified libraries were purified and size-selected using SPRIselect beads (Beckman Coulter) to remove unincorporated primers and other reagents. Libraries were sequenced on an Illumina NextSeq 2000 sequencer as single read 50 base reads. Image analysis and base calling were performed using RTA version 2.7.7 and BCL Convert version 3.8.4.

Xenograft models

4- to 6-week-old NSG mice were subcutaneously implanted into their right flank with human melanoma cell suspensions (501mel, 501mel^{VemuR}, or SKmel28). When tumors began to develop, these were measured 2-3 times per week. Tumor volume was calculated with the equation $(a \times b^2)/2$, where “a” and “b” referred to the longest and shortest diameters, respectively. When tumors reached a size of 150 mm³, tumor bearing animals (N = 8/group) were treated with Placebo (saline solution) or PM14 or PM54 at 1.2 mg/kg weekly. Tumor volume and animal body weights were measured 2-3 times per week, starting from the first day of treatment. The median was determined for tumor volume/size on each measurement day. Treatment tolerability was assessed by monitoring body weight evolution, clinical signs of systemic toxicity, as well as evidences of local damage in the injection site. Treatments which produced >20% lethality and/or 20% net body weight loss were considered toxic. Furthermore, animals were euthanized when their tumors reached ca. 1500 mm³ and/or severe necrosis was seen. Differences on antitumor effect were evaluated by comparing tumor volume data as well as median survival time from the placebo treated group with PM54 or PM14 treated groups. For this, a two-tailed Mann-Whitney U test was used.

Tumor Immunofluorescence

Tumors were grown as mentioned above and were extracted after 24h following a single dose of placebo treatment or 1.2 mg/kg of PM14, PM54. In parallel, untreated tumors were extracted. The tumors were fixed in 10% formalin and embedded in paraffin for histology. Slides prepared from 5µm-thick paraffin sections were processed for antigen retrieval in 10 mM sodium citrate buffer (PH = 6.0) for 45 min at 95°C in a water bath. The slides were cooled down at room temperature (RT) for 15 min. They were rinsed in PBS and then incubated in a humidified chamber for 16 h at 4 °C, with the primary antibodies diluted in PBS containing 0.1% (v/v) Tween 20 (PBST) to detect mitotic (pHH3-positive) and apoptotic (cleaved caspase 3-positive) cells. After rinsing in PBST, detection of the bound primary antibodies was performed for 1 hour at room temperature in a humidified chamber using 555-conjugated secondary rabbit IgG antibody. The sections were then counterstained with DAPI to label nuclei. Stained sections were digitalized using a slide scanner (Nanozoomer 2.0-HT, Hamamatsu, Japan) and analyzed with the corresponding ND.view2 software.

Large 8-Bits digital scanned images of tumors stained for nuclei (10 000 to 30 000 nuclei per section) and pHH3 or cleaved caspase 3 were processed through an inhouse python (v3.8) algorithm to quantify positive cells. Basically, blue channels were proposed to a Cellpose2

model (deep learning model backbone by pytorch process) to segment nuclei. Subsequently, nuclei were analyzed for specific signals. For pHH3, a nucleus was considered positive if total pixels above 50 in intensity value exceeds 20% of nuclei surface (in 8 Bits image values range from 0 [no signal] to 255). Hence, we ensured that we did not consider unspecific background signals or insignificantly bright signals. The same procedure was applied to Caspase3 with pixel value set to 50 and minimal covered surface set to 30%. For each image, a ratio of positive cells/total nuclei was returned as the experimental variable. Statistics were produced using python's pingouin library (v0.5.3) with two-way ANOVA and post hoc tests being built-in functions.

Statistics and reproducibility

Experimental data was plotted and analyzed using either Excel (Microsoft) or GraphPad Prism (GraphPad Software Inc.). The number of samples and replicates are indicated in the respective figure legends. The P-values are indicated, * < 0.05 ** < 0.01 *** < 0.001 **** < 0.0001 and ns (non-significant) > 0.05.

Acknowledgements: The authors declare no competing financial interests. This study was supported by the Ligue contre le cancer (Equipe Labélisée 2022-2024) and the grant ANR-10-LABX-0030-INRT, a French State fund managed by the Agence Nationale de la Recherche under the frame program Investissements d'Avenir ANR-10-IDEX-0002-02.

References

- Akbani, R., The Cancer Genome Atlas Network, 2015. Genomic Classification of Cutaneous Melanoma. *Cell* 161, 1681–1696. <https://doi.org/10.1016/j.cell.2015.05.044>
- Anders, S., Huber, W., 2010. Differential expression analysis for sequence count data. *Genome Biol.* 11, 1–12. <https://doi.org/10.1186/GB-2010-11-10-R106/COMMENTS>
- Arozarena, I., Wellbrock, C., 2019. Phenotype plasticity as enabler of melanoma progression and therapy resistance. *Nat. Rev. Cancer* 19, 377–391. <https://doi.org/10.1038/s41568-019-0154-4>
- Atkins, M.B., Curiel-Lewandrowski, C., Fisher, D.E., Swetter, S.M., Tsao, H., Aguirre-Ghiso, J.A., Soengas, M.S., Weeraratna, A.T., Flaherty, K.T., Herlyn, M., Sosman, J.A., Tawbi, H.A., Pavlick, A.C., Cassidy, P.B., Chandra, S., Chapman, P.B., Daud, A., Eroglu, Z., Ferris, L.K., Fox, B.A., Gershenwald, J.E., Gibney, G.T., Grossman, D., Hanks, B.A., Hanniford, D., Hernando, E., Jeter, J.M., Johnson, D.B., Khleif, S.N., Kirkwood, J.M., Leachman, S.A., Mays, D., Nelson, K.C., Sondak, V.K., Sullivan, R.J., Merlino, G., 2021. The State of Melanoma: Emergent Challenges and Opportunities. *Clin. Cancer Res.* 27, 2678–2697. <https://doi.org/10.1158/1078-0432.CCR-20-4092>
- Benboubker, V., Boivin, F., Dalle, S., Caramel, J., 2022. Cancer Cell Phenotype Plasticity as a Driver of Immune Escape in Melanoma. *Front. Immunol.* 13, 873116. <https://doi.org/10.3389/fimmu.2022.873116>
- Benjamini, Y., Hochberg, Y., 1995. Controlling the False Discovery Rate: A Practical and Powerful Approach to Multiple Testing. *J. R. Stat. Soc. Ser. B Methodol.* 57, 289–300. <https://doi.org/10.1111/J.2517-6161.1995.TB02031.X>
- Berico, P., Cigrang, M., Davidson, G., Braun, C., Sandoz, J., Legras, S., Vokshi, B.H., Slovic, N., Peyresaubes, F., Gene Robles, C.M., Egly, J., Compe, E., Davidson, I., Coin, F., 2021. CDK7 and MITF repress a transcription program involved in survival and drug tolerance in melanoma. *EMBO Rep.* <https://doi.org/10.15252/embr.202051683>

- Bradner, J.E., Hnisz, D., Young, R.A., 2017. Transcriptional Addiction in Cancer. *Cell* 168, 629–643. <https://doi.org/10.1016/j.cell.2016.12.013>
- Bushweller, J.H., 2019. Targeting transcription factors in cancer — from undruggable to reality. *Nat. Rev. Cancer* 19, 611–624. <https://doi.org/10.1038/s41568-019-0196-7>
- Carlino, M.S., Larkin, J., Long, G.V., 2021. Immune checkpoint inhibitors in melanoma. *The Lancet* 398, 1002–1014. [https://doi.org/10.1016/S0140-6736\(21\)01206-X](https://doi.org/10.1016/S0140-6736(21)01206-X)
- Casper, D.J., Ross, K.I., Messina, J.L., Sondak, V.K., Bodden, C.N., McCardle, T.W., Glass, L.F., 2010. Use of Anti-phosphohistone H3 Immunohistochemistry to Determine Mitotic Rate in Thin Melanoma. *Am. J. Dermatopathol.* 32, 650–654. <https://doi.org/10.1097/DAD.0b013e3181cf7cc1>
- Chauhan, J.S., Hölzel, M., Lambert, J., Buffa, F.M., Goding, C.R., 2022. The MITF regulatory network in melanoma. *Pigment Cell Melanoma Res.* 35, 517–533. <https://doi.org/10.1111/pcmr.13053>
- Comandante-Lou, N., Baumann, D.G., Fallahi-Sichani, M., 2022. AP-1 transcription factor network explains diverse patterns of cellular plasticity in melanoma cells. *Cell Rep.* 40, 111147. <https://doi.org/10.1016/j.celrep.2022.111147>
- Costanzo, F., Martínez Díez, M., Santamaría Nuñez, G., Díaz-Hernández, J.I., Genes Robles, C.M., Díez Pérez, J., Compe, E., Ricci, R., Li, T., Coin, F., Martínez Leal, J.F., Garrido-Martin, E.M., Egly, J.M., 2022. Promoters of ASCL1- and NEUROD1-dependent genes are specific targets of lurbectedin in SCLC cells. *EMBO Mol. Med.* <https://doi.org/10.15252/emmm.202114841>
- Curti, B.D., Faries, M.B., 2021. Recent Advances in the Treatment of Melanoma. *N. Engl. J. Med.* 384, 2229–2240. <https://doi.org/10.1056/NEJMra2034861>
- De Velasco, G., Je, Y., Bossé, D., Awad, M.M., Ott, P.A., Moreira, R.B., Schutz, F., Bellmunt, J., Sonpavde, G.P., Hodi, F.S., Choueiri, T.K., 2017. Comprehensive Meta-analysis of Key Immune-Related Adverse Events from CTLA-4 and PD-1/PD-L1 Inhibitors in Cancer Patients. *Cancer Immunol. Res.* 5, 312–318. <https://doi.org/10.1158/2326-6066.CIR-16-0237>
- Delyon, J., Lebbe, C., Dumaz, N., 2020. Targeted therapies in melanoma beyond BRAF: targeting NRAS-mutated and KIT-mutated melanoma. *Curr. Opin. Oncol.* 32, 79–84. <https://doi.org/10.1097/CCO.0000000000000606>
- Dickson, P.V., Gershenwald, J.E., 2011. Staging and Prognosis of Cutaneous Melanoma. *Surg. Oncol. Clin. N. Am.* 20, 1–17. <https://doi.org/10.1016/j.soc.2010.09.007>
- Donati, B., Lorenzini, E., Ciarrocchi, A., 2018. BRD4 and Cancer: going beyond transcriptional regulation. *Mol. Cancer* 17, 164. <https://doi.org/10.1186/s12943-018-0915-9>
- Fontanals-Cirera, B., Hasson, D., Vardabasso, C., Di Micco, R., Agrawal, P., Chowdhury, A., Gantz, M., de Pablos-Aragoneses, A., Morgenstern, A., Wu, P., Filipescu, D., Valle-Garcia, D., Darvishian, F., Roe, J.-S., Davies, M.A., Vakoc, C.R., Hernando, E., Bernstein, E., 2017. Harnessing BET Inhibitor Sensitivity Reveals AMIGO2 as a Melanoma Survival Gene. *Mol. Cell* 68, 731–744.e9. <https://doi.org/10.1016/j.molcel.2017.11.004>
- Guo, W., Wang, H., Li, C., 2021. Signal pathways of melanoma and targeted therapy. *Signal Transduct. Target. Ther.* 6, 424. <https://doi.org/10.1038/s41392-021-00827-6>
- Hoek, K.S., Goding, C.R., 2010. Cancer stem cells versus phenotype-switching in melanoma. *Pigment Cell Melanoma Res* 23, 746–59. <https://doi.org/10.1111/j.1755-148X.2010.00757.x>
- Hogg, S.J., Beavis, P.A., Dawson, M.A., Johnstone, R.W., 2020. Targeting the epigenetic regulation of antitumour immunity. *Nat. Rev. Drug Discov.* 19, 776–800. <https://doi.org/10.1038/s41573-020-0077-5>
- Huang, A.C., Zappasodi, R., 2022. A decade of checkpoint blockade immunotherapy in melanoma: understanding the molecular basis for immune sensitivity and resistance. *Nat. Immunol.* 23, 660–670. <https://doi.org/10.1038/s41590-022-01141-1>
- Jenkins, R.W., Fisher, D.E., 2021. Treatment of Advanced Melanoma in 2020 and Beyond. *J. Invest. Dermatol.* 141, 23–31. <https://doi.org/10.1016/j.jid.2020.03.943>
- Jerby-Amon, L., Shah, P., Cuoco, M.S., Rodman, C., Su, M.J., Melms, J.C., Leeson, R., Kanodia, A., Mei, S., Lin, J.R., Wang, S., Rabasha, B., Liu, D., Zhang, G., Margolais, C., Ashenberg, O., Ott, P.A., Buchbinder, E.I., Haq, R., Hodi, F.S., Boland, G.M., Sullivan, R.J., Frederick, D.T., Miao, B., Moll, T., Flaherty, K.T., Herlyn, M., Jenkins, R.W., Thummalapalli, R., Kowalczyk, M.S., Canadas, I., Schilling, B., Cartwright, A.N.R., Luoma, A.M., Malu, S., Hwu, P., Bernatchez, C., Forget, M.A., Barbie, D.A., Shalek, A.K., Tirosh, I., Sorger, P.K., Wucherpennig, K., Van Allen, E.M., Schadendorf, D., Johnson, B.E., Rotem, A., Rozenblatt-Rosen, O., Garraway, L.A., Yoon, C.H., Izar, B., Regev, A., 2018. A Cancer Cell Program Promotes T Cell Exclusion and Resistance to Checkpoint Blockade. *Cell* 175, 984–+. <https://doi.org/10.1016/j.cell.2018.09.006>
- Karras, P., Bordeu, I., Pozniak, J., Nowosad, A., Pazzi, C., Van Raemdonck, N., Landeloos, E., Van Herck, Y., Pedri, D., Bervoets, G., Makhzami, S., Khoo, J.H., Pavie, B., Lamote, J., Marin-Bejar, O., Dewaele, M., Liang, H., Zhang, X., Hua, Y., Wouters, J., Browaeys, R., Bergers, G., Saeys, Y., Bosisio, F., van den Oord, J., Lambrechts, D., Rustgi, A.K., Bechter, O., Blanpain, C., Simons, B.D., Rambow, F., Marine, J.-C., 2022. A cellular hierarchy in melanoma uncouples growth and metastasis. *Nature* 610, 190–198. <https://doi.org/10.1038/s41586-022-05242-7>
- Kozar, I., Margue, C., Rothengatter, S., Haan, C., Kreis, S., 2019. Many ways to resistance: How melanoma cells evade targeted therapies. *Biochim. Biophys. Acta BBA - Rev. Cancer* 1871, 313–322. <https://doi.org/10.1016/j.bbcan.2019.02.002>

- Kwiatkowski, N., Zhang, T., Rahl, P.B., Abraham, B.J., Reddy, J., Ficarro, S.B., Dastur, A., Amzallag, A., Ramaswamy, S., Tesar, B., Jenkins, C.E., Hannett, N.M., McMillin, D., Sanda, T., Sim, T., Kim, N.D., Look, T., Mitsiades, C.S., Weng, A.P., Brown, J.R., Benes, C.H., Marto, J.A., Young, R.A., Gray, N.S., 2014. Targeting transcription regulation in cancer with a covalent CDK7 inhibitor. *Nature* 511, 616–20. <https://doi.org/10.1038/nature13393>
- Laham-Karam, N., Pinto, G.P., Poso, A., Kokkonen, P., 2020. Transcription and Translation Inhibitors in Cancer Treatment. *Front. Chem.* 8, 276. <https://doi.org/10.3389/fchem.2020.00276>
- Leonardi, G., Falzone, L., Salemi, R., Zanghì, A., Spandidos, D., Mccubrey, J., Candido, S., Libra, M., 2018. Cutaneous melanoma: From pathogenesis to therapy (Review). *Int. J. Oncol.* <https://doi.org/10.3892/ijo.2018.4287>
- Love, M.I., Huber, W., Anders, S., 2014. Moderated estimation of fold change and dispersion for RNA-seq data with DESeq2. *Genome Biol.* 15, 1–21. <https://doi.org/10.1186/S13059-014-0550-8/FIGURES/9>
- Luke, J.J., Flaherty, K.T., Ribas, A., Long, G.V., 2017. Targeted agents and immunotherapies: optimizing outcomes in melanoma. *Nat. Rev. Clin. Oncol.* 14, 463–482. <https://doi.org/10.1038/nrclinonc.2017.43>
- Luskin, M.R., Murakami, M.A., Manalis, S.R., Weinstock, D.M., 2018. Targeting minimal residual disease: a path to cure? *Nat. Rev. Cancer* 18, 255–263. <https://doi.org/10.1038/nrc.2017.125>
- Marin-Bejar, O., Rogiers, A., Dewaele, M., Femel, J., Karras, P., Pozniak, J., Bervoets, G., Van Raemdonck, N., Pedri, D., Swings, T., Demeulemeester, J., Borghs, S.V., Lehnert, S., Bosisio, F., van den Oord, J.J., Bempt, I.V., Lambrechts, D., Voet, T., Bechter, O., Rizos, H., Levesque, M.P., Leucci, E., Lund, A.W., Rambow, F., Marine, J.-C., 2021. Evolutionary predictability of genetic versus nongenetic resistance to anticancer drugs in melanoma. *Cancer Cell* 39, 1135–1149.e8. <https://doi.org/10.1016/j.ccell.2021.05.015>
- Mehta, A., Kim, Y.J., Robert, L., Tsoi, J., Comin-Anduix, B., Berent-Maoz, B., Cochran, A.J., Economou, J.S., Tumei, P.C., Puig-Saus, C., Ribas, A., 2018. Immunotherapy Resistance by Inflammation-Induced Dedifferentiation. *Cancer Discov.* 8, 935–943. <https://doi.org/10.1158/2159-8290.CD-17-1178>
- Newell, F., Johansson, P.A., Wilmott, J.S., Nones, K., Lakis, V., Pritchard, A.L., Lo, S.N., Rawson, R.V., Kazakoff, S.H., Colebatch, A.J., Koufariotis, L.T., Ferguson, P.M., Wood, S., Leonard, C., Law, M.H., Brooks, K.M., Broit, N., Palmer, J.M., Coutts, K.L., Vergara, I.A., Long, G.V., Barbour, A.P., Nieweg, O.E., Shivalingam, B., Robinson, W.A., Stretch, J.R., Spillane, A.J., Saw, R.P.M., Shannon, K.F., Thompson, J.F., Mann, G.J., Pearson, J.V., Scolyer, R.A., Waddell, N., Hayward, N.K., 2022. Comparative Genomics Provides Etiologic and Biological Insight into Melanoma Subtypes. *Cancer Discov.* 12, 2856–2879. <https://doi.org/10.1158/2159-8290.CD-22-0603>
- Radke, J., Schumann, E., Onken, J., Koll, R., Acker, G., Bodnar, B., Senger, C., Tierling, S., Möbs, M., Vajkoczy, P., Vidal, A., Högl, S., Kodajova, P., Westphal, D., Meier, F., Heppner, F., Kreuzer-Redmer, S., Grebien, F., Jürchott, K., Redmer, T., 2022. Decoding molecular programs in melanoma brain metastases. *Nat. Commun.* 13, 7304. <https://doi.org/10.1038/s41467-022-34899-x>
- Rambow, F., Marine, J.C., Goding, C.R., 2019. Melanoma plasticity and phenotypic diversity: therapeutic barriers and opportunities. *Genes Dev* 33, 1295–1318. <https://doi.org/10.1101/gad.329771.119>
- Rambow, F., Rogiers, A., Marin-Bejar, O., Aibar, S., Femel, J., Dewaele, M., Karras, P., Brown, D., Chang, Y.H., Debiec-Rychter, M., Adriaens, C., Radaelli, E., Wolter, P., Bechter, O., Dummer, R., Levesque, M., Piris, A., Frederick, D.T., Boland, G., Flaherty, K.T., van den Oord, J., Voet, T., Aerts, S., Lund, A.W., Marine, J.C., 2018. Toward Minimal Residual Disease-Directed Therapy in Melanoma. *Cell* 174, 843+. <https://doi.org/ARTN.855.e19.10.1016/j.cell.2018.06.025>
- Rebecca, V.W., Herlyn, M., 2020. Nongenetic Mechanisms of Drug Resistance in Melanoma. *Annu. Rev. Cancer Biol.* 4, 315–330. <https://doi.org/10.1146/annurev-cancerbio-030419-033533>
- Ribas, A., Hodi, F.S., Callahan, M., Chmielowski, B., Lawrence, D., Konto, C., McHenry, M.B., Choong, N., Wolchok, J., 2013. Phase I trial evaluating concurrent vemurafenib and ipilimumab in patients with advanced BRAF-mutant melanoma. *Eur. J. Cancer* 49, S867–S867.
- Robert, C., Grob, J.J., Stroyakovskiy, D., Karaszewska, B., Hauschild, A., Levchenko, E., Chiarion Sileni, V., Schachter, J., Garbe, C., Bondarenko, I., Gogas, H., Mandalá, M., Haanen, J.B.A.G., Lebbé, C., Mackiewicz, A., Rutkowski, P., Nathan, P.D., Ribas, A., Davies, M.A., Flaherty, K.T., Burgess, P., Tan, M., Gasal, E., Voi, M., Schadendorf, D., Long, G.V., 2019. Five-Year Outcomes with Dabrafenib plus Trametinib in Metastatic Melanoma. *N. Engl. J. Med.* 381, 626–636. <https://doi.org/10.1056/NEJMoa1904059>
- Rubanov, A., Berico, P., Hernando, E., 2022. Epigenetic Mechanisms Underlying Melanoma Resistance to Immune and Targeted Therapies. *Cancers* 14, 5858. <https://doi.org/10.3390/cancers14235858>
- Saginala, K., Barsouk, Adam, Aluru, J.S., Rawla, P., Barsouk, Alexander, 2021. Epidemiology of Melanoma. *Med. Sci.* 9, 63. <https://doi.org/10.3390/medsci9040063>
- Santamaria Nunez, G., Robles, C.M., Giraudo, C., Martinez-Leal, J.F., Compe, E., Coin, F., Aviles, P., Galmarini, C.M., Egly, J.M., 2016. Lurbinectedin Specifically Triggers the Degradation of Phosphorylated RNA Polymerase II and the Formation of DNA Breaks in Cancer Cells. *Mol Cancer Ther* 15, 2399–2412. <https://doi.org/10.1158/1535-7163.MCT-16-0172>
- Schadendorf, D., van Akkooi, A.C.J., Berking, C., Griewank, K.G., Gutzmer, R., Hauschild, A., Stang, A., Roesch, A., Ugurel, S., 2018. Melanoma. *The Lancet* 392, 971–984. [https://doi.org/10.1016/S0140-6736\(18\)31559-9](https://doi.org/10.1016/S0140-6736(18)31559-9)
- Sengupta, S., George, R.E., 2017. Super-Enhancer-Driven Transcriptional Dependencies in Cancer. *Trends Cancer* 3, 269–281. <https://doi.org/10.1016/j.trecan.2017.03.006>
- Shain, A.H., Bastian, B.C., 2016. From melanocytes to melanomas. *Nat Rev Cancer* 16, 345–58. <https://doi.org/10.1038/nrc.2016.37>

Sung, H., Ferlay, J., Siegel, R.L., Laversanne, M., Soerjomataram, I., Jemal, A., Bray, F., 2021. Global Cancer Statistics 2020: GLOBOCAN Estimates of Incidence and Mortality Worldwide for 36 Cancers in 185 Countries. *CA. Cancer J. Clin.* 71, 209–249. <https://doi.org/10.3322/caac.21660>

Switzer, B., Puzanov, I., Skitzki, J.J., Hamad, L., Ernstoff, M.S., 2022. Managing Metastatic Melanoma in 2022: A Clinical Review. *JCO Oncol. Pract.* 18, 335–351. <https://doi.org/10.1200/OP.21.00686>

Tirosh, I., Izar, B., Prakadan, S.M., Wadsworth, M.H., Treacy, D., Trombetta, J.J., Rotem, A., Rodman, C., Lian, C., Murphy, G., Fallahi-Sichani, M., Dutton-Regester, K., Lin, J.R., Cohen, O., Shah, P., Lu, D., Genshaft, A.S., Hughes, T.K., Ziegler, C.G., Kazer, S.W., Gaillard, A., Kolb, K.E., Villani, A.C., Johannessen, C.M., Andreev, A.Y., Van Allen, E.M., Bertagnolli, M., Sorger, P.K., Sullivan, R.J., Flaherty, K.T., Frederick, D.T., Jane-Valbuena, J., Yoon, C.H., Rozenblatt-Rosen, O., Shalek, A.K., Regev, A., Garraway, L.A., 2016. Dissecting the multicellular ecosystem of metastatic melanoma by single-cell RNA-seq. *Science* 352, 189–96. <https://doi.org/10.1126/science.aad0501>

Tsoi, J., Robert, L., Paraiso, K., Galvan, C., Sheu, K.M., Lay, J., Wong, D.J.L., Atefi, M., Shirazi, R., Wang, X., Braas, D., Grasso, C.S., Palaskas, N., Ribas, A., Graeber, T.G., 2018. Multi-stage Differentiation Defines Melanoma Subtypes with Differential Vulnerability to Drug-Induced Iron-Dependent Oxidative Stress. *Cancer Cell* 33, 890–904.e5. <https://doi.org/10.1016/j.ccell.2018.03.017>

Verfaillie, A., Imrichova, H., Atak, Z.K., Dewaele, M., Rambow, F., Hulselmans, G., Christiaens, V., Svetlichnyy, D., Luciani, F., Van den Mooter, L., Claerhout, S., Fiers, M., Journe, F., Ghanem, G.E., Herrmann, C., Halder, G., Marine, J.C., Aerts, S., 2015. Decoding the regulatory landscape of melanoma reveals TEADS as regulators of the invasive cell state. *Nat Commun* 6, 6683. <https://doi.org/10.1038/ncomms7683>

Vervoort, S.J., Devlin, J.R., Kwiatkowski, N., Teng, M., Gray, N.S., Johnstone, R.W., 2022. Targeting transcription cycles in cancer. *Nat. Rev. Cancer* 22, 5–24. <https://doi.org/10.1038/s41568-021-00411-8>

Widmer, D.S., Cheng, P.F., Eichhoff, O.M., Belloni, B.C., Zipser, M.C., Schlegel, N.C., Javelaud, D., Mauviel, A., Dummer, R., Hoek, K.S., 2012. Systematic classification of melanoma cells by phenotype-specific gene expression mapping. *Pigment Cell Melanoma Res* 25, 343–53. <https://doi.org/10.1111/j.1755-148X.2012.00986.x>

Wouters, J., Kalender-Atak, Z., Minnoye, L., Spanier, K.I., De Waegeneer, M., Bravo Gonzalez-Blas, C., Mauduit, D., Davie, K., Hulselmans, G., Najem, A., Dewaele, M., Pedri, D., Rambow, F., Makhzami, S., Christiaens, V., Ceyssens, F., Ghanem, G., Marine, J.C., Poovathingal, S., Aerts, S., 2020. Robust gene expression programs underlie recurrent cell states and phenotype switching in melanoma. *Nat Cell Biol* 22, 986–998. <https://doi.org/10.1038/s41566-020-0547-3>

Zanconato, F., Battilana, G., Forcato, M., Filippi, L., Azzolin, L., Manfrin, A., Quaranta, E., Di Biagio, D., Sigismondo, G., Guzzardo, V., Lejeune, P., Haendler, B., Krijgsvelde, J., Fassan, M., Bicciato, S., Cordenonsi, M., Piccolo, S., 2018. Transcriptional addiction in cancer cells is mediated by YAP/TAZ through BRD4. *Nat. Med.* 24, 1599–1610. <https://doi.org/10.1038/s41591-018-0158-8>

Figure legends

Figure 1: Melanoma cells show high sensitivity to Lurb, PM14 and PM54

a. Protein lysates from either the differentiated melanoma cells 501mel, MM011, MM074, MM117, IGR37 and SKMel-28 or the undifferentiated melanoma cells MM029, MM047, MM099 and IGR39 were immuno-blotted for proteins as indicated. Molecular mass of the proteins is indicated (kDa).

b-g. Melanoma cells were treated with increasing concentrations of Vemu (**b**), Dabra (**c**), Tram (**d**), Lurb (**e**), PM14 (**f**) or PM54 (**g**) for 72h. Mean growth is shown relative to vehicle (DMSO)-treated cells. Error bars indicate mean values \pm Standard Deviation (SD) for three biological triplicates. Differentiated (MITF-High, proliferative) melanoma cells are shown in blue, while undifferentiated (MITF-low, invasive) melanoma cells are shown in red. Differentiated melanoma cells with acquired resistance to Vemu are shown in green. Immortalized Hermes3A melanocytes are shown in violet. P-values are shown (Ordinary one-way ANOVA using Dunnett's multiple comparisons test).

Figure 2: Lurb, PM14 and PM54 induce cell cycle arrest and apoptosis

a. Indicated melanoma cells were treated with either vehicle (DMSO), Lurb, PM14 or PM54 for 48h at respective IC₅₀ concentrations and then allowed to grow for additional 10 days in the absence of the drugs. Results are shown as the mean colony numbers \pm SD for three biological triplicates. P-values are shown (Ordinary one-way ANOVA using Dunnett's multiple comparisons test).

b. Indicated melanoma cells were incubated with CellTrace and subsequently treated with either vehicle (DMSO), Lurb, PM14 or PM54 for 72h at respective IC₅₀ concentrations. Quantifications of populations with high CellTrace signal in DMSO or drug-treated cells are shown as mean values \pm SD for three biological triplicates. Proliferative cells show low CellTrace signal while non proliferative cells show high CellTrace signal. P-values are shown (Ordinary one-way ANOVA using Dunnett's multiple comparisons test).

c. Indicated melanoma cells were treated with either vehicle (DMSO), Lurb, PM14 or PM54 for 72h at respective IC₅₀ concentrations. Cell cycle was studied by flow cytometry, and results are shown as mean values \pm SD for three biological triplicates.

d. Indicated melanoma cells were treated with either vehicle (DMSO), Lurb, PM14 or PM54 for 72h at respective IC₅₀ concentrations. Apoptosis was studied by flow cytometry using annexin V-APC staining. Results are shown as mean values \pm SD for three biological triplicates. P-values are shown (Ordinary one-way ANOVA using Dunnett's multiple comparisons test).

e. Protein lysates from the differentiated melanoma cell 501mel treated with either Lurb, PM14 or PM54 for 24h at 5xIC₅₀ concentrations were immuno-blotted for proteins as indicated. Molecular mass of the proteins is indicated (kDa).

f. MM029 and MM099 melanoma cells were treated with either vehicle (DMSO), Lurb, PM14 or PM54 for 48h at respective IC₅₀ concentrations. Invasion was determined using Boyden chamber assays. Results are shown as mean values of coverage index \pm SD for three biological triplicates. P-values are shown (Ordinary one-way ANOVA using Dunnett's multiple comparisons test).

g. Confluent monolayers of melanoma cells were scratched and fresh medium containing reduced FCS % and either vehicle (DMSO), Lurb, PM14 or PM54 (IC₅₀ concentrations) was added. Size of the wound was measured at the indicated times and results are shown as mean values of fold changes of wound area versus DMSO treatment \pm SD for three biological triplicates. P-values are shown (Ordinary one-way ANOVA using Dunnett's multiple comparisons test).

Figure 3: Melanospheres have high sensitivity to Lurb, PM14 and PM54 compared with targeted therapies

a-b. MM074 melanospheres were treated with drug as indicated for 72h, and cell viability was measured with CellTiter-Glo assay. Results are shown as mean values of viability vs. DMSO +/- SD for three biological triplicates. P-values are shown (Ordinary one-way ANOVA using Dunnett's multiple comparisons test).

c. MM074 melanospheres were treated with either vehicle (DMSO), Lurb, PM14, PM54 or Vemu for 72h. Apoptosis was studied by flow cytometry with annexin V-APC and propidium iodide staining. Results are shown as mean values +/- SD for three biological triplicates

Figure 4: Lurb, PM14 and PM54 impair crucial melanoma genes

a. qRT-PCR analysis showing average 18S-normalized expression of *MITF* and *ACTB* in the differentiated MM074 cells treated with either vehicle (DMSO), Lurb, PM14 or PM54 for 12h at 5xIC50 concentrations. Error bars indicate mean values + SD for three biological triplicates. P-values are shown (Ordinary one-way ANOVA using Dunnett's multiple comparisons test).

b. qRT-PCR analysis showing average 18S-normalized expression of *AXL* and *ACTB* in the undifferentiated MM029 treated with either vehicle (DMSO), Lurb, PM14 or PM54 for 12h at 5xIC50 concentrations. Error bars indicate the mean values +/- SD for three biological triplicates. P-values are shown (Ordinary one-way ANOVA using Dunnett's multiple comparisons test).

c-d. The differentiated MM074 (**c**) or undifferentiated MM099 (**d**) cells were treated with either vehicle (DMSO), Lurb, PM14 or PM54 for 24h at 5xIC50 concentrations. Protein lysates were immuno-blotted for proteins as indicated. Molecular mass of the proteins is indicated (kDa).

e. qRT-PCR analysis showing average 18S-normalized expression of *RPL13A*, *TBP*, *MITF* and *SOX10* in MM074 melanospheres or *RPL13a*, *TBP* or *AXL* in MM029 melanospheres treated with either vehicle (DMSO), Lurb, PM14 or PM54 for 24h at 5xIC50 concentrations. Results are shown as the mean values +/- SD for three biological triplicates. P-values are shown (Ordinary one-way ANOVA using Dunnett's multiple comparisons test).

Figure 5: Lurb, PM14 and PM54 impair transcription-associated genes

a. Venn diagrams between significantly down-regulated (left) and up-regulated (right) genes identified by RNA-seq in MM074 (top) and MM029 (bottom) upon treatment with either Lurb, PM14 or PM54 for 8h with 10xIC50 concentrations.

- b.** Venn diagrams between genes identified by RNA-seq as being commonly down-regulated (left) or up-regulated (right) in both MM074 and MM029 by the three compounds. Representation factor and hypergeometric p-values are represented.
- c.** Gene ontology analysis of the 757 genes significantly down-regulated (left) and 110 genes significantly up-regulated (right) in both MM074 and MM029 by the three compounds, as identified in (b). The histogram shows the top deregulated biological pathways according to the FDR and fold enrichment.

Figure 6: Lurb, PM14 and PM54 impair different sets of transcribed genes

- a.** Heatmap depicting all deregulated genes from either Lurb, PM14, or PM54 treatments, in MM074 cells (left) or MM029 cells (right), from the RNA-Seq described in Figure 5. RPKM values are represented as z-score.
- b-c.** Volcano plots showing differentially expressed genes between Lurbi and PM14 treatment (**b**) or between Lurbi and PM54 treatment (**c**) in MM074 (left) and MM029 (right) as determined by RNA-seq as described in Figure 5. Deregulated genes were defined as genes with $\log_2(\text{Fold change}) > 1$ or < -1 and adjusted P-value < 0.05 .

Figure 7: Potent in vivo effects of PM14 and PM54 in melanoma CDX models

- a.** Representative images of pHH3-positive cells (red) in tumor sections of 501mel, 501mel^{VemuR} and SKMel28 CDX models after 24h treatment with a one-time dose of Placebo, PM14 or PM54 at 1.2 mg/kg (left). Quantification of mitotic index (% of pHH3-positive cells/tumor section) of indicated CDX models (right), in which results are shown as mean values \pm SD for tumor sections from three tumors per condition. P-values are shown (Ordinary one-way ANOVA using Dunnett's multiple comparisons test).
- b.** Representative images of cleaved caspase-3-positive cells (red) in tumor sections of 501mel, 501mel^{VemuR} and SKMel28 CDX models after 24h treatment with a one-time dose of Placebo, PM14 or PM54 at 1.2 mg/kg (left). Quantification of apoptotic index (% of cleaved caspase-3-positive cells/tumor section) of indicated CDX models (right), in which results are shown as mean values \pm SD for tumor sections from three tumors per condition. P-values are shown (Ordinary one-way ANOVA using Dunnett's multiple comparisons test).
- c.** Indicated CDX models (n=8/condition) were treated with Placebo, PM14 or PM54 at 1.2 mg/kg weekly and tumor volumes were measured.
- d.** Indicated CDX models (n=8/condition) were treated weekly with Placebo, PM14 or PM54 at 1.2 mg/kg and survival was assessed. P-values are shown (logrank (Mantel-Cox) test).

Supplemental Figure 1: Clonogenicity assays

Indicated differentiated or undifferentiated cells were treated as explained in Figure 2.a. Representative photographs of technical triplicates are shown.

Supplemental Figure 2: Lurb, PM14 and PM54 potently induce DSB

a-d. 501mel (**a-b**) or MM099 (**c-d**) cells were treated with indicated drugs for 24h at 5xIC50 concentrations, and gH2AX induction was assessed by immunofluorescence. Representative images are shown (**a+c**) as well as gH2AX signal quantification for three biological triplicates (**b+d**). P-values are shown (Ordinary one-way ANOVA using Dunnett's multiple comparisons test).

e. Protein lysates from differentiated MM074 or undifferentiated MM099 treated with either Lurb, PM14 or PM54 for 24h at 5xIC50 concentrations were immuno-blotted for proteins as indicated. Molecular mass of the proteins is indicated (kDa).

Supplemental Figure 3: Lurb, PM14 and PM54 potently inhibit invasive capacities

Undifferentiated MM029 and MM099 were treated as explained in Figure 2.f. Representative photographs of are shown.

Supplemental Figure 4: Lurb, PM14 and PM54 affect melanoma MRGs expression

a-b. qRT-PCR analysis showing average 18S-normalized expression of *SOX10* in indicated differentiated cells (**a**) and of *EGFR* in indicated undifferentiated cells (**b**) treated with either vehicle (DMSO), Lurb, PM14 or PM54 for 12h at 5xIC50 concentrations. Error bars indicate mean values + SD for three biological triplicates. P-values are shown (Ordinary one-way ANOVA using Dunnett's multiple comparisons test).

c-e. 501mel (**c**) or MM099 (**e**) cells were treated with vehicle (DMSO), Lurb, PM14 or PM54 for indicated durations at 5xIC50 concentrations, and gH2AX induction was assessed by immunofluorescence. gH2AX signal quantification for three biological triplicates are represented. P-values are shown (Ordinary one-way ANOVA using Dunnett's multiple comparisons test).

d-f. qRT-PCR analysis showing average 18S-normalized expression of *MITF* in 501mel (**d**) and of *AXL* in MM099 cells (**f**) treated with either vehicle (DMSO), Lurb, PM14 or PM54 for indicated durations at 5xIC50 concentrations. Error bars indicate mean values + SD for three biological triplicates. P-values are shown (Ordinary one-way ANOVA using Dunnett's multiple comparisons test).

Supplemental Figure 5: Transcriptional effects of short Lurb, PM14 and PM54 treatment

- a.** Volcano plots showing differentially expressed genes between DMSO-treated versus Lurbi-PM14-, or PM54-treated MM074 (left) or MM029 (right) cells, determined by RNA-seq as described in Figure 5. Examples of deregulated genes are shown, which were defined as genes with $\log_2(\text{Fold change}) > 1$ or < -1 and adjusted P-value < 0.05 .
- b.** GSEA analysis of deregulated genes in MM074 or MM029 cells treated with Lurb, PM14 or PM54, determined by RNA-seq as described in Figure 5.

Supplemental Figure 6: Specific effect of PM54 vs. Lurb on gene expression

- a.** GSEA analysis of differentially deregulated genes in MM074 and MM029 cells treated either with Lurb or PM54, determined by RNA-seq as described in Figure 5.
- b.** Gene ontology analysis of the genes significantly up-regulated (up) or down-regulated (bottom) in MM074 (left) and MM029 (right) cells treated with Lurb vs PM54. The histogram shows the top deregulated biological pathways according to the FDR and fold enrichment.

Supplemental Figure 7: Preferential binding of Lurb and PM54 on transcriptionally active genes

- a.** Indicated melanoma cells were treated with increasing concentrations of Lurbi, biotinylated Lurbi (Bio-Lurbi), PM54 or biotinylated PM54 (Bio-PM54) for 72h. Mean growth is shown relative to vehicle (DMSO)-treated cells. Error bars indicate mean values \pm Standard Deviation (SD) for three biological triplicates. IC50 values are indicated.
- b.** 501mel cell were treated for 8h with 10xIC50 concentrations of Bio-Lurb or Bio-PM54, before Chem-Seq analysis was performed to study drug binding sites. Indicated are UCSC genome browser captures showing the Chem-seq profiles of Bio-Lurb and Bio-PM54 in the genomic regions of *MITF* and *HRPT1*, as well as publicly available ATAC-Seq and H3K27ac ChIP-Seq data (Fontanals-Cirera et al., 2017).

Table 1: IC50s of Vemu, Dabra, Trame, Lurb, PM14 and PM54 towards various melanoma cells. The phenotype and genotype of these cells are indicated. Hermes3A are melanocytes.

Table 2: Statistical results by Mann-Whitney U test. Comparison of tumor volumes in placebo-treated group vs. PM54 or PM14 groups following injection in tumours formed following 501mel, 501melVemuR or SKMEL28 melanoma cells injection in NSG mice.

Figure 1

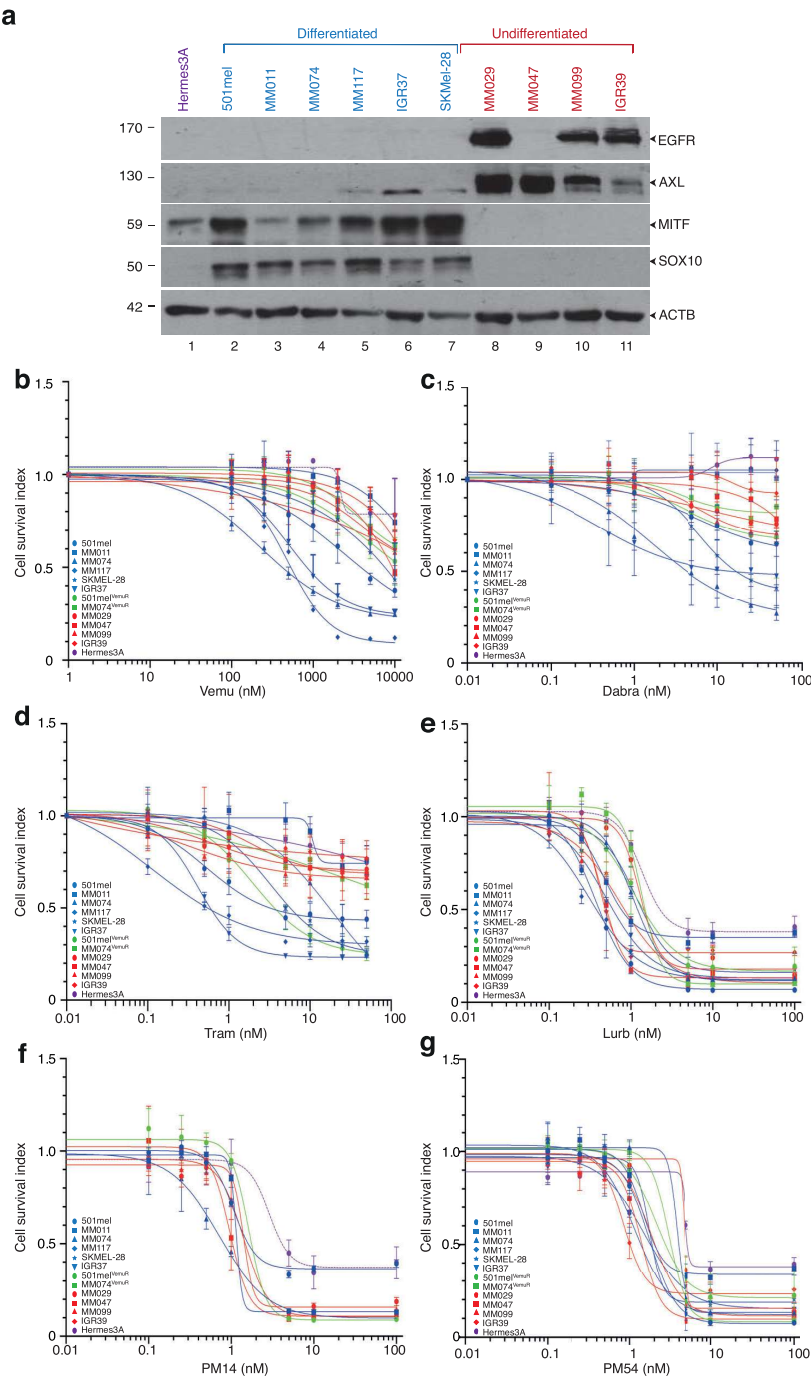


Figure 2

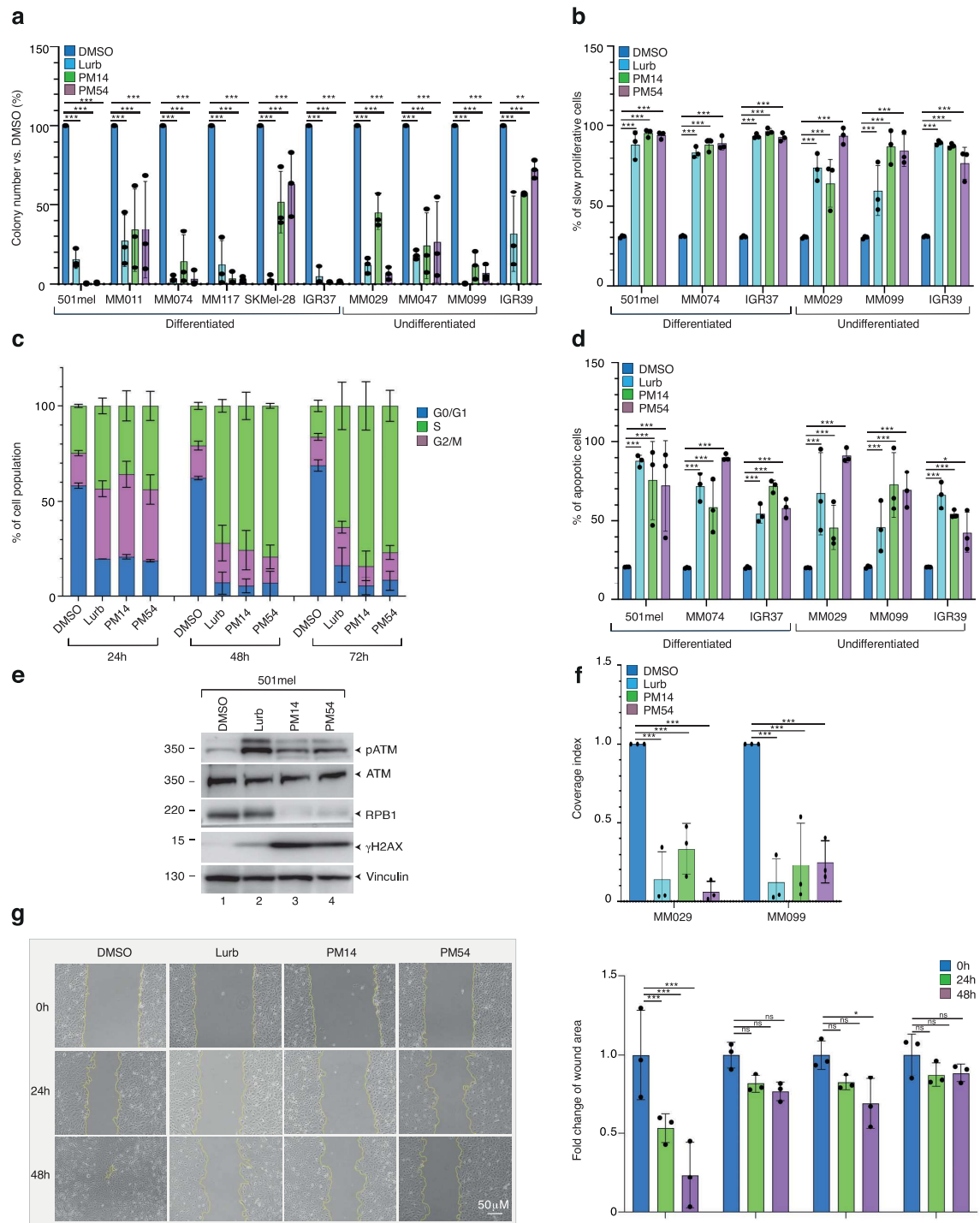


Figure 3

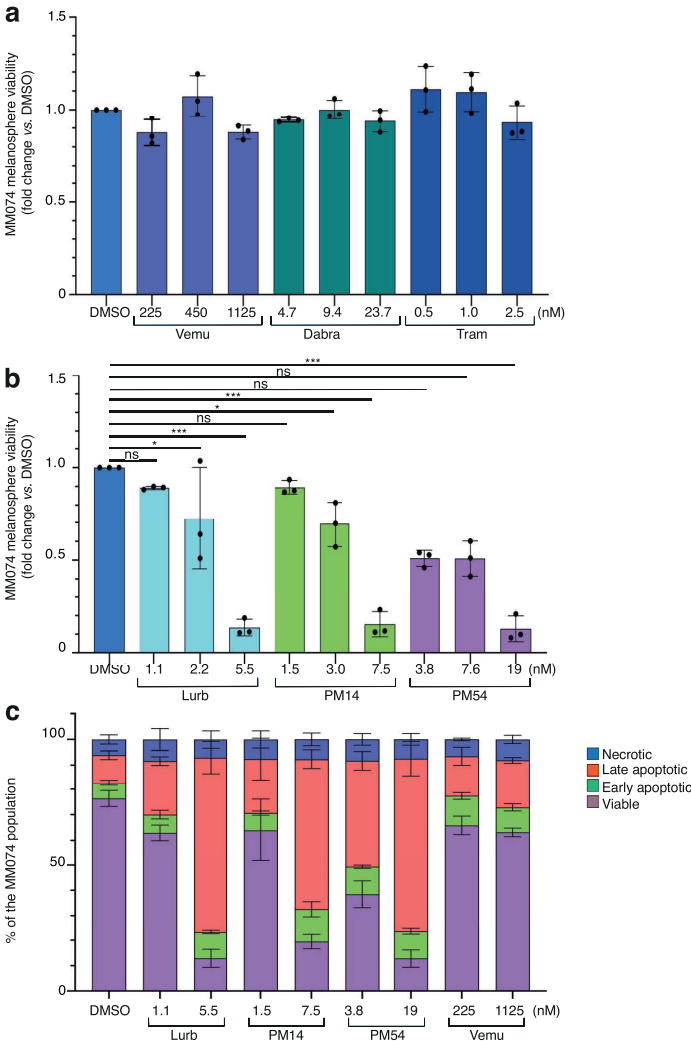


Figure 4

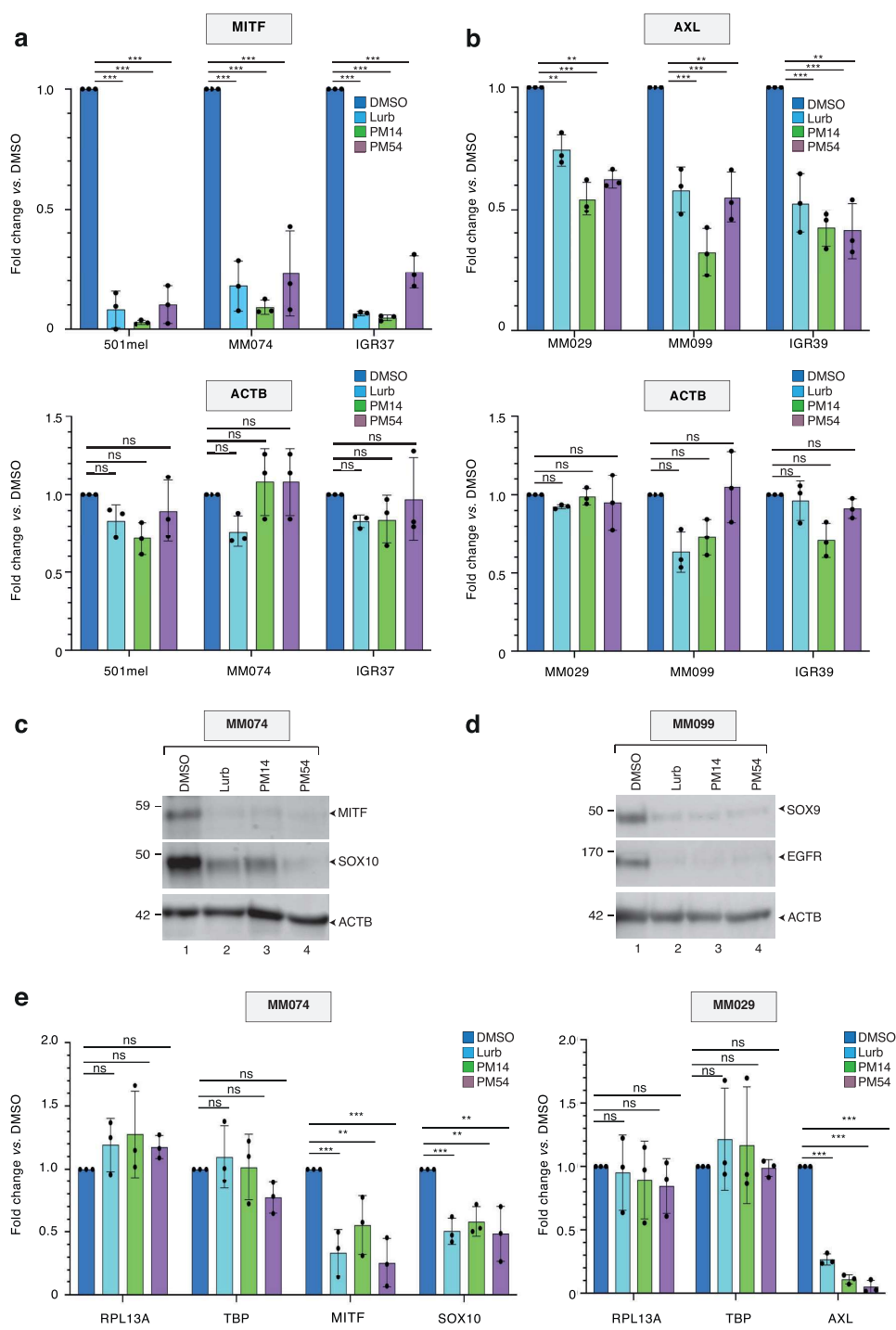


Figure 5

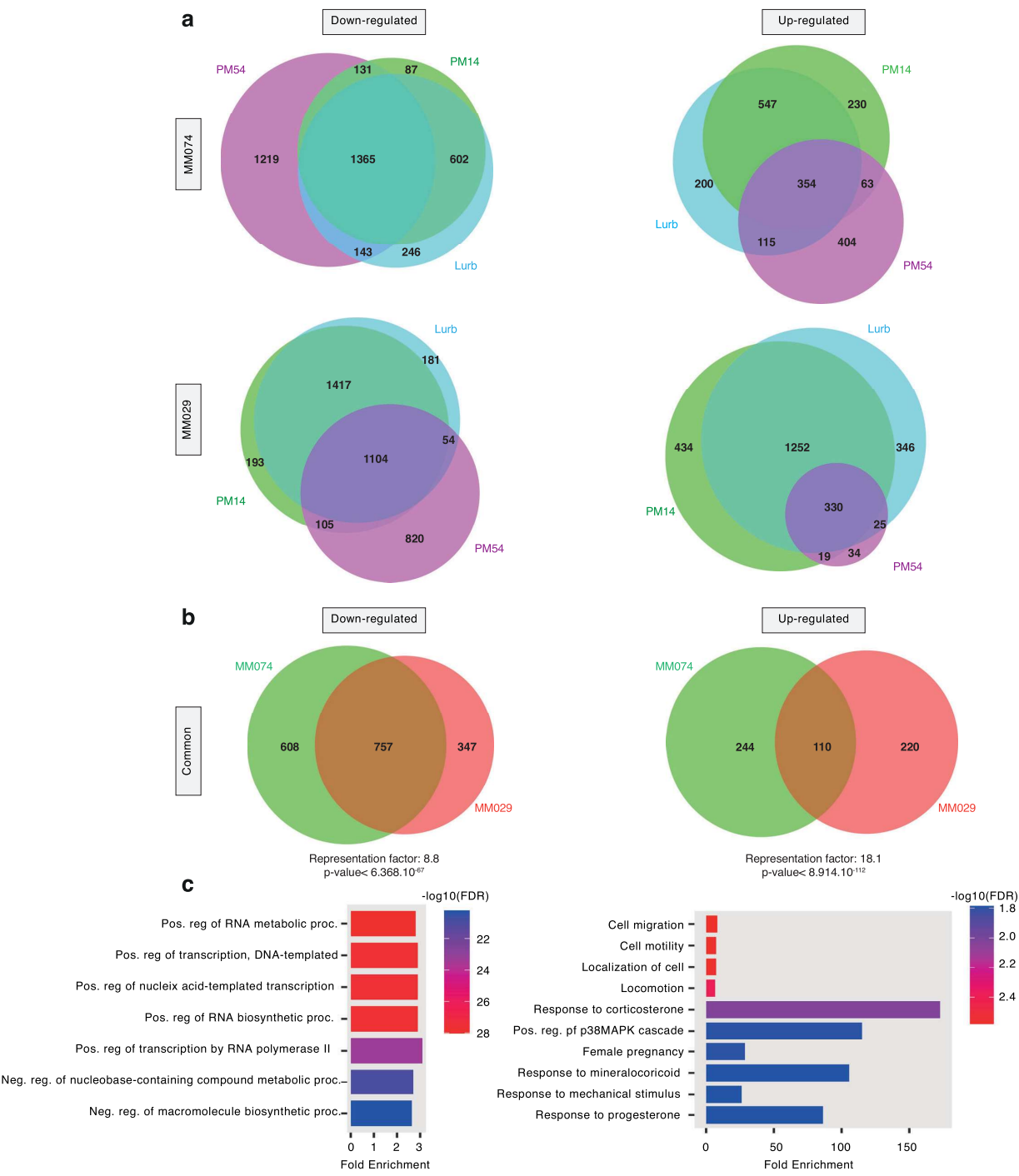


Figure 6

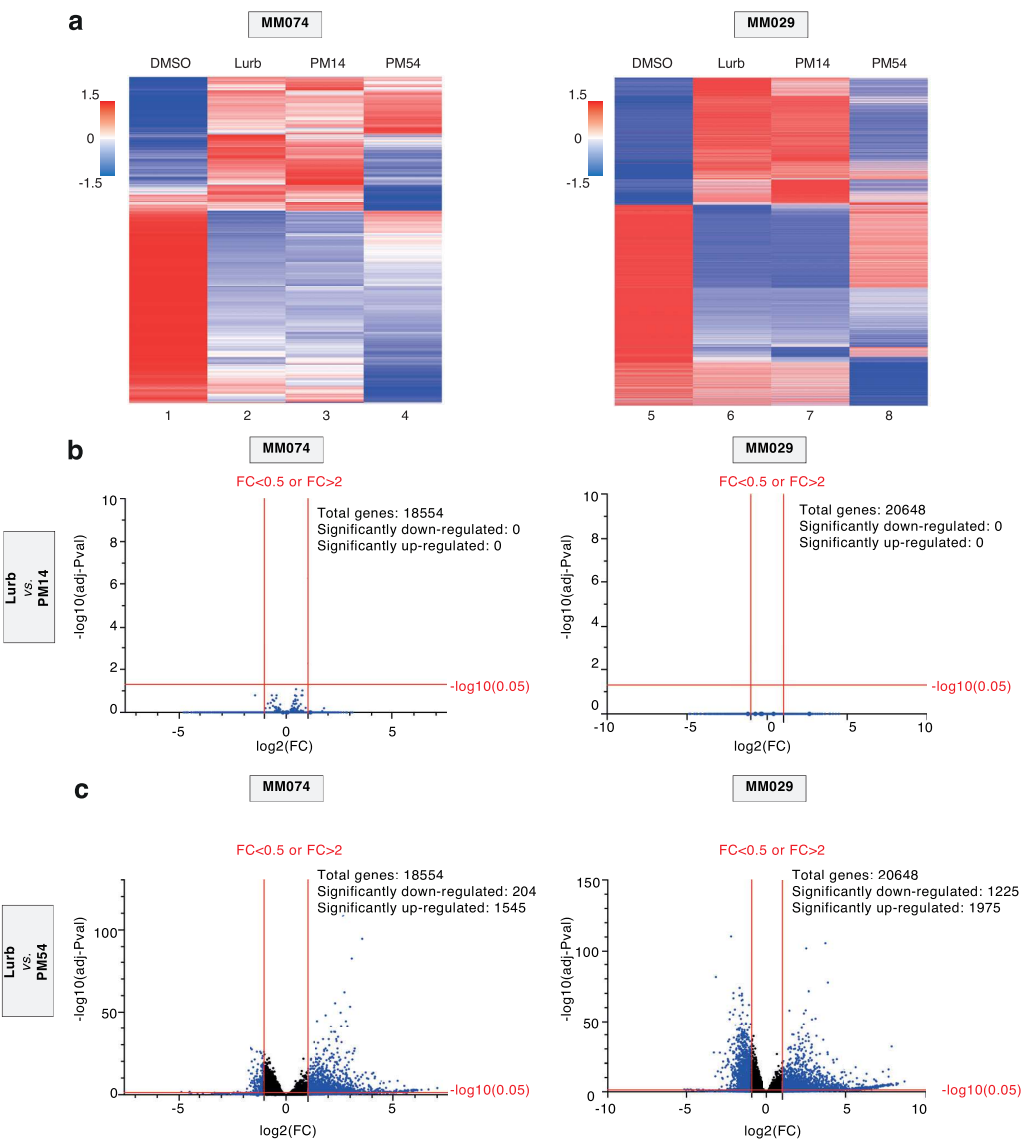
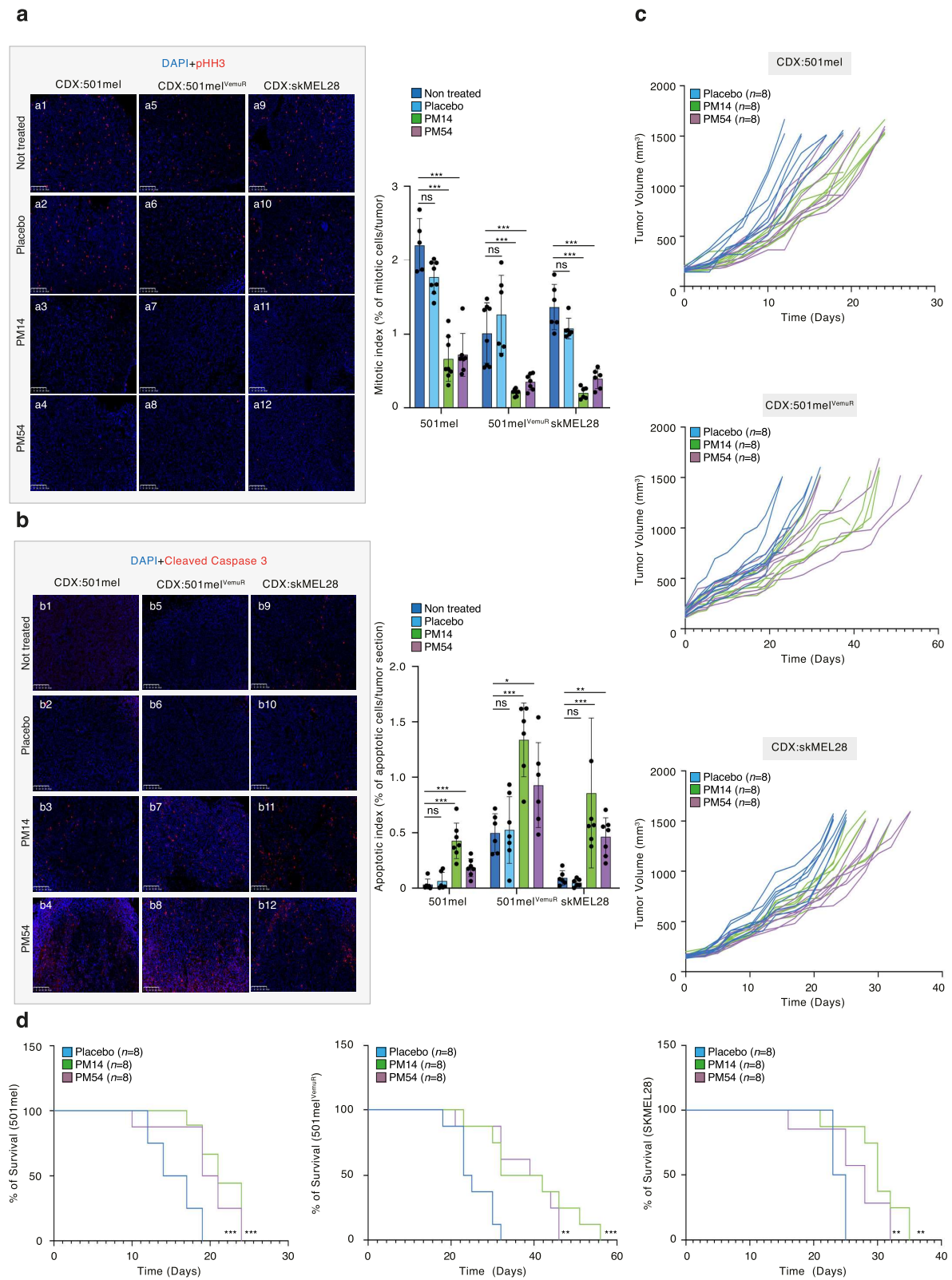
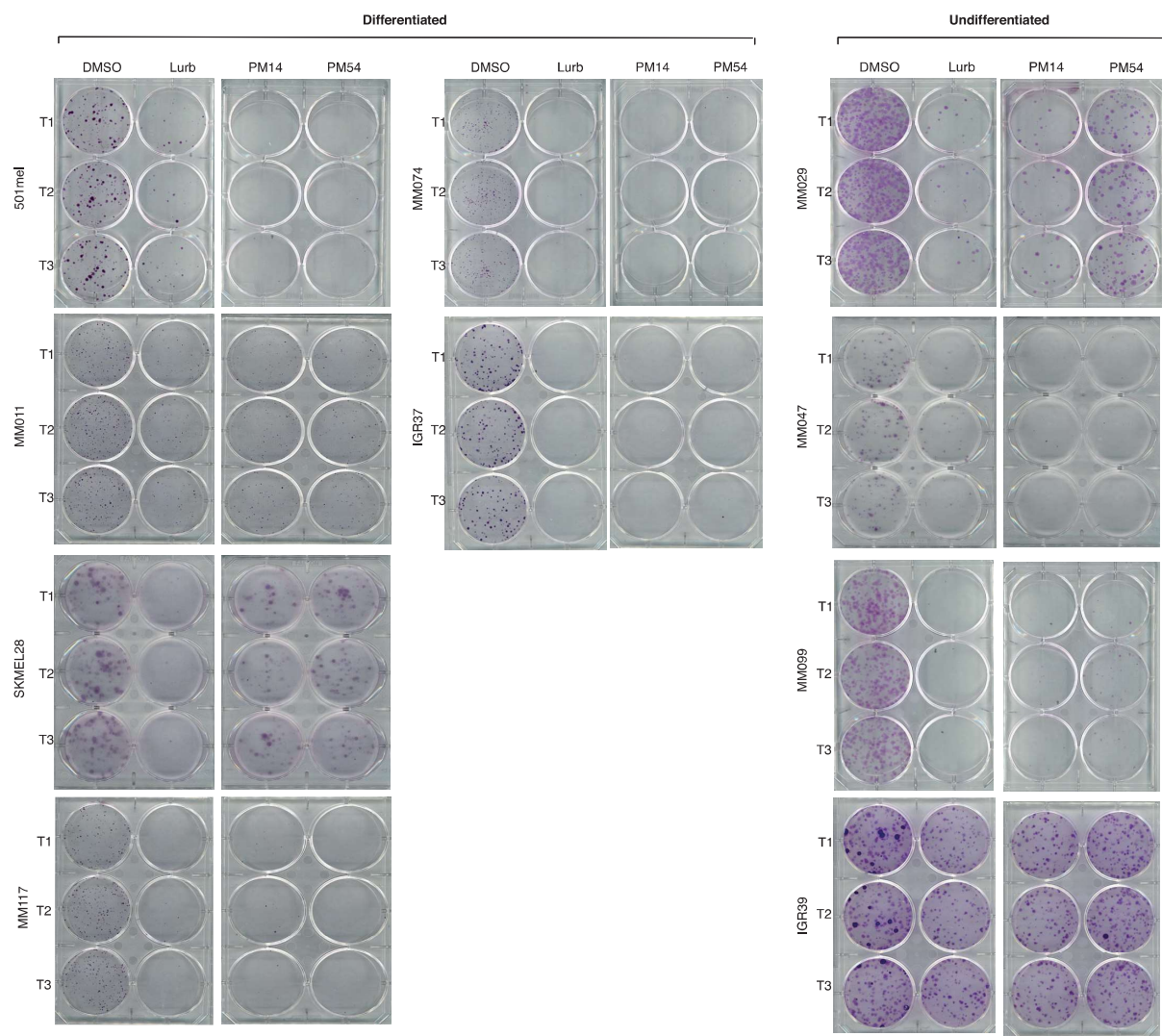


Figure 7

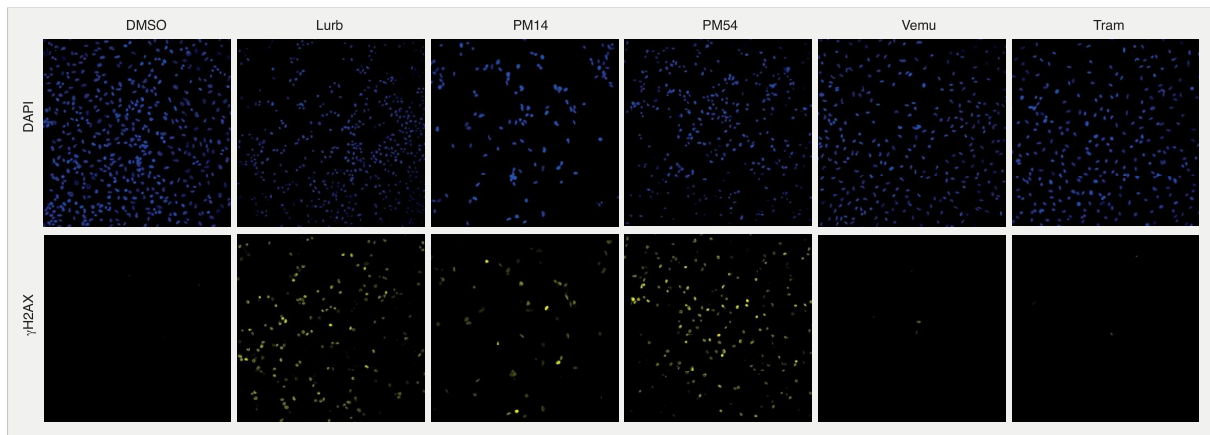


Supplemental Figure 1

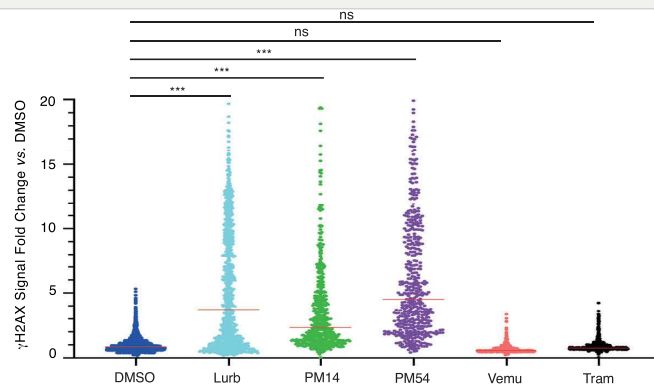


Supplemental Figure 2

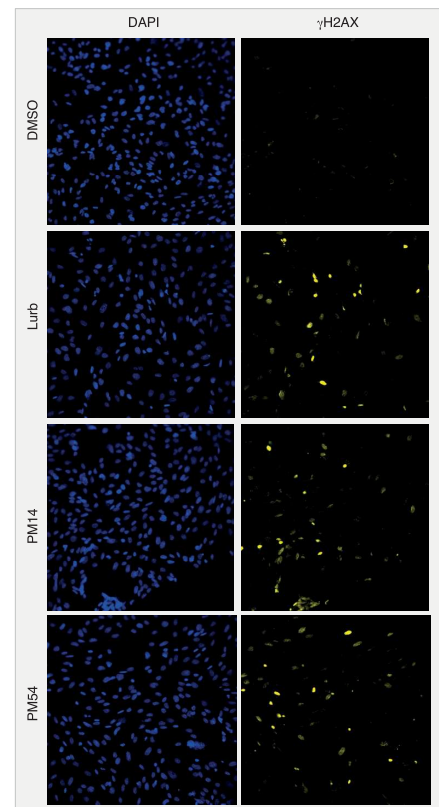
a



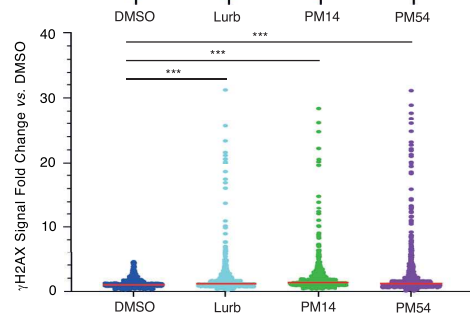
b



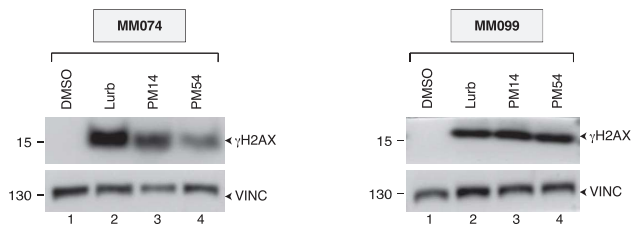
c



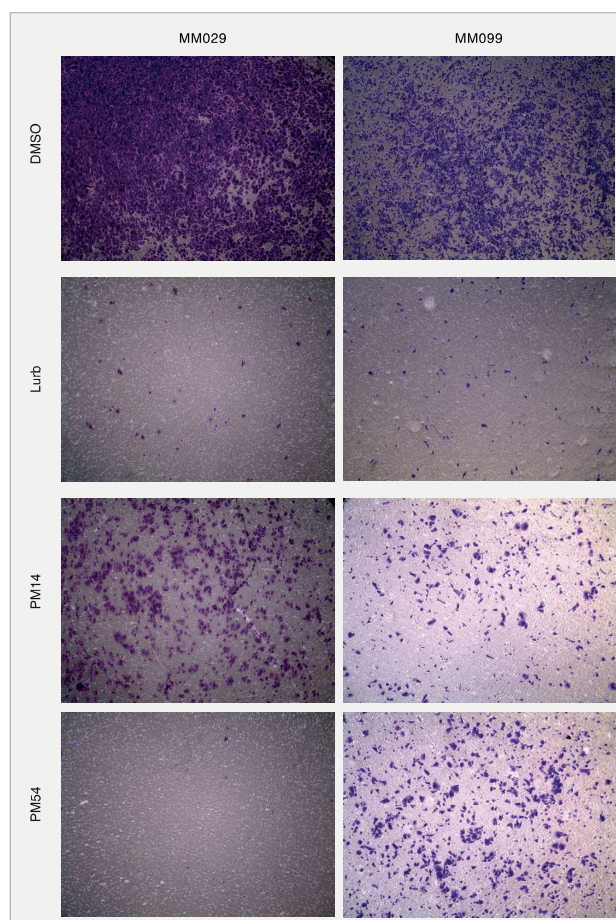
d



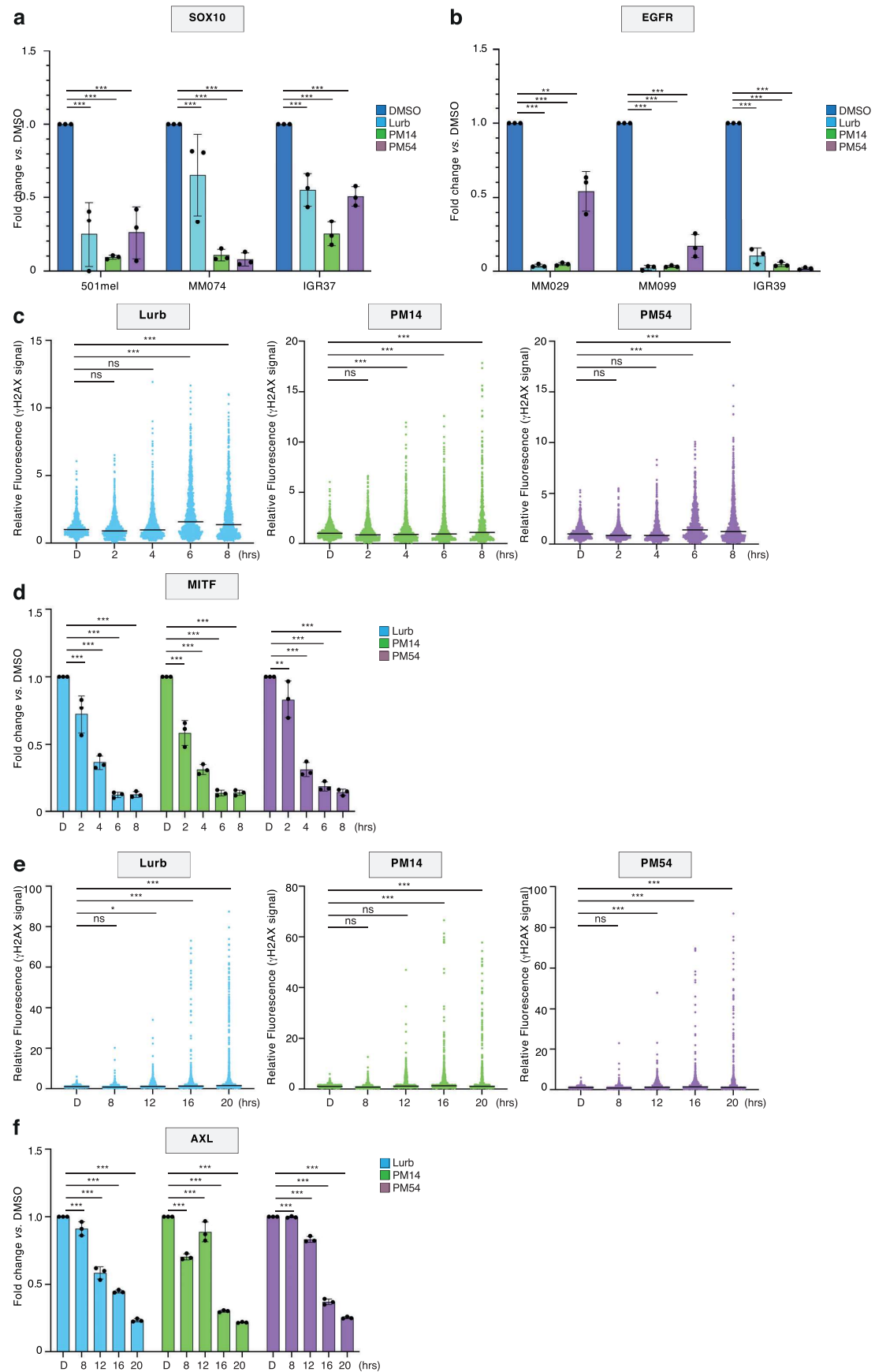
e



Supplemental Figure 3

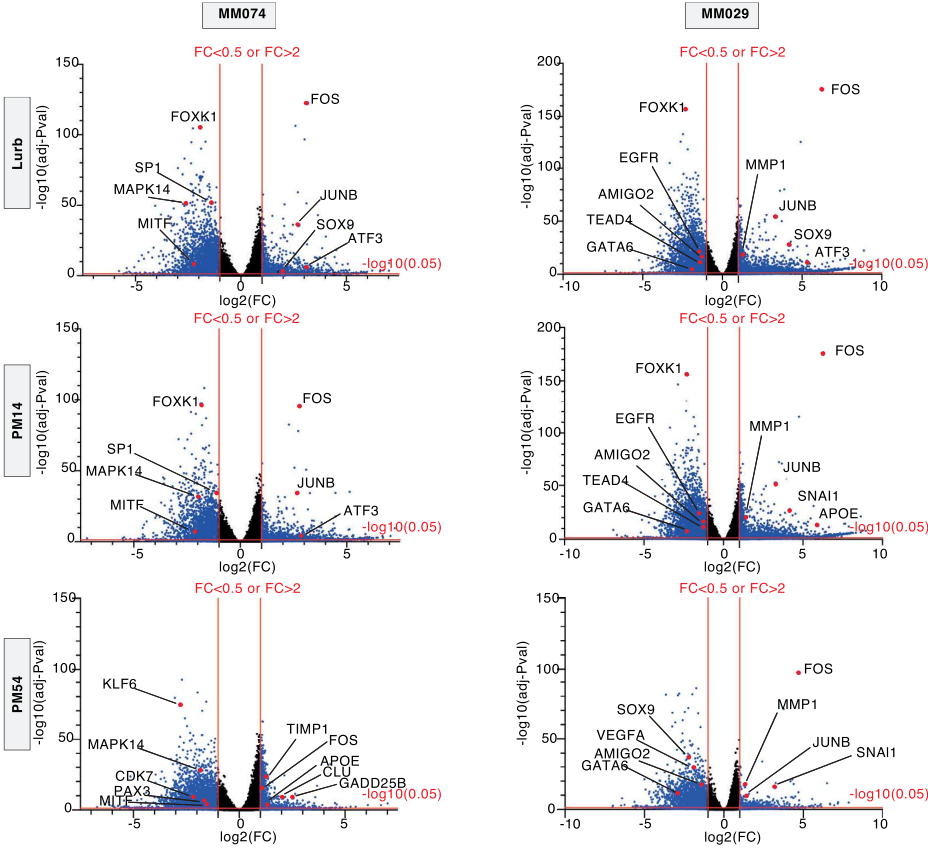


Supplemental Figure 4



Supplemental Figure 5

a



b

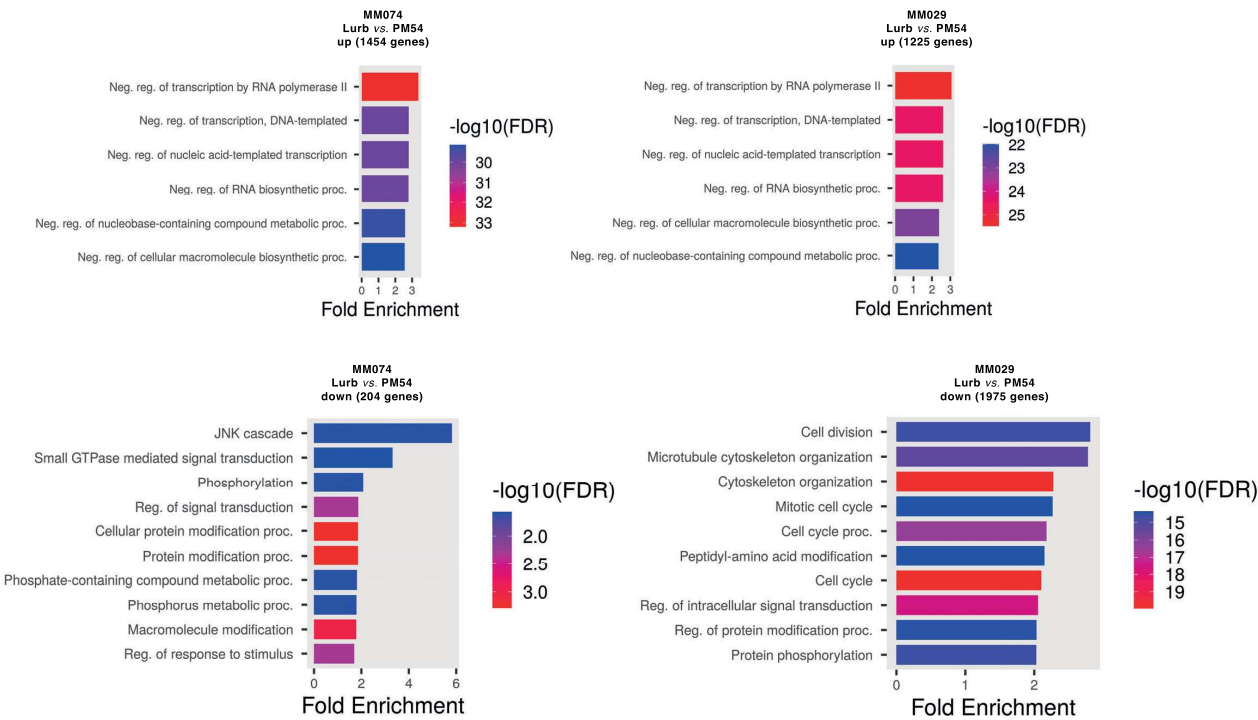
GSEA Nom p-val <0/05	MM074 Lurb vs. DMSO	MM074 PM14 vs. DMSO	MM074 PM54 vs. DMSO	MM029 Lurb vs. DMSO	MM029 PM14 vs. DMSO	MM029 PM54 vs. DMSO
Positive correlation	Adipogenesis Coagulation EMT Fatty acid metabolism Glycolysis Oxidative phosphorylation TNFA signaling via NFkB UV response UP Xenobiotic metabolism	Coagulation EMT Fatty acid metabolism Myogenesis Oxidative phosphorylation	Adipogenesis EMT Fatty acid metabolism Glycolysis Xenobiotic metabolism	No significant correlation found	Myogenesis UV response up	Apical junction EMT Fatty acid metabolism Glycolysis Xenobiotic metabolism
Negative correlation	G2M checkpoint Interferon alpha response Interferon gamma response Mitotic spindle MYC targets V2 Notch signaling UV response down WNT beta catenin signaling	E2F targets G2M checkpoint Interferon alpha response Interferon gamma response Mitotic spindle MYC targets V2 Notch signaling TGF beta signaling UV response down WNT beta catenin signaling	G2M checkpoint Mitotic spindle MYC targets V2 TNFA signaling via NFkB UV response down WNT beta catenin signaling	Androgen response Apical surface E2F targets Estrogen response early G2M checkpoint Hedgehog signaling Heme metabolism Inflammatory response Interferon alpha response Interferon gamma response Mitotic spindle MYC targets V2 Notch signaling PI3 AKT mitor signaling Protein secretion TGF beta signaling UV response down WNT beta catenin signaling	Androgen response E2F targets Estrogen response early G2M checkpoint Hedgehog signaling Heme metabolism Interferon alpha response Interferon gamma response Mitotic spindle MYC targets V2 Notch signaling PI3 AKT mitor signaling Protein secretion TGF beta signaling UV response down WNT beta catenin signaling	G2M checkpoint TNFA signaling via NFkB UV response down WNT beta catenin signaling

Supplemental Figure 6

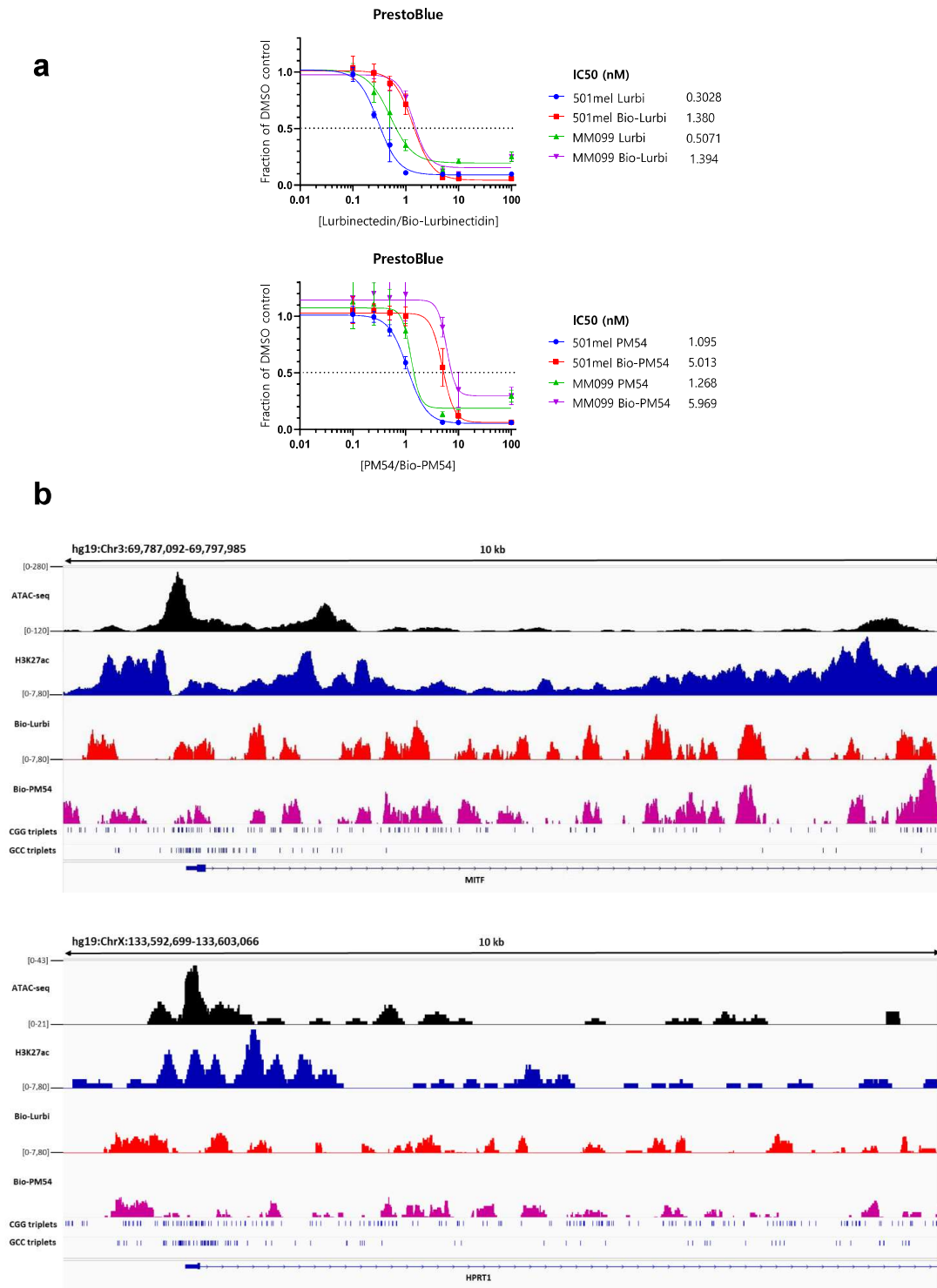
a

GSEA Nom p-val <0/05	MM074 Lurb vs. PM54	MM029 Lurbi vs. PM54
Positive correlation	P53 pathway TNFA signaling via NFKB	TNFA signaling via NFKB
Negative correlation	Androgen response G2M checkpoint Interferon alpha response Mitotic spindle MYC targets V2 Oxydative phosphorylation Protein secretion UV response down	Androgen response E2F targets Hedgehog signaling G2M checkpoint IL6 JAK STAT3 signaling Inflammatory response Interferon alpha response Interferon gamma response Mitotic spindle MYC targets V2 Oxydative phosphorylation PI3 AKT mitor signaling Protein secretion UV response down WNT beta catenin signaling

b



Supplemental Figure 7



Cells	Pheno	Geno	Vemu	Dabra	Trame	Lurb	PM14	PM54
Hermes3A	Mela	WT	>10 μ M	>50nM	>50nM	2.67nM	2.89nM	4.93nM
501mel	Diff	BRAF ^{V600E}	2440nM	>50nM	3nM	0.37nM	1.25nM	1.74nM
MM011	Diff	NRAS ^{Q61R}	>10 μ M	>50nM	>50nM	0.47nM	1.07nM	1.44nM
MM074	Diff	BRAF ^{V600E}	225nM	4.68nM	0.51nM	1.06nM	1.15nM	3.81nM
MM117	Diff	Triple-WT	488nM	>50nM	10.21nM	0.30nM	0.72nM	1.16nM
SKMEL-28	Diff	BRAF ^{V600E}	>10 μ M	1nM	5.12nM	1.17nM	1.31nM	1.74nM
IGR37	Diff	BRAF ^{V600E}	517nM	25.3nM	0.53nM	0.50nM	1.05nM	1.48nM
501mel ^{VemuR}	Diff	BRAF ^{V600E}	>10 μ M	>50nM	>50nM	1.07nM	1.04nM	2.13nM
MM074 ^{VemuR}	Diff	BRAF ^{V600E}	>10 μ M	>50nM	4.65nM	1.36nM	1.63nM	3.08nM
MM029	Undiff	BRAF ^{V600K}	>10 μ M	>50nM	>50nM	1.28nM	1.40nM	4.73nM
MM047	Undiff	NRAS ^{Q61R}	>10 μ M	>50nM	>50nM	0.45nM	0.96nM	1.38nM
MM099	Undiff	BRAF ^{V600E}	>10 μ M	>50nM	>50nM	0.73nM	1.41nM	1.85nM
IGR37	Undiff	BRAF ^{V600E}	>10 μ M	>50nM	>50nM	0.41nM	0.78nM	0.84nM

Table 1 : IC50 of Vemu, Dabra, Trame, Lurb, PM14 and PM54 towards various melanoma cells. The phenotype and genotype of these cells are indicated. Hermes3A are melanocytes.

Cells	Group	P-value*	Days
501mel	PM14	<0.05	D3-D19
501mel	PM54	<0.038	D3-D17
501mel ^{VemuR}	PM14	<0.038	D11-D30
501mel ^{VemuR}	PM54	<0.038	D16-D30
SKMEL28	PM14	<0.01	D14-D25
SKMEL28	PM54	<0.01	D14-D25

Table 2 : Statistical results by Mann-Whitney U test. Comparison of placebo-treated group vs. PM54 or PM14 groups following injection in tumours formed following 501mel, 501melVemuR or SKMEL28 melanoma cells injection in NSG mice.

Addendum: Mechanisms of resistance towards Lurbinectedin and its analogues

Lurbinectedin represents the first drug approved by the FDA in over 20 years in the second line for patients with metastatic SCLC with disease progression on or after platinum-based chemotherapy. The overall response rates range from 30% to 60%, with durations of response spanning from 5 to 10 months when Lurbinectedin is used as a single agent (Hanvesakul et al., 2023), providing a non-negligible, but arguably only moderate survival benefit in SCLC. As such, our ongoing research concerning Lurbinectedin, besides testing its potential use in other cancers such as melanoma and assessing the potency of its analogues, consists also in finding ways to use these novel compounds in more efficient ways. Based on intriguing mechanistic insights we gained, we are currently testing specific co-treatments that might significantly enhance the efficacy of Lurbinectedin and its analogues. However, due to confidentiality reasons concerning PharmaMar, these results will not be further elucidated here, but might be discussed in private.

Another avenue of potentially increasing the efficacy of Lurbinectedin and its analogues is the identification of resistance mechanisms. Strikingly, due to the recent nature of its approval, the topic of Lurbinectedin-resistances is almost unexplored. Although there have been correlative studies implicating the expression of SLFN11 in sensitivity rates (Kundu et al., 2021), no in vitro or in vivo resistance models had ever been generated. Personal communications by PharmaMar indicated that, although they tried, the establishment of Lurbinectedin-resistant SCLC cell lines systematically failed. Thus, considering the high propensity of melanoma cells for developing therapeutic insensitivities, we decided to attempt to generate resistant cells in this different model, hoping that the gained insights might also potentially benefit SCLC patients. Although this was attempted using various types of melanoma cells, only a singular type of cell was able to develop resistances towards Lurbinectedin, PM14 or PM54, representing a first-in-kind in vitro model of insensitivities against these novel compounds. Hereinafter, preliminary findings are presented in which we used the cells with acquired resistances to identify the ABCB1 efflux pump as the main effector of drug resistance. Although there is still important work to be done, particularly regarding in vivo confirmations, this study offers a compelling basis for evaluating ABCB1 biomarker status prior to the clinical administration of Lurbinectedin, and thus directly influences patient care and treatment decisions.

Resistance to novel transcriptional inhibitor Lurbinectedin and its derivatives is mediated by the efflux pump ABCB1

--- Work in progress ---

Max Cigrang^{1, 2, 3, 4}, Jolian Obid^{1, 2, 3, 4}, Clara Maréchal^{1, 2, 3, 4}, Maguelone Nogaret^{1, 2, 3, 4},
Philippe Catez^{1, 2, 3, 4}, Pietro Berico^{1, 2, 3, 4}, Guillaume Davidson^{1, 2, 3, 4}, Jean-Marc Egly^{1, 2, 3,}
⁴, and Frédéric Coin^{1, 2, 3, 4, 5}

¹ Institut de Génétique et de Biologie Moléculaire et Cellulaire Illkirch Cedex, C.U. Equipe
Labélisée Ligue contre le Cancer 2022, Strasbourg, France

² Centre National de la Recherche Scientifique, UMR7104, 67404 Illkirch, France

³ Institut National de la Santé et de la Recherche Médicale, U1258, 67404 Illkirch, France

⁴ Université de Strasbourg, 67404 Illkirch, France

⁵ Corresponding author, fredr@igbmc.fr

Tel: +33 3 88 65 34 49

Key words: Melanoma, Resistance, Lurbinectedin, ABCB1, Drug efflux

Introduction

The last decade has been ground-breaking for melanoma treatment, as the biological understanding of mechanisms driving tumor progression has increased dramatically. Targeted therapy with small molecules inhibiting the MAPK pathway, such as Vemurafenib and Dabrafenib targeting mutated BRAF, or Trametinib and Cobimetinib targeting the downstream MEK kinase, can lead to impressive reductions in tumor sizes (Luke et al., 2017; Jenkins and Fisher, 2021). Immunotherapy, namely CTLA-4 (Ipilimumab) and PD-1 inhibitors (Nivolumab, Pembrolizumab), have in many cases become the first-line regimen for metastatic melanoma, resulting in long-term benefits for 50 % of patients (Ralli et al., 2020; Carlino, Larkin and Long, 2021). Nevertheless, although MAPK and checkpoint inhibitors improve survival in most patients, intrinsic or acquired resistance to treatment is common and represents the biggest obstacle limiting patient survival (Sharma et al., 2017; Kozar et al., 2019; Huang and Zappasodi, 2022).

Both genetic and epigenetic resistance mechanisms are at the root of MAPK inhibitor (MAPKi) insensitivity (Czarnecka et al., 2020; Rubanov, Marin-Bejar et al., 2021; Berico and Hernando, 2022). In 80 % of resistance cases, a reactivation of the MAPK pathway and sustained ERK signaling is observed, even in the presence of MAPKi (Kozar et al., 2019). Secondary alterations in MAPK effectors (such as loss of function of NF-1 or constitutive activation of MEK), BRAF splice variants, or overexpression of RAF isoforms are just some of the mechanisms allowing for maintenance of MAPK signaling. Additionally, melanoma cells can circumvent MAPKi by the hyper-activation of secondary pathways such as PI3K/AKT/mTOR, for example by overexpressing receptors including EGFR, NGFR or AXL. In many cases, these genetic resistance mechanisms are accompanied by epigenetic mechanisms, which lead to the emergence of different melanoma cell states (Rambow, Marine and Goding, 2019; Karras et al., 2022). Indeed, melanoma cells display important phenotypic plasticity. Whereas in drug-naïve tumors, the bulk of cells are of a differentiated, melanocytic, and proliferative nature, expressing lineage transcription factors (TFs) such as MITF and SOX10, treatment-resistant tumors, after patient relapse, have been found to be consistently more heterogeneous in terms of cell populations (Verfaillie et al., 2015; Rambow et al., 2018; Wouters et al., 2020; Pedri et al., 2022). Importantly, more mesenchymal-like, dedifferentiated and invasive cells have been shown to be enriched after prolonged drug treatment. Many traits associated with these cells,

such as their slowly cycling and stem cell-like nature, the overexpression of receptors such as AXL or EGFR, or their reduced immunogenicity, explain why they display intrinsic resistance to both targeted and immunotherapy (Arozarena and Wellbrock, 2017, 2019; Huang et al., 2021). Of note, through a process called phenotype switching, melanoma cells can respond to microenvironmental cues such as drug exposure by adopting an adapted phenotype through transcriptional and epigenetic reprogramming and can thus switch between cell states.

Lurbinectedin (Lurbi), a synthetic alkylating derivative of trabectedin, was approved in 2020 by the FDA as second line treatment for relapsed small cell lung cancer (SCLC) patients after platinum-based therapy (Trigo et al., 2020; Manzo et al., 2022). Lurbi covalently binds to DNA, forming adducts that irreversibly stall elongating RNA polymerase II on highly expressed genes, generating DNA double-strand breaks and apoptosis (Santamaría Nuñez et al., 2016; Costanzo et al., 2022). Lurbi, as well as two synthetic analogs developed by PharmaMar S.A., PM14 and PM54, were recently shown to be very efficient in both in vitro and in vivo melanoma models, causing apoptosis in both melanocytic and mesenchymal-like melanoma cells (Cigrang et al., 2023). PM14 and PM54 displayed similar cell death and DNA damage effects to Lurbi, but PM54 differed greatly in terms of deregulated gene expression, the three molecules thus representing possible alternative treatments for metastatic melanoma. Despite these promising results in both SCLC and melanoma, treatment resistances towards Lurbi, PM14 or PM54 should be anticipated. However, no molecular mechanisms regarding drug insensitivities for these drugs have been elucidated yet, mainly because of the recent nature of clinical approval for Lurbi and the apparent difficulty to generate in vitro SCLC models of resistance (personal communication from PharmaMar S.A.).

Here, we successfully generated mesenchymal-like melanoma cells resistant to either Lurbi, PM14 or PM54, after long-term chronic drug exposure. We show that these cells become cross-resistant to the three drugs by intensely overexpressing the ATP-binding cassette sub-family B member 1 (ABCB1, also known as MDR1 or P-gp), and that the ectopic overexpression of this ABCB1 renders cells of different cancer backgrounds insensitive to drug action. Furthermore, the pharmacological inhibition of this efflux pump completely re-sensitizes cells towards drug exposure, indicating that ABCB1 overexpression is the main culprit behind drug resistance to Lurbi, PM14 and PM54. In contrast to mesenchymal-like melanoma cells, most melanocytic melanoma cells seemed to be unable to become resistant or to overexpress ABCB1, because of proteasomal degradation mechanisms. Although copy number variations were seen for the

ABCB1 gene, epigenetic mechanisms seemed to play an important role as well, which seemed to include increased activity of AP-1/TEAD transcription factors, as evidenced by large-scale transcriptional changes in resistant cells. Overall, a molecular mechanism for Lurbi, PM14 and PM54 is unveiled for the first time, with potential direct repercussions for current clinical Lurbi usage in SCLC and melanoma, or any potential future approval of Lurbi analogues.

Results

Emergence of resistance in mesenchymal-like melanoma cells

In order to explore potential drug resistance mechanisms, we exposed 2 melanocytic (501mel, MM074) as well as 2 mesenchymal-like (MM029, MM099) melanoma cell cultures to increasing doses of either Lurbi, PM14 or PM54, with 1/3 of the respective IC₅₀ values (determined in Cigrang et al., 2023) as starting concentrations (**Figure 1A**). Surprisingly, 3 of the 4 cell types did not survive the treatments for longer than a few weeks, with repeated attempts systematically failing to produce resistances. However, a subset of mesenchymal-like, BRAFV600K-mutated MM029 cells tolerated the treatments, although the acquisition of resistance, as defined by cell proliferation in drug concentrations of at least 10xIC₅₀ values, was a challenging, 8-month long process. Eventually, 3 resistant MM029 cell lines were established, namely the Lurbi-R, PM14-R and PM54-R cells. IC₅₀ determination showed that these cells were from 20- to 100-fold more resistant towards their respective drugs than the MM029 WT cells (**Figure 1B**). Whereas the IC₅₀ values for MM029 WT cells ranged from 1 to 3.3 nM depending on the drug, IC₅₀s for the resistant cells were in all cases superior to 58 nM, with the PM14-R cells displaying the least resistance. Strikingly, drug resistance was not specific to a single molecule, as resistant cells displayed important cross-resistance, meaning for example that Lurbi-R cells were also resistant to PM14 and PM54. This indicated that there might be a shared mechanism of drug resistance.

In terms of cell morphology, Lurbi-R and PM14-R resembled the MM029 WT cells. The PM54-R cells however presented an enlarged morphology, losing the elongated mesenchymal-like shape of MM029 cells (**Supplemental Figure 1A**). β -galactosidase quantification through C12FDG staining revealed that all resistant cells displayed a more pronounced senescent-like state (**Supplemental Figure 1B**). Additionally, Boyden chamber assays showed that the 3 resistant cell lines presented decreased invasion capacities (**Supplemental Figure 1C**). To sum up, of the 4 tested melanoma cell cultures, only a single

one achieved to become insensitive to either Lurbi, PM14 or PM54. The cross-resistant MM029 cells displayed vastly increased IC₅₀ values towards the drugs and presented phenotypical changes.

Overexpression of ABCB1 leads to drug resistance

RNA-Seq analyses revealed important gene expression changes in the resistant cells, with hundreds of genes being either significantly up- or downregulated compared to MM029 WT cells (**Supplemental Figure 2A**). Although the transcriptional changes were quite heterogeneous between the different resistant cell lines (**Supplemental Figure 2B**), sets of common deregulated genes became apparent. Between the deregulated genes, 244 were commonly upregulated and 678 genes were commonly downregulated in Lurbi-R, PM14-R and PM54-R cells (**Supplemental Figure 3A**). Gene Ontology analysis revealed significant common downregulation of genes involved in neuron development and differentiation, as well as cell adhesion and migration genes, indicating a possible loss of the neural-crest stem-like phenotype of these cells (**Supplemental Figure 3B**). Concurrently, GSEA analysis showed significant expression decreases of several gene sets involved in epithelial-to-mesenchymal transition and other important pathways such as p53 or PI3K signaling (**Supplemental Figure 3C**). Regarding upregulated genes, far less significant pathway correlations were observed. Strikingly however, the *ABCB1* gene was systematically found to be heavily overexpressed in all resistant cells (**Supplemental Figures 2A and 3A**). *ABCB1* encodes an ATP-binding cassette transporter, also named MDR1 or P-gp, which is a transmembrane efflux pump known as being implicated in multi-drug resistances (Dean, Rzhetsky and Allikmets, 2001; Amawi et al., 2019; Engle and Kumar, 2022). *ABCB1* transports a wide range of compounds, which tend to be hydrophobic and between 200 and 1900 Da in mass (Chufan, Sim and Ambudkar, 2015; Kodan et al., 2021). Although Lurbi, PM14 and PM54 are not known to be particularly hydrophobic, their molecular weights could potentially make them substrates of *ABCB1*.

RT-qPCR and immunoblot analysis confirmed the overexpression of *ABCB1* in resistant cells (**Figures 2A and 2B**). Of note, in drug-naïve conditions, MM029 cells already presented increased *ABCB1* protein levels compared to the other melanoma cell lines we tried to generate resistances in and displayed also the most mesenchymal nature as evidenced by high SOX9 protein amounts (**Figure 2C**). In order to confirm the potential involvement of *ABCB1* in the insensitivities towards Lurbi, PM14 and PM54, we performed lentivirus-mediated

overexpression of ABCB1 in MM029 cells. Cells infected with ABCB1-encoding lentivirus (LV-ABCB1-29) displayed 1800-fold increased mRNA expression versus MM029 WT or control mCherry-expressing cells (LV-mCherry-29), which by far surpassed ABCB1 mRNA levels in Lurbi-R, PM-14, or PM54-R cells (**Supplemental Figures 4A and 4B**). Despite this, immunoblots from whole-cell extracts of the LV-ABCB1-29 and Lurbi-R, PM14-R and PM54-R cells showed similar ABCB1 protein amounts (**Supplemental Figure 4C**). Strikingly, the LV-ABCB1-29 cells displayed 10-to-20-fold increased IC₅₀ values for either Lurbi, PM14 or PM54, indicating an important role of ABCB1 expression in cross-resistance (**Figure 2D**). Although LV-ABCB1-29 cells became far more drug-resistant compared to MM029 WT or LV-mCherry-29 cells, they didn't reach the IC₅₀ levels of the Lurbi-R, PM14-R and PM54-R cells, despite presenting similar ABCB1 whole-cell protein amounts. In cells overexpressing ABCB1 (Lurbi-R, PM14-R, PM54-R and LV-ABCB1-29), treatment with Lurbi failed to induce DNA double-strand breaks as revealed through γH2AX immunoblotting (**Figure 2E**). However, co-treatment with the specific ABCB1 inhibitor Tariquidar (Fox and Bates, 2007) led to the appearance of γH2AX signal in all Lurbi-treated cells (**Figure 2F**). Collectively, these data show that while resistance to Lurbi and its analogues is accompanied by important transcriptional changes, the main effector behind drug insensitivity could be ABCB1.

Important proteasomal ABCB1 degradation in melanocytic melanoma cells

We next wanted to study whether ABCB1 expression also led to resistances in melanocytic melanoma cells and non-melanoma cells. Melanocytic IGR37, SKMEL28, SKMEL5, 501mel and Vemurafenib-resistant 501mel cells (501mel VemuR), as well as osteosarcoma U2OS cells were infected with ABCB1-encoding lentivirus. Surprisingly, no increased ABCB1 protein levels could be detected in infected IGR37, SKMEL28, and SKMEL5 cells (**Supplemental Figure 4D**), whereas ABCB1 mRNA levels were found to be increased (**Supplemental Figure 4E**). Strikingly, the treatment with MG132, a potent proteasome inhibitor, led to increases in ABCB1 protein levels in these melanocytic cells, whereas little effect was observed for MM029 LV-ABCB1-29 cells (**Supplemental Figure 4F**). Albeit infected 501mel, 501mel VemuR and U2OS cells displayed increased drug-resistances (**Supplemental Figure 5A**) and more elevated ABCB1 protein levels than WT cells, MG132 treatment significantly increased ABCB1 protein amounts in the infected melanocytic 501mel and 501mel VemuR cells, and to a lesser degree in infected U2OS cells (**Supplemental Figure 5B**). In summary, there seem to

be important regulatory mechanisms at play governing ABCB1 protein levels, leading to proteasomal degradation in most melanocytic melanoma cells.

Inhibition of ABCB1 leads to re-sensibilisation of resistant cells

To confirm the involvement of ABCB1 in drug resistance, we first performed Rhodamine123 efflux assays via Flow Cytometry to determine at what concentrations of ABCB1 inhibitors (ABCB1i) the resistant cells became unable to pump out ABCB1 substrates. A short 4h treatment with Tariquidar, a specific ABCB1i, blocked Rhodamine efflux starting at 25 nM, whereas Verapamil, a clinically available calcium channel blocker and non-specific ABCB1i (Wu, Calcagno and Ambudkar, 2008) blocked efflux starting at 100 μ M (**Supplemental Figure 6A**). Strikingly, co-treatments of resistant cells with these concentrations of ABCB1i together with Lurbi, PM14 or PM54 revealed that resistant cells were completely re-sensitized to the effects of the drugs (**Figure 3A**). Whereas treatment with Tariquidar led to IC₅₀ values of resistant cells to resemble those of MM029 WT cells again, the effects of Verapamil were even more pronounced, as even WT cells became more drug-sensitives, displaying IC₅₀ values of less than 1 nM. Additionally, siRNA-mediated knockdown of ABCB1 was performed (**Supplemental Figures 6B and 6C**), also leading to significant re-sensibilisation of resistant cells (**Figure 3B**). However, no complete re-sensibilisation was observed in ABCB1-KD cells, probably due to the remaining ABCB1 activity after RNAi treatment. Collectively, these data confirm the involvement of ABCB1 in drug-resistance and identify drug-efflux as a major mechanism of insensitivity towards Lurbinectedin and its derivatives, which can however be reversed by pharmacological ABCB1 inhibition.

ABCB1 overexpression is mediated by both genetic and epigenetic mechanisms

We next wanted to elucidate the molecular mechanisms driving drug-resistance and ABCB1 overexpression. Intriguingly, analysis of the RNA-Seq data indicated that the resistant cells overexpressed genes located in the genomic 7q21.12 region, where ABCB1 and related multi-drug-resistance-associated genes reside (**Figure 4A**). Chromosomal amplification events at this locus have been associated with drug resistance (Genovese et al., 2017), and indeed, copy number assays indicated a 30-fold increase in *ABCB1* copy numbers in Lurbi-R and PM54-R cells, whereas PM14-R cells only displayed a 5-fold increase versus MM029 WT cells (**Figure 4B**). However, copy number variations alone were unlikely to explain by themselves the important increases in ABCB1 expression and the before-observed potential regulatory

mechanisms at play, for example in the melanocytic cells. We hypothesised that other transcriptional and epigenetic mechanisms may contribute to ABCB1 overexpression, and therefore performed bioinformatical regulon analysis on the differential gene expression signatures determined by RNA-Seq (**Supplemental Figure 7A**). iRegulon analysis (Janky et al., 2014) revealed that the TEAD4 transcription factor may be involved in the gene regulatory network governing the emergence of drug-resistance. Intriguingly, TEADs have been shown to interact with AP-1 transcription factors to regulate the invasive/mesenchymal-like melanoma cell state (Verfaillie et al., 2015). Fittingly, when comparing the transcription factors commonly upregulated in resistant cells with those upregulated upon short drug exposures (Cigrang et al. 2023), the AP-1 factor FOS was identified (**Supplemental Figure 7B**). qPCR analysis confirmed that various AP-1 and TEAD transcription factors were upregulated in drug-resistant cells (**Supplemental Figure 7C**). Finally, treatment with specific AP-1 or TEAD inhibitors SR11302 and CA3, whose IC50 values were quantified (**Supplemental Figure 7D**), induced the downregulation of ABCB1 expression, concomitantly with decreased levels of mesenchymal-like melanoma markers such as AXL or SOX9 (**Figure 4D**). Collectively, these data indicate that both genetic focal amplification events as well as epigenetic and transcriptional regulation by AP-1/TEAD factors are responsible for ABCB1 expression in drug-resistant melanoma cells.

Discussion

The transcriptional addiction of cancer cells has come into light in recent years as an attractive target, as it was stipulated that all cancer cells, regardless of their cell states or phenotypes, would heavily depend on dysregulated gene expression programs (Bradner, Hnisz and Young, 2017). The inhibition of these transcriptional dependencies through small molecules targeting key factors of the gene expression machinery, such as CDK7 or BRD4, have led to impressive initial results in pre-clinical trials (Filippakopoulos et al., 2010; Kwiatkowski et al., 2014). However, as for most other therapeutic strategies, acquired cancer cell resistance mechanisms dampen the effectiveness of transcriptional inhibitors in clinical settings. In order for these novel drugs to be functional, they need to reach their targets inside the cell nucleus. Therefore, drug efflux by ATP-binding cassette transporters has emerged as an important multi-drug resistance mechanism (Choi, 2005; Berico et al., 2021).

Lurbinectedin is a newly clinically approved transcriptional inhibitor for relapsed

SCLC with a unique mechanism of action (Costanzo et al., 2022; Manzo et al., 2022). Along with its structural derivatives PM14 and PM54, Lurbinectedin has also shown impressive potency in targeting different melanoma cell phenotypes in pre-clinical studies (Cigrang et al, 2023). However, to our knowledge, no information is currently available regarding potential drug resistance mechanisms for Lurbinectedin or its derivatives, chiefly because of the recent nature of its approval and because of the absence of in-vitro resistance models.

Here, we report that the long-term, chronic drug exposure of mesenchymal-like melanoma cells led to the first-in-kind generation of cellular models resistant to Lurbinectedin, PM14 and PM54. We identify ABCB1 overexpression as the main molecular mechanism driving drug resistance, which however does not seem to be possible in all cells, as important proteasomal degradation events seem to hinder the emergence of ABCB1 expression, mainly in melanocytic melanoma cells. Furthermore, we prove that the pharmacological inhibition of ABCB1 completely re-sensitizes resistant cells to drug effects. Finally, we show that the overexpression of ABCB1 in our cellular models seems to be dependent on both genetic and epigenetic mechanisms, as we observe the important AP-1/TEAD regulators of the mesenchymal-like melanoma cell state to be involved in ABCB1 overexpression.

Although multiple different melanoma cell types were subjected to the same chronic drug exposures, only a single mesenchymal-like cell type managed to develop resistances. Strikingly, these MM029 cells displayed also the most important expression of mesenchymal markers such as SOX9 and a pre-existing basal expression level of ABCB1, compared to other melanoma cells. As such, our results indicate that for melanoma cells at least, only a certain type of ‘primed’ and very dedifferentiated cell might become resistant to Lurbinectedin and its analogues through overexpression of ABCB1. Indeed, in most differentiated melanoma cells, such as in IGR37, SKMEL5 or SKMEL28 cells, the overexpression of ABCB1 seems to be inhibited by important proteasomal degradation of ABCB1. However, other melanocytic cells such as 501mel were, to a certain extent, able to overexpress ABCB1. The exact mechanism behind this remains to be elucidated in melanoma cells, but in other models, factors such as RSK1 or PIM-1 have been shown to be involved in protecting ABCB1 from degradation (Xie et al., 2010; Katayama et al., 2016). In that regard, differential analysis of transcriptomic data between cells able to tolerate ABCB1 expression and cells degrading ABCB1 might elucidate why most differentiated melanoma cells seem to be unable to overexpress this efflux pump, and which E3 ubiquitin ligases might be involved in this phenomenon. Furthermore, although the Lurbi-R, PM14-R and PM54-R cells share a common genetic background to the MM029 cells, there seem to be important regulatory differences concerning ABCB1 activity. The

ectopic overexpression of ABCB1 allowed for a roughly 20-fold increased mRNA expression in LV-ABCB1-29 cells versus Lurbi-R cells, while only producing similar whole-cell protein levels, and strikingly, a less pronounced drug-resistance. As such, possible explanations for the differences in measured IC50s include a faulty translocation to the membrane or missing post-translational modifications, affecting ABCB1 activity levels. Here, immunofluorescence and protein fractioning followed by immunoblot assays will help determine ABCB1 intracellular localization, and mass spectrometry analysis might elucidate ABCB1 post-translational modification status, giving important insights into how ABCB1 activity is modulated in melanoma cells.

We further demonstrate that both genetic copy number increases as well as AP-1/TEAD transcription factors are involved in ABCB1 overexpression. These results need to be further validated however, for example by siRNA-mediated knockdowns of AP-1/TEAD factors and ChIP assays confirming differential AP-1/TEAD binding in resistant cells. Interestingly, AP-1 factors such as the immediate stress responder FOS are among the most importantly upregulated genes in naïve melanoma cells when exposed to Lurbi or its analogues, potentially contributing to ABCB1 overexpression. Finally, the role of ABCB1 in Lurbi/PM14/PM54-insensitivity will be checked in vivo with melanoma and SCLC mouse models, using adjuvant treatment with Verapamil or Tariquidar to assess the effects of the compounds in ABCB1-overexpressing tumors. Although the clinical use of available ABCB1 inhibitors such as Tariquidar are limited by systemic toxicities, significant effort is currently put into developing new-generation inhibitors with more acceptable safety profiles, potentially paving the way for future adjuvant treatments (Engle and Kumar, 2022). Furthermore, SCLC biopsies from patients after Lurbi relapse should be assayed for ABCB1 overexpression, to confirm its clinical involvement. In conclusion, this study provides a rationale for assessing ABCB1 biomarker status before the clinical use of Lurbinectidin or its analogues in different cancers.

Material and Methods

Cell culture and generation of resistant cells

Cells were grown at 37°C in 5% CO₂ and were regularly checked for mycoplasma contamination. MM patient-derived short-term melanoma cultures (MM074, MM029, MM047, MM099) were grown in HAM-F10 (Gibco, Invitrogen) supplemented with 10% Fetal Calf Serum (FCS), 25 mM HEPES, 5,2 mM GLUTAMAX and penicillin–streptomycin.

Melanoma cell lines 501mel and SKMEL28 were grown in RPMI w/o HEPES (Gibco, Invitrogen) supplemented with 10% FCS and gentamycin. Vemurafenib-resistant 501mel cells (501mel VemuR) were additionally supplemented with 1,5 μ M of Vemurafenib. Melanoma cell line SKMEL5 and osteosarcoma cell line U2OS were grown in DMEM (1g/L Glucose, Gibco, Invitrogen) supplemented with 10% FCS and gentamycin. Melanoma IGR37 cell line was grown in RPMI w/o HEPES (Gibco, Invitrogen) supplemented with 15% FCS and gentamycin. 501mel, SKMELs, U2OS, and IGR37 cells were purchased from ATCC, MM cells were obtained from Dr Ghanem Ghanem. BRAFV600E inhibitor Vemurafenib (PLX4032), ABCB1 inhibitors Tariquidar (XR9576) and Verapamil (HY-14275), AP-1 inhibitor SR11302 (HY-15870), and proteasome inhibitor MG132 (HY-13259) were purchased from MedChemExpress. TEAD inhibitor CA3 (S8661) was purchased from Selleckchem. Lurbinectedin (PM1183), PM14 and PM54 were obtained from PharmaMar S.A. Cells infected with lentivirus were maintained in Puromycin positive medium.

To generate Lurbinectedin-, PM14-, and PM54-resistant cells (Lurbi-R, PM14-R, PM54-R), 501mel, MM074 and IGR37 melanocytic-type cells or MM029, MM099 and IGR39 mesenchymal-like cells were chronically exposed to escalating doses of Lurbinectedin, PM14 or PM54. The starting concentration was 1/3 of the respective IC₅₀ values. In most cases, drug cytotoxicity eliminated all cells within one or two weeks. For the MM029 cells however, the treatments were carried out for over 8 months until the cells proliferated in drug concentrations equal to at least 10 times the original IC₅₀ values, allowing us to generate stable resistant cells. Once established, Lurbi-R, PM14-R and PM54-R cells were grown in HAM-F10 + 10 % FCS, 25 mM HEPES, 5,2 mM GLUTAMAX and penicillin–streptomycin supplemented with 30 nM of Lurbinectedin, PM14 or PM54 respectively, to ensure maintenance of resistance.

IC₅₀ estimation

Cells were seeded at 5,000 cells/well in 96- well plates and treated with increasing concentrations of Lurbinectedin, PM14, or PM54. After 72 h of incubation, cells were treated with PrestoBlue reagent (ThermoFisher) according to the manufacturer's instructions. The absorbance per well was measured with a CellInsight CX5 microplate reader. Determination of IC₅₀ values was performed by nonlinear curve fitting using the Prism9 statistical software (GraphPad).

RNA Extraction and RT-qPCR

Total RNA isolation was performed according to the manufacture protocol with NucleoSpin RNA Plus kit (Macherey-Nagel). RNA was retrotranscribed with Reverse Transcriptase Superscript IV (Invitrogen), qPCR was performed with SYBR Green (Roche) and on a LightCycler 480 (Roche). Primers for RT-qPCR were designed using Primer-BLAST.

Primers

ABCB1	F GGAGGCCAACATACATGCCT R AGGCTGTCTAACAAGGGCAC
FOS	F GCCTCTCTTACTACCACTCACC R AGATGGCAGTGACCGTGGGAAT
FOSB	F TCTGTCTTCGGTGGACTCCTTC R GTTGCACAAGCCACTGGAGGTC
FOSL1	F GGAGGAAGGAACTGACCGACTT R CTCTAGGCGCTCCTTCTGCTTC
FOSL2	F AAGAGGAGGAGAAGCGTCGCAT R GCTCAGCAATCTCCTTCTGCAG
Jun	F CCAACTCATGCTAACGCAGC R TCTCTCCGTCGCAACTTGTC
JunB	F CGATCTGCACAAGATGAACCACG R CTGCTGAGGTTGGTGTAACGG
JunD	F ATCGACATGGACACGCAGGAGC R CTCCGTGTTCTGACTCTTGAGG
TEAD1	F CCTGGCTATCTATCCACCATGTG R TTCTGGTCCTCGTCTTGCCTGT
TEAD2	F CCGCTACATCAAGCTGAGAACG R GGTTGCCATTGTCTGGAAAGCC
TEAD3	F AGGCAGTAGATGTGCGCCAGAT R TCCTGGATGGTGCTGTTGAGGT
TEAD4	F GAAGGTCTGCTCTTTCGGCAAG R GAGGTGCTTGAGCTTGTGGATG
AXL	F CCGTGGACCTACTCTGGCT R CCTTGGCGTTATGGGCTTC
SOX9	F AGGAAGTCGGTGAAGAACGG R CGCCTTGAAGATGGCGTTG
SOX10	F CCAGTTTGACTACTCTGACCATCAG R ATATAGGAGAAGGCCGAGTAGAGG
MITF	F GGCCCTCTGAACAGTTTCAA R ATCCCCATTTTCAGCATGAG
18S	F TCAACTTTCGATGGTAGTCGCCGT R TCCTTGGATGTGGTAGCCGTTTCT

EGFR	F AACACCCTGGTCTGGAAGTACG R TCGTTGGACAGCCTTCAAGACC
SERPINE1	F AGAGCGCTGTCAAGAAGACC R CTCAGAGGTGCCTTGCGATT
AMIGO2	F GCAGTGATAGCTGAGGGCAT R CGCCACAAAAGGTGTGTCAG
ACTb	F ACATCTGCTGGAAGGTGGAC R CCCAGCACAATGAAGATCAA
GAPDH	F ACAACTTTGGTATCGTGGAAGG R GCCATCACGCCACAGTTTC
RPL13a	F TTGAGGACCTCTGTGTATTTGTCAA R CCTGGAGGAGAAGAGGAAAGAGA
TBP	F CGGCTGTTTAACTTCGCTTC R CACACGCCAAGAAACAGTGA

Protein extraction and Western Blotting

For whole cell extracts, cells were rinsed once with cold PBS, before pelleting and resuspension in LSDB 0.5M buffer (500 mM KCl, 50 mM Tris pH 7.9, 20% glycerol, 1% NP-40, 1mM DTT and protease inhibitor cocktail). Afterwards, cells were fully disrupted with 3 cycles of heat shock (liquid nitrogen followed by 37°C water bath). Then, samples were centrifugated for 15min at 14,000rpm to remove cell debris. Lysates were subjected to SDS–polyacrylamide gel electrophoresis (SDS-PAGE) and proteins were transferred onto a nitrocellulose membrane. Membranes were incubated overnight 4 °C with primary antibodies in PBS+ 5% milk powder + 0.01% Tween-20. The membranes were then incubated with HRP-conjugated secondary antibody (Jackson ImmunoResearch) for 1h at room temperature and visualized using the ECL detection system (GE Healthcare).

Antibodies

Western Blots assays were performed following the following antibodies: ABCB1 (sc-55510, Santa Cruz, 1:1000), ACTb (IGBMC House-Made, 1:1000), TUBb (IGBMC House-Made, 1:10000), Vinculin (Sigma, V4505), mCherry (Sigma, V4505, 1:3000), SOX9 (Cell Signaling, 82630, 1:1000), gH2AX (EMD Millipore, JBW301, 1:1000).

siRNA treatment

Cells were transfected with Lipofectamine RNAiMAX following the manufacturer's instructions with 25 nM of siRNA ONTARGETplus SMARTPool (Horizon Discovery), and cells were harvested 48h after transfection.

ABCB1 overexpression

MM029, IGR37, SKMEL5, SKMEL28, 501mel, 501mel VR and U2OS cells constitutively overexpressing ABCB1 were generated as follows. Lentiviral vectors pLenti-pCMV-ABCB1 encoding untagged ABCB1 were transduced in the presence of polybrene, and cells were selected with 3 ug/ml of puromycin. MM029 cells overexpressing mCherry were generated using pLenti-pCMV-mCherry vectors.

Copy number assays

Copy number variations were determined using qBiomarker Copy Number PCR Assays (Qiagen, 337812), using manufacture instructions and qPCR.

Boyden Chamber Invasion Assay

2×10^6 cells were seeded inside Boyden Chamber inserts (Fisher Scientific) with 4% Matrigel (Corning) and covered with Serum free media. The inserts were placed in 24 well plates filled with complete medium. After 24h, the inserts were fixed for 10min with 4% Formaldehyde solution, washed once with PBS and stained with Crystal Violet solution 0.2% for 15min. The wells were finally washed twice with deionized water, air dried, and photos were collected using an EVOS xl Core microscope. The pictures were analyzed with Fiji considering the area of occupancy of the cells.

Senescence assays

2×10^5 cells were seeded in 6 well plates and were incubated 24h later with C12FDG (ThermoFisher) according to manufacture instructions. Senescence was detected on a BD LSRFortessa™ Flow Cytometer. Data were analysed with FlowJo software.

Rhodamine123 Efflux Assays

2×10^5 cells were seeded in 6 well plates and were incubated 24h later with different concentrations of Tariquidar or Verapamil for 24h. Cell medium was removed, and Rhodamine123 diluted in PBS (1 ug/mL, MedChemExpress), supplemented with either Tariquidar or Verapamil, was added for 90 min, before cells were washed with PBS (2 x 5 min). Rho123 signal was then detected on a BD LSRFortessa™ Flow Cytometer and data were analyzed with FlowJo software. Rho123 being a substrate for ABCB1, the detection of Rho123 signal indicated that no drug efflux took place, whereas the absence of Rho123 signal indicated ABCB1 activity and efflux.

Bulk RNA-Sequencing and analysis

Library preparation was performed at the GenomEast platform at the Institute of Genetics and Molecular and Cellular Biology using TruSeq Stranded Total RNA Reference Guide - PN 1000000040499. Total RNA-Seq libraries were generated from 700 ng of total RNA using TruSeq Stranded Total RNA Library Prep Gold kit and TruSeq RNA Single Indexes kits A and B (Illumina, San Diego, USA), according to manufacturer's instructions. Briefly, cytoplasmic and mitochondrial ribosomal RNA (rRNA) was removed using biotinylated, target-specific oligos combined with Ribo-Zero rRNA removal beads. Following purification, the depleted RNA was fragmented into small pieces using divalent cations at 94°C for 8 minutes. Cleaved RNA fragments were then copied into first strand cDNA using reverse transcriptase and random primers followed by second strand cDNA synthesis using DNA Polymerase I and RNase H. Strand specificity was achieved by replacing dTTP with dUTP during second strand synthesis. The double stranded cDNA fragments were blunted using T4 DNA polymerase, Klenow DNA polymerase and T4 PNK. A single 'A' nucleotide was added to the 3' ends of the blunt DNA fragments using a Klenow fragment (3' to 5' exo minus) enzyme. The cDNA fragments were ligated to double stranded adapters using T4 DNA Ligase. The ligated products were enriched by PCR amplification. Surplus PCR primers were further removed by purification using AMPure XP beads (Beckman-Coulter, Villepinte, France) and the final cDNA libraries were checked for quality and quantified using capillary electrophoresis. Libraries were sequenced on an Illumina HiSeq 4000 sequencer as single read 50 base reads. Image analysis and base calling were performed using RTA version 2.7.7 and bcl2fastq version 2.20.0.422.

Reads were preprocessed to remove adapter and low-quality sequences (Phred quality score below 20). After this preprocessing, reads shorter than 40 bases were discarded for further analysis. These preprocessing steps were performed using cutadapt version 1.10. Reads were mapped to rRNA sequences using bowtie version 2.2.8 and reads mapping to rRNA sequences were removed for further analysis. Reads were mapped onto the hg19 assembly of Homo sapiens genome using STAR version 2.5.3a. Gene expression quantification was performed from uniquely aligned reads using htseq-count version 0.6.1p1, with annotations from Ensembl version 75 and 'union' mode. Only non-ambiguously assigned reads have been retained for further analyses. Read counts have been normalized across samples with the median-of-ratios method proposed by Anders and Huber (Anders and Huber, 2010) to make these counts comparable between samples. Comparisons of interest were performed using the Wald test for differential expression proposed by Love et al. (Love et al., 2014) and implemented in the

Bioconductor package DESeq2 version 1.16.1. Genes with high Cook's distance were filtered out and independent filtering based on the mean of normalized counts was performed. P-values were adjusted for multiple testing using the Benjamini and Hochberg method (Benjamini and Hochberg, 1995). Deregulated genes were defined as genes with $\log_2(\text{Fold change}) > 1$ or < -1 and adjusted P-value < 0.05 .

Volcano plots were generated using the Prism9 statistical software (GraphPad). Heatmaps were generated using Morpheus (<https://software.broadinstitute.org/morpheus>). Gene Ontology Analysis was performed using ShinyGO (Ge SX, Jung D & Yao, 2020).

Figure Legends

Figure 1: Generation of MM029 cells resistant to Lurbi, PM14 and PM54

A. 2 melanocytic and 2 mesenchymal-like melanoma cell types were chronically exposed to increasing doses of either Lurbi, PM14 or PM54. IC₅₀ values for the respective cell types are indicated and whether they were able to become drug-resistant, as defined as being able to proliferate in 10xIC₅₀ concentrations of drugs.

B. Naïve MM029 or MM029 cells with acquired resistances to either Lurbi, PM14 or PM54 (Lurbi-R, PM14-R and PM54-R respectively) were treated with increasing concentrations of Lurbi, PM14 or PM54 for 72h. Mean growth is shown relative to vehicle (DMSO)-treated cells and IC₅₀ values are indicated. Error bars indicate mean values \pm Standard Deviation (SD) for three biological triplicates.

Figure 2: The overexpression of ABCB1 leads to insensitivity towards Lurbi, PM14 or PM54

A. qRT-PCR analysis showing average 18S-normalized expression of ABCB1 in indicated cells. Error bars indicate mean values \pm SD for three biological triplicates. P-values are shown (Ordinary one-way ANOVA using Dunnett's multiple comparisons test).

B + C. Protein lysates from the indicated cells were immuno-blotted for proteins as indicated. Molecular mass of the proteins is shown (kDa).

D. Indicated cells were treated with increasing concentrations of Lurbi, PM14 or PM54 for 72h. Mean growth is shown relative to vehicle (DMSO)-treated cells and IC₅₀ values are indicated. Error bars indicate mean values \pm Standard Deviation (SD) for three biological triplicates.

E. Indicated cells were treated with either DMSO or 5 nM of Lurbi (5xIC₅₀ values for MM029 naïve cells) for 24h. Protein lysates were immuno-blotted for proteins as indicated. Molecular mass of the proteins is shown (kDa).

F. Indicated cells were treated with either DMSO or 5 nM of Lurbi (5xIC₅₀ values for MM029 naïve cells), while being co-treated with 100 nM of ABCB1 inhibitor Tariquidar for 24h. Protein lysates were immuno-blotted for proteins as indicated. Molecular mass of the proteins is shown (kDa).

P-values * < 0.05 ** < 0.01 *** < 0.001 **** < 0.0001 and ns (non-significant) > 0.05.

Figure 3: ABCB1 inhibition reverses drug-resistance towards Lurbi, PM14 or PM54

A. Indicated cells were treated with increasing concentrations of Lurbi, PM14 or PM54 for 72h, while being co-treated or not with 100 nM of Tariquidar or 150 uM of Verapamil. Mean growth is shown relative to vehicle (DMSO)-treated cells and IC₅₀ values are indicated. Error bars indicate mean values +/- Standard Deviation (SD) for three biological triplicates.

B. Indicated cells were treated with siSCR or siABCB1 for 48h, before being treated with increasing concentrations of Lurbi, PM14 or PM54 for 72h. Mean growth is shown relative to vehicle (DMSO)-treated cells and IC₅₀ values are indicated. Error bars indicate mean values +/- Standard Deviation (SD) for three biological triplicates.

Figure 4: Both genetic and epigenetic factors contribute to ABCB1 overexpression

A. RPMK value fold changes of indicated genes of the 7q12.12 locus in indicated cells versus MM029 naïve cells are represented as a Heatmap, as determined by RNA-Seq.

B. Copy number assay showing relative ABCB1 gene copy numbers versus MM029 naïve cells. Error bars indicate mean values + SD for three biological triplicates. P-values are shown (Ordinary one-way ANOVA using Dunnett's multiple comparisons test).

C. Lurbi-R cells were treated with 0.5xIC₅₀ values of SR11302 (AP-1 inhibitor) or CA3 (YAP/TEAD inhibitor) for 3 days before RNA extraction. qRT-PCR analysis showing average 18S-normalized expression of indicated genes. Error bars indicate mean values + SD for three biological triplicates. P-values are shown (Ordinary one-way ANOVA using Dunnett's multiple comparisons test).

P-values * < 0.05 ** < 0.01 *** < 0.001 **** < 0.0001 and ns (non-significant) > 0.05.

Supplemental Figure Legends

Supplemental Figure 1: Resistant cells display distinct phenotypical changes

A. Representative images of MM029, Lurbi-R, PM14-R and PM54-R cell morphology.

B. Cell senescence was analyzed using C12FDG staining and flow cytometry in the indicated cells, and the % of senescent-like cells are shown. Error bars indicate mean values + SD for three biological triplicates. P-values are shown (Ordinary one-way ANOVA using Dunnett's multiple comparisons test).

C. Boyden chamber assay for indicated cells. Pictures are representative images of the bottom of the Boyden chamber membrane. Results are shown as mean values of coverage index +/- SD for three biological triplicates. P-values are shown (Ordinary one-way ANOVA using Dunnett's multiple comparisons test).

P-values * < 0.05 ** < 0.01 *** < 0.001 ***** < 0.0001 and ns (non-significant) > 0.05.

Supplemental Figure 2: Transcriptomic changes associated to resistances

A. Volcano plots showing differentially expressed genes between Lurbi-R/PM14-R/PM54-R cells and naïve MM029 cells as determined by RNA-seq. Deregulated genes were defined as genes with $\log_2(\text{Fold change}) > 1$ or < -1 and adjusted P-value < 0.05. Numbers of significantly deregulated genes are shown.

B. Heatmap depicting all deregulated genes from either Lurbi-R, PM14-R, or PM54-R cells, as determined by RNA-Seq. RPKM values are represented as z-score.

Supplemental Figure 3: Genetic signature of drug-resistance

A. Venn diagrams for significantly upregulated (left) or downregulated (right) common genes between Lurbi-R, PM14-R and PM54-R cells as determined by RNA-Seq.

B. Gene Ontology analysis of the significantly upregulated or downregulated common genes between Lurbi-R, PM14-R and PM54-R cells.

C. Gene set enrichment analysis hallmarks commonly affected (either significant negative or positive correlations) between Lurbi-R, PM14-R and PM54-R cells.

Supplemental Figure 4: ABCB1 expression is regulated through proteasomal degradation mechanisms in certain melanoma cells

A + B. qRT-PCR analysis showing average 18S-normalized expression of ABCB1 in indicated cells. Error bars indicate mean values + SD for three biological triplicates. P-values are shown

(Ordinary one-way ANOVA using Dunnett's multiple comparisons test). LV cells are lentivirus infected cells overexpressing either ABCB1 or mCherry.

C + D. Protein lysates from the indicated cells were immuno-blotted for proteins as indicated. Molecular mass of the proteins is shown (kDa).

E. qRT-PCR analysis showing average 18S-normalized expression of ABCB1 in indicated cells. Error bars indicate mean values + SD for three biological triplicates. P-values are shown (Ordinary one-way ANOVA using Dunnett's multiple comparisons test).

F. Indicated cells were exposed to 1 μ M of MG132 for 24h. Protein lysates from the indicated cells were then immuno-blotted for proteins as indicated. Molecular mass of the proteins is shown (kDa).

P-values * < 0.05 ** < 0.01 *** < 0.001 ***** < 0.0001 and ns (non-significant) > 0.05.

Supplemental Figure 5: ABCB1 overexpression in non-mesenchymal-like cells leads to drug insensitivity

A. Indicated cells were treated with increasing concentrations of Lurbi, PM14 or PM54 for 72h. Mean growth is shown relative to vehicle (DMSO)-treated cells and IC50 values are indicated. Error bars indicate mean values +/- Standard Deviation (SD) for three biological triplicates.

B. Indicated cells were exposed to DMSO or 1 μ M of MG132 for 24h. Protein lysates from the indicated cells were then immuno-blotted for proteins as indicated. Molecular mass of the proteins is shown (kDa).

Supplemental Figure 6: Functional inhibition of ABCB1

A. Indicated cells were incubated with increasing concentrations of Tariquidar or Verapamil for 24h, before Rhodamine efflux essays were performed by Flow cytometry. % of Rhodamine123 positive cells are indicated. A cell positive for Rhodamine123 signal does not possess ABCB1 efflux activity.

B. qRT-PCR analysis showing average 18S-normalized expression of ABCB1 or ACTb in indicated cells, after 48h treatment of siSCR or siABCB1. Error bars indicate mean values + SD for three biological triplicates. P-values are shown (Ordinary one-way ANOVA using Dunnett's multiple comparisons test).

C. Protein lysates from the indicated cells were immuno-blotted for proteins as indicated, after 48h treatment of siSCR or siABCB1. Molecular mass of the proteins is shown (kDa).

Supplemental Figure 7: AP-1/TEADs transcription factor involvement in ABCB1 overexpression

A. Venn diagram depicting the overlap of transcription factors identified by iRegulon as being potentially underlying the transcriptomic changes observed in Lurbi-R, PM14-R or PM54-R cells.

B. Venn diagram depicting the overlap of transcription factors commonly upregulated in Lurbi-R, PM14-R and PM54-R cells with the transcription factors commonly upregulated in naïve MM029 cells upon short Lurbi, PM14 or PM54 exposure (10xIC₅₀ for 8h).

C. Heatmap depicting the relative expression of indicated genes in the indicated cells, as determined by RT-qPCR. Values shown as Z-scores to visualize the relative gene expression versus other melanoma cells.

D. Indicated cells were treated with increasing concentrations of SR11302 or CA3 for 72h. Mean growth is shown relative to vehicle (DMSO)-treated cells and IC₅₀ values are indicated. Error bars indicate mean values +/- Standard Deviation (SD) for three biological triplicates.

References

- Amawi, H. *et al.* (2019) 'ABC Transporter-Mediated Multidrug-Resistant Cancer', *Advances in Experimental Medicine and Biology*, 1141, pp. 549–580. Available at: https://doi.org/10.1007/978-981-13-7647-4_12.
- Arozarena, I. and Wellbrock, C. (2017) 'Targeting invasive properties of melanoma cells', *The FEBS journal*, 284(14), pp. 2148–2162. Available at: <https://doi.org/10.1111/febs.14040>.
- Arozarena, I. and Wellbrock, C. (2019) 'Phenotype plasticity as enabler of melanoma progression and therapy resistance', *Nature Reviews. Cancer*, 19(7), pp. 377–391. Available at: <https://doi.org/10.1038/s41568-019-0154-4>.
- Berico, P. *et al.* (2021) 'CDK7 and MITF repress a transcription program involved in survival and drug tolerance in melanoma', *EMBO reports*, 22(9), p. e51683. Available at: <https://doi.org/10.15252/embr.202051683>.
- Bradner, J.E., Hnisz, D. and Young, R.A. (2017) 'Transcriptional Addiction in Cancer', *Cell*, 168(4), pp. 629–643. Available at: <https://doi.org/10.1016/j.cell.2016.12.013>.
- Carlino, M.S., Larkin, J. and Long, G.V. (2021) 'Immune checkpoint inhibitors in melanoma', *Lancet (London, England)*, 398(10304), pp. 1002–1014. Available at: [https://doi.org/10.1016/S0140-6736\(21\)01206-X](https://doi.org/10.1016/S0140-6736(21)01206-X).
- Choi, C.-H. (2005) 'ABC transporters as multidrug resistance mechanisms and the development of chemosensitizers for their reversal', *Cancer Cell International*, 5, p. 30. Available at: <https://doi.org/10.1186/1475-2867-5-30>.
- Chufan, E.E., Sim, H.-M. and Ambudkar, S.V. (2015) 'Molecular Basis of the Polyspecificity of P-Glycoprotein (ABCB1): Recent Biochemical and Structural Studies', *Advances in cancer research*, 125, pp. 71–96. Available at: <https://doi.org/10.1016/bs.acr.2014.10.003>.
- Costanzo, F. *et al.* (2022) 'Promoters of ASCL1- and NEUROD1-dependent genes are specific targets of lurbnectedin in SCLC cells', *EMBO molecular medicine*, 14(4), p. e14841. Available at: <https://doi.org/10.15252/emmm.202114841>.
- Czarnecka, A.M. *et al.* (2020) 'Targeted Therapy in Melanoma and Mechanisms of Resistance', *International Journal of Molecular Sciences*, 21(13), p. 4576. Available at: <https://doi.org/10.3390/ijms21134576>.
- Dean, M., Rzhetsky, A. and Allikmets, R. (2001) 'The human ATP-binding cassette (ABC) transporter superfamily', *Genome Research*, 11(7), pp. 1156–1166. Available at: <https://doi.org/10.1101/gr.184901>.
- Engle, K. and Kumar, G. (2022) 'Cancer multidrug-resistance reversal by ABCB1 inhibition: A recent update', *European Journal of Medicinal Chemistry*, 239, p. 114542. Available at: <https://doi.org/10.1016/j.ejmech.2022.114542>.
- Filippakopoulos, P. *et al.* (2010) 'Selective inhibition of BET bromodomains', *Nature*, 468(7327), pp. 1067–1073. Available at: <https://doi.org/10.1038/nature09504>.

- Fox, E. and Bates, S.E. (2007) 'Tariquidar (XR9576): a P-glycoprotein drug efflux pump inhibitor', *Expert Review of Anticancer Therapy*, 7(4), pp. 447–459. Available at: <https://doi.org/10.1586/14737140.7.4.447>.
- Genovese, I. *et al.* (2017) 'Not only P-glycoprotein: Amplification of the ABCB1-containing chromosome region 7q21 confers multidrug resistance upon cancer cells by coordinated overexpression of an assortment of resistance-related proteins', *Drug Resistance Updates: Reviews and Commentaries in Antimicrobial and Anticancer Chemotherapy*, 32, pp. 23–46. Available at: <https://doi.org/10.1016/j.drug.2017.10.003>.
- Huang, A.C. and Zappasodi, R. (2022) 'A decade of checkpoint blockade immunotherapy in melanoma: understanding the molecular basis for immune sensitivity and resistance', *Nature Immunology*, 23(5), pp. 660–670. Available at: <https://doi.org/10.1038/s41590-022-01141-1>.
- Huang, F. *et al.* (2021) 'Melanoma Plasticity: Promoter of Metastasis and Resistance to Therapy', *Frontiers in Oncology*, 11. Available at: <https://www.frontiersin.org/articles/10.3389/fonc.2021.756001> (Accessed: 10 March 2023).
- Janky, R. *et al.* (2014) 'iRegulon: From a Gene List to a Gene Regulatory Network Using Large Motif and Track Collections', *PLOS Computational Biology*, 10(7), p. e1003731. Available at: <https://doi.org/10.1371/journal.pcbi.1003731>.
- Jenkins, R.W. and Fisher, D.E. (2021) 'Treatment of Advanced Melanoma in 2020 and Beyond', *The Journal of Investigative Dermatology*, 141(1), pp. 23–31. Available at: <https://doi.org/10.1016/j.jid.2020.03.943>.
- Karras, P. *et al.* (2022) 'A cellular hierarchy in melanoma uncouples growth and metastasis', *Nature*, 610(7930), pp. 190–198. Available at: <https://doi.org/10.1038/s41586-022-05242-7>.
- Katayama, K. *et al.* (2016) 'RSK1 protects P-glycoprotein/ABCB1 against ubiquitin–proteasomal degradation by downregulating the ubiquitin-conjugating enzyme E2 R1', *Scientific Reports*, 6(1), p. 36134. Available at: <https://doi.org/10.1038/srep36134>.
- Kodan, A. *et al.* (2021) 'ABCB1/MDR1/P-gp employs an ATP-dependent twist-and-squeeze mechanism to export hydrophobic drugs', *FEBS letters*, 595(6), pp. 707–716. Available at: <https://doi.org/10.1002/1873-3468.14018>.
- Kozar, I. *et al.* (2019) 'Many ways to resistance: How melanoma cells evade targeted therapies', *Biochimica et Biophysica Acta (BBA) - Reviews on Cancer*, 1871(2), pp. 313–322. Available at: <https://doi.org/10.1016/j.bbcan.2019.02.002>.
- Kwiatkowski, N. *et al.* (2014) 'Targeting transcription regulation in cancer with a covalent CDK7 inhibitor', *Nature*, 511(7511), pp. 616–620. Available at: <https://doi.org/10.1038/nature13393>.
- Luke, J.J. *et al.* (2017) 'Targeted agents and immunotherapies: optimizing outcomes in melanoma', *Nature Reviews. Clinical Oncology*, 14(8), pp. 463–482. Available at: <https://doi.org/10.1038/nrclinonc.2017.43>.
- Manzo, A. *et al.* (2022) 'Lurbinectedin in small cell lung cancer', *Frontiers in Oncology*, 12, p. 932105. Available at: <https://doi.org/10.3389/fonc.2022.932105>.
- Marin-Bejar, O. *et al.* (2021) 'Evolutionary predictability of genetic versus nongenetic resistance to anticancer drugs in melanoma', *Cancer Cell*, 39(8), pp. 1135–1149.e8. Available at: <https://doi.org/10.1016/j.ccell.2021.05.015>.
- Pedri, D. *et al.* (2022) 'Epithelial-to-mesenchymal-like transition events in melanoma', *The FEBS Journal*, 289(5), pp. 1352–1368. Available at: <https://doi.org/10.1111/febs.16021>.
- Ralli, M. *et al.* (2020) 'Immunotherapy in the Treatment of Metastatic Melanoma: Current Knowledge and Future Directions', *Journal of Immunology Research*, 2020, p. 9235638. Available at: <https://doi.org/10.1155/2020/9235638>.
- Rambow, F. *et al.* (2018) 'Toward Minimal Residual Disease-Directed Therapy in Melanoma', *Cell*, 174(4), pp. 843–855.e19. Available at: <https://doi.org/10.1016/j.cell.2018.06.025>.
- Rambow, F., Marine, J.-C. and Goding, C.R. (2019) 'Melanoma plasticity and phenotypic diversity: therapeutic barriers and opportunities', *Genes & Development*, 33(19–20), pp. 1295–1318. Available at: <https://doi.org/10.1101/gad.329771.119>.
- Rubanov, A., Berico, P. and Hernando, E. (2022) 'Epigenetic Mechanisms Underlying Melanoma Resistance to Immune and Targeted Therapies', *Cancers*, 14(23), p. 5858. Available at: <https://doi.org/10.3390/cancers14235858>.
- Santamaría Nuñez, G. *et al.* (2016) 'Lurbinectedin Specifically Triggers the Degradation of Phosphorylated RNA Polymerase II and the Formation of DNA Breaks in Cancer Cells', *Molecular Cancer Therapeutics*, 15(10), pp. 2399–2412. Available at: <https://doi.org/10.1158/1535-7163.MCT-16-0172>.
- Sharma, P. *et al.* (2017) 'Primary, Adaptive, and Acquired Resistance to Cancer Immunotherapy', *Cell*, 168(4), pp. 707–723. Available at: <https://doi.org/10.1016/j.cell.2017.01.017>.
- Trigo, J. *et al.* (2020) 'Lurbinectedin as second-line treatment for patients with small-cell lung cancer: a single-arm, open-label, phase 2 basket trial', *The Lancet. Oncology*, 21(5), pp. 645–654. Available at: [https://doi.org/10.1016/S1470-2045\(20\)30068-1](https://doi.org/10.1016/S1470-2045(20)30068-1).
- Verfaillie, A. *et al.* (2015) 'Decoding the regulatory landscape of melanoma reveals TEADS as regulators of the invasive cell state', *Nature Communications*, 6, p. 6683. Available at: <https://doi.org/10.1038/ncomms7683>.
- Wouters, J. *et al.* (2020) 'Robust gene expression programs underlie recurrent cell states and phenotype switching in melanoma', *Nature Cell Biology*, 22(8), pp. 986–998. Available at: <https://doi.org/10.1038/s41556-020-0547-3>.

Wu, C.-P., Calcagno, A.M. and Ambudkar, S.V. (2008) 'Reversal of ABC drug transporter-mediated multidrug resistance in cancer cells: Evaluation of current strategies', *Current molecular pharmacology*, 1(2), pp. 93–105.

Xie, Y. *et al.* (2010) 'Pim-1 Kinase Protects P-Glycoprotein from Degradation and Enables Its Glycosylation and Cell Surface Expression', *Molecular Pharmacology*, 78(2), pp. 310–318. Available at: <https://doi.org/10.1124/mol.109.061713>.

Figure 1

A

Cells	Phenotype	[IC50] for Lurbi	[IC50] for PM14	[IC50] for PM54	Increasing concentrations over 8 months Starting concentration: 1/3 of [IC50]s	Result
501mel	Melanocytic	0.370 nM	1.248 nM	1.743 nM		Unsuccessful
MM074	Melanocytic	1.066 nM	1.151 nM	3.814 nM		Unsuccessful
MM029	Mesenchymal	1.283 nM	1.405 nM	4.735 nM		Resistant
MM099	Mesenchymal	0.733 nM	1.409 nM	1.857 nM		Unsuccessful

B

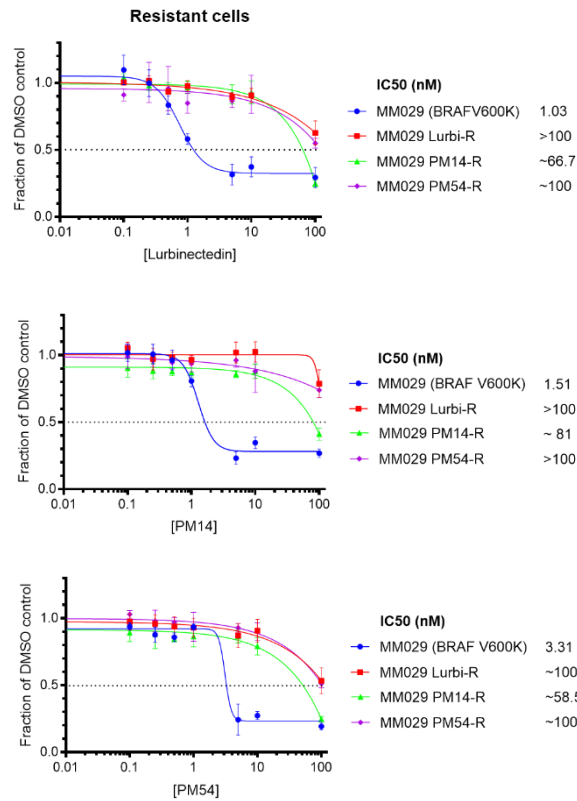


Figure 2

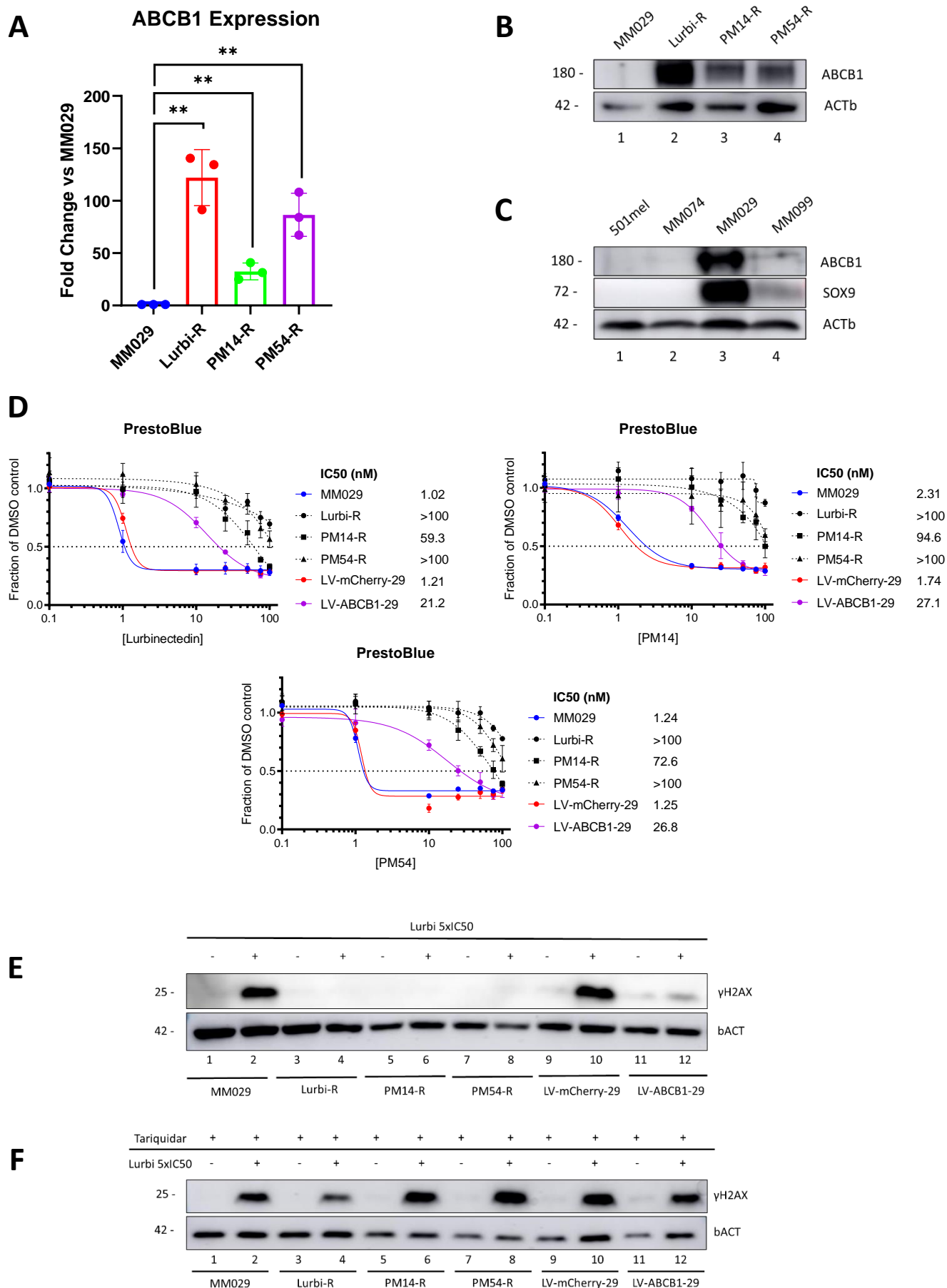
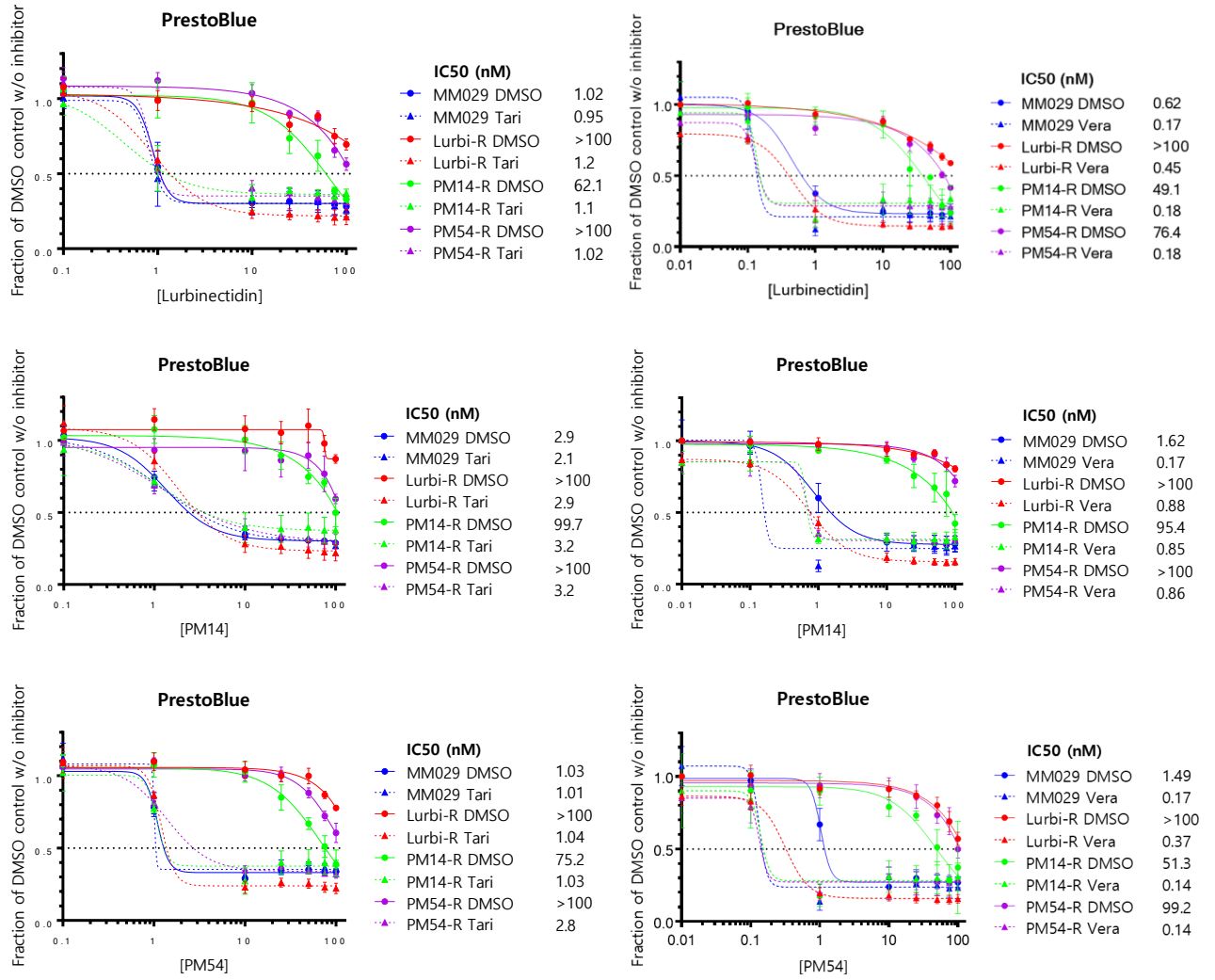


Figure 3

A



B

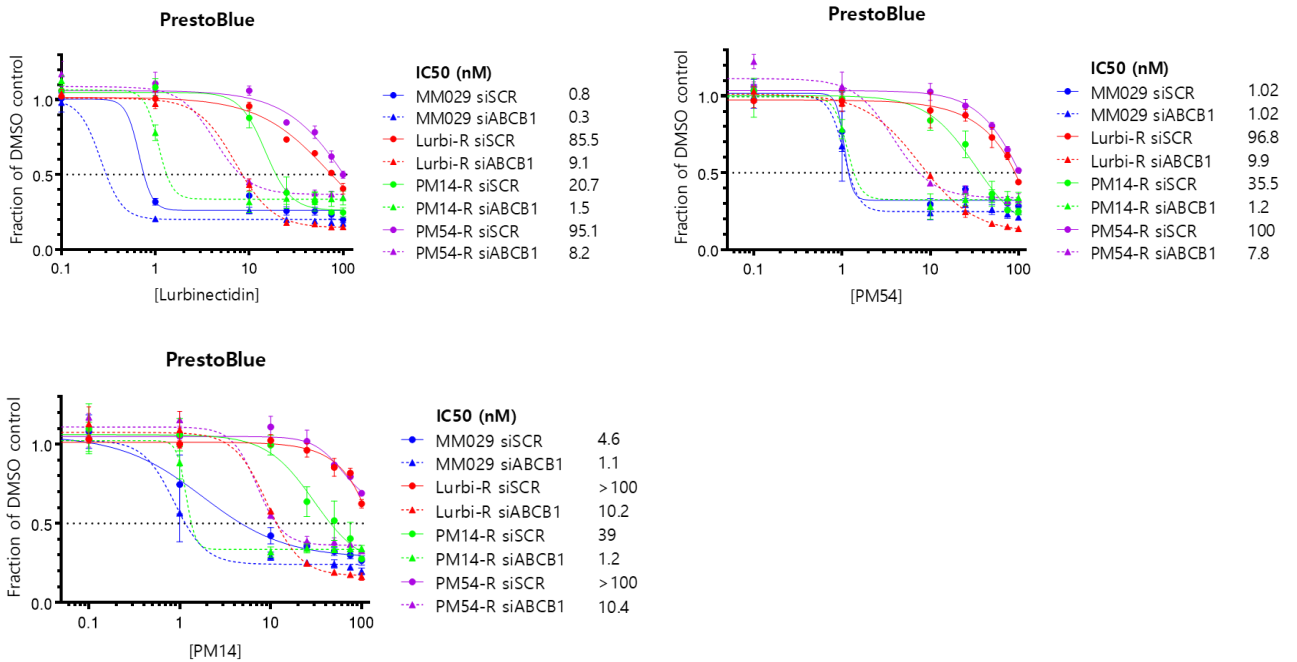
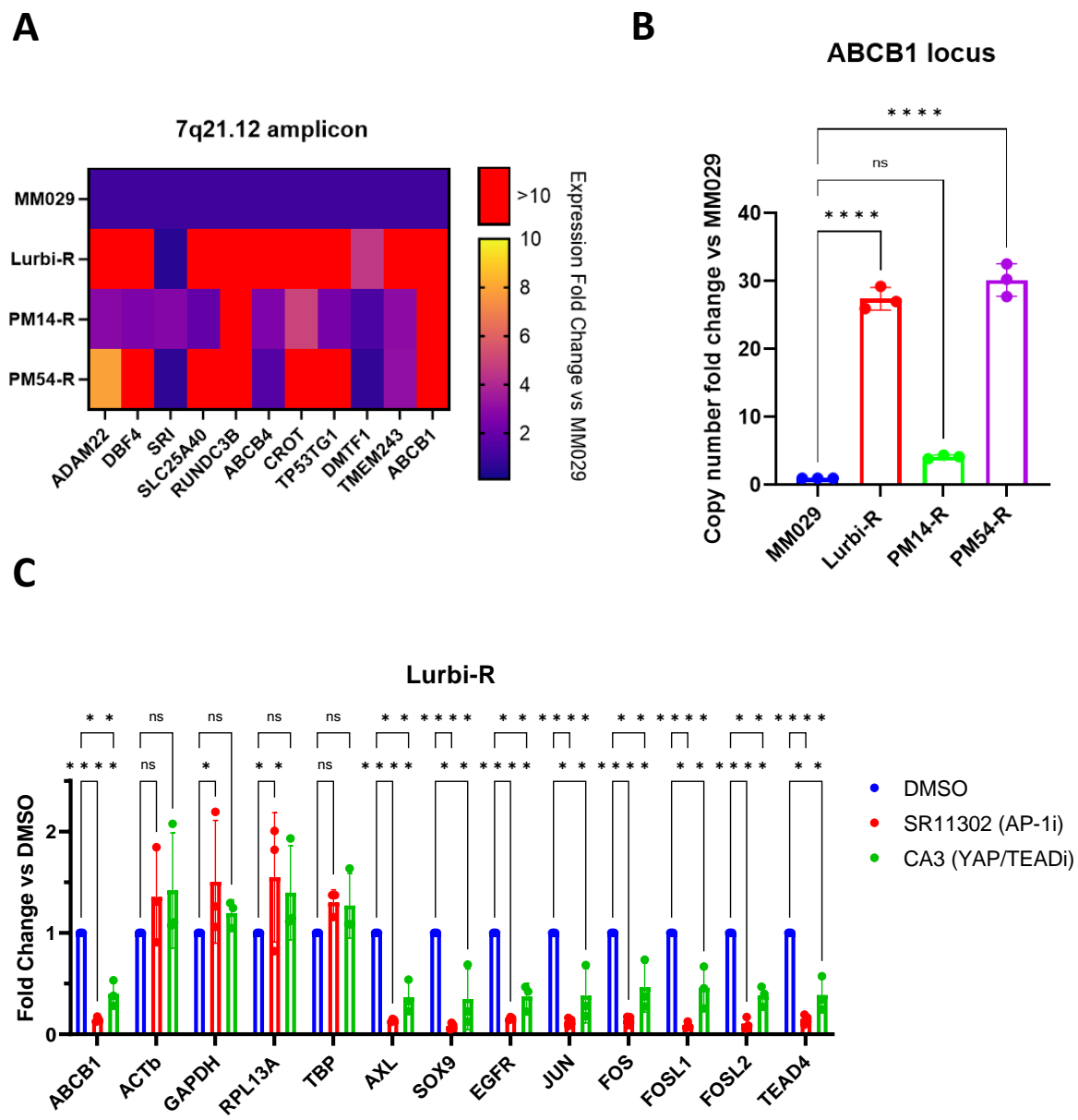
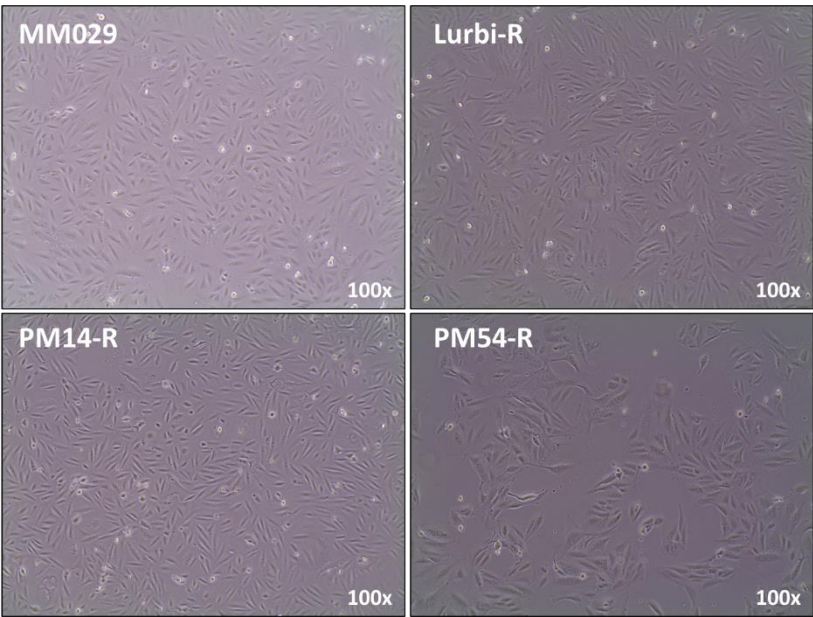


Figure 4

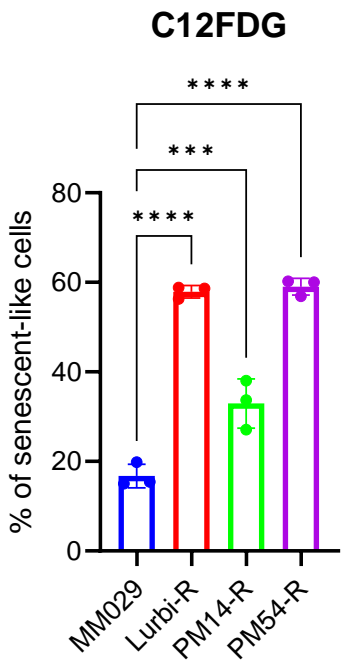


Supplemental Figure 1

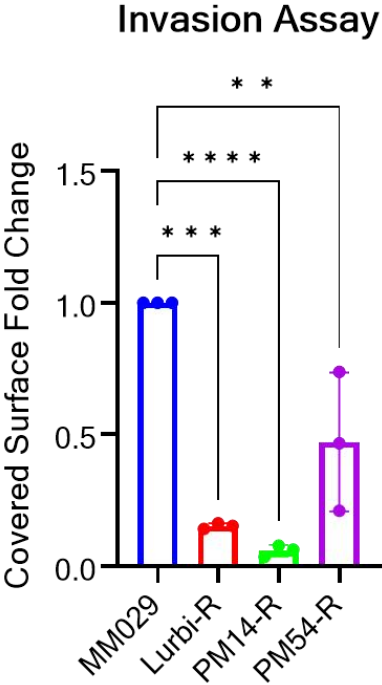
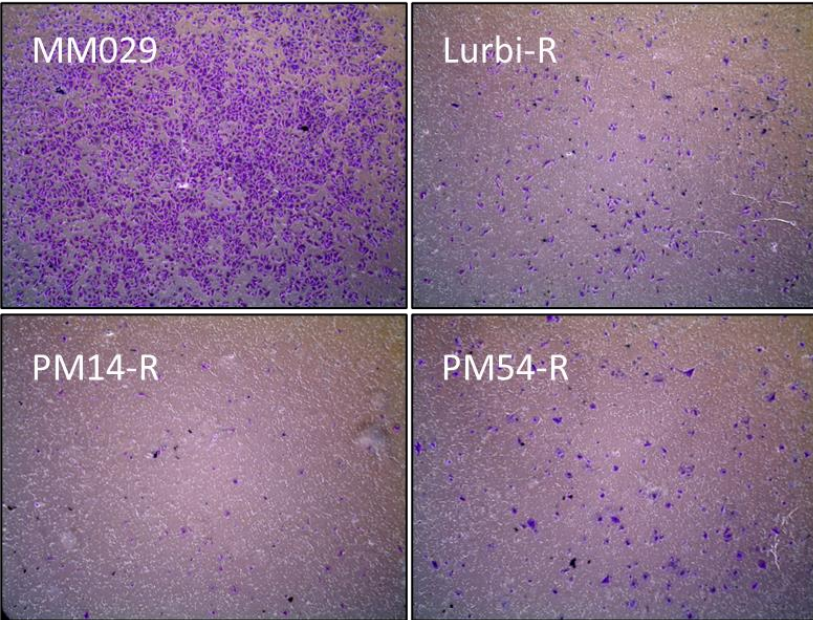
A



B

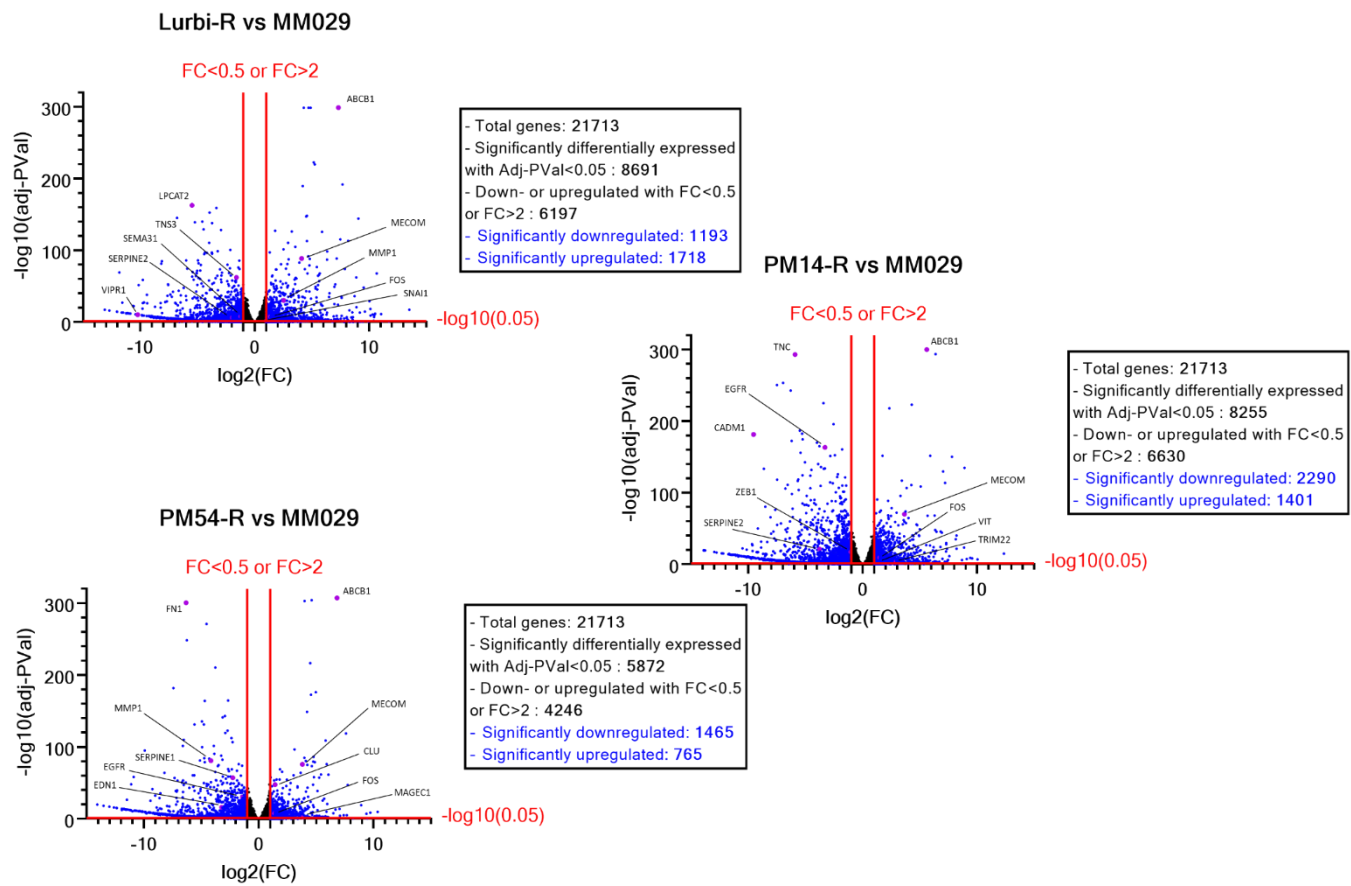


C

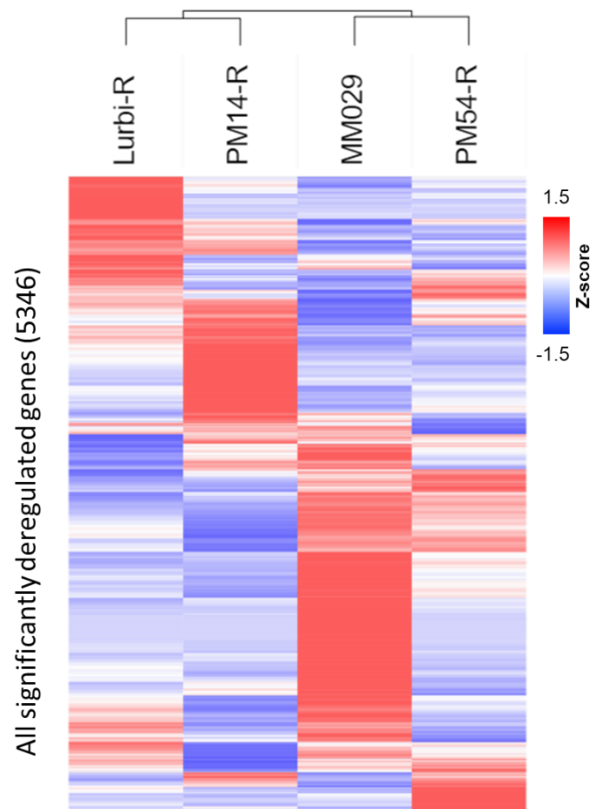


Supplemental Figure 2

A

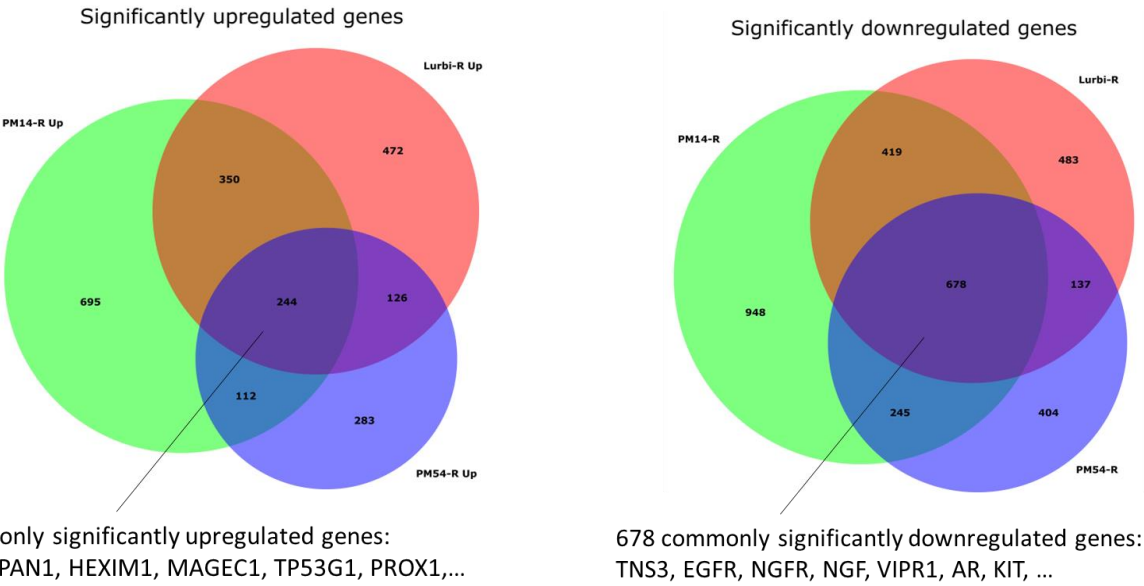


B

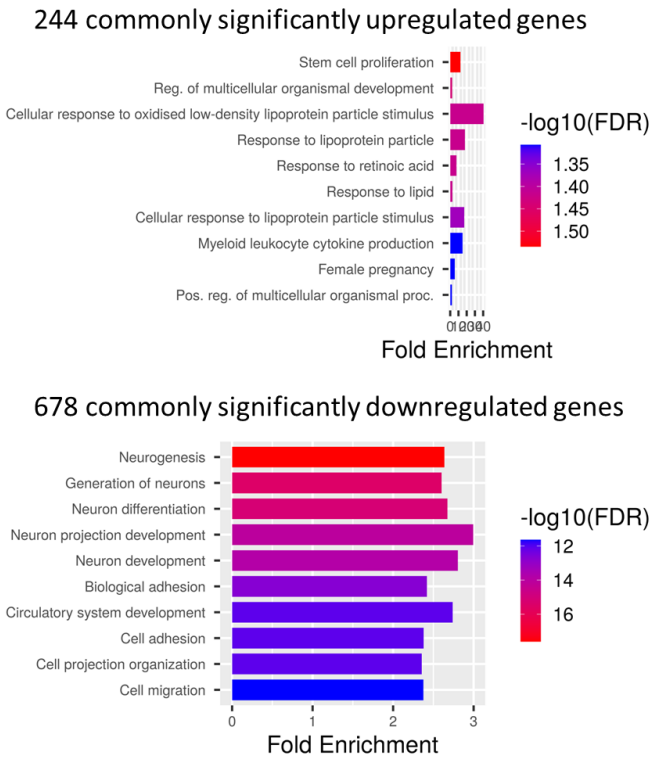


Supplemental Figure 3

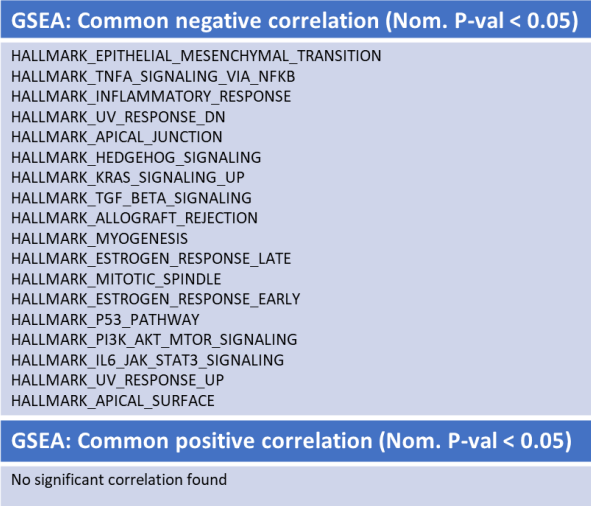
A



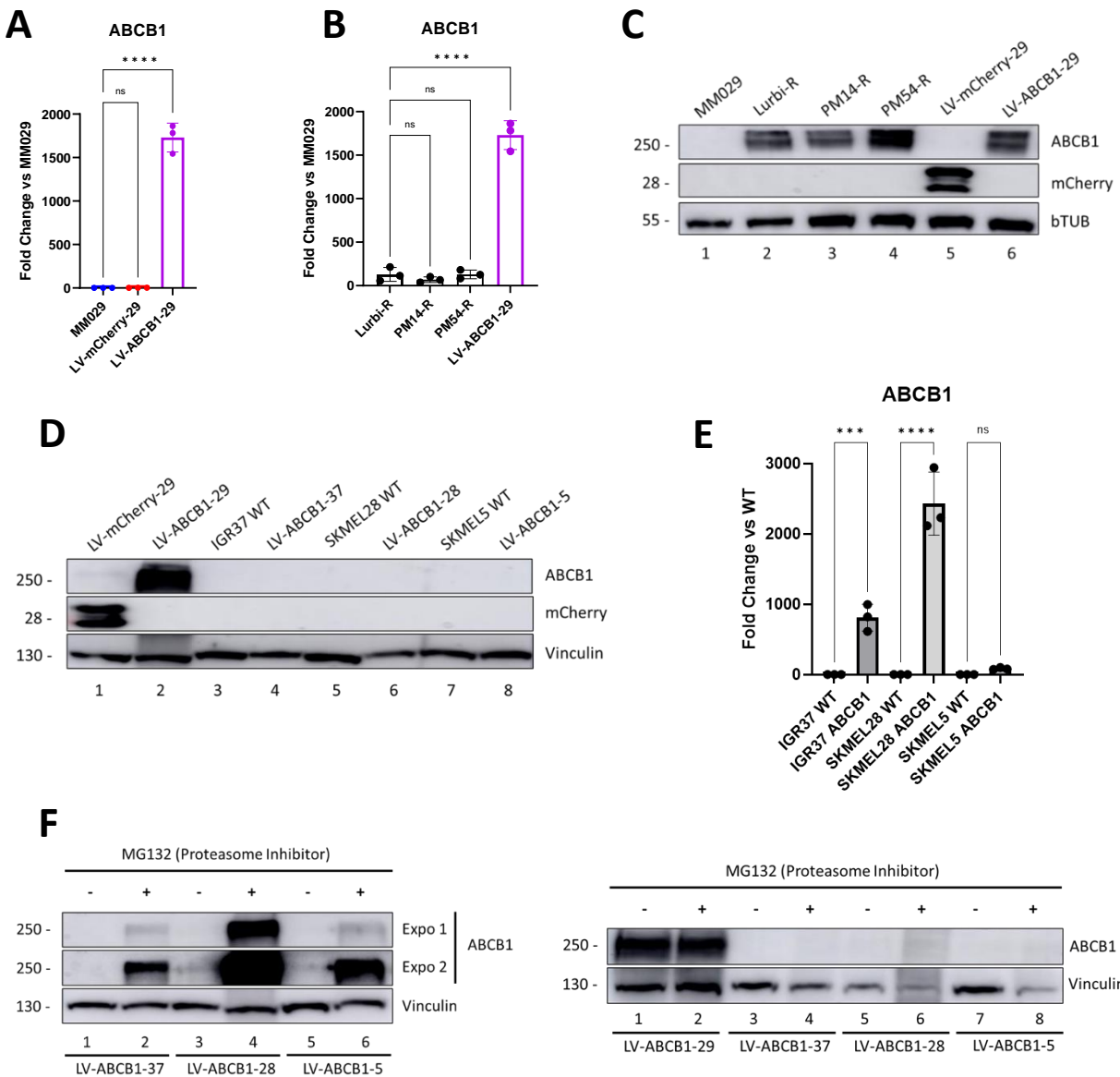
B



C

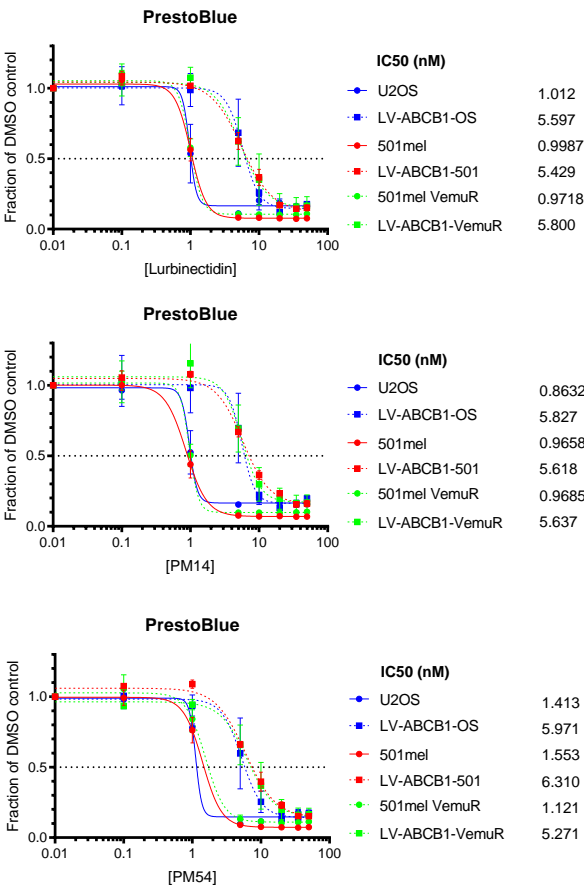


Supplemental Figure 4

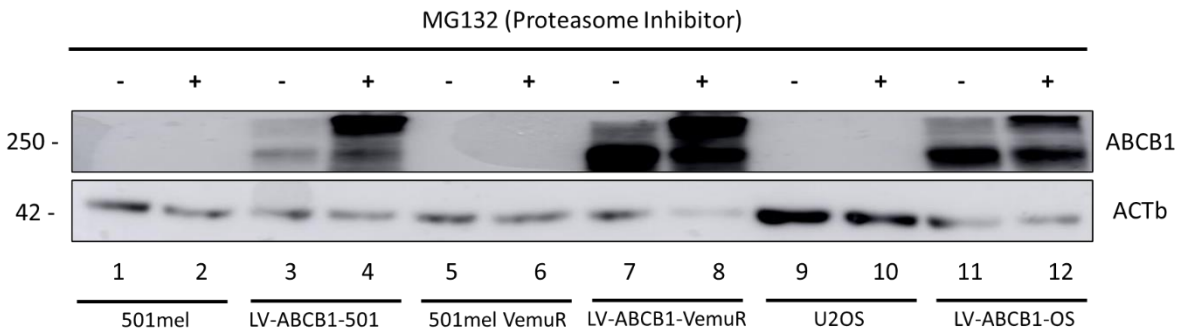


Supplemental Figure 5

A

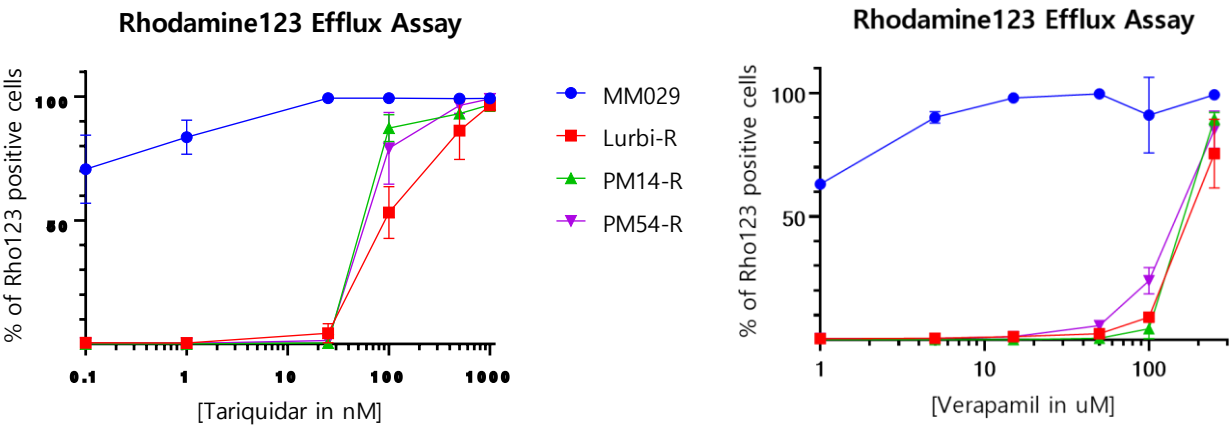


B

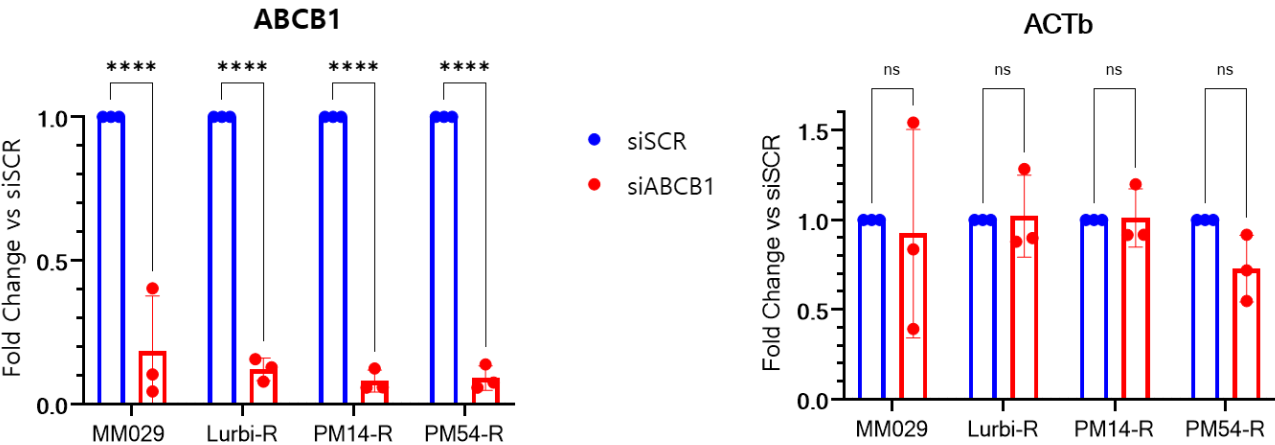


Supplemental Figure 6

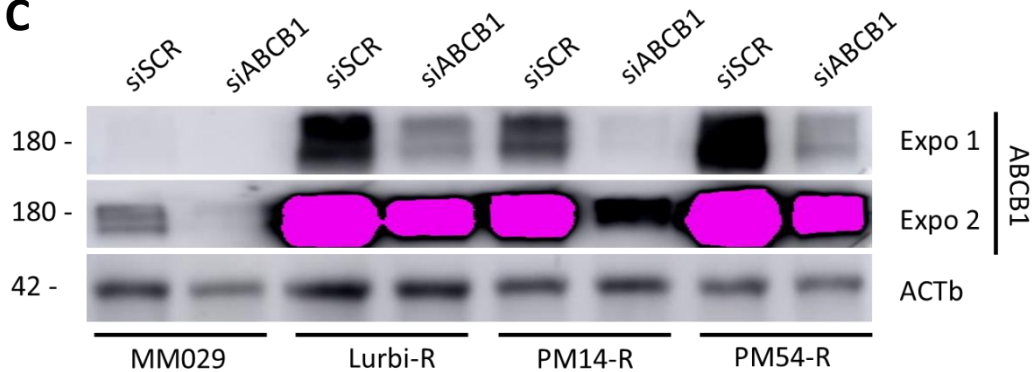
A



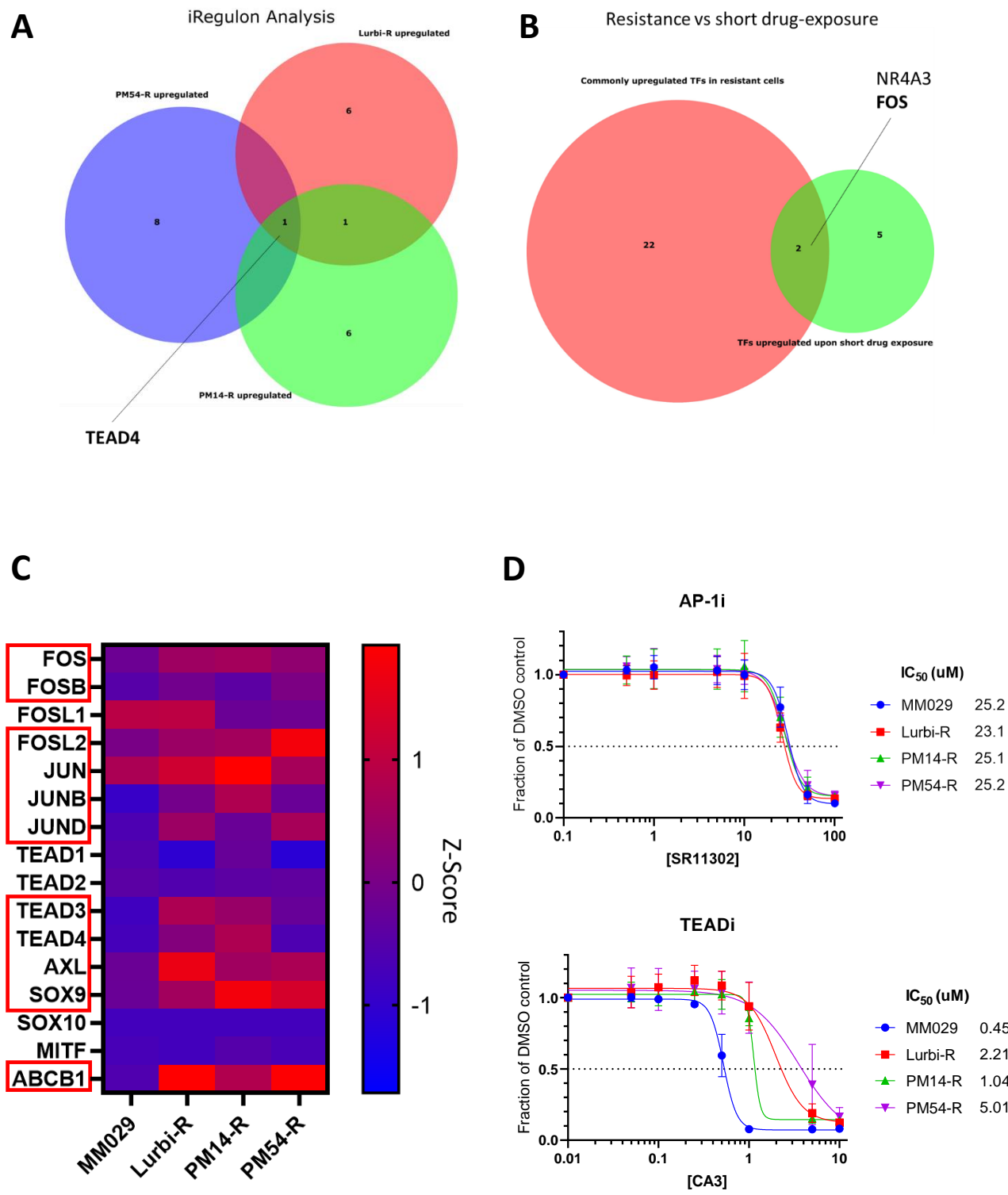
B



C



Supplemental Figure 7



General conclusions and remarks

During the last twenty years, enormous scientific progress has been made in both cancer and molecular biology, respectively resulting in revolutionary new treatments, such as targeted and immunotherapies, as well as a deeper understanding of the underlying drivers of oncogenic gene expression and cancer phenotypes. The convergence of the progress made in those two fields laid the foundation for the concept of ‘transcriptional addiction’, coined by Richard Young in his landmark 2017 paper. Since then, numerous studies have tried to target aberrant cancer-associated transcription programs in different neoplastic diseases through various means, most notably through small-molecule inhibition of epigenetic and gene expression-involved factors. It was in that context that my PhD project initially started, as we hypothesized that melanoma cells, because of their intrinsic phenotypic plasticity, would potentially be promising targets for transcriptional inhibitors. Furthermore, we argued that using these latter ones would help to study the role of transcription regulators such as CDK7 or XPB in melanoma biology, especially considering their emerging roles in SE-dependent oncogene expression. Using two distinct strategies to inhibit transcription in melanoma cells – targeting TFIIH subunits and using a novel type of DNA binders – we elucidated the cellular effects of these drugs, which allowed to find interesting commonalities in cell responses.

The most drastic effect was observed when we exposed melanocytic melanoma cells to the CDK7 inhibitor THZ1. While initially displaying strong anti-proliferative effects for a short period of time, probably due to the downregulation of MITF and SOX10 because of SE decommissioning, long-term exposure triggered a phenotype switch to a mesenchymal-like and multi-drug resistant state. Thus, we demonstrated that the broad inhibition of SE-associated genes through CDK7 inhibition may have an intrinsic therapeutic limitation due to the emergence of multi-drug resistant phenotypes. Interestingly, RNA-Seq analyses revealed that dedifferentiation- and EMT-associated genes were also upregulated when melanoma cells were treated with other transcriptional inhibitors such as Triptolide or Lurbinectedin and its derivatives. In melanocytic cells, short-term exposure to these inhibitors commonly induced the loss of MITF and SOX10 expression while inducing stress signaling, as showcased by the increases in AP-1 factor expression such as JUN or FOS, potentially explaining the observed tendencies for dedifferentiation. As such, a common and immediate response to global transcriptional inhibition seems to be the loss of differentiation.

Intriguingly, while long-term CDK7 inhibition through THZ1 led to the acquisition of a mesenchymal-like cell state dominated by GATA6 activity, long-term TPL exposure did not lead to that fate. As we show in our studies, all tested melanoma cells, regardless of their

phenotypes, were sensitive to XPB inhibition through TPL. Thus, the selection pressure towards phenotype switching might be far less important for cells exposed to TPL as compared to those exposed to THZ1. While the exact molecular mechanisms behind TPL insensitivity are still being studied, it is clear that they are different than those observed in THZ1-resistant cells, in which we showed that the abrogation of the repressive function of MITF at the *GATA6* locus leads to multi-drug resistance. Interestingly, our results suggest that the inhibition of XPB potentially abrogates SE-dependent gene expression, to a more specific degree than THZ1. While important additional studies remain to be performed, such as elucidating if and how XPB is recruited at SEs, we observe that somewhat surprisingly, certain SEs seem to be differently impacted by either XPB or CDK7 inhibition. These results thus warrant deeper investigations into the functions TFIID subunits might have at these loci, as it is still unknown how exactly they contribute to SE functioning. Independently of their exact mechanisms however, our results seem to showcase a clear upside of using XPB inhibitors in melanoma over using CDK7 inhibitors, as TPL potentially targets all tested melanoma cell states and does not seem to lead to phenotype switching. The same benefits were observed for Lurbinectedin and its derivatives, which represent new-generation transcriptional inhibitors combining two distinct mechanisms of action. We showed that the dual downregulation of melanoma master regulator genes and the generation of double-strand breaks potentially led to melanoma cell apoptosis, no matter their phenotype. Lurbinectedin, as a marine-derived molecule, also showcases the potential of investigating oceanic organisms as a previously untapped source of potential bioactive molecules, and the benefits of developing structural analogues of pre-existing drugs to increase their efficacies and safety profiles. Indeed, we find that PM54 seems to exert more elevated specificity for transcription-related genes compared to Lurbi, providing a rationale for further investigating this molecule as a more selective inhibitor of transcriptional addiction in clinical settings, as it may lead to fewer off-target effects and thus reduced systemic toxicity.

Importantly, besides studying the effects of these transcriptional inhibitors, we also investigated potential resistance mechanisms towards these drugs, which represented a relatively unexplored topic when I first began my PhD. Indeed, one of the strongest arguments for using transcriptional inhibitors is the hypothesis that even intrinsically resistant cell populations, such as mesenchymal-like melanoma cells, could still be dependent on increased oncogene expression compared to normal cells and therefore be sensitive to agents abrogating transcriptional processes. However, in order for these drugs to work, they need to reach their targets in the nucleus. By generating resistant cells towards THZ1 and Lurbinectedin and its

analogues, we observed in the two cases that ATP-binding cassette transporters were responsible for the insensitivities, pumping out the drugs before they could inhibit their targets. Strikingly, our studies indicate that the overexpression of efflux pumps could be an adaptive mechanism that is far better tolerated by mesenchymal-like melanoma cells than melanocytic ones. Dedifferentiated melanoma cells, such as MM029 cells, have access to more embryonic and stem-like gene expression programs than differentiated melanoma cells, potentially explaining why the MM029 cells were unique in their capacity to generate resistances against Lurbi, PM14 and PM54. We observed important proteasomal degradation mechanisms in melanocytic melanoma cells, hindering them from overexpressing the ABCB1 efflux pump, likely elucidating why these cells seemed unable to become drug-resistant. This underscores once again the dangers of melanoma phenotype switching, and the urgent need to understand the molecular mechanisms driving the distinct cell states, in order to find ways to target them effectively.

In conclusion, the results presented in this manuscript provide novel insights into the intricacies of targeting the transcriptional addiction of melanoma cells through different classes of small-molecule inhibitors. Indeed, we describe how molecules such as THZ1 and TPL can be used as tools to identify important regulators of melanoma cell states, and elucidate how these drugs differently impact SE-dependent gene expression in melanoma cells while characterizing some of the molecular factors involved in cellular responses to transcriptional inhibition. Furthermore, we identify potentially beneficial effects of drugs such as Triptolide and Lurbinectedin for treating melanoma, and suggest that these drugs be further investigated in clinical settings, especially for relapsed or treatment-resistant melanoma cases. Particular attention should be given to Lurbinectedin and its analogues, as Lurbinectedin is a molecule already used for SCLC patients and represents thus a potentially promising drug to be repurposed for melanoma cases. Importantly however, our results indicate that PM54 could provide enhanced patient benefits compared to Lurbinectedin. Thus, the encouraging results described in this manuscript contributed to PharmaMar S.A. patenting and initiating Phase I clinical trials for PM54 in advanced solid tumors, including melanoma (ClinicalTrials.gov Identifier: NCT05841563). Finally, we uncover ABC-transporter overexpression as a major resistance mechanism against the tested transcriptional inhibitors, and urge that future drug developments should systematically include the evaluation of drug interactions with efflux pumps, and that ABC-transporter biomarker status should be considered before administering molecules such as Lurbinectedin and its analogues to patients.

Annexes

Preface to annexed Articles 5 and 6: Context and contributions

Besides my two main assignments, concerning the role of TFIIH and the efficacy of Lurbinectedin and its analogues in melanoma, I was also actively involved in two other projects of the lab during my PhD.

The first study I was a part of identified and characterized the role of BAHCC1, a novel, melanoma-specific transcriptional regulator encoded by a SE-dependent gene and involved in melanoma cell proliferation and DNA repair. We observed that the inhibition of BAHCC1 greatly synergized with PARP inhibitors and might thus be leveraged as a therapeutic target to impair melanoma cell proliferation, especially in combination with DNA damage-inducing agents. My concrete contributions to this study, which is in revision at *Cell Reports*, consisted in assisting Pietro Berico, the main author, in performing RT-qPCRs, Boyden chamber assays, synergy studies and Cut&Tag assay wet lab work.

The second study I participated in was not directly related to melanoma biology, but concerned how cells transcriptionally respond to genotoxic attacks. Efficient repair of DNA damage, caused by UV mutations for example, requires the global downregulation of transcription, which is followed by its restart after the DNA lesions have been removed. However, the molecular actors and mechanisms behind this recovery of RNA synthesis remained elusive. In this study, I helped Jérémy Sandoz, a former postdoctoral researcher in our lab, to uncover the involvement of the EXD2 RNA/DNA nuclease in this process, by performing various survival and 5-Ethynyl Uridine (EU) incorporation assays. This study was published in *Nature Communications* in January 2023.

Super-enhancer driven expression of BAHCC1 promotes melanoma

cell proliferation and genome stability

Pietro Berico^{1, 2, 3, 4, 7, 8}, Maguelone Nogaret^{1, 2, 3, 4}, Max Cigrang^{1, 2, 3, 4}, Antonin Lallement^{1, 2, 3, 4}, Fatemeh Vand Rajabpour^{7, 8}, Amanda Flores-Yanke^{7, 8}, Giovanni Gambi^{1, 2, 3, 4}, Guillaume Davidson^{1, 2, 3, 4}, Leane Seno^{1, 2, 3, 4}, Julian Obid^{1, 2, 3, 4}, Bujamin H Vokshi^{1, 2, 3, 4}, Stephanie Le Gras^{1, 2, 3, 4}, Gabrielle Mengus^{1, 2, 3, 4}, Tao Ye^{1, 2, 3, 4}, Carlos Fernandez Cordero^{7, 8}, Mélanie Dalmasso^{5, 6}, Emmanuel Compe^{1, 2, 3, 4}, Corine Bertolotto^{5, 6}, Eva Hernando^{7, 8}, Irwin Davidson^{1, 2, 3, 4, 9}, Frédéric Coin^{1, 2, 3, 4, 9}

¹ Institut de Génétique et de Biologie Moléculaire et Cellulaire, Equipe Labéllisée « Ligue contre le Cancer 2022 » 2022. BP 163, 67404 Illkirch Cedex, C.U. Strasbourg, France

² Centre National de la Recherche Scientifique, UMR7104, 67404 Illkirch, France

³ Institut National de la Santé et de la Recherche Médicale, U1258, 67404 Illkirch, France

⁴ Université de Strasbourg, 67404 Illkirch, France

⁵ Université Côte d'Azur, Nice, France

⁶ Inserm, Biology and Pathologies of melanocytes, team1, Equipe labellisée « Ligue contre le Cancer 2020 » and Equipe labellisée « Fondation ARC 2022 », Centre Méditerranéen de Médecine Moléculaire, Nice, France

⁷ Department of Pathology, New York University Grossman School of Medicine, New York, NY 10016, USA.

⁸ Interdisciplinary Melanoma Cooperative Group, Perlmutter Cancer Center, New York University School of Medicine, New York, NY 10016, USA.

⁹ Corresponding authors: fredr@igbmc.fr, irwin@igbmc.fr

Keywords: Melanoma, Super-enhancer, BAHCC1, gene expression, genome stability

Abstract

Super enhancers (SE) are stretches of active enhancers ensuring high expression levels of key genes associated with cell function and survival. The identification of cancer-specific SE-driven genes and their functional characterization may prove to be a powerful means for the development of innovative therapeutic strategies. By performing epigenomic profiling in patient-derived short-term melanoma cultures, we identify a MITF/SOX10/TFIIH-dependent SE promoting the specific expression of BAHCC1 in a broad panel of cutaneous and uveal melanoma cells. BAHCC1 is highly expressed in metastatic melanoma, correlates with decreased patient survival and is required for tumor engraftment, growth and metastasis dissemination. Integrative genomics analyses reveal that BAHCC1 is a transcriptional regulator controlling expression of a subset of E2F/KLF-dependent cell cycle and DNA repair genes. BAHCC1 associates with BRG1-containing remodeling complexes at the promoters of these genes. In agreement, BAHCC1 silencing leads to decreased cell proliferation and delay in DNA repair. Consequently, BAHCC1 deficiency cooperates with PARP inhibition to induce melanoma cell death. Our study identifies a novel SE-driven gene expressed in cutaneous and uveal melanoma and demonstrates how its inhibition can be exploited as a therapeutic target, alone or in combination with DNA damage-inducing agents.

Introduction

Transcriptional deregulation represents a key mechanism for cancer initiation and progression (Bradner et al., 2017). A combination of somatic mutations and microenvironmental cues leads to the overexpression of epigenetic regulators promoting aberrant gene expression programs, ultimately resulting in cancer hallmarks (Hnisz et al., 2013). A key epigenetic mechanism promoting tumor-specific gene expression programs is the aberrant activation of Super-Enhancers (SEs), broad gene regulatory elements highly dependent on the activity of general co-activators compared to canonical enhancers (Pott and Lieb, 2015). Consequently, transcriptional inhibitors targeting co-activators such as BRD4 (Bromodomain-containing protein 4) and the cyclin-dependent kinase 7 (CDK7) of the basal transcription factor TFIID are widely used to disrupt SE-associated genes in cancer cells (Filippakopoulos et al., 2010), (Kwiatkowski et al., 2014). However, the presence of SE-associated genes in normal cells, together with the poor pharmacokinetics and efficacy of transcriptional inhibitors in human clinical trials, underscore the need for alternative strategies (Postel-Vinay et al., 2016), (Ameratunga et al., 2020) such as the identification of cancer-specific SE-driven genes (Fontanals-Cirera et al., 2017).

Cutaneous melanoma remains the most lethal skin cancer whose incidence continues to increase over the past few decades (Ribas et al., 2015), (Mitchell et al., 2020). Despite the significant improvement in 5-years overall survival provided by therapies targeting mitogen-activated protein kinase (MAPK) including Vemurafenib and Trametinib (respectively BRAF and MEK inhibitors) (Chapman et al., 2011), (Robert et al., 2019) or by immune checkpoint inhibitors anti-PD1 and anti-CTLA4 (Curti and Faries, 2021), many patients still develop resistance in part due to melanoma phenotypic plasticity, a dynamic and non-mutational mechanism of adaptation to micro-environmental changes and drug exposure (Marin-Bejar et al., 2021), (Rubanov et al., 2022). Plasticity results in an important tumor heterogeneity involving multiple cell states with distinct transcriptional signatures and different proliferative, invasive and drug resistance phenotypes. Melanoma phenotype plasticity depends in part on two opposing gene expression programs, governed by the transcription factors MITF (microphthalmia-associated transcription factor) and SOX10 (SRY-box transcription factor 10) or AP-1 (Activating Protein 1) and TEAD (Transcriptional enhancer associate domain transcription factor), respectively, whose activities modulate melanoma cell state transition (Verfaillie et al., 2015), (Rambow et al., 2018), (Rambow et al., 2019), (Wouters et al., 2020).

Other forms of melanoma include uveal melanoma, the most common primary intraocular tumor in adults that is intrinsically different from cutaneous melanoma. In uveal melanoma, the most frequent driver mutations are those involving the heterotrimeric G-protein subunits GNAQ or GNA11 (Onken et al., 2008), (Van Raamsdonk et al., 2010). Despite successful treatment of primary uveal melanoma, 50% of patients will develop metastasis that are highly refractory to existing treatments (Yang et al., 2018). Therefore, there is an urgent need to better understand the molecular mechanisms involved in these two cancers in order to develop efficient treatments.

Here, we characterized the SE landscapes of patient-derived short-term cutaneous melanoma cultures. Integrative epigenomic analyses revealed a melanoma-specific SE regulating the expression of the Bromo Adjacent Homology and Coiled Coil Domain-Containing 1 (BAHCC1) protein in a broad panel of cutaneous, but also in uveal melanoma cells. BAHCC1 drives cutaneous and uveal melanoma cell proliferation and is required for tumor growth of cutaneous melanoma xenografts *in vivo*. Loss-of-function and genomic profiling experiments show that BAHCC1 is a transcriptional regulator controlling the expression of a subset of E2F (E2 factor)/KLF (Krüppel-like factor)-dependent cell cycle and DNA repair genes in melanoma cells. BAHCC1 associates with BRG1 (BRM/SWI2-related gene 1)-containing remodeling complexes at the promoters of these genes. Consistent with the involvement of BAHCC1 in the regulation of DNA repair genes, including the crucial cell cycle kinase ATM (Ataxia Telangiectasia Mutated), BAHCC1 depletion delays DNA repair and cooperates with PARP (Poly ADP-ribose polymerase) inhibition to induce melanoma cell death. We thus identify a SE-dependent pan-melanoma expressed gene and demonstrate how its inhibition can be leveraged as a therapeutic target to impair melanoma cell proliferation, alone or in combination with DNA damage-inducing agents.

Results

SE17q25 regulates BAHCC1 expression in melanoma

To identify cutaneous melanoma (SKCM) specific SEs, we performed *in silico* ROSE analysis of H3K27ac ChIP-seq data from short-term melanoma cultures (MM) (Verfaillie et al., 2015) and two normal human melanocytes samples (NHEM1 and 2) (Fontanals-Cirera et al., 2017). The MM panel covered the two main phenotypes and most common driver mutations (Ext. Table 1). We further ranked SEs using DiffBind according to the enrichment in the binding of

the lineage-specific transcription factors MITF and SOX10 that are recruited to long and short enhancers in melanocytic-like melanoma cells (Ext. Figure 1a) (Strub et al., 2011), (Laurette et al., 2015), (Berico et al., 2021), (Mauduit et al., 2021). Using these criteria, we identified a collection of potential SEs active in MM cells (Ext. Table 2). We further defined *bona fide* melanoma-specific SEs as active in at least 5 MM cell cultures. A SE at chr17q25.3 (hereafter referred to as SE17q25) met these criteria and was absent from NHEM (Figure 1a, left panel and Ext. Figure 1c). The SE17q25 region measured around 20kb and was recurrent not only in many of the MM cells, but also in melanoma cell lines such as SK-MEL-5 and 501mel (Figure 1a, left and right panels) (Ext. Table 2).

SE17q25 localized in close proximity to the promoter of the protein-coding gene BAHCC1 (Figure 1a). The Cancer Genome Atlas (TCGA) reports that high SE17q25 activity, as measured by the level of ATAC-seq signal, correlated with high BAHCC1 expression in several tumors and that the highest SE17q25 activity was observed in SKCM, with the highest BAHCC1 expression (Figure 1b). Quantitative RT-PCR and Western blotting showed that BAHCC1 displayed higher RNA and protein levels in melanoma cells highly expressing MITF and SOX10, including melanocytic-like melanoma cells (501mel, MM117, IGR-37, SK-MEL-28, SK-MEL-5, MM011) and uveal melanoma (UVM) cells (OMM1, OMM1.3, OMM2.5) (Ext. Figures 1c and 1d). In agreement with these observations, analyses of the Cancer Cell Lines Encyclopedia (CCLE) revealed that BAHCC1 expression correlated with that of MITF in melanoma cell lines (n=49) (Figure 1c). Furthermore, depletion of SOX10 or MITF strongly reduced BAHCC1 mRNA and protein expression in melanocytic-like melanoma cells (Figures 1d-e). Note that MITF depletion reduced BRG1 deposition at SE17q25, suggesting the decommission of this SE (Ext. Figure 1e).

Compared to melanocytic-like melanoma cells, BAHCC1 was less expressed in dedifferentiated mesenchymal-like MITF^{LOW} melanoma cells (MM099, MM047, IGR-39 and MM029) (Ext. Figures 1c and 1d). Note, however, that BAHCC1 expression remained significantly higher in MITF^{LOW} melanoma cells compared to non-transformed Hermes3A melanocytes (which expresses MITF) or U-2 OS cells (non-melanoma cell line) (Ext. Figure 1d).

In addition to MITF and SOX10, the ATP-dependent chromatin remodeler BRG1 and the TFIIH kinase CDK7 that is known to associate with SEs (Chipumuro et al., 2014), also bound SE17q25 in 501mel cells (Figure 1a, right panel). Interestingly, treatment of 501mel cells for a short period of time with THZ1 (an inhibitor targeting CDK7) (Kwiatkowski et al., 2014) or Triptolide (an inhibitor of the XPB subunit of TFIIH) (Titov et al., 2011), (Noel et al., 2020)

significantly diminished BAHCC1 expression (Figure 1f). In parallel, CRISPR interference (CRISPRi) of SE17q25 in 501mel using a dead Cas9 (dCas9) fused with the repressive Krüppel associated box (KRAB) domain (dCas9^{KRAB}) and guide RNAs targeting SE17q25 (gSE17q25), diminished BAHCC1 expression compared to GAPDH control gene (Figure 1g). Altogether these data link SE17q25 activity to BAHCC1 expression in melanoma cells.

BAHCC1 expression increases during melanoma progression

To explore BAHCC1 expression in tumors, we analyzed public transcriptional data and observed first that BAHCC1 was more strongly expressed in melanoma cell lines compared to other tumors cells (Figure 2a). In agreement, SKCM and UVM tumors from TCGA displayed higher levels of BAHCC1 compared to other tumors and normal tissues (Figure 2b). Furthermore, BAHCC1 overexpression was a marker of poor prognosis in SKCM or UVM patients (Figure 2c-d) and its expression was independent from the BRAF, NRAS or NF1 mutation status in SKCM patients (Figure 2e).

To trace the evolution of BAHCC1 expression along melanoma initiation and progression, different published bulk and single-cell transcriptomic datasets coming from normal cells, pre-malignant and malignant lesions were combined. Notably, we observed that BAHCC1 expression progressively increased going from normal skin to primary melanoma and metastatic lesions specifically in malignant cells (Ext. Figure 2a-d) and that BAHCC1 was higher expressed in melanoma cells vs. melanocyte stem cells in BRAF mouse melanoma model (Ext. Figure 2e). Using RNA *in situ* hybridization on a cohort of patient samples including benign nevi, cutaneous and uveal melanoma, we confirmed the increased expression of BAHCC1 mRNA in SOX10-positive malignant cells (Fig 2f and Ext. Figure 2f-g). Overall, these results indicate that BAHCC1 expression progressively increases during melanoma progression from primary tumors to metastasis.

BAHCC1 is required for melanoma cell proliferation and tumor growth

To investigate the functional consequences of BAHCC1 knock down (BAHCC1 KD), we transfected melanoma cells with two independent custom antisense oligonucleotides (ASO, locked nucleic acid GapmeRs) targeting the pre-mRNA. GapmeR^{#1} and GapmeR^{#2} efficiently silenced BAHCC1 expression in 501mel cells (Ext. Figure 3a). We observed that BAHCC1 KD reduced proliferation of cutaneous melanocytic-like (501mel and MM117) and mesenchymal-like (MM047 and MM029) melanoma cells but also of uveal melanoma cell lines (OMM1.3 and OMM2.5) (Figure 3a, Ext. Figure 3b). In contrast, BAHCC1 KD did not affect

proliferation of U-2 OS cells excluding an off-target effect (Ext. Figure 3b). Given the anti-proliferative role of MAPKi inhibitors (MAPKi) used in the clinic, we wondered whether BAHCC1 KD could increase their effect. Indeed, BAHCC1 KD further reduced the proliferation of a melanocytic cell line upon treatment with Trametinib or Vemurafenib (Figure 3b). We also evaluated the effect of BAHCC1 KD on melanoma cell invasive capacity and observed that BAHCC1 KD significantly impaired migration of 501mel, MM099 and MM029 melanoma cells (Figure 3c). All together, these results highlight the importance of BAHCC1 for melanoma cells proliferation and invasion *in vitro*.

To test the effects of BAHCC1 silencing *in vivo*, we injected the MITF^{HIGH} 501mel melanoma cell line expressing Luciferase together with GFP and a non-targeting shRNA (SH^{NTC}) or two independent shRNAs against BAHCC1 (SH^{#1} and SH^{#2}) in immune compromised mice (Ext. Figure 4a). KD of BAHCC1 in intradermally injected cells dramatically prevent CDX tumors' engraftment and growth compared to the non-targeting shRNA (Figure 4a-b). In parallel, 501mel cells were also injected intracardiac to evaluate melanoma cells capacity to disseminate and establish metastatic lesions in presence and absence of BAHCC1. Concordant with our previous observation in the invasion *in vitro* assay, BAHCC1 KD completely prevent the formation of metastasis in liver, lungs and brain as shown by a strong reduction of Luciferase luminescence (Figures 4c-d and Ext. Figure 4b). These data point to the critical role of BAHCC1 in melanoma tumor engraftment, growth and metastatic progression *in vivo*.

BAHCC1 regulates E2F/KLF target genes involved in DNA repair and cell cycle

To better understand BAHCC1 function in melanoma cell proliferation, we first checked its localization by immunofluorescence in 501mel cells and observed its nuclear localization (Ext. Figure 5a). Analysis of subcellular protein fractions by immunoblot confirmed BAHCC1 accumulation in the nuclear soluble and insoluble fractions (Ext. Figures 5b). We then investigated the potential role of BAHCC1 to regulate melanoma gene expression first by transcriptome profiling of 501mel and MM047 cells before and after BAHCC1 KD. RNA-seq revealed that several hundred genes were deregulated in the absence of BAHCC1 (absolute log2 fold change >0.5 and adjusted P-value<0.05) (Figure 5a) with a significant overlap of 200 genes between the 501mel and MM047 cells (Figure 5b and Ext. Table 3). Gene Ontology (GO) analyses of the 200 co-downregulated and 82 co-upregulated genes revealed their enrichment in cell cycle (MCM7, TOP2A, CNTRL), DNA repair (RAD51B, FANCG, ATM), regulation of MAPK-pathway (MAP2K1, CDKN1B, CDKN2C) as well as mitochondria biogenesis (MTFR1, IMM2P2L, DNA2) and cell migration (MMP2, COL18A1, BMP1) (Figure

5c and Ext. Figures 5c), consistent with the anti-proliferative and anti-invasive effects of BAHCC1 KD observed above. Note that no modification of the melanocytic and mesenchymal signature of 501mel and MM047 was observed after BAHCC1 KD (Ext. Figures 5d).

To evaluate if BAHCC1 directly regulated gene expression by chromatin binding, we profiled endogenous BAHCC1 (BAHCC1^{WT}) genome-wide occupancy using CUT&Tag followed by deep sequencing in 501mel cells. We identified 31,280 peaks for endogenous BAHCC1^{WT}, localizing mostly in proximal gene promoters (37.62%) and distal intergenic (24.28%) regions (Ext. Figures 5e). Read density clustering of BAHCC1^{WT}, H3K27ac ChIP-seq and ATAC-seq in the 31,280 BAHCC1-occupied regions demonstrated that BAHCC1^{WT} mostly binds to active chromatin at the nucleosome depleted regions between two H3K27ac-marked nucleosomes (Figure 5d). Moreover, a large fraction of the 41,088 annotated transcription start-sites (TSS) showed a TSS-centered BAHCC1 and ATAC peaks flanked by H3K27ac chromatin marks (Figure 5e). Consistent with these data, analysis of the 1,000 best scoring BAHCC1-occupied sites with RSAT to identify transcription factor DNA binding motifs and transcription factors that may cooperate with or recruit BAHCC1 to regulate gene expression revealed strong enrichment of the NFY and SP family factors known to be enriched at proximal promoters (Ext. Table 4). Integrating BAHCC1 RNA-seq and CUT&Tag data, we observed that amongst the 11,385 genes associated with a TSS-centered BAHCC1 peaks, 783 genes were deregulated upon BAHCC1 KD in 501mel cells, of which 539 (70%) were down-regulated and 244 (30%) were up-regulated (Figure 5f). RSAT analyses of the DNA motifs under the BAHCC1 bound sites at the down-regulated promoters showed enrichment of NFY as above but also for motifs for KLF-family factors. Analyses at the promoters of up-regulated genes also showed KLF-family factors, but also SOX10 (Ext. Table 4).

Further evidence for the role of BAHCC1 in cell cycle gene regulation came from mining of single cell RNA-sequencing (scRNA-seq) from melanoma patient derived xenografts (PDXs) (Rambow et al., 2018), (Berico et al., 2021) where BAHCC1 seemed to be preferentially expressed in the “mitotic” melanoma cell subpopulation (Ext. Figures 5f) also significantly enriched in E2F and SP/KLF regulons (Ext. Figures 5g). Similarly, scRNA-seq from uveal and cutaneous tumors (Tirosh et al., 2016), (Pandiani et al., 2021) were separated into “Slow” or “Fast” cycling cells according to the Tirosh cell cycle signature (95 genes) (Ext. Table 5) (Tirosh et al., 2016). We observed that BAHCC1 was significantly enriched in fast cycling cells (Ext. Figures 5h), confirming its potential role in the control of the melanoma cell cycle. Similar observations were made using TCGA datasets from UVM or SKCM patients, in which BAHCC1 expression significantly correlated with the Tirosh cell cycle signature (Ext. Figures

5i). Together, these results demonstrate that BAHCC1 regulates the expression of a set of E2F/KLF-dependent genes involved in cell cycle and DNA repair.

BAHCC1 interacts with BRG1-containing complexes

Protein Blast and AlphaFold tools revealed the presence of a Coiled Coil (CC) region in the central part of the protein together with two well conserved TUDOR and Bromo-Adjacent Homology (BAH) domains at the C-terminal (Figure 6a). CCs are involved in protein-protein interactions, while BAH and TUDOR domains are found in a wide range of chromatin binding proteins where they are readers of histone modifications and act as chromatin co-activators/repressors (Ciani et al., 2010), (Musselman et al., 2012). We profiled genome occupancy of a FLAG-tagged truncated form of BAHCC1 missing the N-terminal CC domain and bearing only the short C-terminal region containing the TUDOR and BAH domains (BAHCC1^{TUDOR-BAH}) (Figure 6a). Genome-wide BAHCC1^{TUDOR-BAH} occupancy pattern highly overlapped with endogenous BAHCC1^{WT} as shown by seqMINER read density heatmap (Ext. Figures 6a), further validating the CUT&Tag data obtained above with the full-length endogenous protein. However, a limited cluster of sites was selectively occupied by endogenous BAHCC1^{WT}, but not the truncated form (Ext. Figures 6a and Ext. Table 6). This BAHCC1 N-terminal region-dependent cluster included 222 of the 539 genes down-regulated after BAHCC1 KD, including DNA repair or cell cycle genes such as ATM or CDKN1A (Ext. Figure 6b, and Ext. Table 6). In agreement with this, RSAT analyses showed that N-terminal region-dependent sites were preferentially enriched in KLF-family DNA binding motifs similar to the down-regulated promoters (Ext. Table 4).

We previously demonstrated that the BRG1 subunit of the PBAF chromatin remodeling complex occupied H3K27ac marked nucleosomes in 501mel melanoma cells (Laurette et al., 2015). Comparison of genome wide occupancy of both BRG1 and BAHCC1 showed that most BAHCC1 peaks were flanked by nucleosomes bound by BRG1 and marked by H3K27ac (Figure 6b). SeqMINER read density clustering allowed the identification of several BAHCC1-BRG1 clusters amongst which cluster 3 (C3) was associated with DNA repair and cell cycle genes including ATM that was strongly enriched in BAHCC1, BRG1 and H3K27ac at its promoter (Ext. Figure 6b). Moreover, a significant fraction of genes down-regulated upon BAHCC1 KD in 501mel were also down-regulated by BRG1 silencing (Figure 6c, left panel) including 75 of the 200 genes down-regulated in both 501mel and MM047 (Figure 6c, right panel). Most of these genes were found to be involved in mitosis and DNA repair, including ATM (Ext. Figures 6c-d and Ext. Table 3).

We next aimed to investigate whether a physical interaction could be observed between BAHCC1 and BRG1-containing complexes. BRG1 co-immunoprecipitated with endogenous BAHCC1, together with the BAF and pBAF subunits PBRM1, SMARCC1 and SMARCC2 in 501mel cells (Figure 6d). In parallel, pull down of BRG1 co-precipitated the FLAG-tagged BAHCC1^{TUDOR-BAH} deletion mutant overexpressed in HEK293T cells (Figure 6e). We further observed that BRG1 co-precipitated specifically with the BAH domain of BAHCC1 but not with the TUDOR domain (Figure 6f). The BAHCC1^{BAH}-BRG1 co-precipitation was confirmed in 501mel melanoma cells stably expressing HA-tagged BAHCC1^{BAH} domain (Ext. Figures 6d).

Finally, both H3K27ac and BRG1 genomic occupancy was reduced around BAHCC1-binding sites when BAHCC1 was invalidated in 501mel (Figure 6g). Altogether, these data highlight a direct physical interaction between BAHCC1 and BRG1-containing BAF and PBAF complexes, which impacts BRG1 recruitment and H3K27ac deposition around BAHCC1-binding sites.

BAHCC1 KD cooperates with PARP inhibition to induce melanoma cell death

The above results suggested a role of BAHCC1 in genome stability through its regulation of DNA repair proteins, including the master DNA damage repair sensor ATM. In agreement, RT-qPCR and immunoblotting showed that BAHCC1 KD decreased expression of ATM at the mRNA and protein levels (Figures 7a and b), which can be explained by a loose of H3K27ac deposition and BRG1 recruitment at its promoter (Ext. Figure 7a). Furthermore, BAHCC1 expression positively correlated with genome alteration frequencies in human melanoma tumors (Figure 7c). We then tested the effect of BAHCC1 KD on the ability of 501mel cells to repair DNA following treatment with Neocarzinostatin (NCS) that induces DNA double strand breaks (Figure 7d). Strikingly, BAHCC1 KD led to higher numbers of γ H2AX foci during the repair time course, indicating a delay in the repair of DNA double strand breaks in the absence of BAHCC1 (Figure 7e and Ext. Figure 7b).

Poly (ADP-ribose) polymerase 1 (PARP1) is the main PARP-family protein involved in DNA damage response where it acts as a DNA damage sensor. PARP1 inhibition (PARPi) has been shown to increase DNA replication fork destabilization leading to accumulation of DNA breaks (Caron et al., 2019). Since the PARP-pathway acts independently from ATM, it has been postulated that ATM-deficient cancer cells become addicted to PARP-dependent DNA repair, making them highly sensitive to PARPi (Pilié et al., 2019). Therefore, we queried whether BAHCC1 KD might potentiate the effect of PARPi in melanoma cells. Strikingly, co-treatment

with the PARPi Olaparib and BAHCC1 KD showed a significant cooperative effect on viability of 501mel (MITF^{HIGH}, BRAF^{V600E}), MM117 (MITF^{HIGH}, Triple-wt) and MM047 (MITF^{LOW}, NRAS^{Q61R}) melanoma cells due to increased apoptosis (Figure 7f). Finally, we tested the impact of the combination of PARPi and targeted therapies on the viability of 501mel cells with or without BAHCC1 with SynergyFinder, using the Zero Interaction Potency (ZIP) model. In the absence of BAHCC1, the overall positive ZIP score of 4.45 suggested moderate synergy between the two drugs, which was highest at intermediate and high concentrations of Olaparib (ZIP \geq 10), regardless of the concentration of Trametinib (Figure 7g, right panel). The negative ZIP score in the presence of BAHCC1 (Figure 7g, left panel) suggested that it was the absence of BAHCC1 that induced the moderate synergism observed above. Overall, these findings demonstrate the important role of BAHCC1 in the expression of DNA repair genes such as ATM, the kinetics of DNA-repair and are in line with the idea that melanoma cells may be sensitized to PARPi by BAHCC1 depletion.

Discussion

Deregulation of gene expression in cancer cells is well established and cannot be explained solely by genomic alterations such as mutations or copy number variations. Cancer cells undergo significant changes in their transcriptional program through extensive rewiring that includes the acquisition of alternative gene regulatory elements such as SEs (Lee and Young, 2013), (Lovén et al., 2013), (Bradner et al., 2017). Here, using several H3K27ac ChIP-seq data sets from short-term patient-derived cutaneous melanoma cultures, we identified melanoma-specific SEs and their associated genes that could also be exploited in therapy. We further integrated the H3K27ac profile with the binding profiles of master regulators in melanoma cells such as SOX10 and MITF, which occupy long and short enhancers found in cutaneous melanocytic-like melanoma cells with SOX10 being required to achieve high levels of activity (Mauduit et al., 2021). Our analysis converged on the SE17q25 element that was activated in most of the melanocytic-like melanoma cells but also in SKCM and UVM biopsies regardless of driver mutation status (BRAF, NRAS, Triple-WT in cutaneous and GNAQ or GNA11 in uveal melanoma). In cutaneous melanoma cells, the SE17q25 element was not only highly occupied by MITF and SOX10, but also by the TFIIH kinase CDK7 and BRG1, all of which are known to occupy relevant SEs (Kwiatkowski et al., 2014), (Barutcu et al., 2016), (Eliades et al., 2018). Depletion of MITF or SOX10 as well as TFIIH inhibition decommissioned

SE17q25 and reduced the expression of BAHCC1, a gene located in close vicinity to SE17q25. In addition, selective CRISPR-mediated silencing of SE17q25 significantly affected BAHCC1 expression strongly supporting the idea that SE17q25 regulated BAHCC1 expression. TCGA data on human tumors consolidated these observations and showed that SE17q25 activity in various tumors correlates with BAHCC1 expression. Importantly, SKCM are the tumors in which SE17q25 activity and BAHCC1 expression are highest.

In agreement with its dependency on MITF and SOX10 observed *in vitro*, high BAHCC1 expression correlated with high MITF and SOX10 expression in melanoma biopsies and with poor prognosis in both SKCM and UVM patients (Gao et al., 2020). Consistent with these findings, an extensive analysis of single cell transcriptomic data from melanoma PDX demonstrated that BAHCC1 expression was the highest in “mitotic-like” melanoma cells, (Berico et al., 2021). “Mitotic” melanoma cells have been found in metastatic SKCM and UVM biopsies and are characterized by the expression of E2F-dependent genes. E2F transcription factors are known to promote melanoma progression and metastasis (Ma et al., 2008), (Alla et al., 2010). These data are consistent with the fact that our *in vitro* and *in vivo* functional studies showed that BAHCC1 was involved in melanoma cell proliferation and metastatic progression by regulating a set of E2F/KLF-dependent genes. Although MITF^{LOW} cells have significantly reduced SE17q25 activity and BAHCC1 expression, we observed that they also depend on SE17q25 and BAHCC1, whose expression may be differently regulated by other TFs important for the mesenchymal state such as TFAP2A, FOSL2 and TEAD4 that bind within SE17q25 (Verfaillie et al., 2015), (Fontanals-Cirera et al., 2017), (Wouters et al., 2020) (Mauduit et al., 2021) .

BAH domains are known to bind post-translation modifications (PTMs) of histones such as H3K27me3 (Zhao et al., 2016), (Fan et al., 2020) and H4K20me2 (Kuo et al., 2012), (Dai et al., 2018). A previous study characterized the BAHCC1 BAH domain showing that it bound H3K27me3 and that BAHCC1 interacted with Histone de-acetylases (HDACs) and SAP30BP proteins of the polycomb repressor complex 1 (PRC1) in Acute Myeloid Leukemia (AML) to repress a large number of genes involved in myeloid differentiation and promote cell proliferation (Fan et al., 2020). In melanoma, BAHCC1 did not show a predominant repressive role, as an equivalent number of genes were up and down regulated after BAHCC1 KD. CUT&Tag performed on H3K27me3 in 501mel demonstrated that this mark was not present around the BAHCC1 binding sites (Ext. Figure 8). These observations support the idea that BAHCC1 activity in melanoma does not depend on BAH-H3K27me3 interactions. Our data demonstrated a novel interaction between BAHCC1 and the SWI/SNF chromatin remodeling

complexes, occurring through the BAHCC1^{BAH} domain. We suppose that BRG1 may act upstream to remodel the chromatin, creating the nucleosome-depleted regions to be occupied by BAHCC1. Alternatively, BAHCC1 may be recruited to chromatin via interaction with transcription factors such as those of the KLF/SP/E2F families to regulate their target genes. Moreover, the N-terminal region of BAHCC1, containing the CC domain, appears to be important for the recruitment of BAHCC1 to a set of genes involved in cell proliferation and DNA repair again suggesting that the BAH domain is not the only determinant of genomic recruitment. We therefore propose that either or both of the above mechanisms drive BAHCC1 genomic recruitment in melanoma in stark contrast to the BAH-H3K27me3 pathway in AML. Metastatic melanoma is characterized by the overexpression of genes involved in the DNA damage response (DDR), which makes this tumor stage highly refractory to chemo- and radio-therapies (Kauffmann et al., 2008). DDR is essential for maintaining genomic stability to face genotoxic stress resulting from environmental and endogenous DNA damage. In the DDR, ATM, the pivotal mediator of genotoxic stress, phosphorylates histone H2AX to γ H2AX to generate docking sites for proteins involved in DNA break repair. ATM also links DNA damage to the cell cycle by controlling key DNA damage checkpoints to regulate DNA break repair directly or indirectly through the control of cell cycle checkpoints. On the other hand, PARP1 is able to bind to damaged DNA sites to promote the PARylation of surrounding proteins, thus creating new scaffolds for the recruitment of DNA repair proteins involved in an alternative DNA break repair pathway. This dual DNA repair mechanism ensures that DNA breaks are repaired efficiently. However, the loss of one DNA repair pathway results in increased reliance on the other that is not essential under normal settings. Therefore, a high response rate to the PARP inhibitor Olaparib was found in patients with metastatic prostate (Mateo et al., 2015) or gastric (Bang et al., 2015) cancers harboring low expression or mutations of ATM. Since ATM was one of the E2F-dependent genes strongly regulated by BAHCC1, we wondered if this dependence could be exploited therapeutically. Interestingly, BAHCC1 KD cooperates with PARP inhibition by Olaparib to impact cell survival, associated with increased apoptosis. In addition to their potential clinical application, these data clearly demonstrate the involvement of BAHCC1 in the control of genes involved in DDR in melanoma cells and suggest that metastatic melanoma upregulates BAHCC1 to promote genomic stability and cellular fitness necessary to sustain high mitotic rates. Accordingly, melanoma brain metastases have higher genomic instability underpinning an increased copy number variation rate compared to extracranial metastasis (ECMs) (Biermann et al., 2022). scRNA-seq data mining in Biermann cohort of 22 melanoma brain metastases and 10

melanoma extracranial metastasis demonstrate indeed that both ATM and BAHCC1 are significantly upregulated in MBMs vs. ECMs in melanoma proliferating cells. In agreement with that, our *in vivo* metastatic studies have proven the complete incapacity of melanoma cells to seed and form secondary lesions in liver, lungs and brain in absence of BAHCC1. Finally, the presence of a gene expressed in both cutaneous and uveal melanoma cells make it possible to envisage common treatments for these two cancers.

Limitations of the study

Our study shows the involvement of BAHCC1 in melanoma progression and metastasis. We show that BAHCC1 is a transcription factor involved in regulating the expression of genes involved in cell cycle progression and DNA repair. Although we have shown the link between BAHCC1 and BRG1- containing transcription complexes, we have not demonstrated the precise molecular role of BAHCC1 in melanoma. We assume that it interacts with BAF/pBAF complexes to facilitate their recruitment to the promoters of these genes, but we have not demonstrated this hypothesis.

Acknowledgments

We thank the IGBMC facilities, in particular Paola Rossolillo and Karim Essabri for the isolation of BAHCC1 cDNA, and Dr Catherine Birck and Dr Nathalie Troffer-Charlier for the purification of the BAH and Tudor domains. We thank Prof D. Lipsker and the staff of the Strasbourg University Hospital dermatology clinic for tumour sections and Prof. G. Ghanem and Prof. J-C Marine for providing us the MM-series melanoma cultures. This study was supported by the Institut National Du Cancer (INCa) (2017-11537), the Ligue contre le Cancer (Equipe labélisée 2022, FC and ID), the Fondation ARC, and the ANR-10-LABX-0030-INRT, a French State fund managed by the Agence Nationale de la Recherche under the frame program Investissements d’Avenir ANR-10- IDEX-0002-02. Sequencing was performed by the IGBMC GenomEast platform, a member of the “France Génomique” consortium (ANR-10-INBS-0009). E.H. is founded by R01CA243446, R01CA274100, U54 CA263001 and R01CA277425 (NCI/NIH). P.B. is supported by the Ligue contre le Cancer and the National Cancer Center.

Conflict of interest

The authors declare no competing financial interest in relation to the work described.

Author Contributions

P.B., I.D. and F.C. conceived the study. P.B., I.D. and F.C. analyzed the data. P.B. performed most of the *in vitro* functional studies, the RNA-seq and RNAScope. P.B., and M.N. performed the RT-qPCR, and the WB. S.L., G.D., T.Y and P.B., performed bioinformatic analyses. B.V., A.L. and M.C. performed wet lab of CUT&Tag experiments. M.C. performed the boyden-chamber experiments. M.C. performed the SynergyFinder experiment. L.S performed immunoprecipitation. E.H. supervised the *in vivo* studies and gives inputs to the manuscript. P.B., F.V.R, A.Y.F and C.C.F performed *in vivo* experiments. G.M., G.G., M. D., E.C. and C.B. provided valuable materials. F.C., I.D. and P.B wrote the manuscript.

Lead Contact

Further information and requests for resources and reagents should be directed to and will be fulfilled by the Lead Contact, Frédéric Coin (fredr@igbmc.fr).

Materials availability

Reagent generated in this study will be made available on request, but we may require a payment and/or a completed Materials Transfer Agreement if there is potential for commercial application.

Data availability. Next generation sequencing raw and processed data have been deposited in the SuperSeries Gene Expression Omnibus under accession number GSE205463: RNA-seq GSE201702, CUT&Tag GSE205462.

Competing Financial Interests

Authors declare no competing financial interests.

STAR Methods

Sample collection

Tumors 1, 2 and 3 for cutaneous melanoma were described in (Ennen et al., 2017) as tumors 4, 5 and 6. Tumor for uveal melanoma (#A-D) were described in (Pandiani et al., 2021).

Cell culture

Patient-derived short-term cultures MM cells have been grown in HAM-F10 (Gibco, Invitrogen) supplemented with 10% Fetal Calf Serum (FCS) and penicillin-streptomycin. 501mel and SK-MEL-28 cells were grown in RPMI w/o HEPES (Gibco, Invitrogen) supplemented with 10% FCS and gentamycin and IGR37 and IGR39 were grown in RPMI w/o HEPES supplemented with 15% of FCS and gentamycin. Uveal melanoma cells OMM1.3 and OMM2.5 were cultured respectively in DMEM (4.5g/l glucose) supplemented with 10% FCS, penicillin-streptomycin, Sodium Pyruvate, MEM essential vitamin mixture, NEAA mixture and Hepes, and RPMI w/o HEPES supplemented with 2gr/l glucose, 10% FCS and penicillin-streptomycin. U-2 OS cells were grown in DMEM/Ham-F10 (1:1) supplemented with 10% FCS and gentamicin. HEK293T cell were grown in DMEM (1g/l glucose) supplemented with 10% FCS and penicillin-streptomycin. All cell lines were grown in 5% CO₂ at 37°C. Melanocyte cell line Hermes3A was grown in 10% CO₂ at 37°C in RPMI w/o HEPES supplemented with 10% FCS, penicillin-streptomycin, 200nM TPA (Sigma Aldrich), 200pM Cholera Toxin (Sigma Aldrich), 10ng/mL hSCF (Life Technologies), 10nM EDN-1 (Sigma Aldrich) and 2mM Glutamine (Invitrogen). All cell lines used were mycoplasma negative.

501mel for in vivo studies were generated in the Hernando Lab transducing cells first with lentiviral vector pEIGW-SK II Luc-GFP (kindly provided by Dr. Iannis Aifantis) followed by a second transduction with MISSION® shRNA lentiviral vectors shNTC (Millipore Sigma, SHC002), shBAHCC1^{#1} (Millipore Sigma, TRCN0000230988) and shBAHCC1^{#2} (Millipore Sigma, TRCN0000217993) as previously described (Fan et al., 2020)

501mel HA-BAHCC1^{BAH} were generated by transducing cells with lentiviral vectors pLenti-TET-3HA-BAHCC1^{BAH} and selected with 0.5ug/mL of puromycin.

Cells carrying a doxycycline-inducible system were treated with 1ug/mL of doxycycline for at least 24h.

GapmeRs or siRNAs were transfected in cells with Lipofectamine RNAiMAX following the manufacture instructions using an oligos final concentration of 25nM and cells were harvested 48h and/or 72h after transfection.

For CRISPRi experiments, 501mel cells were co-transfected with pX629_dCas9_KRAB_mScarlet (plasmid obtained from the IGBMC BioMol service) and pCDNA-GFP (gCTRL) or pCDNA-GFP-SE17q25 (gSE17q25) using Fugene6 following manufacture instructions. Afterward, double positive GFP+/mScarlet+ cells were sorted with

a FACSAria Fusion BD Biosciences Cell sorter and RNA extraction was performed 72h post sorting.

BAHCC1^{TUDOR} and BAHCC1^{BAH} were cloned into a pcDNA-FLAG vector. pcDNA-FLAG, pcDNA-FLAG-BAHCC1^{TUDOR}, pcDNA-FLAG-BAHCC1^{BAH}, pLenti6-GFP and pLenti6-3HA-BAHCC1^{BAH-TUDOR} vectors were transiently transfected in HEK293T cells with Lipofectamine 2000 following the manufacture instructions.

Synergy assay

24 hours after transfection with GAPMERs, 501mel or MM047 cells were seeded into 96-well plates at 5.000 cells/well. 24 hours later, cells were incubated with combinations of increasing concentrations of the MEK inhibitor Trametinib or the PARP inhibitor Olaparib, for 72 hours. Cell viabilities were cells assessed using PrestoBlue reagent (ThermoFisher) according to the manufacturer's instructions. The absorbance was measured with a Cell-Insight CX5 microplate reader. Synergy scoring was then determined using the SynergyFinder software (<https://synergyfinder.fimm.fi>) and by implementing the ZIP calculation method (Ianevski et al., 2022).

Identification of SEs

H3K27ac ChIP-seq data from 12 different melanoma cell lines (MM001, MM011, MM031, MM034, MM057, MM074, MM047, MM087, MM099, MM118, SK-MEL-5, 501mel) and 3 melanocytes cell lines (NHEM1, NHEM2, Foreskin) were retrieved from GEO GSE60666, GSM958157 and GSE94488 and mapped to the Homo Sapiens genome (assembly hg19) using Bowtie v1.0.0 with default parameters except for “-p 3 -m 1 -strata -best -chunkmbs 128”. Normalized BigWig files were generated using Homer makeUCSCfile v4.9.1 with the following parameter ‘-norm 20e6’ meaning that data were normalized to 20M reads. The genome was divided into bins of 10Kb long with Deeptools multiBamSummary v2.5.0. The number of reads for each bin was computed for each sample. The following figure was made with Deeptools plotCorrelation and shows the pairwise correlation values (Spearman) for all samples of this project. Peaks were called using MACS2 with default parameters except for “-g hs -f BAM -broad -broad-cutoff 0.1”. Peaks falling into ENCODE blacklisted regions (“An Integrated Encyclopedia of DNA Elements in the Human Genome” 2012–9AD) were removed. Peaks were annotated relative to genomic features using Homer v4.9.1 (annotations got extracted from gtf file downloaded from ensembl v75). ROSE was used to differentiate SEs from typical enhancers (detected from H3K27ac data). SEs were annotated relative to genomic

features using Homer v4.9.1 (annotations got extracted from gtf file downloaded from ensembl v75). Finally, SEs were filtered according to their position relative to the one of SOX10 and MITF (ChIP-seq tracks in 501mel) (Strub et al., 2011),(Laurette et al., 2015) using the bioconductor package DiffBind v1.12.3.

RNA FISH

Assays were performed following the manufacturer's instructions (<https://acdbio.com/manual-assays-rnascope>). For the detection of BAHCC1 and SOX10, cells and paraffin tissue sections were treated following the RNAScopeTM manufacture protocol. Cells and tissue samples were counterstained with DAPI and visualized using confocal microscope Spinning disk Leica CSU W1. The sequences of the probes were not provided by the manufacture.

Protein extraction

For the production of whole cell extracts, cells were washed once with cold PBS, rinsed with a cell scraper, pelleted and resuspended in LSDB 0.5M buffer (0.5M KCl, 50mM Tris HCl pH 7.9, 20% Glycerol, 1% NP40, 1mM DTT, PIC). Afterwards cells were fully disrupted with 3 cycles of heat shock in liquid nitrogen and 37°C water bath and centrifugated 15min at 14,000rpm to pellet cell debris.

To obtain cytoplasmic and nuclear protein fractions, cells were first lysed in hypotonic buffer (10 mM Tris-HCl at pH 7.65, 1.5 mM MgCl₂, 10 mM KCl) and disrupted by Dounce homogenizer. The cytosolic fraction was separated from the pellet by centrifugation at 4°C. The nuclear soluble fraction was obtained by incubation of the pellet in high salt buffer (final NaCl concentration of 300 mM) and then separated by centrifugation at 4°C. To obtain the nuclear insoluble fraction (chromatin fraction), the remaining pellet was digested with micrococcal nuclease and sonicated.

Co-immunoprecipitation

Whole cell extract was prepared by resuspending cells in LSDB buffer (50mM Tris HCl pH 7.9, 20% Glycerol, 1% NP40, 1mM DTT, PIC) containing 150mM KCl, followed by sonication in Q800R3 sonicator. Between 250ug-1mg of protein extract was used to performed IP with 1-10ug of primary antibody overnight at 4°C on rotation. Following, 50ul of Dynabeads protein A/G were added to the samples for 2h at 4°C. In alternative, FLAG-tagged proteins were immunoprecipitated directly using Affinity Gel FLAG M2 conjugated beads. Beads were washed five times with TGEN buffer (20mM Tris-HCl pH 7.65, 3mM MgCl₂, 0.1mM EDTA,

10% glycerol, 0.01% NP-40, PIC) containing 150mM NaCl. Samples were loaded on NuPage gel to perform western blot

RNA extraction and RT-qPCR

Total RNA isolation was performed according to the manufacture protocol with NucleoSpin RNA Plus kit. RNA was retrotranscribed with Reverse Transcriptase Superscript IV and qPCR was performed with SYBR Green and monitored by LightCycler 480. Gene expression results were normalized according to four housekeeping genes (HMBS, TBP, UBC and RPL13a). Primers for RT-qPCR and ChIP-qPCR were designed using Primer-BLAST.

Immunofluorescence

Immunofluorescence assay was performed as previously described (Laurette et al., 2015). Human tissue sections were deparaffinized and dehydrated with Histosol and dilutions of ethanol 100%, 90%, 70% and 30% and rehydrated with demineralized water. Subsequently sections were boiled in Sodium Citrate buffer (0.1M Citric acid, 0.1M Sodium citrate) for 15min to unmask antigens. In parallel, 2D culture cells were grown on LAB-TEK II chamber slides and fixed with 4% formaldehyde or 100% methanol. Afterward, both tissues and cells were permeabilized and saturated in blocking buffer (1% BSA, PBS, 0.3% TritonX-100). Primary antibodies were diluted in blocking buffer and incubate ON at 4°C in wet chamber. Secondary antibody staining was carried out in blocking buffer for 1h and 30min at room temperature. Nuclei were marked with DAPI and slides were mounted with ProLong™ Gold antifade reagent before microscope image acquisition.

For γ H2AX foci quantification, transfected or naïve cells were plated in 96 well plates OptiPlates-96 and eventually treated with NCS (150nM) for 1h at 37°C followed by 1h, 8h or 24h of recovery in complete medium. Afterward, cells were labeled for γ H2AX following a classic immunofluorescence protocol. Image acquisition was done using high-throughput imaging system CX7 using 20X objective (50 fields per well). Image segmentation was done with HCS studio. Nuclei were identified using DAPI staining and γ H2AX foci were identified within nuclei mask. Foci number and intensity were quantified automatically.

Cell proliferation assay

To measure cell proliferation, cells were incubated first with CellTrace Violet according to the manufacture instructions. Cell proliferation, were detected on a FORTESSA BD Biosciences Cytofluorometer. Data were analyzed with FlowJo software. To define slow proliferating cells, we proceeded as follows: We considered that slow proliferating cells represented the 30% of

cells with the highest concentration of BV421 in the control treatment. We then calculated the % of cells that had a concentration greater than or equal to this value after treatment.

Cell death assay

To measure cell death, cells were rinsed and incubated 15min with AnnexinV-APC after treatment. Cell death was detected on a FORTESSA BD Biosciences Cytofluorometer. Data were analyzed with FlowJo software.

Cell density assay

Cell density assay was performed as previously described (Berico et al., 2021). Briefly, following transfection, between $5 \cdot 10^4$ to $1 \cdot 10^5$ cells were grown in 6 wells plate for up to 1 week. Afterward cells were fixed for 10min with 4% Formaldehyde solution, washed once with PBS and stained with Crystal Violet solution 0.2% for 15min at room temperature. The wells were finally washed twice with deionized water, air dried, scanned and analyzed with Fiji considering the area occupancy of the cells.

Cell invasion assay

Boyden-Chamber invasion assay was performed as previously described (Berico et al., 2021). Briefly, between 1 and $2 \cdot 10^5$ cells were seeded inside a Boyden Chamber insert covered with Serum free media and 4% Matrigel. The inserts were placed in 24 wells plate filled with complete medium. After 12-24h, the inserts were fixed with 4% Formaldehyde solution for 10min, gently cleaned inside with a cotton stick and stained for 15min at room temperature with a Crystal Violet solution 0.2%. Afterward the inserts were washed twice in deionized water, air dried and photos were collected using an EVOS xl Core microscope. The pictures were analyzed with Fiji considering the area occupancy of the cells.

CUT&Tag and deep sequencing

Assays were performed following the manufacturer's instructions (<https://www.activemotif.com/catalog/1318/cut-tag-it-kit>). Briefly, $5 \cdot 10^5$ cells per condition were used. The cells were washed 2 time before the binding on Concavalin A beads and then incubated overnight with BAHCC1 (BAHCC1^{WT}) or HA (BAHCC1^{TUDOR-BAH}) primary antibodies at the recommended dilution (1:50) or without antibody (negative control). The next day the corresponding secondary antibody, a guinea pig Anti-rabbit antibody was used following a 1:100 dilution in digitonin buffer and incubated at room temperature for 1h. The

CUT&Tag-IT™ Assembled pA-Tn5 Transposomes were incubated for 1h at room temperature before tagmentation. Cells were resuspended in Tagmentation buffer and incubated at 37°C for 1h, then the Tagmentation process was stopped by addition of EDTA and SDS. Protein digestion was performed by the addition of 80ug/mL of proteinase K and incubated at 55°C for 60min. DNA was retrieved on DNA purification columns provided by the manufacturer. Library preparation and PCR amplification were done using the Kit primers and purified by 2 successive washes with SPRI beads. Samples were subjected to paired-end sequencing by the IGBMC GenomEast platform on Illumina HiSeq 4000 instrument.

Deep sequencing analysis

ChIP-seq data for BRG1 (Laurette et al., 2015), H3K27ac and ATAC-seq (Fontanals-Cirera et al., 2017) and CUT&Tag-seq for BAHCC1 (this work) were analyzed as previously described (Berico et al., 2021). Briefly, after reads mapping onto hg19 human genome, peak calling was performed using MACS2 according to specific negative control inputs (Zhang et al., 2008). Peak annotation was carried out using HOMER and ChIPseeker. Peak genome distribution and correlation between BAHCC1 and BRG1, H3K27ac and ATAC was performed using deepTool2. Peak enrichment for BRG1, H3K27ac, ATAC and BAHCC1 was done using seqMINER. Top 500 macs peaks summits for BAHCC1 alone or co-bound by BAHCC1 and BRG1 (identified with seqMINER) were subsequently extended of 100bp upstream and downstream using “bedtools slop” followed by extraction of FASTA format sequences with “bedtools getfasta”. DNA binding motif analysis was carried out with Simple Enrichment Analysis (SEA) (Bailey and Grant, 2021) and by the pipeline “peak-motifs” available online as part of the Regulatory Sequence Analysis Tools (RSAT) web server using +/- 400bp around the center to cut peak sequences and the non-redundant vertebrate Jaspar core database for motif comparison.

Bulk RNA-seq analysis

Reads were preprocessed to remove adapter and low-quality sequences (Phred quality score below 20). After this preprocessing, reads shorter than 40 bases were discarded for further analysis. These preprocessing steps were performed using cutadapt version 1.10. Reads were mapped to rRNA sequences using bowtie version 2.2.8 and reads mapping to rRNA sequences were removed for further analysis. Reads were mapped onto the hg19 assembly of Homo sapiens genome using STAR version 2.5.3a. Gene expression quantification was performed from uniquely aligned reads using htseq-count version 0.6.1p1, with annotations from Ensembl

version 75 and “union” mode. Only non-ambiguously assigned reads have been retained for further analyses. Read counts have been normalized across samples with the median-of-ratios method proposed by Anders and Huber (Anders and Huber, 2010) to make these counts comparable between samples. Comparisons of interest were performed using the Wald test for differential expression proposed by Love (Love et al., 2014) and implemented in the Bioconductor package DESeq2 version 1.16.1. Genes with high Cook’s distance were filtered out and independent filtering based on the mean of normalized counts was performed. P-values were adjusted for multiple testing using the Benjamini and Hochberg method (Benjamini and Hochberg, 1995). iRegulon plugin of Cytoscape was used to analyze the co-deregulated genes between iBAHCC1 and iBRG1.

Single cell data analysis

Expression matrix with row reads counts for the single cell experiment was retrieved from GEO GSE116237, GSE115978, GSE151091, GSE138665, GSE185386 and GSE113502 datasets. Then, data were normalized and clustered using the Seurat software package version 3.1.4 in R version 3.6.1. Data were filtered and only genes detected in at least 3 cells and cells with at least 350 detected genes were kept for further analysis. Expression of 26,661 transcripts in single cells was quantified. To cluster cells, read counts were normalized using the method “LogNormalize” of the Seurat function NormalizeData. It divides gene expression counts by the total expression, multiplies this by a scale factor (10,000 was used), and log-transforms the result. Then, 2000 variable features were selected with the variance stabilizing transformation method using the Seurat function FindVariableGenes with default parameters. Integrated expression matrices were scaled (linear transformation) followed by principal component analysis (PCA) for linear dimensional reduction. The first 20 principal components (PCs) were used to cluster the cells with a resolution of 0.5 and as input to tSNE to visualize the dataset in two dimensions. The Bioconductor package AUCell v 1.6.1 was used to assess whether some cells from the different datasets were enriched in gene sets of interest.

Other publicly available datasets used in this work

BAHCC1 RNA expression was quantified in available datasets including GEO GSE12391 (Scatolini et al., 2010), GSE80829 (Tsoi et al., 2018), GSE98394 (Badal et al., 2017), GSE114445 (Yan et al., 2019), GSE46517 (Kabbarah et al., 2010), GSE8401 (Xu et al., 2008) and in the CCLE portal. TCGA and GTEx data were obtained through UCSC Xena browser, cBioPortal and Gene Expression Profiling Interactive Analysis 2 (GEPIA2). PCA profile of

TCGA and melanoma cell lines according to their phenotypic profile was obtained from the Graeber Lab software

Mouse xenograft studies

Animal experiments in NYU Langone Health were approved by the Institutional Animal Care and Use Committee (IACUC) under the protocol number IA16-00051. Immunodeficient mice NOD.Cg-Prkdc^{scid} IL2rg^{tm1Wjl}/SzJ (NSG) were purchased from Jackson Laboratories and maintained in the NYU Langone Health SBCAF animal facility germ-free. For primary tumor formation, 1×10^5 501mel cells were resuspended in 50ml of PBS + 50ml of Corning Matrigel® Matrix Basement Membrane (ref 354234) and injected intradermally in the flank of the animal. For metastasis formation, 1×10^5 501mel cells were resuspended in 100ml of PBS mice and injected in the heart left ventricle of the animal through ultrasound imaging-guided intracardiac injection. Metastatic progression was quantified once per week through luciferase radiance bioluminescence with In Vivo Imaging System (IVIS) imager at the NYU Langone's Experimental Animal and Exposure Core. Animals were euthanized when the body weight reached a 20% decrease. Primary tumor volume was measured every 3 days after becoming palpable using a two-dimensional caliper (volume = $(\pi/6) \times \text{length} \times \text{wide}^2$) and animals were euthanized when tumors reached 1cm³ volume.

After euthanasia, mouse organs were collected and analyzed for GFP fluorescence using a Zeiss AxioObserver microscope in the NYU Langone's Microscopy Laboratory. Afterward, organs were fixed in 10% Formalin for 72hrs followed by 72hrs in ethanol 70% before paraffin inclusion, sectioning, hematoxylin & eosin staining and imaging at the NYU Langone's Experimental Pathology Research Laboratory.

Statistical analysis

Statistical analysis was mostly performed using Prism 9. Briefly, for absolute quantification comparison, Student's t-test and ordinary one-way ANOVA unpaired were used; paired test was used for relative quantification comparisons. Grouped sample analysis was carried out through two-way ANOVA test. Kaplan-Meier survival curves were analyzed using Mantel-Cox test. For correlation analysis, Spearman analysis was performed together with linear regression curve fit. Statistical analysis on RNA-seq and ChIP-seq is listed in their dedicated sections. For Venn diagram statistic, hypergeometric test was performed using Nemates software (nemates.org). P values are represented as ns (p>0.05), * (p<0.05), ** (p<0.01), *** (p<0.005) and **** (p<0.001).

References

- Alla, V., Engelmann, D., Niemetz, A., Pahnke, J., Schmidt, A., Kunz, M., Emmrich, S., Steder, M., Koczan, D., Pützer, B.M., 2010. E2F1 in Melanoma Progression and Metastasis. *JNCI: Journal of the National Cancer Institute* 102, 127–133. <https://doi.org/10.1093/jnci/djp458>
- Ameratunga, M., Braña, I., Bono, P., Postel-Vinay, S., Plummer, R., Aspegren, J., Korjamo, T., Snapir, A., de Bono, J.S., 2020. First-in-human Phase 1 open label study of the BET inhibitor ODM-207 in patients with selected solid tumours. *British Journal of Cancer* 123, 1730–1736. <https://doi.org/10.1038/s41416-020-01077-z>
- Anders, S., Huber, W., 2010. Differential expression analysis for sequence count data. *Genome Biology* 11, 1–12. <https://doi.org/10.1186/GB-2010-11-10-R106/COMMENTS>
- Badal, B., Solovyov, A., Di Cecilia, S., Chan, J.M., Chang, L.W., Iqbal, R., Aydin, I.T., Rajan, G.S., Chen, C., Abbate, F., Arora, K.S., Tanne, A., Gruber, S.B., Johnson, T.M., Fullen, D.R., Raskin, L., Phelps, R., Bhardwaj, N., Bernstein, E., Ting, D.T., Brunner, G., Schadt, E.E., Greenbaum, B.D., Celebi, J.T., 2017. Transcriptional dissection of melanoma identifies a high-risk subtype underlying TP53 family genes and epigenome deregulation. *JCI Insight* 2. <https://doi.org/10.1172/jci.insight.92102>
- Bailey, T.L., Grant, C.E., 2021. SEA: Simple Enrichment Analysis of motifs. *bioRxiv* 2021.08.23.457422. <https://doi.org/10.1101/2021.08.23.457422>
- Bang, Y.-J., Im, S.-A., Lee, K.-W., Cho, J.Y., Song, E.-K., Lee, K.H., Kim, Y.H., Park, J.O., Chun, H.G., Zang, D.Y., Fielding, A., Rowbottom, J., Hodgson, D., O'Connor, M.J., Yin, X., Kim, W.H., 2015. Randomized, Double-Blind Phase II Trial With Prospective Classification by ATM Protein Level to Evaluate the Efficacy and Tolerability of Olaparib Plus Paclitaxel in Patients With Recurrent or Metastatic Gastric Cancer. *JCO* 33, 3858–3865. <https://doi.org/10.1200/JCO.2014.60.0320>
- Barutcu, A.R., Lajoie, B.R., Fritz, A.J., McCord, R.P., Nickerson, J.A., Van Wijnen, A.J., Lian, J.B., Stein, J.L., Dekker, J., Stein, G.S., Imbalzano, A.N., 2016. SMARCA4 regulates gene expression and higherorder chromatin structure in proliferating mammary epithelial cells. *Genome Research* 26, 1188–1201. <https://doi.org/10.1101/gr.201624.115>
- Benjamini, Y., Hochberg, Y., 1995. Controlling the False Discovery Rate: A Practical and Powerful Approach to Multiple Testing. *Journal of the Royal Statistical Society: Series B (Methodological)* 57, 289–300. <https://doi.org/10.1111/J.2517-6161.1995.TB02031.X>
- Berico, P., Cigrang, M., Davidson, G., Braun, C., Sandoz, J., Legras, S., Vokshi, B.H., Slovic, N., Peyresaubes, F., Gene Robles, C.M., Egly, J., Compe, E., Davidson, I., Coin, F., 2021. CDK7 and MITF repress a transcription program involved in survival and drug tolerance in melanoma. *EMBO reports* 22, 1–18. <https://doi.org/10.15252/embr.202051683>
- Biermann, J., Melms, J.C., Amin, A.D., Wang, Y., Caprio, L.A., Karz, A., Tagore, S., Barrera, I., Ibarra-Arellano, M.A., Andreatta, M., Fullerton, B.T., Gretarsson, K.H., Sahu, V., Mangipudy, V.S., Nguyen, T.T.T., Nair, A., Rogava, M., Ho, P., Koch, P.D., Banu, M., Humala, N., Mahajan, A., Walsh, Z.H., Shah, S.B., Vaccaro, D.H., Caldwell, B., Mu, M., Wünnemann, F., Chazotte, M., Berhe, S., Luoma, A.M., Driver, J., Ingham, M., Khan, S.A., Rapisuwon, S., Slingluff, C.L., Eigentler, T., Röcken, M., Carvajal, R., Atkins, M.B., Davies, M.A., Agustinus, A., Bakhoun, S.F., Azizi, E., Siegelin, M., Lu, C., Carmona, S.J., Hibshoosh, H., Ribas, A., Canoll, P., Bruce, J.N., Bi, W.L., Agrawal, P., Schapiro, D., Hernando, E., Macosko, E.Z., Chen, F., Schwartz, G.K., Izar, B., 2022. Dissecting the treatment-naïve ecosystem of human melanoma brain metastasis. *Cell* 185, 2591–2608.e30. <https://doi.org/10.1016/j.cell.2022.06.007>
- Bradner, J.E., Hnisz, D., Young, R.A., 2017. Transcriptional Addiction in Cancer. *Cell*. <https://doi.org/10.1016/j.cell.2016.12.013>
- Caron, M.C., Sharma, A.K., O'Sullivan, J., Myler, L.R., Ferreira, M.T., Rodrigue, A., Coulombe, Y., Ethier, C., Gagné, J.P., Langelier, M.F., Pascal, J.M., Finkelstein, I.J., Hendzel, M.J., Poirier, G.G., Masson, J.Y., 2019. Poly(ADP-ribose) polymerase-1 antagonizes DNA resection at double-strand breaks. *Nature Communications* 10. <https://doi.org/10.1038/s41467-019-10741-9>
- Chapman, P.B., Hauschild, A., Robert, C., Haanen, J.B., Ascierto, P., Larkin, J., Dummer, R., Garbe, C., Testori, A., Maio, M., Hogg, D., Lorigan, P., Lebbe, C., Jouary, T., Schadendorf, D., Ribas, A., O'Day, S.J., Sosman, J.A., Kirkwood, J.M., Eggermont, A.M.M., Dreno, B., Nolop, K., Li, J., Nelson, B., Hou, J., Lee, R.J., Flaherty, K.T., McArthur, G.A., 2011. Improved Survival with Vemurafenib in Melanoma with BRAF V600E Mutation. *N Engl J Med* 364, 2507–2516. <https://doi.org/10.1056/NEJMoa1103782>
- Chipumuro, E., Marco, E., Christensen, C.L., Kwiatkowski, N., Zhang, T., Hatheway, C.M., Abraham, B.J., Sharma, B., Yeung, C., Altabel, A., Perez-Atayde, A., Wong, K.K., Yuan, G.C., Gray, N.S., Young, R.A., George, R.E., 2014. CDK7 inhibition suppresses super-enhancer-linked oncogenic transcription in MYCN-driven cancer. *Cell* 159, 1126–39. <https://doi.org/10.1016/j.cell.2014.10.024>
- Ciani, B., Bjelić, S., Honnappa, S., Jawhari, H., Jaussi, R., Payapilly, A., Jowitt, T., Steinmetz, M.O., Kammerer, R.A., 2010. Molecular basis of coiled-coil oligomerization-state specificity. *Proc. Natl. Acad. Sci. U.S.A.* 107, 19850–19855. <https://doi.org/10.1073/pnas.1008502107>
- Curti, B.D., Faries, M.B., 2021. Recent Advances in the Treatment of Melanoma. *New England Journal of Medicine* 384, 2229–2240. <https://doi.org/10.1056/NEJMra2034861>
- Dai, Y., Zhang, A., Shan, S., Gong, Z., Zhou, Z., 2018. Structural basis for recognition of 53BP1 tandem Tudor domain by TIRR. *Nature Communications* 9. <https://doi.org/10.1038/s41467-018-04557-2>
- Eliades, P., Abraham, B.J., Ji, Z., Miller, D.M., Christensen, C.L., Kwiatkowski, N., Kumar, R., Njauw, C.N., Taylor, M., Miao, B., Zhang, T., Wong, K.K., Gray, N.S., Young, R.A., Tsao, H., 2018. High MITF Expression Is Associated with Super-Enhancers and Suppressed by CDK7 Inhibition in Melanoma. *Journal of Investigative Dermatology* 138, 1582–1590. <https://doi.org/10.1016/j.jid.2017.09.056>
- Ennen, M., Keime, C., Gambi, G., Kieny, A., Coassolo, S., Thibault-Carpentier, C., Margerin-Schaller, F., Davidson, G., Vagne, C., Lipsker, D., Davidson, I., 2017. MITF-High and MITF-Low Cells and a Novel Subpopulation Expressing Genes

of Both Cell States Contribute to Intra- and Intertumoral Heterogeneity of Primary Melanoma. *Clinical Cancer Research* 23, 7097–7107. <https://doi.org/10.1158/1078-0432.Ccr-17-0010>

Fan, H., Lu, J., Guo, Y., Li, D., Zhang, Z.M., Tsai, Y.H., Pi, W.C., Ahn, J.H., Gong, W., Xiang, Y., Allison, D.F., Geng, H., He, S., Diao, Y., Chen, W.Y., Strahl, B.D., Cai, L., Song, J., Wang, G.G., 2020. BAHCC1 binds H3K27me3 via a conserved BAH module to mediate gene silencing and oncogenesis. *Nature Genetics*. <https://doi.org/10.1038/s41588-020-00729-3>

Filippakopoulos, P., Qi, J., Picaud, S., Shen, Y., Smith, W.B., Fedorov, O., Morse, E.M., Keates, T., Hickman, T.T., Felletar, I., Philpott, M., Munro, S., McKeown, M.R., Wang, Y., Christie, A.L., West, N., Cameron, M.J., Schwartz, B., Heightman, T.D., La Thangue, N., French, C.A., Wiest, O., Kung, A.L., Knapp, S., Bradner, J.E., 2010. Selective inhibition of BET bromodomains. *Nature* 468, 1067–1073. <https://doi.org/10.1038/nature09504>

Fontanals-Cirera, B., Hasson, D., Vardabasso, C., Di Micco, R., Agrawal, P., Chowdhury, A., Gantz, M., de Pablos-Aragoneses, A., Morgenstern, A., Wu, P., Filipescu, D., Valle-Garcia, D., Darvishian, F., Roe, J.S., Davies, M.A., Vakoc, C.R., Hernandez, E., Bernstein, E., 2017. Harnessing BET Inhibitor Sensitivity Reveals AMIGO2 as a Melanoma Survival Gene. *Molecular Cell* 68, 731–744.e9. <https://doi.org/10.1016/j.molcel.2017.11.004>

Gao, Y., Li, Y., Niu, X., Wu, Y., Guan, X., Hong, Y., Chen, H., Song, B., 2020. Identification and Validation of Prognostically Relevant Gene Signature in Melanoma. *BioMed Research International* 2020. <https://doi.org/10.1155/2020/5323614>

Hnisz, D., Abraham, B.J., Lee, T.I., Lau, A., Saint-André, V., Sigova, A.A., Hoke, H.A., Young, R.A., 2013. Super-enhancers in the control of cell identity and disease. *Cell* 155, 934. <https://doi.org/10.1016/j.cell.2013.09.053>

Ianevski, A., Giri, A.K., Aittokallio, T., 2022. SynergyFinder 3.0: an interactive analysis and consensus interpretation of multi-drug synergies across multiple samples. *Nucleic Acids Research* 50, W739–W743. <https://doi.org/10.1093/nar/gkac382>

Kabbarah, O., Nogueira, C., Feng, B., Nazarian, R.M., Bosenberg, M., Wu, M., Scott, K.L., Kwong, L.N., Xiao, Y., Cordon-Cardo, C., Granter, S.R., Ramaswamy, S., Golub, T., Duncan, L.M., Wagner, S.N., Brennan, C., Chin, L., 2010. Integrative Genome Comparison of Primary and Metastatic Melanomas. *PLoS ONE* 5, e10770. <https://doi.org/10.1371/journal.pone.0010770>

Kauffmann, A., Rosselli, F., Lazar, V., Winneppinckx, V., Mansuet-Lupo, A., Dessen, P., Van Den Oord, J.J., Spatz, A., Sarasin, A., 2008. High expression of DNA repair pathways is associated with metastasis in melanoma patients. *Oncogene* 27, 565–573. <https://doi.org/10.1038/sj.onc.1210700>

Kuo, A.J., Song, J., Cheung, P., Ishibe-Murakami, S., Yamazoe, S., Chen, J.K., Patel, D.J., Or, G., 2012. ORC1 BAH domain links H4K20 to DNA replication licensing and Meier-Gorlin syndrome. *Nature* 484, 115–119. <https://doi.org/10.1038/nature10956>

Kwiatkowski, N., Zhang, T., Rahl, P.B., Abraham, B.J., Reddy, J., Ficarro, S.B., Dastur, A., Amzallag, A., Ramaswamy, S., Tesar, B., Jenkins, C.E., Hannett, N.M., McMillin, D., Sanda, T., Sim, T., Kim, N.D., Look, T., Mitsiades, C.S., Weng, A.P., Brown, J.R., Benes, C.H., Marto, J.A., Young, R.A., Gray, N.S., 2014. Targeting transcription regulation in cancer with a covalent CDK7 inhibitor. *Nature* 511, 616–620. <https://doi.org/10.1038/nature13393>

Laurette, P., Strub, J., Koludrovic, D., Keime, C., Le Gras, S., Seberg, H., Van Otterloo, E., Imrichova, H., Siddaway, R., Aerts, S., Cornell, R.A., Mengus, G., Davidson, I., 2015. Transcription factor MITF and remodeler BRG1 define chromatin organisation at regulatory elements in melanoma cells. *Elife* 4. <https://doi.org/10.7554/eLife.06857>

Lee, T.I., Young, R.A., 2013. Transcriptional regulation and its misregulation in disease. *Cell* 152, 1237–1251. <https://doi.org/10.1016/j.cell.2013.02.014>

Love, M.I., Huber, W., Anders, S., 2014. Moderated estimation of fold change and dispersion for RNA-seq data with DESeq2. *Genome Biology* 15, 1–21. <https://doi.org/10.1186/S13059-014-0550-8/FIGURES/9>

Lovén, J., Hoke, H.A., Lin, C.Y., Lau, A., Orlando, D.A., Vakoc, C.R., Bradner, J.E., Lee, T.I., Young, R.A., 2013. Selective inhibition of tumor oncogenes by disruption of super-enhancers. *Cell* 153, 320–334. <https://doi.org/10.1016/j.cell.2013.03.036>

Ma, Y., Kurtyka, C.A., Boyapalle, S., Sung, S.-S., Lawrence, H., Guida, W., Cress, W.D., 2008. A Small-Molecule E2F Inhibitor Blocks Growth in a Melanoma Culture Model. *Cancer Research* 68, 6292–6299. <https://doi.org/10.1158/0008-5472.CAN-08-0121>

Marin-Bejar, O., Rogiers, A., Dewaele, M., Femel, J., Karras, P., Pozniak, J., Bervoets, G., Van Raemdonck, N., Pedri, D., Swings, T., Demeulemeester, J., Borgh, S. Vander, Lehnert, S., Bosisio, F., van den Oord, J.J., Bempt, I., Vanden, Lambrechts, D., Voet, T., Bechter, O., Rizos, H., Levesque, M.P., Leucci, E., Lund, A.W., Rambow, F., Marine, J.C., 2021. Evolutionary predictability of genetic versus nongenetic resistance to anticancer drugs in melanoma. *Cancer Cell* 39, 1135–1149.e8. <https://doi.org/10.1016/j.ccell.2021.05.015>

Mateo, J., Carreira, S., Sandhu, S., Miranda, S., Mossop, H., Perez-Lopez, R., Nava Rodrigues, D., Robinson, D., Omlin, A., Tunariu, N., Boysen, G., Porta, N., Flohr, P., Gillman, A., Figueiredo, I., Paulding, C., Seed, G., Jain, S., Ralph, C., Protheroe, A., Hussain, S., Jones, R., Elliott, T., McGovern, U., Bianchini, D., Goodall, J., Zafeiriou, Z., Williamson, C.T., Ferraldeschi, R., Riisnaes, R., Ebbs, B., Fowler, G., Roda, D., Yuan, W., Wu, Y.-M., Cao, X., Brough, R., Pemberton, H., A'Hern, R., Swain, A., Kunju, L.P., Eeles, R., Attard, G., Lord, C.J., Ashworth, A., Rubin, M.A., Knudsen, K.E., Feng, F.Y., Chinnaiyan, A.M., Hall, E., de Bono, J.S., 2015. DNA-Repair Defects and Olaparib in Metastatic Prostate Cancer. *N Engl J Med* 373, 1697–1708. <https://doi.org/10.1056/NEJMoa1506859>

Mauduit, D., Taskiran, I.I., Minnoye, L., de Waegeneer, M., Christiaens, V., Hulselmans, G., Demeulemeester, J., Wouters, J., Aerts, S., 2021. Analysis of long and short enhancers in melanoma cell states. *eLife* 10, e71735. <https://doi.org/10.7554/eLife.71735>

Mitchell, T., Karakousis, G., Schuchter, L., 2020. Melanoma, in: Niederhuber, J.E., Armitage, J.O., Doroshow, J.H., Kastan, M.B., Tepper, J.E. (Eds.), *Abeloff's Clinical Oncology*. Elsevier, Philadelphia, PA.

Musselman, C.A., Lalonde, M.-E., Côté, J., Kutateladze, T.G., 2012. Perceiving the epigenetic landscape through histone readers. *Nat Struct Mol Biol* 19, 1218–1227. <https://doi.org/10.1038/nsmb.2436>

Noel, P., Hussein, S., Ng, S., Antal, C.E., Lin, W., Rodela, E., Delgado, P., Naveed, S., Downes, M., Lin, Y., Evans, R.M., Von Hoff, D.D., Han, H., 2020. Triptolide targets super-enhancer networks in pancreatic cancer cells and cancer-associated fibroblasts. *Oncogenesis* 9. <https://doi.org/10.1038/s41389-020-00285-9>

Onken, M.D., Worley, L.A., Long, M.D., Duan, S., Council, M.L., Bowcock, A.M., Harbour, J.W., 2008. Oncogenic Mutations in *GNAQ* Occur Early in Uveal Melanoma. *Invest. Ophthalmol. Vis. Sci.* 49, 5230. <https://doi.org/10.1167/iops.08-2145>

Pandiani, C., Strub, T., Nottet, N., Cheli, Y., Gambi, G., Bille, K., Husser, C., Dalmasso, M., Béranger, G., Lassalle, S., Magnone, V., Pédeutour, F., Irondele, M., Maschi, C., Nahon-Estève, S., Martel, A., Caujolle, J.P., Hofman, P., LeBrigand, K., Davidson, I., Baillif, S., Barbry, P., Ballotti, R., Bertolotto, C., 2021. Single-cell RNA sequencing reveals intratumoral heterogeneity in primary uveal melanomas and identifies HES6 as a driver of the metastatic disease. *Cell Death and Differentiation* 28, 1990–2000. <https://doi.org/10.1038/s41418-020-00730-7>

Pilié, P.G., Gay, C.M., Byers, L.A., O'Connor, M.J., Yap, T.A., 2019. PARP Inhibitors: Extending Benefit Beyond *BRCA* - Mutant Cancers. *Clinical Cancer Research* 25, 3759–3771. <https://doi.org/10.1158/1078-0432.CCR-18-0968>

Postel-Vinay, S., Herbschleb, K., Massard, C., Woodcock, V., Soria, J.-C., Walter, A.O., Ewerton, F., Poelman, M., Benson, N., Ocker, M., Wilkinson, G., Middleton, M., 2016. First-in-human phase I study of the bromodomain and extraterminal motif inhibitor BAY 1238097: emerging pharmacokinetic/pharmacodynamic relationship and early termination due to unexpected toxicity. *European Journal of Cancer*.

Pott, S., Lieb, J.D., 2015. What are super-enhancers? *Nature Genetics* 47, 8–12. <https://doi.org/10.1038/ng.3167>

Rambow, F., Marine, J.C., Goding, C.R., 2019. Melanoma plasticity and phenotypic diversity: Therapeutic barriers and opportunities. *Genes and Development* 33, 1295–1318. <https://doi.org/10.1101/gad.329771.119>

Rambow, F., Rogiers, A., Marin-Bejar, O., Aibar, S., Femel, J., Dewaele, M., Karras, P., Brown, D., Chang, Y.H., Debiec-Rychter, M., Adriaens, C., Radaelli, E., Wolter, P., Bechter, O., Dummer, R., Levesque, M., Piris, A., Frederick, D.T., Boland, G., Flaherty, K.T., van den Oord, J., Voet, T., Aerts, S., Lund, A.W., Marine, J.C., 2018. Toward Minimal Residual Disease-Directed Therapy in Melanoma. *Cell* 174, 843–855.e19. <https://doi.org/10.1016/j.cell.2018.06.025>

Ribas, A., Read, P., Slingluff, C., 2015. Cutaneous Melanoma, in: DeVita, Hellman, and Rosenberg's Cancer: Principles and Practice of Oncology. Wolters Kluwer, Philadelphia.

Robert, C., Grob, J.J., Stroyakovskiy, D., Karaszewska, B., Hauschild, A., Levchenko, E., Chiarion Sileni, V., Schachter, J., Garbe, C., Bondarenko, I., Gogas, H., Mandalá, M., Haanen, J.B.A.G., Lebbé, C., Mackiewicz, A., Rutkowski, P., Nathan, P.D., Ribas, A., Davies, M.A., Flaherty, K.T., Burgess, P., Tan, M., Gasal, E., Voi, M., Schadendorf, D., Long, G.V., 2019. Five-Year Outcomes with Dabrafenib plus Trametinib in Metastatic Melanoma. *N Engl J Med* 381, 626–636. <https://doi.org/10.1056/NEJMoa1904059>

Rubanov, A., Berico, P., Hernando, E., 2022. Epigenetic Mechanisms Underlying Melanoma Resistance to Immune and Targeted Therapies. *Cancers* 14, 5858. <https://doi.org/10.3390/cancers14235858>

Scatolini, M., Grand, M.M., Grosso, E., Venesio, T., Pisacane, A., Balsamo, A., Sirovich, R., Risio, M., Chiorino, G., 2010. Altered molecular pathways in melanocytic lesions: Altered Molecular Pathways in Melanocytic Lesions. *Int. J. Cancer* 126, 1869–1881. <https://doi.org/10.1002/ijc.24899>

Strub, T., Giuliano, S., Ye, T., Bonet, C., Keime, C., Kobi, D., Le Gras, S., Cormont, M., Ballotti, R., Bertolotto, C., Davidson, I., 2011. Essential role of microphthalmia transcription factor for DNA replication, mitosis and genomic stability in melanoma. *Oncogene* 30, 2319–2332. <https://doi.org/10.1038/onc.2010.612>

Tirosch, I., Izar, B., Prakadan, S.M., Wadsworth, M.H., Treacy, D., Trombetta, J.J., Rotem, A., Rodman, C., Lian, C., Murphy, G., Fallahi-Sichani, M., Dutton-Regeister, K., Lin, J.R., Cohen, O., Shah, P., Lu, D., Genshaft, A.S., Hughes, T.K., Ziegler, C.G.K., Kazer, S.W., Gaillard, A., Kolb, K.E., Villani, A.C., Johannessen, C.M., Andreev, A.Y., Van Allen, E.M., Bertagnolli, M., Sorger, P.K., Sullivan, R.J., Flaherty, K.T., Frederick, D.T., Jané-Valbuena, J., Yoon, C.H., Rozenblatt-Rosen, O., Shalek, A.K., Regev, A., Garraway, L.A., 2016. Dissecting the multicellular ecosystem of metastatic melanoma by single-cell RNA-seq. *Science* 352, 189–196. <https://doi.org/10.1126/science.1250000>

Titov, D.V., Gilman, B., He, Q.L., Bhat, S., Low, W.K., Dang, Y., Smeaton, M., Demain, A.L., Miller, P.S., Kugel, J.F., Goodrich, J.A., Liu, J.O., 2011. XPB, a subunit of TFIIH, is a target of the natural product triptolide. *Nat Chem Biol* 7, 182–8. <https://doi.org/nchembio.522> [pii] 10.1038/nchembio.522

Tsoi, J., Robert, L., Paraiso, K., Galvan, C., Sheu, K.M., Lay, J., Wong, D.J.L., Atefi, M., Shirazi, R., Wang, X., Braas, D., Grasso, C.S., Palaskas, N., Ribas, A., Graeber, T.G., 2018. Multi-stage Differentiation Defines Melanoma Subtypes with Differential Vulnerability to Drug-Induced Iron-Dependent Oxidative Stress. *Cancer Cell* 33, 890–904.e5. <https://doi.org/10.1016/j.ccell.2018.03.017>

Van Raamsdonk, C.D., Griewank, K.G., Crosby, M.B., Garrido, M.C., Vemula, S., Wiesner, T., Obenaus, A.C., Wackernagel, W., Green, G., Bouvier, N., Sozen, M.M., Baimukanova, G., Roy, R., Heguy, A., Dolgalev, I., Khanin, R., Busam, K., Speicher, M.R., O'Brien, J., Bastian, B.C., 2010. Mutations in *GNAI1* in Uveal Melanoma. *N Engl J Med* 363, 2191–2199. <https://doi.org/10.1056/NEJMoa1000584>

Verfaillie, A., Imrichova, H., Atak, Z.K., Dewaele, M., Rambow, F., Hulselmans, G., Christiaens, V., Svetlichnyy, D., Luciani, F., Van Den Mooter, L., Claerhout, S., Fiers, M., Journe, F., Ghanem, G.E., Herrmann, C., Halder, G., Marine, J.C., Aerts, S., 2015. Decoding the regulatory landscape of melanoma reveals TEADS as regulators of the invasive cell state. *Nature Communications* 6. <https://doi.org/10.1038/ncomms7683>

Wouters, J., Kalender-Atak, Z., Minnoye, L., Spanier, K.I., De Waegeneer, M., Bravo González-Blas, C., Mauduit, D., Davie, K., Hulselmans, G., Najem, A., Dewaele, M., Pedri, D., Rambow, F., Makhzami, S., Christiaens, V., Ceysens, F., Ghanem, G., Marine, J.C., Poovathingal, S., Aerts, S., 2020. Robust gene expression programs underlie recurrent cell states and phenotype switching in melanoma. *Nature Cell Biology* 22, 986–998. <https://doi.org/10.1038/s41556-020-0547-3>

Xu, L., Shen, S.S., Hoshida, Y., Subramanian, A., Ross, K., Brunet, J.P., Wagner, S.N., Ramaswamy, S., Mesirov, J.P., Hynes, R.O., 2008. Gene expression changes in an animal melanoma model correlate with aggressiveness of human melanoma metastases. *Mol Cancer Res* 6, 760–9. <https://doi.org/10.1158/1541-7786.MCR-07-0344>

Yan, B.Y., Garcet, S., Gulati, N., Kiecker, F., Fuentes-Duculan, J., Gilleaudeau, P., Sullivan-Whalen, M., Shemer, A., Mitsui, H., Krueger, J.G., 2019. Novel immune signatures associated with dysplastic naevi and primary cutaneous melanoma in human skin. *Exp Dermatol* 28, 35–44. <https://doi.org/10.1111/exd.13805>

Yang, J., Manson, D.K., Marr, B.P., Carvajal, R.D., 2018. Treatment of uveal melanoma: where are we now? *Ther Adv Med Oncol* 10, 175883401875717. <https://doi.org/10.1177/1758834018757175>

Zhang, Y., Liu, T., Meyer, C.A., Eeckhoute, J., Johnson, D.S., Bernstein, B.E., Nussbaum, C., Myers, R.M., Brown, M., Li, W., Shirley, X.S., 2008. Model-based analysis of ChIP-Seq (MACS). *Genome Biology* 9, 1–9. <https://doi.org/10.1186/GB-2008-9-9-R137/FIGURES/3>

Zhao, D., Zhang, X., Guan, H., Xiong, X., Shi, X., Deng, H., Li, H., 2016. The BAH domain of BAHD1 is a histone H3K27me3 reader. *Protein and Cell* 7, 222–226. <https://doi.org/10.1007/s13238-016-0243-z>

Figure legends

Figure 1: SE17q25 regulates BAHCC1 expression in melanoma

a. Left panel; Captures of the UCSC genome browser (GRCh38/hg19) showing the ChIP-seq profiles of H3K27ac in the genomic region of SE17q25 in several MM cell lines, normal melanocytes (NHEM = Normal Human Epidermal Melanocytes, Foreskin = Human Foreskin Melanocytes) and other tumor and normal cell lines (Layered = H3K27ac mark on 7 cell lines from ENCODE project). **Right panel;** Captures of the UCSC genome browser (GRCh38/hg19) showing the ChIP-seq profiles of H3K27ac, CDK7, BRG1, MITF and SOX10 at SE17q25 in mel501 cells. RefSeq annotated genes are displayed at the bottom.

b. Spearman correlation between BAHCC1 RNA expression and SE17q25 activity, as defined by the ATAC-seq signal (normalized count), measured in different TCGA tumor samples (n=399). The SKCM samples are highlighted in light blue and have the higher expression of BAHCC1 and SE17q25 activity. “Spearman r” and p-value are shown on bottom right.

c. Dot plot of BAHCC1 vs. MITF expression (RPKM) determined by RNA-seq from melanoma cell lines obtained from the CCLE data sets (n=49). The linear regression curve is shown in blue. “Spearman r” and p-value are shown on bottom right.

d. BAHCC1 mRNA fold change (Condition vs. shControl) upon SOX10 or MITF KD in normal melanocytes (Hermes3A) or 501mel melanoma cells obtained from the GEO dataset GSE61967.

e. 501mel melanoma cells were transfected with siSCR, siMITF and siSOX10 for 24 hours. Total extracts were resolved by SDS-PAGE and immuno-blotted against proteins as indicated. Molecular sizes are indicated.

f. 501mel cells were treated with DMSO, THZ1 or Triptolide for 2, 4, 6 and 12 hours, as indicated and the relative amount of BAHCC1 mRNA was quantified by RT-qPCR. Bars represent mean values of three different experiments (Biological triplicates) (+/- SEM), Two-way ANOVA Šídák's multiple comparisons test.

g. RT-qPCR for GAPDH and BAHCC1 in 501mel cells co-transfected with CRISPR-dCas9^{KRAB} and guide RNAs (gRNA) against SE17q25 (gSE17q25) or a non-targeting genomic

region (gCTRL). Bars represent mean values of three different experiments (Biological triplicates) (+/- SEM); paired t-test.

Figure 2: BAHCC1 is overexpressed in melanoma

a. Violin plot of BAHCC1 levels in melanoma vs. non-melanoma cell lines (RPKM) obtained from CCLE (n=1019); unpaired t-test.

b. Normalized RNA levels of BAHCC1 in normal tissues (n=8156), non-melanoma tumors (n=10416), SKCM (n=469), UVM (n=79) obtained from TCGA and The Genotype-Tissue Expression (GTEx) datasets. Ordinary One-Way ANOVA using Dunnett's multiple comparisons test all vs. all.

c-d. Kaplan-Meier analysis of TCGA data from SKCM (n=302) (**c**) or UVM (n=80) (**d**) patients with high or low BAHCC1 expression (Lower and Upper percentile = 50); Log-rank Mantel-Cox test.

e. Box and Whiskers plot representation of BAHCC1 expression (RPKM) in TCGA data from SKCM patients (n=469) according to the BRAF, NRAS and NF1 mutational status. Bars show the min and max values, box represent mean +/- SEM.

f. RNA FISH against BAHCC1 and SOX10 mRNA in naevus, cutaneous and uveal melanomas tissue biopsies. Scale bars are indicated. Additional samples are shown in Ext. Figures 2e and f.

Figure 3: BAHCC1 depletion impairs melanoma cell proliferation

a. Left panel; Quantification of crystal violet staining of cells transfected with GapmeR^{NEG} (NEG), GapmeR^{#1} (GR^{#1}) and GapmeR^{#2} (GR^{#2}) in SKCM cells (501mel and MM117) and UVM (OMM1.3) cells. **Middle panel;** CellTrace staining was measured by FACS in the cells used in the left panel and results are represented as % of slow proliferative cells considering an arbitrary threshold between 20-30% in the GapmeR^{NEG} (GR^{NEG}) control. **Right panel;** Relative BAHCC1 expression upon transfection with GapmeR^{NEG} (GR^{NEG}), GapmeR^{#1} (GR^{#1}) and GapmeR^{#2} (GR^{#2}) were measured by RT-qPCR in the cells used in the left panel. Bars represent mean values of three different experiments (Biological triplicates) (+/- SEM). Ordinary one-way ANOVA using Dunnett's multiple comparisons test.

b. Cell coverage quantification of crystal violet staining of 501mel cells transfected with GapmeR^{NEG} (GR^{NEG}) or GapmeR^{#1} (GR^{#1}) upon treatment with DMSO, Trametinib (10nM) or Vemurafenib (5uM). Bars represent mean values of three different experiments (Biological triplicates) (+/- SEM); Ordinary one-way ANOVA using Dunnett's multiple comparisons test.

c. Cell coverage quantification of the Boyden-Chamber transwell after crystal violet staining of 501mel, MM099 and MM029 cells transfected with GapmeR^{NEG} (GR^{NEG}), GapmeR^{#1} (GR^{#1}) and GapmeR^{#2} (GR^{#2}). Bars represent mean values of three different experiments (Biological triplicates) (+/- SEM); Two-way ANOVA using Tukey's multiple comparisons test.

Figure 4: BAHCC1 depletion impairs melanoma tumor engraftments and metastases.

- a. Kinetic of tumor growth obtained following xenografting of 501mel melanoma cells stably expressing shNTC (SH^{NTC}) or shBAHCC1 (SH^{#1} and SH^{#2}) in NSG mice (+/- SEM); number of mice per group are shown. Two-way ANOVA Dunnet's multiple comparisons test.
- b. Animal weights were measured in the three intracardiac group every three days starting at day 21. Weight has been scaled to day 21 for each mouse to evaluate the relative changing. Two-way ANOVA Dunnet's multiple comparisons test.
- c. Luciferase luminescence was measured in the three intracardiac groups as indicated at days 2, 12 and 26 post injection. Luminescence is expressed as Radiance per mouse. Number of animals per group are displayed. Two-way ANOVA Dunnet's multiple comparisons test.
- d. Animal weights were measured in the three intracardiac group as indicated at days 7, 13, 16, 21, 23, 26 and 28 post injection. Weight has been scaled to day 7 for each mouse to evaluate the relative changing. Two-way ANOVA Dunnet's multiple comparisons test.

Figure 5: BAHCC1 is a transcriptional regulator

- a. Scatter plot of the significantly (p-value<0.05) deregulated genes (normalized count) upon BAHCC1 KD in 501mel and MM047. Red dots highlight BAHCC1 which is one of the top downregulated genes.
- b. Venn diagram between significantly down-regulated (top) and up-regulated (bottom) genes identified by RNA-seq in 501mel and MM047 upon BAHCC1 KD. Representation factor and p-values were calculated using hypergeometric test.
- c. GO analysis of the 200 co-downregulated genes between 501mel and MM047 upon BAHCC1 KD. The first 10 most significant annotation groups are listed from top to bottom according to the -log₁₀(q-value).
- d. **Upper panel;** Read density clustering obtained with seqMINER for the 31,280 BAHCC1 occupied sites relative to BAHCC1, H3K27ac and ATAC-seq signals in 501mel cells in a genomic window of 10 kb around the peaks. **Lower panel;** Merge meta-profiles distribution of BAHCC1, H3K27ac and ATAC enrichment relative to the 31,280 BAHCC1 peaks.

e. Upper panel; Read density clustering obtained with seqMINER for BAHCC1, H3K27ac and ATAC-seq signals relative to the 41,088 annotated TSS. **Lower panel;** Merge meta-profiles distribution of BAHCC1, H3K27ac and ATAC in a +/- 5 kb window around the TSS. **f.** Venn diagram between genes showing a TSS-associated BAHCC1 protein and the significantly down- or up-regulated genes following BAHCC1 KD, as determined by RNA-seq.

Figure 6: BAHCC1 interacts with BRG1-containing chromatin remodeler complexes

a. Domain architecture of BAHCC1. CC; Coiled Coil. The deletion mutants used below are shown.

b. Upper panel; Read density clustering using SeqMINER showing the colocalization between BAHCC1^{WT}, BRG1, H3K27ac and ATAC signal in the 31,280 BAHCC1-occupied sites. Cluster 3 (C3) is highlighted. **Bottom panel;** Meta-profile of BAHCC1, BRG1, H3K27ac and ATAC signals around the 31,280 BAHCC1 peaks.

c. Left panel: Venn diagram showing the overlap between the down regulated genes in 501mel following either BRG1 or BAHCC1 KD. **Right panel** Venn diagram showing the overlap between the down-regulated genes in mel501 after BRG1 KD and the common down-regulated genes in 501mel and MM047 after BAHCC1 KD. Representation factor and p-values were calculated using hypergeometric test.

d. BRG1 was immunoprecipitated (IP-BRG1) from nuclear extracts of 501mel cells. Following SDS-PAGE, proteins were immunoblotted as indicated, including subunits of the pBAF/BAF complexes. IP-IgG was performed as a negative control. Molecular sizes are indicated.

e. HEK293T cells were transfected to express HA-BAHCC1^{TUDOR-BAH} protein and BRG1 was immunoprecipitated (IP-BRG1). Following SDS-PAGE, proteins were immunoblotted as indicated. IP-IgG was performed as a negative control. Molecular sizes are indicated.

f. HEK293T cells were transfected to express FLAG-BAHCC1^{BAH} and FLAG-BAHCC1^{TUDOR} domains and FLAG-IP was performed. Following SDS-PAGE, proteins were immunoblotted as indicated. Molecular sizes are indicated.

g. Upper panel; Read density clustering using SeqMINER showing the colocalization between H3K27ac and BRG1 signal in the 31,280 H3K27ac-deposition sites with (GR^{NEG}) or without BAHCC1 (GR^{#2}). **Bottom panel;** Meta-profile of H3K27ac and BRG1 signals around the 31,280 H3K27ac peaks with (GR^{NEG}) or without (GR^{#2}) BAHCC1.

Figure 7: BAHCC1 depletion cooperates with PARPi to induce cell death

- a.** Relative ATM expression upon transfection with GapmeR^{NEG} (NEG), GapmeR^{#1} (#1) and shBAHCC1 was measured by RT-qPCR in 501mel or MM047. Bars represent mean values of three different experiments (Biological triplicates) (+/- SEM); two-way ANOVA using Šídák's multiple comparisons test.
- b.** 501mel or MM047 were transfected with GapmeR^{NEG} (GR^{NEG}), GapmeR^{#1} (GR^{#1}), siCTRL (SI^{NEG}) or shBAHCC1 (SI^{#1}). Whole cell extracts were resolved by SDS-PAGE and proteins were immunoblotted as indicated.
- c.** Spearman correlation between BAHCC1 expression and the fraction of genomic alteration (FGA) in TCGA melanoma samples (n=443) where FGA is considered as the percentage of copy number alterations found in the tumor compared to the normal karyotype. The linear regression curve is shown in red.
- d.** Schematic representation of the *in vitro* experiments using Neocarzinostatin (NCS).
- e.** Immunofluorescence quantification of the number of γ H2AX foci per cell in 501mel and MM047 transfected either with GapmeR^{NEG} (GR^{NEG}), GapmeR^{#1} (GR^{#1}) or GapmeR^{#2} (GR^{#2}) and treated or not (NT) with NCS (1, 8 and 24 hours of recovery). Bars represent the means obtained from six biological replicates (+/-SEM) (501mel n1=45338, n2=46604, n3=47365, n4=39185, n5=61975, n6=85783; MM047 n1=26535, n2=26284, n3=28105, n4=8559, n5=13342, n6=18296); Two-way ANOVA test.
- f. Left panel;** Crystal violet quantification expressed as fold change relative to GapmeR (NEG)-transfected cells treated with DMSO. Bars represent mean values of three different experiments (Biological triplicates) (+/- SEM); Two-way ANOVA using Dunnett's multiple comparisons test. **Right panel;** Percentage of Annexin V positive cell in 501mel, MM117 and MM047 transfected with GapmeR^{NEG} (GR^{NEG}) and GapmeR^{#1} (GR^{#1}) and treated for 96 hours with DMSO or 10uM of Olaparib. Bars represent mean values of three different experiments (Biological triplicates) (+/- SEM); Two-way ANOVA using Dunnett's multiple comparisons test.
- g.** Surface plot in three-dimensional views, showing synergy scores for impact of Trametinib plus Olaparib combination on 501mel cell viability. Cells were transfected with GapmeR^{NEG} (GR^{NEG}) and GapmeR^{#1} (GR^{#1}). ZIP synergy scores (shown as d-scores) were calculated from the % of inhibition of 501mel cell viability in the dose combination matrix. Black arrows indicate the areas of the most synergistic scores (ZIP>10). Areas in red, white and green show region of synergy, additivity and antagonism, respectively.

Ext. Figure 1: BAHCC1 overexpression in melanoma cells

- a.** Schematic representation of the SE pipeline analysis used to identify SE17q25.
- b.** Dot plot representing the H3K27ac signal at SEs as a function of the ROSE ranking. We used the distribution of SEs in MM011 cells as a representative distribution. In different shape and colors are the specific positions of SE17q25 in the corresponding melanoma cell lines.
- c.** Immunoblot against BAHCC1, MITF, AXL and ACTIN in U-2 OS, immortalized melanocyte Hermes3A and several SKCM and UVM cell lines as indicated.
- d.** Relative expression of BAHCC1, MITF and AXL determined by RT-qPCR in a large panel of melanoma and non-melanoma cell lines as indicated. Bars represent mean values of three different experiments (Biological triplicates) (+/- SEM).
- e.** BRG1 ChIP-seq tracks in 501mel treated with siCTRL or siMITF, scaled in the region of SE17q25. The decommission of SE17q25 is illustrated by the loss of BRG1 binding. Values were retrieved from the GEO dataset GSE61967 (Laurette et al., 2015). The red box indicates the SE17q25 localization.

Ext. Figure 2: BAHCC1 expression increases during melanoma progression

- a.** BAHCC1 expression in human nevi (n=27) and primary melanomas (n=51). Values were retrieved from the GEO dataset GSE98394 (Badal et al., 2017); unpaired t-test.
- b.** BAHCC1 expression in primary (n=31) and metastatic (n=73) melanoma. Values were retrieved from the GEO dataset GSE46517 (Kabbarah et al., 2010); unpaired t-test.
- c.** Expression levels of BAHCC1 in human biopsies of nevus (n=36), dysplastic nevus (n=22), melanoma radial growth phase (RGP) (n=16), vertical growth phase (VGP) (n=30) and metastatic melanoma (n=10). Values were retrieved from the GEO dataset GSE12391 (Scatolini et al., 2010). Ordinary One-Way ANOVA using Dunnett's multiple comparisons test all vs. all.
- d.** BAHCC1 expression in normal skin (n=6), common nevus (n=5), dysplastic nevus (n=7) and melanoma (n=16). Values were retrieved from the GEO dataset GSE114445 (Yan et al., 2019); Ordinary One-Way ANOVA using Dunnett's multiple comparisons test all vs. all.
- e.** BAHCC1 expression in melanocyte stem cells vs. melanoma cells in BRAF melanoma mouse model. Values were retrieved from the GEO dataset GSE113502 (Sun et al., 2019); unpaired t-test.
- f-g.** RNA FISH for SOX10 and BAHCC1 in human tissue samples of nevi (n=2), cutaneous (n=2) and uveal melanomas (n=3, same samples than (Pandiani et al., 2021)). Scale bar is indicated for each image.

Ext. Figure 3: BAHCC1 depletion impairs SKCM and UVM cells proliferation

a. RNA FISH was performed for BAHCC1 in 501mel and MM047 transfected with GapmeR^{NEG} (GR^{NEG}), GapmeR^{#1} (GR^{#1}) and GapmeR^{#2} (GR^{#2}). Scale bars are indicated.

b. Left panel; Cell coverage quantification of crystal violet staining of cells transfected with GapmeR^{NEG} (GR^{NEG}), GapmeR^{#1} (GR^{#1}) and GapmeR^{#2} (GR^{#2}) in SKCM cells (MM047 and MM029) or UVM cells (OMM2.5). **Middle panel;** CellTrace staining was measured by FACS in the cells used in the left panel and results are represented as % of slow proliferative cells considering an arbitrary threshold between 20-30% in the GapmeR^{NEG} (NEG) control. **Right panel;** Relative BAHCC1 expressions upon transfection with GapmeR^{NEG} (NEG), GapmeR^{#1} (GR^{#1}) and GapmeR^{#2} (GR^{#2}) were measured by RT-qPCR in the cells used in the left panel (with the exception of U-2 OS cells that do not express BAHCC1). Bars represent mean values of three different experiments (Biological triplicates) (+/- SEM). Two-way ANOVA using Šídák's multiple comparisons test.

Ext Figure 4: Cell derived xenografts engraftment and metastases require BAHCC1.

a. Invalidation of BAHCC1 using SH^{#1} and SH^{#2} was evaluated in 501mel cells right before injection in animals through RT-qPCR, using shNTC as control. Two-way ANOVA Dunnet's multiple comparisons test.

b. Bioluminescence imaging with IVIS of intracardiac group mice at day 2, day 12 and day 26 post injection.

Ext. Figure 5: BAHCC1 localizes at the promoter of E2F/KLF dependent genes

a. Immunostaining of BAHCC1 in 501mel cells using an anti-BAHCC1 antibody together with DAPI staining. Scale bars are indicated.

b. Immunoblot of the indicated proteins in 501mel protein sub fractions corresponding to cytoplasm (Cyto), nuclear soluble (NS) and nuclear insoluble (NI). BRG1 and Actin were used as positive controls for NS/NI and Cyto respectively.

c. GO analysis of the 82 co-upregulated genes between 501mel and MM047 upon BAHCC1 KD. The first 10 most significant annotation groups are listed from top to bottom according to the -log₁₀(q-value).

d. Genes characterizing the melanocytic-type and mesenchymal-like transcription signatures (Widmer et al., 2012) have been plotted on a heatmap and are shown in relation to their expression in 501mel or MM047 following expression of controlled or anti-BAHCC1

GAPMER. RPKM values are represented as z-score. The color key shows the \log_2 expression values. Green color stands for high expression and dark violet for low expression.

e. Pie chart displaying the distribution of 31,280 BAHCC1 peaks identified in this work with respect of genomic annotations.

f. BAHCC1 expression among the different transcriptional states previously identified in Rambow melanoma PDXs (n=674 cells) (Rambow et al., 2018), (Berico et al., 2021).

g. Heatmap representing the regulon activity of E2F, Sp/KLF transcription factor family members obtained by SCENIC analysis in the different transcriptional states of Rambow PDX described in (e).

h. BAHCC1 single cell expression retrieved from the GEO dataset GSE138433 (Pandiani et al., 2021) and GSE72056 (Tirosh et al., 2016) was separated in two groups of “Slow” and “Fast” cell cycle cells based on cell enrichment of 95 cell cycle genes identified by Tirosh and colleagues (4) (Ext. Table 6).

i. SKCM (n=469) and UVM (n=81) Spearman correlation between BAHCC1 expression and Tirosh cell cycle signature (95 genes). Values were retrieved from TCGA. Analysis was done using GEPIA2.

Ext. Figure 6: BAHCC1 and BRG1 co-regulate expression of cell cycle and DNA repair genes

a. Upper panel; Read density clustering using SeqMINER showing the colocalization between BAHCC1^{WT} and BAHCC1^{TUDOR-BAH} in the 31,280 BAHCC1^{WT} occupied sites. Red box indicates the cluster of BAHCC1 N-terminal region dependent peaks. **Lower panel;** Meta-profiles of BAHCC1^{WT} and BAHCC1^{TUDOR-BAH} signals around the 31,280 BAHCC1 peaks.

b. Captures of the UCSC genome browser (GRCh38/hg19) showing the ChIP-seq profiles for BAHCC1^{WT}, BAHCC1^{TUDOR-BAH}, BRG1, H3K27ac and ATAC-seq in 501mel corresponding to the promoter regions of ATM, ZZE1 and CDKN1 genes. ZZE1 is used as a control gene recruiting both BAHCC1^{WT} and BAHCC1^{TUDOR-BAH}. RefSeq annotated genes are displayed at the bottom.

c. Gene annotation analysis of the 266 genes co-regulated by BRG1 and BAHCC1 in 501mel. The histogram shows the top 10 deregulated biological pathways according to the $-\log_{10}(q\text{-value})$.

d. Heatmap of the genes involved in DNA repair and/or mitosis and significantly co-regulated by BAHCC1 and BRG1 in melanoma cells as indicated. GapmeR^{#2} (GR^{#2}) was used to knock-down BAHCC1. GapmeR^{NEG} (GR^{NEG}) was used as negative control.

e. Following the stable overexpression of a HA-BAHCC1^{BAH} domain in 501mel cells, immunoprecipitation was carried out using anti-IgG (control), anti-BRG1 and anti-HA antibodies. Following SDS-PAGE, proteins were immunoblotted as indicated. Molecular sizes are indicated.

Ext. Figure 7: BAHCC1 depletion impairs double-stranded DNA repair

- a. Genome Browser overview of H3K27ac, H3K27me3 and BRG1 at ATM's promoter. Overview obtained with GapmeR control (GR^{NEG}) was compared to that obtained with GapmeR against BAHCC1 (GR^{#2}).
- b. Immunofluorescence for γ H2AX in 501mel and MM047 in basal conditions or upon DNA damage in presence or absence of BAHCC1. Images are representative of the quantification of Figure 7. DAPI staining is shown. Scale bars are shown.

Ext. Figure 8: BAHCC1 does not co-localized with H3K27me3

Left panel; Read density clustering using SeqMINER showing the colocalization between BAHCC1^{WT}, H3K27me3 and H3K27ac at the 31,280 BAHCC1^{WT} occupied sites. Red box indicates the cluster of BAHCC1 N-terminal region dependent peaks. **Right panel;** Meta-profiles of BAHCC1^{WT}, H3K27me3 and H3K27ac around the 31,280 BAHCC1^{WT} occupied sites.

Extended Table 1: Melanoma cells used in this study

The melanoma cells, their driver mutations and phenotypes are indicated.

Extended Table 2: Putative SEs identified in melanoma cells

The top 19 putative SEs identified in 10 different melanoma cells, including the 501mel melanoma cell line and MM cells, are shown. SE17q25 is highlighted in red and is among the top 19 SEs of the 10 cells considered.

Extended Table 3: Down-regulated genes

A list of genes down-regulated both in 501mel and MM047 after BAHCC1 KD is provided page 1. A list of down-regulated genes both in 501mel after BRG1 KD and after BAHCC1 KD in 501mel and MM047 is provided page 2.

Extended Table 4: BAHCC1 binding sites

RSAT was carried out on the BAHCC1 occupied sites according to MACS2 ranking on the top peaks (page 1), on BAHCC1 N-ter dependent peaks (page 2), on TSS of up-regulated genes in BAHCC1^{KD} cells (page 3) and on TSS of down-regulated genes on BAHCC1^{KD} (page 4).

Extended Table 5: Gene cell cycle

List of 95 melanoma cell cycle genes identified by Tirosh and colleagues and used in this work to separate in “Slow” or “Fast” cell cycle either single cells or bulk RNA-seq data.

Extended Table 6: BAHCC1^{WT} vs. BAHCC1^{TUDOR-BAH} binding sites

A list of genes bound by BAHCC1^{WT} but not by BAHCC1^{TUDOR-BAH} as determined by CUT&Tag is provided page 1. A list of down- and up-regulated genes belonging to this cluster is provided page 2.

Supplementary References:

- Badal, B., Solovyov, A., Di Cecilia, S., Chan, J.M., Chang, L.W., Iqbal, R., Aydin, I.T., Rajan, G.S., Chen, C., Abbate, F., Arora, K.S., Tanne, A., Gruber, S.B., Johnson, T.M., Fullen, D.R., Raskin, L., Phelps, R., Bhardwaj, N., Bernstein, E., Ting, D.T., Brunner, G., Schadt, E.E., Greenbaum, B.D., Celebi, J.T., 2017. Transcriptional dissection of melanoma identifies a high-risk subtype underlying TP53 family genes and epigenome deregulation. *JCI Insight* 2. <https://doi.org/10.1172/jci.insight.92102>
- Berico, P., Cigrang, M., Davidson, G., Braun, C., Sandoz, J., Legras, S., Vokshi, B.H., Slovic, N., Peyresaubes, F., Gene Robles, C.M., Egly, J., Compe, E., Davidson, I., Coin, F., 2021. CDK7 and MITF repress a transcription program involved in survival and drug tolerance in melanoma. *EMBO reports* 22, 1–18. <https://doi.org/10.15252/embr.202051683>
- Kabbarah, O., Nogueira, C., Feng, B., Nazarian, R.M., Bosenberg, M., Wu, M., Scott, K.L., Kwong, L.N., Xiao, Y., Cordon-Cardo, C., Granter, S.R., Ramaswamy, S., Golub, T., Duncan, L.M., Wagner, S.N., Brennan, C., Chin, L., 2010. Integrative Genome Comparison of Primary and Metastatic Melanomas. *PLoS ONE* 5, e10770. <https://doi.org/10.1371/journal.pone.0010770>
- Laurette, P., Strub, T., Koludrovic, D., Keime, C., Le Gras, S., Seberg, H., Van Otterloo, E., Imrichova, H., Siddaway, R., Aerts, S., Cornell, R.A., Mengus, G., Davidson, I., 2015. Transcription factor MITF and remodeller BRG1 define chromatin organisation at regulatory elements in melanoma cells. *Elife* 4. <https://doi.org/10.7554/eLife.06857>
- Pandiani, C., Strub, T., Nottet, N., Cheli, Y., Gambi, G., Bille, K., Husser, C., Dalmaso, M., Béranger, G., Lassalle, S., Magnone, V., Pédeutour, F., Irondelle, M., Maschi, C., Nahon-Estève, S., Martel, A., Caujolle, J.P., Hofman, P., LeBrigand, K., Davidson, I., Baillif, S., Barbry, P., Ballotti, R., Bertolotto, C., 2021. Single-cell RNA sequencing reveals intratumoral heterogeneity in primary uveal melanomas and identifies HES6 as a driver of the metastatic disease. *Cell Death and Differentiation* 28, 1990–2000. <https://doi.org/10.1038/s41418-020-00730-7>
- Rambow, F., Rogiers, A., Marin-Bejar, O., Aibar, S., Femel, J., Dewaele, M., Karras, P., Brown, D., Chang, Y.H., Debiec-Rychter, M., Adriaens, C., Radaelli, E., Wolter, P., Bechter, O., Dummer, R., Levesque, M., Piris, A., Frederick, D.T., Boland, G., Flaherty, K.T., van den Oord, J., Voet, T., Aerts, S., Lund, A.W., Marine, J.C., 2018. Toward Minimal Residual Disease-Directed Therapy in Melanoma. *Cell* 174, 843–855.e19. <https://doi.org/10.1016/j.cell.2018.06.025>
- Scatolini, M., Grand, M.M., Grosso, E., Venesio, T., Pisacane, A., Balsamo, A., Sirovich, R., Risio, M., Chiorino, G., 2010. Altered molecular pathways in melanocytic lesions: Altered Molecular Pathways in Melanocytic Lesions. *Int. J. Cancer* 126, 1869–1881. <https://doi.org/10.1002/ijc.24899>
- Sun, Q., Lee, W., Mohri, Y., Takeo, M., Lim, C.H., Xu, X., Myung, P., Atit, R.P., Taketo, M.M., Moubarak, R.S., Schober, M., Osman, I.,

Gay, D.L., Saur, D., Nishimura, E.K., Ito, M., 2019. A novel mouse model demonstrates that oncogenic melanocyte stem cells engender melanoma resembling human disease. *Nat Commun* 10, 5023. <https://doi.org/10.1038/s41467-019-12733-1>

Tirosh, I., Izar, B., Prakadan, S.M., Wadsworth, M.H., Treacy, D., Trombetta, J.J., Rotem, A., Rodman, C., Lian, C., Murphy, G., Fallahi-Sichani, M., Dutton-Regester, K., Lin, J.R., Cohen, O., Shah, P., Lu, D., Genshaft, A.S., Hughes, T.K., Ziegler, C.G., Kazer, S.W., Gaillard, A., Kolb, K.E., Villani, A.C., Johannessen, C.M., Andreev, A.Y., Van Allen, E.M., Bertagnolli, M., Sorger, P.K., Sullivan, R.J., Flaherty, K.T., Frederick, D.T., Jane-Valbuena, J., Yoon, C.H., Rozenblatt-Rosen, O., Shalek, A.K., Regev, A., Garraway, L.A., 2016. Dissecting the multicellular ecosystem of metastatic melanoma by single-cell RNA-seq. *Science* 352, 189–96. <https://doi.org/10.1126/science.aad0501>

Widmer, D.S., Cheng, P.F., Eichhoff, O.M., Belloni, B.C., Zipser, M.C., Schlegel, N.C., Javelaud, D., Mauviel, A., Dummer, R., Hoek, K.S., 2012. Systematic classification of melanoma cells by phenotype-specific gene expression mapping. *Pigment Cell Melanoma Res* 25, 343–53. <https://doi.org/10.1111/j.1755-148X.2012.00986.x>

Yan, B.Y., Garcet, S., Gulati, N., Kiecker, F., Fuentes-Duculan, J., Gilleaudeau, P., Sullivan-Whalen, M., Shemer, A., Mitsui, H., Krueger, J.G., 2019. Novel immune signatures associated with dysplastic naevi and primary cutaneous melanoma in human skin. *Exp Dermatol* 28, 35–44. <https://doi.org/10.1111/exd.13805>

KEY RESOURCES TABLE

REAGENT or RESOURCE	SOURCE	IDENTIFIER
Antibodies		
ACTB	IGBMC house-made	
ATM	Cell Signaling	D2E2
AXL	Proteintech	13196-AP
BAHCC1	ThermoFisher	PA5-54785
BRG1	Abcam	ab110641
FLAG	Sigma Aldrich	F7425
GFP	Abcam	ab290
H3K27ac	Abcam	ab4729
HA	Abcam	ab9110
γ H2AX	Sigma Aldrich	05-636
IgG control	Abcam	ab171870
c-JUN	Cell Signaling	60A8
Ki67	Abcam	ab15580
LUCIFERASE	Santa Cruz	SC-57604
MITF	Cell Signaling	D5G7V
SOX9	Cell Signaling	D8G8H
SOX10	Cell Signaling	D5V9L
VINCULIN	Sigma Aldrich	V4505
Biological samples		
Histological sections of nevi and cutaneous melanoma samples	Prof. B. Cribier, head of the <i>Laboratoire d'histopathologie et d'immunopathologie cutanees</i> , Strasbourg CHU hospital	
Histological sections primary uveal melanoma tumor sections	Nice CHU hospital.	(Pandiani et al., 2021)
Chemicals, peptides, and recombinant proteins		
CellTrace™ Violet Proliferation Kit	Fisher Scientific	C34557
Doxycycline	ENVIGO	TD.00502
Fugene6	Roche Diagnostics	1815075
Lipofectamine 2000	Fisher Scientific	11668027
Lipofectamine RNAiMAX	Fisher Scientific	13778030
NCS	Sigma Aldrich	N9162
SYBR Green	Roche Diagnostics	4887352001
Critical commercial assays		
Affinity Gel FLAG M2 conjugated beads	Sigma Aldrich	M8823
AnnexinV-APC	BD Biosciences	88-8007-72
CUT&Tag-IT™ Assay Kit	Active motif	#53165, #53160
Culturex® Basement Membrane Extract	R&D systems	3434-001-02
GentleMACS C-tubes	Miltenyibiotec	130-096-334

Human Tumor dissociation kit	Miltenyibiotec	130-095-929
LAB-TEK II chamber slides	Thermo Fisher Scientific	154461
Matrigel	Corning	356231
NucleoSpin RNA Plus kit	Macherey-Nagel	740990
ProLong™ Gold antifade reagent	Invitrogen	P36930
Reverse Transcriptase Superscript IV	Life Technologies	18090050
Deposited data		
CUT&Tag	This paper	GSE205462
RNA-seq	This paper	GSE201702
Experimental models: Cell lines		
All MM melanoma cells	Dr. G. Ghanem (Institute Jules Bordet, Brussels, Belgium) and J-C Marine (VIB-KU Leuven, Belgium)	(Verfaillie et al., 2015)
OMM1.3	(Pandiani et al., 2021)	
OMM2.5	(Pandiani et al., 2021)	
Hermes3A	Dr. C Bennett, University of London (UK)	
U-2 OS	ATCC	
501mel HA-BAHCC1 ^{BAH}	This paper	
501mel	Dr. C Goding, University of Oxford (UK)	
HEK293T	ATCC	
SKMEL-28	Dr. L Larue, Institut Curie, (France)	
IGR37	Dr. C Goding, University of Oxford (UK)	
Experimental models: Organisms/strains		
Mouse: Crl:NU(lco)-Foxn1nu (Nude)	Charles River Lab	
Oligonucleotides		
GR ^{NEG} : TCATACTATATGACAG	This paper	
GR ^{#1} : AGATTGGCGGTAGGAA	This paper	
GR ^{#2} : TCCGTGGAATTTAGAT	This paper	
gRNA SE17q25 ^{#1} : GGCACGAGGCGCATAGCTA	This paper, CRISPOR	(Concordet and Haeussler, 2018)
gRNA SE17q25 ^{#2} : TGCACGCCCTCTTGTTTCAG	This paper, CRISPOR	(Concordet and Haeussler, 2018)
gRNA SE17q25 ^{#3} : CTGATTTCTACCCTTCCGTG	This paper, CRISPOR	(Concordet and Haeussler, 2018)

SI ^{NEG}	ON-TARGETplus SMARTpool L-001830-10	Orizon Discovery
SI ^{#1}	ON-TARGETplus SMARTpool L-023331-02	Orizon Discovery
siMITF	ON-TARGETplus SMARTpool L-008674-00	Orizon Discovery
siSOX10	ON-TARGETplus SMARTpool L-017192-00	Orizon Discovery
Recombinant DNA		
pcDNA-FLAG	This study	
pX629_dCas9_KRAB_mScarlet	This study	
pCDNA-GFP	This study	
pcDNA-GFP-SE17q25	This study	
pcDNA-FLAG-BAHCC1 ^{TUDOR}	This study	
pcDNA-FLAG-BAHCC1 ^{BAH}	This study	
pLT3_shCTRL	This study	
pLT3_sh4 (shBAHCC1)	This study	
pGL4.10Luc2	This study	
pLenti6-GFP	This study	
pLenti-TET-3HA-BAHCC1 ^{BAH}	This study	
pLenti6-3HA-BAHCC1 ^{BAH-TUDOR}	This study	
Software and algorithms		
FlowJo software	https://www.flowjo.com/solutions/flowjo/downloads	
Seurat software package version 3.1.4	(Butler et al., 2018)	
Fiji	https://imagej.net/software/fiji/downloads	
DeepTool2	(Ramírez et al., 2016)	
DiffBind v1.12.3	(Ross-Innes et al., 2012)	
ROSE	(Whyte et al., 2013), (Lovén et al., 2013)	
Homer v4.9.1	(Heinz et al., 2010)	
ChIPseeker	(Yu et al., 2015)	
Seq-MINER	(Ye et al., 2011)	
Homer makeUCSCfile v4.9.1	(Heinz et al., 2010)	
Cutadapt version 1.10	https://cutadapt.readthedocs.io/en/v1.10/	
Bowtie v1.0.0	(Langmead et al., 2009)	
STAR version 2.5.3a	(Dobin et al., 2013)	
Scope	https://scope.aertslab.org	

Bioconductor package AUCell v 1.6.1	https://www.bioconductor.org/packages/release/bioc/html/AUCell.html	
Deeptools multiBamSummary v2.5.0	(Ramírez et al., 2016)	
Htseq-count version 0.6.1p1	https://htseq.readthedocs.io/en/master/history.html	
Bioconductor package DESeq2 version 1.16.1	https://bioconductor.org/packages/release/bioc/html/DESeq2.html	
Prism 9	https://www.graphpad.com/scientific-software/prism/	
iRegulon plugin of Cytoscape	https://apps.cytoscape.org/apps/iregulon	
Graeber Lab software	https://systems.crumpp.ucla.edu/	
CCLE portal	https://sites.broadinstitute.org/ccle	
Regulatory Sequence Analysis Tools (RSAT) web server	(Thomas-Chollier et al., 2012)	
Non-redundant vertebrate Jaspar core database	(Fornes et al., 2019)	
Bedtools getfasta	(Quinlan and Hall, 2010)	
Other		
High-throughput imaging system CX7	ThermoFisher	
EVOS xl Core microscope	ThermoFisher	
IVIS imager	Perkin Elmer	
Q800R3 sonicator	Qsonica	
LightCycler 480	Roche	
Illumina HiSeq 4000	Illumina	
gentleMACS™ Dissociator	Miltenyibiotec	

References

- Butler, A., Hoffman, P., Smibert, P., Papalexi, E., Satija, R., 2018. Integrating single-cell transcriptomic data across different conditions, technologies, and species. *Nature biotechnology* 36, 411–420. <https://doi.org/10.1038/NBT.4096>
- Concordet, J.-P., Haeussler, M., 2018. CRISPOR: intuitive guide selection for CRISPR/Cas9 genome editing experiments and screens. *Nucleic Acids Research* 46, W242–W245. <https://doi.org/10.1093/nar/gky354>
- Dobin, A., Davis, C.A., Schlesinger, F., Drenkow, J., Zaleski, C., Jha, S., Batut, P., Chaisson, M., Gingeras, T.R., 2013. STAR: ultrafast universal RNA-seq aligner. *Bioinformatics* 29, 15–21. <https://doi.org/10.1093/bioinformatics/bts635>
- Fellmann, C., Hoffmann, T., Sridhar, V., Hopfgartner, B., Muhar, M., Roth, M., Lai, D.Y., Barbosa, I.A.M., Kwon, J.S., Guan, Y., Sinha, N., Zuber, J., 2013. An Optimized microRNA Backbone for Effective Single-Copy RNAi. *Cell Reports* 5, 1704–1713. <https://doi.org/10.1016/j.celrep.2013.11.020>
- Fornes, O., Castro-Mondragon, J.A., Khan, A., van der Lee, R., Zhang, X., Richmond, P.A., Modi, B.P., Correard, S., Gheorghe, M., Baranašić, D., Santana-Garcia, W., Tan, G., Chèneby, J., Ballester, B., Parcy, F., Sandelin, A., Lenhard, B., Wasserman, W.W., Mathelier, A., 2019. JASPAR 2020: update of the open-access database of transcription factor binding profiles. *Nucleic Acids Research* gkz1001. <https://doi.org/10.1093/nar/gkz1001>

- Heinz, S., Benner, C., Spann, N., Bertolino, E., Lin, Y.C., Laslo, P., Cheng, J.X., Murre, C., Singh, H., Glass, C.K., 2010. Simple combinations of lineage-determining transcription factors prime cis-regulatory elements required for macrophage and B cell identities. *Molecular cell* 38, 576. <https://doi.org/10.1016/J.MOLCEL.2010.05.004>
- Langmead, B., Trapnell, C., Pop, M., Salzberg, S.L., 2009. Ultrafast and memory-efficient alignment of short DNA sequences to the human genome. *Genome Biology* 10, 1–10. <https://doi.org/10.1186/GB-2009-10-3-R25/TABLES/5>
- Lovén, J., Hoke, H.A., Lin, C.Y., Lau, A., Orlando, D.A., Vakoc, C.R., Bradner, J.E., Lee, T.I., Young, R.A., 2013. Selective inhibition of tumor oncogenes by disruption of super-enhancers. *Cell* 153, 320–334. <https://doi.org/10.1016/j.cell.2013.03.036>
- Pandiani, C., Strub, T., Nottet, N., Cheli, Y., Gambi, G., Bille, K., Husser, C., Dalmasso, M., Béranger, G., Lassalle, S., Magnone, V., Pédeutour, F., Irondelle, M., Maschi, C., Nahon-Estève, S., Martel, A., Caujolle, J.-P., Hofman, P., LeBrigand, K., Davidson, I., Baillif, S., Barbry, P., Ballotti, R., Bertolotto, C., 2021. Single-cell RNA sequencing reveals intratumoral heterogeneity in primary uveal melanomas and identifies HES6 as a driver of the metastatic disease. *Cell Death Differ* 28, 1990–2000. <https://doi.org/10.1038/s41418-020-00730-7>
- Quinlan, A.R., Hall, I.M., 2010. BEDTools: a flexible suite of utilities for comparing genomic features. *Bioinformatics (Oxford, England)* 26, 841–842. <https://doi.org/10.1093/BIOINFORMATICS/BTQ033>
- Ramírez, F., Ryan, D.P., Grüning, B., Bhardwaj, V., Kilpert, F., Richter, A.S., Heyne, S., Dündar, F., Manke, T., 2016. deepTools2: a next generation web server for deep-sequencing data analysis. *Nucleic acids research* 44, W160–W165. <https://doi.org/10.1093/NAR/GKW257>
- Ross-Innes, C.S., Stark, R., Teschendorff, A.E., Holmes, K.A., Ali, H.R., Dunning, M.J., Brown, G.D., Gojis, O., Ellis, I.O., Green, A.R., Ali, S., Chin, S.F., Palmieri, C., Caldas, C., Carroll, J.S., 2012. Differential oestrogen receptor binding is associated with clinical outcome in breast cancer. *Nature* 481, 389. <https://doi.org/10.1038/NATURE10730>
- Thomas-Chollier, M., Darbo, E., Herrmann, C., Defrance, M., Thieffry, D., van Helden, J., 2012. A complete workflow for the analysis of full-size ChIP-seq (and similar) data sets using peak-motifs. *Nat Protoc* 7, 1551–1568. <https://doi.org/10.1038/nprot.2012.088>
- Verfaillie, A., Imrichova, H., Atak, Z.K., Dewaele, M., Rambow, F., Hulselmans, G., Christiaens, V., Svetlichnyy, D., Luciani, F., Van den Mooter, L., Claerhout, S., Fiers, M., Journe, F., Ghanem, G.E., Herrmann, C., Halder, G., Marine, J.C., Aerts, S., 2015. Decoding the regulatory landscape of melanoma reveals TEADS as regulators of the invasive cell state. *Nat Commun* 6, 6683. <https://doi.org/10.1038/ncomms7683>
- Whyte, W.A., Orlando, D.A., Hnisz, D., Abraham, B.J., Lin, C.Y., Kagey, M.H., Rahl, P.B., Lee, T.I., Young, R.A., 2013. Master transcription factors and mediator establish super-enhancers at key cell identity genes. *Cell* 153, 307–319. <https://doi.org/10.1016/j.cell.2013.03.035>
- Ye, T., Krebs, A.R., Choukrallah, M.A., Keime, C., Plewniak, F., Davidson, I., Tora, L., 2011. seqMINER: an integrated ChIP-seq data interpretation platform. *Nucleic acids research* 39. <https://doi.org/10.1093/NAR/GKQ1287>
- Yu, G., Wang, L.G., He, Q.Y., 2015. ChIPseeker: an R/Bioconductor package for ChIP peak annotation, comparison and visualization. *Bioinformatics (Oxford, England)* 31, 2382–2383. <https://doi.org/10.1093/BIOINFORMATICS/BTV145>

Figure 1

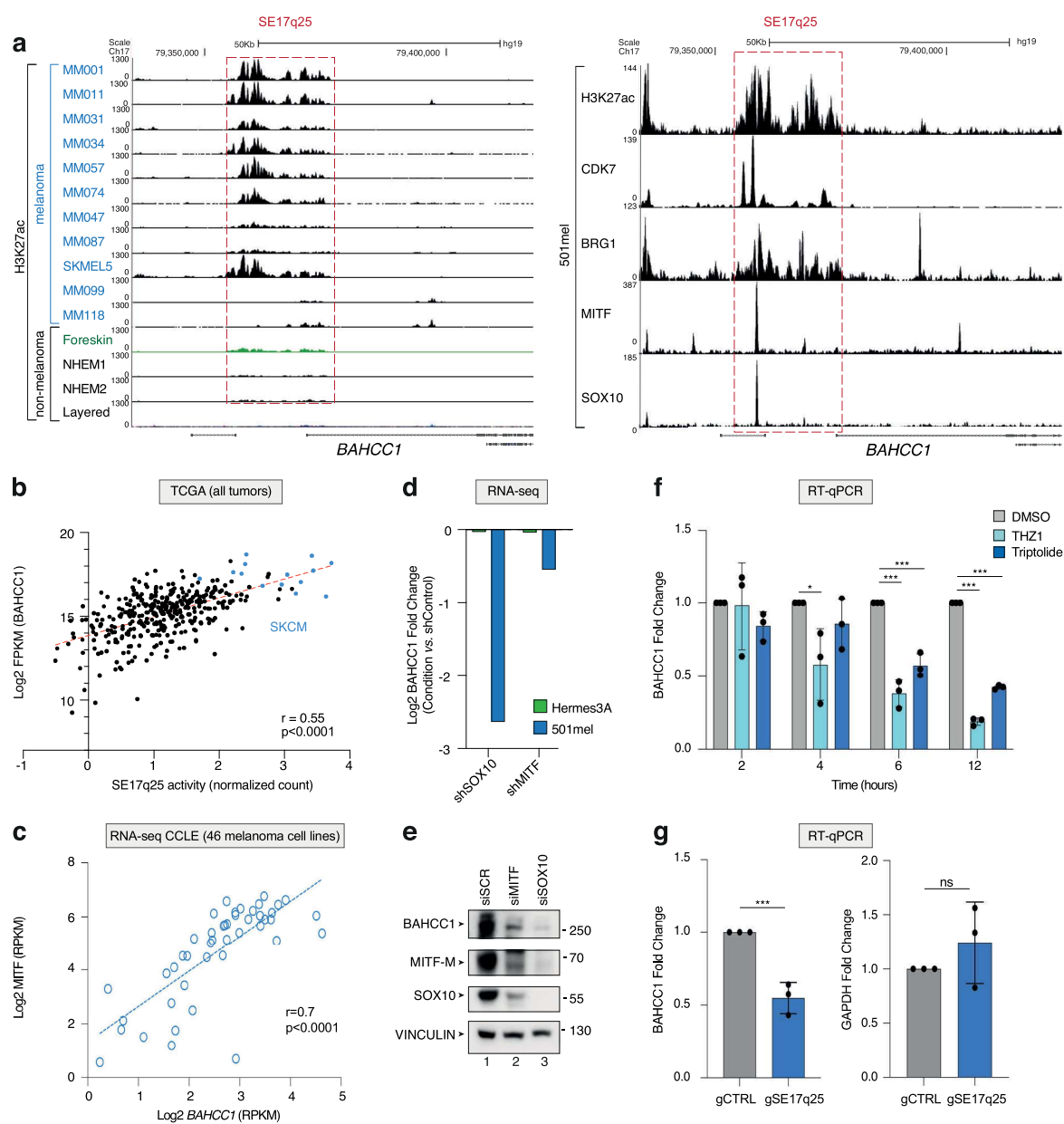


Figure 2

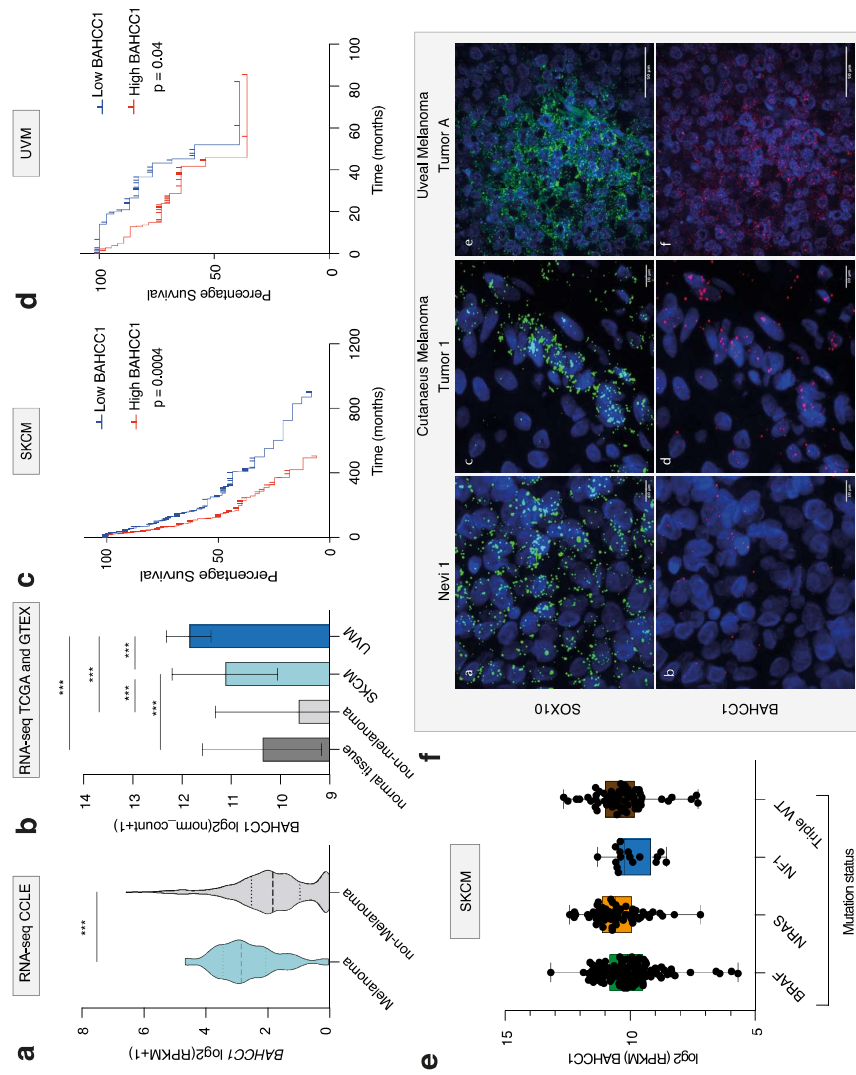


Figure 3

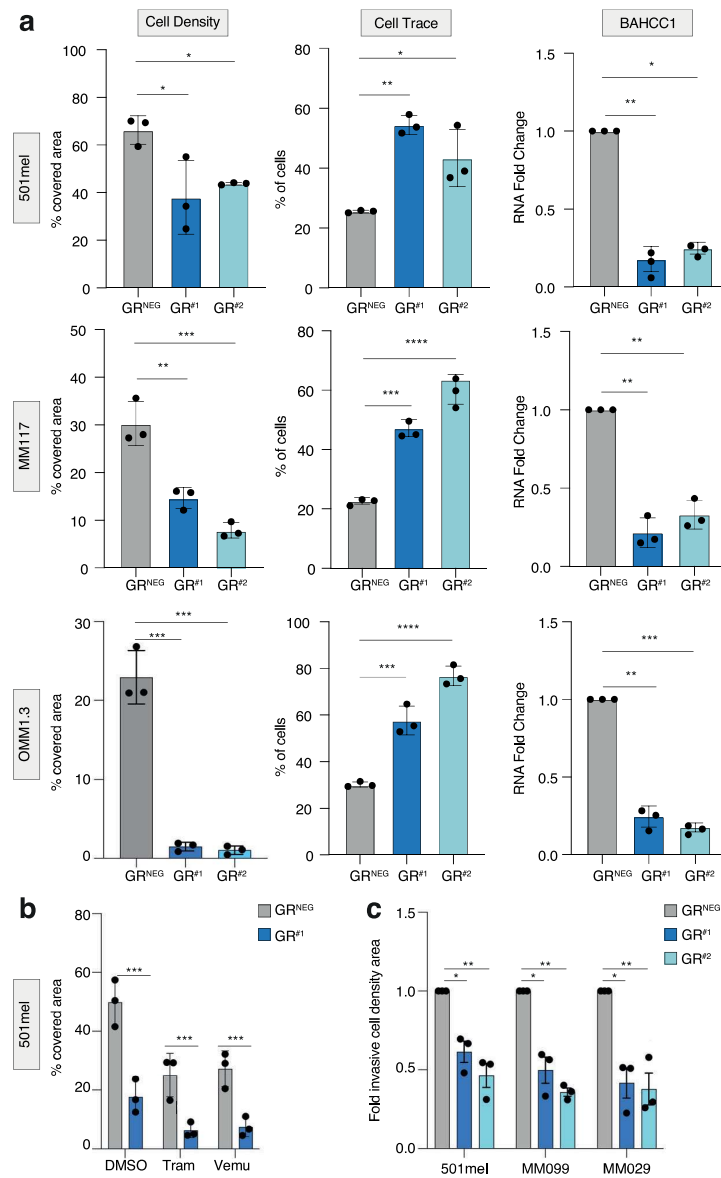


Figure 4

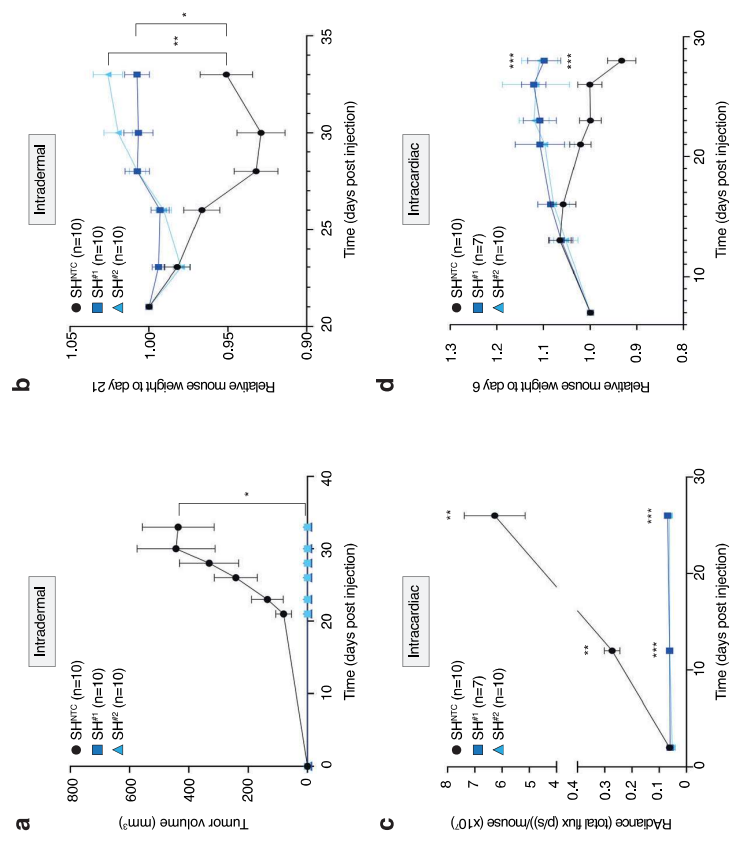


Figure 5

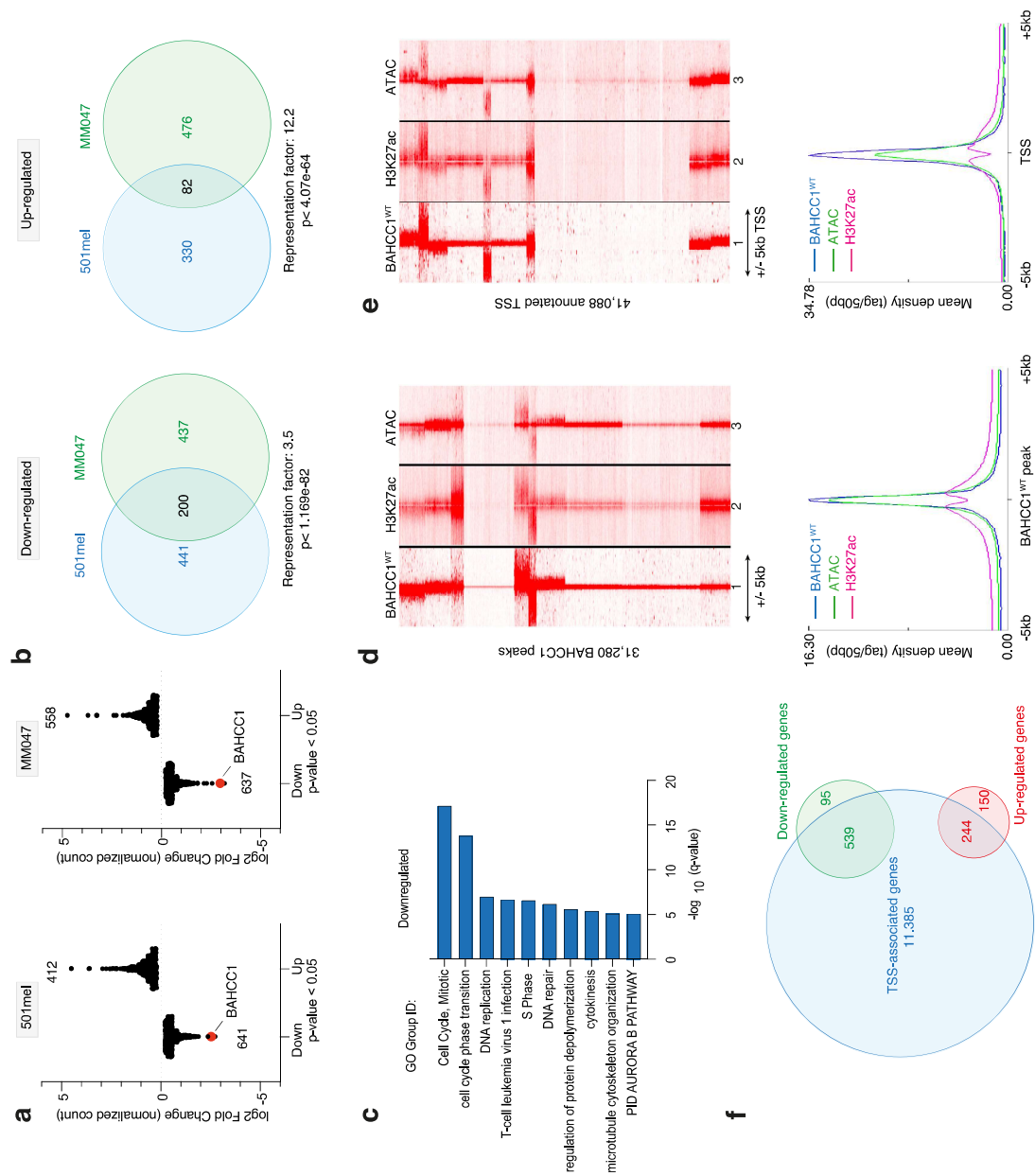


Figure 6

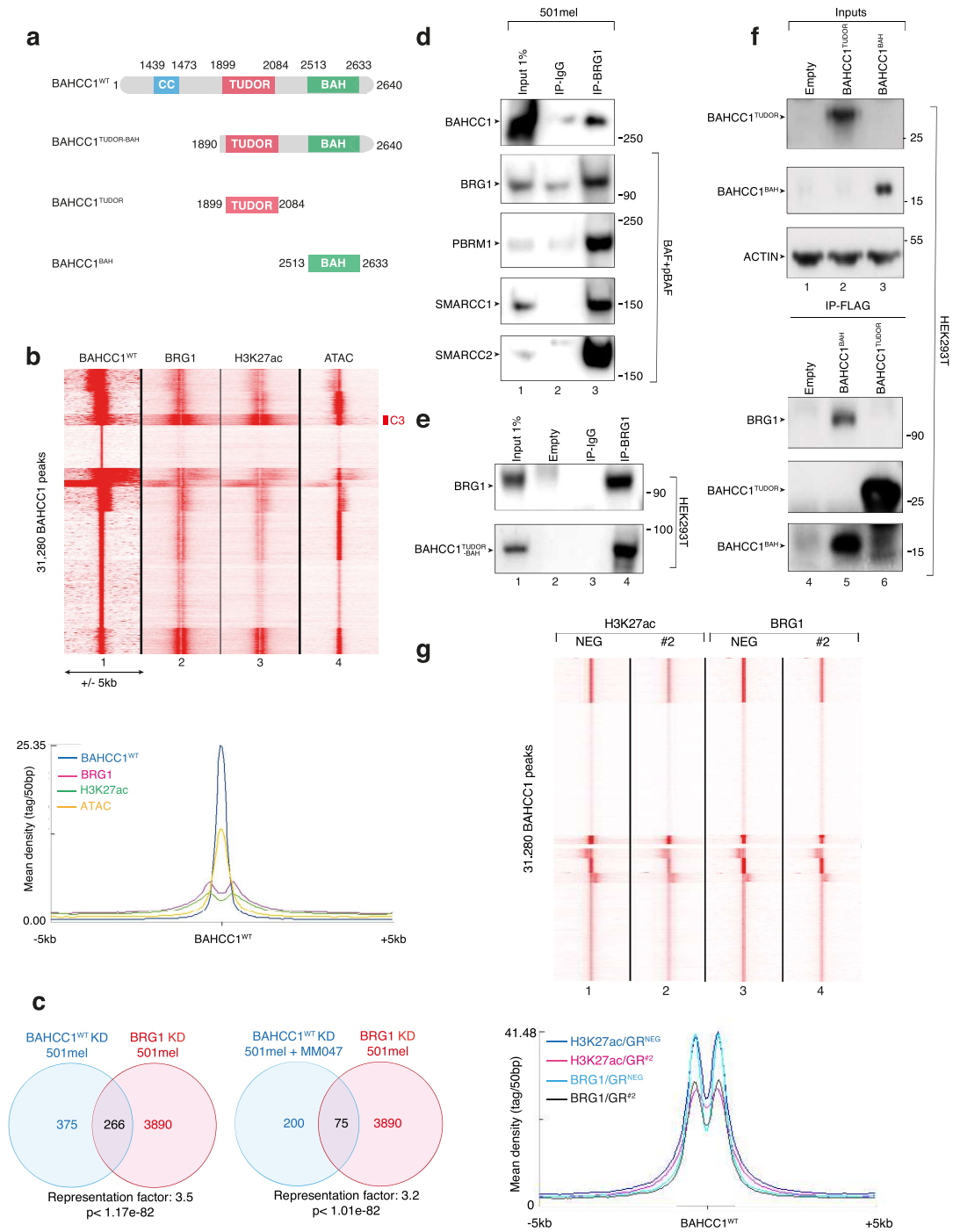
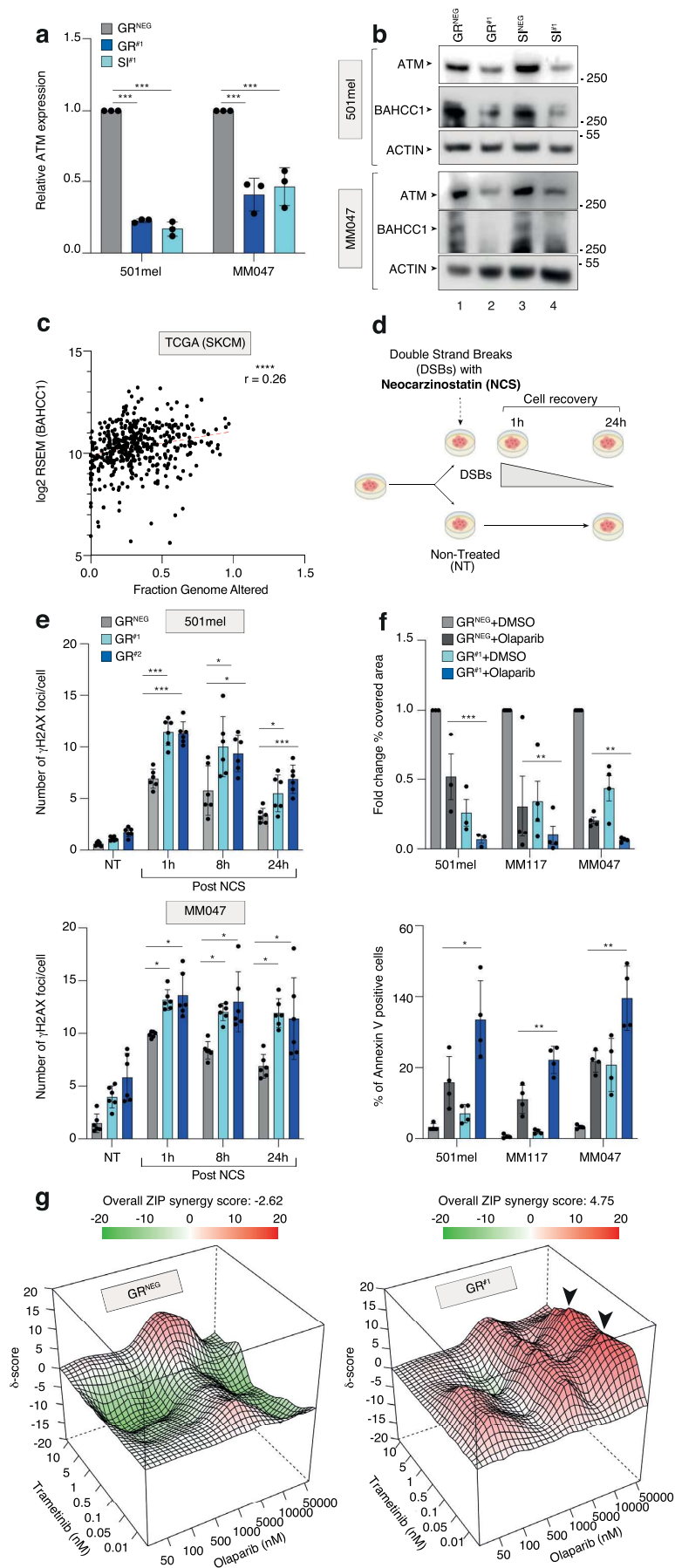
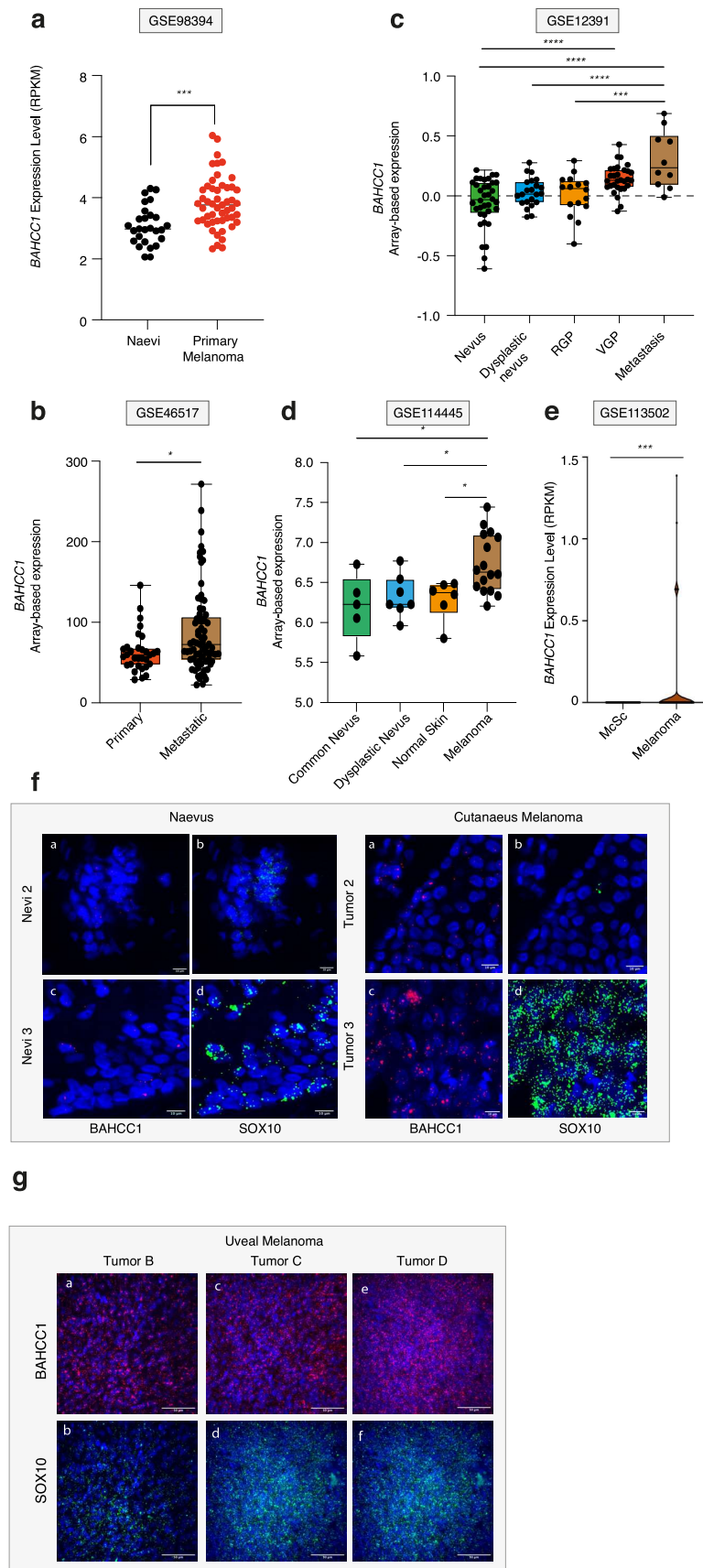


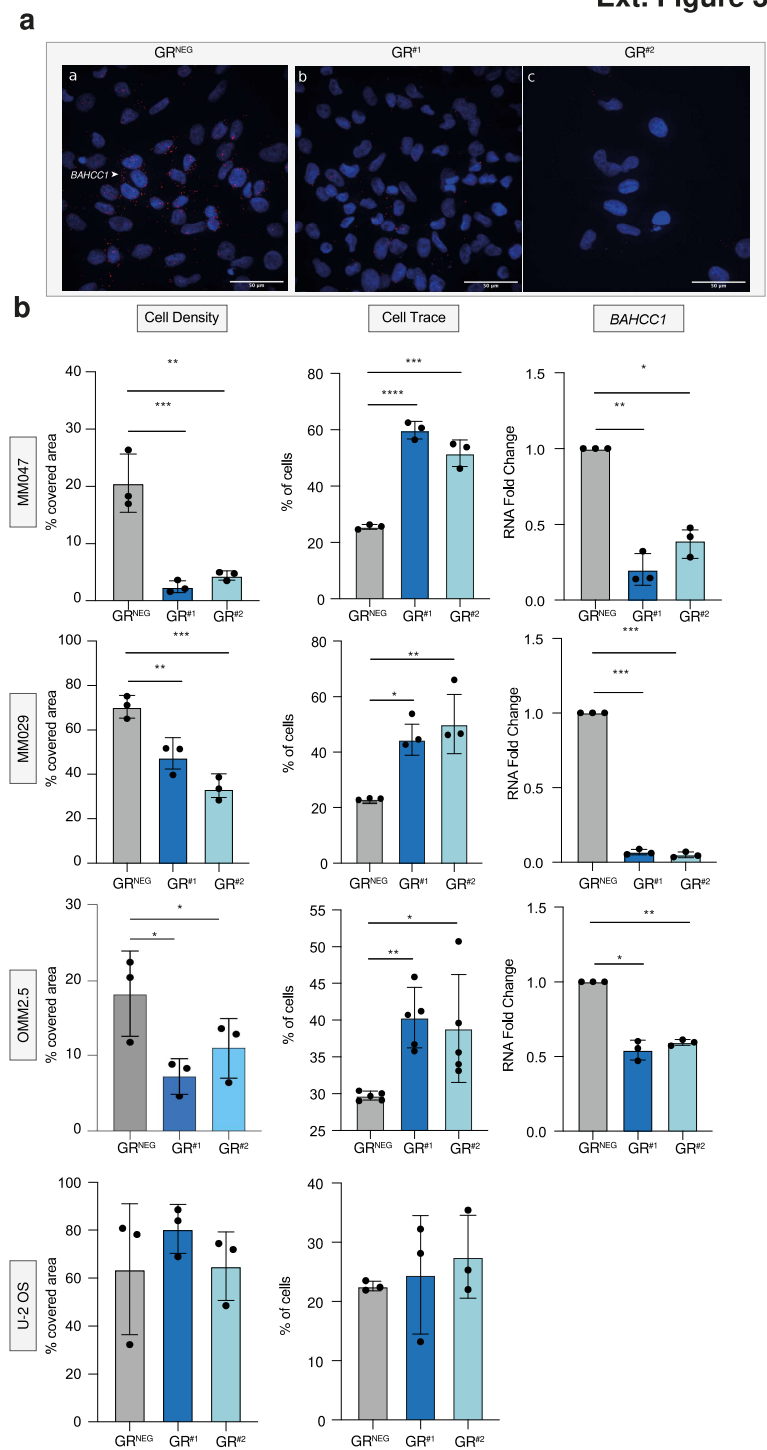
Figure 7



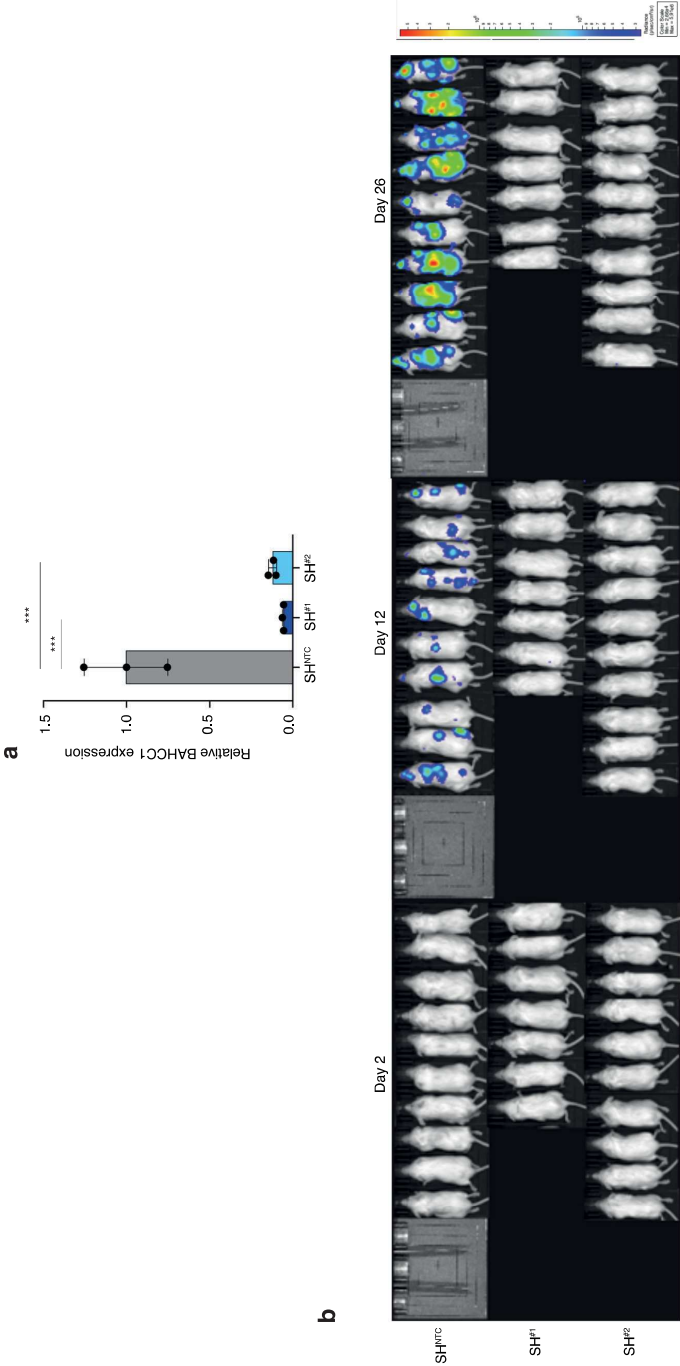
Ext. Figure 2



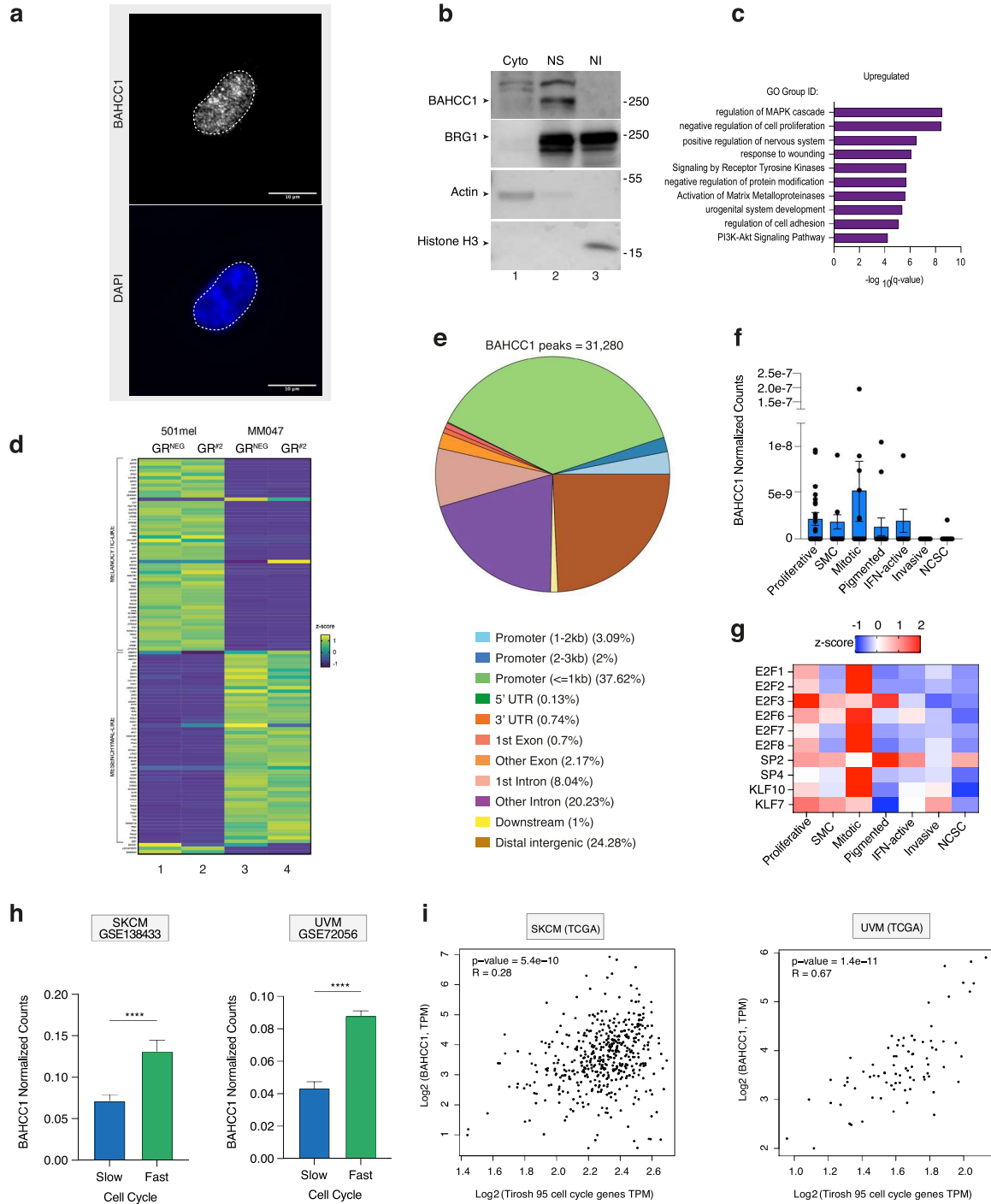
Ext. Figure 3



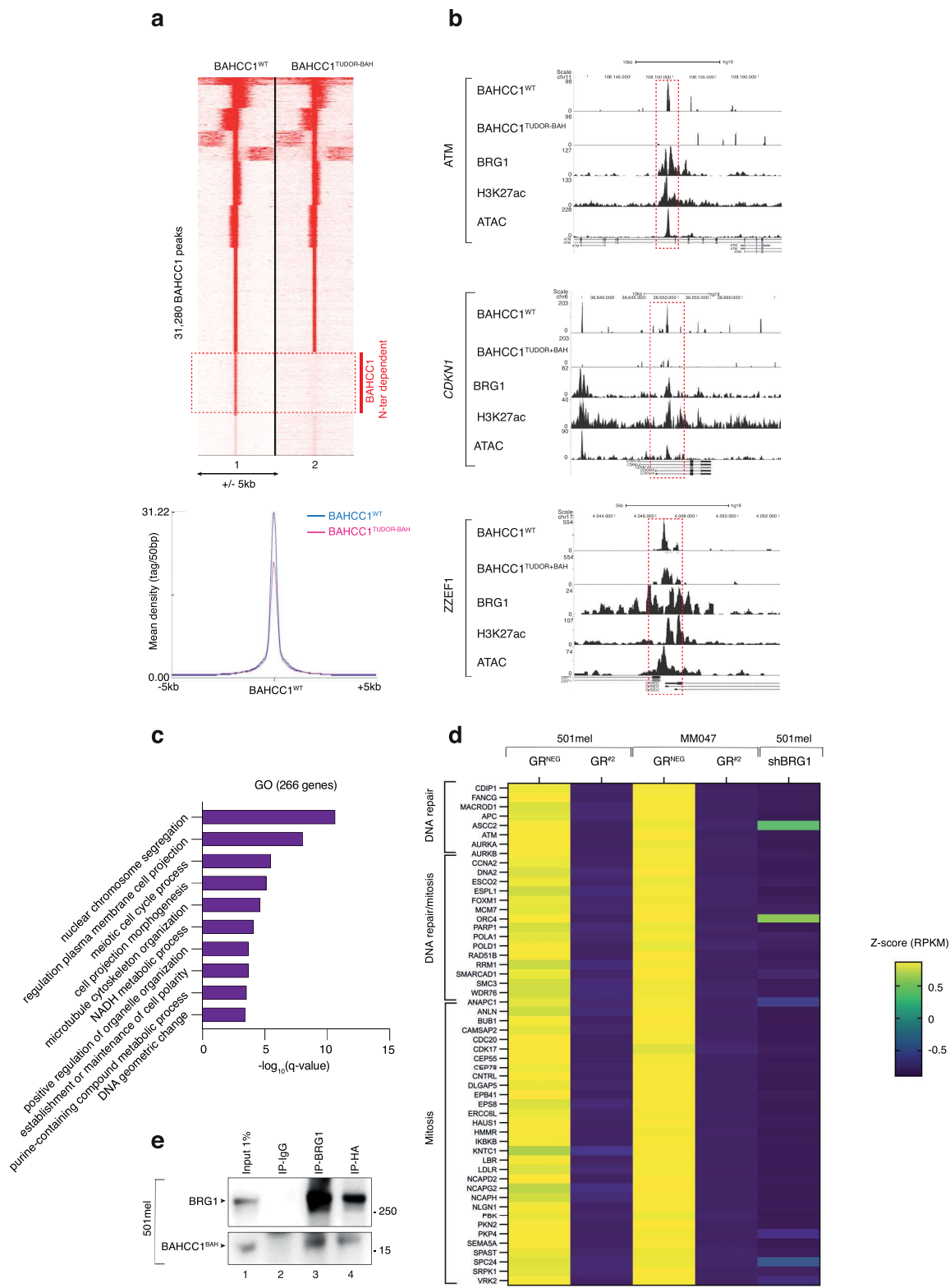
Ext. Figure 4



Ext. Figure 5

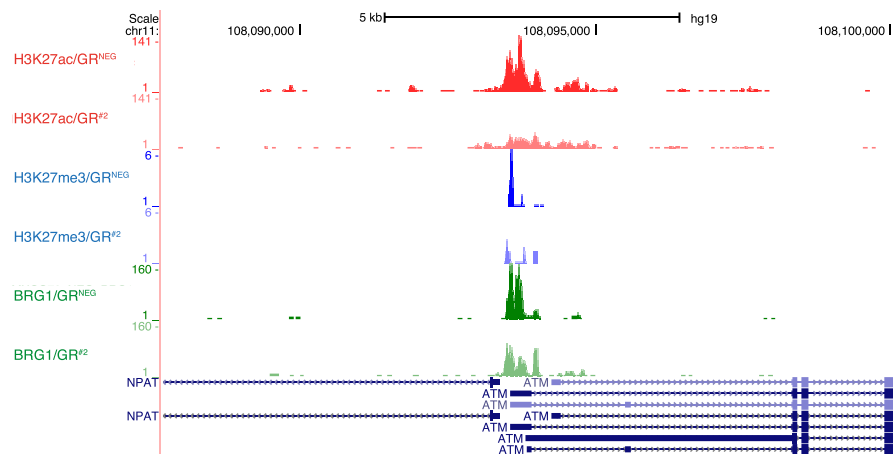


Ext. Figure 6

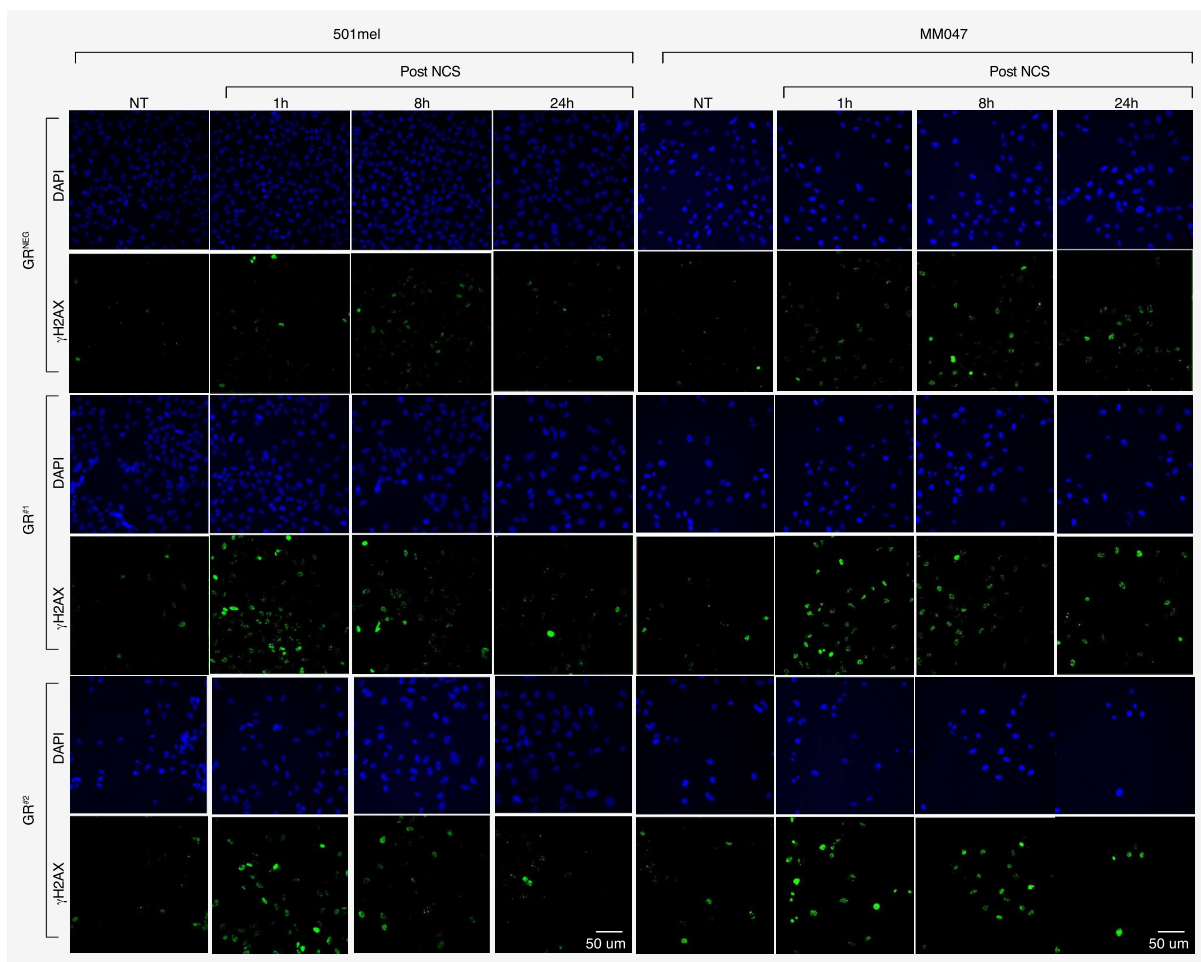


Extended Figure 7

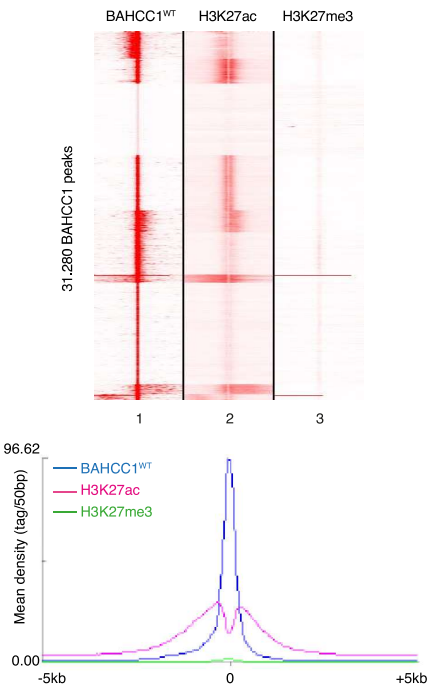
a



b



Extended Figure 8




Active mRNA degradation by EXD2 nuclease elicits recovery of transcription after genotoxic stress

Received: 20 June 2022

Accepted: 6 January 2023

Published online: 20 January 2023

 Check for updates

Jérémy Sandoz^{1,2,3,4}, Max Cigrang^{1,2,3,4}, Amélie Zachayus^{1,2,3,4},
Philippe Catez^{1,2,3,4}, Lise-Marie Donnio⁵, Clémence Elly^{1,2,3,4},
Jadwiga Nieminuszczy⁶, Pietro Berico^{1,2,3,4}, Cathy Braun^{1,2,3,4},
Sergey Alekseev^{1,2,3,4}, Jean-Marc Egly^{1,2,3,4}, Wojciech Niedzwiedz⁶,
Giuseppina Giglia-Mari⁵, Emmanuel Compe^{1,2,3,4} & Frédéric Coin^{1,2,3,4}✉

The transcriptional response to genotoxic stress involves gene expression arrest, followed by recovery of mRNA synthesis (RRS) after DNA repair. We find that the lack of the EXD2 nuclease impairs RRS and decreases cell survival after UV irradiation, without affecting DNA repair. Overexpression of wild-type, but not nuclease-dead EXD2, restores RRS and cell survival. We observe that UV irradiation triggers the relocation of EXD2 from mitochondria to the nucleus. There, EXD2 is recruited to chromatin where it transiently interacts with RNA Polymerase II (RNAPII) to promote the degradation of nascent mRNAs synthesized at the time of genotoxic attack. Reconstitution of the EXD2-RNAPII partnership on a transcribed DNA template in vitro shows that EXD2 primarily interacts with an elongation-blocked RNAPII and efficiently digests mRNA. Overall, our data highlight a crucial step in the transcriptional response to genotoxic attack in which EXD2 interacts with elongation-stalled RNAPII on chromatin to potentially degrade the associated nascent mRNA, allowing transcription restart after DNA repair.

Cells are regularly exposed to endogenous and exogenous genotoxic attacks that induce damage in the DNA molecule^{1,2}. The generation of DNA damage can potentially challenge several fundamental cellular processes such as transcription or replication and can ultimately cause diseases such as cancer if not repaired^{3–5}. The identification of several protective mechanisms against genotoxic stress highlights the importance of maintaining genome integrity to ensure low mutation frequencies in the genome⁶. One such mechanism, the nucleotide excision repair (NER) pathway, removes DNA adducts such as pyrimidine (6–4) pyrimidone (6–4PP) or cyclobutane pyrimidine dimers (CPD) that are produced by UV light^{7–9}. Two NER sub-pathways co-exist in cells: global genome NER (GG-NER), which removes DNA damage

from the entire genome, and transcription-coupled NER (TC-NER), which corrects lesions located on actively transcribed genes^{8,10–12}. In GG-NER, the concerted action of XPC and/or DDB2-containing complexes enables the detection of DNA damage in the genome, whereas in TC-NER, an actively transcribing RNA Polymerase II (RNAPII), which is stalled by a lesion, triggers efficient removal of cytotoxic damage^{13,14}.

To protect the integrity of gene expression under genotoxic attack, cells undergo a transcription stress response that includes global inhibition of transcription occurring in two steps: rapid and local inhibition of elongation due to the stalling of RNAPII in front of transcription-blocking DNA damage¹⁵ which is followed by a global inhibition of transcription initiation occurring on both damaged and

¹Institut de Génétique et de Biologie Moléculaire et Cellulaire Illkirch Cedex, C.U. Equipe Labellisée Ligue contre le Cancer, 2022 Strasbourg, France. ²Centre National de la Recherche Scientifique, UMR7104 Illkirch, France. ³Institut National de la Santé et de la Recherche Médicale, U1258 Illkirch, France. ⁴Université de Strasbourg, Strasbourg, France. ⁵Institut NeuroMyogène (INMG) – Laboratoire Physiopathologie et Génétique du Neurone et du Muscle, Université Claude Bernard Lyon 1, CNRS UMR 5261, INSERM U1315, Lyon, France. ⁶The Institute of Cancer Research, London SW3 6JB, UK. ✉e-mail: fredr@igbmc.fr

undamaged genes^{16,17}. Recent evidence has shown that global inhibition takes place after the degradation of the pool of RNAPII^{18,19}. After DNA repair, cells recover transcription in an active process involving transcription and chromatin remodeling factors^{20–24}. Recovery of RNA synthesis (RRS) encompasses both the re-initiation of expression at the promoters of actively transcribed genes and the restart of RNAPII molecules already in elongation. Despite recent advances in our understanding of the transcriptional stress response to genotoxic attack, the actors and mechanisms responsible for RRS after DNA repair remain largely elusive. Finding new players involved in RRS is therefore crucial to better understand this process at the molecular level and its role in genome stability.

We unveil here that EXD2, a RNA/DNA nuclease previously shown to be involved in homologous recombination and in the replication fork protection pathway^{25,26}, is essential for RRS after the genotoxic attack. Cells lacking EXD2 or expressing a nuclease-dead version of the enzyme are unable to restore global RNAPII-dependent transcription after UV irradiation, resulting in decreased resistance to genotoxic attack. Mechanistically, we demonstrated that EXD2 is not involved in the removal of UV-induced photoproducts. Instead, UV irradiation provokes the re-localization of EXD2 from mitochondria to the nucleus and its translocation to chromatin. There EXD2 transiently interacts with RNAPII and potentially promotes the degradation, during the recovery phase of transcription, of nascent mRNA being synthesized at the time of the genotoxic attack. Using a reconstituted transcription system *in vitro*, we reconstructed the dynamic association of EXD2 to RNAPII on a transcribed DNA template and demonstrated that EXD2 preferentially interacts with an elongation-blocked RNAPII. In such system, the ribonuclease activity of purified EXD2 efficiently processes mRNA. Accordingly, the interaction between EXD2 and a stalled-RNAPII was also observed *in vivo* using proximal ligation assay (PLA). These findings unveil a crucial role for EXD2 in the transcription stress response and are the first to assign a nuclear function to the ribonuclease activity of EXD2 by showing its involvement in the degradation of mRNA under synthesis at the time of the genotoxic attack. This degradation is necessary for an efficient recovery of gene expression after DNA repair.

Results

UV-induced inhibition and recovery of transcription at a defined genomic locus

In order to identify factors required for transcription recovery after a genotoxic attack, we first sought to develop a sensitive assay to easily monitor transcription inhibition and recovery after UV irradiation. As depicted in Supplementary Fig. 1a, we used a doxycyclin (dox)-inducible transcription/translation reporter system integrated at a single site on genomic DNA in the human osteosarcoma U-2 OS cell line. This system allows visualization of the genomic locus, its nascent mRNA transcript (CFP-SKL), and protein product (CPF-SKL)^{27,28}. After a 2-h dox treatment, we detected transcription of CFP-SKL in 80% of the cells (Supplementary Fig. 1b). A 2-h dox treatment followed by a recovery period in the absence of dox (1- to 4-h) triggered an accumulation of CFP-SKL protein expression (Supplementary Fig. 1c). The plasticity of this system also allowed us to measure the transcriptional activity of the cells in a specific time window after UV-irradiation. For this purpose, cells were irradiated with UV (30 J/m²) and pulsed with dox for 2 h at different times after the genotoxic attack. Under these conditions, we noticed a strong inhibition of CPF-SKL mRNA expression at early times after UV irradiation (Supplementary Fig. 1d, right panel, lanes 1 and 2). Interestingly, CPF-SKL mRNA expression recovered over time after irradiation (lane 3) and knockdown of the TC- and GG-NER factor XPA prevented this recovery (lanes 4–6 and left panel). CPF-SKL protein expression followed that of its mRNA with a strong inhibition early after irradiation and a progressive recovery that was completed 18 h after irradiation (Supplementary Fig. 1e). These data indicate that CPF-SKL expression recapitulates the rapid inhibition and

progressive recovery of global transcription that is generally completed 20 h after a genotoxic attack when DNA repair is efficient^{29,30}.

EXD2 is a critical factor for RRS

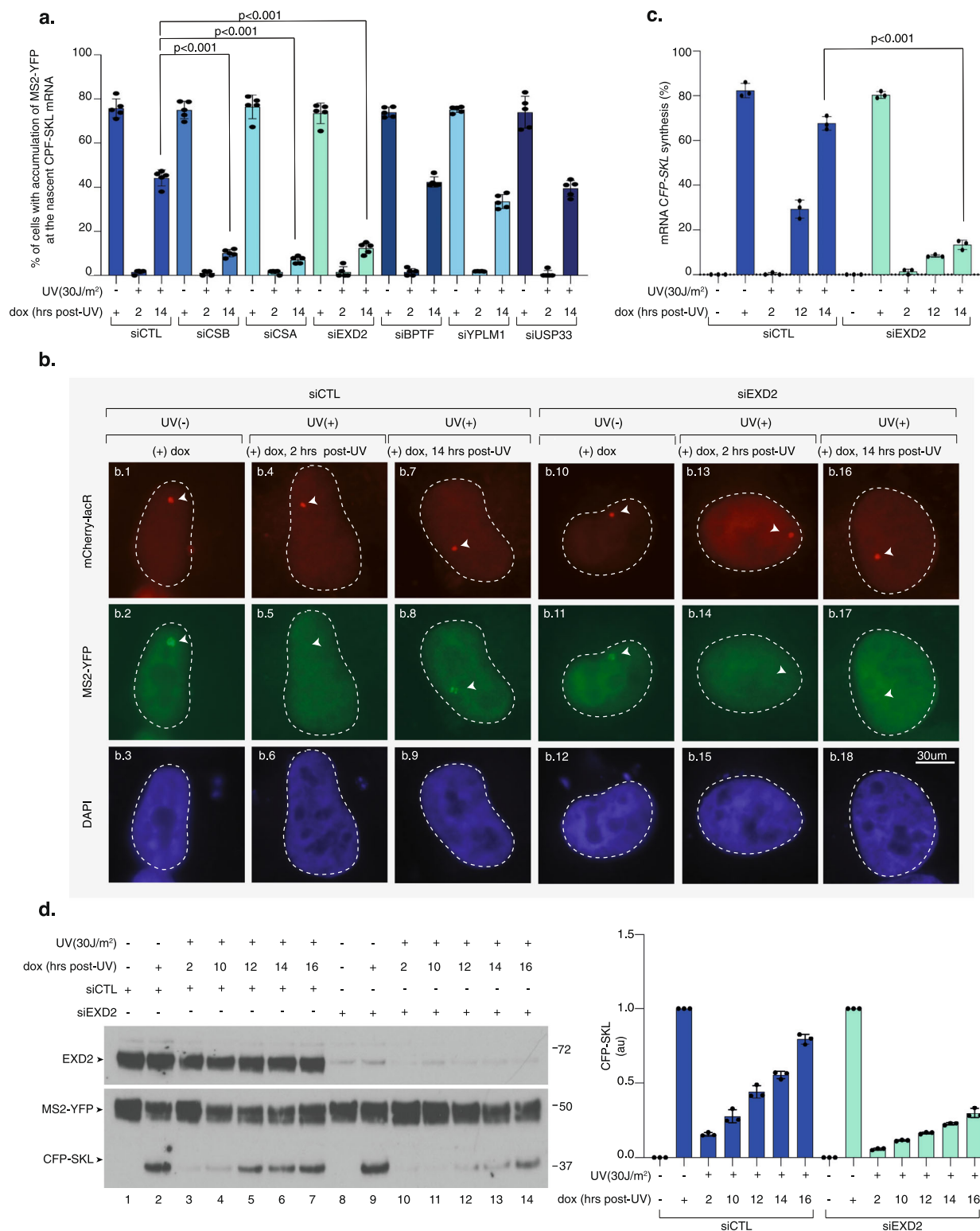
To explore the mechanism of transcription recovery after genotoxic stress, we used the reporter assay described above and tested a small number of selected candidates for their potential involvement in RRS. As expected, knockdown of the TC-NER factors CSA and CSB inhibited recovery of CFP-SKL expression (Fig. 1a). Interestingly, the 3' to 5' DNA/RNA exonuclease EXD2 emerged as a potential effector of transcription recovery after UV irradiation (Fig. 1a, b). The lack of recovery of CFP-SKL expression in the absence of EXD2 was confirmed by RT-qPCR (Fig. 1c) and resulted in 70% inhibition of *de novo* translation of CFP-SKL over time after UV irradiation (Fig. 1d, compare lanes 10–14 and 3–7). Of note, we observed that the accumulation of nascent CFP-SKL mRNA or *de novo* CFP-SKL protein was not impaired by the knockdown of EXD2 in the mock-treated cells (Fig. 1b, compare panels b1-b2-b3 with b10-b11-b12 and Fig. 1d, compare lane 2 and 9). These data suggest that EXD2 is required for RRS following a genotoxic stress.

EXD2 nuclease activity is required for RRS

We next used HeLa EXD2 CRISPR knock-out cells (EXD2^{-/-}-cl1)²⁵ (Fig. 2a, compare lanes 1 and 2) to measure the impact of EXD2 on global RRS. We pulse-labeled nascent mRNAs at various time points after UV irradiation (15 J/m²) using 5-ethynyluridine (EU)³¹. At this UV dose, all transcribed gene strands should contain at least one lesion that blocks RNAPII elongation³². We pre-treated the cells with a low concentration of actinomycin D (0.05 µg/ml) to abolish the intense nucleolar EU staining due to RNAPI-dependent ribosomal RNA synthesis. In these conditions, EU incorporation mainly reflects RNAPII-dependent RNA transcription³¹. Within the first hour after UV irradiation, we observed a strong inhibition (50%) of mRNA synthesis in both EXD2^{+/+} and EXD2^{-/-}-cl1 cells (Fig. 2b and Supplementary Fig. 2a, panels a.1-a.2 and a.5-a.6). In agreement with the above data, RRS was progressively restored in wild-type EXD2^{+/+} cells over time, whereas it remained deficient in EXD2^{-/-}-cl1 cells (Fig. 2b and Supplementary Fig. 2a panels a.3-a.4 and a.7-a.8). This defect was similar to the RRS defect observed in the CS1ANSV cell line from CS-B patient (in which the TC-NER factor CSB was deficient)³³ (Supplementary Fig. 2b).

To explore the role of the exonuclease activity of EXD2 in RRS, EXD2^{-/-}-cl1 cells were subsequently complemented with either FLAG-HA-tagged wild-type (EXD2^{-/-} + EXD2^{WT}-cl1) or dominant negative nuclease-dead EXD2 containing two substitutions at positions D108 and E110 (EXD2^{-/-} + EXD2^{D108A/E110A}-cl1). These two amino-acids are located in the active site of EXD2 and are known to be essential for its nuclease activity^{25,34}. RRS was restored in EXD2^{-/-} + EXD2^{WT}-cl1 cells but not in the nuclease-dead EXD2^{-/-} + EXD2^{D108A/E110A}-cl1 cells (Fig. 2b, c, compare panels c.1, c.2, c.3 with c.4, c.5, c.6), showing that RRS requires the nuclease activity of EXD2. We noted that the stability of the RPB1 subunit of RNAPII after UV-irradiation was not affected by the depletion of EXD2 or the lack of its exonuclease activity (Supplementary Fig. 2c). As noted above, we also observed that mRNA synthesis was indistinguishable in all four mock-treated HeLa cells, suggesting that EXD2 is not required for RNAPII-dependent transcription in the absence of genotoxic attack (Fig. 2c, panels c.1 and c.4, and Supplementary Fig. 2a, panels a.1 and a.5). Similar results were obtained with an additional set of HeLa clones (EXD2^{-/-}-cl2, EXD2^{-/-} + EXD2^{WT}-cl2 and EXD2^{-/-} + EXD2^{D108A/E110A}-cl2) (Supplementary Fig. 2d–e), but also under conditions in which cells were synchronized at G0-G1 to prevent cell division (Supplementary Fig. 2f). Thus, the knockdown as well as overexpression studies complement one another and establish that EXD2 exonuclease activity has a crucial function in RRS following UV irradiation.

In a second set of experiments, we evaluated the role of EXD2 in response to various treatments provoking transcription arrest without



generating DNA damage. We either treated the cells with the transcriptional inhibitor 5,6-dichloro-1-beta-D-ribofuranosylbenzimidazole (DRB) for 30 min³¹ or incubated them for 15 min at 4 °C to block transcription. Following the chase of DRB or the re-incubation at 37 °C, we observed similar transcriptional recovery in EXD2^{-/-} + EXD2^{WT}-c1 and EXD2^{-/-} + EXD2^{D108A/E110A}-c1 (Supplementary Fig. 3). Taken together, these results suggest that EXD2 specifically contributes to the global transcription recovery operating after a genotoxic stress such as UV irradiation.

Lack of EXD2 nuclease activity leads to mild UV sensitivity

To further examine the consequences of a lack of EXD2 activity on cell homeostasis, we measured the UV sensitivity of EXD2^{-/-}-c1, EXD2^{-/-} + EXD2^{WT}-c1, and EXD2^{-/-} + EXD2^{D108A/E110A}-c1 cells in comparison with the parental EXD2^{+/+} cells as well as the CS-B patient CS1ANSV cell line and the HeLa XPC^{-/-} (in which the GG-NER factor XPC was depleted)³⁵. Upon increasing doses of UV irradiation, knockdown of EXD2 activity resulted in hypersensitivity of EXD2^{-/-}-c1 and EXD2^{-/-} + EXD2^{D108A/E110A}-c1 cells, compared to EXD2^{+/+} and EXD2^{-/-} + EXD2^{WT}-c1.

Fig. 1 | Knockdown of EXD2 impairs RRS of CFP-SKL. **a** U-2 OS cells were transfected with siRNA for 24 h, then with a construct expressing mCherry-lacR for 24 h before UV irradiation (30 J/m²) and 2-h pulse-incubation with dox starting at various time points post-UV. Nascent CFP-SKL mRNAs were detected at the reporter locus by accumulation of the MS2-YFP protein to the MS2 RNA loop. Quantification of the transcribing locus is expressed as % of cells showing YFP-MS2 accumulation at a single locus (n = at least 250 cells in five independent experiments). Bars represent mean values of three different experiments (Biological triplicates) (\pm SD). One-way ANOVA with post-hoc Tukey adjustment comparisons were used to determine the p -values. Source data are provided as a Source Data file. **b** Representative confocal images of cells treated with siCTL or siEXD2. Images of the cells were obtained with the same microscopy system and constant acquisition parameters. **c** Cells were treated as described above and after the 2-h pulse-incubation with dox, the relative amount of CFP-SKL mRNA was quantified by RT-qPCR. Bars represent

mean values of three different experiments (Biological triplicates) (\pm SEM). One-way ANOVA with post-hoc Tukey adjustment comparisons were used to determine the p -values. Source data are provided as a Source Data file. **d** U-2 OS cells were treated as described above. After the 2-h pulse-incubation with dox, the cells were let to recover for 4 h before lysis. Extracts were resolved by SDS-PAGE and immunoblotted with anti-GFP (recognizing both the MS2-YFP and CFP-SKL proteins) and anti-EXD2. Lanes 1 and 8 are negative controls in which cells were not treated with dox. Lanes 2 and 9 are positive controls in which cells were treated with dox for 2 h before to recover 4 h in the absence of dox. Molecular sizes are indicated (kDa). CFP-SKL signals were quantified using ImageJ software (NIH), normalized with YFP-MS2 signals and reported on the graph (1 is the value for dox (+) for siCTL or siEXD2). Bars represent mean values of three different experiments (Biological triplicates) (\pm SEM). Source data are provided as a Source Data file.

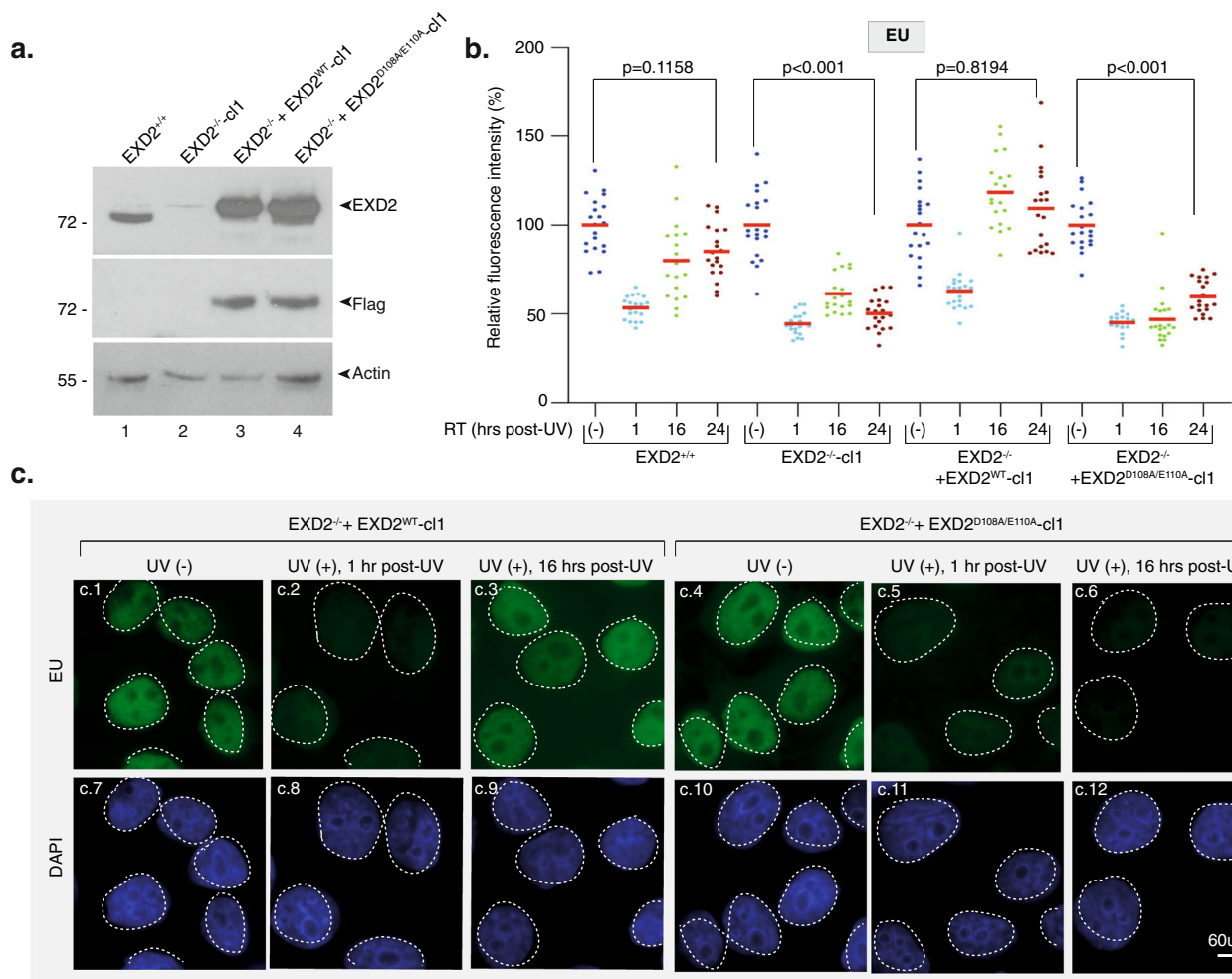


Fig. 2 | Knockdown of EXD2 nuclease activity impairs global RRS. **a** Protein lysates from EXD2^{+/+}, EXD2^{-/-}-cl1, EXD2^{-/-} + EXD2^{WT}-cl1 and EXD2^{-/-} + EXD2^{D108A/E110A}-cl1 cells were immuno-blotted for proteins as indicated. Molecular mass of the proteins is indicated (kDa). Source data are provided as a Source Data file. **b** Cells were mock- or UV-irradiated (15 J/m²) and mRNA was labeled with EU at the indicated time points post-UV. EU signal was quantified by ImageJ and relative integrated densities, normalized to mock-treated level set to 100%, are reported on the

graph (n = at least 20 cells per conditions). Red bars indicate mean integrated density. RT recovery time. One-way ANOVA with post-hoc Tukey adjustment comparisons were used to determine the p -values. Source data are provided as a Source Data file. **c** Representative confocal images of EXD2^{-/-} + EXD2^{WT}-cl1 and EXD2^{-/-} + EXD2^{D108A/E110A}-cl1 treated like in **b**. Images of the cells were obtained with the same microscopy system and constant acquisition parameters.

cl1 cells (Fig. 3a). Interestingly, UV sensitivity of EXD2^{-/-}-cl1 and EXD2^{-/-} + EXD2^{D108A/E110A}-cl1 cells was similar to that found in the TC-NER deficient CS-B cells but not as pronounced as the one found in the highly sensitive GG-NER deficient XPC^{-/-} cells.

To determine whether EXD2 was involved in the removal of UV-induced DNA damage by NER, we measured GG- and TC-NER in cells depleted of EXD2 activity. To this end, we first performed immunofluorescence-based quantification of UV lesions directly in cell

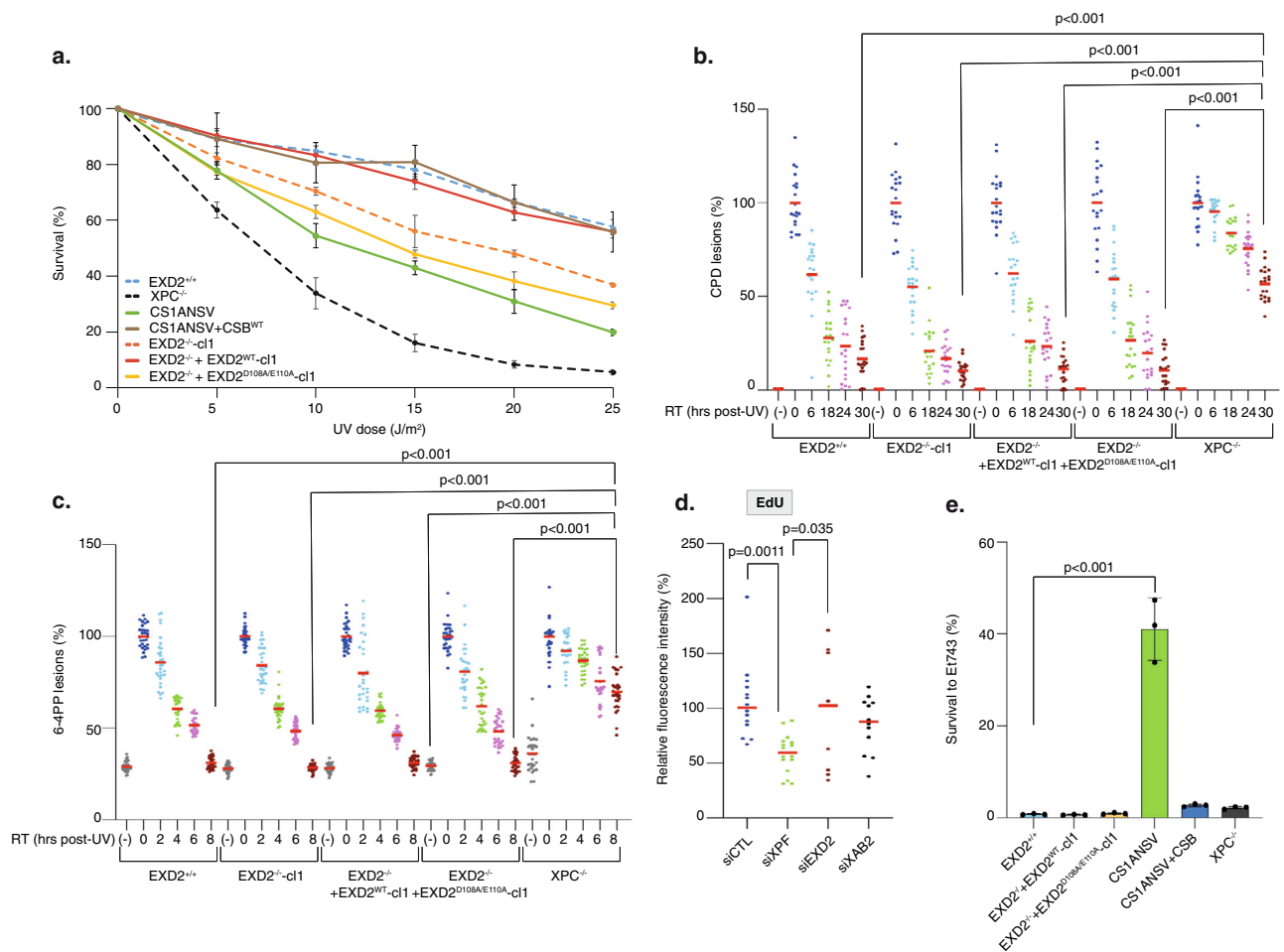


Fig. 3 | Knockdown of EXD2 nuclease activity sensitizes cells to UV irradiation.

a Cells were treated with increasing doses of UV irradiation and survival was determined 48 h later. Data were normalized to the mock treatment controls (as value of 100). The values are the means of three independent experiments (\pm SEM) (Technical triplicates). Source data are provided as a Source Data file. **b, c** Removal of UV lesions was measured in cells, harvested at different time points post-UV (15 J/m²) as indicated. Cells were labeled with anti-CPD (**b**) or anti-6-4PP (**c**) antibodies and signals were quantified using ImageJ at the different times indicated in the figure. Graph represents the % of lesions remaining in the genome at different time points normalized to the amounts of lesions measured immediately after UV irradiation (as a value of 100%). For each time point, a mean of 30 cells has been analyzed. Red bars indicate mean integrated density. RT; recovery time. (-); cells were mock-irradiated. 0; cells were irradiated and fixed immediately. One-way ANOVA with post-hoc Tukey adjustment comparisons were used to determine the

p -values. Source data are provided as a Source Data file. **d** GG-NER deficient XPC^{-/-} cells were treated either with siRNA against the TC-NER factor XAB2, the TC- and GG-NER factor XPF or against EXD2 for 24 h before local UV irradiation (50 J/m²) and EdU staining. The local TCR-UDS signals were quantified by ImageJ and reported on the graph. At least 15 cells were quantified for each situation. Red bars indicate mean integrated density. One-way ANOVA with post-hoc Tukey adjustment comparisons were used to determine the p -values. Source data are provided as a Source Data file. **e** Cells were treated with Et743 (0.5 nM) and survival was determined 48 h later. Data were normalized to the mock treatment controls (as a value of 100). The values are the means of three independent experiments (\pm SEM) (Biological triplicates). One-way ANOVA with post-hoc Tukey adjustment comparisons were used to determine the p -values. Source data are provided as a Source Data file.

nuclei³¹. The removal rate of the two main types of UV lesions in EXD2^{-/-}-cl1 and EXD2^{-/-}+EXD2^{D108A/E110A}-cl1 cells was higher to that of HeLa XPC^{-/-} cells and identical to that of EXD2^{+/+} or EXD2^{-/-}+EXD2^{WT}-cl1 cells, implying that GG-NER was efficient in cells lacking EXD2 nuclease activity (Fig. 3b, c). We used two different assays to measure TC-NER. We first performed unscheduled DNA repair synthesis (UDS) during TC-NER (TCR-UDS)³⁶. Using GG-NER deficient XPC^{-/-} cells to ensure that repair replication in the UV-damage area was due to ongoing TC-NER, we measured repair replication via incorporation of EdU into newly synthesized DNA after local UV irradiation. Loss of the TC-NER specific factor XAB2 or TC/GG-NER factor XPF using siRNA knockdown induced similar deficiency in TCR-UDS, while loss of EXD2 had no impact (Fig. 3d). We next used the particularity of TC-NER deficient cells to be resistant to the DNA binder and anti-cancer drug Ecteinascidin 743 (Et743)³⁷. Indeed, the TC-NER deficient CS1ANSV cells showed high resistance to Et743 that was abolished in the

recovered CS1ANSV+CSB cells (Fig. 3e). In contrast, knockdown of EXD2 exonuclease activity did not impact the sensitivity of the corresponding cells to Et743. Finally, while γ H2AX accumulated after UV irradiation and persisted in NER deficient cells³⁸, no accumulation of γ H2AX after knockdown of EXD2 was observed over time after UV irradiation (Supplementary Fig. 4). Altogether, these results suggest that while the knockdown of EXD2 sensitizes cells to UV irradiation, the nuclease is not involved in GG- or TC-NER.

EXD2 degrades nascent mRNA under synthesis at the time of UV irradiation

The above data point to a direct processing of mRNA by EXD2 nuclease activity during transcription recovery. To study this function, we first wanted to analyze the fate of mRNA under synthesis at the time of UV irradiation and developed the assay described in Fig. 4a, upper panel. We inhibited ribosomal RNA synthesis with a low

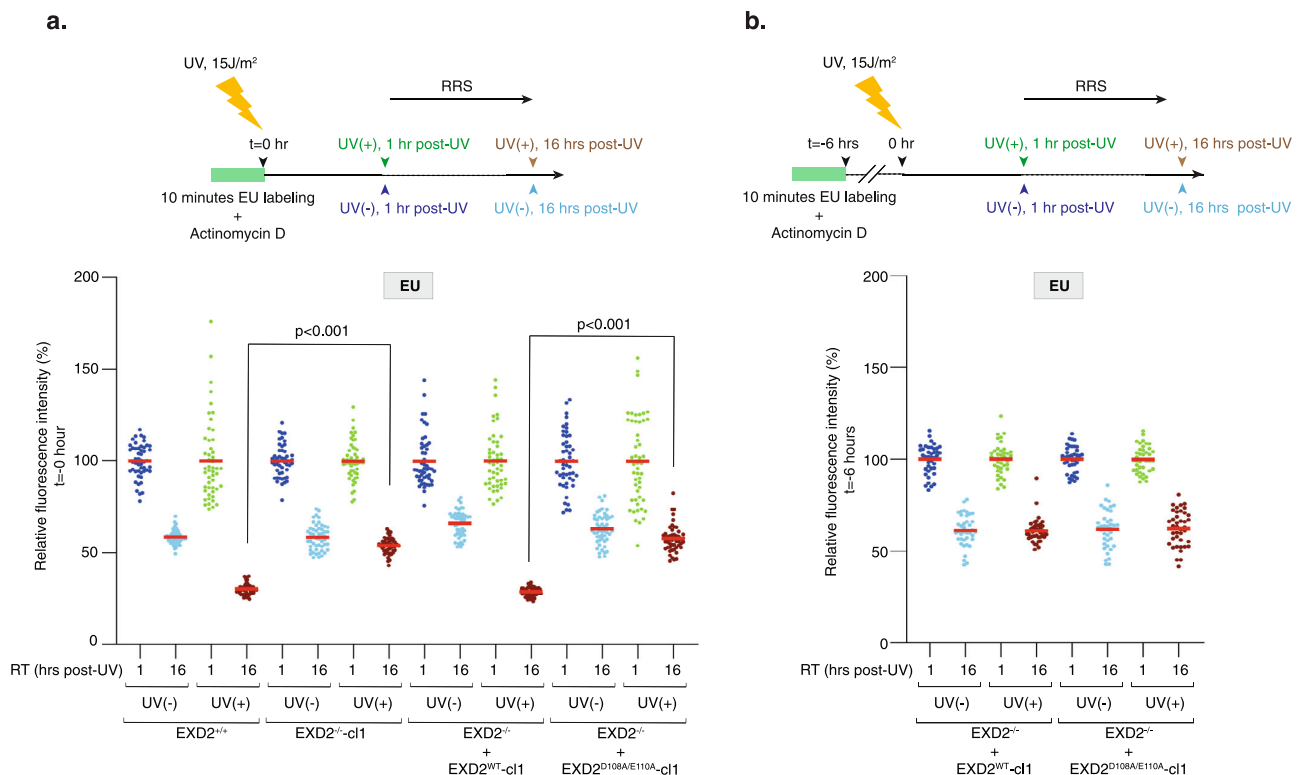


Fig. 4 | EXD2 degrades mRNA under synthesis at the time of UV irradiation.

a Upper panel; Scheme of the EU pulse-chase method used to analyze the fate of mRNA being synthesized at the moment of UV irradiation. Cells were incubated for 30 min with Actinomycin D (0.05 $\mu\text{g}/\text{ml}$) to specifically inhibit RNAPII transcription and mRNAs were pulse-labeled with EU for 10 min prior to UV irradiation (15 J/m^2). Cells were let to recover for 1 h or 16 h post-UV before fixation. Actinomycin D was maintained during the experiment. Lower panel; Cells were treated as indicated in the upper panel and EU signals were quantified using ImageJ and normalized to the value obtained at 1 h set to 100%. Values are reported on the graph ($n =$ at least 50 cells). Red bars indicate mean integrated density. RT; recovery time. One-way ANOVA with post-hoc Tukey adjustment comparisons were used to determine the

p -values. Source data are provided as a Source Data file. **b** Upper panel; Compare to panel **a**, UV irradiation (15 J/m^2) was performed 6 h after EU labeling and cells were let to recover for either 1 h or 16 h post-UV before fixation. Actinomycin D was maintained during the experiment. Lower panel; Cells were treated as indicated in upper panel and EU signals were quantified using ImageJ. Values are reported on the graph ($n =$ at least 50 cells). Red bars indicate mean integrated density. RT recovery time. One-way ANOVA with post-hoc Tukey adjustment comparisons were used to determine the p -values. No statistically significant differences were detected at 16 h post-UV between $\text{EXD2}^{-/-} + \text{EXD2}^{\text{WT-cl1}}$ and $\text{EXD2}^{-/-} + \text{EXD2}^{\text{D108A/E110A-cl1}}$ cells. Source data are provided as a Source Data file.

concentration of actinomycin D and subsequently labeled nascent mRNAs with a 10 min EU pulse. We then chased EU and immediately UV-irradiated the cells (15 J/m^2). Fixing them 1 or 16 h post-chase, we were able to follow, during the recovery phase, the fate of mRNAs under synthesis when cells were subject to a genotoxic attack. In the four mock-treated cells, we observed a 50–40% reduced fraction size of EU-labeled mRNAs between 1 and 16 h of culture (probably reflecting both the turn-over of mRNAs and their dilution during cell division) (Fig. 4a and Supplementary Fig. 5a). Interestingly, UV irradiation of wild-type $\text{EXD2}^{+/+}$ and $\text{EXD2}^{-/-} + \text{EXD2}^{\text{WT-cl1}}$ cells provoked a 70% reduced fraction size of EU-labeled mRNAs between 1 and 16 h of culture, while $\text{EXD2}^{-/-}\text{-cl1}$ and $\text{EXD2}^{-/-} + \text{EXD2}^{\text{D108A/E110A-cl1}}$ cells were refractory to this reduction and showed a situation similar to mock-treated cells with a 50–40% reduced fraction size of EU-labeled mRNAs (Fig. 4a and Supplementary Fig. 5a). Similarly, TCR-deficient CS-B cells were refractory to UV-induced reduction of EU-labeled mRNAs, which was restored after CSB^{WT} expression (Supplementary Fig. 5b). In another set of experiments, we performed UV-irradiation long after EU labeling (6 h) so that the labeled mRNAs were synthesized long before the UV treatment (Fig. 4b, upper panel). In these conditions, the reduced fraction size of labeled mRNAs between 1 and 16 h after irradiation was 50–40% for the four cell lines, regardless of whether EXD2 nuclease activity was present or not, a situation that resembles that of the mock treatment (Fig. 4b). These experiments suggest that the EXD2 nuclease degrades, during the recovery

phase, a large fraction of the nascent mRNAs (30%) that were being synthesized at the time of UV irradiation.

EXD2 translocates to nucleus to interact with RNAPII after UV irradiation

After having established the involvement of EXD2, during the recovery phase, in the degradation of mRNA under synthesis at the time of UV irradiation, we studied the potential connection of the nuclease with RNAPII. Since the literature on EXD2 suggests that the protein has a mitochondrial localization that seems incompatible with a potential nuclear role, we first determined the localization of EXD2 in wild-type $\text{EXD2}^{+/+}$ cells in normal conditions and after UV irradiation. Interestingly, whereas the localization of endogenous EXD2 appeared mostly mitochondrial in the absence of genotoxic stress, UV irradiation triggered the re-localization of a large fraction of the endogenous protein from the mitochondria to the nucleus (Fig. 5a, panels a.1–a.10). Similarly, the exogenous flag-tagged EXD2 protein in $\text{EXD2}^{-/-} + \text{EXD2}^{\text{WT-cl1}}$ cells also appeared to partially re-localize to the nucleus after irradiation, although a fraction appeared to localize to the nucleus even in the absence of genotoxic stress (Fig. 5a, panels a.21–a.30). To confirm these observations, we also performed a cell fractionation experiment on $\text{EXD2}^{+/+}$ cells. We observed that while EXD2 was mainly localized in mitochondria in the absence of genotoxic stress (although a small fraction was found in the chromatin), a decrease in the amount of EXD2 in this organelle was observed after UV irradiation, coupled

with an increase in the amount of EXD2 associated with chromatin (Fig. 5b). Next, we analyzed the potential interaction between EXD2 and RNAPII and its timing in EXD2^{-/-} + EXD2^{WT}-cl1 cells. Following UV irradiation (15 J/m²), we observed transient coprecipitation between flag-EXD2 and the RPB1 subunit of RNAPII, which was maximal at 1 h after treatment (Fig. 5c, lanes 9–12) and then begins to decrease at later time points to reach the level of mock-treated cells 24 h after UV irradiation (compare lanes 12–14–16). Note that an interaction between endogenous EXD2 and RNAPII was also observed in HeLa EXD2^{+/+}, 1 h after UV irradiation (Fig. 5d). We next expressed the full-length GST-tagged EXD2^{WT} in bacteria and performed a GST pull-down assay with purified RNAPII from HeLa cells³⁹. GST-EXD2^{WT} pulldown coprecipitated RPB1, suggesting a direct interaction between EXD2 and RNAPII (Fig. 5e). These data highlight a transient direct interaction between EXD2 and RNAPII taking place quickly after UV irradiation and persisting during the recovery phase.

EXD2 interacts with a subset of RNAPII that stalls persistently on DNA

We then asked whether we could reconstitute EXD2 recruitment in vitro on an elongation-blocked RNAPII. We approached this question using a protein/DNA binding assay consisting of a biotinylated DNA template containing the AdMLP promoter and a transcribed region of 309 base pairs. The template was immobilized to streptavidin beads and incubated with purified RNAPII fraction from HeLa cells as well as with the recombinant general transcription factors (GTF: TFIIB, TBP, TFIIE, TFIIIF, TFIIH) to form the pre-initiation complex (PIC). Bacterially purified recombinant EXD2 (rEXD2, without GST) was added at different stages of the assay (Fig. 6a, left panel). Addition of NTP induced transcription initiation, whereas their subsequent chase induced RNAPII elongation arrest⁴⁰ (Fig. 6a, middle panel). While western blot analysis of the remaining DNA-bound proteins revealed a very weak background signal of EXD2 to the DNA template in the absence of RNAPII and its GTF (Fig. 6a, right panel, lane 1), a clear recruitment of EXD2 occurred to the PIC in the absence of NTP (lane 3). In contrast, the presence of EXD2 did not improve the recruitment of RNAPII or GTFs (as observed for TFIIE α) (compare lane 2 and 3). The addition of NTP (lane 4) induced the initiation of transcription and the beginning of the elongation step characterized by the emergence of RNAPII as well as the release of the basal transcription factor TFIIE α from the DNA template (Fig. 6a, middle panel)⁴⁰. Under these conditions of transcription elongation, EXD2 was released from the RNAPII complex (compare lane 3 with lane 5). Interestingly, the chase of NTP, which blocks RNAPII in elongation, caused EXD2 to be recruited again to the DNA template (compare lane 5 with lane 7). In another set of experiments, we determined whether NTP or ATP were required to induce EXD2 release from RNAPII during initiation. The addition of ATP triggered EXD2 release that was clearly enhanced by the presence of the four NTP (Fig. 6b).

To further demonstrate the association of EXD2 with stalled RNAPII in vivo, we used the proximity-ligation assay (PLA). U-2 OS cells stably expressing C-terminally tagged EXD2-GFP, in which EXD2 localized mainly in mitochondria (Supplementary Fig. 6a), were treated with Flavopiridol, which inhibits RNAPII elongation and causes a slight relocation of EXD2-GFP to the nucleus (Supplementary Fig. 6a, b). After Flavopiridol treatment, we detected a nuclear PLA signal indicating EXD2-RNAPII interaction, which was significantly enriched compared to untreated cells and did not occur with GFP alone (Fig. 6c). These data indicate that EXD2 preferentially interacts with an elongation-blocked RNAPII.

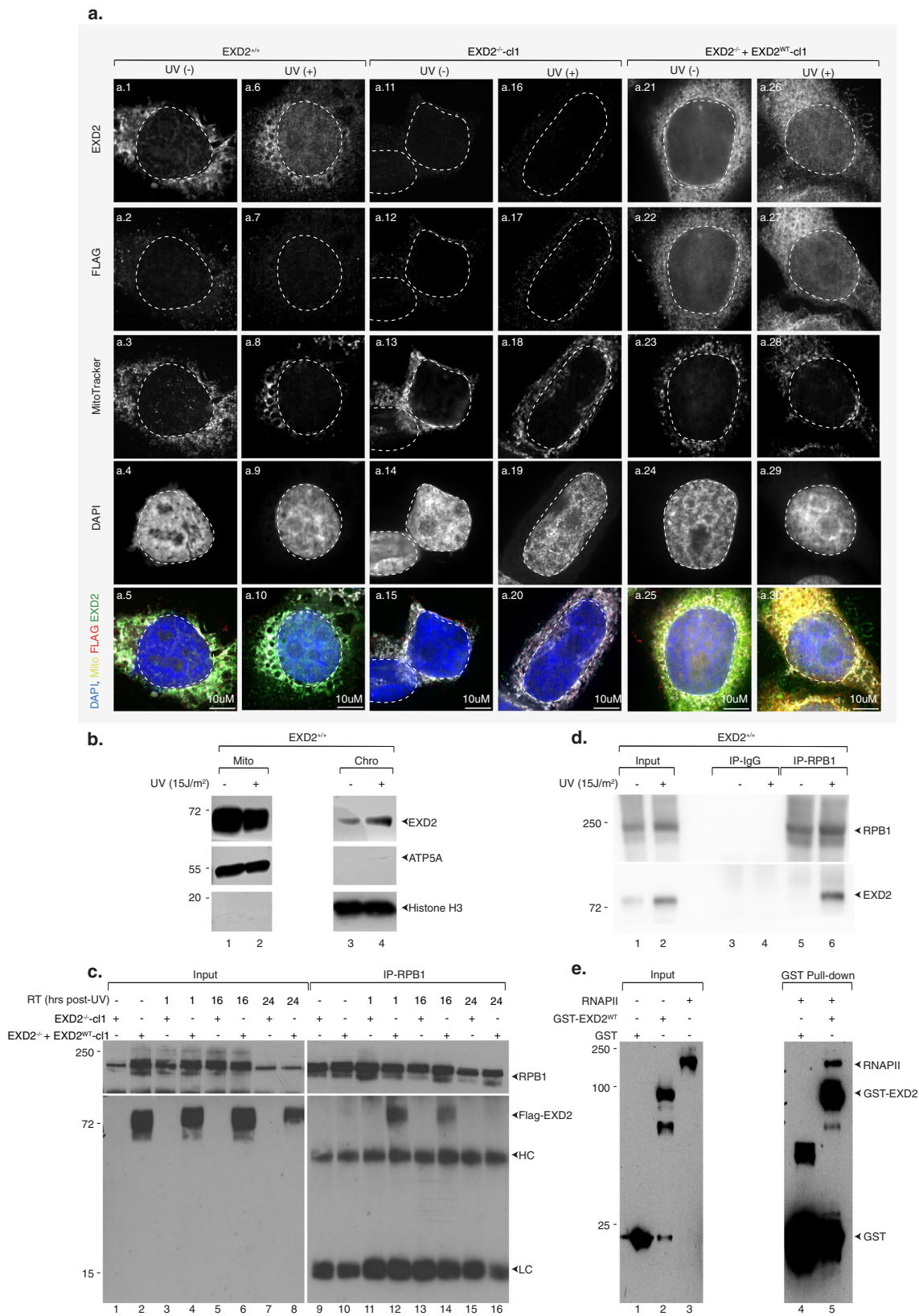
We subsequently examined the impact of the exonuclease activity of EXD2 on newly synthesized mRNA. To detect mRNA, we complemented the above in vitro system with radio-labeled CTP³¹. Note that the purified RNAPII fraction from HeLa cells was devoid of EXD2

(Fig. 6d, left panel). Recombinant human EXD2^{WT} and nuclease-dead EXD2^{D108A/E110A} were purified from insect cells in parallel (Fig. 6d, right panel). Transcription of the AdMLP-containing DNA template led to the production of an mRNA transcript of 309 nucleotides length in 30 min (Fig. 6e, lane 1). The addition of increasing amounts of recombinant purified EXD2^{WT} for the last 10 min of the reaction induced the degradation of the mRNA transcript whereas EXD2^{D108A/E110A} had no impact (compare lanes 3–5 to 6–8). Taken together, these data suggest that a fraction of EXD2 is recruited to chromatin after UV-irradiation to directly interact with elongation-blocked RNAPII and degrade mRNA under synthesis.

Discussion

Transcription is controlled in time and space by complex epigenetic and signaling-mediated regulatory networks at each step of the process. When cells are subjected to genotoxic attack, DNA damage impacts several crucial cellular functions, including transcription. Indeed, if these lesions are bulky and located in the transcribed strand of an active gene, they become a major complication during its transcription because they constitute a strong barrier to RNAPII forward translocation and result in its blockage, generating transcriptional genotoxic stress^{41,42}. Cells cope with this stress firstly by inhibiting global gene expression, then by removing lesions that block RNAPII progression using the TC-NER pathway, and finally by initiating RRS at both promoters and damaged sites. How cells resume transcription after an acute genotoxic attack is crucial because inappropriate restarting is toxic and leads to cellular dysfunction and apoptosis, as observed in cells from patients with CS, which show intermediate sensitivity to UV irradiation coupled with a defect in RRS⁴³. With this in mind, we sought to find new players involved in RNAPII-dependent gene expression recovery after genotoxic attack and unveiled a key role for the 3'–5' exonuclease activity of EXD2 in this process. Recent studies have shown that RNAPII-dependent ribosomal gene transcription is also blocked shortly after a genotoxic stress and recovers over time. A TC-NER machinery removes lesions in ribosomal genes with the participation of CSA and CSB⁴⁴. We tested whether EXD2 was involved in RNAPII-dependent transcription recovery but did not detect a defect in this process in cells lacking EXD2 (Dr. Mari-Giglia, personal information), suggesting a specific involvement of EXD2 in RNAPII-dependent transcription recovery after UV irradiation.

Cells lacking EXD2 nuclease activity exhibited deficient in RRS and intermediate sensitivity to UV irradiation, reminiscent of the phenotype observed in TC-NER deficient cells^{10,42}, including CS-B cells in our study. At first glance, this could indicate that EXD2 is involved in TC-NER and in the removal of DNA lesions that block RNAPII during elongation. However, sensitivity to Et743, which required an active TC-NER pathway³⁷, and the TCR-UDS assay indicate that TC-NER is unaffected by the absence of EXD2, suggesting an uncoupling of efficient TC-NER from deficient RRS in these conditions. Recently, regulation of the RNAPII pool by ubiquitination was shown to be central in the inhibition and restart of transcription in response to genotoxic stress^{18,19}. Persistent depletion of RNAPII was shown to be largely responsible for the lack of transcriptional recovery observed in CS-B cells. Under our conditions, the RNAPII pool was not affected after UV irradiation by the lack of EXD2 nuclease activity, and we ruled out that a direct impact of EXD2 on RNAPII stability was involved in the RRS defect observed in EXD2-deficient cells. Instead, our observations suggest that EXD2 nuclease acts on mRNA, which was observed both in vivo, using pulse-labeling of nascent mRNA, and in vitro, using the transcription/nuclease run-off assay. These assays suggest that the EXD2 nuclease processes, during the recovery phase, a fraction of mRNA representing 30% of the nascent mRNA being synthesized at the time of the genotoxic attack. During RNAPII backtracking, the ability of RNAPII to cleave its transcript potentially allows transcription to resume and cells to survive when the lesions are removed. A plethora



of transcription factors, such as TFIIS, are known to stimulate transcript cleavage⁴⁵. Similarly, it seems reasonable to suggest that the exonuclease activity of EXD2 is involved in the mRNA processing associated with RNAPII backtracking in front of DNA lesion as illustrated by the dynamic interaction we observed between them, which transiently kicks in after the genotoxic attack. Moreover, this activity is

likely limited to a genotoxic attack situation because mRNA transcription was efficiently recovered after cold-shock treatment in cells lacking EXD2. Our observations also suggest that EXD2 is probably not involved in transcription per se, as EU incorporation or reporter expression was hardly affected in mock-treated cells in our assay and cell viability was largely not affected by EXD2 knockdown in the

Fig. 5 | EXD2 transiently interacts with RNAPII after UV irradiation.

a Representative confocal images of HeLa EXD2^{+/+}, EXD2^{-/-} and EXD2^{-/-} + EXD2^{WT}-c11 mock- or UV-irradiated (15 J/m²) and left to recover for an hour. Cells were labeled with anti-EXD2 and anti-FLAG and stained with MitoTracker. Images of the cells were obtained with the same microscopy system and constant acquisition parameters for a given labeling/staining. **b** EXD2^{+/+} cells were mock- or UV-irradiated (15 J/m²) and let to recover for 1 h. Cells were fractionated in mitochondria (Mito) and chromatin (Chro) fractions, which were resolved by SDS-PAGE and immunoblotted against the indicated proteins. Molecular sizes are indicated (kDa). ATP5A is a marker of mitochondria. Histone H3 is a marker of chromatin. Source data are provided as a Source Data file. **c** EXD2^{-/-}-c11 or EXD2^{-/-} + EXD2^{WT}-c11 cells were mock- or UV-irradiated (15 J/m²) and let to recover for the indicated period of time post-UV (RT). RNAPII was immunoprecipitated using anti-RPB1 from total extracts and

protein were resolved by SDS-PAGE and immunoblotted using anti-RPB1 or anti-EXD2 antibodies. HC antibody heavy chain, LC antibody light chain, RT recovery time. Molecular sizes are indicated (kDa). Source data are provided as a Source Data file. **d**. RNAPII was immunoprecipitated from chromatin fractions obtained in panel **b**, using anti-RPB1 in the presence of Benzonase. IP using IgG was performed as controls. Proteins were resolved by SDS-PAGE and immunoblotted using anti-RPB1 or anti-EXD2 antibodies. RT recovery time. Molecular sizes are indicated (kDa). Source data are provided as a Source Data file. **e** Purified RNAPII from HeLa cells³⁹ was incubated with recombinant pulldown GST-EXD2^{WT}. Following washes, fractions were resolved by SDS-PAGE and immunoblotted against the indicated proteins. Controls IP was performed with GST alone (lane 4). Molecular sizes are indicated (kDa). Source data are provided as a Source Data file.

absence of genotoxic stress (our data and ref.²⁵). This is similar to other genes encoding transcript cleavage stimulatory factors, such a TFIS, that becomes essential for cell viability only in the presence of a genotoxic stress⁴⁶, which may reflect a potential redundancy in the function of these factors in the absence of stress. The involvement of EXD2 in the recovery of transcription after a genotoxic attack, as well as its role in the repair of double-strand breaks^{25,26} seems to contradict its mitochondrial location^{47,48} that we confirmed in this work. However, our results may potentially reconcile these observations as they suggest that a genotoxic stress such as UV-irradiation leads to a significant re-location of EXD2 from the mitochondria to the nucleus. The molecular aspects of this relocation, and the generalization of this observation to other genotoxic attacks, are not yet known but it suggests post-translational modifications or new protein interactions allowing EXD2 to travel from the mitochondria to the nucleus.

Because EXD2 is known to be a regulator of homologous recombination in double-strand break repair²⁶ and double-strand breaks can occur following replication stress, we were also concerned that the lack of RRS might be due to replication stress and not directly to UV irradiation-induced DNA damage. However, we observed first that confluent EXD2-deficient cells synchronized in G0-G1 were also unable to recover transcription after UV irradiation and second that RNAPII-EXD2 interaction occurred when RNAPII is blocked in elongation, even in the absence of genotoxic stress. These data argue for a direct role of EXD2 in transcription recovery in relation to its interaction with RNAPII.

RNAPII backtracking in front of a lesion likely occurs over several nucleotides, such that the 3' end of the RNA is no longer aligned with the RNAPII active site, preventing transcription restart. Therefore, the data presented here advocate for a scenario in which EXD2, after its relocation to the nucleus, transiently associates with an RNAPII that is stopped persistently on a gene during elongation by the presence of a transcription-blocking lesion, to potentially assist RNAPII in degrading mRNA from 3' to 5' when backtracking occurs^{41,49}. This activity, alone or in combination with that of RNAPII, could reactivate backtracked RNAPII by providing a new 3' end to the mRNA to realign RNAPII active site with the ongoing mRNA. Why cells would require the 3' to 5' exonuclease activities of RNAPII and EXD2 to process mRNA at a damaged site is unclear, but consistent with this scenario, EXD2 is essential for cell viability after UV irradiation but is not required for NER to occur, demonstrating that UV sensitivity reflects the toxicity of the absence of RRS rather than a defect in DNA damage removal. To better understand the molecular mechanism of EXD2 involvement in RRS, the association of EXD2 with RNAPII was reconstituted in vitro using a transcribed DNA template and highly purified and recombinant transcription factors. Consistent with our hypothesis, we observed that elongation-active RNAPII associated less with EXD2 than elongation-blocked RNAPII on transcribed DNA. It is known that EXD2 discriminates RNA and DNA substrates via metal coordination (Mn²⁺ vs Mg²⁺)³⁴. We show that under the physicochemical conditions allowing in vitro transcription and the presence of Mg²⁺, EXD2

exonuclease activity processes newly synthesized long mRNA molecules (309nts length), reinforcing our model of UV-induced recruitment of EXD2 to stalled RNAPII, followed by degradation of nascent mRNA before transcription resumes. Interestingly, these data are also the only ones to assign a ribonuclease function to EXD2 in the nucleus since previous work implicated it in the degradation of nuclear DNA either during DNA double strand break resection in non-homologous end joining or in the protection of stressed replication forks^{25,26,50}.

Methods

Cell culture

U-2 OS cells were cultured in DMEM (1 g/l Glucose) containing 10% FCS and gentamycin. U-2 OS pTuner 263 cells were cultured in DMEM (1 g/l Glucose) containing 10% Tet-system approved FBS, 1% Penicillin/Streptomycin, 400 µg/ml G418, and 100 µg/ml hygromycin B and 2 µg/ml puromycin. The clones of each cell type (HeLa EXD2^{-/-}-c11 and 2, HeLa EXD2^{-/-} + EXD2^{WT}-c11 and 2 and HeLa EXD2^{-/-} + EXD2^{D108A/E110A}-c11 and 2) were cultured in DMEM (1 g/l Glucose) containing 10% FCS and gentamycin supplemented with 0.25 µg/ml of puromycin for HeLa EXD2^{-/-} + EXD2^{WT}-c11 and 2 and HeLa EXD2^{-/-} + EXD2^{D108A/E110A}-c11 and 2. XP4PA-SV, CS1ANSV, CS1ANSV + CSB, and XPC Hela Silencix were cultured as described^{33,36,51} in Dulbecco/HamF10 medium containing 10% FCS. U-2 OS^{EXD2-GFP} and U-2 OS^{GFP} cells were cultured as described²⁵ in DMEM medium containing 10% FCS.

Quantification of actively transcribing cells

U-2 OS pTuner 263 cells were induced by 1 µg/ml of dox for the indicated time intervals. Cells were fixed and the number of cells harboring an YFP-MS2 spot counted.

CFP-SKL mRNA quantification

Total RNA was purified using TriReagent following the manufacturer's protocol (Molecular Research Center, TRI18) and cDNA was prepared by the SuperScript IV kit (Invitrogen, 18090050). qPCR reactions were carried out using the LightCycler480 (Roche) machine and the LightCycler 480 SYBR Green I Master (Roche, 04887352001).

EU incorporation assay/RRS assay

RNA labeling by EU incorporation was performed with Click-iT RNA Alexa Fluor 488 Imaging Kit (Invitrogen, C10329) following the manufacturer protocol with the following modifications; SEU was used at 0.1 mM and labeling was performed during 1 h (with the exception of the RNA degradation assay in which mRNAs were labeled during 10 min) to obtain a good linear EU signal as a function of the incubation time³¹. Microscopy pictures were taken with Leica DM 4000 B equipped with a CoolSnap FX monochrome camera and EU signal intensity was quantified by ImageJ software.

Immunofluorescence-based DNA lesion quantification

Cells were plated in a 24-well plate. 24 h later, cells were UV-irradiated with UV-C lamp (15 J/m²) and recovered for different recovery time

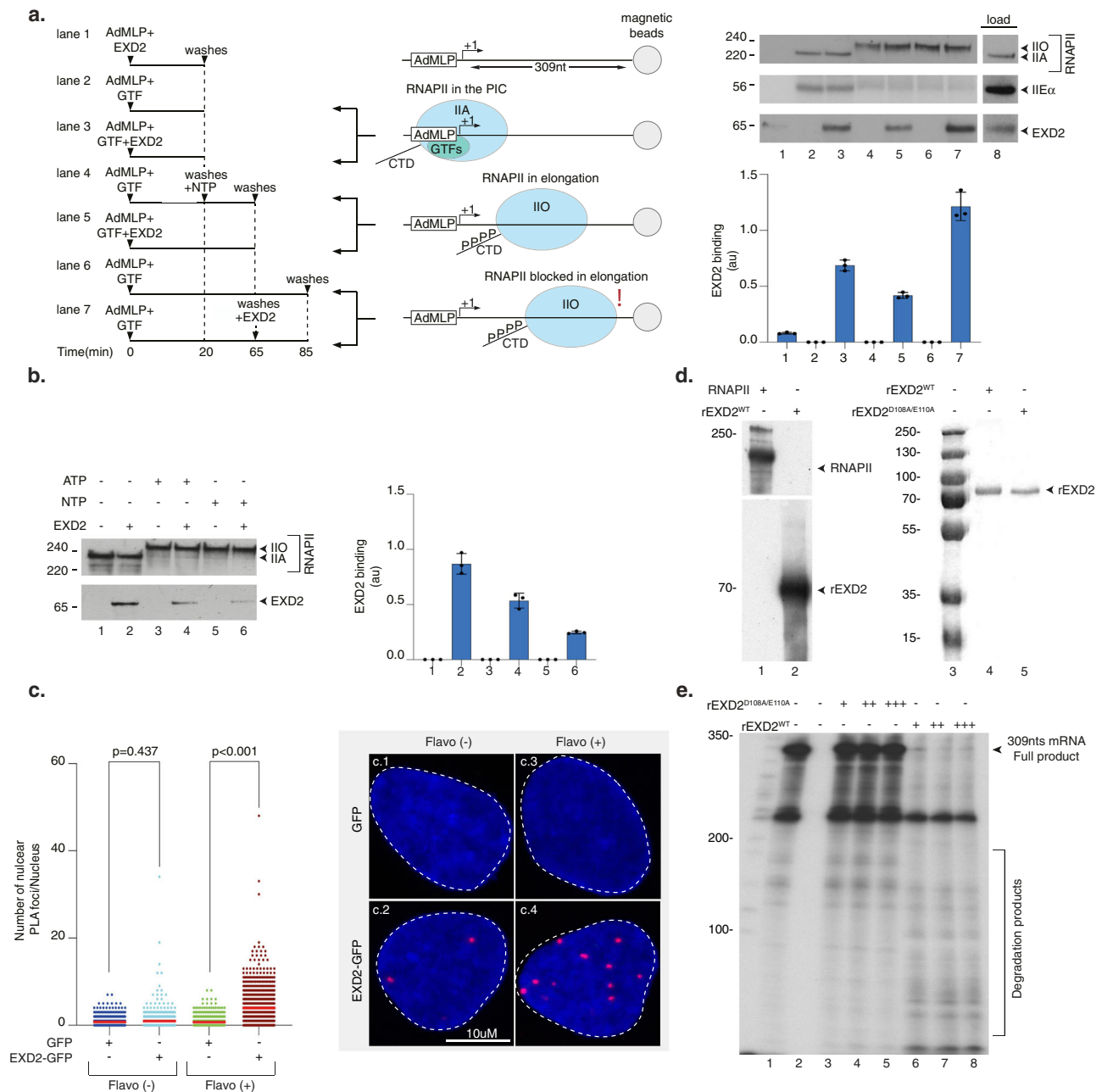


Fig. 6 | EXD2 preferentially interacts with RNAPII stopped in elongation. **a** Left panel; biotinylated DNA template was bound to streptavidin magnetic beads and incubated for 20 min with purified RNAPII and GTFs. After washes, NTPs were added to initiate RNAPII elongation for 45 min. Middle panel; Three conditions were used: in the absence of NTPs where PIC is formed, in the presence of NTPs in which RNAPII is in elongation, and after the chase of NTPs in which RNAPII is blocked from elongating. Right panel; the binding of different factors was evaluated by immunoblotting. The signals for rEXD2 were quantified and plotted in arbitrary units (au). The values are the means of three independent experiments (+/-SD) (Technical triplicates). Molecular sizes are indicated (kDa). Source data are provided as a Source Data file. **b** The biotinylated DNA template was bound to streptavidin magnetic beads and incubated for 20 min with purified RNAPII and GTFs with or without EXD2 as indicated. After washes, ATP or NTPs were added for 45 min. The binding of different factors was evaluated by immunoblotting and the signals for EXD2 were quantified and plotted in arbitrary units (au). The values are the means of three independent experiments (+/-SD) (Technical triplicates).

Molecular sizes are indicated (kDa). Source data are provided as a Source Data file. **c** Number of nuclear GFP/RNAPII PLA foci in U-2 OS cells expressing either GFP or EXD2-GFP with or without Flavopiridol treatment ($n =$ at least 100 cells per conditions from three independent experiments). Red bars indicate mean integrated density. One-way ANOVA with post-hoc Tukey adjustment comparisons were used to determine the p -values. **d** Left panel; rEXD2^{WT} and purified RNAPII were resolved by SDS-PAGE and immunoblotted with anti-EXD2 and anti-RPB1 antibodies. Molecular sizes are indicated (kDa). Right panel; Coomassie staining of recombinant EXD2^{WT} and EXD2^{D108A/E110A}. Lane 3 is the protein markers. Source data are provided as a Source Data file. **e** RNA (309nts) was transcribed from a linear template containing the AdML promoter using a reconstituted RNAPII run-off transcription assay. Then, increasing amount of recombinant EXD2^{WT} or EXD2^{D108A/E110A} (10, 20 and 30 ng) was added to the reaction for an additional 10 min incubation period before the reaction was stopped. Molecular sizes are indicated (Nucleotides). Source data are provided as a Source Data file.

intervals at 37 °C, 5% CO₂. Immuno-labeling of cyclobutane pyrimidine dimers (CPD) and 6–4 photoproducts (6–4PP) was performed using mouse anti-CPD and anti-6–4PP antibodies. DNA was denatured with 2 M HCl for 20 min at RT and blocked in 10% FCS in PBS for 30 min prior to labeling. Microscopy pictures were taken with Leica DM 4000 B equipped with a CoolSnap FX monochrome camera and EU signal intensity was quantified by ImageJ software to determine the percentage of CPD and 6–4PP removal (100% represents the % of lesions measured just after UV irradiation).

Immunofluorescence

Twenty-four hours after plating, cells were irradiated with UV-C lamps (15 J/m²) and recovered for 1 h at 37 °C, 5% CO₂. Thirty minutes before fixation, cells were treated with MitoTracker Red CMXRos according to the manufacturer's instructions. After permeabilization (0.02% Triton X-100 for 10 min) and blocking (4% bovine serum albumin, 20 min), cells were immuno-labeled to visualize either endogenous or tag-FLAG EXD2 using rabbit anti-EXD2 (HPA005848, 1/2000) and mouse anti-FLAG M2 antibodies. Slides were mounted with Vectashield containing DAPI. Microscopy pictures were taken with Leica Spinning Disk CSU-W1 and processed with ImageJ software.

Proximity-ligation assay

U-2 OS cells stably expressing GFP or EXD2-GFP were treated with Flavopiridol (1 μM for 1 h) before permeabilization in 0.5% Triton in PBS for 10 min at 4 °C followed by two washes with PBS, fixation with 3% formaldehyde, 2% sucrose in PBS for 10 min at room temperature and two washes with PBS. Blocking, primary antibody incubation and the PLA assay were then carried out as described²⁵. Antibodies employed for the PLA assay were as follows: GFP (Roche, 11814460001, 1:500) and RNAPII (Bethyl, A300-653A, 1:1000). Images were acquired with Zeiss Axio Observer Z1 Marianas™ Microscope attached with a CSU-W spinning disk unit (built by Intelligent Imaging Innovations (3i)) using a 63x objective. Image analysis was carried out with Fiji (ImageJ) and CellProfiler (Broad Institute) software.

Transfections

Plasmid transfections were conducted using X-tremeGene DNA Transfection Reagent (Roche) according to the manufacturer's protocols. siRNA transfections were conducted using Lipofectamine RNAiMAX Transfection Reagent (Invitrogen) according to the manufacturer's protocols.

TCR-Unscheduled DNA synthesis (TCR-UDS)

GG-NER-deficient XP4PA-SV cells (XP-C) were grown on 18 mm coverslips. siRNA transfections were performed 24 h and 48 h before TCR-UDS assays. After local irradiation at 50 J/m² with UV-C through a 5 μm pore polycarbonate membrane filter, cells were incubated for 8 h with 5-ethynyl-2'-deoxyuridine (EdU), fixed and permeabilized with PBS and 0.5% triton X-100. Then, cells were blocked with PBS + solution (PBS containing 0.15% glycine and 0.5% bovine serum albumin) for 30 min and subsequently incubated for 1 h with mouse monoclonal anti-yH2AX antibody 1:500 diluted in PBS. After extensive washes with PBS containing 0.5% Triton X100, cells were incubated for 45 min with secondary antibodies conjugated with Alexa Fluor 594 fluorescent dyes (Molecular Probes, 1:400 dilution in PBS). Next, cells were washed several times and then incubated for 30 min with the Click-iT reaction cocktail containing Alexa Fluor Azide 488. After washing, the coverslips were mounted with Vectashield containing DAPI (Vector). Images of the cells were obtained with the same microscopy system and constant acquisition parameters. Images were analyzed as follows using ImageJ and a circle of constant size for all images: (i) the background signal was estimated in the nucleus (avoiding the damage, nucleoli and other non-specific signal) and subtracted, (ii) the locally damaged area was defined by using the yH2AX staining, (iii) the mean

fluorescence correlated to the EdU incorporation was then measured and thus an estimate of DNA synthesis after the repair was obtained. For each sample, three independent experiments were performed.

Cell sub-fractionation and IP

Cell fractionation was performed by using the Qproteome Mitochondria Isolation Kit (Qiagen) with some modifications. 2 × 10⁷ HeLa cells were collected 1-h post UV irradiation (20 J/m²) and resuspended in cold lysis buffer. Following centrifugation (1000 × g, 4 °C), the supernatant was removed and the pellet was resuspended in cold disruption buffer using dounce homogenizer. After centrifugation (1000 × g, 4 °C), while the supernatant was treated according to the manufacturer's instruction to collect mitochondrial fraction, the pellet has been washed three times with PBS and resuspended in sucrose buffer (20 mM Tris pH 7.6, 15 mM KCl, 60 mM NaCl, 0.34 M sucrose). Under vortex agitation, high salt buffer (20 mM Tris pH 7.6, 25% glycerol, 1.5 mM MgCl₂, 0.1 mM EDTA, 300 mM NaCl final concentration) was added (30 min at 4 °C). Following centrifugation (2500 × g, 4 °C), the supernatant was removed and the pellet (containing the chromatin fraction) was resuspended in sucrose buffer supplemented with 1 mM CaCl₂. Digestion with Micrococcal Nuclease (25 u, Biolabs) was next performed 5 min at 37 °C and stopped by adding 4 mM EDTA. Sonication was carried out with a Q800R2 sonicator (Qsonica, 3 s on/2 s off during 3 min). The chromatin fraction was collected after centrifugation (16,000 × g, 30 min at 4 °C). Bradford protein assays were used to measure the final concentration of the mitochondrial and chromatin fraction. IP experiments were performed with the chromatin fraction using anti-RPB1 monoclonal antibody in the presence or not of Benzonase.

Protein-DNA binding assay

Biotinylated AdMLP DNA template bound to streptavidin magnetic beads was incubated 20 min at 25 °C with purified RNAPII, TFIIA, IIB, IIF, TBP, IIH and EXD2 in transcription buffer (20 mM HEPES (pH 7.9), 7 mM MgCl₂, 55 mM KCl). After three washings at 50 mM NaCl, bound fractions were resolved by SDS-PAGE for immunoblottings and others were incubated 45 min at 25 °C with NTP (200 μM). After washings, these fractions were in turn resolved by SDS-PAGE or were further incubated 20 min with EXD2. The abundance of EXD2 was assessed by immunoblot densitometry analysis (using ImageJ software). Each signal was quantified three times and plotted in arbitrary units (au).

Reconstituted run-off transcription

Reaction mixtures of 12 μL containing 50 ng of linear AdMLP DNA template and recombinant TFIIH, TFIIIB, TFIIIE, TFIIIF, TBP together with purified RNA pol II as described⁵² were pre-incubated for 20 min at 25 °C in transcription buffer (20 mM HEPES (pH 7.9), 7 mM MgCl₂, 55 mM KCl) and transcription was initiated by the addition of 2 μL nucleotide solution to final concentrations of 600 μM UTP, ATP, GTP and 0.6 μM (α-³²P) CTP. Reactions were carried out for 30 min and recombinant EXD2 was added for another 10 min. Reaction was stopped by the addition of 0.5 μL of 0.5 M EDTA (pH 8). The resulting RNA transcripts were analyzed on an 8% denaturing polyacrylamide gel.

Statistics and reproducibility

Experimental data were plotted and analyzed using GraphPad Prism (GraphPad Software Inc.). The number of samples and replicates are indicated in the respective figure legends. Each experiment was repeated a least three times with similar results.

Extended resource table

An extended resource table with antibodies, oligonucleotide sequences, chemicals, and reagents used in this work is provided in Supplementary Table 1.

Reporting summary

Further information on research design is available in the Nature Portfolio Reporting Summary linked to this article.

Data availability

All data generated or analyzed during this study are included in this published article (and its supplementary information files) and are available from the corresponding author on request. An extended resource table with antibodies, oligonucleotide sequences, chemicals and reagents used in this work is provided in Supplemental Table 1. Source data are provided with this paper.

References

- Hoeijmakers, J. H. J. DNA damage, aging, and cancer. *N. Engl. J. Med.* **361**, 1475–1485 (2009).
- Vermeij, W. P., Hoeijmakers, J. H. & Pothof, J. Aging: not all DNA damage is equal. *Curr. Opin. Genet. Dev.* **26**, 124–130 (2014).
- Kotsantis, P., Petermann, E. & Boulton, S. J. Mechanisms of oncogene-induced replication stress: Jigsaw falling into place. *Cancer Discov.* **8**, 537–555 (2018).
- Lee, T. I. & Young, R. A. Transcriptional regulation and its misregulation in disease. *Cell* **152**, 1237–1251 (2013).
- Jackson, S. P. & Bartek, J. The DNA-damage response in human biology and disease. *Nature* **461**, 1071–1078 (2009).
- Edifizi, D. & Schumacher, B. Genome instability in development and aging: insights from nucleotide excision repair in humans, mice, and worms. *Biomolecules* **5**, 1855–1869 (2015).
- Sancar, A. & Reardon, J. T. Nucleotide excision repair in *E. Coli* and man. *Adv. Protein Chem.* **69**, 43–71 (2004).
- Marteijn, J. A., Lans, H., Vermeulen, W. & Hoeijmakers, J. H. Understanding nucleotide excision repair and its roles in cancer and ageing. *Nat. Rev. Mol. Cell Biol.* **15**, 465–481 (2014).
- Scharer, O. D. Nucleotide excision repair in eukaryotes. *Cold Spring Harb. Perspect. Biol.* **5**, a012609 (2013).
- van den Heuvel, D., van der Weegen, Y., Boer, D. E. C., Ogi, T. & Luijsterburg, M. S. Transcription-coupled DNA repair: from mechanism to human disorder. *Trends Cell Biol.* **31**, 359–371 (2021).
- Ljungman, M. & Lane, D. P. Transcription—guarding the genome by sensing DNA damage. *Nat. Rev. Cancer* **4**, 727–737 (2004).
- Hanawalt, P. C. & Spivak, G. Transcription-coupled DNA repair: two decades of progress and surprises. *Nat. Rev. Mol. Cell Biol.* **9**, 958–970 (2008).
- Foster, M. & Mullenders, L. H. Transcription-coupled nucleotide excision repair in mammalian cells: molecular mechanisms and biological effects. *Cell Res.* **18**, 73–84 (2008).
- Lans, H., Hoeijmakers, J. H. J., Vermeulen, W. & Marteijn, J. A. The DNA damage response to transcription stress. *Nat. Rev. Mol. Cell Biol.* **20**, 766–784 (2019).
- Lavigne, M. D., Konstantopoulos, D., Ntakou-Zamplara, K. Z., Liakos, A. & Foster, M. Global unleashing of transcription elongation waves in response to genotoxic stress restricts somatic mutation rate. *Nat. Commun.* **8**, 2076 (2017).
- Gyenis, Á. et al. UVB induces a genome-wide acting negative regulatory mechanism that operates at the level of transcription initiation in human cells. *PLoS Genet.* **10**, e1004483 (2014).
- Rockx, D. A. et al. UV-induced inhibition of transcription involves repression of transcription initiation and phosphorylation of RNA polymerase II. *Proc. Natl Acad. Sci. USA* **97**, 10503–10508 (2000).
- Tufegdžić Vidaković, A. et al. Regulation of the RNAPII pool is integral to the DNA damage response. *Cell* **180**, 1245–1261.e21 (2020).
- Nakazawa, Y. et al. Ubiquitination of DNA damage-stalled RNAPII promotes transcription-coupled repair. *Cell* **180**, 1228–1244.e24 (2020).
- Oksenyshyn, V. et al. Histone methyltransferase DOT1L drives recovery of gene expression after a genotoxic attack. *PLoS Genet.* **9**, e1003611 (2013).
- Mourgues, S. et al. ELL, a novel TFIIH partner, is involved in transcription restart after DNA repair. *Proc. Natl Acad. Sci. USA* **110**, 17927–17932 (2013).
- Adam, S., Polo, S. E. & Almouzni, G. Transcription recovery after DNA damage requires chromatin priming by the H3.3 histone chaperone HIRA. *Cell* **155**, 94–106 (2013).
- Dinant, C. et al. Enhanced chromatin dynamics by FACT promotes transcriptional restart after UV-induced DNA damage. *Mol. Cell* **51**, 469–479 (2013).
- Geijer, M. E. et al. Elongation factor ELOF1 drives transcription-coupled repair and prevents genome instability. *Nat. Cell Biol.* **23**, 608–619 (2021).
- Nieminszczy, J. et al. EXD2 protects stressed replication forks and is required for cell viability in the absence of BRCA1/2. *Mol. Cell* **75**, 605–619.e6 (2019).
- Broderick, R. et al. EXD2 promotes homologous recombination by facilitating DNA end resection. *Nat. Cell Biol.* **18**, 271–280 (2016).
- Janicki, S. M. et al. From silencing to gene expression: real-time analysis in single cells. *Cell* **116**, 683–698 (2004).
- Shanbhag, N. M., Rafalska-Metcalf, I. U., Balane-Bolivar, C., Janicki, S. M. & Greenberg, R. A. ATM-dependent chromatin changes silence transcription in cis to DNA double-strand breaks. *Cell* **141**, 970–981 (2010).
- Mayne, L. V. & Lehmann, A. R. Failure of RNA synthesis to recover after UV radiation: an early defect in cells from individuals with Cockayne's syndrome and xeroderma pigmentosum. *Cancer Res.* **42**, 1473–1478 (1982).
- Williamson, L. et al. UV irradiation induces a non-coding RNA that functionally opposes the protein encoded by the same gene. *Cell* **168**, 843–855.e13 (2017).
- Alekseev, S. et al. Transcription without XPB establishes a unified helicase-independent mechanism of promoter opening in eukaryotic gene expression. *Mol. Cell* **65**, 504–514.e4 (2017).
- van Hoffen, A., Venema, J., Meschini, R., van Zeeland, A. A. & Mullenders, L. H. Transcription-coupled repair removes both cyclobutane pyrimidine dimers and 6-4 photoproducts with equal efficiency and in a sequential way from transcribed DNA in xeroderma pigmentosum group C fibroblasts. *Embo J.* **14**, 360–367 (1995).
- Kristensen, U. et al. Regulatory interplay of Cockayne syndrome B ATPase and stress-response gene ATF3 following genotoxic stress. *Proc. Natl Acad. Sci. U.S.A.* **110**, E2261–E2270 (2013).
- Park, J. et al. The structure of human EXD2 reveals a chimeric 3' to 5' exonuclease domain that discriminates substrates via metal coordination. *Nucleic Acids Res.* **47**, 7078–7093 (2019).
- Biard, D. S. F., Despras, E., Sarasin, A. & Angulo, J. F. Development of new EBV-based vectors for stable expression of small interfering RNA to mimic human syndromes: application to NER gene silencing. *Mol. Cancer Res.* **3**, 519–529 (2005).
- Donnio, L.-M., Lagarou, A., Sueur, G., Mari, P.-O. & Giglia-Mari, G. CSB-dependent cyclin-dependent kinase 9 degradation and RNA polymerase II phosphorylation during transcription-coupled repair. *Mol. Cell Biol.* **39**, e00225-18 (2019).
- Takebayashi, Y. et al. Antiproliferative activity of ecteinascidin 743 is dependent upon transcription-coupled nucleotide-excision repair. *Nat. Med.* **7**, 961–966 (2001).
- Oh, K.-S., Bustin, M., Mazur, S. J., Appella, E. & Kraemer, K. H. UV-induced histone H2AX phosphorylation and DNA damage related proteins accumulate and persist in nucleotide excision repair-deficient XP-B cells. *DNA Repair* **10**, 5–15 (2011).

39. Gerard, M. et al. Purification and interaction properties of the human RNA polymerase B(II) general transcription factor BTF2. *J. Biol. Chem.* **266**, 20940–20945 (1991).
40. Compe, E., Genes, C. M., Braun, C., Coin, F. & Egly, J. M. TFIIIE orchestrates the recruitment of the TFIIH kinase module at promoter before release during transcription. *Nat. Commun.* **10**, 2084 (2019).
41. Noe Gonzalez, M., Blears, D. & Svejstrup, J. Q. Causes and consequences of RNA polymerase II stalling during transcript elongation. *Nat. Rev. Mol. Cell Biol.* **22**, 3–21 (2021).
42. Jia, N. et al. Dealing with transcription-blocking DNA damage: repair mechanisms, RNA polymerase II processing and human disorders. *DNA Repair* **106**, 103192 (2021).
43. Gregersen, L. H. & Svejstrup, J. Q. The cellular response to transcription-blocking DNA damage. *Trends Biochem. Sci.* **43**, 327–341 (2018).
44. Daniel, L. et al. Mechanistic insights in transcription-coupled nucleotide excision repair of ribosomal DNA. *Proc. Natl Acad. Sci. USA* **115**, E6770–E6779 (2018).
45. Sigurdsson, S., Dirac-Svejstrup, A. B. & Svejstrup, J. Q. Evidence that transcript cleavage is essential for RNA polymerase II transcription and cell viability. *Mol. Cell* **38**, 202–210 (2010).
46. Jensen, A. & Mullenders, L. H. F. Transcription factor IIS impacts UV-inhibited transcription. *DNA Repair* **9**, 1142–1150 (2010).
47. Hensen, F., Moretton, A., van Esvelde, S., Farge, G. & Spelbrink, J. N. The mitochondrial outer-membrane location of the EXD2 exonuclease contradicts its direct role in nuclear DNA repair. *Sci. Rep.* **8**, 5368 (2018).
48. Silva, J. et al. EXD2 governs germ stem cell homeostasis and lifespan by promoting mitoribosome integrity and translation. *Nat. Cell Biol.* **20**, 162–174 (2018).
49. Geijer, M. E. & Marteijn, J. A. What happens at the lesion does not stay at the lesion: Transcription-coupled nucleotide excision repair and the effects of DNA damage on transcription in cis and trans. *DNA Repair* **71**, 56–68 (2018).
50. Biehs, R. et al. DNA double-strand break resection occurs during non-homologous end joining in G1 but is distinct from resection during homologous recombination. *Mol. Cell* **65**, 671–684.e5 (2017).
51. Le May, N. et al. NER factors are recruited to active promoters and facilitate chromatin modification for transcription in the absence of exogenous genotoxic attack. *Mol. Cell* **38**, 54–66 (2010).
52. Coin, F. et al. p8/TTD-A as a repair-specific TFIIH subunit. *Mol. Cell* **21**, 215–226 (2006).

Acknowledgements

We thank Dr. Patrick Reilly for the critical reading of the article and Dr. Roger Greenberg (University of Pennsylvania) for the U-2 OS-pTuner263 cells and Karolina Chabowska (ICR London) for recombinant EXD2^{WT} and EXD2^{D108A/E110A} proteins expressed in and purified from insect cells. We thank Amélie Freismuth and the cell culture service of IGBMC. This study was supported by ANR (TFIIH-2021), by the Ligue contre le cancer (Equipe Labélisée 2022-2024) and the grant ANR-10-LABX-0030-INRT, a French State fund managed by the Agence Nationale de la Recherche

under the frame program Investissements d’Avenir ANR-10-IDEX-0002-02. M.C. is supported by the “Ligue contre le Cancer”. C.E. by the “Région Réunion”. LMD is supported by Agence Nationale de la Recherche (ANR-14-CE10-0009) and Institut National du Cancer (PLBIO17-043 and PLBIO19-126). Work in WN’s laboratory is funded by Cancer Research UK Programme (A24881).

Author contributions

J.S. (EU, WB, mRNA degradation), M.C. (EU, mRNA degradation), A.Z., (Confocal microscopy), P.C. (IP, Fractionation assay), L.-M.D. (TCR-UDS), P.B. (WB), C.E. (CFP-SKL reporter assay), J.N. (PLA assay), C.B. (In vitro binding assay) and S.A. (CFP-SKL assay) conducted the experiments. J.S., W.N., J.M.-E., G.G.-M., E.C., and F.C. analyzed the results and/or provided valuable material. F.C. designed the experiments and wrote the paper.

Competing interests

The authors declare no competing interests.

Additional information

Supplementary information The online version contains supplementary material available at <https://doi.org/10.1038/s41467-023-35922-5>.

Correspondence and requests for materials should be addressed to Frédéric Coin.

Peer review information *Nature Communications* thanks Björn Schumacher and the other, anonymous, reviewer(s) for their contribution to the peer review of this work.

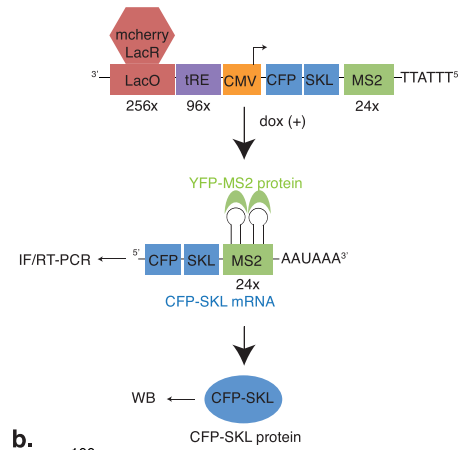
Reprints and permissions information is available at <http://www.nature.com/reprints>

Publisher’s note Springer Nature remains neutral with regard to jurisdictional claims in published maps and institutional affiliations.

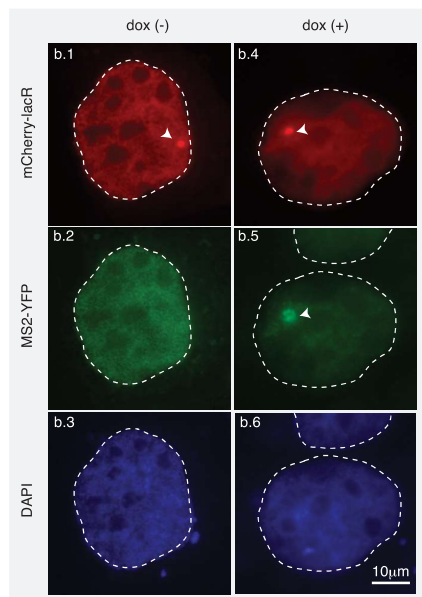
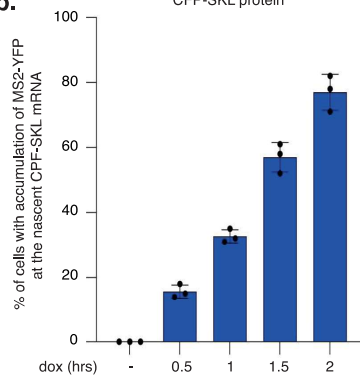
Open Access This article is licensed under a Creative Commons Attribution 4.0 International License, which permits use, sharing, adaptation, distribution and reproduction in any medium or format, as long as you give appropriate credit to the original author(s) and the source, provide a link to the Creative Commons license, and indicate if changes were made. The images or other third party material in this article are included in the article’s Creative Commons license, unless indicated otherwise in a credit line to the material. If material is not included in the article’s Creative Commons license and your intended use is not permitted by statutory regulation or exceeds the permitted use, you will need to obtain permission directly from the copyright holder. To view a copy of this license, visit <http://creativecommons.org/licenses/by/4.0/>.

© The Author(s) 2023

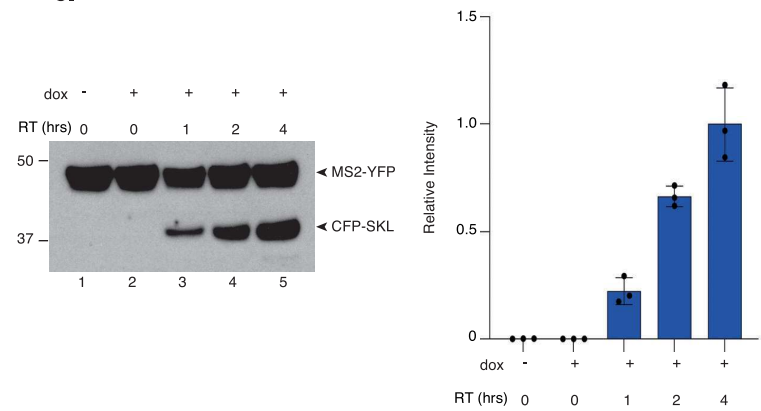
a.



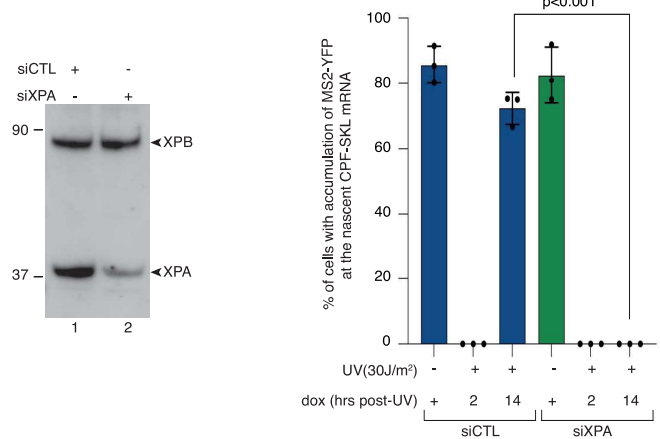
b.



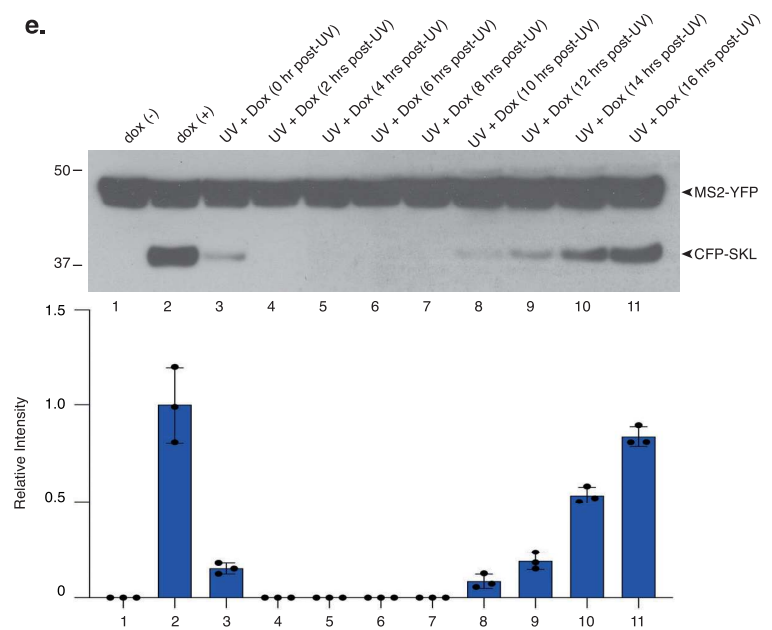
c.



d.



e.



Supplementary Figure 1: The CFP-SKL reporter assay

a. 256 copies of lacO array provide examination of the reporter through a mCherry protein fused to lacR. Tetracycline response elements (TREs) control expression of the unique *CFP-SKL* mRNA transcript upon dox treatment. *CFP-SKL* transcription is detected through the binding of YFP-MS2 and encoded CFP-SKL protein that can be detected by WB.

b. U-2 OS were treated with dox as indicated and *CFP-SKL* mRNA expression was quantified. Results are expressed as % of cells showing YFP-MS2 accumulation at a single locus (n= 3x20 cells, biological triplicates). Bars represent mean values of three different experiments (Biological triplicates) (+/- SD). Representative confocal images of MS2-YFP accumulation at *CFP-SKL* is shown. The reporter locus is detected with a mCherry-LacR fusion construct.

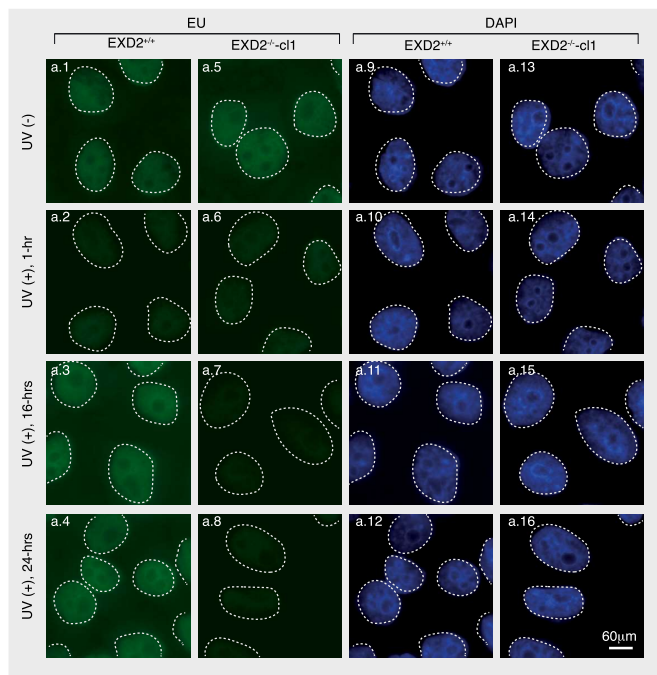
c. Immuno-blot for CFP-SKL and YFP-MS2 in U-2 OS cells treated with dox and subsequently let to recover in dox-free medium. Extracts were immuno-blotted with anti-GFP. CFP-SKL signals were normalized with YFP-MS2 signals (+/-SEM). Three independent immunoblots were performed (technical triplicates). Source data are provided as a Source Data file.

d. U-2 OS cells were transfected with siCTL or siXPA for 24 hours and with a construct expressing mCherry-lacR for 24 hours before UV irradiation (30J/m²) and subsequent 2-hour pulse-incubation with dox. **Left panel;** cell extracts were immunoblotted against XPB and XPA. **Right panel;** Newly transcribed *CFP-SKL* were detected at the reporter locus. Quantification of the transcribing locus was done and results are expressed as % of cells showing YFP-MS2 accumulation at a single locus (n= 3x20 cells, biological triplicates). Bars represent mean values of three different experiments (Biological triplicates) (+/- SD). One-way ANOVA with post-hoc Tukey adjustment comparisons were used to determine the p-values. Source data are provided as a Source Data file.

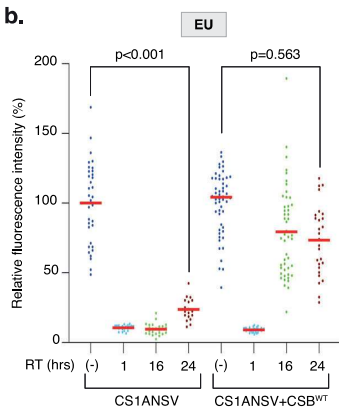
e. U-2 OS cells were UV-irradiated (30 J/m²) and pulse-incubated for 2 hours with dox. Cells were allowed to recover for 4 hours in the absence of dox. Extracts were immuno-blotted with anti-GFP antibody. Lane 1; cells were not treated with dox. Lane 2; cells were treated with dox for 2 hours before to recover 4 hours in the absence of dox. CFP-SKL signals were normalized

with YFP-MS2 signals (\pm SEM). Three independent immunoblots were performed (technical triplicates). Source data are provided as a Source Data file.

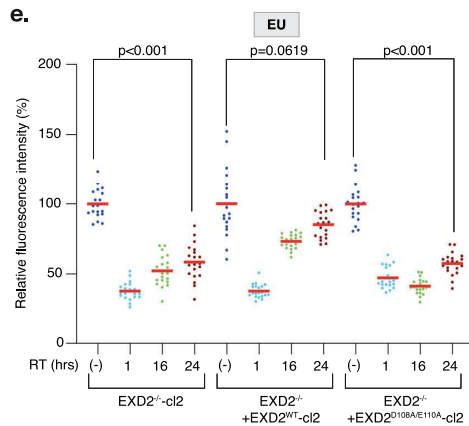
a.



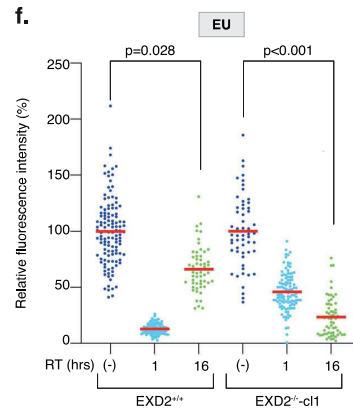
b.



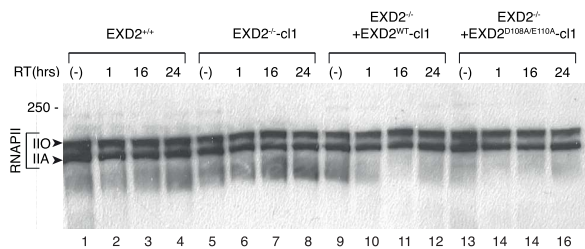
e.



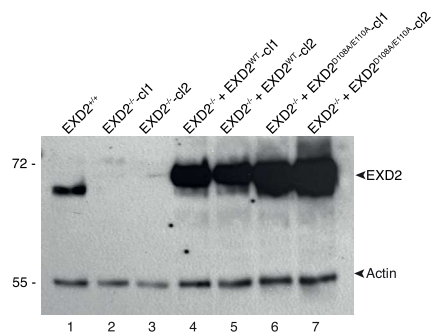
f.



c.



d.



Supplementary Figure 2: Lack of EXD2 induces inhibition of RRS

a. Representative confocal images of EXD2^{+/+} and EXD2^{-/-}-cl1. Cells were mock or UV-irradiated (15J/m²) and mRNA was labelled with EU 1, 16 and 24 hours after UV-irradiation. Images of the cells were obtained with the same microscopy system and constant acquisition parameters.

b. CS1ANSV and CS1ANSV+CSB^{WT} were UV-irradiated (15J/m²) and mRNA was labelled with EU at 1, 16 and 24 hours after UV-irradiation. EU signal was quantified by ImageJ and relative integrated density normalized to mock-treated level set to 100% are reported on the graph (n=at least 20 cells per condition). Red bars indicate mean integrated density. One-way ANOVA with post-hoc Tukey adjustment comparisons were used to determine the p-values. Source data are provided as a Source Data file.

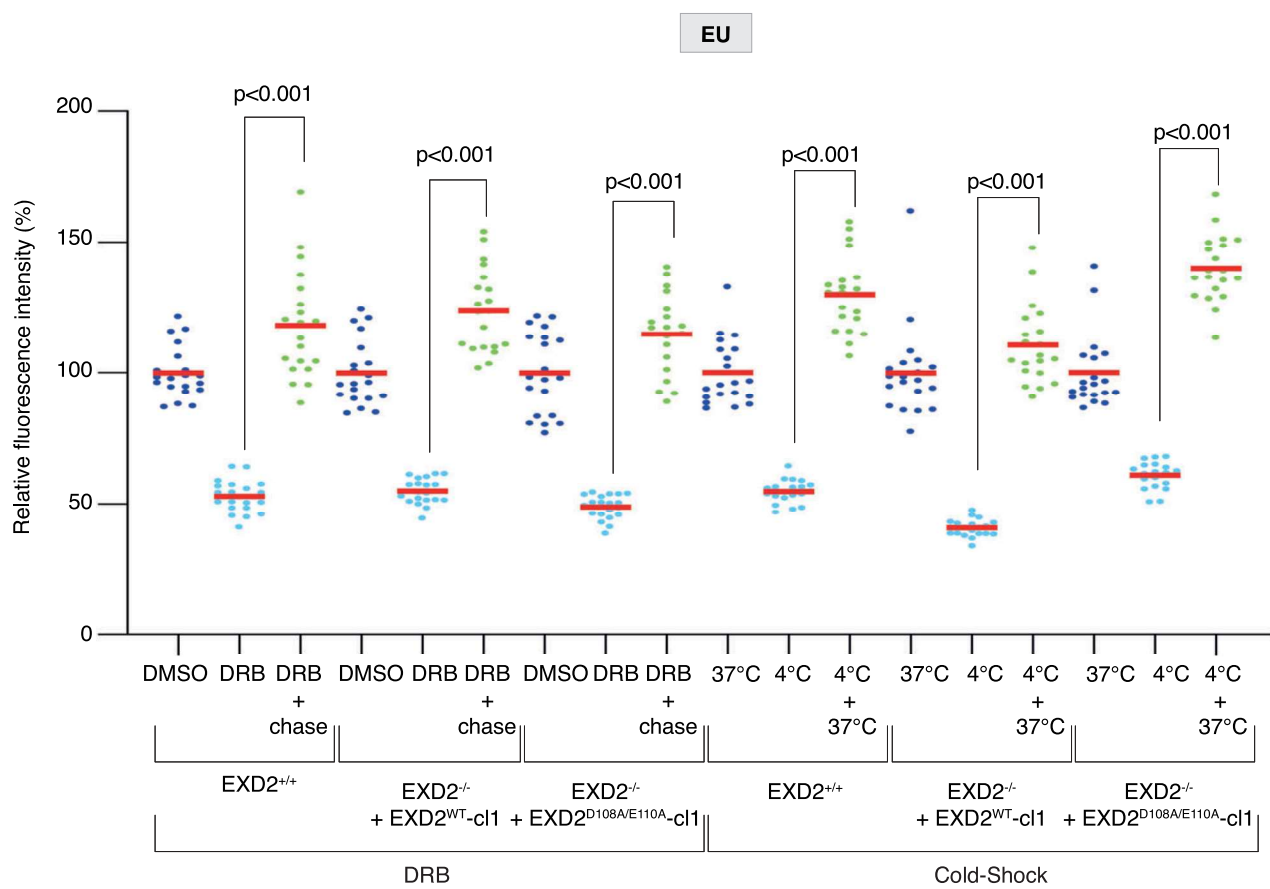
c. HeLa were mock or UV-irradiated (15J/m²) and let to recover for the indicated times before lysis. Protein lysates were immuno-blotted for RPB1 subunit of RNAPII. Molecular mass of the proteins is indicated on the left (kDa). RT; recovery time. IIO, phosphorylated form of RPB1. IIA non-phosphorylated form. Source data are provided as a Source Data file.

d. Protein lysates were immuno-blotted for proteins as indicated. Molecular mass of the proteins is indicated (kDa). Source data are provided as a Source Data file.

e. HeLa cells were mock or UV-irradiated (15J/m²) and mRNA was labelled with EU 1, 16 and 24 hours after UV-irradiation. EU signal was quantified by ImageJ and relative integrated density normalized to mock-treated level set to 100% are reported on the graph (n=at least 20 cells per condition). Red bars indicate mean integrated density. One-way ANOVA with post-hoc Tukey adjustment comparisons were used to determine the p-values. Source data are provided as a Source Data file.

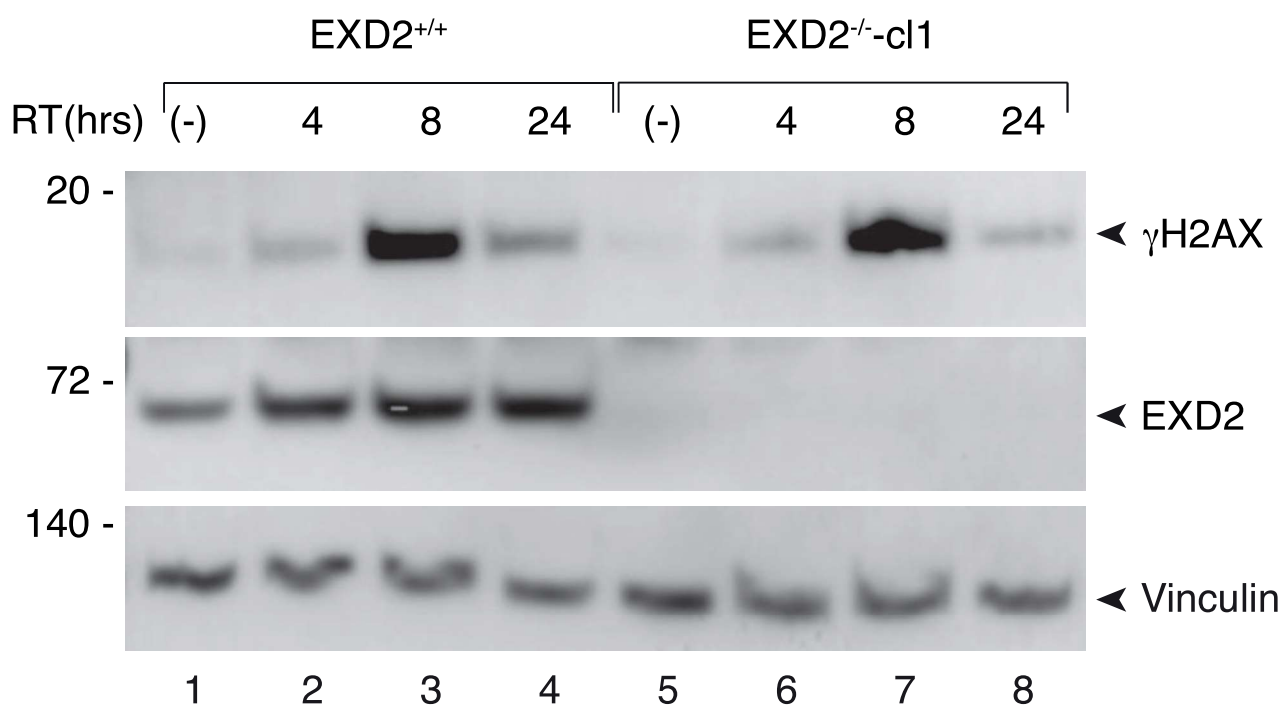
f. EXD2^{+/+} and EXD2^{-/-}-cl 1 cells were grown to 80% confluence and further incubated 24 hours in medium containing 0.5% FCS. Cells were mock or UV-irradiated (15J/m²) and mRNA was labelled with EU at 1 and 16 hours after UV-irradiation. EU signal was quantified by ImageJ and relative integrated density normalized to mock-treated level set to 100% are reported on the graph (n= at least 50 cells per condition). Red bars indicate mean integrated density. One-

way ANOVA with post-hoc Tukey adjustment comparisons were used to determine the p-values. Source data are provided as a Source Data file.



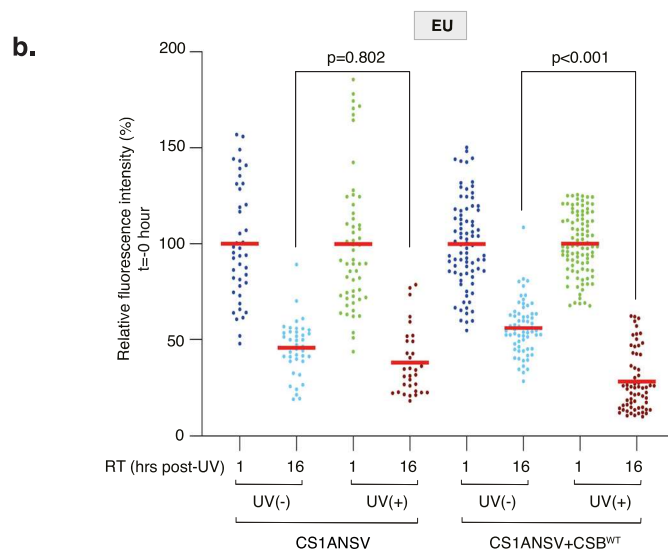
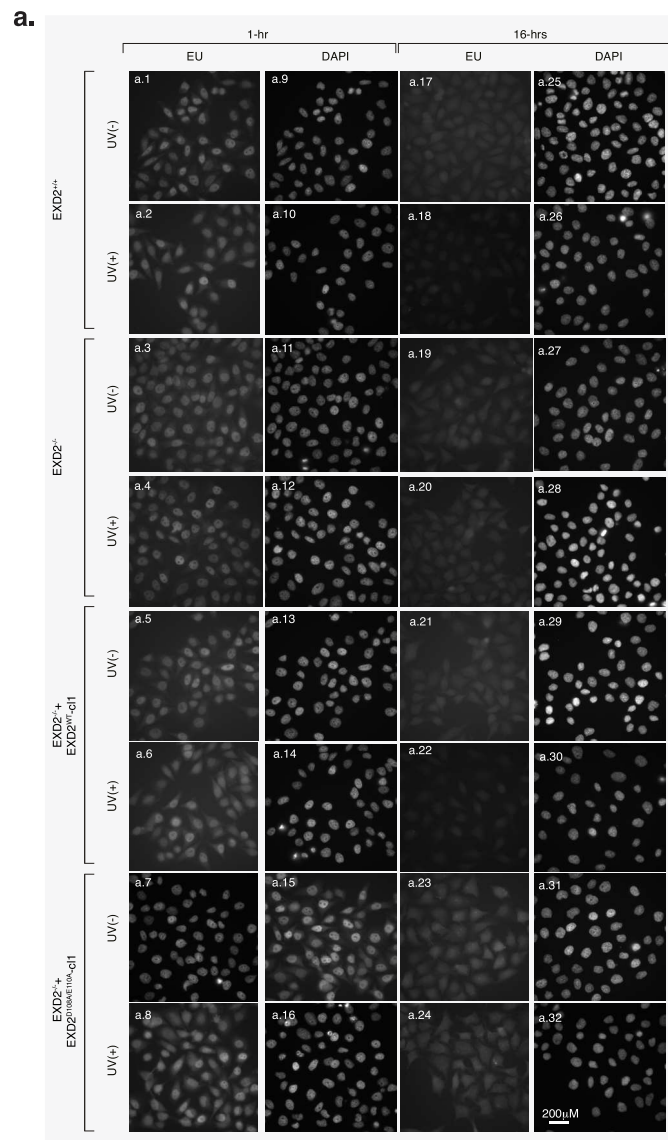
Supplementary Figure 3: EXD2 is not involved in RRS after DRB or cold-shock treatment

DRB: EXD2^{+/+}, EXD2^{-/-} + EXD2^{WT}-cl1 and EXD2^{-/-} + EXD2^{D108A/E110A}-cl1 were treated with DRB (100 μ M) for 1 hour before chase and cells were let to recover for 30 minutes. mRNA was labelled with EU before (DMSO), during (DRB) or after the chase (DRB + chase) of DRB treatment. **Cold-Shock:** EXD2^{+/+}, EXD2^{-/-} + EXD2^{WT}-cl1 and EXD2^{-/-} + EXD2^{D108A/E110A}-cl1 were incubated at 4°C for 15 minutes and let to recover at 37°C for 30 minutes. mRNA was labelled with EU before (37°C), after 15 minutes at 4°C (4°C) or after the recovery at 37°C (4°C+37°C). For both experiments, EU signal was quantified by ImageJ and relative integrated densities normalized to mock-treated level set to 100% are reported on the graph (n= at least 20 cells per condition). Red bars indicate mean integrated density. One-way ANOVA with post-hoc Tukey adjustment comparisons were used to determine the p-values. Source data are provided as a Source Data file.



Supplementary Figure 4: NER is not affected by the lack of EXD2

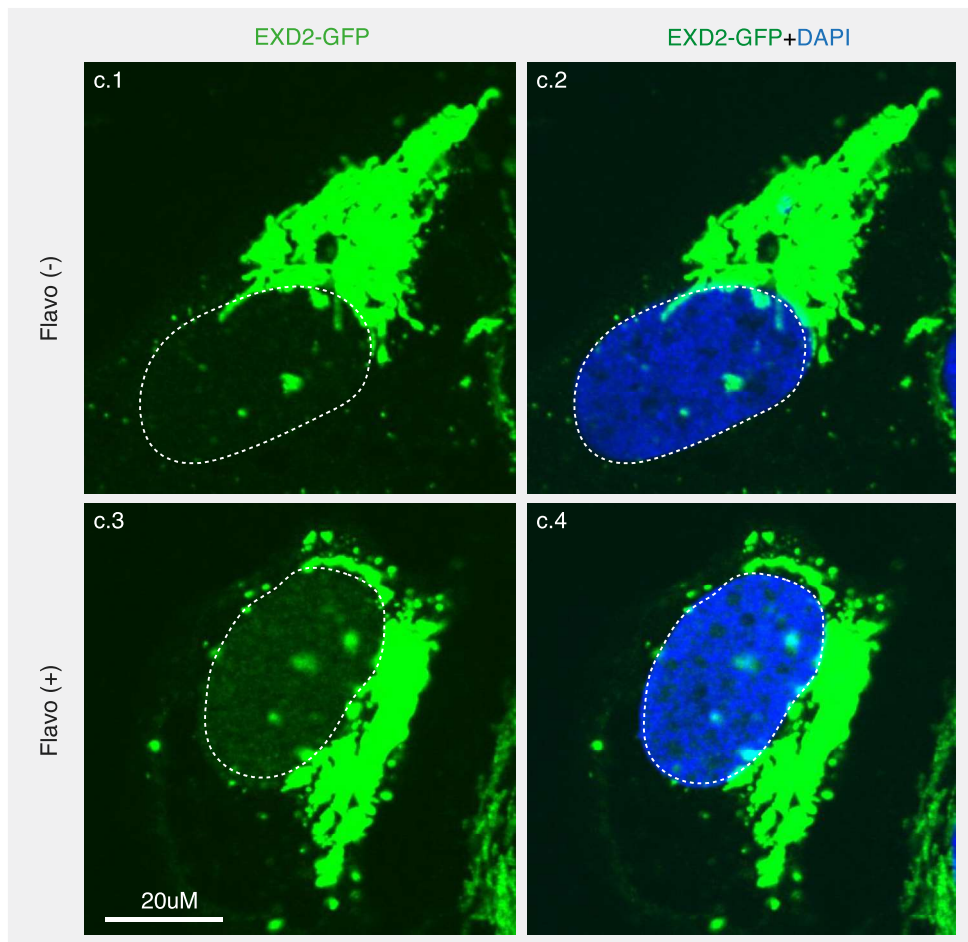
EXD2^{+/+} and EXD2^{-/-}-cl1 were mock or UV-irradiated (15J/m²) and let to recover for the indicated times before lysis. Protein lysates were immuno-blotted for EXD2, γ H2AX or Vinculin. Molecular mass of the proteins is indicated (kDa). RT; recovery time. Source data are provided as a Source Data file.



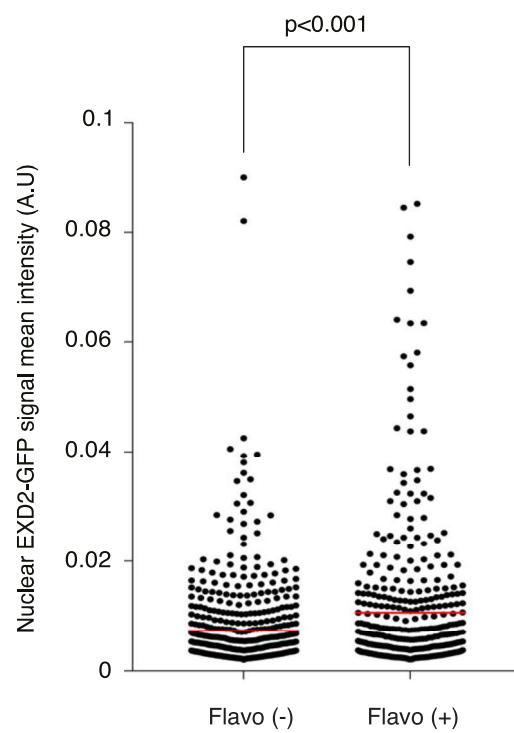
Supplementary Figure 5: mRNAs under synthesis are degraded by EXD2 following UV irradiation

- a.** Representative confocal images of EXD2^{+/+}, EXD2^{-/-}, EXD2^{-/-} + EXD2^{WT}-cl1 and EXD2^{-/-} + EXD2^{D108A/E110A}-cl1 showing newly synthesized mRNA (1 hour or 16 hours after mock-treatment or UV irradiation at 15J/m²). Images of the cells were obtained with the same microscopy system and constant acquisition parameters.
- b.** CS1ANSV and CS1ANSV+CSB^{WT} were treated as indicated in Figure 4a, upper panel, and EU signals were quantified using ImageJ and normalized to the value obtained at 1 hour set to 100%. Values are reported on the graph (n= at least 50 cells). Red bars indicate mean integrated density. *RT*; recovery time. One-way ANOVA with post-hoc Tukey adjustment comparisons were used to determine the p-values. Source data are provided as a Source Data file.

a.



b.



Supplementary Figure 6: EXD2^{WT}-GFP localization in U-2 OS cell

a. Representative confocal images of U-2 OS cells stably expressing EXD2^{WT}-GFP with or without Flavopiridol treatment. Images of the cells were obtained with the same microscopy system and constant acquisition parameters.

b. Quantification of the EXD2-GFP nuclear signal in U-2 OS cells treated or not with Flavopiridol (n= at least 400 cells). Red bars indicate mean integrated density. One-way ANOVA with post-hoc Tukey adjustment comparisons were used to determine the p-values. Source data are provided as a Source Data file.

Supplementary Table 1: Reagents and chemicals

REAGENT or RESOURCE	SOURCE	IDENTIFIER
Antibodies		
ACTIN 1/1000	Abcam	AB209856
CPD 1/500	Cosmo Bio	CAC-NM-DND-001
ATP5A 1/1000	ProteinTech Europe	66037-1-IG
EXD2 1/2000	Sigma-Aldrich	HPA005848
FLAG M2 1/1000	Sigma-Aldrich	F1804
GAPDH 1/2000	Abcam	AB8245
GFP 1/2000	Amsbio	TP401
GFP (PLA)	Roche	11814460001
GST 1/1000	Abcam	ab19256
γ H2AX 1/1000	Abcam	ab22551
Histone H3 1/5000	Abcam	ab1791100
RPB1 1/5000	Homemade IGBMC	7C2
RNA Pol II (PLA)	Bethyl	A300-653A
TFIIE α 1/1000	Homemade, IGBMC	2A1
Vinculin 1/1000	Sigma Aldrich	V9131
XPA 1/500	SCBT	SC-853
6-4PP 1/1000	Cosmo Bio	CAC-NM-DND-002
Chemicals, peptides, and recombinant proteins		
Actinomycin D	Sigma Aldrich	A-1410
DRB	Merck Chemicals	287891
Et743	PharmaMar	(Feuerhahn et al., 2011)
LightCycler 480 SYBR Green I Master	Roche	04887352001
MitoTracker Red CMXRos	Invitrogen	M7512
Streptavidin magnetic beads	Fisher Scientific SAS	88816
TriReagent	Molecular Research Center	TR118
Vectashield	VectorLaboratories	H-1000-10
Critical commercial assays		
Click-iT EU Alexa Fluor 488 Imaging Kit	ThermoFisher	C10329
Click-iT EdU Alexa Fluor 488 Imaging Kit	ThermoFisher	C10337
Lipofectamine RNAiMAX Transfection Reagent	Fisher Scientific SAS	13778030
SuperScript IV kit	Invitrogen	18090050
X-tremeGene DNA Transfection Reagent	Roche	063657870001
Qproteome Mitochondria Isolation Kit	Qiagen	37612
Experimental models: Cell lines		
U-2 OS and U-2 OS pTuner 263		(Nagy et al., 2016)
CS1ANSV and CS1ANSV+CSB		(Kristensen et al., 2013)
HeLa		Nieminuszczy et al., 2019)
HeLa EXD2 ^{-/-} -cl1 and 2		(Nieminuszczy et al., 2019)

HeLa EXD2 ^{-/-} +EXD2 ^{WT} -cl1 and 2		(Nieminuszczy et al., 2019)
HeLa EXD2 ^{-/-} +EXD2 ^{D108A/E110A} -cl1 and 2		(Nieminuszczy et al., 2019)
U-2 OS ^{GFP}		(Nieminuszczy et al., 2019)
U-2 OS ^{EXD2-GFP}		(Nieminuszczy et al., 2019)
XP4PA-SV		(Donnio et al., 2019)
XPC HeLa Silencix		(Le May et al., 2010)
Oligonucleotides		
F: GCAGAAGAACGGCATCAAGG	<i>CFP-SKL</i>	This paper
R: GTCCATGCCGAGAGTGATCC	<i>CFP-SKL</i>	This paper
F: CTTCCCCGATGAGAACTTCAAACCT	<i>CycB</i>	This paper
R: CACCTCCATGCCCTCTAGAACCTTT	<i>CycB</i>	This paper
siXPF	Dharmacon	019946-00
siXAB2	Dharmacon	004914-01
siEXD2	Dharmacon	020899-02
siCTL	Dharmacon	001810-02
siXPA	Dharmacon	005067-01
siCSB	Dharmacon	004888-00
siCSA	Dharmacon	011008-00
siUSP33	Dharmacon	006081-00
siBPTF	Dharmacon	004025-00
siYLP1	Dharmacon	032696-00
Recombinant DNA		
mCherry-LacR		(Nagy et al., 2016)
Software and algorithms		
GraphPad Prism	GraphPad Software Inc.	
ImageJ	NIH	
CellProfiler	Broad Institut	CellProfiler
Other		
Leica DM 4000 B equipped with a CoolSnap FX monochrome camera	Leica	

Supplementary References

- Donnio, L.-M., Lagarou, A., Sueur, G., Mari, P.-O., Giglia-Mari, G., 2019. CSB-Dependent Cyclin-Dependent Kinase 9 Degradation and RNA Polymerase II Phosphorylation during Transcription-Coupled Repair. *Mol Cell Biol* 39. <https://doi.org/10.1128/MCB.00225-18>
- Feuerhahn, S., Giraudon, C., Martinez-Diez, M., Bueren-Calabuig, J.A., Galmarini, C.M., Gago, F., Egly, J.M., 2011. XPF-dependent DNA breaks and RNA polymerase II arrest induced by antitumor DNA interstrand crosslinking-mimetic alkaloids. *Chem Biol* 18, 988–99. [https://doi.org/S1074-5521\(11\)00227-4](https://doi.org/S1074-5521(11)00227-4) [pii] 10.1016/j.chembiol.2011.06.007

- Kristensen, U., Epanchintsev, A., Rauschendorf, M.A., Laugel, V., Stevnsner, T., Bohr, V.A., Coin, F., Egly, J.M., 2013. Regulatory interplay of Cockayne syndrome B ATPase and stress-response gene ATF3 following genotoxic stress. *Proceedings of the National Academy of Sciences of the United States of America* 110, E2261-70. <https://doi.org/10.1073/pnas.1220071110>
- Le May, N., Mota-Fernandes, D., Velez-Cruz, R., Iltis, I., Biard, D., Egly, J.M., 2010. NER factors are recruited to active promoters and facilitate chromatin modification for transcription in the absence of exogenous genotoxic attack. *Mol Cell* 38, 54–66. [https://doi.org/S1097-2765\(10\)00211-X](https://doi.org/S1097-2765(10)00211-X) [pii] 10.1016/j.molcel.2010.03.004
- Nagy, Z., Kalousi, A., Furst, A., Koch, M., Fischer, B., Soutoglou, E., 2016. Tankyrases Promote Homologous Recombination and Check Point Activation in Response to DSBs. *PLoS Genet* 12, e1005791. <https://doi.org/10.1371/journal.pgen.1005791>
- Nieminuszczy, J., Broderick, R., Bellani, M.A., Smethurst, E., Schwab, R.A., Cherdyntseva, V., Evmorfopoulou, T., Lin, Y.-L., Minczuk, M., Pasero, P., Gagos, S., Seidman, M.M., Niedzwiedz, W., 2019. EXD2 Protects Stressed Replication Forks and Is Required for Cell Viability in the Absence of BRCA1/2. *Molecular Cell* 75, 605-619.e6. <https://doi.org/10.1016/j.molcel.2019.05.026>
- Shanbhag, N.M., Rafalska-Metcalf, I.U., Balane-Bolivar, C., Janicki, S.M., Greenberg, R.A., 2010. ATM-dependent chromatin changes silence transcription in cis to DNA double-strand breaks. *Cell* 141, 970–81. <https://doi.org/10.1016/j.cell.2010.04.038>

Bibliography

- Abdella, R. et al. (2021) 'Structure of the human Mediator-bound transcription preinitiation complex', *Science* (New York, N.Y.), 372(6537), pp. 52–56. Available at: <https://doi.org/10.1126/science.abg3074>.
- Abd-Elrahman, I. et al. (2009) 'The Inhibitor of Apoptosis Protein Livin (ML-IAP) Plays a Dual Role in Tumorigenicity', *Cancer Research*, 69(13), pp. 5475–5480. Available at: <https://doi.org/10.1158/0008-5472.CAN-09-0424>.
- Abril-Garrido, J. et al. (2023) 'Structural basis of transcription reduction by a promoter-proximal +1 nucleosome', *Molecular Cell* [Preprint]. Available at: <https://doi.org/10.1016/j.molcel.2023.04.011>.
- Abuhashem, A., Garg, V. and Hadjantonakis, A.-K. (2022) 'RNA polymerase II pausing in development: orchestrating transcription', *Open Biology*, 12(1), p. 210220. Available at: <https://doi.org/10.1098/rsob.210220>.
- Adam, R.C. et al. (2015) 'Pioneer factors govern super-enhancer dynamics in stem cell plasticity and lineage choice', *Nature*, 521(7552), pp. 366–370. Available at: <https://doi.org/10.1038/nature14289>.
- Adameyko, I. et al. (2009) 'Schwann Cell Precursors from Nerve Innervation Are a Cellular Origin of Melanocytes in Skin', *Cell*, 139(2), pp. 366–379. Available at: <https://doi.org/10.1016/j.cell.2009.07.049>.
- Adameyko, I. and Lallemand, F. (2010) 'Glial versus melanocyte cell fate choice: Schwann cell precursors as a cellular origin of melanocytes', *Cellular and Molecular Life Sciences*, 67(18), pp. 3037–3055. Available at: <https://doi.org/10.1007/s00018-010-0390-y>.
- Adelman, K. and Lis, J.T. (2012) 'Promoter-proximal pausing of RNA polymerase II: emerging roles in metazoans', *Nature Reviews Genetics*, 13(10), pp. 720–731. Available at: <https://doi.org/10.1038/nrg3293>.
- Ahn, A., Chatterjee, A. and Eccles, M.R. (2017) 'The Slow Cycling Phenotype: A Growing Problem for Treatment Resistance in Melanoma', *Molecular Cancer Therapeutics*, 16(6), pp. 1002–1009. Available at: <https://doi.org/10.1158/1535-7163.MCT-16-0535>.
- Akbani, R. et al. (2015) 'Genomic Classification of Cutaneous Melanoma', *Cell*, 161(7), pp. 1681–1696. Available at: <https://doi.org/10.1016/j.cell.2015.05.044>.
- Al Hashmi, M. et al. (2020) 'Differential responsiveness to BRAF inhibitors of melanoma cell lines BRAF V600E-mutated', *Journal of Translational Medicine*, 18(1), p. 192. Available at: <https://doi.org/10.1186/s12967-020-02350-8>.
- Alekseev, S. et al. (2017) 'Transcription without XPB Establishes a Unified Helicase-Independent Mechanism of Promoter Opening in Eukaryotic Gene Expression', *Molecular Cell*, 65(3), pp. 504–514.e4. Available at: <https://doi.org/10.1016/j.molcel.2017.01.012>.
- Alexandrov, L.B. et al. (2013) 'Signatures of mutational processes in human cancer', *Nature*, 500(7463), pp. 415–421. Available at: <https://doi.org/10.1038/nature12477>.
- Allavena, P. et al. (2022) 'Effects of the Anti-Tumor Agents Trabectedin and Lurbinectedin on Immune Cells of the Tumor Microenvironment', *Frontiers in Oncology*, 12, p. 851790. Available at: <https://doi.org/10.3389/fonc.2022.851790>.
- Allen, B.L. and Taatjes, D.J. (2015) 'The Mediator complex: a central integrator of transcription', *Nature Reviews. Molecular Cell Biology*, 16(3), pp. 155–166. Available at: <https://doi.org/10.1038/nrm3951>.
- Allshire, R.C. and Madhani, H.D. (2018) 'Ten principles of heterochromatin formation and function', *Nature Reviews Molecular Cell Biology*, 19(4), pp. 229–244. Available at: <https://doi.org/10.1038/nrm.2017.119>.
- Aloia, A. et al. (2019) 'A Fatty Acid Oxidation-dependent Metabolic Shift Regulates the Adaptation of BRAF-mutated Melanoma to MAPK Inhibitors', *Clinical Cancer Research: An Official Journal of the American Association for Cancer Research*, 25(22), pp. 6852–6867. Available at: <https://doi.org/10.1158/1078-0432.CCR-19-0253>.
- Alver, B.H. et al. (2017) 'The SWI/SNF chromatin remodelling complex is required for maintenance of lineage specific enhancers', *Nature Communications*, 8(1), p. 14648. Available at: <https://doi.org/10.1038/ncomms14648>.
- Anastasiadou, E., Jacob, L.S. and Slack, F.J. (2018) 'Non-coding RNA networks in cancer', *Nature Reviews Cancer*, 18(1), pp. 5–18. Available at: <https://doi.org/10.1038/nrc.2017.99>.
- Anbar, T.S., Hegazy, R.A. and Shalaby, S. (2019) 'Extra-Cutaneous Melanocytes', in M. Picardo and A. Taïeb (eds) *Vitiligo*. Cham: Springer International Publishing, pp. 103–113. Available at: https://doi.org/10.1007/978-3-319-62960-5_10.
- Andersson, R. et al. (2014) 'An atlas of active enhancers across human cell types and tissues', *Nature*, 507(7493), pp. 455–461. Available at: <https://doi.org/10.1038/nature12787>.
- Andersson, R. et al. (2015) 'Human Gene Promoters Are Intrinsically Bidirectional', *Molecular Cell*, 60(3), pp. 346–347. Available at: <https://doi.org/10.1016/j.molcel.2015.10.015>.
- Andrades, A. et al. (2023) 'SWI/SNF complexes in hematological malignancies: biological implications and therapeutic opportunities', *Molecular Cancer*, 22(1), p. 39. Available at: <https://doi.org/10.1186/s12943-023-01736-8>.
- Andreucci, E. et al. (2020) 'The acidic tumor microenvironment drives a stem-like phenotype in melanoma cells', *Journal of Molecular Medicine*, 98(10), pp. 1431–1446. Available at: <https://doi.org/10.1007/s00109-020-01959-y>.
- Andrews, L.P., Yano, H. and Vignali, D.A.A. (2019) 'Inhibitory receptors and ligands beyond PD-1, PD-L1 and CTLA-4: breakthroughs or backups', *Nature Immunology*, 20(11), pp. 1425–1434. Available at: <https://doi.org/10.1038/s41590-019-0512-0>.
- Annual Report to the Nation 2022: National Trends in Rates of New Cancer Cases (no date) SEER. Available at: https://seer.cancer.gov/report_to_nation/infographics/trends_incidence.html (Accessed: 9 February 2023).

- Ansary, T.M. et al. (2021) 'Inflammatory Molecules Associated with Ultraviolet Radiation-Mediated Skin Aging', *International Journal of Molecular Sciences*, 22(8), p. 3974. Available at: <https://doi.org/10.3390/ijms22083974>.
- Anshabo, A.T. et al. (2021) 'CDK9: A Comprehensive Review of Its Biology, and Its Role as a Potential Target for Anti-Cancer Agents', *Frontiers in Oncology*, 11. Available at: <https://www.frontiersin.org/articles/10.3389/fonc.2021.678559> (Accessed: 26 April 2023).
- Aoi, Y. et al. (2020) 'NELF Regulates a Promoter-Proximal Step Distinct from RNA Pol II Pause-Release', *Molecular Cell*, 78(2), pp. 261–274.e5. Available at: <https://doi.org/10.1016/j.molcel.2020.02.014>.
- Aprile-Garcia, F. et al. (2019) 'Nascent-protein ubiquitination is required for heat shock-induced gene downregulation in human cells', *Nature Structural & Molecular Biology*, 26(2), pp. 137–146. Available at: <https://doi.org/10.1038/s41594-018-0182-x>.
- Arafteh, R. et al. (2015) 'Recurrent inactivating RASA2 mutations in melanoma', *Nature Genetics*, 47(12), pp. 1408–1410. Available at: <https://doi.org/10.1038/ng.3427>.
- Arango Duque, G. and Descoteaux, A. (2014) 'Macrophage Cytokines: Involvement in Immunity and Infectious Diseases', *Frontiers in Immunology*, 5. Available at: <https://www.frontiersin.org/articles/10.3389/fimmu.2014.00491> (Accessed: 24 March 2023).
- Arkin, M.R., Tang, Y. and Wells, J.A. (2014) 'Small-Molecule Inhibitors of Protein-Protein Interactions: Progressing toward the Reality', *Chemistry & Biology*, 21(9), pp. 1102–1114. Available at: <https://doi.org/10.1016/j.chembiol.2014.09.001>.
- Arozarena, I. and Wellbrock, C. (2017) 'Targeting invasive properties of melanoma cells', *The FEBS journal*, 284(14), pp. 2148–2162. Available at: <https://doi.org/10.1111/febs.14040>.
- Arozarena, I. and Wellbrock, C. (2019) 'Phenotype plasticity as enabler of melanoma progression and therapy resistance', *Nature Reviews. Cancer*, 19(7), pp. 377–391. Available at: <https://doi.org/10.1038/s41568-019-0154-4>.
- Arts, N. et al. (2015) 'microRNA-155, induced by interleukin-1 β , represses the expression of microphthalmia-associated transcription factor (MITF-M) in melanoma cells', *PloS One*, 10(4), p. e0122517. Available at: <https://doi.org/10.1371/journal.pone.0122517>.
- Atkins, M.B. et al. (2021) 'The State of Melanoma: Emergent Challenges and Opportunities', *Clinical Cancer Research: An Official Journal of the American Association for Cancer Research*, 27(10), pp. 2678–2697. Available at: <https://doi.org/10.1158/1078-0432.CCR-20-4092>.
- Atkins, M.B. et al. (2023) 'Combination Dabrafenib and Trametinib Versus Combination Nivolumab and Ipilimumab for Patients With Advanced BRAF-Mutant Melanoma: The DREAMseq Trial—ECOG-ACRIN EA6134', *Journal of Clinical Oncology*, 41(2), pp. 186–197. Available at: <https://doi.org/10.1200/JCO.22.01763>.
- Attieh, Y. et al. (2017) 'Cancer-associated fibroblasts lead tumor invasion through integrin- β 3-dependent fibronectin assembly', *Journal of Cell Biology*, 216(11), pp. 3509–3520. Available at: <https://doi.org/10.1083/jcb.201702033>.
- Augert, A. and MacPherson, D. (2014) 'Treating transcriptional addiction in small cell lung cancer', *Cancer Cell*, 26(6), pp. 783–784. Available at: <https://doi.org/10.1016/j.ccell.2014.11.012>.
- Avagliano, A. et al. (2020) 'Metabolic Plasticity of Melanoma Cells and Their Crosstalk With Tumor Microenvironment', *Frontiers in Oncology*, 10, p. 722. Available at: <https://doi.org/10.3389/fonc.2020.00722>.
- de Azevedo, S.J. et al. (2021) 'First-line atezolizumab monotherapy in patients with advanced BRAFV600 wild-type melanoma', *Pigment Cell & Melanoma Research*, 34(5), pp. 973–977. Available at: <https://doi.org/10.1111/pcmr.12960>.
- Bacabac, M. and Xu, W. (2023) 'Oncogenic super-enhancers in cancer: mechanisms and therapeutic targets', *Cancer Metastasis Reviews* [Preprint]. Available at: <https://doi.org/10.1007/s10555-023-10103-4>.
- Bafaloukos, D. et al. (2023) 'Evolution and Progress of mRNA Vaccines in the Treatment of Melanoma: Future Prospects', *Vaccines*, 11(3), p. 636. Available at: <https://doi.org/10.3390/vaccines11030636>.
- Baggiolini, A. et al. (2021) 'Developmental chromatin programs determine oncogenic competence in melanoma', *Science*, 373(6559), p. eabc1048. Available at: <https://doi.org/10.1126/science.abc1048>.
- Bagrodia, S., Smeal, T. and Abraham, R.T. (2012) 'Mechanisms of intrinsic and acquired resistance to kinase-targeted therapies', *Pigment Cell & Melanoma Research*, 25(6), pp. 819–831. Available at: <https://doi.org/10.1111/pcmr.12007>.
- Bal, E. et al. (2022) 'Super-enhancer hypermutation alters oncogene expression in B cell lymphoma', *Nature*, 607(7920), pp. 808–815. Available at: <https://doi.org/10.1038/s41586-022-04906-8>.
- Balch, C.M. et al. (2009) 'Final Version of 2009 AJCC Melanoma Staging and Classification', *Journal of Clinical Oncology*, 27(36), pp. 6199–6206. Available at: <https://doi.org/10.1200/JCO.2009.23.4799>.
- Bald, T. et al. (2014) 'Ultraviolet-radiation-induced inflammation promotes angiogenesis and metastasis in melanoma', *Nature*, 507(7490), pp. 109–113. Available at: <https://doi.org/10.1038/nature13111>.
- Balsalobre, A. and Drouin, J. (2022) 'Pioneer factors as master regulators of the epigenome and cell fate', *Nature Reviews Molecular Cell Biology*, 23(7), pp. 449–464. Available at: <https://doi.org/10.1038/s41580-022-00464-z>.
- Baluapuri, A., Wolf, E. and Eilers, M. (2020) 'Target gene-independent functions of MYC oncoproteins', *Nature Reviews Molecular Cell Biology*, 21(5), pp. 255–267. Available at: <https://doi.org/10.1038/s41580-020-0215-2>.
- Banani, S.F. et al. (2017) 'Biomolecular condensates: organizers of cellular biochemistry', *Nature Reviews. Molecular Cell Biology*, 18(5), pp. 285–298. Available at: <https://doi.org/10.1038/nrm.2017.7>.

- Banerji, J., Rusconi, S. and Schaffner, W. (1981) 'Expression of a beta-globin gene is enhanced by remote SV40 DNA sequences', *Cell*, 27(2 Pt 1), pp. 299–308. Available at: [https://doi.org/10.1016/0092-8674\(81\)90413-x](https://doi.org/10.1016/0092-8674(81)90413-x).
- Bannister, A.J. and Kouzarides, T. (2011) 'Regulation of chromatin by histone modifications', *Cell Research*, 21(3), pp. 381–395. Available at: <https://doi.org/10.1038/cr.2011.22>.
- Baptista, T. et al. (2017) 'SAGA Is a General Cofactor for RNA Polymerase II Transcription', *Molecular Cell*, 68(1), pp. 130–143.e5. Available at: <https://doi.org/10.1016/j.molcel.2017.08.016>.
- Barone, A. et al. (2017) 'FDA Approval Summary: Trabectedin for Unresectable or Metastatic Liposarcoma or Leiomyosarcoma Following an Anthracycline-Containing Regimen', *Clinical Cancer Research: An Official Journal of the American Association for Cancer Research*, 23(24), pp. 7448–7453. Available at: <https://doi.org/10.1158/1078-0432.CCR-17-0898>.
- Bastian, B.C. (2014) 'The molecular pathology of melanoma: an integrated taxonomy of melanocytic neoplasia', *Annual Review of Pathology*, 9, pp. 239–271. Available at: <https://doi.org/10.1146/annurev-pathol-012513-104658>.
- Batlle, E. and Clevers, H. (2017) 'Cancer stem cells revisited', *Nature Medicine*, 23(10), pp. 1124–1134. Available at: <https://doi.org/10.1038/nm.4409>.
- Batlle, E. and Massagué, J. (2019) 'Transforming Growth Factor- β Signaling in Immunity and Cancer', *Immunity*, 50(4), pp. 924–940. Available at: <https://doi.org/10.1016/j.immuni.2019.03.024>.
- Bauer, J. and Bastian, B.C. (2006) 'Distinguishing melanocytic nevi from melanoma by DNA copy number changes: comparative genomic hybridization as a research and diagnostic tool', *Dermatologic Therapy*, 19(1), pp. 40–49. Available at: <https://doi.org/10.1111/j.1529-8019.2005.00055.x>.
- Baumeister, S.H. et al. (2016) 'Coinhibitory Pathways in Immunotherapy for Cancer', *Annual Review of Immunology*, 34, pp. 539–573. Available at: <https://doi.org/10.1146/annurev-immunol-032414-112049>.
- Belgiovine, C. et al. (2017) 'Lurbinectedin reduces tumour-associated macrophages and the inflammatory tumour microenvironment in preclinical models', *British Journal of Cancer*, 117(5), pp. 628–638. Available at: <https://doi.org/10.1038/bjc.2017.205>.
- Belkaid, Y. and Segre, J.A. (2014) 'Dialogue between skin microbiota and immunity', *Science (New York, N.Y.)*, 346(6212), pp. 954–959. Available at: <https://doi.org/10.1126/science.1260144>.
- Bell, C.C. and Gilan, O. (2020) 'Principles and mechanisms of non-genetic resistance in cancer', *British Journal of Cancer*, 122(4), pp. 465–472. Available at: <https://doi.org/10.1038/s41416-019-0648-6>.
- Bell, R.J.A. et al. (2016) 'Understanding TERT Promoter Mutations: A Common Path to Immortality', *Molecular Cancer Research*, 14(4), pp. 315–323. Available at: <https://doi.org/10.1158/1541-7786.MCR-16-0003>.
- Bellei, B., Migliano, E. and Picardo, M. (2020) 'A Framework of Major Tumor-Promoting Signal Transduction Pathways Implicated in Melanoma-Fibroblast Dialogue', *Cancers*, 12(11), p. 3400. Available at: <https://doi.org/10.3390/cancers12113400>.
- Belote, R.L. et al. (2021) 'Human melanocyte development and melanoma dedifferentiation at single-cell resolution', *Nature Cell Biology*, 23(9), pp. 1035–1047. Available at: <https://doi.org/10.1038/s41556-021-00740-8>.
- Benboubker, V. et al. (2022) 'Cancer Cell Phenotype Plasticity as a Driver of Immune Escape in Melanoma', *Frontiers in Immunology*, 13, p. 873116. Available at: <https://doi.org/10.3389/fimmu.2022.873116>.
- Benci, J.L. et al. (2016) 'Tumor Interferon Signaling Regulates a Multigenic Resistance Program to Immune Checkpoint Blockade', *Cell*, 167(6), pp. 1540–1554.e12. Available at: <https://doi.org/10.1016/j.cell.2016.11.022>.
- Benci, J.L. et al. (2019) 'Opposing Functions of Interferon Coordinate Adaptive and Innate Immune Responses to Cancer Immune Checkpoint Blockade', *Cell*, 178(4), pp. 933–948.e14. Available at: <https://doi.org/10.1016/j.cell.2019.07.019>.
- Benjamin, R.S. (1979) 'Chemotherapy of malignant melanoma', *World Journal of Surgery*, 3(3), pp. 321–328. Available at: <https://doi.org/10.1007/BF01556584>.
- Bennett, D.C. (1983) 'Differentiation in mouse melanoma cells: Initial reversibility and an on-off stochastic model', *Cell*, 34(2), pp. 445–453. Available at: [https://doi.org/10.1016/0092-8674\(83\)90378-1](https://doi.org/10.1016/0092-8674(83)90378-1).
- Bentley, N.J., Eisen, T. and Goding, C.R. (1994) 'Melanocyte-specific expression of the human tyrosinase promoter: activation by the microphthalmia gene product and role of the initiator', *Molecular and Cellular Biology*, 14(12), pp. 7996–8006. Available at: <https://doi.org/10.1128/mcb.14.12.7996-8006.1994>.
- Berghoff, A.S. et al. (2013) 'Evaluation of invasion patterns and their correlation with integrin α v β 3 expression in brain metastases of solid cancers', *Journal of Clinical Oncology*, 31(15_suppl), pp. 2059–2059. Available at: https://doi.org/10.1200/jco.2013.31.15_suppl.2059.
- Berico, P. and Coin, F. (2018) 'Is TFIIH the new Achilles heel of cancer cells?', *Transcription*, 9(1), pp. 47–51. Available at: <https://doi.org/10.1080/21541264.2017.1331723>.
- Berk-Krauss, J. et al. (2020) 'New Systematic Therapies and Trends in Cutaneous Melanoma Deaths Among US Whites, 1986–2016', *American Journal of Public Health*, 110(5), pp. 731–733. Available at: <https://doi.org/10.2105/AJPH.2020.305567>.
- Bernecky, C., Plitzko, J.M. and Cramer, P. (2017) 'Structure of a transcribing RNA polymerase II-DSIF complex reveals a multidentate DNA-RNA clamp', *Nature Structural & Molecular Biology*, 24(10), pp. 809–815. Available at: <https://doi.org/10.1038/nsmb.3465>.

- Berthenet, K. et al. (2020) 'Failed Apoptosis Enhances Melanoma Cancer Cell Aggressiveness', *Cell Reports*, 31(10), p. 107731. Available at: <https://doi.org/10.1016/j.celrep.2020.107731>.
- Betancur, P., Bronner-Fraser, M. and Sauka-Spengler, T. (2010) 'Assembling Neural Crest Regulatory Circuits into a Gene Regulatory Network', *Annual Review of Cell and Developmental Biology*, 26(1), pp. 581–603. Available at: <https://doi.org/10.1146/annurev.cellbio.042308.113245>.
- Bhan, A., Soleimani, M. and Mandal, S.S. (2017) 'Long Noncoding RNA and Cancer: A New Paradigm', *Cancer Research*, 77(15), pp. 3965–3981. Available at: <https://doi.org/10.1158/0008-5472.CAN-16-2634>.
- Bhat, P., Honson, D. and Guttman, M. (2021) 'Nuclear compartmentalization as a mechanism of quantitative control of gene expression', *Nature Reviews Molecular Cell Biology*, 22(10), pp. 653–670. Available at: <https://doi.org/10.1038/s41580-021-00387-1>.
- Bikle, D.D. (2011) 'Vitamin D metabolism and function in the skin', *Molecular and Cellular Endocrinology*, 347(1), pp. 80–89. Available at: <https://doi.org/10.1016/j.mce.2011.05.017>.
- Binnewies, M. et al. (2018) 'Understanding the tumor immune microenvironment (TIME) for effective therapy', *Nature Medicine*, 24(5), pp. 541–550. Available at: <https://doi.org/10.1038/s41591-018-0014-x>.
- Birkeland, E. et al. (2018) 'Patterns of genomic evolution in advanced melanoma', *Nature Communications*, 9(1), p. 2665. Available at: <https://doi.org/10.1038/s41467-018-05063-1>.
- Bleich, R.M. and Arthur, J.C. (2021) 'Microbiome and the Hallmarks of Cancer', in J. Sun (ed.) *Inflammation, Infection, and Microbiome in Cancers: Evidence, Mechanisms, and Implications*. Cham: Springer International Publishing (Physiology in Health and Disease), pp. 1–26. Available at: https://doi.org/10.1007/978-3-030-67951-4_1.
- Blobel, G.A. et al. (2021) 'Testing the super-enhancer concept', *Nature Reviews Genetics*, 22(12), pp. 749–755. Available at: <https://doi.org/10.1038/s41576-021-00398-w>.
- Bockhorn, M., Jain, R.K. and Munn, L.L. (2007) 'Active versus passive mechanisms in metastasis: do cancer cells crawl into vessels, or are they pushed?', *The Lancet. Oncology*, 8(5), pp. 444–448. Available at: [https://doi.org/10.1016/S1470-2045\(07\)70140-7](https://doi.org/10.1016/S1470-2045(07)70140-7).
- Boehning, M. et al. (2018) 'RNA polymerase II clustering through carboxy-terminal domain phase separation', *Nature Structural & Molecular Biology*, 25(9), pp. 833–840. Available at: <https://doi.org/10.1038/s41594-018-0112-y>.
- Boija, A. et al. (2018) 'Transcription Factors Activate Genes through the Phase-Separation Capacity of Their Activation Domains', *Cell*, 175(7), pp. 1842–1855.e16. Available at: <https://doi.org/10.1016/j.cell.2018.10.042>.
- Boija, A., Klein, I.A. and Young, R.A. (2021) 'Biomolecular Condensates and Cancer', *Cancer Cell*, 39(2), pp. 174–192. Available at: <https://doi.org/10.1016/j.ccell.2020.12.003>.
- Bojszuk, D., Nagy, G. and Balint, B.L. (2017) 'Inducible super-enhancers are organized based on canonical signal-specific transcription factor binding elements', *Nucleic Acids Research*, 45(7), pp. 3693–3706. Available at: <https://doi.org/10.1093/nar/gkw1283>.
- Bollag, G. et al. (2010) 'Clinical efficacy of a RAF inhibitor needs broad target blockade in BRAF-mutant melanoma', *Nature*, 467(7315), pp. 596–599. Available at: <https://doi.org/10.1038/nature09454>.
- Bonaventura, P. et al. (2019) 'Cold Tumors: A Therapeutic Challenge for Immunotherapy', *Frontiers in Immunology*, 10, p. 168. Available at: <https://doi.org/10.3389/fimmu.2019.00168>.
- Bondeson, D.P. et al. (2015) 'Catalytic in vivo protein knockdown by small-molecule PROTACs', *Nature Chemical Biology*, 11(8), pp. 611–617. Available at: <https://doi.org/10.1038/nchembio.1858>.
- Bondurand, N. et al. (2000) 'Interaction among SOX10, PAX3 and MITF, three genes altered in Waardenburg syndrome', *Human Molecular Genetics*, 9(13), pp. 1907–1917. Available at: <https://doi.org/10.1093/hmg/9.13.1907>.
- Boshuizen, J. et al. (2018) 'Cooperative targeting of melanoma heterogeneity with an AXL antibody-drug conjugate and BRAF/MEK inhibitors', *Nature Medicine*, 24(2), pp. 203–212. Available at: <https://doi.org/10.1038/nm.4472>.
- Boshuizen, J. et al. (2020) 'Reversal of pre-existing NGFR-driven tumor and immune therapy resistance', *Nature Communications*, 11(1), p. 3946. Available at: <https://doi.org/10.1038/s41467-020-17739-8>.
- Boumahdi, S. and de Sauvage, F.J. (2020) 'The great escape: tumour cell plasticity in resistance to targeted therapy', *Nature Reviews Drug Discovery*, 19(1), pp. 39–56. Available at: <https://doi.org/10.1038/s41573-019-0044-1>.
- Boutros, A. et al. (2020) 'Case Report: Immune-Related Toxicity During Adjuvant Treatment With BRAF Plus MEK Inhibitors in a Melanoma Patient', *Frontiers in Immunology*, 11. Available at: <https://www.frontiersin.org/articles/10.3389/fimmu.2020.579523> (Accessed: 4 April 2023).
- Boxer, L.M. and Dang, C.V. (2001) 'Translocations involving c-myc and c-myc function', *Oncogene*, 20(40), pp. 5595–5610. Available at: <https://doi.org/10.1038/sj.onc.1204595>.
- Bozsányi, S. et al. (2022) 'Multispectral Imaging Algorithm Predicts Breslow Thickness of Melanoma', *Journal of Clinical Medicine*, 11(1), p. 189. Available at: <https://doi.org/10.3390/jcm11010189>.
- Brabletz, T. et al. (2018) 'EMT in cancer', *Nature Reviews Cancer*, 18(2), pp. 128–134. Available at: <https://doi.org/10.1038/nrc.2017.118>.
- Bradner, J.E., Hnisz, D. and Young, R.A. (2017) 'Transcriptional Addiction in Cancer', *Cell*, 168(4), pp. 629–643. Available at: <https://doi.org/10.1016/j.cell.2016.12.013>.

- Brahmer, J.R. et al. (2018) 'Management of Immune-Related Adverse Events in Patients Treated With Immune Checkpoint Inhibitor Therapy: American Society of Clinical Oncology Clinical Practice Guideline', *Journal of Clinical Oncology: Official Journal of the American Society of Clinical Oncology*, 36(17), pp. 1714–1768. Available at: <https://doi.org/10.1200/JCO.2017.77.6385>.
- Brash, D.E. (2015) 'UV signature mutations', *Photochemistry and Photobiology*, 91(1), pp. 15–26. Available at: <https://doi.org/10.1111/php.12377>.
- Brighton, H.E. et al. (2018) 'New Mechanisms of Resistance to MEK Inhibitors in Melanoma Revealed by Intravital Imaging', *Cancer Research*, 78(2), pp. 542–557. Available at: <https://doi.org/10.1158/0008-5472.CAN-17-1653>.
- Bronner, M.E. and LeDouarin, N.M. (2012) 'Development and evolution of the neural crest: An overview', *Developmental Biology*, 366(1), pp. 2–9. Available at: <https://doi.org/10.1016/j.ydbio.2011.12.042>.
- Broussard, L. et al. (2018) 'Melanoma Cell Death Mechanisms', *Chonnam Medical Journal*, 54(3), pp. 135–142. Available at: <https://doi.org/10.4068/cmj.2018.54.3.135>.
- Brown, J.D. et al. (2014) 'NF- κ B directs dynamic super enhancer formation in inflammation and atherogenesis', *Molecular Cell*, 56(2), pp. 219–231. Available at: <https://doi.org/10.1016/j.molcel.2014.08.024>.
- Brown, M. et al. (2018) 'Lymph node blood vessels provide exit routes for metastatic tumor cell dissemination in mice', *Science (New York, N.Y.)*, 359(6382), pp. 1408–1411. Available at: <https://doi.org/10.1126/science.aal3662>.
- Brozyna, A. et al. (2007) 'Mechanism of UV-related carcinogenesis and its contribution to nevi/melanoma', *Expert Review of Dermatology*, 2(4), pp. 451–469. Available at: <https://doi.org/10.1586/17469872.2.4.451>.
- Buckels, A. et al. (2019) 'Autocrine/paracrine actions of growth hormone in human melanoma cell lines', *Biochemistry and Biophysics Reports*, 21, p. 100716. Available at: <https://doi.org/10.1016/j.bbrep.2019.100716>.
- Buitrago, D. et al. (2021) 'Impact of DNA methylation on 3D genome structure', *Nature Communications*, 12(1), p. 3243. Available at: <https://doi.org/10.1038/s41467-021-23142-8>.
- Bulut-Karslioglu, A. et al. (2018) 'The transcriptionally permissive chromatin state of embryonic stem cells is acutely tuned to translational output', *Cell stem cell*, 22(3), pp. 369–383.e8. Available at: <https://doi.org/10.1016/j.stem.2018.02.004>.
- Burris, T.P. et al. (2013) 'Nuclear Receptors and Their Selective Pharmacologic Modulators', *Pharmacological Reviews*. Edited by D.M. Perez, 65(2), pp. 710–778. Available at: <https://doi.org/10.1124/pr.112.006833>.
- Burslem, G.M. et al. (2018) 'The Advantages of Targeted Protein Degradation Over Inhibition: An RTK Case Study', *Cell Chemical Biology*, 25(1), pp. 67–77.e3. Available at: <https://doi.org/10.1016/j.chembiol.2017.09.009>.
- Bushnell, D.A. et al. (2004) 'Structural Basis of Transcription: An RNA Polymerase II-TFIIB Cocrystal at 4.5 Ångströms', *Science*, 303(5660), pp. 983–988. Available at: <https://doi.org/10.1126/science.1090838>.
- Bushweller, J.H. (2019) 'Targeting transcription factors in cancer — from undruggable to reality', *Nature Reviews Cancer*, 19(11), pp. 611–624. Available at: <https://doi.org/10.1038/s41568-019-0196-7>.
- Busse, A. and Keilholz, U. (2011) 'Role of TGF- β in melanoma', *Current Pharmaceutical Biotechnology*, 12(12), pp. 2165–2175. Available at: <https://doi.org/10.2174/138920111798808437>.
- Butler, J.M., Kobayashi, H. and Rafii, S. (2010) 'Instructive role of the vascular niche in promoting tumour growth and tissue repair by angiocrine factors', *Nature Reviews. Cancer*, 10(2), pp. 138–146. Available at: <https://doi.org/10.1038/nrc2791>.
- Byers, H.R. et al. (2003) 'Role of cytoplasmic dynein in perinuclear aggregation of phagocytosed melanosomes and supranuclear melanin cap formation in human keratinocytes', *The Journal of Investigative Dermatology*, 121(4), pp. 813–820. Available at: <https://doi.org/10.1046/j.1523-1747.2003.12481.x>.
- Cai, Y. et al. (2021) 'H3K27me3-rich genomic regions can function as silencers to repress gene expression via chromatin interactions', *Nature Communications*, 12(1), p. 719. Available at: <https://doi.org/10.1038/s41467-021-20940-y>.
- Caksa, S., Baqai, U. and Aplin, A.E. (2022) 'The future of targeted kinase inhibitors in melanoma', *Pharmacology & Therapeutics*, 239, p. 108200. Available at: <https://doi.org/10.1016/j.pharmthera.2022.108200>.
- Calabrese, C. et al. (2020) 'Genomic basis for RNA alterations in cancer', *Nature*, 578(7793), pp. 129–136. Available at: <https://doi.org/10.1038/s41586-020-1970-0>.
- Callahan, M.K. et al. (2012) 'Progression of RAS-Mutant Leukemia during RAF Inhibitor Treatment', *New England Journal of Medicine*, 367(24), pp. 2316–2321. Available at: <https://doi.org/10.1056/NEJMoa1208958>.
- Campbell, N.R. et al. (2021) 'Cooperation between melanoma cell states promotes metastasis through heterotypic cluster formation', *Developmental Cell*, 56(20), pp. 2808–2825.e10. Available at: <https://doi.org/10.1016/j.devcel.2021.08.018>.
- del Campo, A.B. et al. (2014) 'Immune escape of cancer cells with beta2-microglobulin loss over the course of metastatic melanoma', *International Journal of Cancer*, 134(1), pp. 102–113. Available at: <https://doi.org/10.1002/ijc.28338>.
- Cancer Hotspots (no date). Available at: <https://www.cancerhotspots.org/#/home> (Accessed: 12 February 2023).
- Caramel, J. et al. (2013) 'A switch in the expression of embryonic EMT-inducers drives the development of malignant melanoma', *Cancer Cell*, 24(4), pp. 466–480. Available at: <https://doi.org/10.1016/j.ccr.2013.08.018>.

- Carcamo, S. et al. (2022) 'Altered BAF occupancy and transcription factor dynamics in PBAF-deficient melanoma', *Cell Reports*, 39(1), p. 110637. Available at: <https://doi.org/10.1016/j.celrep.2022.110637>.
- Carlino, M.S., Larkin, J. and Long, G.V. (2021) 'Immune checkpoint inhibitors in melanoma', *Lancet* (London, England), 398(10304), pp. 1002–1014. Available at: [https://doi.org/10.1016/S0140-6736\(21\)01206-X](https://doi.org/10.1016/S0140-6736(21)01206-X).
- Carninci, P. et al. (2006) 'Genome-wide analysis of mammalian promoter architecture and evolution', *Nature Genetics*, 38(6), pp. 626–635. Available at: <https://doi.org/10.1038/ng1789>.
- Carreira, S. et al. (2006) 'Mitf regulation of D1a1 controls melanoma proliferation and invasiveness', *Genes & Development*, 20(24), pp. 3426–3439. Available at: <https://doi.org/10.1101/gad.406406>.
- Carter, B. and Zhao, K. (2021) 'The epigenetic basis of cellular heterogeneity', *Nature Reviews Genetics*, 22(4), pp. 235–250. Available at: <https://doi.org/10.1038/s41576-020-00300-0>.
- Casey, S.C. et al. (2016) 'MYC regulates the antitumor immune response through CD47 and PD-L1', *Science*, 352(6282), pp. 227–231. Available at: <https://doi.org/10.1126/science.aac9935>.
- Castellano-Pellicena, I. et al. (2021) 'Melanin Distribution in Human Skin: Influence of Cytoskeletal, Polarity, and Centrosome-Related Machinery of Stratum basale Keratinocytes', *International Journal of Molecular Sciences*, 22(6), p. 3143. Available at: <https://doi.org/10.3390/ijms22063143>.
- Castro-Mondragon, J.A. et al. (2022) 'Cis-regulatory mutations associate with transcriptional and post-transcriptional deregulation of gene regulatory programs in cancers', *Nucleic Acids Research*, 50(21), pp. 12131–12148. Available at: <https://doi.org/10.1093/nar/gkac1143>.
- Cavallini, B. et al. (1988) 'A yeast activity can substitute for the HeLa cell TATA box factor', *Nature*, 334(6177), pp. 77–80. Available at: <https://doi.org/10.1038/334077a0>.
- cBioPortal for Cancer Genomics (no date). Available at: <http://www.cbioportal.org/> (Accessed: 12 February 2023).
- Centore, R.C. et al. (2020) 'Mammalian SWI/SNF Chromatin Remodeling Complexes: Emerging Mechanisms and Therapeutic Strategies', *Trends in Genetics*, 36(12), pp. 936–950. Available at: <https://doi.org/10.1016/j.tig.2020.07.011>.
- Cerezo, M. et al. (2018) 'Translational control of tumor immune escape via the eIF4F–STAT1–PD-L1 axis in melanoma', *Nature Medicine*, 24(12), pp. 1877–1886. Available at: <https://doi.org/10.1038/s41591-018-0217-1>.
- Cernilogar, F.M. et al. (2011) 'Chromatin-associated RNA interference components contribute to transcriptional regulation in *Drosophila*', *Nature*, 480(7377), pp. 391–395. Available at: <https://doi.org/10.1038/nature10492>.
- Cesi, G. et al. (2017) 'ROS production induced by BRAF inhibitor treatment rewires metabolic processes affecting cell growth of melanoma cells', *Molecular Cancer*, 16(1), p. 102. Available at: <https://doi.org/10.1186/s12943-017-0667-y>.
- Cesi, G. et al. (2018) 'A new ALK isoform transported by extracellular vesicles confers drug resistance to melanoma cells', *Molecular Cancer*, 17(1), p. 145. Available at: <https://doi.org/10.1186/s12943-018-0886-x>.
- Chacón, M. et al. (2020) 'Uncommon Subtypes of Malignant Melanomas: A Review Based on Clinical and Molecular Perspectives', *Cancers*, 12(9), p. 2362. Available at: <https://doi.org/10.3390/cancers12092362>.
- Chalkley, G.E. and Verrijzer, C.P. (1999) 'DNA binding site selection by RNA polymerase II TAFs: a TAF(II)250-TAF(II)150 complex recognizes the initiator', *The EMBO journal*, 18(17), pp. 4835–4845. Available at: <https://doi.org/10.1093/emboj/18.17.4835>.
- Chan, L.-C. et al. (2019) 'IL-6/JAK1 pathway drives PD-L1 Y112 phosphorylation to promote cancer immune evasion', *The Journal of Clinical Investigation*, 129(8), pp. 3324–3338. Available at: <https://doi.org/10.1172/JCI126022>.
- Chapman, A. et al. (2014) 'Heterogeneous Tumor Subpopulations Cooperate to Drive Invasion', *Cell Reports*, 8(3), pp. 688–695. Available at: <https://doi.org/10.1016/j.celrep.2014.06.045>.
- Chapman, P.B. et al. (2011) 'Improved survival with vemurafenib in melanoma with BRAF V600E mutation', *The New England Journal of Medicine*, 364(26), pp. 2507–2516. Available at: <https://doi.org/10.1056/NEJMoa1103782>.
- Chapuy, B. et al. (2013) 'Discovery and characterization of super-enhancer-associated dependencies in diffuse large B cell lymphoma', *Cancer Cell*, 24(6), pp. 777–790. Available at: <https://doi.org/10.1016/j.ccr.2013.11.003>.
- Chatterjee, S. and Ahituv, N. (2017) 'Gene Regulatory Elements, Major Drivers of Human Disease', *Annual Review of Genomics and Human Genetics*, 18(1), pp. 45–63. Available at: <https://doi.org/10.1146/annurev-genom-091416-035537>.
- Chauhan, J.S. et al. (2022) 'The MITF regulatory network in melanoma', *Pigment Cell & Melanoma Research*, 35(5), pp. 517–533. Available at: <https://doi.org/10.1111/pcmr.13053>.
- Cheli, Y. et al. (2010) 'Fifteen-year quest for microphthalmia-associated transcription factor target genes', *Pigment Cell & Melanoma Research*, 23(1), pp. 27–40. Available at: <https://doi.org/10.1111/j.1755-148X.2009.00653.x>.
- Cheli, Y. et al. (2012) 'Hypoxia and MITF control metastatic behaviour in mouse and human melanoma cells', *Oncogene*, 31(19), pp. 2461–2470. Available at: <https://doi.org/10.1038/onc.2011.425>.
- Cheli, Y. et al. (2021) 'ITGBL1 is a new immunomodulator that favors development of melanoma tumors by inhibiting natural killer cells cytotoxicity', *Molecular Cancer*, 20(1), p. 12. Available at: <https://doi.org/10.1186/s12943-020-01306-2>.

- Chen, A. and Koehler, A.N. (2020) 'Transcription Factor Inhibition: Lessons Learned and Emerging Targets', *Trends in molecular medicine*, 26(5), pp. 508–518. Available at: <https://doi.org/10.1016/j.molmed.2020.01.004>.
- Chen, D.S. and Mellman, I. (2013) 'Oncology meets immunology: the cancer-immunity cycle', *Immunity*, 39(1), pp. 1–10. Available at: <https://doi.org/10.1016/j.immuni.2013.07.012>.
- Chen, F., Gao, X. and Shilatifard, A. (2015) 'Stably paused genes revealed through inhibition of transcription initiation by the TFIID inhibitor triptolide', *Genes & Development*, 29(1), pp. 39–47. Available at: <https://doi.org/10.1101/gad.246173.114>.
- Chen, F.X., Smith, E.R. and Shilatifard, A. (2018) 'Born to run: control of transcription elongation by RNA polymerase II', *Nature Reviews Molecular Cell Biology*, 19(7), pp. 464–478. Available at: <https://doi.org/10.1038/s41580-018-0010-5>.
- Chen, G. et al. (2018) 'Exosomal PD-L1 contributes to immunosuppression and is associated with anti-PD-1 response', *Nature*, 560(7718), pp. 382–386. Available at: <https://doi.org/10.1038/s41586-018-0392-8>.
- Chen, H. et al. (2018) 'Dynamic interplay between enhancer–promoter topology and gene activity', *Nature Genetics*, 50(9), pp. 1296–1303. Available at: <https://doi.org/10.1038/s41588-018-0175-z>.
- Chen, K.G. et al. (2006) 'Melanosomal sequestration of cytotoxic drugs contributes to the intractability of malignant melanomas', *Proceedings of the National Academy of Sciences*, 103(26), pp. 9903–9907. Available at: <https://doi.org/10.1073/pnas.0600213103>.
- Chen, K.G. et al. (2009) 'Involvement of ABC Transporters in Melanogenesis and the Development of Multidrug Resistance of Melanoma', *Pigment cell & melanoma research*, 22(6), pp. 740–749. Available at: <https://doi.org/10.1111/j.1755-148X.2009.00630.x>.
- Chen, X., Qi, Y., et al. (2021) 'Structural insights into preinitiation complex assembly on core promoters', *Science*, 372(6541), p. eaba8490. Available at: <https://doi.org/10.1126/science.aba8490>.
- Chen, X., Yin, X., et al. (2021) 'Structures of the human Mediator and Mediator-bound preinitiation complex', *Science (New York, N.Y.)*, 372(6546), p. eabg0635. Available at: <https://doi.org/10.1126/science.abg0635>.
- Chen, Y. et al. (2020) 'Core transcriptional regulatory circuitries in cancer', *Oncogene*, 39(43), pp. 6633–6646. Available at: <https://doi.org/10.1038/s41388-020-01459-w>.
- Chen, Y.-Y. et al. (2022) 'Recognition of Melanocytes in Immuno-Neuroendocrinology and Circadian Rhythms: Beyond the Conventional Melanin Synthesis', *Cells*, 11(13), p. 2082. Available at: <https://doi.org/10.3390/cells11132082>.
- Cheng, P.F. et al. (2015) 'Methylation-dependent SOX9 expression mediates invasion in human melanoma cells and is a negative prognostic factor in advanced melanoma', *Genome Biology*, 16(1), p. 42. Available at: <https://doi.org/10.1186/s13059-015-0594-4>.
- Cheng, Z. et al. (2021) 'Cis-regulatory mutations with driver hallmarks in major cancers', *iScience*, 24(3), p. 102144. Available at: <https://doi.org/10.1016/j.isci.2021.102144>.
- Cheung, K.J. and Ewald, A.J. (2016) 'A collective route to metastasis: Seeding by tumor cell clusters', *Science (New York, N.Y.)*, 352(6282), pp. 167–169. Available at: <https://doi.org/10.1126/science.aaf6546>.
- Chiba, K. et al. (2017) 'Mutations in the promoter of the telomerase gene TERT contribute to tumorigenesis by a two-step mechanism', *Science (New York, N.Y.)*, 357(6358), pp. 1416–1420. Available at: <https://doi.org/10.1126/science.aao0535>.
- Chin, A.R. and Wang, S.E. (2016) 'Cancer Tills the Premetastatic Field: Mechanistic Basis and Clinical Implications', *Clinical Cancer Research*, 22(15), pp. 3725–3733. Available at: <https://doi.org/10.1158/1078-0432.CCR-16-0028>.
- Chipumuro, E. et al. (2014) 'CDK7 Inhibition Suppresses Super-Enhancer-Linked Oncogenic Transcription in MYCN-Driven Cancer', *Cell*, 159(5), pp. 1126–1139. Available at: <https://doi.org/10.1016/j.cell.2014.10.024>.
- Cho, E.-J. et al. (1997) 'mRNA capping enzyme is recruited to the transcription complex by phosphorylation of the RNA polymerase II carboxy-terminal domain', *Genes & Development*, 11(24), pp. 3319–3326.
- Cho, W.C., Jour, G. and Aung, P.P. (2019) 'Role of angiogenesis in melanoma progression: Update on key angiogenic mechanisms and other associated components', *Seminars in Cancer Biology*, 59, pp. 175–186. Available at: <https://doi.org/10.1016/j.semcancer.2019.06.015>.
- Cho, W.-K. et al. (2016) 'RNA Polymerase II cluster dynamics predict mRNA output in living cells', *eLife*, 5, p. e13617. Available at: <https://doi.org/10.7554/eLife.13617>.
- Cho, W.-K. et al. (2018) 'Mediator and RNA polymerase II clusters associate in transcription-dependent condensates', *Science*, 361(6400), pp. 412–415. Available at: <https://doi.org/10.1126/science.aar4199>.
- Chocarro, L. et al. (2022) 'Cutting-Edge: Preclinical and Clinical Development of the First Approved Lag-3 Inhibitor', *Cells*, 11(15), p. 2351. Available at: <https://doi.org/10.3390/cells11152351>.
- Chong, S. et al. (2018) 'Imaging dynamic and selective low-complexity domain interactions that control gene transcription', *Science*, 361(6400), p. eaar2555. Available at: <https://doi.org/10.1126/science.aar2555>.
- Chowell, D. et al. (2018) 'Patient HLA class I genotype influences cancer response to checkpoint blockade immunotherapy', *Science (New York, N.Y.)*, 359(6375), pp. 582–587. Available at: <https://doi.org/10.1126/science.aao4572>.
- Christensen, C.L. et al. (2014) 'Targeting Transcriptional Addictions in Small Cell Lung Cancer with a Covalent CDK7 Inhibitor', *Cancer Cell*, 26(6), pp. 909–922. Available at: <https://doi.org/10.1016/j.ccell.2014.10.019>.

- Ciążyńska, M. et al. (2021) 'The incidence and clinical analysis of non-melanoma skin cancer', *Scientific Reports*, 11(1), p. 4337. Available at: <https://doi.org/10.1038/s41598-021-83502-8>.
- Cidre-Aranaz, F. and Alonso, J. (2015) 'EWS/FLI1 Target Genes and Therapeutic Opportunities in Ewing Sarcoma', *Frontiers in Oncology*, 5. Available at: <https://www.frontiersin.org/articles/10.3389/fonc.2015.00162> (Accessed: 3 May 2023).
- Cirenajwis, H. et al. (2017) 'NF1-mutated melanoma tumors harbor distinct clinical and biological characteristics', *Molecular Oncology*, 11(4), pp. 438–451. Available at: <https://doi.org/10.1002/1878-0261.12050>.
- Cisowski, J. et al. (2016) 'Oncogene-induced senescence underlies the mutual exclusive nature of oncogenic KRAS and BRAF', *Oncogene*, 35(10), pp. 1328–1333. Available at: <https://doi.org/10.1038/onc.2015.186>.
- Cives, M. et al. (2020) 'Non-Melanoma Skin Cancers: Biological and Clinical Features', *International Journal of Molecular Sciences*, 21(15), p. 5394. Available at: <https://doi.org/10.3390/ijms21155394>.
- Claringbould, A. and Zaugg, J.B. (2021) 'Enhancers in disease: molecular basis and emerging treatment strategies', *Trends in Molecular Medicine*, 27(11), pp. 1060–1073. Available at: <https://doi.org/10.1016/j.molmed.2021.07.012>.
- Clark, C.A. et al. (2016) 'Tumor-Intrinsic PD-L1 Signals Regulate Cell Growth, Pathogenesis, and Autophagy in Ovarian Cancer and Melanoma', *Cancer Research*, 76(23), pp. 6964–6974. Available at: <https://doi.org/10.1158/0008-5472.CAN-16-0258>.
- Clark, W.H. et al. (1984) 'A study of tumor progression: the precursor lesions of superficial spreading and nodular melanoma', *Human Pathology*, 15(12), pp. 1147–1165. Available at: [https://doi.org/10.1016/s0046-8177\(84\)80310-x](https://doi.org/10.1016/s0046-8177(84)80310-x).
- Cleaver, J.E. (2008) 'Diagnosis of Xeroderma Pigmentosum and Related DNA Repair-Deficient Cutaneous Diseases', *Current medical literature. Dermatology*, 13(2), pp. 41–48.
- Coe, E.A. et al. (2019) 'The MITF-SOX10 regulated long non-coding RNA DIRC3 is a melanoma tumour suppressor', *PLoS genetics*, 15(12), p. e1008501. Available at: <https://doi.org/10.1371/journal.pgen.1008501>.
- Coin, F. et al. (1998) 'Mutations in the XPD helicase gene result in XP and TTD phenotypes, preventing interaction between XPD and the p44 subunit of TFIIH', *Nature Genetics*, 20(2), pp. 184–188. Available at: <https://doi.org/10.1038/2491>.
- Coin, F. et al. (1999) 'Mutations in XPB and XPD helicases found in xeroderma pigmentosum patients impair the transcription function of TFIIH', *The EMBO journal*, 18(5), pp. 1357–1366. Available at: <https://doi.org/10.1093/emboj/18.5.1357>.
- Coin, F. et al. (2004) 'Phosphorylation of XPB helicase regulates TFIIH nucleotide excision repair activity', *The EMBO journal*, 23(24), pp. 4835–4846. Available at: <https://doi.org/10.1038/sj.emboj.7600480>.
- Coin, F. et al. (2008) 'Nucleotide Excision Repair Driven by the Dissociation of CAK from TFIIH', *Molecular Cell*, 31(1), pp. 9–20. Available at: <https://doi.org/10.1016/j.molcel.2008.04.024>.
- Coin, F. and Egly, J.-M. (2015) 'Revisiting the Function of CDK7 in Transcription by Virtue of a Recently Described TFIIH Kinase Inhibitor', *Molecular Cell*, 59(4), pp. 513–514. Available at: <https://doi.org/10.1016/j.molcel.2015.08.006>.
- Coin, F., Oksenysh, V. and Egly, J.-M. (2007) 'Distinct roles for the XPB/p52 and XPD/p44 subcomplexes of TFIIH in damaged DNA opening during nucleotide excision repair', *Molecular Cell*, 26(2), pp. 245–256. Available at: <https://doi.org/10.1016/j.molcel.2007.03.009>.
- Colombo, S. et al. (2011) 'Classical and Nonclassical Melanocytes in Vertebrates', in *Melanins and Melanosomes*. John Wiley & Sons, Ltd, pp. 21–61. Available at: <https://doi.org/10.1002/9783527636150.ch2>.
- Colombo, S. et al. (2022) 'Stabilization of β -catenin promotes melanocyte specification at the expense of the Schwann cell lineage', *Development*, 149(2), p. dev194407. Available at: <https://doi.org/10.1242/dev.194407>.
- Compe, E. et al. (2005) 'Dysregulation of the peroxisome proliferator-activated receptor target genes by XPD mutations', *Molecular and Cellular Biology*, 25(14), pp. 6065–6076. Available at: <https://doi.org/10.1128/MCB.25.14.6065-6076.2005>.
- Compe, E. et al. (2007) 'Neurological defects in trichothiodystrophy reveal a coactivator function of TFIIH', *Nature Neuroscience*, 10(11), pp. 1414–1422. Available at: <https://doi.org/10.1038/nn1990>.
- Compe, E. et al. (2019) 'TFIIE orchestrates the recruitment of the TFIIH kinase module at promoter before release during transcription', *Nature Communications*, 10(1), p. 2084. Available at: <https://doi.org/10.1038/s41467-019-10131-1>.
- Compe, E. et al. (2022) 'Phosphorylation of XPD drives its mitotic role independently of its DNA repair and transcription functions', *Science Advances*, 8(33), p. eabp9457. Available at: <https://doi.org/10.1126/sciadv.abp9457>.
- Compe, E. and Egly, J.-M. (2012) 'TFIIH: when transcription met DNA repair', *Nature Reviews Molecular Cell Biology*, 13(6), p. 343. Available at: <https://doi.org/10.1038/nrm3350>.
- Compe, E. and Egly, J.-M. (2016) 'Nucleotide Excision Repair and Transcriptional Regulation: TFIIH and Beyond', *Annual Review of Biochemistry*, 85(1), pp. 265–290. Available at: <https://doi.org/10.1146/annurev-biochem-060815-014857>.
- Compe, E. and Egly, J.-M. (2021) 'The Long Road to Understanding RNAPII Transcription Initiation and Related Syndromes', *Annual Review of Biochemistry*, 90(1), pp. 193–219. Available at: <https://doi.org/10.1146/annurev-biochem-090220-112253>.
- Constantin, T.A. et al. (2022) 'Transcription associated cyclin-dependent kinases as therapeutic targets for prostate cancer', *Oncogene*, 41(24), pp. 3303–3315. Available at: <https://doi.org/10.1038/s41388-022-02347-1>.

- Cook, D.P. and Vanderhyden, B.C. (2020) 'Context specificity of the EMT transcriptional response', *Nature Communications*, 11(1), p. 2142. Available at: <https://doi.org/10.1038/s41467-020-16066-2>.
- Cooke, V.G. et al. (2012) 'Pericyte depletion results in hypoxia-associated epithelial-to-mesenchymal transition and metastasis mediated by met signaling pathway', *Cancer Cell*, 21(1), pp. 66–81. Available at: <https://doi.org/10.1016/j.ccr.2011.11.024>.
- Coppé, J.-P. et al. (2010) 'The Senescence-Associated Secretory Phenotype: The Dark Side of Tumor Suppression', *Annual review of pathology*, 5, pp. 99–118. Available at: <https://doi.org/10.1146/annurev-pathol-121808-102144>.
- Core, L. and Adelman, K. (2019) 'Promoter-proximal pausing of RNA polymerase II: a nexus of gene regulation', *Genes & Development*, 33(15–16), pp. 960–982. Available at: <https://doi.org/10.1101/gad.325142.119>.
- Core, L.J. et al. (2014) 'Analysis of nascent RNA identifies a unified architecture of initiation regions at mammalian promoters and enhancers', *Nature Genetics*, 46(12), pp. 1311–1320. Available at: <https://doi.org/10.1038/ng.3142>.
- Cortazar, M.A. et al. (2019) 'Control of RNA Pol II Speed by PNUTS-PP1 and Spt5 Dephosphorylation Facilitates Termination by a "Sitting Duck Torpedo" Mechanism', *Molecular Cell*, 76(6), pp. 896–908.e4. Available at: <https://doi.org/10.1016/j.molcel.2019.09.031>.
- Cossa, G. et al. (2021) 'Protein phosphatases in the RNAPII transcription cycle: erasers, sculptors, gatekeepers, and potential drug targets', *Genes & Development*, 35(9–10), pp. 658–676. Available at: <https://doi.org/10.1101/gad.348315.121>.
- Costanzo, F. et al. (2022) 'Promoters of ASCL1- and NEUROD1-dependent genes are specific targets of lurbicetectedin in SCLC cells', *EMBO molecular medicine*, 14(4), p. e14841. Available at: <https://doi.org/10.15252/emmm.202114841>.
- Couvillion, M. et al. (2022) 'Transcription elongation is finely tuned by dozens of regulatory factors', *eLife*. Edited by J.L. Workman, J.L. Manley, and J.L. Workman, 11, p. e78944. Available at: <https://doi.org/10.7554/eLife.78944>.
- Cramer, P. (2019) 'Organization and regulation of gene transcription', *Nature*, 573(7772), pp. 45–54. Available at: <https://doi.org/10.1038/s41586-019-1517-4>.
- Cremer, T. and Cremer, M. (2010) 'Chromosome territories', *Cold Spring Harbor Perspectives in Biology*, 2(3), p. a003889. Available at: <https://doi.org/10.1101/cshperspect.a003889>.
- Creyghton, M.P. et al. (2010) 'Histone H3K27ac separates active from poised enhancers and predicts developmental state', *Proceedings of the National Academy of Sciences*, 107(50), pp. 21931–21936. Available at: <https://doi.org/10.1073/pnas.1016071107>.
- Crosetto, N. and Bienko, M. (2020) 'Radial Organization in the Mammalian Nucleus', *Frontiers in Genetics*, 11, p. 33. Available at: <https://doi.org/10.3389/fgene.2020.00033>.
- Cui, R. et al. (2007) 'Central role of p53 in the suntan response and pathologic hyperpigmentation', *Cell*, 128(5), pp. 853–864. Available at: <https://doi.org/10.1016/j.cell.2006.12.045>.
- Curran, K. et al. (2010) 'Interplay between Foxd3 and Mitf regulates cell fate plasticity in the zebrafish neural crest', *Developmental Biology*, 344(1), pp. 107–118. Available at: <https://doi.org/10.1016/j.ydbio.2010.04.023>.
- Curti, B.D. and Faries, M.B. (2021) 'Recent Advances in the Treatment of Melanoma', *New England Journal of Medicine*. Edited by D.L. Longo, 384(23), pp. 2229–2240. Available at: <https://doi.org/10.1056/NEJMr2034861>.
- Curtin, J.A. et al. (2005) 'Distinct sets of genetic alterations in melanoma', *The New England Journal of Medicine*, 353(20), pp. 2135–2147. Available at: <https://doi.org/10.1056/NEJMoa050092>.
- Czudnochowski, N., Böskén, C.A. and Geyer, M. (2012) 'Serine-7 but not serine-5 phosphorylation primes RNA polymerase II CTD for P-TEFb recognition', *Nature Communications*, 3, p. 842. Available at: <https://doi.org/10.1038/ncomms1846>.
- Czyz, M. (2018) 'HGF/c-MET Signaling in Melanocytes and Melanoma', *International Journal of Molecular Sciences*, 19(12), p. 3844. Available at: <https://doi.org/10.3390/ijms19123844>.
- D'Alba, L. and Shawkey, M.D. (2019) 'Melanosomes: Biogenesis, Properties, and Evolution of an Ancient Organelle', *Physiological Reviews*, 99(1), pp. 1–19. Available at: <https://doi.org/10.1152/physrev.00059.2017>.
- D'Alessio, A.C. et al. (2015) 'A Systematic Approach to Identify Candidate Transcription Factors that Control Cell Identity', *Stem Cell Reports*, 5(5), pp. 763–775. Available at: <https://doi.org/10.1016/j.stemcr.2015.09.016>.
- Damsky, W. et al. (2015) 'mTORC1 Activation Blocks BrafV600E-Induced Growth Arrest but Is Insufficient for Melanoma Formation', *Cancer Cell*, 27(1), pp. 41–56. Available at: <https://doi.org/10.1016/j.ccell.2014.11.014>.
- Damsky, W.E. et al. (2011) 'β-catenin signaling controls metastasis in Braf-activated Pten-deficient melanomas', *Cancer Cell*, 20(6), pp. 741–754. Available at: <https://doi.org/10.1016/j.ccr.2011.10.030>.
- Damsky, W.E. and Bosenberg, M. (2017) 'Melanocytic nevi and melanoma: unraveling a complex relationship', *Oncogene*, 36(42), pp. 5771–5792. Available at: <https://doi.org/10.1038/onc.2017.189>.
- Damsky, W.E., Rosenbaum, L.E. and Bosenberg, M. (2010) 'Decoding Melanoma Metastasis', *Cancers*, 3(1), pp. 126–163. Available at: <https://doi.org/10.3390/cancers3010126>.
- Damsky, W.E., Theodosakis, N. and Bosenberg, M. (2014) 'Melanoma metastasis: new concepts and evolving paradigms', *Oncogene*, 33(19), pp. 2413–2422. Available at: <https://doi.org/10.1038/onc.2013.194>.
- Dang, C.V. (2012) 'MYC on the Path to Cancer', *Cell*, 149(1), pp. 22–35. Available at: <https://doi.org/10.1016/j.cell.2012.03.003>.

- Dankort, D. et al. (2009) 'BrafV600E cooperates with Pten loss to induce metastatic melanoma', *Nature Genetics*, 41(5), pp. 544–552. Available at: <https://doi.org/10.1038/ng.356>.
- Daoud, M. et al. (2022) 'XIAP promotes melanoma growth by inducing tumour neutrophil infiltration', *EMBO reports*, 23(6), p. e53608. Available at: <https://doi.org/10.15252/embr.202153608>.
- Dar, A.A. et al. (2011) 'miRNA-205 Suppresses Melanoma Cell Proliferation and Induces Senescence via Regulation of E2F1 Protein **', *Journal of Biological Chemistry*, 286(19), pp. 16606–16614. Available at: <https://doi.org/10.1074/jbc.M111.227611>.
- Darnell, J.E. (2002) 'Transcription factors as targets for cancer therapy', *Nature Reviews Cancer*, 2(10), pp. 740–749. Available at: <https://doi.org/10.1038/nrc906>.
- Das, A. et al. (2017) 'MMP proteolytic activity regulates cancer invasiveness by modulating integrins', *Scientific Reports*, 7(1), p. 14219. Available at: <https://doi.org/10.1038/s41598-017-14340-w>.
- Das, S.K., Lewis, B.A. and Levens, D. (2023) 'MYC: a complex problem', *Trends in Cell Biology*, 33(3), pp. 235–246. Available at: <https://doi.org/10.1016/j.tcb.2022.07.006>.
- Dasari, S. and Tchounwou, P.B. (2014) 'Cisplatin in cancer therapy: molecular mechanisms of action', *European journal of pharmacology*, 740, pp. 364–378. Available at: <https://doi.org/10.1016/j.ejphar.2014.07.025>.
- Davidson, L., Muniz, L. and West, S. (2014) '3' end formation of pre-mRNA and phosphorylation of Ser2 on the RNA polymerase II CTD are reciprocally coupled in human cells', *Genes & Development*, 28(4), pp. 342–356. Available at: <https://doi.org/10.1101/gad.231274.113>.
- Davies, H. et al. (2002) 'Mutations of the BRAF gene in human cancer', *Nature*, 417(6892), pp. 949–954. Available at: <https://doi.org/10.1038/nature00766>.
- Davies, M.A. (2012) 'The role of the PI3K-AKT pathway in melanoma', *Cancer Journal (Sudbury, Mass.)*, 18(2), pp. 142–147. Available at: <https://doi.org/10.1097/PPO.0b013e31824d448c>.
- Davison, B.L. et al. (1983) 'Formation of stable preinitiation complexes between eukaryotic class B transcription factors and promoter sequences', *Nature*, 301(5902), pp. 680–686. Available at: <https://doi.org/10.1038/301680a0>.
- De Blander, H. et al. (2021) 'Cellular Plasticity: A Route to Senescence Exit and Tumorigenesis', *Cancers*, 13(18), p. 4561. Available at: <https://doi.org/10.3390/cancers13184561>.
- De Palma, M., Biziato, D. and Petrova, T.V. (2017) 'Microenvironmental regulation of tumour angiogenesis', *Nature Reviews Cancer*, 17(8), pp. 457–474. Available at: <https://doi.org/10.1038/nrc.2017.51>.
- DeBerardinis, R.J. and Chandel, N.S. (2020) 'We need to talk about the Warburg effect', *Nature Metabolism*, 2(2), pp. 127–129. Available at: <https://doi.org/10.1038/s42255-020-0172-2>.
- Dekker, J. and Mirny, L. (2016) 'The 3D Genome as Moderator of Chromosomal Communication', *Cell*, 164(6), pp. 1110–1121. Available at: <https://doi.org/10.1016/j.cell.2016.02.007>.
- Dekker, J. and Misteli, T. (2015) 'Long-Range Chromatin Interactions', *Cold Spring Harbor Perspectives in Biology*, 7(10), p. a019356. Available at: <https://doi.org/10.1101/cshperspect.a019356>.
- Del Fiore, P. et al. (2021) 'Melanoma in Adolescents and Young Adults: Evaluation of the Characteristics, Treatment Strategies, and Prognostic Factors in a Monocentric Retrospective Study', *Frontiers in Oncology*, 11. Available at: <https://www.frontiersin.org/articles/10.3389/fonc.2021.725523> (Accessed: 10 February 2023).
- Deplancke, B., Alpern, D. and Gardeux, V. (2016) 'The Genetics of Transcription Factor DNA Binding Variation', *Cell*, 166(3), pp. 538–554. Available at: <https://doi.org/10.1016/j.cell.2016.07.012>.
- Deschamps, A. and Magder, S. (1990) 'Skin vascular bed is a potential blood reservoir during heat stress', *The American Journal of Physiology*, 259(6 Pt 2), pp. H1796–1802. Available at: <https://doi.org/10.1152/ajpheart.1990.259.6.H1796>.
- Dhall, A. and Chatterjee, C. (2011) 'Chemical approaches to understand the language of histone modifications', *ACS chemical biology*, 6(10), pp. 987–999. Available at: <https://doi.org/10.1021/cb200142c>.
- Dharanipragada, P. et al. (2023) 'Blocking Genomic Instability Prevents Acquired Resistance to MAPK Inhibitor Therapy in Melanoma', *Cancer Discovery*, pp. OF1–OF30. Available at: <https://doi.org/10.1158/2159-8290.CD-22-0787>.
- Di Micco, R. et al. (2021) 'Cellular senescence in ageing: from mechanisms to therapeutic opportunities', *Nature Reviews Molecular Cell Biology*, 22(2), pp. 75–95. Available at: <https://doi.org/10.1038/s41580-020-00314-w>.
- Di Nardo, M., Pallotta, M.M. and Musio, A. (2022) 'The multifaceted roles of cohesin in cancer', *Journal of Experimental & Clinical Cancer Research*, 41(1), p. 96. Available at: <https://doi.org/10.1186/s13046-022-02321-5>.
- Diazzi, S., Tartare-Deckert, S. and Deckert, M. (2020) 'Bad Neighborhood: Fibrotic Stroma as a New Player in Melanoma Resistance to Targeted Therapies', *Cancers*, 12(6), p. 1364. Available at: <https://doi.org/10.3390/cancers12061364>.
- Diazzi, S., Tartare-Deckert, S. and Deckert, M. (2023) 'The mechanical phenotypic plasticity of melanoma cell: an emerging driver of therapy cross-resistance', *Oncogenesis*, 12(1), pp. 1–7. Available at: <https://doi.org/10.1038/s41389-023-00452-8>.
- Dienemann, C. et al. (2019) 'Promoter Distortion and Opening in the RNA Polymerase II Cleft', *Molecular Cell*, 73(1), pp. 97–106.e4. Available at: <https://doi.org/10.1016/j.molcel.2018.10.014>.

- Diener, J. and Sommer, L. (2020) 'Reemergence of neural crest stem cell-like states in melanoma during disease progression and treatment', *Stem Cells Translational Medicine*, 10(4), pp. 522–533. Available at: <https://doi.org/10.1002/sctm.20-0351>.
- Dietrich, P. et al. (2018) 'Wild-type KRAS is a novel therapeutic target for melanoma contributing to primary and acquired resistance to BRAF inhibition', *Oncogene*, 37(7), pp. 897–911. Available at: <https://doi.org/10.1038/onc.2017.391>.
- Dignon, G.L., Best, R.B. and Mittal, J. (2020) 'Biomolecular Phase Separation: From Molecular Driving Forces to Macroscopic Properties', *Annual Review of Physical Chemistry*, 71(1), pp. 53–75. Available at: <https://doi.org/10.1146/annurev-physchem-071819-113553>.
- Ding, L. et al. (2014) 'Clonal architectures and driver mutations in metastatic melanomas', *PloS One*, 9(11), p. e111153. Available at: <https://doi.org/10.1371/journal.pone.0111153>.
- Ding, Q. et al. (2013) 'Discovery of RG7388, a Potent and Selective p53–MDM2 Inhibitor in Clinical Development', *Journal of Medicinal Chemistry*, 56(14), pp. 5979–5983. Available at: <https://doi.org/10.1021/jm400487c>.
- Dittmar, T. et al. (2008) 'Adhesion molecules and chemokines: the navigation system for circulating tumor (stem) cells to metastasize in an organ-specific manner', *Clinical & Experimental Metastasis*, 25(1), pp. 11–32. Available at: <https://doi.org/10.1007/s10585-007-9095-5>.
- Dixon, J.R. et al. (2012) 'Topological domains in mammalian genomes identified by analysis of chromatin interactions', *Nature*, 485(7398), pp. 376–380. Available at: <https://doi.org/10.1038/nature11082>.
- D'Mello, S.A.N. et al. (2016) 'Signaling Pathways in Melanogenesis', *International Journal of Molecular Sciences*, 17(7), p. 1144. Available at: <https://doi.org/10.3390/ijms17071144>.
- Dollinger, R. and Gilmour, D.S. (2021) 'Regulation of Promoter Proximal Pausing of RNA Polymerase II in Metazoans', *Journal of Molecular Biology*, 433(14), p. 166897. Available at: <https://doi.org/10.1016/j.jmb.2021.166897>.
- Domingues, B. et al. (2018) 'Melanoma treatment in review', *ImmunoTargets and Therapy*, Volume 7, pp. 35–49. Available at: <https://doi.org/10.2147/ITT.S134842>.
- Donati, B., Lorenzini, E. and Ciarrocchi, A. (2018) 'BRD4 and Cancer: going beyond transcriptional regulation', *Molecular Cancer*, 17(1), p. 164. Available at: <https://doi.org/10.1186/s12943-018-0915-9>.
- D'Orazio, J. et al. (2013) 'UV radiation and the skin', *International Journal of Molecular Sciences*, 14(6), pp. 12222–12248. Available at: <https://doi.org/10.3390/ijms140612222>.
- Doudican, N.A. and Orlow, S.J. (2017) 'Inhibition of the CRAF/prohibitin interaction reverses CRAF-dependent resistance to vemurafenib', *Oncogene*, 36(3), pp. 423–428. Available at: <https://doi.org/10.1038/onc.2016.214>.
- Douglass, S.M. et al. (2021) 'Myeloid-Derived Suppressor Cells Are a Major Source of Wnt5A in the Melanoma Microenvironment and Depend on Wnt5A for Full Suppressive Activity', *Cancer Research*, 81(3), pp. 658–670. Available at: <https://doi.org/10.1158/0008-5472.CAN-20-1238>.
- Drané, P. et al. (2004) 'Selective regulation of vitamin D receptor-responsive genes by TFIIH', *Molecular Cell*, 16(2), pp. 187–197. Available at: <https://doi.org/10.1016/j.molcel.2004.10.007>.
- Dratwa, M. et al. (2020) 'TERT—Regulation and Roles in Cancer Formation', *Frontiers in Immunology*, 11. Available at: <https://www.frontiersin.org/articles/10.3389/fimmu.2020.589929> (Accessed: 18 March 2023).
- Drier, Y. et al. (2016) 'An oncogenic MYB feedback loop drives alternate cell fates in adenoid cystic carcinoma', *Nature Genetics*, 48(3), pp. 265–272. Available at: <https://doi.org/10.1038/ng.3502>.
- Duan, Q. et al. (2020) 'Turning Cold into Hot: Firing up the Tumor Microenvironment', *Trends in Cancer*, 6(7), pp. 605–618. Available at: <https://doi.org/10.1016/j.trecan.2020.02.022>.
- Dubaele, S. et al. (2003) 'Basal transcription defect discriminates between xeroderma pigmentosum and trichothiodystrophy in XPD patients', *Molecular Cell*, 11(6), pp. 1635–1646. Available at: [https://doi.org/10.1016/s1097-2765\(03\)00182-5](https://doi.org/10.1016/s1097-2765(03)00182-5).
- Dueva, R. et al. (2019) 'Neutralization of the Positive Charges on Histone Tails by RNA Promotes an Open Chromatin Structure', *Cell Chemical Biology*, 26(10), pp. 1436–1449.e5. Available at: <https://doi.org/10.1016/j.chembiol.2019.08.002>.
- Duffy, D.L. et al. (2010) 'IRF4 variants have age-specific effects on nevus count and predispose to melanoma', *American Journal of Human Genetics*, 87(1), pp. 6–16. Available at: <https://doi.org/10.1016/j.ajhg.2010.05.017>.
- Duffy, K. and Grossman, D. (2012) 'The dysplastic nevus: From historical perspective to management in the modern era: Part I. Historical, histologic, and clinical aspects', *Journal of the American Academy of Dermatology*, 67(1), p. 1.e1–1.e16. Available at: <https://doi.org/10.1016/j.jaad.2012.02.047>.
- Dugo, M. et al. (2015) 'A melanoma subtype with intrinsic resistance to BRAF inhibition identified by receptor tyrosine kinases gene-driven classification', *Oncotarget*, 6(7), pp. 5118–5133. Available at: <https://doi.org/10.18632/oncotarget.3007>.
- Dummer, R. et al. (2017) 'Binimetinib versus dacarbazine in patients with advanced NRAS-mutant melanoma (NEMO): a multicentre, open-label, randomised, phase 3 trial', *The Lancet Oncology*, 18(4), pp. 435–445. Available at: [https://doi.org/10.1016/S1470-2045\(17\)30180-8](https://doi.org/10.1016/S1470-2045(17)30180-8).
- Dunn, G.P., Old, L.J. and Schreiber, R.D. (2004) 'The Immunobiology of Cancer Immunosurveillance and Immunoediting', *Immunity*, 21(2), pp. 137–148. Available at: <https://doi.org/10.1016/j.immuni.2004.07.017>.

- Dupin, E. et al. (2003) 'Reversal of developmental restrictions in neural crest lineages: Transition from Schwann cells to glial-melanocytic precursors in vitro', *Proceedings of the National Academy of Sciences*, 100(9), pp. 5229–5233. Available at: <https://doi.org/10.1073/pnas.0831229100>.
- Durbin, A.D. et al. (2018) 'Selective gene dependencies in MYCN-amplified neuroblastoma include the core transcriptional regulatory circuitry', *Nature Genetics*, 50(9), pp. 1240–1246. Available at: <https://doi.org/10.1038/s41588-018-0191-z>.
- Dzieran, J. et al. (2018) 'MYCN-amplified neuroblastoma maintains an aggressive and undifferentiated phenotype by deregulation of estrogen and NGF signaling', *Proceedings of the National Academy of Sciences*, 115(6), pp. E1229–E1238. Available at: <https://doi.org/10.1073/pnas.1710901115>.
- Eaton, J.D. et al. (2018) 'Xrn2 accelerates termination by RNA polymerase II, which is underpinned by CPSF73 activity', *Genes & Development*, 32(2), pp. 127–139. Available at: <https://doi.org/10.1101/gad.308528.117>.
- Eaton, J.D. et al. (2020) 'A unified allosteric/torpedo mechanism for transcriptional termination on human protein-coding genes', *Genes & Development*, 34(1–2), pp. 132–145. Available at: <https://doi.org/10.1101/gad.332833.119>.
- Eaton, J.D. and West, S. (2020) 'Termination of Transcription by RNA Polymerase II: BOOM!', *Trends in Genetics*, 36(9), pp. 664–675. Available at: <https://doi.org/10.1016/j.tig.2020.05.008>.
- Eddy, K. and Chen, S. (2020) 'Overcoming Immune Evasion in Melanoma', *International Journal of Molecular Sciences*, 21(23), p. 8984. Available at: <https://doi.org/10.3390/ijms21238984>.
- Eddy, K., Shah, R. and Chen, S. (2021) 'Decoding Melanoma Development and Progression: Identification of Therapeutic Vulnerabilities', *Frontiers in Oncology*, 10. Available at: <https://www.frontiersin.org/articles/10.3389/fonc.2020.626129> (Accessed: 14 February 2023).
- Eggermont, A.M.M. et al. (2019) 'Adjuvant ipilimumab versus placebo after complete resection of stage III melanoma: long-term follow-up results of the European Organisation for Research and Treatment of Cancer 18071 double-blind phase 3 randomised trial', *European Journal of Cancer*, 119, pp. 1–10. Available at: <https://doi.org/10.1016/j.ejca.2019.07.001>.
- Egly, J.-M. and Coin, F. (2011) 'A history of TFIIH: Two decades of molecular biology on a pivotal transcription/repair factor', *DNA Repair*, 10(7), pp. 714–721. Available at: <https://doi.org/10.1016/j.dnarep.2011.04.021>.
- Eick, D. (2018) 'Getting to grips with c-Myc', *eLife*, 7, p. e32010. Available at: <https://doi.org/10.7554/eLife.32010>.
- Eick, D. and Geyer, M. (2013) 'The RNA Polymerase II Carboxy-Terminal Domain (CTD) Code', *Chemical Reviews*, 113(11), pp. 8456–8490. Available at: <https://doi.org/10.1021/cr400071f>.
- El Rayes, T. et al. (2015) 'Lung inflammation promotes metastasis through neutrophil protease-mediated degradation of Tsp-1', *Proceedings of the National Academy of Sciences*, 112(52), pp. 16000–16005. Available at: <https://doi.org/10.1073/pnas.1507294112>.
- Elder, D.E. et al. (2020) 'The 2018 World Health Organization Classification of Cutaneous, Mucosal, and Uveal Melanoma: Detailed Analysis of 9 Distinct Subtypes Defined by Their Evolutionary Pathway', *Archives of Pathology & Laboratory Medicine*, 144(4), pp. 500–522. Available at: <https://doi.org/10.5858/arpa.2019-0561-RA>.
- Elia, I., Doglioni, G. and Fendt, S.-M. (2018) 'Metabolic Hallmarks of Metastasis Formation', *Trends in Cell Biology*, 28(8), pp. 673–684. Available at: <https://doi.org/10.1016/j.tcb.2018.04.002>.
- Eliades, P. et al. (2018) 'High MITF Expression Is Associated with Super-Enhancers and Suppressed by CDK7 Inhibition in Melanoma', *Journal of Investigative Dermatology*, 138(7), pp. 1582–1590. Available at: <https://doi.org/10.1016/j.jid.2017.09.056>.
- Elinav, E. et al. (2013) 'Inflammation-induced cancer: crosstalk between tumours, immune cells and microorganisms', *Nature Reviews Cancer*, 13(11), pp. 759–771. Available at: <https://doi.org/10.1038/nrc3611>.
- Elinav, E. et al. (2019) 'The cancer microbiome', *Nature Reviews. Cancer*, 19(7), pp. 371–376. Available at: <https://doi.org/10.1038/s41568-019-0155-3>.
- Elwood, J.M. and Gallagher, R.P. (1998) 'Body site distribution of cutaneous malignant melanoma in relationship to patterns of sun exposure', *International Journal of Cancer*, 78(3), pp. 276–280. Available at: [https://doi.org/10.1002/\(SICI\)1097-0215\(19981029\)78:3<276::AID-IJC2>3.0.CO;2-S](https://doi.org/10.1002/(SICI)1097-0215(19981029)78:3<276::AID-IJC2>3.0.CO;2-S).
- van Emmerik, C.L. and van Ingen, H. (2019) 'Unspinning chromatin: Revealing the dynamic nucleosome landscape by NMR', *Progress in Nuclear Magnetic Resonance Spectroscopy*, 110, pp. 1–19. Available at: <https://doi.org/10.1016/j.pnmrs.2019.01.002>.
- Emmons, M.F. et al. (2019) 'HDAC8 Regulates a Stress Response Pathway in Melanoma to Mediate Escape from BRAF Inhibitor Therapy', *Cancer Research*, 79(11), pp. 2947–2961. Available at: <https://doi.org/10.1158/0008-5472.CAN-19-0040>.
- Emran, T.B. et al. (2022) 'Multidrug Resistance in Cancer: Understanding Molecular Mechanisms, Immunoprevention and Therapeutic Approaches', *Frontiers in Oncology*, 12. Available at: <https://www.frontiersin.org/articles/10.3389/fonc.2022.891652> (Accessed: 6 April 2023).
- Ennen, M. et al. (2017) 'MITF -High and MITF -Low Cells and a Novel Subpopulation Expressing Genes of Both Cell States Contribute to Intra- and Intertumoral Heterogeneity of Primary Melanoma', *Clinical Cancer Research*, 23(22), pp. 7097–7107. Available at: <https://doi.org/10.1158/1078-0432.CCR-17-0010>.
- Erba, E. et al. (2001) 'Ecteinascidin-743 (ET-743), a natural marine compound, with a unique mechanism of action', *European Journal of Cancer*, 37(1), pp. 97–105. Available at: [https://doi.org/10.1016/S0959-8049\(00\)00357-9](https://doi.org/10.1016/S0959-8049(00)00357-9).

- Erickson, C.A. and Goins, T.L. (1995) 'Avian neural crest cells can migrate in the dorsolateral path only if they are specified as melanocytes', *Development*, 121(3), pp. 915–924. Available at: <https://doi.org/10.1242/dev.121.3.915>.
- Erkurt, M.A. et al. (2009) 'Nodular melanoma presenting with rapid progression and widespread metastases: a case report', *Journal of Medical Case Reports*, 3(1), p. 50. Available at: <https://doi.org/10.1186/1752-1947-3-50>.
- Ernfors, P. (2010) 'Cellular origin and developmental mechanisms during the formation of skin melanocytes', *Experimental Cell Research*, 316(8), pp. 1397–1407. Available at: <https://doi.org/10.1016/j.yexcr.2010.02.042>.
- Ernst, M. and Giubellino, A. (2022) 'The Current State of Treatment and Future Directions in Cutaneous Malignant Melanoma', *Biomedicines*, 10(4), p. 822. Available at: <https://doi.org/10.3390/biomedicines10040822>.
- Escors, D. (2014) 'Tumour immunogenicity, antigen presentation and immunological barriers in cancer immunotherapy', *New Journal of Science*, 2014, p. 734515. Available at: <https://doi.org/10.1155/2014/734515>.
- Eye Melanoma - Statistics (2023) Cancer.Net. Available at: <https://www.cancer.net/cancer-types/eye-melanoma/statistics> (Accessed: 16 February 2023).
- Eyles, J. et al. (2010) 'Tumor cells disseminate early, but immunosurveillance limits metastatic outgrowth, in a mouse model of melanoma', *The Journal of Clinical Investigation*, 120(6), pp. 2030–2039. Available at: <https://doi.org/10.1172/JCI42002>.
- Fabrega, C. et al. (2003) 'Structure of an mRNA capping enzyme bound to the phosphorylated carboxy-terminal domain of RNA polymerase II', *Molecular Cell*, 11(6), pp. 1549–1561. Available at: [https://doi.org/10.1016/s1097-2765\(03\)00187-4](https://doi.org/10.1016/s1097-2765(03)00187-4).
- Faget, D.V., Ren, Q. and Stewart, S.A. (2019) 'Unmasking senescence: context-dependent effects of SASP in cancer', *Nature Reviews Cancer*, 19(8), pp. 439–453. Available at: <https://doi.org/10.1038/s41568-019-0156-2>.
- Faghri, S. et al. (2008) 'Trichothiodystrophy: a systematic review of 112 published cases characterises a wide spectrum of clinical manifestations', *Journal of Medical Genetics*, 45(10), pp. 609–621. Available at: <https://doi.org/10.1136/jmg.2008.058743>.
- Fallahi-Sichani, M. et al. (2017) 'Adaptive resistance of melanoma cells to RAF inhibition via reversible induction of a slowly dividing de-differentiated state', *Molecular Systems Biology*, 13(1), p. 905. Available at: <https://doi.org/10.1525/msb.20166796>.
- Falletta, P. et al. (2017) 'Translation reprogramming is an evolutionarily conserved driver of phenotypic plasticity and therapeutic resistance in melanoma', *Genes & Development*, 31(1), pp. 18–33. Available at: <https://doi.org/10.1101/gad.290940.116>.
- Falletta, P., Goding, C.R. and Vivas-García, Y. (2022) 'Connecting Metabolic Rewiring With Phenotype Switching in Melanoma', *Frontiers in Cell and Developmental Biology*, 10. Available at: <https://www.frontiersin.org/articles/10.3389/fcell.2022.930250> (Accessed: 19 March 2023).
- Fan, Z. et al. (2020) 'CDK13 cooperates with CDK12 to control global RNA polymerase II processivity', *Science Advances*, 6(18), p. eaaz5041. Available at: <https://doi.org/10.1126/sciadv.aaz5041>.
- Fane, M.E. et al. (2019) 'BRN2, a POUerful driver of melanoma phenotype switching and metastasis', *Pigment Cell & Melanoma Research*, 32(1), pp. 9–24. Available at: <https://doi.org/10.1111/pcmr.12710>.
- Fane, M.E. et al. (2022) 'Stromal changes in the aged lung induce an emergence from melanoma dormancy', *Nature*, 606(7913), pp. 396–405. Available at: <https://doi.org/10.1038/s41586-022-04774-2>.
- Fanelli, M. et al. (2020) 'Cisplatin Resistance in Osteosarcoma: In vitro Validation of Candidate DNA Repair-Related Therapeutic Targets and Drugs for Tailored Treatments', *Frontiers in Oncology*, 10, p. 331. Available at: <https://doi.org/10.3389/fonc.2020.00331>.
- Fang, C. et al. (2020) 'Cancer-specific CTCF binding facilitates oncogenic transcriptional dysregulation', *Genome Biology*, 21(1), p. 247. Available at: <https://doi.org/10.1186/s13059-020-02152-7>.
- Fang, F. et al. (2022) 'Super-enhancer profiling identifies novel critical and targetable cancer survival gene LYL1 in pediatric acute myeloid leukemia', *Journal of experimental & clinical cancer research: CR*, 41(1), p. 225. Available at: <https://doi.org/10.1186/s13046-022-02428-9>.
- Fang, M. et al. (2013) 'MEN1 Is a Melanoma Tumor Suppressor That Preserves Genomic Integrity by Stimulating Transcription of Genes That Promote Homologous Recombination-Directed DNA Repair', *Molecular and Cellular Biology*, 33(13), pp. 2635–2647. Available at: <https://doi.org/10.1128/MCB.00167-13>.
- Farago, A.F. et al. (2019) 'ATLANTIS: a Phase III study of lurbinectedin/doxorubicin versus topotecan or cyclophosphamide/doxorubicin/vincristine in patients with small-cell lung cancer who have failed one prior platinum-containing line', *Future Oncology*, 15(3), pp. 231–239. Available at: <https://doi.org/10.2217/fon-2018-0597>.
- Faries, M.B. et al. (2017) 'Completion Dissection or Observation for Sentinel-Node Metastasis in Melanoma', *The New England Journal of Medicine*, 376(23), pp. 2211–2222. Available at: <https://doi.org/10.1056/NEJMoa1613210>.
- Fattore, L. et al. (2019) 'Single cell analysis to dissect molecular heterogeneity and disease evolution in metastatic melanoma', *Cell Death & Disease*, 10(11), pp. 1–12. Available at: <https://doi.org/10.1038/s41419-019-2048-5>.
- Faubert, B., Solmonson, A. and DeBerardinis, R.J. (2020) 'Metabolic reprogramming and cancer progression', *Science*, 368(6487), p. eaaw5473. Available at: <https://doi.org/10.1126/science.aaw5473>.
- Fazal, F.M. et al. (2015) 'Real-time observation of the initiation of RNA polymerase II transcription', *Nature*, 525(7568), pp. 274–277. Available at: <https://doi.org/10.1038/nature14882>.

- Feichtinger, R.G. et al. (2018) 'Melanoma tumors exhibit a variable but distinct metabolic signature', *Experimental Dermatology*, 27(2), pp. 204–207. Available at: <https://doi.org/10.1111/exd.13465>.
- Feichtinger, R.G. and Lang, R. (2019) 'Targeting L-Lactate Metabolism to Overcome Resistance to Immune Therapy of Melanoma and Other Tumor Entities', *Journal of Oncology*, 2019, p. 2084195. Available at: <https://doi.org/10.1155/2019/2084195>.
- Feige, E. et al. (2011) 'Hypoxia-induced transcriptional repression of the melanoma-associated oncogene MITF', *Proceedings of the National Academy of Sciences of the United States of America*, 108(43), pp. E924–933. Available at: <https://doi.org/10.1073/pnas.1106351108>.
- Feinberg, A.P. and Levchenko, A. (2023) 'Epigenetics as a mediator of plasticity in cancer', *Science*, 379(6632), p. eaaw3835. Available at: <https://doi.org/10.1126/science.aaw3835>.
- Felsenfeld, G. and Groudine, M. (2003) 'Controlling the double helix', *Nature*, 421(6921), pp. 448–453. Available at: <https://doi.org/10.1038/nature01411>.
- Felsher, D.W. (2008) 'Oncogene Addiction versus Oncogene Amnesia: Perhaps More than Just a Bad Habit?', *Cancer Research*, 68(9), pp. 3081–3086. Available at: <https://doi.org/10.1158/0008-5472.CAN-07-5832>.
- Feng, C. et al. (2023) 'Landscape and significance of human super enhancer-driven core transcription regulatory circuitry', *Molecular Therapy - Nucleic Acids*, 32, pp. 385–401. Available at: <https://doi.org/10.1016/j.omtn.2023.03.014>.
- Fenouil, R. et al. (2012) 'CpG islands and GC content dictate nucleosome depletion in a transcription-independent manner at mammalian promoters', *Genome Research*, 22(12), pp. 2399–2408. Available at: <https://doi.org/10.1101/gr.138776.112>.
- Ferguson, J. et al. (2017) 'Glucose availability controls ATF4-mediated MITF suppression to drive melanoma cell growth', *Oncotarget*, 8(20), pp. 32946–32959. Available at: <https://doi.org/10.18632/oncotarget.16514>.
- Fernández-Cortés, M., Delgado-Bellido, D. and Oliver, F.J. (2019) 'Vasculogenic Mimicry: Become an Endothelial Cell “But Not So Much”', *Frontiers in Oncology*, 9. Available at: <https://www.frontiersin.org/articles/10.3389/fonc.2019.00803> (Accessed: 10 March 2023).
- Fidler, I.J. et al. (1981) 'Demonstration of Multiple Phenotypic Diversity in a Murine Melanoma of Recent Origin²³⁴', *JNCI: Journal of the National Cancer Institute*, 67(4), pp. 947–956. Available at: <https://doi.org/10.1093/jnci/67.4.947>.
- Field, A. and Adelman, K. (2020) 'Evaluating Enhancer Function and Transcription', *Annual Review of Biochemistry*, 89, pp. 213–234. Available at: <https://doi.org/10.1146/annurev-biochem-011420-095916>.
- Filippakopoulos, P. et al. (2010) 'Selective inhibition of BET bromodomains', *Nature*, 468(7327), pp. 1067–1073. Available at: <https://doi.org/10.1038/nature09504>.
- Fillingham, J. and Greenblatt, J.F. (2008) 'A Histone Code for Chromatin Assembly', *Cell*, 134(2), pp. 206–208. Available at: <https://doi.org/10.1016/j.cell.2008.07.007>.
- Finn, L., Markovic, S.N. and Joseph, R.W. (2012) 'Therapy for metastatic melanoma: the past, present, and future', *BMC Medicine*, 10(1), p. 23. Available at: <https://doi.org/10.1186/1741-7015-10-23>.
- Fischer, G.M. et al. (2018) 'Metabolic strategies of melanoma cells: Mechanisms, interactions with the tumor microenvironment, and therapeutic implications', *Pigment Cell & Melanoma Research*, 31(1), pp. 11–30. Available at: <https://doi.org/10.1111/pcmr.12661>.
- Fischer, G.M. et al. (2019) 'Molecular Profiling Reveals Unique Immune and Metabolic Features of Melanoma Brain Metastases', *Cancer Discovery*, 9(5), pp. 628–645. Available at: <https://doi.org/10.1158/2159-8290.CD-18-1489>.
- Fishburn, J. et al. (2015) 'Double-stranded DNA translocase activity of transcription factor TFIID and the mechanism of RNA polymerase II open complex formation', *Proceedings of the National Academy of Sciences of the United States of America*, 112(13), pp. 3961–3966. Available at: <https://doi.org/10.1073/pnas.1417709112>.
- Fisher, R.P. (2005) 'Secrets of a double agent: CDK7 in cell-cycle control and transcription', *Journal of Cell Science*, 118(22), pp. 5171–5180. Available at: <https://doi.org/10.1242/jcs.02718>.
- Fisher, R.P. (2018) 'Cdk7: a kinase at the core of transcription and in the crosshairs of cancer drug discovery', *Transcription*, 10(2), pp. 47–56. Available at: <https://doi.org/10.1080/21541264.2018.1553483>.
- Flaherty, K.T. et al. (2012) 'Improved survival with MEK inhibition in BRAF-mutated melanoma', *The New England Journal of Medicine*, 367(2), pp. 107–114. Available at: <https://doi.org/10.1056/NEJMoa1203421>.
- Flavahan, W.A. et al. (2016) 'Insulator dysfunction and oncogene activation in IDH mutant gliomas', *Nature*, 529(7584), pp. 110–114. Available at: <https://doi.org/10.1038/nature16490>.
- Flavahan, W.A., Gaskell, E. and Bernstein, B.E. (2017) 'Epigenetic plasticity and the hallmarks of cancer', *Science (New York, N.Y.)*, 357(6348), p. eaal2380. Available at: <https://doi.org/10.1126/science.aal2380>.
- Flesher, J.L. et al. (2020) 'Delineating the role of MITF isoforms in pigmentation and tissue homeostasis', *Pigment Cell & Melanoma Research*, 33(2), pp. 279–292. Available at: <https://doi.org/10.1111/pcmr.12828>.
- Flores, G. and Grohar, P.J. (2021) 'One oncogene, several vulnerabilities: EWS/FLI targeted therapies for Ewing sarcoma', *Journal of Bone Oncology*, 31, p. 100404. Available at: <https://doi.org/10.1016/j.jbo.2021.100404>.
- Forgie, B.N., Prakash, R. and Telleria, C.M. (2022) 'Revisiting the Anti-Cancer Toxicity of Clinically Approved Platinating Derivatives', *International Journal of Molecular Sciences*, 23(23), p. 15410. Available at: <https://doi.org/10.3390/ijms232315410>.

- Fowler, J.C. et al. (2021) 'Selection of Oncogenic Mutant Clones in Normal Human Skin Varies with Body Site', *Cancer Discovery*, 11(2), pp. 340–361. Available at: <https://doi.org/10.1158/2159-8290.CD-20-1092>.
- Franceschi, C. et al. (2018) 'Inflammaging: a new immune–metabolic viewpoint for age-related diseases', *Nature Reviews Endocrinology*, 14(10), pp. 576–590. Available at: <https://doi.org/10.1038/s41574-018-0059-4>.
- Franco, H.L. and Kraus, W.L. (2015) 'No Driver behind the Wheel? Targeting Transcription in Cancer', *Cell*, 163(1), pp. 28–30. Available at: <https://doi.org/10.1016/j.cell.2015.09.013>.
- Frantz, W.T. and Ceol, C.J. (2021) 'Working together: Heterotypic clusters and collective cell migration in melanoma metastasis', *Developmental Cell*, 56(20), pp. 2783–2784. Available at: <https://doi.org/10.1016/j.devcel.2021.10.003>.
- Fraser, J. et al. (2015) 'Hierarchical folding and reorganization of chromosomes are linked to transcriptional changes in cellular differentiation', *Molecular Systems Biology*, 11(12), p. 852. Available at: <https://doi.org/10.15252/msb.20156492>.
- Fredriksson, N.J. et al. (2014) 'Systematic analysis of noncoding somatic mutations and gene expression alterations across 14 tumor types', *Nature Genetics*, 46(12), pp. 1258–1263. Available at: <https://doi.org/10.1038/ng.3141>.
- Fredriksson, N.J. et al. (2017) 'Recurrent promoter mutations in melanoma are defined by an extended context-specific mutational signature', *PLOS Genetics*, 13(5), p. e1006773. Available at: <https://doi.org/10.1371/journal.pgen.1006773>.
- Fuda, N.J., Ardehali, M.B. and Lis, J.T. (2009) 'Defining mechanisms that regulate RNA polymerase II transcription in vivo', *Nature*, 461(7261), pp. 186–192. Available at: <https://doi.org/10.1038/nature08449>.
- Fudenberg, G. et al. (2016) 'Formation of Chromosomal Domains by Loop Extrusion', *Cell Reports*, 15(9), pp. 2038–2049. Available at: <https://doi.org/10.1016/j.celrep.2016.04.085>.
- Fufa, T.D. et al. (2019) 'MEK inhibition remodels the active chromatin landscape and induces SOX10 genomic recruitment in BRAF(V600E) mutant melanoma cells', *Epigenetics & Chromatin*, 12(1), p. 50. Available at: <https://doi.org/10.1186/s13072-019-0297-2>.
- Fujinaga, K., Huang, F. and Peterlin, B.M. (2023) 'P-TEFb: The master regulator of transcription elongation', *Molecular Cell*, 83(3), pp. 393–403. Available at: <https://doi.org/10.1016/j.molcel.2022.12.006>.
- Fulbright, L.E., Ellermann, M. and Arthur, J.C. (2017) 'The microbiome and the hallmarks of cancer', *PLoS Pathogens*, 13(9), p. e1006480. Available at: <https://doi.org/10.1371/journal.ppat.1006480>.
- Fung, J.M.-W. et al. (2009) 'Identification and Characterization of a Novel Melanoma Tumor Suppressor Gene on Human Chromosome 6q21', *Clinical Cancer Research*, 15(3), pp. 797–803. Available at: <https://doi.org/10.1158/1078-0432.CCR-08-1472>.
- Gabay, M., Li, Y. and Felsher, D.W. (2014) 'MYC Activation Is a Hallmark of Cancer Initiation and Maintenance', *Cold Spring Harbor Perspectives in Medicine*, 4(6), p. a014241. Available at: <https://doi.org/10.1101/cshperspect.a014241>.
- Gadducci, A. and Cosio, S. (2022) 'Trabectedin and lurbectedin: Mechanisms of action, clinical impact, and future perspectives in uterine and soft tissue sarcoma, ovarian carcinoma, and endometrial carcinoma', *Frontiers in Oncology*, 12, p. 914342. Available at: <https://doi.org/10.3389/fonc.2022.914342>.
- Gajos-Michniewicz, A. and Czyz, M. (2020) 'WNT Signaling in Melanoma', *International Journal of Molecular Sciences*, 21(14), p. 4852. Available at: <https://doi.org/10.3390/ijms21144852>.
- Galli, G.G. et al. (2015) 'YAP Drives Growth by Controlling Transcriptional Pause Release from Dynamic Enhancers', *Molecular Cell*, 60(2), pp. 328–337. Available at: <https://doi.org/10.1016/j.molcel.2015.09.001>.
- Gallo, R.L. (2017) 'Human Skin Is the Largest Epithelial Surface for Interaction with Microbes', *The Journal of Investigative Dermatology*, 137(6), pp. 1213–1214. Available at: <https://doi.org/10.1016/j.jid.2016.11.045>.
- Gambi, G. et al. (2022) 'The LncRNA LENOX Interacts with RAP2C to Regulate Metabolism and Promote Resistance to MAPK Inhibition in Melanoma', *Cancer Research*, 82(24), pp. 4555–4570. Available at: <https://doi.org/10.1158/0008-5472.CAN-22-0959>.
- Gandini, S. et al. (2005) 'Meta-analysis of risk factors for cutaneous melanoma: I. Common and atypical naevi', *European Journal of Cancer*, 41(1), pp. 28–44. Available at: <https://doi.org/10.1016/j.ejca.2004.10.015>.
- García-Díaz, A. et al. (2017) 'Interferon Receptor Signaling Pathways Regulating PD-L1 and PD-L2 Expression', *Cell Reports*, 19(6), pp. 1189–1201. Available at: <https://doi.org/10.1016/j.celrep.2017.04.031>.
- García-Jiménez, C. and Goding, C.R. (2019) 'Starvation and Pseudo-Starvation as Drivers of Cancer Metastasis through Translation Reprogramming', *Cell Metabolism*, 29(2), pp. 254–267. Available at: <https://doi.org/10.1016/j.cmet.2018.11.018>.
- Garnock-Jones, K.P. (2015) 'Cobimetinib: First Global Approval', *Drugs*, 75(15), pp. 1823–1830. Available at: <https://doi.org/10.1007/s40265-015-0477-8>.
- Garraway, L.A. et al. (2005) 'Integrative genomic analyses identify MITF as a lineage survival oncogene amplified in malignant melanoma', *Nature*, 436(7047), pp. 117–122. Available at: <https://doi.org/10.1038/nature03664>.
- Gasque, P. and Jaffar-Bandjee, M.C. (2015) 'The immunology and inflammatory responses of human melanocytes in infectious diseases', *The Journal of Infection*, 71(4), pp. 413–421. Available at: <https://doi.org/10.1016/j.jinf.2015.06.006>.
- Gavish, A. et al. (2023) 'Hallmarks of transcriptional intratumour heterogeneity across a thousand tumours', *Nature*, pp. 1–9. Available at: <https://doi.org/10.1038/s41586-023-06130-4>.

- Gay, L.J. and Felding-Habermann, B. (2011) 'Contribution of platelets to tumour metastasis', *Nature Reviews Cancer*, 11(2), pp. 123–134. Available at: <https://doi.org/10.1038/nrc3004>.
- Geimer Le Lay, A.-S. et al. (2014) 'The Tumor Suppressor Ikaros Shapes the Repertoire of Notch Target Genes in T Cells', *Science Signaling*, 7(317), pp. ra28–ra28. Available at: <https://doi.org/10.1126/scisignal.2004545>.
- Gelato, K.A. et al. (2018) 'Super-enhancers define a proliferative PGC-1 α -expressing melanoma subgroup sensitive to BET inhibition', *Oncogene*, 37(4), pp. 512–521. Available at: <https://doi.org/10.1038/onc.2017.325>.
- Gelis, L. et al. (2016) 'Functional Characterization of the Odorant Receptor 51E2 in Human Melanocytes', *The Journal of Biological Chemistry*, 291(34), pp. 17772–17786. Available at: <https://doi.org/10.1074/jbc.M116.734517>.
- Gelmi, M.C. et al. (2022) 'MITF in Normal Melanocytes, Cutaneous and Uveal Melanoma: A Delicate Balance', *International Journal of Molecular Sciences*, 23(11), p. 6001. Available at: <https://doi.org/10.3390/ijms23116001>.
- Genes Robles, C.M. and Coin, F. (2019) 'Conducting the CTD orchestra', *Nature Chemical Biology*, 15(2), pp. 97–98. Available at: <https://doi.org/10.1038/s41589-018-0201-6>.
- Gerard, M. et al. (1991) 'Purification and interaction properties of the human RNA polymerase B(II) general transcription factor BTF2', *The Journal of Biological Chemistry*, 266(31), pp. 20940–20945.
- Ghiraldini, F.G., Filipescu, D. and Bernstein, E. (2021) 'Solid tumours hijack the histone variant network', *Nature Reviews Cancer*, 21(4), pp. 257–275. Available at: <https://doi.org/10.1038/s41568-020-00330-0>.
- Ghoneim, H.E. et al. (2017) 'De Novo Epigenetic Programs Inhibit PD-1 Blockade-Mediated T Cell Rejuvenation', *Cell*, 170(1), pp. 142–157.e19. Available at: <https://doi.org/10.1016/j.cell.2017.06.007>.
- Ghosh, K. and Capell, B.C. (2016) 'The Senescence-Associated Secretory Phenotype: Critical Effector in Skin Cancer and Aging', *The Journal of investigative dermatology*, 136(11), pp. 2133–2139. Available at: <https://doi.org/10.1016/j.jid.2016.06.621>.
- Giancotti, F.G. (2013) 'Mechanisms Governing Metastatic Dormancy and Reactivation', *Cell*, 155(4), pp. 750–764. Available at: <https://doi.org/10.1016/j.cell.2013.10.029>.
- Gibney, G.T. and Smalley, K.S.M. (2013) 'An unholy alliance: cooperation between BRAF and NF1 in melanoma development and BRAF inhibitor resistance', *Cancer Discovery*, 3(3), pp. 260–263. Available at: <https://doi.org/10.1158/2159-8290.CD-13-0017>.
- Gil-Bernabé, A.M. et al. (2012) 'Recruitment of monocytes/macrophages by tissue factor-mediated coagulation is essential for metastatic cell survival and premetastatic niche establishment in mice', *Blood*, 119(13), pp. 3164–3175. Available at: <https://doi.org/10.1182/blood-2011-08-376426>.
- Gillgren, P. et al. (2011) '2-cm versus 4-cm surgical excision margins for primary cutaneous melanoma thicker than 2 mm: a randomised, multicentre trial', *The Lancet*, 378(9803), pp. 1635–1642. Available at: [https://doi.org/10.1016/S0140-6736\(11\)61546-8](https://doi.org/10.1016/S0140-6736(11)61546-8).
- Gilmour, D.S. and Lis, J.T. (1986) 'RNA polymerase II interacts with the promoter region of the noninduced hsp70 gene in *Drosophila melanogaster* cells', *Molecular and Cellular Biology*, 6(11), pp. 3984–3989. Available at: <https://doi.org/10.1128/mcb.6.11.3984-3989.1986>.
- Girbig, M., Misiaszek, A.D. and Müller, C.W. (2022) 'Structural insights into nuclear transcription by eukaryotic DNA-dependent RNA polymerases', *Nature Reviews Molecular Cell Biology*, 23(9), pp. 603–622. Available at: <https://doi.org/10.1038/s41580-022-00476-9>.
- Glatz, K. et al. (2010) 'Frequent mitotic activity in banal melanocytic nevi uncovered by immunohistochemical analysis', *The American Journal of Dermatopathology*, 32(7), pp. 643–649. Available at: <https://doi.org/10.1097/DAD.0b013e3181d7ce6f>.
- Glover-Cutter, K. et al. (2009) 'TFIIH-associated Cdk7 kinase functions in phosphorylation of C-terminal domain Ser7 residues, promoter-proximal pausing, and termination by RNA polymerase II', *Molecular and Cellular Biology*, 29(20), pp. 5455–5464. Available at: <https://doi.org/10.1128/MCB.00637-09>.
- Glyde, R. et al. (2017) 'Structures of RNA Polymerase Closed and Intermediate Complexes Reveal Mechanisms of DNA Opening and Transcription Initiation', *Molecular Cell*, 67(1), pp. 106–116.e4. Available at: <https://doi.org/10.1016/j.molcel.2017.05.010>.
- Gobeil, S. et al. (2008) 'A genome-wide shRNA screen identifies GAS1 as a novel melanoma metastasis suppressor gene', *Genes & Development*, 22(21), pp. 2932–2940. Available at: <https://doi.org/10.1101/gad.1714608>.
- Goding, C.R. and Arnheiter, H. (2019) 'MITF-the first 25 years', *Genes & Development*, 33(15–16), pp. 983–1007. Available at: <https://doi.org/10.1101/gad.324657.119>.
- Goel, V.K. et al. (2006) 'Examination of Mutations in BRAF, NRAS, and PTEN in Primary Cutaneous Melanoma', *Journal of Investigative Dermatology*, 126(1), pp. 154–160. Available at: <https://doi.org/10.1038/sj.jid.5700026>.
- Golan, T. et al. (2015) 'Interactions of Melanoma Cells with Distal Keratinocytes Trigger Metastasis via Notch Signaling Inhibition of MITF', *Molecular Cell*, 59(4), pp. 664–676. Available at: <https://doi.org/10.1016/j.molcel.2015.06.028>.
- Golan, T. et al. (2019) 'Adipocytes sensitize melanoma cells to environmental TGF- β cues by repressing the expression of miR-211', *Science Signaling*, 12(591), p. eaav6847. Available at: <https://doi.org/10.1126/scisignal.aav6847>.
- Gonda, T.J. and Ramsay, R.G. (2015) 'Directly targeting transcriptional dysregulation in cancer', *Nature Reviews Cancer*, 15(11), pp. 686–694. Available at: <https://doi.org/10.1038/nrc4018>.
- Gopalakrishnan, V. et al. (2018) 'Gut microbiome modulates response to anti-PD-1 immunotherapy in melanoma patients', *Science (New York, N.Y.)*, 359(6371), pp. 97–103. Available at: <https://doi.org/10.1126/science.aan4236>.

- Gorgoulis, V.G. et al. (2005) 'Activation of the DNA damage checkpoint and genomic instability in human precancerous lesions', *Nature*, 434(7035), pp. 907–913. Available at: <https://doi.org/10.1038/nature03485>.
- Gould, J. (2018) 'Superpowered skin', *Nature*, 563(7732), pp. S84–S85. Available at: <https://doi.org/10.1038/d41586-018-07429-3>.
- Grasso, C.S. et al. (2020) 'Conserved Interferon- γ Signaling Drives Clinical Response to Immune Checkpoint Blockade Therapy in Melanoma', *Cancer Cell*, 38(4), pp. 500–515.e3. Available at: <https://doi.org/10.1016/j.ccell.2020.08.005>.
- Green, S.A., Simoes-Costa, M. and Bronner, M.E. (2015) 'Evolution of vertebrates as viewed from the crest', *Nature*, 520(7548), pp. 474–482. Available at: <https://doi.org/10.1038/nature14436>.
- Gressel, S., Schwab, B. and Cramer, P. (2019) 'The pause-initiation limit restricts transcription activation in human cells', *Nature Communications*, 10(1), p. 3603. Available at: <https://doi.org/10.1038/s41467-019-11536-8>.
- Greten, F.R. and Grivnenkov, S.I. (2019) 'Inflammation and Cancer: Triggers, Mechanisms, and Consequences', *Immunity*, 51(1), pp. 27–41. Available at: <https://doi.org/10.1016/j.immuni.2019.06.025>.
- Griffin, M. et al. (2017) 'BRAF inhibitors: resistance and the promise of combination treatments for melanoma', *Oncotarget*, 8(44), pp. 78174–78192. Available at: <https://doi.org/10.18632/oncotarget.19836>.
- Griss, J. et al. (2019) 'B cells sustain inflammation and predict response to immune checkpoint blockade in human melanoma', *Nature Communications*, 10(1), p. 4186. Available at: <https://doi.org/10.1038/s41467-019-12160-2>.
- Gröschel, S. et al. (2014) 'A Single Oncogenic Enhancer Rearrangement Causes Concomitant EVI1 and GATA2 Deregulation in Leukemia', *Cell*, 157(2), pp. 369–381. Available at: <https://doi.org/10.1016/j.cell.2014.02.019>.
- Grosveld, F., van Staaldin, J. and Stadhouders, R. (2021) 'Transcriptional Regulation by (Super)Enhancers: From Discovery to Mechanisms', *Annual Review of Genomics and Human Genetics*, 22(1), pp. 127–146. Available at: <https://doi.org/10.1146/annurev-genom-122220-093818>.
- Grünberg, S., Warfield, L. and Hahn, S. (2012) 'Architecture of the RNA polymerase II preinitiation complex and mechanism of ATP-dependent promoter opening', *Nature Structural & Molecular Biology*, 19(8), pp. 788–796. Available at: <https://doi.org/10.1038/nsmb.2334>.
- Grüner, B.M. and Fendt, S.-M. (2020) 'Cancer cells stock up in lymph vessels to survive', *Nature*, 585(7823), pp. 36–37. Available at: <https://doi.org/10.1038/d41586-020-02383-5>.
- Gruosso, T. et al. (2015) 'MAP3K8/TPL-2/COT is a potential predictive marker for MEK inhibitor treatment in high-grade serous ovarian carcinomas', *Nature Communications*, 6(1), p. 8583. Available at: <https://doi.org/10.1038/ncomms9583>.
- Grzywa, T.M., Paskal, W. and Włodarski, P.K. (2017) 'Intratumor and Intertumor Heterogeneity in Melanoma', *Translational Oncology*, 10(6), pp. 956–975. Available at: <https://doi.org/10.1016/j.tranon.2017.09.007>.
- Guan, J., Gupta, R. and Filipp, F.V. (2015) 'Cancer systems biology of TCGA SKCM: efficient detection of genomic drivers in melanoma', *Scientific Reports*, 5, p. 7857. Available at: <https://doi.org/10.1038/srep07857>.
- Gubin, M.M. and Vesely, M.D. (2022) 'Cancer Immunoediting in the Era of Immuno-oncology', *Clinical Cancer Research*, 28(18), pp. 3917–3928. Available at: <https://doi.org/10.1158/1078-0432.CCR-21-1804>.
- Gudjohnsen, S.A.H. et al. (2015) 'Meningeal Melanocytes in the Mouse: Distribution and Dependence on Mitf', *Frontiers in Neuroanatomy*, 9. Available at: <https://www.frontiersin.org/articles/10.3389/fnana.2015.00149> (Accessed: 29 January 2023).
- Guerry, D. et al. (1993) 'Lessons from tumor progression: the invasive radial growth phase of melanoma is common, incapable of metastasis, and indolent', *The Journal of Investigative Dermatology*, 100(3), pp. 342S–345S. Available at: <https://doi.org/10.1111/1523-1747.ep12470248>.
- Gunnell, A. et al. (2016) 'RUNX super-enhancer control through the Notch pathway by Epstein-Barr virus transcription factors regulates B cell growth', *Nucleic Acids Research*, 44(10), pp. 4636–4650. Available at: <https://doi.org/10.1093/nar/gkw085>.
- Guo, W., Wang, H. and Li, C. (2021) 'Signal pathways of melanoma and targeted therapy', *Signal Transduction and Targeted Therapy*, 6(1), pp. 1–39. Available at: <https://doi.org/10.1038/s41392-021-00827-6>.
- Guo, Y. et al. (2022) 'TERT Promoter Mutations and Telomerase in Melanoma', *Journal of Oncology*, 2022, p. 6300329. Available at: <https://doi.org/10.1155/2022/6300329>.
- Guo, Y.A. et al. (2018) 'Mutation hotspots at CTCF binding sites coupled to chromosomal instability in gastrointestinal cancers', *Nature Communications*, 9(1), p. 1520. Available at: <https://doi.org/10.1038/s41467-018-03828-2>.
- Guo, Y.E. et al. (2019) 'Pol II phosphorylation regulates a switch between transcriptional and splicing condensates', *Nature*, 572(7770), pp. 543–548. Available at: <https://doi.org/10.1038/s41586-019-1464-0>.
- Güvenç, C. et al. (2021) 'Bona Fide Tumor Suppressor Genes Hypermethylated in Melanoma: A Narrative Review', *International Journal of Molecular Sciences*, 22(19), p. 10674. Available at: <https://doi.org/10.3390/ijms221910674>.
- Guzder, S.N. et al. (1994) 'RAD25 is a DNA helicase required for DNA repair and RNA polymerase II transcription', *Nature*, 369(6481), pp. 578–581. Available at: <https://doi.org/10.1038/369578a0>.
- Ha, L. et al. (2007) 'ARF functions as a melanoma tumor suppressor by inducing p53-independent senescence', *Proceedings of the National Academy of Sciences*, 104(26), pp. 10968–10973. Available at: <https://doi.org/10.1073/pnas.0611638104>.

- Haas, L. et al. (2021) 'Acquired resistance to anti-MAPK targeted therapy confers an immune-evasive tumour microenvironment and cross-resistance to immunotherapy in melanoma', *Nature cancer*, 2(7), pp. 693–708. Available at: <https://doi.org/10.1038/s43018-021-00221-9>.
- Haass, N.K. et al. (2005) 'Adhesion, migration and communication in melanocytes and melanoma', *Pigment Cell Research*, 18(3), pp. 150–159. Available at: <https://doi.org/10.1111/j.1600-0749.2005.00235.x>.
- Haberle, V. and Stark, A. (2018) 'Eukaryotic core promoters and the functional basis of transcription initiation', *Nature Reviews Molecular Cell Biology*, 19(10), pp. 621–637. Available at: <https://doi.org/10.1038/s41580-018-0028-8>.
- Hall, B.J. and LeBoit, P.E. (2014) 'Suprabasal Spread of Melanocytes in Dysplastic Nevi and Melanoma In Situ: Ki-67-labeling Rate of Junctional Melanocytes and Suprabasal Cells May Be a Helpful Clue to the Diagnosis', *The American Journal of Surgical Pathology*, 38(8), p. 1111. Available at: <https://doi.org/10.1097/PAS.0000000000000224>.
- Halling-Overgaard, A.-S. et al. (2017) 'Skin absorption through atopic dermatitis skin: a systematic review', *The British Journal of Dermatology*, 177(1), pp. 84–106. Available at: <https://doi.org/10.1111/bjd.15065>.
- Hamm, M. et al. (2021) 'BRN2 is a non-canonical melanoma tumor-suppressor', *Nature Communications*, 12(1), p. 3707. Available at: <https://doi.org/10.1038/s41467-021-23973-5>.
- Hanahan, D. (2022) 'Hallmarks of Cancer: New Dimensions', *Cancer Discovery*, 12(1), pp. 31–46. Available at: <https://doi.org/10.1158/2159-8290.CD-21-1059>.
- Hanahan, D. and Weinberg, R.A. (2000) 'The Hallmarks of Cancer', *Cell*, 100(1), pp. 57–70. Available at: [https://doi.org/10.1016/S0092-8674\(00\)81683-9](https://doi.org/10.1016/S0092-8674(00)81683-9).
- Hanahan, D. and Weinberg, R.A. (2011) 'Hallmarks of Cancer: The Next Generation', *Cell*, 144(5), pp. 646–674. Available at: <https://doi.org/10.1016/j.cell.2011.02.013>.
- Hanvesakul, R. et al. (2023) 'Indirect treatment comparison of lurbinectedin versus other second-line treatments for small-cell lung cancer', *Journal of Comparative Effectiveness Research*, 12(5), p. e220098. Available at: <https://doi.org/10.57264/ceer-2022-0098>.
- Hao, L. et al. (2012) 'Cadherin switch from E- to N-cadherin in melanoma progression is regulated by the PI3K/PTEN pathway through Twist and Snail', *The British Journal of Dermatology*, 166(6), pp. 1184–1197. Available at: <https://doi.org/10.1111/j.1365-2133.2012.10824.x>.
- Haq, R. et al. (2013) 'Oncogenic BRAF Regulates Oxidative Metabolism via PGC1 α and MITF', *Cancer Cell*, 23(3), pp. 302–315. Available at: <https://doi.org/10.1016/j.ccr.2013.02.003>.
- Harbst, K. et al. (2016) 'Multiregion Whole-Exome Sequencing Uncovers the Genetic Evolution and Mutational Heterogeneity of Early-Stage Metastatic Melanoma', *Cancer Research*, 76(16), pp. 4765–4774. Available at: <https://doi.org/10.1158/0008-5472.CAN-15-3476>.
- Harlen, K.M. and Churchman, L.S. (2017) 'The code and beyond: transcription regulation by the RNA polymerase II carboxy-terminal domain', *Nature Reviews Molecular Cell Biology*, 18(4), pp. 263–273. Available at: <https://doi.org/10.1038/nrm.2017.10>.
- Harlow, M.L. et al. (2016) 'Lurbinectedin Inactivates the Ewing Sarcoma Oncoprotein EWS-FLI1 by Redistributing It within the Nucleus', *Cancer Research*, 76(22), pp. 6657–6668. Available at: <https://doi.org/10.1158/0008-5472.CAN-16-0568>.
- Hartley, G.P. et al. (2018) 'Programmed Cell Death Ligand 1 (PD-L1) Signaling Regulates Macrophage Proliferation and Activation', *Cancer Immunology Research*, 6(10), pp. 1260–1273. Available at: <https://doi.org/10.1158/2326-6066.CIR-17-0537>.
- Hartman, M.L. (2020) 'Non-Apoptotic Cell Death Signaling Pathways in Melanoma', *International Journal of Molecular Sciences*, 21(8), p. 2980. Available at: <https://doi.org/10.3390/ijms21082980>.
- Hartman, M.L. and Czyz, M. (2015) 'MITF in melanoma: mechanisms behind its expression and activity', *Cellular and molecular life sciences: CMLS*, 72(7), pp. 1249–1260. Available at: <https://doi.org/10.1007/s00018-014-1791-0>.
- Hartsough, E., Shao, Y. and Aplin, A.E. (2014) 'Resistance to RAF inhibitors revisited', *The Journal of Investigative Dermatology*, 134(2), pp. 319–325. Available at: <https://doi.org/10.1038/jid.2013.358>.
- Hasanau, T. et al. (2022) 'Detection of TERT Promoter Mutations as a Prognostic Biomarker in Gliomas: Methodology, Prospects, and Advances', *Biomedicines*, 10(3), p. 728. Available at: <https://doi.org/10.3390/biomedicines10030728>.
- Hatzivassiliou, G. et al. (2010) 'RAF inhibitors prime wild-type RAF to activate the MAPK pathway and enhance growth', *Nature*, 464(7287), pp. 431–435. Available at: <https://doi.org/10.1038/nature08833>.
- Hauschild, A. et al. (2012) 'Dabrafenib in BRAF-mutated metastatic melanoma: a multicentre, open-label, phase 3 randomised controlled trial', *Lancet (London, England)*, 380(9839), pp. 358–365. Available at: [https://doi.org/10.1016/S0140-6736\(12\)60868-X](https://doi.org/10.1016/S0140-6736(12)60868-X).
- Hay, D. et al. (2016) 'Genetic dissection of the α -globin super-enhancer in vivo', *Nature Genetics*, 48(8), pp. 895–903. Available at: <https://doi.org/10.1038/ng.3605>.
- Hayward, N.K. et al. (2017) 'Whole-genome landscapes of major melanoma subtypes', *Nature*, 545(7653), pp. 175–180. Available at: <https://doi.org/10.1038/nature22071>.
- He, Q.-L. et al. (2015) 'Covalent Modification of a Cysteine Residue in the XPB Subunit of the General Transcription Factor TFIID Through Single Epoxide Cleavage of the Transcription Inhibitor Triptolide', *Angewandte Chemie (International ed. in English)*, 54(6), pp. 1859–1863. Available at: <https://doi.org/10.1002/anie.201408817>.
- He, Y. et al. (2016) 'Near-atomic resolution visualization of human transcription promoter opening', *Nature*, 533(7603), pp. 359–365. Available at: <https://doi.org/10.1038/nature17970>.

- Heizmann, B., Kastner, P. and Chan, S. (2018) 'The Ikaros family in lymphocyte development', *Current Opinion in Immunology*, 51, pp. 14–23. Available at: <https://doi.org/10.1016/j.coi.2017.11.005>.
- Hendrix, M.J.C. et al. (2003) 'Vasculogenic mimicry and tumour-cell plasticity: lessons from melanoma', *Nature Reviews Cancer*, 3(6), pp. 411–421. Available at: <https://doi.org/10.1038/nrc1092>.
- Hernando, B. et al. (2021) 'The effect of age on the acquisition and selection of cancer driver mutations in sun-exposed normal skin', *Annals of Oncology*, 32(3), pp. 412–421. Available at: <https://doi.org/10.1016/j.annonc.2020.11.023>.
- Hibino, S. et al. (2021) 'Inflammation-Induced Tumorigenesis and Metastasis', *International Journal of Molecular Sciences*, 22(11), p. 5421. Available at: <https://doi.org/10.3390/ijms22115421>.
- Hida, T. et al. (2020) 'Elucidation of Melanogenesis Cascade for Identifying Pathophysiology and Therapeutic Approach of Pigmentary Disorders and Melanoma', *International Journal of Molecular Sciences*, 21(17), p. 6129. Available at: <https://doi.org/10.3390/ijms21176129>.
- Hill, C.H. et al. (2019) 'Activation of the Endonuclease that Defines mRNA 3' Ends Requires Incorporation into an 8-Subunit Core Cleavage and Polyadenylation Factor Complex', *Molecular Cell*, 73(6), pp. 1217–1231.e11. Available at: <https://doi.org/10.1016/j.molcel.2018.12.023>.
- Hinohara, K. and Polyak, K. (2019) 'Intratumoral Heterogeneity: More Than Just Mutations', *Trends in Cell Biology*, 29(7), pp. 569–579. Available at: <https://doi.org/10.1016/j.tcb.2019.03.003>.
- Hnisz, D. et al. (2013) 'Super-Enhancers in the Control of Cell Identity and Disease', *Cell*, 155(4), pp. 934–947. Available at: <https://doi.org/10.1016/j.cell.2013.09.053>.
- Hnisz, D. et al. (2015) 'Convergence of developmental and oncogenic signaling pathways at transcriptional super-enhancers', *Molecular Cell*, 58(2), pp. 362–370. Available at: <https://doi.org/10.1016/j.molcel.2015.02.014>.
- Hnisz, D. et al. (2016) 'Activation of proto-oncogenes by disruption of chromosome neighborhoods', *Science (New York, N.Y.)*, 351(6280), pp. 1454–1458. Available at: <https://doi.org/10.1126/science.aad9024>.
- Hnisz, D. et al. (2017) 'A Phase Separation Model for Transcriptional Control', *Cell*, 169(1), pp. 13–23. Available at: <https://doi.org/10.1016/j.cell.2017.02.007>.
- Hodgkinson, C.A. et al. (1993) 'Mutations at the mouse microphthalmia locus are associated with defects in a gene encoding a novel basic-helix-loop-helix-zipper protein', *Cell*, 74(2), pp. 395–404. Available at: [https://doi.org/10.1016/0092-8674\(93\)90429-t](https://doi.org/10.1016/0092-8674(93)90429-t).
- Hodi, F.S. et al. (2010) 'Improved survival with ipilimumab in patients with metastatic melanoma', *The New England Journal of Medicine*, 363(8), pp. 711–723. Available at: <https://doi.org/10.1056/NEJMoa1003466>.
- Hodi, F.S. et al. (2018) 'Nivolumab plus ipilimumab or nivolumab alone versus ipilimumab alone in advanced melanoma (CheckMate 067): 4-year outcomes of a multicentre, randomised, phase 3 trial', *The Lancet Oncology*, 19(11), pp. 1480–1492. Available at: [https://doi.org/10.1016/S1470-2045\(18\)30700-9](https://doi.org/10.1016/S1470-2045(18)30700-9).
- Hodis, E. et al. (2012) 'A landscape of driver mutations in melanoma', *Cell*, 150(2), pp. 251–263. Available at: <https://doi.org/10.1016/j.cell.2012.06.024>.
- Hodis, E. et al. (2022) 'Stepwise-edited, human melanoma models reveal mutations' effect on tumor and microenvironment', *Science*, 376(6592), p. eabi8175. Available at: <https://doi.org/10.1126/science.abi8175>.
- Hoek, K.S. et al. (2006) 'Metastatic potential of melanomas defined by specific gene expression profiles with no BRAF signature', *Pigment Cell Research*, 19(4), pp. 290–302. Available at: <https://doi.org/10.1111/j.1600-0749.2006.00322.x>.
- Hoek, K.S. et al. (2008) 'In vivo switching of human melanoma cells between proliferative and invasive states', *Cancer Research*, 68(3), pp. 650–656. Available at: <https://doi.org/10.1158/0008-5472.CAN-07-2491>.
- Hoek, K.S. and Goding, C.R. (2010) 'Cancer stem cells versus phenotype-switching in melanoma: Phenotype-switching in melanoma', *Pigment Cell & Melanoma Research*, 23(6), pp. 746–759. Available at: <https://doi.org/10.1111/j.1755-148X.2010.00757.x>.
- Holderfield, M., Nagel, T.E. and Stuart, D.D. (2014) 'Mechanism and consequences of RAF kinase activation by small-molecule inhibitors', *British Journal of Cancer*, 111(4), pp. 640–645. Available at: <https://doi.org/10.1038/bjc.2014.139>.
- Hölzel, M., Bovier, A. and Tüting, T. (2013) 'Plasticity of tumour and immune cells: a source of heterogeneity and a cause for therapy resistance?', *Nature Reviews Cancer*, 13(5), pp. 365–376. Available at: <https://doi.org/10.1038/nrc3498>.
- Hölzel, M. and Tüting, T. (2016) 'Inflammation-Induced Plasticity in Melanoma Therapy and Metastasis', *Trends in Immunology*, 37(6), pp. 364–374. Available at: <https://doi.org/10.1016/j.it.2016.03.009>.
- Homann, L. et al. (2022) 'IFN- γ and TNF Induce Senescence and a Distinct Senescence-Associated Secretory Phenotype in Melanoma', *Cells*, 11(9), p. 1514. Available at: <https://doi.org/10.3390/cells11091514>.
- Horak, C.E. et al. (2008) 'The role of metastasis suppressor genes in metastatic dormancy', *APMIS: acta pathologica, microbiologica, et immunologica Scandinavica*, 116(7–8), pp. 586–601. Available at: <https://doi.org/10.1111/j.1600-0463.2008.01213.x>.
- Horn, S. et al. (2013) 'TERT promoter mutations in familial and sporadic melanoma', *Science (New York, N.Y.)*, 339(6122), pp. 959–961. Available at: <https://doi.org/10.1126/science.1230062>.
- Hoshino, A. et al. (2015) 'Tumour exosome integrins determine organotropic metastasis', *Nature*, 527(7578), pp. 329–335. Available at: <https://doi.org/10.1038/nature15756>.

- Hossain, S.M. and Eccles, M.R. (2023) 'Phenotype Switching and the Melanoma Microenvironment; Impact on Immunotherapy and Drug Resistance', *International Journal of Molecular Sciences*, 24(2), p. 1601. Available at: <https://doi.org/10.3390/ijms24021601>.
- Hou, L. and Pavan, W.J. (2008) 'Transcriptional and signaling regulation in neural crest stem cell-derived melanocyte development: do all roads lead to Mitf?', *Cell Research*, 18(12), pp. 1163–1176. Available at: <https://doi.org/10.1038/cr.2008.303>.
- Howard, T.P. and Roberts, C.W.M. (2020) 'Partitioning of Chemotherapeutics into Nuclear Condensates—Opening the Door to New Approaches for Drug Development', *Molecular Cell*, 79(4), pp. 544–545. Available at: <https://doi.org/10.1016/j.molcel.2020.07.029>.
- Hsieh, T.-H.S. et al. (2020) 'Resolving the 3D Landscape of Transcription-Linked Mammalian Chromatin Folding', *Molecular Cell*, 78(3), pp. 539–553.e8. Available at: <https://doi.org/10.1016/j.molcel.2020.03.002>.
- Hsin, J.-P. and Manley, J.L. (2012) 'The RNA polymerase II CTD coordinates transcription and RNA processing', *Genes & Development*, 26(19), pp. 2119–2137. Available at: <https://doi.org/10.1101/gad.200303.112>.
- Hu, L. et al. (2022) 'Why Senescent Cells Are Resistant to Apoptosis: An Insight for Senolytic Development', *Frontiers in Cell and Developmental Biology*, 10. Available at: <https://www.frontiersin.org/articles/10.3389/fcell.2022.822816> (Accessed: 23 March 2023).
- Huang, A.C. and Zappasodi, R. (2022) 'A decade of checkpoint blockade immunotherapy in melanoma: understanding the molecular basis for immune sensitivity and resistance', *Nature Immunology*, 23(5), pp. 660–670. Available at: <https://doi.org/10.1038/s41590-022-01141-1>.
- Huang, F., Gonçalves, C., et al. (2021) 'Inhibiting the MNK1/2-eIF4E axis impairs melanoma phenotype switching and potentiates antitumor immune responses', *The Journal of Clinical Investigation*, 131(8). Available at: <https://doi.org/10.1172/JCI140752>.
- Huang, F., Santinon, F., et al. (2021) 'Melanoma Plasticity: Promoter of Metastasis and Resistance to Therapy', *Frontiers in Oncology*, 11. Available at: <https://www.frontiersin.org/articles/10.3389/fonc.2021.756001> (Accessed: 10 March 2023).
- Huang, F.W. et al. (2013) 'Highly recurrent TERT promoter mutations in human melanoma', *Science (New York, N.Y.)*, 339(6122), pp. 957–959. Available at: <https://doi.org/10.1126/science.1229259>.
- Huang, L. et al. (2021) 'Targeting regulatory T cells for immunotherapy in melanoma', *Molecular Biomedicine*, 2, p. 11. Available at: <https://doi.org/10.1186/s43556-021-00038-z>.
- Huang, Q. et al. (2020) 'A Highlight of the Mechanisms of Immune Checkpoint Blocker Resistance', *Frontiers in Cell and Developmental Biology*, 8. Available at: <https://www.frontiersin.org/articles/10.3389/fcell.2020.580140> (Accessed: 9 April 2023).
- Huang, R. and Rofstad, E.K. (2018) 'Integrins as therapeutic targets in the organ-specific metastasis of human malignant melanoma', *Journal of Experimental & Clinical Cancer Research*, 37, p. 92. Available at: <https://doi.org/10.1186/s13046-018-0763-x>.
- Huang, S. et al. (2022) 'Genetic insights, disease mechanisms, and biological therapeutics for Waardenburg syndrome', *Gene Therapy*, 29(9), pp. 479–497. Available at: <https://doi.org/10.1038/s41434-021-00240-2>.
- Huang, Y. et al. (2009) 'Pulmonary Vascular Destabilization in the Premetastatic Phase Facilitates Lung Metastasis', *Cancer Research*, 69(19), pp. 7529–7537. Available at: <https://doi.org/10.1158/0008-5472.CAN-08-4382>.
- Huergo-Zapico, L. et al. (2018) 'NK-cell Editing Mediates Epithelial-to-Mesenchymal Transition via Phenotypic and Proteomic Changes in Melanoma Cell Lines', *Cancer Research*, 78(14), pp. 3913–3925. Available at: <https://doi.org/10.1158/0008-5472.CAN-17-1891>.
- Hughes, A.E. et al. (1994) 'A gene for Waardenburg Syndrome type 2 maps close to the human homologue of the microphthalmia gene at chromosome 3p12–p14.1', *Nature Genetics*, 7(4), pp. 509–512. Available at: <https://doi.org/10.1038/ng0894-509>.
- Hugo, W. et al. (2015) 'Non-genomic and Immune Evolution of Melanoma Acquiring MAPKi Resistance', *Cell*, 162(6), pp. 1271–1285. Available at: <https://doi.org/10.1016/j.cell.2015.07.061>.
- Hugo, W. et al. (2016) 'Genomic and Transcriptomic Features of Response to Anti-PD-1 Therapy in Metastatic Melanoma', *Cell*, 165(1), pp. 35–44. Available at: <https://doi.org/10.1016/j.cell.2016.02.065>.
- Huilgol, D. et al. (2019) 'Transcription Factors That Govern Development and Disease: An Achilles Heel in Cancer', *Genes*, 10(10), p. 794. Available at: <https://doi.org/10.3390/genes10100794>.
- Hunter, K.W. et al. (2018) 'Genetic insights into the morass of metastatic heterogeneity', *Nature Reviews Cancer*, 18(4), pp. 211–223. Available at: <https://doi.org/10.1038/nrc.2017.126>.
- Hwang, H. et al. (2015) 'Cardiac melanocytes influence atrial reactive oxygen species involved with electrical and structural remodeling in mice', *Physiological Reports*, 3(9), p. e12559. Available at: <https://doi.org/10.14814/phy2.12559>.
- Hyun, Y.-M. et al. (2020) 'Endogenous DEL-1 restrains melanoma lung metastasis by limiting myeloid cell-associated lung inflammation', *Science Advances*, 6(45), p. eabc4882. Available at: <https://doi.org/10.1126/sciadv.abc4882>.
- I, D.-J. and At, S. (2018) 'Tumour heterogeneity and resistance to cancer therapies', *Nature reviews. Clinical oncology*, 15(2). Available at: <https://doi.org/10.1038/nrclinonc.2017.166>.
- Ibrahim, A.A.E. et al. (2020) 'Anatomy and Organization of Human Skin', in B. Smoller and Nooshin Bagherani (eds) *Atlas of Dermatology, Dermatopathology and Venereology*. Cham: Springer International Publishing, pp. 1–24. Available at: https://doi.org/10.1007/978-3-319-45134-3_3-1.
- Igolkina, A.A. et al. (2019) 'H3K4me3, H3K9ac, H3K27ac, H3K27me3 and H3K9me3 Histone Tags Suggest Distinct Regulatory Evolution of Open and Condensed Chromatin Landmarks', *Cells*, 8(9), p. 1034. Available at: <https://doi.org/10.3390/cells8091034>.

- Ikedo, Y. et al. (2021) 'Melanocyte progenitor cells reside in human subcutaneous adipose tissue', *PloS One*, 16(8), p. e0256622. Available at: <https://doi.org/10.1371/journal.pone.0256622>.
- Ikehata, H. et al. (2018) 'Quantitative analysis of UV photolesions suggests that cyclobutane pyrimidine dimers produced in mouse skin by UVB are more mutagenic than those produced by UVC', *Photochemical & Photobiological Sciences: Official Journal of the European Photochemistry Association and the European Society for Photobiology*, 17(4), pp. 404–413. Available at: <https://doi.org/10.1039/c7pp00348j>.
- Ikehata, H. and Ono, T. (2011) 'The mechanisms of UV mutagenesis', *Journal of Radiation Research*, 52(2), pp. 115–125. Available at: <https://doi.org/10.1269/jrr.10175>.
- Illendula, A. et al. (2015) 'A small-molecule inhibitor of the aberrant transcription factor CBF β -SMMHC delays leukemia in mice', *Science*, 347(6223), pp. 779–784. Available at: <https://doi.org/10.1126/science.aaa0314>.
- Ilsley, M.D. et al. (2019) 'Corrupted DNA-binding specificity and ectopic transcription underpin dominant neomorphic mutations in KLF/SP transcription factors', *BMC Genomics*, 20(1), p. 417. Available at: <https://doi.org/10.1186/s12864-019-5805-z>.
- Imodoye, S.O. et al. (2021) 'Understanding the Complex Milieu of Epithelial-Mesenchymal Transition in Cancer Metastasis: New Insight Into the Roles of Transcription Factors', *Frontiers in Oncology*, 11. Available at: <https://www.frontiersin.org/articles/10.3389/fonc.2021.762817> (Accessed: 10 March 2023).
- Irvine, M. et al. (2018) 'Oncogenic PI3K/AKT promotes the step-wise evolution of combination BRAF/MEK inhibitor resistance in melanoma', *Oncogenesis*, 7(9), pp. 1–11. Available at: <https://doi.org/10.1038/s41389-018-0081-3>.
- Islam, Z. et al. (2021) 'Transcription Factors: The Fulcrum Between Cell Development and Carcinogenesis', *Frontiers in Oncology*, 11. Available at: <https://www.frontiersin.org/articles/10.3389/fonc.2021.681377> (Accessed: 3 May 2023).
- Isola, A.L., Eddy, K. and Chen, S. (2016) 'Biology, Therapy and Implications of Tumor Exosomes in the Progression of Melanoma', *Cancers*, 8(12), p. 110. Available at: <https://doi.org/10.3390/cancers8120110>.
- Ito, S. et al. (2010) 'MMXD, a TFIIH-independent XPD-MMS19 protein complex involved in chromosome segregation', *Molecular Cell*, 39(4), pp. 632–640. Available at: <https://doi.org/10.1016/j.molcel.2010.07.029>.
- Ito, S. and Wakamatsu, K. (2003) 'Quantitative analysis of eumelanin and pheomelanin in humans, mice, and other animals: a comparative review', *Pigment Cell Research*, 16(5), pp. 523–531. Available at: <https://doi.org/10.1034/j.1600-0749.2003.00072.x>.
- Itzen, F. et al. (2014) 'Brd4 activates P-TEFb for RNA polymerase II CTD phosphorylation', *Nucleic Acids Research*, 42(12), pp. 7577–7590. Available at: <https://doi.org/10.1093/nar/gku449>.
- Ives, N.J. et al. (2017) 'Adjuvant interferon- α for the treatment of high-risk melanoma: An individual patient data meta-analysis', *European Journal of Cancer (Oxford, England: 1990)*, 82, pp. 171–183. Available at: <https://doi.org/10.1016/j.ejca.2017.06.006>.
- Jackson, D.A. et al. (1993) 'Visualization of focal sites of transcription within human nuclei.', *The EMBO Journal*, 12(3), pp. 1059–1065.
- Jacob, F. and Monod, J. (1961) 'Genetic regulatory mechanisms in the synthesis of proteins', *Journal of Molecular Biology*, 3(3), pp. 318–356. Available at: [https://doi.org/10.1016/S0022-2836\(61\)80072-7](https://doi.org/10.1016/S0022-2836(61)80072-7).
- Jacquelot, N. et al. (2018) 'Targeting Chemokines and Chemokine Receptors in Melanoma and Other Cancers', *Frontiers in Immunology*, 9. Available at: <https://www.frontiersin.org/articles/10.3389/fimmu.2018.02480> (Accessed: 12 March 2023).
- Jain, T. et al. (2021) 'New Insights Into the Cancer–Microbiome–Immune Axis: Decrypting a Decade of Discoveries', *Frontiers in Immunology*, 12. Available at: <https://www.frontiersin.org/articles/10.3389/fimmu.2021.622064> (Accessed: 24 March 2023).
- Janji, B. and Chouaib, S. (2021) '“Suffocating” tumors by blocking adaptation to hypoxia: a new headway in melanoma immunotherapy', *Oncoimmunology*, 10(1), p. 1968611. Available at: <https://doi.org/10.1080/2162402X.2021.1968611>.
- Janssen, A., Colmenares, S.U. and Karpen, G.H. (2018) 'Heterochromatin: Guardian of the Genome', *Annual Review of Cell and Developmental Biology*, 34, pp. 265–288. Available at: <https://doi.org/10.1146/annurev-cellbio-100617-062653>.
- Jardim, D.L. et al. (2021) 'The Challenges of Tumor Mutational Burden as an Immunotherapy Biomarker', *Cancer cell*, 39(2), pp. 154–173. Available at: <https://doi.org/10.1016/j.ccell.2020.10.001>.
- Javelaud, D. et al. (2011) 'GLI2 and M-MITF transcription factors control exclusive gene expression programs and inversely regulate invasion in human melanoma cells', *Pigment Cell & Melanoma Research*, 24(5), pp. 932–943. Available at: <https://doi.org/10.1111/j.1755-148X.2011.00893.x>.
- Jeannot, R. et al. (2010) 'Oncogenic activation of the Notch1 gene by deletion of its promoter in Ikaros-deficient T-ALL', *Blood*, 116(25), pp. 5443–5454. Available at: <https://doi.org/10.1182/blood-2010-05-286658>.
- Jeggo, P.A., Pearl, L.H. and Carr, A.M. (2016) 'DNA repair, genome stability and cancer: a historical perspective', *Nature Reviews. Cancer*, 16(1), pp. 35–42. Available at: <https://doi.org/10.1038/nrc.2015.4>.
- Jenkins, R.W. and Fisher, D.E. (2021) 'Treatment of Advanced Melanoma in 2020 and Beyond', *The Journal of Investigative Dermatology*, 141(1), pp. 23–31. Available at: <https://doi.org/10.1016/j.jid.2020.03.943>.
- Jenuwein, T. and Allis, C.D. (2001) 'Translating the Histone Code', *Science*, 293(5532), pp. 1074–1080. Available at: <https://doi.org/10.1126/science.1063127>.

- Jeronimo, C., Bataille, A.R. and Robert, F. (2013) 'The Writers, Readers, and Functions of the RNA Polymerase II C-Terminal Domain Code', *Chemical Reviews*, 113(11), pp. 8491–8522. Available at: <https://doi.org/10.1021/cr4001397>.
- Jia, Q. et al. (2020) 'Oncogenic super-enhancer formation in tumorigenesis and its molecular mechanisms', *Experimental & Molecular Medicine*, 52(5), pp. 713–723. Available at: <https://doi.org/10.1038/s12276-020-0428-7>.
- Jia, Y., Chng, W.-J. and Zhou, J. (2019) 'Super-enhancers: critical roles and therapeutic targets in hematologic malignancies', *Journal of Hematology & Oncology*, 12(1), p. 77. Available at: <https://doi.org/10.1186/s13045-019-0757-y>.
- Jiang, H. et al. (2015) 'Elevated chronic inflammatory factors and myeloid-derived suppressor cells indicate poor prognosis in advanced melanoma patients', *International Journal of Cancer*, 136(10), pp. 2352–2360. Available at: <https://doi.org/10.1002/ijc.29297>.
- Jiang, Y., Jiang, Y.-Y. and Lin, D.-C. (2021) 'Super-enhancer-mediated core regulatory circuitry in human cancer', *Computational and Structural Biotechnology Journal*, 19, pp. 2790–2795. Available at: <https://doi.org/10.1016/j.csbj.2021.05.006>.
- Jimbow, K. et al. (1975) 'Mitotic activity in non-neoplastic melanocytes in vivo as determined by histochemical, autoradiographic, and electron microscope studies', *The Journal of Cell Biology*, 66(3), pp. 663–670.
- Jin, C. et al. (2009) 'H3.3/H2A.Z double variant-containing nucleosomes mark "nucleosome-free regions" of active promoters and other regulatory regions', *Nature Genetics*, 41(8), pp. 941–945. Available at: <https://doi.org/10.1038/ng.409>.
- Johnson, K.M. et al. (2002) 'TFIID and human mediator coactivator complexes assemble cooperatively on promoter DNA', *Genes & Development*, 16(14), pp. 1852–1863. Available at: <https://doi.org/10.1101/gad.995702>.
- Joly-Tonetti, N. et al. (2018) 'An explanation for the mysterious distribution of melanin in human skin: a rare example of asymmetric (melanin) organelle distribution during mitosis of basal layer progenitor keratinocytes', *British Journal of Dermatology*, 179(5), pp. 1115–1126. Available at: <https://doi.org/10.1111/bjd.16926>.
- Jonge, W.J. de et al. (2022) 'Following the tracks: How transcription factor binding dynamics control transcription', *Biophysical Journal*, 121(9), pp. 1583–1592. Available at: <https://doi.org/10.1016/j.bpj.2022.03.026>.
- Jonkers, I. and Lis, J.T. (2015) 'Getting up to speed with transcription elongation by RNA polymerase II', *Nature Reviews. Molecular Cell Biology*, 16(3), pp. 167–177. Available at: <https://doi.org/10.1038/nrm3953>.
- Joseph, E.W. et al. (2010) 'The RAF inhibitor PLX4032 inhibits ERK signaling and tumor cell proliferation in a V600E BRAF-selective manner', *Proceedings of the National Academy of Sciences*, 107(33), pp. 14903–14908. Available at: <https://doi.org/10.1073/pnas.1008990107>.
- Joyce, K.M. (2017) 'Surgical Management of Melanoma', in W.H. Ward and J.M. Farma (eds) *Cutaneous Melanoma: Etiology and Therapy*. Brisbane (AU): Codon Publications. Available at: <http://www.ncbi.nlm.nih.gov/books/NBK481850/> (Accessed: 2 April 2023).
- Jr, C.W. (1967) 'A classification of malignant melanoma in man correlated with histogenesis and clinical behavior', *Advances in Biology of the Skin: The Pigmentary System*, 8, pp. 621–645.
- Kabashima, K. et al. (2019) 'The immunological anatomy of the skin', *Nature Reviews. Immunology*, 19(1), pp. 19–30. Available at: <https://doi.org/10.1038/s41577-018-0084-5>.
- Kadoch, C. and Crabtree, G.R. (2015) 'Mammalian SWI/SNF chromatin remodeling complexes and cancer: Mechanistic insights gained from human genomics', *Science Advances*, 1(5), p. e1500447. Available at: <https://doi.org/10.1126/sciadv.1500447>.
- Kadonaga, J.T. (2012) 'Perspectives on the RNA polymerase II core promoter', *Wiley Interdisciplinary Reviews. Developmental Biology*, 1(1), pp. 40–51. Available at: <https://doi.org/10.1002/wdev.21>.
- Kalbasi, A. and Ribas, A. (2020) 'Tumour-intrinsic resistance to immune checkpoint blockade', *Nature Reviews Immunology*, 20(1), pp. 25–39. Available at: <https://doi.org/10.1038/s41577-019-0218-4>.
- Kandaswamy, R. et al. (2016) 'Genetic Predisposition to Chronic Lymphocytic Leukemia Is Mediated by a BMF Super-Enhancer Polymorphism', *Cell Reports*, 16(8), pp. 2061–2067. Available at: <https://doi.org/10.1016/j.celrep.2016.07.053>.
- Kang, K. et al. (2020) 'Significance of Tumor Mutation Burden in Immune Infiltration and Prognosis in Cutaneous Melanoma', *Frontiers in Oncology*, 10. Available at: <https://www.frontiersin.org/articles/10.3389/fonc.2020.573141> (Accessed: 5 April 2023).
- Kanitakis, J. (2002) 'Anatomy, histology and immunohistochemistry of normal human skin', *European journal of dermatology: EJD*, 12(4), pp. 390–399; quiz 400–401.
- Kaplan, R.N. et al. (2005) 'VEGFR1-positive haematopoietic bone marrow progenitors initiate the pre-metastatic niche', *Nature*, 438(7069), pp. 820–827. Available at: <https://doi.org/10.1038/nature04186>.
- Kapoor, A. et al. (2010) 'The histone variant macroH2A suppresses melanoma progression through regulation of CDK8', *Nature*, 468(7327), pp. 1105–1109. Available at: <https://doi.org/10.1038/nature09590>.
- Kapranov, P. et al. (2007) 'RNA maps reveal new RNA classes and a possible function for pervasive transcription', *Science (New York, N.Y.)*, 316(5830), pp. 1484–1488. Available at: <https://doi.org/10.1126/science.1138341>.
- Karras, P. et al. (2022) 'A cellular hierarchy in melanoma uncouples growth and metastasis', *Nature*, 610(7930), pp. 190–198. Available at: <https://doi.org/10.1038/s41586-022-05242-7>.
- Kastner, P. and Chan, S. (2011) 'Role of Ikaros in T-cell acute lymphoblastic leukemia', *World Journal of Biological Chemistry*, 2(6), pp. 108–114. Available at: <https://doi.org/10.4331/wjbc.v2.i6.108>.

- Katainen, R. et al. (2015) 'CTCF/cohesin-binding sites are frequently mutated in cancer', *Nature Genetics*, 47(7), pp. 818–821. Available at: <https://doi.org/10.1038/ng.3335>.
- Kataoka, K. et al. (2016) 'Aberrant PD-L1 expression through 3'-UTR disruption in multiple cancers', *Nature*, 534(7607), pp. 402–406. Available at: <https://doi.org/10.1038/nature18294>.
- Katlinskaya, Y.V. et al. (2016) 'Suppression of Type I Interferon Signaling Overcomes Oncogene-Induced Senescence and Mediates Melanoma Development and Progression', *Cell Reports*, 15(1), pp. 171–180. Available at: <https://doi.org/10.1016/j.celrep.2016.03.006>.
- Kaufman, C.K. et al. (2016) 'A zebrafish melanoma model reveals emergence of neural crest identity during melanoma initiation', *Science*, 351(6272), p. aad2197. Available at: <https://doi.org/10.1126/science.aad2197>.
- Kaur, A. et al. (2019) 'Remodeling of the Collagen Matrix in Aging Skin Promotes Melanoma Metastasis and Affects Immune Cell Motility', *Cancer Discovery*, 9(1), pp. 64–81. Available at: <https://doi.org/10.1158/2159-8290.CD-18-0193>.
- Kawakami, A. and Fisher, D.E. (2017) 'The master role of microphthalmia-associated transcription factor in melanocyte and melanoma biology', *Laboratory Investigation*, 97(6), pp. 649–656. Available at: <https://doi.org/10.1038/labinvest.2017.9>.
- Kelderman, S., Schumacher, T.N.M. and Haanen, J.B.A.G. (2014) 'Acquired and intrinsic resistance in cancer immunotherapy', *Molecular Oncology*, 8(6), pp. 1132–1139. Available at: <https://doi.org/10.1016/j.molonc.2014.07.011>.
- Keller, L. and Pantel, K. (2019) 'Unravelling tumour heterogeneity by single-cell profiling of circulating tumour cells', *Nature Reviews Cancer*, 19(10), pp. 553–567. Available at: <https://doi.org/10.1038/s41568-019-0180-2>.
- Kenny, G.P. and McGinn, R. (2017) 'Restoration of thermoregulation after exercise', *Journal of Applied Physiology (Bethesda, Md.: 1985)*, 122(4), pp. 933–944. Available at: <https://doi.org/10.1152/japplphysiol.00517.2016>.
- Keung, E.Z. and Gershenwald, J.E. (2018) 'The eighth edition American Joint Committee on Cancer (AJCC) melanoma staging system: implications for melanoma treatment and care', *Expert review of anticancer therapy*, 18(8), pp. 775–784. Available at: <https://doi.org/10.1080/14737140.2018.1489246>.
- Kfoury, A. et al. (2018) 'AMPK promotes survival of c-Myc-positive melanoma cells by suppressing oxidative stress', *The EMBO Journal*, 37(5), p. e97673. Available at: <https://doi.org/10.15252/embj.201797673>.
- Kiel, C. et al. (2016) 'The yin–yang of kinase activation and unfolding explains the peculiarity of Val600 in the activation segment of BRAF', *eLife*. Edited by Y. Shan, 5, p. e12814. Available at: <https://doi.org/10.7554/eLife.12814>.
- Kilgore, H.R. and Young, R.A. (2022) 'Learning the chemical grammar of biomolecular condensates', *Nature Chemical Biology*, 18(12), pp. 1298–1306. Available at: <https://doi.org/10.1038/s41589-022-01046-y>.
- Killela, P.J. et al. (2013) 'TERT promoter mutations occur frequently in gliomas and a subset of tumors derived from cells with low rates of self-renewal', *Proceedings of the National Academy of Sciences of the United States of America*, 110(15), pp. 6021–6026. Available at: <https://doi.org/10.1073/pnas.1303607110>.
- Kim, M.-Y. et al. (2009) 'Tumor self-seeding by circulating cancer cells', *Cell*, 139(7), pp. 1315–1326. Available at: <https://doi.org/10.1016/j.cell.2009.11.025>.
- Kim, P. et al. (2016) 'ccmGDB: a database for cancer cell metabolism genes', *Nucleic Acids Research*, 44(D1), pp. D959–968. Available at: <https://doi.org/10.1093/nar/gkv1128>.
- Kim, S. and Shendure, J. (2019) 'Mechanisms of Interplay between Transcription Factors and the 3D Genome', *Molecular Cell*, 76(2), pp. 306–319. Available at: <https://doi.org/10.1016/j.molcel.2019.08.010>.
- Kim, Y.K. et al. (2002) 'Phosphorylation of the RNA Polymerase II Carboxyl-Terminal Domain by CDK9 Is Directly Responsible for Human Immunodeficiency Virus Type 1 Tat-Activated Transcriptional Elongation', *Molecular and Cellular Biology*, 22(13), pp. 4622–4637. Available at: <https://doi.org/10.1128/MCB.22.13.4622-4637.2002>.
- Kinde, I. et al. (2013) 'TERT Promoter Mutations Occur Early in Urothelial Neoplasia and Are Biomarkers of Early Disease and Disease Recurrence in Urine', *Cancer Research*, 73(24), pp. 7162–7167. Available at: <https://doi.org/10.1158/0008-5472.CAN-13-2498>.
- Kleffel, S. et al. (2015) 'Melanoma Cell-Intrinsic PD-1 Receptor Functions Promote Tumor Growth', *Cell*, 162(6), pp. 1242–1256. Available at: <https://doi.org/10.1016/j.cell.2015.08.052>.
- Klein, I.A. et al. (2020) 'Partitioning of cancer therapeutics in nuclear condensates', *Science*, 368(6497), pp. 1386–1392. Available at: <https://doi.org/10.1126/science.aaz4427>.
- Klemm, S.L., Shipony, Z. and Greenleaf, W.J. (2019) 'Chromatin accessibility and the regulatory epigenome', *Nature Reviews Genetics*, 20(4), pp. 207–220. Available at: <https://doi.org/10.1038/s41576-018-0089-8>.
- Kluza, J. et al. (2012) 'Inactivation of the HIF-1 α /PDK3 Signaling Axis Drives Melanoma toward Mitochondrial Oxidative Metabolism and Potentiates the Therapeutic Activity of Pro-Oxidants', *Cancer Research*, 72(19), pp. 5035–5047. Available at: <https://doi.org/10.1158/0008-5472.CAN-12-0979>.
- Knezetic, J.A. and Luse, D.S. (1986) 'The presence of nucleosomes on a DNA template prevents initiation by RNA polymerase II in vitro', *Cell*, 45(1), pp. 95–104. Available at: [https://doi.org/10.1016/0092-8674\(86\)90541-6](https://doi.org/10.1016/0092-8674(86)90541-6).
- Knight, A., Karapetyan, L. and Kirkwood, J.M. (2023) 'Immunotherapy in Melanoma: Recent Advances and Future Directions', *Cancers*, 15(4), p. 1106. Available at: <https://doi.org/10.3390/cancers15041106>.

- Knippel, R.J., Drewes, J.L. and Sears, C.L. (2021) 'The Cancer Microbiome: Recent Highlights and Knowledge Gaps', *Cancer Discovery*, 11(10), pp. 2378–2395. Available at: <https://doi.org/10.1158/2159-8290.CD-21-0324>.
- Kobayashi, N. et al. (1998) 'Supranuclear melanin caps reduce ultraviolet induced DNA photoproducts in human epidermis', *The Journal of Investigative Dermatology*, 110(5), pp. 806–810. Available at: <https://doi.org/10.1046/j.1523-1747.1998.00178.x>.
- Koelblinger, P., Thuerigen, O. and Dummer, R. (2018) 'Development of encorafenib for BRAF-mutated advanced melanoma', *Current Opinion in Oncology*, 30(2), pp. 125–133. Available at: <https://doi.org/10.1097/CCO.0000000000000426>.
- Köhler, C. et al. (2017) 'Mouse Cutaneous Melanoma Induced by Mutant BRAF Arises from Expansion and Dedifferentiation of Mature Pigmented Melanocytes', *Cell Stem Cell*, 21(5), pp. 679–693.e6. Available at: <https://doi.org/10.1016/j.stem.2017.08.003>.
- Kokic, G. et al. (2019) 'Structural basis of TFIIH activation for nucleotide excision repair', *Nature Communications*, 10(1), p. 2885. Available at: <https://doi.org/10.1038/s41467-019-10745-5>.
- Koludrovic, D. et al. (2015) 'Chromatin-Remodelling Complex NURF Is Essential for Differentiation of Adult Melanocyte Stem Cells', *PLOS Genetics*, 11(10), p. e1005555. Available at: <https://doi.org/10.1371/journal.pgen.1005555>.
- Konieczkowski, D.J. et al. (2014) 'A melanoma cell state distinction influences sensitivity to MAPK pathway inhibitors', *Cancer Discovery*, 4(7), pp. 816–827. Available at: <https://doi.org/10.1158/2159-8290.CD-13-0424>.
- Kornberg, R.D. and Thomas, J.O. (1974) 'Chromatin structure; oligomers of the histones', *Science (New York, N.Y.)*, 184(4139), pp. 865–868. Available at: <https://doi.org/10.1126/science.184.4139.865>.
- Kostrewa, D. et al. (2009) 'RNA polymerase II-TFIIIB structure and mechanism of transcription initiation', *Nature*, 462(7271), pp. 323–330. Available at: <https://doi.org/10.1038/nature08548>.
- Kozar, I. et al. (2019) 'Many ways to resistance: How melanoma cells evade targeted therapies', *Biochimica et Biophysica Acta (BBA) - Reviews on Cancer*, 1871(2), pp. 313–322. Available at: <https://doi.org/10.1016/j.bbcan.2019.02.002>.
- Krauthammer, M. et al. (2015) 'Exome sequencing identifies recurrent mutations in NF1 and RASopathy genes in sun-exposed melanomas', *Nature Genetics*, 47(9), pp. 996–1002. Available at: <https://doi.org/10.1038/ng.3361>.
- Kress, T.R., Sabò, A. and Amati, B. (2015) 'MYC: connecting selective transcriptional control to global RNA production', *Nature Reviews Cancer*, 15(10), pp. 593–607. Available at: <https://doi.org/10.1038/nrc3984>.
- Krietenstein, N. et al. (2020) 'Ultrastructural Details of Mammalian Chromosome Architecture', *Molecular Cell*, 78(3), pp. 554–565.e7. Available at: <https://doi.org/10.1016/j.molcel.2020.03.003>.
- Krumm, A. et al. (1992) 'The block to transcriptional elongation within the human c-myc gene is determined in the promoter-proximal region', *Genes & Development*, 6(11), pp. 2201–2213. Available at: <https://doi.org/10.1101/gad.6.11.2201>.
- Kuczynski, E.A. et al. (2019) 'Vessel co-option in cancer', *Nature Reviews Clinical Oncology*, 16(8), pp. 469–493. Available at: <https://doi.org/10.1038/s41571-019-0181-9>.
- Kugel, J.F. and Goodrich, J.A. (2017) 'Finding the start site: redefining the human initiator element', *Genes & Development*, 31(1), pp. 1–2. Available at: <https://doi.org/10.1101/gad.295980.117>.
- Kumar, A. et al. (2019) 'Mechanistic insights into mRNA 3'-end processing', *Current Opinion in Structural Biology*, 59, pp. 143–150. Available at: <https://doi.org/10.1016/j.sbi.2019.08.001>.
- Kumar, P.R. et al. (2021) 'Mitochondrial oxidative phosphorylation in cutaneous melanoma', *British Journal of Cancer*, 124(1), pp. 115–123. Available at: <https://doi.org/10.1038/s41416-020-01159-y>.
- Kundu, K. et al. (2021) 'SLFN11 biomarker status predicts response to lurbinectedin as a single agent and in combination with ATR inhibition in small cell lung cancer', *Translational Lung Cancer Research*, 10(11), pp. 4095–4105. Available at: <https://doi.org/10.21037/tlcr-21-437>.
- Kunz, M. (2013) 'MicroRNAs in melanoma biology', *Advances in Experimental Medicine and Biology*, 774, pp. 103–120. Available at: https://doi.org/10.1007/978-94-007-5590-1_6.
- Kupchan, S.M. et al. (1972) 'Triptolide and triptidiolide, novel antileukemic diterpenoid triepoxides from *Tripterygium wilfordii*', *Journal of the American Chemical Society*, 94(20), pp. 7194–7195. Available at: <https://doi.org/10.1021/ja00775a078>.
- Kuper, J. and Kisker, C. (2021) 'Three targets in one complex: A molecular perspective of TFIIH in cancer therapy', *DNA Repair*, 105, p. 103143. Available at: <https://doi.org/10.1016/j.dnarep.2021.103143>.
- Kwiatkowski, N. et al. (2014) 'Targeting transcription regulation in cancer with a covalent CDK7 inhibitor', *Nature*, 511(7511), pp. 616–620. Available at: <https://doi.org/10.1038/nature13393>.
- Kwong, L.N. et al. (2017) 'Modeling Genomic Instability and Selection Pressure in a Mouse Model of Melanoma', *Cell reports*, 19(7), pp. 1304–1312. Available at: <https://doi.org/10.1016/j.celrep.2017.04.065>.
- Kyjacova, L. et al. (2021) 'IER2-induced senescence drives melanoma invasion through osteopontin', *Oncogene*, 40(47), pp. 6494–6512. Available at: <https://doi.org/10.1038/s41388-021-02027-6>.
- Labelle, M., Begum, S. and Hynes, R.O. (2014) 'Platelets guide the formation of early metastatic niches', *Proceedings of the National Academy of Sciences*, 111(30), pp. E3053–E3061. Available at: <https://doi.org/10.1073/pnas.1411082111>.

- Lafontaine, D.L.J. et al. (2021) 'The nucleolus as a multiphase liquid condensate', *Nature Reviews Molecular Cell Biology*, 22(3), pp. 165–182. Available at: <https://doi.org/10.1038/s41580-020-0272-6>.
- Laham-Karam, N. et al. (2020) 'Transcription and Translation Inhibitors in Cancer Treatment', *Frontiers in Chemistry*, 8. Available at: <https://www.frontiersin.org/articles/10.3389/fchem.2020.00276> (Accessed: 23 January 2023).
- Lai, A.C. and Crews, C.M. (2017) 'Induced protein degradation: an emerging drug discovery paradigm', *Nature Reviews Drug Discovery*, 16(2), pp. 101–114. Available at: <https://doi.org/10.1038/nrd.2016.211>.
- Lambert, A.W., Pattabiraman, D.R. and Weinberg, R.A. (2017) 'Emerging Biological Principles of Metastasis', *Cell*, 168(4), pp. 670–691. Available at: <https://doi.org/10.1016/j.cell.2016.11.037>.
- Lammerding, J. (2011) 'Mechanics of the Nucleus', *Comprehensive Physiology*, 1(2), pp. 783–807. Available at: <https://doi.org/10.1002/cphy.c100038>.
- Lancho, O. and Herranz, D. (2018) 'The MYC enhancer-ome: Long-range transcriptional regulation of MYC', *Trends in cancer*, 4(12), pp. 810–822. Available at: <https://doi.org/10.1016/j.trecan.2018.10.003>.
- Landolin, J.M. et al. (2010) 'Sequence features that drive human promoter function and tissue specificity', *Genome Research*, 20(7), pp. 890–898. Available at: <https://doi.org/10.1101/gr.100370.109>.
- Landsberg, J. et al. (2012) 'Melanomas resist T-cell therapy through inflammation-induced reversible dedifferentiation', *Nature*, 490(7420), pp. 412–416. Available at: <https://doi.org/10.1038/nature11538>.
- Landsberg, J. et al. (2016) 'The Role of Neutrophilic Inflammation, Angiotropism, and Pericytic Mimicry in Melanoma Progression and Metastasis', *Journal of Investigative Dermatology*, 136(2), pp. 372–377. Available at: <https://doi.org/10.1016/j.jid.2015.11.013>.
- Larkin, J. et al. (2019) 'Five-Year Survival with Combined Nivolumab and Ipilimumab in Advanced Melanoma', *New England Journal of Medicine*, 381(16), pp. 1535–1546. Available at: <https://doi.org/10.1056/NEJMoa1910836>.
- Larochelle, S. et al. (2012) 'Cyclin-dependent kinase control of the initiation-to-elongation switch of RNA polymerase II', *Nature Structural & Molecular Biology*, 19(11), pp. 1108–1115. Available at: <https://doi.org/10.1038/nsmb.2399>.
- Larribère, L. and Utikal, J. (2019) 'Stem Cell-Derived Models of Neural Crest Are Essential to Understand Melanoma Progression and Therapy Resistance', *Frontiers in Molecular Neuroscience*, 12, p. 111. Available at: <https://doi.org/10.3389/fnmol.2019.00111>.
- Lassam, N.J., From, L. and Kahn, H.J. (1993) 'Overexpression of p53 is a late event in the development of malignant melanoma', *Cancer Research*, 53(10 Suppl), pp. 2235–2238.
- Laughery, M.F. et al. (2020) 'Atypical UV Photoproducts Induce Non-canonical Mutation Classes Associated with Driver Mutations in Melanoma', *Cell Reports*, 33(7), p. 108401. Available at: <https://doi.org/10.1016/j.celrep.2020.108401>.
- Laurette, P. et al. (2015) 'Transcription factor MITF and remodeler BRG1 define chromatin organisation at regulatory elements in melanoma cells', *eLife*, 4. Available at: <https://doi.org/10.7554/eLife.06857>.
- Laurette, P. et al. (2020) 'Chromatin remodellers Brg1 and Bptf are required for normal gene expression and progression of oncogenic Braf-driven mouse melanoma', *Cell Death and Differentiation*, 27(1), pp. 29–43. Available at: <https://doi.org/10.1038/s41418-019-0333-6>.
- Le Gal, K. et al. (2015) 'Antioxidants can increase melanoma metastasis in mice', *Science Translational Medicine*, 7(308), p. 308re8. Available at: <https://doi.org/10.1126/scitranslmed.aad3740>.
- Le Poole, I.C. et al. (1993) 'A novel, antigen-presenting function of melanocytes and its possible relationship to hypopigmentary disorders', *Journal of Immunology (Baltimore, Md.: 1950)*, 151(12), pp. 7284–7292.
- Leal, J.F.M. et al. (2010) 'PM01183, a new DNA minor groove covalent binder with potent in vitro and in vivo anti-tumour activity', *British Journal of Pharmacology*, 161(5), pp. 1099–1110. Available at: <https://doi.org/10.1111/j.1476-5381.2010.00945.x>.
- Lebrun, J.-J. (2012) 'The Dual Role of TGFβ in Human Cancer: From Tumor Suppression to Cancer Metastasis', *ISRN molecular biology*, 2012, p. 381428. Available at: <https://doi.org/10.5402/2012/381428>.
- Leclerc, J., Ballotti, R. and Bertolotto, C. (2017) 'Pathways from senescence to melanoma: focus on MITF sumoylation', *Oncogene*, 36(48), pp. 6659–6667. Available at: <https://doi.org/10.1038/onc.2017.292>.
- Lee, C. et al. (2019) 'Tumor metastasis to lymph nodes requires YAP-dependent metabolic adaptation', *Science*, 363(6427), pp. 644–649. Available at: <https://doi.org/10.1126/science.aav0173>.
- Lee, J.H. et al. (2020) 'Transcriptional downregulation of MHC class I and melanoma de-differentiation in resistance to PD-1 inhibition', *Nature Communications*, 11(1), p. 1897. Available at: <https://doi.org/10.1038/s41467-020-15726-7>.
- Lee, J.W. et al. (2020) 'Deciphering UV-induced DNA Damage Responses to Prevent and Treat Skin Cancer', *Photochemistry and Photobiology*, 96(3), pp. 478–499. Available at: <https://doi.org/10.1111/php.13245>.
- Lee, K.A. et al. (2022) 'Cross-cohort gut microbiome associations with immune checkpoint inhibitor response in advanced melanoma', *Nature Medicine*, 28(3), pp. 535–544. Available at: <https://doi.org/10.1038/s41591-022-01695-5>.
- Lee, K.J. et al. (2021) 'On Naevi and Melanomas: Two Sides of the Same Coin?', *Frontiers in Medicine*, 8. Available at: <https://www.frontiersin.org/articles/10.3389/fmed.2021.635316> (Accessed: 22 February 2023).

- Lee, T.I. and Young, R.A. (2013) 'Transcriptional Regulation and its Misregulation in Disease', *Cell*, 152(6), pp. 1237–1251. Available at: <https://doi.org/10.1016/j.cell.2013.02.014>.
- Lehmann, A.R., McGibbon, D. and Stefanini, M. (2011) 'Xeroderma pigmentosum', *Orphanet Journal of Rare Diseases*, 6(1), p. 70. Available at: <https://doi.org/10.1186/1750-1172-6-70>.
- Leiter, U. et al. (2016) 'Complete lymph node dissection versus no dissection in patients with sentinel lymph node biopsy positive melanoma (DeCOG-SLT): a multicentre, randomised, phase 3 trial', *The Lancet. Oncology*, 17(6), pp. 757–767. Available at: [https://doi.org/10.1016/S1470-2045\(16\)00141-8](https://doi.org/10.1016/S1470-2045(16)00141-8).
- Leonardi, G. et al. (2018) 'Cutaneous melanoma: From pathogenesis to therapy (Review)', *International Journal of Oncology* [Preprint]. Available at: <https://doi.org/10.3892/ijo.2018.4287>.
- Lequeux, A. et al. (2019) 'Impact of hypoxic tumor microenvironment and tumor cell plasticity on the expression of immune checkpoints', *Cancer Letters*, 458, pp. 13–20. Available at: <https://doi.org/10.1016/j.canlet.2019.05.021>.
- Lequeux, A. et al. (2021) 'Targeting HIF-1 alpha transcriptional activity drives cytotoxic immune effector cells into melanoma and improves combination immunotherapy', *Oncogene*, 40(28), pp. 4725–4735. Available at: <https://doi.org/10.1038/s41388-021-01846-x>.
- Leucci, E. et al. (2016) 'Melanoma addiction to the long non-coding RNA SAMMSON', *Nature*, 531(7595), pp. 518–522. Available at: <https://doi.org/10.1038/nature17161>.
- Levin, M.D. et al. (2009) 'Melanocyte-like cells in the heart and pulmonary veins contribute to atrial arrhythmia triggers', *The Journal of Clinical Investigation*, 119(11), pp. 3420–3436. Available at: <https://doi.org/10.1172/JCI39109>.
- Levine, M. (2011) 'Paused RNA Polymerase II as a Developmental Checkpoint', *Cell*, 145(4), pp. 502–511. Available at: <https://doi.org/10.1016/j.cell.2011.04.021>.
- Levine, M. and Tjian, R. (2003) 'Transcription regulation and animal diversity', *Nature*, 424(6945), pp. 147–151. Available at: <https://doi.org/10.1038/nature01763>.
- Lewis, L.M. et al. (2018) 'Replication Study: Transcriptional amplification in tumor cells with elevated c-Myc', *eLife*, 7, p. e30274. Available at: <https://doi.org/10.7554/eLife.30274>.
- Li, G.-H. et al. (2021) 'Super-enhancers: a new frontier for epigenetic modifiers in cancer chemoresistance', *Journal of Experimental & Clinical Cancer Research*, 40(1), p. 174. Available at: <https://doi.org/10.1186/s13046-021-01974-y>.
- Li, J. and Gilmour, D.S. (2011) 'Promoter proximal pausing and the control of gene expression', *Current opinion in genetics & development*, 21(2), pp. 231–235. Available at: <https://doi.org/10.1016/j.gde.2011.01.010>.
- Li, M. et al. (2021) 'Fatty acid oxidation: driver of lymph node metastasis', *Cancer Cell International*, 21(1), p. 339. Available at: <https://doi.org/10.1186/s12935-021-02057-w>.
- Li, M., Knapp, S.K. and Iden, S. (2020) 'Mechanisms of melanocyte polarity and differentiation: What can we learn from other neuroectoderm-derived lineages?', *Current Opinion in Cell Biology*, 67, pp. 99–108. Available at: <https://doi.org/10.1016/j.ccb.2020.09.001>.
- Li, X. et al. (2018) 'Long non-coding RNA PANDAR promotes melanoma cell invasion through regulating epithelial-mesenchymal transition', *International Journal of Clinical and Experimental Pathology*, 11(5), pp. 2430–2439.
- Li, X. et al. (2020) 'Disseminated Melanoma Cells Transdifferentiate into Endothelial Cells in Intravascular Niches at Metastatic Sites', *Cell Reports*, 31(11), p. 107765. Available at: <https://doi.org/10.1016/j.celrep.2020.107765>.
- Li, Y. et al. (2019) 'Gut microbiota dependent anti-tumor immunity restricts melanoma growth in Rnf5^{-/-} mice', *Nature Communications*, 10(1), p. 1492. Available at: <https://doi.org/10.1038/s41467-019-09525-y>.
- Liberti, M.V. and Locasale, J.W. (2016) 'The Warburg Effect: How Does it Benefit Cancer Cells?', *Trends in biochemical sciences*, 41(3), pp. 211–218. Available at: <https://doi.org/10.1016/j.tibs.2015.12.001>.
- Lieberman-Aiden, E. et al. (2009) 'Comprehensive mapping of long-range interactions reveals folding principles of the human genome', *Science (New York, N.Y.)*, 326(5950), pp. 289–293. Available at: <https://doi.org/10.1126/science.1181369>.
- Liguoro, D. et al. (2020) 'Drug tolerance to target therapy in melanoma revealed at single cell level: What next?', *Biochimica et Biophysica Acta (BBA) - Reviews on Cancer*, 1874(2), p. 188440. Available at: <https://doi.org/10.1016/j.bbcan.2020.188440>.
- Lim, S.Y. et al. (2023) 'The molecular and functional landscape of resistance to immune checkpoint blockade in melanoma', *Nature Communications*, 14(1), p. 1516. Available at: <https://doi.org/10.1038/s41467-023-36979-y>.
- Lim, S.Y., Menzies, A.M. and Rizos, H. (2017) 'Mechanisms and strategies to overcome resistance to molecularly targeted therapy for melanoma', *Cancer*, 123(S11), pp. 2118–2129. Available at: <https://doi.org/10.1002/cnrc.30435>.
- Lima, M. et al. (2016) 'Dual inhibition of ATR and ATM potentiates the activity of trabectedin and lurbinectedin by perturbing the DNA damage response and homologous recombination repair', *Oncotarget*, 7(18), pp. 25885–25901. Available at: <https://doi.org/10.18632/oncotarget.8292>.
- Lin, C.Y. et al. (2012) 'Transcriptional Amplification in Tumor Cells with Elevated c-Myc', *Cell*, 151(1), pp. 56–67. Available at: <https://doi.org/10.1016/j.cell.2012.08.026>.
- Lin, J.Y. and Fisher, D.E. (2007) 'Melanocyte biology and skin pigmentation', *Nature*, 445(7130), pp. 843–850. Available at: <https://doi.org/10.1038/nature05660>.

- Lin, Y.C., Choi, W.S. and Gralla, J.D. (2005) 'TFIIH XPB mutants suggest a unified bacterial-like mechanism for promoter opening but not escape', *Nature Structural & Molecular Biology*, 12(7), pp. 603–607. Available at: <https://doi.org/10.1038/nsmb949>.
- Lines, J.L. et al. (2014) 'VISTA Is an Immune Checkpoint Molecule for Human T Cells', *Cancer Research*, 74(7), pp. 1924–1932. Available at: <https://doi.org/10.1158/0008-5472.CAN-13-1504>.
- Lis, J.T. (2019) 'A 50 year history of technologies that drove discovery in eukaryotic transcription regulation', *Nature Structural & Molecular Biology*, 26(9), pp. 777–782. Available at: <https://doi.org/10.1038/s41594-019-0288-9>.
- Littlewood, T.D., Kreuzaler, P. and Evan, G.I. (2012) 'All Things to All People', *Cell*, 151(1), pp. 11–13. Available at: <https://doi.org/10.1016/j.cell.2012.09.006>.
- Liu, D. et al. (2021) 'Evolution of delayed resistance to immunotherapy in a melanoma responder', *Nature Medicine*, 27(6), pp. 985–992. Available at: <https://doi.org/10.1038/s41591-021-01331-8>.
- Liu, Jianglan et al. (2021) 'Neural Crest-Like Stem Cell Transcriptome Analysis Identifies LPAR1 in Melanoma Progression and Therapy Resistance', *Cancer Research*, 81(20), pp. 5230–5241. Available at: <https://doi.org/10.1158/0008-5472.CAN-20-1496>.
- Liu, Jing et al. (2021) 'TF-PROTACs Enable Targeted Degradation of Transcription Factors', *Journal of the American Chemical Society*, 143(23), pp. 8902–8910. Available at: <https://doi.org/10.1021/jacs.1c03852>.
- Liu, R. et al. (2021) 'Molecular Mechanisms of MYCN Dysregulation in Cancers', *Frontiers in Oncology*, 10. Available at: <https://www.frontiersin.org/articles/10.3389/fonc.2020.625332> (Accessed: 3 May 2023).
- Loercher, A.E. et al. (2005) 'MITF links differentiation with cell cycle arrest in melanocytes by transcriptional activation of INK4A', *The Journal of Cell Biology*, 168(1), pp. 35–40. Available at: <https://doi.org/10.1083/jcb.200410115>.
- Lomberk, G., Wallrath, L. and Urrutia, R. (2006) 'The Heterochromatin Protein 1 family', *Genome Biology*, 7(7), p. 228. Available at: <https://doi.org/10.1186/gb-2006-7-7-228>.
- Long, G.V. et al. (2012) 'Dabrafenib in patients with Val600Glu or Val600Lys BRAF-mutant melanoma metastatic to the brain (BREAK-MB): a multicentre, open-label, phase 2 trial', *The Lancet. Oncology*, 13(11), pp. 1087–1095. Available at: [https://doi.org/10.1016/S1470-2045\(12\)70431-X](https://doi.org/10.1016/S1470-2045(12)70431-X).
- Loras, A. et al. (2022) 'UV-Induced Somatic Mutations Driving Clonal Evolution in Healthy Skin, Nevus, and Cutaneous Melanoma', *Life*, 12(9), p. 1339. Available at: <https://doi.org/10.3390/life12091339>.
- Lorch, Y. and Kornberg, R.D. (2017) 'Chromatin-remodeling for transcription', *Quarterly Reviews of Biophysics*, 50, p. e5. Available at: <https://doi.org/10.1017/S003358351700004X>.
- Lorentzen, C.L. et al. (2022) 'Clinical advances and ongoing trials of mRNA vaccines for cancer treatment', *The Lancet Oncology*, 23(10), pp. e450–e458. Available at: [https://doi.org/10.1016/S1470-2045\(22\)00372-2](https://doi.org/10.1016/S1470-2045(22)00372-2).
- Lorenzi, L. et al. (2021) 'The RNA Atlas expands the catalog of human non-coding RNAs', *Nature Biotechnology*, 39(11), pp. 1453–1465. Available at: <https://doi.org/10.1038/s41587-021-00936-1>.
- Louder, R.K. et al. (2016) 'Structure of promoter-bound TFIID and model of human pre-initiation complex assembly', *Nature*, 531(7596), pp. 604–609. Available at: <https://doi.org/10.1038/nature17394>.
- Louphrasitthiphol, P. et al. (2019) 'MITF controls the TCA cycle to modulate the melanoma hypoxia response', *Pigment Cell & Melanoma Research*, 32(6), pp. 792–808. Available at: <https://doi.org/10.1111/pcmr.12802>.
- Louphrasitthiphol, P. et al. (2020) 'Tuning Transcription Factor Availability through Acetylation-Mediated Genomic Redistribution', *Molecular Cell*, 79(3), pp. 472–487.e10. Available at: <https://doi.org/10.1016/j.molcel.2020.05.025>.
- Lourenco, C. et al. (2021) 'MYC protein interactors in gene transcription and cancer', *Nature Reviews Cancer*, 21(9), pp. 579–591. Available at: <https://doi.org/10.1038/s41568-021-00367-9>.
- Lovén, J. et al. (2013) 'Selective Inhibition of Tumor Oncogenes by Disruption of Super-Enhancers', *Cell*, 153(2), pp. 320–334. Available at: <https://doi.org/10.1016/j.cell.2013.03.036>.
- Lowings, P., Yavuzer, U. and Goding, C.R. (1992) 'Positive and negative elements regulate a melanocyte-specific promoter', *Molecular and Cellular Biology*, 12(8), pp. 3653–3662. Available at: <https://doi.org/10.1128/mcb.12.8.3653-3662.1992>.
- Lu, H. et al. (1992) 'Human general transcription factor IIH phosphorylates the C-terminal domain of RNA polymerase II', *Nature*, 358(6388), pp. 641–645. Available at: <https://doi.org/10.1038/358641a0>.
- Lu, H. et al. (1997) 'The CDK7-cycH-p36 complex of transcription factor IIH phosphorylates p53, enhancing its sequence-specific DNA binding activity in vitro.', *Molecular and Cellular Biology*, 17(10), pp. 5923–5934. Available at: <https://doi.org/10.1128/MCB.17.10.5923>.
- Lu, H. et al. (2018) 'Phase-separation mechanism for C-terminal hyperphosphorylation of RNA polymerase II', *Nature*, 558(7709), pp. 318–323. Available at: <https://doi.org/10.1038/s41586-018-0174-3>.
- Lui, Y. and Davis, S.J. (2018) 'LAG-3: a very singular immune checkpoint', *Nature Immunology*, 19(12), pp. 1278–1279. Available at: <https://doi.org/10.1038/s41590-018-0257-1>.
- Luke, J.J. et al. (2017) 'Targeted agents and immunotherapies: optimizing outcomes in melanoma', *Nature Reviews. Clinical Oncology*, 14(8), pp. 463–482. Available at: <https://doi.org/10.1038/nrclinonc.2017.43>.

- Luo, C. et al. (2015) 'Expression of oncogenic BRAFV600E in melanocytes induces Schwannian differentiation in vivo', *Pigment cell & melanoma research*, 28(5), pp. 603–606. Available at: <https://doi.org/10.1111/pcmr.12384>.
- Luo, Z. et al. (2012) 'The super elongation complex family of RNA polymerase II elongation factors: gene target specificity and transcriptional output', *Molecular and Cellular Biology*, 32(13), pp. 2608–2617. Available at: <https://doi.org/10.1128/MCB.00182-12>.
- Lüönd, F. et al. (2022) 'Hierarchy of TGF β /SMAD, Hippo/YAP/TAZ, and Wnt/ β -catenin signaling in melanoma phenotype switching', *Life Science Alliance*, 5(2). Available at: <https://doi.org/10.26508/lsa.202101010>.
- Luse, D.S. (2013) 'Promoter clearance by RNA polymerase II', *Biochimica et Biophysica Acta (BBA) - Gene Regulatory Mechanisms*, 1829(1), pp. 63–68. Available at: <https://doi.org/10.1016/j.bbgrm.2012.08.010>.
- Lyden, D. et al. (2001) 'Impaired recruitment of bone-marrow-derived endothelial and hematopoietic precursor cells blocks tumor angiogenesis and growth', *Nature Medicine*, 7(11), pp. 1194–1201. Available at: <https://doi.org/10.1038/nm1101-1194>.
- Lyon, A.S., Peebles, W.B. and Rosen, M.K. (2021) 'A framework for understanding the functions of biomolecular condensates across scales', *Nature Reviews Molecular Cell Biology*, 22(3), pp. 215–235. Available at: <https://doi.org/10.1038/s41580-020-00303-z>.
- Lyons, H. et al. (2023) 'Functional partitioning of transcriptional regulators by patterned charge blocks', *Cell*, 186(2), pp. 327–345.e28. Available at: <https://doi.org/10.1016/j.cell.2022.12.013>.
- Ma, Y. et al. (2021) 'Mucosal Melanoma: Pathological Evolution, Pathway Dependency and Targeted Therapy', *Frontiers in Oncology*, 11. Available at: <https://www.frontiersin.org/articles/10.3389/fonc.2021.702287> (Accessed: 30 January 2023).
- Mack, S.C. et al. (2018) 'Therapeutic targeting of ependymoma as informed by oncogenic enhancer profiling', *Nature*, 553(7686), pp. 101–105. Available at: <https://doi.org/10.1038/nature25169>.
- Madan, V., Lear, J.T. and Szeimies, R.-M. (2010) 'Non-melanoma skin cancer', *Lancet (London, England)*, 375(9715), pp. 673–685. Available at: [https://doi.org/10.1016/S0140-6736\(09\)61196-X](https://doi.org/10.1016/S0140-6736(09)61196-X).
- Maeshima, K., Ide, S. and Babokhov, M. (2019) 'Dynamic chromatin organization without the 30-nm fiber', *Current Opinion in Cell Biology*, 58, pp. 95–104. Available at: <https://doi.org/10.1016/j.ceb.2019.02.003>.
- Makaranka, S. et al. (2022) 'The gut microbiome and melanoma: A review', *Experimental Dermatology*, 31(9), pp. 1292–1301. Available at: <https://doi.org/10.1111/exd.14639>.
- Mäkinen, N. et al. (2011) 'MED12, the mediator complex subunit 12 gene, is mutated at high frequency in uterine leiomyomas', *Science (New York, N.Y.)*, 334(6053), pp. 252–255. Available at: <https://doi.org/10.1126/science.1208930>.
- Malekan, M., Ebrahimzadeh, M.A. and Sheida, F. (2021) 'The role of Hypoxia-Inducible Factor-1 α and its signaling in melanoma', *Biomedicine & Pharmacotherapy*, 141, p. 111873. Available at: <https://doi.org/10.1016/j.biopha.2021.111873>.
- Mandel, C.R. et al. (2006) 'Polyadenylation factor CPSF-73 is the pre-mRNA 3'-end-processing endonuclease', *Nature*, 444(7121), pp. 953–956. Available at: <https://doi.org/10.1038/nature05363>.
- Mann, R. and Notani, D. (2023) 'Transcription factor condensates and signaling driven transcription', *Nucleus*, 14(1), p. 2205758. Available at: <https://doi.org/10.1080/19491034.2023.2205758>.
- Mansisor, A.R. and Risca, V.I. (2022) 'Chromatin accessibility: methods, mechanisms, and biological insights', *Nucleus*, 13(1), pp. 238–278. Available at: <https://doi.org/10.1080/19491034.2022.2143106>.
- Mansour, M.R. et al. (2014) 'Oncogene regulation. An oncogenic super-enhancer formed through somatic mutation of a noncoding intergenic element', *Science (New York, N.Y.)*, 346(6215), pp. 1373–1377. Available at: <https://doi.org/10.1126/science.1259037>.
- Mantovani, A. et al. (2022) 'Macrophages as tools and targets in cancer therapy', *Nature Reviews Drug Discovery*, 21(11), pp. 799–820. Available at: <https://doi.org/10.1038/s41573-022-00520-5>.
- Marchetti, P. et al. (2018) 'Melanoma metabolism contributes to the cellular responses to MAPK/ERK pathway inhibitors', *Biochimica et Biophysica Acta (BBA) - General Subjects*, 1862(4), pp. 999–1005. Available at: <https://doi.org/10.1016/j.bbagen.2018.01.018>.
- Maresca, V., Flori, E. and Picardo, M. (2015) 'Skin phototype: a new perspective', *Pigment Cell & Melanoma Research*, 28(4), pp. 378–389. Available at: <https://doi.org/10.1111/pcmr.12365>.
- Margue, C. et al. (2019) 'Kinase inhibitor library screening identifies synergistic drug combinations effective in sensitive and resistant melanoma cells', *Journal of experimental & clinical cancer research: CR*, 38(1), p. 56. Available at: <https://doi.org/10.1186/s13046-019-1038-x>.
- Mariathasan, S. et al. (2018) 'TGF β attenuates tumour response to PD-L1 blockade by contributing to exclusion of T cells', *Nature*, 554(7693), pp. 544–548. Available at: <https://doi.org/10.1038/nature25501>.
- Marin-Bejar, O. et al. (2021) 'Evolutionary predictability of genetic versus nongenetic resistance to anticancer drugs in melanoma', *Cancer Cell*, 39(8), pp. 1135–1149.e8. Available at: <https://doi.org/10.1016/j.ccell.2021.05.015>.
- Marine, J.-C., Dawson, S.-J. and Dawson, M.A. (2020) 'Non-genetic mechanisms of therapeutic resistance in cancer', *Nature Reviews. Cancer*, 20(12), pp. 743–756. Available at: <https://doi.org/10.1038/s41568-020-00302-4>.
- Marshall, G.M. et al. (2014) 'The prenatal origins of cancer', *Nature Reviews Cancer*, 14(4), pp. 277–289. Available at: <https://doi.org/10.1038/nrc3679>.

- Marteijn, J.A. et al. (2014) 'Understanding nucleotide excision repair and its roles in cancer and ageing', *Nature Reviews Molecular Cell Biology*, 15(7), pp. 465–481. Available at: <https://doi.org/10.1038/nrm3822>.
- Martincorena, I. et al. (2015) 'High burden and pervasive positive selection of somatic mutations in normal human skin', *Science*, 348(6237), pp. 880–886. Available at: <https://doi.org/10.1126/science.aaa6806>.
- Martincorena, I. (2020) 'Seeds of cancer in normal skin', *Nature*, 586(7830), pp. 504–506. Available at: <https://doi.org/10.1038/d41586-020-02749-9>.
- Martincorena, I. and Campbell, P.J. (2015) 'Somatic mutation in cancer and normal cells', *Science*, 349(6255), pp. 1483–1489. Available at: <https://doi.org/10.1126/science.aab4082>.
- Martins, F. et al. (2019) 'Adverse effects of immune-checkpoint inhibitors: epidemiology, management and surveillance', *Nature Reviews Clinical Oncology*, 16(9), pp. 563–580. Available at: <https://doi.org/10.1038/s41571-019-0218-0>.
- Martire, S. and Banaszynski, L.A. (2020) 'The roles of histone variants in fine-tuning chromatin organization and function', *Nature Reviews Molecular Cell Biology*, 21(9), pp. 522–541. Available at: <https://doi.org/10.1038/s41580-020-0262-8>.
- Marusyk, A., Janiszewska, M. and Polyak, K. (2020) 'Intratumor Heterogeneity: The Rosetta Stone of Therapy Resistance', *Cancer Cell*, 37(4), pp. 471–484. Available at: <https://doi.org/10.1016/j.ccell.2020.03.007>.
- Masri, S. et al. (2022) 'Cellular Interaction of Human Skin Cells towards Natural Bioink via 3D-Bioprinting Technologies for Chronic Wound: A Comprehensive Review', *International Journal of Molecular Sciences*, 23(1), p. 476. Available at: <https://doi.org/10.3390/ijms23010476>.
- Matharu, N. and Ahituv, N. (2020) 'Modulating gene regulation to treat genetic disorders', *Nature Reviews Drug Discovery*, 19(11), pp. 757–775. Available at: <https://doi.org/10.1038/s41573-020-0083-7>.
- Matson, V. et al. (2018) 'The commensal microbiome is associated with anti-PD-1 efficacy in metastatic melanoma patients', *Science (New York, N.Y.)*, 359(6371), pp. 104–108. Available at: <https://doi.org/10.1126/science.aao3290>.
- Maurus, K. et al. (2017) 'The AP-1 transcription factor FOSL1 causes melanocyte reprogramming and transformation', *Oncogene*, 36(36), pp. 5110–5121. Available at: <https://doi.org/10.1038/onc.2017.135>.
- Max, T., Søgaard, M. and Svejstrup, J.Q. (2007) 'Hyperphosphorylation of the C-terminal Repeat Domain of RNA Polymerase II Facilitates Dissociation of Its Complex with Mediator *', *Journal of Biological Chemistry*, 282(19), pp. 14113–14120. Available at: <https://doi.org/10.1074/jbc.M701345200>.
- Maxon, M.E., Goodrich, J.A. and Tjian, R. (1994) 'Transcription factor IIE binds preferentially to RNA polymerase IIa and recruits TFIID: a model for promoter clearance', *Genes & Development*, 8(5), pp. 515–524. Available at: <https://doi.org/10.1101/gad.8.5.515>.
- May, W.A. et al. (1993) 'The Ewing's sarcoma EWS/FLI-1 fusion gene encodes a more potent transcriptional activator and is a more powerful transforming gene than FLI-1', *Molecular and Cellular Biology*, 13(12), pp. 7393–7398. Available at: <https://doi.org/10.1128/mcb.13.12.7393-7398.1993>.
- Mayer, A., Landry, H.M. and Churchman, L.S. (2017) 'Pause & go: from the discovery of RNA polymerase pausing to its functional implications', *Current Opinion in Cell Biology*, 46, pp. 72–80. Available at: <https://doi.org/10.1016/j.ceb.2017.03.002>.
- Mazurkiewicz, J. et al. (2022) 'Melanoma cells with diverse invasive potential differentially induce the activation of normal human fibroblasts', *Cell Communication and Signaling*, 20(1), p. 63. Available at: <https://doi.org/10.1186/s12964-022-00871-x>.
- McArthur, G.A. et al. (2014) 'Safety and efficacy of vemurafenib in BRAF(V600E) and BRAF(V600K) mutation-positive melanoma (BRIM-3): extended follow-up of a phase 3, randomised, open-label study', *The Lancet. Oncology*, 15(3), pp. 323–332. Available at: [https://doi.org/10.1016/S1470-2045\(14\)70012-9](https://doi.org/10.1016/S1470-2045(14)70012-9).
- McConnell, A.T. et al. (2016) 'The prognostic significance and impact of the CXCR4–CXCR7–CXCL12 axis in primary cutaneous melanoma', *British Journal of Dermatology*, 175(6), pp. 1210–1220. Available at: <https://doi.org/10.1111/bjd.14720>.
- McGinty, R.K. and Tan, S. (2015) 'Nucleosome structure and function', *Chemical Reviews*, 115(6), pp. 2255–2273. Available at: <https://doi.org/10.1021/cr500373h>.
- Mckenzie, J.A. and Grossman, D. (2012) 'Role of the Apoptotic and Mitotic Regulator Survivin in Melanoma', *Anticancer Research*, 32(2), pp. 397–404.
- Medema, J.P. (2018) 'Escape from senescence boosts tumour growth', *Nature*, 553(7686), pp. 37–38. Available at: <https://doi.org/10.1038/d41586-017-08652-0>.
- Medicine, N. (no date) Treatment, Northwestern Medicine. Available at: <https://www.nm.org/conditions-and-care-areas/dermatology/moles-and-melanoma/treatment> (Accessed: 27 February 2023).
- Mehta, A. et al. (2018) 'Immunotherapy Resistance by Inflammation-Induced Dedifferentiation', *Cancer Discovery*, 8(8), pp. 935–943. Available at: <https://doi.org/10.1158/2159-8290.CD-17-1178>.
- Mehta, S. and Zhang, J. (2022) 'Liquid–liquid phase separation drives cellular function and dysfunction in cancer', *Nature Reviews Cancer*, 22(4), pp. 239–252. Available at: <https://doi.org/10.1038/s41568-022-00444-7>.
- Mekadim, C. et al. (2022) 'Dysbiosis of skin microbiome and gut microbiome in melanoma progression', *BMC Microbiology*, 22(1), p. 63. Available at: <https://doi.org/10.1186/s12866-022-02458-5>.

Melanoma Skin Cancer Statistics (no date). Available at: <https://www.cancer.org/cancer/melanoma-skin-cancer/about/key-statistics.html> (Accessed: 10 February 2023).

Mele, L. et al. (2020) 'The role of autophagy in resistance to targeted therapies', *Cancer Treatment Reviews*, 88, p. 102043. Available at: <https://doi.org/10.1016/j.ctrv.2020.102043>.

Melnikova, V.O. and Bar-Eli, M. (2009) 'Inflammation and melanoma metastasis', *Pigment Cell & Melanoma Research*, 22(3), pp. 257–267. Available at: <https://doi.org/10.1111/j.1755-148X.2009.00570.x>.

Mgrditchian, T. et al. (2017) 'Targeting autophagy inhibits melanoma growth by enhancing NK cells infiltration in a CCL5-dependent manner', *Proceedings of the National Academy of Sciences of the United States of America*, 114(44), pp. E9271–E9279. Available at: <https://doi.org/10.1073/pnas.1703921114>.

Michael, A.K. and Thomä, N.H. (2021) 'Reading the chromatinized genome', *Cell*, 184(14), pp. 3599–3611. Available at: <https://doi.org/10.1016/j.cell.2021.05.029>.

Michaloglou, C. et al. (2005) 'BRAF^{E600}-associated senescence-like cell cycle arrest of human naevi', *Nature*, 436(7051), pp. 720–724. Available at: <https://doi.org/10.1038/nature03890>.

Milanovic, M. et al. (2018) 'Senescence-associated reprogramming promotes cancer stemness', *Nature*, 553(7686), pp. 96–100. Available at: <https://doi.org/10.1038/nature25167>.

Milet, C. and Monsoro-Burq, A.H. (2012) 'Neural crest induction at the neural plate border in vertebrates', *Developmental Biology*, 366(1), pp. 22–33. Available at: <https://doi.org/10.1016/j.ydbio.2012.01.013>.

Miller, A.J. and Mihm, M.C. (2006) 'Melanoma', *New England Journal of Medicine*, 355(1), pp. 51–65. Available at: <https://doi.org/10.1056/NEJMra052166>.

Misteli, T. (2020) 'The Self-Organizing Genome: Principles of Genome Architecture and Function', *Cell*, 183(1), pp. 28–45. Available at: <https://doi.org/10.1016/j.cell.2020.09.014>.

Mittal, P. and Roberts, C.W.M. (2020) 'The SWI/SNF complex in cancer — biology, biomarkers and therapy', *Nature Reviews Clinical Oncology*, 17(7), pp. 435–448. Available at: <https://doi.org/10.1038/s41571-020-0357-3>.

Mo, X. et al. (2018) 'Interferon- γ Signaling in Melanocytes and Melanoma Cells Regulates Expression of CTLA-4', *Cancer Research*, 78(2), pp. 436–450. Available at: <https://doi.org/10.1158/0008-5472.CAN-17-1615>.

Mohammad, R.M. et al. (2015) 'Broad targeting of resistance to apoptosis in cancer', *Seminars in cancer biology*, 35(0), pp. S78–S103. Available at: <https://doi.org/10.1016/j.semcancer.2015.03.001>.

Mohammed Ismail, W. et al. (2023) 'MacroH2A histone variants modulate enhancer activity to repress oncogenic programs and cellular reprogramming', *Communications Biology*, 6(1), pp. 1–19. Available at: <https://doi.org/10.1038/s42003-023-04571-1>.

Molhoek, K.R. et al. (2011) 'Comprehensive analysis of RTK activation in human melanomas reveals autocrine signaling through IGF-1R', *Melanoma research*, 21(4), pp. 274–284. Available at: <https://doi.org/10.1097/CMR.0b013e328343a1d6>.

Monk, M. and Holding, C. (2001) 'Human embryonic genes re-expressed in cancer cells', *Oncogene*, 20(56), pp. 8085–8091. Available at: <https://doi.org/10.1038/sj.onc.1205088>.

Montagnani, V. et al. (2016) 'Thin and thick primary cutaneous melanomas reveal distinct patterns of somatic copy number alterations', *Oncotarget*, 7(21), pp. 30365–30378. Available at: <https://doi.org/10.18632/oncotarget.8758>.

Moon, H. et al. (2017) 'Melanocyte Stem Cell Activation and Translocation Initiate Cutaneous Melanoma in Response to UV Exposure', *Cell Stem Cell*, 21(5), pp. 665–678.e6. Available at: <https://doi.org/10.1016/j.stem.2017.09.001>.

Moore, J.E. et al. (2020) 'Expanded encyclopaedias of DNA elements in the human and mouse genomes', *Nature*, 583(7818), pp. 699–710. Available at: <https://doi.org/10.1038/s41586-020-2493-4>.

Moreira, A. et al. (2021) 'Current Melanoma Treatments: Where Do We Stand?', *Cancers*, 13(2), p. 221. Available at: <https://doi.org/10.3390/cancers13020221>.

Moreiras, H., Seabra, M.C. and Barral, D.C. (2021) 'Melanin Transfer in the Epidermis: The Pursuit of Skin Pigmentation Control Mechanisms', *International Journal of Molecular Sciences*, 22(9), p. 4466. Available at: <https://doi.org/10.3390/ijms22094466>.

Morgan, M.A.J. and Shilatifard, A. (2020) 'Reevaluating the roles of histone-modifying enzymes and their associated chromatin modifications in transcriptional regulation', *Nature Genetics*, 52(12), pp. 1271–1281. Available at: <https://doi.org/10.1038/s41588-020-00736-4>.

Moriceau, G. et al. (2015) 'Tunable-combinatorial mechanisms of acquired resistance limit the efficacy of BRAF/MEK cotargeting but result in melanoma drug addiction', *Cancer Cell*, 27(2), pp. 240–256. Available at: <https://doi.org/10.1016/j.ccell.2014.11.018>.

Moro, N., Mauch, C. and Zigrino, P. (2014) 'Metalloproteinases in melanoma', *European Journal of Cell Biology*, 93(1–2), pp. 23–29. Available at: <https://doi.org/10.1016/j.ejcb.2014.01.002>.

Mort, R.L., Jackson, I.J. and Patton, E.E. (2015) 'The melanocyte lineage in development and disease', *Development*, 142(4), pp. 620–632. Available at: <https://doi.org/10.1242/dev.106567>.

Morton, D.L. et al. (2014) 'Final trial report of sentinel-node biopsy versus nodal observation in melanoma', *The New England Journal of Medicine*, 370(7), pp. 599–609. Available at: <https://doi.org/10.1056/NEJMoa1310460>.

- Mueller, B. et al. (2017) 'Widespread changes in nucleosome accessibility without changes in nucleosome occupancy during a rapid transcriptional induction', *Genes & Development*, 31(5), pp. 451–462. Available at: <https://doi.org/10.1101/gad.293118.116>.
- Mullenders, L.H.F. (2018) 'Solar UV damage to cellular DNA: from mechanisms to biological effects', *Photochemical & Photobiological Sciences: Official Journal of the European Photochemistry Association and the European Society for Photobiology*, 17(12), pp. 1842–1852. Available at: <https://doi.org/10.1039/c8pp00182k>.
- Müller, F. and Tora, L. (2014) 'Chromatin and DNA sequences in defining promoters for transcription initiation', *Biochimica Et Biophysica Acta*, 1839(3), pp. 118–128. Available at: <https://doi.org/10.1016/j.bbagr.2013.11.003>.
- Müller, J. et al. (2014) 'Low MITF/AXL ratio predicts early resistance to multiple targeted drugs in melanoma', *Nature Communications*, 5(1), p. 5712. Available at: <https://doi.org/10.1038/ncomms6712>.
- Muniz, L., Nicolas, E. and Trouche, D. (2021) 'RNA polymerase II speed: a key player in controlling and adapting transcriptome composition', *The EMBO Journal*, 40(15), p. e105740. Available at: <https://doi.org/10.15252/embj.2020105740>.
- Murakami, K. et al. (2015) 'Structure of an RNA polymerase II preinitiation complex', *Proceedings of the National Academy of Sciences*, 112(44), pp. 13543–13548. Available at: <https://doi.org/10.1073/pnas.1518255112>.
- Murisier, F., Guichard, S. and Beermann, F. (2007) 'The tyrosinase enhancer is activated by Sox10 and Mitf in mouse melanocytes', *Pigment Cell Research*, 20(3), pp. 173–184. Available at: <https://doi.org/10.1111/j.1600-0749.2007.00368.x>.
- Nabet, B. et al. (2015) 'Deregulation of the Ras-Erk Signaling Axis Modulates the Enhancer Landscape', *Cell Reports*, 12(8), pp. 1300–1313. Available at: <https://doi.org/10.1016/j.celrep.2015.06.078>.
- Nagarajan, P. et al. (2019) 'Keratinocyte Carcinomas: Current concepts and future research priorities', *Clinical cancer research : an official journal of the American Association for Cancer Research*, 25(8), pp. 2379–2391. Available at: <https://doi.org/10.1158/1078-0432.CCR-18-1122>.
- Nagy, J.A. et al. (2010) 'Heterogeneity of the tumor vasculature', *Seminars in Thrombosis and Hemostasis*, 36(3), pp. 321–331. Available at: <https://doi.org/10.1055/s-0030-1253454>.
- Najem, A. et al. (2022) 'Understanding Molecular Mechanisms of Phenotype Switching and Crosstalk with TME to Reveal New Vulnerabilities of Melanoma', *Cells*, 11(7), p. 1157. Available at: <https://doi.org/10.3390/cells11071157>.
- Nakamura, Y. et al. (2017) 'Targeting of super-enhancers and mutant BRAF can suppress growth of BRAF-mutant colon cancer cells via repression of MAPK signaling pathway', *Cancer Letters*, 402, pp. 100–109. Available at: <https://doi.org/10.1016/j.canlet.2017.05.017>.
- Nath, S. and Villadsen, J. (2015) 'Oxidative phosphorylation revisited', *Biotechnology and Bioengineering*, 112(3), pp. 429–437. Available at: <https://doi.org/10.1002/bit.25492>.
- Naumov, G.N. et al. (2006) 'A model of human tumor dormancy: an angiogenic switch from the nonangiogenic phenotype', *Journal of the National Cancer Institute*, 98(5), pp. 316–325. Available at: <https://doi.org/10.1093/jnci/djj068>.
- Nazarov, P.V. et al. (2013) 'Interplay of microRNAs, transcription factors and target genes: linking dynamic expression changes to function', *Nucleic Acids Research*, 41(5), pp. 2817–2831. Available at: <https://doi.org/10.1093/nar/gks1471>.
- Nejman, D. et al. (2020) 'The human tumor microbiome is composed of tumor type–specific intracellular bacteria', *Science*, 368(6494), pp. 973–980. Available at: <https://doi.org/10.1126/science.aay9189>.
- Neophytou, C.M. et al. (2021) 'Apoptosis Deregulation and the Development of Cancer Multi-Drug Resistance', *Cancers*, 13(17), p. 4363. Available at: <https://doi.org/10.3390/cancers13174363>.
- Ng, M.F., Simmons, J.L. and Boyle, G.M. (2022) 'Heterogeneity in Melanoma', *Cancers*, 14(12), p. 3030. Available at: <https://doi.org/10.3390/cancers14123030>.
- Ngeow, K.C. et al. (2018) 'BRAF/MAPK and GSK3 signaling converges to control MITF nuclear export', *Proceedings of the National Academy of Sciences*, 115(37), pp. E8668–E8677. Available at: <https://doi.org/10.1073/pnas.1810498115>.
- Nguyen, V.Q. et al. (2021) 'Spatiotemporal coordination of transcription preinitiation complex assembly in live cells', *Molecular Cell*, 81(17), pp. 3560–3575.e6. Available at: <https://doi.org/10.1016/j.molcel.2021.07.022>.
- Nie, Z. et al. (2012) 'c-Myc Is a Universal Amplifier of Expressed Genes in Lymphocytes and Embryonic Stem Cells', *Cell*, 151(1), pp. 68–79. Available at: <https://doi.org/10.1016/j.cell.2012.08.033>.
- Niknafs, N. et al. (2023) 'Persistent mutation burden drives sustained anti-tumor immune responses', *Nature Medicine*, 29(2), pp. 440–449. Available at: <https://doi.org/10.1038/s41591-022-02163-w>.
- Nilson, K.A. et al. (2015) 'THZ1 Reveals Roles for Cdk7 in Co-transcriptional Capping and Pausing', *Molecular Cell*, 59(4), pp. 576–587. Available at: <https://doi.org/10.1016/j.molcel.2015.06.032>.
- Ning, B. et al. (2022) 'The Predictive Value of Tumor Mutation Burden on Clinical Efficacy of Immune Checkpoint Inhibitors in Melanoma: A Systematic Review and Meta-Analysis', *Frontiers in Pharmacology*, 13, p. 748674. Available at: <https://doi.org/10.3389/fphar.2022.748674>.
- Noel, P. et al. (2019) 'Triptolide and Its Derivatives as Cancer Therapies', *Trends in Pharmacological Sciences*, 40(5), pp. 327–341. Available at: <https://doi.org/10.1016/j.tips.2019.03.002>.
- Noel, P. et al. (2020) 'Triptolide targets super-enhancer networks in pancreatic cancer cells and cancer-associated fibroblasts', *Oncogenesis*, 9(11), pp. 1–12. Available at: <https://doi.org/10.1038/s41389-020-00285-9>.

- Nogales, E. and Greber, B.J. (2019) 'High-resolution cryo-EM structures of TFIIF and their functional implications', *Current opinion in structural biology*, 59, pp. 188–194. Available at: <https://doi.org/10.1016/j.sbi.2019.08.002>.
- Noman, M.Z. et al. (2020) 'Inhibition of Vps34 reprograms cold into hot inflamed tumors and improves anti-PD-1/PD-L1 immunotherapy', *Science Advances*, 6(18), p. eaax7881. Available at: <https://doi.org/10.1126/sciadv.aax7881>.
- Noman, M.Z. et al. (2022) 'The β -carboline Harmine improves the therapeutic benefit of anti-PD1 in melanoma by increasing the MHC-I-dependent antigen presentation', *Frontiers in Immunology*, 13, p. 980704. Available at: <https://doi.org/10.3389/fimmu.2022.980704>.
- Northcott, P.A. et al. (2014) 'Enhancer hijacking activates GFI1 family oncogenes in medulloblastoma', *Nature*, 511(7510), pp. 428–434. Available at: <https://doi.org/10.1038/nature13379>.
- O'Boyle, G. et al. (2013) 'Inhibition of CXCR4–CXCL12 chemotaxis in melanoma by AMD11070', *British Journal of Cancer*, 108(8), pp. 1634–1640. Available at: <https://doi.org/10.1038/bjc.2013.124>.
- O'Connell, M.P. et al. (2013) 'Hypoxia Induces Phenotypic Plasticity and Therapy Resistance in Melanoma via the Tyrosine Kinase Receptors ROR1 and ROR2', *Cancer Discovery*, 3(12), pp. 1378–1393. Available at: <https://doi.org/10.1158/2159-8290.CD-13-0005>.
- O'Donnell, J.S., Teng, M.W.L. and Smyth, M.J. (2019) 'Cancer immunoediting and resistance to T cell-based immunotherapy', *Nature Reviews Clinical Oncology*, 16(3), pp. 151–167. Available at: <https://doi.org/10.1038/s41571-018-0142-8>.
- Okabe, A. and Kaneda, A. (2021) 'Transcriptional dysregulation by aberrant enhancer activation and rewiring in cancer', *Cancer Science*, 112(6), pp. 2081–2088. Available at: <https://doi.org/10.1111/cas.14884>.
- Oksenysh, V. et al. (2009) 'Molecular insights into the recruitment of TFIIF to sites of DNA damage', *The EMBO Journal*, 28(19), pp. 2971–2980. Available at: <https://doi.org/10.1038/emboj.2009.230>.
- Oksenysh, V. and Coin, F. (2010) 'The long unwinding road: XPB and XPD helicases in damaged DNA opening', *Cell Cycle*, 9(1), pp. 90–96. Available at: <https://doi.org/10.4161/cc.9.1.10267>.
- Oladipupo, S. et al. (2011) 'VEGF is essential for hypoxia-inducible factor-mediated neovascularization but dispensable for endothelial sprouting', *Proceedings of the National Academy of Sciences of the United States of America*, 108(32), pp. 13264–13269. Available at: <https://doi.org/10.1073/pnas.1101321108>.
- Oldridge, D.A. et al. (2015) 'Genetic predisposition to neuroblastoma mediated by a LMO1 super-enhancer polymorphism', *Nature*, 528(7582), pp. 418–421. Available at: <https://doi.org/10.1038/nature15540>.
- Olvedy, M. et al. (2017) 'Comparative oncogenomics identifies tyrosine kinase FES as a tumor suppressor in melanoma', *The Journal of Clinical Investigation*, 127(6), pp. 2310–2325. Available at: <https://doi.org/10.1172/JCI91291>.
- Ong, C.-T. and Corces, V.G. (2011) 'Enhancer function: new insights into the regulation of tissue-specific gene expression', *Nature Reviews Genetics*, 12(4), pp. 283–293. Available at: <https://doi.org/10.1038/nrg2957>.
- Oren, Y. et al. (2021) 'Cycling cancer persister cells arise from lineages with distinct programs', *Nature*, 596(7873), pp. 576–582. Available at: <https://doi.org/10.1038/s41586-021-03796-6>.
- Orgaz, J.L. and Sanz-Moreno, V. (2020) 'What does not kill you makes you stronger: surviving anti-cancer therapies by cytoskeletal remodeling and Myosin II reactivation', *Molecular & Cellular Oncology*, 7(3), p. 1735911. Available at: <https://doi.org/10.1080/23723556.2020.1735911>.
- Orphanides, G., Lagrange, T. and Reinberg, D. (1996) 'The general transcription factors of RNA polymerase II', *Genes & Development*, 10(21), pp. 2657–2683. Available at: <https://doi.org/10.1101/gad.10.21.2657>.
- Osrodek, M. and Wozniak, M. (2021) 'Targeting Genome Stability in Melanoma—A New Approach to an Old Field', *International Journal of Molecular Sciences*, 22(7), p. 3485. Available at: <https://doi.org/10.3390/ijms22073485>.
- Ott, C.J. et al. (2018) 'Enhancer Architecture and Essential Core Regulatory Circuitry of Chronic Lymphocytic Leukemia', *Cancer Cell*, 34(6), pp. 982–995.e7. Available at: <https://doi.org/10.1016/j.ccell.2018.11.001>.
- Otte, J. et al. (2021) 'MYCN Function in Neuroblastoma Development', *Frontiers in Oncology*, 10. Available at: <https://www.frontiersin.org/articles/10.3389/fonc.2020.624079> (Accessed: 3 May 2023).
- Ottema, S. et al. (2021) 'The leukemic oncogene EVI1 hijacks a MYC super-enhancer by CTCF-facilitated loops', *Nature Communications*, 12(1), p. 5679. Available at: <https://doi.org/10.1038/s41467-021-25862-3>.
- Ouzounova, M. et al. (2017) 'Monocytic and granulocytic myeloid derived suppressor cells differentially regulate spatiotemporal tumour plasticity during metastatic cascade', *Nature Communications*, 8, p. 14979. Available at: <https://doi.org/10.1038/ncomms14979>.
- Ozer, J. et al. (1998) 'Transcription factor IIA derepresses TATA-binding protein (TBP)-associated factor inhibition of TBP-DNA binding', *The Journal of Biological Chemistry*, 273(23), pp. 14293–14300. Available at: <https://doi.org/10.1074/jbc.273.23.14293>.
- Pagliuca, C., Di Leo, L. and De Zio, D. (2022) 'New Insights into the Phenotype Switching of Melanoma', *Cancers*, 14(24), p. 6118. Available at: <https://doi.org/10.3390/cancers14246118>.
- Paik, J. (2022) 'Nivolumab Plus Relatlimab: First Approval', *Drugs*, 82(8), pp. 925–931. Available at: <https://doi.org/10.1007/s40265-022-01723-1>.
- Pal, S. et al. (2022) 'The microbiome restrains melanoma bone growth by promoting intestinal NK and Th1 cell homing to bone', *The Journal of Clinical Investigation*, 132(12). Available at: <https://doi.org/10.1172/JCI157340>.

- Palacio, M. and Taatjes, D.J. (2022) 'Merging Established Mechanisms with New Insights: Condensates, Hubs, and the Regulation of RNA Polymerase II Transcription', *Journal of Molecular Biology*, 434(1), p. 167216. Available at: <https://doi.org/10.1016/j.jmb.2021.167216>.
- Paluncic, J. et al. (2016) 'Roads to melanoma: Key pathways and emerging players in melanoma progression and oncogenic signaling', *Biochimica Et Biophysica Acta*, 1863(4), pp. 770–784. Available at: <https://doi.org/10.1016/j.bbamcr.2016.01.025>.
- Papaccio, F. et al. (2021) 'Profiling Cancer-Associated Fibroblasts in Melanoma', *International Journal of Molecular Sciences*, 22(14), p. 7255. Available at: <https://doi.org/10.3390/ijms22147255>.
- Papai, G. et al. (2020) 'Structure of SAGA and mechanism of TBP deposition on gene promoters', *Nature*, 577(7792), pp. 711–716. Available at: <https://doi.org/10.1038/s41586-020-1944-2>.
- Pardoll, D.M. (2012) 'The blockade of immune checkpoints in cancer immunotherapy', *Nature Reviews Cancer*, 12(4), pp. 252–264. Available at: <https://doi.org/10.1038/nrc3239>.
- Parua, P.K. et al. (2018) 'A Cdk9-PP1 switch regulates the elongation-termination transition of RNA polymerase II', *Nature*, 558(7710), pp. 460–464. Available at: <https://doi.org/10.1038/s41586-018-0214-z>.
- Parua, P.K. and Fisher, R.P. (2020) 'Dissecting the Pol II transcription cycle and derailing cancer with CDK inhibitors', *Nature Chemical Biology*, 16(7), pp. 716–724. Available at: <https://doi.org/10.1038/s41589-020-0563-4>.
- Pastushenko, I. et al. (2018) 'Identification of the tumour transition states occurring during EMT', *Nature*, 556(7702), pp. 463–468. Available at: <https://doi.org/10.1038/s41586-018-0040-3>.
- Pastwińska, J. et al. (2022) 'Targeting EGFR in melanoma – The sea of possibilities to overcome drug resistance', *Biochimica et Biophysica Acta (BBA) - Reviews on Cancer*, 1877(4), p. 188754. Available at: <https://doi.org/10.1016/j.bbcan.2022.188754>.
- Patange, S. et al. (2022) 'MYC amplifies gene expression through global changes in transcription factor dynamics', *Cell Reports*, 38(4), p. 110292. Available at: <https://doi.org/10.1016/j.celrep.2021.110292>.
- Patel, A.B. et al. (2018) 'Structure of human TFIID and mechanism of TBP loading onto promoter DNA', *Science (New York, N.Y.)*, 362(6421), p. eaau8872. Available at: <https://doi.org/10.1126/science.aau8872>.
- Patel, H. et al. (2018) 'ICEC0942, an Orally Bioavailable Selective Inhibitor of CDK7 for Cancer Treatment', *Molecular Cancer Therapeutics*, 17(6), pp. 1156–1166. Available at: <https://doi.org/10.1158/1535-7163.MCT-16-0847>.
- Patel, R.P. et al. (2023) 'The therapeutic potential of targeting minimal residual disease in melanoma', *Clinical and Translational Medicine*, 13(3), p. e1197. Available at: <https://doi.org/10.1002/ctm2.1197>.
- Pathmanathan, S. et al. (2022) 'Drugging the undruggable proteins in cancer: A systems biology approach', *Current Opinion in Chemical Biology*, 66, p. 102079. Available at: <https://doi.org/10.1016/j.cbpa.2021.07.004>.
- Pathria, G. et al. (2019) 'Translational reprogramming marks adaptation to asparagine restriction in cancer', *Nature Cell Biology*, 21(12), pp. 1590–1603. Available at: <https://doi.org/10.1038/s41556-019-0415-1>.
- Pavey, S.J. et al. (2002) 'Loss of p16 expression is associated with histological features of melanoma invasion', *Melanoma Research*, 12(6), pp. 539–547. Available at: <https://doi.org/10.1097/00008390-200212000-00003>.
- Pavlova, N.N. and Thompson, C.B. (2016) 'The Emerging Hallmarks of Cancer Metabolism', *Cell Metabolism*, 23(1), pp. 27–47. Available at: <https://doi.org/10.1016/j.cmet.2015.12.006>.
- Pawlik, L., Morgenroth, S. and Dummer, R. (2023) 'Recent Progress in the Diagnosis and Treatment of Melanoma and Other Skin Cancers', *Cancers*, 15(6), p. 1824. Available at: <https://doi.org/10.3390/cancers15061824>.
- Pedri, D. et al. (2022) 'Epithelial-to-mesenchymal-like transition events in melanoma', *The FEBS Journal*, 289(5), pp. 1352–1368. Available at: <https://doi.org/10.1111/febs.16021>.
- Peinado, H. et al. (2012) 'Melanoma exosomes educate bone marrow progenitor cells toward a pro-metastatic phenotype through MET', *Nature Medicine*, 18(6), pp. 883–891. Available at: <https://doi.org/10.1038/nm.2753>.
- Peinado, H. et al. (2017) 'Pre-metastatic niches: organ-specific homes for metastases', *Nature Reviews Cancer*, 17(5), pp. 302–317. Available at: <https://doi.org/10.1038/nrc.2017.6>.
- Penagos-Puig, A. and Furlan-Magaril, M. (2020) 'Heterochromatin as an Important Driver of Genome Organization', *Frontiers in Cell and Developmental Biology*, 8. Available at: <https://www.frontiersin.org/articles/10.3389/fcell.2020.579137> (Accessed: 19 April 2023).
- Peng, Y. and Croce, C.M. (2016) 'The role of MicroRNAs in human cancer', *Signal Transduction and Targeted Therapy*, 1(1), pp. 1–9. Available at: <https://doi.org/10.1038/sigtrans.2015.4>.
- Perego, M. et al. (2018) 'A slow-cycling subpopulation of melanoma cells with highly invasive properties', *Oncogene*, 37(3), pp. 302–312. Available at: <https://doi.org/10.1038/ncr.2017.341>.
- Pereira, E.R. et al. (2018) 'Lymph node metastases can invade local blood vessels, exit the node, and colonize distant organs in mice', *Science (New York, N.Y.)*, 359(6382), pp. 1403–1407. Available at: <https://doi.org/10.1126/science.aal3622>.
- Pereira, R.B. et al. (2019) 'Marine-Derived Anticancer Agents: Clinical Benefits, Innovative Mechanisms, and New Targets', *Marine Drugs*, 17(6), p. 329. Available at: <https://doi.org/10.3390/md17060329>.

- Pérez-Guijarro, E. et al. (2016) 'Lineage-specific roles of the cytoplasmic polyadenylation factor CPEB4 in the regulation of melanoma drivers', *Nature Communications*, 7(1), p. 13418. Available at: <https://doi.org/10.1038/ncomms13418>.
- Pham, D. (Daniel) M., Guhan, S. and Tsao, H. (2020) 'KIT and Melanoma: Biological Insights and Clinical Implications', *Yonsei Medical Journal*, 61(7), pp. 562–571. Available at: <https://doi.org/10.3349/ymj.2020.61.7.562>.
- Phatnani, H.P. and Greenleaf, A.L. (2006) 'Phosphorylation and functions of the RNA polymerase II CTD', *Genes & Development*, 20(21), pp. 2922–2936. Available at: <https://doi.org/10.1101/gad.1477006>.
- Philippidou, D. et al. (2010) 'Signatures of MicroRNAs and Selected MicroRNA Target Genes in Human Melanoma', *Cancer Research*, 70(10), pp. 4163–4173. Available at: <https://doi.org/10.1158/0008-5472.CAN-09-4512>.
- Phung, B. et al. (2019) 'The X-Linked DDX3X RNA Helicase Dictates Translation Reprogramming and Metastasis in Melanoma', *Cell Reports*, 27(12), pp. 3573–3586.e7. Available at: <https://doi.org/10.1016/j.celrep.2019.05.069>.
- Pierrat, M.-J. et al. (2012) 'Expression of microphthalmia-associated transcription factor (MITF), which is critical for melanoma progression, is inhibited by both transcription factor GLI2 and transforming growth factor- β ', *The Journal of Biological Chemistry*, 287(22), pp. 17996–18004. Available at: <https://doi.org/10.1074/jbc.M112.358341>.
- Pillai, M. et al. (2022) 'Quantitative landscapes reveal trajectories of cell-state transitions associated with drug resistance in melanoma', *iScience*, 25(12), p. 105499. Available at: <https://doi.org/10.1016/j.isci.2022.105499>.
- Piskounova, E. et al. (2015) 'Oxidative stress inhibits distant metastasis by human melanoma cells', *Nature*, 527(7577), pp. 186–191. Available at: <https://doi.org/10.1038/nature15726>.
- Pistillo, M.P. et al. (2020) 'Phenotypic characterization of tumor CTLA-4 expression in melanoma tissues and its possible role in clinical response to Ipilimumab', *Clinical Immunology (Orlando, Fla.)*, 215, p. 108428. Available at: <https://doi.org/10.1016/j.clim.2020.108428>.
- Pizzimenti, S. et al. (2021) 'Oxidative Stress-Related Mechanisms in Melanoma and in the Acquired Resistance to Targeted Therapies', *Antioxidants*, 10(12), p. 1942. Available at: <https://doi.org/10.3390/antiox10121942>.
- Plaschka, C. et al. (2016) 'Transcription initiation complex structures elucidate DNA opening', *Nature*, 533(7603), pp. 353–358. Available at: <https://doi.org/10.1038/nature17990>.
- Plaschka, M. et al. (2022) 'ZEB1 transcription factor promotes immune escape in melanoma', *Journal for Immunotherapy of Cancer*, 10(3), p. e003484. Available at: <https://doi.org/10.1136/jitc-2021-003484>.
- Pleasant, E.D. et al. (2010) 'A comprehensive catalogue of somatic mutations from a human cancer genome', *Nature*, 463(7278), pp. 191–196. Available at: <https://doi.org/10.1038/nature08658>.
- Plet, A., Eick, D. and Blanchard, J.M. (1995) 'Elongation and premature termination of transcripts initiated from c-fos and c-myc promoters show dissimilar patterns', *Oncogene*, 10(2), pp. 319–328.
- Plonka, P.M. et al. (2009) 'What are melanocytes really doing all day long...?', *Experimental Dermatology*, 18(9), pp. 799–819. Available at: <https://doi.org/10.1111/j.1600-0625.2009.00912.x>.
- Pogenberg, V. et al. (2012) 'Restricted leucine zipper dimerization and specificity of DNA recognition of the melanocyte master regulator MITF', *Genes & Development*, 26(23), pp. 2647–2658. Available at: <https://doi.org/10.1101/gad.198192.112>.
- Pollard, T.D. et al. (2016) *Cell Biology: Third Edition*. Elsevier Inc. Available at: <https://www.research.ed.ac.uk/en/publications/cell-biology-third-edition> (Accessed: 18 April 2023).
- Popovic, A. and Tartare-Deckert, S. (2022) 'Role of extracellular matrix architecture and signaling in melanoma therapeutic resistance', *Frontiers in Oncology*, 12. Available at: <https://www.frontiersin.org/articles/10.3389/fonc.2022.924553> (Accessed: 18 March 2023).
- Pott, S. and Lieb, J.D. (2015) 'What are super-enhancers?', *Nature Genetics*, 47(1), pp. 8–12. Available at: <https://doi.org/10.1038/ng.3167>.
- Potterf, S.B. et al. (2000) 'Transcription factor hierarchy in Waardenburg syndrome: regulation of MITF expression by SOX10 and PAX3', *Human Genetics*, 107(1), pp. 1–6. Available at: <https://doi.org/10.1007/s004390000328>.
- Poulikakos, P.I. et al. (2010) 'RAF inhibitors transactivate RAF dimers and ERK signalling in cells with wild-type BRAF', *Nature*, 464(7287), pp. 427–430. Available at: <https://doi.org/10.1038/nature08902>.
- Poulos, R.C. et al. (2015) 'The search for cis-regulatory driver mutations in cancer genomes', *Oncotarget*, 6(32), pp. 32509–32525. Available at: <https://doi.org/10.18632/oncotarget.5085>.
- Psaila, B. and Lyden, D. (2009) 'The metastatic niche: adapting the foreign soil', *Nature Reviews Cancer*, 9(4), pp. 285–293. Available at: <https://doi.org/10.1038/nrc2621>.
- Puente, X.S. et al. (2015) 'Non-coding recurrent mutations in chronic lymphocytic leukaemia', *Nature*, 526(7574), pp. 519–524. Available at: <https://doi.org/10.1038/nature14666>.
- Pugh, B.F. and Tjian, R. (1991) 'Transcription from a TATA-less promoter requires a multisubunit TFIID complex', *Genes & Development*, 5(11), pp. 1935–1945. Available at: <https://doi.org/10.1101/gad.5.11.1935>.
- Pulikkan, J.A. et al. (2018) 'CBF β -SMMHC Inhibition Triggers Apoptosis by Disrupting MYC Chromatin Dynamics in Acute Myeloid Leukemia', *Cell*, 174(1), pp. 172–186.e21. Available at: <https://doi.org/10.1016/j.cell.2018.05.048>.

- Pyo, S.M. and Maibach, H.I. (2019) 'Skin Metabolism: Relevance of Skin Enzymes for Rational Drug Design', *Skin Pharmacology and Physiology*, 32(5), pp. 283–294. Available at: <https://doi.org/10.1159/000501732>.
- Qian, H., Yang, C. and Yang, Y. (2017) 'MicroRNA-26a inhibits the growth and invasiveness of malignant melanoma and directly targets on MITF gene', *Cell Death Discovery*, 3(1), pp. 1–9. Available at: <https://doi.org/10.1038/cddiscovery.2017.28>.
- Qiao, Y. et al. (2016) 'AP-1 Is a Key Regulator of Proinflammatory Cytokine TNF α -mediated Triple-negative Breast Cancer Progression', *The Journal of Biological Chemistry*, 291(10), pp. 5068–5079. Available at: <https://doi.org/10.1074/jbc.M115.702571>.
- Quail, D.F. and Dannenberg, A.J. (2019) 'The obese adipose tissue microenvironment in cancer development and progression', *Nature Reviews. Endocrinology*, 15(3), pp. 139–154. Available at: <https://doi.org/10.1038/s41574-018-0126-x>.
- Quaresmini, D. and Guida, M. (2020) 'Neoangiogenesis in Melanoma: An Issue in Biology and Systemic Treatment', *Frontiers in Immunology*, 11. Available at: <https://www.frontiersin.org/articles/10.3389/fimmu.2020.584903> (Accessed: 22 March 2023).
- Rabbie, R. et al. (2019) 'Melanoma subtypes: genomic profiles, prognostic molecular markers and therapeutic possibilities', *The Journal of Pathology*, 247(5), pp. 539–551. Available at: <https://doi.org/10.1002/path.5213>.
- Radhakrishnan, S.K. and Gartel, A.L. (2006) 'A novel transcriptional inhibitor induces apoptosis in tumor cells and exhibits antiangiogenic activity', *Cancer Research*, 66(6), pp. 3264–3270. Available at: <https://doi.org/10.1158/0008-5472.CAN-05-3940>.
- Radke, J. et al. (2022) 'Decoding molecular programs in melanoma brain metastases', *Nature Communications*, 13(1), p. 7304. Available at: <https://doi.org/10.1038/s41467-022-34899-x>.
- Rajabi, P., Karimian, P. and Heidarpour, M. (2012) 'The relationship between MDM2 expression and tumor thickness and invasion in primary cutaneous malignant melanoma', *Journal of Research in Medical Sciences: The Official Journal of Isfahan University of Medical Sciences*, 17(5), pp. 452–455.
- Rak, J. et al. (1995) 'Mutant ras oncogenes upregulate VEGF/VPF expression: implications for induction and inhibition of tumor angiogenesis', *Cancer Research*, 55(20), pp. 4575–4580.
- Rambow, F. et al. (2018) 'Toward Minimal Residual Disease-Directed Therapy in Melanoma', *Cell*, 174(4), pp. 843–855.e19. Available at: <https://doi.org/10.1016/j.cell.2018.06.025>.
- Rambow, F., Marine, J.-C. and Goding, C.R. (2019) 'Melanoma plasticity and phenotypic diversity: therapeutic barriers and opportunities', *Genes & Development*, 33(19–20), pp. 1295–1318. Available at: <https://doi.org/10.1101/gad.329771.119>.
- Ramirez, R.D. et al. (1999) 'Progressive increase in telomerase activity from benign melanocytic conditions to malignant melanoma', *Neoplasia (New York, N.Y.)*, 1(1), pp. 42–49. Available at: <https://doi.org/10.1038/sj.neo.7900004>.
- Randic, T. et al. (2021) 'NRAS mutant melanoma: Towards better therapies', *Cancer Treatment Reviews*, 99, p. 102238. Available at: <https://doi.org/10.1016/j.ctrv.2021.102238>.
- Ratnikov, B.I. et al. (2017) 'Metabolic rewiring in melanoma', *Oncogene*, 36(2), pp. 147–157. Available at: <https://doi.org/10.1038/onc.2016.198>.
- Ravi, R. et al. (2000) 'Regulation of tumor angiogenesis by p53-induced degradation of hypoxia-inducible factor 1 α ', *Genes & Development*, 14(1), pp. 34–44.
- Rawat, P. et al. (2021) 'Stress-induced nuclear condensation of NELF drives transcriptional downregulation', *Molecular Cell*, 81(5), pp. 1013–1026.e11. Available at: <https://doi.org/10.1016/j.molcel.2021.01.016>.
- Rebecca, V.W. and Herlyn, M. (2020) 'Nongenetic Mechanisms of Drug Resistance in Melanoma', *Annual Review of Cancer Biology*, 4(1), pp. 315–330. Available at: <https://doi.org/10.1146/annurev-cancerbio-030419-033533>.
- Reddy, J. et al. (2021) 'Predicting master transcription factors from pan-cancer expression data', *Science Advances*, 7(48), p. eabf6123. Available at: <https://doi.org/10.1126/sciadv.abf6123>.
- Reed, J.A. et al. (1995) 'Loss of expression of the p16/cyclin-dependent kinase inhibitor 2 tumor suppressor gene in melanocytic lesions correlates with invasive stage of tumor progression', *Cancer Research*, 55(13), pp. 2713–2718.
- Regazzetti, C. et al. (2018) 'Melanocytes Sense Blue Light and Regulate Pigmentation through Opsin-3', *The Journal of Investigative Dermatology*, 138(1), pp. 171–178. Available at: <https://doi.org/10.1016/j.jid.2017.07.833>.
- Reid, A.L. et al. (2013) 'Markers of circulating tumour cells in the peripheral blood of patients with melanoma correlate with disease recurrence and progression', *The British Journal of Dermatology*, 168(1), pp. 85–92. Available at: <https://doi.org/10.1111/bjd.12057>.
- Reiter, F., Wienerroither, S. and Stark, A. (2017) 'Combinatorial function of transcription factors and cofactors', *Current Opinion in Genetics & Development*, 43, pp. 73–81. Available at: <https://doi.org/10.1016/j.gde.2016.12.007>.
- Reiter, J.G. et al. (2018) 'Minimal functional driver gene heterogeneity among untreated metastases', *Science*, 361(6406), pp. 1033–1037. Available at: <https://doi.org/10.1126/science.aat7171>.
- Reiter, J.G. et al. (2019) 'An analysis of genetic heterogeneity in untreated cancers', *Nature Reviews Cancer*, 19(11), pp. 639–650. Available at: <https://doi.org/10.1038/s41568-019-0185-x>.
- Rengachari, S. et al. (2021) 'Structure of the human Mediator-RNA polymerase II pre-initiation complex', *Nature*, 594(7861), pp. 129–133. Available at: <https://doi.org/10.1038/s41586-021-03555-7>.

- Restivo, G. et al. (2017) 'The low affinity neurotrophin receptor CD271 regulates phenotype switching in melanoma', *Nature Communications*, 8(1), p. 1988. Available at: <https://doi.org/10.1038/s41467-017-01573-6>.
- Revach, O.-Y. et al. (2019) 'Cross-Talk between Receptor Tyrosine Kinases AXL and ERBB3 Regulates Invadopodia Formation in Melanoma Cells', *Cancer Research*, 79(10), pp. 2634–2648. Available at: <https://doi.org/10.1158/0008-5472.CAN-18-2316>.
- Rheinbay, E. et al. (2017) 'Recurrent and functional regulatory mutations in breast cancer', *Nature*, 547(7661), pp. 55–60. Available at: <https://doi.org/10.1038/nature22992>.
- Ribas, A. et al. (2015) 'P0116 Updated clinical efficacy of the anti-PD-1 monoclonal antibody pembrolizumab (MK-3475) in 411 patients with melanoma', *European Journal of Cancer*, 51, p. e24. Available at: <https://doi.org/10.1016/j.ejca.2015.06.072>.
- Ribas, A. et al. (2020) 'PD-L1 blockade in combination with inhibition of MAPK oncogenic signaling in patients with advanced melanoma', *Nature Communications*, 11(1), p. 6262. Available at: <https://doi.org/10.1038/s41467-020-19810-w>.
- Richard, G. et al. (2016) 'ZEB1-mediated melanoma cell plasticity enhances resistance to MAPK inhibitors', *EMBO molecular medicine*, 8(10), pp. 1143–1161. Available at: <https://doi.org/10.1525/emmm.201505971>.
- Richter, W.F. et al. (2022) 'The Mediator complex as a master regulator of transcription by RNA polymerase II', *Nature Reviews Molecular Cell Biology*, 23(11), pp. 732–749. Available at: <https://doi.org/10.1038/s41580-022-00498-3>.
- Rickman, D.S., Schulte, J.H. and Eilers, M. (2018) 'The Expanding World of N-MYC-Driven Tumors', *Cancer Discovery*, 8(2), pp. 150–163. Available at: <https://doi.org/10.1158/2159-8290.CD-17-0273>.
- Riesenberg, S. et al. (2015) 'MITF and c-Jun antagonism interconnects melanoma dedifferentiation with pro-inflammatory cytokine responsiveness and myeloid cell recruitment', *Nature Communications*, 6, p. 8755. Available at: <https://doi.org/10.1038/ncomms9755>.
- Rimel, J.K. et al. (2020) 'Selective inhibition of CDK7 reveals high-confidence targets and new models for TFIIF function in transcription', *Genes & Development*, 34(21–22), pp. 1452–1473. Available at: <https://doi.org/10.1101/gad.341545.120>.
- Rimel, J.K. and Taatjes, D.J. (2018) 'The essential and multifunctional TFIIF complex', *Protein Science*, 27(6), pp. 1018–1037. Available at: <https://doi.org/10.1002/pro.3424>.
- Robert, C. et al. (2015) 'Nivolumab in Previously Untreated Melanoma without BRAF Mutation', *New England Journal of Medicine*, 372(4), pp. 320–330. Available at: <https://doi.org/10.1056/NEJMoa1412082>.
- Robert, C. et al. (2019) 'Pembrolizumab versus ipilimumab in advanced melanoma (KEYNOTE-006): post-hoc 5-year results from an open-label, multicentre, randomised, controlled, phase 3 study', *The Lancet Oncology*, 20(9), pp. 1239–1251. Available at: [https://doi.org/10.1016/S1470-2045\(19\)30388-2](https://doi.org/10.1016/S1470-2045(19)30388-2).
- Robert, F. et al. (1998) 'Wrapping of promoter DNA around the RNA polymerase II initiation complex induced by TFIIF', *Molecular Cell*, 2(3), pp. 341–351. Available at: [https://doi.org/10.1016/S1097-2765\(00\)80278-6](https://doi.org/10.1016/S1097-2765(00)80278-6).
- Rochette-Egly, C. et al. (1997) 'Stimulation of RAR α Activation Function AF-1 through Binding to the General Transcription Factor TFIIF and Phosphorylation by CDK7', *Cell*, 90(1), pp. 97–107. Available at: [https://doi.org/10.1016/S0092-8674\(00\)80317-7](https://doi.org/10.1016/S0092-8674(00)80317-7).
- Rodríguez-Molina, J.B., West, S. and Passmore, L.A. (2023) 'Knowing when to stop: Transcription termination on protein-coding genes by eukaryotic RNAPII', *Molecular Cell*, 83(3), pp. 404–415. Available at: <https://doi.org/10.1016/j.molcel.2022.12.021>.
- Roeder, R.G. (2019) '50+ years of eukaryotic transcription: an expanding universe of factors and mechanisms', *Nature Structural & Molecular Biology*, 26(9), pp. 783–791. Available at: <https://doi.org/10.1038/s41594-019-0287-x>.
- Roeder, R.G. and Rutter, W.J. (1969) 'Multiple forms of DNA-dependent RNA polymerase in eukaryotic organisms', *Nature*, 224(5216), pp. 234–237. Available at: <https://doi.org/10.1038/224234a0>.
- Roesch, A. et al. (2013) 'Overcoming intrinsic multidrug resistance in melanoma by blocking the mitochondrial respiratory chain of slow-cycling JARID1B(high) cells', *Cancer Cell*, 23(6), pp. 811–825. Available at: <https://doi.org/10.1016/j.ccr.2013.05.003>.
- Roesch, A. (2015) 'Tumor heterogeneity and plasticity as elusive drivers for resistance to MAPK pathway inhibition in melanoma', *Oncogene*, 34(23), pp. 2951–2957. Available at: <https://doi.org/10.1038/onc.2014.249>.
- Rogiers, A. et al. (2022) 'The Genetic Evolution of Metastasis', *Cancer Research*, 82(10), pp. 1849–1857. Available at: <https://doi.org/10.1158/0008-5472.CAN-21-3863>.
- Roh, M.R. et al. (2015) 'Genetics of melanocytic nevi', *Pigment Cell & Melanoma Research*, 28(6), pp. 661–672. Available at: <https://doi.org/10.1111/pcmr.12412>.
- Roh, M.R. et al. (2016) 'Promoter Methylation of PTEN Is a Significant Prognostic Factor in Melanoma Survival', *The Journal of Investigative Dermatology*, 136(5), pp. 1002–1011. Available at: <https://doi.org/10.1016/j.jid.2016.01.024>.
- Rolver, M.G. and Pedersen, S.F. (2021) 'Putting Warburg to work: how imaging of tumour acidosis could help predict metastatic potential in breast cancer', *British Journal of Cancer*, 124(1), pp. 1–2. Available at: <https://doi.org/10.1038/s41416-020-01171-2>.
- Romano, M. et al. (2013) 'Comparison of in vitro and in vivo biological effects of trabectedin, lurbectedin (PM01183) and Zalypsis® (PM00104)', *International Journal of Cancer*, 133(9), pp. 2024–2033. Available at: <https://doi.org/10.1002/ijc.28213>.
- Romano, V. et al. (2021) 'Influence of Tumor Microenvironment and Fibroblast Population Plasticity on Melanoma Growth, Therapy Resistance and Immunoescape', *International Journal of Molecular Sciences*, 22(10), p. 5283. Available at: <https://doi.org/10.3390/ijms22105283>.

- Rose, A.A.N. et al. (2016) 'MAPK Pathway Inhibitors Sensitize BRAF-Mutant Melanoma to an Antibody-Drug Conjugate Targeting GPNMB', *Clinical Cancer Research*, 22(24), pp. 6088–6098. Available at: <https://doi.org/10.1158/1078-0432.CCR-16-1192>.
- Rosenbaum, S.R. et al. (2021) 'SOX10 requirement for melanoma tumor growth is due, in part, to immune-mediated effects', *Cell Reports*, 37(10), p. 110085. Available at: <https://doi.org/10.1016/j.celrep.2021.110085>.
- Rossi, S. et al. (2018) 'TNF-alpha and metalloproteases as key players in melanoma cells aggressiveness', *Journal of experimental & clinical cancer research: CR*, 37(1), p. 326. Available at: <https://doi.org/10.1186/s13046-018-0982-1>.
- Rotte, A. (2019) 'Combination of CTLA-4 and PD-1 blockers for treatment of cancer', *Journal of Experimental & Clinical Cancer Research*, 38(1), p. 255. Available at: <https://doi.org/10.1186/s13046-019-1259-z>.
- Rougvie, A.E. and Lis, J.T. (1988) 'The RNA polymerase II molecule at the 5' end of the uninduced hsp70 gene of *D. melanogaster* is transcriptionally engaged', *Cell*, 54(6), pp. 795–804. Available at: [https://doi.org/10.1016/s0092-8674\(88\)91087-2](https://doi.org/10.1016/s0092-8674(88)91087-2).
- Routy, B. et al. (2018) 'Gut microbiome influences efficacy of PD-1-based immunotherapy against epithelial tumors', *Science (New York, N.Y.)*, 359(6371), pp. 91–97. Available at: <https://doi.org/10.1126/science.aan3706>.
- Rowley, M.J. and Corces, V.G. (2018) 'Organizational principles of 3D genome architecture', *Nature Reviews. Genetics*, 19(12), pp. 789–800. Available at: <https://doi.org/10.1038/s41576-018-0060-8>.
- Rowling, E.J. et al. (2020) 'Cooperative behaviour and phenotype plasticity evolve during melanoma progression', *Pigment Cell & Melanoma Research*, 33(5), pp. 695–708. Available at: <https://doi.org/10.1111/pcmr.12873>.
- Rubanov, A., Berico, P. and Hernando, E. (2022) 'Epigenetic Mechanisms Underlying Melanoma Resistance to Immune and Targeted Therapies', *Cancers*, 14(23), p. 5858. Available at: <https://doi.org/10.3390/cancers14235858>.
- Ruocco, M.R. et al. (2019) 'Metabolic flexibility in melanoma: A potential therapeutic target', *Seminars in Cancer Biology*, 59, pp. 187–207. Available at: <https://doi.org/10.1016/j.semcancer.2019.07.016>.
- Russo, A.A., Jeffrey, P.D. and Pavletich, N.P. (1996) 'Structural basis of cyclin-dependent kinase activation by phosphorylation', *Nature Structural Biology*, 3(8), pp. 696–700. Available at: <https://doi.org/10.1038/nsb0896-696>.
- Ryan, R.J.H. et al. (2015) 'Detection of Enhancer-Associated Rearrangements Reveals Mechanisms of Oncogene Dysregulation in B-cell Lymphoma', *Cancer Discovery*, 5(10), pp. 1058–1071. Available at: <https://doi.org/10.1158/2159-8290.CD-15-0370>.
- Saba, J. et al. (2019) 'The elemental mechanism of transcriptional pausing', *eLife*. Edited by J.L. Workman and J.L. Manley, 8, p. e40981. Available at: <https://doi.org/10.7554/eLife.40981>.
- Sabari, B.R. et al. (2018) 'Coactivator condensation at super-enhancers links phase separation and gene control', *Science*, 361(6400), p. eaar3958. Available at: <https://doi.org/10.1126/science.aar3958>.
- Sager, R. (1997) 'Expression genetics in cancer: Shifting the focus from DNA to RNA', *Proceedings of the National Academy of Sciences of the United States of America*, 94(3), pp. 952–955.
- Saginala, K. et al. (2021) 'Epidemiology of Melanoma', *Medical Sciences (Basel, Switzerland)*, 9(4), p. 63. Available at: <https://doi.org/10.3390/medsci9040063>.
- Sainsbury, S., Niesser, J. and Cramer, P. (2013) 'Structure and function of the initially transcribing RNA polymerase II–TFIIB complex', *Nature*, 493(7432), pp. 437–440. Available at: <https://doi.org/10.1038/nature11715>.
- Saint-André, V. et al. (2016) 'Models of human core transcriptional regulatory circuitries', *Genome Research*, 26(3), pp. 385–396. Available at: <https://doi.org/10.1101/gr.197590.115>.
- Sanborn, J.Z. et al. (2015) 'Phylogenetic analyses of melanoma reveal complex patterns of metastatic dissemination', *Proceedings of the National Academy of Sciences of the United States of America*, 112(35), pp. 10995–11000. Available at: <https://doi.org/10.1073/pnas.1508074112>.
- Sanchez-Vega, F. et al. (2018) 'Oncogenic Signaling Pathways in The Cancer Genome Atlas', *Cell*, 173(2), pp. 321–337.e10. Available at: <https://doi.org/10.1016/j.cell.2018.03.035>.
- Sanda, T. et al. (2012) 'Core Transcriptional Regulatory Circuit Controlled by the TAL1 Complex in Human T Cell Acute Lymphoblastic Leukemia', *Cancer Cell*, 22(2), pp. 209–221. Available at: <https://doi.org/10.1016/j.ccr.2012.06.007>.
- Sandoz, J. et al. (2019) 'Functional interplay between TFIH and KAT2A regulates higher-order chromatin structure and class II gene expression', *Nature Communications*, 10(1), p. 1288. Available at: <https://doi.org/10.1038/s41467-019-09270-2>.
- Sandoz, J. and Coin, F. (2017) 'Unified promoter opening steps in eukaryotic gene expression', *Oncotarget*, 8(49), pp. 84614–84615. Available at: <https://doi.org/10.18632/oncotarget.21387>.
- Sang, N. et al. (2003) 'MAPK Signaling Up-regulates the Activity of Hypoxia-inducible Factors by Its Effects on p300', *The Journal of biological chemistry*, 278(16), pp. 14013–14019. Available at: <https://doi.org/10.1074/jbc.M209702200>.
- Sansó, M. et al. (2016) 'P-TEFb regulation of transcription termination factor Xrn2 revealed by a chemical genetic screen for Cdk9 substrates', *Genes & Development*, 30(1), pp. 117–131. Available at: <https://doi.org/10.1101/gad.269589.115>.
- Santamaría Nuñez, G. et al. (2016) 'Lurbinectedin Specifically Triggers the Degradation of Phosphorylated RNA Polymerase II and the Formation of DNA Breaks in Cancer Cells', *Molecular Cancer Therapeutics*, 15(10), pp. 2399–2412. Available at: <https://doi.org/10.1158/1535-7163.MCT-16-0172>.

- Sato, S. et al. (1997) 'CBP/p300 as a co-factor for the Microphthalmia transcription factor', *Oncogene*, 14(25), pp. 3083–3092. Available at: <https://doi.org/10.1038/sj.onc.1201298>.
- Sava, G.P. et al. (2020) 'CDK7 inhibitors as anticancer drugs', *Cancer Metastasis Reviews*, 39(3), pp. 805–823. Available at: <https://doi.org/10.1007/s10555-020-09885-8>.
- Scatena, C., Murtas, D. and Tomei, S. (2021) 'Cutaneous Melanoma Classification: The Importance of High-Throughput Genomic Technologies', *Frontiers in Oncology*, 11. Available at: <https://www.frontiersin.org/articles/10.3389/fonc.2021.635488> (Accessed: 10 February 2023).
- Schachter, M.M. et al. (2013) 'A Cdk7-Cdk4 T-Loop Phosphorylation Cascade Promotes G1 Progression', *Molecular Cell*, 50(2), pp. 250–260. Available at: <https://doi.org/10.1016/j.molcel.2013.04.003>.
- Schadendorf, D. et al. (2015) 'Pooled Analysis of Long-Term Survival Data From Phase II and Phase III Trials of Ipilimumab in Unresectable or Metastatic Melanoma', *Journal of Clinical Oncology*, 33(17), pp. 1889–1894. Available at: <https://doi.org/10.1200/JCO.2014.56.2736>.
- Schadendorf, D. et al. (2018) 'Melanoma', *The Lancet*, 392(10151), pp. 971–984. Available at: [https://doi.org/10.1016/S0140-6736\(18\)31559-9](https://doi.org/10.1016/S0140-6736(18)31559-9).
- Schadendorf, D., Kochs, C. and Livingstone, E. (2013) 'Clinical Features and Classification', in D. Schadendorf, C. Kochs, and E. Livingstone (eds) *Handbook of Cutaneous Melanoma: A Guide to Diagnosis and Treatment*. Tarpoley: Springer Healthcare Ltd., pp. 13–27. Available at: https://doi.org/10.1007/978-1-908517-98-2_2.
- Schaeffer, L. et al. (1993) 'DNA repair helicase: a component of BTF2 (TFIIH) basic transcription factor', *Science (New York, N.Y.)*, 260(5104), pp. 58–63. Available at: <https://doi.org/10.1126/science.8465201>.
- Schärer, O.D. (2008) 'The molecular basis for different disease states caused by mutations in TFIIH and XPG', *DNA repair*, 7(2), pp. 339–344. Available at: <https://doi.org/10.1016/j.dnarep.2007.10.007>.
- Schilbach, S. et al. (2021) 'Structure of RNA polymerase II pre-initiation complex at 2.9 Å defines initial DNA opening', *Cell*, 184(15), pp. 4064–4072.e28. Available at: <https://doi.org/10.1016/j.cell.2021.05.012>.
- Schmidt, K. et al. (2016) 'The lncRNA SLNCR1 Mediates Melanoma Invasion through a Conserved SRA1-like Region', *Cell Reports*, 15(9), pp. 2025–2037. Available at: <https://doi.org/10.1016/j.celrep.2016.04.018>.
- Schmidt, M. et al. (2022) 'Reconstitution of 3' end processing of mammalian pre-mRNA reveals a central role of RBBP6', *Genes & Development*, 36(3–4), pp. 195–209. Available at: <https://doi.org/10.1101/gad.349217.121>.
- Schor, I.E. et al. (2017) 'Promoter shape varies across populations and affects promoter evolution and expression noise', *Nature Genetics*, 49(4), pp. 550–558. Available at: <https://doi.org/10.1038/ng.3791>.
- Schrieck, A. et al. (2014) 'RNA polymerase II termination involves C-terminal-domain tyrosine dephosphorylation by CPF subunit Glc7', *Nature Structural & Molecular Biology*, 21(2), pp. 175–179. Available at: <https://doi.org/10.1038/nsmb.2753>.
- Schröder, S. et al. (2013) 'Acetylation of RNA polymerase II regulates growth-factor-induced gene transcription in mammalian cells', *Molecular Cell*, 52(3), pp. 314–324. Available at: <https://doi.org/10.1016/j.molcel.2013.10.009>.
- Schuijers, J. et al. (2018) 'Transcriptional Dysregulation of MYC Reveals Common Enhancer-Docking Mechanism', *Cell Reports*, 23(2), pp. 349–360. Available at: <https://doi.org/10.1016/j.celrep.2018.03.056>.
- Schultz, P. et al. (2000) 'Molecular Structure of Human TFIIH', *Cell*, 102(5), pp. 599–607. Available at: [https://doi.org/10.1016/S0092-8674\(00\)00082-9](https://doi.org/10.1016/S0092-8674(00)00082-9).
- Scoyler, R.A., Long, G.V. and Thompson, J.F. (2011) 'Evolving concepts in melanoma classification and their relevance to multidisciplinary melanoma patient care', *Molecular Oncology*, 5(2), pp. 124–136. Available at: <https://doi.org/10.1016/j.molonc.2011.03.002>.
- Seberg, H.E., Van Otterloo, E. and Cornell, R.A. (2017) 'Beyond MITF: Multiple transcription factors directly regulate the cellular phenotype in melanocytes and melanoma', *Pigment cell & melanoma research*, 30(5), pp. 454–466. Available at: <https://doi.org/10.1111/pcmr.12611>.
- Ségal-Bendirdjian, E. and Geli, V. (2019) 'Non-canonical Roles of Telomerase: Unraveling the Imbroglia', *Frontiers in Cell and Developmental Biology*, 7. Available at: <https://www.frontiersin.org/articles/10.3389/fcell.2019.00332> (Accessed: 18 March 2023).
- Segura, M.F. et al. (2009) 'Aberrant miR-182 expression promotes melanoma metastasis by repressing FOXO3 and microphthalmia-associated transcription factor', *Proceedings of the National Academy of Sciences of the United States of America*, 106(6), pp. 1814–1819. Available at: <https://doi.org/10.1073/pnas.0808263106>.
- Semer, M. et al. (2019) 'DNA repair complex licenses acetylation of H2A.Z.1 by KAT2A during transcription', *Nature Chemical Biology*, 15(10), pp. 992–1000. Available at: <https://doi.org/10.1038/s41589-019-0354-y>.
- Senft, D. and Ronai, Z.A. (2016) 'Immunogenic, cellular, and angiogenic drivers of tumor dormancy-a melanoma view', *Pigment Cell & Melanoma Research*, 29(1), pp. 27–42. Available at: <https://doi.org/10.1111/pcmr.12432>.
- Sengupta, S. and George, R.E. (2017) 'Super-Enhancer-Driven Transcriptional Dependencies in Cancer', *Trends in Cancer*, 3(4), pp. 269–281. Available at: <https://doi.org/10.1016/j.trecan.2017.03.006>.
- Sensi, M. et al. (2011) 'Human Cutaneous Melanomas Lacking MITF and Melanocyte Differentiation Antigens Express a Functional Axl Receptor Kinase', *Journal of Investigative Dermatology*, 131(12), pp. 2448–2457. Available at: <https://doi.org/10.1038/jid.2011.218>.

- Sever, R. and Brugge, J.S. (2015) 'Signal Transduction in Cancer', *Cold Spring Harbor Perspectives in Medicine*, 5(4), p. a006098. Available at: <https://doi.org/10.1101/cshperspect.a006098>.
- Sexton, T. et al. (2007) 'The role of transcription factories in large-scale structure and dynamics of interphase chromatin', *Seminars in Cell & Developmental Biology*, 18(5), pp. 691–697. Available at: <https://doi.org/10.1016/j.semcdb.2007.08.008>.
- Shaban, H.A. and Seeber, A. (2020) 'Monitoring the spatio-temporal organization and dynamics of the genome', *Nucleic Acids Research*, 48(7), pp. 3423–3434. Available at: <https://doi.org/10.1093/nar/gkaa135>.
- Shachar, S. and Misteli, T. (2017) 'Causes and consequences of nuclear gene positioning', *Journal of Cell Science*, 130(9), pp. 1501–1508. Available at: <https://doi.org/10.1242/jcs.199786>.
- Shaffer, S.M. et al. (2017) 'Rare cell variability and drug-induced reprogramming as a mode of cancer drug resistance', *Nature*, 546(7658), pp. 431–435. Available at: <https://doi.org/10.1038/nature22794>.
- Shain, A.H. et al. (2015) 'The Genetic Evolution of Melanoma from Precursor Lesions', *The New England Journal of Medicine*, 373(20), pp. 1926–1936. Available at: <https://doi.org/10.1056/NEJMoa1502583>.
- Shain, A.H. et al. (2018) 'Genomic and Transcriptomic Analysis Reveals Incremental Disruption of Key Signaling Pathways during Melanoma Evolution', *Cancer Cell*, 34(1), pp. 45–55.e4. Available at: <https://doi.org/10.1016/j.ccell.2018.06.005>.
- Shain, A.H. and Bastian, B.C. (2016) 'From melanocytes to melanomas', *Nature Reviews Cancer*, 16(6), pp. 345–358. Available at: <https://doi.org/10.1038/nrc.2016.37>.
- Shao, H. et al. (2021) 'Converting melanoma-associated fibroblasts into a tumor-suppressive phenotype by increasing intracellular Notch1 pathway activity', *PLOS ONE*, 16(3), p. e0248260. Available at: <https://doi.org/10.1371/journal.pone.0248260>.
- Sharma, M. et al. (2022) 'Trial in progress: Phase I study of SY-5609, a potent, selective CDK7 inhibitor, with initial expansion in adults with metastatic pancreatic cancer.', *Journal of Clinical Oncology*, 40(16_suppl), pp. TPS4180–TPS4180. Available at: https://doi.org/10.1200/JCO.2022.40.16_suppl.TPS4180.
- Sharma, P. et al. (2017) 'Primary, Adaptive, and Acquired Resistance to Cancer Immunotherapy', *Cell*, 168(4), pp. 707–723. Available at: <https://doi.org/10.1016/j.cell.2017.01.017>.
- Sharma, P. et al. (2020) 'Melanoma cell-derived exosomes in plasma of melanoma patients suppress functions of immune effector cells', *Scientific Reports*, 10(1), p. 92. Available at: <https://doi.org/10.1038/s41598-019-56542-4>.
- Sharma, S.V. et al. (2010) 'A chromatin-mediated reversible drug-tolerant state in cancer cell subpopulations', *Cell*, 141(1), pp. 69–80. Available at: <https://doi.org/10.1016/j.cell.2010.02.027>.
- Shellard, A. and Mayor, R. (2019) 'Integrating chemical and mechanical signals in neural crest cell migration', *Current Opinion in Genetics & Development*, 57, pp. 16–24. Available at: <https://doi.org/10.1016/j.gde.2019.06.004>.
- Shen, S., Vagner, S. and Robert, C. (2020) 'Persistent Cancer Cells: The Deadly Survivors', *Cell*, 183(4), pp. 860–874. Available at: <https://doi.org/10.1016/j.cell.2020.10.027>.
- Shi, H. et al. (2014) 'Acquired resistance and clonal evolution in melanoma during BRAF inhibitor therapy', *Cancer Discovery*, 4(1), pp. 80–93. Available at: <https://doi.org/10.1158/2159-8290.CD-13-0642>.
- Shi, J. and Vakoc, C.R. (2014) 'The mechanisms behind the therapeutic activity of BET bromodomain inhibition', *Molecular Cell*, 54(5), pp. 728–736. Available at: <https://doi.org/10.1016/j.molcel.2014.05.016>.
- Shi, Y. et al. (2009) 'Molecular Architecture of the Human Pre-mRNA 3' Processing Complex', *Molecular Cell*, 33(3), pp. 365–376. Available at: <https://doi.org/10.1016/j.molcel.2008.12.028>.
- Shi, Y. et al. (2023) 'BRD4-targeting PROTAC as a unique tool to study biomolecular condensates', *Cell Discovery*, 9(1), p. 47. Available at: <https://doi.org/10.1038/s41421-023-00544-0>.
- Shi, Z.-D. et al. (2023) 'Tumor cell plasticity in targeted therapy-induced resistance: mechanisms and new strategies', *Signal Transduction and Targeted Therapy*, 8(1), pp. 1–21. Available at: <https://doi.org/10.1038/s41392-023-01383-x>.
- Shibuya, M. (2011) 'Vascular Endothelial Growth Factor (VEGF) and Its Receptor (VEGFR) Signaling in Angiogenesis', *Genes & Cancer*, 2(12), pp. 1097–1105. Available at: <https://doi.org/10.1177/1947601911423031>.
- Shin, D.S. et al. (2017) 'Primary Resistance to PD-1 Blockade Mediated by JAK1/2 Mutations', *Cancer Discovery*, 7(2), pp. 188–201. Available at: <https://doi.org/10.1158/2159-8290.CD-16-1223>.
- Shin, H.Y. et al. (2016) 'Hierarchy within the mammary STAT5-driven Wap super-enhancer', *Nature Genetics*, 48(8), pp. 904–911. Available at: <https://doi.org/10.1038/ng.3606>.
- Shin, H.Y. (2018) 'Targeting Super-Enhancers for Disease Treatment and Diagnosis', *Molecules and Cells*, 41(6), pp. 506–514. Available at: <https://doi.org/10.14348/MOLCELLS.2018.2297>.
- Shlyueva, D., Stampfel, G. and Stark, A. (2014) 'Transcriptional enhancers: from properties to genome-wide predictions', *Nature Reviews. Genetics*, 15(4), pp. 272–286. Available at: <https://doi.org/10.1038/nrg3682>.
- Shreberk-Hassidim, R., Ostrowski, S.M. and Fisher, D.E. (2023) 'The Complex Interplay between Nevi and Melanoma: Risk Factors and Precursors', *International Journal of Molecular Sciences*, 24(4), p. 3541. Available at: <https://doi.org/10.3390/ijms24043541>.

- Shrinivas, K. et al. (2019) 'Enhancer Features that Drive Formation of Transcriptional Condensates', *Molecular Cell*, 75(3), pp. 549–561.e7. Available at: <https://doi.org/10.1016/j.molcel.2019.07.009>.
- Shu, S.L. et al. (2018) 'Metabolic reprogramming of stromal fibroblasts by melanoma exosome microRNA favours a pre-metastatic microenvironment', *Scientific Reports*, 8(1), p. 12905. Available at: <https://doi.org/10.1038/s41598-018-31323-7>.
- Shull, A.Y. et al. (2012) 'Novel somatic mutations to PI3K pathway genes in metastatic melanoma', *PloS One*, 7(8), p. e43369. Available at: <https://doi.org/10.1371/journal.pone.0043369>.
- Siena, Á.D.D. et al. (2019) 'Whole transcriptome analysis reveals correlation of long noncoding RNA ZEB1-AS1 with invasive profile in melanoma', *Scientific Reports*, 9(1), p. 11350. Available at: <https://doi.org/10.1038/s41598-019-47363-6>.
- Simiczyjew, A. et al. (2020) 'The Influence of Tumor Microenvironment on Immune Escape of Melanoma', *International Journal of Molecular Sciences*, 21(21), p. 8359. Available at: <https://doi.org/10.3390/ijms21218359>.
- Simões-Costa, M. and Bronner, M.E. (2015) 'Establishing neural crest identity: a gene regulatory recipe', *Development*, 142(2), pp. 242–257. Available at: <https://doi.org/10.1242/dev.105445>.
- Simon, J.D. and Peles, D.N. (2010) 'The red and the black', *Accounts of Chemical Research*, 43(11), pp. 1452–1460. Available at: <https://doi.org/10.1021/ar100079y>.
- Simons, M., Gordon, E. and Claesson-Welsh, L. (2016) 'Mechanisms and regulation of endothelial VEGF receptor signalling', *Nature Reviews Molecular Cell Biology*, 17(10), pp. 611–625. Available at: <https://doi.org/10.1038/nrm.2016.87>.
- Singh, A. et al. (2015) 'TFIIH subunit alterations causing xeroderma pigmentosum and trichothiodystrophy specifically disturb several steps during transcription', *American Journal of Human Genetics*, 96(2), pp. 194–207. Available at: <https://doi.org/10.1016/j.ajhg.2014.12.012>.
- Singh, J. and Padgett, R.A. (2009) 'Rates of in situ transcription and splicing in large human genes', *Nature Structural & Molecular Biology*, 16(11), pp. 1128–1133. Available at: <https://doi.org/10.1038/nsmb.1666>.
- Singh, K. et al. (2019) 'c-MYC regulates mRNA translation efficiency and start-site selection in lymphoma', *The Journal of Experimental Medicine*, 216(7), pp. 1509–1524. Available at: <https://doi.org/10.1084/jem.20181726>.
- Singh, S. et al. (2021) 'FDA Approval Summary: Lurbinectedin for the Treatment of Metastatic Small Cell Lung Cancer', *Clinical Cancer Research: An Official Journal of the American Association for Cancer Research*, 27(9), pp. 2378–2382. Available at: <https://doi.org/10.1158/1078-0432.CCR-20-3901>.
- Skin Cancer (Non-Melanoma) - Statistics (2022) Cancer.Net. Available at: <https://www.cancer.net/cancer-types/skin-cancer-non-melanoma/statistics> (Accessed: 10 February 2023).
- Skorupan, N. et al. (2022) 'A phase II trial of the super-enhancer inhibitor Minnelide™ in advanced refractory adenocarcinoma of the pancreas', *Future Oncology (London, England)*, 18(20), pp. 2475–2481. Available at: <https://doi.org/10.2217/fon-2021-1609>.
- Skrypek, N. et al. (2017) 'Epithelial-to-Mesenchymal Transition: Epigenetic Reprogramming Driving Cellular Plasticity', *Trends in genetics: TIG*, 33(12), pp. 943–959. Available at: <https://doi.org/10.1016/j.tig.2017.08.004>.
- Slack, F.J. and Chinnaiyan, A.M. (2019) 'The Role of Non-coding RNAs in Oncology', *Cell*, 179(5), pp. 1033–1055. Available at: <https://doi.org/10.1016/j.cell.2019.10.017>.
- Sleeman, J.P. (2012) 'The metastatic niche and stromal progression', *Cancer and Metastasis Reviews*, 31(3), pp. 429–440. Available at: <https://doi.org/10.1007/s10555-012-9373-9>.
- Slominski, A. (2009) 'Neuroendocrine activity of the melanocyte', *Experimental Dermatology*, 18(9), pp. 760–763. Available at: <https://doi.org/10.1111/j.1600-0625.2009.00892.x>.
- Slominski, A., Paus, R. and Schauder, D. (1993) 'Melanocytes as "Sensory" and Regulatory Cells in the Epidermis', *Journal of Theoretical Biology*, 164(1), pp. 103–120. Available at: <https://doi.org/10.1006/jtbi.1993.1142>.
- Smale, S.T. and Baltimore, D. (1989) 'The "initiator" as a transcription control element', *Cell*, 57(1), pp. 103–113. Available at: [https://doi.org/10.1016/0092-8674\(89\)90176-1](https://doi.org/10.1016/0092-8674(89)90176-1).
- Śmiech, M. et al. (2020) 'Emerging BRAF Mutations in Cancer Progression and Their Possible Effects on Transcriptional Networks', *Genes*, 11(11), p. 1342. Available at: <https://doi.org/10.3390/genes11111342>.
- Smith, E. and Shilatifard, A. (2014) 'Enhancer biology and enhanceropathies', *Nature Structural & Molecular Biology*, 21(3), pp. 210–219. Available at: <https://doi.org/10.1038/nsmb.2784>.
- Smith, L.K. et al. (2020) 'Obesity and the Impact on Cutaneous Melanoma: Friend or Foe?', *Cancers*, 12(6), p. 1583. Available at: <https://doi.org/10.3390/cancers12061583>.
- Smith, L.K., Sheppard, K.E. and McArthur, G.A. (2021) 'Is resistance to targeted therapy in cancer inevitable?', *Cancer Cell*, 39(8), pp. 1047–1049. Available at: <https://doi.org/10.1016/j.ccell.2021.07.013>.
- Smith, M.P. et al. (2016) 'Inhibiting Drivers of Non-mutational Drug Tolerance Is a Salvage Strategy for Targeted Melanoma Therapy', *Cancer Cell*, 29(3), pp. 270–284. Available at: <https://doi.org/10.1016/j.ccell.2016.02.003>.
- Smith, M.P. et al. (2019) 'A PAX3/BRN2 rheostat controls the dynamics of BRAF mediated MITF regulation in MITFhigh/AXLlow melanoma', *Pigment Cell & Melanoma Research*, 32(2), pp. 280–291. Available at: <https://doi.org/10.1111/pcmr.12741>.

- Snyder, A. et al. (2014) 'Genetic Basis for Clinical Response to CTLA-4 Blockade in Melanoma', *New England Journal of Medicine*, 371(23), pp. 2189–2199. Available at: <https://doi.org/10.1056/NEJMoa1406498>.
- Soengas, M.S. et al. (2001) 'Inactivation of the apoptosis effector Apaf-1 in malignant melanoma', *Nature*, 409(6817), pp. 207–211. Available at: <https://doi.org/10.1038/35051606>.
- Soengas, M.S. and Lowe, S.W. (2003) 'Apoptosis and melanoma chemoresistance', *Oncogene*, 22(20), pp. 3138–3151. Available at: <https://doi.org/10.1038/sj.onc.1206454>.
- Solano, F. (2014) 'Melanins: Skin Pigments and Much More—Types, Structural Models, Biological Functions, and Formation Routes', *New Journal of Science*, 2014, p. e498276. Available at: <https://doi.org/10.1155/2014/498276>.
- Solit, D.B. et al. (2006) 'BRAF mutation predicts sensitivity to MEK inhibition', *Nature*, 439(7074), pp. 358–362. Available at: <https://doi.org/10.1038/nature04304>.
- Sommer, L. (2011) 'Generation of melanocytes from neural crest cells', *Pigment Cell & Melanoma Research*, 24(3), pp. 411–421. Available at: <https://doi.org/10.1111/j.1755-148X.2011.00834.x>.
- Sosa, M.S., Bragado, P. and Aguirre-Ghiso, J.A. (2014) 'Mechanisms of disseminated cancer cell dormancy: an awakening field', *Nature Reviews. Cancer*, 14(9), pp. 611–622. Available at: <https://doi.org/10.1038/nrc3793>.
- Soutourina, J. (2018) 'Transcription regulation by the Mediator complex', *Nature Reviews Molecular Cell Biology*, 19(4), pp. 262–274. Available at: <https://doi.org/10.1038/nrm.2017.115>.
- Spencer, C.N. et al. (2021) 'Dietary fiber and probiotics influence the gut microbiome and melanoma immunotherapy response', *Science*, 374(6575), pp. 1632–1640. Available at: <https://doi.org/10.1126/science.aaz7015>.
- Spitz, F. and Furlong, E.E.M. (2012) 'Transcription factors: from enhancer binding to developmental control', *Nature Reviews. Genetics*, 13(9), pp. 613–626. Available at: <https://doi.org/10.1038/nrg3207>.
- Spranger, S. et al. (2017) 'Tumor-Residing Batf3 Dendritic Cells Are Required for Effector T Cell Trafficking and Adoptive T Cell Therapy', *Cancer Cell*, 31(5), pp. 711–723.e4. Available at: <https://doi.org/10.1016/j.ccell.2017.04.003>.
- Spranger, S., Bao, R. and Gajewski, T.F. (2015) 'Melanoma-intrinsic β -catenin signalling prevents anti-tumour immunity', *Nature*, 523(7559), pp. 231–235. Available at: <https://doi.org/10.1038/nature14404>.
- Staněk, D. and Fox, A.H. (2017) 'Nuclear bodies: news insights into structure and function', *Current Opinion in Cell Biology*, 46, pp. 94–101. Available at: <https://doi.org/10.1016/j.ccb.2017.05.001>.
- van Steensel, B. and Furlong, E.E.M. (2019) 'The role of transcription in shaping the spatial organization of the genome', *Nature Reviews Molecular Cell Biology*, 20(6), pp. 327–337. Available at: <https://doi.org/10.1038/s41580-019-0114-6>.
- Steurer, B. et al. (2018) 'Live-cell analysis of endogenous GFP-RPB1 uncovers rapid turnover of initiating and promoter-paused RNA Polymerase II', *Proceedings of the National Academy of Sciences of the United States of America*, 115(19), pp. E4368–E4376. Available at: <https://doi.org/10.1073/pnas.1717920115>.
- Straussman, R. et al. (2012) 'Tumour micro-environment elicits innate resistance to RAF inhibitors through HGF secretion', *Nature*, 487(7408), pp. 500–504. Available at: <https://doi.org/10.1038/nature11183>.
- Strub, T. et al. (2011) 'Essential role of microphthalmia transcription factor for DNA replication, mitosis and genomic stability in melanoma', *Oncogene*, 30(20), pp. 2319–2332. Available at: <https://doi.org/10.1038/nc.2010.612>.
- Strub, T., Ballotti, R. and Bertolotto, C. (2020) 'The "ART" of Epigenetics in Melanoma: From histone "Alterations, to Resistance and Therapies"', *Theranostics*, 10(4), pp. 1777–1797. Available at: <https://doi.org/10.1515/thno.36218>.
- Sturm, R.A., Teasdale, R.D. and Box, N.F. (2001) 'Human pigmentation genes: identification, structure and consequences of polymorphic variation', *Gene*, 277(1–2), pp. 49–62. Available at: [https://doi.org/10.1016/S0378-1119\(01\)00694-1](https://doi.org/10.1016/S0378-1119(01)00694-1).
- Su, Y. et al. (2017) 'Single-cell analysis resolves the cell state transition and signaling dynamics associated with melanoma drug-induced resistance', *Proceedings of the National Academy of Sciences*, 114(52), pp. 13679–13684. Available at: <https://doi.org/10.1073/pnas.1712064115>.
- Subbiah, V., Baik, C. and Kirkwood, J.M. (2020) 'Clinical Development of BRAF plus MEK Inhibitor Combinations', *Trends in Cancer*, 6(9), pp. 797–810. Available at: <https://doi.org/10.1016/j.trecan.2020.05.009>.
- Sulaimon, S.S. and Kitchell, B.E. (2003) 'The biology of melanocytes', *Veterinary Dermatology*, 14(2), pp. 57–65. Available at: <https://doi.org/10.1046/j.1365-3164.2003.00327.x>.
- Sullivan, R.J. and Flaherty, K. (2013) 'MAP kinase signaling and inhibition in melanoma', *Oncogene*, 32(19), pp. 2373–2379. Available at: <https://doi.org/10.1038/nc.2012.345>.
- Sun, C. et al. (2014) 'Reversible and adaptive resistance to BRAF(V600E) inhibition in melanoma', *Nature*, 508(7494), pp. 118–122. Available at: <https://doi.org/10.1038/nature13121>.
- Sun, X. et al. (2018) 'Senescence-associated secretory factors induced by cisplatin in melanoma cells promote non-senescent melanoma cell growth through activation of the ERK1/2-RSK1 pathway', *Cell Death & Disease*, 9(3), pp. 1–15. Available at: <https://doi.org/10.1038/s41419-018-0303-9>.

- Sun, Y., Hamilton, K. and Tong, L. (2020) 'Recent molecular insights into canonical pre-mRNA 3'-end processing', *Transcription*, 11(2), pp. 83–96. Available at: <https://doi.org/10.1080/21541264.2020.1777047>.
- Sundararajan, S. et al. (2022) 'Metastatic Melanoma', in StatPearls. Treasure Island (FL): StatPearls Publishing. Available at: <http://www.ncbi.nlm.nih.gov/books/NBK470358/> (Accessed: 12 March 2023).
- Sunkel, B.D. et al. (2021) 'Evidence of pioneer factor activity of an oncogenic fusion transcription factor', *iScience*, 24(8), p. 102867. Available at: <https://doi.org/10.1016/j.isci.2021.102867>.
- Suresh, S. et al. (2023) 'Identifying the Transcriptional Drivers of Metastasis Embedded within Localized Melanoma', *Cancer Discovery*, 13(1), pp. 194–215. Available at: <https://doi.org/10.1158/2159-8290.CD-22-0427>.
- Suter, D.M. (2020) 'Transcription Factors and DNA Play Hide and Seek', *Trends in Cell Biology*, 30(6), pp. 491–500. Available at: <https://doi.org/10.1016/j.tcb.2020.03.003>.
- Suzuki, H.I. and Onimaru, K. (2022) 'Biomolecular condensates in cancer biology', *Cancer Science*, 113(2), pp. 382–391. Available at: <https://doi.org/10.1111/cas.15232>.
- Takahashi, H. et al. (2011) 'Human mediator subunit MED26 functions as a docking site for transcription elongation factors', *Cell*, 146(1), pp. 92–104. Available at: <https://doi.org/10.1016/j.cell.2011.06.005>.
- Takeda, K., Takahashi, N.-H. and Shibahara, S. (2007) 'Neuroendocrine Functions of Melanocytes: Beyond the Skin-Deep Melanin Maker', *The Tohoku Journal of Experimental Medicine*, 211(3), pp. 201–221. Available at: <https://doi.org/10.1620/tjem.211.201>.
- Takizawa, T., Meaburn, K.J. and Misteli, T. (2008) 'The meaning of gene positioning', *Cell*, 135(1), pp. 9–13. Available at: <https://doi.org/10.1016/j.cell.2008.09.026>.
- Talty, R. and Bosenberg, M. (2022) 'The role of ferroptosis in melanoma', *Pigment Cell & Melanoma Research*, 35(1), pp. 18–25. Available at: <https://doi.org/10.1111/pcmr.13009>.
- Tam, I., Dzierżęga-Lęcznar, A. and Stępień, K. (2019) 'Differential expression of inflammatory cytokines and chemokines in lipopolysaccharide-stimulated melanocytes from lightly and darkly pigmented skin', *Experimental Dermatology*, 28(5), pp. 551–560. Available at: <https://doi.org/10.1111/exd.13908>.
- Tanda, E.T. et al. (2020) 'Current State of Target Treatment in BRAF Mutated Melanoma', *Frontiers in Molecular Biosciences*, 7. Available at: <https://www.frontiersin.org/articles/10.3389/fmolb.2020.00154> (Accessed: 3 April 2023).
- Tang, C. et al. (2023) 'Cisplatin nephrotoxicity: new insights and therapeutic implications', *Nature Reviews Nephrology*, 19(1), pp. 53–72. Available at: <https://doi.org/10.1038/s41581-022-00631-7>.
- Tang, F. et al. (2020) 'Super-enhancer function and its application in cancer targeted therapy', *npj Precision Oncology*, 4(1), pp. 1–7. Available at: <https://doi.org/10.1038/s41698-020-0108-z>.
- Tang, J. et al. (2020) 'The genomic landscapes of individual melanocytes from human skin', *Nature*, 586(7830), pp. 600–605. Available at: <https://doi.org/10.1038/s41586-020-2785-8>.
- Tang, Y. et al. (2020) 'EMT-Inducing Transcription Factors, Drivers of Melanoma Phenotype Switching, and Resistance to Treatment', *Cancers*, 12(8), p. 2154. Available at: <https://doi.org/10.3390/cancers12082154>.
- Tasdogan, A. et al. (2020) 'Metabolic heterogeneity confers differences in melanoma metastatic potential', *Nature*, 577(7788), pp. 115–120. Available at: <https://doi.org/10.1038/s41586-019-1847-2>.
- Taub, R. et al. (1982) 'Translocation of the c-myc gene into the immunoglobulin heavy chain locus in human Burkitt lymphoma and murine plasmacytoma cells', *Proceedings of the National Academy of Sciences of the United States of America*, 79(24), pp. 7837–7841. Available at: <https://doi.org/10.1073/pnas.79.24.7837>.
- Tengesdal, I.W. et al. (2021) 'Targeting tumor-derived NLRP3 reduces melanoma progression by limiting MDSCs expansion', *Proceedings of the National Academy of Sciences*, 118(10), p. e2000915118. Available at: <https://doi.org/10.1073/pnas.2000915118>.
- Teves, S.S., Weber, C.M. and Henikoff, S. (2014) 'Transcribing through the nucleosome', *Trends in Biochemical Sciences*, 39(12), pp. 577–586. Available at: <https://doi.org/10.1016/j.tibs.2014.10.004>.
- Thandapani, P. (2019) 'Super-enhancers in cancer', *Pharmacology & Therapeutics*, 199, pp. 129–138. Available at: <https://doi.org/10.1016/j.pharmthera.2019.02.014>.
- The Cancer Genome Atlas Program - NCI (2018). Available at: <https://www.cancer.gov/about-nci/organization/ccg/research/structural-genomics/tcga> (Accessed: 12 February 2023).
- Theocharidis, G. et al. (2022) 'Single-cell transcriptomics in human skin research: available technologies, technical considerations and disease applications', *Experimental Dermatology*, 31(5), pp. 655–673. Available at: <https://doi.org/10.1111/exd.14547>.
- Theveneau, E. and Mayor, R. (2012) 'Neural crest delamination and migration: from epithelium-to-mesenchyme transition to collective cell migration', *Developmental Biology*, 366(1), pp. 34–54. Available at: <https://doi.org/10.1016/j.ydbio.2011.12.041>.
- Thomas, A.J. and Erickson, C.A. (2009) 'FOXO3 regulates the lineage switch between neural crest-derived glial cells and pigment cells by repressing MITF through a non-canonical mechanism', *Development (Cambridge, England)*, 136(11), pp. 1849–1858. Available at: <https://doi.org/10.1242/dev.031989>.

- Thomas, L.R. and Tansey, W.P. (2011) 'Proteolytic control of the oncoprotein transcription factor Myc', *Advances in Cancer Research*, 110, pp. 77–106. Available at: <https://doi.org/10.1016/B978-0-12-386469-7.00004-9>.
- Thompson, B.J. (2020) 'YAP/TAZ: Drivers of Tumor Growth, Metastasis, and Resistance to Therapy', *BioEssays: News and Reviews in Molecular, Cellular and Developmental Biology*, 42(5), p. e1900162. Available at: <https://doi.org/10.1002/bies.201900162>.
- Thompson, J.F., Mozzillo, N. and Ross, M.I. (2020) 'Local Melanoma Recurrence, Satellitosis, and In-transit Metastasis: Incidence, Outcomes, and Selection of Treatment Options', in C.M. Balch et al. (eds) *Cutaneous Melanoma*. Cham: Springer International Publishing, pp. 867–894. Available at: https://doi.org/10.1007/978-3-030-05070-2_32.
- Thornton, J. et al. (2022) 'Mechanisms of Immunotherapy Resistance in Cutaneous Melanoma: Recognizing a Shapeshifter', *Frontiers in Oncology*, 12. Available at: <https://www.frontiersin.org/articles/10.3389/fonc.2022.880876> (Accessed: 6 April 2023).
- Thurman, R.E. et al. (2012) 'The accessible chromatin landscape of the human genome', *Nature*, 489(7414), pp. 75–82. Available at: <https://doi.org/10.1038/nature11232>.
- Tirosh, I. et al. (2016) 'Dissecting the multicellular ecosystem of metastatic melanoma by single-cell RNA-seq', *Science (New York, N.Y.)*, 352(6282), pp. 189–196. Available at: <https://doi.org/10.1126/science.aad0501>.
- Titov, D.V. et al. (2011) 'XPB, a subunit of TFIIH, is a target of the natural product triptolide', *Nature Chemical Biology*, 7(3), pp. 182–188. Available at: <https://doi.org/10.1038/nchembio.522>.
- Todd, R.C. and Lippard, S.J. (2009) 'Inhibition of transcription by platinum antitumor compounds', *Metallomics: integrated biometal science*, 1(4), pp. 280–291. Available at: <https://doi.org/10.1039/b907567d>.
- Tomela, K. et al. (2023) 'Myeloid-Derived Suppressor Cells (MDSC) in Melanoma Patients Treated with Anti-PD-1 Immunotherapy', *Cells*, 12(5), p. 789. Available at: <https://doi.org/10.3390/cells12050789>.
- Torre, E.A. et al. (2021) 'Genetic screening for single-cell variability modulators driving therapy resistance', *Nature genetics*, 53(1), pp. 76–85. Available at: <https://doi.org/10.1038/s41588-020-00749-z>.
- Tortora's Principles of Anatomy and Physiology, 15th Edition, Global Edition | Wiley (no date) Wiley.com. Available at: <https://www.wiley.com/en-ie/Tortora%27s+Principles+of+Anatomy+and+Physiology%2C+15th+Edition%2C+Global+Edition-p-9781119400066> (Accessed: 25 January 2023).
- Tovar, C. et al. (2013) 'MDM2 small-molecule antagonist RG7112 activates p53 signaling and regresses human tumors in preclinical cancer models', *Cancer Research*, 73(8), pp. 2587–2597. Available at: <https://doi.org/10.1158/0008-5472.CAN-12-2807>.
- Tran, B. and Cohen, M.S. (2020) 'The discovery and development of binimetinib for the treatment of melanoma', *Expert Opinion on Drug Discovery*, 15(7), pp. 745–754. Available at: <https://doi.org/10.1080/17460441.2020.1746265>.
- Triana-Martínez, F., Loza, M.I. and Domínguez, E. (2020) 'Beyond Tumor Suppression: Senescence in Cancer Stemness and Tumor Dormancy', *Cells*, 9(2), p. 346. Available at: <https://doi.org/10.3390/cells9020346>.
- Trigo, J. et al. (2020) 'Lurbinectedin as second-line treatment for patients with small-cell lung cancer: a single-arm, open-label, phase 2 basket trial', *The Lancet. Oncology*, 21(5), pp. 645–654. Available at: [https://doi.org/10.1016/S1470-2045\(20\)30068-1](https://doi.org/10.1016/S1470-2045(20)30068-1).
- Trojer, P. and Reinberg, D. (2007) 'Facultative Heterochromatin: Is There a Distinctive Molecular Signature?', *Molecular Cell*, 28(1), pp. 1–13. Available at: <https://doi.org/10.1016/j.molcel.2007.09.011>.
- Trompouki, E. et al. (2011) 'Lineage Regulators Direct BMP and Wnt Pathways to Cell-Specific Programs during Differentiation and Regeneration', *Cell*, 147(3), pp. 577–589. Available at: <https://doi.org/10.1016/j.cell.2011.09.044>.
- Trujillo, J.A. et al. (2019) 'Secondary resistance to immunotherapy associated with β -catenin pathway activation or PTEN loss in metastatic melanoma', *Journal for Immunotherapy of Cancer*, 7(1), p. 295. Available at: <https://doi.org/10.1186/s40425-019-0780-0>.
- Tsai, C.-H. et al. (2023) 'Immunoediting instructs tumor metabolic reprogramming to support immune evasion', *Cell Metabolism*, 35(1), pp. 118–133.e7. Available at: <https://doi.org/10.1016/j.cmet.2022.12.003>.
- Tsao, H. et al. (2003) 'The transformation rate of moles (melanocytic nevi) into cutaneous melanoma: a population-based estimate', *Archives of Dermatology*, 139(3), pp. 282–288. Available at: <https://doi.org/10.1001/archderm.139.3.282>.
- Tsoi, J. et al. (2018) 'Multi-stage Differentiation Defines Melanoma Subtypes with Differential Vulnerability to Drug-Induced Iron-Dependent Oxidative Stress', *Cancer Cell*, 33(5), pp. 890–904.e5. Available at: <https://doi.org/10.1016/j.ccell.2018.03.017>.
- Tsuji, T., Ibaragi, S. and Hu, G. (2009) 'Epithelial-Mesenchymal Transition and Cell Cooperativity in Metastasis', *Cancer Research*, 69(18), pp. 7135–7139. Available at: <https://doi.org/10.1158/0008-5472.CAN-09-1618>.
- Tsakamoto, H. et al. (2018) 'Combined Blockade of IL6 and PD-1/PD-L1 Signaling Abrogates Mutual Regulation of Their Immunosuppressive Effects in the Tumor Microenvironment', *Cancer Research*, 78(17), pp. 5011–5022. Available at: <https://doi.org/10.1158/0008-5472.CAN-18-0118>.
- Tucker, M.A. et al. (1997) 'Clinically Recognized Dysplastic Nevi: A Central Risk Factor for Cutaneous Melanoma', *JAMA*, 277(18), pp. 1439–1444. Available at: <https://doi.org/10.1001/jama.1997.03540420035026>.
- Tumini, E. et al. (2019) 'The Antitumor Drugs Trabectedin and Lurbinectedin Induce Transcription-Dependent Replication Stress and Genome Instability', *Molecular cancer research: MCR*, 17(3), pp. 773–782. Available at: <https://doi.org/10.1158/1541-7786.MCR-18-0575>.

- Tuna, M., Amos, C.I. and Mills, G.B. (2019) 'Molecular mechanisms and pathobiology of oncogenic fusion transcripts in epithelial tumors', *Oncotarget*, 10(21), pp. 2095–2111. Available at: <https://doi.org/10.18632/oncotarget.26777>.
- Turajlic, S. et al. (2014) 'Whole-genome sequencing reveals complex mechanisms of intrinsic resistance to BRAF inhibition', *Annals of Oncology: Official Journal of the European Society for Medical Oncology*, 25(5), pp. 959–967. Available at: <https://doi.org/10.1093/annonc/mdl049>.
- Turajlic, S. et al. (2019) 'Resolving genetic heterogeneity in cancer', *Nature Reviews. Genetics*, 20(7), pp. 404–416. Available at: <https://doi.org/10.1038/s41576-019-0114-6>.
- Tyser, R.C.V. and Srinivas, S. (2022) 'Recent advances in understanding cell types during human gastrulation', *Seminars in Cell & Developmental Biology*, 131, pp. 35–43. Available at: <https://doi.org/10.1016/j.semcdb.2022.05.004>.
- Ubellacker, J.M. et al. (2020) 'Lymph protects metastasizing melanoma cells from ferroptosis', *Nature*, 585(7823), pp. 113–118. Available at: <https://doi.org/10.1038/s41586-020-2623-z>.
- Van Allen, E.M. et al. (2014) 'The genetic landscape of clinical resistance to RAF inhibition in metastatic melanoma', *Cancer discovery*, 4(1), pp. 94–109. Available at: <https://doi.org/10.1158/2159-8290.CD-13-0617>.
- Van Oss, S.B. et al. (2016) 'The Histone Modification Domain of Paf1 Complex Subunit Rtf1 Directly Stimulates H2B Ubiquitylation through an Interaction with Rad6', *Molecular Cell*, 64(4), pp. 815–825. Available at: <https://doi.org/10.1016/j.molcel.2016.10.008>.
- Vandamme, N. et al. (2020) 'The EMT Transcription Factor ZEB2 Promotes Proliferation of Primary and Metastatic Melanoma While Suppressing an Invasive, Mesenchymal-Like Phenotype', *Cancer Research*, 80(14), pp. 2983–2995. Available at: <https://doi.org/10.1158/0008-5472.CAN-19-2373>.
- Vandamme, N. and Berx, G. (2019) 'From neural crest cells to melanocytes: cellular plasticity during development and beyond', *Cellular and molecular life sciences: CMLS*, 76(10), pp. 1919–1934. Available at: <https://doi.org/10.1007/s00018-019-03049-w>.
- Vander Velde, R. et al. (2020) 'Resistance to targeted therapies as a multifactorial, gradual adaptation to inhibitor specific selective pressures', *Nature Communications*, 11(1), p. 2393. Available at: <https://doi.org/10.1038/s41467-020-16212-w>.
- Vandyck, H.H. et al. (2021) 'Rethinking the biology of metastatic melanoma: a holistic approach', *Cancer and Metastasis Reviews*, 40(2), pp. 603–624. Available at: <https://doi.org/10.1007/s10555-021-09960-8>.
- Vannini, A. et al. (2019) 'αvβ3-integrin regulates PD-L1 expression and is involved in cancer immune evasion', *Proceedings of the National Academy of Sciences*, 116(40), pp. 20141–20150. Available at: <https://doi.org/10.1073/pnas.1901931116>.
- Vardabasso, C. et al. (2015) 'Histone variant H2A.Z.2 mediates proliferation and drug sensitivity of malignant melanoma', *Molecular cell*, 59(1), pp. 75–88. Available at: <https://doi.org/10.1016/j.molcel.2015.05.009>.
- Vareki, S.M. (2018) 'High and low mutational burden tumors versus immunologically hot and cold tumors and response to immune checkpoint inhibitors', *Journal for ImmunoTherapy of Cancer*, 6(1), p. 157. Available at: <https://doi.org/10.1186/s40425-018-0479-7>.
- Varrone, F. and Caputo, E. (2020) 'The miRNAs Role in Melanoma and in Its Resistance to Therapy', *International Journal of Molecular Sciences*, 21(3), p. 878. Available at: <https://doi.org/10.3390/ijms21030878>.
- Vartanian, A. et al. (2011) 'VEGFR1 and PKCα signaling control melanoma vasculogenic mimicry in a VEGFR2 kinase-independent manner', *Melanoma Research*, 21(2), pp. 91–98. Available at: <https://doi.org/10.1097/CMR.0b013e328343a237>.
- Veglia, F., Sanseviero, E. and Gabrilovich, D.I. (2021) 'Myeloid-derived suppressor cells in the era of increasing myeloid cell diversity', *Nature Reviews Immunology*, 21(8), pp. 485–498. Available at: <https://doi.org/10.1038/s41577-020-00490-y>.
- Verastegui, C. et al. (2000) 'Regulation of the microphthalmia-associated transcription factor gene by the Waardenburg syndrome type 4 gene, SOX10', *The Journal of Biological Chemistry*, 275(40), pp. 30757–30760. Available at: <https://doi.org/10.1074/jbc.C000445200>.
- Verfaillie, A. et al. (2015) 'Decoding the regulatory landscape of melanoma reveals TEADS as regulators of the invasive cell state', *Nature Communications*, 6, p. 6683. Available at: <https://doi.org/10.1038/ncomms7683>.
- Vergara, I.A. et al. (2021) 'Evolution of late-stage metastatic melanoma is dominated by aneuploidy and whole genome doubling', *Nature Communications*, 12(1), p. 1434. Available at: <https://doi.org/10.1038/s41467-021-21576-8>.
- Vergara, I.A. et al. (2022) 'Genetic drivers of non-cutaneous melanomas: Challenges and opportunities in a heterogeneous landscape', *Experimental Dermatology*, 31(1), pp. 13–30. Available at: <https://doi.org/10.1111/exd.14287>.
- Vermunt, M.W., Zhang, D. and Blobel, G.A. (2019) 'The interdependence of gene-regulatory elements and the 3D genome', *The Journal of Cell Biology*, 218(1), pp. 12–26. Available at: <https://doi.org/10.1083/jcb.201809040>.
- Vervoort, S.J. et al. (2022) 'Targeting transcription cycles in cancer', *Nature Reviews Cancer*, 22(1), pp. 5–24. Available at: <https://doi.org/10.1038/s41568-021-00411-8>.
- Vesely, M.D. and Schreiber, R.D. (2013) 'Cancer Immunoediting: antigens, mechanisms and implications to cancer immunotherapy', *Annals of the New York Academy of Sciences*, 1284(1), pp. 1–5. Available at: <https://doi.org/10.1111/nyas.12105>.
- Vessoni, A.T. et al. (2020) 'Cockayne Syndrome: The many challenges and approaches to understand a multifaceted disease', *Genetics and Molecular Biology*, 43(1 Suppl 1), p. e20190085. Available at: <https://doi.org/10.1590/1678-4685-GMB-2019-0085>.

- Vidal, A. et al. (2012) 'Lurbinectedin (PM01183), a new DNA minor groove binder, inhibits growth of orthotopic primary graft of cisplatin-resistant epithelial ovarian cancer', *Clinical Cancer Research: An Official Journal of the American Association for Cancer Research*, 18(19), pp. 5399–5411. Available at: <https://doi.org/10.1158/1078-0432.CCR-12-1513>.
- Vido, M.J. et al. (2018) 'BRAF Splice Variant Resistance to RAF Inhibitor Requires Enhanced MEK Association', *Cell Reports*, 25(6), pp. 1501–1510.e3. Available at: <https://doi.org/10.1016/j.celrep.2018.10.049>.
- Vihervaara, A., Duarte, F.M. and Lis, J.T. (2018) 'Molecular mechanisms driving transcriptional stress responses', *Nature Reviews Genetics*, 19(6), pp. 385–397. Available at: <https://doi.org/10.1038/s41576-018-0001-6>.
- Villanueva, J., Vultur, A. and Herlyn, M. (2011) 'Resistance to BRAF inhibitors: Unraveling mechanisms and future treatment options', *Cancer research*, 71(23), pp. 7137–7140. Available at: <https://doi.org/10.1158/0008-5472.CAN-11-1243>.
- Villemin, C. et al. (2023) 'The heightened importance of the microbiome in cancer immunotherapy', *Trends in Immunology*, 44(1), pp. 44–59. Available at: <https://doi.org/10.1016/j.it.2022.11.002>.
- Villicaña, C., Cruz, G. and Zurita, M. (2014) 'The basal transcription machinery as a target for cancer therapy', *Cancer Cell International*, 14(1), p. 18. Available at: <https://doi.org/10.1186/1475-2867-14-18>.
- Visel, A. et al. (2009) 'ChIP-seq accurately predicts tissue-specific activity of enhancers', *Nature*, 457(7231), pp. 854–858. Available at: <https://doi.org/10.1038/nature07730>.
- Vitali, F. et al. (2022) 'Early melanoma invasivity correlates with gut fungal and bacterial profiles', *The British Journal of Dermatology*, 186(1), pp. 106–116. Available at: <https://doi.org/10.1111/bjd.20626>.
- Vittoria, M.A. et al. (2022) 'Inactivation of the Hippo tumor suppressor pathway promotes melanoma', *Nature Communications*, 13(1), p. 3732. Available at: <https://doi.org/10.1038/s41467-022-31399-w>.
- Vivas-García, Y. et al. (2020) 'Lineage-Restricted Regulation of SCD and Fatty Acid Saturation by MITF Controls Melanoma Phenotypic Plasticity', *Molecular Cell*, 77(1), pp. 120–137.e9. Available at: <https://doi.org/10.1016/j.molcel.2019.10.014>.
- Vo Ngoc, L. et al. (2017) 'The punctilious RNA polymerase II core promoter', *Genes & Development*, 31(13), pp. 1289–1301. Available at: <https://doi.org/10.1101/gad.303149.117>.
- Vogelstein, B. and Kinzler, K.W. (1993) 'The multistep nature of cancer', *Trends in Genetics*, 9(4), pp. 138–141. Available at: [https://doi.org/10.1016/0168-9525\(93\)90209-Z](https://doi.org/10.1016/0168-9525(93)90209-Z).
- Vos, S.M., Farnung, L., Boehning, M., et al. (2018) 'Structure of activated transcription complex Pol II-DSIF-PAF-SPT6', *Nature*, 560(7720), pp. 607–612. Available at: <https://doi.org/10.1038/s41586-018-0440-4>.
- Vos, S.M., Farnung, L., Urlaub, H., et al. (2018) 'Structure of paused transcription complex Pol II-DSIF-NELF', *Nature*, 560(7720), pp. 601–606. Available at: <https://doi.org/10.1038/s41586-018-0442-2>.
- Wagner, E.J., Tong, L. and Adelman, K. (2023) 'Integrator is a global promoter-proximal termination complex', *Molecular Cell*, 83(3), pp. 416–427. Available at: <https://doi.org/10.1016/j.molcel.2022.11.012>.
- Walbrech, G. et al. (2020) 'Distinct Cargos of Small Extracellular Vesicles Derived from Hypoxic Cells and Their Effect on Cancer Cells', *International Journal of Molecular Sciences*, 21(14), p. 5071. Available at: <https://doi.org/10.3390/ijms21145071>.
- Wang, C. et al. (2022) 'Lineage-selective super enhancers mediate core regulatory circuitry during adipogenic and osteogenic differentiation of human mesenchymal stem cells', *Cell Death & Disease*, 13(10), pp. 1–12. Available at: <https://doi.org/10.1038/s41419-022-05309-3>.
- Wang, G., Wang, X. and Xu, X. (2015) 'Triptolide potentiates lung cancer cells to cisplatin-induced apoptosis by selectively inhibiting the NER activity', *Biomarker Research*, 3, p. 17. Available at: <https://doi.org/10.1186/s40364-015-0043-2>.
- Wang, H. et al. (2023) 'Structures of transcription preinitiation complex engaged with the +1 nucleosome', *Nature Structural & Molecular Biology*, 30(2), pp. 226–232. Available at: <https://doi.org/10.1038/s41594-022-00865-w>.
- Wang, J. et al. (2022) 'Exploring Tumor Immune Microenvironment and Its Associations With Molecular Characteristics in Melanoma', *Frontiers in Oncology*, 12, p. 821578. Available at: <https://doi.org/10.3389/fonc.2022.821578>.
- Wang, K.C. and Chang, H.Y. (2011) 'Molecular Mechanisms of Long Noncoding RNAs', *Molecular Cell*, 43(6), pp. 904–914. Available at: <https://doi.org/10.1016/j.molcel.2011.08.018>.
- Wang, S. et al. (2016) 'Spatial organization of chromatin domains and compartments in single chromosomes', *Science*, 353(6299), pp. 598–602. Available at: <https://doi.org/10.1126/science.aaf8084>.
- Wang, X., Haswell, J.R. and Roberts, C.W.M. (2014) 'Molecular Pathways: SWI/SNF (BAF) Complexes Are Frequently Mutated in Cancer—Mechanisms and Potential Therapeutic Insights', *Clinical Cancer Research*, 20(1), pp. 21–27. Available at: <https://doi.org/10.1158/1078-0432.CCR-13-0280>.
- Wang, Y. et al. (2015) 'CDK7-Dependent Transcriptional Addiction in Triple-Negative Breast Cancer', *Cell*, 163(1), pp. 174–186. Available at: <https://doi.org/10.1016/j.cell.2015.08.063>.
- Wang, Y. et al. (2020) 'The emerging role of super enhancer-derived noncoding RNAs in human cancer', *Theranostics*, 10(24), pp. 11049–11062. Available at: <https://doi.org/10.7150/thno.49168>.
- Wang, Z.-H. et al. (2021) 'Lactate in the tumour microenvironment: From immune modulation to therapy', *eBioMedicine*, 73. Available at: <https://doi.org/10.1016/j.ebiom.2021.103627>.

- Wanzel, M. et al. (2008) 'A ribosomal protein L23-nucleophosmin circuit coordinates Miz1 function with cell growth', *Nature Cell Biology*, 10(9), pp. 1051–1061. Available at: <https://doi.org/10.1038/ncb1764>.
- Warburg, O. (1924) 'Über den Stoffwechsel der Carcinomzelle', *Naturwissenschaften*, 12(50), pp. 1131–1137. Available at: <https://doi.org/10.1007/BF01504608>.
- Watson, I.R. et al. (2014) 'The RAC1 P29S hotspot mutation in melanoma confers resistance to pharmacological inhibition of RAF', *Cancer Research*, 74(17), pp. 4845–4852. Available at: <https://doi.org/10.1158/0008-5472.CAN-14-1232-T>.
- Weber, C.M., Ramachandran, S. and Henikoff, S. (2014) 'Nucleosomes are context-specific, H2A.Z-modulated barriers to RNA polymerase', *Molecular Cell*, 53(5), pp. 819–830. Available at: <https://doi.org/10.1016/j.molcel.2014.02.014>.
- Weber, J.S. et al. (2017) 'Safety Profile of Nivolumab Monotherapy: A Pooled Analysis of Patients With Advanced Melanoma', *Journal of Clinical Oncology: Official Journal of the American Society of Clinical Oncology*, 35(7), pp. 785–792. Available at: <https://doi.org/10.1200/JCO.2015.66.1389>.
- Wei, L. et al. (2021) 'Ultra-deep sequencing differentiates patterns of skin clonal mutations associated with sun-exposure status and skin cancer burden', *Science Advances*, 7(1), p. eabd7703. Available at: <https://doi.org/10.1126/sciadv.abd7703>.
- Wei, M.-T. et al. (2020) 'Nucleated transcriptional condensates amplify gene expression', *Nature Cell Biology*, 22(10), pp. 1187–1196. Available at: <https://doi.org/10.1038/s41556-020-00578-6>.
- Weidemüller, P. et al. (2021) 'Transcription factors: Bridge between cell signaling and gene regulation', *PROTEOMICS*, 21(23–24), p. 2000034. Available at: <https://doi.org/10.1002/pmic.202000034>.
- Weinhold, N. et al. (2014) 'Genome-wide analysis of noncoding regulatory mutations in cancer', *Nature Genetics*, 46(11), pp. 1160–1165. Available at: <https://doi.org/10.1038/ng.3101>.
- Weinstein, I.B. and Joe, A.K. (2006) 'Mechanisms of Disease: oncogene addiction—a rationale for molecular targeting in cancer therapy', *Nature Clinical Practice Oncology*, 3(8), pp. 448–457. Available at: <https://doi.org/10.1038/ncponc0558>.
- WEINSTOCK, M.A. and SOBER, A.J. (1987) 'The risk of progression of lentigo maligna to lentigo maligna melanoma', *British Journal of Dermatology*, 116(3), pp. 303–310. Available at: <https://doi.org/10.1111/j.1365-2133.1987.tb05843.x>.
- Weis, S.M. and Cheresch, D.A. (2011) 'Tumor angiogenesis: molecular pathways and therapeutic targets', *Nature Medicine*, 17(11), pp. 1359–1370. Available at: <https://doi.org/10.1038/nm.2537>.
- Weiss, J.M. et al. (2022) 'Anatomic position determines oncogenic specificity in melanoma', *Nature*, 604(7905), pp. 354–361. Available at: <https://doi.org/10.1038/s41586-022-04584-6>.
- Welti, M. et al. (2022) 'Triple Combination of Immune Checkpoint Inhibitors and BRAF/MEK Inhibitors in BRAFV600 Melanoma: Current Status and Future Perspectives', *Cancers*, 14(22), p. 5489. Available at: <https://doi.org/10.3390/cancers14225489>.
- Werner-Klein, M. et al. (2018) 'Genetic alterations driving metastatic colony formation are acquired outside of the primary tumour in melanoma', *Nature Communications*, 9(1), p. 595. Available at: <https://doi.org/10.1038/s41467-017-02674-y>.
- Wessely, A. et al. (2021) 'How Neural Crest Transcription Factors Contribute to Melanoma Heterogeneity, Cellular Plasticity, and Treatment Resistance', *International Journal of Molecular Sciences*, 22(11), p. 5761. Available at: <https://doi.org/10.3390/ijms22115761>.
- West, S., Gromak, N. and Proudfoot, N.J. (2004) 'Human 5' → 3' exonuclease Xrn2 promotes transcription termination at co-transcriptional cleavage sites', *Nature*, 432(7016), pp. 522–525. Available at: <https://doi.org/10.1038/nature03035>.
- Whyte, W.A. et al. (2013) 'Master transcription factors and mediator establish super-enhancers at key cell identity genes', *Cell*, 153(2), pp. 307–319. Available at: <https://doi.org/10.1016/j.cell.2013.03.035>.
- Widmer, D.S. et al. (2012) 'Systematic classification of melanoma cells by phenotype-specific gene expression mapping', *Pigment Cell & Melanoma Research*, 25(3), pp. 343–353. Available at: <https://doi.org/10.1111/j.1755-148X.2012.00986.x>.
- Wilson, B.G. et al. (2010) 'Epigenetic Antagonism between Polycomb and SWI/SNF Complexes during Oncogenic Transformation', *Cancer Cell*, 18(4), pp. 316–328. Available at: <https://doi.org/10.1016/j.ccr.2010.09.006>.
- Winkler, J. et al. (2020) 'Concepts of extracellular matrix remodelling in tumour progression and metastasis', *Nature Communications*, 11(1), p. 5120. Available at: <https://doi.org/10.1038/s41467-020-18794-x>.
- Winter, G.E. et al. (2015) 'Phthalimide conjugation as a strategy for in vivo target protein degradation', *Science*, 348(6241), pp. 1376–1381. Available at: <https://doi.org/10.1126/science.aab1433>.
- Wong, K.H., Jin, Y. and Struhl, K. (2014) 'TFIIH phosphorylation of the Pol II CTD stimulates mediator dissociation from the preinitiation complex and promoter escape', *Molecular Cell*, 54(4), pp. 601–612. Available at: <https://doi.org/10.1016/j.molcel.2014.03.024>.
- Wong, R. et al. (2016) 'The dynamic anatomy and patterning of skin', *Experimental Dermatology*, 25(2), pp. 92–98. Available at: <https://doi.org/10.1111/exd.12832>.
- Woo, Y.R. et al. (2022) 'The Human Microbiota and Skin Cancer', *International Journal of Molecular Sciences*, 23(3), p. 1813. Available at: <https://doi.org/10.3390/ijms23031813>.
- Wouters, J. et al. (2020) 'Robust gene expression programs underlie recurrent cell states and phenotype switching in melanoma', *Nature Cell Biology*, 22(8), pp. 986–998. Available at: <https://doi.org/10.1038/s41556-020-0547-3>.

- Wozniak, M. and Czyz, M. (2021) 'The Functional Role of Long Non-Coding RNAs in Melanoma', *Cancers*, 13(19), p. 4848. Available at: <https://doi.org/10.3390/cancers13194848>.
- Wu, M. and Shen, J. (2019) 'From Super-Enhancer Non-coding RNA to Immune Checkpoint: Frameworks to Functions', *Frontiers in Oncology*, 9. Available at: <https://www.frontiersin.org/articles/10.3389/fonc.2019.01307> (Accessed: 12 May 2023).
- Wu, R. et al. (2020) 'SOX2 promotes resistance of melanoma with PD-L1 high expression to T-cell-mediated cytotoxicity that can be reversed by SAHA', *Journal for Immunotherapy of Cancer*, 8(2), p. e001037. Available at: <https://doi.org/10.1136/jitc-2020-001037>.
- Wu, Y. et al. (2023) 'Disrupting the phase separation of KAT8–IRF1 diminishes PD-L1 expression and promotes antitumor immunity', *Nature Cancer*, 4(3), pp. 382–400. Available at: <https://doi.org/10.1038/s43018-023-00522-1>.
- Xi, C. et al. (2017) 'Toxicity of triptolide and the molecular mechanisms involved', *Biomedicine & Pharmacotherapy = Biomedecine & Pharmacotherapie*, 90, pp. 531–541. Available at: <https://doi.org/10.1016/j.biopha.2017.04.003>.
- Xiao, D. et al. (2016) 'Melanoma cell-derived exosomes promote epithelial–mesenchymal transition in primary melanocytes through paracrine/autocrine signaling in the tumor microenvironment', *Cancer Letters*, 376(2), pp. 318–327. Available at: <https://doi.org/10.1016/j.canlet.2016.03.050>.
- Xiao, M. et al. (2018) 'Driving Cytotoxic Natural Killer Cells into Melanoma: If CCL5 Plays the Music, Autophagy Calls the Shots', *Critical Reviews in Oncogenesis*, 23(5–6), pp. 321–332. Available at: <https://doi.org/10.1615/CritRevOnc.2018027526>.
- Xie, F. et al. (2019) 'The role of exosomal PD-L1 in tumor progression and immunotherapy', *Molecular Cancer*, 18(1), p. 146. Available at: <https://doi.org/10.1186/s12943-019-1074-3>.
- Xie, Q. et al. (2023) 'Phase separation in cancer at a glance', *Journal of Translational Medicine*, 21(1), p. 237. Available at: <https://doi.org/10.1186/s12967-023-04082-x>.
- Xie, W. et al. (2019) 'Lurbinectedin synergizes with immune checkpoint blockade to generate anticancer immunity', *Oncoimmunology*, 8(11), p. e1656502. Available at: <https://doi.org/10.1080/2162402X.2019.1656502>.
- Xie, Y. et al. (2022) 'Identification of Lactate-Related Gene Signature for Prediction of Progression and Immunotherapeutic Response in Skin Cutaneous Melanoma', *Frontiers in Oncology*, 12. Available at: <https://www.frontiersin.org/articles/10.3389/fonc.2022.818868> (Accessed: 18 March 2023).
- Xu, Y. et al. (2012) 'Differential expression of microRNAs during melanoma progression: miR-200c, miR-205 and miR-211 are downregulated in melanoma and act as tumour suppressors', *British Journal of Cancer*, 106(3), pp. 553–561. Available at: <https://doi.org/10.1038/bjc.2011.568>.
- Yajima, I. and Larue, L. (2008) 'The location of heart melanocytes is specified and the level of pigmentation in the heart may correlate with coat color', *Pigment Cell & Melanoma Research*, 21(4), pp. 471–476. Available at: <https://doi.org/10.1111/j.1755-148X.2008.00483.x>.
- Yamaguchi, Y. and Hearing, V.J. (2014) 'Melanocytes and Their Diseases', *Cold Spring Harbor Perspectives in Medicine*, 4(5), p. a017046. Available at: <https://doi.org/10.1101/cshperspect.a017046>.
- Yang, C. et al. (2021) 'Melanoma subpopulations that rapidly escape MAPK pathway inhibition incur DNA damage and rely on stress signalling', *Nature Communications*, 12(1), p. 1747. Available at: <https://doi.org/10.1038/s41467-021-21549-x>.
- Yang, H. et al. (2010) 'RG7204 (PLX4032), a selective BRAFV600E inhibitor, displays potent antitumor activity in preclinical melanoma models', *Cancer Research*, 70(13), pp. 5518–5527. Available at: <https://doi.org/10.1158/0008-5472.CAN-10-0646>.
- Yang, J. et al. (2021) 'The Paradoxical Role of Cellular Senescence in Cancer', *Frontiers in Cell and Developmental Biology*, 9. Available at: <https://www.frontiersin.org/articles/10.3389/fcell.2021.722205> (Accessed: 23 March 2023).
- Yang, M.-H. et al. (2008) 'Direct regulation of TWIST by HIF-1 α promotes metastasis', *Nature Cell Biology*, 10(3), pp. 295–305. Available at: <https://doi.org/10.1038/ncb1691>.
- Yang, Z., Sharma, K. and de Lange, T. (2022) 'TRF1 uses a noncanonical function of TFIIF to promote telomere replication', *Genes & Development*, 36(17–18), pp. 956–969. Available at: <https://doi.org/10.1101/gad.349975.122>.
- Yao, D., Dai, C. and Peng, S. (2011) 'Mechanism of the mesenchymal-epithelial transition and its relationship with metastatic tumor formation', *Molecular cancer research: MCR*, 9(12), pp. 1608–1620. Available at: <https://doi.org/10.1158/1541-7786.MCR-10-0568>.
- Yao, Z. et al. (2017) 'Tumours with class 3 BRAF mutants are sensitive to the inhibition of activated RAS', *Nature*, 548(7666), pp. 234–238. Available at: <https://doi.org/10.1038/nature23291>.
- Yeh, I. and Bastian, B.C. (2021) 'Melanoma pathology: new approaches and classification*', *British Journal of Dermatology*, 185(2), pp. 282–293. Available at: <https://doi.org/10.1111/bjd.20427>.
- Yeh, I., von Deimling, A. and Bastian, B.C. (2013) 'Clonal BRAF mutations in melanocytic nevi and initiating role of BRAF in melanocytic neoplasia', *Journal of the National Cancer Institute*, 105(12), pp. 917–919. Available at: <https://doi.org/10.1093/jnci/djt119>.
- Yokoyama, S. et al. (2021) 'SOX10 regulates melanoma immunogenicity through an IRF4-IRF1 axis', *Cancer research*, 81(24), pp. 6131–6141. Available at: <https://doi.org/10.1158/0008-5472.CAN-21-2078>.
- Yu, C. et al. (2019) 'Combination of Immunotherapy With Targeted Therapy: Theory and Practice in Metastatic Melanoma', *Frontiers in Immunology*, 10, p. 990. Available at: <https://doi.org/10.3389/fimmu.2019.00990>.

- Yu, X. and Xu, J. (2020) 'A "Goldmine" for digging cancer-specific targets: the genes essential for embryo development but non-essential for adult life', *Journal of Molecular Cell Biology*, 12(9), pp. 669–673. Available at: <https://doi.org/10.1093/jmcb/mjaa024>.
- Yuan, K. et al. (2019) 'Application and Mechanisms of Triptolide in the Treatment of Inflammatory Diseases—A Review', *Frontiers in Pharmacology*, 10, p. 1469. Available at: <https://doi.org/10.3389/fphar.2019.01469>.
- Zabidi, M.A. and Stark, A. (2016) 'Regulatory Enhancer-Core-Promoter Communication via Transcription Factors and Cofactors', *Trends in genetics: TIG*, 32(12), pp. 801–814. Available at: <https://doi.org/10.1016/j.tig.2016.10.003>.
- Zamudio, A.V. et al. (2019) 'Mediator Condensates Localize Signaling Factors to Key Cell Identity Genes', *Molecular Cell*, 76(5), pp. 753–766.e6. Available at: <https://doi.org/10.1016/j.molcel.2019.08.016>.
- Zanconato, F. et al. (2018) 'Transcriptional addiction in cancer cells is mediated by YAP/TAZ through BRD4', *Nature Medicine*, 24(10), pp. 1599–1610. Available at: <https://doi.org/10.1038/s41591-018-0158-8>.
- Zanconato, F., Cordenonsi, M. and Piccolo, S. (2016) 'YAP/TAZ at the Roots of Cancer', *Cancer Cell*, 29(6), pp. 783–803. Available at: <https://doi.org/10.1016/j.ccell.2016.05.005>.
- Zaretsky, J.M. et al. (2016) 'Mutations Associated with Acquired Resistance to PD-1 Blockade in Melanoma', *The New England Journal of Medicine*, 375(9), pp. 819–829. Available at: <https://doi.org/10.1056/NEJMoa1604958>.
- Zeid, R. et al. (2018) 'Enhancer invasion shapes MYCN-dependent transcriptional amplification in neuroblastoma', *Nature Genetics*, 50(4), pp. 515–523. Available at: <https://doi.org/10.1038/s41588-018-0044-9>.
- Zeng, H. et al. (2018) 'Bi-allelic Loss of CDKN2A Initiates Melanoma Invasion via BRN2 Activation', *Cancer Cell*, 34(1), pp. 56–68.e9. Available at: <https://doi.org/10.1016/j.ccell.2018.05.014>.
- Zhang, C. et al. (2015) 'RAF inhibitors that evade paradoxical MAPK pathway activation', *Nature*, 526(7574), pp. 583–586. Available at: <https://doi.org/10.1038/nature14982>.
- Zhang, C. et al. (2020) 'Super-enhancer-driven AJUBA is activated by TCF4 and involved in epithelial-mesenchymal transition in the progression of Hepatocellular Carcinoma', *Theranostics*, 10(20), pp. 9066–9082. Available at: <https://doi.org/10.7150/thno.45349>.
- Zhang, F. et al. (2013) 'Perivascular macrophage-like melanocyte responsiveness to acoustic trauma—a salient feature of stria vascularis associated hearing loss', *FASEB journal: official publication of the Federation of American Societies for Experimental Biology*, 27(9), pp. 3730–3740. Available at: <https://doi.org/10.1096/fj.13-232892>.
- Zhang, K. et al. (2012) 'A Notch1–neuregulin1 autocrine signaling loop contributes to melanoma growth', *Oncogene*, 31(43), pp. 4609–4618. Available at: <https://doi.org/10.1038/onc.2011.606>.
- Zhang, Q. et al. (2018) 'Blockade of the checkpoint receptor TIGIT prevents NK cell exhaustion and elicits potent anti-tumor immunity', *Nature Immunology*, 19(7), pp. 723–732. Available at: <https://doi.org/10.1038/s41590-018-0132-0>.
- Zhang, T. et al. (2020) 'Aberrant super-enhancer landscape reveals core transcriptional regulatory circuitry in lung adenocarcinoma', *Oncogenesis*, 9(10), pp. 1–12. Available at: <https://doi.org/10.1038/s41389-020-00277-9>.
- Zhang, X. et al. (2016) 'Identification of focally amplified lineage-specific super-enhancers in human epithelial cancers', *Nature Genetics*, 48(2), pp. 176–182. Available at: <https://doi.org/10.1038/ng.3470>.
- Zhang, Z. et al. (2019) 'The role of vascular mimicry as a biomarker in malignant melanoma: a systematic review and meta-analysis', *BMC Cancer*, 19(1), p. 1134. Available at: <https://doi.org/10.1186/s12885-019-6350-5>.
- Zhou, B. et al. (2016) 'INO80 governs superenhancer-mediated oncogenic transcription and tumor growth in melanoma', *Genes & Development*, 30(12), pp. 1440–1453. Available at: <https://doi.org/10.1101/gad.277178.115>.
- Zhou, J. et al. (2020) 'Tumor-Associated Macrophages: Recent Insights and Therapies', *Frontiers in Oncology*, 10. Available at: <https://www.frontiersin.org/articles/10.3389/fonc.2020.00188> (Accessed: 20 March 2023).
- Zhou, R.W. et al. (2022) 'A local tumor microenvironment acquired super-enhancer induces an oncogenic driver in colorectal carcinoma', *Nature Communications*, 13(1), p. 6041. Available at: <https://doi.org/10.1038/s41467-022-33377-8>.
- Zhovmer, A., Oksenysh, V. and Coin, F. (2010) 'Two sides of the same coin: TFIIH complexes in transcription and DNA repair', *TheScientificWorldJournal*, 10, pp. 633–643. Available at: <https://doi.org/10.1100/tsw.2010.46>.
- Zhuang, D. et al. (2008) 'C-MYC overexpression is required for continuous suppression of oncogene-induced senescence in melanoma cells', *Oncogene*, 27(52), pp. 6623–6634. Available at: <https://doi.org/10.1038/onc.2008.258>.
- Zimmer, L. et al. (2020) 'Adjuvant nivolumab plus ipilimumab or nivolumab monotherapy versus placebo in patients with resected stage IV melanoma with no evidence of disease (IMMUNED): a randomised, double-blind, placebo-controlled, phase 2 trial', *The Lancet*, 395(10236), pp. 1558–1568. Available at: [https://doi.org/10.1016/S0140-6736\(20\)30417-7](https://doi.org/10.1016/S0140-6736(20)30417-7).
- Zimmerman, A., Bai, L. and Ginty, D.D. (2014) 'The gentle touch receptors of mammalian skin', *Science (New York, N.Y.)*, 346(6212), pp. 950–954. Available at: <https://doi.org/10.1126/science.1254229>.
- Zitvogel, L., Tesniere, A. and Kroemer, G. (2006) 'Cancer despite immunosurveillance: immunoselection and immunosubversion', *Nature Reviews Immunology*, 6(10), pp. 715–727. Available at: <https://doi.org/10.1038/nri1936>.
- Zuo, Q. et al. (2018) 'AXL/AKT axis mediated-resistance to BRAF inhibitor depends on PTEN status in melanoma', *Oncogene*, 37(24), pp. 3275–3289. Available at: <https://doi.org/10.1038/s41388-018-0205-4>.

- Zurita, M. and Cruz-Becerra, G. (2016) 'TFIIH: New Discoveries Regarding its Mechanisms and Impact on Cancer Treatment', *Journal of Cancer*, 7(15), pp. 2258–2265. Available at: <https://doi.org/10.7150/jca.16966>.
- Zylicz, J.J. and Heard, E. (2020) 'Molecular Mechanisms of Facultative Heterochromatin Formation: An X-Chromosome Perspective', *Annual Review of Biochemistry*, 89(1), pp. 255–282. Available at: <https://doi.org/10.1146/annurev-biochem-062917-012655>.

Targeting transcriptional addiction in cutaneous melanoma

Résumé

Malgré de récentes avancées thérapeutiques révolutionnaires, le mélanome métastatique constitue toujours un problème de santé publique important, caractérisé par l'émergence rapide de sous-populations cellulaires résistantes aux traitements. Les cellules de mélanome se distinguent des cellules normales par une caractéristique associée au cancer que l'on peut cibler. En effet, les cellules de mélanome présentent un état de 'dépendance transcriptionnelle', par lequel elles deviennent dépendantes de l'expression intense d'oncogènes clés. Nous cherchons ici à déterminer si l'utilisation d'inhibiteurs de la transcription pourrait constituer une stratégie efficace de traitement du mélanome. Nous constatons qu'un inhibiteur de CDK7, THZ1, n'affecte pas tous les types de cellules de mélanome de la même manière et qu'une inhibition prolongée de CDK7 conduit à des cellules de mélanome plus dédifférenciées, plus invasives et plus résistantes aux traitements. Cependant, l'inhibition de XPB, un partenaire moléculaire de CDK7, ne provoque pas un tel changement de phénotype et cible efficacement l'expression des gènes oncogènes, ce qui justifie des études plus approfondies. En outre, nous établissons que l'utilisation de la Lurbinectedine et de ses dérivés structuraux pourrait être bénéfique sur le plan clinique dans le mélanome, mais nous élucidons également pour la première fois des mécanismes de résistance potentiels contre ce nouveau type d'inhibiteur transcriptionnel. En conclusion, ce travail met en lumière des questions fondamentales concernant la régulation de l'expression des gènes dans les cellules de mélanome et leurs réponses moléculaires et cellulaires aux inhibiteurs de la transcription, tout en élucidant leurs avantages et inconvénients cliniques potentiels pour les patients.

Mots-clés : Cancer, Mélanome, Expression génétique, Dépendance transcriptionnelle, Nouvelles thérapies

Abstract

Despite revolutionary recent advances in therapeutics, metastatic melanoma still poses a significant public health problem, characterized by rapidly emerging treatment-resistant cell subpopulations. In a fashion distinguishing them from normal cells and representing thus a targetable cancer-associated hallmark, melanoma cells display a state of 'transcriptional addiction', by which they become dependent on the intense expression of key oncogenes. Here, we elucidate whether the use of transcriptional inhibitors might be a useful addition to the existing framework of melanoma treatments. We find that the CDK7 inhibitor THZ1 does not affect all melanoma cell types equally, and that prolonged CDK7 inhibition leads to melanoma cells becoming more dedifferentiated, invasive and treatment-resistant. However, the inhibition of XPB, a molecular partner of CDK7, does not elicit such a phenotype switch, and potently targets oncogenic gene expression, thus warranting more extensive studies. Furthermore, we establish that the use of Lurbinectedin and its structural derivatives might be of clinical benefit in melanoma, but also elucidate for the first time potential resistance mechanisms against this new type of transcriptional inhibitors. In conclusion, this work sheds light on fundamental questions concerning gene expression regulation in melanoma cells and their molecular and cellular responses to transcriptional inhibitors, while also elucidating their potential clinical patient-related benefits and shortcomings.

Keywords: Cancer, Melanoma, Gene Expression, Transcriptional Addiction, Novel Therapeutics